

## **Applied Gas Dynamics**

# Applied Gas Dynamics

*Second Edition*

*Ethirajan Rathakrishnan*

Indian Institute of Technology Kanpur, India

**WILEY**



This edition first published 2019

© 2019 John Wiley & Sons Ltd

1e 2010 Wiley

All rights reserved. No part of this publication may be reproduced, stored in a retrieval system, or transmitted, in any form or by any means, electronic, mechanical, photocopying, recording or otherwise, except as permitted by law. Advice on how to obtain permission to reuse material from this title is available at <http://www.wiley.com/go/permissions>.

The right of Ethirajan Rathakrishnan to be identified as the author of this work has been asserted in accordance with law.

#### *Registered Office*

John Wiley & Sons, Inc., 111 River Street, Hoboken, NJ 07030, USA

John Wiley & Sons Ltd., The Atrium, Southern Gate, Chichester, West Sussex, PO19 8SQ, UK

#### *Editorial Office*

The Atrium, Southern Gate, Chichester, West Sussex, PO19 8SQ, UK

For details of our global editorial offices, customer services, and more information about Wiley products visit us at [www.wiley.com](http://www.wiley.com).

Wiley also publishes its books in a variety of electronic formats and by print-on-demand. Some content that appears in standard print versions of this book may not be available in other formats.

#### *Limit of Liability/Disclaimer of Warranty*

While the publisher and authors have used their best efforts in preparing this work, they make no representations or warranties with respect to the accuracy or completeness of the contents of this work and specifically disclaim all warranties, including without limitation any implied warranties of merchantability or fitness for a particular purpose. No warranty may be created or extended by sales representatives, written sales materials or promotional statements for this work. The fact that an organization, website, or product is referred to in this work as a citation and/or potential source of further information does not mean that the publisher and authors endorse the information or services the organization, website, or product may provide or recommendations it may make. This work is sold with the understanding that the publisher is not engaged in rendering professional services. The advice and strategies contained herein may not be suitable for your situation. You should consult with a specialist where appropriate. Further, readers should be aware that websites listed in this work may have changed or disappeared between when this work was written and when it is read. Neither the publisher nor authors shall be liable for any loss of profit or any other commercial damages, including but not limited to special, incidental, consequential, or other damages.

#### *Library of Congress Cataloging-in-Publication Data*

Names: Rathakrishnan, Ethirajan, author.

Title: Applied gas dynamics / Ethirajan Rathakrishnan.

Description: 2e. | Hoboken, NJ : John Wiley & Sons, 2019. | Includes bibliographical references and index. |

Identifiers: LCCN 2018041528 (print) | LCCN 2019002833 (ebook) | ISBN 9781119500384 (Adobe PDF) | ISBN 9781119500391 (ePub) | ISBN 9781119500452 (hardcover)

Subjects: LCSH: Gas dynamics.

Classification: LCC QC168 (ebook) | LCC QC168 .R38 2019 (print) | DDC 620.1/074—dc23

LC record available at <https://lcn.loc.gov/2018041528>

Cover Design: Wiley

Cover Image: © 3DSculptor/iStock.com

Set in 10/12pt WarnockPro by SPi Global, Chennai, India

10 9 8 7 6 5 4 3 2 1

*This book is dedicated to my parents,*  
*Mr Thammanur Shunmugam Ethirajan*  
*and*  
*Mrs Aandaal Ethirajan*

*Ethirajan Rathakrishnan*

## Contents

**Preface** *xv*

**Author Biography** *xvii*

**About the Companion Website** *xix*

<b>1</b>	<b>Basic Facts</b>	<b>1</b>
1.1	Definition of Gas Dynamics	1
1.2	Introduction	1
1.3	Compressibility	2
1.3.1	Limiting Conditions for Compressibility	3
1.4	Supersonic Flow – What Is it?	4
1.5	Speed of Sound	5
1.6	Temperature Rise	7
1.7	Mach Angle	8
1.7.1	Small Disturbance	10
1.7.2	Finite Disturbance	10
1.8	Thermodynamics of Fluid Flow	11
1.9	First Law of Thermodynamics (Energy Equation)	11
1.9.1	Energy Equation for an Open System	12
1.9.2	Adiabatic Flow Process	14
1.10	The Second Law of Thermodynamics (Entropy Equation)	15
1.11	Thermal and Calorical Properties	16
1.11.1	Thermally Perfect Gas	16
1.12	The Perfect Gas	17
1.12.1	Entropy Calculation	18
1.12.2	Isentropic Relations	20
1.12.3	Limitations on Air as a Perfect Gas	25
1.13	Wave Propagation	26
1.14	Velocity of Sound	26
1.15	Subsonic and Supersonic Flows	27
1.16	Similarity Parameters	28
1.17	Continuum Hypothesis	28
1.18	Compressible Flow Regimes	30
1.19	Summary	31
	Exercise Problems	34
<b>2</b>	<b>Steady One-Dimensional Flow</b>	<b>43</b>
2.1	Introduction	43

2.2	Fundamental Equations	43
2.3	Discharge from a Reservoir	45
2.3.1	Mass Flow Rate per Unit Area	47
2.3.2	Critical Values	51
2.4	Streamtube Area–Velocity Relation	54
2.5	de Laval Nozzle	57
2.5.1	Mass Flow Relation in Terms of Mach Number	65
2.5.2	Maximum Mass Flow Rate per Unit Area	65
2.6	Supersonic Flow Generation	66
2.6.1	Nozzles	68
2.6.2	Physics of the Nozzle Flow Process	69
2.7	Performance of Actual Nozzles	71
2.7.1	Nozzle Efficiency	71
2.7.2	Nozzle Discharge Coefficient	73
2.8	Diffusers	75
2.8.1	Special Features of Supersonic Diffusers	77
2.8.2	Supersonic Wind Tunnel Diffusers	78
2.8.3	Supersonic Inlets	81
2.8.4	Fixed-Geometry Inlet	82
2.8.5	Variable-Geometry Inlet	83
2.8.6	Diffuser Efficiency	84
2.9	Dynamic Head Measurement in Compressible Flow	88
2.9.1	Compressibility Correction to Dynamic Pressure	91
2.10	Pressure Coefficient	95
2.11	Summary	97
	Exercise Problems	99
<b>3</b>	<b>Normal Shock Waves</b>	<b>113</b>
3.1	Introduction	113
3.2	Equations of Motion for a Normal Shock Wave	113
3.3	The Normal Shock Relations for a Perfect Gas	115
3.4	Change of Stagnation or Total Pressure Across a Shock	118
3.5	Hugoniot Equation	121
3.5.1	Moving Shocks	123
3.6	The Propagating Shock Wave	123
3.6.1	Weak Shock	128
3.6.2	Strong Shock	130
3.7	Reflected Shock Wave	133
3.8	Centered Expansion Wave	138
3.9	Shock Tube	139
3.9.1	Shock Tube Applications	142
3.10	Summary	145
	Exercise Problems	148
<b>4</b>	<b>Oblique Shock and Expansion Waves</b>	<b>155</b>
4.1	Introduction	155
4.2	Oblique Shock Relations	156
4.3	Relation Between $\beta$ and $\theta$	158
4.4	Shock Polar	160

4.5	Supersonic Flow Over a Wedge	162
4.6	Weak Oblique Shocks	165
4.7	Supersonic Compression	167
4.8	Supersonic Expansion by Turning	169
4.9	The Prandtl–Meyer Expansion	170
4.9.1	Velocity Components $V_r$ and $V_\phi$	172
4.9.2	The Prandtl–Meyer Function	175
4.9.3	Compression	177
4.10	Simple and Nonsimple Regions	178
4.11	Reflection and Intersection of Shocks and Expansion Waves	178
4.11.1	Intersection of Shocks of the Same Family	181
4.11.2	Wave Reflection from a Free Boundary	183
4.12	Detached Shocks	189
4.13	Mach Reflection	191
4.14	Shock-Expansion Theory	197
4.15	Thin Airfoil Theory	202
4.15.1	Application of Thin Aerofoil Theory	203
4.16	Summary	210
	Exercise Problems	212
<b>5</b>	<b>Compressible Flow Equations</b>	<b>221</b>
5.1	Introduction	221
5.2	Crocco's Theorem	221
5.2.1	Basic Solutions of Laplace's Equation	224
5.3	General Potential Equation for Three-Dimensional Flow	225
5.4	Linearization of the Potential Equation	226
5.4.1	Small Perturbation Theory	227
5.5	Potential Equation for Bodies of Revolution	229
5.5.1	Conclusions	230
5.5.2	Solution of Nonlinear Potential Equation	231
5.6	Boundary Conditions	231
5.6.1	Bodies of Revolution	232
5.7	Pressure Coefficient	233
5.7.1	Bodies of Revolution	234
5.8	Summary	234
	Exercise Problems	237
<b>6</b>	<b>Similarity Rule</b>	<b>239</b>
6.1	Introduction	239
6.2	Two-Dimensional Flow: The Prandtl–Glauert Rule for Subsonic Flow	239
6.2.1	Prandtl–Glauert Transformations	239
6.2.2	The Direct Problem (Version I)	241
6.2.3	The Indirect Problem (Case of Equal Potentials): P–G Transformation (Version II)	243
6.2.4	Streamline Analogy (Version III): Gothert's Rule	244
6.3	Prandtl–Glauert Rule for Supersonic Flow: Versions I and II	245
6.3.1	Subsonic Flow	246
6.3.2	Supersonic Flow	246
6.3.2.1	Analogy Version I	246

6.3.2.2	Analogy Version II	247
6.3.2.3	Analogy Version III: Gothert's Rule	247
6.4	The von Karman Rule for Transonic Flow	248
6.4.1	Use of the von Karman Rule	249
6.5	Hypersonic Similarity	250
6.6	Three-Dimensional Flow: Gothert's Rule	252
6.6.1	General Similarity Rule	252
6.6.2	Gothert's Rule	254
6.6.3	Application to Wings of Finite Span	255
6.6.3.1	Planform	255
6.6.3.2	Profile	255
6.6.4	Application to Bodies of Revolution and Fuselages	255
6.6.4.1	Comparison of Two-Dimensional Symmetric Body and Axially Symmetric Body	256
6.6.5	The Prandtl–Glauert Rule	257
6.6.5.1	General Considerations	258
6.6.5.2	P–G Rule for Two-Dimensional Flow, Using Eqs. (6.46) and (6.47)	258
6.6.5.3	Application to Wings	259
6.6.5.4	Application to Wings of Finite Span	260
6.6.5.5	Application to Bodies of Revolution	261
6.6.6	The von Karman Rule for Transonic Flow	261
6.6.6.1	Application to Wings	261
6.6.6.2	Application to Bodies of Revolution	261
6.7	Critical Mach Number	261
6.7.1	Calculation of $M_{\infty}^*$	264
6.8	Summary	266
	Exercise Problems	269
<b>7</b>	<b>Two-Dimensional Compressible Flows</b>	<b>271</b>
7.1	Introduction	271
7.2	General Linear Solution for Supersonic Flow	271
7.2.1	Existence of Characteristics in a Physical Problem	273
7.2.2	Equation for the Streamlines from Kinematic Flow Condition	274
7.3	Flow over a Wave-Shaped Wall	276
7.3.1	Incompressible Flow	276
7.3.2	Compressible Subsonic Flow	277
7.3.3	Supersonic Flow	278
7.3.4	Pressure Coefficient	278
7.4	Summary	280
	Exercise Problems	280
<b>8</b>	<b>Flow with Friction and Heat Transfer</b>	<b>283</b>
8.1	Introduction	283
8.2	Flow in Constant Area Duct with Friction	283
8.2.1	The Fanno Line	284
8.3	Adiabatic, Constant-Area Flow of a Perfect Gas	285
8.3.1	Definition of Friction Coefficient	286
8.3.2	Effects of Wall Friction on Fluid Properties	287
8.3.3	Second Law of Thermodynamics	288

8.3.4	Working Relations	289
8.4	Flow with Heating or Cooling in Ducts	294
8.4.1	Governing Equations	294
8.4.2	Simple-Heating Relations for a Perfect Gas	295
8.5	Summary	300
	Exercise Problems	303
<b>9</b>	<b>Method of Characteristics</b>	<b>309</b>
9.1	Introduction	309
9.2	The Concepts of Characteristics	309
9.3	The Compatibility Relation	310
9.4	The Numerical Computational Method	312
9.4.1	Solid and Free Boundary Points	313
9.4.2	Sources of Error	316
9.4.3	Axisymmetric Flow	316
9.4.4	Nonisentropic Flow	317
9.5	Theorems for Two-Dimensional Flow	318
9.6	Numerical Computation with Weak Finite Waves	320
9.6.1	Reflection of Waves	320
9.7	Design of Supersonic Nozzle	323
9.7.1	Contour Design Details	324
9.8	Summary	328
<b>10</b>	<b>Measurements in Compressible Flow</b>	<b>329</b>
10.1	Introduction	329
10.2	Pressure Measurements	329
10.2.1	Liquid Manometers	329
10.2.2	Measuring Principle of Manometers	330
10.2.3	Dial-Type Pressure Gauges	332
10.2.4	Pressure Transducers	333
10.3	Temperature Measurements	335
10.4	Velocity and Direction	338
10.5	Density Problems	339
10.6	Compressible Flow Visualization	339
10.6.1	Supersonic Flows	340
10.7	Interferometer	341
10.7.1	Formation of Interference Patterns	341
10.7.2	Quantitative Evaluation	342
10.7.3	Fringe-Displacement Method	344
10.8	Schlieren System	344
10.8.1	Range and Sensitivity of the Schlieren System	347
10.8.2	Optical Components Quality Requirements	347
10.8.2.1	Schlieren Mirrors	347
10.8.2.2	Light Source	348
10.8.2.3	Condenser Lens	348
10.8.2.4	Focusing Lens	348
10.8.2.5	Knife-Edge	348
10.8.2.6	Color Schlieren	348
10.8.2.7	Short-Duration Light Source	348

10.8.3	Sensitivity of the Schlieren Method for Shock and Expansion Studies	350
10.9	Shadowgraph	352
10.9.1	Comparison of the Schlieren and Shadowgraph Methods	353
10.10	Wind Tunnels	354
10.10.1	High-Speed Wind Tunnels	354
10.10.2	Blowdown Type Wind Tunnels	354
10.10.2.1	Advantages	355
10.10.2.2	Disadvantages	355
10.10.3	Induction Type Tunnels	355
10.10.3.1	Advantages	356
10.10.3.2	Disadvantages	356
10.10.4	Continuous Supersonic Wind Tunnels	356
10.10.5	Losses in Supersonic Tunnels	357
10.10.6	Supersonic Wind Tunnel Diffusers	358
10.10.6.1	Polytropic Efficiency	358
10.10.6.2	Isentropic Efficiency	359
10.10.7	Effects of Second Throat	360
10.10.8	Compressor Tunnel Matching	362
10.10.9	The Mass Flow Rate	365
10.10.10	Blowdown Tunnel Operation	369
10.10.10.1	Reynolds Number Control	370
10.10.11	Optimum Conditions	372
10.10.12	Running Time of Blowdown Wind Tunnels	373
10.11	Hypersonic Tunnels	375
10.11.1	Hypersonic Nozzle	377
10.12	Instrumentation and Calibration of Wind Tunnels	380
10.12.1	Calibration of Supersonic Wind Tunnels	380
10.12.2	Calibration	381
10.12.3	Mach Number Determination	381
10.12.4	Pitot Pressure Measurement	382
10.12.5	Static Pressure Measurement	382
10.12.6	Determination of Flow Angularity	383
10.12.7	Determination of Turbulence Level	383
10.12.8	Determination of Test-Section Noise	384
10.12.9	Use of Calibration Results	384
10.12.10	Starting of Supersonic Tunnels	384
10.12.11	Starting Loads	385
10.12.12	Reynolds Number Effects	385
10.12.13	Model Mounting-Sting Effects	385
10.13	Calibration and Use of Hypersonic Tunnels	386
10.13.1	Calibration of Hypersonic Tunnels	386
10.13.2	Mach Number Determination	386
10.13.3	Determination of Flow Angularity	388
10.13.4	Determination of Turbulence Level	388
10.13.4.1	Blockage Tests	388
10.13.4.2	Starting Loads	388
10.13.5	Reynolds Number Effects	389
10.13.6	Force Measurements	389
10.14	Flow Visualization	390



10.15	Summary	390
	Exercise Problems	393
<b>11</b>	<b>Ramjet</b>	<b>395</b>
11.1	Introduction	395
11.2	The Ideal Ramjet	396
11.3	Aerodynamic Losses	401
11.4	Aerothermodynamics of Engine Components	404
11.4.1	Engine Inlets	404
11.4.1.1	Subsonic Inlets	404
11.5	Flow Through Inlets	405
11.5.1	Inlet Flow Process	406
11.5.2	Boundary Layer Separation	406
11.5.3	Flow Over the Inlet	406
11.6	Performance of Actual Intakes	410
11.6.1	Isentropic Efficiency	410
11.6.2	Stagnation Pressure Ratio	411
11.6.3	Supersonic Inlets	411
11.6.4	Supersonic Diffusers	412
11.6.5	Starting Problem	413
11.7	Shock–Boundary Layer Interaction	418
11.8	Oblique Shock Wave Incident on Flat Plate	419
11.9	Normal Shocks in Ducts	420
11.10	External Supersonic Compression	422
11.11	Two-Shock Intakes	423
11.12	Multi-Shock Intakes	427
11.13	Isentropic Compression	429
11.14	Limits of External Compression	431
11.15	External Shock Attachment	433
11.16	Internal Shock Attachment	433
11.17	Pressure Loss	434
11.18	Supersonic Combustion	442
11.19	Summary	444
	Exercise Problems	447
<b>12</b>	<b>Jets</b>	<b>451</b>
12.1	Introduction	451
12.1.1	Subsonic Jets	453
12.2	Mathematical Treatment of Jet Profiles	454
12.3	Theory of Turbulent Jets	455
12.3.1	Mean Velocity and Mean Temperature	456
12.3.2	Turbulence Characteristics of Free Jets	457
12.3.3	Mixing Length	458
12.4	Experimental Methods for Studying Jets and the Techniques Used for Analysis	461
12.4.1	Pressure Measurement	462
12.4.1.1	Precautions Observed	463
12.5	Expansion Levels of Jets	464
12.5.1	Overexpanded Jets	464

12.5.2	Correctly Expanded Jets	467
12.5.3	Underexpanded Jets	469
12.6	Control of Jets	471
12.6.1	Classification of Control Methods	473
12.6.1.1	Active Control	473
12.6.1.2	Passive Control	473
12.6.2	Role of Shear Layer in Flow Control	474
12.6.2.1	Large-Scale Structure in Subsonic Shear Layers	474
12.6.2.2	Role of Large-Scale Structures in Subsonic Mixing Enhancement	475
12.6.3	Supersonic Shear Layers	475
12.6.4	Use of Tabs for Jet Control	477
12.6.5	Evaluation of the Effectiveness of Some Specific Passive Controls	481
12.6.5.1	Jet Control with the Limiting Tab	481
12.6.5.2	Centerline Decay	482
12.6.5.3	Flow Development	487
12.6.5.4	Acoustic Characteristics of a Mach 1.6 Jet	490
12.6.5.5	Acoustic Characteristics of a Mach 1.79 Jet	496
12.6.5.6	Acoustic Characteristics of a Mach 2 Jet	496
12.6.5.7	Use of Corrugated Tabs	497
12.6.5.8	Pressure Profiles	504
12.6.5.9	Optical Flow Visualization	511
12.6.5.10	Water Flow Visualization	517
12.6.6	Grooves and Cutouts	519
12.7	Noncircular Jets and Shifted Tabs	519
12.7.1	Jet Control with Tabs	523
12.7.2	Shifted Tabs	527
12.7.3	Ventilated Triangular Tabs	532
12.7.4	Tab Edge Effect	535
12.8	Summary	541
<b>Appendix A</b>		547
<b>References</b>		619
<b>Index</b>		625

## Preface

The first edition of this book, developed to serve as the text for a course on gas dynamics at the introductory level for undergraduates and an advanced level at the graduate level was well received all over the world, because of its completeness and proper balance between the theoretical aspects and application of this science.

Over the years, the feedback received from the faculty and students made the author realize the need for adding solved examples and exercise problems at the end of the chapter on ramjets.

Some faculty suggested adding more examples at appropriate locations in various chapters and adding exercise problems on moving waves and similarity would make the book more effective for practicing the theory presented in the book.

Considering the feedback from faculty and students, the following material has been added to this edition.

- A number of new examples to different chapters of the book.
- A section on critical Mach number in Chapter 6.
- Examples using the theory of ramjet and a list of exercise problems along with answers in Chapter 11.
- A subsection highlighting new developments in the field of noncircular jets and the control of jets with shifted tab, which keeps the nozzle exit clean so that the jet will enjoy full momentum thrust potential in Chapter 12.

I would like to thank the faculty and students all over the world for adopting this book for their courses. I thank my doctoral student Maruthupandiyan and master's student Kaustubh Hirve for checking the material added in this edition and the Solutions Manual.

For instructors, a companion Solutions Manual that contains typed solutions to all the end-of-chapter problems and lecture slides for the complete book are available from the publisher.

*Ethirajan Rathakrishnan*

## Author Biography

Ethirajan Rathakrishnan is professor of Aerospace Engineering at the Indian Institute of Technology Kanpur. He is well known internationally for his research in the area of high-speed jets. The limit for the passive control of jets, called the *Rathakrishnan Limit*, is his contribution to the field of jet research, and the concept of *breathing blunt nose (BBN)*, which reduces the positive pressure at the nose and increases the low pressure at the base simultaneously, is his contribution to drag reduction at hypersonic speeds. Positioning the twin-vortex Reynolds number at around 5000, by changing the geometry from cylinder, for which the maximum limit for the Reynolds number for positioning the twin-vortex was found to be around 160, by von Karman, to flat plate, is his addition to vortex flow theory. He has published a large number of research articles in many highly regarded international journals. He is a Fellow of many professional societies, including the Royal Aeronautical Society. Professor Rathakrishnan serves as the editor-in-chief of the *International Review of Aerospace Engineering* (IREASE) and *International Review of Mechanical Engineering* (IREME) journals. He has authored 12 other books: *Gas Dynamics*, 6th ed. (PHI Learning, New Delhi, 2017); *Fundamentals of Engineering Thermodynamics*, 2nd ed. (PHI Learning, New Delhi, 2005); *Fluid Mechanics: An Introduction*, 3rd ed. (PHI Learning, New Delhi, 2012); *Gas Tables*, 3rd ed. (Universities Press, Hyderabad, India, 2012); *Theory of Compressible Flows* (Maruzen Co., Ltd., Tokyo, 2008); *Gas Dynamics Workbook*, 2nd ed. (Praise Worthy Prize, Napoli, 2013); *Elements of Heat Transfer* (CRC Press, Boca Raton, FL, 2012); *Theoretical Aerodynamics* (Wiley, Hoboken, NJ, 2013); *High Enthalpy Gas Dynamics* (Wiley, Hoboken, NJ, 2015); *Dynamique Des Gaz* (Praise Worthy Prize, Napoli, Italy, 2015); *Instrumentation, Measurements and Experiments in Fluids*, 2nd ed. (CRC Press, Boca Raton, FL, 2017); and *Helicopter Aerodynamics* (PHI Learning, New Delhi, 2019).

*At least two trees are planted for each one used for paper production.*

*Ethirajan Rathakrishnan*

## About the Companion Website

This book is accompanied by a companion website:

[www.wiley.com/go/gasdyn](http://www.wiley.com/go/gasdyn)



The website includes:

- Lecture slides for the complete book
- Solutions Manual containing detailed solutions for the problems listed at the end of different chapters

## 1

## Basic Facts

### 1.1 Definition of Gas Dynamics

*Gas dynamics* is the science of fluid flow in which both density and temperature changes become significant. Taking 5% change in temperature as significant, it can be stated that, at standard sea level, Mach number 0.5 is the lower limit of gas dynamics. Thus, gas dynamics is the science of flow fields with speeds of Mach 0.5 and above. Therefore, gas dynamic regimes consist of both subsonic and supersonic Mach numbers. Further, when the flow is supersonic, any change of flow property or direction is caused by waves. These waves are isentropic and nonisentropic compression waves (shock waves), expansion waves, and Mach waves. Among these, the compression and expansion waves can cause finite changes but the flow property changes caused by a Mach wave are insignificant. The essence of gas dynamics is that, when the flow speed is supersonic, the entire flow field is dominated by Mach waves, expansion waves, and shock waves. It is through these waves that the change of flow properties, from one state to another, takes place.

### 1.2 Introduction

*Compressible flow* is the science of fluid flow where the density change associated with pressure change is significant. *Fluid mechanics* is the science of fluid flow in which the temperature changes associated with the flow are insignificant. Fluid mechanics is essentially the science of *isenthalpic* flows, and thus the main equations governing a fluid dynamic stream are only the continuity and momentum equations plus the second law of thermodynamics. The energy equation is passive as far as fluid dynamic streams are concerned. At standard sea level conditions, considering less than 5% change in temperature as insignificant, flow with a Mach number of less than 0.5 can be termed a *fluid mechanic stream*. A fluid mechanic stream may be compressible or incompressible. For an incompressible flow, both temperature and density changes are insignificant. For a compressible flow, the temperature change may be insignificant but density change is finite.

However, in many engineering applications, such as the design of airplanes, missiles, and launch vehicles, the flow Mach numbers associated are more than 0.5. Hence both temperature and density changes associated with the flow become significant. The study of such flows where both density and temperature changes associated with pressure change become appreciable is called *gas dynamics*. In other words, gas dynamics is the science of fluid flow in which both density and temperature changes are significant. The essence of gas dynamics is that the entire flow field is dominated by Mach waves, expansion waves, and shock waves, when the flow speed is supersonic. It is through these waves that the change of flow properties

from one state to another takes place. In the theory of gas dynamics, a change of state in flow properties is achieved by three means: (i) with area change, treating the fluid as inviscid and passage to be frictionless; (ii) with friction, treating the heat transfer between the surroundings and the system to be negligible; and (iii) with heat transfer, assuming the fluid to be inviscid. These three types of flows are called *isentropic flow*, *frictional* or *Fanno type flow*, and *Rayleigh type flow*, respectively.

All problems in gas dynamics can be classified under the three flow processes described above, while, of course, bearing in mind the previously stated assumptions. Although it is impossible in practice to have a flow process which is purely isentropic or Fanno type or Rayleigh type, these assumptions are justified, since the results obtained with these treatments prove to be accurate enough for most practical problems in gas dynamics.

### 1.3 Compressibility

Fluids such as water are incompressible under normal conditions. But under conditions of high pressure (e.g. 1000 atm) they are compressible. The change in volume is the characteristic feature of a compressible medium under static conditions. Under dynamic conditions, that is when the medium is moving, the characteristic feature for incompressible and compressible flow situations are: the volume flow rate,  $\dot{Q} = AV = \text{constant}$  at any cross-section of a streamtube for incompressible flow, and the mass flow rate,  $\dot{m} = \rho AV = \text{constant}$  at any cross-section of a streamtube for compressible flow. In these relations,  $A$  is the cross-sectional area of the streamtube and  $V$  and  $\rho$  are, respectively, the velocity and density of the fluid at that cross-section (Figure 1.1).

In general, the flow of an incompressible medium is called *incompressible flow* and that of a compressible medium is called *compressible flow*. Though this statement is true for incompressible media under normal conditions of pressure and temperature, for compressible media, like gases, it has to be modified.

As long as a gas flows at a sufficiently low speed from one cross-section of a passage to another the change in volume (or density) can be neglected and, therefore, the flow can be treated as incompressible. Although the fluid is compressible, this property may be neglected when the flow is taking place at low speeds. In other words, although there is some density change associated with every physical flow, it is often possible (for low-speed flows) to neglect it and idealize the flow as incompressible. This approximation is applicable to many practical flow situations, such as low-speed flow around an airplane and flow through a vacuum cleaner.

From the above discussion it is clear that compressibility is the phenomenon by virtue of which the flow changes its density with changes in speed. Now, we may ask, what are the precise conditions under which density changes must be considered? We will try to answer this question now.

A quantitative measure of compressibility is the volume modulus of elasticity  $E$ , defined as

$$E = -\frac{\Delta p}{\Delta V/V_i} \quad (1.1)$$

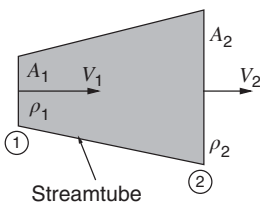


Figure 1.1 Elemental streamtube.

where  $\Delta p$  is the change in static pressure,  $\Delta V$  is the change in volume, and  $V_i$  is the initial volume. For ideal gases, the equation of state is

$$pV = RT$$

For isothermal flows, this reduces to

$$pV = p_i V_i = \text{constant}$$

where  $p_i$  is the initial pressure.

The above equation may be written as

$$(p_i + \Delta p)(V_i + \Delta V) = p_i V_i$$

Expanding this equation, and neglecting the second-order terms, we get

$$\Delta p V_i + \Delta V p_i = 0$$

Therefore,

$$\Delta p = -p_i \frac{\Delta V}{V_i} \quad (1.2)$$

For gases, from Eqs. (1.1) and (1.2), we get

$$E = p_i \quad (1.3)$$

Hence, by Eq. (1.2), the compressibility may be defined as the volume modulus of the pressure.

### 1.3.1 Limiting Conditions for Compressibility

By mass conservation, we have  $\dot{m} = \rho V = \text{constant}$ , where  $\dot{m}$  is mass flow rate per unit area,  $V$  is the flow velocity, and  $\rho$  is the corresponding density. This can also be written as

$$(V_i + \Delta V)(\rho_i + \Delta \rho) = \rho_i V_i$$

Considering only first-order terms, this simplifies to

$$\frac{\Delta \rho}{\rho_i} = -\frac{\Delta V}{V_i}$$

Substituting this into Eq. (1.1) and noting that  $V = \mathbf{V}$  for unit area per unit time in the present case, we get

$$\Delta p = E \frac{\Delta \rho}{\rho_i} \quad (1.4)$$

From Eq. (1.4), it can be seen that the compressibility may also be defined as the *density modulus* of the pressure.

For incompressible flows, by Bernoulli's equation, we have

$$p + \frac{1}{2} \rho V^2 = \text{constant} = p_{\text{stag}}$$

where the subscript "stag" refers to *stagnation condition*. The above equation may also be written as

$$p_{\text{stag}} - p = \Delta p = \frac{1}{2} \rho V^2$$

that is the change of pressure from stagnation to static states is equal to  $\frac{1}{2} \rho V^2$ . Using Eq. (1.4) in the above relation, we obtain

$$\frac{\Delta p}{E} = \frac{\Delta \rho}{\rho_i} = \frac{\rho_i V_i^2}{2E} = \frac{q_i}{E} \quad (1.5)$$



where  $q_i = \frac{1}{2}\rho_i V_i^2$  is the dynamic pressure. Equation (1.5) relates the density change to the flow speed.

The compressibility effects can be neglected if the density changes are very small, that is if

$$\frac{\Delta\rho}{\rho_i} \ll 1$$

From Eq. (1.5) it is seen that for neglecting compressibility

$$q/E \ll 1$$

For gases, the speed of sound  $a$  may be expressed in terms of pressure and density changes as (see Eq. (1.11))

$$a^2 = \frac{\Delta p}{\Delta\rho}$$

Using Eq. (1.4) in the above relation, we get

$$a^2 = \frac{E}{\rho_i}$$

With this, Eq. (1.5) reduces to

$$\frac{\Delta\rho}{\rho_i} = \frac{\rho_i}{2} \frac{V_i^2}{E} = \frac{1}{2} \left( \frac{V}{a} \right)^2 \quad (1.6)$$

The ratio  $V/a$  is called the Mach number  $M$ . Therefore, the condition of incompressibility for gases becomes

$$M^2/2 \ll 1$$

Thus, the criterion determining the effect of compressibility for gases is that the magnitude of the Mach number  $M$  should be negligibly small. Indeed, mathematics would stipulate this limit as  $M \rightarrow 0$ . But Mach number zero corresponds to stagnation state. Therefore, in engineering sciences flows with very small Mach numbers are treated as incompressible. To have a quantification of this limiting value of the Mach number to treat a flow as incompressible, a Mach number corresponding to a 5% change in flow density is usually taken as the limit.

It is widely accepted that compressibility can be neglected when

$$\frac{\Delta\rho}{\rho_i} \leq 0.05 \text{ or } 5\%$$

that is when  $M \leq 0.3$ . In other words, the flow may be treated as incompressible when  $V \leq 100 \text{ m s}^{-1}$ , that is when  $V \leq 360 \text{ kmph}$  under standard sea level conditions. The above values of  $M$  and  $V$  are widely accepted values and they may be re-fixed at different levels, depending upon the flow situation and the degree of accuracy desired.

## 1.4 Supersonic Flow – What Is it?

The Mach number  $M$  is defined as the ratio of the local flow speed  $V$  to the local speed of sound  $a$

$$M = \frac{V}{a} \quad (1.7)$$

Thus,  $M$  is a dimensionless quantity. In general, both  $V$  and  $a$  are functions of position and time. Therefore, the Mach number is not just the flow speed made nondimensional by dividing

by a constant. In other words, the flow Mach number is the ratio of  $V$  to  $a$  and this relation should not be viewed as  $M$  proportional to  $V$ , or inversely proportional to  $a$ , in isolation. That is, we cannot write  $M \propto V$  or  $M \propto 1/a$  in isolation. However, it is almost always true that  $M$  increases monotonically with  $V$ .

A flow with a Mach number greater than unity is termed *supersonic flow*. In a supersonic flow  $V > a$  and the flow upstream of a given point remains unaffected by changes in conditions at that point.

## 1.5 Speed of Sound

Sound waves are infinitely small pressure disturbances. The speed with which sound propagates in a medium is called the *speed of sound* and is denoted by  $a$ . If an infinitesimal disturbance is created by the piston, as shown in Figure 1.2, the wave propagates through the gas at the velocity of sound relative to the gas into which the disturbance is moving. Let the stationary gas at pressure  $p_i$  and density  $\rho_i$  in the pipe be set in motion by moving the piston. The infinitesimal pressure wave created by the piston movement travels with speed  $a$ , leaving the medium behind it at pressure  $p_1$  and density  $\rho_1$  to move with velocity  $V$ .

As a result of compression created by the piston, the pressure and density next to the piston are infinitesimally greater than the pressure and density of the gas at rest ahead of the wave. Therefore,

$$\Delta p = p_1 - p_i, \quad \Delta \rho = \rho_1 - \rho_i$$

are small.

Choose a control volume of length  $b$ , as shown in Figure 1.2. Compression of volume  $Ab$  causes the density to rise from  $\rho_i$  to  $\rho_1$  in time  $t = b/a$ . The mass flow into volume  $Ab$  is

$$\dot{m} = \rho_1 AV \quad (1.8)$$

For mass conservation,  $\dot{m}$  must also be equal to the mass flow rate  $A b(\rho_1 - \rho_i)/t$  through the control volume. Thus,

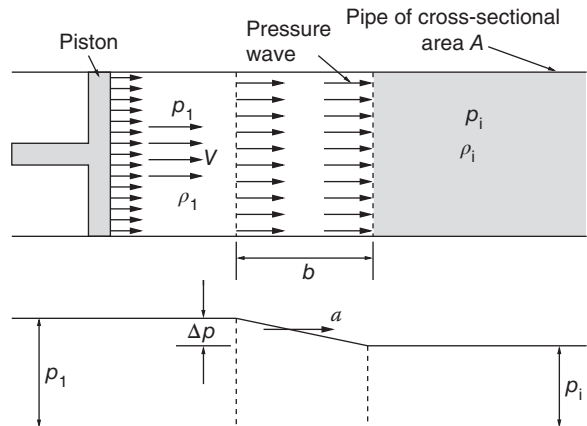
$$Ab(\rho_1 - \rho_i)/t = \rho_1 AV$$

or

$$a(\rho_1 - \rho_i) = \rho_1 V \quad (1.9)$$

because  $b/t = a$ .

**Figure 1.2** Propagation of pressure disturbance.



The compression wave caused by the piston motion travels and accelerates the gas from zero velocity to  $V$ . The acceleration is given by

$$\frac{V}{t} = V \frac{a}{b}$$

The mass in the control volume  $Ab$  is

$$m = Ab\bar{\rho}$$

where

$$\bar{\rho} = \frac{\rho_i + \rho_1}{2}$$

The force acting on the control volume is  $F = A(p_1 - p_i)$ . Therefore, by Newton's law,

$$\begin{aligned} A(p_1 - p_i) &= m \left( V \frac{a}{b} \right) \\ A(p_1 - p_i) &= (Ab\bar{\rho}) \left( V \frac{a}{b} \right) \end{aligned}$$

or

$$\bar{\rho}Va = p_1 - p_i \quad (1.10)$$

Because the disturbance is very weak,  $\rho_1$  on the right-hand side of Eq. (1.9) may be replaced by  $\bar{\rho}$  to result in

$$a(\rho_1 - \rho_i) = \bar{\rho}V$$

Using this relation, Eq. (1.10) can be written as

$$a^2 = \frac{p_1 - p_i}{\rho_1 - \rho_i} = \frac{\Delta p}{\Delta \rho}$$

In the limiting case of  $\Delta p$  and  $\Delta \rho$  approaching zero, the above equation leads to

$$\boxed{a^2 = \frac{dp}{d\rho}} \quad (1.11)$$

This is the *Laplace equation* and is valid for any fluid.

The sound wave is an isentropic pressure wave, across which only infinitesimal changes in fluid properties occur. Further, the wave itself is extremely thin, and changes in properties occur very rapidly. The rapidity of the process rules out the possibility of any heat transfer between the system of fluid particles and its surrounding.

For very strong pressure waves, the traveling speed of a disturbance may be greater than that of sound. The pressure can be expressed as

$$p = p(\rho) \quad (1.12)$$

For an isentropic process of a gas,

$$\frac{p}{\rho^\gamma} = \text{constant}$$

where the isentropic index  $\gamma$  is the ratio of specific heats and is a constant for a perfect gas. Using the above relation in Eq. (1.11), we get

$$a^2 = \gamma p / \rho \quad (1.13)$$

For a perfect gas, by the state equation

$$p = \rho RT \quad (1.14)$$

where  $R$  is the gas constant and  $T$  the static temperature of the gas in absolute units.

Equations (1.13) and (1.14) together lead to the following expression for the speed of sound.

$$a = \sqrt{\gamma RT} \quad (1.15)$$

The perfect gas assumption is valid so long as the speed of the gas stream is not too high. However, at hypersonic speeds the assumption of a perfect gas is not valid and we must consider Eq. (1.11) to calculate the speed of sound.

## 1.6 Temperature Rise

For a perfect gas,

$$p = \rho RT, \quad R = c_p - c_v$$

where  $c_p$  and  $c_v$  are specific heats at constant pressure and constant volume, respectively. Also,  $\gamma = c_p/c_v$ ; therefore,

$$R = \frac{\gamma - 1}{\gamma} c_p \quad (1.16)$$

For an isentropic change of state, an equation not involving  $T$  can be written as

$$p/\rho^\gamma = \text{constant}$$

Now, between state 1 and any other state the relation between the pressures and densities can be written as

$$\left(\frac{p}{p_1}\right) = \left(\frac{\rho}{\rho_1}\right)^\gamma \quad (1.17)$$

Combining Eqs. (1.17) and (1.14), we get

$$\frac{T}{T_1} = \left(\frac{\rho}{\rho_1}\right)^{\gamma-1} = \left(\frac{p}{p_1}\right)^{(\gamma-1)/\gamma} \quad (1.18)$$

The above relations are very useful for gas dynamic studies. The temperature, density, and pressure ratios in Eq. (1.18) can be expressed in terms of the flow Mach number.

Let us examine the flow around a symmetrical body, as shown in Figure 1.3.

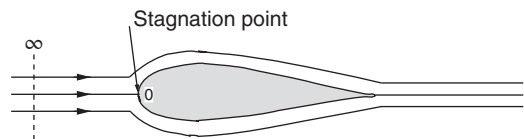
In a compressible medium, there will be a change in density and temperature at point 0. The temperature rise at the stagnation point can be obtained from the energy equation.

The energy equation for an isentropic flow is

$$h + \frac{V^2}{2} = \text{constant} \quad (1.19)$$

where  $h$  is the enthalpy.

**Figure 1.3** Flow around a symmetrical body.



Equating the energy at far upstream,  $\infty$ , and the stagnation point 0, we get

$$h_{\infty} + \frac{V_{\infty}^2}{2} = h_0 + \frac{V_0^2}{2}$$

But  $V_0 = 0$ , thus

$$h_0 - h_{\infty} = \frac{V_{\infty}^2}{2}$$

For a perfect gas  $h = c_p T$ ; therefore, from the above relation we obtain

$$c_p(T_0 - T_{\infty}) = \frac{V_{\infty}^2}{2}$$

that is

$$\Delta T = T_0 - T_{\infty} = \frac{V_{\infty}^2}{2c_p} \quad (1.20)$$

Combining Eqs. (1.15) and (1.16), we get

$$c_p = \frac{1}{\gamma - 1} \frac{a_{\infty}^2}{T_{\infty}}$$

Hence,

$$\Delta T = \frac{\gamma - 1}{2} T_{\infty} M_{\infty}^2 \quad (1.21)$$

that is

$$T_0 = T_{\infty} \left( 1 + \frac{\gamma - 1}{2} M_{\infty}^2 \right) \quad (1.22)$$

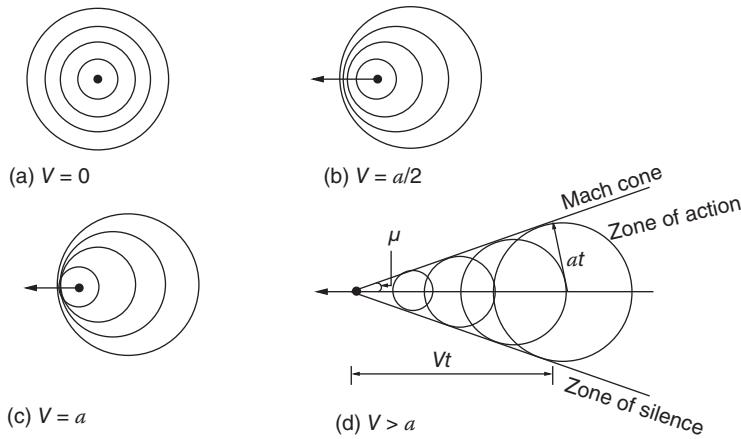
For air,  $\gamma = 1.4$ , and hence

$$T_0 = T_{\infty} (1 + 0.2 M_{\infty}^2) \quad (1.23)$$

where  $T_0$  is the temperature at the stagnation point on the body. It is also referred to as *total temperature*. For example, at the stagnation point 0 on the body shown in Figure 1.3, the flow will attain the stagnation temperature.

## 1.7 Mach Angle

The presence of a small disturbance is felt throughout the field by means of disturbance waves traveling at the local velocity of sound relative to the medium. Let us examine the propagation of pressure disturbances created by a moving object, shown in Figure 1.4. The propagation of disturbance waves created by an object moving with velocity  $V = 0$ ,  $V = a/2$ ,  $V = a$ , and  $V > a$  is shown in Figures 1.4a–d, respectively. In a subsonic flow the disturbance waves reach a stationary observer before the source of disturbance could reach him, as shown in Figures 1.4a and b. But in supersonic flows it takes a considerable amount of time for an observer to perceive the pressure disturbance, after the source has passed. This is one of the fundamental differences between subsonic and supersonic flows. Therefore, in a subsonic flow the streamlines sense the presence of any obstacle in the flow field and adjust themselves well ahead of the obstacle and flow around it smoothly.



**Figure 1.4** Propagation of disturbance waves.

But in a supersonic flow, the streamlines feel the obstacle only when they hit it. The obstacle acts as a source, and the streamlines deviate at the Mach cone, as shown in Figure 1.4d. Thus, in a supersonic flow, the disturbance due to an obstacle is sudden and the flow behind the obstacle has to change abruptly.

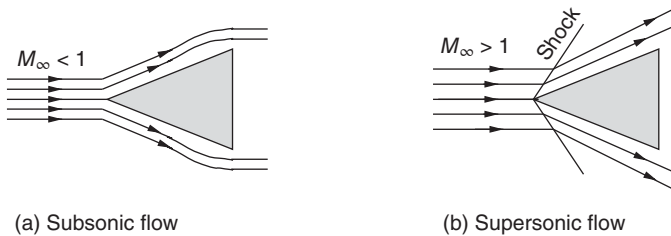
Flow around a wedge shown in Figures 1.5a and b illustrates the smooth and abrupt change in flow direction for subsonic and supersonic flow, respectively. For  $M_\infty < 1$ , the flow direction changes smoothly and the pressure decreases with acceleration. For  $M_\infty > 1$ , there is a sudden change in flow direction at the body, and the pressure increases downstream of the shock.

In Figure 1.4d, it is shown that for supersonic motion of an object there is a well-defined conical zone in the flow field with the object located at the nose of the cone, and the disturbance created by the moving object is confined only to the field included inside the cone. The flow field zone outside the cone does not even feel the disturbance. For this reason, von Karman termed the region inside the cone as the *zone of action*, and the region outside the cone as the *zone of silence*. The lines at which the pressure disturbance is concentrated and which generate the cone are called *Mach waves* or *Mach lines*. The angle between the Mach line and the direction of motion of the body is called the *Mach angle*  $\mu$ . From Figure 1.4d, we have

$$\sin \mu = \frac{at}{Vt} = \frac{a}{V}$$

that is

$$\boxed{\sin \mu = \frac{1}{M}} \quad (1.24)$$



**Figure 1.5** Flow around a wedge.

From the propagation of the disturbance waves shown in Figure 1.4, we can infer the following features of the flow regimes.

- When the medium is *incompressible* ( $M = 0$ , Figure 1.4a) or when the speed of the moving disturbance is negligibly small compared to the local sound speed, the pressure pulse created by the disturbance spreads uniformly in all directions.
- When the disturbance source moves with a *subsonic speed* ( $M < 1$ , Figure 1.4b), the pressure disturbance is felt in all directions and at all points in space (neglecting viscous dissipation), but the pressure pattern is no longer symmetrical.
- For *sonic velocity* ( $M = 1$ , Figure 1.4c) the pressure pulse is at the boundary between subsonic and supersonic flow and the wavefront is a plane.
- For *supersonic speeds* ( $M > 1$ , Figure 1.4d) the disturbance wave propagation phenomenon is totally different from those at subsonic speeds. All the pressure disturbances are included in a cone that has the disturbance source at its apex, and the effect of the disturbance is not felt upstream of the disturbance source.

### 1.7.1 Small Disturbance

When the apex angle of wedge  $\delta$  is vanishingly small, the disturbances will be small, and we can consider these disturbance waves identical to sound pulses. In such a case, the deviation of streamlines will be small and there will be an infinitesimally small increase of pressure across the Mach cone, as shown in Figure 1.6.

### 1.7.2 Finite Disturbance

When the wedge angle  $\delta$  is finite, the disturbances introduced are finite, then the wave is not called a Mach wave but a *shock* or shock wave (see Figure 1.7). The angle of shock  $\beta$  is always smaller than the Mach angle. The deviation of the streamlines is finite and the pressure increase across a shock wave is finite.

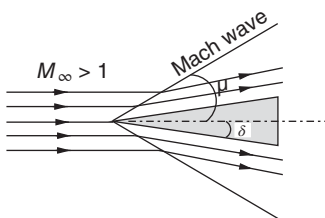


Figure 1.6 Mach cone.

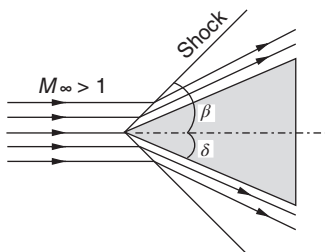


Figure 1.7 Shock wave.

## 1.8 Thermodynamics of Fluid Flow

Entropy and temperature are the two fundamental concepts of thermodynamics. Unlike low-speed or incompressible flows, the energy change associated with a compressible flow is substantial enough to strongly interact with other properties of the flow. Hence, the energy concept plays an important role in the study of compressible flows. In other words, the study of thermodynamics which deals with energy (and entropy) is an essential component in the study of compressible flow.

The following are the broad divisions of fluid flow based on thermodynamic considerations.

(i) Fluid mechanics of perfect fluids – fluids without viscosity and heat (transfer) conductivity – is an extension of equilibrium thermodynamics to moving fluids. The kinetic energy of the fluid has to be considered in addition to the internal energy which the fluid possesses, even when at rest. (ii) Fluid mechanics of real fluids (those that go beyond the scope of classical thermodynamics). The transport processes of momentum and heat (energy) are of primary interest here. But, even though thermodynamics is not fully and directly applicable to all phases of real fluid flow, it is often extremely helpful in relating the initial and final conditions.

For low-speed flow problems, thermodynamic considerations are not needed, because the heat content of the fluid flow is so large compared to the kinetic energy of the flow that the temperature remains nearly constant even if the whole of the kinetic energy is transformed into heat. In other words, the difference between the static and stagnation temperatures is not significant in low-speed flows. But in high-speed flows, the kinetic energy content of the fluid can be so large compared to its heat content that the difference between the static and stagnation temperature can become substantial. Hence, emphasis on the thermodynamic concepts assumes importance in high-speed flow analysis.

## 1.9 First Law of Thermodynamics (Energy Equation)

Consider a closed system, consisting of a certain amount of gas at rest, across whose boundaries no transfer of mass is possible. Let  $\delta Q$  be an incremental amount of heat added to the system across the boundary (by thermal conduction or by direct radiation). Also, let  $\delta W$  denote the work done on the system by the surroundings (or by the system on the surroundings). The sign convention is positive when the work is done by the system and negative when the work is done on the system. Owing to the molecular motion of the gas, the system has an internal energy  $U$ . The first law of thermodynamics states that the *heat added minus work done by the system is equal to the change in the internal energy of the system*:

$$\boxed{\delta Q - \delta W = dU} \quad (1.25)$$

This is an empirical result confirmed by laboratory experiments and practical experience. In Eq. (1.25), the internal energy  $U$  is a state variable (thermodynamic property). Hence, the change in internal energy  $dU$  is an exact differential and its value depends only on the initial and final states of the system. In contrast (the nonthermodynamic properties),  $\delta Q$  and  $\delta W$  depend on the process by which the system attained its final state from the initial state.

In general, for any given  $dU$ , there are an infinite number of ways (processes) by which heat can be added and work can be done on the system. In the present course of study, we will mainly be concerned with the following three types of processes only.



- **Adiabatic process:** A process in which no heat is added to or taken away from the system.
- **Reversible process:** A process which can be reversed without leaving any trace on the surroundings, that is both the system and the surroundings are returned to their initial states at the end of the reverse process.
- **Isentropic process:** A process which is adiabatic and reversible.

For an open system (e.g. pipe flow), there is always a term  $(U + p V)$  instead of just  $U$ . This term is referred to as *enthalpy* or *heat function*  $H$ , and is given by

$$H = U + p V \quad (1.26)$$

$$H_2 - H_1 = U_2 - U_1 + p_2 V_2 - p_1 V_1 \quad (1.27)$$

where  $(p_2 V_2 - p_1 V_1)$  is termed *flow work*, and subscripts 1 and 2 represent states 1 and 2.

In general, we can say that the following are the major differences between the open and closed systems.

- The mass that enters or leaves an open system has kinetic energy, whereas there is no mass transfer possible across the boundaries of a closed system.
- The mass can enter and leave an open system at different levels of potential energy.
- Open systems are capable of delivering work continuously, because in the system the medium which transforms energy is continuously replaced. This useful work, which a machine continuously delivers, is called the *shaft work*.

### 1.9.1 Energy Equation for an Open System

Consider the system shown in Figure 1.8. The total energy  $E$  at the inlet station 1 and the outlet station 2 is given by

$$E_1 = U_1 + \frac{1}{2} m V_1^2 + m g z_1 \quad (1.28)$$

$$E_2 = U_2 + \frac{1}{2} m V_2^2 + m g z_2 \quad (1.29)$$

For an open system, the first-law expression given by Eq. (1.25) has to be rewritten with the total energy  $E$  in place of the internal energy  $U$ . Thus, we have

$$Q_{12} - W_{12} = E_2 - E_1 \quad (1.30)$$

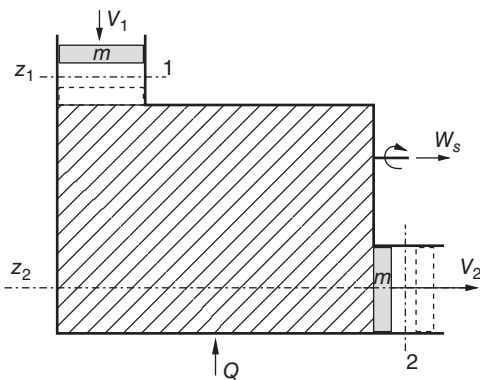


Figure 1.8 Open system.

Substituting for  $E_1$  and  $E_2$  from Eqs. (1.28) and (1.29), respectively, we get

$$Q_{12} - W_{12} = \left( U_2 + \frac{m}{2} V_2^2 + m g z_2 \right) - \left( U_1 + \frac{m}{2} V_1^2 + m g z_1 \right) \quad (1.31)$$

For an open system, the shaft (useful) work is not just equal to  $W_{12}$ , because the work done to move the pistons at 1 and 2 must also be considered. Work done with respect to the system by the piston at state 1 is

$$\begin{aligned} W'_1 &= -F_1 \Delta_1 & (F_1 = \text{force and } \Delta_1 = \text{displacement}) \\ W'_1 &= -p_1 A_1 \Delta_1 & (p_1 = \text{pressure at 1; } A_1 = \text{cross-sectional area of piston}) \\ W'_1 &= -p_1 V_1 \end{aligned}$$

Work delivered at 2 is  $W'_2 = p_2 V_2$ . Therefore,

$$W_{12} = W_s + p_2 V_2 - p_1 V_1 \quad (1.32)$$

In Eq. (1.32),  $W_s$  is the shaft work, which can be extracted from the system, and  $(p_2 V_2 - p_1 V_1)$  is the flow work necessary to maintain the flow. Substituting Eq. (1.32) into Eq. (1.31), we get

$$Q_{12} - W_s = \left( U_2 + p_2 V_2 + \frac{m}{2} V_2^2 + m g z_2 \right) - \left( U_1 + p_1 V_1 + \frac{m}{2} V_1^2 + m g z_1 \right)$$

or

$$Q_{12} - W_s = \left( H_2 + \frac{m}{2} V_2^2 + m g z_2 \right) - \left( H_1 + \frac{m}{2} V_1^2 + m g z_1 \right)$$

where  $H_1 = U_1 + p_1 V_1$  and  $H_2 = U_2 + p_2 V_2$ . This is the fundamental equation for an open system. If there are any other forms of energy, such as electrical energy or magnetic energy, their initial and final values should be added properly to this equation. The energy equation for an open system

$$\boxed{H_1 + \frac{m}{2} V_1^2 + m g z_1 = H_2 + \frac{m}{2} V_2^2 + m g z_2 + W_s - Q_{12}} \quad (1.33)$$

is universally valid. This is the expression of the first law of thermodynamics for any open system. In most applications of gas dynamics, the gravitational energy is negligible compared to the kinetic energy. For working processes such as flow in turbines and compressors, the shaft work  $W_s$  in Eq. (1.33) is finite and for flow processes like flow around an airplane,  $W_s = 0$ . Therefore, for a gas dynamic working process, Eq. (1.33) becomes

$$H_1 + \frac{m}{2} V_1^2 = H_2 + \frac{m}{2} V_2^2 + W_s - Q_{12} \quad (1.34)$$

This is usually the case with systems such as turbo machines and internal combustion engines, where the process is assumed to be adiabatic (that is,  $Q_{12} = 0$ ). For a gas dynamic adiabatic flow process, the energy Eq. (1.33) becomes

$$H_1 + \frac{m}{2} V_1^2 = H_2 + \frac{m}{2} V_2^2 \quad (1.35)$$

or

$$\boxed{H_1 + \frac{m}{2} V_1^2 = H_0 = \text{constant}} \quad (1.36)$$

where  $H_0$  is the stagnation enthalpy and  $H_1$  is the static enthalpy. That is, the sum of static enthalpy and kinetic energy is constant in an adiabatic flow.

### 1.9.2 Adiabatic Flow Process

For an adiabatic process, the heat transfer is associated with the process,  $Q = 0$ . Therefore, the energy equation is given by Eqs. (1.35) and (1.36). Dividing Eqs. (1.35) and (1.36) by  $m$ , we can rewrite them as

$$h_1 + \frac{V_1^2}{2} = h_2 + \frac{V_2^2}{2} \quad (1.37)$$

$$h_1 + \frac{V_1^2}{2} = h_0 \quad (1.38)$$

or, in general,

$$\boxed{h + \frac{V^2}{2} = h_0 = \text{constant}} \quad (1.39)$$

where  $h = H/m$  is called *specific static enthalpy* and  $h_0$  is the specific stagnation enthalpy. With  $h = p/\rho$ , Eq. (1.39) represents Bernoulli's equation for incompressible flow,

$$p + \frac{1}{2} \rho V^2 = p_0 = \text{constant}$$

where  $p_0$  is the stagnation pressure. That is, for the incompressible flow of air the energy equation happens to be the Bernoulli equation, because we are not interested in the internal energy and the temperature for such flows. In other words, Bernoulli's equation is the limiting case of the energy equation for incompressible flows. Here it is important to realize that, even though Bernoulli's equation for the incompressible flow of a gas is shown to be the limiting case of the energy equation, it is essentially a momentum equation. For a closed system,

$$Q_{12} - W_{12} = U_2 - U_1$$

In terms of specific quantities this becomes

$$q_{12} - w_{12} = u_2 - u_1$$

For the processes of a closed system there is no shaft work, that is no useful work can be extracted from the working medium. There will only be compression or expansion work. Therefore,  $w_{12}$  may be expressed as

$$w_{12} = \int_1^2 p \, dv$$

where  $v$  is the specific volume.

Thus, the change in internal energy becomes

$$du = \delta q - p \, dv \quad (1.40a)$$

Also,  $h = u + pv$ ;  $dh = du + p \, dv + v \, dp$ . Using relation (1.40a), we can write the change in enthalpy as

$$dh = \delta q + v \, dp \quad (1.40b)$$

For adiabatic changes of state, Eqs. (1.40a) and (1.40b) reduce to

$$du = -p \, dv, \quad dh = v \, dp \quad (1.40c)$$

where  $u$ ,  $q$ , and  $v$  in Eqs. (1.40) stand for specific quantities of internal energy, heat energy, and volume, respectively.

## 1.10 The Second Law of Thermodynamics (Entropy Equation)

Consider a cold body coming into contact with a hot body. From experience, we can say that the cold body will get heated up and the hot body will cool down. However, Eq. (1.25) does not necessarily imply that this will happen. In fact, the first law allows the cold body to become cooler and the hot body to become hotter as long as energy is conserved during the process. However, in practice this does not happen; instead, the law of nature imposes another condition on the process, a condition that stipulates the direction in which a process should take place. To ascertain the proper direction of a process, let us define a new state variable, the entropy, as follows.

$$ds = \frac{\delta q_{\text{rev}}}{T} \quad (1.41)$$

where  $s$  is the entropy (amount of disorder) of the system,  $\delta q_{\text{rev}}$  is an incremental amount of heat added reversibly to the system, and  $T$  is the system temperature. The above definition gives the change in entropy in terms of a reversible addition of heat,  $\delta q_{\text{rev}}$ . Since entropy is a state variable, it can be used in conjunction with any type of process, reversible or irreversible. The quantity  $\delta q_{\text{rev}}$  is just an artifice; an effective value of  $\delta q_{\text{rev}}$  can always be assigned to relate the initial and final states of an irreversible process, where the actual amount of heat added is  $\delta q$ . Indeed, an alternative and probably more lucid relation is

$$ds = \frac{\delta q}{T} + ds_{\text{irrev}} \quad (1.42)$$

Equation (1.42) applies in general to all processes. It states that the change in entropy during any process is equal to the actual heat added,  $\delta q$ , divided by the temperature,  $\delta q/T$ , plus a contribution from the irreversible dissipative phenomena of viscosity, thermal conductivity, and mass diffusion occurring within the system,  $ds_{\text{irrev}}$ . These dissipative phenomena always cause an increase in of entropy:

$$ds_{\text{irrev}} \geq 0 \quad (1.43)$$

The equals sign in the inequality (1.43) denotes a reversible process where, by definition, the above dissipative phenomena are absent. Hence, a combination of Eqs. (1.42) and (1.43) yields

$$ds \geq \frac{\delta q}{T} \quad (1.44)$$

Further, if the process is adiabatic,  $\delta q = 0$ , and Eq. (1.44) reduces to

$$ds \geq 0 \quad (1.45)$$

Equations (1.44) and (1.45) are two forms of the second law of thermodynamics. The second law gives the direction in which a process will take place. Equations (1.44) and (1.45) imply that a process will always proceed in a direction such that the entropy of the system plus its surroundings always increases, or at least remains unchanged. That is, in an adiabatic process the entropy can never decrease. This aspect of the second law of thermodynamics is important because it distinguishes between reversible and irreversible processes.

If  $ds > 0$ , the process is called an *irreversible process*, and when  $ds = 0$ , the process is called a *reversible process*. A reversible and adiabatic process is called an *isentropic process*. However, in a nonadiabatic process, we can extract heat from the system and thus decrease the entropy of the system.

## 1.11 Thermal and Calorical Properties

The equation  $p\nu = RT$  or  $p/\rho = RT$  is called the *thermal equation of state*, where  $p$ ,  $T$ , and  $\nu (=1/\rho)$  are *thermal properties* and  $R$  is the gas constant. A gas that obeys the thermal equation of state is called a *thermally perfect gas*. Any relation between the calorical properties  $u$ ,  $h$ , and  $s$  and any two thermal properties is called a *calorical equation of state*. In general, the thermodynamic properties (the properties do not depend on process) can be grouped into thermal properties ( $p$ ,  $T$ ,  $\nu$ ) and calorical properties ( $u$ ,  $h$ ,  $s$ ). From Eqs. (1.40), we have

$$u = u(T, \nu), \quad h = h(T, p)$$

In terms of exact differentials, the above relations become

$$du = \left( \frac{\partial u}{\partial T} \right)_\nu dT + \left( \frac{\partial u}{\partial \nu} \right)_T d\nu \quad (1.46)$$

$$dh = \left( \frac{\partial h}{\partial T} \right)_p dT + \left( \frac{\partial h}{\partial p} \right)_T dp \quad (1.47)$$

For a constant volume process, Eq. (1.46) reduces to

$$du = \left( \frac{\partial u}{\partial T} \right)_\nu dT$$

where  $\left( \frac{\partial u}{\partial T} \right)_\nu$  is the specific heat at constant volume represented as  $c_\nu$ ; therefore,

$$du = c_\nu dT \quad (1.48)$$

For an isobaric process, Eq. (1.47) reduces to

$$dh = \left( \frac{\partial h}{\partial T} \right)_p dT$$

where  $\left( \frac{\partial h}{\partial T} \right)_p$  is the specific heat at constant pressure represented by  $c_p$ ; therefore,

$$dh = c_p dT \quad (1.49)$$

From Eq. (1.40a) for a constant volume (isochoric) process, we get

$$\delta q = du = c_\nu dT \quad (1.50a)$$

and for a constant pressure (isobaric) process,

$$\delta q = dh = c_p dT, \quad \delta q = dh = c_\nu dT + p d\nu \quad (1.50b)$$

For an adiabatic flow process ( $q = 0$ ), from Eq. (1.40c) we have

$$dh = \nu dp \quad (1.50c)$$

From Eqs. (1.50) it can be inferred that:

- If heat is added at constant volume, it only raises the internal energy.
- If heat is added at constant pressure, it not only increases the internal energy but also does some external work, that is it increases the enthalpy.
- If the change is adiabatic, the change in enthalpy is equal to the external work  $\nu dp$ .

### 1.11.1 Thermally Perfect Gas

A gas is said to be thermally perfect when its internal energy and enthalpy are functions of temperature alone, that is for a thermally perfect gas,

$$u = u(T), \quad h = h(T) \quad (1.51a)$$

Therefore, from Eqs. (1.48) and (1.49), we get

$$c_v = c_v(T), \quad c_p = c_p(T) \quad (1.51b)$$

Further, from Eqs. (1.46), (1.47), and (1.51a), we obtain

$$\left(\frac{\partial u}{\partial v}\right)_T = 0, \quad \left(\frac{\partial h}{\partial p}\right)_T = 0 \quad (1.51c)$$

The important relations of this section are

$$\boxed{du = c_v dT, \quad dh = c_p dT}$$

These equations are universally valid so long as the gas is thermally perfect. Otherwise, in order to have equations of universal validity, we must add  $\left(\frac{\partial u}{\partial v}\right)_T dv$  to the first equation and  $\left(\frac{\partial h}{\partial p}\right)_T dp$  to the second equation.

The state equation for a thermally perfect gas is

$$pv = RT$$

In the differential form, this equation becomes

$$p dv + v dp = R dT$$

Also,

$$h = u + pv$$

$$dh = du + p dv + v dp$$

Therefore,

$$dh - du = p dv + v dp = R dT$$

that is

$$R dT = c_p dT - c_v dT$$

Thus,

$$R = c_p(T) - c_v(T) \quad (1.52)$$

For thermally perfect gases, Eq. (1.52) shows that, though  $c_p$  and  $c_v$  are functions of temperature, their difference is a constant with reference to temperature.

## 1.12 The Perfect Gas

This is an even greater specialization than a thermally perfect gas. For a perfect gas, both  $c_p$  and  $c_v$  are constants and are independent of temperature, that is

$$c_v = \text{constant} \neq c_v(T), \quad c_p = \text{constant} \neq c_p(T) \quad (1.53)$$

Such a gas, with constant  $c_p$  and  $c_v$ , is called a *calorically perfect gas*. Therefore, a perfect gas should be thermally as well as calorically perfect.

From the above discussions it is evident that:

- A perfect gas must be both thermally and calorically perfect.
- A perfect gas must satisfy both the *thermal equation of state*:  $p = \rho R T$ , and the *caloric equations of state*:  $c_p = (\partial h / \partial T)_p$ ,  $c_v = (\partial u / \partial T)_v$ .

- A calorically perfect gas must be thermally perfect, but a thermally perfect gas need not be calorically perfect. That is, thermal perfectness is a prerequisite for caloric perfectness.
- For a thermally perfect gas,  $c_p = c_p(T)$  and  $c_v = c_v(T)$ ; that is, both  $c_p$  and  $c_v$  are functions of temperature. But even though the specific heats  $c_p$  and  $c_v$  vary with temperature, their ratio,  $\gamma$ , becomes a constant and is independent of temperature, that is  $\gamma = \text{constant} \neq \gamma(T)$ .
- For a calorically perfect gas,  $c_p$  and  $c_v$ , as well as  $\gamma$  are constants and independent of temperature.

### 1.12.1 Entropy Calculation

Entropy is defined by the relation (for a reversible process)

$$\delta q = T ds$$

Using Eq. (1.40), we can write

$$T ds = du + p dv \quad (1.54)$$

$$T ds = dh - v dp \quad (1.55)$$

Equations (1.54) and (1.55) are as important and useful as the original form of the first law of thermodynamics, Eq. (1.25).

For a thermally perfect gas, from Eq. (1.49), we have  $dh = c_p dT$ . Substituting this relation into Eq. (1.55), we obtain

$$ds = c_p \frac{dT}{T} - \frac{v dp}{T} \quad (1.56)$$

Substituting the perfect gas equation of state,  $p v = R T$ , into Eq. (1.56), we get

$$ds = c_p \frac{dT}{T} - R \frac{dp}{p} \quad (1.57)$$

Integrating Eq. (1.57) between states 1 and 2, we obtain

$$s_2 - s_1 = \int_{T_1}^{T_2} c_p \frac{dT}{T} - R \ln \left( \frac{p_2}{p_1} \right) \quad (1.58)$$

Equation (1.58) holds for a thermally perfect gas. The integral can be evaluated if  $c_p$  is known as a function of  $T$ . Further, assuming the gas to be calorically perfect, for which  $c_p$  is constant, Eq. (1.58) reduces to

$$s_2 - s_1 = c_p \ln \left( \frac{T_2}{T_1} \right) - R \ln \left( \frac{p_2}{p_1} \right) \quad (1.59)$$

Using  $du = c_v dT$  in Eq. (1.54), the change in entropy can also be expressed as

$$s_2 - s_1 = c_v \ln \left( \frac{T_2}{T_1} \right) + R \ln \left( \frac{v_2}{v_1} \right) \quad (1.60)$$

From the above discussion, we can summarize that a perfect gas is both thermally and calorically perfect. Further, a calorically perfect gas must also be thermally perfect, whereas a thermally perfect gas need not be calorically perfect.

For a thermally perfect gas,  $p = \rho RT$ ,  $c_v = c_v(T)$ ,  $c_p = c_p(T)$ , and for a perfect gas,  $p = \rho RT$ ,  $c_v = \text{constant}$  and  $c_p = \text{constant}$ . Further, for a perfect gas, all equations get simplified, resulting in the following simple relations for  $u$ ,  $h$ , and  $s$ .

$$u = u_1 + c_v T \quad (1.61a)$$

$$h = h_1 + c_p T \quad (1.61b)$$

$$s = s_1 + c_v \ln \left( \frac{p}{p_1} \right) - c_p \ln \left( \frac{\rho}{\rho_1} \right) \quad (1.61c)$$

where the subscript 1 refers to the initial state.

Equations (1.61a), (1.61b), and (1.52), combined with the thermal equation of state ( $p = \rho RT$ ), result in

$$u = u_1 + \frac{1}{\gamma - 1} \frac{p}{\rho}, \quad h = h_1 + \frac{\gamma}{\gamma - 1} \frac{p}{\rho}$$

where  $\gamma$  is the ratio of specific heats,  $c_p/c_v$ . For the simplest molecular model, the kinetic theory of gases gives the specific heats ratio  $\gamma$  as

$$\gamma = \frac{n + 2}{n}$$

where  $n$  is the number of degrees of freedom of the gas molecules. Thus, for monatomic gases with  $n = 3$  (only three translational degrees of freedom), the specific heats ratio becomes

$$\gamma = \frac{3 + 2}{3} = 1.67$$

Diatomic gases, such as oxygen and nitrogen, have  $n = 5$  (three translational degrees of freedom and two rotational degrees of freedom), thus,

$$\gamma = \frac{5 + 2}{5} = 1.4$$

Gases with extremely complex molecules, such as freon and gaseous compounds of uranium, have large values of  $n$ , resulting in values of  $\gamma$  only slightly greater than unity. Thus, the value of specific heats ratio  $\gamma$  varies from 1 to 1.67, depending on the molecular nature of the gas:

$$1 \leq \gamma \leq 1.67$$

The above relations for  $u$  and  $h$  are important, because they connect the quantities used in thermodynamics with those used in gas dynamics. With the aid of these relations, the energy equation can be written in two different forms, as follows.

- The energy equation for an adiabatic process, as given by Eq. (1.39), is

$$h + \frac{V^2}{2} = h_0 = \text{constant}$$

When the gas is perfect, it becomes

$$c_p T + \frac{V^2}{2} = c_p T_0 = \text{constant} \quad (1.62a)$$

- Equation (1.62a), when combined with the state equation, yields

$$\frac{\gamma}{\gamma - 1} \frac{p}{\rho} + \frac{V^2}{2} = \text{constant} \quad (1.62b)$$



Equation (1.62b) is the form of energy equation commonly used in gas dynamics. This is popularly known as the *compressible Bernoulli's equation* for isentropic flows.

From Eq. (1.62a), we infer that for an adiabatic process of a perfect gas,

$$T_{01} = T_{02} = T_0 = \text{constant} \quad (1.63)$$

So far, we have not made any assumption about the reversibility or irreversibility of the process. Equation (1.63) implies that the stagnation temperature  $T_0$  remains constant for an adiabatic process of a perfect gas, irrespective of the process being reversible or irreversible.

Consider the flow of gas in a tube with an orifice, as shown in Figure 1.9. In such a flow process, there will be pressure loss. But if the stagnation temperature is measured before and after the orifice plate and if it remains constant, then the gas can be treated as a perfect gas and all the simplified equations (Eqs. (1.61a)–(1.61c)) can be used. Otherwise, it cannot be treated as a perfect gas, and Eq. (1.61c) can be rewritten as

$$\frac{p_2}{p_1} = \left( \frac{\rho_2}{\rho_1} \right)^\gamma \exp[(s_2 - s_1)/c_v] \quad (1.64)$$

### 1.12.2 Isentropic Relations

An adiabatic and reversible process is called an *isentropic process*. For an adiabatic process,  $\delta q = 0$ , and for a reversible process,  $ds_{\text{irrev}} = 0$ . Hence, from Eq. (1.42), an isentropic process is one for which  $ds = 0$ , that is the entropy is constant. Important relations for an isentropic process can be directly obtained from Eqs. (1.59), (1.60), and (1.64) by setting  $s_2 = s_1$ . For example, from Eq. (1.59) we have

$$\begin{aligned} 0 &= c_p \ln \left( \frac{T_2}{T_1} \right) - R \ln \left( \frac{p_2}{p_1} \right) \\ \ln \left( \frac{p_2}{p_1} \right) &= \frac{c_p}{R} \ln \left( \frac{T_2}{T_1} \right) \\ \frac{p_2}{p_1} &= \left( \frac{T_2}{T_1} \right)^{c_p/R} \end{aligned} \quad (1.65)$$

From Eq. (1.52),

$$\begin{aligned} c_p - c_v &= R \\ 1 - \frac{c_v}{c_p} &= \frac{R}{c_p} \\ \frac{\gamma - 1}{\gamma} &= \frac{R}{c_p} \end{aligned}$$

since  $c_p/c_v = \gamma$ . Therefore,

$$\frac{c_p}{R} = \frac{\gamma}{\gamma - 1}$$

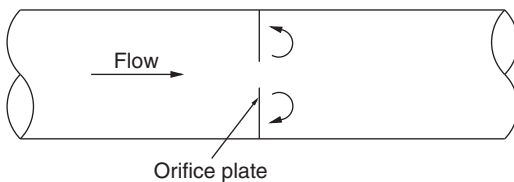


Figure 1.9 Flow through an orifice plate.

Substituting this relation into Eq. (1.65), we obtain

$$\frac{p_2}{p_1} = \left( \frac{T_2}{T_1} \right)^{\gamma/(\gamma-1)} \quad (1.66)$$

Similarly, from Eq. (1.60),

$$\begin{aligned} 0 &= c_v \ln \left( \frac{T_2}{T_1} \right) + R \ln \left( \frac{v_2}{v_1} \right) \\ \ln \left( \frac{v_2}{v_1} \right) &= -\frac{c_v}{R} \ln \left( \frac{T_2}{T_1} \right) \\ \frac{v_2}{v_1} &= \left( \frac{T_2}{T_1} \right)^{-c_v/R} \end{aligned} \quad (1.67)$$

But it can be shown that

$$\frac{c_v}{R} = \frac{1}{\gamma - 1}$$

Substituting the above relation into Eq. (1.67), we get

$$\frac{v_2}{v_1} = \left( \frac{T_2}{T_1} \right)^{-1/(\gamma-1)} \quad (1.68)$$

Since  $\rho_2/\rho_1 = v_1/v_2$ , Eq. (1.68) becomes

$$\frac{\rho_2}{\rho_1} = \left( \frac{T_2}{T_1} \right)^{1/(\gamma-1)} \quad (1.69)$$

Substituting  $s_1 = s_2$  into Eq. (1.64), we obtain

$$\frac{p_2}{p_1} = \left( \frac{\rho_2}{\rho_1} \right)^{\gamma} \quad (1.70)$$

This relation is also called *Poisson's equation*. Summarizing Eqs. (1.66), (1.69), and (1.70), we can write

$$\boxed{\frac{p_2}{p_1} = \left( \frac{\rho_2}{\rho_1} \right)^{\gamma} = \left( \frac{T_2}{T_1} \right)^{\gamma/(\gamma-1)}} \quad (1.71)$$

Equation (1.71) is an important equation and is used very frequently in the analysis of compressible flows.

Using the isentropic relations discussed above, several useful equations of total (stagnation) conditions can be obtained as follows. From Eqs. (1.62a) and (1.15),

$$\frac{T_0}{T} = 1 + \frac{V^2}{2c_p T} = 1 + \frac{V^2}{2\gamma R T/(\gamma - 1)} = 1 + \frac{V^2}{2a^2/(\gamma - 1)}$$

where  $T$  is the static temperature,  $T_0$  is the stagnation temperature and  $V$  is the flow velocity. Hence,

$$\boxed{\frac{T_0}{T} = 1 + \frac{\gamma - 1}{2} M^2} \quad (1.72)$$

Equation (1.72) gives the ratio of total to static temperature at a point in an isentropic flow field as a function of the flow Mach number  $M$  at that point. Combining Eqs. (1.71) and (1.72), we get

$$\frac{p_0}{p} = \left(1 + \frac{\gamma - 1}{2} M^2\right)^{\gamma/(\gamma-1)} \quad (1.73)$$

$$\frac{\rho_0}{\rho} = \left(1 + \frac{\gamma - 1}{2} M^2\right)^{1/(\gamma-1)} \quad (1.74)$$

Equations (1.73) and (1.74) give the ratio of total to static pressure and total and static density, respectively, at a point in an isentropic flow field as a function of the flow Mach number  $M$  at that point. Equations (1.72)–(1.74) form a set of most important equations for total properties, which are often used in gas dynamic studies. Their values as a function of  $M$  for  $\gamma = 1.4$  (air at standard conditions) are tabulated in Table A.1 of the Appendix.

At this stage we may ask how Eq. (1.71), which is derived from the concept of an isentropic change of state, which is so restrictive (adiabatic as well as reversible) that it may find only limited applications – is so important, and why it is frequently used. In compressible flow processes, such as flow through a rocket engine, flow over an airfoil, etc., large regions of the flow fields are isentropic. In the region adjacent to the rocket nozzle walls and the airfoil surface, a boundary layer is formed wherein the dissipative mechanisms of viscosity, thermal conduction, and diffusion are strong. Hence, the entropy increases within these boundary layers. On the other hand, for fluid elements outside the boundary layer, the dissipative effects are negligible. Further, no heat is being added to or removed from the fluid element at these points, hence the flow is adiabatic. Therefore, the fluid elements outside the boundary layer experience a reversible adiabatic process, hence the flow is isentropic. Moreover, the boundary layers are usually thin, hence large regime of flow fields are isentropic. Therefore, a study of isentropic flow is directly applicable to many types of practical flow problems. Equation (1.71) is a powerful relation, connecting pressure, density, and temperature, and is valid for calorically perfect gases.

Expressing all the quantities as stagnation quantities, Eq. (1.61c) can be written as

$$s_{02} - s_{01} = c_v \ln \left( \frac{p_{02}}{p_{01}} \right) - c_p \ln \left( \frac{\rho_{02}}{\rho_{01}} \right) \quad (1.75)$$

Also, from Eq. (1.52),

$$R = c_p - c_v$$

and from the state equation

$$\frac{p_{01}}{p_{02}} = \frac{\rho_{01}}{\rho_{02}} \frac{T_{01}}{T_{02}}$$

Substitution of the above relations into Eq. (1.75) yields

$$s_{02} - s_{01} = R \ln \left( \frac{p_{01}}{p_{02}} \right) + c_p \ln \left( \frac{T_{02}}{T_{01}} \right)$$

For an adiabatic process of a perfect gas,

$$T_{01} = T_{02}$$

Therefore,

$$s_{02} - s_{01} = R \ln \left( \frac{p_{01}}{p_{02}} \right) \quad (1.76)$$

From Eq. (1.76) it is obvious that the entropy changes only when there are losses in pressure. It does not change with velocity, and hence there is nothing like static and stagnation entropy. Also, by Eq. (1.63), the stagnation temperature does not change even when there are pressure losses. There is always an increase in entropy associated with pressure loss. In other words, when there are losses, there will be an increase in entropy, leading to a drop in stagnation pressure. These losses can be due to friction, separation, shocks, etc.

### Example 1.1

Argon is compressed adiabatically in a steady-flow compressor from 101 kPa and 25 °C to 505 kPa. If the compression work required is 475 kJ kg<sup>-1</sup>, show that the compression process is irreversible. Assume argon to be an ideal gas.

#### Solution:

As we know, the work required for a process is minimum when the process is isentropic, that is when the process is adiabatic and reversible. Also, any process requiring more work than that required for an isentropic process is irreversible.

For an isentropic process, work transfer can be expressed as

$$w_{12} = \frac{\gamma}{\gamma - 1} R T_1 \left[ 1 - \left( \frac{p_2}{p_1} \right)^{\frac{\gamma-1}{\gamma}} \right]$$

Given that

$$T_1 = 25^\circ \text{C} = 298.15 \text{ K}, \quad p_1 = 101 \text{ kPa}, \quad p_2 = 505 \text{ kPa}$$

For argon,  $\gamma = 1.67$  and  $R = 8314/39.944 = 208.14 \text{ J (kg K)}^{-1}$ , since the molecular weight of argon is 39.944.

Substituting these values into the work transfer equation, we get

$$\begin{aligned} w_{12} &= \frac{1.67 \times 208.14}{0.67} \times 298.15 \left[ 1 - \left( \frac{505}{101} \right)^{\frac{0.67}{1.67}} \right] \\ &= \boxed{-140.34 \text{ kJ kg}^{-1}} \end{aligned}$$

The actual work required, 475 kJ kg<sup>-1</sup>, is more than the isentropic work transfer. Hence, the process is irreversible.

### Example 1.2

The Mach number of an aircraft is the same at all altitudes. If its speed is 90 kmph slower at 7000 m altitude than at sea level, what is its Mach number?

#### Solution:

From the standard atmospheric table, at 7000 m altitude, we get the local temperature  $T_h$  as

$$T_h = 242.65 \text{ K}$$

Therefore, the speed of sound at 7000 m altitude is

$$a_h = \sqrt{\gamma R T_h} = \sqrt{1.4 \times 287 \times 242.65} = 312.24 \text{ m s}^{-1}$$

At sea level,

$$T_0 = 15^\circ\text{C} = 288.15\text{ K}$$

The speed of sound at sea level is

$$a_0 = \sqrt{\gamma R T_0} = \sqrt{1.4 \times 287 \times 288.15} = 340.26\text{ m s}^{-1}$$

The Mach number is the same at these two altitudes. Thus,

$$\begin{aligned}\frac{V_0}{a_0} &= \frac{V_h}{a_h} = \frac{\left(V_0 - \frac{90}{3.6}\right)}{a_h} \\ V_0 \frac{a_h}{a_0} &= V_0 - \frac{90}{3.6} \\ V_0 \left(\frac{a_h}{a_0} - 1\right) &= -\frac{90}{3.6} \\ V_0 \left(\frac{312.24}{340.26} - 1\right) &= -25 \\ V_0 &= 303.59\text{ m s}^{-1} \\ M &= \frac{V_0}{a_0} = \frac{303.59}{340.26} \\ &= \boxed{0.892}\end{aligned}$$

### Example 1.3

Air enters a compressor at a stagnation state of 100 kPa and  $27^\circ\text{C}$ . If it has to be compressed to a stagnation pressure of 900 kPa, calculate the power input to the compressor when the mass flow rate is  $0.02\text{ kg s}^{-1}$ . Assume the compression process to be isentropic.

#### Solution:

Given,

$$p_{01} = 100\text{ kPa}, \quad T_{01} = 27^\circ\text{C} = 300\text{ K}, \quad p_{02} = 900\text{ kPa}$$

The entropy change can be expressed as

$$s_2 - s_1 = c_p \ln \left( \frac{T_{02}}{T_{01}} \right) - R \ln \left( \frac{p_{02}}{p_{01}} \right)$$

For an isentropic compression,  $s_2 - s_1 = 0$ . Therefore,

$$\begin{aligned}c_p \ln \left( \frac{T_{02}}{T_{01}} \right) &= R \ln \left( \frac{p_{02}}{p_{01}} \right) \\ \ln \left( \frac{T_{02}}{T_{01}} \right) &= \frac{R}{c_p} \ln \left( \frac{p_{02}}{p_{01}} \right) \\ &= \frac{287}{1004.5} \ln \left( \frac{900}{100} \right) = 0.628 \\ T_{02} &= (e^{0.628}) T_{01} = 562.16\text{ K}\end{aligned}$$

The power required is

$$\begin{aligned}\text{Power} &= \dot{m} \Delta h = \dot{m} c_p (T_{02} - T_{01}) \\ &= 0.02 \times 1004.5 \times (562.16 - 300) \\ &= \boxed{5.27\text{ kW}}\end{aligned}$$

**Example 1.4**

Show that for air the difference between stagnation and static temperature in the Kelvin scale is approximately  $5 \times (\text{speed in hundreds of meters per second})^2$ .

**Solution:**

By energy equation, we have

$$h + \frac{V^2}{2} = h_0$$

where  $h$  and  $h_0$  are the static and stagnation enthalpies, and  $V$  is the flow speed. For a perfect gas, this equation can be written as

$$c_p T + \frac{V^2}{2} = c_p T_0$$

Therefore, the stagnation temperature rise is

$$T_0 - T = \frac{V^2}{2c_p} = \frac{(\gamma - 1) V^2}{2 \gamma R}$$

since

$$c_p = \frac{\gamma}{\gamma - 1} R$$

For air,  $R = 287 \text{ J (kg K)}^{-1}$  and  $\gamma = 1.4$ , under normal temperatures. Substituting for  $R$  and  $\gamma$  in the above equation, we get

$$\begin{aligned} T_0 - T &= \frac{0.4}{2 \times 1.4 \times 287} V^2 \\ &= 4.9776 \times 10^{-4} V^2 \text{ K} \\ &\approx 5(V \times 10^{-2})^2 \text{ K} \\ &\approx \boxed{5 (\text{speed in hundreds of meters per seconds})^2} \end{aligned}$$

**1.12.3 Limitations on Air as a Perfect Gas**

- When the temperature is less than 500 K, air can be treated as a perfect gas, and the ratio of specific heats,  $\gamma$ , takes a constant value of 1.4.
- When the temperature lies between 500 and 2000 K, air is only thermally perfect (but calorically imperfect), and the state equation  $p = \rho R T$  is valid, but  $c_p$  and  $c_v$  become functions of temperature,  $c_p = c_p(T)$  and  $c_v = c_v(T)$ . Even though  $c_p$  and  $c_v$  are functions of temperature, their ratio  $\gamma$  continues to be independent of temperature. That is,  $c_p$  and  $c_v$  vary with temperature in such a manner that their ratio continues to be the same constant as in temperatures below 500 K.
- For temperatures more than 2000 K, air becomes both thermally and calorically imperfect. That is,  $c_p$ ,  $c_v$ , as well as  $\gamma$  become functions of temperature.

In supersonic flight with a Mach number of, say, 2.0 at sea level, the temperature reached is already about  $245^\circ\text{C}$  (more than 500 K). But, for  $500 \text{ K} \leq T \leq 700 \text{ K}$ , we can still use perfect gas equations and the error involved in doing so will be negligible; that is, for a Mach number of less than 2.68, perfect gas equations can be used with slight error. For temperatures of more than 700 K, we must go for thermally perfect gas equations.

At this stage, we may have some doubt about the possible values of the isentropic index  $\gamma$ , when the flow medium is at a temperature which is quite high and where the medium cannot

be assumed as perfect. This doubt can be removed if we consider the flow medium as an ideal gas, which satisfies perfect gas equations, and has  $\gamma = \text{constant}$ , independent of temperature. For a monatomic gas (such as He, Ar, Ne, etc.), the simplest possible molecular structure gives  $\gamma = 5/3$ . This prediction is well confirmed by experiment. At the other extreme of molecular complexity, very complicated molecules have a large number of degrees of freedom, and  $\gamma$  may approach unity, which represents the minimum possible value, since  $c_p \geq c_v$  by virtue of a general thermodynamic argument [1]. So  $\gamma$  necessarily has a range of values

$$\frac{5}{3} \geq \gamma \geq 1$$

Experimental results show that most diatomic gases, and nitrogen, and oxygen in particular, have  $\gamma = 7/5$  at room temperature, gradually tending to  $\gamma = 9/7$  at a few thousand kelvin.

### 1.13 Wave Propagation

We have already seen that in incompressible flows the fluid particles are able to sense the presence of a body before actually reaching it. This fact suggests that a signaling mechanism exists, whereby the fluid particles can be informed, in advance, about the presence of a body ahead of it. The velocity of propagation of this signal must apparently be greater than the fluid velocity, since the flow is able to adjust to the presence of a body before reaching it. On the other hand, if the fluid particles were to move faster than the signal waves, as in the case of supersonic flows, the fluid would not be able to sense the body before actually reaching it, and abrupt changes in velocity and other properties would take place.

An understanding of the mechanism by which the signal waves propagate through a fluid medium along with an expression for the velocity of propagation of those waves will be extremely useful in deriving significant conclusions concerning the fundamental differences between incompressible and compressible flows.

When a fluid medium is allowed to vary its density, the consequence is that the fluid elements could occupy varying volumes in space. This possibility means that a set of fluid elements can spread into a larger region of space without requiring a simultaneous shift to be made to all fluid elements in the flow field, as would be required in the case of incompressible flow, in order to keep the density constant. From studies of physics, we know that a small shift of fluid elements in compressible media will induce, in due course, similar small movements in adjacent elements and in this way a disturbance, referred to as an *acoustic wave*, propagates at a relatively high speed through the medium. Furthermore, in incompressible flows these waves propagate with infinitely large velocity; in other words, adjustments take place instantaneously throughout the flow and so, in the conventional sense, there are no acoustic or elastic waves to be considered. With the introduction of compressibility, we thus permit the possibility of elastic waves having a finite velocity, and the magnitude of this wave velocity is of great importance in compressible flow theory.

### 1.14 Velocity of Sound

A sound wave is a weak compression wave across which only infinitesimal changes in flow properties occur, that is across these waves there will be only infinitesimal pressure variations. In the ensuing chapters, we shall study waves where comparatively large pressure variation occurs over

a very narrow front. Such waves are shock waves (as introduced above), the flow process across them is nonisentropic, and they move relative to the fluid at speeds that exceed the speed of sound. At this stage one may think of the sound waves as limiting cases of compression waves where the change in pressure across the wave becomes infinitesimal.

From Eq. (1.15), we have the speed of sound as  $a = \sqrt{\gamma RT}$ , where  $T$  is the static temperature of the medium in absolute units. The speed of sound in a perfect gas may be computed by employing Eq. (1.15) and for the other fluids by employing Eq. (1.11).

## 1.15 Subsonic and Supersonic Flows

The velocity of sound is used as the limiting value for differentiating the subsonic flow from the supersonic flow. Flows with velocity more than the speed of sound are called *supersonic flows*, and those with velocities less than the speed of sound are called *subsonic flows*. Flows with velocity close to the speed of sound are classified under a special category called *transonic flows*.

We saw the propagation of disturbance waves in flow fields with velocities from zero level to a level greater than the speed of sound, and that these disturbances will propagate along a *Mach cone*. For supersonic flow over two-dimensional objects, we will have a *Mach wedge* instead of a Mach cone. The angle  $\mu$  for such waves is measured in a counter-clockwise manner from an axis taken parallel to the direction of freestream, as shown in Figure 1.10.

For an observer looking in the direction of flow toward the disturbance, the wave to the left is called the *left-running wave* and the wave to the right is called the *right-running wave* (Figure 1.10). Usually, the disturbance arises at a solid boundary where the fluid, having arrived supersonically without prior warning through pressure or sound signals, is made to undergo a change in direction, thus initiating a disturbance at the boundary which propagates along the Mach waves.

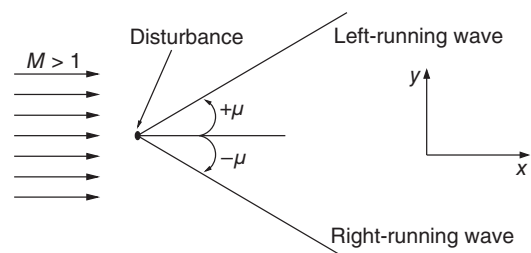
For historical interest, we should mention that Newton was the first to calculate the propagation speed of pressure waves. Based on the assumed isothermal process in a perfect gas, he found the speed of the propagation of sound to be equal to the square root of the ratio of the pressure to the corresponding density involved in the process, that is

$$a = \sqrt{p/\rho}$$

Because the science of thermodynamics was not known in Newton's time, the 18% difference between his theory and experiment was never justified.

Nearly a century later, the Marquis de Laplace rectified Newton's calculation. The basic difference between Laplace's theory and Newton's theory is that the former considered an adiabatic process for the propagation of pressure waves. This is fully justified since the compressions taking place in the propagation of pressure waves produce a very small temperature gradient, and

**Figure 1.10** Waves in supersonic flows.





hence it is not possible for heat due to compression to be transferred to the surrounding region. The correction by Laplace using the adiabatic process model multiplied Newton's formula by  $\sqrt{\gamma}$ . The correct expression for the speed of sound is  $a = \sqrt{\gamma RT}$ , which is the same as Eq. (1.15).

## 1.16 Similarity Parameters

In our discussions in the previous sections, we saw the Mach number  $M$  as a primary parameter which dictates the flow pattern in the compressible regime of flow. In the chapters that follow, it will be seen that  $M$  is also a parameter that appears in almost all equations of motion. Here the aim is to show that  $M$  is an important parameter for experimental studies too.

Let us consider a prototype and a model which are geometrically similar. Now, it is our interest to find the condition that must be met in order for the flow pattern around the model to be similar to that around the prototype. Examining the energy equation and taking into account the effect of viscosity and heat conductivity, it can be shown that the specific heats ratio,  $\gamma$ , must be the same for both the model and the prototype. Thus, it can be concluded that the Mach number,  $M$ , must be the same for the model and the prototype, if the flows are to be similar. When viscosity is present, an analysis applied to the inertia and viscosity terms in the momentum equation leads to the criterion that the Reynolds number must be the same for ensuring similarity of flow pattern around the model and the prototype.

Thus, by considering all the physical equations that govern the flow – namely the continuity, momentum, and energy equation and the equations of state – it is possible to arrive at four dimensionless parameters that must be the same for the dynamic similarity of the model and the prototype flow fields. They are

- Mach number,  $M = \frac{V}{a}$
- Reynolds number,  $Re_L = \frac{\rho VL}{\mu}$
- Ratio of specific heats,  $\gamma = \frac{c_p}{c_v}$
- Prandtl number,  $Pr = \frac{\mu c_p}{k}$

where  $V$  is the flow velocity,  $a$  is speed of sound,  $\rho$  is the flow density,  $L$  is a characteristic dimension of the body in the flow,  $\mu$  is the viscosity coefficient,  $c_p$  is the specific heat at constant pressure,  $c_v$  is the specific heat at constant volume, and  $k$  is the thermal conductivity of the fluid.

In the potential flow region outside the boundary layer, where the viscous and heat conduction effects are relatively unimportant, it is usually necessary that only  $M$  and  $\gamma$  are the same between the model and prototype flow fields to establish similarity. Of the two, similarity in  $M$  is more important than  $\gamma$ , since  $\gamma$  has a relatively weak influence on the flow pattern.

Within the boundary layer, or in the interior of shock waves, viscous and heat conduction effects are significant. Hence, the Reynolds number and Prandtl number must also be included in the similarity conditions. But the Prandtl number is nearly the same for all gases and varies only slowly with temperature.

## 1.17 Continuum Hypothesis

From the kinetic theory of gases, we know that matter is made up of a large number of molecules which are in constant motion and collision. But in problems of engineering interest, we are concerned only with the gross behavior of the fluid, thought of as a continuous material, and not in the motion of the individual molecules of the fluid. Even though the postulation

of continuous fluid (continuum) is only a convenient assumption, it is a valid approach to many practical problems where only the macroscopic or phenomenological information is of interest. The assumption of fluids as continua is valid only when the smallest volume of fluid of interest contains large numbers of molecules so that the statistical averages are meaningful. The advantage of continuum treatment is that, instead of dealing with the instantaneous states of large number of molecules, we only have to deal with certain properties describing the gross behavior of the substance. In compressible flows the relevant properties are the density, pressure, temperature, velocity, shear stress, coefficient of viscosity, internal energy, entropy, and coefficient of thermal conductivity. The macroscopic approach with its continuum hypothesis will fail whenever the mean free path of the molecules is of the same order as the smallest significant dimension of the problem under consideration. The flow in which the mean free path of the molecules is of the same order or more than the characteristic dimension of the problem is termed *rarefied flow*. To deal with highly rarefied gases, we should resort to the microscopic approach of kinetic theory, since the continuum approach of classical fluid mechanics and thermodynamics is not valid here.

In order to determine whether the condition of continuum is valid, let us consider a steady flow and perform some approximate calculations of an order-of-magnitude nature.

With kinetic theory, it can be shown, using an order-of-magnitude approach, that the viscosity coefficient  $\mu$  can be expressed as

$$\mu \approx \rho \bar{c} \lambda$$

and

$$\bar{c} \approx a$$

where  $\bar{c}$  is the mean molecular velocity,  $\lambda$  is the mean free path, and  $a$  is the speed of sound.

The Reynolds number of a flying vehicle can be expressed as

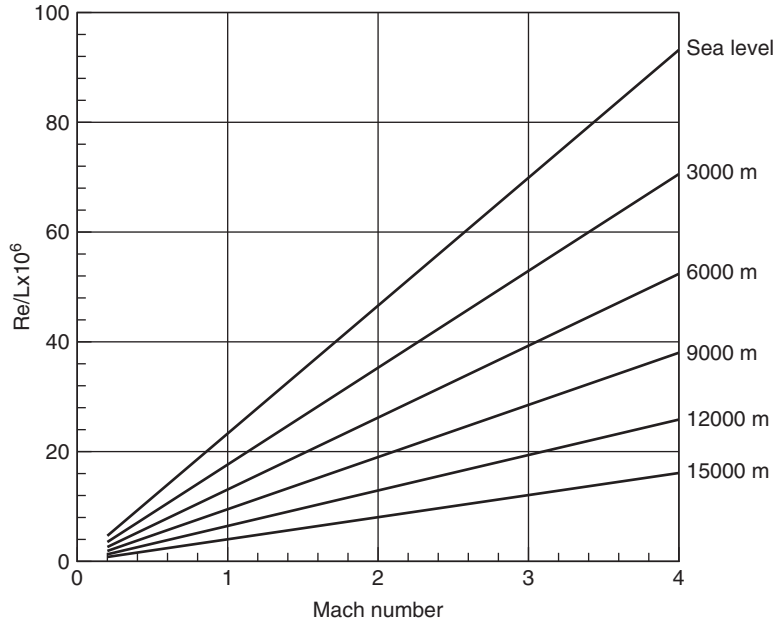
$$\begin{aligned} \text{Re}_L &= \frac{\rho V L}{\mu} = \frac{\rho \bar{c} \lambda}{\mu} \frac{V}{a} \frac{a}{\bar{c}} \frac{L}{\lambda} \\ &\approx \frac{V}{a} \frac{L}{\lambda} \end{aligned}$$

where  $L$  is a characteristic length of the vehicle. But  $V/a = M$ ; therefore,

$$\frac{L}{\lambda} \approx \frac{\text{Re}_L}{M} \quad (1.77)$$

Equation (1.77) shows that the ratio of the Reynolds number to the Mach number is a dimensionless parameter indicative of whether a given problem is amenable to the continuum approach or not. From this ratio it is seen that the continuum hypothesis is likely to fail when the Mach number is very large or the Reynolds number is extremely low. But we have to exercise caution when using Eq. (1.77), since  $\text{Re}_L$  and  $M$  depend on the nature of the problem considered. For example, when  $\text{Re}_L$  is very low owing to low density, the continuum hypothesis is not valid, whereas when it is very low owing to high viscosity, the continuum concept is perfectly valid and such a flow is termed a *stratified flow*. However, the rules for determining the validity of the continuum concept in terms of  $\text{Re}_L$  and  $M$  can be illustrative by supposing that, in a given problem, the smallest *significant* body dimension is of the order of the boundary layer thickness,  $\delta$ . If  $\text{Re}_L$  is large compared to unity, and if the boundary layer flow is also laminar, then the boundary layer relations for a flat plate give

$$\frac{\delta}{L} \approx \frac{1}{\sqrt{\text{Re}_L}}$$



**Figure 1.11** Reynolds number per meter versus Mach number, based on standard atmosphere. Source: Data extracted from Rathakrishnan 2004 [3] © 2004.

Using Eq. (1.77), this can be expressed as

$$\frac{\delta}{\lambda} \approx \frac{\sqrt{\text{Re}_L}}{M}$$

For this case Tsien [2] suggests that the realm of continuum gas dynamics be limited to instances where the boundary layer thickness is at least 100 times the mean free path. That is

$$\frac{\sqrt{\text{Re}_L}}{M} > 100$$

Figure 1.11 shows the Reynolds number per unit length as a function of flight Mach number for various altitudes, based on the standard atmosphere.

## 1.18 Compressible Flow Regimes

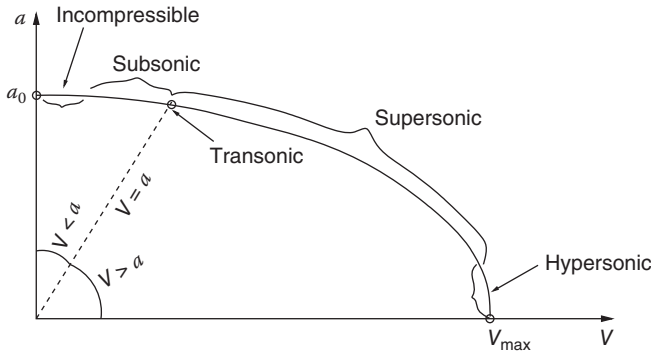
The compressible flow regime can be subdivided into different zones based on the local flow velocity and the local speed of sound. To do this classification, we can make use of the energy equation, as follows.

Consider a streamtube in a steady compressible flow in which the flow does not exchange heat with the fluid in neighboring streamtubes, that is the flow process is adiabatic. The steady-flow energy equation for the adiabatic flow through such a streamtube is

$$h + \frac{V^2}{2} = h_0$$

where  $h$  and  $h_0$  are the static and stagnation enthalpies and  $V$  is the flow velocity. For a perfect gas,  $h = c_p T$ ; therefore

$$c_p T + \frac{V^2}{2} = c_p T_0$$



**Figure 1.12** Steady-flow adiabatic ellipse.

But,  $c_p = \frac{\gamma}{\gamma-1}R$  for perfect gases, thus

$$\frac{\gamma}{\gamma-1}RT + \frac{V^2}{2} = \frac{\gamma}{\gamma-1}RT_0$$

This simplifies to

$$V^2 + \frac{2}{\gamma-1}a^2 = \frac{2}{\gamma-1}a_0^2 = V_{\max}^2 \quad (1.78)$$

since  $a = \sqrt{\gamma RT}$ , the local speed of sound, and  $a_0 = \sqrt{\gamma RT_0}$ , the speed of sound at the stagnation state (where  $V = 0$ ) and  $V_{\max}$  is the maximum possible flow velocity in the fluid (where the absolute temperature is zero).

Equation (1.78) represents an ellipse and is called as *adiabatic steady-flow ellipse*. The adiabatic ellipse can be plotted as in Figure 1.12.

Different realms of compressible flow, having significantly different physical characteristics, are represented schematically on the adiabatic ellipse. The zones highlighted on the adiabatic ellipse are the following.

- *Incompressible flow* is the flow in which the flow speed,  $V$ , is small compared to the speed of sound,  $a$ , in the flow medium. The changes in  $a$  are very small compared to the changes in  $V$ .
- *Compressible subsonic flow* is that in which the flow speed and speed of sound are of comparable magnitude, but  $V < a$ . Changes in flow Mach number  $M$  are mainly due to changes in  $V$ .
- *Transonic flow* is that in which the difference between the flow speed and the speed of sound is small compared to either  $V$  or  $a$ . Changes in  $V$  and  $a$  are of comparable magnitude.
- *Supersonic flow* is that with flow speed and speed of sound of comparable magnitude, but where  $V > a$ . Changes in Mach number  $M$  take place through substantial variation in both  $V$  and  $a$ .
- *Hypersonic flow* is that where the flow speed is very large compared with the speed of sound. Changes in flow velocity are very small, and thus variations in Mach number  $M$  are almost exclusively due to changes in the speed of sound  $a$ .

## 1.19 Summary

Compressible flow is defined as *variable density flow*; this is in contrast to incompressible flow, where the density is assumed to be invariant. Usually, flows with a Mach number of less than 0.3 are treated as constant density (incompressible) flows.

*Gas dynamics* is a science that primarily deals with the behavior of gas flows in which compressibility and temperature change become significant. *Compressibility* is a phenomenon by virtue of which the flow changes its density with change in speed. Compressibility may also be defined as the volume modulus of the pressure.

The Mach number is the ratio of the local flow speed to the local speed of sound:

$$M = \frac{V}{a}$$

Flows with Mach number greater than unity are called *supersonic flows*.

Sound waves are infinitesimally small pressure disturbances. The speed with which sound waves propagate in a medium is called the *speed of sound*  $a$ . The speed of sound is given by

$$a^2 = \frac{dp}{d\rho}$$

For a perfect gas, the speed of sound can be expressed as

$$a = \sqrt{\gamma RT}$$

For a perfect gas, the state equation is

$$p = \rho RT$$

For an isentropic flow of a perfect gas, the relation between the pressure, temperature, and density between state 1 and any other state can be expressed as

$$\frac{T}{T_1} = \left( \frac{\rho}{\rho_1} \right)^{\gamma-1} = \left( \frac{p}{p_1} \right)^{(\gamma-1)/\gamma}$$

For supersonic motion of an object, there is a well-defined conical zone in the flow field with the object located at the nose of the cone. The region inside the cone is called the *zone of action*, and the region outside the cone is termed the *zone of silence*. The lines at which the pressure difference is concentrated and which generate the cone are *Mach waves* or *Mach lines*. Therefore, Mach waves may be defined as weak pressure waves across which there is only insignificant change in flow properties. The angle between the Mach line and the direction of motion of the body (flow direction) is called the *Mach angle*  $\mu$ , given by

$$\sin \mu = \frac{1}{M}$$

Modern classification of the flow regimes is as follows.

- Fluid flow with  $0 < M < 0.8$  is called *subsonic flow*.
- Flow in the Mach number range  $0.8 < M < 1.2$  is called *transonic flow*.
- Flow in the Mach number range  $1.2 < M < 5$  is called *supersonic flow*.
- Flow with  $M > 5$  is called *hypersonic flow*.

Linearized theory can be used for studying subsonic and supersonic flows; the study of transonic and hypersonic flows is, however, complicated.

When a body is kept in transonic flow, it experiences subsonic flow over some portions of its surface and supersonic flow over other portions. There is also a possibility of shock formation on the body. It is this mixed nature of the flow field that makes the study of transonic flows complicated.

The temperature at stagnation point and over the surface of an object in hypersonic flow becomes very high and, therefore, requires special treatment. That is, we must consider the thermodynamic aspects of the flow along with gas dynamic aspects. That is why hypersonic

flow theory is also called *aerothermodynamic theory*. Besides, because of the high temperature, the specific heats become functions of temperature and hence the gas cannot be treated as a perfect gas. If the temperature is quite high (of the order of more than 2000 K), even dissociation of gas can take place. The complexities due to high temperatures associated with hypersonic flow make its study complicated.

*Thermodynamics* is the science that primarily deals with energy. The *first law of thermodynamics* is simply an expression of the conservation of energy principle.

The second law of thermodynamics asserts that actual processes occur in the direction of increasing entropy.

A system of fixed mass is called a *closed system*, or *control mass*, and a system that involves mass transfer across its boundaries is called an *open system*, or *control volume*.

For an open system, by the first law of thermodynamics, the energy equation can be expressed as

$$H_1 + \frac{m}{2} V_1^2 + m g z_1 = H_2 + \frac{m}{2} V_2^2 + m g z_2 + W_s - Q_{12}$$

For a gas dynamic working process this equation becomes

$$H_1 + \frac{m}{2} V_1^2 = H_2 + \frac{m}{2} V_2^2 + W_s - Q_{12}$$

A process during which there is no heat transfer is called an *adiabatic process*.

A reversible process is a process that can be reversed to its initial state without leaving any trace on the surroundings. That is, both the system and the surroundings are returned to their initial states at the end of the reverse process. Processes that are not reversible are called *irreversible processes*.

A process that is adiabatic and reversible is called an *isentropic process*. The factors that change the entropy of a system are heat transfer and irreversibility. Many engineering systems or devices such as nozzles, diffusers, and turbines are essentially adiabatic in their operation, and they perform best when the irreversibilities, such as the friction associated with the process, are minimized. Therefore, an isentropic process can serve as an appropriate model for actual processes.

A perfect gas is an *imaginary* substance that obeys the relation  $p = \rho RT$ .

The amount of energy needed to raise the temperature of a unit mass of a substance by one degree is called the specific heat at constant volume,  $c_v$ , for a constant volume process and the specific heat at constant pressure,  $c_p$ , for a constant pressure process. They are defined as

$$c_v = \left( \frac{\partial u}{\partial T} \right)_v, \quad c_p = \left( \frac{\partial h}{\partial T} \right)_p$$

The specific heats ratio  $\gamma$  is defined as

$$\gamma = \frac{c_p}{c_v}$$

A gas is said to be perfect when it is *thermally* as well as *calorically* perfect. For a thermally perfect gas,  $u$ ,  $h$ ,  $c_v$ , and  $c_p$  are functions of temperature alone.

For a calorically perfect gas,  $c_p$  and  $c_v$  are constants and are independent of temperature, that is a perfect gas has to be thermally as well as calorically perfect.

Entropy may be viewed as a measure of *disorder* or *randomness* in a system. The change in entropy can be expressed as

$$ds = \frac{\delta q}{T} + ds_{\text{irrev}}$$

The value of  $ds$  can be used to determine whether a process is reversible, irreversible, or impossible.

For the isentropic flow of a perfect gas,

$$\begin{aligned}\frac{p_2}{p_1} &= \left(\frac{\rho_2}{\rho_1}\right)^\gamma = \left(\frac{T_2}{T_1}\right)^{\gamma/(\gamma-1)} \\ \frac{T_0}{T} &= 1 + \frac{\gamma-1}{2}M^2 \\ \frac{p_0}{p} &= \left(1 + \frac{\gamma-1}{2}M^2\right)^{\gamma/(\gamma-1)} \\ \frac{\rho_0}{\rho} &= \left(1 + \frac{\gamma-1}{2}M^2\right)^{1/(\gamma-1)}\end{aligned}$$

For an adiabatic process of a perfect gas, the entropy change in terms of stagnation pressure becomes

$$s_{02} - s_{01} = R \ln \left( \frac{p_{01}}{p_{02}} \right)$$

Entropy changes only when there are losses in pressure. Entropy does not change with velocity and there is nothing like stagnation or static entropy.

The ratio of specific heats varies from 1 to 1.67. For monatomic gases like argon,  $\gamma = 1.67$ . Diatomic gases such as oxygen and nitrogen have  $\gamma = 1.4$ ; for gases with extremely complex molecular structures,  $\gamma$  is slightly more than unity.

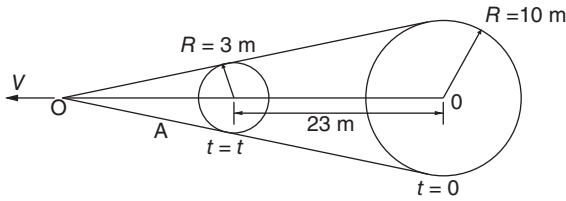
When an object moves through a fluid medium, waves are emitted from each point on the object which travel outward at the speed of sound. In an incompressible fluid, the speed of sound is infinite; therefore, the entire flow field could be able to feel the motion of the object instantaneously. In a compressible medium, the speed of sound has a finite value, and hence, if a body travels at a velocity greater than that of sound, the fluid ahead of the body is not able to sense the motion of the object. However, for the subsonic motion of an object the fluid ahead of the object could be able to sense the motion of the object. Therefore, for subsonic motion, the fluid elements adjust and move smoothly around the object, resulting in smooth, continuous streamline patterns. For supersonic motion, the fluid is forced to adjust rapidly to flow around a moving object, resulting in the formation of shock waves.

## Exercise Problems

- 1.1 A gas has  $p = 1 \text{ atm}$ ,  $T = 0^\circ\text{C}$ , and  $\rho = 0.09 \text{ kg m}^{-3}$ . Determine (a) the characteristic gas constant and molecular weight of the gas and (b) the specific volume of the gas at  $70^\circ\text{C}$  and  $2.3 \text{ atm}$ . Assume the gas to be thermally perfect.  
[Answer: (a)  $4.1217 \text{ kJ (kg K)}^{-1}$ ,  $2.017 \text{ kg}$ , (b)  $6.07 \text{ m}^3 \text{ kg}^{-1}$ ]
- 1.2 A rigid tank contains a certain amount of nitrogen gas at  $120 \text{ kPa}$  and  $30^\circ\text{C}$ , initially. Two kilograms of nitrogen gas are then added to the tank. If the final pressure and temperature of the gas in the tank are  $240 \text{ kPa}$  and  $30^\circ\text{C}$ , respectively, what is the volume of the tank?  
[Answer:  $1.5 \text{ m}^3$ ]
- 1.3 A barometer reads a local atmospheric pressure as  $735 \text{ mm}$  of mercury. How much is this pressure in pascals?  
[Answer:  $98.061 \text{ kPa}$ ]

- 1.4** A mercury manometer reads the pressure inside a vessel as 200 mm above atmosphere. The barometer reading is 750 mm Hg. Determine the absolute pressure in the vessel in kPa.  
[Answer: 126.75 kPa]
- 1.5** A U-tube mercury manometer has its one limb connected to a pressure tank. The other end of the manometer is open to the atmosphere. If the manometer height difference measures 250 cm, determine the pressure in the tank.  
[Answer: 434.63 kPa]
- 1.6** A water manometer reads the pressure inside a vessel as 500 mm below atmospheric pressure. If the atmospheric pressure is 760 mm of Hg, determine the absolute pressure in the vessel in kPa.  
[Answer: 96.49 kPa]
- 1.7** A Bourdon pressure gauge records a pressure of 1.5 MPa gauge. If the atmospheric pressure is 740 mm Hg, determine the absolute value of the pressure read by the Bourdon gauge.  
[Answer: 1.5987 MPa]
- 1.8** Determine the column height of a mercury manometer connected to a gas tank at a pressure of 50 kPa. Find the difference in the fluid level if water is used instead of mercury. Assume  $\rho_{Hg} = 13\,600\text{ kg m}^{-3}$  and  $\rho_w = 1000\text{ kg m}^{-3}$ .  
[Answer:  $\Delta h = 4.7223\text{ m}$ ]
- 1.9** A force of 8000 N is exerted uniformly on a piston of 100 mm diameter. Determine the pressure at the piston face.  
[Answer: 1018.6 kPa]
- 1.10** An oil of specific gravity 0.8 is contained in a vessel to a depth of 2.2 m. Determine the gauge pressure at the bottom of the vessel.  
[Answer: 17.27 kPa]
- 1.11** If the speed of sound at an altitude in Earth's atmosphere is  $299\text{ m s}^{-1}$ , determine the altitude.  
[Answer: 10 076.9 m]
- 1.12** The noise of an aircraft in level flight flown overhead is only heard by an observer at sea level altitude when the aircraft has traveled 1 km from the location of the observer. Ignoring the temperature variation with altitude, estimate the flight altitude if the aircraft is flying at Mach 3.0.  
[Answer: 333.45 m]
- 1.13** Two disturbance spheres created by an object moving at supersonic speed are as shown in Figure 1.13. Assuming the medium to be at standard sea level atmosphere, calculate the Mach number and velocity of the object and the Mach angle of the cone created by the disturbance.  
[Answer: 3.286,  $1117.24\text{ m s}^{-1}$ ,  $17.7^\circ$ ]





**Figure 1.13** Disturbance spheres created by a moving object.

- 1.14** A jet plane flies at 1100 kmph. Determine the flight Mach number for (a) sea-level operation with an air temperature of  $25^\circ\text{C}$  and (b) high-altitude operation with an air temperature of  $-55^\circ\text{C}$ .  
[Answer: (a) 0.883, (b) 1.03]
- 1.15** A stream of air drawn from a reservoir is flowing through an irreversible adiabatic process into a second reservoir in which the pressure is half of that in the first. Calculate the entropy difference between the two reservoirs, at the beginning of the process.  
[Answer:  $198.933 \text{ J (kg K)}^{-1}$ ]
- 1.16** Air is expanded in an insulated cylinder equipped with a frictionless piston. The initial temperature of the air is 1400 K. The original volume is  $1/10$  of the final volume. Calculate (a) the change in temperature, (b) the work removed from the gas, and (c) the pressure ratio.  
[Answer: (a)  $-842.65 \text{ K}$ , (b)  $6.04 \times 10^5 \text{ J kg}^{-1}$ , (c) 25.1189]
- 1.17** A tank of volume  $15 \text{ m}^3$  contains air at  $p_1 = 5.0 \times 10^5 \text{ Pa}$  and  $T_1 = 500 \text{ K}$ . The air is discharged into the atmosphere through a nozzle until the mass of air in the tank is reduced to one-half of its original value. Assuming the discharge process to be adiabatic and frictionless, calculate the pressure and temperature of the air remaining in the tank. Assume the air to be a perfect gas.  
[Answer:  $1.8946 \times 10^5 \text{ Pa}$ ,  $378.92 \text{ K}$ ]
- 1.18** Air is compressed isentropically in a centrifugal compressor from a pressure of  $1.0 \times 10^5 \text{ Pa}$  to a pressure of  $6.0 \times 10^5 \text{ Pa}$ . The initial temperature is  $290 \text{ K}$ . Calculate (a) the change in temperature, (b) the change in internal energy, and (c) the work imparted to the air, neglecting the velocity change.  
[Answer: (a)  $193.868 \text{ K}$ , (b)  $1.39 \times 10^5 \text{ J kg}^{-1}$ , (c)  $-1.39 \times 10^5 \text{ J kg}^{-1}$ ]
- 1.19** A perfect gas enclosed by an insulated (upright) cylinder and piston is in equilibrium at conditions  $p_1, v_1, T_1$ . A weight is placed on the piston. After a number of oscillations, the motion subsides and the gas reaches a new equilibrium at conditions  $p_2, v_2, T_2$ . Find the temperature ratio  $T_2/T_1$  in terms of the pressure ratio  $\lambda = p_2/p_1$ . Show that the change of entropy is given by

$$s_2 - s_1 = R \ln \left( \frac{1 + (\gamma - 1)\lambda}{\gamma} \right)^{\gamma/(\gamma-1)} \frac{1}{\lambda}$$

Also show that, if the initial disturbance is small, that is  $\lambda = 1 + \epsilon$ ,  $\epsilon \ll 1$ , then

$$\frac{s_2 - s_1}{R} \approx \frac{\epsilon^2}{2\gamma}$$

$$\left[ \text{Answer : } \frac{T_2}{T_1} = \frac{1 + (\gamma - 1)\lambda}{\gamma} \right]$$

- 1.20** The unit weight of air is compressed adiabatically from an initial state with  $p_1 = 10^5$  Pa and  $T_1 = 303$  K to a final state of  $p_2 = 2 p_1$  and  $T_2$ . If the air enters and leaves the compressor with same velocity, calculate the shaft work necessary. Assume air as an ideal gas. [Answer:  $w_s = -66.66$  kJ kg<sup>-1</sup>]
- 1.21** A fluid in a cylinder at a pressure of 6 atm and volume 0.3 m<sup>3</sup> is expanded at constant pressure to a volume of 2 m<sup>3</sup>. Determine the work done by this expansion. [Answer: 1.0335 MJ]
- 1.22** A gas at pressure 150 kPa and density 1.5 kg m<sup>-3</sup> is compressed to 690 kPa isentropically. Determine the final density. Assume the isentropic index to be 1.3. [Answer: 4.85 kg m<sup>-3</sup>]
- 1.23** Air undergoes a change of state isentropically. The initial pressure and temperature are 101 kPa and 298 K, respectively. The final pressure is seven times the initial pressure. Determine the final temperature. Assume air to be an ideal gas with specific heats ratio  $\gamma = 1.4$ . [Answer: 519.9 K]
- 1.24** Air at 30 °C is compressed isentropically to occupy a volume that is 1/30 of its initial volume. Assuming air to be an ideal gas, determine the final temperature. [Answer: 908.55 °C]
- 1.25** An ideal gas is cooled under constant pressure from 200 to 50 °C. Assuming constant specific heats with  $c_p = 1000$  J (kg K)<sup>-1</sup>, and  $\gamma = 1.4$ , determine (a) the molecular weight of the gas and (b) the ratio of final to initial volume of the gas. [Answer: (a) 29.1, (b) 0.683]
- 1.26** If the velocity of sound in an ideal gas of molecular weight 29 is measured to be 400 m s<sup>-1</sup> at 100 °C, determine the  $c_p$  and  $c_v$  of the gas at 100 °C. [Answer:  $c_p = 860.1$  J (kg K)<sup>-1</sup>,  $c_v = 573.4$  J (kg K)<sup>-1</sup>]
- 1.27** Air flows isentropically through a nozzle. If the speed and temperature at the nozzle exit are 390 m s<sup>-1</sup> and 28 °C, respectively, determine the Mach number and stagnation temperature there. What will be the Mach number just upstream of a station where the temperature is 92.5 °C? [Answer: 1.12, 103.29 °C, 0.387]
- 1.28** Hydrogen gas at 7 atm and 300 K in a cylinder is expanded isentropically through a nozzle to a final pressure of 1 atm. Assuming hydrogen to be a perfect gas with  $\gamma = 1.4$ , determine the velocity and Mach number corresponding to the final pressure. Also, find the mass flow rate through the nozzle if the exit area is 10 cm<sup>2</sup>. [Answer: 1923 m s<sup>-1</sup>, 1.93, 0.275 kg s<sup>-1</sup>]
- 1.29** Air in a cylinder changes state from 101 kPa and 310 K to a pressure of 1100 kPa according to the process
- $$pv^{1.32} = \text{constant}$$
- Determine the entropy change associated with this process. Assume air to be an ideal gas with  $c_p = 1004$  J (kg K)<sup>-1</sup> and  $\gamma = 1.4$ . [Answer: -103.8 J (kg K)<sup>-1</sup>]

- 1.30** Oxygen gas is heated from 25 to 125 °C. Determine the increase in its internal energy and enthalpy. Take  $\gamma = 1.4$ .  
[Answer: 64 950 J (kg K)<sup>-1</sup>, 90 930 J (kg K)<sup>-1</sup>]
- 1.31** Air enters a compressor at 100 kPa and 1.175 kg m<sup>-3</sup> and exits at 500 kPa and 5.875 kg m<sup>-3</sup>. Determine the enthalpy difference between the outlet and inlet states.  
[Answer: 0]
- 1.32** Show that the entropy change for an ideal gas can be expressed as  $ds = c_p \frac{dv}{v} + c_v \frac{dp}{p}$ . Using this result, show that for an ideal gas undergoing an isentropic change of state with constant specific heats,  $p v^\gamma = \text{constant}$ .
- 1.33** A certain quantity of air at 0.7 MPa and 150 °C occupies a volume of 0.014 m<sup>3</sup>. If the gas is expanded isothermally to a volume of 0.084 m<sup>3</sup>, calculate the change of entropy.  
[Answer: 513.4 J (kg K)<sup>-1</sup>]
- 1.34** A mass of 0.3 kg of air at 350 kPa and 35 °C receives heat energy at constant volume until its pressure becomes 700 kPa. It then receives heat energy at constant pressure until its volume becomes 0.2289 m<sup>3</sup>. Calculate the entropy change associated with each process.  
[Answer: 149.2 J K<sup>-1</sup>, 333 J K<sup>-1</sup>]
- 1.35** Air is flowing through a frictionless diffuser. At a station in the diffuser the temperature, pressure, and velocity are 0 °C, 140 kPa and 900 m s<sup>-1</sup>, respectively. At a downstream station the velocity decreases to 300 m s<sup>-1</sup>. Assuming the flow to be adiabatic, calculate the increase in pressure and temperature of the flow between these stations.  
[Answer: 358.39 K, 2.491 MPa]
- 1.36** Nitrogen gas is compressed reversibly and isothermally from 100 kPa and 25 °C to a final pressure of 300 kPa. Calculate the change in entropy.  
[Answer: - 0.3263 kJ (kg K)<sup>-1</sup>]
- 1.37** Air undergoes a change of state isentropically from 300 K and 110 kPa to a final pressure of 550 kPa. Assuming ideal gas behavior, determine the change in enthalpy.  
[Answer: 176.19 kJ kg<sup>-1</sup>]
- 1.38** Air at low pressure inside a rigid tank is heated from 50 to 125 °C. What is the change in entropy associated with this heating process?  
[Answer: 149.75 J (kg K)<sup>-1</sup>]
- 1.39** Compute the temperature rise at the nose of an aircraft flying with Mach number 2 at an altitude of 10 000 m.  
[Answer: 178.52]
- 1.40** A gas at an initial volume of 0.06 m<sup>3</sup> and 15 °C is expanded to a volume of 0.12 m<sup>3</sup> while the pressure remains constant. Determine the final temperature of the gas.  
[Answer: 303.15 °C]

- 1.41** A certain quantity of a gas at 140 kPa and volume of  $0.15 \text{ m}^3$  is compressed to 700 kPa at constant temperature. Determine the final volume of the gas.  
[Answer:  $0.03 \text{ m}^3$ ]
- 1.42** Calculate the speed of sound in nitrogen gas at  $100^\circ\text{C}$ .  
[Answer:  $393.85 \text{ m s}^{-1}$ ]
- 1.43** Find the value of the gas constant  $R$  for air in SI units.  
[Answer:  $287.2 \text{ J (kg K)}^{-1}$  or  $287.2 \text{ m}^2 (\text{s}^2 \text{ K})^{-1}$ ]
- 1.44** Methane gas enters a constant area duct at 4 atm,  $200^\circ\text{C}$ , and  $150 \text{ m s}^{-1}$ . At a downstream station 2,  $T_2 = 400^\circ\text{C}$  and  $V_2 = 250 \text{ m s}^{-1}$ . Determine  $p_2$ , the mass flow rate and the entropy change between these stations.  
[Answer: 3.414 atm,  $247.9 \text{ kg (m}^2 \text{ s)}^{-1}$ ,  $835.86 \text{ J (kg K)}^{-1}$ ]
- 1.45** Gas flows through an insulated duct. At station 1 in the duct  $p_1 = 5 \text{ atm}$ ,  $T_1 = 350 \text{ K}$ , and  $V_1 = 55 \text{ m s}^{-1}$ . At a downstream station 2, if  $p_2 = 1 \text{ atm}$  and  $V_2 = 300 \text{ m s}^{-1}$ , determine  $T_2$  and the entropy difference  $s_2 - s_1$  if the gas is (a) air and (b) argon.  
[Answer: (a) 306.7 K,  $329.25 \text{ J (kg K)}^{-1}$ , (b) 266.11 K,  $192.71 \text{ J (kg K)}^{-1}$ ]
- 1.46** Helium gas at 200 kPa, kept in a closed tank, is heated from  $50$  to  $100^\circ\text{C}$ . If the change in entropy is  $1000 \text{ J K}^{-1}$ , determine the new pressure and the mass of helium in the tank.  
[Answer: 230.94 kPa, 2.21 kg]
- 1.47** An aircraft flying at an altitude of 10 000 m experiences a temperature of  $500^\circ\text{C}$  at its nose. Determine the flight Mach number.  
[Answer: 3.51]
- 1.48** Helium gas expands isentropically through a nozzle from state 1 to state 2. If the pressure and temperature at state 1 are 108 kPa and  $92^\circ\text{C}$ , respectively, and the pressure and velocity at state 2 are 60 kPa and  $903 \text{ m s}^{-1}$ , respectively, determine  $T_2$ ,  $M_2$ ,  $V_1$ ,  $M_1$ ,  $p_0$ , and  $T_0$ .  
[Answer: 289.05 K, 0.904,  $139.02 \text{ m s}^{-1}$ , 0.124, 109.38 kPa, 367 K]
- 1.49** Derive an expression for the entropy change in terms of pressures for a polytropic process of an ideal gas with constant specific heats.

$$\left[ \text{Answer : } s_2 - s_1 = \frac{(n - \gamma)R}{n(\gamma - 1)} \ln \left( \frac{p_2}{p_1} \right) \right]$$

- 1.50** The temperature and pressure of an unknown ideal gas in a cylinder of volume  $1 \text{ m}^3$  are found to be 300 K and 6 atm, respectively. The mass of the gas in the cylinder is 975 g. Find the molecular weight of the gas.  
[Answer:  $4 \text{ kg kmol}^{-1}$ ]

- 1.51** Ten grams of oxygen gas undergo a change of state at constant internal energy. Initial pressure and temperature are 2 atm and 330 K, respectively. The final volume occupied by the gas is twice the initial volume. Calculate the final temperature and pressure and the change in entropy due to the state change. Assume oxygen to be an ideal gas.  
[Answer: 330 K, 1 atm,  $1.8 \text{ J K}^{-1}$ ]
- 1.52** A cylinder of capacity  $2 \text{ m}^3$  contains oxygen gas at 600 kPa and  $30^\circ\text{C}$ . The gas is discharged from the cylinder until the pressure drops to 350 kPa, keeping the temperature at the same level. Assuming ideal gas behavior, determine the quantity of oxygen discharged.  
[Answer: 6.35 kg]
- 1.53** Determine the specific volume of an ideal gas at 1 atm and  $0^\circ\text{C}$ .  
[Answer:  $22.4 \text{ m}^3 \text{ kgmol}^{-1}$ ]
- 1.54** An ideal gas has a molecular weight of 39.948. If its specific heats ratio at a given temperature is 1.67, determine  $c_p$  and  $c_v$  of the gas at that temperature.  
[Answer:  $c_p = 518.4 \text{ J (kg K)}^{-1}$ ,  $c_v = 310.4 \text{ J (kg K)}^{-1}$ ]
- 1.55** A rigid tank of volume  $2 \text{ m}^3$  contains oxygen gas at 50 kPa and  $50^\circ\text{C}$ . Another rigid tank of the same volume contains oxygen gas at 30 kPa and  $25^\circ\text{C}$ . The two tanks are then connected. If the final equilibrium temperature of the gas in both tanks is  $25^\circ\text{C}$ , what is the final pressure in both the tanks? Treat the process as being isentropic.  
[Answer: 37.7 kPa]
- 1.56** If an airplane flies at 90 kmph at an altitude of 10 000 m, find whether it flies at supersonic speed or subsonic speed?  
[Answer: Flies at subsonic speed at Mach 0.835]
- 1.57** Calculate the speed of sound in (a) air, (b) hydrogen, (c) methane, (d) oxygen, (e) carbon dioxide, and (f) helium, at  $100^\circ\text{C}$ .  
[Answer: (a)  $387.21 \text{ m s}^{-1}$ , (b)  $1473.03 \text{ m s}^{-1}$ , (c)  $505.27 \text{ m s}^{-1}$ , (d)  $368.4 \text{ m s}^{-1}$ , (e)  $302.71 \text{ m s}^{-1}$ , (f)  $1134.25 \text{ m s}^{-1}$ ]
- 1.58** A missile in flight experiences a pressure and a temperature of 4 atm and 500 K, respectively, at its nose. Determine the density of air at its nose.  
[Answer:  $2.824 \text{ kg m}^{-3}$ ]
- 1.59** A pressure vessel of volume  $15 \text{ m}^3$  is filled with dry air at pressure 10 atm and temperature 300 K. Compute the mass of air in the tank.  
[Answer: 176.52 kg]
- 1.60** Calculate the enthalpy of the air stored in the pressure vessel in Problem 1.59.  
[Answer: 53.19 MJ]
- 1.61** For a calorically perfect gas show that  
$$c_p - c_v = R$$
- 1.62** A gas initially at 140 kPa,  $0.012 \text{ m}^3$ , and  $100^\circ\text{C}$  is compressed to a final state with a pressure and volume of 2.8 MPa and  $0.0012 \text{ m}^3$ , respectively, according to the law

$pV^n = \text{constant}$ . Determine (a) the value of  $n$ , (b) temperature of the final state, (c) the work transfer, and (d) the change of internal energy of the gas if  $R = 0.287 \text{ kJ (kg K)}^{-1}$  and  $c_v = 0.717 \text{ kJ (kg K)}^{-1}$ .

[Answer: (a) 1.3, (b)  $472.54^\circ\text{C}$ , (c)  $-5.6 \text{ kJ}$ , (d)  $4.194 \text{ kJ}$ ]

- 1.63** One kilogram of gas at an initial pressure of  $0.11 \text{ MPa}$  and a temperature of  $15^\circ\text{C}$  is compressed isothermally until the volume becomes  $0.1 \text{ m}^3$ . Determine (a) the final pressure, (b) the final temperature, and (c) the heat transfer associated with the process. Assume  $c_p = 0.92 \text{ kJ (kg K)}^{-1}$  and  $c_v = 0.66 \text{ kJ (kg K)}^{-1}$ , for the gas.

[Answer: (a)  $0.749 \text{ MPa}$ , (b)  $15^\circ\text{C}$ , (c)  $-143.724 \text{ kJ}$ ]

- 1.64** A certain quantity of gas has an initial volume and temperature of  $1.2 \text{ l}$  and  $150^\circ\text{C}$ , respectively. If it is expanded to a volume of  $3.6 \text{ l}$  according to the law  $pV^{1.4} = \text{constant}$ , determine the final temperature of the gas.

[Answer:  $-0.486^\circ\text{C}$ ]

- 1.65** A certain quantity of gas at an initial pressure of  $0.1 \text{ MPa}$  and volume  $0.1 \text{ m}^3$  is compressed to a pressure of  $1.4 \text{ MPa}$  according to the law  $pV^{1.26} = \text{constant}$ . Determine the final volume of the gas.

[Answer:  $12.31 \text{ l}$ ]

- 1.66** A certain mass of air initially at  $1.3 \text{ MPa}$ ,  $0.014 \text{ m}^3$ , and  $135^\circ\text{C}$  is expanded to a state where the pressure is  $275 \text{ kPa}$  and the volume is  $0.056 \text{ m}^3$ . Determine the mass and final temperature of the air.

[Answer:  $0.1554 \text{ kg}$ ,  $72.14^\circ\text{C}$ ]

- 1.67** Argon gas flows through a nozzle. At the nozzle inlet the pressure and density are  $200 \text{ kPa}$  and  $1.2 \text{ kg m}^{-3}$ , respectively. At the nozzle exit the pressure and temperature are  $100 \text{ kPa}$  and  $500^\circ\text{C}$ , respectively. Calculate the initial temperature, the final density, and the changes in entropy and enthalpy of the gas due to the flow process.

[Answer:  $800.74 \text{ K}$ ,  $0.621 \text{ kg m}^{-3}$ ,  $126.08 \text{ J (kg K)}^{-1}$ ,  $-14.31 \text{ kJ kg}^{-1}$ ]

- 1.68** An insulated tank is divided into two compartments of equal volume by a diaphragm. One of the compartments is kept empty at vacuum and the other contains a gas of unit mass. The diaphragm is burst so that the gas fills both compartments. Assuming the gas to be a perfect gas, show that the final temperature of the gas is the same as the initial temperature and that the entropy increases by an amount  $\frac{\gamma-1}{\gamma} c_p \ln(2)$ .

- 1.69** Show that, for an ideal gas, the entropy change can be expressed as

$$\Delta s = c_p \ln \left( \frac{v_2}{v_1} \right) + c_v \ln \left( \frac{p_2}{p_1} \right)$$

- 1.70** Air flowing isentropically through a duct has a velocity and temperature of  $100 \text{ m s}^{-1}$  and  $20^\circ\text{C}$ , respectively, at a particular station. Find the velocity at a downstream station where the temperature is  $5^\circ\text{C}$ .

[Answer:  $200.34 \text{ m s}^{-1}$ ]

- 1.71** A pitot-static probe placed in an air stream measures  $214 \text{ mm}$  of mercury. If the stream pressure and temperature are  $66 \text{ kPa}$  and  $9^\circ\text{C}$ , calculate its velocity.

[Answer:  $247.5 \text{ m s}^{-1}$ ]

## 2

## Steady One-Dimensional Flow

### 2.1 Introduction

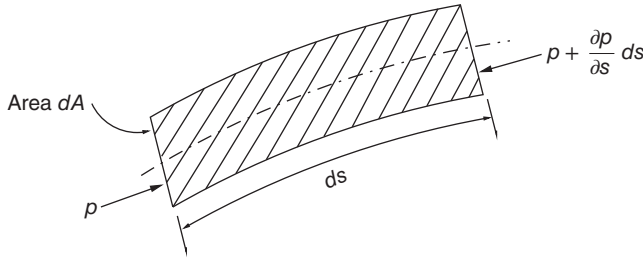
The complications associated with compressible flows are much more than those with incompressible flows. Hence, it seems appropriate to begin with the simplest types of flow rather than with a general flow analysis. Therefore, in this chapter we shall consider steady flows with constant properties normal to the flow direction. The three state variables  $p$ ,  $\rho$ ,  $T$ , and the flow speed  $V$ , now depend on a single parameter only, e.g. the arc length measured in the direction of the flow. These conditions are approximately realized in flow through constant area ducts and ducts with a gradually varying cross-section. The state of the flow (including the speed) is often found constant over the whole cross-section except for a narrow zone in the immediate vicinity of the wall, thus the use of mean values in the calculations makes physical sense. The following remarks not only refer to the above case but are also useful for steady flows of a more general spatial character.

Streamlines, in general, are imaginary curves in the flow field that have their tangents everywhere in the (instantaneous) direction of the flow. They can be bundled into streamtubes and when sufficiently small cross-sections are chosen the assumption of a uniform state of flow over the cross-section is almost satisfied. Also, in steady flows, a specified fluid element is at all times either inside or outside a specified streamtube. Therefore, the steady flow within a streamtube can be considered strictly one-dimensional. For flows with gradually varying finite cross-sections, we speak of *quasi-one-dimensional flow*, to distinguish it from strictly one-dimensional flow.

### 2.2 Fundamental Equations

Consider a streamtube differential in equilibrium in a one-dimensional flow field, as represented by the shaded area in Figure 2.1.  $p$  is the pressure acting at the left face of the streamtube and  $\left(p + \frac{\partial p}{\partial s} ds\right)$  is the pressure at the right face. Therefore, the pressure force in the positive  $s$ -direction,  $F_p$ , is given by

$$F_p = p dA - \left[ p + \frac{\partial p}{\partial s} ds \right] dA = - \frac{\partial p}{\partial s} ds dA$$



**Figure 2.1** Forces acting on streamtube.

For equilibrium,  $dm(dV/dt) = \text{sum of all the forces acting on the streamtube differential}$ , where  $dm$  is the mass of fluid in the streamtube element considered and  $dV/dt$  is the substantial acceleration.

$$dV = \frac{\partial V}{\partial t} dt + \frac{\partial V}{\partial s} ds$$

$$\frac{dV}{dt} = \frac{\partial V}{\partial t} \frac{dt}{dt} + \frac{\partial V}{\partial s} \frac{ds}{dt}$$

In the above equation for substantial acceleration,  $\partial V/\partial t$  is the local acceleration or acceleration at a point, that is the change of velocity at a fixed point in space with time. The convective acceleration  $\frac{\partial V}{\partial s} \frac{ds}{dt} = V \frac{\partial V}{\partial s}$  is the acceleration between two points in space, that is the change of velocity at a fixed time with space. It is present even in a steady flow.

The substantial derivative is expressed as

$$\frac{dV}{dt} = \frac{\partial V}{\partial t} + V \frac{\partial V}{\partial s} \quad (2.1)$$

Therefore, the equilibrium equation becomes

$$-\frac{\partial p}{\partial s} ds dA = dm \frac{dV}{dt}$$

But  $dm = \rho dA ds$ . Substituting this into the above equation, we get

$$\frac{dV}{dt} = -\frac{1}{\rho} \frac{\partial p}{\partial s} \quad (2.2)$$

that is

$$\frac{\partial V}{\partial t} + V \frac{\partial V}{\partial s} + \frac{1}{\rho} \frac{\partial p}{\partial s} = 0$$

Equation (2.2) is applicable for incompressible flows also; the only difference comes in solution. For steady flow, Eq. (2.2) becomes

$$V \frac{\partial V}{\partial s} + \frac{1}{\rho} \frac{\partial p}{\partial s} = 0 \quad (2.3)$$

Integration of Eq. (2.3) yields

$$\boxed{\frac{V^2}{2} + \int \frac{1}{\rho} \frac{\partial p}{\partial s} ds = \text{constant}} \quad (2.4)$$

This equation is often called the *compressible form of Bernoulli's equation for inviscid flows*. If  $\rho$  is expressible as a function of  $p$  only, that is  $\rho = \rho(p)$ , the second expression is



integrable. Fluids having these characteristics are called *barotropic fluids*. For an isentropic flow process,

$$\frac{p}{\rho^\gamma} = \text{constant} \quad (2.5)$$

$$\frac{\rho_2}{\rho_1} = \left( \frac{p_2}{p_1} \right)^{1/\gamma} \quad (2.6)$$

where subscripts 1 and 2 refer to two different states. Therefore, integrating  $dp/\rho$  between pressure limits  $p_1$  and  $p_2$ , we get

$$\int_{p_1}^{p_2} \frac{dp}{\rho} = \frac{\gamma}{\gamma-1} \frac{p_1}{\rho_1} \left[ \left( \frac{p_2}{p_1} \right)^{(\gamma-1)/\gamma} - 1 \right] \quad (2.7)$$

Using Eq. (2.7), Bernoulli's equation can be written as

$$\frac{V_2^2}{2} - \frac{V_1^2}{2} + \frac{\gamma}{\gamma-1} \frac{p_1}{\rho_1} \left[ \left( \frac{p_2}{p_1} \right)^{(\gamma-1)/\gamma} - 1 \right] = 0 \quad (2.8)$$

Equation (2.8) is a form of energy equation for the isentropic flow process of gases.

For an adiabatic flow of perfect gases, the energy equation can be written as

$$c_p T_2 + \frac{V_2^2}{2} = c_p T_1 + \frac{V_1^2}{2} \quad (2.9a)$$

or

$$\frac{\gamma}{\gamma-1} \frac{p_2}{\rho_2} + \frac{V_2^2}{2} = \frac{\gamma}{\gamma-1} \frac{p_1}{\rho_1} + \frac{V_1^2}{2} \quad (2.9b)$$

or

$$\frac{\gamma}{\gamma-1} \frac{p}{\rho} + \frac{V^2}{2} = \frac{\gamma}{\gamma-1} \frac{p_0}{\rho_0} \quad (2.9c)$$

Equations (2.9a)–(2.9c) are more general in nature than Eq. (2.8); the restrictions on Eq. (2.8) are more severe than those of Eq. (2.9).

Equations (2.9a)–(2.9c) can be applied to shock, but not Eq. (2.8), because the flow across the shock is nonisentropic. With a Laplace equation  $a^2 = \gamma p/\rho$ , Eq. (2.9c) can be written as

$$\frac{V^2}{2} + \frac{a^2}{\gamma-1} = \frac{\gamma}{\gamma-1} \frac{p_0}{\rho_0} \quad (2.9d)$$

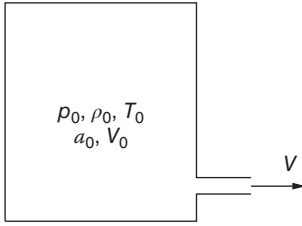
or

$$\frac{V^2}{2} + \frac{a^2}{\gamma-1} = \frac{a_0^2}{\gamma-1} \quad (2.9e)$$

The subscript 0 refers to the stagnation condition when the flow is brought to rest isentropically or when the flow is connected to a large reservoir. All these relations are valid only for a perfect gas.

## 2.3 Discharge from a Reservoir

Consider a reservoir as shown in Figure 2.2, containing air at high pressure  $p_0$ . Let the density, temperature, speed of sound, and velocity of air be  $\rho_0$ ,  $T_0$ ,  $a_0$ , and  $V_0$ , respectively.



**Figure 2.2** Discharge of high pressure air through a small opening.

Because of the large volume of the reservoir, the velocity of air inside is  $V_0 = 0$ . Let the high pressure air be discharged to ambient atmosphere at pressure  $p_a$  and velocity  $V = 0$ , through an opening, as shown in Figure 2.2. Now the velocity  $V$  at the opening, at which the air is discharged, can be obtained by substituting  $V_1 = 0, p_1 = p_0, \rho_1 = \rho_0$ , and  $p_2 = p_a$  into Eq. (2.8) as

$$V = \sqrt{\frac{2\gamma}{\gamma - 1} \frac{p_0}{\rho_0} \left[ 1 - \left( \frac{p_a}{p_0} \right)^{(\gamma-1)/\gamma} \right]} \quad (2.10)$$

For discharge into vacuum, that is if  $p_a = 0$ , Eq. (2.10) results in the maximum velocity

$$V_{\max} = \sqrt{\frac{2\gamma}{\gamma - 1} \frac{p_0}{\rho_0}} = a_0 \sqrt{\frac{2}{\gamma - 1}} \quad (2.11)$$

$V_{\max}$  is the limiting velocity that may be achieved by expanding a gas at any given stagnation condition into vacuum. For air at  $T_0 = 288$  K,  $V_{\max} = 760.7 \text{ m s}^{-1} = 2.236 a_0$ . This is the maximum velocity that can be obtained by discharge into vacuum in a frictionless flow. From Equation (2.11), we can see that  $V_{\max}$  is independent of the reservoir pressure but it depends only on the reservoir temperature. For incompressible flow, by Bernoulli's equation,

$$p + \frac{1}{2} \rho V^2 = p_0, \quad V = \sqrt{2 \left( \frac{p_0 - p}{\rho} \right)} \quad (2.12a)$$

Therefore,

$$V_{\max} = \sqrt{2 \frac{p_0}{\rho_0}} \quad (2.12b)$$

In this relation  $\rho$  is replaced by  $\rho_0$ , because  $\rho$  is constant for incompressible flow. Combining Eqs. (2.11) and (2.12b), we get

$$V_{\max(\text{comp.})} = \sqrt{\frac{\gamma}{\gamma - 1}} V_{\max(\text{incomp.})}$$

For air, with  $\gamma = 1.4$ ,

$$V_{\max(\text{comp.})} \approx 1.9 V_{\max(\text{incomp.})}$$

That is, the error involved in treating air as an incompressible medium is 90%.

For the case when the flow is not into vacuum,  $p_a/p_0 \neq 0$ , and Equations (2.10) and (2.12a) may be expressed by dividing them by  $a_0$  as

$$\frac{V}{a_0} = \sqrt{\frac{2}{\gamma - 1} \left[ 1 - \left( \frac{p_a}{p_0} \right)^{(\gamma-1)/\gamma} \right]} \quad (\text{compressible}) \quad (2.13)$$

$$\frac{V}{a_0} = \sqrt{\frac{2}{\gamma} \left[ 1 - \left( \frac{p_a}{p_0} \right) \right]} \quad (\text{incompressible}) \quad (2.14)$$

### 2.3.1 Mass Flow Rate per Unit Area

For a streamtube in a compressible flow field,

$$\dot{m} = \rho AV = \text{constant}$$

or

$$\frac{\dot{m}}{A} = \rho V = \frac{\text{constant}}{A} \quad (2.15)$$

The mass flow rate per unit area  $\propto \frac{1}{\text{sectional area of the streamtube}}$

With Eqs. (1.71), (2.13), and (2.15), we can write

$$\frac{\rho V}{\rho_0 a_0} = \sqrt{\frac{2}{\gamma - 1} \left( \frac{p_a}{p_0} \right)^{1/\gamma}} \sqrt{1 - \left( \frac{p_a}{p_0} \right)^{(\gamma-1)/\gamma}} \quad (2.16)$$

Variation of  $V/a_0$ , temperature ratio  $T/T_0$ , density ratio  $\rho/\rho_0$ , and  $\rho V/(\rho_0 a_0)$  with the pressure ratio  $p/p_0$  for the isentropic flow of a high-pressure air discharged from a reservoir at the stagnation state at  $p_0$  and  $T_0$  are all shown in Figure 2.3.

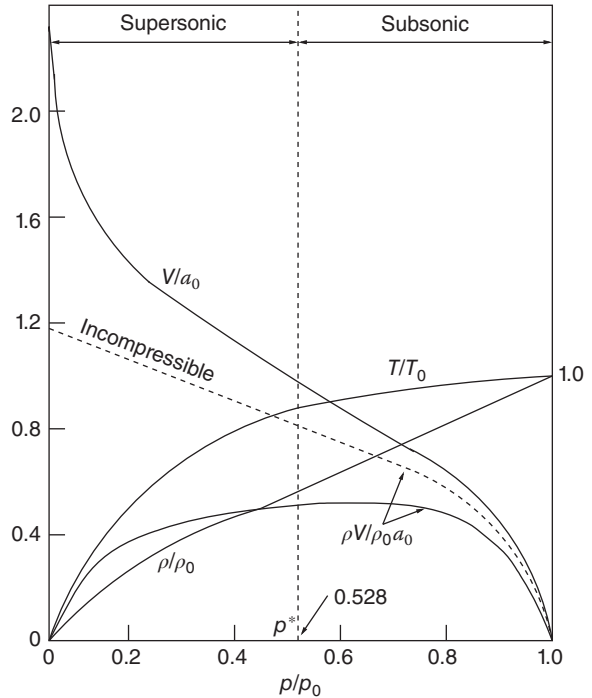
The peculiar shape of the curve represented by Eq. (2.16) is of the utmost importance;  $\rho V/(\rho_0 a_0)$  has a definite maximum, because at  $p_a/p_0 = 1.0$ ,  $V/a_0 = 0$ , and  $\rho/\rho_0$  is finite as seen from Figure 2.3. Therefore,

$$\frac{\rho V}{\rho_0 a_0} = 0$$

At  $p_a/p_0 = 0$ ,  $V/a_0$  is finite and  $\rho/\rho_0 = 0$ . Thus,

$$\frac{\rho V}{\rho_0 a_0} = 0$$

**Figure 2.3** Flow properties variation with pressure ratio for isentropic flow discharged from a reservoir.



That is, for the two limiting values of pressure ratio,  $\rho V/(\rho_0 a_0)$  becomes zero and therefore it should have a definite maximum value at a pressure ratio between the two limiting pressure ratios. Also, as  $p/p_0$  decreases,  $V/a_0$  increases and  $\rho/\rho_0$  decreases; therefore, there should be a point where their product  $(\rho V)/(\rho_0 a_0)$  is a maximum.

From the above discussion we can say that, in the range

- $\frac{p^*}{p_0} \leq \frac{p}{p_0} \leq 1$ ,  $V$  increases faster than  $\rho$  decreases, and for
- $0 \leq \frac{p}{p_0} \leq \frac{p^*}{p_0}$ , the increase of  $V$  is slower than the decrease of  $\rho$ .

Also, at this point of maximum  $\rho V/(\rho_0 a_0)$ , the mass flow rate is maximum and the streamtube area is a minimum, that is:

- $\rho V$  is a maximum at  $p = p^*$
- $A$  is minimum at  $p = p^*$
- $V^* = a$  or  $M^* = 1$  at  $p = p^*$

Now, consider Bernoulli's equation

$$\frac{V^2}{2} + \int \frac{dp}{\rho} = \text{constant}$$

Differentiating and rearranging, we get

$$\rho V = -\frac{dp}{dV} \quad (2.17)$$

The condition for  $\rho V$  to be maximum may be written as

$$\frac{d(\rho V)}{dp} = 0$$

that is

$$\rho \frac{dV}{dp} + V \frac{d\rho}{dp} = 0$$

Substituting for  $dV/dp$  from Eq. (2.17), we get

$$-\frac{1}{V} + V \frac{d\rho}{dp} = 0, \quad \frac{dp}{d\rho} = V^2$$

But  $dp/d\rho = a^2$ , from the Laplace Eq. (1.11). Therefore,  $V^2 = a^2$  or

$$V^* = a \quad (2.18a)$$

$$M^* = 1 \quad (2.18b)$$

In Eq. (2.18a),  $V$  is replaced by  $V^*$  in order to make this velocity correspond to the condition of  $\rho V$  maximum. The values with superscript  $*$  are called *critical values*, because if a reservoir at high pressure is connected to a pipe then, depending on the backpressure (the pressure of the surrounding atmosphere to which the high pressure gas in the reservoir is discharged through the pipe), the velocity at the exit of the pipe changes. If the backpressure is more than  $p^*$ , the velocity at the pipe exit is subsonic; if it is equal to  $p^*$ , the velocity will be sonic and if it is less than  $p^*$ , the velocity will be supersonic in the core region in the vicinity of the pipe exit.

**Example 2.1**

Helium gas from a storage tank at 1000 kPa and 310 K is flowing out through a convergent nozzle of exit area 3 cm<sup>2</sup> to another tank. When the mass flow rate is 0.15 kg s<sup>-1</sup>, determine the pressure in the second tank.

**Solution:**

Given,  $p_0 = 1000$  kPa and  $T_0 = 310$  K. The maximum mass flow through the nozzle is at choked condition with  $M_e = 1$  and is given by

$$\dot{m}_{\max} = \sqrt{\gamma \left( \frac{2}{\gamma + 1} \right)^{(\gamma+1)/(\gamma-1)} \frac{p_0^2}{RT_0}} A^*$$

For helium gas,  $\gamma = 1.67$  and the gas constant is given by

$$R = \frac{R_u}{\text{molecular weight}} = \frac{8314}{4.003} = 2077 \text{ J (kg K)}^{-1}$$

Therefore,

$$\dot{m}_{\max} = \frac{0.7266 \times 1000 \times 10^3}{\sqrt{2077 \times 310}} 3 \times 10^{-4} = 0.27 \text{ kg s}^{-1}$$

The given mass flow rate 0.15 kg s<sup>-1</sup> is less than the critical value and hence  $M_e$  is subsonic.

$$\begin{aligned} \dot{m} &= 0.15 = \rho_e A_e V_e \\ &= \left( \frac{\rho_e}{\rho_0} \right) \rho_0 A_e M_e \left( \frac{a_e}{a_0} \right) a_0 \\ &= \rho_0 a_0 A_e M_e \left( \frac{\rho_e}{\rho_0} \right) \left( \frac{T_e}{T_0} \right)^{1/2} \\ &= \rho_0 a_0 A_e M_e \left( 1 + \frac{\gamma - 1}{2} M_e^2 \right)^{-\frac{1}{\gamma-1}} \left( 1 + \frac{\gamma - 1}{2} M_e^2 \right)^{-0.5} \end{aligned}$$

For helium,  $\gamma = 1.67$ , so

$$0.15 = \rho_0 a_0 A_e M_e (1 + 0.33 M_e^2)^{-2}$$

Also,

$$\begin{aligned} \rho_0 &= \frac{p_0}{RT_0} \\ &= \frac{1000 \times 10^3}{2077 \times 310} \\ &= 1.553 \text{ kg m}^{-3} \\ a_0 &= \sqrt{\gamma RT_0} \\ &= \sqrt{1.67 \times 2077 \times 310} \\ &= 1036.95 \text{ m s}^{-1} \\ A_e &= 3 \times 10^{-4} \text{ m}^2 \end{aligned}$$

Thus,

$$0.15 = \frac{0.4831 M_e}{(1 + 0.335 M_e^2)^2}$$

Now let us solve for  $M_e$  by trial and error.

*Trial 1* Let  $M_e = 0.3$ .

$$\text{RHS} \approx 0.145$$

*Trial 2* Let  $M_e = 0.32$ .

$$\text{RHS} \approx 0.15$$

Hence,  $M_e = 0.32$ .

By isentropic relation, we have

$$\begin{aligned} \frac{p_0}{p_e} &= \left(1 + \frac{\gamma - 1}{2} M_e^2\right)^{\frac{\gamma}{\gamma - 1}} \\ &= (1 + 0.335 M_e^2)^{2.493} \\ &= 1.087 \end{aligned}$$

Thus, the pressure in the second tank is

$$\begin{aligned} p_e &= \frac{p_0}{1.087} \\ &= \frac{1000 \times 10^3}{1.087} \\ &= \boxed{919.96 \text{ kPa}} \end{aligned}$$

### Example 2.2

A flow at  $60 \text{ m s}^{-1}$  enters a nozzle kept horizontal. The specific enthalpy at the nozzle inlet and exit is  $3025$  and  $2790 \text{ kJ kg}^{-1}$ , respectively. Neglecting the heat loss from the nozzle, calculate (a) the flow velocity at the nozzle exit, (b) the mass flow rate through the nozzle, if the inlet area is  $0.1 \text{ m}^2$  and the specific volume at inlet is  $0.19 \text{ m}^3 \text{ kg}^{-1}$ , and (c) the exit area of the nozzle when the specific volume at the exit is  $0.5 \text{ m}^3 \text{ kg}^{-1}$ .

#### Solution:

Let the inlet and the exit of the nozzle be denoted by subscripts 1 and 2, respectively.

(a) By energy equation, we have

$$\begin{aligned} h_1 + \frac{V_1^2}{2} &= h_2 + \frac{V_2^2}{2} \\ 3025 \times 10^3 + \frac{60^2}{2} &= 2790 \times 10^3 + \frac{V_2^2}{2} \\ V_2^2 &= 473600 \\ V_2 &= \boxed{688.2 \text{ m s}^{-1}} \end{aligned}$$

(b) The mass flow rate is

$$\begin{aligned} \dot{m} &= \rho AV \\ &= \frac{A_1 V_1}{v_1} \\ &= \frac{0.1 \times 60}{0.19} \\ &= \boxed{31.58 \text{ kg s}^{-1}} \end{aligned}$$

(c) Mass flow rate is also given by

$$\dot{m} = \rho_2 A_2 V_2 = \frac{A_2 V_2}{v_2}$$

Thus,

$$\begin{aligned} A_2 &= \frac{\dot{m} v_2}{V_2} \\ &= \frac{31.58 \times 0.5}{688.2} \\ &= \boxed{0.0229 \text{ m}^2} \end{aligned}$$

### 2.3.2 Critical Values

The critical value of pressure ratio,  $p^*/p_0$ , is obtained from Eq. (2.13) by replacing  $V$  by  $V^* = a$ . With  $V = a$ , Eq. (2.13) becomes

$$\frac{a}{a_0} = \sqrt{\frac{2}{\gamma - 1} \left( 1 - \left( \frac{p_0}{p} \right)^{(\gamma-1)/\gamma} \right)}$$

With the speed of sound  $a = \sqrt{\gamma RT}$ , we get

$$\sqrt{\frac{T}{T_0}} = \left[ \frac{2}{\gamma - 1} \left( 1 - \left( \frac{p_a}{p_0} \right)^{(\gamma-1)/\gamma} \right) \right]^{1/2}$$

By Eq. (1.71),

$$\frac{T}{T_0} = \left( \frac{p}{p_0} \right)^{(\gamma-1)/\gamma} = \left( \frac{a}{a_0} \right)^2 \quad (2.19)$$

Therefore,

$$\left( \frac{p}{p_0} \right)^{(\gamma-1)/\gamma} = \frac{2}{\gamma - 1} \left[ 1 - \left( \frac{p_a}{p_0} \right)^{(\gamma-1)/\gamma} \right]$$

or

$$\begin{aligned} \left( \frac{p^*}{p_0} \right)^{(\gamma-1)/\gamma} &= \frac{2}{\gamma + 1} \\ \frac{p^*}{p_0} &= \left( \frac{2}{\gamma + 1} \right)^{\gamma/(\gamma-1)} \end{aligned} \quad (2.20)$$

Because Eq. (2.20) is derived on the assumption that  $V = a$ , which is the critical condition, the static pressure  $p$  is replaced by  $p^*$ . Also, note that pressure  $p$  is the same as  $p_a$  in Eq. (2.13).

Equation (2.20) gives the value of the critical pressure ratio; other critical values are obtained by introducing Eq. (2.20) into Eqs. (1.71), (2.16), and (2.19) as

$$\frac{\rho^*}{\rho_0} = \left( \frac{2}{\gamma + 1} \right)^{1/(\gamma-1)} \quad (2.21)$$

$$\frac{T^*}{T_0} = \frac{2}{\gamma + 1} \quad (2.22)$$

$$\frac{V^*}{a_0} = \frac{a^*}{a_0} = \sqrt{\frac{2}{\gamma + 1}} \quad (2.23)$$

$$\frac{\rho^* V^*}{\rho_0 a_0} = \left( \frac{2}{\gamma + 1} \right)^{(\gamma+1)/2(\gamma-1)} \quad (2.24)$$

All these critical values depend only on the specific heats ratio  $\gamma$ . For air at standard conditions, with  $\gamma = 1.4$ , these ratios are

$$\frac{p^*}{p_0} = 0.528$$

$$\frac{T^*}{T_0} = 0.833$$

$$\frac{\rho^*}{\rho_0} = 0.634$$

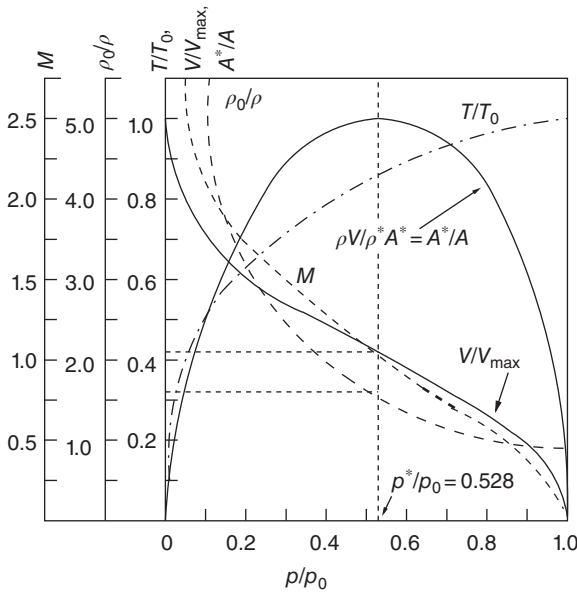
$$\frac{V^*}{a_0} = \frac{a^*}{a_0} = 0.913$$

$$\frac{\rho^* V^*}{\rho_0 a_0} = 0.578$$

It will be useful if we keep these values in mind for subsequent discussions. Some of the important relations of compressible flow are shown in graphical form in Figure 2.4.

Finally, from Eq. (1.62b) we have

$$\frac{a^2}{\gamma - 1} + \frac{V^2}{2} = \frac{\gamma + 1}{2(\gamma - 1)} a^{*2}$$



**Figure 2.4** Variation of Mach number, density ratio, temperature ratio, area ratio, and  $V/V_{\max}$  with pressure ratio.



Dividing throughout by  $V^2$ , we get

$$\begin{aligned} \frac{\left(\frac{a}{V}\right)^2}{\gamma - 1} + \frac{1}{2} &= \frac{\gamma + 1}{2(\gamma - 1)} \left(\frac{a^*}{V}\right)^2 \\ \frac{\left(\frac{1}{M^2}\right)}{\gamma - 1} &= \frac{\gamma + 1}{2(\gamma - 1)} \left(\frac{1}{M^*}\right)^2 - \frac{1}{2} \\ \boxed{M^2} &= \frac{2}{((\gamma + 1)/M^{*2}) - (\gamma - 1)} \end{aligned} \quad (2.25)$$

where  $M^*$ , which is the ratio of local flow speed ( $V$ ) and critical speed of sound ( $a^*$ ), is called the *characteristic Mach number*. Equation (2.25) provides a direct relation between the actual Mach number  $M$  and the characteristic Mach number  $M^*$ . From Eq. (2.25), it is seen that

$$\begin{aligned} M^* &= 1 \text{ if } M = 1 \\ M^* &< 1 \text{ if } M < 1 \\ M^* &> 1 \text{ if } M > 1 \\ M^* &\rightarrow \sqrt{\frac{\gamma+1}{\gamma-1}} \text{ if } M \rightarrow \infty \end{aligned}$$

Hence, qualitatively,  $M^*$  behaves in the same manner as  $M$ , except when  $M$  goes to infinity.  $M^*$  will be a useful parameter for further building of the subject involving shocks and expansion waves because it approaches a finite value as  $M$  approaches infinity.

In the course of discussion in this section we repeatedly came across three speeds:  $V_{\max}$ ,  $a_0$ , and  $V^*(=a^*)$ . These three speeds serve as standard reference speeds for gas dynamic study. We know that for adiabatic flow of a perfect gas the velocity can be expressed as

$$V = \sqrt{2c_p(T_0 - T)} = \sqrt{\frac{2\gamma}{\gamma - 1}R(T_0 - T)}$$

where  $T_0$  is the stagnation temperature. Since negative temperatures on absolute scales are not attainable, it is evident from the above equation that there is a maximum velocity corresponding to a given stagnation temperature. This maximum velocity, which is often used for reference purposes, is given by

$$V_{\max} = \sqrt{\frac{2\gamma}{\gamma - 1}RT_0}$$

Another useful reference velocity is the speed of sound at the stagnation temperature, given by

$$a_0 = \sqrt{\gamma RT_0}$$

Yet another convenient reference velocity is the critical speed  $V^*$ , that is velocity at Mach number unity, or

$$V^* = a^*$$

This may also be written as

$$\sqrt{\frac{2\gamma}{\gamma - 1}R(T_0 - T^*)} = \sqrt{\gamma RT^*}$$

This results in

$$\frac{T^*}{T_0} = \frac{2}{\gamma + 1}$$

Therefore, in terms of stagnation temperature, the critical speed becomes

$$V_0^* = a^* = \sqrt{\frac{2\gamma}{\gamma + 1} RT_0}$$

From this equation, we can get the following relations between the three reference velocities (with  $\gamma = 1.4$ ):

$$\begin{aligned}\frac{a^*}{a_0} &= \sqrt{\frac{2}{\gamma + 1}} = 0.913 \\ \frac{V_{\max}}{a_0} &= \sqrt{\frac{2}{\gamma - 1}} = 2.24 \\ \frac{V_{\max}}{a^*} &= \sqrt{\frac{\gamma + 1}{\gamma - 1}} = 2.45\end{aligned}$$

## 2.4 Streamtube Area–Velocity Relation

In this section, let us consider quasi-one-dimensional flow, allowing the streamtube area  $A$  to vary with distance  $x$ , as shown in Figure 2.5.

Let us continue to assume that all flow properties are uniform across any given cross-section of the streamtube and are functions of  $x$  only for steady flows. Such a flow, where  $A = A(x)$ ,  $p = p(x)$ ,  $\rho = \rho(x)$ , and  $V = V(x)$  for steady flow, is defined as a quasi-one-dimensional flow. Algebraic equations for steady quasi-one-dimensional flow can be obtained by applying the integral form of the conservation equations.

For any streamtube of area  $A$ , the continuity equation is given by

$$\rho AV = \text{constant} \quad (2.26)$$

Differentiating with respect to  $V$ , we obtain

$$\frac{d(\rho AV)}{dV} = \rho V \frac{dA}{dV} + A \frac{d(\rho V)}{dV} = 0$$

The term

$$A \frac{d(\rho V)}{dV} = A \left( \rho + V \frac{d\rho}{dp} \frac{dp}{dV} \right) = A\rho(1 - M^2)$$

Since, from Eq. (2.17),

$$\frac{dp}{dV} = -\rho V$$

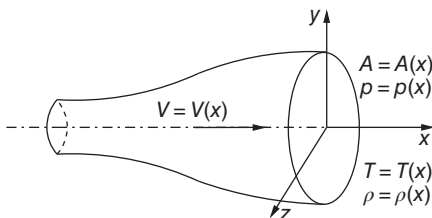


Figure 2.5 Quasi-one-dimensional flow.

and from the Laplace equation, we have

$$\frac{dp}{d\rho} = a^2$$

therefore

$$\rho V \frac{dA}{dV} + A\rho(1 - M^2) = 0$$

$$\boxed{\frac{dA}{dV} = -\frac{A}{V}(1 - M^2)} \quad (2.27)$$

Equation (2.27) is an important result. It is called the *area–velocity relation*.

The following information can be derived from the area–velocity relation:

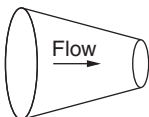
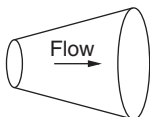
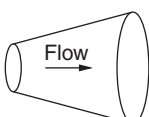
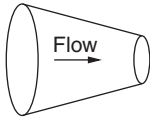
- For incompressible flow limit, that is for  $M \rightarrow 0$ , Eq. (2.27) shows that  $AV = \text{constant}$ . This is the famous volume conservation equation or continuity equation for incompressible flow.
- For  $0 \leq M \leq 1$ , a decrease in area results in an increase of velocity and vice versa. Therefore, the velocity increases in a convergent duct and decreases in a divergent duct. This result for compressible subsonic flows is the same as that for incompressible flows.
- For  $M > 1$ , an increase in area results in an increase of velocity and vice versa, that is the velocity increases in a divergent duct and decreases in a convergent duct. This is directly opposite to the behavior of subsonic flow in divergent and convergent ducts.
- For  $M = 1$ , by Eq. (2.27),  $dA/A = 0$ , which implies that at the location where the Mach number is unity the area of the passage is either minimum or maximum. We can easily show that the minimum in area is the only physically realistic solution.

The above results can be schematically shown as in Figure 2.6.

At this stage it is essential to understand why a supersonic flow accelerates in a divergent duct. The answer to this behavior of supersonic flow is as follows. By continuity, the mass flow rate through the passage is  $\dot{m} = \rho AV$ , where  $\rho$ ,  $A$ , and  $V$  are the local density, area, and velocity of the flow, respectively. Among these, the density is the most sensitive parameter in the supersonic regime. That is, when  $M > 1$  the decrease of density with Mach number increase becomes very rapid compared to the increase of flow velocity and duct area. Therefore, to keep the mass flow rate  $\dot{m}$  constant in a diverging passage, both the flow velocity and the passage area must increase together to compensate for the drastic decrease of density. This physics of the flow causes supersonic flow to accelerate in divergent passages.

From the above discussion, it is clear that for a gas to expand isentropically from subsonic to supersonic speeds it must flow through a convergent–divergent duct, as shown in Figure 2.7.

**Figure 2.6** Flow in convergent and divergent ducts.

Velocity, $V$	Subsonic, $M < 1$	Supersonic, $M > 1$
Increases		
Decreases		

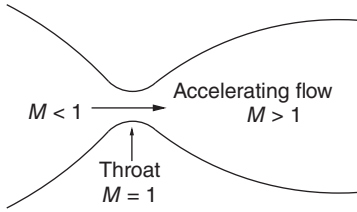


Figure 2.7 Flow in a convergent–divergent duct.

The minimum area that divides the convergent and divergent sections of the duct is called the *throat*. From point 4 above, we know that the flow at the throat must be sonic with  $M = 1$ . Conversely, for a gas to be compressed isentropically from supersonic to subsonic speeds, it must again flow through a convergent–divergent duct, with a throat where sonic flow occurs.

### Example 2.3

Air from a reservoir at 10 atm and  $80^\circ\text{C}$  is discharged through a convergent–divergent nozzle fitted to the reservoir. The thrust exerted by the jet issuing from the nozzle is 11.12 kN. If the backpressure is 1 atm, calculate the nozzle throat and exit areas and Mach number of the jet issuing from the nozzle. Assume the flow through the nozzle to be isentropic and correctly expanded.

### Solution:

Given,  $p_0 = 10$  atm,  $T_0 = 80 + 273.15 = 353.15$  K, and  $p_b = 1$  atm. The flow is correctly expanded; therefore,  $p_b = p_e$ .

The pressure ratio across the nozzle is

$$\frac{p_e}{p_0} = \frac{1}{10} = 0.1$$

For  $p_e/p_0 = 0.1$ , from the isentropic table we have the Mach number of the jet issuing from the nozzle as

$$M_e = \boxed{2.16}$$

Also,

$$\frac{T_e}{T_0} = 0.5173$$

$$\frac{A_e}{A_{th}} = 1.935$$

Therefore,

$$T_e = 0.5173 \times 353.15 = 182.68 \text{ K}$$

$$a_e = \sqrt{1.4 \times 287 \times 182.68} = 270.93 \text{ m s}^{-1}$$

The velocity at the nozzle exit is

$$V_e = M_e a_e = 2.16 \times 270.93 = 585.2 \text{ m s}^{-1}$$

The thrust generated by the jet issuing from the nozzle is

$$F = 11.12 \times 10^3 = \dot{m} V_e$$

Therefore,

$$\dot{m} = \frac{11120}{585.2} = 19 \text{ kg s}^{-1}$$

The mass flow rate  $\dot{m}$  is also given by

$$\dot{m} = \frac{0.6847}{\sqrt{RT_0}} p_0 A_{th}$$

Therefore, the throat area becomes

$$\begin{aligned} A_{th} &= \frac{19\sqrt{287 \times 353.15}}{0.6847 \times 10 \times 101325} \\ &= 0.0087188 \text{ m}^2 = \boxed{87.19 \text{ cm}^2} \end{aligned}$$

The nozzle exit area is

$$\begin{aligned} A_e &= 1.935 \times 87.19 \\ &= \boxed{168.71 \text{ cm}^2} \end{aligned}$$

## 2.5 de Laval Nozzle

A nozzle is a passage used to transform pressure energy into kinetic energy. A convergent–divergent nozzle used to generate supersonic flow is sometimes called a *de Laval nozzle*, after Carl G.P. de Laval, who first used such a configuration in his steam turbines in the late nineteenth century. Therefore, we can say that the de Laval nozzle is the only means to generate supersonic flow. A nozzle that does not have an expanding portion can never produce supersonic flow. In Section 2.6, detailed discussion about supersonic flow generation; the de Laval nozzle, which is a contoured nozzle capable of generating uniform and unidirectional supersonic flow; and the straight convergent–divergent nozzle, which can generate uniform but not unidirectional supersonic flow, is given.

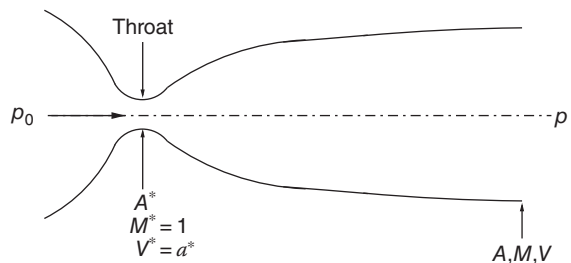
Consider the de Laval nozzle shown in Figure 2.8. At the throat, the flow is sonic. Hence, denoting conditions at sonic speed by an asterisk, we have at the throat,  $M^* = 1$  and  $V^* = a^*$ . The area of the throat is  $A^*$ . At any other section of the duct, the local area, Mach number, and velocity are  $A$ ,  $M$ , and  $V$ , respectively. By continuity equation,

$$\rho^* V^* A^* = \rho A V \quad (2.28)$$

With  $V^* = a^*$ , Eq. (2.28) becomes

$$\frac{A}{A^*} = \frac{\rho^* a^*}{\rho V} = \frac{\rho^* \rho_0 a^*}{\rho_0 \rho V} \quad (2.29)$$

**Figure 2.8** The de Laval nozzle.



where  $\rho_0$  is the stagnation density and is constant throughout the isentropic flow. By Eq. (1.74),

$$\frac{\rho_0}{\rho} = \left(1 + \frac{\gamma - 1}{2} M^2\right)^{1/(\gamma - 1)}$$

and applying this to sonic conditions ( $M = 1$ ), we get

$$\frac{\rho_0}{\rho^*} = \left(\frac{\gamma + 1}{2}\right)^{1/(\gamma - 1)} \quad (2.30)$$

Also, by definition,  $V/a^* = M^*$ . From Eq. (2.25),

$$M^{*2} = \frac{\left(\frac{\gamma + 1}{2}\right) M^2}{1 + \left(\frac{\gamma - 1}{2}\right) M^2} \quad (2.31)$$

Squaring Eq. (2.29) and substituting for  $\left(\frac{\rho^*}{\rho_0}\right)^2$ ,  $\left(\frac{\rho_0}{\rho}\right)^2$ , and  $\left(\frac{a^*}{V}\right)^2$  from Eqs. (2.30), (1.74), and (2.31), respectively, we have

$$\left(\frac{A}{A^*}\right)^2 = \left(\frac{\rho^*}{\rho_0}\right)^2 \left(\frac{\rho_0}{\rho}\right)^2 \left(\frac{a^*}{V}\right)^2$$

$$\left(\frac{A}{A^*}\right)^2 = \frac{1}{M^2} \left(\frac{2}{\gamma + 1} \left(1 + \frac{\gamma - 1}{2} M^2\right)\right)^{(\gamma + 1)/(\gamma - 1)} \quad (2.32)$$

Equation (2.32) is called the *Area–Mach number relation*. From this equation we get the striking result  $M = f(A/A^*)$ , that is the Mach number at any location in the duct is a function of the ratio of the local area of the duct to the sonic throat area. As can be seen from Eq. (2.27), the local duct area,  $A$ , must be larger than or at least equal to  $A^*$ , and the case in which  $A < A^*$  is physically impossible in an isentropic flow. Further, from Eq. (2.32), for any given  $A/A^* > 1$ , two values of  $M$  are obtained: a subsonic value and a supersonic value. The plot given in Figure 2.9 is the solution of Eq. (2.32) showing the subsonic and supersonic branches. Values of  $A/A^*$  as a function of  $M$  are tabulated in Table A.1 of the Appendix, for both subsonic and supersonic

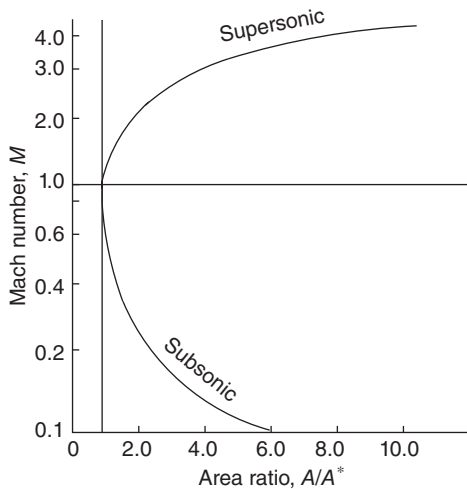


Figure 2.9 Area–Mach number relation.

flows. Once the variation of Mach number through the nozzle is known, the variations of static temperature, pressure, and density follow from Eqs. (1.72)–(1.74), respectively. The pressure, temperature, and density decrease continuously throughout the nozzle. Also, the exit pressure, density, and temperature ratios,  $p_e/p_0$ ,  $\rho_e/\rho_0$ , and  $T_e/T_0$  depend only on the exit area ratio  $A_e/A^*$ . That is, if the nozzle is part of a supersonic wind tunnel, the test-section conditions are completely determined by  $A_e/A^*$  (geometry of the nozzle) and  $p_0$  and  $T_0$  (properties of the gas in the reservoir).

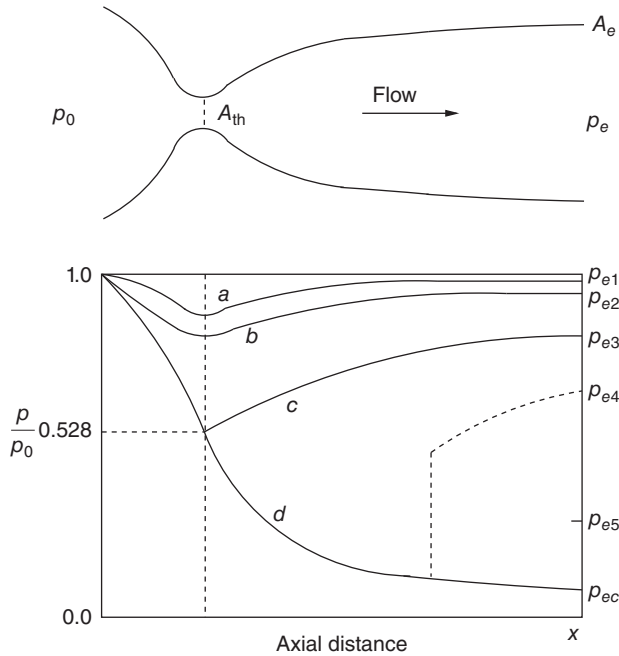
If a de Laval nozzle, designed for a particular Mach number, is kept in still atmosphere and nothing else is done, obviously the air will not start accelerating through the nozzle of its own accord. To accelerate the air, a favorable pressure gradient must be exerted across the nozzle. Therefore, in order to establish a flow through any duct, the pressure at the exit must be lower than the inlet pressure, that is  $p_e/p_0 < 1$ . Indeed, supersonic velocity can be reached only if  $p_e/p_0 < 0.528$ . For such pressure ratios, the contracting portion of the nozzle accelerates the flow up to  $M = 1$  and the divergent portion further accelerates the flow beyond  $M = 1$ .

It is important to realize that the statement “supersonic velocity can be reached only if  $p_e/p_0 < 0.528$ ” is the essential requirement for the nozzle to choke at the throat (that is to have  $M^* = 1$  at the throat). Thus, in the strict sense it should be stated that a nozzle will have  $M_{th} = 1$  at the throat only if  $p_{th}/p_0 < 0.528$ , and the flow in the divergent portion of the nozzle will accelerate to increasing supersonic Mach numbers only if  $p/p_{th} < 1$ , where  $p$  is the local static pressure in the divergent portion of the nozzle. The flow after choking at the nozzle throat will continue to accelerate to progressively higher supersonic Mach numbers only if  $p_e/p_{th} < 1$ . In other words, for the flow to accelerate, a favorable pressure gradient should exist. Therefore, for a convergent–divergent nozzle to experience supersonic flow from downstream of the throat up to the exit, the limiting pressure ratio  $p_e/p_0$  required across the nozzle is dictated by the presence of normal shock at the exit. This  $p_e/p_0$  can also be greater than 0.528. A detailed discussion on the limiting  $p_e/p_0$  required for every nozzle exit Mach number  $M_e$  to establish supersonic flow throughout the divergent portion of the nozzle, with a normal shock at the nozzle exit plane, is given in Section 2.6.2.

A variety of flow fields can be generated in the convergent–divergent or de Laval nozzle by independently governing the backpressure downstream of the nozzle exit. Consider the flow through a de Laval nozzle, as shown in Figure 2.10.

When  $p_e = p_0$ , there will be no flow through the nozzle. Let the exit pressure be reduced to a value ( $p_{e1}$ ) slightly below  $p_0$ . This small favorable pressure gradient will cause a flow through the nozzle at low subsonic speeds. The local Mach number will increase continuously through the convergent portion of the nozzle, reaching the maximum at the throat. In other words, the static pressure will decrease continuously in the convergent portion of the nozzle, reaching a minimum at the throat, as shown by curve *a* in Figure 2.10. Assume that  $p_e$  is reduced further ( $p_{e2}$ ). Then the pressure gradient will be stronger, flow acceleration will be faster, and the variation of Mach number and static pressure through the duct will be larger, as shown by curve *b*. Similarly, if  $p_e$  is reduced continuously, at some value of  $p_e$  the flow will reach sonic velocity at the throat, as shown by curve *c*. For this case,  $A_{th} = A^*$ . Now, the sonic flow at the throat will expand further in the divergent portion of the nozzle as a supersonic flow if  $p_e/p_{th} < 1$  and will decelerate as a subsonic flow, as shown by curve *c*, for  $p_e/p_{th} > 1$ .

For the cases discussed above, the mass flow through the duct increases as  $p_e$  decreases. This mass flow can be calculated by evaluating Eq. (2.15) at the throat,  $\dot{m} = \rho_{th} A_{th} V_{th}$ . When  $p_e$  is equal to  $p_{e3}$ , where sonic flow is attained at the throat,  $\dot{m} = \rho^* A^* a^*$ ; also, the Mach number at the throat is unity; this is dictated by Eq. (2.27). Hence, the flow properties at the throat and, indeed, throughout the subsonic (convergent) section of the duct become “frozen” when  $p_e < p_{e3}$ , that is the subsonic flow in the convergent portion of the nozzle becomes unaffected



**Figure 2.10** Flow in a convergent–divergent nozzle.

and the mass flow remains constant for  $p_e < p_{e3}$ . This condition for sonic flow at the throat is called *choked flow*. For further reduction of  $p_e$  below  $p_{e3}$ , after the flow becomes choked, the mass flow remains constant.

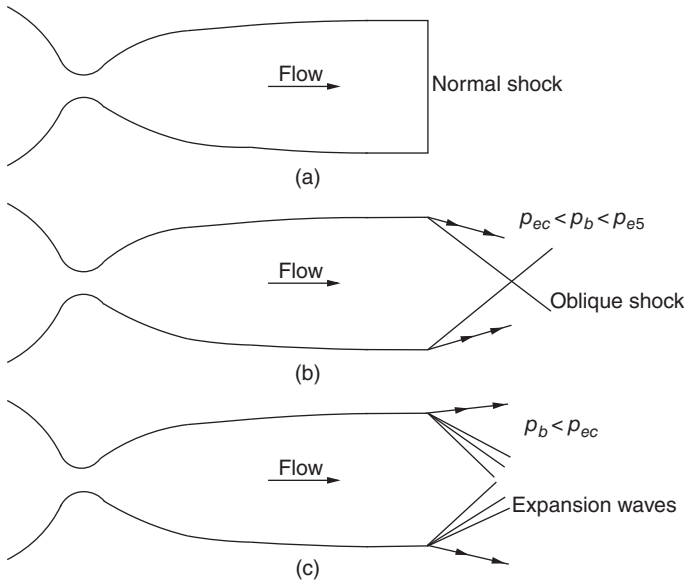
At this stage it is important to realize that the choked mass flow rate  $\dot{m}^*$  is the maximum only for a given  $p_0$  and  $T_0$ . However, when the stagnation pressure and temperature are altered,  $\dot{m}^*$  will have different maxima corresponding to every set of  $p_0$  and  $T_0$ .

From the foregoing discussion, it is clear that, in the convergent portion of the duct, flow remains unchanged for backpressures below  $p_{e3}$ . But in the divergent portion of the duct the flow expands as a supersonic flow for  $p_e < p_{e3}$ . However,  $p_e$  should be adequately reduced to a specified low value,  $p_{ec}$ , for establishing isentropic expansion of flow throughout the divergent portion of the nozzle, resulting in shock-free supersonic flow; the variation of pressure for such an isentropic expansion is shown by curve *d* in Figure 2.10.

For values of exit pressure between  $p_{ec}$  and  $p_{e3}$ , a normal shock wave exists inside the divergent portion of the nozzle. The flow behind the normal shock is subsonic, hence the static pressure increases to  $p_{e4}$  at the exit. The normal shock moves downstream with a decrease of  $p_e$  below  $p_{e4}$  and will stand precisely at the exit when  $p_e = p_{e5}$ , where  $p_{e5}$  is the static pressure behind a normal shock at the design Mach number of the nozzle; this is shown in Figure 2.11a.

When  $p_e$  is further reduced such that  $p_{ec} < p_b < p_{e5}$ , the flow inside the nozzle is fully supersonic and isentropic, where  $p_b$ , the pressure of the ambient atmosphere to which the flow is discharged, is called the *backpressure*. For this case, the static pressure  $p_e$  at the nozzle exit is less than the backpressure  $p_b$ . Therefore, the static pressure of the flow should increase to come to an equilibrium with the backpressure. The process leading to an increase of the flow pressure, resulting in equilibrium with  $p_b$ , takes place across an oblique shock attached to the nozzle exit outside the duct, as shown in Figure 2.11b. For further reduction in backpressure below  $p_{ec}$ , equilibration of the flow pressure takes place across expansion waves outside the duct, as illustrated in Figure 2.11c.



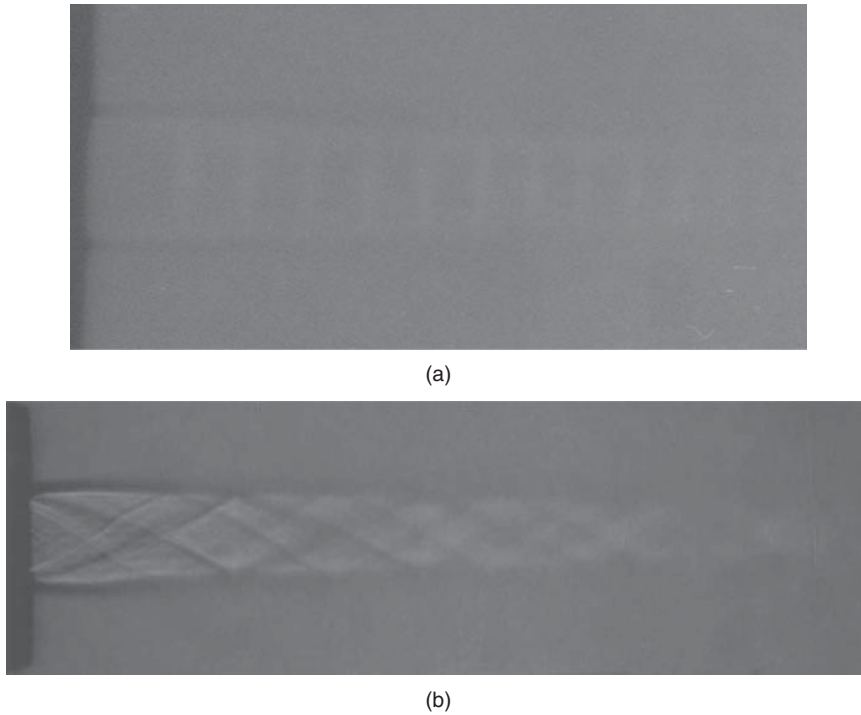


**Figure 2.11** Flow with shock and expansion waves at the exit of a convergent–divergent nozzle.

When the flow situation is as shown in Figure 2.11b, the nozzle is said to be *overexpanded*, since the pressure at the exit has expanded below the backpressure,  $p_e < p_b$ , and hence the flow experiences compression after leaving the nozzle. Conversely, when the situation is as shown in Figure 2.11c, the nozzle is said to be *underexpanded*, since the exit pressure is higher than the backpressure, that is  $p_e > p_b$ , and hence the flow experiences additional expansion after leaving the nozzle.

The above results can be summarized as follows.

- For  $p_{e1}/p_0 < 1$ , the flow is subsonic at the throat; therefore, the divergent portion acts as a diffuser. This is the case of flow through a venturi.
- For  $p_{e3}/p_0 < 1$ , the pressure at the throat is  $p^*$  and so  $M = 1$  at the throat. But  $p_{e3}/p_{th} > 1$ , so the divergent portion acts as a diffuser and the flow does not become supersonic.
- For pressure at the exit equal to  $p_{ec}$ , the flow expands isentropically throughout the nozzle and there is shock-free supersonic flow in the divergent portion of the nozzle.
- For  $p_{e3}/p_0 < p_e/p_0 < p_{ec}/p_0$ , there will be supersonic velocity locally, but at the exit it cannot be supersonic and so there will be a jump in static pressure at some section of the nozzle, that is there is a shock in the divergent portion of the nozzle. Therefore, there is a certain backpressure  $p_{ec}$ , above which there cannot be supersonic flow at the exit. Only below  $p_{ec}$  can there be shock-free supersonic flow up to the exit. This backpressure  $p_b = p_{ec}$  for which the flow in the nozzle is accelerated throughout the nozzle (both in the convergent and divergent portions), and the nozzle delivers uniform supersonic flow, is termed the *design pressure*. This is referred to as *correctly expanded operation*.
- For the correctly expanded condition, the nozzle exit pressure  $p_e$  is equal to the backpressure ( $p_e = p_b$ ). Therefore, there is no need for the flow to be compressed or expanded after exiting the nozzle, as in the case of overexpanded or underexpanded states, respectively, to come to equilibrium with the backpressure. This gives the impression that, when the flow is correctly expanded, there are no compression or expansion waves generated at the nozzle exit. Indeed, we tend to think that the correctly expanded sonic and supersonic flow exiting a nozzle is wave free. But in the actual flow process it is not true. This is because, even though the



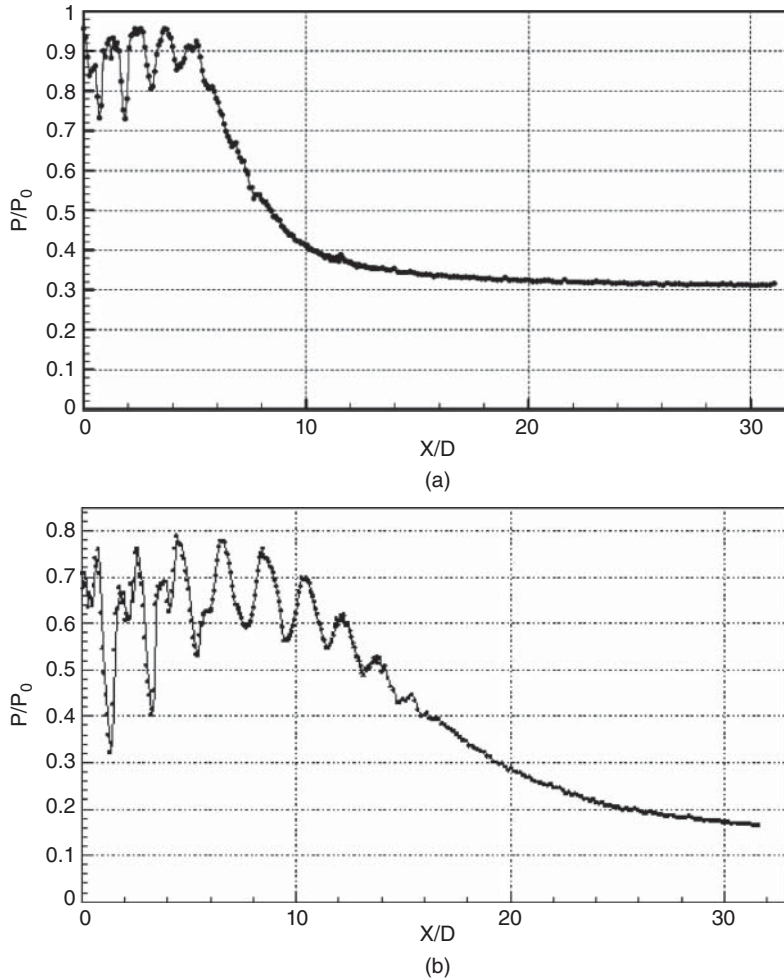
**Figure 2.12** (a) Waves in a correctly expanded Mach 1.43 jet. (b) Waves in a correctly expanded Mach 2 jet.

flow is correctly expanded, soon after exiting the nozzle the flow encounters a large space to relax. Therefore, the flow turns away from the nozzle axis in a bid to occupy the space available at the nozzle exit. We know that supersonic flow is essentially wave dominated, and any change in the state (change of  $p$ ,  $T$ ,  $\rho$ ) or mode (direction) of the flow will take place only through these waves. In the case of correctly expanded flow exiting a nozzle, the flow has to turn away from the nozzle axis to occupy the free space available. This leads to the formation of expansion waves at the nozzle exit. It is important to note that the expansion strength in the case of correctly expanded flow is much less than that for an underexpanded flow. Thus, both correctly expanded and underexpanded flows encounter expansion at the nozzle exit. However, the expansion for a correctly expanded flow is to turn the flow away from the nozzle axis, but for an underexpanded flow the expansion has to reduce the static pressure and turn the flow away from the nozzle axis. The expansion rays formed at the nozzle exit will travel some distance and be reflected from the jet boundary as compression waves, as illustrated in Figures 2.12a and b. To quantify the effect of expansion of correctly expanded sonic and supersonic flows, some representative experimental results of centerline pitot pressure distribution are shown in Figures 2.13a and b.

It is seen from Figures 2.12 and 2.13 that there are expansion and compression processes in the core of correctly expanded supersonic flows exiting nozzles possessing waves.

The equations that are useful for calculating the cross-sectional averaged properties inside a nozzle of a given shape are

$$\frac{p}{p_0} = \left( 1 + \frac{\gamma - 1}{2} M^2 \right)^{-\gamma/(\gamma-1)} \quad (2.33a)$$



**Figure 2.13** (a) Centerline decay of correctly expanded Mach 1.43 jet. (b) Centerline decay of correctly expanded Mach 2 jet.

$$\frac{\rho}{\rho_0} = \left(1 + \frac{\gamma - 1}{2} M^2\right)^{-1/(\gamma - 1)} \quad (2.33b)$$

$$\frac{T}{T_0} = \left(1 + \frac{\gamma - 1}{2} M^2\right)^{-1} \quad (2.33c)$$

$$\frac{A}{A^*} = \frac{1}{M} \left(\frac{\gamma + 1}{2}\right)^{-(\gamma + 1)/2(\gamma - 1)} \left(1 + \frac{\gamma - 1}{2} M^2\right)^{(\gamma + 1)/2(\gamma - 1)} \quad (2.33d)$$

For air at standard conditions ( $\gamma = 1.4$ ), Eqs. (2.33a)–(2.33d) reduce to

$$\frac{p}{p_0} = \left(1 + \frac{M^2}{5}\right)^{-7/2} \quad (2.34a)$$

$$\frac{\rho}{\rho_0} = \left(1 + \frac{M^2}{5}\right)^{-5/2} \quad (2.34b)$$

$$\frac{T}{T_0} = \left(1 + \frac{M^2}{5}\right)^{-1} \tag{2.34c}$$

$$\frac{A}{A^*} = \frac{1}{M} \left(\frac{5 + M^2}{6}\right)^3 \tag{2.34d}$$

From Eq. (2.34d), it can be seen that, for a required exit Mach number, there is only one ratio of exit area to throat area for a de Laval nozzle. That is, for a given de Laval nozzle, there is only one exit supersonic Mach number that can be produced. Therefore, for a supersonic wind tunnel, it is necessary to have a separate nozzle for every test-section Mach number of interest. However, this requirement of a separate nozzle for every Mach number can be avoided if there is a provision in the tunnel to vary the exit area for a given throat area, or both throat and exit areas, to achieve the required area ratio  $A_e/A_{th}$  for a specific test-section Mach number. Though this type of variable geometry nozzle will result in different test-section Mach numbers with a single nozzle, it is very expensive. Furthermore, it is evident from Eq. (2.34d) that the higher the exit Mach number, the larger should be the exit area.

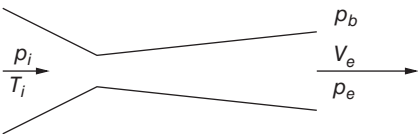
We can see from Eqs. (2.34a)–(2.34d) that for high exit Mach numbers the exit pressure, temperature, and density will be very small. Also, because the exit temperature is very low, it is sometimes necessary to heat the tunnel or increase the stagnation temperature of the air in the storage tank so that there is a reasonable temperature at the test-section. This requirement of maintaining moderate temperature becomes important if the temperature in the test-section goes to nearly  $-270^\circ\text{C}$ , as no conventional material can withstand such low temperatures. Therefore, for high Mach numbers (say hypersonic flows), the air is heated to thousands of degrees before expanding into the tunnel. For example, consider the values of pressure and temperature at the exit section of a de Laval nozzle for Mach numbers 2 and 4. From isentropic tables we have the data in Table 2.1.

Let the stagnation temperature be  $20^\circ\text{C}$ . The corresponding test-section static temperatures are  $-110.2$  and  $-203.2^\circ\text{C}$  for Mach numbers 2 and 4, respectively. At  $M = 4$ , we are forced to heat the air since the nitrogen in air liquefies at  $-180^\circ\text{C}$ , for the air properties to be the same as those in atmosphere.

It is important to note that the convergent–divergent nozzles shown in Figures 2.10 and 2.11 are de Laval or contoured nozzles with their wall near the exit parallel to the nozzle's axis. The flow phenomenon discussed for these nozzles can also be achieved with convergent–divergent nozzles without a contoured shape. Such nozzles will have straight walls for both convergent and divergent portions, as shown in Figure 2.14.

**Table 2.1** Pressure and temperature ratio for Mach 2 and 4 flows.

$M_{TS}$	$p_{TS}/p_0$	$T_{TS}/T_0$
2	0.1278	0.5556
4	0.0066	0.2381



**Figure 2.14** Straight convergent–divergent nozzle.

The straight convergent–divergent nozzle can also deliver correctly expanded, underexpanded, and overexpanded flow when suitable  $p_0$  and  $p_b$  are maintained. However, there is a distinct difference between a de Laval nozzle and a straight convergent–divergent nozzle. That is, the de Laval nozzle can deliver uniform as well as unidirectional supersonic flow, but a straight convergent–divergent nozzle can deliver only uniform Mach number flow and the flow will not be unidirectional. The flow streamlines will diverge away from the nozzle axis and the divergence is dictated by the semi-divergence angle of the nozzle's divergent portion.

### 2.5.1 Mass Flow Relation in Terms of Mach Number

From our discussions so far, it is clear that, by and large, the flow Mach number  $M$  is the most convenient parameter in terms of which all other parameters can be expressed. Indeed,  $p/p_0$ ,  $\rho/\rho_0$ ,  $T/T_0$ , and  $A/A^*$  are all expressed in terms of  $M$  in Eq. (2.33). Therefore, the mass flow rate through the nozzle can also be expressed in terms of  $M$ . The mass flow rate per unit area is

$$\begin{aligned}
 \frac{\dot{m}}{A} &= \rho V \\
 &= \frac{\rho}{\rho_0} \rho_0 \frac{V}{a} a \\
 &= \frac{\rho}{\rho_0} \frac{p_0}{RT_0} M \sqrt{\gamma RT} \\
 &= \frac{\rho}{\rho_0} \sqrt{\frac{T}{T_0}} \sqrt{T_0} \frac{p_0 M}{RT_0} \sqrt{\gamma R} \\
 &= \frac{p_0 M \sqrt{\gamma / RT_0}}{\left(1 + \frac{\gamma - 1}{2} M^2\right)^{1/(\gamma - 1)} \left(1 + \frac{\gamma - 1}{2} M^2\right)^{1/2}} \\
 &= \frac{p_0 M \sqrt{\gamma / RT_0}}{\left(1 + \frac{\gamma - 1}{2} M^2\right)^{\frac{\gamma + 1}{2(\gamma - 1)}}} \quad (2.35)
 \end{aligned}$$

where subscript 0 refers to the stagnation state. This relation shows that the mass flow rate per unit area at a given Mach number is proportional to stagnation pressure and inversely proportional to the square root of the stagnation temperature.

### 2.5.2 Maximum Mass Flow Rate per Unit Area

To find the condition of maximum mass flow rate per unit area, we can differentiate  $\dot{m}/A$  with respect to  $M$  and equate that derivative to zero. At this condition we find that  $M = 1$ . The mass flow rate per unit area is maximum where the Mach number is unity. We know that this can happen only at the throat of a convergent–divergent nozzle or at the exit of a convergent nozzle or orifice, and it is referred to as the *choked state*. For this condition of  $M = 1$ , we get from Eq. (2.35) that

$$\left(\frac{\dot{m}}{A}\right)_{\max} = \frac{\dot{m}}{A^*} = \sqrt{\frac{\gamma}{RT_0} \left(\frac{2}{\gamma + 1}\right)^{\frac{\gamma + 1}{\gamma - 1}}} p_0 \quad (2.36)$$

Equation (2.36) shows that, for a given gas (that is a given  $\gamma$ ), the maximum mass flow rate per unit area depends only on the ratio of  $p_0/\sqrt{RT_0}$ . This also implies that for a given  $p_0$  and  $T_0$  the mass flow rate through a passage with a given minimum area (given throat) is relatively large for gases of high molecular weight (that is gas of low gas constant,  $R$ ) and relatively small for gases of low molecular weight. Also, doubling the stagnation pressure level would double the maximum flow rate, whereas doubling the stagnation temperature would reduce the maximum mass flow rate by about 29%. For a gas with  $\gamma = 1.4$ , the maximum mass flow rate through a convergent–divergent nozzle becomes

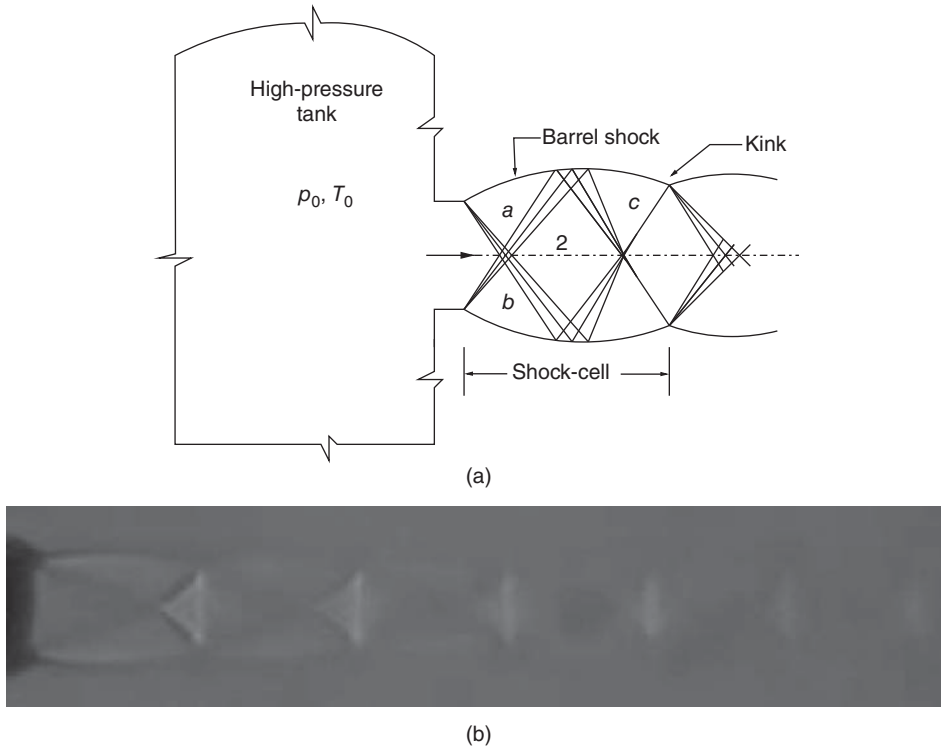
$$\dot{m}_{\max} = \frac{0.6847}{\sqrt{RT_0}} p_0 A^*$$

The area  $A^*$  is the area at the choked location with  $M = 1$ , which is the minimum cross-sectional area location of the passage. For a convergent–divergent nozzle, this is the throat area.

## 2.6 Supersonic Flow Generation

We saw in Section 2.5 that “a nozzle that does not have an expanding portion can never produce supersonic flow.” Now, we may ask, what will be the Mach number of a flow that comes out through a straight hole from a high pressure tank at a pressure, say  $p_{01} = 10$  atm, to an environment at standard sea level condition,  $p_a$ , as shown in Figure 2.15a?

It is important to note that the pressure ratio across the hole,  $p_a/p_{01} = 0.1$ , is much less than the isentropic choking pressure ratio of 0.528. Therefore, the flow leaving the hole would be choked and the exit velocity would be sonic. Also, the choked flow leaving the hole is highly underexpanded and finds a large space to expand further. Therefore, the flow on free expansion can attain a Mach number corresponding to the pressure ratio of 0.1. For this pressure ratio, isentropic expansion would result in Mach 2.15. This simply implies that the underexpanded flow exiting the hole at Mach 1 will pass through an expansion fan and attain Mach 2.15. At zones *a* and *b* the flow experiences only half the expansion and hence the Mach number would be less than the full expansion Mach number of 2.15, which the flow attains at zone 2, after passing through the full expansion zone. Soon after leaving the hole the sonic flow passes through the expansion fan and becomes supersonic. But at every point in the expansion fan the flow has a different supersonic Mach number. Also, since the flow at the apex of the expansion fan is turned almost suddenly to move away from the hole axis, it has to be turned toward the axis to become axial at a downstream distance. This turning is caused by the shock, which is essentially an oblique shock. But on either side of the axis for two-dimensional flow and around the axis for axisymmetric flow, the shape of the shock assumes the form of a barrel and thus is referred to as a *barrel shock*. Outside of the barrel shock, the flow is a mixture of supersonic and subsonic Mach numbers. The expansion rays get reflected from the free boundary as compression waves, since the reflection of a wave from a free boundary is *unlike*. The supersonic flow in zone *a* gets decelerated on passing through these reflected compression waves and hence the flow Mach number at *c* is less than that at *a*. These compression waves may coalesce to form shock waves that cross each other at the axis and meet the barrel shock and reflect back as expansion waves, as shown in Figure 2.15a. The distance from hole exit to the first kink location on the barrel shock, where the shocks get reflected as expansion waves, is called a *shock-cell*, in jet literature. Therefore, what is meant by the statement in the beginning of Section 2.5, that “a nozzle which does not have an expanding portion can never produce supersonic flow” is that, to generate a uniform supersonic flow of a specific Mach number, a divergent duct of specific exit area ( $A_e$ ) run by a convergent duct with choked throat ( $A^*$ ), as shown in Figure 2.8, is essential.

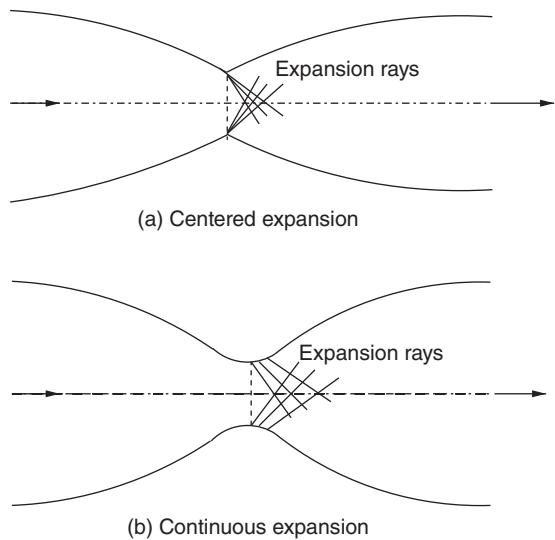


**Figure 2.15** (a) Flow pattern of the discharge from a tank. (b) Wave pattern in a sonic underexpanded free jet issuing from a tube run at nozzle pressure ratio 2.73.

The wave pattern described above (Figure 2.15a) can be clearly seen in the shadowgraph picture of a sonic underexpanded jet issuing from a circular tube, shown in Figure 2.15b.

If the nozzle has a contoured divergent portion, as in Figure 2.16, it will deliver a uniform supersonic Mach number,  $M_e$ , corresponding to the area ratio  $A_e/A^*$ . Also, the supersonic flow delivered by a contoured nozzle will be a uniform flow parallel to the nozzle axis. This kind of

**Figure 2.16** Contoured convergent-divergent (de Laval) nozzle.



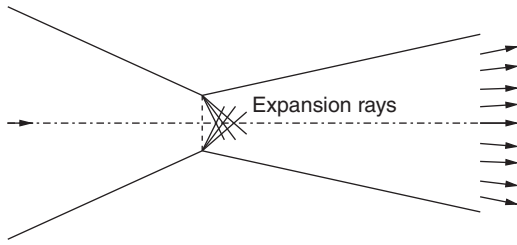


Figure 2.17 Straight convergent–divergent nozzle.

contoured nozzle is called a *de Laval nozzle*, in honor of de Laval, who was the first to use such a configuration. The details of the design procedure and the associated wave cancellation process of contoured nozzles will be seen in our discussions on *method of characteristics* in Chapter 9.

A defined supersonic flow can also be generated using a convergent–divergent nozzle with straight walls, as shown in Figure 2.17. But the flow delivered by a straight convergent–divergent nozzle will be of uniform Mach number but will not be unidirectional. The flow exiting a straight convergent–divergent nozzle will diverge away from the nozzle axis, as shown in Figure 2.17. That is, a straight convergent–divergent nozzle can deliver uniform supersonic Mach number but the flow will not be unidirectional, whereas a contoured or de Laval nozzle can generate uniform as well as unidirectional supersonic flow.

### 2.6.1 Nozzles

A nozzle is a passage in which the flow accelerates. From our discussions above, it is evident that a convergent–divergent nozzle is essential for generating a supersonic flow of desired properties. Also, a convergent nozzle can accelerate a flow to a maximum of Mach 1.0 only. For accelerating the flow choked at the exit of a convergent nozzle to supersonic level, a divergent portion must be added to the convergent duct, with the convergent nozzle exit with sonic condition becoming the throat of the convergent–divergent nozzle. The convergent–divergent nozzles are of two types: straight convergent–divergent nozzle and contoured or de Laval nozzle. For generating uniform as well as unidirectional supersonic flow, a de Laval nozzle should be used and if only the uniform Mach number is of interest and unidirectional quality is not mandatory, straight convergent–divergent nozzles can be employed. Of these, the fabrication of contoured nozzles is the more involved and the more expensive. Therefore, it is common practice to use straight convergent–divergent nozzles for thrust production in rockets and missiles, where the unidirectional flow requirement is not mandatory. But in devices such as supersonic tunnels, the flow in the test-section must be uniform and unidirectional and hence the only option is to use a de Laval nozzle.

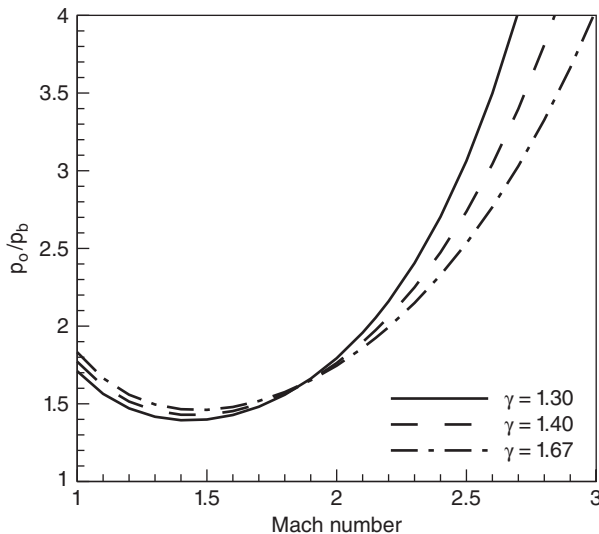
It is important to recognize that, even though it is desirable to use straight convergent–divergent nozzles for thrust generation it does result in some thrust penalty, owing to the diverging nature of the flow. But this loss can be made marginal by keeping the semi-divergence angle of the duct to 6 or 7°. The semi-divergence angle around 7° is an almost universally used value. Even smaller values for this angle are possible, but such small values will result in very long nozzles, which is undesirable and will cause drastic reduction in the thrust/weight ratio. The thrust/weight ratio is a crucial parameter in missile and launch vehicle design, not only from a performance point of view but also from the mission cost point of view. Each kilogram of weight increase will result in many thousands of dollars increase in the mission cost for a launch vehicle.



### 2.6.2 Physics of the Nozzle Flow Process

At this stage, it is important to have a clear understanding of the physics of the nozzle flow process, illustrated in Figure 2.18. First of all we should answer the question: for a convergent–divergent nozzle of given area ratio ( $A_e/A_{th}$ ), what is the limiting minimum value of the ratio of stagnation pressure,  $p_0$ , to the backpressure,  $p_b$ , of the environment to which the nozzle is discharging, required for starting a nozzle to accelerate the flow to sonic at its throat and continue to accelerate the sonic flow at the throat to higher Mach numbers and establish supersonic flow throughout its divergent portion and continue to run with supersonic flow up to the end of its divergent portion? The pressure ratio  $p_0/p_b$  is popularly known as the *nozzle pressure ratio* (NPR). We ask this question because, throughout the discussion on nozzle flow, we saw that, having started the flow through the nozzle, soon after choking at the throat, there is a formation of normal shock just downstream of the throat where the flow becomes supersonic. This shock has to be pushed progressively downstream in order to establish supersonic flow downstream of the throat. Therefore, for a convergent–divergent nozzle of fixed geometry, the minimum NPR necessary to establish supersonic flow throughout its divergent portion corresponds to that with normal shock at the nozzle exit. For example, for a fixed geometry convergent–divergent Mach 2 nozzle with a backpressure of 101 kPa, the NPR required to run it with a normal shock at the exit is 1.734. Note that this NPR is less than the choking NPR of 1.89, for a sonic throat.

One important point to be noted here is that, in the above limiting value of NPR for running of a convergent–divergent nozzle, we were focusing on the nozzle performance with supersonic flow throughout its divergent portion. But there is always a normal shock at the exit. Such operation will result in subsonic flow leaving the nozzle. Therefore, if the nozzle has to discharge supersonic flow, the normal shock has to be pushed out of the nozzle, by suitable adjustment of the NPR. In such a case, since the nozzle exit pressure is lower than the backpressure, static pressure increase of the supersonic flow leaving the nozzle in order to come to an equilibrium



**Figure 2.18** Variation of limiting NPR to position normal shock at nozzle exit with nozzle exit Mach number.

with the back pressure has to be achieved through compression waves positioned outside the exit. These compression waves will be oblique shocks attached to the nozzle exit lip. The flow delivered by a nozzle operating with oblique shocks at its exit is termed *overexpanded*.

Thus, a gas of specific heats ratio,  $\gamma = 1.4$ , at a stagnation state of  $p_0$  and  $T_0$ , flowing through a convergent or convergent–divergent passage will have the following features.

- For a convergent nozzle, the flow at the exit will be choked for  $p_b/p_0 \leq 0.528$ .
- Flow exiting a convergent nozzle will be underexpanded for  $p_b/p_0 < 0.528$ .
- For a convergent–divergent nozzle, the throat will have sonic state for  $p_{th}/p_0 < 0.528$ . Note that the ratio for choking the throat of a convergent–divergent nozzle is dictated by the ratio of static pressure at the throat to the upstream stagnation pressure,  $p_{th}/p_0$ , and not by the NPR,  $p_b/p_0$ .
- For the flow in the entire divergent portion of a convergent–divergent nozzle to be supersonic, the minimum limiting pressure ratio,  $(p_b/p_0)_{\min}$ , is dictated by the presence of normal shock at the nozzle exit. This  $(p_b/p_0)_{\min}$  can also be more than 0.528. For a given area ratio, that is for a given nozzle of design exit Mach number  $M_e$  discharging into a backpressure  $p_b$ , the pressure ratio  $(p_{th}/p_0)_{\min}$  can be determined as follows.

For a given  $M_e$ , from the isentropic relation, we have

$$\frac{p_0}{p_e} = \left(1 + \frac{\gamma - 1}{2} M_e^2\right)^{\frac{\gamma}{\gamma - 1}}$$

When there is a normal shock at the nozzle exit, the pressure ratio across the shock, from Eq. (3.16), is given by

$$\frac{p_b}{p_e} = 1 + \frac{2\gamma}{\gamma + 1} (M_e^2 - 1)$$

where  $p_e$  is the static pressure at the nozzle exit. Therefore, for the nozzle to experience supersonic flow throughout the divergent portion (with a normal shock at the exit), the pressure ratio required is

$$\frac{p_0}{p_b} = \frac{p_0}{p_e} \times \frac{p_e}{p_b}$$

For a known  $\gamma$ , the right-hand side of this equation is a function of the nozzle exit Mach number,  $M_e$ , only. Therefore, for every  $M_e$ , there is a specific value of NPR at which the nozzle will run with a normal shock at its exit. Variation of  $p_0/p_b$  with  $M_e$ , for  $\gamma = 1.4$ , is shown in Figure 2.18.

For a given  $\gamma = 1.4$  and  $p_b$ , the required  $p_0$  which will enable the nozzle to experience acceleration from inlet to exit can be obtained from the above relation. For example, for a convergent–divergent nozzle to accelerate a flow of air with supersonic flow throughout its divergent portion, to have a normal shock at its exit, and to discharge to ambient atmosphere at a pressure of 101 kPa, its area ratio must correspond to  $M_e = 2.15$ , if the  $(p_0/p_b)_{\min}$  is fixed as 1.89, and this is the choking limit for a sonic nozzle, as shown below. This limiting Mach number is based on the assumption that the flow process through the nozzle is isentropic up to the exit.

For a convergent–divergent nozzle with supersonic flow throughout its divergent portion and a normal shock at the exit, it should satisfy

$$\frac{p_0}{p_b} = \frac{p_0}{p_e} \times \frac{p_e}{p_b}$$

We fixed the  $(p_0/p_b)_{\min}$  as 1.89 and  $\gamma = 1.4$ ; therefore,

$$\frac{p_0}{p_b} = \left(1 + \frac{\gamma - 1}{2} M_e^2\right)^{\frac{\gamma}{\gamma - 1}} \times \left(1 + \frac{2\gamma}{\gamma + 1} (M_e^2 - 1)\right)^{-1}$$

$$1.89 = (1 + 0.2M_e^2)^{3.5} \times (1 + 1.167(M_e^2 - 1))^{-1}$$

Solving for  $M_e$ , we get  $M_e = 2.15$ .

The corresponding limiting Mach number for the above nozzle accelerating gases with  $\gamma = 1.3$  is 2.07, if  $(p_0/p_b)_{\min}$  is fixed at 1.83, and for  $\gamma = 1.67$ , the nozzle Mach number has to be 2.38, if  $(p_0/p_b)_{\min}$  is fixed as 2.05 [4].

Another important aspect of the convergent–divergent nozzle flow process is the area–velocity variation. In the convergent portion of the nozzle, area decrease causes increase of flow velocity and an associated decrease of density. In other words, in the subsonic region of flow, increase of velocity alone balances the decrease of both area and density, maintaining the mass conservation ( $\dot{m} = \rho AV$ ). But in the supersonic regime (in the divergent portion of the nozzle), both the area and the velocity increase together to compensate for the decrease of density, to satisfy mass conservation. This is because, in the supersonic regime of flow, the decrease of density is so *rapid* that both the velocity and area must increase to compensate for the density decrease in order to satisfy mass conservation.

## 2.7 Performance of Actual Nozzles

So far, all our discussions have been based on the assumption that

- The flow process through the nozzle is adiabatic and reversible, that is the heat transfer and viscous effects are absent (or negligible). In other words, the nozzle flow is isentropic.

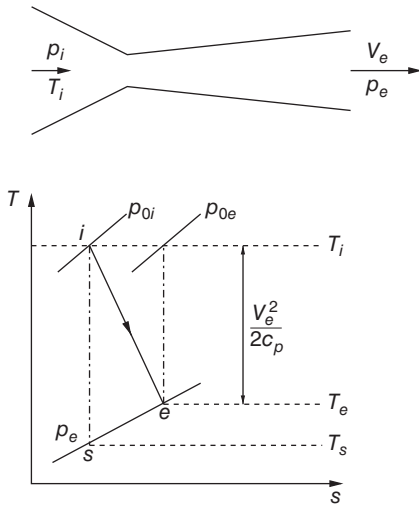
Because of frictional effects, the performance of real nozzles differs slightly from that determined from the isentropic flow relations. However, the departure of the actual performance from that computed using the isentropic assumption is usually small. Therefore, the usual design procedure is based on the use of isentropic relations modified by two types of empirically determined coefficients, namely the *nozzle efficiency* and the *coefficient of discharge*.

### 2.7.1 Nozzle Efficiency

Nozzle efficiency,  $\eta_N$ , is defined as the ratio of actual kinetic energy at nozzle exit to the kinetic energy that would be obtained in a frictionless nozzle expanding the gas to the same final pressure. In other words,  $\eta_N$  is the ratio of actual to ideal kinetic energy at the nozzle exit. The nozzle efficiency plays a dominant role in turbine design where it is important to estimate accurately the average velocity of flow leaving the nozzle. Consider a convergent–divergent nozzle shown in Figure 2.16 supplied with a gas at very low velocity and at pressure  $p_i$  and temperature  $T_i$ , so that  $p_i$  and  $T_i$  can be regarded as stagnation values.

The gas expands adiabatically, but with increasing entropy, to a state  $e$  (Figure 2.19) at the nozzle exit. If the expansion were isentropic, the end state would have been  $s$  (Figure 2.19). Using the steady-flow energy equation, the efficiency of the nozzle can be expressed as

$$\eta_N \equiv \frac{V_e^2/2}{c_p(T_i - T_s)} \quad (2.37)$$



**Figure 2.19**  $T$ - $s$  diagram for flow through a convergent-divergent nozzle.

This may be written as

$$\eta_N = \frac{\frac{V_e^2}{2c_p T_i}}{1 - \frac{T_s}{T_i}}$$

For an isentropic process from  $i$  to  $s$ ,

$$\left( \frac{T_s}{T_i} \right) = \left( \frac{p_s}{p_i} \right)^{\frac{\gamma-1}{\gamma}}$$

But  $p_e = p_s$ . Therefore,

$$\begin{aligned} \eta_N &= \frac{\frac{V_e^2}{2} \left( \frac{\gamma-1}{\gamma R T_i} \right)}{1 - \left( \frac{p_e}{p_i} \right)^{\frac{\gamma-1}{\gamma}}} \\ &= \frac{\left( \frac{\gamma-1}{2} \right) \frac{V_e^2}{a_i^2}}{1 - \left( \frac{p_e}{p_i} \right)^{\frac{\gamma-1}{\gamma}}} \end{aligned} \quad (2.38)$$

When the nozzle efficiency, pressure ratio, and stagnation temperature are known, the actual velocity at the nozzle exit can be determined with Eq. (2.38).

Friction effects in the nozzle are confined to the thin boundary layers adjacent to the walls. Since the boundary layer thickness depends primarily on the Reynolds number, based on some equivalent nozzle length and on the pressure distribution in the nozzle, no single expression which is applicable for all nozzles is possible. In general, the nozzle efficiency becomes nearly unity for extremely large nozzles, because the boundary layer thickness is very small compared to the size of the nozzle passage. But for very small nozzles, the boundary layer can even fill the passage, and for such cases the efficiency will drop drastically. Well-designed nozzles with

straight axes, when operated at the design pressure ratio and high Reynolds numbers, are found to have efficiencies ranging from 94 to 99%. Properly designed wind tunnel nozzles can run with efficiencies of nearly 100%. Properly designed turbine nozzles with curved axes have efficiencies of around 90–95%, when operated with suitable pressure ratios at high Reynolds numbers.

### 2.7.2 Nozzle Discharge Coefficient

The nozzle discharge coefficient  $C_d$  is the ratio of the actual mass flow rate through the nozzle to the mass flow calculated from the isentropic relations for the initial and final pressures of the actual nozzle, that is

$$C_d = \frac{\dot{m}_{\text{actual}}}{\dot{m}_{\text{isentropic}}}$$

For both convergent and convergent–divergent nozzles:

- If the overall pressure ratio of the nozzle is such that the velocity at the minimum section (throat) is subsonic, then the isentropic mass flow is calculated in terms of nozzle exit conditions.
- If the pressure ratio is such that the flow at the minimum section is sonic, then the isentropic flow is calculated using the relation for choked flow at the throat.
- For properly designed nozzles with straight axes running with measured Reynolds number of  $10^6$  or more at the minimum area,  $C_d$  is of the order of 0.99. For low Reynolds numbers,  $C_d$  may be considerably less than unity.

#### Example 2.4

A rocket nozzle has an exit/throat area ratio of 3. The combustion gas mixture at 20 bar and 2500 K is expanded through the nozzle to an atmosphere at 1 bar. The molar mass of the gas mixture is  $33.5 \text{ kg kmol}^{-1}$  and  $\gamma = 1.2$ . Assuming the flow process to be isentropic, estimate the momentum thrust generated by the nozzle per unit area.

#### Solution:

For the gas mixture,  $R = 8314/33.5 = 248 \text{ J (kg K)}^{-1}$ . For the given pressure ratio, the flow through the nozzle should be choked. Therefore, the mass flow rate per unit throat area is given by

$$\begin{aligned} \frac{\dot{m}}{A_{\text{th}}} &= \rho_{\text{th}} V_{\text{th}} = \rho^* a^* \\ &= \frac{\rho^*}{\rho_0} \rho_0 \sqrt{\gamma R T^*} \\ &= \frac{\rho^*}{\rho_0} \sqrt{\frac{T^*}{T_0}} \sqrt{\gamma R T_0} \rho_0 \\ &= \left( \frac{2}{\gamma + 1} \right)^{1/(\gamma-1)} \left( \frac{2}{\gamma + 1} \right)^{1/2} \sqrt{1.2 \times 248 \times 2500} \rho_0 \\ &\quad \left( \frac{2}{2.2} \right)^{1/0.2} \left( \frac{2}{2.2} \right)^{1/2} \sqrt{1.2 \times 248 \times 2500} \rho_0 \\ &= 510.654 \rho_0 \\ \rho_0 &= p_0 / R T_0 \end{aligned}$$

$$\begin{aligned}
&= \frac{20 \times 10^5}{248 \times 2500} \\
&= 3.226 \text{ kg m}^{-3}
\end{aligned}$$

Therefore,

$$\begin{aligned}
\frac{\dot{m}}{A_{\text{th}}} &= (510.654)(3.226) \\
&= \boxed{1647.37 \text{ kg (s m}^2\text{)}^{-1}}
\end{aligned}$$

The momentum thrust  $\text{Th}$  generated by the nozzle per unit area is given by

$$\text{Th} = \dot{m} V_e$$

where  $V_e$  is the flow velocity at the nozzle exit, given by  $V_e = M_e a_e$ . To determine the nozzle exit Mach number  $M_e$  we have to solve the area–Mach number relation,

$$\frac{A_e}{A^*} = \frac{1}{M_e} \left[ \frac{2}{\gamma + 1} \left( 1 + \frac{\gamma - 1}{2} M_e^2 \right) \right]^{(\gamma+1)/2(\gamma-1)}$$

For  $\gamma = 1.2$ , this relation simplifies to

$$\begin{aligned}
3 &= \frac{1}{M_e} \left( 0.91 \left( 1 + 0.1 M_e^2 \right) \right)^{5.5} \\
(3M_e)^{1/5.5} &= 0.91 + 0.091 M_e^2 \\
1.22 M_e^{1/5.5} &= 0.91 + 0.091 M_e^2 \\
M_e^{1/5.5} &= 0.746 + 0.075 M_e^2
\end{aligned}$$

Solving this by trial and error, we get  $M_e = 2.4$ . The temperature ratio becomes

$$\begin{aligned}
\frac{T_0}{T_e} &= 1 + \frac{\gamma - 1}{2} M_e^2 \\
&= 1 + 0.1(2.4)^2 = 1.576 \\
T_e &= 2500/1.576 = 1586.3 \text{ K}
\end{aligned}$$

Therefore,

$$V_e = 2.4 \sqrt{1.2 \times 248 \times 1586.3} = 1649 \text{ m s}^{-1}$$

Thus,

$$\begin{aligned}
\text{Th} &= \dot{m} V_e = 1647.37 \times 1649 \\
&= \boxed{2.717 \text{ MN}}
\end{aligned}$$

### Example 2.5

An aluminum pitot probe is placed in a supersonic air stream of temperature  $30^\circ\text{C}$ . If the melting temperature of aluminum is about  $660^\circ\text{C}$ , determine the flow velocity at which the probe will begin to melt. Assume air to be an ideal gas.

### Solution:

Given that aluminum will melt at  $660^\circ\text{C}$ , the probe will start melting at a stream stagnation temperature  $T_0$  of  $660^\circ\text{C}$ .

$$T_0 = 660^\circ\text{C} = 660 + 273.15 = 933.15 \text{ K}$$

The static temperature of the stream is  $T = 30^\circ\text{C} = 303.15\text{ K}$ . From isentropic relation, we have

$$\frac{T_0}{T} = 1 + \frac{\gamma - 1}{2} M^2$$

where  $M$  is the stream Mach number. For the present problem, we have

$$\frac{933.15}{303.15} = 1 + 0.2M^2$$

since  $\gamma = 1.4$ . Thus, we get

$$M = 3.22$$

The speed of sound in the air stream is

$$\begin{aligned} a &= \sqrt{\gamma RT} \\ &= \sqrt{1.4 \times 287 \times 303.15} = 349\text{ m s}^{-1} \end{aligned}$$

Thus, the velocity at which the probe will just begin to melt is

$$\begin{aligned} V &= Ma = 3.22 \times 349 \\ &= \boxed{1123.78\text{ m s}^{-1}} \end{aligned}$$

*Alternatively*

This problem can also be solved using the energy equation, as follows.

$$h_0 = h + \frac{V^2}{2}$$

where  $h_0$  and  $h$  are the stagnation and static enthalpies of the air stream. For a perfect gas,

$$h_0 = c_p T_0, \quad h = c_p T$$

where  $c_p = 1004.5\text{ J (kg K)}^{-1}$ , for air. Therefore,

$$\begin{aligned} T_0 - T &= \frac{V^2}{2c_p} \\ V &= \sqrt{2c_p(T_0 - T)} \\ &= \sqrt{2 \times 1004.5(933.15 - 303.15)} \\ &= \boxed{1125.02\text{ m s}^{-1}} \end{aligned}$$

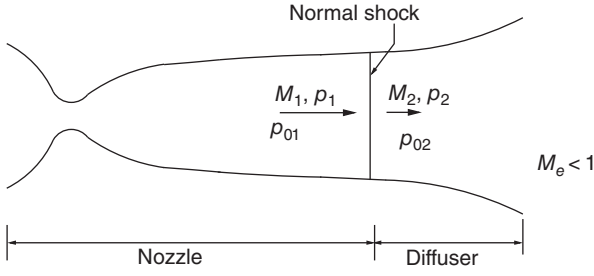
This is the stream velocity at which the probe will start melting.

*Note:* The difference between these two answers is due to the fact that the value of Mach number  $M$  was terminated at the second decimal place. For this problem, the accurate answer is  $V = 1125.02\text{ m s}^{-1}$ .

## 2.8 Diffusers

Diffusers are passages in which flow decelerates. If the de Laval nozzle shown in Figure 2.10 discharges directly into a receiver, the minimum value of stagnation to static pressure ratio at which the nozzle will deliver supersonic flow is

$$\left(\frac{p_0}{p_e}\right)_{\min} = \frac{p_0}{p_{e5}}$$



**Figure 2.20** Nozzle exhausting into diffuser through a normal shock.

where  $p_{e5}$  is the value of static pressure at the nozzle exit ( $p_e$ ) at which a normal shock will stand at the nozzle exit (Figure 2.11a). However, if a diffuser is attached at the nozzle exit, as shown in Figure 2.20, the nozzle can be operated to generate shock-free supersonic flow at the nozzle exit, even at a lower pressure ratio ( $p_0/p_b$ ). This is because the subsonic flow downstream of the normal shock may be decelerated isentropically to the stagnation pressure  $p_{02}$ .

The pressure ratio required then is the ratio of stagnation pressures across a normal shock wave at the test-section Mach number  $M_1$ , that is

$$\frac{p_{02}}{p_{01}} = \left( 1 + \frac{2\gamma}{\gamma+1}(M_1^2 - 1) \right)^{-1/(\gamma-1)} \left( \frac{(\gamma+1)M_1^2}{(\gamma-1)M_1^2 + 2} \right)^{\gamma/(\gamma-1)}$$

This ratio is given in Eq. (3.22).

It can be shown that  $p_{02}/p_{01}$  is equal to the ratio of the first throat area  $A_1^*$  to that of the second throat  $A_2^*$ , as follows.

By continuity,

$$\dot{m}_1^* = \dot{m}_2^* \\ \rho_1^* A_1^* V_1^* = \rho_2^* A_2^* V_2^*$$

But  $V_1^* = V_2^* = a^*$ ; therefore,

$$\rho_1^* A_1^* = \rho_2^* A_2^* \\ \frac{A_1^*}{A_2^*} = \frac{\rho_2^*}{\rho_1^*} = \frac{p_2^*}{p_1^*}$$

Because  $T_1^* = T_2^*$ , the second equation above can be written as

$$\frac{A_1^*}{A_2^*} = \frac{p_2^*}{p_{02}} \frac{p_{02}}{p_{01}} \frac{1}{p_1^*/p_{01}}$$

By isentropic relations, for  $M = 1$ ,

$$\frac{p^*}{p_0} = \left( \frac{\gamma+1}{2} \right)^{-\gamma/(\gamma-1)}$$

Hence,

$$\frac{p_2^*}{p_{02}} = \frac{p_1^*}{p_{01}}$$

Thus,

$$\boxed{\frac{A_1^*}{A_2^*} = \frac{p_{02}}{p_{01}}}$$



This pressure ratio is based on the assumption of isentropic expansion of the subsonic flow in the diffuser and hence it does not account for losses in the diffuser. But, in practice, the diffuser of Figure 2.20 does not give the expected recovery, owing to the interaction of shock wave and boundary layer, which produces a flow different from the above isentropic model. Therefore, design of a perfect isentropic diffuser is impossible. In other words, design of a diffuser that can give complete pressure recovery, that is that can expand the flow isentropically so that the tunnel can be run with stagnation pressure ratio  $p_{02}/p_{01}$ , is physically not possible. The other way of looking at it is that no diffuser can expand the flow with a stagnation pressure  $p_{02}$  at its entrance (just behind the shock in Figure 2.20), taking the static pressure value from  $p_2$  at its entrance to the ambient atmospheric pressure value,  $p_a$  (also called backpressure), at its exit. Hence, the stagnation pressure required for practical operation is definitely much larger than the pressure required for isentropic operation,  $p_{01}$ .

From the above discussion, it is clear that a perfect diffuser cannot be built. However, we can visualize with our basic knowledge about shocks that the normal shock is the strongest one, and the flow experiences more pressure loss across it compared to an oblique shock. Therefore, modification of the diffuser so as to compress the supersonic flow to subsonic level through a series of oblique shocks instead of through a single normal shock, as shown in Figure 2.20, before it is being actually expanded as a subsonic flow, will result in a better pressure recovery. Therefore, it would be advantageous to replace the normal shock diffuser in Figure 2.20 with an oblique shock diffuser, as illustrated in Figure 2.21, where the test-section Mach number  $M_1$  is slowed down through a series of oblique shock waves initiated by a compression corner at the diffuser inlet and finally by a weak normal shock at the end of the constant area section before entering the subsonic portion of the diffuser, where it is subsonically compressed by the divergent section which exhausts to the atmosphere. At the diffuser exit, the static pressure  $p_e$ , in principle, can be made equal to the ambient atmospheric pressure  $p_a$ , by suitably designing the diffuser. Conceptually, this oblique shock diffuser should provide better pressure recovery (lower loss in total pressure) than a normal shock diffuser. But, in practice, the interaction of the shock waves (Figure 2.21) with the viscous boundary layer on the diffuser walls creates an additional total pressure loss, which tends to partially reduce the advantages of an oblique shock diffuser. The net effect is that the full potential of an oblique shock diffuser is never achieved.

### 2.8.1 Special Features of Supersonic Diffusers

At the beginning of Section 2.8, we saw some aspects of the diffusion process in a diffuser which is fed with a supersonic stream by a supersonic nozzle preceding the diffuser. This kind of diffuser is typical in a supersonic wind tunnel circuit. But diffusers, or passages that decelerate a flow to a low velocity, are important elements in devices such as compressors, ram jets, etc., in addition to wind tunnels. Further, supersonic diffusers pose certain special problems that are

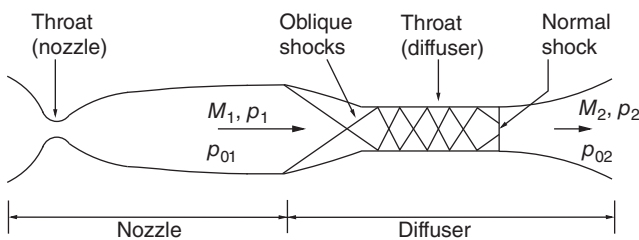


Figure 2.21 Nozzle exhausting into diffuser through oblique shocks.

not encountered in the design of subsonic diffusers. Two important difficulties associated with supersonic diffusers are:

- If the diffuser is in a closed system and is preceded by a supersonic nozzle, as in the case of a wind tunnel, frictional effects between the nozzle and the diffuser require that the diffuser throat be larger than the nozzle throat. If the diffuser throat is smaller than the nozzle throat, supersonic flow will not be attained in the nozzle. If the diffuser throat is too large, there will be a shock positioned somewhere within the diffuser. Also, even if the nozzle and diffuser are made such that the diffuser throat is larger than the nozzle throat to the required level so that the two throats match perfectly, it appears that the combined system would be unstable and that flow oscillations would occur.
- In most systems flow starts from rest and accelerates to the operating velocity. During the starting period, a normal shock wave passes through the system. Across a normal shock there is no change in mass flow rate or in stagnation temperature. Therefore,  $A_1^* p_{01} = A_2^* p_{02}$ , where the areas  $A_1^*$  and  $A_2^*$  are the sonic throat area ahead of and behind the shock, and  $p_{01}$  and  $p_{02}$  are the total pressures ahead of and behind the shock, respectively. As the total pressure is reduced by a normal shock, it follows that there is a corresponding increase in the sonic or minimum area,  $A_2^*$ , through which the flow can be made to pass. The design problems associated with this aspect will be discussed for two important applications, namely wind tunnel diffusers and propulsion engine diffusers.

## 2.8.2 Supersonic Wind Tunnel Diffusers

Supersonic wind tunnel diffusers are essentially convergent–divergent ducts attached to the end of the test-section. Here it is our aim to address the essential features of the flow process in such a diffuser. In order to focus our attention only on these features, let us assume the flow to be isentropic everywhere in the diffuser, except across the shocks, where the entropy increases considerably. Also, let us assume the flow to be quasi-one-dimensional and quasi-steady during the starting of the flow.

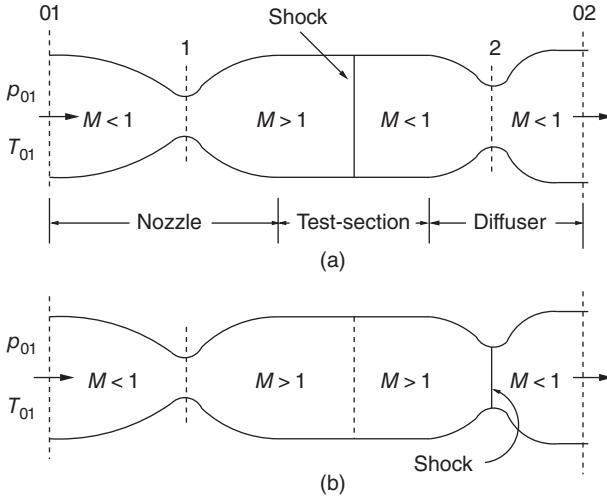
Let us examine the flow through the supersonic tunnel circuit shown in Figure 2.22 consisting of a de Laval nozzle, a test-section, and a diffuser, run with constant stagnation pressure,  $p_{01}$ , and constant stagnation temperature,  $T_{01}$ , at its settling chamber.

Let us assume that the tunnel is discharging to atmosphere at pressure  $p_a$ . When the tunnel is started by letting high pressure air from a storage tank into a settling chamber and from the settling chamber to the tunnel, flow through the tunnel is taking place since  $p_{01}/p_a > 1$ . At the time of starting, the flow enters the inlet and accelerates through the nozzle. If the pressure ratio  $p_{01}/p_a$  is large enough for the flow to choke, the Mach number at the nozzle throat becomes unity. Soon after that, a shock is generated just downstream of the nozzle throat and the shock moves down the diverging portion of the nozzle. During this period, the nozzle throat is passing the maximum possible mass flow of air, since it is choked. The mass flow rate through the nozzle for a given value of specific heats ratio, say  $\gamma = 1.4$ , becomes

$$\dot{m}^* = \frac{0.6847 p_{01} A_1^*}{\sqrt{R T_{01}}}$$

where  $A_1^*$  is the nozzle throat area. For gases with  $\gamma$  other than 1.4 we can express the mass flow rate as

$$\dot{m}^* \propto \frac{p_{01} A_1^*}{\sqrt{R T_{01}}}$$



**Figure 2.22** Schematic of a part of a supersonic tunnel circuit: (a) running with a normal shock in the test-section and (b) running with a normal shock at the diffuser throat.

The flow process across the shock is adiabatic, hence  $T_{01} = T_{02} = \text{constant}$ . Therefore, to maintain the mass flow rate  $\dot{m}^*$ ,  $p_{01}A_1^*$  must be equal to  $p_{02}A_2^*$ , across the shock. This implies that the flow can pass through the diffuser only if  $A_2^* > A_1^*$ , that is if the diffuser throat area  $A_2^*$  is larger than the nozzle throat area  $A_1^*$ . The worst situation in this operation is the flow process causing maximum pressure loss and hence forcing the design to have the limiting minimum  $A_2^*$ , for a given test-section Mach number. This corresponds to operation with a shock positioned in the test-section (Figure 2.22a). Therefore, the diffuser throat area should be at least the limiting minimum  $A_2^*$  corresponding to the state with the shock in the test-section, that is

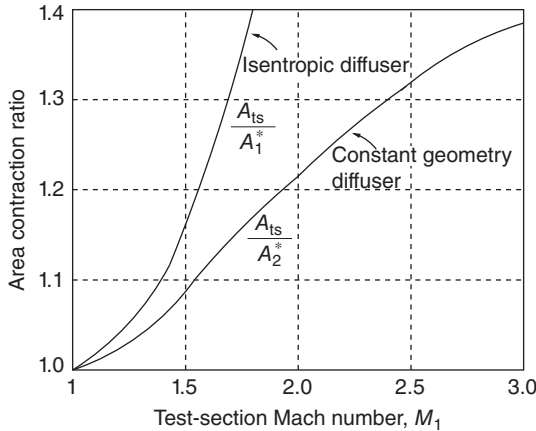
$$\frac{A_{2\min}^*}{A_1^*} = \left( \frac{p_{01}}{p_{02}} \right)_{\text{Mts}}$$

where  $\left( \frac{p_{02}}{p_{01}} \right)_{\text{Mts}}$  is the stagnation pressure ratio across the shock in the test-section. The limiting contraction ratio for the convergent portion of the diffuser is

$$\frac{A_{ts}}{A_2^*} = \frac{A_{ts}}{A_1^*} \frac{p_{02}}{p_{01}} \quad (2.39)$$

The area ratio  $A_{ts}/A_1^*$  is given in terms of  $M_{ts} = M_1$  by the isentropic area–Mach number relation Eq. (2.32) and  $p_{02}/p_{01}$  is the total pressure ratio across the normal shock in the test-section, which is again given in terms of  $M_1$  by the normal shock relation Eq. (3.22). Hence, the limiting contraction ratio of the diffuser  $A_{ts}/A_2^*$  depends on the test-section Mach number.

Variation of  $A_{ts}/A_1^*$  with test-section Mach number  $M_1$  is shown in Figure 2.23. This plot shows the maximum possible contraction for a supersonic wind tunnel of fixed geometry that will permit supersonic flow to be established in the test-section. With the limiting diffuser throat area corresponding to Eq. (2.39), the diffuser will barely be able to “swallow” the flow in the test-section during start-up and the flow at the diffuser will be exactly sonic when the shock is in the test-section. If the diffuser throat is even slightly smaller than that dictated by Eq. (2.39), a normal shock will be standing in the diverging portion of the nozzle and only subsonic flow will prevail in the test-section. With a progressive decrease of the second throat area, for a given test-section area, the shock in the diverging portion of the nozzle will travel even to the



**Figure 2.23** Maximum area contraction for a supersonic wind tunnel diffuser with test-section Mach number.

nozzle throat and ultimately be sucked into the convergent portion of the nozzle and disappear, causing the entire nozzle to experience only subsonic flow.

From the above discussions it is evident that:

- During the start-up of a supersonic tunnel, there is a large loss of stagnation pressure during the worst phase of the starting process with a normal shock in the test-section. At this time an increase of upstream stagnation pressure ( $p_{01}$ ), or increase of diffuser throat area ( $A_2^*$ ), is required to pass the flow through the tunnel circuit.
- If the diffuser throat area is large enough for supersonic flow to be established in the test-section, a sufficient increase of  $p_{01}$ , or lowering of the backpressure, will cause the shock to move through the test-section and to be swallowed by the diffuser throat.
- The position at which the shock comes to rest depends on the manner in which the operating characteristics of the backpressure is matched to the pressure-flow characteristics of the remainder of the system.
- For best efficiency of the tunnel the backpressure should be such that the equilibrium position of the shock is at the diffuser throat, with an upstream Mach number just greater than unity.
- The stagnation pressure loss for best operation is less than that for starting up because of the lower Mach number at which the shock occurs during operation.
- The pressure ratio across the tunnel unit, ( $p_{01}/p_b$ ), is determined by the starting condition rather than the operating condition.

In actual operation, the shock is maintained slightly downstream of the diffuser throat, since with a fixed backpressure the shock is unstable in the converging portion of the diffuser. For example, if the shock is positioned exactly at the second throat, even a slight disturbance can make the shock move temporarily into the converging portion of the diffuser. This will result in increased stagnation pressure loss; also, if the backpressure is fixed, transient waves will cause the shock to move further upstream, making the situation even worse. The shock will keep moving further upstream until it comes to rest in the diverging portion of the nozzle at a point where the stagnation pressure loss in the system matches the backpressure of the system. With this condition, to obtain supersonic flow in the test-section, the pressure ratio  $p_{01}/p_b$  has to be taken to the start-up level, either by increasing  $p_{01}$  or by lowering  $p_b$ , or by adjusting both the pressures suitably.

To ensure that a supersonic diffuser of fixed geometry will start, the throat area  $A_2^*$  must be kept slightly larger than the theoretical minimum value to account for the inaccuracies in the estimate of frictional loss, and for the error caused by departure from the assumption of one-dimensional flow, and so on.

The practically attainable efficiencies of supersonic diffusers are always less than the efficiencies that seem possible theoretically. In general, the theoretical considerations discussed here are confirmed by experimental studies, although there are modifications due to viscous effects. The friction caused by viscosity results in a marginally additional loss in stagnation pressure. The major effect of viscosity is to make the shock occur over a length of several diameters of the passage, rather than abruptly, adversely influencing the efficiency of the diffuser. Hence, this feature of shock prevailing over a portion of the diffuser length must be accounted for in the design, in order to achieve a reasonable extent of design efficiency in practical application.

It is advisable to avoid the problems that adversely influence the diffuser performance, rather than accounting for their effects. Some of the popular means which can be employed to avoid some of the adverse effects are

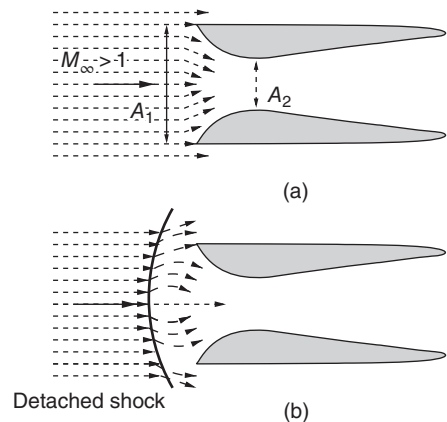
- using variable-geometry diffusers, capable of larger  $A_2^*$  during start-up
- using variable-geometry diffusers in conjunction with variable-geometry nozzles, so that both  $A_2^*$  and  $A_1^*$  can be adjusted to enable easy start-up and efficient running
- driving the shock through the diffuser throat by means of a large-amplitude pressure pulse, that is sudden increase of  $p_{01}$  during start-up
- taking advantage of effects that are not one-dimensional.

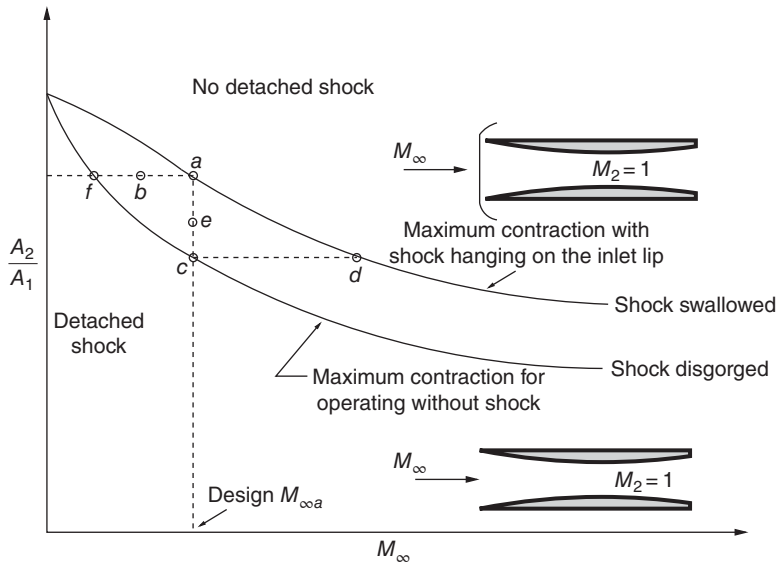
### 2.8.3 Supersonic Inlets

Supersonic inlets are essentially diffusers located at the inlet of turbojets and ram jets to decelerate the freestream air at supersonic speeds entering the inlet to the required level of incompressible Mach number at the combustion chamber, where fuel is mixed with the air and ignited. Let us consider such air-breathing propulsion engine intakes operating at supersonic speeds. It is important to note that such engines always reach their operating speeds by being accelerated from lower speeds. Therefore, it is essential to investigate the performance of supersonic inlets during starting phase where the flow entering the inlet is subsonic, and during supersonic operating speeds, where the speed at the inlet entry is also supersonic. But, for simplicity, in our discussions here, we consider the performance of supersonic inlets during the operating phase only. Also, let us treat the flow to be quasi-static and ignore all losses except those across the normal shocks.

Consider a converging–diverging supersonic inlet of entrance area  $A_1$  and minimum area  $A_2$ , as shown in Figure 2.24.

**Figure 2.24** (a) No detached shock and all freestream flow through area  $A_1$ , entering the inlet. (b) Detached shock causing spillover at the inlet entry.





**Figure 2.25** Limiting contraction area ratio variation with freestream Mach number.

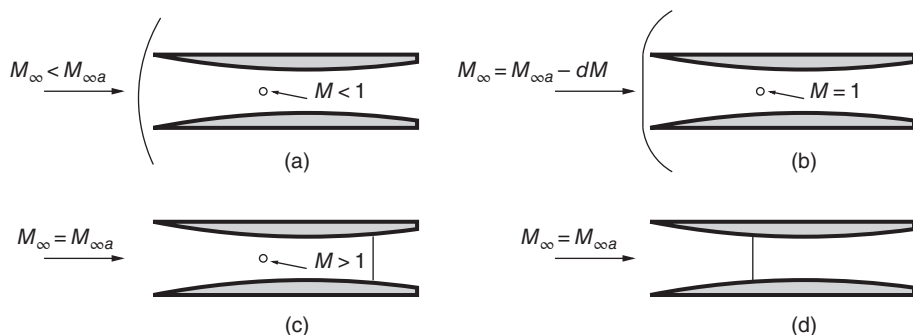
When the inlet travels at supersonic speeds, if we assume that there is no shock ahead of the inlet, as in Figure 2.24a, there is no possibility of air being diverted before reaching the inlet, and all the freestream flow corresponding to the inlet area  $A_1$  will enter the engine. But because of the above impossible assumption of a supersonic flow entering the intake without a shock (Figure 2.24a), this is impracticable since, with decreasing area in the convergent portion, the inlet cannot pass the amount of flow entering area  $A_1$  at the entrance. This physical condition of the flow process dictates the formation of a detached shock ahead of the inlet (as schematically shown in Figure 2.24b), as then the flow behind the shock is subsonic and may spill over the inlet tip of the diffuser.

Figure 2.25 shows the maximum contraction,  $A_2/A_1$ , possible when there is no shock at the diffuser inlet, based on isentropic theory, and also the maximum contraction for a specific case where a detached normal shock hangs on the inlet lip and forces all the air mass over the inlet area  $A_1$ , through the engine, but with a reduced stagnation pressure as a function of freestream Mach number,  $M_\infty$ .

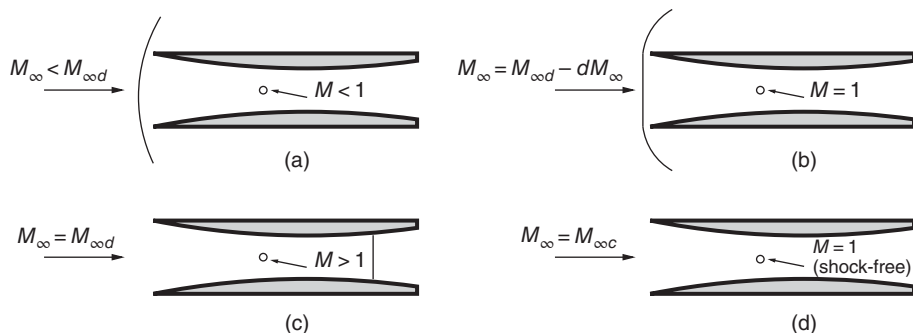
#### 2.8.4 Fixed-Geometry Inlet

Let us examine the flow through a fixed-geometry supersonic inlet of area ratio  $(A_2/A_1)_a$  at a freestream Mach number  $M_{\infty a}$ , where the subscript *a* refers to the operating point *a* in Figure 2.25. The flow field of the inlet at various stages during starting are shown in Figure 2.26.

In Figure 2.26a, the freestream Mach number is too low for the flow to be swallowed and a detached shock is positioned upstream of the inlet mouth. This situation corresponds to point *b* in Figure 2.25. When the flight Mach number is slightly less than the design value, the normal shock hangs on the inlet lip, as shown in Figure 2.26b. A slight increase in freestream Mach number would make the shock move into the inlet, provided the backpressure is sufficiently low. The equilibrium position of the shock depends on the performance of the rest of the engine. If the shock is too far downstream from the minimum area, as shown in Figure 2.26c, the inlet efficiency will be poor, since the Mach number upstream of the shock will be high and the



**Figure 2.26** Starting of fixed-geometry supersonic inlet of area ratio  $(A_2/A_1)_a$  and design Mach number  $M_{\infty a}$ .



**Figure 2.27** Over-speed starting of fixed-geometry supersonic inlet of contraction ratio  $(A_2/A_1)_c$  and design freestream Mach number  $M_{\infty a}$ .

stagnation pressure loss associated with such a strong shock will be severe. In Figure 2.26d the shock is in the farthest upstream position for which the flow is stable. A slight disturbance in the flow pattern of Figure 2.26d would cause the shock to be disorged.

During starting, if the backpressure is sufficiently low, the shock will not be swallowed during acceleration until the Mach number reaches  $M_{\infty a}$  in Figure 2.25. Also, once the shock is swallowed, it will not be disorged upon deceleration until the Mach number  $M_{\infty f}$ , marked on Figure 2.25, is reached.

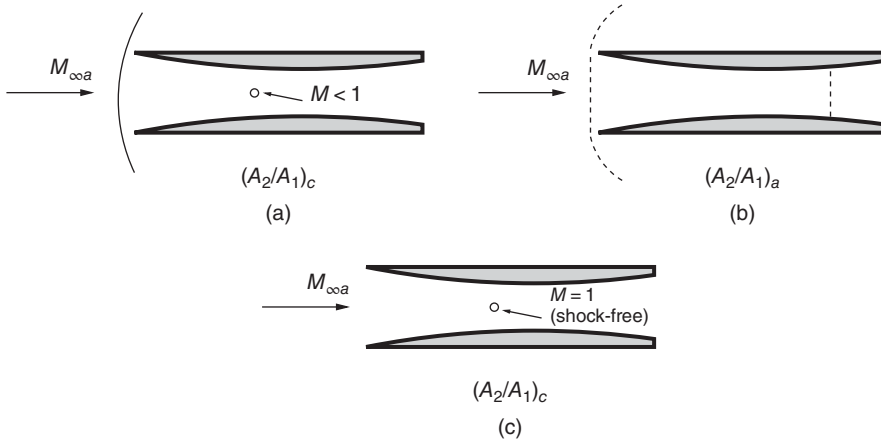
The operating shock of a fixed-geometry supersonic inlet may be eliminated completely by over-speeding the engine. For a fixed geometry inlet of area ratio  $(A_2/A_1)_c$  (Figure 2.25) and designed for  $M_{\infty a}$ , various stages of the accelerating phase during starting are shown in Figure 2.27.

By over-speeding the engine to Mach number  $M_{\infty d}$  in Figure 2.25, the shock can be swallowed and then the engine may be decelerated to at least  $M_{\infty a}$  before the shock is disorged.

### 2.8.5 Variable-Geometry Inlet

The operating shock of a supersonic inlet may also be eliminated by using a variable geometry of the duct. Let us consider a variable-geometry intake operating at Mach number  $M_{\infty a}$  in Figure 2.25. The flow field through the inlet for  $(A_2/A_1)_c$  and  $(A_2/A_1)_a$  in Figure 2.25 will be as shown in Figure 2.28.

If the throat area ( $A_2$ ) is too small, corresponding to point  $c$  in Figure 2.25, a detached shock will stand ahead of the inlet, as shown in Figure 2.25a. By increasing the throat area, the shock can be moved to the inlet lip. When the operating point  $a$  of Figure 2.25 is reached, the



**Figure 2.28** Starting of a variable-geometry supersonic inlet.

shock will reach the inlet lip and may be swallowed, as shown in Figure 2.28b. Now, the throat area may be reduced without disgorge the shock until point  $c$  of Figure 2.25 is reached. At this stage, by properly adjusting the backpressure, the diffuser can be made to operate without shock, as shown in Figure 2.28c.

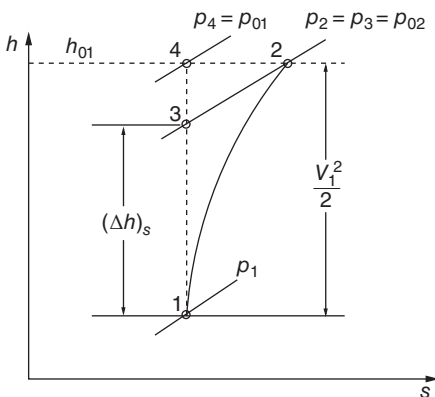
The operating condition at which a shock hangs at the inlet lip is called the *critical operation*. The operating condition for which the shock is swallowed is called the *supercritical operation* and that with a detached shock upstream of the inlet is called the *subcritical operation*.

### 2.8.6 Diffuser Efficiency

We can characterize the differences between actual and ideal performances of engine inlets by a *diffuser efficiency* or by a stagnation pressure ratio. Figure 2.29 shows the enthalpy–entropy ( $h$ – $s$ ) diagram of the flow diffusion process through the inlet, with state 1 referring to the actual state of the flow entering the diffuser, state 2 to the state of the flow leaving the diffuser, and state 3 to a fictitious state at the leaving pressure but at the entering entropy.

Assuming that the velocity leaving the diffuser is negligible, the diffuser efficiency can be expressed as

$$\eta_D = \frac{(\Delta h)_s}{V_1^2/2} = \frac{h_3 - h_1}{h_2 - h_1} \quad (2.40)$$



**Figure 2.29** Definition of the flow states in the inlet.



For a perfect gas,  $h = c_p T$ , therefore, assuming air to be a perfect gas, the diffuser efficiency can be expressed as

$$\eta_D = \frac{T_3 - T_1}{T_2 - T_1} = \frac{T_1(T_3/T_1 - 1)}{V_1^2/2c_p}$$

Also, the process 1–3 is isentropic, thus

$$\frac{T_3}{T_1} = \left(\frac{p_2}{p_1}\right)^{\frac{\gamma-1}{\gamma}}$$

Therefore,

$$\begin{aligned} \eta_D &= \frac{\left(\frac{p_2}{p_1}\right)^{\frac{\gamma-1}{\gamma}} - 1}{V_1^2 / \left(2 \frac{\gamma}{\gamma-1} RT_1\right)} \\ &= \frac{\left(\frac{p_2}{p_1}\right)^{\frac{\gamma-1}{\gamma}} - 1}{\frac{\gamma-1}{2} M_1^2} \end{aligned} \quad (2.41)$$

since  $c_p = \frac{\gamma}{\gamma-1} R$ , speed of sound  $a_1^2 = \gamma RT_1$  and  $V_1^2/a_1^2 = M_1^2$ . Also,  $p_2 \approx p_{02}$ ; therefore,

$$\frac{p_2}{p_1} = \frac{p_{01}}{p_1} \frac{p_{02}}{p_{01}}$$

Hence,

$$\eta_D = \frac{\left(\frac{p_{01}}{p_1}\right)^{\frac{\gamma-1}{\gamma}} \left(\frac{p_{02}}{p_{01}}\right)^{\frac{\gamma-1}{\gamma}} - 1}{\frac{\gamma-1}{2} M_1^2}$$

But, by isentropic relation, we have

$$\frac{p_{01}}{p_1} = \left(1 + \frac{\gamma-1}{2} M_1^2\right)^{\frac{\gamma}{\gamma-1}}$$

Thus,

$$\boxed{\eta_D = \frac{\left(1 + \frac{\gamma-1}{2} M_1^2\right) \left(\frac{p_{02}}{p_{01}}\right)^{\frac{\gamma-1}{\gamma}} - 1}{\frac{\gamma-1}{2} M_1^2}} \quad (2.42)$$

This relation shows that, for a given Mach number  $M_1$ , the diffuser efficiency depends only on the stagnation pressure ratio  $p_{02}/p_{01}$ . We know that, for complete isentropic diffusion the stagnation pressure ratio  $p_{02}/p_{01} = 1$  and for diffusion with shock, the diffusion efficiency can be maximized if the Mach number upstream of the shock is just above 1.

For a better understanding of the arguments given in this section, the reader is advised to consult Chapters 3 and 4.

**Example 2.6**

Helium gas at 250 kPa and 100 °C flows through a rectangular duct of cross-section 40 cm × 50 cm, with a velocity of 500 m s<sup>-1</sup>. Determine the Mach number, stagnation temperature, stagnation pressure, and the mass flow rate. Assume helium to be an ideal gas.

**Solution:**

Given,  $p = 250$  kPa,  $T = 100$  °C = 373.15 K, Area =  $0.40 \times 0.50 = 0.2$  m<sup>2</sup>,  $V = 500$  m s<sup>-1</sup>

The gas constant for helium (of molecular weight 4.003) is

$$R = \frac{8314}{4.003} = 2077 \text{ J (kg K)}^{-1}$$

The speed of sound is

$$\begin{aligned} a &= \sqrt{\gamma RT} \\ &= \sqrt{1.66 \times 2077 \times 373.15} = 1134.3 \text{ m s}^{-1} \end{aligned}$$

since  $\gamma = 1.66$  for helium gas. Thus,

$$M = \frac{V}{a} = \frac{500}{1134.3} = \boxed{0.44}$$

By isentropic relation, we have the temperature ratio as

$$\frac{T_0}{T} = 1 + \frac{\gamma - 1}{2} M^2$$

Therefore,

$$\begin{aligned} T_0 &= T \left( 1 + \frac{\gamma - 1}{2} M^2 \right) \\ &= 373.15(1 + 0.33 \times 0.44^2) = \boxed{397 \text{ K}} \end{aligned}$$

By isentropic relation, the pressure ratio is given by

$$\frac{p_0}{p} = \left( 1 + \frac{\gamma - 1}{2} M^2 \right)^{\frac{\gamma}{\gamma - 1}}$$

Thus,

$$\begin{aligned} p_0 &= 250 \left( 1 + 0.33 \times 0.44^2 \right)^{2.515} \\ &= \boxed{292.13 \text{ kPa}} \end{aligned}$$

The mass flow rate through the duct is

$$\begin{aligned} \dot{m} &= \rho AV = \frac{p}{RT} AV \\ &= \frac{250 \times 10^3}{2077 \times 373.15} \times 0.2 \times 500 = \boxed{32.26 \text{ kg s}^{-1}} \end{aligned}$$

**Example 2.7**

Compressed air at 40 °C and 145 kPa from a large tank is discharged to ambient atmosphere at 101 kPa, through a convergent nozzle of 10 cm<sup>2</sup> exit area. Calculate the mass flow rate through the nozzle when the ambient atmosphere is at (a) 101 kPa, (b) 50 kPa, and (c) 30 kPa.

**Solution:**

Given,  $p_0 = 145$  kPa and  $T_0 = 40$  °C = 40 + 273.15 = 313.15 K.

- (a) When  $p_a = 101$  kPa, the pressure ratio across the nozzle is

$$\frac{p_0}{p_a} = \frac{145}{101} = 1.44$$

The pressure ratio has to be above 1.89 for the flow to choke at the nozzle exit. Therefore, for pressure ratio 1.44 the flow at the nozzle exit is only subsonic. By isentropic relation,

$$\begin{aligned} \frac{p_0}{p_a} &= \left( 1 + \frac{\gamma - 1}{2} M^2 \right)^{\frac{\gamma}{\gamma - 1}} \\ 1.44 &= \left( 1 + 0.2 M^2 \right)^{3.5} \end{aligned}$$

This gives  $M = 0.74$ . From the isentropic table (Table A.1 in the Appendix), for  $M = 0.74$ , we get

$$\frac{\rho}{\rho_0} = 0.7712, \quad \frac{T}{T_0} = 0.9013$$

Therefore,

$$\begin{aligned} \rho &= 0.7712 \rho_0 = 0.7712 \frac{p_0}{RT_0} \\ &= \frac{0.7712 \times 145 \times 10^3}{287 \times 313.15} = 1.244 \text{ kg m}^{-3} \\ T &= 0.9013 T_0 = 0.9013 \times 313.15 = 282.24 \text{ K} \\ a &= \sqrt{\gamma RT} \\ &= \sqrt{1.4 \times 287 \times 282.24} = 336.75 \text{ m s}^{-1} \\ V &= Ma = 0.74 \times 336.75 = 249.2 \text{ m s}^{-1} \end{aligned}$$

The mass flow rate is

$$\begin{aligned} \dot{m} &= \rho AV \\ &= 1.244 \times 10 \times 10^{-4} \times 249.2 \\ &= \boxed{0.31 \text{ kg s}^{-1}} \end{aligned}$$

- (b) Given:  $p_a = 50$  kPa. Therefore,  $\frac{p_0}{p_a} = \frac{145}{50} = 2.9$  and hence the flow is choked and the nozzle exit Mach number is 1.

From the isentropic table, for  $M = 1$ , we get

$$\begin{aligned} \frac{\rho}{\rho_0} &= 0.6339, \quad \frac{T}{T_0} = 0.8333 \\ \rho &= 0.6339 \rho_0 = 0.6339 \frac{p_0}{RT_0} \\ &= \frac{0.6339 \times 145 \times 10^3}{287 \times 313.15} = 1.023 \text{ kg m}^{-3} \\ T &= 0.8333 T_0 = 0.8333 \times 313.15 = 260.95 \text{ K} \\ a &= \sqrt{\gamma RT} \\ &= \sqrt{1.4 \times 287 \times 260.95} = 323.8 \text{ m s}^{-1} \\ V &= Ma = 1.0 \times 323.8 = 323.8 \text{ m s}^{-1} \end{aligned}$$

$$\begin{aligned}
 \dot{m} &= \rho AV \\
 &= 1.023 \times 10 \times 10^{-4} \times 323.8 \\
 &= \boxed{0.331 \text{ kg s}^{-1}}
 \end{aligned}$$

- (c) Given:  $p_a = 30 \text{ kPa}$ . Here again  $M = 1$ . After choking, any change in the conditions downstream of the nozzle cannot influence the flow in the nozzle. This is because, for a given stagnation condition, the nozzle flow is frozen once it is choked. Only changes in the stagnation condition can influence the nozzle flow and not the downstream condition of the nozzle. Therefore, for  $p_a = 30 \text{ kPa}$  also,

$$\dot{m} = \boxed{0.331 \text{ kg s}^{-1}}$$

## 2.9 Dynamic Head Measurement in Compressible Flow

In any flow field, basically there are three pressures that are of interest to gas dynamic studies. However, in fluid mechanics we use a fourth pressure in parallel flow studies, which we call the *geometric pressure*. Also, we know that this pressure is due only to the gravitational action on a static fluid having the same geometry as the actual flow.

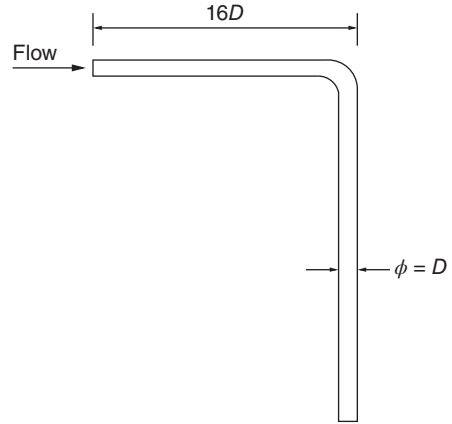
The three pressures that are of interest in gas dynamics are (i) total or stagnation pressure, (ii) static pressure, and (iii) dynamic pressure. The *total pressure* is the pressure that results when the flow is brought to rest isentropically, that is at a position in the flow where the actual fluid velocity is zero; the total pressure corresponds to the undisturbed static pressure  $p$ . The *static pressure* is the pressure acting in the direction normal to the flow. The static pressure acts equally in all directions in space. The third pressure, *dynamic pressure*, may be associated with the flow conditions at a point by taking the difference between the stagnation pressure  $p_0$  and the undisturbed static pressure  $p$ .

For incompressible flows, these three pressures are linked together by Bernoulli's equation:

$$p_0 - p = \frac{1}{2} \rho V^2 = q \text{ (incomp.)} \quad (2.43)$$

where  $p_0$  is the total pressure,  $p$  the static pressure, and  $\frac{1}{2} \rho V^2$  the dynamic pressure. The total pressure  $p_0$  will be the same everywhere in an incompressible flow with no losses. For a constant  $p_0$ , it is seen from Eq. (2.43) that an increase in flow velocity results in a decrease of static pressure, and vice versa. The dynamic pressure  $q$  is linked to the kinetic energy of the flow and it has the same direction as that of the flow. Also, we know that the static pressure of a flow is that pressure which is acting normal to the flow direction. Therefore, the total pressure also has a definite direction. The total pressure is measured by using a simple device called a *pitot (total) probe*. The pitot probe is simply a tube with a blunt end facing into the gas stream. The tube will normally have an inside-to-outside diameter ratio of 1/2 to 3/4 and a length aligned with the gas stream of 15–20 tube diameters. The pressure hole is formed by the inside diameter of the tube at the blunt end. A typical pitot tube is shown in Figure 2.30.

In subsonic flows, the open-ended tube facing into the flow always measures the stagnation pressure of the flow. But for supersonic flows, there will be a detached shock formed and standing in front of the blunt end. This means that the tube does not measure the actual stagnation pressure but only the stagnation pressure behind a normal shock. This new value is called *pitot pressure* and in modern terminology denotes the total pressure in supersonic streams.

**Figure 2.30** Pitot probe.

This indicated pitot pressure  $p_{02}$ , the stagnation pressure behind the normal shock, may be used for calculating the flow Mach number, as follows: multiply the equation

$$\frac{p_{01}}{p_1} = \left( 1 + \frac{\gamma - 1}{2} M_1^2 \right)^{\gamma/(\gamma-1)}$$

by Eq. (3.22) to obtain

$$\frac{p_1}{p_{02}} = \frac{\left( \frac{2\gamma}{\gamma+1} M_1^2 - \frac{\gamma-1}{\gamma+1} \right)^{1/(\gamma-1)}}{\left( \frac{\gamma+1}{2} M_1^2 \right)^{\gamma/(\gamma-1)}}$$

This relation is called the *Rayleigh supersonic pitot formula*. Once the static pressure  $p$  and pitot pressure  $p_{02}$  are known, the flow Mach number  $M$  can be calculated.

When the Reynolds number of the flow (based on probe diameter) is very low ( $< 500$ ), the measured pitot pressures are unreliable. However, this effect is seldom a problem in supersonic flows, because a reasonably sized probe will usually have a Reynolds number of well above 500.

The measurement of static pressure in a supersonic flow is much more difficult than in a subsonic flow. Though static probes are not used extensively for calibrating supersonic tunnels, a considerable amount of study has been made for the development of accurate static pressure probes for other applications. The major problem in the use of static probes at supersonic speeds is that any probe will have a shock wave at its nose, which causes a rise in static pressure.

In subsonic flows if the probe has a conical tip followed by a cylinder, the air passing the shoulder will be expanded to a pressure below the freestream static pressure. Then, as the distance from the shoulder is increased, the pressure on the probe will approach the true static pressure on the stream. The sharp-nosed tip of the probe facing the flow is closed and holes are drilled perpendicular to the axis of the tube at a specified distance from the sharp nose. The included angle of the sharp cone should be small for good results. Also, it is established that a static hole located beyond  $8D$  from the nose is good enough for reasonably accurate measurements. A typical L-shaped static probe is shown in Figure 2.31. Static pressure measurements are very sensitive to any inclination of the tube to the flow direction.

Inclinations beyond  $5^\circ$  result in a large error in the measured static pressure. In order to minimize this error, it is a common practice to have static probes with four holes in mutually perpendicular directions. When a static pressure probe is placed in a subsonic flow field, flow

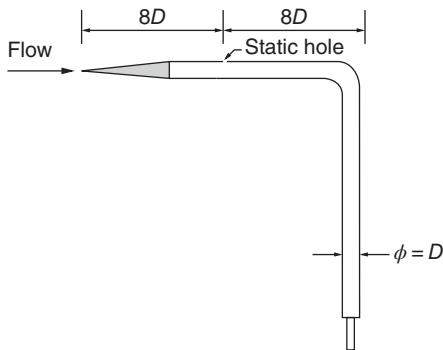


Figure 2.31 Static pressure probe.

is accelerated because of the horizontal portion of the probe and decelerated because of the vertical stem of the probe; therefore, the holes are located at such a location that these two effects cancel each other and the probe measures the correct pressure.

For measurement of static pressure in supersonic flow, the hole should be located beyond  $8D$  from the nose, and the acceleration due to the probe should be kept to a minimum; for this, the nose should be very sharp with an included angle of less than  $10^\circ$ . Also, it is usual practice to employ a straight probe for measurement in supersonic flows.

Starting from an incompressible regime of flow, up to Mach 0.8 a static pressure probe aligned with the flow direction continues to record the freestream static pressure correctly. Once the freestream Mach number reaches a level such that the flow near the probe becomes transonic, the pressure reading is severely affected by the waves generated. For further increases of the freestream Mach number, there are shock wave formations on the probe and the pressure measured by the probe becomes something totally different from the actual value. Therefore, locating the static pressure orifice at the proper place for measuring static pressure with reasonable accuracy poses serious problems in the probe design. In general, static probes with a measuring orifice located sufficiently far downstream are suitable for the measurement of static pressure in supersonic flows. A typical probe, shown in Figure 2.32, can measure static pressure within  $\pm 0.5\%$  at Mach 1.6 [5], provided the pressure tapings are located more than 10 tube diameters downstream of the shoulder. This distance increases with increase of Mach number, in the supersonic regime.

The yaw sensitivity of this probe with sting support is about 1% reduction in the measured pressure for  $3\text{--}5^\circ$  yaw. If it is used with a stem support, the support should be at least 13 tube diameters away from the static orifice.

Even though a lot of investigations have been done on supersonic static probes, we can see from the fundamental nature of the supersonic stream that it is a flow stream dominated by waves in the form of Mach waves, expansion waves, and shock waves. It may be possible to develop a static probe for a particular Mach number, but development of a static probe for use at all supersonic Mach numbers with a reasonable accuracy will prove to be a futile task. Therefore, in practice, one can make use of the boundary walls of nozzles, like a de Laval nozzle, which develops supersonic flow – this is mostly the case in laboratories – to locate an orifice (on

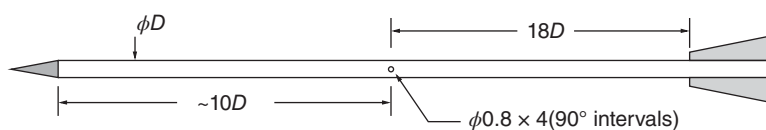
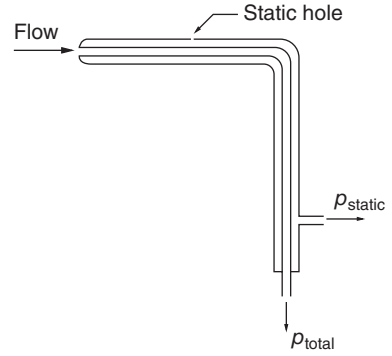


Figure 2.32 Supersonic static tube.

**Figure 2.33** Pitot-static tube.

the nozzle wall) for measuring the stream static pressure. For instance, a pressure tap located at the wall is capable of measuring the stream static pressure almost exactly, provided the nozzle is properly made with smooth inner surfaces to generate a shock-free supersonic stream.

The dynamic pressure of a subsonic flow can be measured directly by a special probe called a *pitot-static probe*, which is a combination of a pitot and a static probe. A typical pitot-static probe is shown in Figure 2.33.

### 2.9.1 Compressibility Correction to Dynamic Pressure

For an incompressible flow, the velocity of the flow can be calculated from the measured dynamic pressure  $q$  by the relation

$$V = \sqrt{\frac{2}{\rho}q}$$

However, for compressible flow, the above formula cannot be used for calculating flow velocity, because, in compressible flow, the relation  $p_0 - p = q$  is not valid. Also, it may be noted that in the supersonic regime of the compressible flow the Mach number is more important than the velocity itself. For compressible flows, the dynamic pressure can be expressed in terms of  $M$  as follows.

$$\begin{aligned} q &= \frac{1}{2}\rho V^2 = \frac{\rho}{2}M^2\gamma RT \\ &= \frac{\gamma p}{2}M^2 \end{aligned} \quad (2.44a)$$

From Eq. (2.44a), we get

$$p = \frac{2}{\gamma M^2}q \quad (2.44b)$$

Also, by Eq. (1.73),

$$\begin{aligned} p_0 &= p \left( 1 + \frac{\gamma-1}{2}M^2 \right)^{\gamma/(\gamma-1)} \\ p_0 - p &= p \left[ \left( 1 + \frac{\gamma-1}{2}M^2 \right)^{\gamma/(\gamma-1)} - 1 \right] \end{aligned}$$

Now, replacing the  $p$  on the right-hand side of this equation from Eq. (2.44b), we get

$$p_0 - p = \frac{2}{\gamma M^2}q \left[ \left( 1 + \frac{\gamma-1}{2}M^2 \right)^{\gamma/(\gamma-1)} - 1 \right] \quad (2.45a)$$

For air at standard conditions, that is  $\gamma = 7/5$ , Eq. (2.45a) becomes

$$p_0 - p = q \frac{2}{\gamma M^2} \left[ \left( 1 + \frac{M^2}{5} \right)^{7/2} - 1 \right] \quad (2.45b)$$

Expanding Eq. (2.45b) binomially and retaining terms only up to fourth power in  $M$ , we get

$$p_0 - p = q \left( 1 + \frac{M^2}{4} + \frac{M^4}{40} \right) \quad (2.46)$$

For  $M = 0$ , Eq. (2.46) gives Bernoulli's equation for incompressible flow. From this equation, we get the dynamic pressure  $q$  as

$$q = \frac{p_0 - p}{K} \quad (2.47)$$

where  $K = 1 + M^2/4 + M^4/40$  is called the *correction coefficient for dynamic pressure in compressible flow*.

Equation (2.46) is accurate enough up to  $M = 2$ , and for Mach numbers up to 1, even without the last term, the equation should prove to be reasonably accurate.

For any Mach number more than 2, Eq. (2.45a) should be used for the proper estimation of dynamic pressure.

For dynamics pressure  $q$  measured with a pitot-static tube,

the error in  $q$  with Equation (2.47) = 20% at  $M = 1$ , with  $K = 1$

Error in  $q = 2.5\%$  at  $M = 1$ , with  $K = \left( 1 + \frac{M^2}{4} \right)$

Error in  $q = 4\%$  at  $M = 2$  with  $K = 1 + \frac{M^2}{4} + \frac{M^4}{40}$

Beyond  $M = 2$ , use of Eq. (2.47) results in a large error in  $q$ .

### Example 2.8

A perfect gas flows isentropically through a nozzle. If the ratio of the nozzle exit to the throat is 3.0, and the exit Mach number is also 3.0, find the specific heats ratio of the gas.

#### Solution:

Given,  $A_e/A_{th} = 3.0$  and  $M_e = 3.0$ .

For isentropic flow, the area–Mach number relation is

$$\frac{A_e}{A_{th}} = \frac{1}{M_e} \left[ \frac{2}{\gamma + 1} \left( 1 + \frac{\gamma - 1}{2} M_e^2 \right) \right]^{\frac{\gamma + 1}{2(\gamma - 1)}}$$

The only way to solve for  $\gamma$  from the above equation is by trial and error.

By trial and error it can be found that  $\gamma = 1.67$

This gas is a monatomic gas like helium or argon.

### Example 2.9

A convergent–divergent nozzle of throat area  $10 \text{ cm}^2$  and exit area  $24 \text{ cm}^2$  is run from an air storage tank at 300 kPa and 300 K. Calculate the range of backpressure for which (a) the entire divergent portion will be supersonic and (b) the exit Mach number is less than 1. (c) Are the mass flow and exit pressure independent of the backpressure?



**Solution:**

- (a) After choking, if the pressure  $p^*$  at the throat is larger than the backpressure  $p_b$ , the flow will expand further downstream as a supersonic stream in the divergent portion of the nozzle. This will continue as long as the backpressure  $p_b$  is less than the pressure that will compel the flow to establish a normal shock at the nozzle exit. Therefore, this problem essentially becomes a determination of the backpressure required for the formation of a normal shock at the nozzle exit.

Given:

$$\frac{A_e}{A_{th}} = \frac{24}{10} = 2.4$$

For this area ratio, from the isentropic table, we have

$$M_e = 2.4, \quad \frac{p_e}{p_0} = 0.0684$$

This becomes the upstream Mach number  $M_1$  for the normal shock at the nozzle exit. Therefore, from the normal shock table (Table A.2 in the Appendix), for  $M_1 = 2.4$ ,

$$\frac{p_2}{p_1} = 6.5533$$

Thus,

$$\begin{aligned} p_2 &= 6.5533 p_1 = 6.5533 p_e, \quad \text{since } p_e = p_1 \\ &= 6.5533 \times 0.0684 \times p_0 \\ &= 6.5533 \times 0.0684 \times 300 \\ &= \boxed{134.47 \text{ kPa}} \end{aligned}$$

Hence, the flow in the complete divergent portion of the nozzle will be supersonic in the range of backpressures

$$\boxed{0 \leq p_b \leq 134.47 \text{ kPa}}$$

- (b) The nozzle exit Mach number will be subsonic when the flow in the entire divergent portion of the nozzle is subsonic or if there is a normal shock in the divergent portion. For this to happen, the given area ratio will have to give a subsonic Mach number at the exit. Thus, for  $A_e/A_{th} = 2.4$ , from the isentropic table, we get

$$\begin{aligned} M_e &= 0.25, \quad \frac{p_e}{p_0} = 0.9575 \\ p_e &= 0.9575 \times 300 = 287.25 \text{ kPa} \end{aligned}$$

When  $p_b \geq 287.25$  the entire divergent portion of the nozzle is subsonic flow. When  $p_b = 134.47$  there will be a normal shock at the nozzle exit. Therefore, for the subsonic flow in the divergent portion the backpressure has to be in the range

$$\boxed{134.47 < p_b \leq 287.25 \text{ kPa}}$$

- (c) The throat will be choked for  $\frac{p_{th}}{p_0} \leq 0.528$ , thus

$$\begin{aligned} p_{th} &\leq 0.528 \times 300 \\ &\leq 158.40 \text{ kPa} \end{aligned}$$

The choked flow will make the flow in the convergent portion frozen for any change in the downstream condition. Therefore,  $\dot{m}$  is independent of  $p_b$  for

$$0 \leq p_b \leq 158.40 \text{ kPa}$$

The exit pressure is independent of  $p_b$  for

$$0 \leq p_b \leq 134.97 \text{ kPa}$$

This is because when the entire divergent duct flow is supersonic, for any fixed area ratio  $A_e/A_{th}$ ,  $M_e$  is constant and, therefore, for a fixed  $p_0$  and  $A_e/A_{th}$ ,  $p_e$  becomes independent of  $p_b$  as long as the above conditions are maintained.

### Example 2.10

Air flows isentropically through a nozzle of throat area  $12 \text{ cm}^2$  and exit area  $50.19 \text{ cm}^2$ . If the stagnation pressure and temperature are  $300 \text{ kPa}$  and  $35^\circ\text{C}$ , compute the velocity and pressure at the nozzle exit and the mass flow rate through the nozzle if the flow at the nozzle exit is subsonic. Also, determine the pressure of the ambient atmosphere to which the nozzle is discharging.

#### Solution:

Given that the nozzle area ratio is

$$\frac{A_e}{A_{th}} = \frac{50.19}{12} = 4.18$$

For this area ratio both subsonic and supersonic Mach numbers are possible at the nozzle exit. Thus, from the isentropic table, for  $A_e/A_{th} = 4.18$ , we get

$$M_e = 0.14$$

and

$$\frac{p_e}{p_0} = 0.9864, \frac{T_e}{T_0} = 0.9961, \frac{\rho_e}{\rho_0} = 0.9903$$

Therefore,

$$\begin{aligned} p_e &= 0.9864 \times p_0 \\ &= 0.9864 \times 300 \\ &= \boxed{295.92 \text{ kPa}} \\ \rho_e &= 0.9903 \times \frac{p_0}{RT_0} \\ &= 0.9903 \times \frac{300 \times 10^3}{287 \times 308.15} = 3.359 \text{ kg m}^{-3} \end{aligned}$$

$$\begin{aligned} T_e &= 0.9961 \times T_0 \\ &= 0.9961 \times 308.15 = 306.95 \text{ K} \end{aligned}$$

$$\begin{aligned} a_e &= \sqrt{\gamma RT_e} \\ &= \sqrt{1.4 \times 287 \times 306.95} = 351.19 \text{ m s}^{-1} \end{aligned}$$

$$\begin{aligned} V_e &= M_e a_e = 0.14 \times 351.19 \\ &= \boxed{49.17 \text{ m s}^{-1}} \end{aligned}$$

$$\begin{aligned}
 \dot{m} &= \rho_e A_e V_e \\
 &= 3.359 \times 50.19 \times 10^{-4} \times 49.17 \\
 &= \boxed{0.829 \text{ kg s}^{-1}}
 \end{aligned}$$

In this problem the nozzle is correctly expanded, since  $M_e$  is subsonic. Therefore, the ambient atmosphere to which the nozzle is discharging has to be at a pressure of 295.92 kPa.

### Example 2.11

If the overexpansion level of a Laval nozzle run by a settling chamber at 5 atm and discharging to sea level atmosphere is 36.1%, determine the design Mach number of the nozzle, treating the flow through the nozzle as adiabatic and reversible.

#### Solution:

Given,  $p_0 = 5 \text{ atm}$ ,  $p_b = 1 \text{ atm}$  and expansion level is 0.361.

The expansion level can be expressed as

$$\frac{p_b - p_e}{p_b}$$

Therefore,

$$\frac{p_b - p_e}{p_b} = 0.361$$

$$1 - \frac{p_e}{p_b} = 0.361$$

$$\frac{p_e}{p_b} = 1 - 0.361$$

$$= 0.639$$

$$p_e = 0.639 \text{ atm}$$

The pressure ratio at the nozzle exit is

$$\begin{aligned}
 \frac{p_e}{p_0} &= \frac{0.639}{5} \\
 &= 0.1278
 \end{aligned}$$

For  $\frac{p_e}{p_0} = 0.1278$ , from isentropic table,  $M_e = 2.0$ . Thus, the design Mach number of the nozzle is 2.0.

## 2.10 Pressure Coefficient

The pressure coefficient  $C_p$ , an extremely useful quantity in fluid dynamics, is defined as

$$C_p = \frac{p - p_\infty}{\frac{1}{2} \rho_\infty V_\infty^2} \quad (2.48)$$

where  $p$  is the local static pressure and  $p_\infty$ ,  $\rho_\infty$ , and  $V_\infty$  are the pressure, density, and velocity in the freestream. The pressure coefficient is essentially a nondimensional pressure difference.

An alternative form of the pressure coefficient, convenient for compressible flows, can be obtained as follows: Eq. (2.48) can be written as

$$C_p = \frac{p - p_\infty}{\left(\frac{\gamma}{2}\right) p_\infty M_\infty^2} = \frac{p_\infty \left(\frac{p}{p_\infty} - 1\right)}{\left(\frac{\gamma}{2}\right) p_\infty M_\infty^2}$$

Therefore,

$$C_p = \frac{2}{\gamma M_\infty^2} \left( \frac{p}{p_\infty} - 1 \right) \quad (2.49)$$

Equation (2.49) is an exact representation of Eq. (2.48) expressed in terms of the freestream Mach number  $M_\infty$ .

We now proceed to obtain an expression for a pressure coefficient at the stagnation point in a compressible flow. Let us recall that, in an incompressible flow, the pressure coefficient at a stagnation point is  $C_{p0} = 1$ . But in compressible flows, because of the basic fact that, unlike for incompressible flows, the dynamic pressure is not simply the difference between stagnation and static pressures, it is given from Eq. (2.45a) as

$$q = \frac{\gamma M^2 (p_0 - p)}{2 \left( \left( 1 + \frac{\gamma-1}{2} M^2 \right)^{\gamma/(\gamma-1)} - 1 \right)} \quad (2.50)$$

Therefore, the stagnation pressure coefficient for compressible flow can be expressed as

$$C_{p0} = \frac{p_0 - p}{q} = \frac{2}{\gamma M^2} \left( \left( 1 + \frac{\gamma-1}{2} M^2 \right)^{\gamma/(\gamma-1)} - 1 \right) \quad (2.51)$$

By Eq. (2.46),  $C_{p0}$  can also be expressed as

$$C_{p0} = 1 + \frac{M^2}{4} + \frac{M^4}{40} \quad (2.52)$$

Equation (2.52) is accurate enough only for Mach numbers up to 2.0. For Mach numbers of less than 1.0, it may further be simplified without loss of accuracy as

$$C_{p0} = 1 + \frac{M^2}{4} \quad (2.53)$$

Equation (2.49) may also be expressed in another form in terms of velocities and Mach number as follows. From Eq. (2.49), we get

$$\frac{p}{p_\infty} = 1 + \frac{\gamma}{2} M_\infty^2 C_p$$

Combining this with Eq. (2.8), we can obtain

$$C_p = \frac{2}{\gamma M_\infty^2} \left[ \left( \frac{\gamma-1}{2} M_\infty^2 \left\{ 1 - \left( \frac{V}{V_\infty} \right)^2 \right\} + 1 \right)^{\gamma/(\gamma-1)} - 1 \right] \quad (2.54)$$

where  $V$  and  $V_\infty$  are the local and freestream velocities, respectively.

For small values of the factor  $\frac{\gamma-1}{2} M_\infty^2 \left( 1 - \left( \frac{V}{V_\infty} \right)^2 \right)$ , Eq. (2.54) may be simplified further to result in

$$C_p = \left( 1 - \left( \frac{V}{V_\infty} \right)^2 \right) \left( 1 + \frac{M_\infty^4}{4} \left\{ 1 - \left( \frac{V}{V_\infty} \right)^2 \right\} \right) \quad (2.55)$$

The first term on the right-hand side of Eq. (2.55) gives the pressure coefficient for incompressible flows in terms of velocity, namely

$$C_{p_{\text{inc}}} = 1 - \left( \frac{V}{V_{\infty}} \right)^2 \quad (2.56)$$

## 2.11 Summary

In this chapter the equations of continuity, momentum, and energy are applied to one-dimensional and quasi-one-dimensional isentropic flow through constant area ducts and ducts with gradually varying cross-sections. The effects of Mach number on pressure, temperature, and density are demonstrated; the variations of pressure, velocity, and temperature with area change for supersonic flow are totally different from those for subsonic flow.

For supersonic flow in a divergent channel, any decrease in density is so rapid that both the area and velocity must increase together in order to keep the mass conservation rule,  $\rho AV = \text{constant}$ , which is an essential feature for continuum flows.

The phenomenon of *choking* is discussed in detail and the reason why choking should occur only at the minimum area, and the reason for maximum mass flow rate per unit area at the throat, may be argued as follows. As the backpressure for a running nozzle is lowered for a constant reservoir pressure, mass flow through the nozzle keeps increasing until a maximum flow rate is reached. Further decrease in backpressure has no effect on the mass flow rate and at this condition the nozzle is said to be *choked*. That is, after choking, the decrease in backpressure cannot be sensed by the fluid in the reservoir. For subsonic flow, any change in backpressure is sensed in the reservoir by means of signal waves that are traveling with speed equal to the *velocity of sound*. Once the flow velocity at a point in the nozzle becomes equal to the velocity of sound, the signals carrying the information about backpressure changes are not able to travel to the reservoir crossing the sonic speed location. This is because the *effective velocity* with which the signals can travel back into the convergent portion of the nozzle *becomes zero* at the sonic location. Therefore, the reservoir is unable to sense any further decrease in backpressure.

The nozzles whose flow area decrease in the flow direction are called *convergent nozzles*. Nozzles whose flow area first decreases and then increases are called *convergent–divergent nozzles*. The converging–diverging nozzle with a *contoured shape* that leads to a uniform parallel flow at the exit is called a *de Laval nozzle*. The location of the smallest flow area of a nozzle is called the *throat*. The highest velocity to which the flow can be accelerated in a convergent nozzle is the sonic velocity. Accelerating a flow to supersonic velocities is possible only in convergent–divergent nozzles. In all convergent–divergent nozzles delivering supersonic flow, the flow velocity at the throat is the velocity of sound.

For steady inviscid flow the *compressible* Bernoulli's equation is

$$\frac{V^2}{2} + \int \frac{1}{\rho} \frac{\partial p}{\partial s} ds = \text{constant}$$

The limiting maximum velocity that can be achieved by expanding a gas at any given stagnation condition into vacuum is

$$V_{\text{max}} = a_0 \sqrt{\frac{2}{\gamma - 1}}$$

When  $M = 1$ , the resulting static-to-stagnation property ratios for pressure, density, and temperature are called *critical ratios* and are denoted by a superscript asterisk.

$$\begin{aligned}\frac{p^*}{p_0} &= \left( \frac{2}{\gamma + 1} \right)^{\gamma/(\gamma-1)} \\ \frac{\rho^*}{\rho_0} &= \left( \frac{2}{\gamma + 1} \right)^{1/(\gamma-1)} \\ \frac{T^*}{T_0} &= \frac{2}{\gamma + 1}\end{aligned}$$

The pressure of the surrounding environment to which the flow through the nozzle is discharged is called the *backpressure*. For all backpressures lower than  $p^*$ , the pressure at the exit plane of the converging nozzle is equal to  $p^*$ , the Mach number at the exit plane is unity, and the mass flow rate is the maximum (or choked) flow rate. Under steady flow conditions, the mass flow rate through the nozzle is constant and can be expressed as

$$\dot{m} = \frac{A M p_0 \sqrt{\frac{\gamma}{R T_0}}}{\left( 1 + \frac{\gamma-1}{2} M^2 \right)^{\frac{\gamma+1}{2(\gamma-1)}}}$$

For air with  $\gamma = 1.4$ , the maximum mass flow rate becomes

$$\dot{m}_{\max} = \frac{0.6847 p_0 A^*}{\sqrt{R T_0}}$$

The variation of flow area  $A$  through the nozzle relative to the throat area  $A^*$  for the same mass flow rate and stagnation properties of a perfect gas is

$$\frac{A}{A^*} = \frac{1}{M} \left( \left( \frac{2}{\gamma + 1} \right) \left( 1 + \frac{\gamma-1}{2} M^2 \right) \right)^{(\gamma+1)/2(\gamma-1)}$$

This is called the *area–Mach number relation*.

The parameter  $M^*$  is defined as the ratio of the local velocity to the velocity of sound at the choked condition ( $M = 1$ ). It can be expressed as

$$M^* = M \sqrt{\frac{\gamma + 1}{2 + (\gamma - 1) M^2}}$$

The three standard reference speeds for gas dynamic study are  $V_{\max}$  corresponding to a given stagnation state, the speed of sound  $a_0$  at the stagnation temperature, and the critical speed  $V^*$ . These can be expressed as

$$\begin{aligned}V_{\max} &= \sqrt{\frac{2\gamma}{\gamma-1} R T_0} \\ a_0 &= \sqrt{\gamma R T_0} \\ V^* &= a^* = \sqrt{\gamma R T^*}\end{aligned}$$

A nozzle is said to be *overexpanded* when the pressure at the nozzle exit  $p_e$  is less than the backpressure  $p_b$ . When the exit pressure is higher than the backpressure, the nozzle is said to be *underexpanded*.

Basically, diffusers are passages in which flow decelerates. In a diffuser with a normal shock, it can be shown that

$$\frac{p_{02}}{p_{01}} = \frac{A_1^*}{A_2^*}$$

where  $p_{01}$  and  $p_{02}$  are the stagnation pressures just upstream and downstream of the normal shock, respectively, and  $A_1^*$  is the area of the first throat and  $A_2^*$  is the second throat area.

The pressures that are of interest in gas dynamics are the total or stagnation pressure, the static pressure, and the dynamic pressure. In incompressible flows, these three pressures are linked by the *incompressible* Bernoulli equation

$$p_0 - p = \frac{1}{2} \rho V^2$$

This equation is used for the measurement of flow velocity with pitot-static tube in incompressible flows. But for compressible flows, the Bernoulli's equation becomes

$$\frac{\gamma}{\gamma - 1} \frac{p}{\rho} + \frac{1}{2} V^2 = \frac{\gamma}{\gamma - 1} \frac{p_0}{\rho_0}$$

This is the *compressible* Bernoulli equation for isentropic flow of perfect fluids.

In a supersonic flow, the indicated pitot-pressure  $p_{02}$  is measured by a pitot probe; the stagnation pressure behind a normal shock may be used for calculating the flow Mach number with the relation

$$\frac{p_1}{p_{02}} = \frac{\left( \frac{2\gamma}{\gamma+1} M_1^2 - \frac{\gamma-1}{\gamma+1} \right)^{1/(\gamma-1)}}{\left( \frac{\gamma+1}{2} M_1^2 \right)^{\gamma/(\gamma-1)}}$$

The relation is called the *Rayleigh supersonic pitot formula*.

The dynamic pressure  $q$  in compressible flow can be expressed as

$$q = \frac{p_0 - p}{K}$$

where

$$K = 1 + \frac{M^2}{4} + \frac{M^4}{40}$$

is called the *correction coefficient*.

For compressible flows, the pressure coefficient, which is a dimensionless pressure difference, can be expressed as

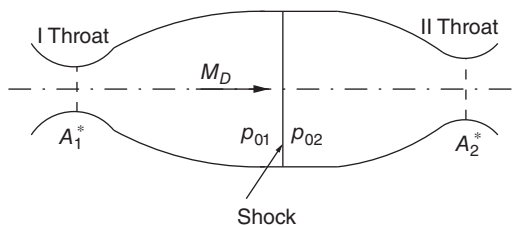
$$C_p = \frac{2}{\gamma M_\infty^2} \left( \frac{p}{p_\infty} - 1 \right)$$

## Exercise Problems

- 2.1 A storage chamber of a compressor is maintained at 1.8 atm absolute and 20 °C. The surrounding ambient pressure is 1 atm. Calculate (a) the velocity with which airflow will take place from the outside through a unit area hole and (b) the mass flow rate per unit area. Assume air as a perfect gas.

[Answer: (a) 301.8 m s<sup>-1</sup>, (b) 430 kg (m<sup>2</sup> s)<sup>-1</sup>]

- 2.2** A ramjet flies at 11 km altitude with a flight Mach number of 0.9. In the inlet diffuser, the air is brought to the stagnation condition so that it is stationary just before the combustion chamber. Combustion takes place at constant pressure and a temperature increase of 1500 K results. The combustion products are then ejected through the nozzle. (a) Calculate the stagnation pressure and temperature. (b) What will be the nozzle exit velocity? (At inlet  $p_\infty = 0.3$  atm and  $T_\infty = 213$  K, at exit  $p_{\text{exit}} = 0.3$  atm.)  
[Answer: (a) 0.507 atm, 247.5 K, (b) 699 m s<sup>-1</sup>]
- 2.3** A storage chamber supplies high-pressure air to a pneumatic machine. It is found that there is an unavoidable leak at the joints and the total area through which leakage occurs is estimated to be 1 cm<sup>2</sup>. Calculate the quantity of air leaking out of the chamber to the sea-level atmosphere, if the chamber is maintained at 5 atm and 20 °C.  
[Answer: 0.12 kg s<sup>-1</sup>]
- 2.4** A de Laval nozzle has to be designed for an exit Mach number of 1.5 with an exit diameter of 200 mm. (a) Find the ratio of the necessary throat area/exit area. The air reservoir conditions are given as  $p_0 = 1$  atm (gauge) and  $T_0 = 20$  °C. (b) Find the maximum mass flow rate through the nozzle. (c) What will be the exit pressure and temperature?  
[Answer: (a) 0.85, (b) 12.78 kg s<sup>-1</sup>, (c) 0.545 atm, 202.07 K]
- 2.5** A convergent–divergent nozzle is designed to operate with an exit Mach number of 1.75. The nozzle is supplied from an air reservoir at  $68 \times 10^5$  N m<sup>-2</sup> (abs). Assuming one-dimensional flow, calculate (a) the maximum backpressure to choke the nozzle, (b) the range of backpressure over which a normal shock will appear in the nozzle, (c) the backpressure for the nozzle to be perfectly expanded to design  $M$ , and (d) the range of backpressure for supersonic flow at the nozzle exit plane.  
[Answer: (a) 58 atm, (b) 43.53 to 58 atm, (c) 12.78 atm, (d) 43.53 atm]
- 2.6** A supersonic convergent–divergent diffuser, shown in Figure 2.34, is designed to operate at a Mach number of 1.7. To what Mach number should the inlet be accelerated in order to swallow the shock during the start-up?  
[Answer: 1.94]
- 2.7** A convergent–divergent diffuser is to be used at Mach 3.0. The diffuser has to use a variable throat area so as to swallow the starting shock. What percentage increase in throat area will be necessary?  
[Answer: 204.6%]
- 2.8** Calculate the dynamic pressure of the air flow if  $V_\infty = 175$  m s<sup>-1</sup>,  $p_\infty = 1$  atm, and  $T_\infty = 298$  K. What will be the percentage error if the flow is treated as incompressible?  
[Answer: 6.16%]



**Figure 2.34** A supersonic convergent–divergent diffuser.



- 2.9** The working section of a wind tunnel of cross-sectional area  $0.6 \text{ m}^2$  has a Mach number of 0.80. In the settling chamber of cross-sectional area  $4.0 \text{ m}^2$  the pressure, density, and temperature are  $1.014 \times 10^5 \text{ Pa}$ ,  $1.144 \text{ kg m}^{-3}$ , and  $35^\circ\text{C}$ , respectively. Calculate the pressure, density, and temperature in the working section, neglecting the effects of viscosity and treating the flow as one-dimensional.  
[Answer:  $0.665 \times 10^5 \text{ Pa}$ ,  $0.847 \text{ kg m}^{-3}$ ,  $272.88 \text{ K}$ ]
- 2.10** Air from a storage tank exhausts through a convergent nozzle of exit area  $0.5 \text{ cm}^2$  to an environment at 1 atm pressure. If the tank is at 500 kPa and  $30^\circ\text{C}$ , compute the mass flow rate at the beginning of discharge.  
[Answer:  $0.058 \text{ kg s}^{-1}$ ]
- 2.11** Air at stagnation state of 700 kPa and  $180^\circ\text{C}$  enters a nozzle. The pressure at the nozzle exit is 100 kPa. Flow expands isentropically through the nozzle. Determine the flow velocity at the nozzle exit if the flow expands isentropically. Assume air to be a perfect gas with  $\gamma = 1.4$ .  
[Answer:  $623.4 \text{ m s}^{-1}$ ]
- 2.12** Calculate the maximum mass flow possible through a frictionless, insulated convergent nozzle of exit area  $6.5 \text{ cm}^2$  operating at sea level, if the stagnation conditions are 5 bar and  $15^\circ\text{C}$ . Also, calculate the exit temperature.  
[Answer:  $0.774 \text{ kg s}^{-1}$ ,  $240.12 \text{ K}$ ]
- 2.13** Air at 101 kPa and  $20^\circ\text{C}$  is drawn isentropically through a convergent–divergent nozzle of exit area  $0.033 \text{ m}^2$ . If the pressure at the nozzle exit is 91.4 kPa, determine the mass flow rate through the nozzle. What is the pressure at the location with area  $0.022 \text{ m}^2$ ?  
[Answer:  $4.74 \text{ kg s}^{-1}$ ,  $73.5 \text{ kPa}$ ]
- 2.14** A rocket nozzle has to generate 9 kN thrust at an altitude of 16 km above the earth, with its chamber pressure and temperature of 15 atm and  $2600^\circ\text{C}$ , respectively. Calculate its exit and throat areas and the velocity and temperature at the nozzle exit. Take  $\gamma = 1.4$  and  $R = 287 \text{ J (kg K)}^{-1}$ . Assume the nozzle to operate at the adapted condition.  
[Answer:  $0.0394 \text{ m}^2$ ,  $0.00374 \text{ m}^2$ ,  $2094.6 \text{ m s}^{-1}$ ,  $689.33 \text{ K}$ ]
- 2.15** Determine the stagnation pressure  $p_0$ , temperature  $T_0$ , and density  $\rho_0$  of an air stream at a speed of  $200 \text{ m s}^{-1}$ . The air temperature is  $15^\circ\text{C}$  and pressure is 101 kPa.  
[Answer:  $127.8 \text{ kPa}$ ,  $308.2 \text{ K}$ ,  $1.445 \text{ kg m}^{-3}$ ]
- 2.16** Air flows through a convergent duct. At station 1 in the duct,  $A_1 = 10 \text{ cm}^2$ ,  $p_1 = 100 \text{ kPa}$ ,  $T_1 = 30^\circ\text{C}$ , and  $V_1 = 90.5 \text{ m s}^{-1}$ . Calculate  $M_2$ ,  $p_2$ , and  $T_2$  at station 2 where  $A_2 = 6.9 \text{ cm}^2$ . Assume the flow to be one-dimensional and isentropic.  
[Answer: 0.4,  $93.86 \text{ kPa}$ ,  $297.72 \text{ K}$ ]
- 2.17** Carbon dioxide from a large reservoir at 6 atm and  $30^\circ\text{C}$  is discharged to an ambient atmosphere through an orifice of diameter 1 mm. Determine the temperature of the carbon dioxide stream and the mass flow rate.  
[Answer:  $-9.55^\circ\text{C}$ ,  $0.00133 \text{ kg s}^{-1}$ ]

- 2.18** Air flows through a convergent–divergent nozzle of inlet area  $12\text{ cm}^2$  at a rate of  $0.7\text{ kg s}^{-1}$ . The conditions at the inlet and exit of the nozzle are  $8\text{ kg m}^{-3}$  and  $400\text{ K}$ , and  $4\text{ kg m}^{-3}$  and  $300\text{ K}$ , respectively. Find the cross-sectional area, pressure, and the Mach number at the nozzle exit. Assume isentropic flow.  
[Answer:  $3.9\text{ cm}^2$ ,  $344.4\text{ kPa}$ ,  $1.29$ ]
- 2.19** An air stream at  $200\text{ kPa}$  and  $400\text{ K}$  enters a convergent axisymmetric nozzle at a velocity of  $100\text{ m s}^{-1}$  and expands isentropically to an exit pressure of  $150\text{ kPa}$ . If the inlet diameter is  $75\text{ mm}$ , find the temperature, Mach number, and the diameter at the nozzle exit. Also estimate the mass flow rate through the nozzle.  
[Answer:  $368.85\text{ K}$ ,  $0.7$ ,  $50.7\text{ mm}$ ,  $0.77\text{ kg s}^{-1}$ ]
- 2.20** Air enters a nozzle at a pressure of  $3\text{ MPa}$  with a temperature of  $400^\circ\text{C}$ . At the nozzle exit,  $A_2 = 5000\text{ mm}^2$  and  $p_2 = 0.5\text{ MPa}$ . Expansion through the nozzle is isentropic according to the law  $pV^\gamma = \text{constant}$ . Determine (a) the Mach number at nozzle exit, (b) the throat area, and (c) the mass flow through the nozzle.  
[Answer: (a)  $1.83$ , (b)  $3415\text{ mm}^2$ , (c)  $15.89\text{ kg s}^{-1}$ ]
- 2.21** Air stream at  $80\text{ kPa}$  and  $5^\circ\text{C}$  enters an adiabatic diffuser of circular cross-section with an entrance area of  $0.2\text{ m}^2$  at  $200\text{ m s}^{-1}$ . If the semi-divergence angle of the diffuser is  $8^\circ$ , find the  $dp/dx$ ,  $dV/dx$ , and  $d\rho/dx$ , where  $x$  is the axial direction of the diffuser, assuming the flow to be (a) incompressible and (b) compressible.  
[Answer: (a)  $44.53\text{ kPa m}^{-1}$ ,  $-222\text{ (m s}^{-1})\text{ m}^{-1}$ ,  $0$ , (b)  $69.3\text{ kPa m}^{-1}$ ,  $-345.6\text{ (m s}^{-1})\text{ m}^{-1}$ ,  $0.621\text{ (kg m}^{-3})\text{ m}^{-1}$ ]
- 2.22** An aircraft flies at Mach  $0.8$  at an altitude where the pressure and temperature are  $44\text{ kPa}$  and  $-15^\circ\text{C}$ , respectively. Determine the isentropic stagnation pressure and temperature recorded on the aircraft. Assume air to be an ideal gas. Solve the problem using property relations as well as by using gas tables.  
[Answer:  $67.08\text{ kPa}$ ,  $291.2\text{ K}$ ]
- 2.23** The pressure and temperature in the test-section of a supersonic wind tunnel are  $0.55\text{ atm}$  and  $216\text{ K}$ , respectively. If the total temperature is  $40^\circ\text{C}$ , calculate the test-section Mach number and the total pressure.  
[Answer:  $1.5$ ,  $2.019\text{ atm}$ ]
- 2.24** Air flow in a duct has  $V_1 = 100\text{ m s}^{-1}$ ,  $T_1 = 70^\circ\text{C}$ ,  $p_1 = 2.5\text{ atm}$  at station 1. At a downstream station 2, if  $V_2 = 400\text{ m s}^{-1}$  and  $p_2 = 0.5\text{ atm}$ , compute  $M_2$ ,  $V_{\text{max}}$ , and  $p_{02}/p_{01}$ . Treat the flow as being isentropic.  
[Answer:  $1.218$ ,  $836.3\text{ m s}^{-1}$ ,  $0.471$ ]
- 2.25** Air from a high pressure tank at  $350\text{ kPa}$  and  $420\text{ K}$  expands isentropically through a nozzle of exit area  $A_e = 0.22\text{ m}^2$ . If  $V_e = 525\text{ m s}^{-1}$ , determine  $M_e$ ,  $p_e$ ,  $\dot{m}_e$ , and  $A^*$ .  
[Answer:  $1.56$ ,  $87.35\text{ kPa}$ ,  $124.3\text{ kg s}^{-1}$ ,  $0.18\text{ m}^2$ ]
- 2.26** Air flows through a convergent–divergent nozzle of throat area  $25\text{ cm}^2$ . At station 1 upstream of the throat  $V_1 = 150\text{ m s}^{-1}$ ,  $T_1 = 315\text{ K}$ , and  $p_1 = 152\text{ kPa}$ . If the flow velocity at the nozzle exit is supersonic, compute the nozzle cross-sectional area at station 1 and the mass flow rate  $\dot{m}$ . Assume the flow to be isentropic.  
[Answer:  $38.22\text{ cm}^2$ ,  $0.9637\text{ kg s}^{-1}$ ]

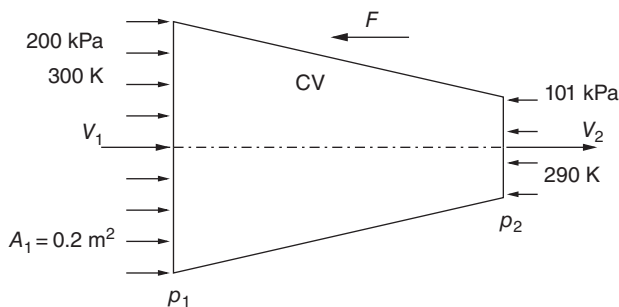
- 2.27** Compressed dry air at  $40^\circ\text{C}$  from a large reservoir exhausts through a nozzle with an exit velocity of  $200\text{ m s}^{-1}$ . A mercury manometer (with standard sea level pressure reference) reads the corresponding pressure as 2.27 cm compression. Determine the exit Mach number, the tank, and the atmospheric pressure. Assume the flow through the nozzle to be isentropic.  
[Answer: 0.583, 131, 381.11 Pa, 104, 353.54 Pa]
- 2.28** At a particular section of a duct, air at  $32^\circ\text{C}$  and 80 kPa flows with a velocity of  $365\text{ m s}^{-1}$ . Assuming the process to be isentropic, calculate the  $T$  and  $V$  at a section where the pressure is 120 kPa. Determine the Mach number at both sections.  
[Answer:  $69.91^\circ\text{C}$ ,  $237.6\text{ m s}^{-1}$ , 1.04, 0.64]
- 2.29** Calculate the mass flow rate of air, the nozzle throat area, and the reservoir pressure and temperature required for a supersonic wind tunnel operation with test-section conditions of Mach 3, static pressure of 0.2 atm, and static temperature 300 K. The test-section area is  $0.05\text{ m}^2$ ; assume the flow to be isentropic.  
[Answer:  $12.25\text{ kg s}^{-1}$ ,  $0.0118\text{ m}^2$ , 744.38 kPa, 840 K]
- 2.30** Air enters a de Laval nozzle of a supersonic wind tunnel at 1 MPa and 300 K with a very low velocity. The nozzle exit area  $A_e = 0.15\text{ m}^2$ , which is the same as the test-section area  $A_{\text{TS}}$ . Calculate the  $p$ ,  $T$ ,  $V$ , and  $\dot{m}$  in the test-section for Mach number 2.  
[Answer: 127.8 kPa, 166.67 K,  $517.56\text{ m s}^{-1}$ ,  $207.43\text{ kg s}^{-1}$ ]
- 2.31** In an intermittently operated supersonic wind tunnel, atmospheric air at stationary conditions is taken into a constant pressure heat exchanger, where it is heated to  $T_1$  K. The air leaves the heat exchanger with velocity  $V_1 = 15\text{ m s}^{-1}$  and is then expanded in a de Laval nozzle to attain the test-section Mach number  $M_T = 2.5$  and temperature  $T_T$  K. Calculate the necessary temperature rise in the heat exchanger so that  $T_T = T_0$ . Given  $T_0 = 300\text{ K}$  and  $\rho_0 = 1.25\text{ kg m}^{-3}$ .  
[Answer:  $T_1 - T_0 = 375\text{ K}$ ]
- 2.32** Dry heated air is supplied from a storage chamber to a blowdown type wind tunnel through a suitable nozzle. The nozzle throat area is  $80\text{ cm}^2$  and is designed for  $M = 2.0$ . The storage chamber conditions are  $p_0 = 3.12\text{ atm}$  and  $T_0 = 100^\circ\text{C}$ . Find the test-section temperature and the mass flow rate.  
[Answer:  $T_{\text{TS}} = 207.3\text{ K}$ ,  $\dot{m} = 5.288\text{ kg s}^{-1}$ ]
- 2.33** A supersonic stream at  $M_1 = 3.0$  is decelerated in a convergent nozzle to sonic condition at the exit of the nozzle. Calculate the pressure and temperature at the nozzle entry and the mass flow rate. What will be the temperature indicated by a thermocouple held in the flow direction at the entry? The conditions at nozzle exit are:  $p_e = 0.8\text{ atm}$ ,  $T_e = 293\text{ K}$ , and  $A_e = 40\text{ cm}^2$ .  
[Answer:  $p_1 = 0.04123\text{ atm}$ ,  $T_1 = 125.57\text{ K}$ ,  $\dot{m} = 1.323\text{ kg s}^{-1}$ ,  $T_0 = 351.6\text{ K}$ ]
- 2.34** In a continuous-operation supersonic wind tunnel, the inlet area  $A_1 = 600 \times 400\text{ mm}^2$ , the throat area of the nozzle is  $300 \times 400\text{ mm}^2$ , and the test-section is  $h_2 \times 400\text{ mm}^2$ . The test-section conditions are  $M_2 = 2.5$ ,  $T_2 = -10^\circ\text{C}$ , and  $p_2 = 0.15\text{ atm}$ . Calculate  $h_2$ ,  $T_1$ ,  $M_1$ ,  $V_1$ , and the temperature at the stagnation point of a model in the test-section.  
[Answer:  $h_2 = 791\text{ mm}$ ,  $T_1 = 581.5\text{ K}$ ,  $M_1 = 0.3$ ,  $V_1 = 145\text{ m s}^{-1}$ ,  $T_0 = 592\text{ K}$ ]

- 2.35** For the operation of a supersonic test-section, air flow at  $p_1$ ,  $T_1$ , and  $M_1$  is led through a de Laval nozzle of inlet area  $A_1$  which expands the flow to a pressure of  $p_2$  at the test-section. If  $p_1 = 6.5$  atm,  $T_1 = 440$  K,  $M_1 = 0.5$ ,  $A_1 = 160$  cm<sup>2</sup>,  $p_2 = 1.0$  atm, what will be  $M_2$ ,  $A^*/A_2$ , and  $\dot{m}$ ?  
[Answer:  $M_2 = 2.0$ ,  $A^*/A_2 = 0.6$ ,  $\dot{m} = 17.54$  kg s<sup>-1</sup>]
- 2.36** To find the flow Mach number in a pipe, a venturi nozzle is built into the pipe, the measured value of pressures  $p_1$  and  $p_2$  at inlet and throat of venturi are 1.5 atm and 1.2 atm, respectively. Inlet area/throat area = 4/3. Find  $M_1$  and  $M_{\text{throat}}$ .  
[Answer:  $M_1 = 0.46$ ,  $M_{\text{throat}} = 0.74$ ]
- 2.37** A pitot-static tube shows a pressure difference of 490 mm of mercury, when placed in a flow. The static pressure is measured separately to be 0.35 atm (gauge). If the stagnation temperature of the flow is 25 °C, calculate the flow velocity.  
[Answer:  $V = 253.69$  m s<sup>-1</sup>]
- 2.38** Air is compressed isentropically in a centrifugal compressor from 1 atm to 6 atm. If the initial temperature is 290 K, calculate (a) the change in temperature, (b) the change in internal energy, and (c) the work imparted to the air, neglecting the velocity change.  
[Answer: (a)  $\Delta T = 194$  K, (b)  $\Delta e = 1.39 \times 10^5$  J kg<sup>-1</sup>, (c)  $\Delta w = 1.39 \times 10^5$  J kg<sup>-1</sup>]
- 2.39** Air at atmospheric pressure and at a temperature of 300 K expands in an ideal diffuser. The entrance speed is 180 m s<sup>-1</sup>. Calculate the maximum pressure (ram pressure) that can be achieved if the air is diffused to zero speed.  
[Answer:  $p_0 = 1.217 \times 10^5$  Pa]
- 2.40** Air at a stagnation temperature and pressure of 200.9 K and  $6.895 \times 10^5$  Pa respectively flows from a reservoir through a converging nozzle that exhausts into an atmosphere where the pressure is  $1.014 \times 10^5$  Pa. Calculate (a) the pressure in the nozzle exit plane, (b) the minimum stagnation pressure for which the flow is choked, and (c) the exit plane pressure if the stagnation pressure is reduced to  $1.724 \times 10^5$  Pa.  
[Answer: (a)  $3.64 \times 10^5$  Pa, (b)  $1.92 \times 10^5$  Pa, (c)  $1.014 \times 10^5$  Pa]
- 2.41** The diffuser of a turbojet engine operating at 10 000 m passes a mass flow rate of 25 kg s<sup>-1</sup>. The velocity, pressure, and the temperature at the inlet are 200 m s<sup>-1</sup>,  $0.35 \times 10^5$  Pa, 230 K. The exit area of the diffuser is 0.5 m<sup>2</sup>. Assuming frictionless flow, calculate the reaction force acting on the diffuser if the exit Mach number is 0.2.  
[Answer: 10.815 kN]
- 2.42** Air enters a tank at a speed of 100 m s<sup>-1</sup> and leaves it at 200 m s<sup>-1</sup>. If no heat is added to and no work is done by the air, show that the temperature of the air at the exit is 15 °C below that at the entrance.
- 2.43** Air enters a machine at 373 K with a speed of 200 m s<sup>-1</sup> and leaves at standard sea level temperature (15 °C). Show that, (a) if the machine has to deliver 100 000 Nm kg<sup>-1</sup> of work without any heat input, the air speed at the exit has to be 103.3 m s<sup>-1</sup> and (b) the exit speed becomes 459 m s<sup>-1</sup> when the machine is idling.

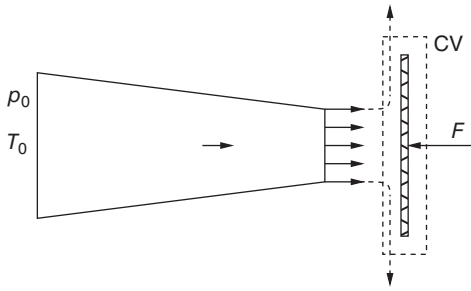
- 2.44** Two jets of air of equal mass flow rate mix thoroughly before entering a large reservoir. One jet is at 400 K and  $100 \text{ m s}^{-1}$  and the other is at 200 K and  $300 \text{ m s}^{-1}$ . In the absence of heat addition or work done, show that the temperature of air in the reservoir is 324.9 K.
- 2.45** When air is released adiabatically from a tire, the temperature of the air at the nozzle exit is found to be  $37^\circ\text{C}$  below that inside the tire. Show that the air speed at the nozzle exit is  $272.57 \text{ m s}^{-1}$ .
- 2.46** An airplane flies at  $800 \text{ km h}^{-1}$  at 15 000 m altitude. Calculate (a) the maximum possible temperature at the airplane skin, (b) the maximum possible pressure intensity on the airplane body, (c) the critical velocity of the air relative to the airplane, and (d) the maximum possible velocity of the air relative to the airplane.  
[Answer: (a) 240.83 K, (b)  $1.751 \times 10^4 \text{ Pa}$ , (c)  $283.97 \text{ m s}^{-1}$ , (d)  $695.58 \text{ m s}^{-1}$ ]
- 2.47** A perfect gas having  $c_p = 1017 \text{ Nm (kg K)}^{-1}$  flows adiabatically in a converging passage with a mass flow rate  $\dot{m} = 29.188 \text{ kg s}^{-1}$ . At a particular cross-section,  $M = 0.6$ ,  $T_0 = 550 \text{ K}$ , and  $p_0 = 2.0 \times 10^5 \text{ Pa}$ . Calculate the area of the passage at that location.  
[Answer:  $0.10125 \text{ m}^2$ ]
- 2.48** Sea-level air is being drawn isentropically through a duct into a vacuum tank. The cross-sectional areas of the duct at the mouth, the throat, and the entrance to the vacuum tank are 2, 1, and  $4 \text{ m}^2$ , respectively. Show that (a) the maximum amount of air that can be drawn into the vacuum tank is  $241.25 \text{ kg s}^{-1}$  and (b) for maximum mass flow rate through the duct, the pressure in the vacuum tank has to be 3018.7 Pa.
- 2.49** A supersonic wind tunnel nozzle is to be designed for  $M = 2$  with a  $1 \text{ m}^2$  throat section. The supply pressure and temperature at the nozzle inlet, where the velocity is negligible, are  $7 \times 10^5 \text{ Pa}$  and  $40^\circ\text{C}$ , respectively. The preliminary design is to be based on the assumption that the flow is one-dimensional at the throat and the test-section. Compute the mass flow rate, the test-section area, and the flow properties at the throat and the test-section.  
[Answer:  $\dot{m} = 1599.13 \text{ kg s}^{-1}$ ,  $A = 1.688 \text{ m}^2$ ; at the throat:  $p = 3.7 \times 10^5 \text{ Pa}$ ,  $T = 261 \text{ K}$ ,  $\rho = 4.944 \text{ kg m}^{-3}$ ; at the test-section:  $p = 8.946 \times 10^4 \text{ Pa}$ ,  $T = 173.9 \text{ K}$ ,  $\rho = 1.794 \text{ kg m}^{-3}$ ]
- 2.50** Air at 300 K and  $1 \times 10^5 \text{ Pa}$  enters a diffuser with a velocity of  $245 \text{ m s}^{-1}$ . The diffuser is to be designed to reduce the velocity of the air to  $60 \text{ m s}^{-1}$ . The mass flow rate through the diffuser is  $13.6 \text{ kg s}^{-1}$ . Assuming the flow to be isentropic, determine (a) the inlet diameter, (b) the outlet diameter, and (c) the rise in static temperature.  
[Answer: (a) 0.2467 m, (b) 0.459 m, (c) 28.2 K]
- 2.51** A blunt-nosed pitot tube is placed in a supersonic wind tunnel to determine the flow Mach number. The stagnation pressure  $p_0$  at the entrance to the pitot tube is  $2.0 \times 10^5 \text{ Pa}$ . The freestream static pressure  $p_1$  ahead of the shock wave, measured by a static pressure tap in the wall of the tunnel, is  $0.15 \times 10^5 \text{ Pa}$ . Estimate the Mach number in the tunnel.  
[Answer:  $M = 3.16$ ]

- 2.52** Consider Problem 2.48. If a normal shock is detected (by Schlieren photography) in the divergence portion of the duct where the cross-sectional area is  $3 \text{ m}^2$ , show that the pressure in the reservoir is  $41\,442.5 \text{ Pa}$ .
- 2.53** A subsonic diffuser of inlet area  $0.15 \text{ m}^2$  operates isentropically. The inlet conditions are  $V_1 = 240 \text{ m s}^{-1}$ ,  $T_1 = 300 \text{ K}$ , and  $p_1 = 0.70 \times 10^5 \text{ Pa}$ . The flow leaves the diffuser at  $120 \text{ m s}^{-1}$ . Calculate (a) the mass flow rate, (b) the stagnation pressure at the exit, (c) the stagnation temperature at the exit, (d) the static pressure at the exit, (e) the entropy change across the diffuser, and (f) the exit area.  
[Answer: (a)  $29.26 \text{ kg s}^{-1}$ , (b)  $0.9624 \times 10^5 \text{ Pa}$ , (c)  $328.6 \text{ K}$ , (d)  $8.91 \times 10^4 \text{ Pa}$ , (e) 0, (f)  $0.2518 \text{ m}^2$ ]
- 2.54** The cross-sectional area of the working section of a Mach 0.8 wind tunnel is  $0.6 \text{ m}^2$ . The cross-sectional area of the settling chamber is  $4.0 \text{ m}^2$ . If the pressure, density, and temperature in the settling chamber are  $0.1014 \text{ MPa}$ ,  $1.144 \text{ kg m}^{-3}$ , and  $35^\circ\text{C}$ , respectively, determine the pressure, density, and temperature in the working section, neglecting the effects of viscosity and treating the flow as one-dimensional.  
[Answer:  $0.665 \times 10^5 \text{ Pa}$ ,  $0.847 \text{ kg m}^{-3}$ ,  $273 \text{ K}$ ]
- 2.55** Air flows through a frictionless adiabatic convergent–divergent nozzle. The air stagnation pressure and temperature are  $7.0 \times 10^5 \text{ Pa}$  and  $500 \text{ K}$ , respectively. The diverging portion of the nozzle has an area ratio of  $A_{\text{exit}}/A_{\text{throat}} = 11.91$ . A normal shock wave stands in the divergent portion of the nozzle, where the Mach number is 3.0. Determine the Mach number, static pressure, and temperature at the nozzle exit plane.  
[Answer:  $M_e = 0.15$ ,  $p_e = 2.2622 \times 10^5 \text{ Pa}$ ,  $T_e = 497.8 \text{ K}$ ]
- 2.56** The pressure coefficient  $C_p = (p - p_\infty)/q_\infty$  is used to denote the local pressure coefficient near a body placed in a freestream under conditions  $p_\infty$ ,  $V_\infty$ ,  $M_\infty$ . Show that the value of  $C_p$  at which critical velocity occurs somewhere on the body can be written as
- $$C_p^* = \frac{[(2 + (\gamma - 1)M_\infty^2)/(\gamma + 1)]^{\gamma/(\gamma-1)} - 1}{(\gamma/2)M_\infty^2}$$
- 2.57** Air at a stagnation state of  $700 \text{ kPa}$  and  $180^\circ\text{C}$  expands isentropically through a nozzle. If the pressure at the nozzle exit is  $100 \text{ kPa}$ , determine the flow velocity at the nozzle exit. Assume air to be a perfect gas with  $\gamma = 1.4$ .  
[Answer:  $623.4 \text{ m s}^{-1}$ ]
- 2.58** Calculate the maximum mass flow rate possible through a frictionless, insulated convergent nozzle of exit area  $6.5 \text{ cm}^2$  operating at sea level, if the stagnation conditions are  $5 \text{ bar}$  and  $15^\circ\text{C}$ . Also, calculate the exit temperature.  
[Answer:  $0.774 \text{ kg s}^{-1}$ ,  $240.12 \text{ K}$ ]
- 2.59** Atmospheric air at  $101 \text{ kPa}$  and  $20^\circ\text{C}$  is drawn isentropically through a convergent–divergent nozzle of exit area  $0.033 \text{ m}^2$ . If the pressure at the nozzle exit is  $91.4 \text{ kPa}$ , determine the mass flow rate through the nozzle. What is the pressure at the location where the cross-sectional area is  $0.022 \text{ m}^2$ ?  
[Answer:  $4.74 \text{ kg s}^{-1}$ ,  $73.5 \text{ kPa}$ ]

- 2.60** Determine the stagnation pressure  $p_0$ , temperature  $T_0$ , and density  $\rho_0$  of an air stream at  $200 \text{ m s}^{-1}$ ,  $15^\circ\text{C}$ , and  $101 \text{ kPa}$ .  
[Answer:  $127.8 \text{ kPa}$ ,  $308.2 \text{ K}$ ,  $1.445 \text{ kg m}^{-3}$ ]
- 2.61** Air flows through a convergent duct. At station 1 in the duct,  $A_1 = 10 \text{ cm}^2$ ,  $p_1 = 100 \text{ kPa}$ ,  $T_1 = 30^\circ\text{C}$ , and  $V_1 = 90.5 \text{ m s}^{-1}$ . Calculate  $M_2$ ,  $p_2$ , and  $T_2$  at station 2, where  $A_2 = 6.9 \text{ cm}^2$ . Assume the flow to be one-dimensional and the process to be isentropic.  
[Answer:  $0.4$ ,  $93.86 \text{ kPa}$ ,  $297.72 \text{ K}$ ]
- 2.62** Sea level air is drawn through a convergent duct of inlet area  $A_1$ . If the velocity at the inlet is  $4 \text{ m s}^{-1}$ , determine the exit area required to accelerate the flow to  $75 \text{ m s}^{-1}$ .  
[Answer:  $0.05516 A_1$ ]
- 2.63** An air stream at  $200 \text{ kPa}$  and  $400 \text{ K}$  enters a convergent axisymmetric nozzle at a velocity of  $100 \text{ m s}^{-1}$  and expands isentropically to an exit pressure of  $150 \text{ kPa}$ . If the inlet diameter is  $75 \text{ mm}$ , find the temperature, Mach number, and diameter at the nozzle exit. Also, estimate the mass flow rate through the nozzle.  
[Answer:  $368.85 \text{ K}$ ,  $0.7$ ,  $50.7 \text{ mm}$ ,  $0.77 \text{ kg s}^{-1}$ ]
- 2.64** Air flows through a convergent nozzle, as shown in Figure 2.35, at a rate of  $5 \text{ kg s}^{-1}$ . Determine the force experienced by the inner surface of the nozzle.  
[Answer:  $36\,414.15 \text{ N}$ ]
- 2.65** Air at a stagnation state of  $3.5 \text{ MPa}$  and  $500^\circ\text{C}$  is expanded isentropically through a de Laval nozzle to a pressure of  $0.7 \text{ MPa}$  at the nozzle exit. If the mass flow rate through the nozzle is  $1.3 \text{ kg s}^{-1}$ , determine (a) the exit Mach number, (b) the exit area, and (c) the throat area.  
[Answer: (a)  $1.71$ , (b)  $3.5 \text{ cm}^2$ , (c)  $2.6 \text{ cm}^2$ ]
- 2.66** Subsonic air flow from a nozzle of exit area  $15 \text{ cm}^2$  strikes a vertical plate, as shown in Figure 2.36. A force of  $100 \text{ N}$  is required to hold the plate in position. If the stagnation temperature of the nozzle flow is  $25^\circ\text{C}$ , determine the Mach number  $M_e$  and velocity  $V_e$  at the nozzle exit and the stagnation pressure  $p_0$  of the flow.  
[Answer:  $0.69$ ,  $228.2 \text{ m s}^{-1}$ ,  $1.37 \text{ atm}$ ]



**Figure 2.35** Air flow through a convergent nozzle.



**Figure 2.36** Subsonic air flow from a nozzle striking a vertical plate.

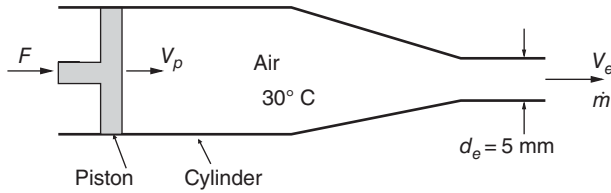
- 2.67** Air at  $p_0 = 700$  kPa and  $T_0 = 325$  K flows isentropically through a de Laval nozzle with a mass flow rate of  $1 \text{ kg s}^{-1}$ . If the nozzle is correctly expanded to standard atmosphere, determine  $A^*$ ,  $M_e$ , and  $V_e$ .  
[Answer:  $6.37 \text{ cm}^2$ ,  $1.92$ ,  $526.27 \text{ m s}^{-1}$ ]
- 2.68** Air flows isentropically through a convergent–divergent nozzle. The flow conditions at the inlet are  $V_1 = 100 \text{ m s}^{-1}$ ,  $p_1 = 1 \text{ atm}$ ,  $T_1 = 300 \text{ K}$ , and  $A_1 = 5 \text{ cm}^2$ . If the nozzle delivers supersonic flow, find  $p_{02}$  and  $T_{02}$  at the exit. Also determine the static pressure, temperature, and area at the throat.  
[Answer:  $1.06 \text{ atm}$ ,  $305 \text{ K}$ ,  $0.56 \text{ atm}$ ,  $254 \text{ K}$ ,  $2.36 \text{ cm}^2$ ]
- 2.69** Determine the exit area of an ideal convergent nozzle for a mass flow rate of air at  $0.5 \text{ kg s}^{-1}$  flowing from a reservoir at  $6 \text{ atm}$  and  $30^\circ\text{C}$  and discharging into a second reservoir maintained at a pressure of  $3 \text{ atm}$ . Assume air to be a perfect gas.  
[Answer:  $3.544 \text{ cm}^2$ ]
- 2.70** A convergent–divergent nozzle discharges air from a reservoir at  $1 \text{ MPa}$  to a surrounding at  $100 \text{ kPa}$ . The throat and exit areas of the nozzle are  $8 \text{ cm}^2$  and  $13.5 \text{ cm}^2$ , respectively. Determine the exit Mach number.  
[Answer:  $2.0$ ]
- 2.71** Air initially at standard sea-level pressure and temperature flows into an evacuated tank through a convergent nozzle of exit diameter  $0.04 \text{ m}$ . What pressure must be maintained in the tank to produce a sonic jet. What will be the corresponding mass flow rate.  
[Answer:  $53.5 \text{ kPa}$ ,  $0.303 \text{ kg s}^{-1}$ ]
- 2.72** A convergent–divergent nozzle fed from a reservoir has an exit area four times the throat area. What is the ratio of the exit pressure to reservoir pressure for isentropic flow of air if the Mach number at the exit is supersonic and correctly expanded?  
[Answer:  $0.029795$ ]
- 2.73** A convergent–divergent nozzle is designed to operate at an exit Mach number of  $1.63$ . If the stagnation pressure is maintained at  $10 \text{ atm}$ , assuming one-dimensional flow, calculate (a) the backpressure for correct expansion, (b) the range of backpressure for supersonic flow at the nozzle exit, and (c) the maximum backpressure for the flow to remain choked.  
[Answer: (a)  $228 \text{ kPa}$ , (b)  $< 228 \text{ kPa}$ , (c)  $830.87 \text{ kPa}$ ]



- 2.74** Show that the limiting values of density ratio and downstream Mach number for a normal shock in air when the upstream Mach number becomes very large are 6 and 0.378, respectively.
- 2.75** Determine the suction indicated by a mercury manometer connected to a wall static pressure located in a Mach 2 supersonic tunnel test-section, if the stagnation pressure and atmospheric pressure are 3 atm and 760 mm of mercury, respectively. Treat the flow as being one-dimensional and isentropic.  
[Answer: 468.61 mm]
- 2.76** The barometer of a mountain hiker reads 1000 mbar at the beginning of a hiking trip and 500 mbar at the end. Determine the vertical distance climbed by the hiker. Neglect the effect of altitude on local gravitational acceleration. Take an average air density of  $1.10 \text{ kg m}^{-3}$  and gravitational acceleration  $g = 9.81 \text{ m s}^{-2}$ .  
[Answer: 4633.49 m]
- 2.77** A barometer in an airplane cockpit shows 600 mm Hg at a particular altitude. If the pressure on the ground right below the airplane is 755 mm Hg, calculate the altitude of the airplane from ground level. Take the average air density to be  $1.20 \text{ kg m}^{-3}$  and mercury density to be  $13.6 \text{ kg m}^{-3}$ .  
[Answer: 1756.7 m]
- 2.78** Carbon dioxide gas at  $50^\circ\text{C}$  and 5 atm is compressed isentropically to 10 atm. Compute the new temperature.  
[Answer:  $106.05^\circ\text{C}$ ]
- 2.79** Air flows with conditions  $V = 400 \text{ m s}^{-1}$ ,  $p = 109 \text{ kPa}$ , and  $T = 100^\circ\text{C}$ . Determine the maximum velocity attainable by adiabatic expansion of this stream.  
[Answer:  $953.76 \text{ m s}^{-1}$ ]
- 2.80** In an air stream, the measured values of static pressure, stagnation pressure, and stagnation temperature are 100 kPa, 212 kPa, and  $95^\circ\text{C}$ , respectively. Calculate the flow velocity assuming the flow to be (a) incompressible and (b) compressible. Also, estimate the error in the velocity due to the incompressible assumption.  
[Answer: (a)  $334.16 \text{ m s}^{-1}$ , (b)  $378.02 \text{ m s}^{-1}$ , 11.64%]
- 2.81** Air flows isentropically through a nozzle. At station 1 upstream of the throat  $M_1 = 0.52$ ,  $T_1 = 190^\circ\text{C}$ , and  $p_1 = 288 \text{ kPa}$ . If the Mach number at station 2 downstream of the throat is 3.6, compute  $p_2$ ,  $T_2$ , and  $p_{02}$ . Also, express pressure  $p_2$  in terms of mercury column height.  
[Answer: 3.94 kPa, 135.9 K, 346.3 kPa, 29.55 mm Hg]
- 2.82** Show that, for isentropic flow of a perfect gas, the flow velocity can be expressed as
- $$V^2 = 2c_p T_0 \left( 1 - \left( \frac{p}{p_0} \right)^{\frac{\gamma-1}{\gamma}} \right)$$
- 2.83** Air enters a constant area duct of cross-section 25 cm by 40 cm at 110 kPa and  $24^\circ\text{C}$ , with a velocity of  $50 \text{ m s}^{-1}$ . It leaves the duct at 108 kPa and  $240^\circ\text{C}$ . If the flow is steady,

- determine (a) the velocity at the exit and (b) the mass flow rate. Assume air to be an ideal gas.  
[Answer: (a)  $88 \text{ m s}^{-1}$ , (b)  $6.45 \text{ kg s}^{-1}$ ]
- 2.84** Air expands isentropically from the stagnation state at 1500 kPa and  $100^\circ\text{C}$  to 500 kPa. Determine the ratio of the final to initial velocity of sound. Assume  $\gamma = 1.4$ .  
[Answer: 0.854]
- 2.85** Air expands isentropically through a nozzle from 4 MPa and  $300^\circ\text{C}$  to 2 MPa. If the mass flow rate is  $5 \text{ kg s}^{-1}$ , determine the nozzle exit area and velocity.  
[Answer:  $7.42 \text{ cm}^2$ ,  $456.12 \text{ m s}^{-1}$ ]
- 2.86** A rocket motor is designed to produce 500 N thrust at 12 000 m altitude and at that height the flow in the motor nozzle and subsequent jet is isentropic. The combustion chamber pressure  $p_c$  and temperature  $T_c$  are 25 atm and 3000 K, respectively. The value of  $\gamma$  of combustion products is 1.3 and their gas constant is the same as that of air. Compute the nozzle exit Mach number and the cross-sectional areas of the exit and throat of the nozzle, treating the flow as one-dimensional and inviscid.  
[Answer: 3.72,  $0.0014285 \text{ m}^2$ ,  $0.0001223 \text{ m}^2$ ]
- 2.87** Estimate the settling chamber pressure and temperature and the area ratio required to operate a supersonic wind tunnel at Mach 2 under standard sea-level conditions. Assume the flow to be one-dimensional and that the tunnel is operating with correct expansion.  
[Answer: 792.77 kPa, 518.67 K, 1.687]
- 2.88** Carbon dioxide gas at a stagnation state of 500 kPa and 400 K is accelerated isentropically to Mach 0.6. Calculate the temperature and pressure of the carbon dioxide after acceleration. Take  $\gamma = 1.252$  for carbon dioxide.  
[Answer: 382.64 K, 401.09 kPa]
- 2.89** Air enters a de Laval nozzle at a pressure of 2 MPa with negligible velocity. Determine the lowest pressure that can be obtained at the nozzle throat. Assume the flow to be isentropic.  
[Answer: 1.057 MPa]
- 2.90** Carbon dioxide enters an adiabatic nozzle at 1000 K with a velocity of  $50 \text{ m s}^{-1}$  and exits at 400 K. Determine the Mach number at the inlet and exit of the nozzle. Assume  $\gamma = 1.181$  at 1000 K and 1.252 at 400 K.  
[Answer: 0.106, 3.45]
- 2.91** Air at a stagnation state at 0.6 MPa and  $400^\circ\text{C}$  is expanded isentropically through a nozzle. Determine the static pressure and temperature at the nozzle exit, if the velocity after expansion is  $570 \text{ m s}^{-1}$ .  
[Answer: 0.2285 MPa, 511.43 K]
- 2.92** Air enters a nozzle at 0.2 MPa, 350 K, and  $150 \text{ m s}^{-1}$ . Assuming isentropic flow, determine the pressure and temperature of air at a location where the air velocity equals the speed of sound. Find the ratio of the area at this location to the nozzle entry area.  
[Answer: 0.1178 MPa, 300.99 K, 0.6289]

- 2.93** A pitot-static tube of an aircraft flying at 3000 m altitude measures the difference between the stagnation and static pressures as 14 kPa. Calculate the flight speed and Mach number.  
[Answer:  $184.45 \text{ m s}^{-1}$ , 0.58]
- 2.94** Determine the stagnation temperature and stagnation pressure of air flowing at  $470 \text{ m s}^{-1}$ , 245.9 K, and 44 kPa.  
[Answer: 356.53 K, 161.53 kPa]
- 2.95** Air enters a convergent–divergent nozzle at 0.8 MPa with negligible velocity. Determine the backpressure necessary for Mach 1.5 at the nozzle exit. Treat the flow as being isentropic.  
[Answer: 0.2179 MPa]
- 2.96** An aircraft is cruising at 10 000 m altitude. If a pitot tube is mounted at the nose of the aircraft, what will be the pressure measured by the pitot tube when the flight speed is 2000 kmph?  
[Answer: 130.96 kPa]
- 2.97** Determine the local values of  $p_0$ ,  $T_0$ ,  $T^*$ ,  $M^*$ , and  $a^*$  at a point in a supersonic flow field with Mach number, pressure, and temperature as 3.0, 0.5 atm, and 200 K, respectively.  
[Answer: 18.382 atm, 560 K, 466.66 K, 1.964,  $433 \text{ m s}^{-1}$ ]
- 2.98** If the local Mach number, pressure, and temperature at a point in a flow field are 0.7, 0.9 atm and 300 K, respectively, calculate the values of  $p^*$ ,  $T^*$ ,  $a^*$ , and  $T_0$  at that point.  
[Answer: 0.6593 atm, 274.5 K,  $332.1 \text{ m s}^{-1}$ , 329.41 K]
- 2.99** A supersonic nozzle with an exit area of  $10 \text{ cm}^2$  discharges air at  $M_e = 3$ ,  $p_e = 101 \text{ kPa}$ , and  $T_e = 300 \text{ K}$ . Determine  $V_e$ ,  $p_0$ ,  $T_0$ , and  $\dot{m}$ . Assume the flow to be isentropic.  
[Answer:  $1041.6 \text{ m s}^{-1}$ , 3.71 MPa, 840 K,  $1.22 \text{ kg s}^{-1}$ ]
- 2.100** Air flows in a convergent–divergent nozzle of throat area  $90 \text{ cm}^2$ . The pressure at the throat is 405 kPa and the exit Mach number is supersonic. Calculate the pressure at sections 1 and 2 which are upstream and downstream of a throat whose area is  $150 \text{ cm}^2$ . Assume the flow to be one-dimensional and isentropic.  
[Answer: 693.96 kPa, 101.04 kPa]
- 2.101** Air at  $30^\circ\text{C}$  contained in an insulated cylinder of 20 cm inside diameter is compressed by applying a force of 3000 N on a piston which is sliding in the cylinder. At the end of the cylinder there is a vent of 5 mm diameter, as shown in Figure 2.37. The compressed air exhausts through the vent to an ambient atmosphere at 1 atm. Compute  $V_p$ ,  $\dot{m}_e$ , and  $V_e$ . Also, find the minimum force  $F$  for which the piston velocity will be independent of the applied force.  
[Answer:  $0.123 \text{ m s}^{-1}$ ,  $0.00897 \text{ kg s}^{-1}$ ,  $318.6 \text{ m s}^{-1}$ , 2831.62 N]
- 2.102** Compressed air from a large reservoir is leaking through a small hole of diameter 3 mm. Determine the mass flow of air through the hole when the reservoir is at 300 kPa and 300 K and the ambient atmosphere is at 100 kPa. Also, compute the percentage increase in the mass flow when the reservoir pressure is increased to 600 kPa.  
[Answer:  $0.00495 \text{ kg s}^{-1}$ , 100%]



**Figure 2.37** Compressed air exhausting from a piston-cylinder device.

- 2.103** Air flows adiabatically through a frictionless duct. At station 1 in the duct  $A_1 = 0.3 \text{ m}^2$ ,  $V_1 = 200 \text{ m s}^{-1}$ ,  $p_1 = 80 \text{ kPa}$ , and  $T_1 = 400 \text{ K}$ . Calculate (a) the stagnation pressure and temperature of the flow. (b) Find  $M_2$  and  $p_2$  at a downstream station 2 where  $A_2 = 0.25 \text{ m}^2$ , when  $V_2$  is (i) subsonic and (ii) supersonic.  
[Answer: (a) 94.9 kPa, 420 K, (b) (i) 0.67, 70.24 kPa, (ii) 1.4, 29.81 kPa]
- 2.104** Air from a reservoir at 10 atm and 400 K is expanded through a convergent nozzle of exit area  $2 \text{ cm}^2$ . Determine the nozzle exit pressure and the mass flow rate through the nozzle if the backpressure is 1 atm.  
[Answer: 535.279 kPa,  $0.4095 \text{ kg s}^{-1}$ ]
- 2.105** Stagnant air at 200 kPa and 500 K is expanded isentropically through a de Laval nozzle to Mach 3.8. If the mass flow rate is  $2 \text{ kg s}^{-1}$ , calculate the throat area,  $p$ ,  $\rho$ ,  $T$ ,  $V$ , and area at the nozzle exit.  
[Answer:  $0.005533 \text{ m}^2$ , 1.72 kPa,  $0.0467 \text{ kg m}^{-3}$ , 128.6 K,  $863.79 \text{ m s}^{-1}$ ,  $0.04952 \text{ m}^2$ ]
- 2.106** The pressure, temperature, and velocity of a high speed gas flow are 100 kPa,  $100^\circ \text{C}$ , and  $930 \text{ m s}^{-1}$ , respectively. Determine the pressure and temperature that would result if the gas is brought to rest isentropically. Take the gas to be air.  
[Answer: 1.462 MPa, 803 K]
- 2.107** At a particular section in a duct through which air is flowing adiabatically, the pressure, temperature, and velocity are 2 atm,  $10^\circ \text{C}$ , and  $200 \text{ m s}^{-1}$ , respectively. If the pressure and velocity at a downstream location are 1.5 atm and  $250 \text{ m s}^{-1}$ , calculate the Mach number and the stagnation pressure, density, and temperature at the first location. Also, calculate the maximum velocity, sonic velocity, and the stagnation pressure and density at station 2. What is the percentage pressure loss between stations 1 and 2? Assume flow to be incompressible.  
[Answer: 0.593, 2.49 atm,  $2.9 \text{ kg m}^{-3}$ , 303.06 K,  $780.29 \text{ m s}^{-1}$ ,  $318.55 \text{ m s}^{-1}$ , 2.10 atm,  $2.45 \text{ kg m}^{-3}$ , 15.66%]
- 2.108** Show that the maximum mass flow rate in terms of the stagnation pressure  $p_0$ , stagnation temperature  $T_0$ , and throat area  $A_{\text{th}}$  for the isentropic flow of a perfect gas through a nozzle can be expressed as

$$\dot{m}_{\text{max}} = A_{\text{th}} \sqrt{\frac{\gamma}{RT_0}} p_0 \left( \frac{2}{\gamma + 1} \right)^{\frac{\gamma+1}{2(\gamma-1)}}$$

## 3

## Normal Shock Waves

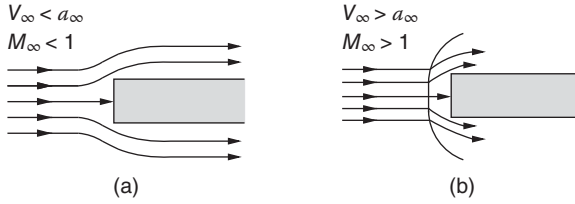
### 3.1 Introduction

Shock is a compression front across which the flow properties jump. Shock may also be described as a front in a supersonic flow field, and the flow processing across the front results in an abrupt change in fluid properties. In other words, shock is a thin region where large gradients in temperature, pressure, and velocity occur and where the transport phenomena of momentum and energy are important. The thickness of the shocks is comparable to the mean free path of the gas molecules in the flow field. To have some physical feel about the formation of such shock waves, consider a cylinder placed in a flow, as shown in Figure 3.1

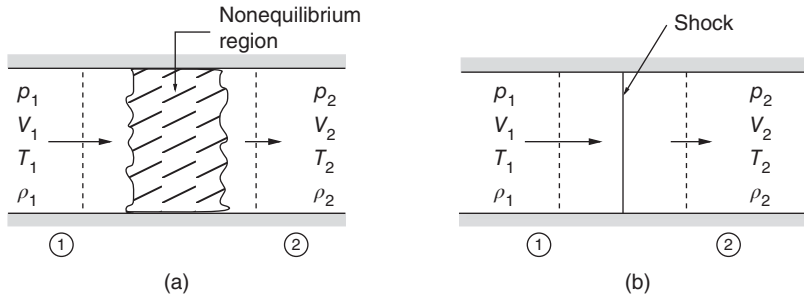
We know from kinetic theory that the flows consist of a large number of fluid molecules in unit volume and the transport of mass, momentum, and energy takes place through the motion of these molecules. Also, the molecules carry the signals about the presence of the cylinder around the flow field at a speed equal to the speed of sound. In Figure 3.1a, the incoming stream is subsonic,  $V_\infty < a_\infty$  and the molecules far upstream of the cylinder get information about the presence of the cylinder through the signals which travel with speed  $a_\infty$ , well before reaching the cylinder. Therefore, the molecules orient themselves in order to flow around the cylinder, as shown in Figure 3.1a. But when the incoming stream is supersonic, the molecules travel faster than the signals and there is no possibility that they will be informed of the presence of the cylinder before they reach it. Also, the reflected signals from the cylinder face tend to coalesce at a short distance ahead of the cylinder. Their coalescence forms a thin compression front called a *shock wave*, as shown in Figure 3.1b. Upstream of the shock, the flow has no information about the presence of the cylinder. However, the streamlines behind the shock quickly compensate for the obstruction, since the flow is subsonic after a detached shock, as shown in the figure. Although the shock formation discussed above is for a specific situation, the mechanism described is, in general, valid. However, we should realize that, when the flow just starts, there is no shock. The formation of shock takes place after the fluid molecules impinge on the cylinder face and rebound.

### 3.2 Equations of Motion for a Normal Shock Wave

For a quantitative analysis of changes across a normal shock wave, let us consider an adiabatic, constant-area flow through a nonequilibrium region, as shown in Figure 3.2a. Let sections 1 and 2 be sufficiently away from the nonequilibrium region so that we can define flow properties at these stations, as shown in Figure 3.2a. Now we can write the equations of motion for the flow considered as follows.



**Figure 3.1** Streamlines around a blunt-faced cylinder in (a) subsonic and (b) supersonic flows.



**Figure 3.2** Flow through a normal shock.

By continuity

$$\rho_1 V_1 = \rho_2 V_2 \quad (3.1)$$

The momentum equation is

$$p_1 + \rho_1 V_1^2 = p_2 + \rho_2 V_2^2 \quad (3.2)$$

The energy equation is

$$h_1 + \frac{1}{2} V_1^2 = h_2 + \frac{1}{2} V_2^2 \quad (3.3)$$

Equations (3.1)–(3.3) are general: they apply to all gases. Also, there is no restriction on the size or details of the nonequilibrium region as long as the reference sections 1 and 2 are outside of it. The solution of these equations gives the relations that must exist between the flow parameters at these two sections.

Since there are no restrictions on the size or details of the nonequilibrium region, it may be idealized as a vanishingly thin region, as shown in Figure 3.2b, across which the flow parameters *jump*. The control sections 1 and 2 may also be brought arbitrarily close to the thin region. Such a compression front across which the flow properties change suddenly is called a *shock wave*. Heat is neither added to nor taken away from the flow as it traverses the shock wave, hence the flow process across the shock wave is adiabatic.

In many textbooks, *shock* is defined as a discontinuity. From our discussions above the question obviously arises: is it possible to have a discontinuity in a continuum flow field of a real fluid? We should realize that the above consideration is only an idealization of the very high gradients of flow properties that actually occur in a shock wave, in the transition from state 1 to state 2. These large gradients produce viscous stress and heat transfer, i.e. nonequilibrium conditions inside the shock. The processes taking place inside the shock wave itself are extremely complex, and cannot be studied on the basis of equilibrium thermodynamics. Temperature and velocity gradients inside the shock provide heat conduction and viscous dissipation that render the flow process inside the shock internally irreversible. In most practical applications, primary interest is not generally focused on the internal mechanism of the shock wave but on the net changes in

fluid properties taking place across the wave. However, there are situations where the detailed information about the flow mechanism inside the shock describing its structure is essential for studying practical problems. But since such conditions occur only in flow regimes like rarefied flow fields, it is not of any interest for the present study. Thus, shock is not a discontinuity but an active continuum compression front causing sudden changes to the flow properties.

### 3.3 The Normal Shock Relations for a Perfect Gas

For a calorically perfect gas, we have the equation of state, namely

$$p = \rho RT \quad (3.4)$$

and the enthalpy is given by

$$h = c_p T \quad (3.5)$$

Equations (3.1)–(3.5) form a set of five equations with five unknowns:  $p_2$ ,  $\rho_2$ ,  $T_2$ ,  $V_2$ , and  $h_2$ . Hence, they can be solved algebraically. In other words, Eqs. (3.1)–(3.3) are the general equations for a normal shock wave, and for a perfect gas it is possible to obtain explicit solutions in terms of Mach number,  $M_1$ , ahead of the shock using Eqs. (3.4) and (3.5) along with Eqs. (3.1)–(3.3), as follows. Dividing Eq. (3.2) by Eq. (3.1), we get

$$\frac{p_1}{\rho_1 V_1} - \frac{p_2}{\rho_2 V_2} = V_2 - V_1 \quad (3.6)$$

Recalling that the speed of sound  $a = \sqrt{\gamma p / \rho}$ , Eq. (3.6) becomes

$$\frac{a_1^2}{\gamma V_1} - \frac{a_2^2}{\gamma V_2} = V_2 - V_1 \quad (3.7)$$

Now,  $a_1^2$  and  $a_2^2$  in Eq. (3.7) may be replaced with an energy equation for a perfect gas as follows.

By energy equation, we have

$$\frac{V_1^2}{2} + \frac{a_1^2}{\gamma - 1} = \frac{V_2^2}{2} + \frac{a_2^2}{\gamma - 1} = \frac{1}{2} \frac{\gamma + 1}{\gamma - 1} a^{*2}$$

From the above relation,  $a_1^2$  and  $a_2^2$  can be expressed as

$$a_1^2 = \frac{\gamma + 1}{2} a^{*2} - \frac{\gamma - 1}{2} V_1^2$$

$$a_2^2 = \frac{\gamma + 1}{2} a^{*2} - \frac{\gamma - 1}{2} V_2^2$$

Because the flow process across the shock wave is adiabatic,  $a^*$  in the above relations for  $a_1^2$  and  $a_2^2$  has the same constant value.

Substituting these relations into Eq. (3.7), we get

$$\begin{aligned} \frac{\gamma + 1}{2} \frac{a^{*2}}{\gamma V_1} - \frac{\gamma - 1}{2\gamma} V_1 - \frac{\gamma + 1}{2} \frac{a^{*2}}{\gamma V_2} + \frac{\gamma - 1}{2\gamma} V_2 &= V_2 - V_1 \\ \frac{\gamma + 1}{2\gamma V_1 V_2} (V_2 - V_1) a^{*2} + \frac{\gamma - 1}{2\gamma} (V_2 - V_1) &= V_2 - V_1 \end{aligned}$$

Dividing this equation by  $(V_2 - V_1)$ , we obtain

$$\frac{\gamma + 1}{2\gamma V_1 V_2} a^{*2} + \frac{\gamma - 1}{2\gamma} = 1$$

This may be solved to result in

$$a^{*2} = V_1 V_2 \quad (3.8)$$

which is called the *Prandtl relation*.

In terms of the speed ratio  $M^* = V/a^*$ , Eq. (3.8) can be expressed as

$$M_2^* = \frac{1}{M_1^*} \quad (3.9)$$

Equation (3.9) implies that the velocity change across a normal shock must be from supersonic to subsonic and vice versa. But, it will be shown later in this section that only the former is possible. Hence, the *Mach number behind a normal shock is always subsonic*. This is a general result, and is not limited just to a calorically perfect gas.

The relation between the characteristic Mach number  $M^*$  and actual Mach number  $M$  is given by Eq. (2.25) as

$$M^{*2} = \frac{(\gamma + 1)M^2}{(\gamma - 1)M^2 + 2} \quad (3.10)$$

Using Eq. (3.10) to replace  $M_1^*$  and  $M_2^*$  in Eq. (3.9), we get

$$M_2^2 = \frac{1 + \frac{\gamma - 1}{2}M_1^2}{\gamma M_1^2 - \frac{\gamma - 1}{2}} \quad (3.11)$$

Equation (3.11) shows that, for a perfect gas, the Mach number behind the shock is a function of only the Mach number  $M_1$  ahead of the shock. It also shows that, when  $M_1 = 1$ ,  $M_2 = 1$ . This is the case of an infinitely weak normal shock, which is identical to a *Mach wave*. It is essential to realize that the Mach waves in a supersonic flow field are at an angle  $\mu = \sin^{-1}(1/M)$ , which is always less than  $\pi/2$ . In other words, a Mach wave is essentially an isentropic wave degenerated to a level that the flow across it will not experience any significant change of property. But, as  $M_1$  increases above 1, the normal shock becomes stronger and  $M_2$  becomes progressively less than 1, and in the limit, as  $M_1 \rightarrow \infty$ ,  $M_2$  approaches a finite minimum value,  $M_2 \rightarrow \sqrt{(\gamma - 1)/2\gamma}$ , which for air (at standard conditions), with  $\gamma = 1.4$  is 0.378.

The ratio of velocities may also be written as

$$\frac{V_1}{V_2} = \frac{V_1^2}{V_1 V_2} = \frac{V_1^2}{a^{*2}} = M_1^{*2} \quad (3.12)$$

Equations (3.10) and (3.12) are useful for the derivation of other normal shock relations.

From Eq. (3.1), we can write

$$\frac{\rho_2}{\rho_1} = \frac{V_1}{V_2} = \frac{(\gamma + 1)M_1^2}{(\gamma - 1)M_1^2 + 2} \quad (3.13)$$

To obtain the pressure ratio across the shock, consider the momentum relation Eq. (3.2)

$$p_2 - p_1 = \rho_1 V_1^2 - \rho_2 V_2^2$$

Which, combined with Eq. (3.1), gives

$$\begin{aligned} p_2 - p_1 &= \rho_1 V_1 (V_1 - V_2) \\ &= \rho_1 V_1^2 \left( 1 - \frac{V_2}{V_1} \right) \end{aligned}$$



Dividing throughout by  $p_1$ , we get

$$\frac{p_2 - p_1}{p_1} = \frac{\rho_1 V_1^2}{p_1} \left( 1 - \frac{V_2}{V_1} \right)$$

Now, recalling  $a_1^2 = (\gamma p_1)/\rho_1$ , we obtain

$$\frac{p_2 - p_1}{p_1} = \gamma M_1^2 \left( 1 - \frac{V_2}{V_1} \right) \quad (3.14)$$

Substituting for  $V_2/V_1$  from Eq. (3.13), we get

$$\frac{p_2 - p_1}{p_1} = \gamma M_1^2 \left[ 1 - \frac{2 + (\gamma - 1)M_1^2}{(\gamma + 1)M_1^2} \right] \quad (3.15)$$

Equation (3.15) may also be written as

$$\boxed{\frac{p_2}{p_1} = 1 + \frac{2\gamma}{\gamma + 1}(M_1^2 - 1)} \quad (3.16)$$

The ratio  $(p_2 - p_1)/p_1 = \Delta p/p_1$  is called the *shock strength*.

The state equation  $p = \rho RT$  can be used to get the temperature ratio. With the state equation, we can write

$$\frac{T_2}{T_1} = \left( \frac{p_2}{p_1} \right) \left( \frac{\rho_1}{\rho_2} \right) \quad (3.17)$$

Substituting Eqs. (3.16) and (3.13) into Eq. (3.17) and, rearranging, we get

$$\frac{T_2}{T_1} = \frac{h_2}{h_1} = \frac{a_2^2}{a_1^2} = 1 + \frac{2(\gamma - 1)}{(\gamma + 1)^2} \frac{(\gamma M_1^2 + 1)}{M_1^2} (M_1^2 - 1) \quad (3.18)$$

By Eq. (1.59), we have

$$s_2 - s_1 = c_p \ln \frac{T_2}{T_1} - R \ln \frac{p_2}{p_1}$$

From Eqs. (3.16) and (3.18),

$$s_2 - s_1 = c_p \ln \left[ 1 + \frac{2(\gamma - 1)}{(\gamma + 1)^2} \frac{\gamma M_1^2 + 1}{M_1^2} (M_1^2 - 1) \right] - R \ln \left( 1 + \frac{2\gamma}{\gamma + 1} (M_1^2 - 1) \right) \quad (3.19)$$

From Eqs. (3.11), (3.13), (3.16), (3.18), and (3.19), it is obvious that, for a perfect gas with a given  $\gamma$ ,  $M_2$ ,  $\rho_2/\rho_1$ ,  $p_2/p_1$ ,  $T_2/T_1$ , and  $(s_2 - s_1)$  are all functions of  $M_1$  only. This explains the importance of Mach number in the quantitative governance of compressible flows. At this stage, we should realize that the simplicity of the above equations arises from the fact that the gas is assumed to be perfect. For high-temperature gas dynamic problems, closed-form expressions such as Eqs. (3.11)–(3.18) are generally not possible and the normal shock properties must be computed numerically. The results of this section hold reasonably accurately up to about  $M_1 = 5$  for air at standard conditions. Beyond Mach 5, the temperature behind the normal shock becomes high enough that the specific heats ratio  $\gamma$  is no longer a constant.

The limiting case of  $M_1 \rightarrow \infty$  can be considered either as  $V_1 \rightarrow \infty$ , where, because of high temperatures, the perfect gas assumption becomes invalid, or as  $a_1 \rightarrow 0$ , where, because of extremely low temperatures, the perfect gas assumption becomes invalid. That is, when  $M_1 \rightarrow \infty$  (either by  $V_1 \rightarrow \infty$  or by  $a \rightarrow 0$ ), the perfect gas assumption is not valid. But, it is

interesting to examine the variation of properties across the normal shock, for this limiting case. When  $M_1 \rightarrow \infty$ , we find, for  $\gamma = 1.4$ ,

$$\begin{aligned}\lim_{M_1 \rightarrow \infty} M_2 &= \sqrt{\frac{\gamma - 1}{2\gamma}} = 0.378 \\ \lim_{M_1 \rightarrow \infty} \frac{\rho_2}{\rho_1} &= \frac{\gamma + 1}{\gamma - 1} = 6 \\ \lim_{M_1 \rightarrow \infty} \frac{p_2}{p_1} &= \infty \\ \lim_{M_1 \rightarrow \infty} \frac{T_2}{T_1} &= \infty\end{aligned}$$

At the other extreme case of an infinitely weak normal shock degenerating into a Mach wave, i.e. at  $M_1 = 1$ , Eqs. (3.11), (3.13), (3.16), and (3.18) yield  $M_2 = \rho_2/\rho_1 = p_2/p_1 = T_2/T_1 = 1$ . That is, when  $M_1 = 1$ , no finite changes occur across the wave.

Equation (3.19) justifies the statement we made earlier that the Prandtl relation, although it is possible for the flow to decelerate from supersonic to subsonic and vice versa across a normal shock wave, only the former is physically feasible. From Eq. (3.19), if  $M_1 = 1$ , then  $\Delta s = 0$ ; if  $M_1 < 1$ ,  $\Delta s < 0$ ; and if  $M_1 > 1$ ,  $\Delta s > 0$ . Therefore, since it is necessary that  $\Delta s \geq 0$  for a physically possible process, from the second law of thermodynamics,  $M_1$  must be greater than or equal to 1. When  $M_1$  is subsonic, the entropy across the wave decreases, which is impossible. Therefore, the only physically possible flow is  $M_1 > 1$ , and from the above results we have  $M_2 < 1$ ,  $\rho_2/\rho_1 > 1$ ,  $p_2/p_1 > 1$ , and  $T_2/T_1 > 1$ .

The changes in flow properties across the shock take place within a very short distance, of the order of  $10^{-5}$  cm. Hence, the velocity and temperature gradients inside the shock structure are very large. These large gradients result in an increase of entropy across the shock. Also, these gradients internal to the shock provide heat conduction and viscous dissipation that render the shock process internally irreversible.

### 3.4 Change of Stagnation or Total Pressure Across a Shock

There is no heat added to or taken away from the flow as it traverses a shock wave, i.e. the flow process across the shock wave is adiabatic. Therefore, the total temperature remains the same ahead of and behind the wave,

$$T_{02} = T_{01} \quad (3.20)$$

Now, it is important to note that Eq. (3.20), valid for a perfect gas, is a special case of the more general result that the total enthalpy is constant across a normal shock, as given by Eq. (3.3). For a stationary normal shock, the total enthalpy is always constant across the wave, which, for calorically or thermally perfect gases, translates into a constant total temperature across the shock. However, for a chemically reacting gas, the total temperature is not constant across the shock. Also, *if the shock wave is not stationary (i.e. for a moving shock), neither the total enthalpy nor the total temperature is constant across the shock wave.*

For an adiabatic process of a perfect gas, by Eq. (1.76), we have

$$s_{02} - s_{01} = R \ln \frac{p_{01}}{p_{02}}$$

In the above equation, all the quantities are expressed as stagnation quantities. It is seen from the equation that the entropy varies only when there are losses in pressure. It is independent of

velocity and hence there is nothing like stagnation entropy. Therefore, the entropy difference between states 1 and 2 is expressed, without any reference to the velocity level, as

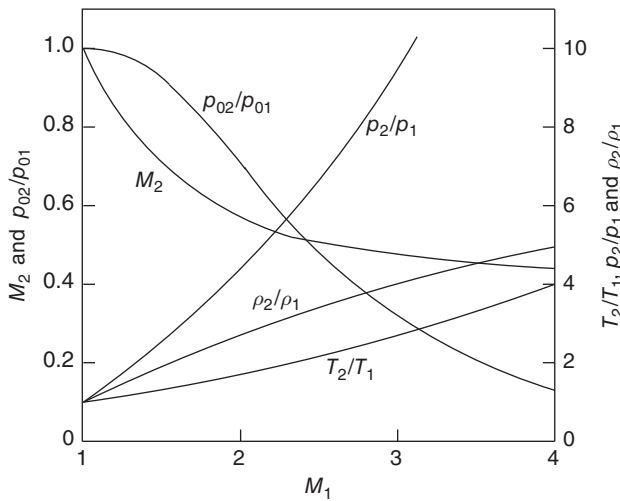
$$s_2 - s_1 = R \ln \frac{p_{01}}{p_{02}} \quad (3.21)$$

The exact expression for the ratio of total pressure may be obtained from Eqs. (3.21) and (3.19) as

$$\frac{p_{02}}{p_{01}} = \left( 1 + \frac{2\gamma}{\gamma+1}(M_1^2 - 1) \right)^{-1/(\gamma-1)} \left\{ \frac{(\gamma+1)M_1^2}{(\gamma-1)M_1^2 + 2} \right\}^{\gamma/(\gamma-1)} \quad (3.22)$$

Equation (3.22) is an important and useful equation, since it connects the stagnation pressures on either side of a normal shock to flow Mach number ahead of the shock. Also, we can see the usefulness of Eq. (3.22) from the application aspect. When a pitot probe is placed in a supersonic flow facing the flow, there would be a detached shock standing ahead of the probe's nose and, therefore, the probe measures the total pressure behind that detached shock. However, the portion of the shock ahead of a pitot probe's mouth can be approximated as a normal shock. Thus, what a pitot probe facing a supersonic flow measures is the total pressure  $p_{02}$  behind a normal shock. Knowing the stagnation pressure ahead of the shock, which is the pressure in the reservoir, for isentropic flow up to the shock, we can determine the flow Mach number ahead of the shock with Eq. (3.22).

The variation of  $p_2/p_1$ ,  $\rho_2/\rho_1$ ,  $T_2/T_1$ ,  $p_{02}/p_{01}$ , and  $M_2$  with  $M_1$  as obtained from the above equations are tabulated in Table A.2 in the Appendix. These variations are also given in graphical form in Figure 3.3. From the figure it can be seen that, as  $M_1$  becomes very large,  $T_2/T_1$  and  $p_2/p_1$  also become very large, whereas  $\rho_2/\rho_1$  and  $M_2$  approach finite limits, as already stated. However, the rate of increase of  $p_2/p_1$  is significantly greater than the rate of increase of  $\rho_2/\rho_1$  and  $T_2/T_1$ . It is seen from Figure 3.3 that, at  $M = 4$ ,  $T_2/T_1 \approx 4$  whereas  $\rho_2/\rho_1 = 4.57$ . However, the temperature ratio continues to increase with increase of  $M_1$  but the density ratio becomes 6 when  $M_1 \rightarrow \infty$ . Further, it is seen that the  $p_{02}/p_{01}$  across a normal shock decreases steeply with an increase of the upstream Mach number  $M_1$ . This clearly reveals that the total pressure loss  $(p_{01} - p_{02})/p_{01}$  caused by a normal shock increases with an increase of  $M_1$ . At this stage it



**Figure 3.3** Properties behind a normal shock wave as a function of upstream Mach number.

is essential to note that, what is meant by *pressure loss* is the total pressure loss, and there is no such thing as static pressure loss.

### Example 3.1

If the flow Mach number, pressure, and temperature ahead of a normal shock are 2.0, 0.5 atm, and 300 K, respectively, determine  $M_2$ ,  $p_2$ ,  $T_2$ , and  $V_2$  behind the wave.

#### Solution:

From the normal shock table (Table A.2) for  $M_1 = 2.0$ ,

$$\frac{p_2}{p_1} = 4.5, \frac{T_2}{T_1} = 1.687, M_2 = \boxed{0.5774}$$

Therefore,

$$p_2 = (4.500)(0.5) = \boxed{2.250 \text{ atm}}$$

$$T_2 = (1.687)(300) = \boxed{506.1 \text{ K}}$$

For  $T_2 = 506.1 \text{ K}$  the speed of sound  $a_2 = \sqrt{\gamma RT_2}$ , i.e.

$$a_2 = \sqrt{1.4 \times 287 \times 506.1} = 450.94 \text{ m s}^{-1}$$

Thus,

$$V_2 = M_2 a_2 = (0.5774)(450.94) = \boxed{260.37 \text{ m s}^{-1}}$$

### Example 3.2

A re-entry vehicle (RV) is at an altitude of 15 000 m and has a velocity of  $1850 \text{ m s}^{-1}$ . A bow shock wave envelops the RV. Neglecting dissociation, determine the static pressure and temperature and the stagnation pressure and temperature just behind the shock wave on the RV center line where the shock wave may be treated as a normal shock. Assume that the air behaves as perfect gas, with  $\gamma = 1.4$  and  $R = 287 \text{ J (kg K)}^{-1}$ .

#### Solution:

Let subscripts 1 and 2 refer to conditions before and after the shock. At 15 000 m altitude [3]

$$p_1 = 1.2108 \times 10^4 \text{ N m}^{-2}, T_1 = -56.5^\circ \text{C} = 216.5 \text{ K}$$

The speed of sound ahead of the shock is

$$a_1 = \sqrt{\gamma RT_1} = 295 \text{ m s}^{-1}$$

Therefore,

$$M_1 = \frac{V_1}{a_1} = 6.27$$

By the Rayleigh supersonic pitot relation (Section 2.9),

$$\frac{p_1}{p_{02}} = \frac{\left( \frac{2\gamma}{\gamma+1} M_1^2 - \frac{\gamma-1}{\gamma+1} \right)^{1/(\gamma-1)}}{\left( \frac{\gamma+1}{2} M_1^2 \right)^{\gamma/(\gamma-1)}} = \frac{1}{51.08}$$

$$p_{02} = 51.08 p_1 = \boxed{6.18 \times 10^5 \text{ Pa}}$$

$$T_{01} = T_{02} = T_1 \left( 1 + \frac{\gamma-1}{2} M_1^2 \right) \text{ from isentropic relation}$$

$$T_{01} = T_{02} = 216.5(1 + 0.2M_1^2)$$

$$= \boxed{1918.75 \text{ K}}$$

By Eq. (3.16),

$$\frac{p_2}{p_1} = 1 + \frac{2\gamma}{\gamma+1}(M_1^2 - 1) = 45.7$$

Therefore,

$$p_2 = 45.7p_1$$

$$= \boxed{5.53 \times 10^5 \text{ Pa}}$$

By Eq. (3.18),

$$\frac{T_2}{T_1} = 1 + \frac{2(\gamma-1)}{(\gamma+1)^2} \frac{\gamma M_1^2 + 1}{M_1^2} (M_1^2 - 1) = 8.63$$

Thus,

$$T_2 = \boxed{1868.4 \text{ K}}$$

### 3.5 Hugoniot Equation

As already discussed, the static pressure always increases across a shock wave; therefore, the shock can be visualized as a thermodynamic device which compresses the gas. With this consideration, the changes across a normal shock wave can be expressed purely in terms of thermodynamic variables, without explicit reference to a velocity or Mach number, as follows. By the continuity Eq. (3.1),

$$V_2 = V_1 \left( \frac{\rho_1}{\rho_2} \right) \quad (3.23)$$

Substituting Eq. (3.23) into Eq. (3.2), we get

$$p_1 + \rho_1 V_1^2 = p_2 + \rho_2 \left( \frac{\rho_1}{\rho_2} V_1 \right)^2 \quad (3.24)$$

Solving Eq. (3.24) for  $V_1^2$ , we obtain

$$V_1^2 = \frac{p_2 - p_1}{\rho_2 - \rho_1} \left( \frac{\rho_2}{\rho_1} \right) \quad (3.25)$$

Also, substituting  $V_1 = V_2(\rho_2/\rho_1)$  from Eq. (3.1) into Eq. (3.2) and solving for  $V_2$ , we get

$$V_2^2 = \frac{p_2 - p_1}{\rho_2 - \rho_1} \left( \frac{\rho_1}{\rho_2} \right) \quad (3.26)$$

Replacing  $h$  by  $\left( e + \frac{p}{\rho} \right)$  in the energy Eq. (3.3), we obtain

$$e_1 + \frac{p_1}{\rho_1} + \frac{V_1^2}{2} = e_2 + \frac{p_2}{\rho_2} + \frac{V_2^2}{2} \quad (3.27)$$

Substituting for  $V_1$  and  $V_2$  from Eqs. (3.25) and (3.26) into Eq. (3.27), we get

$$e_1 + \frac{p_1}{\rho_1} + \frac{1}{2} \left( \frac{p_2 - p_1}{\rho_2 - \rho_1} \right) \left( \frac{\rho_2}{\rho_1} \right) = e_2 + \frac{p_2}{\rho_2} + \frac{1}{2} \left( \frac{p_2 - p_1}{\rho_2 - \rho_1} \right) \left( \frac{\rho_1}{\rho_2} \right) \quad (3.28)$$

On simplification, Eq. (3.28) yields

$$e_2 - e_1 = \frac{p_1 + p_2}{2} \left( \frac{1}{\rho_1} - \frac{1}{\rho_2} \right) \quad (3.29)$$

Replacing  $\rho_1$  and  $\rho_2$  in Eq. (3.29) by specific volumes  $v_1$  and  $v_2$ , we obtain

$$e_2 - e_1 = \frac{p_1 + p_2}{2} (v_1 - v_2) \quad (3.30)$$

Equation (3.30) is called a *Hugoniot equation*. It has certain advantages because it relates only thermodynamic quantities across the shock. Also, since there was no assumption made about the type of gas in deriving Eq. (3.30), it is a general relation that holds for a perfect gas, real gas, chemically reacting gas, etc. Further, the form of Eq. (3.30),  $\Delta e = -p_{\text{ave}} \Delta v$ , implies that the change in internal energy is equal to the mean pressure across the shock times the change in specific volume, and this strongly reminds us of the first law of thermodynamics in the form of Eq. (1.25), with  $\delta q = 0$  for an adiabatic process across the shock.

We know that in equilibrium thermodynamics any state variable can be expressed as a function of any other two state variables. Therefore, the specific energy  $e$  can be expressed as

$$e = e(p, v)$$

Substituting this into Eq. (3.30), we get

$$p_2 = f(p_1, v_1, v_2) \quad (3.31)$$

For given  $p_1$  and  $v_1$ , Eq. (3.31) represents  $p_2$  as a function of  $v_2$ . A plot of this relation on a  $p$ - $v$  diagram is called the *Hugoniot curve*, shown in Figure 3.4. This curve is the locus of all possible pressure volume conditions behind normal shocks of different strength for a given set of upstream values for  $p_1$  and  $v_1$  (point 1 in Figure 3.4). Therefore, each point on the Hugoniot curve in Figure 3.4 corresponds to a shock with a specific upstream velocity  $V_1$ .

Now, choosing a specific shock with a specific upstream velocity  $V_1$ , we can locate the specific point on the Hugoniot curve, point 2, which corresponds to this particular shock, as follows. Replacing  $1/\rho$  by  $v$  in Eq. (3.25), we get

$$V_1^2 = \frac{p_2 - p_1}{1/v_1 - 1/v_2} \left( \frac{v_1}{v_2} \right)$$

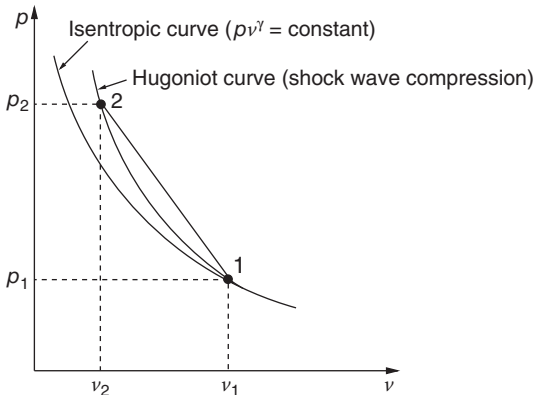


Figure 3.4 Hugoniot curve.

This equation may be expressed as

$$\frac{p_2 - p_1}{v_2 - v_1} = - \left( \frac{V_1}{v_1} \right)^2 \quad (3.32)$$

In Eq. (3.32), the left-hand side gives the slope of the straight line through points 1 and 2 in Figure 3.4. The right-hand side is a known value, given by the upstream velocity and the specific volume. That is, Eq. (3.32) connects the geometry of the Hugoniot curve to the flow velocity and specific volume upstream of the shock. Further, for calorically perfect gas, it is possible to write Eq. (3.30) as

$$\frac{p_2}{p_1} = \frac{\left( \frac{\gamma + 1}{\gamma - 1} \right) \left( \frac{v_1}{v_2} \right) - 1}{\left( \frac{\gamma + 1}{\gamma - 1} \right) - \left( \frac{v_1}{v_2} \right)}$$

noting  $e = c_v T$  and  $T = pv/R$ .

### 3.5.1 Moving Shocks

We are familiar with the fact that a moving body in a flow field creates disturbances and these disturbances propagate throughout the flow field. The motion of these disturbances relative to the fluid is called *wave motion*. The speed of propagation of the disturbances is termed *wave speed*. Through these waves only the various parts of the body interact with the fluid and with each other, and by which the forces on the body are established.

For our discussion, let us consider the case of the one-dimensional motion of a shock wave in a tube of constant area. These waves are called *plane waves*. Since this sort of wave may be generated by the motion of a piston in a tube, it is also referred to as a *piston problem*.

## 3.6 The Propagating Shock Wave

The study of equations of motion for a normal shock wave in Section 3.2 assumed the shock to be stationary, as shown in Figure 3.5a. The fluid flows through the shock with velocity  $V_1$ . We may say that, relatively, the shock is propagating through the fluid with speed  $V_1$ . Let us call this shock speed  $C_s$ . This situation is shown in Figure 3.5b, where the shock is moving with speed  $C_s$  and the fluid ahead of it is at rest. Therefore, we have

$$C_s = V_1 \quad (3.33a)$$

The fluid behind the shock wave is following the shock with speed

$$V_p = V_1 - V_2 \quad (3.33b)$$

For the stationary normal shock wave shown in Figure 3.5a, we know from Eqs. (3.1)–(3.3) that the continuity, momentum, and energy equations, respectively, are

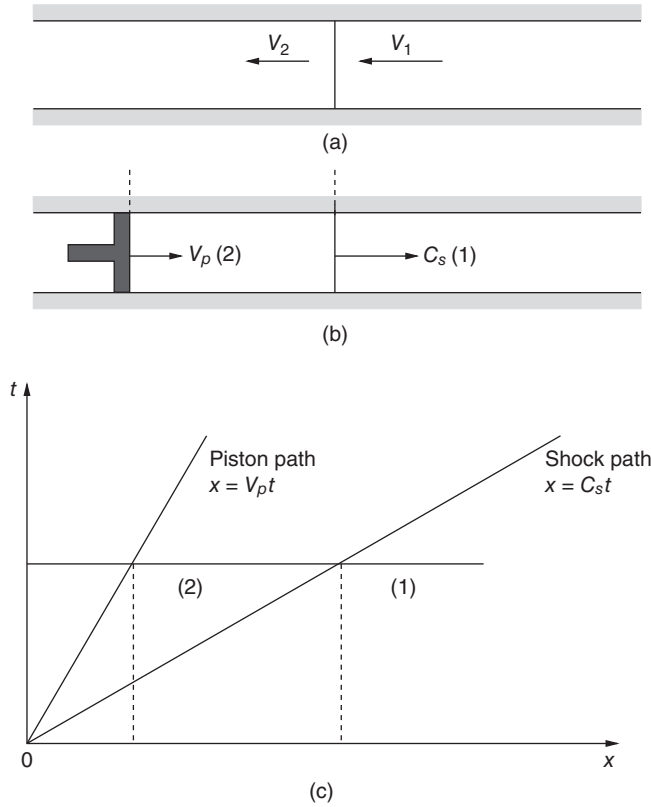
$$\rho_1 V_1 = \rho_2 V_2 \quad (3.1)$$

$$p_1 + \rho_1 V_1^2 = p_2 + \rho_2 V_2^2 \quad (3.2)$$

$$h_1 + \frac{V_1^2}{2} = h_2 + \frac{V_2^2}{2} \quad (3.3)$$

From Figure 3.5c, it can be seen that

- $V_1$  = velocity of the fluid ahead of the shock wave, relative to the wave.
- $V_2$  = velocity of the fluid behind the shock wave, relative to the wave.



**Figure 3.5** Stationary and moving shock waves.

Equations (3.1)–(3.3) always hold for flow velocities relative to the shock wave, whether the shock is stationary or moving. Therefore, from Figure 3.5b, we deduce from the geometry of a moving shock that

- $C_s$  = velocity of the gas ahead of the shock wave, relative to the wave.
- $C_s - V_p$  = velocity of the gas behind the shock wave, relative to the wave.

It may be assumed that the fluid behind the shock wave is followed by a driving piston, moving at the speed  $V_p$ , as illustrated in Figure 3.5b. In Figure 3.5c, the position time diagram of piston and shock wave is illustrated. At time  $t = 0$  the piston is started impulsively with speed  $V_p$ . It establishes a shock which runs ahead at the speed  $C_s$ . The pressure on the piston face is  $p_2$ . The region of compressed fluid between the shock wave and piston increases in length at the rate  $(C_s - V_p)$ . Therefore, the normal shock continuity, momentum, and energy equations, namely Eqs. (3.1)–(3.3), for the moving shock wave, shown in Figure 3.5b, become

$$\rho_1 C_s = \rho_2 (C_s - V_p) \quad (3.34)$$

$$p_1 + \rho_1 C_s^2 = p_2 + \rho_2 (C_s - V_p)^2 \quad (3.35)$$

$$h_1 + \frac{C_s^2}{2} = h_2 + \frac{(C_s - V_p)^2}{2} \quad (3.36)$$

Equations (3.34)–(3.36) are the governing normal shock equations for a shock moving with velocity  $C_s$  into a stagnant gas.



For convenience, the above equations may be rearranged as follows. From Eq. (3.34), we get

$$C_s - V_p = C_s \left( \frac{\rho_1}{\rho_2} \right) \quad (3.37)$$

Substitution of Eq. (3.37) into (3.35) yields

$$\begin{aligned} p_1 + \rho_1 C_s^2 &= p_2 + \rho_2 C_s^2 \left( \frac{\rho_1}{\rho_2} \right)^2 \\ p_2 - p_1 &= \rho_1 C_s^2 \left( 1 - \frac{\rho_1}{\rho_2} \right) \\ C_s^2 &= \frac{p_2 - p_1}{\rho_1 (1 - \rho_1/\rho_2)} \end{aligned}$$

Solving, we get

$$C_s^2 = \frac{p_2 - p_1}{\rho_2 - \rho_1} \left( \frac{\rho_2}{\rho_1} \right) \quad (3.38)$$

Equation (3.34) can also be expressed as

$$C_s = (C_s - V_p) \left( \frac{\rho_2}{\rho_1} \right) \quad (3.39)$$

Substituting Eq. (3.39) into Eq. (3.38), we get

$$(C_s - V_p)^2 \left( \frac{\rho_2}{\rho_1} \right)^2 = \frac{p_2 - p_1}{\rho_1 - \rho_2} \left( \frac{\rho_2}{\rho_1} \right)$$

that is

$$(C_s - V_p)^2 = \frac{p_2 - p_1}{\rho_2 - \rho_1} \left( \frac{\rho_1}{\rho_2} \right) \quad (3.40)$$

Substitution of Eqs. (3.38) and (3.40) into relation (3.36), with  $h = e + p/\rho$ , results in

$$e_1 + \frac{p_1}{\rho_1} + \frac{1}{2} \left[ \frac{p_2 - p_1}{\rho_2 - \rho_1} \left( \frac{\rho_2}{\rho_1} \right) \right] = e_2 + \frac{p_2}{\rho_2} + \frac{1}{2} \left[ \frac{p_2 - p_1}{\rho_2 - \rho_1} \left( \frac{\rho_1}{\rho_2} \right) \right] \quad (3.41)$$

On simplification, Eq. (3.41) reduces to

$$e_2 - e_1 = \frac{p_1 + p_2}{2} \left( \frac{1}{\rho_1} - \frac{1}{\rho_2} \right)$$

or

$$\boxed{e_2 - e_1 = \frac{p_1 + p_2}{2} (v_1 - v_2)} \quad (3.42)$$

Equation (3.42) is the Hugoniot equation and is identically the same as Eq. (3.30) for stationary shock. This is naturally expected, since the Hugoniot equation relates changes of thermodynamic variables across a normal shock wave and these are physically independent of shock motion.

In general, Eqs. (3.34)–(3.36) must be solved numerically. However, for the special case of calorically perfect gas with  $e = c_v T$  and  $v = RT/p$ , Eq. (3.42) becomes

$$\frac{T_2}{T_1} = \frac{p_2}{p_1} \left( \frac{\frac{\gamma+1}{\gamma-1} + \frac{p_2}{p_1}}{1 + \frac{\gamma+1}{\gamma-1} \frac{p_2}{p_1}} \right) \quad (3.43)$$

Similarly, density ratio  $\rho_2/\rho_1$  becomes

$$\frac{\rho_2}{\rho_1} = \frac{1 + \frac{\gamma + 1}{\gamma - 1} \frac{p_2}{p_1}}{\frac{\gamma + 1}{\gamma - 1} + \frac{p_2}{p_1}} \quad (3.44)$$

The temperature ratio and density ratio across a moving shock wave are given as functions of the pressure ratio. Unlike a stationary shock wave where it is conventional to think of Mach number  $M_1$ , upstream of a shock wave as the governing parameter for changes across the wave, for a moving shock wave it now becomes convenient to keep  $p_2/p_1$  as the basic parameter governing changes across the wave.

Now, even the moving shock Mach number  $M_s$  is defined as

$$M_s = \frac{C_s}{a_1}$$

where  $a_1^2 = (dp/d\rho)_1$  can also be expressed in terms of  $p_2/p_1$ .

With Eq. (3.16) to relate  $p_2/p_1$  to the Mach number, the shock velocity for a perfect gas can be expressed as

$$C_s = a_1 \sqrt{\frac{\gamma + 1}{2\gamma} \left( \frac{p_2}{p_1} - 1 \right) + 1} \quad (3.45)$$

Equation (3.45) is important; it relates the wave velocity of the moving shock wave to the pressure ratio across the wave and the *speed of sound* in the gas into which the wave is moving. The fluid velocity behind the shock is

$$V_p = V_1 - V_2 = C_s \left( 1 - \frac{V_2}{V_1} \right)$$

or

$$V_p = C_s \left( 1 - \frac{\rho_1}{\rho_2} \right)$$

because  $\frac{\rho_1}{\rho_2} = \frac{V_2}{V_1}$  from continuity. Substituting Eqs. (3.44) and (3.45) for density ratio and shock speed in the equation for  $V_p$ , we get

$$V_p = \frac{a_1}{\gamma} \left( \frac{p_2}{p_1} - 1 \right) \left( \frac{\frac{2\gamma}{\gamma + 1}}{\frac{p_2}{p_1} + \frac{\gamma - 1}{\gamma + 1}} \right)^{1/2} \quad (3.46)$$

It can be seen from Eq. (3.46) that, like the shock velocity  $C_s$ , the fluid velocity behind the shock, which is sometimes called a *mass-motion velocity*  $V_p$ , also depends on the pressure ratio across the shock wave and the speed of sound ahead of the wave.

Now let us study the above jump relations and shock speed and mass-motion velocity for the moving shock wave for the extreme cases of weak and strong shocks.

### Example 3.3

Consider a shock of strength 0.382 generated by a piston which moves in a cylinder with still air at 300 K. Determine the shock speed and the piston speed.

**Solution:**

Given,  $\Delta p/p_1 = 0.382$ ,  $T_1 = 300$  K, where subscripts 1 and 2 respectively refer to the states ahead of and behind the shock.

Therefore,

$$\begin{aligned}\frac{p_2 - p_1}{p_1} &= 0.382 \\ \frac{p_2}{p_1} - 1 &= 0.382 \\ \frac{p_2}{p_1} &= 1.382 \\ a_1 &= \sqrt{1.4 \times 287 \times 300} \\ &= 347.19 \text{ m s}^{-1}\end{aligned}$$

By Eq. (3.16),

$$\begin{aligned}\frac{p_2}{p_1} &= 1 + \frac{2\gamma}{\gamma + 1}(M_s^2 - 1) \\ M_s^2 - 1 &= \left(\frac{p_2}{p_1} - 1\right) \times \frac{\gamma + 1}{2\gamma} \\ &= 0.382 \times \frac{2.4}{2.8} \\ &= 0.3274 \\ M_s &= \sqrt{1.3274} \\ &= 1.152\end{aligned}$$

Therefore,

$$\begin{aligned}C_s &= M_s a_1 = 1.152 \times 347.19 \\ &= \boxed{400 \text{ m s}^{-1}}\end{aligned}$$

By Eq. (3.46)

$$\begin{aligned}V_p &= \frac{a_1}{\gamma} \left(\frac{p_2}{p_1} - 1\right) \left[ \frac{\frac{2\gamma}{\gamma + 1}}{\frac{p_2}{p_1} + \frac{\gamma - 1}{\gamma + 1}} \right]^{1/2} \\ &= \frac{347.19}{1.4} \times 0.382 \times \left[ \frac{2.8/2.4}{1.382 + 0.4/2.4} \right]^{1/2} \\ &= 248 \times 0.382 \times \left[ \frac{1.167}{1.549} \right]^{1/2} \\ &= \boxed{82.23 \text{ m s}^{-1}}\end{aligned}$$

The piston speed is also given by

$$V_p = C_s \left(1 - \frac{\rho_1}{\rho_2}\right)$$

By Eq. (3.44)

$$\begin{aligned}
 \frac{\rho_2}{\rho_1} &= \frac{1 + \frac{\gamma + 1}{\gamma - 1} \frac{p_2}{p_1}}{\frac{\gamma + 1}{\gamma - 1} + \frac{p_2}{p_1}} \\
 &= \frac{1 + \frac{2.4}{0.4} \times 1.382}{\frac{2.4}{0.4} + 1.382} \\
 &= \frac{9.292}{7.382} \\
 &= 1.2587
 \end{aligned}$$

Thus,

$$\begin{aligned}
 V_p &= C_s \left( 1 - \frac{1}{1.2587} \right) \\
 &= 400 \times 0.20553 \\
 &= \boxed{82.21 \text{ m s}^{-1}}
 \end{aligned}$$

### 3.6.1 Weak Shock

A weak shock is that for which the pressure jump across it is very small. In other words, a weak shock is that for which the normalized *pressure jump is very small*, i.e.

$$\frac{\Delta p}{p_1} = \frac{p_2 - p_1}{p_1} \ll 1$$

where  $p_1$  and  $p_2$  are the pressures ahead of and behind the shock, respectively. The other property's jumps are then correspondingly small. The temperature and density jump across a weak shock in terms of the normalized pressure jump  $\frac{\Delta p}{p_1}$  can be expressed, by expanding Eqs. (3.43) and (3.44) as a series and retaining only the first-order terms in  $\Delta p/p_1$ , as

$$\frac{\Delta T}{T_1} \approx \frac{\gamma - 1}{\gamma} \frac{\Delta p}{p_1} \quad (3.47a)$$

$$\frac{\Delta \rho}{\rho_1} \approx \frac{1}{\gamma} \frac{\Delta p}{p_1} \approx \frac{V_p}{a_1} \quad (3.47b)$$

Similarly, from Eq. (3.45), we get the shock speed in terms of the pressure jump as

$$C_s \approx a_1 \left( 1 + \frac{\gamma + 1}{4\gamma} \frac{\Delta p}{p_1} \right) \quad (3.47c)$$

Note from Eq. (3.47c) that the speed of very weak shocks is nearly equal to the speed of sound  $a_1$  in the flow field upstream of the shock.

### Example 3.4

A weak shock is generated by a piston in a tube containing still air at 300 K. If the temperature of the air traversed by the shock is 5% more than the initial temperature, determine the piston speed and the shock Mach number.

**Solution:**

Given,  $T_1 = 300 \text{ K}$ ,  $T_2 = 1.05 T_1$ .

By Eq. (3.47a),

$$\begin{aligned}\frac{\Delta T}{T} &\approx \frac{\gamma - 1}{\gamma} \frac{\Delta p}{p_1} \\ \frac{T_2 - T_1}{T_1} &= \frac{1.4 - 1}{1.4} \frac{\Delta p}{p_1} \\ \frac{T_2}{T_1} - 1 &= \frac{1.4 - 1}{1.4} \frac{\Delta p}{p_1} \\ 1.05 - 1 &= \frac{0.4}{1.4} \frac{\Delta p}{p_1} \\ \frac{\Delta p}{p_1} &= \frac{1.4 \times 0.05}{0.4} \\ \frac{p_2 - p_1}{p_1} &= 0.175 \\ \frac{p_2}{p_1} &= 1.175\end{aligned}$$

By Eq. (3.47b),

$$\begin{aligned}\frac{V_p}{a_1} &\approx \frac{1}{\gamma} \frac{\Delta p}{p_1} \\ &= \frac{1}{1.4} \times 0.175 \\ &= 0.125 \\ V_p &= 0.125 \sqrt{\gamma R T_1} \\ &= 0.125 \times \sqrt{1.4 \times 287 \times 300} \\ &= \boxed{43.4 \text{ m s}^{-1}}\end{aligned}$$

By Eq. (3.47c),

$$\begin{aligned}C_s &\approx a_1 \left( 1 + \frac{\gamma + 1}{4\gamma} \frac{\Delta p}{p_1} \right) \\ &= \sqrt{1.4 \times 287 \times 300} \times \left( 1 + \frac{2.4}{4 \times 1.4} \times 0.175 \right) \\ &= 373.23 \text{ m s}^{-1}\end{aligned}$$

The shock Mach number is

$$\begin{aligned}M_s &= \frac{C_s}{a_1} \\ &= \frac{373.23}{347.19} \\ &= \boxed{1.075}\end{aligned}$$

### 3.6.2 Strong Shock

A strong shock is one for which  $p_2/p_1$  is very large. It may also be stated that a strong shock is that with very large upstream Mach numbers (i.e.  $M_1 \rightarrow \infty$ ). For this case we can show that

$$\frac{T_2}{T_1} \rightarrow \frac{\gamma - 1}{\gamma + 1} \frac{p_2}{p_1} \quad (3.48a)$$

$$\frac{\rho_2}{\rho_1} \rightarrow \frac{\gamma + 1}{\gamma - 1} \quad (3.48b)$$

$$C_s \rightarrow a_1 \left( \frac{\gamma + 1}{2\gamma} \frac{p_2}{p_1} \right)^{1/2} \quad (3.48c)$$

$$V_p \rightarrow a_1 \left( \frac{2}{\gamma(\gamma + 1)} \frac{p_2}{p_1} \right)^{1/2} \quad (3.48d)$$

It is interesting to note that for a strong shock the temperature ratio  $T_2/T_1$  across the shock, the shock speed  $C_s$ , and the piston speed  $V_p$  also become very large. Indeed, when the flow Mach number  $M_1$  ahead of the shock tends to  $\infty$ , these parameters also tend to  $\infty$ . But the density ratio  $\rho_2/\rho_1$ , as seen from Eq. (3.48b), becomes only  $(\gamma + 1)/(\gamma - 1)$  even when  $M_1 \rightarrow \infty$ . For air with specific heats ratio  $\gamma = 1.4$ , the density ratio becomes 6 when  $M_1 \rightarrow \infty$ . A closer look at this limit would reveal many interesting facts about gas dynamic flow physics. Even though the range of the density ratio across a shock is narrow (only from 0 to 6), it plays the most dominant role than the pressure and temperature ratios, whose theoretical range is from 0 to  $\infty$ , in practical applications. For example, when a flying machine keeps gaining altitude, the pressure, temperature, and density of the atmosphere fall continuously. Above a certain altitude, the continuum hypothesis becomes invalid. From such an altitude onwards, we need to look at the ratio of the mean free path,  $\lambda$ , and a characteristic geometric parameter, say  $D$ , termed the *Knudsen number*,  $Kn$ , to characterize the nature of the flow. The continuum hypothesis is valid till  $Kn < 0.01$ . When  $Kn > 0.01$  the flow transits to a regime where the number of gas molecules prevailing in unit volume is not sufficient to represent the state with two average thermodynamic properties such as  $p$ ,  $T$ , and  $\rho$ . The transition regime continues up to  $Kn \approx 0.1$ . When  $Kn > 0.1$ , the intermolecular collisions become rare and the flow regime is termed *nearly free molecular*, emphasizing that the gas molecules are almost free to move without encountering intermolecular collision. This continues till  $Kn \approx 1$ . When  $Kn > 1$  the molecules rarely encounter any intermolecular collision and the flow is termed *free molecular flow*. In the transition, nearly free molecular, and free molecular regimes of flow, even though the pressure is very low, the flow is not referred to by the pressure. The regime of flow encompassing the transition, nearly free molecular, and free molecular regimes is called *rarefied gas dynamics* or *low-density flow*, in terms of density. This is because the momentum parameter  $p$  is less significant than the density  $\rho$  in this field. Because of this, even the Mach number loses its importance in low-density flows and the Knudsen number  $Kn$  becomes the dominant parameter. Thus, even though a narrow range parameter, density plays a dominant role, beginning from continuum gas dynamics to rarefied flows, whereas pressure is dominant only in the continuum regime of flow.

#### Example 3.5

If a strong shock of strength 60 is to be generated by piston motion in a cylinder filled with nitrogen gas at 290 K, (a) what should be the piston speed? (b) What will be the static temperature behind the shock? (c) What will be the Mach number behind the shock, if the field traversed by this strong shock is assumed to be isentropic with specific heats ratio  $\gamma = 1.4$ ?

**Solution:**

Given,  $\frac{\Delta p}{p_1} = 60$ ,  $T_1 = 290$  K.

The pressure ratio across the shock is

$$\begin{aligned}\frac{\Delta p}{p_1} &= 60 \\ \frac{p_2 - p_1}{p_1} &= 60 \\ \frac{p_2}{p_1} - 1 &= 60 \\ \frac{p_2}{p_1} &= 61\end{aligned}$$

For nitrogen gas, the gas constant is

$$\begin{aligned}R &= \frac{R_u}{28} \\ &= \frac{8314}{28} \\ &= 296.93 \text{ m}^2 (\text{s}^2 \text{ K})^{-1}\end{aligned}$$

The speed of sound in the undisturbed zone is

$$\begin{aligned}a_1 &= \sqrt{\gamma R T_1} \\ &= \sqrt{1.4 \times 296.93 \times 290} \\ &= 347.21 \text{ m s}^{-1}\end{aligned}$$

(a) The piston speed for a strong shock, by Eq. (3.48d), is

$$\begin{aligned}V_p &= a_1 \sqrt{\frac{2}{\gamma(\gamma+1)} \frac{p_2}{p_1}} \\ &= 347.21 \times \sqrt{\frac{2}{1.4 \times 2.4} \times 61} \\ &= \boxed{2092.2 \text{ m s}^{-1}}\end{aligned}$$

(b) The temperature across the shock, by Eq. (3.48a), is

$$\begin{aligned}\frac{T_2}{T_1} &= \frac{\gamma-1}{\gamma+1} \frac{p_2}{p_1} \\ &= \frac{0.4}{2.4} \times 61 \\ &= 10.17 \\ T_2 &= 10.17 \times 290 \\ &= \boxed{2949.3 \text{ K}}\end{aligned}$$

(c) By Eq. (3.48c)

$$\begin{aligned}C_s &= a_1 \sqrt{\frac{\gamma+1}{2\gamma} \frac{p_2}{p_1}} \\ &= 347.21 \times \sqrt{\frac{2.4}{2.8} \times 61} \\ &= 2510.64 \text{ m s}^{-1}\end{aligned}$$

Assuming the nitrogen behind the shock to be a perfect gas, we have the speed of sound behind the shock as

$$\begin{aligned} a_2 &= \sqrt{\gamma RT_2} \\ &= \sqrt{1.4 \times 296.93 \times 2949.3} \\ &= 1107.26 \text{ m s}^{-1} \end{aligned}$$

The Mach number behind the shock is

$$\begin{aligned} M_2 &= \frac{V_2}{a_2} \\ &= \frac{C_s - V_p}{a_2} \\ &= \frac{2510.64 - 2092.2}{1107.26} \\ &= \frac{418.44}{1107.26} \\ &= \boxed{0.378} \end{aligned}$$

Note that this Mach number is the limiting value for  $M_1 \rightarrow \infty$ .

### Example 3.6

A normal shock moves in a constant area tube, as shown in Figure 3.6a. In region 1,  $V_1 = 100 \text{ m s}^{-1}$ ,  $T_1 = 30^\circ \text{C}$ , and  $p_1 = 0.7 \text{ atm}$ . Shock speed  $C_s$  with respect to a fixed coordinate system is  $600 \text{ m s}^{-1}$ . Find fluid properties in region 2.

### Solution:

Referring to a coordinate system which is moving at velocity  $600 \text{ m s}^{-1}$  to the left, the flow field becomes as in Figure 3.6 with shock stationary.

The speed of sound is given by

$$\begin{aligned} a_1 &= \sqrt{\gamma RT_1} = 348.9 \text{ m s}^{-1} \\ V_1 &= 500 \text{ m s}^{-1} \\ M_1 &= \frac{500}{348.9} = 1.433 \end{aligned}$$

From Eq. (3.11), we have

$$M_2^2 = \frac{1 + 0.2M_1^2}{1.4M_1^2 - 0.2} = 0.527$$

Hence,  $M_2 = 0.726$ . From Eq. (3.13),

$$\frac{\rho_2}{\rho_1} = \frac{2.4M_1^2}{0.4M_1^2 + 2} = 1.747$$

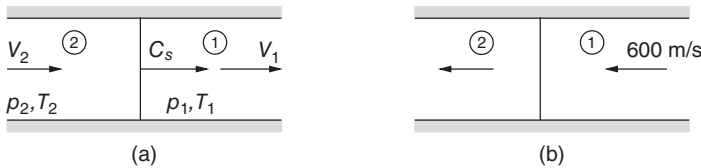


Figure 3.6 Normal shock moving in a tube.



Again, from Eq. (3.16),

$$\frac{p_2}{p_1} = 1 + \frac{2.8}{2.4}(M_1^2 - 1) = 2.229$$

Further, from Eq. (3.17),

$$\frac{T_2}{T_1} = \frac{p_2}{p_1} \frac{\rho_1}{\rho_2} = 1.276$$

Therefore,

$$p_2 = 2.229 \times 0.7$$

$$= \boxed{1.56 \text{ atm}}$$

$$T_2 = 1.276 \times (30 + 273.15)$$

$$= \boxed{386.81 \text{ K}}$$

$$V_2 = M_2 a_2 = 0.726 \sqrt{1.4 \times 287 \times 386.81}$$

$$= \boxed{286.21 \text{ m s}^{-1}} \text{ to the left w.r.t. the fixed coordinate system}$$

$$= -286.21 + 600 = \boxed{313.8 \text{ m s}^{-1}} \text{ to the right}$$

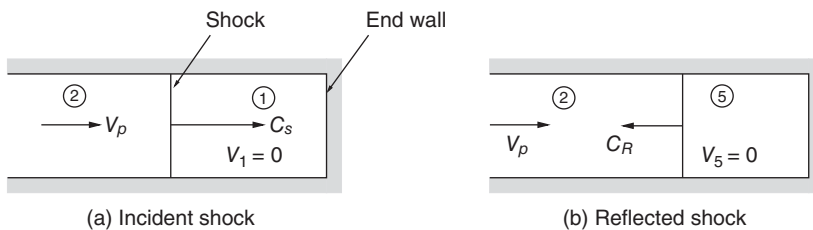
### 3.7 Reflected Shock Wave

Consider a normal shock wave moving with velocity  $C_s$  to the right inside a tube, as shown in Figure 3.7a. Let the shock be incident on a flat end wall. Ahead of the incident shock, the mass motion velocity  $V_1 = 0$ . Behind the incident shock, the mass velocity is  $V_p$  toward the end wall. The shock gets reflected from the wall and travels to the left with velocity  $C_R$ , as shown in Figure 3.7b.

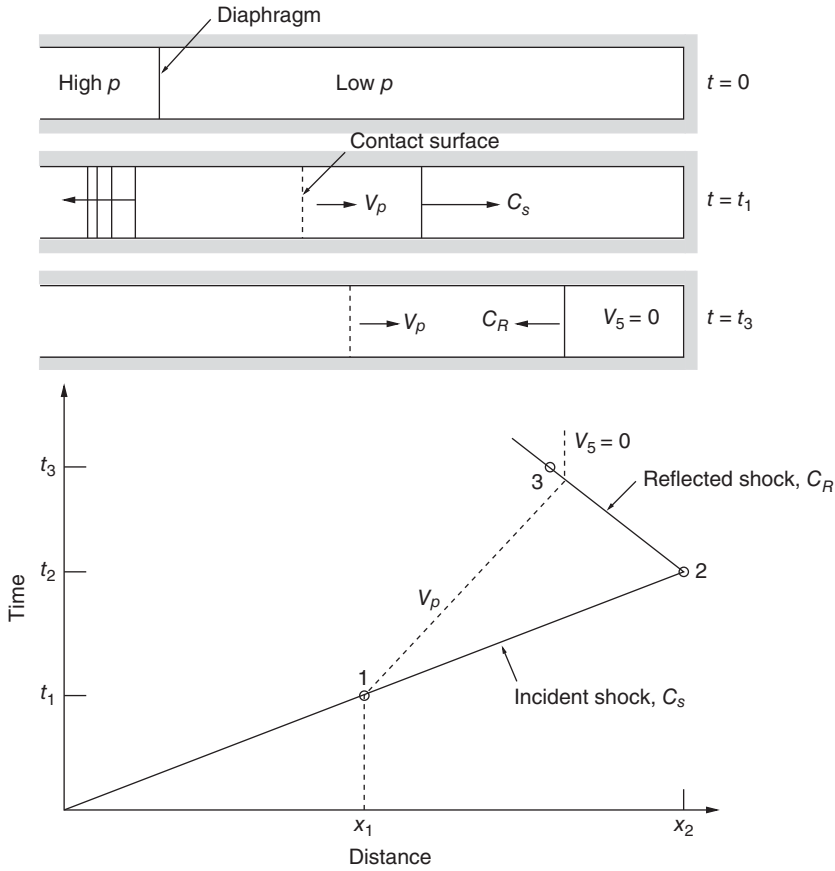
The strength of this reflected shock is such that the originally induced mass motion with velocity  $V_p$  is stopped completely in its track. Therefore, the mass motion behind the reflected shock should be zero, i.e.  $V_5 = 0$  in Figure 3.7b. Thus, the zero-velocity boundary condition is kept by the reflected shock wave. Indeed, for an incident normal shock of specified strength, the reflected normal shock strength is completely determined by imposing the boundary condition  $V_5 = 0$ .

The shock wave reflection considered above is illustrated as an  $x - t$  diagram in Figure 3.8. The plot showing the wave motion on a graph of  $x$  versus  $t$  is called a *wave diagram*. At time  $t = 0$ , the incident shock just starts from the diaphragm location. Therefore, at  $t = 0$  the incident shock is at location  $x = 0$ .

The shock wave travels to the right with increasing  $t$  and is located at  $x = x_1$ , at  $t = t_1$ . This is marked as point 1 in Figure 3.8. After hitting the wall at  $x = x_2$ , the shock reflects toward the left with velocity  $C_R$ . At time  $t = t_3$ , the reflected shock is at  $x = x_3$ . The incident and reflected



**Figure 3.7** Incident and reflected shock waves.



**Figure 3.8**  $x - t$  diagram.

shock paths are straight in the wave diagram. The slopes of the incident and reflected shock paths are  $1/C_s$  and  $1/C_R$ , respectively. Also,  $C_R < C_s$  because of the general characteristics of reflected shock; therefore, the reflected shock path is more steeply inclined than the incident shock path.

The path of the fluid particles behind the shock, traveling with velocity  $V_p$ , is shown by the dashed lines in Figure 3.8. In Figure 3.7b, it can be seen that

$$C_R + V_p = \text{Velocity of the gas ahead of the shockwave relative to the wave.}$$

$$C_R = \text{velocity of the gas behind the shock wave relative to the wave.}$$

Hence, following Eqs. (3.1)–(3.3) for the reflected shock, we have

$$\rho_2(C_R + V_p) = \rho_5 C_R \quad (3.49)$$

$$p_2 + \rho_2(C_R + V_p)^2 = p_5 + \rho_5 C_R^2 \quad (3.50)$$

$$h_2 + \frac{(C_R + V_p)^2}{2} = h_5 + \frac{C_R^2}{2} \quad (3.51)$$

Equations (3.49)–(3.51) are the continuity, momentum, and energy equations, respectively, for a reflected shock wave.

The incident shock propagates into the gas ahead of it with a Mach number  $M_s = C_s/a_1$ . The reflected shock propagates into the gas ahead of it with a Mach number  $M_R = (C_R + V_p)/a_2$ . With the incident shock Eqs. (3.1)–(3.3) and the reflected shock Eqs. (3.49)–(3.51), for a perfect gas, a relation between  $M_R$  and  $M_s$  can be obtained as

$$\frac{M_R}{M_R^2 - 1} = \frac{M_s}{M_s^2 - 1} \left[ 1 + \frac{2(\gamma - 1)}{(\gamma + 1)^2} (M_s^2 - 1) \left( (\gamma + 1) \frac{1}{M_s^2} \right) \right]^{1/2} \quad (3.52)$$

Detailed derivation of this relation is given in [6].

### Example 3.7

A normal shock wave with a pressure ratio of 4.5 impinges on a plane wall. Determine the static pressure ratio for the reflected normal shock wave (see Figure 3.9). The air temperature in front of the incident wave is 280 K.

#### Solution:

The flow field for incident shock illustrated in Figure 3.9 is equivalent to one with velocities as shown in Figure 3.10.

Given,

$$\begin{aligned} \frac{p_2}{p_1} &= 4.5 \\ a_1 &= \sqrt{\gamma RT_1} = 335.4 \text{ m s}^{-1} \end{aligned}$$

From normal shock table, for  $p_2/p_1 = 4.5$

$$\begin{aligned} M_1 &= 2.0, T_2/T_1 = 1.688 \\ T_2 &= 1.688 \times 280 = 472.64 \text{ K} \end{aligned}$$

Therefore,  $C_{si} = M_1 a_1 = 670.8 \text{ m s}^{-1}$ .

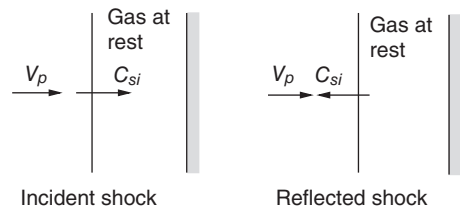
From Eqs. (3.33a) and (3.13), we get

$$\begin{aligned} \frac{C_{si} - V_p}{C_{si}} &= \frac{2 + (\gamma - 1)M_1^2}{(\gamma + 1)M_1^2} \\ &= 0.375 \\ C_{si} - V_p &= 0.375 C_{si} \end{aligned}$$

But

$$\begin{aligned} C_{si} &= M_1 a_1 = 2 \times 335.4 \\ &= 670.8 \text{ m s}^{-1} \end{aligned}$$

**Figure 3.9** A normal shock impinging on a plane wall.



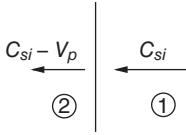


Figure 3.10 Flow field for incident shock.

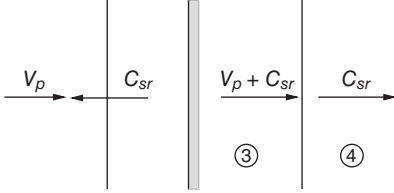


Figure 3.11 Flow field for reflected shock.

Therefore,

$$\begin{aligned}
 670.8 - V_p &= 0.375 \times 670.8 \\
 &= 251.55 \\
 V_p &= 670.8 - 251.55 \\
 &= 419.25 \text{ m s}^{-1}
 \end{aligned}$$

The flow field for the reflected shock is equivalent to that shown in Figure 3.11. The speed of sound in zone 3 is given by

$$\begin{aligned}
 a_3 &= \sqrt{\gamma R T_2} = \sqrt{1.4 \times 287 \times 472.64} \\
 &= 435.78 \text{ m s}^{-1}
 \end{aligned}$$

Therefore,

$$M_3 = \frac{C_{sr} + 419.25}{435.78}$$

From Eq. (3.13)

$$\frac{V_3}{V_4} = \frac{(\gamma + 1)M_3^2}{2 + (\gamma - 1)M_3^2} = \frac{C_{sr} + 419.25}{C_{sr}}$$

Substituting for  $C_{sr}$  from these two equations, we obtain

$$\frac{2.4M_3^2}{2 + 0.4M_3^2} = \frac{435.78M_3}{435.78M_3 - 419.25}$$

This results in  $M_3 = 1.73$ . Therefore, the static pressure ratio across the reflected shock is

$$\begin{aligned}
 \frac{p_4}{p_3} &= 1 + \frac{2\gamma}{\gamma + 1}(M_3^2 - 1) \\
 &= \boxed{3.32}
 \end{aligned}$$

### Example 3.8

A normal shock, generated by impulsively moving the piston in a cylinder piston device with stagnant air at 300K and 1 atm, moves toward the closed end of the cylinder and reflects back. If the pressure losses caused by the incident and reflected shocks are 23.26 and 14.01%, respectively, determine (a) the speed of the incident shock and piston speed and (b) the pressure behind the reflected shock and the speed of sound ahead of the reflected shock.

**Solution:**

- (a) Let subscripts 1 and 2, respectively, refer to the fields ahead of and behind the incident shock and subscripts 3 and 4 refer to the fields ahead of and behind the reflected shock.

Given,  $T_1 = 300$  K and  $p_1 = 1$  atm and

$$\begin{aligned}\frac{p_{01} - p_{02}}{p_{01}} \times 100 &= 23.26 \\ 1 - \frac{p_{02}}{p_{01}} &= 0.2326 \\ \frac{p_{02}}{p_{01}} &= 0.7674\end{aligned}$$

For  $p_{02}/p_{01} = 0.7674$ , from the normal shock table (Table A.2), we have

$$M_1 = 1.9, \frac{p_2}{p_1} = 4.045, \frac{T_2}{T_1} = 1.6079, \frac{\rho_2}{\rho_1} = 2.5157$$

Thus,

$$\begin{aligned}V_1 &= M_1 a_1 = 1.9 \times \sqrt{\gamma R T_1} \\ &= 1.9 \times \sqrt{1.4 \times 287 \times 300} \\ &= \boxed{659.66 \text{ m s}^{-1}} \\ \frac{V_1}{V_2} &= \frac{V_1}{V_1 - V_p} = \frac{\rho_2}{\rho_1} = 2.5157 \\ V_p &= V_1 - \frac{V_1}{2.5157} \\ &= 659.66 - \frac{659.66}{2.5157} \\ &= \boxed{397.44 \text{ m s}^{-1}}\end{aligned}$$

- (b) Temperature  $T_3$  ahead of the reflected shock is the same as  $T_2$ , the temperature behind the incident shock. Thus,

$$\begin{aligned}T_3 &= 1.6079 \times T_1 = 1.6079 \times 300 \\ &= 482.37 \text{ K}\end{aligned}$$

Thus, the speed of sound ahead of the reflected shock is

$$\begin{aligned}a_3 &= \sqrt{\gamma R T_3} = \sqrt{1.4 \times 287 \times 482.37} \\ &= \boxed{440.25 \text{ m s}^{-1}}\end{aligned}$$

Given,

$$\frac{p_{04}}{p_{03}} = 1 - 0.1401 = 0.8599$$

For  $p_{04}/p_{03} = 0.8599$ , from the normal shock table (Table A.2),

$$\frac{p_4}{p_3} = 3.1654$$

But pressure  $p_3$  ahead of the reflected shock is equal to pressure  $p_2$  behind the incident shock. Therefore,

$$\begin{aligned} p_4 &= 3.1654 \times p_2 = 3.1654 \times 4.045 \\ &= 12.804 \text{ atm} \\ &= 12.804 \times 101325 \\ &= \boxed{1.297 \text{ MPa}} \end{aligned}$$

### 3.8 Centered Expansion Wave

If, instead of moving the piston into the fluid, the piston is withdrawn, an expansion wave is generated. The wave diagram of such a motion is shown in Figure 3.12. The front of the expansion wave travels with speed  $a_4$  into the undisturbed fluid, i.e. in the direction opposite to the piston and fluid motion (note that any isentropic wave will travel at the speed of sound in the undisturbed fluid).

The wave speed in the portions of the wave behind the front is given by [6]

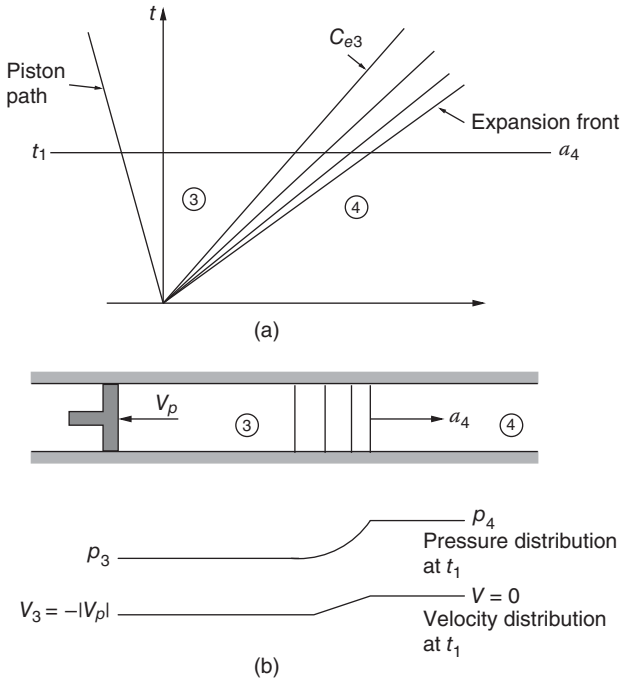
$$C_e = a_4 + \frac{\gamma + 1}{2} V$$

Here,  $V < 0$  and, therefore,  $C_e$  decreases continuously through the wave. The fan of straight lines shown are lines of constant  $C_e$  and thus of constant  $V$  and  $\rho$ . These lines are called *characteristics*.

With increasing time the fan becomes wider, i.e. the gradients of  $V$ ,  $\rho$ , etc. become smaller. Thus, the wave *remains isentropic*. The terminating characteristic is given by

$$x/t = C_{e3} = a_4 - \frac{\gamma + 1}{2} |V_p|$$

and slopes to right or left, depending on whether  $a_4 >$  or  $< \frac{\gamma+1}{2} |V_p|$



**Figure 3.12** (a)  $x-t$  diagram of centered expansion, (b) variation of pressure and velocity across the expansion zone.

Between the terminating characteristic and piston, the fluid properties have the uniform value of  $p_3$ ,  $\rho_3$ ,  $a_3$ , etc. For a perfect gas, the density ratio  $\rho_3/\rho_4$  and pressure ratio  $p_3/p_4$  are given by the isentropic relations

$$\frac{\rho_3}{\rho_4} = \left(1 - \frac{\gamma - 1}{2} \frac{|V_p|}{a_4}\right)^{2/(\gamma-1)} \quad (3.53)$$

$$\frac{p_3}{p_4} = \left(1 - \frac{\gamma - 1}{2} \frac{|V_p|}{a_4}\right)^{2\gamma/(\gamma-1)} \quad (3.54)$$

The derivation of the above relations is available in [6].

The pressure ratio  $p_3/p_4$  is called the *strength of the expansion fan*. The maximum expansion that can be obtained corresponds to  $\rho_3 = 0$  and is obtained when  $|V_p| = 2a_4/(\gamma - 1)$ . For this case,  $p_3 = T_3 = 0$ , i.e. all the fluid energy is converted to kinetic energy of flow. If the piston velocity is more than this limiting value (causing  $\rho_3 = 0$ ), it has no further effect on the flow.

### Example 3.9

An expansion wave generated by the withdrawal of piston in a tube travels into the still air at  $T_4 = 23^\circ\text{C}$ . If the piston speed is  $275 \text{ m s}^{-1}$ , determine whether the expansion characteristics will slope to the right or left.

#### Solution:

Given,

$$\begin{aligned} |V_p| &= 275 \text{ m s}^{-1} \\ T_4 &= 23^\circ\text{C} = 23 + 273.15 \\ &= 296.15 \text{ K} \end{aligned}$$

Therefore,

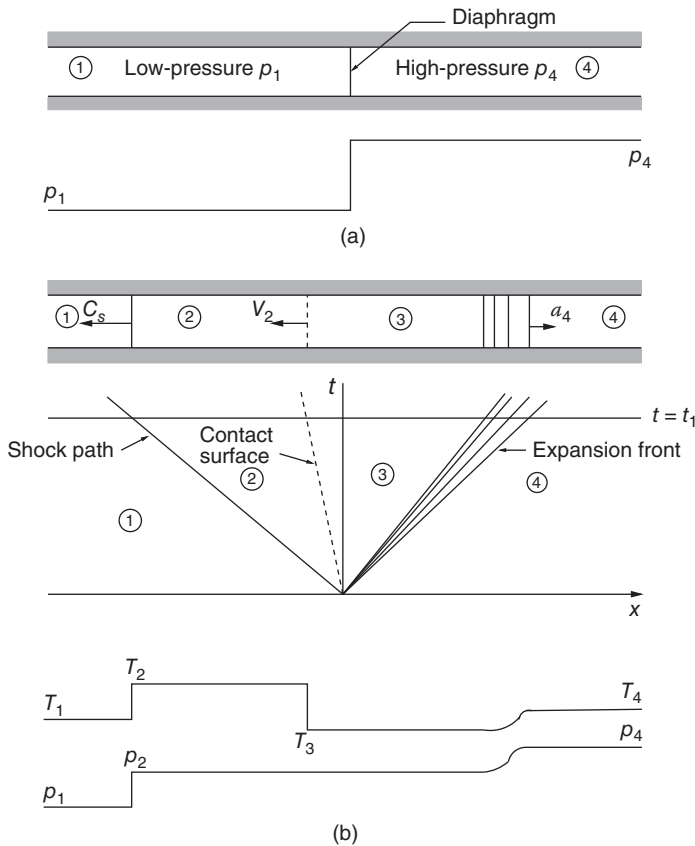
$$\begin{aligned} a_4 &= \sqrt{\gamma RT} = \sqrt{1.4 \times 287 \times 296.15} \\ &= 344.95 \text{ m s}^{-1} \\ \frac{\gamma + 1}{2} |V_p| &= \frac{1.4 + 1}{2} \times 275 \\ &= 330 \text{ m s}^{-1} \end{aligned}$$

i.e.  $a_4 > \frac{\gamma+1}{2} |V_p|$ ; therefore, the characteristics will slope to the right.

## 3.9 Shock Tube

The shock tube is a device to generate a high-speed flow with high temperatures, by traversing normal shock waves which are generated by the rupture of a diaphragm separating a high-pressure gas from a low-pressure gas. The shock tube is a very useful research tool for investigating not only the shock phenomena but also the behavior of materials and objects when subjected to extreme conditions of pressure and temperature. Thus, problems such as the kinetics of a chemical reaction taking place at high temperature, the performance, for example, of a body during re-entry into the earth's atmosphere and so on, can be studied with a shock tube.

In general, shock tubes are thick-walled tubes made out of stainless steel or aluminum alloy with circular, square, or rectangular cross-section with a very smooth inner surface, which is divided by a membrane or diaphragm into two chambers in which the pressures are different.



**Figure 3.13** Flow motion in a shock tube.

When the membrane is suddenly removed, a wave motion is set up. A shock tube and a fluid motion in it are shown in Figure 3.13. The studies made in the preceding sections, for shock waves and expansion waves, may be used to analyze flow conditions in the shock tube.

For shock tube operation, it is of prime importance to develop an expression for shock strength  $p_2/p_1$  as a function of the diaphragm pressure ratio  $p_4/p_1$ . Once the shock strength is known, all other flow parameters (quantities) can be easily determined from the normal shock relations.

A diaphragm at  $x=0$  separates the high-pressure (compression) and low-pressure (expansion) regions in a tube, as shown in Figure 3.13a.

The basic parameter of the shock tube is the *diaphragm pressure ratio*  $p_4/p_1$ . The high pressure and low pressure separated by the diaphragm may be at different temperatures,  $T_1$  and  $T_4$ , and may contain different gases with gas constants  $R_1$  and  $R_4$ .

At time  $t = 0$  when the diaphragm is burst, the pressure distribution is a step, as illustrated in Figure 3.13a. The shock wave propagates into the low-pressure chamber with speed  $C_s$  and an expansion wave propagates into the high-pressure chamber with speed  $a_4$  at its front.

The condition of the fluid which is traversed by the shock is denoted by subscript 2 and that of the fluid traversed by the expansion fan (waves) is denoted by subscript 3. The interface between regions 2 and 3 (Figure 3.13b) is called the *contact surface*. It makes the boundary between the fluids which were initially on either side of the diaphragm. Neglecting diffusion, it can be inferred that the high-pressure and low-pressure gases do not mix, but are permanently



separated by the contact surface, which is like the front of a piston, driving into the low-pressure chamber.

On either side of the contact surface, the temperatures  $T_2$  and  $T_3$  and the densities  $\rho_2$  and  $\rho_3$  may be different, but it is necessary that the pressure and fluid velocity be the same, that is

$$p_2 = p_3, V_2 = V_3$$

Thus,  $V_2$  is the velocity of the contact surface. With the above two conditions, the shock strength  $p_2/p_1$  and the expansion strength  $p_3/p_4$  in terms of the diaphragm pressure ratio  $p_4/p_1$  are determined as follows.

The values of  $V_2$  and  $V_3$  may be calculated from Eqs. (3.46), (3.53), and (3.54), which are the relations for the mass-motion velocity  $V_p$ , the density ratio  $\rho_3/\rho_4$ , and pressure ratio  $p_3/p_4$  across the expansion wave, respectively. By rearranging the above equations, and with subscripts to correspond to the present case, we get

$$V_2 = a_1 \left( \frac{p_2}{p_1} - 1 \right) \left( \frac{2/\gamma_1}{(\gamma_1 + 1)p_2/p_1 + (\gamma_1 - 1)} \right)^{1/2} \quad (3.55)$$

$$V_3 = \frac{2a_4}{\gamma_4 - 1} \left( 1 - \left( \frac{p_3}{p_4} \right)^{(\gamma_4 - 1)/2\gamma_4} \right) \quad (3.56)$$

But  $V_2 = V_3$  and  $p_2 = p_3$ ; therefore, from Eqs. (3.55) and (3.56) we can write the *basic shock tube equation* or the diaphragm pressure ratio  $p_4/p_1$  as

$$\frac{p_4}{p_1} = \frac{p_2}{p_1} \left( 1 - \frac{(\gamma_4 - 1)(a_1/a_4)(p_2/p_1 - 1)}{\sqrt{2\gamma_1}\sqrt{2\gamma_1 + (\gamma_1 + 1)(p_2/p_1 - 1)}} \right)^{-2\gamma_4/(\gamma_4 - 1)} \quad (3.57)$$

Equation (3.57) gives the shock strength  $p_2/p_1$  as a function of the diaphragm pressure ratio  $p_4/p_1$ . The expansion strength is obtained from

$$\frac{p_3}{p_4} = \frac{p_3}{p_1} \frac{p_1}{p_4} = \frac{p_2/p_1}{p_4/p_1} \quad (3.58)$$

From the above shock tube relations it is evident that, once the shock strength  $p_2/p_1$  is known, all other flow quantities can be determined from the normal shock relations.

The thermodynamic properties immediately behind the expansion fan can be found from the isentropic relations

$$\frac{p_3}{p_4} = \left( \frac{\rho_3}{\rho_4} \right)^{\gamma_4} = \left( \frac{T_3}{T_4} \right)^{\gamma_4/(\gamma_4 - 1)}$$

This can be rearranged as

$$\frac{T_3}{T_4} = \left( \frac{p_3}{p_4} \right)^{(\gamma_4 - 1)/\gamma_4} = \left( \frac{p_2/p_1}{p_4/p_1} \right)^{(\gamma_4 - 1)/\gamma_4} \quad (3.59)$$

The temperature  $T_2$  behind the shock wave is given by Eq. (3.43), as

$$\frac{T_2}{T_1} = \frac{1 + \frac{\gamma_1 - 1}{\gamma_1 + 1} \frac{p_2}{p_1}}{1 + \frac{\gamma_1 - 1}{\gamma_1 + 1} \frac{p_1}{p_2}} \quad (3.60)$$

The velocity of contact surface may be obtained from either Eq. (3.55) or Eq. (3.56).

### 3.9.1 Shock Tube Applications

The shock tube, being a device capable of producing established flow with uniform temperatures and pressure at high values that cannot be achieved with conventional tunnels, finds application in numerous fields in science and engineering.

- The uniform flow behind the shock wave may be used as a short-duration wind tunnel. In this role, the shock tube is similar to an intermittent or blowdown tunnel, but the duration of flow is much shorter, usually of the order of a millisecond. But the operating conditions (particularly the high stagnation enthalpies) which are possible cannot be easily obtained with other types of facility.
- The abrupt changes of flow condition at the shock front may be utilized for studying transient aerodynamic effects, and for studies of dynamic and thermal response.
- Shock tubes can also be used for studies on relaxation effects, reaction rates, dissociation, ionization, etc.

Finally, note that in the shock tube relations we use different  $\gamma$  for every flow zone. This is because in most of the applications the temperatures experienced by the gas at these zones are appreciably above the level mentioned in Section 1.12, describing perfect gas, and hence  $\gamma$  takes different values corresponding to the local temperature.

#### Example 3.10

A shock tube may be used as a short-duration wind tunnel by utilizing the flow behind the shock wave. Show that, in terms of the shock Mach number  $M_s = C_s/a_1$ , the density ratio  $\eta = \rho_2/\rho_1$  and conditions in the expansion chamber (1), the flow conditions behind the shock in region (2) are given by the following.

- $\frac{p_2}{p_1} = 1 + \gamma_1 M_s^2 \left(1 - \frac{1}{\eta}\right)$
- $\frac{h_2}{h_1} = 1 + \frac{\gamma_1 - 1}{2} M_s^2 \left(1 - \frac{1}{\eta^2}\right)$
- $\frac{V_p}{a_1} = M_s \left(1 - \frac{1}{\eta}\right)$
- $\frac{h_{02}}{h_1} = 1 + (\gamma_1 - 1) M_s^2 \left(1 - \frac{1}{\eta}\right)$

#### Solution:

The flow field is as shown in Figure 3.14.

- (a) From the continuity equation, we have

$$\rho_1 V_1 = \rho_2 V_2$$

$$\frac{V_2}{V_1} = \frac{\rho_1}{\rho_2} = \frac{1}{\eta}$$



Figure 3.14 Normal shock moving in a tube.

By the momentum equation,

$$\begin{aligned} p_2 - p_1 &= \rho_1 V_1^2 - \rho_2 V_2^2 \\ &= \rho_1 V_1^2 \left( 1 - \frac{V_2}{V_1} \right) \\ &= \rho_1 V_1^2 \left( 1 - \frac{1}{\eta} \right) \end{aligned}$$

Dividing throughout by  $p_1$ , we get

$$\begin{aligned} \frac{p_2}{p_1} - 1 &= \frac{\gamma_1 \rho_1}{\gamma_1 p_1} V_1^2 \left( 1 - \frac{1}{\eta} \right) \\ &= \gamma_1 M_s^2 \left( 1 - \frac{1}{\eta} \right) \\ \frac{p_2}{p_1} &= 1 + \gamma_1 M_s^2 \left( 1 - \frac{1}{\eta} \right) \end{aligned}$$

since  $\gamma p / \rho = a^2$ .

(b) By the energy equation,

$$\begin{aligned} h_1 + \frac{V_1^2}{2} &= h_2 + \frac{V_2^2}{2} \\ h_2 - h_1 &= \frac{V_1^2 - V_2^2}{2} \\ &= \frac{V_1^2}{2} \left( 1 - \frac{V_2^2}{V_1^2} \right) \\ &= \frac{a_1^2}{2} M_s^2 \left( 1 - \frac{1}{\eta^2} \right) \end{aligned}$$

Dividing throughout by  $h_1$ , we get

$$\frac{h_2}{h_1} = 1 + \frac{a_1^2}{2h_1} M_s^2 \left( 1 - \frac{1}{\eta^2} \right)$$

$h_1$  can be written as

$$h_1 = c_p T_1 = \frac{\gamma_1}{\gamma_1 - 1} R T_1 = \frac{a_1^2}{\gamma_1 - 1}$$

Therefore,

$$\frac{h_2}{h_1} = 1 + \frac{\gamma_1 - 1}{2} M_s^2 \left( 1 - \frac{1}{\eta^2} \right)$$

(c) By continuity,

$$\rho_1 V_1 = \rho_2 V_2, \quad V_2 = \frac{\rho_1}{\rho_2} V_1$$

The piston speed

$$V_p = V_1 - V_2 = \left( 1 - \frac{\rho_1}{\rho_2} \right) V_1$$

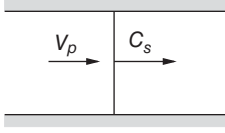


Figure 3.15 Normal shock moving in a tube.

Therefore,

$$\frac{V_p}{a_1} = M_s \left( 1 - \frac{1}{\eta} \right)$$

(d)

$$\begin{aligned} h_{02} &= h_2 + \frac{V_p^2}{2} \\ \frac{h_{02}}{h_1} &= \frac{h_2}{h_1} + \frac{1}{2} \frac{V_p^2}{h_1} \\ &= \frac{h_2}{h_1} + \frac{\gamma_1 - 1}{2} \frac{V_p^2}{a_1^2} \\ &= 1 + \frac{\gamma_1 - 1}{2} M_s^2 \left( 1 - \frac{1}{\eta^2} \right) + \frac{\gamma_1 - 1}{2} M_s^2 \left( 1 - \frac{1}{\eta} \right)^2 \\ &= 1 + (\gamma_1 - 1) M_s^2 \left( 1 - \frac{1}{\eta} \right) \end{aligned}$$

Refer to Figure 3.15 for the above solution.

### Example 3.11

If a shock tube filled with air at 300 and 400 K at its low- and high-pressure chambers, respectively, has to generate a shock to traverse the air to attain 600 K, what should be the shock strength? Also, determine the velocity of the contact surface and the shock speed.

#### Solution:

Given,  $T_1 = 300$  K,  $T_4 = 400$  K,  $T_2 = 600$  K. Also,  $\gamma_1 = \gamma_4 = 1.4$ .

By Eq. (3.60),

$$\begin{aligned} \frac{T_2}{T_1} &= \frac{1 + \frac{\gamma_1 - 1}{\gamma_1 + 1} \frac{p_2}{p_1}}{1 + \frac{\gamma_1 - 1}{\gamma_1 + 1} \frac{p_1}{p_2}} \\ 2 &= \frac{1 + \frac{0.4}{1.4} \frac{p_2}{p_1}}{1 + \frac{0.4}{1.4} \frac{p_1}{p_2}} \\ 2 \left( 1 + \frac{1}{6} \frac{p_1}{p_2} \right) &= 1 + \frac{1}{6} \frac{p_2}{p_1} \\ 2 \left( 6 + \frac{p_1}{p_2} \right) &= 6 + \frac{p_2}{p_1} \end{aligned}$$

$$\begin{aligned}
\frac{p_1}{p_2} &= -6 + 3 + \frac{1}{2} \frac{p_2}{p_1} \\
1 &= -3 \frac{p_2}{p_1} + \frac{1}{2} \left( \frac{p_2}{p_1} \right)^2 \\
\left( \frac{p_2}{p_1} \right)^2 - 6 \frac{p_2}{p_1} - 2 &= 0 \\
\frac{p_2}{p_1} &= \frac{6 \pm \sqrt{36 + 8}}{2} \\
&= \frac{6 + 6.633}{2} \\
&= 6.32
\end{aligned}$$

Note that the negative value of  $\frac{p_2}{p_1}$  is not a feasible solution. Thus, the shock strength is

$$\begin{aligned}
\frac{\Delta p}{p_1} &= \frac{p_2 - p_1}{p_1} \\
&= \frac{p_2}{p_1} - 1 \\
&= 6.32 - 1 \\
&= \boxed{5.32}
\end{aligned}$$

The contact surface speed, by Eq. (3.55), is

$$\begin{aligned}
V_2 &= a_1 \left( \frac{p_2}{p_1} - 1 \right) \left[ \frac{2/\gamma_1}{(\gamma_1 + 1) \frac{p_2}{p_1} + (\gamma_1 - 1)} \right]^{1/2} \\
&= \sqrt{1.4 \times 287 \times 300} \times (6.32 - 1) \times \left[ \frac{2/1.4}{2.4 \times 6.32 + 0.4} \right]^{1/2} \\
&= 347.19 \times 5.32 \times \sqrt{\frac{1.429}{15.568}} \\
&= \boxed{559.60 \text{ m s}^{-1}}
\end{aligned}$$

By Eq. (3.45), the shock speed is

$$\begin{aligned}
C_s &= a_1 \sqrt{\frac{\gamma_1 + 1}{2\gamma_1} \left( \frac{p_2}{p_1} - 1 \right) + 1} \\
&= 347.19 \times \sqrt{\frac{2.4}{2.8} \times (6.32 - 1) + 1} \\
&= \boxed{818.66 \text{ m s}^{-1}}
\end{aligned}$$

### 3.10 Summary

Shock is a compression front, in a supersonic flow field, across which there is an abrupt change in flow properties. The flow process through a shock wave is highly irreversible and cannot

be approximated as being isentropic. The flow is supersonic upstream of a normal shock and subsonic downstream of it. The larger the Mach number before the shock, the stronger the shock will be. In the limiting case of  $M_1 = 1$ , the shock wave simply becomes a sonic wave. The flow through the shock wave is adiabatic and irreversible.

The conservation of energy principle (Eq. 3.3) requires that the stagnation enthalpy remains constant across the shock;  $h_{01} = h_{02}$ . For ideal gases,  $h_0 = c_p T_0$  and hence

$$T_{01} = T_{02}$$

That is, the stagnation temperature of a perfect gas also remains constant across the shock. However, it should be noted that the stagnation pressure decreases across the shock because of the irreversibilities.

In terms of the speed ratio  $M^* = V/a^*$ , the Prandtl relation can be expressed as

$$M_2^* = \frac{1}{M_1^*}$$

This implies that the velocity change across a normal shock must be from supersonic to subsonic and vice versa. But if we consider entropy, it can be shown that only the former is the practical solution. Hence, *the Mach number behind a normal shock is always subsonic*. This is a general result, not limited to calorically perfect gases alone.

The Mach number behind a normal shock is given by

$$M_2^2 = \frac{1 + \frac{\gamma - 1}{2} M_1^2}{\gamma M_1^2 - \frac{\gamma - 1}{2}}$$

The ratios of density, pressure, and temperature across a normal shock are given by

$$\begin{aligned} \frac{\rho_2}{\rho_1} &= \frac{(\gamma + 1)M_1^2}{(\gamma - 1)M_1^2 + 2} \\ \frac{p_2}{p_1} &= 1 + \frac{2\gamma}{\gamma + 1}(M_1^2 - 1) \\ \frac{T_2}{T_1} &= 1 + \frac{2(\gamma - 1)}{(\gamma + 1)^2} \frac{\gamma M_1^2 + 1}{M_1^2} (M_1^2 - 1) \end{aligned}$$

The entropy change across a shock is given by

$$s_2 - s_1 = c_p \ln \frac{T_2}{T_1} - R \ln \frac{p_2}{p_1}$$

The variations in properties across a normal shock, for the limiting case of  $M_1 \rightarrow \infty$ , in a gas with  $\gamma = 1.4$  are

$$\begin{aligned} \lim_{M_1 \rightarrow \infty} M_2 &= \sqrt{\frac{\gamma - 1}{2\gamma}} = 0.378 \\ \lim_{M_1 \rightarrow \infty} \frac{\rho_2}{\rho_1} &= \frac{\gamma + 1}{\gamma - 1} = 6 \\ \lim_{M_1 \rightarrow \infty} \frac{p_2}{p_1} &= \infty \\ \lim_{M_1 \rightarrow \infty} \frac{T_2}{T_1} &= \infty \end{aligned}$$

The ratio of stagnation pressure across a normal shock is

$$\frac{p_{02}}{p_{01}} = \left( 1 + \frac{2\gamma}{\gamma+1}(M_1^2 - 1) \right)^{-1/(\gamma-1)} \left( \frac{(\gamma+1)M_1^2}{(\gamma-1)M_1^2 + 2} \right)^{\gamma/(\gamma-1)}$$

The change in flow properties across a normal shock can also be expressed only in terms of thermodynamic variables, without explicit reference to velocity or Mach number, as

$$e_2 - e_1 = \frac{p_1 + p_2}{2}(v_1 - v_2)$$

This is called the *Hugoniot equation*. It is a general relation valid for perfect gases, real gases, chemically reacting gases, etc., since there is no assumption made about the type of gas in deriving it.

A moving body in a flow field creates disturbances. The motion of these disturbances relative to the fluid is called *wave motion*. The speed of propagation of the disturbances is known as *wave speed*.

The wave or shock velocity in a perfect gas can be expressed as

$$C_s = a_1 \sqrt{\frac{\gamma+1}{2\gamma} \left( \frac{p_2}{p_1} - 1 \right) + 1}$$

The fluid velocity behind a moving shock, also called the *mass-motion velocity*  $V_p$  is given by

$$V_p = \frac{a_1}{\gamma} \left( \frac{p_2}{p_1} - 1 \right) \left( \frac{\frac{2\gamma}{\gamma-1}}{\frac{p_2}{p_1} + \frac{\gamma-1}{\gamma+1}} \right)^{1/2}$$

The wave produced by an impulsive withdrawal of the piston is called a *centered expansion wave*. The front of the wave propagates in the direction opposite to the piston and fluid motion. The maximum expansion that can be obtained corresponds to the state of *zero density* behind the terminating characteristic. This situation corresponds to the state where all the fluid energy is converted into kinetic energy of flow.

The shock tube consists of a long duct of constant cross-section divided into two chambers by a diaphragm. The high-pressure chamber is called the *driver section* and the low-pressure chamber is called the *expansion section*. The low-pressure gas may be the same as or different from the high-pressure gas. Also, the temperature of the gases at the two chambers may be the same or different. The *basic equation for a shock tube* is

$$\frac{p_4}{p_1} = \frac{p_2}{p_1} \left( 1 - \frac{(\gamma_4 - 1)(a_1/a_4)(p_2/p_1 - 1)}{\sqrt{2\gamma_1}\sqrt{2\gamma_1 + (\gamma_1 + 1)(p_2/p_1 - 1)}} \right)^{-2\gamma_4/(\gamma_4 - 1)}$$

This equation gives the shock strength  $p_2/p_1$  as a function of the diaphragm pressure ratio  $p_4/p_1$ . The expansion strength is given by

$$\frac{p_3}{p_4} = \frac{p_2/p_1}{p_4/p_1}$$

A shock tube can be used for studying unsteady short-duration phenomena in various fields of aerodynamics, physics, and chemistry. Because of the high-stagnation enthalpies that can be attained, the shock tube provides a means to study phenomena such as the thermodynamic properties of gases at high temperatures, dissociation, ionization, and chemical kinetics. Temperatures as high as 8000 °C have been attained in shock tubes.

The flow process across a normal shock is shown to be adiabatic. But we have seen that there are large gradients of flow properties across the shock. We also know that these severe gradients produce viscous stress and heat transfer, i.e. nonequilibrium conditions inside the shock. It is no wonder, then, that we ask how the process across a shock can be treated as adiabatic. The answer to this question is that the shock is a very thin compression front with thickness of the order of  $10^{-5}$  cm. Also, the flow crosses the shock wave at a very high velocity. The combination of this high velocity of the flow and extremely small thickness of the wave makes the fluid particles cross the wave in an infinitesimal time, thereby ruling out the possibility of any exchange of energy of the fluid particles with the surroundings. In other words, even though the fluid particles attain a high temperature while passing through the shock, they do not have any significant energy exchange with the surroundings since they have only an infinitesimal contact time with the surroundings, while passing through the shock.

It is interesting to recall that the flow through a normal shock is one-dimensional. The change of flow properties occur in the same direction as that of the flow. The flow properties and their derivatives across a shock wave are discontinuous. Shock waves propagate faster than Mach waves do, and they show large gradients in pressure, temperature, and density. Finally, we should realize that any formation of proper normal shock (the shock front which is strictly normal to the flow) is possible only in internal flows, such as flow in a wind tunnel and shock tubes. Normal shocks formed without a solid confinement are only close to normal shock and are not strictly normal to the flow.

## Exercise Problems

- 3.1 The Mach number, pressure, and temperature of air stream ahead of a normal shock are 2.0, 0.5 atm, and 300 K, respectively. Determine  $M_2$ ,  $p_2$ ,  $T_2$ , and  $V_2$  behind the wave.  
[Answer: 0.5774, 2.250 atm, 506.1 K, 260.37 m s<sup>-1</sup>]
- 3.2 A re-entry vehicle (RV) flies at 15 000 m altitude with a velocity of 1850 m s<sup>-1</sup>. A bow shock wave envelops the RV. Neglecting dissociation, determine the static and stagnation pressure and temperature just behind the shock wave on the RV center line where the shock wave may be treated as normal shock. Assume that the air behaves as perfect gas, with  $\gamma = 1.4$  and  $R = 287$  J (kg K)<sup>-1</sup>.  
[Answer:  $5.51 \times 10^5$  N m<sup>-2</sup>,  $6.16 \times 10^5$  N m<sup>-2</sup>, 1859.74 K, 1918.75 K]
- 3.3 A Mach 3 intermittent wind tunnel is operated by expanding atmospheric air at 15 °C through the test-section into an evacuated tank. Determine the static pressure and the total pressure that a pitot tube placed in the test-section would indicate.  
[Answer: 2758 Pa, 33.265 kPa]
- 3.4 Upstream of a normal shock in air,  $M_1 = 2.5$ ,  $p_1 = 1$  atm,  $\rho_1 = 1.225$  kg m<sup>-3</sup>. Determine  $p_2$ ,  $\rho_2$ ,  $T_2$ ,  $M_2$ ,  $V_2$ ,  $p_{02}$  and  $T_{02}$  downstream of it.  
[Answer: 7.125 atm, 4.083 kg m<sup>-3</sup>, 616.03 K, 0.513, 255.22 m s<sup>-1</sup>, 8.5261 atm, 648.45 K]
- 3.5 Nitrogen gas passes through a normal shock with upstream conditions of  $p_1 = 300$  kPa,  $T_1 = 303$  K, and  $V_1 = 923$  m s<sup>-1</sup>. Determine the velocity  $V_2$  and pressure  $p_2$  downstream of the shock. If the same deceleration from  $V_1$  to  $V_2$  takes place isentropically, what will be the resultant  $p_2$ ?  
[Answer: 267.64 m s<sup>-1</sup>, 2.316 MPa, 5.036 MPa]



- 3.6** A blunt-nosed model is placed in a Mach 3 supersonic tunnel test-section. If the settling chamber pressure and temperature of the tunnel are 10 atm and 315 K, respectively, calculate the pressure, temperature, and density at the nose of the model. Assume the flow to be one-dimensional and the gas to be air.  
[Answer: 332.69 kPa, 315 K,  $3.68 \text{ kg m}^{-3}$ ]
- 3.7** A convergent–divergent nozzle of exit area  $4 \text{ cm}^2$  is to be designed to generate Mach 2.5 air stream. The nozzle is correctly expanded and discharging to standard atmosphere. The stagnation temperature at the entry is 500 K. Determine the backpressure required to position a normal shock at the nozzle exit plane.  
[Answer: 863.91 kPa]
- 3.8** Suppose the backpressure were increased for the nozzle in Problem 3.7 until a normal shock wave was formed in the divergent section where  $M = 1.5$ . What backpressure would be necessary to accomplish this and what would be the resulting velocity and temperature at the nozzle exit?  
[Answer: 15.89 atm,  $108.71 \text{ m s}^{-1}$ , 490 K]
- 3.9** Air at 700 kPa and 530 K from a storage tank is expanded through a frictionless convergent–divergent duct of throat area  $5 \text{ cm}^2$  and exit area  $12.5 \text{ cm}^2$ . The backpressure is 350 kPa. There is a normal shock in the divergent portion and the Mach number just upstream of the shock is 2.32. Determine (a) the cross-sectional area at the shock location, (b) the exit Mach number, and (c) the backpressure required for the flow to be isentropic throughout the duct.  
[Answer: (a)  $11.165 \text{ cm}^2$ , (b) 0.45, (c) 45.01 kPa]
- 3.10** A normal shock is formed in an air stream at a static temperature of 22 K. If the total temperature is 400 K, determine the Mach number and static temperature behind the shock.  
[Answer: 0.3893, 382.8 K]
- 3.11** The velocity, pressure, and temperature of air flow upstream of a normal shock are  $500 \text{ m s}^{-1}$ , 100 kPa, and 300 K. Determine the velocity, pressure, and temperature just behind the shock and the increase of entropy caused by the shock.  
[Answer:  $284.27 \text{ m s}^{-1}$ , 225.25 kPa, 384.21 K,  $15.45 \text{ J (kg K)}^{-1}$ ]
- 3.12** Stagnant air at 1 MPa and 300 K is expanded through a nozzle. If a normal shock wave is formed at the nozzle exit plane, determine the pressure, temperature, Mach number, velocity, and the stagnation pressure of the flow just behind the shock.  
[Answer: 0.5751 MPa, 281.3 K,  $0.5774 \text{ m s}^{-1}$ , 0.7209 MPa]
- 3.13** Air at  $30^\circ\text{C}$  and 101 kPa is drawn through a convergent–divergent nozzle with throat area  $0.025 \text{ m}^2$  and exit area  $0.0724 \text{ m}^2$ , discharging into a large vacuum tank. Determine the conditions (a) upstream and (b) downstream of a normal shock which is positioned at the nozzle exit.  
[Answer: (a) 2.6, 5.06 kPa, 128.9 K, (b) 0.504, 39.06 kPa, 288.5 K]
- 3.14** Air from a reservoir at 200 kPa and 350 K is expanded through a convergent–divergent nozzle of throat area  $0.2 \text{ m}^2$  and exit area  $0.8 \text{ m}^2$ . If a normal shock wave is positioned

in the nozzle where the cross-sectional area is  $0.6 \text{ m}^2$ , compute the static and stagnation pressures on either side of the shock. What will be the static and stagnation pressures and temperatures at the nozzle exit?

[Answer: Upstream of shock:  $p_1 = 9.42 \text{ kPa}$ ,  $p_{01} = 200 \text{ kPa}$ . Downstream of shock:  $p_2 = 75.03 \text{ kPa}$ ,  $p_{02} = 89.04 \text{ kPa}$ . At exit:  $p_3 = 81.81 \text{ kPa}$ ,  $p_{03} = 89.04 \text{ kPa}$ ,  $T_3 = 341.63 \text{ K}$ ]

- 3.15** A convergent–divergent nozzle connects two air reservoirs at pressures 5 atm and 3.6 atm. If a normal shock has to stand at the nozzle exit, find the backpressure required.  
[Answer: 2.876 atm]
- 3.16** A pitot tube is placed in an air stream of static pressure 0.95 atm. Determine the flow Mach number if the pitot tube records (a) 1.1 atm, (b) 2.5 atm, and (c) 10 atm.  
[Answer: (a) 0.465, (b) 1.275, (c) 2.79]
- 3.17** A convergent–divergent nozzle with  $A_{\text{th}} = 1000 \text{ mm}^2$  and  $A_e = 3000 \text{ mm}^2$  operates under a stagnation condition of 200 kPa and  $45^\circ\text{C}$ . If a normal shock is formed in the nozzle at a location with area  $2000 \text{ mm}^2$ , determine (a) the exit pressure and (b) the pressure loss experienced by the nozzle flow.  
[Answer: (a) 116.75 kPa, (b) 74.38 kPa]
- 3.18** Mach 2 air stream at 80 kPa and 290 K enters a divergent channel with a ratio of inlet to exit area of 0.25. Determine the backpressure required to position a normal shock in the channel at an area equal to twice the inlet area.  
[Answer: 243.77 kPa]
- 3.19** A normal shock moves at a constant speed of  $500 \text{ m s}^{-1}$  into still air at  $0^\circ\text{C}$  and 0.7 atm. Determine the static and stagnation conditions present in the air after passage of the wave.  
[Answer:  $p = 1.745 \text{ atm}$ ,  $T = 362.27 \text{ K}$ ,  $V = 233.9 \text{ m s}^{-1}$ ,  $p_0 = 2.25 \text{ atm}$ ,  $T_0 = 389.5 \text{ K}$ ]
- 3.20** A horizontal tube contains stationary air at 1 atm and 300 K. The left end of the tube is closed by a movable piston, which at time  $t = 0$  is moved impulsively at a speed of  $V_p = 100 \text{ m s}^{-1}$  to the right. Find the wave speed and pressure on the face of the piston.  
[Answer:  $C_s = 413 \text{ m s}^{-1}$ ,  $p_{\text{pistonface}} = 1.505 \times 10^5 \text{ N m}^{-2}$ ]
- 3.21** A horizontal tube contains stationary air at 1 atm and 300 K. The left end of the tube is closed by a movable piston, which at time  $t = 0$  is moved impulsively at a speed of  $120 \text{ m s}^{-1}$  to the left. Find the pressure on the face of the piston, if (a) the piston motion is to the left, and (b) the piston motion is to the right.  
[Answer: (a) 0.605 atm, (b) 1.57 atm]
- 3.22** Consider a pipe in which air at 300 K and  $1.50 \times 10^5 \text{ N m}^{-2}$  flows uniformly with a speed of  $150 \text{ m s}^{-1}$ . The end of the pipe is suddenly closed by a valve and a shock wave is propagated back into the pipe. Compute the speed of the wave and the pressure and temperature of the air which has been brought to rest.  
[Answer:  $C_s = 297.63 \text{ m s}^{-1}$ ,  $p_2 = 2.66 \times 10^5 \text{ N m}^{-2}$ ,  $T_2 = 355.5 \text{ K}$ ]
- 3.23** A shock wave is formed in a tube of initially stagnant air (state 1) by the sudden acceleration of a piston to the speed  $V_p$ . Show that the following relation holds between the

dimensionless shock speed  $C_s/a_1$  and the dimensionless piston speed  $V_p/a_1$ :

$$\frac{C_s}{a_1} = \frac{\gamma + 1}{4} \frac{V_p}{a_1} + \left[ 1 + \frac{1}{4} \left( \frac{\gamma + 1}{2} \right)^2 \left( \frac{V_p}{a_1} \right)^2 \right]^{1/2}$$

Determine the limiting form of this relation as

$$\frac{V_p}{a_1} \rightarrow \infty, \quad \frac{V_p}{a_1} \rightarrow 0$$

[Answer: as  $\frac{V_p}{a_1} \rightarrow \infty$ ,  $\frac{C_s}{a_1} \rightarrow \infty$ ; as  $\frac{V_p}{a_1} \rightarrow 0$ ,  $\frac{C_s}{a_1} \rightarrow 1$ ]

- 3.24** A horizontal tube contains stationary air at 1 atm and at a temperature such that the velocity of sound is  $360 \text{ m s}^{-1}$ . It has a movable piston which at instant  $t = 0$  is withdrawn impulsively from the tube with a constant velocity of  $300 \text{ m s}^{-1}$ . If the piston is suddenly stopped after a distance of 30 m, a shock runs into the tube. Calculate (a) the pressure on the face of the piston and (b) the time for the shock to hit the terminating characteristic after stoppage of the piston, and then (c) draw an  $x - t$  diagram for the above process, showing the piston path, shock path, expansion wave, and the particle path.

[Answer: (a) 0.969 atm, (b) 0.0566 s]

- 3.25** Calculate the pressure required in the driver (or higher-pressure) section of a shock tube to produce a shock of  $M_s = 5.0$  in the driven section which contains air (perfect gas) at an initial temperature of  $27^\circ\text{C}$  and pressure 0.01 atm if the driver gas is air at  $27^\circ\text{C}$ ,  $\gamma = 1.4$ ,  $R = 287 \text{ m}^2 (\text{s}^2 \text{K})^{-1}$ .

[Answer:  $2.26 \times 10^4 \text{ atm}$ ]

- 3.26** If the flow behind the shock wave in Problem 3.25 is to be used as a short-duration wind tunnel flow, calculate (a) the static temperature and pressure, (b) the stagnation temperature and pressure, (c) the testing time available, given that the test-section is 8 m, from the bursting diaphragm (assume that the contact surface is disturbance which limits testing time), and (d) the angle of a Mach line in this flow.

[Answer: (a) 1740 K, 0.29 atm, (b) 2699 K, 1.349 atm, (c)  $1.15 \times 10^{-3} \text{ s}$ , (d)  $37^\circ$ ]

- 3.27** If the conditions behind the shock after its relation from the end of the tube are denoted by (5) and the shock speed relative to the tube is  $U_R$ , show that, in terms of the density ratios  $\eta = \rho_2/\rho_1$  and  $\zeta = \rho_5/\rho_1$ ,

$$\begin{aligned} \frac{U_R}{C_s} &= \frac{\eta - 1}{\zeta - \eta} \\ \frac{p_5}{p_1} &= 1 + \gamma_1 M_s^2 \frac{(\eta - 1)(\zeta - 1)}{\zeta - \eta} \\ \frac{h_5}{h_1} &= 1 + (\gamma_1 - 1) M_s^2 \frac{(\eta - 1)(\zeta - 1)}{\zeta - \eta} \frac{1}{\eta} \end{aligned}$$

- 3.28** An intermittent wind tunnel is operated by expanding atmospheric air at  $15^\circ\text{C}$  through the test-section into an evacuated tank. Determine the static pressure and the pressure a pitot tube placed in the test-section would measure, if the Mach number there is 3.0.

[Answer: 2756 Pa, 33.265 kPa]

- 3.29** Nitrogen gas passes through a normal shock with upstream conditions of  $p_1 = 300$  kPa,  $T_1 = 303$  K, and  $V_1 = 923$  m s<sup>-1</sup>. Determine the velocity  $V_2$  and pressure  $p_2$  downstream of the shock. If the same deceleration from  $V_1$  to  $V_2$  takes place isentropically, what will be the resultant  $p_2$ ?  
[Answer: 2.316 MPa, 267.64 m s<sup>-1</sup>, 5.034 MPa]
- 3.30** A blunt-nosed model is placed in a Mach 3 supersonic tunnel test-section. If the settling chamber pressure and temperature of the tunnel are 10 atm and 315 K, respectively, calculate the pressure, temperature, and density at the nose of the model. Assume the flow to be one-dimensional.  
[Answer: 332.65 kPa, 315 K, 3.68 kg m<sup>-3</sup>]
- 3.31** A normal shock travels with velocity  $C_s$  in a still atmosphere at 101 kPa and 330 K. If the pressure just downstream of the shock is 5000 kPa, determine the velocity  $C_s$  and the velocity of the field traversed by the shock just downstream of it.  
[Answer: 2374.16 m s<sup>-1</sup>, 1932.24 m s<sup>-1</sup>]
- 3.32** There is a normal shock in a uniform air stream. The properties upstream of the shock are  $V_1 = 412$  m s<sup>-1</sup>,  $p_1 = 92$  kPa, and  $T_1 = 300$  K. Determine  $V_2$ ,  $p_2$ ,  $T_2$ ,  $T_{02}$ , and  $p_{02}$  downstream of the shock. Also, calculate the entropy increase across the shock.  
[Answer: 311.99 m s<sup>-1</sup>, 136.66 kPa, 336.51 K, 384.96 K, 218.81 kPa, 1.817 J (kg K)<sup>-1</sup>]
- 3.33** In a supersonic wind tunnel test-section a wall pressure tap and a pitot tube were used to measure the pressures. They indicate 112 kPa and 2895 kPa, respectively. If the stagnation temperature is 500 K, determine the test-section Mach number and velocity.  
[Answer: 4.44, 895.1 m s<sup>-1</sup>]
- 3.34** A continuous supersonic wind tunnel is designed to operate at a test-section Mach number of 2.4, with static conditions of those at 10 000 m altitude. The test-section is of circular cross-section with 250 mm in diameter. Neglecting friction and boundary layer effects, determine the power requirements of the compressor (a) during steady-state operation and (b) during start-up. Assume an isentropic compression, with a cooler located between compressor and nozzle, so that the compressor inlet temperature is maintained equal to the test-section stagnation temperature.  
[Answer: (a) 376.3 hp, (b) 1815 hp]
- 3.35** If a weak shock to move with Mach 1.05 is to be generated, by moving a piston, in a cylinder filled with air at 300 K, what should be the piston speed?  
[Answer: 29.02 m s<sup>-1</sup>]
- 3.36** What is the minimum (maximum negative) limiting speed of the piston withdrawal at which the expansion characteristics will begin to slant to the left in a cylinder filled with nitrogen gas at 40 °C?  
[Answer: 300.67 m s<sup>-1</sup>]

- 3.37** If the speed of the terminating characteristics generated by piston withdrawal in a cylinder filled with oxygen at 310 K is  $212 \text{ m s}^{-1}$ , determine the piston speed. Also, find whether the characteristics are sloping to the left or right.  
[Answer:  $103.16 \text{ m s}^{-1}$ , the characteristics will slope to the right.]
- 3.38** In a piston-cylinder device containing helium at 10 kPa and 50 K, the piston is suddenly moved with  $1000 \text{ m s}^{-1}$ . Find the shock speed and the pressure, density, and temperature behind the shock.  
[Answer:  $1454.62 \text{ m s}^{-1}$ , 150 kPa,  $0.308 \text{ kg m}^{-3}$ , 234.31 K]

## 4

## Oblique Shock and Expansion Waves

### 4.1 Introduction

The normal shock wave, a compression front normal to the flow direction, was studied in some detail in Chapters 2 and 3. However, in a wide variety of physical situations, a compression wave inclined at an angle to the flow occurs. Such a wave is called an *oblique shock*. Indeed, all naturally occurring shocks in external flows are oblique.

In steady subsonic flows, we generally do not think in terms of wave motion. It is usually much simpler to view the motion from a frame of reference in which the body is stationary and the fluid flows over it. If the relative speed is supersonic, the disturbance waves cannot propagate ahead of the immediate vicinity of the body and the wave system travels with the body. Thus, in the reference frame in which the body is stationary, the wave system is also stationary; then the correspondence between the wave system and the flow field is direct.

The normal shock wave is a special case of oblique shock waves, with shock angle  $\beta = 90^\circ$ . Also, it can be shown that the superposition of a uniform velocity, which is normal to the upstream flow, on the flow field of the normal shock will result in a flow field through an oblique shock wave. This phenomenon will be employed later in this chapter to get the oblique shock relations. Oblique shocks are usually generated when a supersonic flow is turned into itself. The opposite of this, i.e. when a supersonic flow is turned away from itself, results in the formation of an expansion fan. These two families of waves play a dominant role in all flow fields involving supersonic velocities. Typical flows with oblique shock and expansion fan are illustrated in Figure 4.1.

In Figure 4.1a the flow is deflected into itself by the oblique shock formed at the compression corner, to become parallel to the solid wall downstream of the corner. All the streamlines are deflected to the same angle  $\theta$  at the shock, resulting in uniform parallel flow downstream of shock. The angle  $\theta$  is referred to as the *flow deflection angle*. Across the shock wave, the Mach number decreases and the pressure, density, and temperature increase. The corner which turns the flow into itself is called the *compression* or *concave corner*. In contrast, in an expansion or convex corner, the flow is turned away from itself through an expansion fan, as illustrated in Figure 4.1b. All the streamlines are deflected to the same angle  $\theta$  after the expansion fan, resulting in uniform parallel flow downstream of the fan. Across the expansion wave, the Mach number increases and the pressure, density, and temperature decrease. From Figure 4.1, it is seen that the flow turns suddenly across the shock and the turning is gradual across the expansion fan and hence all flow properties through the expansion fan change smoothly, with the exception of the wall streamline, which changes suddenly.

Oblique shock and expansion waves prevail in two- and three-dimensional supersonic flows, in contrast to normal shock waves, which are one-dimensional. In this chapter, we shall focus our attention only on steady, two-dimensional (plane) supersonic flows.

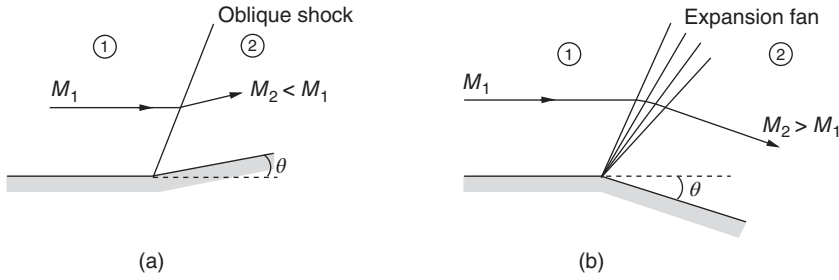


Figure 4.1 Supersonic flow over (a) Compression corner and (b) Expansion corner.

## 4.2 Oblique Shock Relations

The flow through an oblique shock is illustrated in Figure 4.2b. The flow through a normal shock (Figure 4.1a) has been modified to result in flow through an oblique shock, by superimposing a uniform velocity  $V_y$  (parallel to the normal shock) on the flow field of the normal shock (Figure 4.2a).

The resultant velocity upstream of the shock is  $V_1 = \sqrt{V_{x1}^2 + V_y^2}$  and is inclined at an angle  $\beta = \tan^{-1}(V_{x1}/V_y)$  to the shock. This angle  $\beta$  is called the *shock angle*. The velocity component  $V_{x2}$  is always less than  $V_{x1}$ ; therefore, the inclination of the flow ahead of the shock and after the shock are different. The inclination ahead is always more than that behind the shock wave, i.e. the flow is turned suddenly at the shock. Because  $V_{x1}$  is always more than  $V_{x2}$ , the turning of the flow is always toward the shock. The angle  $\theta$  by which the flow turns toward the shock is called the *flow deflection angle* and is positive as shown in Figure 4.2. The rotation of the flow field in Figure 4.2a by an angle  $\beta$  results in the field shown in Figure 4.2b, with  $V_1$  in the horizontal direction. The shock in that field inclined at an angle  $\beta$  to the incoming supersonic flow is called the *oblique shock*.

The relations between the flow parameters upstream and downstream of the flow field through the oblique shock, illustrated in Figure 4.2b, can be obtained from the normal shock relations in Chapter 3, since the superposition of uniform velocity  $V_y$  on the normal shock flow field in Figure 4.2a does not affect the flow parameters (e.g. static pressure) defined for normal shock. The only change is that in the present case the upstream Mach number is

$$M_1 = \frac{\text{Resultant velocity}}{\text{Speed of sound}} = \frac{V_1}{a_1}$$

The component of the upstream Mach number  $M_1$  normal to the shock wave is

$$M_{n1} = M_1 \sin \beta \quad (4.1)$$

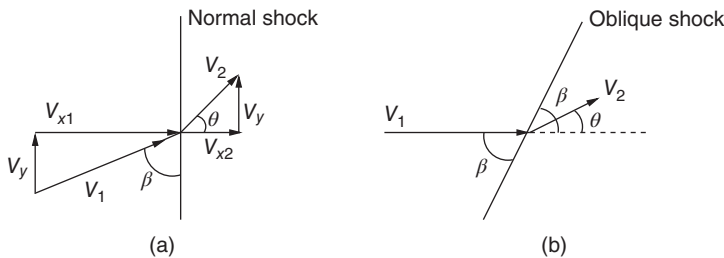


Figure 4.2 Flow through an oblique shock wave.

Thus, replacement of  $M_1$  with  $M_1 \sin \beta$  in normal shock relations given by Eqs. (3.13), (3.16), (3.18), and (3.19) results in the following relations for an oblique shock.

$$\frac{\rho_2}{\rho_1} = \frac{(\gamma + 1)M_1^2 \sin^2 \beta}{(\gamma - 1)M_1^2 \sin^2 \beta + 2} \quad (4.2)$$

$$\frac{p_2}{p_1} = 1 + \frac{2\gamma}{\gamma + 1}(M_1^2 \sin^2 \beta - 1) \quad (4.3)$$

$$\frac{T_2}{T_1} = \frac{a_2^2}{a_1^2} = 1 + \frac{2(\gamma - 1)}{(\gamma + 1)^2} \frac{M_1^2 \sin^2 \beta - 1}{M_1^2 \sin^2 \beta} (\gamma M_1^2 \sin^2 \beta + 1) \quad (4.4)$$

$$\begin{aligned} \frac{s_2 - s_1}{R} &= \ln \left( \left[ 1 + \frac{2\gamma}{\gamma + 1}(M_1^2 \sin^2 \beta - 1) \right]^{1/(\gamma-1)} \left[ \frac{(\gamma + 1)M_1^2 \sin^2 \beta}{(\gamma - 1)M_1^2 \sin^2 \beta + 2} \right]^{-\gamma/(\gamma-1)} \right) \\ &= \ln \left( \frac{p_{01}}{p_{02}} \right) \end{aligned} \quad (4.5)$$

The normal component of Mach number behind the shock  $M_{n2}$  is given by

$$M_{n2}^2 = \frac{M_1^2 \sin^2 \beta + \frac{2}{\gamma-1}}{\frac{2\gamma}{\gamma-1} M_1^2 \sin^2 \beta - 1} \quad (4.6)$$

From the geometry of the oblique shock flow field shown in Figure 4.2, it can be seen that the Mach number behind the oblique shock,  $M_2$ , is related to  $M_{n2}$  by

$$M_2 = \frac{M_{n2}}{\sin(\beta - \theta)} \quad (4.7)$$

In the above equations,  $M_2 = V_2/a_2$  and  $M_{n2} = V_{x2}/a_2$ . The Mach number  $M_2$  after a shock can be obtained by combining Eqs. (4.6) and (4.7).

Numerical values of the oblique shock relations for a perfect gas, with  $\gamma = 1.4$ , are presented in graphical form. The same in tabular form is given in Table A.3 in the Appendix.

It is seen from the oblique shock relations given by Eqs. (4.1)–(4.5) that the ratio of thermodynamic variables depends only on the normal component of velocity ( $M_1 \sin \beta$ ) ahead of the shock. But, from normal shock analysis we know that this component must be supersonic, i.e.  $M_1 \sin \beta \geq 1$ . This requirement imposes the restriction on the wave angle  $\beta$  that it cannot go below a limiting minimum value for any given  $M_1$ . At this minimum limiting value of shock angle, the shock gets degenerated to an isentropic wave across which the change of flow properties become negligibly small. Such a weak isentropic wave is also termed a *Mach wave*. The maximum value of  $\beta$  is that for a normal shock,  $\beta = \pi/2$ . Thus, for a given initial Mach number,  $M_1$ , the possible range of wave angle is

$$\sin^{-1} \left( \frac{1}{M_1} \right) \leq \beta \leq \frac{\pi}{2} \quad (4.8)$$

The limiting values of the wave angle in Eq. (4.8) are of special significance. The limiting minimum value is  $\sin^{-1} \left( \frac{1}{M} \right)$  is the Mach angle  $\mu$  and the maximum value  $\frac{\pi}{2}$  corresponds to normal shock. Thus, the strongest wave possible in a given supersonic flow is the normal shock corresponding to the given  $M_1$ . The weakest wave is the Mach wave corresponding to the given  $M_1$ . It is essential to note that the shock wave formation is not mandatory in a supersonic flow. For example, in uniform supersonic streams such as the flow in a supersonic wind tunnel test-section, no shocks are formed when the test-section is empty. Whereas, the weakest limiting isentropic waves, namely the Mach waves, are always present in all supersonic flows.



Even in the empty test-section of a supersonic tunnel the Mach waves are present. But we know that the waves in a supersonic flow are due to perturbations in the flow field. Therefore, it is natural to ask, "In an undisturbed uniform supersonic flow, why should there be Mach waves present?" The answer to this question is the following. In a uniform supersonic flow such as that in a wind tunnel test-section, if the test-section walls are absolutely smooth there will not be any Mach wave present in the flow. However, an absolute smooth surface is only a theoretical assumption. For instance, even a surface such as that of a good-quality Schlieren mirror has a finish of only about  $\lambda/20$ , where  $\lambda$  is the wave length of light. Thus, any practical surface is with some roughness and not absolutely smooth. Therefore, any supersonic flow field generated by a practical device is bound to possess Mach waves. Indeed, the size of the gas molecules are enough to cause Mach wave generation. Therefore, even in a free supersonic flow without any solid confinement Mach waves will be present.

An important feature to be inferred here is that the Mach waves, like characteristics, will be running to the left and right in the flow field. Because of this the Mach waves of opposite families prevailing in the flow field cross each other. But being the weakest degeneration of waves, the Mach waves would continue to propagate as linear waves even after passing through a number of Mach waves. In other words, the Mach waves would continue to be simple waves even after intersecting other Mach waves. Because of this nature of Mach waves, a flow region traversed by the Mach waves is simple throughout (see Section 4.10).

### 4.3 Relation Between $\beta$ and $\theta$

It can be seen from Eq. (4.7) that for determining  $M_2$  the flow deflection angle  $\theta$  must be known. Further, for each value of shock angle  $\beta$  at a given  $M_1$  there is a corresponding flow turning angle  $\theta$ . Therefore,  $\theta$  can also be expressed as a unique function of  $M_1$  and  $\beta$ . From Figure 4.2, we have

$$\tan \beta = \frac{V_{x1}}{V_y} \quad (4.9)$$

$$\tan(\beta - \theta) = \frac{V_{x2}}{V_y} \quad (4.10)$$

Combining Eqs. (4.9) and (4.10), we get

$$\frac{\tan(\beta - \theta)}{\tan \beta} = \frac{V_{x2}}{V_{x1}} \quad (4.11)$$

By continuity,

$$\frac{V_{x2}}{V_{x1}} = \frac{\rho_1}{\rho_2}$$

Now, substituting for  $\rho_1/\rho_2$  from Eq. (4.2), we get

$$\frac{\tan(\beta - \theta)}{\tan \beta} = \frac{(\gamma - 1)M_1^2 \sin^2 \beta + 2}{(\gamma + 1)M_1^2 \sin^2 \beta} \quad (4.12)$$

Equation (4.12) is an implicit relation between  $\theta$  and  $\beta$ , for a given  $M_1$ . With some trigonometric manipulation, this expression can be rewritten to show the dependence of  $\theta$  on Mach number  $M_1$  and shock angle  $\beta$ , as

$$\tan \theta = 2 \cot \beta \frac{M_1^2 \sin^2 \beta - 1}{M_1^2 (\gamma + \cos 2\beta) + 2} \quad (4.13)$$

Equation (4.13) is called the  $\theta$ - $\beta$ - $M$  relation. This relation is important for the analysis of oblique shocks. The expression on the right-hand side of Eq. (4.13) becomes zero at  $\beta = \pi/2$  and  $\beta = \sin^{-1}\left(\frac{1}{M_1}\right)$ , which are the limiting values of  $\beta$ , defined in Eq. (4.8). The deflection angle  $\theta$  is positive in this range and must therefore have a maximum value. The results obtained from Eq. (4.13) are plotted in Figure 4.3, for  $\gamma = 1.4$ . From the plot of  $\theta$ - $\beta$ - $M$  (Figure 4.3) curves, the following observations can be made.

- 1) For any given supersonic Mach number  $M_1$ , there is a maximum value of  $\theta$ . Therefore, at a given  $M_1$ , if  $\theta > \theta_{\max}$ , then no solution is possible for a straight oblique shock wave. In such cases, the shock will be curved and detached, as shown in Figure 4.4.
- 2) When  $\theta < \theta_{\max}$ , there are two possible solutions, for each value of  $\theta$  and  $M$ , having two different wave angles. The larger value of  $\beta$  is called the *strong shock solution* and the smaller value of  $\beta$  is referred to as the *weak shock solution*. For a strong shock solution the flow behind the shock becomes subsonic. For a weak shock solution, the flow behind the oblique shock remains supersonic, except for a small range of  $\theta$  slightly smaller than  $\theta_{\max}$ , the zone bounded by the  $M_2 = 1$  curve and  $\theta = \theta_{\max}$  curve shown in Figure 4.3.
- 3) If  $\theta = 0$ , then  $\beta = \pi/2$ , giving rise to a normal shock, or  $\beta$  decreases to the limiting value  $\mu$ , i.e. shock disappears and only Mach waves prevail in the flow field. That is, when the flow turning angle  $\theta$  is zero, the following two solutions are possible for the shock angle  $\beta$ , for a given  $M_1$ . (a) Either  $\beta = \pi/2$  giving rise to a normal shock which does not cause any flow deflection, but would decelerate the flow to subsonic level, or (b)  $\beta = \sin^{-1}(1/M_1) = \mu$  corresponding a Mach wave, which, even though inclined to the upstream flow, would not cause any flow deflection, being the limiting case of the weakest isentropic wave for a given  $M_1$ .

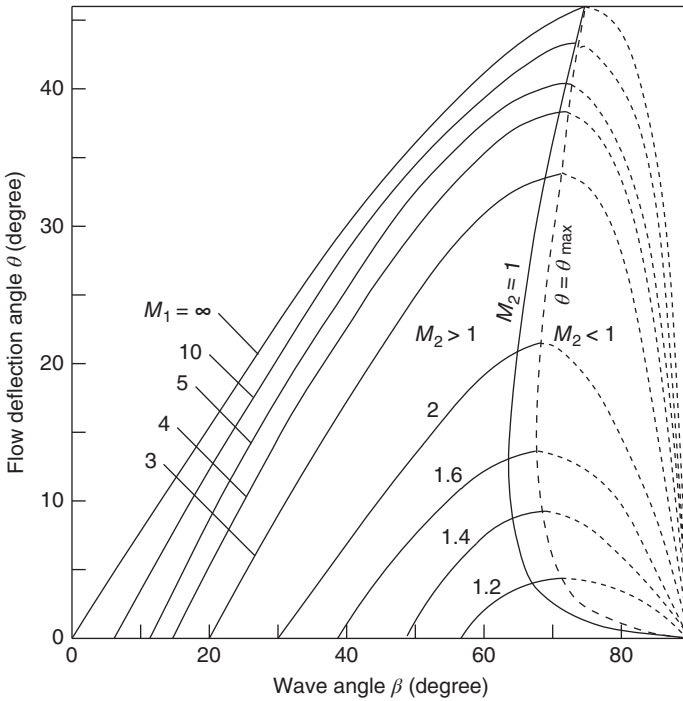
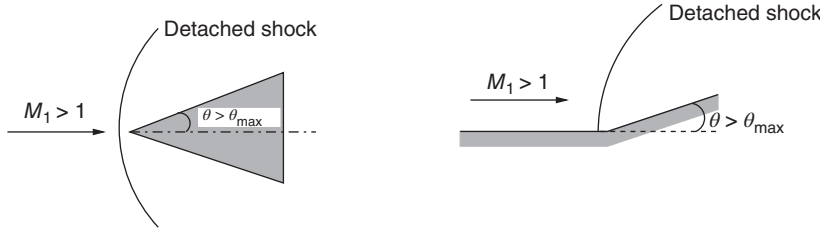


Figure 4.3 Oblique shock solution.



**Figure 4.4** Detached shocks.

A very useful form of  $\theta$ - $\beta$ - $M$  relation can be obtained by rearranging Eq. (4.12) in the following manner. Dividing the numerator and denominator of the right-hand side of Eq. (4.12) by  $2M_1^2 \sin^2 \beta$  and solving, we obtain

$$\frac{1}{M_1^2 \sin^2 \beta} = \frac{\gamma + 1}{2} \frac{\tan(\beta - \theta)}{\tan \beta} - \frac{\gamma - 1}{2}$$

This can be simplified further to result in

$$M_1^2 \sin^2 \beta - 1 = \frac{\gamma + 1}{2} M_1^2 \frac{\sin \beta \sin \theta}{\cos(\beta - \theta)} \quad (4.14)$$

For small deflection angles  $\theta$ , Eq. (4.14) may be approximated as

$$M_1^2 \sin^2 \beta - 1 \approx \left( \frac{\gamma + 1}{2} M_1^2 \tan \beta \right) \theta \quad (4.15)$$

If  $M_1$  is very large, then  $\beta \ll 1$ , but  $M_1 \beta \gg 1$  and Eq. (4.15) reduces to

$$\beta = \frac{\gamma + 1}{2} \theta \quad (4.16)$$

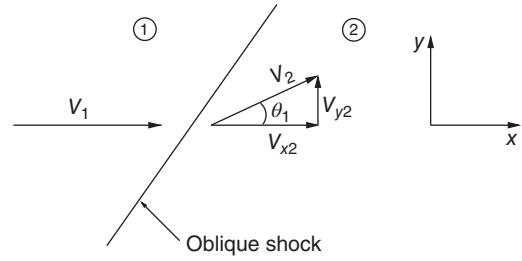
It is important to note that oblique shocks are essentially compression fronts across which the flow decelerates and the static pressure, static temperature, and static density jump to higher values. If the deceleration is such that the Mach number behind the shock continues to be greater than unity, the shock is termed a *weak oblique shock*. If the downstream Mach number becomes less than unity then the shock is called *strong oblique shock*. It is essential to note that only weak oblique shocks are usually formed in any practical flow and it calls for special arrangement to generate strong oblique shocks. One such situation where strong oblique shocks are generated with special arrangements is the engine intakes of supersonic flight vehicles, where the engine has provision to control its backpressure. When the backpressure is increased to an appropriate value, the oblique shock at the engine inlet would become a strong shock and decelerate the supersonic flow passing through it to subsonic level.

## 4.4 Shock Polar

Shock polar is a graphical representation of oblique shock solutions. We have seen in Section 4.3 that, in general, for any specified value of flow turning angle  $\theta$  there are two possible shock angles, giving rise to strong and weak solutions.

The shock polar for the oblique shock geometry illustrated in Figure 4.5 may be drawn as follows.

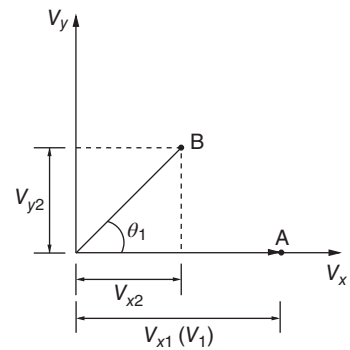
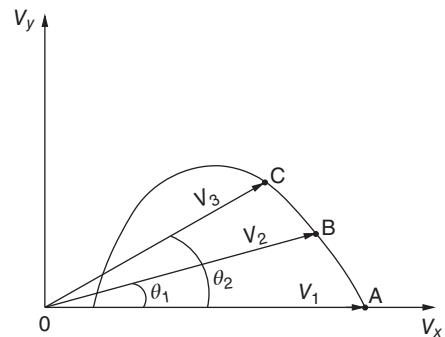
An oblique shock with upstream velocity  $V_1$  in the  $xy$  Cartesian coordinate system, shown in Figure 4.5, has the velocity components  $V_{x2}$  and  $V_{y2}$  in the downstream field, as shown. The

**Figure 4.5** Oblique shock in physical ( $xy$ ) plane.

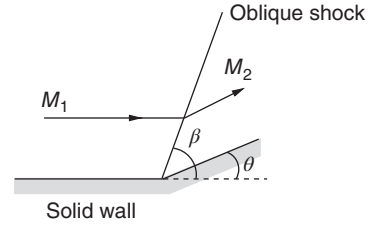
$xy$  plane in Figure 4.5 is called the *physical plane*. Let  $V_{x1}$ ,  $V_{y1}$ ,  $V_{x2}$ , and  $V_{y2}$  be the  $x$  and  $y$  components of flow velocity ahead of and behind the shock. Now, let us represent the oblique shock field in a plane with  $V_x$  and  $V_y$  as the coordinate axes, as shown in Figure 4.6. This plane is called the *hodograph plane*.

In the hodograph plane, point A represents the flow field ahead of the shock marked as region 1 in the physical plane of Figure 4.5. Similarly, region 2 in the physical plane is represented by point B in the hodograph plane. If the deflection angle  $\theta_1$  in Figure 4.6 is increased, then the shock becomes stronger and, therefore, the velocity  $V_2$  decreases. One such point for  $\theta_2$  is shown by point C in Figure 4.7. The loci of all such points for  $\theta$  values from zero to  $\theta_{\max}$ , representing all possible velocities behind the shock, are given in Figure 4.7. Such a locus is defined as a *shock polar*.

We know that the flow process across a shock wave is adiabatic. Therefore, from our definition of  $a^*$  (Section 2.2), it is the same in the fields upstream and downstream of the shock. Hence  $a^*$  can be conveniently used to nondimensionalize the velocities in Figure 4.7 to obtain a shock polar which is the locus of all possible  $M_2^*$  for a given  $M_1^*$ , as shown in Figure 4.8.

**Figure 4.6** Oblique shock geometry in hodograph ( $V_x V_y$ ) plane.**Figure 4.7** Shock polar for a given  $V_1$ .



**Figure 4.10** Supersonic flow over a compression corner.

streamlines can be assumed as solid boundaries. Thus, the oblique shock flow results already described can be used for solving practical problems like supersonic flow over a compression corner, as shown in Figure 4.10. For any given values of  $M_1$  and  $\theta$ , the values of  $M_2$  and  $\beta$  can be determined from oblique shock charts or table (Figures A.1 and A.2 and Table A.3 in the Appendix).

In a similar fashion, problems like supersonic flow over symmetrical and unsymmetrical wedges (Figure 4.11) and so on also can be solved with oblique shock relations, assuming the solid surfaces of the objects as streamlines in accordance with nonviscous (or inviscid) flow theory.

In Figure 4.11b, the flow on each side of the wedge is determined only by the inclination of the surface on that side. If the shocks are attached to the nose, the upper and lower surfaces are independent and there is no influence of wedge on the flow upstream of the shock waves.

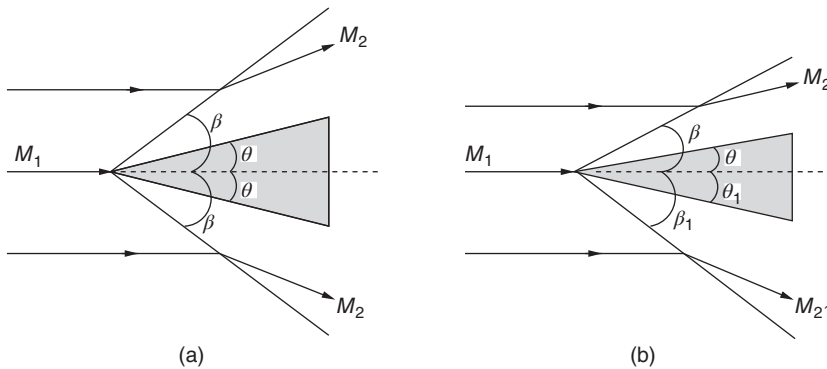
In our discussion on shock angle  $\beta$  and flow turning angle  $\theta$  (Section 4.3), we have seen that when  $\theta$  decreases to zero,  $\beta$  decreases to the limiting value  $\mu$  giving rise to Mach waves in the supersonic flow field (Figure 4.12b), which is given from Eq. (4.14) as

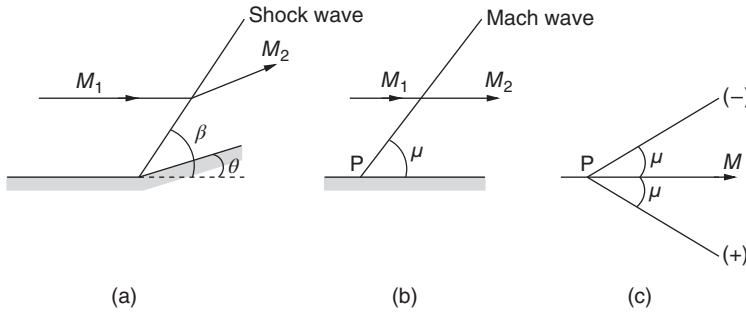
$$M_1^2 \sin^2 \mu - 1 = 0 \quad (4.18)$$

Also, the pressure, temperature, and density jump across the shock ( $p_2 - p_1$ ,  $T_2 - T_1$ , and  $\rho_2 - \rho_1$ ) given by Eqs. (4.2)–(4.5) become zero. There is, in fact, no finite disturbance in the flow. Point P in Figure 4.12b may be any point in the flow field. Then the angle  $\mu$  is simply a characteristic angle associated with the Mach number  $M$  by the relation

$$\mu = \sin^{-1} \left( \frac{1}{M} \right) \quad (4.19)$$

This is called the *Mach angle–Mach number relation*. These lines which may be drawn at any point in the flow field with inclination  $\mu$  are called *Mach lines* or *Mach waves*. It is essential to understand the difference between Mach waves and Mach lines. Mach waves are the weakest

**Figure 4.11** Flow past (a) symmetrical and (b) unsymmetrical wedges.



**Figure 4.12** Waves in a supersonic stream. (a) Oblique shock with deflection angle  $\theta$ , (b) Degeneration to Mach wave  $\theta \rightarrow 0$  and (c) Left (-) and right (+) running characteristics at an arbitrary point in the flow.

isentropic waves in a supersonic flow field and the flow through them will experience only negligible changes of flow properties. Thus, a flow traversed by Mach waves do not experience a change of Mach number. Whereas Mach lines, even though they are weak isentropic waves, will cause small but finite changes to the properties of a flow passing through them. In uniform supersonic flows, the Mach waves and Mach lines are linear and inclined at an angle given by  $\mu = \sin^{-1}(1/M)$ . But in nonuniform supersonic flows the flow Mach number  $M$  varies from point to point and hence the Mach angle  $\mu$ , being a function of the flow Mach number, varies with  $M$  and the Mach lines are curved.

In the flow field at any point P (Figure 4.12c), there are always two lines which are inclined at angle  $\mu$  and intersect the streamline, as shown in Figure 4.12c. In a three-dimensional flow, the Mach wave is in the form of a conical surface, with vertex at P. Thus, a two-dimensional flow of supersonic stream is always associated with two families of Mach lines. These are represented with a plus and minus sign. In Figure 4.12c, the Mach lines with a “+” sign run to the right of the streamline when viewed through the flow direction and those lines with a “-” sign run to the left. These Mach lines which introduce an infinitesimal, but finite, change to flow properties when a flow passes through them are also referred to as *characteristics*, which are not physical unlike the Mach lines and Mach waves. But the mathematical concept of characteristics (taken as identical to the Mach lines), even though not physical forms, the basis for the numerical method termed *method of characteristics*, used to design contoured nozzles to generate uniform and unidirectional supersonic flows. Method of characteristics is presented in Chapter 9.

At this stage it is essential to note the difference between the Mach waves, characteristics, and expansion waves. Even though all these are isentropic waves, there is a distinct difference between them. Mach waves are weak isentropic waves across which the flow experiences *insignificant* change in its properties. Whereas, the expansion waves and characteristics are isentropic waves which introduce small, but *finite*, property changes to a flow passing them. Thus, even though we loosely state that Mach lines and Mach waves are isentropic waves in a supersonic flow, inclined at angle  $\mu$  to the freestream direction, in reality they are distinctly different. Mach waves are the weakest degeneration of isentropic waves to the limiting case of zero strength that a flow across which will not experience any change of property. Whereas, a Mach line is a weak isentropic wave in a supersonic flow field, causing small but finite changes of properties to the flow passing through it.

The characteristic lines play an important role in the compression and expansion processes in the sense that it is only through these lines that it is possible to retard or accelerate a supersonic flow isentropically. Also, this concept will be employed in designing supersonic nozzles with method of characteristics in Chapter 9.

## 4.6 Weak Oblique Shocks

In Section 4.5, we have seen that the compression of supersonic flow without entropy increase is possible only through the Mach lines. In the present discussion on weak shocks also, it will be shown that these weak shocks, which result when the flow deflection angle  $\theta$  is small and Mach number downstream of shock  $M_2 > 1$ , can also compress the flow with entropy increase almost close to zero. It is important to note that, when we discussed about flow through oblique shocks, we considered the shock as weak when the downstream Mach number  $M_2$  is supersonic (even though less than the upstream Mach number  $M_1$ ). When the flow traversed by an oblique shock becomes subsonic (i.e.  $M_2 < 1$ ), the shock is termed *strong*. But when the flow turning  $\theta$  caused by a weak oblique shock is very small, then the weak shock assumes a special significance. These kinds of weak shocks, when both the decrease of flow Mach number ( $M_1 - M_2$ ) and flow turning angle  $\theta$  are small, can be regarded as isentropic compression waves.

For small values of  $\theta$ , the oblique shock relations reduce to very simple forms. For this case,

$$\sin \theta \approx \theta \text{ and } \cos(\beta - \theta) \approx \cos \beta$$

Therefore, Eq. (4.14) simplifies to

$$M_1^2 \sin^2 \beta - 1 \approx \left( \frac{\gamma + 1}{2} M_1^2 \tan \beta \right) \theta$$

Also,  $M_2 > 1$  for weak oblique shocks. Therefore, we may approximate this weak shock with both  $(M_1 - M_2)$  and  $\theta$  extremely small as a Mach line. Thus, the shock angle  $\beta$  can be regarded as almost equal to the Mach angle  $\mu$ . With this approximation, we can express  $\tan \beta$  as follows.

$$\begin{aligned} \sin \beta &\approx \sin \mu = \frac{1}{M} \\ \cos \beta &= \sqrt{1 - \sin^2 \beta} \\ &= \frac{1}{M} \sqrt{M^2 - 1} \\ \tan \beta &= \frac{1}{\sqrt{M^2 - 1}} \end{aligned}$$

Substituting for  $\tan \beta$  in the preceding equation, we get

$$M_1^2 \sin^2 \beta - 1 \approx \frac{\gamma + 1}{2} \frac{M_1^2}{\sqrt{M_1^2 - 1}} \theta \quad (4.20)$$

Equation (4.20) is considered the basic relation for obtaining all other appropriate expressions for weak oblique shocks since all oblique shock relations depend on  $M_1 \sin \beta$ , which is the component of upstream Mach number normal to the shock.

It can be seen from Eqs. (4.3) and (4.20) that the pressure change across a shock  $\frac{\Delta p}{p_1}$ , termed the *shock strength*, can be easily expressed as

$$\frac{p_2 - p_1}{p_1} = \frac{\Delta p}{p_1} \approx \frac{\gamma M_1^2}{\sqrt{M_1^2 - 1}} \theta \quad (4.21)$$

Equation (4.21) shows that the strength of the shock wave is proportional to the flow deflection angle  $\theta$ .



Similarly, it can be shown that the changes in density and temperature are also proportional to  $\theta$ . But the change in entropy, on the other hand, is proportional to the third power of shock strength, as shown below. By Eq. (4.5), we have

$$\frac{s_2 - s_1}{R} = \ln \left[ \left( 1 + \frac{2\gamma}{\gamma + 1} m \right)^{1/(\gamma-1)} (1 + m)^{-\gamma/(\gamma-1)} \left( \frac{\gamma-1}{\gamma+1} m + 1 \right)^{\gamma/(\gamma-1)} \right] \quad (4.22)$$

where  $m = (M_1^2 - 1)$ . (Note that for weak oblique shocks under consideration, i.e. for weak oblique shocks with  $(M_1 - M_2) \ll 1$  and  $\theta$  very small,  $M_1^2 \sin^2 \beta$  is approximated as  $M_1^2$ ). For values of  $M_1$  close to unity,  $m$  is small and the terms within the parentheses are like  $1 + \epsilon$ , with  $\epsilon \ll 1$ . Expanding the terms as logarithmic series, we get

$$\frac{s_2 - s_1}{R} = \frac{2\gamma}{(\gamma + 1)^2} \frac{m^3}{3} + \text{higher-order terms}$$

or

$$\frac{s_2 - s_1}{R} \approx \frac{2\gamma}{(\gamma + 1)^2} \frac{(M_1^2 - 1)^3}{3} \quad (4.23)$$

Because the entropy cannot decrease in an adiabatic flow, Eq. (4.23) stipulates that  $M_1 \geq 1$ . Thus, the increase in entropy is of *third order* in  $(M_1^2 - 1)$ . This may be written in terms of shock strength,  $\Delta p/p$ , with Eq. (3.16) as

$$\frac{s_2 - s_1}{R} \approx \frac{\gamma + 1}{12\gamma^2} \left( \frac{\Delta p}{p_1} \right)^3 \quad (4.24)$$

But by Eq. (4.21), the shock strength is proportional to  $\theta$  and hence

$$\boxed{\Delta s \sim \theta^3} \quad (4.25)$$

Thus, a small but finite change of pressure across a weak oblique shock, for which there are corresponding first-order changes of density and temperature, gives only a third-order change of entropy, i.e. a weak shock produces a nearly isentropic change of state.

Now, let the wave angle  $\beta$  for the weak shock be different from the Mach angle  $\mu$  by a small angle  $\epsilon^\circ$ . That is,

$$\beta = \mu + \epsilon$$

where  $\epsilon \ll \mu$ . Therefore,  $\sin \beta = \sin(\mu + \epsilon) = \sin \mu + \epsilon \cos \mu$ . Also,  $\sin \mu = 1/M_1$  and  $\cot \mu = \sqrt{M_1^2 - 1}$ . Thus,

$$M_1 \sin \beta \approx 1 + \epsilon \sqrt{M_1^2 - 1} \quad (4.26)$$

or

$$M_1^2 \sin^2 \beta \approx 1 + 2\epsilon \sqrt{M_1^2 - 1} \quad (4.27)$$

From Eqs. (4.20) and (4.27), we obtain

$$\epsilon = \frac{\gamma + 1}{4} \frac{M_1^2}{M_1^2 - 1} \theta \quad (4.28)$$

That is, for a finite flow deflection angle  $\theta$ , the direction of weak oblique shock wave differs from the Mach wave direction  $\mu$  by an amount  $\epsilon$ , which is of the same order as  $\theta$ .

## 4.7 Supersonic Compression

Compressions in a supersonic flow are not usually isentropic. Generally, they take place through a shock wave and hence are nonisentropic. But there are certain cases, for which the compression process can be regarded as isentropic. A compression process which can be treated as isentropic is illustrated in Figure 4.13, where the turning of the flow is achieved through a large number of weak oblique shocks. This kind of compression through a large number of weak compression waves is termed *continuous compression*. These kinds of corners are called *continuous compression corners*. Thus, the geometry of the corner should have continuous smooth turning to generate a large number of weak (isentropic) compression waves.

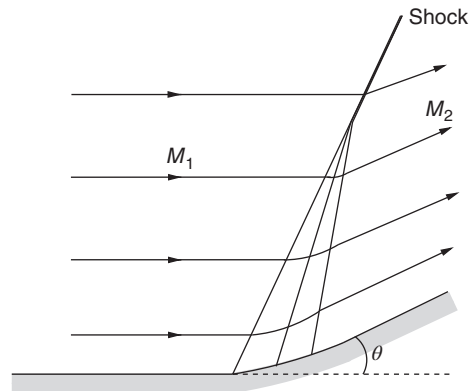
The weak oblique shocks divide the field near the wall into segments of uniform flow. Away from the wall the weak shocks might coalesce and form a strong shock, as illustrated in Figure 4.13. In Section 4.6, we saw that the entropy increase across a weak wave is of the order of third power of deflection angle  $\theta$ . Let the flow turning through an angle, shown in Figure 4.13, be taking place through  $n$  weak compression waves, each wave turning the flow by an angle  $\Delta\theta$ . The overall entropy change for this compression process is

$$(s_n - s_1) \sim n(\Delta\theta)^3 \sim n\Delta\theta(\Delta\theta)^2 \sim \theta(\Delta\theta)^2$$

Thus, if the compression is achieved through a large number of weak compression waves, the entropy increase can be reduced to a very large extent, as compared to a single shock causing the same net deflection. When  $\Delta\theta$  is made vanishingly small, a smooth continuous turning of the flow as shown in Figure 4.13 is achieved. The entropy increase associated with such a continuous smooth compression process is vanishingly small, i.e. the compression can be treated as isentropic.

At this stage it is natural to ask whether this kind of isentropic compression is only of theoretical interest or whether it is used in practical devices too. The answer to this question is that it is used in practical devices too. For example, in the gas turbine engines used to propel supersonic aircraft such as fighters, the freestream supersonic air stream entering the engine intake needs to be decelerated to incompressible Mach numbers (of the order of 0.2) before reaching the combustion chamber, because with the present technology continuous and stable combustion is possible only at low incompressible Mach numbers. This can be achieved by a single normal shock or even with a strong oblique shock to decelerate the supersonic stream to a subsonic Mach number and then the subsonic stream can be decelerated further in a diffuser to reach the required incompressible Mach number before entering the combustion chamber. But both these decelerations will result in a large increase of entropy and the associated large pressure

**Figure 4.13** Smooth continuous compression.



loss. This kind of large increase of entropy is desirable for an efficient mixing of fuel and air in the combustion chamber, but the severe pressure loss with the nonisentropic compression through the shocks is undesirable. We know that the engine is used to generate thrust by reaction. The momentum thrust produced by an engine is

$$\text{Thrust} = \dot{m}V_j$$

where  $\dot{m}$  is the mass flow rate of the combustion products of the fuel–air mixture burnt in the combustion chamber, expanded through the nozzle of the engine and  $V_j$  is the flow velocity at the nozzle exit. Following Bernoulli's principle, it is known that a large velocity  $V_j$  can be generated by expanding a gas at a high stagnation pressure of  $p_0$ . Thus, the aim of the process through the engine is to achieve a high  $p_0$ . If possible, we can use a compressor to achieve the desired level of  $p_0$ . But carrying a compressor in a gas turbine engine is not a practically possible solution, mainly owing to the weight penalty and the need for an additional source of energy to run the compressor. Therefore, as an alternative, the high pressure required is achieved through combustion where liberation of thermal energy by burning a fuel–air mixture results in a large increase of total temperature  $T_0$  and the associated increase of total pressure  $p_0$ . Now, we can notice an interesting point if we keenly observe the process involved. The vehicle is flying at a supersonic Mach number. Because of the skin friction, shock and expansion waves around the vehicle and other drag-producing effects cause the vehicle to encounter drag. This drag has to be compensated with thrust to maintain the supersonic flight speed. Thus, the basic work of the engine is to supply the required momentum to compensate the momentum loss due to the drag. In other words, basically the loss caused by the drag can be viewed as a loss of total pressure  $p_0$ . Therefore, the engine must compensate the pressure loss in order to maintain the constant  $p_0$  required for the supersonic flight at the given altitude. Instead of adding the stagnation pressure equivalent to compensate for the pressure loss due to drag, we are doing the same thing in an indirect manner. This is done through combustion. For performing combustion, the supersonic air entering the engine is decelerated to a low incompressible Mach number, fuel is mixed with the air and combustion is performed at such a low Mach number to increase  $p_0$  through the increase of stagnation temperature  $T_0$ . The combustion products at the low Mach number is accelerated through the engine nozzle to achieve the required jet velocity at the nozzle exit. In the deceleration process through shock/shocks at the engine intake, considerable total pressure is lost. Therefore, it would be appropriate and beneficial if the fuel is added to the air entering the engine with supersonic speed and the combustion is performed at the same freestream supersonic Mach number. But even though this is the most suitable and efficient situation, we are not in a position to do so. This is because the technology for performing stable combustion at supersonic Mach numbers is not yet established. Many research groups in various countries are working on establishing combustion at supersonic Mach numbers. Indeed, stable combustion at a Mach number of around 2 is reported by a few advanced countries, such as USA, China, Britain, France, and Japan. Once the technology for supersonic combustion is established, the pressure lost in decelerating the supersonic air stream to incompressible Mach number to enable combustion with the present technology can be eliminated to a large extent. This will result in a significant increase of engine efficiency. In other words, the pressure loss associated with the deceleration of supersonic or hypersonic flow entering the engine to the required incompressible Mach number for stable combustion with the present technology can be completely eliminated if technology is developed to perform stable combustion at supersonic/hypersonic Mach numbers.

## 4.8 Supersonic Expansion by Turning

Consider the turning of a two-dimensional supersonic flow through a finite angle at a convex corner, as illustrated in Figure 4.14. Let us assume that the flow is turned by an oblique shock at the corner, as shown in the figure.

The flow turning shown in Figure 4.14 is possible only when the normal component of velocity  $V_{2n}$  after the shock is greater than the normal component  $V_{1n}$  ahead of the shock, since  $V_{1t}$  and  $V_{2t}$  on either side of the shock must be equal. Although this would satisfy the equations of motion, it would lead to a decrease of entropy across the shock. Therefore, this turning process is not physically possible. From the geometry of the flow shown in Figure 4.14, it follows that  $V_{2n}$  must be greater than  $V_{1n}$ . The normal momentum equation yields

$$p_1 + \rho_1 V_{1n}^2 = p_2 + \rho_2 V_{2n}^2$$

Combining this with continuity equation

$$\rho_1 V_{1n} = \rho_2 V_{2n}$$

we obtain

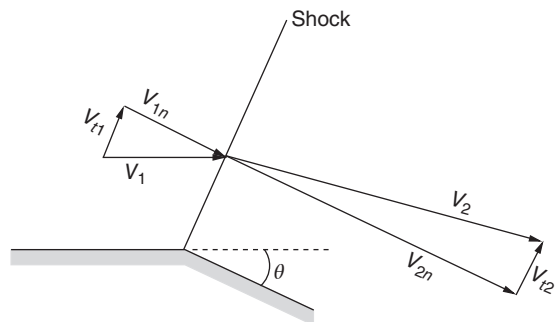
$$p_2 - p_1 = \rho_1 V_{1n}(V_{1n} - V_{2n})$$

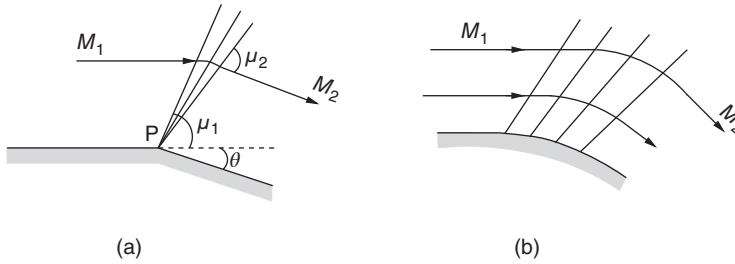
Because  $V_{2n} > V_{1n}$ , it follows that the pressure downstream of the corner should be less than the pressure upstream of the corner ( $p_2 < p_1$ ). For this, the flow should pass through an expansion fan at the corner. Thus, the wave at the convex corner must be an expansion fan, causing the flow to accelerate. In other words, the shock wave shown at the convex corner in Figure 4.14 is a physically impossible solution.

In an expansion process, the Mach lines are divergent, as shown in Figure 4.15, and, consequently, there is a tendency to decrease the pressure, density, and temperature of the flow passing through them. In other words, an expansion is isentropic throughout.

It is essential to note that the statement “expansion is isentropic throughout” is not always true. To gain an insight into the expansion process, let us examine the centered and continuous expansion processes illustrated in Figure 4.15a and b. We know that the expansion rays in an expansion fan are isentropic waves across which the change of pressure, temperature, density, and Mach number is small but finite. But when such small changes coalesce they can give rise to a large change. One such point where such a large change of flow properties occurs due to the amalgamation of the effect due to a large number of isentropic expansion waves is point P, which is the vertex of the centered expansion fan in Figure 4.15a. As illustrated in Figures 4.15a, the

**Figure 4.14** Supersonic flow over a convex corner.





**Figure 4.15** (a) Centered and (b) Continuous (simple) expansion processes.

pressure at the wall suddenly drops from  $p_1$  to  $p_2$  at the vertex of the expansion fan. Similarly, the temperature and density also drop suddenly at point P. The Mach number at P suddenly decreases from  $M_1$  to  $M_2$ . The entropy change across the vertex of the expansion fan is

$$s_2 - s_1 = c_p \ln \frac{T_2}{T_1} - R \ln \frac{p_2}{p_1}$$

It is seen that entropy change associated with the expansion process at point P is finite. Thus, the expansion process at point P is nonisentropic. Therefore, it is essential to realize that a centered expansion process is isentropic everywhere except at the vertex of the expansion fan, where it is nonisentropic. But for the continuous expansion illustrated in Figure 4.15b, there is no sudden change of flow properties. Even at the wall surface, the properties change gradually, as shown in the figure, owing to the absence of any point such as P in Figure 4.15a, where all the expansion rays are concentrated. Therefore, the continuous expansion is isentropic everywhere.

The expansion at a corner (Figure 4.15a) occurs through a centered wave, defined by a “fan” of straight expansion lines. This centered wave, also called a *Prandtl–Meyer expansion fan*, is the counterpart, for a convex corner, of the oblique shock at a concave corner.

A typical expansion over a continuous convex turn is shown in Figure 4.15b. Since the flow is isentropic, it is reversible.

## 4.9 The Prandtl–Meyer Expansion

Now, we are familiar with the fact that the supersonic flow passing through a Prandtl–Meyer expansion would experience a smooth, gradual change of flow properties. The Prandtl–Meyer fan consists of an infinite number of Mach (expansion) lines, centered at the convex corner. The expansion fan has a wedge-like shape with the corner as the apex, as shown in Figure 4.16. There are two Mach lines, one at an angle  $\mu_1$  to the initial flow (upstream of the fan) direction and the other at an angle  $\mu_2$  to the final flow (downstream of the fan) direction. The change in Mach number from  $M_1$  to  $M_2$  takes place through an infinite number of expansion lines. There is a wedge-like space with the corner as the apex, as shown in Figure 4.16, bounded by the two Mach lines, given by  $\mu_1$  and  $\mu_2$ .

As the streamlines turn smoothly across the expansion fan, the flow velocity increases continuously and the pressure, density, and temperature decrease continuously. This type of flow was first studied by Meyer, a student of Prandtl in 1907. This is a turning problem in which the streamlines are continuous and the flow is isentropic everywhere except at the vertex of the expansion fan, where the flow experiences a sudden change of flow properties and the process is nonisentropic. The argument that the expansion process is isentropic holds throughout for expansion over a continuous corner, as shown in Figure 4.17. It is important to note that the flow process across a centered expansion fan is isentropic everywhere except at the vertex of the fan (point A in Figure 4.16), where the flow process is nonisentropic because of the

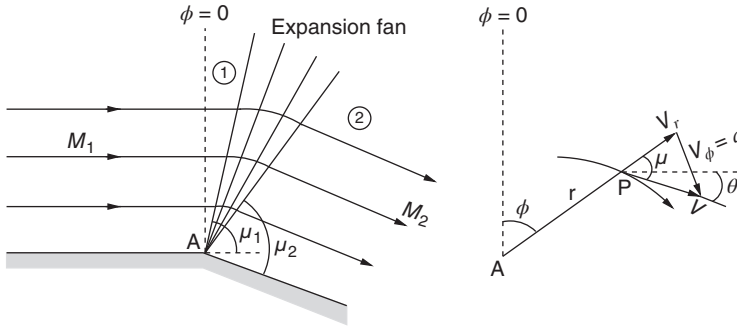


Figure 4.16 Prandtl-Meyer expansion over a sharp corner.

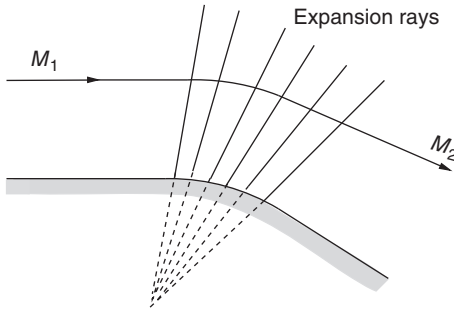


Figure 4.17 Prandtl-Meyer flow over a continuous corner.

accumulated effect of a large number of isentropic ways at a point. As we discussed earlier in this chapter, an important difference between the Mach lines or expansion rays and the Mach wave is the following. Even though all are isentropic rays, across the Mach lines and expansion rays the properties change are *small but finite*. Whereas, across a Mach wave, the flow properties' changes are *insignificant*, i.e. *negligibly small*.

This type of flow process is important from a mathematical point of view, since it is the only problem where an exact solution to the nonlinear compressible flow equation exists. In polar coordinates, the equations of motion for such flow can be written as

$$\frac{\partial}{\partial r}(\rho r V_r) + \frac{\partial}{\partial \phi}(\rho V_\phi) = 0 \quad (4.29)$$

$$V_r \frac{\partial V_r}{\partial r} + \frac{V_\phi}{r} \frac{\partial V_r}{\partial \phi} - \frac{V_\phi^2}{r} = -\frac{1}{\rho} \frac{\partial p}{\partial r} \quad (4.30)$$

$$V_r \frac{\partial V_\phi}{\partial r} + \frac{V_\phi}{r} \frac{\partial V_\phi}{\partial \phi} + \frac{V_r V_\phi}{r} = -\frac{1}{\rho} \frac{1}{r} \frac{\partial p}{\partial \phi} \quad (4.31)$$

Equation (4.29) is the continuity equation and Eqs. (4.30) and (4.31) are the  $r$  and  $\phi$  momentum equations, respectively. Momentum equations of this type for inviscid flow are also called Euler's equations. Note that in the above equations  $r$  and  $\phi$  are used as the variables for polar coordinates instead of the conventional  $r$  and  $\theta$  to avoid being confused with the symbol for a flow deflection angle  $\theta$ .

From the geometry of the flow, it is reasonable to assume that the flow properties do not change along any radial line, i.e. the flow properties vary only with  $\phi$  and are independent of  $r$ . This is a reasonable (also valid) assumption and considerably simplifies the equations.

By the above assumption, the derivatives of flow properties with respect to  $r$  are zero and so Eqs. (4.29)–(4.31) are no longer partial, i.e.

$$\frac{\partial V_r}{\partial r} = \frac{\partial p}{\partial r} = \frac{\partial V_\phi}{\partial r} = 0$$

Equations (4.29)–(4.31) now become

$$\rho V_r + \frac{d}{d\phi}(\rho V_\phi) = 0 \quad (4.32)$$

$$V_\phi = \frac{dV_r}{d\phi} \quad (4.33)$$

$$V_\phi \left( \frac{dV_\phi}{d\phi} + V_r \right) = -\frac{1}{\rho} \frac{dp}{d\phi} \quad (4.34)$$

But  $dp/d\phi$  can be expressed as

$$\frac{dp}{d\phi} = \frac{dp}{d\rho} \frac{d\rho}{d\phi} = a^2 \frac{d\rho}{d\phi}$$

Using this equation and relation (4.32), Eq. (4.34) can be rewritten as

$$\left( V_r + \frac{dV_\phi}{d\phi} \right) \left( 1 - \frac{V_\phi^2}{a^2} \right) = 0 \quad (4.35)$$

This is the governing equation for the Prandtl–Meyer flow. First, let the term in the first set of parentheses in Eq. (4.35) be zero, i.e.

$$V_r + \frac{dV_\phi}{d\phi} = 0$$

Therefore, from Eq. (4.34), we get

$$\frac{dp}{d\phi} = 0$$

This implies that the pressure is constant throughout the flow field and so there can be no expansion. But the basic geometry considered is an expansion field and, therefore, the above solution is impossible. Hence, from Eq. (4.35) we have

$$1 - \frac{V_\phi^2}{a^2} = 0$$

i.e.

$$\boxed{V_\phi = a} \quad (4.36)$$

The velocity is constant along the radial lines and is equal to the local speed of sound. This means that the radial lines must correspond to *Mach lines*. If the Mach lines are assumed to be identical to Mach waves, the Mach angle is given by

$$\sin \mu = \frac{V_\phi}{V} = \frac{a}{V} = \frac{1}{M}$$

Hence, all rays in an expansion field are Mach lines and the entire flow is isentropic.

#### 4.9.1 Velocity Components $V_r$ and $V_\phi$

By the compressible Bernoulli's equation, we have

$$\frac{\gamma}{\gamma - 1} \frac{p}{\rho} + \frac{V^2}{2} = \frac{\gamma}{\gamma - 1} \frac{p_0}{\rho_0} = \frac{V_{\max}^2}{2}$$

where  $p_0$  and  $\rho_0$  are the stagnation pressure and density, respectively. The resultant velocity  $V$  and the  $\phi$  component of velocity  $V_\phi$  are given by

$$\begin{aligned} V^2 &= V_r^2 + V_\phi^2 \\ V_\phi^2 &= a^2 = \frac{\gamma p}{\rho} \end{aligned}$$

With the above two relations, Bernoulli's equation may be rewritten as

$$V_r^2 + \frac{\gamma + 1}{\gamma - 1} V_\phi^2 = V_{\max}^2 \quad (4.37)$$

For the present flow, the velocity and pressure are constants along the radial lines and, therefore, Eq. (4.30) reduces to

$$\frac{dV_r}{d\phi} = V_\phi$$

Substituting the above expression for  $V_\phi$  into Eq. (4.37), we get

$$\frac{dV_r}{d\phi} = V_{\max} \sqrt{\frac{\gamma - 1}{\gamma + 1}} \sqrt{1 - \left( \frac{V_r}{V_{\max}} \right)^2}$$

Integration of the above equation by separation of variables gives

$$\phi \sqrt{\frac{\gamma - 1}{\gamma + 1}} = \arcsin \left( \frac{V_r}{V_{\max}} \right) + \text{constant} \quad (4.38)$$

From Figure 4.16, when  $\phi = 0$ , constant = 0. Therefore, Eq. (4.38) yields

$$V_r = V_{\max} \sin \left( \phi \sqrt{\frac{\gamma - 1}{\gamma + 1}} \right) \quad (4.39)$$

From Eqs. (4.39) and (4.33), we obtain

$$V_\phi = V_{\max} \sqrt{\frac{\gamma - 1}{\gamma + 1}} \cos \left( \phi \sqrt{\frac{\gamma - 1}{\gamma + 1}} \right) \quad (4.40)$$

For  $\phi = 0$ , Eq. (4.40) gives

$$V_\phi = V_{\max} \sqrt{\frac{\gamma - 1}{\gamma + 1}}$$

Substituting for  $V_{\max}$  from Bernoulli's equation, we get

$$V_\phi = \sqrt{\frac{2\gamma}{\gamma + 1} \frac{p_0}{\rho_0}} = \sqrt{\frac{2}{\gamma + 1}} a_0 = a^*$$

That is, at the beginning of the fan the  $\phi$  component of velocity corresponds to the speed of sound at sonic condition.

We can also express the pressure at any point in the Prandtl–Meyer flow in terms of  $\phi$  as follows. With the resultant velocity  $V^2 = V_r^2 + V_\phi^2$ , Bernoulli's equation can be expressed as

$$V_r^2 + V_\phi^2 = V_{\max}^2 \left[ 1 - \left( \frac{p}{p_0} \right)^{\frac{\gamma - 1}{\gamma}} \right]$$



Replacing  $V_r$  and  $V_\phi$  by Eqs. (4.39) and (4.40), we get

$$\begin{aligned}
 \left( V_{\max} \sin \left( \phi \sqrt{\frac{\gamma-1}{\gamma+1}} \right) \right)^2 + \left( V_{\max} \sqrt{\frac{\gamma-1}{\gamma+1}} \cos \left( \phi \sqrt{\frac{\gamma-1}{\gamma+1}} \right) \right)^2 &= V_{\max}^2 \left[ 1 - \left( \frac{p}{p_0} \right)^{\frac{\gamma-1}{\gamma}} \right] \\
 \sin^2 \left( \phi \sqrt{\frac{\gamma-1}{\gamma+1}} \right) + \frac{\gamma-1}{\gamma+1} \cos^2 \left( \phi \sqrt{\frac{\gamma-1}{\gamma+1}} \right) &= 1 - \left( \frac{p}{p_0} \right)^{\frac{\gamma-1}{\gamma}} \\
 1 - \cos^2 \left( \phi \sqrt{\frac{\gamma-1}{\gamma+1}} \right) + \frac{\gamma-1}{\gamma+1} \cos^2 \left( \phi \sqrt{\frac{\gamma-1}{\gamma+1}} \right) &= 1 - \left( \frac{p}{p_0} \right)^{\frac{\gamma-1}{\gamma}} \\
 \cos^2 \left( \phi \sqrt{\frac{\gamma-1}{\gamma+1}} \right) \left( \frac{\gamma-1}{\gamma+1} - 1 \right) &= - \left( \frac{p}{p_0} \right)^{\frac{\gamma-1}{\gamma}} \\
 \cos^2 \left( \phi \sqrt{\frac{\gamma-1}{\gamma+1}} \right) \frac{2}{\gamma+1} &= \left( \frac{p}{p_0} \right)^{\frac{\gamma-1}{\gamma}} \\
 \frac{1}{\gamma+1} \left( 1 + \cos \left( 2\phi \sqrt{\frac{\gamma-1}{\gamma+1}} \right) \right) &= \left( \frac{p}{p_0} \right)^{\frac{\gamma-1}{\gamma}}
 \end{aligned}$$

or

$$\left( \frac{p}{p_0} \right)^{\frac{\gamma-1}{\gamma}} = \frac{1}{\gamma+1} \left( 1 + \cos \left( 2\phi \sqrt{\frac{\gamma-1}{\gamma+1}} \right) \right) \quad (4.41)$$

From Eq. (4.41), it is seen that the flow can be turned by an angle  $\phi_{\max}$  where the pressure  $p$  will become zero. This condition results in

$$\phi_{\max} = \frac{\pi}{2} \sqrt{\frac{\gamma+1}{\gamma-1}} \quad (4.42)$$

For this situation,

$$V_r = V_{\max}, V_\phi = 0$$

For a perfect gas, such as air, with  $\gamma = 1.4$ , the maximum turning angle due to expansion is

$$\boxed{\phi_{\max} = 220.5^\circ}$$

Thus, the limiting maximum flow turning angle associated with Prandtl–Meyer expansion is

$$\boxed{\theta = 130.5^\circ}$$

From the foregoing discussion, it can be seen that the beginning of the Prandtl–Meyer expansion is marked by  $\phi = 0$ , where the radial component of flow velocity is zero and the expansion can go to the maximum extent where the static pressure of the flow goes to zero and the  $\phi$  component of the flow velocity also vanishes. The value of the expansion and flow deflection angles are  $220.5^\circ$  and  $130.5^\circ$ , respectively. The expansion described can be shown graphically, as shown in Figure 4.18. The normal direction to the hodograph curve in the figure gives the Mach line direction in the physical plane.

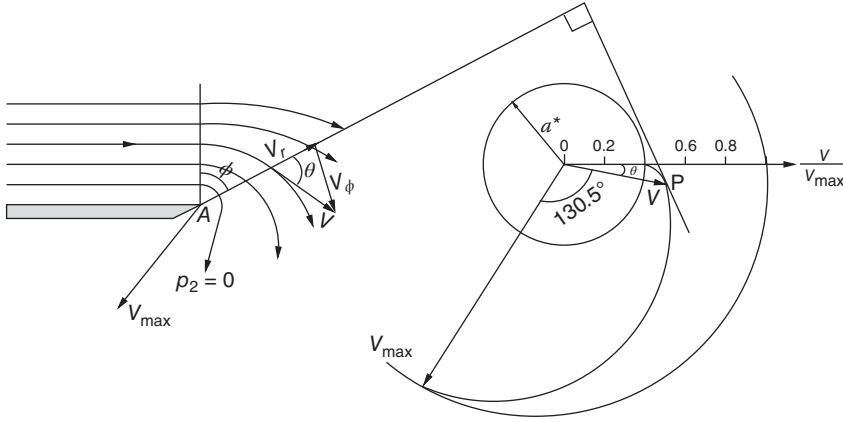


Figure 4.18 Expansion around a corner.

#### 4.9.2 The Prandtl–Meyer Function

It is known from basic studies on fluid flows that a flow which preserves its own geometry in space or time, or both, is called a *self-similar flow*. In the simplest cases of flows, such motions are described by a single independent variable, referred to as a *similarity variable*. The Prandtl–Meyer function is just such a similarity variable.

From the geometry of flow in Figure 4.16,  $\theta = \phi + \mu - \pi/2$ , where  $\theta$  is the isentropic turning angle. Now, we define the quantity  $\nu$  such that  $\nu = \pm\theta$ , where “+” holds across a *right-running characteristic* and “−” across a *left-running characteristic*. This function  $\nu$  is called the *Prandtl–Meyer function*. From the above definition,

$$\nu = \phi + \mu - \pi/2 \quad (4.43)$$

or

$$\phi = \pi/2 + \nu - \mu \quad (4.44)$$

From the flow geometry of Figure 4.16

$$\tan \mu = \frac{V_\phi}{V_r}$$

Substituting for  $V_\phi$  and  $V_r$  from Eqs. (4.39) and (4.40), we get

$$\tan \mu = \sqrt{\frac{\gamma-1}{\gamma+1}} \cot \left( \phi \sqrt{\frac{\gamma-1}{\gamma+1}} \right) \quad (4.45a)$$

or

$$\cot \mu = \sqrt{\frac{\gamma+1}{\gamma-1}} \tan \left( \phi \sqrt{\frac{\gamma-1}{\gamma+1}} \right) \quad (4.45b)$$

However,

$$\cot \mu = \sqrt{M^2 - 1} \quad (4.46)$$

With this the above equation can be expressed as

$$\sqrt{\frac{\gamma-1}{\gamma+1}}(M^2-1) = \tan\left(\phi\sqrt{\frac{\gamma-1}{\gamma+1}}\right)$$

or

$$\phi = \sqrt{\frac{\gamma+1}{\gamma-1}} \arctan \sqrt{\frac{\gamma-1}{\gamma+1}}(M^2-1)$$

Substitution of  $\phi$  from Eq. (4.44) into the above equation results in

$$\nu = \sqrt{\frac{\gamma+1}{\gamma-1}} \arctan \sqrt{\frac{\gamma-1}{\gamma+1}}(M^2-1) + \mu - \frac{\pi}{2}$$

From Eq. (4.46), we have the Mach angle

$$\mu = \arccot \sqrt{(M^2-1)}$$

Also,

$$\arccot \sqrt{(M^2-1)} = \pi/2 - \arctan \sqrt{(M^2-1)}$$

Using the above relations, we obtain the relation for the Prandtl–Meyer function in terms of the Mach number  $M_1$  just upstream of the expansion fan as

$$\nu = \sqrt{\frac{\gamma+1}{\gamma-1}} \arctan \sqrt{\frac{\gamma-1}{\gamma+1}}(M_1^2-1) - \arctan \sqrt{(M_1^2-1)} \quad (4.47)$$

Equation (4.47), expressing the Prandtl–Meyer function  $\nu$  in terms of the Mach number, is a very important result of supersonic flow. From this relation, it can be seen that for a given  $M_1$  there is a fixed  $\nu$ . Physically,  $\nu$  is the flow inclination from  $M_1 = 1$  (i.e.  $\phi = 0$ ) line.

If the wall inclination is  $\theta$ , then  $\nu_2$  can be obtained by adding  $\theta$  to  $\nu_1$ , i.e.  $\nu_2 = \nu_1 + \theta$ . As  $M_1$  varies from 1 to  $\infty$ ,  $\nu$  increases from 0 to  $\nu_{\max}$ . When  $\phi = 0$ ,  $M_1 = 1$ , and  $\nu = 0$ . When  $\phi_1 = 220.5^\circ$  or  $\theta_{\max} = 130.5^\circ$ ,  $M_2 = \infty$ , and  $\nu = \nu_{\max}$ . This maximum for  $\nu$  is

$$\nu_{\max} = \frac{\pi}{2} \left( \sqrt{\frac{\gamma+1}{\gamma-1}} - 1 \right) \quad (4.48)$$

For air with  $\gamma = 1.4$ ,  $\nu_{\max} = 130.5^\circ$  for  $M_1 = \infty$ . The Prandtl–Meyer function is tabulated in the isentropic flow tables (Table A.1 in the Appendix).

### Example 4.1

*Isentropic expansion:*

A Mach 2 air stream passes over a  $10^\circ$  expansion corner. Find the Mach number of the flow downstream of the expansion fan.

### Solution:

Given,  $M_1 = 2$  and  $\theta = 10^\circ$ . From the isentropic table, for  $M_1 = 2$ , the Prandtl–Meyer function is

$$\nu_1 = 26.38^\circ$$

Therefore, the value of the Prandtl–Meyer function  $\nu_2$  downstream of the expansion fan which turns the flow by  $10^\circ$  is

$$\nu_2 = \nu_1 + \theta = 26.38^\circ + 10^\circ = 36.38^\circ$$

Again, from the isentropic table, for  $\nu_2 = 36.38^\circ$ , we get the Mach number  $M_2$  downstream of the expansion fan as

$$M_2 = 2.386$$

### 4.9.3 Compression

The supersonic flow over a continuous compression corner, discussed in Section 4.7, resulting in the isentropic compression of flow is similar to the Prandtl–Meyer expansion except that compression results in isentropic deceleration of flow and expansion accelerates the flow isentropically. In expansion, all Mach lines diverge, whereas in compression, all Mach lines converge. The purpose of Mach lines is to change the direction of the streamlines in such a way that they become parallel to the solid boundary, as shown in Figure 4.13. For isentropic compression also, the Prandtl–Meyer function can be used, but this is restricted to the flow near the wall only. This is because, as illustrated in Figure 4.13, the isentropic compression waves emanating from the continuous compression corners progressively approach each other in the flow field away from the wall and ultimately coalesce to form a shock. As we know, the process across a shock is nonisentropic. Therefore, only in the proximity of the wall of a continuous compression, where the weak compressions waves generated retain their individual identity, can the waves be approximated as isentropic compression waves.

#### Example 4.2

*Isentropic compression:*

A Mach 2 air stream passes over a  $10^\circ$  isentropic compression corner. Find the downstream Mach number of the flow following the  $10^\circ$  turn.

#### Solution:

Given,  $M_1 = 2$ ,  $\theta = 10^\circ$ . From the isentropic table (Table A.1), for  $M_1 = 2$ ,

$$\nu_1 = 26.38^\circ$$

After the compression, the Prandtl–Meyer function becomes

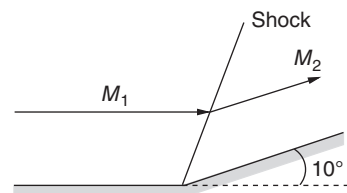
$$\nu_2 = \nu_1 - \theta = 16.38^\circ$$

Again, from the isentropic table, for  $\nu_2 = 16.38^\circ$ , the corresponding Mach number is

$$M_2 = 1.652$$

Instead of continuous change, if the compression is caused by only one kink at the wall of about  $10^\circ$ , the compression cannot be isentropic and the turning of the flow will take place through a shock wave, as shown in Figure 4.19. Only when the compression is continuous, can the process be treated as isentropic. However, for small values of  $\theta$ , the compression through a single compression wave, such as the one shown in Figure 4.19, the process can still be treated

**Figure 4.19** Flow over a compression corner.



as isentropic and reasonably accurate results can be obtained. Flow turning angle  $\theta \leq 5^\circ$  may be taken as the limit for considering the compression to be isentropic.

From the above discussion it is clear that the relation between the Prandtl–Meyer function and the flow turning angle may be expressed as

$$v_n = v_{n-1} + |\theta_n - \theta_{n-1}| \quad (\text{expansion}) \quad (4.49a)$$

$$v_n = v_{n-1} - |\theta_n - \theta_{n-1}| \quad (\text{compression}) \quad (4.49b)$$

## 4.10 Simple and Nonsimple Regions

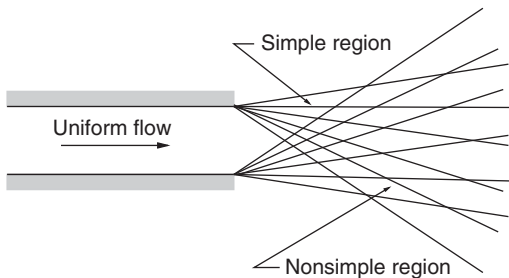
The waves causing isentropic expansion and compression discussed in Section 4.9 are called *simple waves*. A simple wave is a straight Mach line, with constant flow conditions, and is governed by the simple relations Eqs. (4.49a) and (4.49b) between the flow direction and the Prandtl–Meyer function.

A supersonic flow field with simple and nonsimple regions is shown in Figure 4.20. A supersonic expansion or compression zone with Mach lines which are straight is called a *simple region*. Equations (4.49a) and (4.49b) which govern the simple region are not applicable to nonsimple regions. Such a region may be treated by the method of characteristics as discussed in detail in Chapter 9.

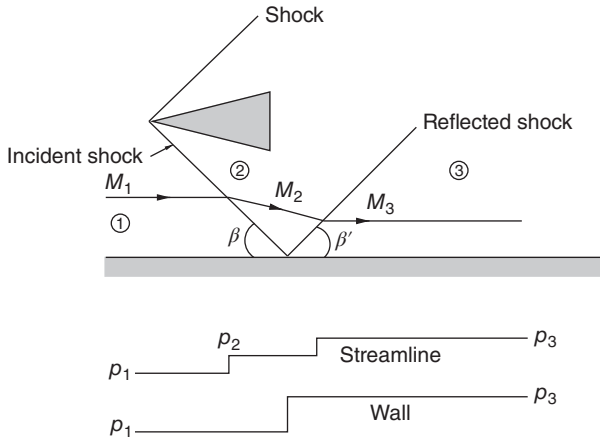
The Mach lines which are straight in the simple region become curved in the nonsimple region, after intersecting with other Mach lines. However, the wave segments between adjacent cross-over points may be treated as linear, without introducing significant error to the calculated results.

## 4.11 Reflection and Intersection of Shocks and Expansion Waves

When an oblique shock is intercepted by a solid wall, it is reflected. A possible flow field is as shown in Figure 4.21. If the incident shock is sufficiently weak, the reflection would be regular and could be treated according to linear theory, giving just a reflected shock of the same strength as the incident shock. For a shock which is not necessarily weak, the incident shock deflects the flow through an angle  $\theta$  toward the wall. A second reflected shock of opposite family is required to turn the flow back again by an amount  $\theta$ , to satisfy the constraint of the wall. That is, the flow passing through the incident shock is deflected by an angle  $\theta$  toward the wall, as shown in Figure 4.21. Therefore, the reflected shock must deflect the flow in the opposite direction to the same angle  $\theta$ , rendering the flow to travel parallel to the solid wall, in accordance with the flow physics that the streamline over a solid wall has to be parallel to the wall surface. Therefore, the Mach number  $M_2$  and wave angle of the reflected shock are dictated by the flow turning angle  $\theta$ .



**Figure 4.20** Simple and nonsimple regions in supersonic flow.



**Figure 4.21** Shock reflection from a rigid wall.

Although the flow deflection  $\theta$ , caused by the incident and reflected shocks, is equal in magnitude, the pressure ratios of the incident and reflected shocks are not equal, since  $M_2 < M_1$ . The pressure distribution along a streamline and along the wall are shown in Figure 4.21. The strength of the reflected shock wave can be defined by the overall pressure ratio

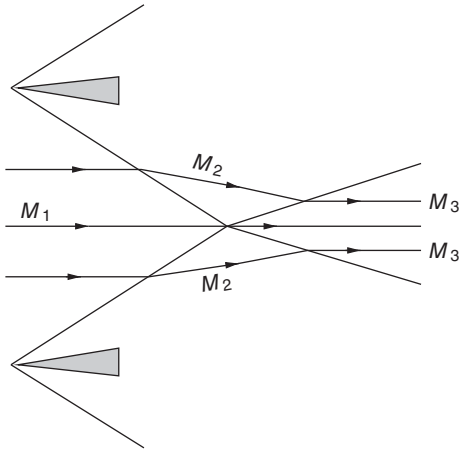
$$\frac{p_3}{p_1} = \frac{p_3}{p_2} \frac{p_2}{p_1}$$

But  $p_3/p_2$  and  $p_2/p_1$  are the strengths of reflected and incident shocks, respectively. Therefore, the strength of reflection is given by the product of individual shock strengths.

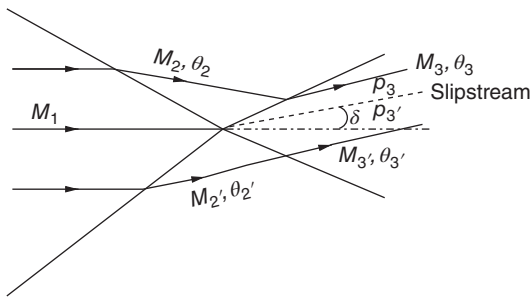
The reflection from a rigid surface, in general, is not specular, that is the reflected shock inclination ( $\beta'$ ) is not equal to the incident shock inclination ( $\beta$ ). Now there exists one of two possibilities: either  $\beta > \beta'$  or  $\beta < \beta'$ . These two cases are opposite, and the net result depends on the particular values of  $M_1$  and  $\theta$ . These results cannot be written explicitly in general form but may easily be obtained, for the particular cases with specified values of  $M_1$  and  $\theta$ , from the oblique shock charts. For high Mach numbers ( $M_1$ ),  $\beta > \beta'$ , whereas for low Mach numbers,  $\beta < \beta'$ . It is important to recall that the reflection of a wave from a surface is governed by the surface roughness. From elementary physics we know that reflection from a surface could be either specular or diffuse. *Specular reflection* is that in which the reflection is like a mirror image. That is, the wave angles of the incident and reflected waves will be the same. For this the surface should be absolutely smooth. But we know that absolute smoothness or zero roughness for a surface is only an imaginary situation. In reality all physical surfaces have some roughness. However, the roughness of a surface can vary depending upon the manufacturing technique used. For example, the surface finish of a high-quality mirror is about  $\lambda/20$ , where  $\lambda$  is the wavelength of light. Therefore, any physical surface is rough enough to cause diffuse reflection. Thus, specular reflection is essentially an assumption made to obtain simplified solutions for most practical problems.

When an oblique shock is intercepted by another oblique shock of the same strength but of opposite family, the possible flow field will look like the one shown in Figure 4.22. Viewing in the flow direction, the shocks running to the left are named as one family (the left-running family) and the shocks running to the right are called the opposite family (the right-running family).

The shocks “pass through” each other, but are slightly “bent” in the process. The flow downstream of the shock system is parallel to the initial flow.



**Figure 4.22** Interaction of oblique shocks of opposite families with equal strength.



**Figure 4.23** Intersection of oblique shocks of opposite families with different strengths.

When two shocks of unequal strength intersect, a new flow geometry is established, as shown in Figure 4.23. The flow field is divided into two portions by the streamline through the intersection point. The two portions experience different changes while passing through the shock wave system. The overall results must be such that, after crossing the wave system, the two portions have the same pressure and same flow direction, that is  $p_3 = p_{3'}$  and  $\theta_3 = \theta_{3'}$ . The flow downstream of the reflected shocks (zone 3) need not be in the freestream direction. These two requirements determine the final direction  $\delta$  and the final pressure  $p_3$ .

The streamline shown with the dashed line in Figure 4.23, having two flow fields of different parameters ( $T$  and  $\rho$ ) on either side of it, is called the *contact surface*. The contact surface may also be *idealized* as a surface of discontinuity. The contact surface can either be stationary or moving. Unlike the shock wave, there is no flow of matter across the contact surface. In the literature, we can find this contact surface being referred to by different names: *material boundary*, *entropy discontinuity*, *slipstream* or *slip surface*, *vortex sheet*, and *tangential discontinuity*. It is essential to note that the contact surface is a fluid boundary across which there is no mass transport. Further, the surface can tolerate temperature and density gradients, but not pressure gradient. In other words, the temperature and density on either side of the slipstream can be different but the pressure on both sides must be equal. This may also be stated as follows. The contact surface can tolerate thermal and concentration imbalance but not pressure imbalance.

### Example 4.3

An oblique from a wedge in a Mach 2 air stream is reflected from a flat surface. If the flow turning caused by the shock is  $11^\circ$ , determine (a) the wave angle of the reflected shock, (b) the Mach number downstream of the reflected shock, and (c) the strength of reflection.

**Solution:**

- (a) For the incident shock,  $M_1 = 2$  and  $\theta = 11^\circ$ . For this Mach number and  $\theta$ , from the oblique shock table (Table A.3), we get

$$\beta_1 = 40.42^\circ, \quad M_2 = 1.6, \quad \frac{p_2}{p_1} = 1.795$$

For  $M_2 = 1.6$  and  $\theta = 11^\circ$ , from the oblique shock chart (Figure A.1), we have

$$\beta_2 = 52.88^\circ$$

The normal component of the Mach number upstream of the reflected shock is

$$\begin{aligned} M_{2n} &= M_2 \sin \beta_2 = 1.6 \times \sin 52.88 \\ &= 1.276 \end{aligned}$$

For  $M_{2n} = 1.276$ , from the normal shock table (Table A.2),

$$M_{3n} = 0.808, \quad \frac{p_3}{p_2} = 1.732$$

- (b) The Mach number downstream of the reflected shock is

$$\begin{aligned} M_3 &= \frac{M_{3n}}{\sin(\beta_2 - \theta_2)} \\ &= \frac{0.808}{\sin(52.88 - 11)} \\ &= 1.213 \end{aligned}$$

- (c) The strength of reflection is

$$\begin{aligned} \frac{p_3}{p_1} &= \frac{p_3}{p_2} \frac{p_2}{p_1} \\ &= 1.732 \times 1.795 \\ &= 3.11 \end{aligned}$$

#### 4.11.1 Intersection of Shocks of the Same Family

When a shock intersects another shock of the same family, the shocks cannot pass through, as in the case of intersection of shocks of an opposite family. The shocks will coalesce to form a single stronger shock, as shown in Figure 4.24, where shocks of the same family are produced by successive corners in the same wall.

If the second shock BO is much weaker than the first one (AO), then OC will be a compression wave. This intersection may also be described as follows. The second shock is partly *transmitted* along OM, thus augmenting the strength of the first one and partly reflected along OC.

Shocks are referred to as *left-running* and *right-running* depending on whether they run to the left or right when viewed in the flow direction. Left-running waves constitute one family and right-running waves constitute the opposite family.

#### Example 4.4

For the flow field shown in Figure 4.25, determine  $\beta_r$  with respect to the flow direction in zone 2,  $M_2$ , and  $M_3$  if  $M_1 = 2.0$  and  $\beta_i = 40^\circ$ .



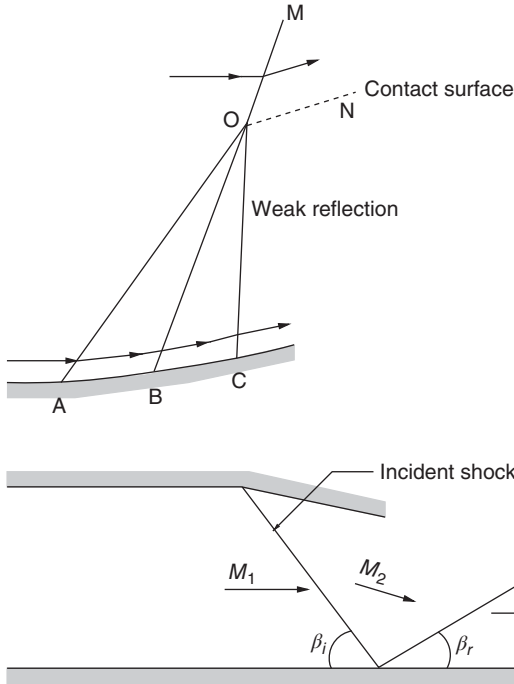


Figure 4.24 Intersection waves of the same family.

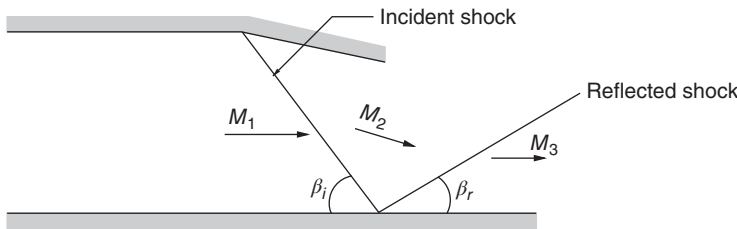


Figure 4.25 Shock reflection from a solid surface.

**Solution:**

From the oblique shock chart 1 (Figure A.1), for  $M_1 = 2.0$  and  $\beta_i = 40^\circ$ , we get  $\theta = 10.5^\circ$ . This  $\theta$  corresponds to the angle through which the flow is turned by the incident shock wave. Also, the angle through which the flow is turned back after the reflected wave should be  $10.5^\circ$ , to satisfy the streamline concept that the flow should be parallel to the surface over which it flows. From oblique shock chart 2 (Figure A.2), we have

$$M_2 = 1.63 \text{ for } M_1 = 2.0, \theta = 10.5^\circ$$

$$M_3 = 1.3 \text{ for } M_2 = 1.63, \theta = 10.5^\circ$$

For  $M_2 = 1.63$  and  $\theta = 10.5^\circ$ , from oblique shock chart 1, we get the corresponding shock angle as  $\beta = 50.2^\circ$ .

The angle between the flow directions of zone 2 and the reflected wave is

$$\beta_r = 50.2 - 10.5 = \boxed{39.7^\circ}$$

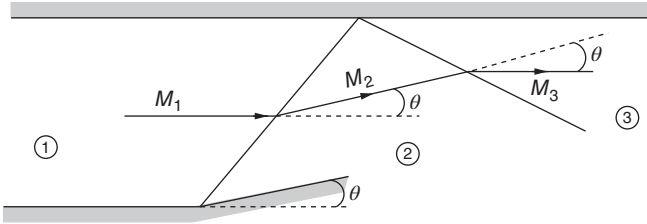
**Example 4.5**

A Mach 4.0 air stream at  $10^5$  Pa is turned abruptly by a wall into the flow with a turning angle of  $20^\circ$ , as shown in Figure 4.26. If the shock is reflected by another wall, determine the Mach number and pressure downstream of the reflected shock.

**Solution:**

For  $M_1 = 4.0$  and  $\theta = 20^\circ$ , from the oblique chart 1 (Figure A.1), the shock angle is

$$\beta_{12} = 32.5^\circ$$



**Figure 4.26** Shock reflection from a solid surface.

Hence,

$$M_{1n} = M_1 \sin \beta = 2.149$$

From the normal shock table, for  $M_{1n} = 2.149$ , we get

$$M_{2n} = 0.554, \frac{p_2}{p_1} = 5.226$$

Therefore,

$$M_2 = \frac{M_{n2}}{\sin(\beta - \theta)} = 2.56$$

Now, for  $M_2 = 2.56$  and  $\theta = 20^\circ$ , from the oblique shock chart,

$$\beta_{23} = 42.11^\circ$$

$$M'_{2n} = M_2 \sin \beta_{23} = 1.72$$

For  $M'_{2n} = 1.72$ , the normal shock table gives

$$M_{3n} = 0.64, \frac{p_3}{p_2} = 3.285$$

Hence, the Mach number downstream of the reflected shock is

$$\begin{aligned} M_3 &= \frac{0.64}{\sin(42.11 - 20)} \\ &= \boxed{1.7} \end{aligned}$$

Thus,

$$\begin{aligned} \frac{p_3}{p_1} &= \frac{p_3}{p_2} \frac{p_2}{p_1} = 3.285 \times 5.226 \\ &= 17.17 \\ p_3 &= \boxed{1.717 \text{ MPa}} \end{aligned}$$

*Note:* Problems involving oblique shocks can also be solved using the oblique shock tables instead of oblique shock charts.

#### 4.11.2 Wave Reflection from a Free Boundary

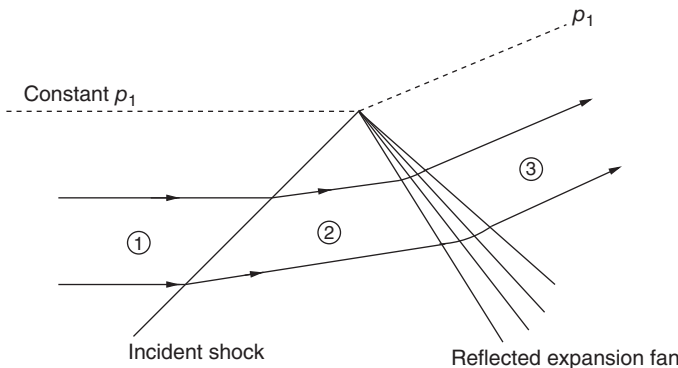
Reflection of shock from a solid wall is shown in Figure 4.21, and based on the analysis of that figure we also know that the reflection from a solid boundary, though generally not specular, is a *like reflection*. That is, an incident shock will be reflected as a shock and an incident expansion wave will be reflected as an expansion wave by a solid boundary. However, when the boundary

is a free boundary (such as a fluid boundary) the reflection will not be a like reflection. The wave patterns shown emanating from the nozzle exit in Figure 2.11b and c experience such reflection from a free boundary. Although they are not inherently quasi-one-dimensional flows, the wave pattern shown is frequently encountered in the study of nozzle flows.

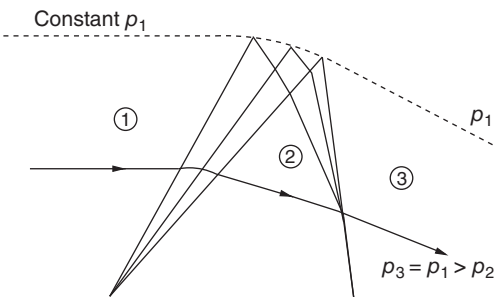
The gas jet emanating from a nozzle and propagating into the surrounding still atmosphere (at pressure  $p_a$ ) has a boundary surface which interfaces with the surroundings still atmosphere. As in the case of the slipstream discussed above the pressure across this boundary must be preserved, i.e. the pressure just below the jet boundary must be equal to the pressure  $p_a$  of the atmosphere in which the jet propagates, along its complete length. Therefore, the waves must reflect from the jet boundary in such a manner to preserve the pressure equilibrium all along the jet boundary. The free boundary, unlike a solid boundary, can change its shape and direction.

Examine the reflection of an oblique shock from a free boundary, as shown in Figure 4.27. The pressure  $p_1$  in region 1 is equal to the surrounding atmosphere. The pressure in the region downstream of the incident shock is  $p_2$ , which is higher than  $p_1$  ( $p_2 > p_1$ ). At the edge of the jet boundary, shown by the dashed line in Figure 4.27, the pressure must always be  $p_1$ . Therefore, when the incident shock impinges on the boundary, it must be reflected in such a manner as to result in  $p_1$  in region 3 behind the reflected wave. Hence, we have  $p_3 = p_1$  and  $p_1 < p_2$ , that is  $p_3 < p_2$ . This situation demands that the reflected wave must be an expansion wave, as shown in Figure 4.27. The flow in turn is deflected upward by both the incident shock and the reflected expansion fan, resulting in the upward deflection of the free boundary, as shown in Figure 4.27.

Reflection of an expansion fan from a free boundary is illustrated in Figure 4.28. The rays of the expansion fan are reflected from the free boundary as compression waves. These waves coalesce, forming a shock wave, as shown. The wave interaction shown in Figure 4.28 can be analyzed by the method of characteristics presented in Chapter 9.



**Figure 4.27** Shock wave reflection from a free boundary.



**Figure 4.28** Reflection of an expansion fan from a free boundary.

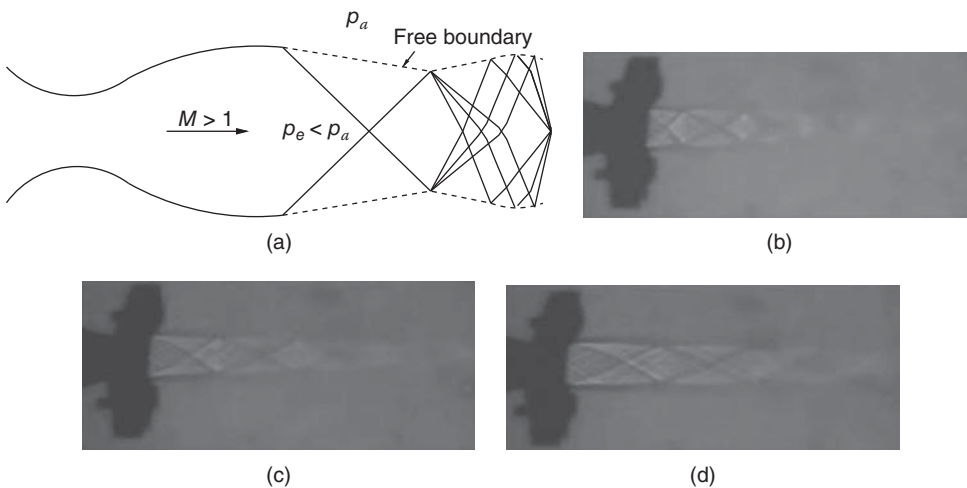
From the above discussions, the following two observations can be made.

- 1) The reflection of an incident wave from a solid boundary is termed *like reflection*, that is a shock wave reflects as a shock wave and an expansion wave reflects as an expansion wave.
- 2) The reflection of an incident wave from a free boundary is called *unlike reflection* (opposite manner), that is a shock wave reflects as an expansion wave and an expansion wave reflects as a shock (a compression wave).

Consider the overexpanded nozzle flow illustrated in Figure 2.11b. The flow pattern downstream of the nozzle exit will appear, as shown in Figure 4.29a. The various reflected waves form a diamond pattern throughout supersonic region of the exhaust jet. Shadowgraph pictures of a Mach 1.8 jet from a straight convergent–divergent nozzle of semi-divergence angle  $7^\circ$ , at overexpanded (nozzle pressure ratio, or NPR 4), correctly expanded (NPR 5.75) and underexpanded (NPR 7) states are shown in Figures 4.29b–d, respectively.

At NPR 4 the Mach 1.8 jet is overexpanded with nozzle exit pressure  $p_e$  less than the back-pressure  $p_a$ , which is the pressure of the ambient atmosphere to which the jet is discharged. Therefore, there is an oblique shock at the nozzle exit to increase  $p_e$  to come to equilibrium with  $p_a$ . This oblique shock formed at the nozzle exit is in the form of an axisymmetric truncated cone. The shock on impingement with the jet boundary reflects as compression waves, as seen in Figure 4.29b, as discussed above for Figure 4.29a. These compression and expansion waves experience back and forth reflections till the flow ceases to become supersonic. Thus, up to some distance downstream of the nozzle exit, waves prevail in the jet field, as seen in Figure 4.29b. The compression and expansion waves exhibit a pattern resembling a diamond.

At NPR 5.75, Mach 1.8 is correctly expanded with  $p_e = p_a$ . In this case, we may tend to think that there will not be any wave in the jet field. But it is not correct. This is because, even though there is pressure equilibrium at the nozzle exit, the supersonic jet issuing from the nozzle finds a large space to relax. This relaxation effect forces the flow to deflect away from the nozzle axis. We know that supersonic flows are wave dominated and any change of flow property or orientation will take place only through waves. In accordance with this flow physics, the relaxation effect causes the formation of an expansion fan at the nozzle exit, as seen in Figure 4.29c [6]. The



**Figure 4.29** (a) Diamond wave pattern in the exhaust from a supersonic nozzle (top), shadowgraph picture of (b) overexpanded (NPR 4) (second), (c) correctly expanded (NPR 5.75) (third), and (d) underexpanded (NPR 7) Mach 1.8 axisymmetric free jet (fourth).

waves of the expansion fan reflect back as compression waves from the jet boundary, coalesce, and become stronger compression waves and cross each other at the jet axis. These waves on reaching the jet boundary reflect back as expansion waves and the process continues. It can be seen in Figure 4.29c that the diamond pattern of waves prevails in the correctly expanded jet also, indicating that the correctly expanded free jet is also wave dominated.

A Mach 1.8 jet at NPR 7 is underexpanded with  $p_e > p_a$ . Therefore, to establish pressure equilibrium  $p_e$  should be reduced to become equal to  $p_a$ . This is caused by the expansion fan positioned at the nozzle exit, as seen in Figure 4.29d. The expansion waves of the fan reflect back as compression waves and the back and forth reflection of these compression and expansion waves establish a diamond pattern in the near field downstream of the nozzle exit. Now we may doubt whether there is any difference between the expansion fan at the nozzle exit for correctly expanded and underexpanded states. The answer to this is that there is a distinct difference between these two expansion fans. For the correctly expanded jet, the expansion fan is only due to the relaxation process. But for the underexpanded jet the expansion is due to the combined effect of pressure inequality and relaxation process. Therefore, the expansion fan for the underexpanded jet is significantly stronger than that of the correctly expanded jet. In fact, even for the overexpanded jet the flow at the nozzle exit would pass through the oblique shock caused by the overexpansion level and an expansion fan caused by the relaxation effect. An elaborate discussion giving a deeper insight into the flow process of correctly and incorrectly expanded free jets with qualitative and quantitative measure of the flow is given in Chapter 12, which discusses jets.

#### Example 4.6

Consider a two-dimensional duct carrying a perfect gas with uniform conditions of  $p_1 = 1$  atm and  $M_1 = 2.0$ . Design a 10 turning elbow to achieve a uniform downstream state 2 for each of the following cases: (a)  $M_2 > M_1$ ,  $s_2 = s_1$ , (b)  $M_2 < M_1$ ,  $s_2 = s_1$ , (c)  $M_2 < M_1$ ,  $s_2 > s_1$ , and (d)  $M_2 = M_1$ ,  $s_2 = s_1$ . For each case find the numerical values for  $M$ ,  $p$ , and the duct area (compared to that of state 1).

#### Solution:

(a) Given,  $M_2 > M_1$ ,  $s_2 = s_1$ . From the isentropic table, for  $M_1 = 2.0$ ,

$$\nu_1 = 26.38^\circ$$

Hence,

$$\nu_2 = \nu_1 + |\Delta\theta| = 26.38 + 10 = 36.38^\circ$$

For  $\nu_2 = 36.38^\circ$ , from the isentropic table,

$$M_2 = \boxed{2.387}$$

For  $M_1 = 2.0$ , again from the isentropic table,

$$\frac{p_1}{p_0} = 0.1278, \quad \frac{A^*}{A_1} = 0.5924$$

For  $M_2 = 2.387$ ,

$$\frac{p_2}{p_0} = 0.06948, \quad \frac{A^*}{A_2} = 0.4236$$

Therefore,

$$\begin{aligned} p_2 &= 0.06948 p_0 \\ &= 0.06948 \times \frac{p_1}{0.1278} \\ &= \boxed{0.544 p_1} \end{aligned}$$

$$\begin{aligned} \frac{d_2^2}{d_1^2} &= \frac{A_2}{A_1} \\ &= \frac{A_2 A^*}{A^* A_1} = 1.40 \\ d_2 &= \boxed{\sqrt{1.4} d_1} \end{aligned}$$

(b) Given,  $M_2 < M_1$ ,  $s_2 = s_1$ . It is an isentropic compression; therefore,

$$v_2 = v_1 - |\Delta\theta| = 16.38^\circ$$

From the isentropic table, for  $v_2 = 16.38^\circ$ ,

$$\begin{aligned} M_2 &= \boxed{1.655} \\ \frac{p_2}{p_0} &= 0.2168 \\ \frac{A^*}{A_2} &= 0.7713 \end{aligned}$$

Therefore,

$$\begin{aligned} p_2 &= 0.2168 p_0 \\ &= 0.2168 \times \frac{p_1}{0.1278} \\ &= \boxed{1.696 p_1} \\ \frac{d_2^2}{d_1^2} &= \frac{A_2 A^*}{A^* A_1} \\ &= \frac{0.5924}{0.7713} \\ &= 0.768 \\ d_2 &= \boxed{\sqrt{0.768} d_1} \end{aligned}$$

(c) Given,  $M_2 < M_1$ ,  $s_2 > s_1$ .

Unlike cases (a) and (b), case (c) is nonisentropic since  $s_2 > s_1$ . Therefore, there should be a shock in the duct to decelerate the flow from  $M_1$  to  $M_2$ . From the oblique shock chart 1, for  $M_1 = 2.0$  and  $\theta = 10^\circ$ ,  $\beta = 39.5^\circ$ . Thus,

$$M_{1n} = M_1 \sin \beta = 1.27$$

From the normal shock table, at  $M_{1n} = 1.27$ , we have

$$\begin{aligned} M_{2n} &= 0.8016, \frac{p_2}{p_1} = 1.715 \\ \frac{\rho_2}{\rho_1} &= 1.463, \frac{a_2}{a_1} = 1.083 \end{aligned}$$

Hence,

$$\begin{aligned} M_2 &= \frac{M_{2n}}{\sin(\beta - \theta)} \\ &= \boxed{1.628} \\ p_2 &= \boxed{1.715 p_1} \end{aligned}$$

By continuity,

$$\rho_2 A_2 V_2 = \rho_1 A_1 V_1$$

Therefore,

$$\begin{aligned} \frac{d_2^2}{d_1^2} &= \frac{A_2}{A_1} = \frac{\rho_1 V_1}{\rho_2 V_2} \\ &= \frac{\rho_1 M_1 a_1}{\rho_2 M_2 a_2} = 0.775 \\ d_2 &= \boxed{\sqrt{0.775} d_1} \end{aligned}$$

(d) Given,  $M_2 = M_1$ ,  $s_2 = s_1$ .

Thus, there is no change in area and flow properties from state 1 to 2.

#### Example 4.7

A Mach 2 uniform air stream at  $p_1 = 800$  kPa and temperature 270 K expands through two convex corners of  $10^\circ$  each, as shown in Figure 4.30. Determine the Mach number  $M_3$  downstream of the second fan and  $p_2$ ,  $T_2$ , and the angle of the second expansion fan.

#### Solution:

From the isentropic table, for  $M_1 = 2.0$ , we get

$$\nu_1 = 26.38^\circ$$

Therefore, the Prandtl–Meyer function after the first fan is

$$\nu_2 = \nu_1 + 10^\circ = 36.38^\circ$$

From the isentropic table, for  $\nu_2 = 36.38^\circ$ ,  $M_2 = 2.38$ . The Prandtl–Meyer function after the second fan is

$$\nu_3 = \nu_2 + 10 = 46.38^\circ$$

For  $\nu_3 = 46.38^\circ$ , from the isentropic table, we get  $M_3 = \boxed{2.83}$  and

$$M_3 = \boxed{2.83}$$

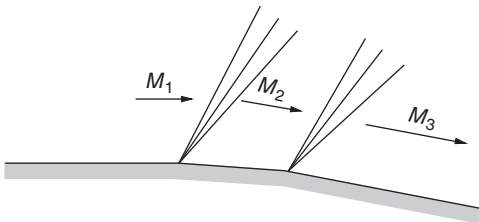


Figure 4.30 Flow expanded by two convex corners.

Also,

$$\frac{p_1}{p_{01}} = 0.1278, \frac{T_1}{T_{01}} = 0.5556 \text{ at } M_1 = 2.0$$

$$\frac{p_2}{p_{02}} = 0.0706, \frac{T_2}{T_{02}} = 0.4688 \text{ at } M_2 = 2.38$$

But for isentropic flow,  $p_{02} = p_{01}$ ,  $T_{02} = T_{01}$ . Therefore,

$$p_2 = \frac{0.0706}{0.1278} \times p_1$$

$$= \frac{0.0706}{0.1278} \times 800$$

$$= \boxed{441.94 \text{ kPa}}$$

$$T_2 = \frac{0.4688}{0.5556} \times 270$$

$$= \boxed{227.82 \text{ K}}$$

After the second fan, following the same procedure as above and using the isentropic table, we get

$$p_3 = 22.03 \text{ kPa}$$

$$T_3 = 186.8 \text{ K}$$

The fan angle for the second fan is

$$\mu_{23} = \theta + \mu_2 - \mu_3$$

$$= 10 + 24.85 - 20.69$$

$$= \boxed{14.16^\circ}$$

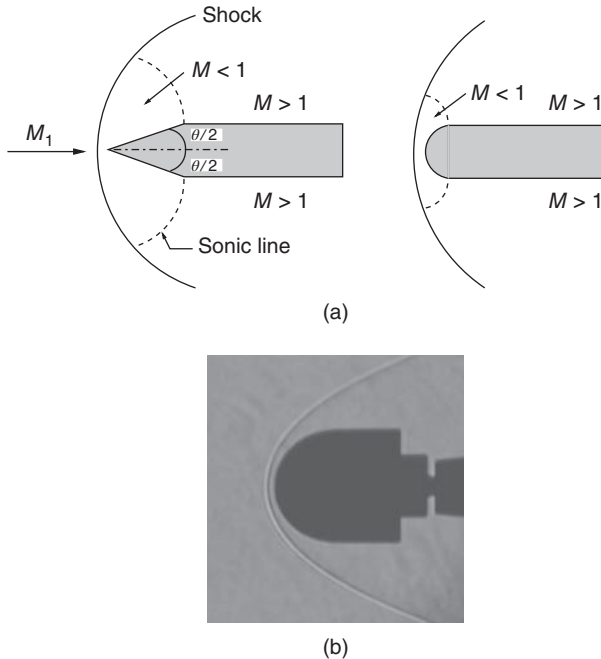
## 4.12 Detached Shocks

Detached shock is a compression front made up of approximately a normal shock followed by an infinite number of strong and weak oblique shocks of varying strengths which finally degenerates to a Mach wave. This is the shock which results when the wall deflection angle  $\theta$  is greater than  $\theta_{\max}$  (Section 4.3). We know from the discussion in Section 4.3 that there is no rigorous analytical procedure available for analyzing problems in which the deflection angles are more than  $\theta_{\max}$ . But experimentally, it has been observed that a flow with  $\theta > \theta_{\max}$  will have a configuration as shown in Figure 4.31a, with the shock wave slightly upstream of the nose even for a sharp-nosed body. The shape of the detached shock and its detachment distance depend on the geometry of the object facing the flow and the Mach number  $M_1$ .

For an object with a blunt nose, as shown in Figure 4.31b, the shock wave is detached at all supersonic and hypersonic Mach numbers. Therefore, even a streamlined body like a cone is a “blunt-nosed” body as far as the oncoming flow is concerned, when  $\theta > \theta_{\max}$ .

From Figure 4.31, it is seen that the shock portion at the nose of the object can be approximated to a normal shock. Therefore, immediately behind it there will be subsonic flow. Hence, the wedge portion of the sharp-nosed body gives rise to acceleration of the flow from subsonic to transonic before the flow reached the shoulder. Because of this acceleration to transonic Mach number, the flow encounters an expansion fan at the shoulder, in order to become parallel to the body downstream of the shoulder, in accordance with the streamline concept. Thus,





**Figure 4.31** Detached shock waves, (a) schematic sketches and (b) detached shock at the nose of a body at Mach 7.

the flow traversed by the expansion fan becomes supersonic. Therefore, there will be a sonic line, which will emanate from the shoulder of the wedge and the blunt-nosed body, as shown in Figure 4.31a. For blunt-nosed bodies, it is difficult to determine the exact position of the sonic line.

For a given wedge angle  $\theta$ , when  $M_1$  is high enough the shock is attached to the nose. As  $M_1$  decreases, the shock angle increases; with a further decrease of the Mach number, a value is reached for which the flow through the shock becomes subsonic. The shoulder of the body, behind the nose, now has an effect on the whole shock, which may be curved, even though attached. These conditions correspond to the region between the lines with  $M_2 = 1$  and  $\theta = \theta_{\max}$  in Figure 4.3. At the Mach number corresponding to  $\theta_{\max}$ , the shock wave begins to detach. This is called the *shock detachment Mach number*. With a further decrease of  $M_1$ , the detached shock moves upstream of the nose.

The analysis of the flow field associated with detached shock becomes very difficult because of the transonic flow, which prevails behind the shock. In this case, we mainly look for the shape of the shock, the detachment distance, and the shape of the sonic line. But such a solution does not exist. The approximation we usually make is that the sonic line is linear.

The strength of the detached shock is at its maximum near the stagnation streamline, where it is approximated as a normal shock and then it continuously decreases by becoming oblique until finally it becomes a Mach line, far away from the object.

It is interesting to note that the detached shock formed ahead of an object is a special compression front consisting of an infinite number of compression wave segments, beginning from nearly normal shock near the stagnation streamline, strong oblique shock segments above that, followed by weak oblique shock segments, and finally terminating into a Mach line, far away from the object.

From our discussions on detached shock it is evident that the higher the freestream Mach number, the closer will be the curved shock to the apex (for conical nose) and nose tip for a

blunt-nosed body. The density near the nose tip will be higher than the rest of the nose portion because the shock is normal near the stagnation point. The flow behind this normal portion of the shock will be subsonic. Hence, the wedge portion gives rise to acceleration of the flow from subsonic to supersonic. Therefore, there will be a sonic line, which will emanate from the shoulder of the wedge. For blunt-nosed bodies determination of the sonic line location is difficult. The problem of detached shock becomes complicated, owing to the presence of sonic flow zone. If at all a solution to the flow exists, it should give the shape of the shock, shock detachment distance, and the shape of the sonic line. But such a solution does not exist. One approximation usually made is that the sonic line is linear.

The shock strength is maximum near the stagnation point and then it decreases continuously by becoming oblique, until finally it becomes a Mach line. Because the strength decreases continuously, the entropy change also continuously decreases and hence the flow behind the detached shock is rotational.

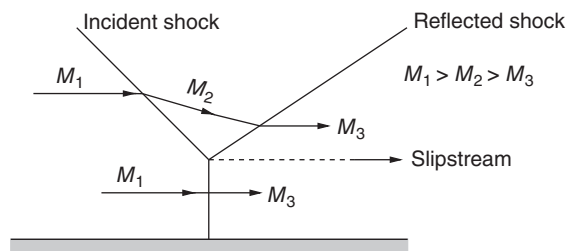
For the conical nose, there is an apex. Therefore, when  $\theta$  is decreased below  $\theta_{\max}$ , the flow detachment angle for the given freestream Mach number, there will be two attached oblique shocks. Also when the freestream Mach number for a conical-nosed body (Figure 4.31a) is greater than the shock detachment Mach number corresponding to its nose angle  $\theta$ , the shock will become attached. But for blunt-nosed bodies (Figure 4.31), the shock is never attached. For these bodies, even for  $M_{\infty} = \infty$ , the shock is detached. This is because the leading edge angle is  $90^\circ$ . For blunt-nosed bodies there is always a detached shock for any Mach number. But for sharp-nosed bodies, provided  $\theta < 45^\circ$ , there is a shock detachment Mach number below which only the shock will be detached. That is, when the Mach number is continuously decreased, the shock, which is oblique so far, gets detached. For  $\theta > 45^\circ$ , the shock detachment Mach number is extremely low.

### 4.13 Mach Reflection

A close look at the detached shock field will reveal that the complications associated with such a flow field are due to the appearance of subsonic regions in the flow. Similar complications, leading to a condition where no solution with a simple oblique shock wave is possible, will arise in a flow field with shock reflections. The intersection of normal shock and the right-running oblique shock gives rise to a reflected left-running oblique shock, in order to bring the flow into the original direction, as illustrated in Figure 4.32, this kind of reflection is termed *Mach reflection*. The left-running shock must have lesser strength compared to the right-running shock because of the flow deflection angle  $\theta$  involved in the compression process associated with the shock, but  $M_1 > M_2$ .

It may so happen that  $M_2$  is less than the shock detachment Mach number for the wall deflection required; in such a case, the entire picture of the flow field changes, all the shocks become curved, and the flow behind the shock system need not be parallel to the wall, as shown in Figure 4.33. Some other phenomenon might take place later on to bring the flow parallel to the wall.

**Figure 4.32** Mach reflection.



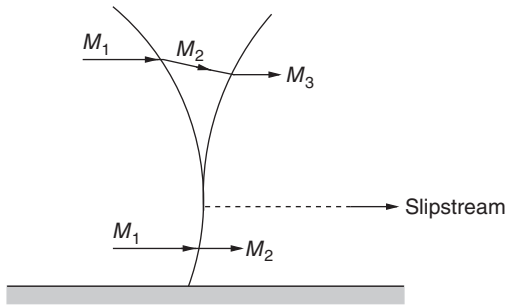


Figure 4.33 Flow past a shock system.

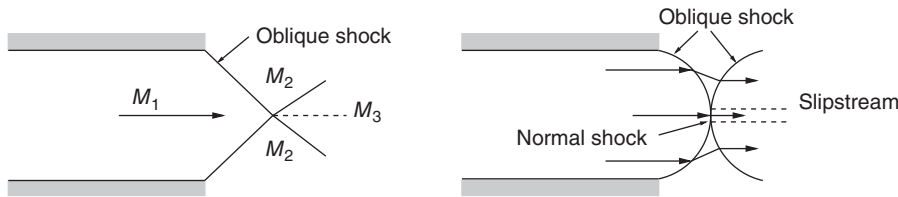


Figure 4.34 Intersection of oblique shocks.

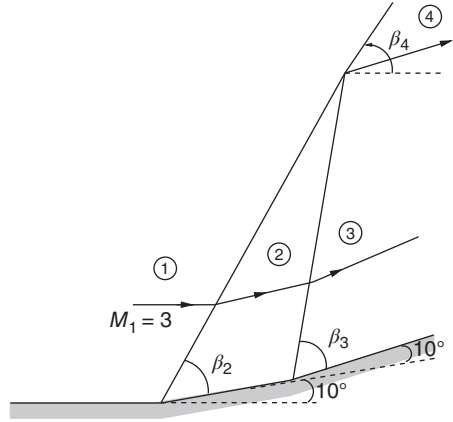
A similar phenomenon also occurs when two oblique shocks of opposite family intersect with a normal shock, bridging them, as shown in Figure 4.34.

From our discussions on shocks we know that, in the case of normally occurring oblique shocks, the strong shock solution is physically impossible. But a detached shock, even though naturally, occurs over blunt-nosed bodies and over sharp-nosed bodies with a nose angle larger than the shock detachment angle at a given supersonic (hypersonic) Mach number, possess both strong and weak oblique shocks at some location of its shape. Thus, detached shock is a special case among naturally occurring shocks, consisting of strong oblique shocks. Therefore, we can state that all naturally occurring oblique shocks are weak when they are just a single shock, but when they appear as a set of oblique shocks, as in the case of detached shock, the combination can have a set of strong and weak oblique shocks.

At this stage, it is important to realize that, as we saw in Section 4.11, the reflection of wave from a free boundary is unlike. In accordance with this, the reflection of the right-running shock from the intersection point of the normal shock in Figure 4.32 should be an expansion fan. But that is not the case in this reflection. This is because, even though the normal shock can be regarded as a free boundary, it is adjacent to a solid wall. Because of this proximity the shock could be able to resist the inertia of the impinging shock without deflecting to an extent to result in a kink at the point of oblique shock incidence. Owing to the absence of any kink, as shown in Figure 4.27, the shock experiences like reflection and gets reflected as a shock. But it is essential to note that the shape of the normal shock near the wall, shown as being linear, is an approximated idealization. In actual flows, the normal shock will assume a shape which is nonlinear, as in Figure 4.33. But it is not possible to predict the exact non-linear shape of the shock in a problem of this kind. The only means to identify the wave shape is through optical flow visualization, such as Schlieren or shadowgraph.

#### Example 4.8

For the flow field shown in Figure 4.35, find the flow Mach number at zones 2, 3, and 4. Assume the slipstream deflection to be negligible.

**Figure 4.35** Flow over two compression corners.**Solution:**

From the oblique shock chart 1, for  $M_1 = 3.0$  and  $\theta_2 = 10^\circ$ , we have

$$\beta_2 = 27.5^\circ$$

Therefore,

$$\begin{aligned} M_{1n2} &= 3 \sin 27.5^\circ \\ &= 1.38 \end{aligned}$$

From the normal shock table, for  $M_{1n2} = 1.38$ , we have

$$\frac{p_2}{p_1} = 2.055, M_{2n1} = 0.7483$$

Therefore,

$$\begin{aligned} M_2 &= \frac{M_{2n1}}{\sin(\beta_2 - \theta_2)} \\ &= \boxed{2.49} \end{aligned}$$

For  $M_2 = 2.49$  and  $\theta_3 = 10^\circ$ , from the oblique shock chart 1 (Figure A.1),

$$\beta_3 = 32^\circ$$

Therefore,

$$\begin{aligned} M_{2n3} &= 2.49 \sin 32^\circ \\ &= 1.32 \end{aligned}$$

From the normal shock table, for  $M_{2n3} = 1.32$ , we get

$$p_3/p_2 = 1.866 \text{ and } M_{3n2} = 0.7760$$

Therefore,

$$\begin{aligned} M_3 &= \frac{0.7760}{\sin(32 - 10)} \\ &= \boxed{2.07} \\ \frac{p_3}{p_1} &= \frac{p_3}{p_2} \times \frac{p_2}{p_1} \\ &= 1.866 \times 2.055 \\ &= 3.835 \end{aligned}$$

With no slipstream deflection,

$$\theta_4 = 20^\circ$$

From oblique shock chart 1, for  $M_1 = 3.0$  and  $\theta_4 = 20^\circ$ , we get

$$\beta_4 = 37.5^\circ$$

Therefore,

$$\begin{aligned} M_{1n4} &= 3 \sin 37.5^\circ \\ &= 1.83 \end{aligned}$$

From the normal shock table, for  $M_{1n4} = 1.83$ ,

$$\frac{p_4}{p_1} = 3.74, M_{n4} = 0.6099$$

Therefore,

$$\begin{aligned} M_4 &= \frac{0.6099}{\sin(37.5 - 20)} \\ &= \boxed{2.03} \end{aligned}$$

#### Example 4.9

Find the slipstream angle  $\delta_s$  for the flow field shown in Figure 4.36, using the oblique shock charts.

#### Solution:

From oblique shock chart 1 (Figure A.1), for  $M_\infty = 2.0$  and  $\theta_1 = 10^\circ$ , we get

$$\beta_1 = 39^\circ$$

For  $M_\infty = 2.0$  and  $\theta_1 = 10^\circ$ , from oblique shock chart 2, we get

$$M_1 = 1.665, \frac{p_1}{p_\infty} = 1.686$$

For  $M_\infty = 2.0$  and  $\theta_2 = 5^\circ$ , from oblique shock chart 1, we get

$$\beta_2 = 34.5^\circ$$

For  $M_\infty = 2.0$  and  $\theta_2 = 5^\circ$ , from oblique shock chart 2, we get

$$M_2 = 1.805 \text{ and } \frac{p_2}{p_\infty} = 1.323$$

Because of the slipstream, the properties in regions 3 and 4 have to be calculated by trial and error only.

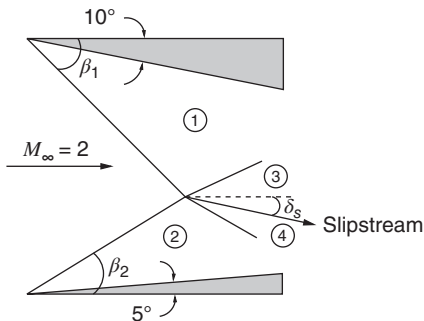


Figure 4.36 Intersection of two oblique shocks.

*Trial 1*

Let the downstream flow be parallel to upstream flow. For  $\theta_3 = 10^\circ$  and  $M_1 = 1.665$ , from oblique shock chart 1,

$$\beta_3 = 48.5^\circ$$

Therefore,

$$\begin{aligned} M_{1n3} &= M_1 \sin \beta_3 \\ &= 1.665 \times \sin 48.5^\circ \\ &= 1.247 \end{aligned}$$

For  $M_{1n3} = 1.247$ , from the normal shock table,

$$p_3/p_1 = 1.656$$

Therefore,

$$\begin{aligned} \frac{p_3}{p_\infty} &= \frac{p_3}{p_1} \times \frac{p_1}{p_\infty} \\ &= 1.656 \times 1.686 \\ &= 2.79 \end{aligned}$$

For  $\theta_4 = 5^\circ$  and  $M_2 = 1.805$ ,

$$\beta_4 = 38^\circ$$

Therefore,

$$\begin{aligned} M_{2n4} &= M_2 \sin \beta_4 \\ &= 1.805 \times \sin 38^\circ \\ &= 1.111 \end{aligned}$$

From the normal shock table, for  $M_{2n4} = 1.111$ ,

$$\frac{p_4}{p_2} = 1.271$$

Therefore,

$$\begin{aligned} \frac{p_4}{p_\infty} &= \frac{p_4}{p_2} \times \frac{p_2}{p_\infty} \\ &= 1.271 \times 1.323 \\ &= 1.68 \end{aligned}$$

Because  $p_3/p_\infty > p_4/p_\infty$ , the slipstream has to be deflected downwards so that the two pressures become equal.

*Trial 2*

Let

$$\frac{p_3}{p_\infty} = \frac{p_4}{p_\infty} = 2.25$$

Therefore,

$$\begin{aligned}\frac{p_3}{p_1} &= \frac{p_3}{p_\infty} \times \frac{p_\infty}{p_1} \\ &= 2.25 \times \frac{1}{1.686} \\ &= 1.334\end{aligned}$$

For  $p_3/p_1 = 1.334$ , from the normal shock table,

$$M_{1n3} = 1.135$$

Therefore,

$$\begin{aligned}\beta_3 &= \sin^{-1} \left( \frac{M_{1n3}}{M_1} \right) \\ &= 43^\circ\end{aligned}$$

For  $M_1 = 1.665$  and  $\beta_3 = 43^\circ$ , from oblique shock chart 1,

$$\theta_3 = 6.5^\circ$$

i.e.  $3.5^\circ$  below freestream direction. Similarly,

$$\begin{aligned}\frac{p_4}{p_2} &= \frac{p_4}{p_\infty} \times \frac{p_\infty}{p_2} \\ &= 2.25 \times \frac{1}{1.323} \\ &= 1.7\end{aligned}$$

For  $p_4/p_2 = 1.7$ , from the normal shock table,

$$M_{2n4} = 1.27$$

Therefore,

$$\begin{aligned}\beta_4 &= \sin^{-1} \left( \frac{M_{2n4}}{M_2} \right) = \sin^{-1} \left( \frac{1.27}{1.805} \right) \\ &= 44.7^\circ\end{aligned}$$

For  $M_2 = 1.805$  and  $\beta_4 = 44.7^\circ$ , from oblique shock chart 2 (Figure A.2),

$$\theta_4 = 11^\circ$$

i.e.  $6^\circ$  below the freestream direction.

### *Trial 3*

With downstream flow  $4.5^\circ$  below upstream flow,

For  $\theta_3 = 5.5^\circ$  and  $M_1 = 1.665$ , from oblique shock chart 1,

$$\beta_3 = 42.5^\circ$$

Therefore,

$$\begin{aligned}M_{1n3} &= M_1 \sin 42.5 = 1.665 \times \sin 42.5 \\ &= 1.125\end{aligned}$$

From the normal shock table, for  $M_{1n3} = 1.125$ ,

$$\frac{p_3}{p_1} = 1.31$$

Therefore,

$$\begin{aligned}\frac{p_3}{p_\infty} &= \frac{p_3}{p_1} \times \frac{p_1}{p_\infty} \\ &= 1.31 \times 1.686 \\ &= 2.21\end{aligned}$$

For  $\theta_4 = 9.5^\circ$  and  $M_2 = 1.805$ , from oblique shock chart 1.

$$\beta_4 = 43.5^\circ$$

Therefore,

$$\begin{aligned}M_{2n4} &= M_2 \sin \beta_4 \\ &= 1.805 \times \sin 43.5^\circ \\ &= 1.242\end{aligned}$$

For  $M_{2n4} = 1.242$ , from the normal shock table,

$$\frac{p_4}{p_2} = 1.63$$

Thus,

$$\begin{aligned}\frac{p_4}{p_\infty} &= \frac{p_4}{p_2} \times \frac{p_2}{p_\infty} \\ &= 1.63 \times 1.323 \\ &= 2.16\end{aligned}$$

In trial 3, it can be seen that pressures  $p_3$  and  $p_4$  are nearly equal, i.e. the assumed slipstream deflection ( $\delta_s$ ) of  $4.5^\circ$  is the correct value.

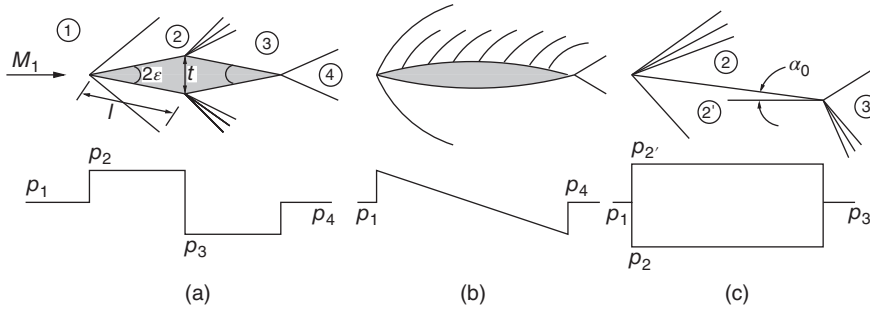
*Note:* This problem could have been solved using oblique shock tables too. But to practice the use oblique shock charts, this example has been solved with charts.

## 4.14 Shock-Expansion Theory

The shock and expansion waves discussed in this chapter are the basis for analyzing large number of two-dimensional supersonic flow problems by simply “patching” together appropriate combinations of two or more solutions. That is, the aerodynamic forces acting on a body present in a supersonic flow are governed by the shock and expansion waves formed at the surface of the body. This can be easily seen from the basic fact that the aerodynamic forces acting on a body depend on the pressure distribution around it, and in supersonic flow, the pressure distribution over an object depends on the wave pattern on it, as shown in Figure 4.37.

Consider the two-dimensional diamond airfoil kept at zero angle of attack in a uniform supersonic flow, as shown in Figure 4.37a. The supersonic flow at  $M_1$  is first compressed and deflected through an angle  $\epsilon$  by the oblique shock wave at the leading edge, forcing the flow to travel parallel to the wedge surface. At the shoulder located at mid-chord, the flow is expanded through an angle  $2\epsilon$  by the expansion fan. At the trailing edge, the flow is again deflected through an





**Figure 4.37** Wave pattern over objects.

angle  $\epsilon$ , in order to bring it back to the original direction. Therefore, the surface pressures on the wedge segments ahead and after the shoulder will be at a constant level over each segment for supersonic flow, according to oblique shock and the Prandtl–Meyer expansion theory.

On the diamond airfoil, at zero angle of attack, the lift is zero because the pressure distributions on the top and bottom surfaces are the same. Therefore, the only aerodynamic force acting on the diamond airfoil is due to the higher pressure on the forward face and lower pressure on the rearward face. The drag per unit span is given by

$$D = 2(p_2 l \sin \epsilon - p_3 l \sin \epsilon) = 2(p_2 - p_3)(t/2)$$

that is

$$D = (p_2 - p_3) t \quad (4.50)$$

Equation (4.50) gives an expression for drag experienced by a two-dimensional diamond airfoil, kept at zero angle of attack in an inviscid flow. This is in contrast to the familiar result from studies on subsonic flow that, for two-dimensional inviscid flow over a wing of infinite span at a subsonic flow, the drag force acting on the wing is zero – a theoretical result called D'Alembert's paradox. In contrast with this, for supersonic flow, drag exists even in the idealized, nonviscous fluid. This new component of drag encountered when the flow is supersonic is called *wave drag*, and is fundamentally different from the skin-friction drag and separation drag which are associated with boundary layer in a viscous fluid. The wave drag is related to the loss of total pressure and increase of entropy across the oblique shock waves generated by the airfoil.

For the flat plate at an angle of attack  $\alpha_0$  in a uniform supersonic flow, shown in Figure 4.37c, from the uniform pressure on the top and bottom sides, the lift and drag are computed very easily, with the following equations.

$$\begin{aligned} L &= (p_{2'} - p_2) c \cos \alpha_0 \\ D &= (p_{2'} - p_2) c \sin \alpha_0 \end{aligned} \quad (4.51)$$

where  $c$  is the chord.

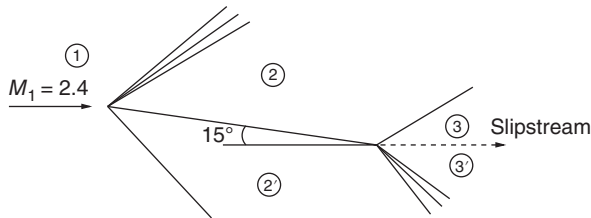
#### Example 4.10

A flat plate is kept at  $15^\circ$  angle of attack to a Mach 2.4 air stream, as shown in Figure 4.38. Solve the flow field around the plate and determine the inclination of slipstream to the freestream direction using shock-expansion theory.

#### Solution:

Using the shock and expansion wave properties, Table 4.1 can be formed.

**Figure 4.38** A flat plate an angle of incidence to Mach 2.4 flow.



**Table 4.1** Flow properties at different regions.

Region	$M$	$\nu$	$\mu$	$p/p_{01}$	$T/T_{01}$
1	2.4	36.8°	24.6°	0.0684	0.465
2	3.11	51.8°	18.8°	0.0231	0.341
3	2.33	35.0°	25.4°	0.0675	0.480
2'	1.80	20.7°	33.8°	0.1629	0.607
3'	2.36	35.7°	25.1°	0.0679	0.473

Table 4.1 lists the flow properties around the flat plate. Slip-surface inclination relative to freestream is negligibly small. The velocity jump across the slip-surface is found to be  $1 \text{ m s}^{-1}$ .

**Example 4.11**

Determine the flow field around a symmetrical double wedge of  $20^\circ$  included angle kept at  $15^\circ$  angle of attack to a Mach 2.4 air stream at a stagnation temperature of 300 K, shown in Figure 4.39, by shock-expansion theory.

**Solution:**

The flow properties are as given in Table 4.2 below.

From the above values, we get

$$a_4 = 258.7 \text{ m s}^{-1}, V_4 = 517.4 \text{ m s}^{-1}$$

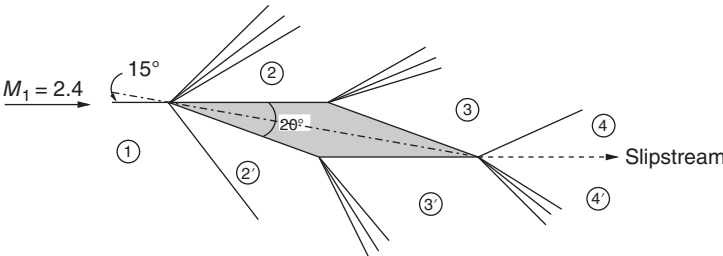
$$a_{4'} = 245.8 \text{ m s}^{-1}, V_{4'} = 548.1 \text{ m s}^{-1}$$

The slipstream surface is inclined at  $\approx 1^\circ$  upward relative to the freestream.

The velocity jump across the slipstream surface is  $= V_{4'} - V_4 = 548.1 - 517.4 = 30.7 \text{ m s}^{-1}$ .

**Example 4.12**

For the flow over the half-diamond wedge shown in Figure 4.40, find the inclinations of shocks and expansion waves and the pressure coefficient over the wedge surfaces 2 and 3.



**Figure 4.39** Flow over a symmetrical double wedge.

**Table 4.2** Flow properties at different regions.

Region	$M$	$\nu$	$\mu$	$p/p_{01}$	$T/T_{01}$
1	2.40	36.8°	24.6°	0.0684	0.465
2	2.62	41.8°	22.5°	0.0486	0.421
3	3.71	61.8°	15.6°	0.0098	0.267
4	2.00	26.5°	30.0°	0.0707	0.555
2'	1.31	6.5°	49.7°	0.2736	0.745
3'	2.00	26.5°	30.0°	0.0986	0.555
4'	2.23	32.5°	26.6°	0.0689	0.501

**Solution:**

## Region 2

From oblique shock chart 1, for  $M_1 = 1.8$  and  $\theta = 15^\circ$ ,

$$\beta_1 = \boxed{51.5^\circ}$$

By Eq. (4.3), we have

$$\begin{aligned} \frac{p_2}{p_1} &= 1 + \frac{2\gamma}{\gamma + 1}(M_1^2 \sin^2 \beta - 1) \\ &= 2.149 \end{aligned}$$

The pressure coefficient over surface 2 is

$$\begin{aligned} C_{p2} &= \frac{p_2 - p_1}{q_1} = \frac{2(p_2/p_1 - 1)}{\gamma M_1^2} \\ &= \boxed{0.506} \end{aligned}$$

By Eq. (4.7),

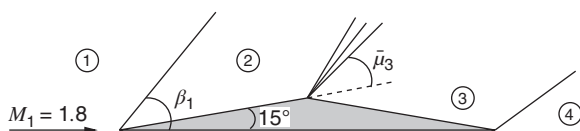
$$M_2 = \frac{M_{n2}}{\sin(\beta_1 - \theta)}$$

From the normal shock table, for  $M_{1n} = M_1 \sin \beta_1 = 1.4$ , we have

$$M_{2n} = 0.7397$$

Therefore,

$$\begin{aligned} M_2 &= \frac{M_{2n}}{\sin(\beta_1 - \theta_1)} \\ &= \frac{0.7397}{\sin(51.5^\circ - 15^\circ)} \\ &= 1.24 \end{aligned}$$

**Figure 4.40** Flow over a half-diamond wedge.

From the isentropic table, for  $M_2 = 1.24$ , we have

$$\nu_2 = 4.569^\circ \text{ and } \mu_2 = 53.751^\circ$$

Therefore,

$$\begin{aligned}\nu_3 &= \nu_2 + \theta_3 = 4.569 + 30 \\ &= 34.569^\circ\end{aligned}$$

For  $\nu_3 = 34.569^\circ$ , from the isentropic table,

$$M_3 = 2.315 \text{ and } \mu_3 = 25.6^\circ$$

Angles  $\mu_2$  and  $\mu_3$  are the inclination angles of the first and last rays of the expansion fan, respectively. Thus, the mean angle of the expansion fan becomes

$$\begin{aligned}\bar{\mu}_3 &= \frac{\mu_2 + \mu_3}{2} \\ &= \boxed{39.68^\circ}\end{aligned}$$

Region 3

For  $M_1 = 1.8$ , from the isentropic table (Table A.1), we have

$$\frac{p_1}{p_{01}} = 0.1740$$

For  $M_3 = 2.315$ , from the isentropic table,

$$\frac{p_3}{p_{03}} = 0.0780, \text{ also } p_{02} = p_{03}$$

The dynamic pressure of the freestream flow is

$$q_1 = \frac{1}{2} \rho_1 V_1^2 = \frac{\gamma p_1 M_1^2}{2}$$

Therefore,

$$\begin{aligned}\frac{q_1}{p_{01}} &= \frac{\gamma M_1^2}{2} \times \frac{p_1}{p_{01}} \\ &= \frac{\gamma M_1^2}{2} \times 0.1740 \\ &= 0.3946 \\ \frac{p_1}{q_1} &= \frac{p_1}{p_{01}} \times \frac{p_{01}}{q_1} \\ &= \frac{0.1740}{0.3946} \\ &= 0.441 \\ \frac{p_2}{q_1} &= C_{p2} + \frac{p_1}{q_1} \\ &= 0.506 + 0.441 \\ &= 0.947\end{aligned}$$

From the normal shock table (Table A.2), for  $M_{1n} = 1.4$ , we have

$$\frac{p_{02}}{p_{01}} = 0.9582$$

Thus,

$$\begin{aligned}\frac{p_3}{q_1} &= \frac{p_3}{p_{02}} \times \frac{p_{02}}{p_{01}} \times \frac{p_{01}}{q_1} \\ &= 0.0780 \times 0.9582 \times \frac{1}{0.3946} \\ &= 0.1894\end{aligned}$$

The pressure coefficient over wedge surface 3 is

$$\begin{aligned}C_{p3} &= \frac{p_3 - p_1}{q_1} \\ &= 0.1894 - 0.441 \\ &= \boxed{-0.2516}\end{aligned}$$

*Note:* It is important to note that the solutions for problems involving oblique shock obtained using oblique shock chart or table are only close to the correct results and are not 100% accurate. For accurate results we have to use the appropriate relations directly. However, the use of chart and table results in a considerable time saving and also the resulting accuracies are adequate for any application.

## 4.15 Thin Airfoil Theory

In Section 4.14 we saw that the shock-expansion theory gives a simple method for computing *lift* and *drag* acting over a body kept in a supersonic stream. This theory is applicable as long as the shocks are attached. This theory may be further simplified by approximating it by using the approximate relations for the weak shocks and expansion, when the airfoil is thin and kept at a small angle of attack, i.e. if the flow inclinations are small. This approximation will result in simple analytical expressions for lift and drag.

From our studies on weak oblique shocks in Section 4.6, we know that the basic approximate expression (Eq. 4.21) for calculating pressure change across a weak shock is

$$\frac{\Delta p}{p_1} \approx \frac{\gamma M_1^2}{\sqrt{M_1^2 - 1}} \Delta \theta$$

Because the wave is weak, the pressure  $p$  behind the shock will not be significantly different from  $p_1$ , nor will the Mach number  $M$  behind the shock be appreciably different from the freestream Mach number  $M_1$ . Therefore, we can express the above relation for pressure change across a weak shock, without any reference to the freestream state (i.e. without subscript 1 to the pressure and Mach number) as

$$\frac{\Delta p}{p} \approx \frac{\gamma M^2}{\sqrt{M^2 - 1}} \Delta \theta$$

Now, assuming all direction changes to the freestream direction to be zero and freestream pressure to be  $p_1$ , we can write

$$\frac{p - p_1}{p_1} = \frac{\gamma M_1^2}{\sqrt{M_1^2 - 1}} (\theta - 0)$$

where  $\theta$  is the local flow inclination relative to the freestream direction.

The pressure coefficient  $C_p$  is defined as

$$C_p = \frac{p - p_1}{q_1}$$

where  $p$  is the local static pressure and  $p_1$  and  $q_1$  are the freestream static pressure and dynamic pressure, respectively. In terms of freestream Mach number  $M_1$ , the pressure coefficient  $C_p$  can be expressed as

$$C_p = \frac{p - p_1}{q_1} = \frac{2}{\gamma M_1^2} \frac{p - p_1}{p_1}$$

Substituting the expression for  $(p - p_1)/p_1$  in terms of  $\theta$  and  $M_1$ , we get

$$C_p = \frac{2\theta}{\sqrt{M_1^2 - 1}} \quad (4.52)$$

The above equation, which states that the *pressure coefficient is proportional to the local flow direction*, is the basic relation for thin airfoil theory.

Thin airfoil theory is also called Ackeret's theory.

#### 4.15.1 Application of Thin Aerofoil Theory

Applying the thin airfoil theory relation, Eq. (4.52), for the flat plate shown in Figure 4.37c at a small angle of attack  $\alpha_0$ , the  $C_p$  on the upper and lower surfaces of the plate can be expressed as

$$C_p = \mp \frac{2\alpha_0}{\sqrt{M_1^2 - 1}} \quad (4.53)$$

where the minus sign is for  $C_p$  on the upper surface and the plus sign is for  $C_p$  on the lower surface. The lift and drag coefficients are respectively given by

$$C_L = \frac{(p_l - p_u) c \cos \alpha_0}{q_1 c} = (C_{pl} - C_{pu}) \cos \alpha_0$$

$$C_D = \frac{(p_l - p_u) c \sin \alpha_0}{q_1 c} = (C_{pl} - C_{pu}) \sin \alpha_0$$

In the above expressions for  $C_L$  and  $C_D$ ,  $\cos \alpha_0 \approx 1$  and  $\sin \alpha_0 \approx \alpha_0$ , since  $\alpha_0$  is small and the subscripts  $l$  and  $u$  refer to the lower and upper surfaces, respectively, and  $c$  is the chord. Therefore,

$$C_L = (C_{pl} - C_{pu})$$

$$C_D = (C_{pl} - C_{pu}) \alpha_0$$

Using Eq. (4.53), the  $C_L$  and  $C_D$  of the flat plate at a small angle of attack may be expressed as

$$C_L = \frac{4\alpha_0}{\sqrt{M_1^2 - 1}}$$

$$C_D = \frac{4\alpha_0^2}{\sqrt{M_1^2 - 1}} \quad (4.54)$$

Now, consider the diamond section airfoil shown in Figure 4.37a, with nose angle  $2\epsilon$ , at zero angle of attack. The pressure coefficient  $C_p$  on the front and rear faces is given by

$$C_p = \pm \frac{2\epsilon}{\sqrt{M_1^2 - 1}}$$

where the plus sign is for the front face where the pressure  $p_2$  is higher than  $p_1$  and the minus sign is for the rear face with pressure  $p_3 < p_1$ . This can be rewritten in terms of pressure difference to give

$$p_2 - p_3 = \frac{4\epsilon}{\sqrt{M_1^2 - 1}} q_1$$

Therefore, the drag is given by

$$D = (p_2 - p_3) t = (p_2 - p_3) \epsilon c$$

$$D = \frac{4\epsilon^2}{\sqrt{M_1^2 - 1}} q_1 c$$

where  $q_1$  is the freestream dynamics pressure and  $c$  is the chord of the airfoil.

In terms of the drag coefficient, the above drag equation becomes

$$C_D = \frac{D}{q_1 c} = \frac{4\epsilon^2}{\sqrt{M_1^2 - 1}} \quad (4.55a)$$

or

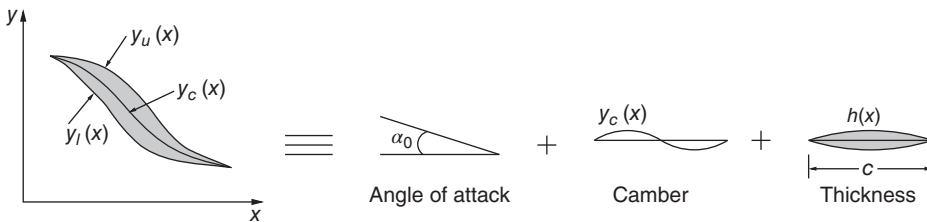
$$C_D = \frac{4}{\sqrt{M_1^2 - 1}} \left( \frac{t}{c} \right)^2 \quad (4.55b)$$

In the above two applications, the thin airfoil theory was used for specific profiles to get expressions for  $C_L$  and  $C_D$ . A general result applicable to any thin airfoil may be obtained as follows. Consider a cambered airfoil with finite thickness at a small angle of attack treated by linear resolution into three components, each of which contributes to lift and drag, as shown in Figure 4.41.

By thin airfoil theory, the  $C_p$  on the upper and lower surfaces is obtained as

$$C_{pu} = \frac{2}{\sqrt{M_1^2 - 1}} \left( \frac{dy_u}{dx} \right)$$

$$C_{pl} = \frac{2}{\sqrt{M_1^2 - 1}} \left( -\frac{dy_l}{dx} \right) \quad (4.56)$$



**Figure 4.41** Linear resolution of airfoil into angle of attack, camber, and thickness.

where  $y_u$  and  $y_l$  are the upper and lower profiles of the airfoil. The profile may be resolved into a symmetrical thickness distribution  $h(x)$  and a camber line of zero thickness  $y_c(x)$ . Thus, we have

$$\frac{dy_u}{dx} = \frac{dy_c}{dx} + \frac{dh}{dx} = -\alpha(x) + \frac{dh}{dx} \quad (4.57a)$$

$$\frac{dy_l}{dx} = \frac{dy_c}{dx} - \frac{dh}{dx} = -\alpha(x) - \frac{dh}{dx} \quad (4.57b)$$

where  $\alpha(x) = \alpha_0 + \alpha_c(x)$  is the local angle of attack of the camber line,  $\alpha_0$  is the angle of attack of the freestream, and  $\alpha_c$  is the angle attack due to the camber. The lift and drag are given by

$$L = q_1 \int_0^c (C_{pl} - C_{pu}) dx \quad (4.58a)$$

$$D = q_1 \int_0^c \left[ C_{pl} \left( -\frac{dy_l}{dx} \right) + C_{pu} \left( \frac{dy_u}{dx} \right) \right] dx \quad (4.58b)$$

Substituting Eqs. (4.56), (4.57a) and (4.57b) into Eqs. (4.58a) and (4.58b), we get

$$\begin{aligned} L &= \frac{2q_1}{\sqrt{M_1^2 - 1}} \int_0^c \left( -2 \frac{dy_c}{dx} \right) dx \\ &= \frac{4q_1}{\sqrt{M_1^2 - 1}} \int_0^c \alpha(x) dx \\ D &= \frac{2q_1}{\sqrt{M_1^2 - 1}} \int_0^c \left[ \left( \frac{dy_l}{dx} \right)^2 + \left( \frac{dy_u}{dx} \right)^2 \right] dx \\ &= \frac{4q_1}{\sqrt{M_1^2 - 1}} \int_0^c \left[ \alpha(x)^2 + \left( \frac{dh}{dx} \right)^2 \right] dx \end{aligned}$$

The integrals may be replaced by average values, e.g.

$$\bar{\alpha} = \frac{1}{c} \int_0^c \alpha(x) dx$$

Also, noting that by definition  $\bar{\alpha}_c = 0$ , we get

$$\begin{aligned} \bar{\alpha} &= \overline{\alpha_0 + \alpha_c} \\ &= \bar{\alpha}_0 + \bar{\alpha}_c \\ &= \alpha_0 \end{aligned}$$

Similarly,

$$\begin{aligned} \overline{\alpha^2} &= \overline{(\alpha_0 + \alpha_c)^2} \\ &= \bar{\alpha}_0^2 + 2\alpha_0 \bar{\alpha}_c + \bar{\alpha}_c^2 \\ &= \alpha_0^2 + \bar{\alpha}_c^2 \end{aligned}$$

Using the above averages in the lift and drag expressions, we obtain the lift and drag coefficients as

$$\boxed{C_L = \frac{4\bar{\alpha}}{\sqrt{M_1^2 - 1}} = \frac{4\alpha_0}{\sqrt{M_1^2 - 1}}} \quad (4.59a)$$



$$C_D = \frac{4}{\sqrt{M_1^2 - 1}} \left[ \overline{\left( \frac{dh}{dx} \right)^2} + \alpha^2(x) \right]$$

$$C_D = \frac{4}{\sqrt{M_1^2 - 1}} \left[ \overline{\left( \frac{dh}{dx} \right)^2} + \alpha_0^2 + \overline{\alpha_c^2(x)} \right] \quad (4.59b)$$

Equations (4.59a) and (4.59b) give the general expressions for lift and drag coefficients of a thin airfoil in a supersonic flow. In thin airfoil theory, the drag is split into *drag due to lift*, *drag due to camber*, and *drag due to thickness*, as given by Eq. (4.59b). But the lift coefficient depends only on the mean angle of attack.

#### Example 4.13

A supersonic, circular arc airfoil, shown in Figure 4.42, has chord  $c$  and a thickness-to-chord ratio of 0.12. Determine the lift and drag coefficients of the airfoil in terms of the angle of attack,  $\alpha$ .

#### Solution:

Let 0 the origin of the  $xy$  coordinate system be at the leading edge of the airfoil. Now, the equation of the circular arc is given by

$$\left( x - \frac{c}{2} \right)^2 + (y + K)^2 = R^2 \quad (4.60)$$

Substituting  $x = 0, y = 0$  in Eq. (4.60), we get

$$\frac{c^2}{4} + K^2 = R^2$$

Also,

$$R - K = t$$

Simplifying the above two equations, we can write

$$R = \frac{1}{8} \frac{c^2}{t} \left[ 1 + \left( \frac{2t}{c} \right)^2 \right]$$

$$K = \frac{1}{8} \frac{c^2}{t} \left[ 1 - \left( \frac{2t}{c} \right)^2 \right]$$

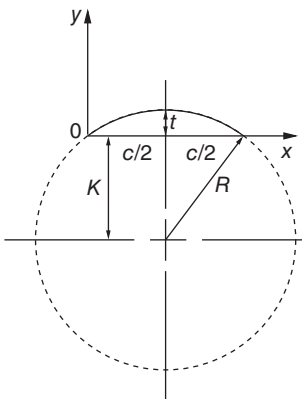


Figure 4.42 A circular arc airfoil in a supersonic stream.

Differentiating Eq. (4.60), the slope  $dy/dx$  can be obtained as

$$\frac{dy}{dx} = \frac{\frac{c}{2} \left(1 - 2\frac{x}{c}\right)}{y + K}$$

For small  $y$ , this can be approximated as

$$\begin{aligned} \frac{dy}{dx} &\approx \left(\frac{dy}{dx}\right)_{y=0} = \frac{4\frac{t}{c} \left(1 - \frac{2x}{c}\right)}{(1 - (2t/c)^2)} \\ &= 0.509 \left(1 - \frac{2x}{c}\right) \end{aligned}$$

For the airfoil considered,

$$\frac{dy_u}{dx} = \frac{dy_c}{dx}, \frac{dy_l}{dx} = \frac{dy_c}{dx}, \frac{dh}{dx} = 0$$

Therefore, when the airfoil is at an angle of attack  $\alpha$ , we have

$$\begin{aligned} \frac{dy_c}{dx} &= -\alpha(x) + \frac{dh}{dx} \\ &= -\alpha(x) + 0.509 \left(1 - \frac{2x}{c}\right) \end{aligned}$$

The coefficient of lift  $C_L$  is given by Eq. (4.58a), in the form

$$\frac{L}{q_1 c} = \frac{1}{c} \int_0^c (C_{pl} - C_{pu}) dx$$

Substituting Eqs. (4.56), (4.57a), and (4.57b) into the above equation, we get

$$\begin{aligned} C_L &= \frac{1}{c} \int_0^c -\frac{4}{\sqrt{M_1^2 - 1}} \left(\frac{dy_c}{dx}\right) dx \\ &= -\frac{4}{c\sqrt{M_1^2 - 1}} \int_0^c \left(-\alpha(x) + 0.509 \left(1 - \frac{2x}{c}\right)\right) dx \end{aligned}$$

On integrating, we obtain the lift coefficient as

$$C_L = \boxed{\frac{4\alpha}{\sqrt{M_1^2 - 1}}}$$

This result of  $C_L$  implies that the lift goes to zero when the angle of attack is zero. The drag coefficient is given by

$$\begin{aligned} C_D &= \frac{1}{c} \int_0^c \left[ C_{pl} \left(-\frac{dy_l}{dx}\right) + C_{pu} \left(\frac{dy_u}{dx}\right) \right] dx \\ &= \frac{2}{c\sqrt{M_1^2 - 1}} \int_0^c \left[ \left(\frac{dy_l}{dx}\right)^2 + \left(\frac{dy_u}{dx}\right)^2 \right] dx \\ &= \frac{4}{c\sqrt{M_1^2 - 1}} \int_0^c \left(\frac{dy_c}{dx}\right)^2 dx \end{aligned}$$

$$\begin{aligned}
 &= \frac{4}{c\sqrt{M_1^2 - 1}} \int_0^c \left[ -\alpha(x) + 0.509 \left( 1 - \frac{2x}{c} \right) \right]^2 dx \\
 &= \frac{4}{c\sqrt{M_1^2 - 1}} \int_0^c \left[ \alpha^2(x) + 0.509^2 \left( 1 - \frac{4x}{c} + \frac{4x^2}{c^2} \right) - 2\alpha(x) \times 0.509 \left( 1 - \frac{2x}{c} \right) \right] dx \\
 &= \frac{4\alpha^2(x)}{\sqrt{M_1^2 - 1}} + \frac{0.3451}{\sqrt{M_1^2 - 1}}
 \end{aligned}$$

**Example 4.14**

An oblique shock of strength 1, in air, meets the free boundary, as shown in Figure 4.43. (a) Describe the reflection of the shock from the boundary, the flow process across the reflected wave, and sketch the reflection. (b) Find the Mach number and total pressure, downstream of the reflection zone. (c) Find the fan angle of the expansion. (d) Determine the deflection angle of the free boundary with reference to the freestream direction, upstream of the shock, and check whether the flow downstream of the expansion satisfies the streamline concept.

**Solution:**

- (a) The reflection of shock from the free boundary is unlike. Thus, the oblique shock will reflect as an expansion fan, as shown in Figure 4.44. The flow process across the expansion fan will be isentropic everywhere, except at the vertex of the fan, where the flow is nonisentropic. Given that the shock strength is 1 that is  $\Delta p/p_1 = 1$ ,

$$\begin{aligned}
 \frac{p_2 - p_1}{p_1} &= 1 \\
 \frac{p_2}{p_1} &= 2
 \end{aligned}$$

- (b) For  $M_1 = 2$  and  $p_2/p_1 = 2$ , from the oblique shock table,

$$M_2 = 1.49, \beta \approx 44^\circ, \theta_{12} = 14^\circ$$

The shock gets reflected as an expansion fan, as shown in Figure 4.44. The free boundary is deflected downwards. A free boundary is identical to a slipstream; therefore, the static

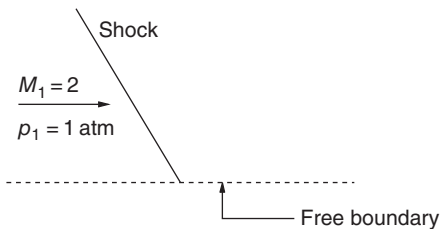


Figure 4.43 Oblique shock incident on a free boundary.

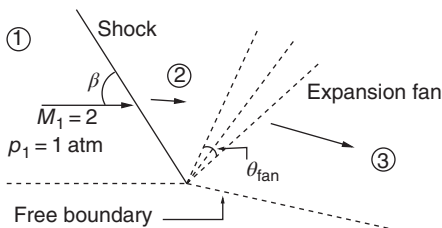


Figure 4.44 Shock reflection from the free boundary.

pressure on either side of the boundary must be equal. Thus, the pressure  $p_3$  at zone 3 will be equal to the atmospheric pressure on the other side of the free boundary.

For  $M_1 = 2$ , from the isentropic table,  $p_1/p_{01} = 0.1278$ . Therefore,

$$\begin{aligned} p_{01} &= \frac{1}{0.1278} \\ &= 7.82 \text{ atm} \end{aligned}$$

The Mach number normal to the shock is

$$\begin{aligned} M_{1n} &= M_1 \sin \beta \\ &= 2 \times \sin 44^\circ \\ &= 1.39 \end{aligned}$$

For  $M_{1n} = 1.39$ , from the normal shock table,  $p_{02}/p_{01} = 0.9607$ . Therefore,

$$\begin{aligned} p_{02} &= 0.9607 \times p_{01} \\ &= 0.9607 \times 7.82 \\ &= 7.513 \text{ atm} \end{aligned}$$

The flow through the expansion fan is isentropic; therefore,

$$p_{03} = p_{02} = \boxed{7.513 \text{ atm}}$$

Thus,

$$\frac{p_{03}}{p_3} = 7.513$$

By isentropic relation, Eq. (1.73),

$$\begin{aligned} \frac{p_{03}}{p_3} &= \left( 1 + \frac{\gamma - 1}{2} M_3^2 \right)^{\gamma/(\gamma-1)} \\ 7.513 &= (1 + 0.2M_3^2)^{3.5} \\ 1 + 0.2M_3^2 &= (7.513)^{1/3.5} \\ 1 + 0.2M_3^2 &= 1.779 \\ M_3 &= \sqrt{\frac{0.779}{0.2}} \\ &= \boxed{1.974} \end{aligned}$$

(c) From the isentropic table,

For  $M_2 = 1.49$ ,  $\mu_2 = 42.155^\circ$ .

For  $M_3 = 1.97$ ,  $\mu_3 = 30.505^\circ$ .

The first leading ray of the expansion fan is the Mach line corresponding to Mach 1.49 and the terminating ray of the fan is the Mach line corresponding to Mach 1.97. Thus, the fan angle of the expansion is

$$\begin{aligned} \theta_{\text{fan}} &= \mu_3 - \mu_2 \\ &= 42.155 - 30.505 \\ &= \boxed{11.65^\circ} \end{aligned}$$

(d) The flow field ahead of and behind the shock, and downstream of the expansion fan, is as shown in Figure 4.45.

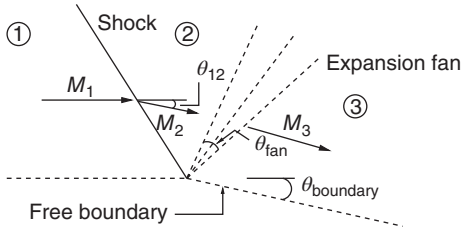


Figure 4.45 Flow through the shock and expansion fan.

The Mach numbers in the three zones of the flow field are

$$M_1 = 2, M_2 = 1.49, M_3 = 1.974$$

For  $M_2 = 1.49$ , from the isentropic table, the Prandtl–Meyer function is

$$v_2 = 11.61^\circ$$

For  $M_3 = 1.974$ , from the isentropic table, the Prandtl–Meyer function is

$$v_3 = 25.66^\circ$$

But

$$v_3 = v_2 + \theta_{\text{boundary}}$$

Thus,

$$\begin{aligned} \theta_{\text{boundary}} &= v_3 - v_2 \\ &= 25.66^\circ - 11.61^\circ \\ &= \boxed{14.05^\circ} \end{aligned}$$

This is the deflection angle of the boundary, with reference to the flow direction in zone 1. This shows that the boundary is deflected by the same angle by which the shock has deflected the flow ( $\theta_{12} = \theta_{\text{boundary}}$ ). It can be seen that the shock turned the flow by  $\theta_{12}$ , downward, and the boundary has also been turned downward by the same angle. This turning of the free boundary ensures that the flow from zone 2 coming downward has been made to flow parallel to the boundary. Thus, the streamlines in zone 3 are parallel to the boundary, satisfying the streamline concept.

## 4.16 Summary

In this chapter we have discussed the flow processes through oblique shock and expansion waves. A shock wave which is inclined at an angle to the flow direction is called an *oblique shock wave*. Oblique shocks usually occur when a supersonic flow is turned into itself. The opposite of this, namely when a supersonic flow is turned away from itself, results in the formation of an expansion fan. Oblique shock and expansion waves prevail in two- and three-dimensional supersonic flows, in contrast to normal shock waves, which are quasi-one-dimensional.

The density, pressure, and temperature ratios across an oblique shock wave are given by

$$\frac{\rho_2}{\rho_1} = \frac{(\gamma + 1)M_1^2 \sin^2 \beta}{(\gamma - 1)M_1^2 \sin^2 \beta + 2}$$

$$\frac{p_2}{p_1} = 1 + \frac{2\gamma}{\gamma + 1}(M_1^2 \sin^2 \beta - 1)$$

$$\frac{T_2}{T_1} = 1 + \frac{2(\gamma - 1)}{(\gamma + 1)^2} \frac{M_1^2 \sin^2 \beta - 1}{M_1^2 \sin^2 \beta} (\gamma M_1^2 \sin^2 \beta + 1)$$

where subscripts 1 and 2 refer to the conditions ahead of and behind the oblique shock and  $\beta$  is the shock angle.

The Mach number behind an oblique shock  $M_2$  is given by

$$M_2 = \frac{M_{n2}}{\sin(\beta - \theta)}$$

where  $M_{n2}$  is the normal component of Mach number behind the shock and  $\theta$  is the flow turning angle.

The maximum and minimum values of shock angle correspond to those for normal shock;  $\beta = \pi/2$  and Mach wave,  $\mu$ . Thus, the possible range of  $\beta$  is

$$\sin^{-1} \left( \frac{1}{M_1} \right) \leq \beta \leq \frac{\pi}{2}$$

The relation between the Mach number, shock angle, and flow turning angle is given by

$$\tan \theta = 2 \cot \beta \left( \frac{M_1^2 \sin^2 \beta - 1}{M_1^2 (\gamma + \cos 2\beta) + 2} \right)$$

This is known as the  $\theta - \beta - M$  relation.

The graphical representation of oblique shock properties is known as *shock polar*.

A two-dimensional flow of supersonic stream is always associated with two families of Mach lines. The Mach lines with (+) sign run to the right of the streamline when viewed through the flow direction are called *right-running characteristics* and those Mach lines with (−) sign that run to the left are called *left-running characteristics*.

Supersonic flow expansion around a convex corner involving a smooth, gradual change in flow properties is known as *Prandtl–Meyer expansion*. The expansion fan, or the Prandtl–Meyer fan, consists of an infinite number of expansion waves, centered at the convex corner. All rays in an expansion fan are isentropic lines and the entire flow (except at the apex of the expansion fan) is isentropic.

The maximum turning of an expanding flow corresponds to the situation where the pressure  $p$  goes to zero. This corresponds to a flow turning angle of  $\theta = 130.5^\circ$ .

The Prandtl–Meyer expansion is a self-similar motion and the Prandtl–Meyer function is a *similarity parameter*. The Prandtl–Meyer function in terms of Mach number is given by

$$v = \sqrt{\frac{\gamma + 1}{\gamma - 1}} \arctan \sqrt{\frac{\gamma - 1}{\gamma + 1} (M_1^2 - 1)} - \arctan \sqrt{M_1^2 - 1}$$

The waves causing isentropic expansion and compression are called *simple waves*. Zones of supersonic expansion or compression with Mach lines which are straight are called *simple regions*. Zones with curved Mach lines are called *nonsimple regions*.

An incident shock gets reflected as a shock from a solid boundary. This kind of reflection is called *like reflection*. On the other hand, an incident shock gets reflected as an expansion fan and the expansion fan gets reflected as compression waves from a free boundary. This kind of reflection is called *unlike reflection*.

For supersonic flows, drag exists even in idealized nonviscous fluid. This new component of drag encountered when the flow is supersonic is called *wave drag* and it is fundamentally

different from the skin-friction drag and separation drag which are associated with boundary layers in a viscous fluid.

Thin airfoil theory gives an expression for the pressure coefficient as

$$C_p = \frac{2\theta}{\sqrt{M_1^2 - 1}}$$

It states that the pressure coefficient is proportional to the local flow direction.

For a flat plate at a small angle of attack  $\alpha_0$ , the lift and drag coefficients may be expressed as

$$C_L = \frac{4\alpha_0}{\sqrt{M_1^2 - 1}}$$

$$C_D = \frac{4\alpha_0^2}{\sqrt{M_1^2 - 1}}$$

The general expressions of lift and drag coefficients of a thin airfoil in supersonic flow may be written as

$$C_L = \frac{4\alpha_0}{\sqrt{M_1^2 - 1}}$$

$$C_D = \frac{4}{\sqrt{M_1^2 - 1}} \left[ \overline{\left( \frac{dh}{dx} \right)^2} + \alpha_0^2 + \overline{\alpha_c^2(x)} \right]$$

where  $h(x)$  gives the symmetrical thickness distribution,  $\alpha_0$  is the freestream angle of attack, and  $\alpha_c(x)$  is the angle of attack due to camber. From the above relation for  $C_D$ , it is seen that the drag is split into *drag due to lift*, *drag due to camber*, and *drag due to thickness*. But the lift coefficient depends only on the mean angle of attack.

From the discussions of shock and expansion waves in this chapter, it is clear that any problem in supersonic flow, in principle, can be analyzed with the relations developed for the oblique shock and expansion fans. However, it must be realized that all relations we have developed are for flow fields with simple regions. For the nonsimple regions with nonlinear wave net there is no exact analytical approach developed so far. But when the wave net pattern is made with tiny segments, the relations developed for linear waves can be applied to nonlinear wave segments in the nonsimple region, without introducing significant error. This kind of approach is adopted in Chapter 9 while designing contoured nozzles to generate uniform and unidirectional supersonic flows. Experimental results with such contoured nozzles prove that, assuming the nonlinear waves to be straight waves within a small wave net does not introduce any significant error. It is essential to realize that in method of characteristics the above approximation is made for expansion waves which are isentropic. When the wave net involves crossing of shocks or compression waves, this assumption is bound to introduce significant errors in our calculations. The development of a theory involving nonsimple regions with shocks or compression waves merits further investigation.

## Exercise Problems

- 4.1** A Mach 2 uniform air flow passes over a wedge. An oblique shock, making an angle of  $40^\circ$  with the flow direction, is attached to the wedge. If the static pressure and temperature

in the freestream are 50 kPa and  $0^\circ\text{C}$ , determine the static pressure and temperature behind the wave, the Mach number of the flow passing over the wedge, and the wedge angle.

[Answer: 88.75 kPa, 323.5 K, 1.61, and  $21.14^\circ$ ]

- 4.2** A Mach 2.0 air stream is isentropically deflected by  $5^\circ$  in a clockwise direction. If the pressure and temperature before deflection are 98 kPa and  $27^\circ\text{C}$ , determine the Mach number, pressure temperature, and density of the deflected flow.

[Answer:  $M = 2.18$ ,  $p = 74$  kPa,  $T = 276.8$  K,  $\rho = 0.9315$  kg  $\text{m}^{-3}$ ]

- 4.3** A Mach 3 axisymmetric wind tunnel nozzle is run by an air reservoir at 7 MPa and the nozzle exhausts to a surrounding at 1 atm. During the operation, the pressure in the supply reservoir decreases. (a) At what supply pressure will an oblique shock wave first appear at the nozzle exit? (b) If a shock-free test-region extending one diameter in length is required, what should be the minimum supply pressure for obtaining this test region? (c) What is the minimum supply pressure for which a normal shock will appear at the nozzle exit?

[Answer: (a)  $\leq 3.725$  MPa, (b) 2.33 MPa, (c) 360 kPa]

- 4.4** Air flows over a symmetrical wedge of semi-vertex angle  $15^\circ$  at a Mach number of 2.0. Determine (a) the wave angle with respect to the freestream direction, (b) the pressure ratio across the wave, (c) the temperature ratio across the wave, (d) the density ratio across the wave, and (e) the Mach number downstream of shock, assuming the shock at the nose to be strong and weak.

[Answer: *Strong shock solution:* (a)  $79.8^\circ$ , (b) 4.355, (c) 1.662, (d) 2.62, (e) 0.646. *Weak shock solution:* (a)  $45.34^\circ$ , (b) 2.186, (c) 1.268, (d) 1.729, (e) 1.448]

- 4.5** An underexpanded, two-dimensional, supersonic nozzle exhausts into a region where  $p = 0.75$  atm. Flow at nozzle exit plane is uniform, with  $p = 1.6$  atm and  $M = 2.0$ . Calculate the flow direction and Mach number after the initial expansion.

[Answer: Flow turning angle =  $12.275^\circ$ ,  $M = 2.48$ ]

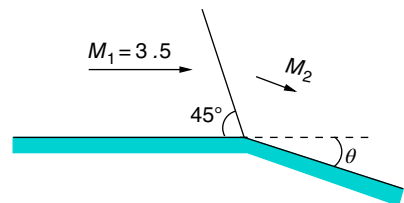
- 4.6** (a) Compute the maximum deflection angles for which the oblique shock remains attached to the wedge when  $M_1 = 2.0$  and 3.0. (b) Compute the minimum values of Mach number  $M_1$  for which the oblique shock remains attached to the wedge for flow deflection angles of  $\theta = 15^\circ$ ,  $25^\circ$ , and  $40^\circ$ .

[Answer: (a)  $22^\circ$ ,  $34^\circ$ , (b) 1.65, 2.11, 4.45]

- 4.7** An oblique shock wave is incident on a solid boundary, as shown in Figure 4.46. The boundary is to be turned through such an angle that there will be no reflected wave. Determine the angle  $\theta$  and the flow Mach angle  $M$ .

[Answer:  $28.158^\circ$ , 1.78]

**Figure 4.46** Oblique shock incident on a solid boundary.





- 4.8** Air flows over a frictionless surface having a sharp corner. The flow angle and Mach number downstream of the corner are  $-60^\circ$  and 4.0, respectively. Calculate the upstream Mach number for flow turning angle of (a)  $15^\circ$  clockwise, (b)  $30^\circ$  clockwise, (c)  $60^\circ$  clockwise, and (d)  $15^\circ$  counter-clockwise.  
[Answer: (a) 1.802, (b) 2.36, (c) 4.0, (d) for this case  $\nu$  is negative, which is not physically possible. Flow can exist only up to  $|\Delta\theta| = 65.785^\circ$ , for which  $\nu_1 = 0$  and  $M_1 = 1.0$ ].
- 4.9** A steady supersonic flow expands from Mach number  $M_1 = 2.0$  and pressure  $p_1$  to pressure  $p_2 = p_1/2$  through a centered expansion. Find the Mach number  $M_2$  and flow direction  $\theta_2$ , after the expansion.  
[Answer:  $2.444, 11.43^\circ$ ]
- 4.10** (a) A nozzle is designed to generate a Mach 3 uniform parallel flow of air. The stagnation pressure of the air supply reservoir  $p_0 = 7$  MPa and the nozzle exhausts to sea level atmosphere. Calculate the flow angle at the exit lip of the nozzle if the atmospheric pressure  $p_e = 1.0$  atm. (b) Determine the stagnation pressure of the air supply for which the flow angle at the exit lip would be zero.  
[Answer: (a)  $7.64^\circ$ , (b) 3.725 MPa]
- 4.11** Air at  $p_1 = 30$  kPa,  $T_1 = 350$  K, and  $M_1 = 1.5$  is to be expanded isentropically to 13 kPa. Determine (a) the flow deflection angle required, (b) final Mach number, and (c) the temperature of air after expansion.  
[Answer: (a)  $15.85^\circ$ , (b) 2.05, (c) 275.7 K]
- 4.12** Mach 2 air stream flows over three sharp corners in succession, having clockwise turning angles of  $5^\circ$ ,  $10^\circ$ , and  $15^\circ$ , respectively. (a) Calculate the Mach number and flow angle after each of the three corners. (b) Find the expansion fan angles and the streamline distances from the solid boundary. (Take freestream streamline distance  $d_1$  from the wall as unity.)  
[Answer: (a) 2.0,  $30^\circ$ , 2.187,  $27.2^\circ$ , 2.6,  $22.62^\circ$ , (b) fan angles:  $7.8^\circ$ ,  $14.6^\circ$ ,  $20.34^\circ$ , distances:  $\frac{d_2}{d_1} = 1.173$ ,  $\frac{d_3}{d_1} = 1.716$ ,  $\frac{d_4}{d_1} = 3.562$ ]
- 4.13** A supersonic inlet is to be designed to handle air at Mach 2.4 with static pressure and temperature of 50 kPa and 280 K, as shown in Figure 4.47. (a) Determine the diffuser inlet area  $A_i$ , if the device has to handle  $20 \text{ kg s}^{-1}$  of air and (b) if the diffuser has to further decelerate the flow behind the normal shock so that the velocity entering the compressor will not exceed  $30 \text{ m s}^{-1}$ . Assuming isentropic flow behind the normal shock, determine the area  $A_e$  required and the static pressure  $p_e$  there.  
[Answer: (a)  $A_i = 0.03126 \text{ m}^2$ , (b)  $A_e = 0.239 \text{ m}^2$ ,  $p_e = 482 \text{ kPa}$ ]
- 4.14** A supersonic inlet is to be designed to operate at Mach 3.0. Two possibilities are considered, as shown in Figure 4.48. In one, the compression and deceleration of the flow takes place through a single normal shock (Figure 4.48a); in the other, a wedge-shaped

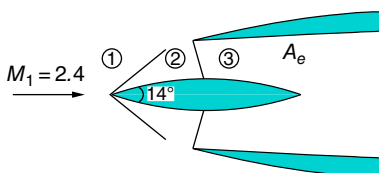
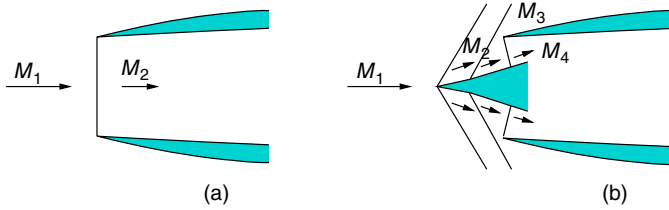


Figure 4.47 A supersonic inlet.



**Figure 4.48** (a) Normal shock diffuser, (b) wedge-shaped diffuser.

diffuser (Figure 4.48b) is used and the deceleration is through two weak oblique shocks followed by a normal shock wave. The wedge turning angles are  $8^\circ$  each. Compare the loss in stagnation pressure for the two cases.

[Ans. (a)  $\frac{p_{02}}{p_{01}} = 0.3283$ ; (b)  $\frac{p_{04}}{p_{01}} = 0.5803$ ]

- 4.15** A two-dimensional flat plate is kept at a positive angle of attack in a Mach 2.0 air stream. Below the plate, an oblique shock wave starts at the leading edge, making an angle of  $42^\circ$  with the freestream direction. On the upper side, an expansion fan is positioned at the leading edge. Find (a) the angle of attack of the plate, (b) the pressure on the lower and upper surfaces of the plate, and (c) the pressure at the trailing edge after the flow leaves the plate, if the freestream static pressure is 1 atm.

[Answer: (a)  $12.3^\circ$ , (b) 1.928 atm and 0.473 atm, (c) 1.0 atm]

- 4.16** High-pressure air maintained at a constant stagnation state of 7 MPa and 300 K runs a Mach 3 blowdown wind tunnel. A symmetrical wedge having a semi-angle  $\alpha = 15^\circ$  is placed in the test-section. Calculate the following flow properties on the face of the wedge: (a) static pressure, density, and temperature, (b) stagnation pressure, (c) flow velocity, and flow Mach number.

[Answer: (a) 536.93 kPa,  $12.58 \text{ kg m}^{-3}$ , 148.7 K, (b) 6.265 MPa, (c)  $552.3 \text{ m s}^{-1}$ , 2.26]

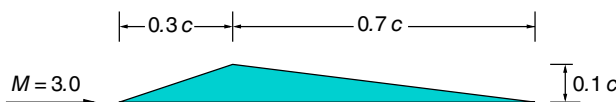
- 4.17** The two-dimensional airfoil shown in Figure 4.49 is traveling at a Mach number of 3 and at an angle of attack of  $2^\circ$ . The thickness to chord ratio of the airfoil is 0.1 and the maximum thickness occurs at 30% of the chord downstream from the leading edge. Using the linearized theory, show that the moment coefficient about the aerodynamic center is  $-0.035$ , the center of pressure is at  $1.217c$ , and the drag coefficient is 0.0354. Show also that the angle of zero lift is  $0^\circ$ .

- 4.18** For the flat plate shown in Figure 4.50, calculate the flow Mach numbers at zones 2, 2', 3, and 3', assuming the slipstream deflection to be negligible.

[Answer:  $M_2 = 3.71$ ,  $M_3 = 2.726$ ,  $M_{2'} = 2.4$ ,  $M_{3'} = 2.95$ ]

- 4.19** For the double-wedge shown in Figure 4.51, calculate the flow Mach numbers at different flow zones and the slipstream.

[Answer:  $M_2 = 3.105$ ,  $M_3 = 4.493$ ,  $M_4 = 2.58$ ,  $M_{2'} = 1.91$ ,  $M_{3'} = 2.71$ ,  $M_{4'} = 2.806$ . Comparing  $p_4/p_{01}$  and  $p_{4'}/p_{01}$  it can be seen that the slipstream is very weak]



**Figure 4.49** A two-dimensional airfoil traveling at Mach 3.

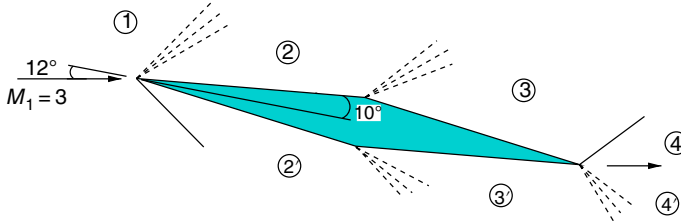
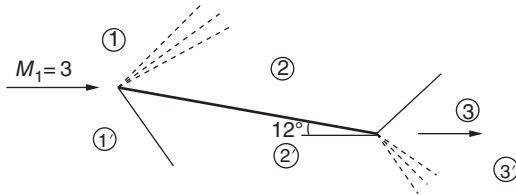
Figure 4.50 A flat plate at  $12^\circ$  to Mach 3 flow.

Figure 4.51 A double-wedge at an incidence to Mach 3 air stream.

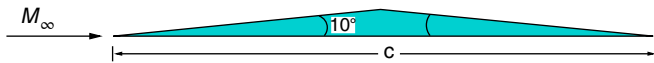


Figure 4.52 A two-dimensional wedge in a supersonic stream.

- 4.20** A two-dimensional wedge shown in Figure 4.52 moves through the atmosphere at sea-level, at zero angle of attack with  $M_\infty = 3.0$ . Calculate  $C_L$  and  $C_D$  using shock-expansion theory.  
[Answer:  $C_L = -0.0389$ ,  $C_D = 0.02266$ ]
- 4.21** For a Prandtl–Meyer expansion, the upstream Mach number is 2 and the pressure ratio across the fan is 0.5. Determine the angles of the front and end Mach lines of the expansion fan relative to the freestream.  
[Answer:  $30^\circ$ ,  $12.86^\circ$ ]
- 4.22** Calculate the ratios of static and total pressures across the shock wave emanating from the leading edge of a wedge of  $5^\circ$  half-angle flying at Mach 2.2.  
[Answer: 1.34, 0.99726]
- 4.23** A uniform supersonic flow of air at Mach 3.0 and  $p_1 = 0.05$  atm passes over a cone of semi-vertex angle  $8^\circ$  kept in line with the flow. Determine the shock angle and the static pressure at the cone surface, just behind the shock.  
[Answer:  $25.61^\circ$ , 9.1 kPa]
- 4.24** A supersonic stream of air at Mach 3 and 1 atm passes through a sudden convex and a sudden concave corner each of turning angle  $15^\circ$ . Determine the Mach number and pressure of the flow downstream of the concave corner.  
[Answer: 2.7, 1.015 atm]
- 4.25** A flat plate wing of chord 1 m experiences a lift of 10 200 N per meter of width. If the flow Mach number and pressure are 1.6 and 25 kPa, respectively, determine the angle of attack and the aerodynamic efficiency ( $C_L/C_D$ ) of the wing.  
[Answer:  $4^\circ$ , 14]

- 4.26** For an oblique shock wave with a wave angle of  $33^\circ$  and upstream Mach number of 2.4, calculate the flow deflection angle  $\theta$ , the pressure and temperature ratios across the shock wave, and the Mach number behind the wave.  
[Answer:  $10^\circ$ , 1.8354, 1.1972, 2.0]

- 4.27** Show that the pressure difference across an oblique shock wave with wave angle  $\beta$  may be expressed in the form

$$\frac{p_2 - p_1}{\frac{1}{2}\rho_1 u_1^2} = \frac{4}{\gamma + 1} \left( \sin^2 \beta - \frac{1}{M_1^2} \right)$$

where subscripts 1 and 2 refer to states upstream and downstream of the shock.

- 4.28** Air flow with a Mach number of 3.0 and pressure of 1 atm passes over a compression corner. If the pressure downstream of the corner is 5 atm, determine the flow turning angle.  
[Answer:  $25.5^\circ$ ]

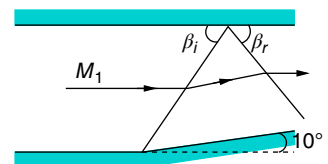
- 4.29** A Mach 2 air stream passes over a  $10^\circ$  compression corner. The oblique shock from the corner is reflected from a flat wall which is parallel to the freestream, as shown in Figure 4.53. Compute the angle of the reflected shock wave relative to the flat wall and the Mach number downstream of the reflected shock.  
[Answer:  $39.5^\circ$ , 1.28]

- 4.30** Mach 2 air stream passes over two compression corners of angles  $7^\circ$  and  $\theta$ , as shown in Figure 4.54. Determine the value of  $\theta$  up to which the second shock will remain attached.  
[Answer:  $18^\circ$ ]

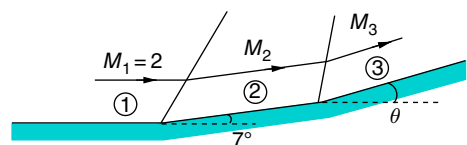
- 4.31** Mach 2 air flow is compressed by turning it through  $15^\circ$ . For each of the possible solutions calculate (a) the shock angle, (b) the Mach number downstream of the shock, and (c) the change of entropy. What is the maximum deflection angle up to which the shock will remain attached?  
[Answer: Weak solution: (a)  $45.34^\circ$ , (b) 1.45, (c)  $13.73 \text{ J (kg K)}^{-1}$ . Strong solution: (a)  $79.83^\circ$ , (b) 0.64, (c)  $88.25 \text{ J (kg K)}^{-1}$ ,  $22.97^\circ$ ]

- 4.32** Mach 3 air stream at 1 atm and 200 K is deflected at a compression corner through  $10^\circ$ . Calculate the Mach number, static and stagnation pressures, and temperatures downstream of the corner.  
[Answer: 2.5, 2.06 atm, 35.4 atm, 248.36 K, 560 K]

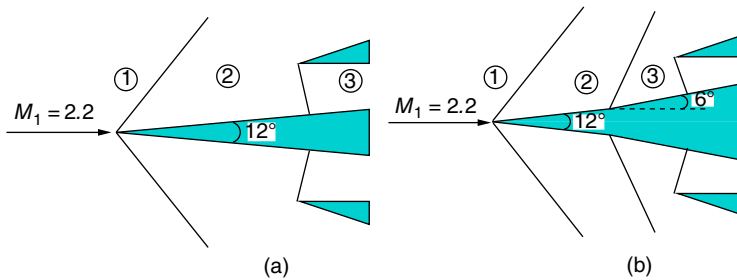
**Figure 4.53** Mach 2 air stream passing over a compression corner.



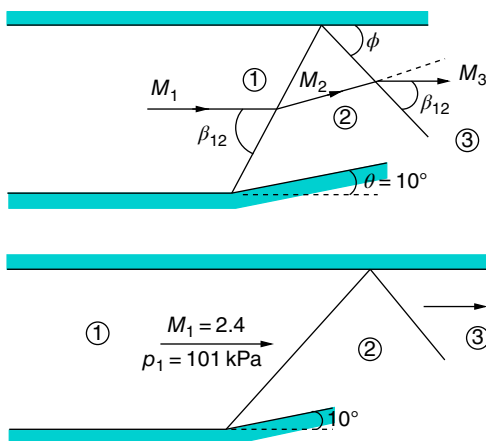
**Figure 4.54** Mach 2 air stream passing over two compression corners.



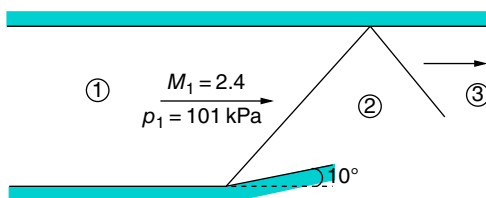
- 4.33** Determine the wave angle and Mach number behind and the pressure ratio across the oblique shock in air with  $M_1 = 3.0$  and  $\theta = 10^\circ$ , treating the shock as (a) weak and (b) strong.  
 [Answer: (a) Weak solution:  $\beta = 27.38^\circ$ , 2.5, 2.05. (b) Strong solution:  $\beta = 86.41^\circ$ , 0.489, 10.292]
- 4.34** Compare the pressure loss experienced by the (a) one-shock and (b) two-shock spikes shown in Figures 4.55a and b.  
 [Answer: 27.3%, 17.2%]
- 4.35** An oblique shock created by the flow of air over a sharp corner, as shown in Figure 4.56, has a wave angle of  $30^\circ$ . If the Mach number upstream of the incident wave is 2.4, determine the Mach number upstream and downstream of the reflected shock wave.  
 [Answer: 2.09, 1.85]
- 4.36** For the flow field shown in Figure 4.57, determine the Mach number and pressure in region 3.  
 [Answer: 1.64, 316.43 kPa]
- 4.37** An oblique shock gets reflected from a solid wall, as shown in Figure 4.58. Calculate the Mach number and pressure downstream of the reflected shock. Also, calculate the angle  $\phi$  made by the reflected shock with the wall. Assume the medium to be air.  
 [Answer: 1.83, 164.7 kPa,  $29^\circ$ ]



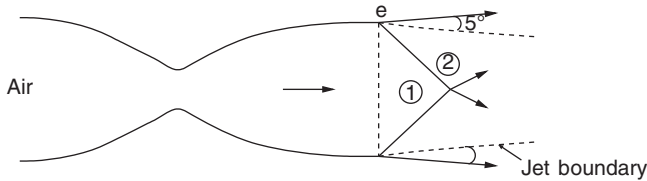
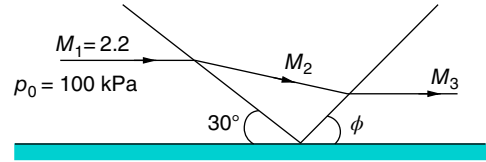
**Figure 4.55** (a) One-shock spike, (b) two-shock spike diffuser.



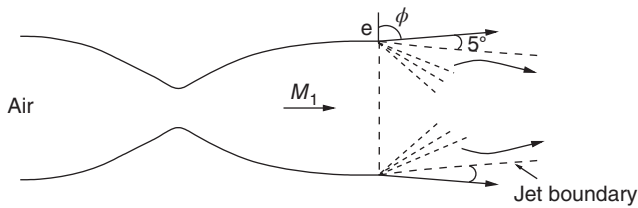
**Figure 4.56** Supersonic flow past a sharp corner.



**Figure 4.57** Flow through incident and reflected oblique shocks.

**Figure 4.58** Oblique shock reflection from a solid wall.**Figure 4.59** Overexpanded jet issuing from a nozzle.

- 4.38** If the boundary of the overexpanded jet issuing from a nozzle with area ratio  $\frac{A_e}{A_t} = 2.0$  and stagnation pressure 300 kPa is as shown in Figure 4.59, determine the backpressure  $p_b$ .  
[Answer: 37.59 kPa]
- 4.39** An incident shock wave with  $\beta = 30^\circ$  impinges on a straight wall. If the flow upstream of the shock is with  $M_1 = 2.8$ ,  $p_1 = 1$  atm, and  $T_1 = 300$  K, calculate the pressure, temperature, Mach number and the stagnation pressure downstream of the reflected shock wave.  
[Answer: 3.83 atm, 441.5 K, 1.93, 25.5 atm]
- 4.40** Mach number 1.46 air stream is expanded through an angle of  $5^\circ$ . Determine the Mach number of the expanded flow. Calculate the pressure coefficient  $C_p = (p_2 - p_1) / \left( \frac{1}{2} \rho_1 V_1^2 \right)$ , where subscript 1 refers to the initial condition. Compare this  $C_p$  with that predicted by linearized (Ackeret's) theory.  
[Answer: 1.63, -0.1474, -0.1645]
- 4.41** Supersonic air stream at Mach 2.2 and 55 kPa is turned by a continuous compression corner by  $10^\circ$ . Determine the Mach number and pressure after the corner.  
[Answer: 1.83, 97.76 kPa]
- 4.42** Mach 2.8 air stream at a pressure of 101 kPa is turned by an expansion fan through  $4^\circ$ . Compute the Mach number and pressure of the turned flow by using (a) the Prandtl–Meyer expansion theory and (b) the small-perturbation theory.  
[Answer: (a) 3.0, 74.65 kPa, (b) 3.03, 71.36 kPa]
- 4.43** Air at Mach 2.82 and at a pressure of 50 kPa flows along a smooth convex wall which gradually turns the flow by  $9^\circ$ . Calculate the Mach number and pressure of the flow downstream of the wall.  
[Answer: 3.3, 24.5 kPa]
- 4.44** Air flow at Mach 2.8 passes over a  $16^\circ$  compression corner. What should be the angle of the expansion corner required to bring the flow back to Mach 2.8?  
[Answer:  $17.73^\circ$ ]
- 4.45** A Laval nozzle of area ratio 1.4 operating in an underexpanded condition exhibits a wave pattern as shown in Figure 4.60. If the stagnation pressure of the air is 490 kPa



**Figure 4.60** Waves at the exit of a Laval nozzle operating in an underexpanded condition.

and the backpressure is 25 kPa, calculate the Mach number and the angle  $\phi$ , assuming  $\gamma = 1.4$ .

[Answer: 2.59, 68.67°]

- 4.46** A flat plate airfoil of 1.4 m chord is placed at an angle of attack of 4° in Mach 2 air stream at 101 kPa. Calculate  $C_L$  and  $C_D$  experienced by the airfoil.

[Answer: 0.1616, 0.0113]

- 4.47** A symmetrical wedge is kept in a supersonic stream of Mach number 2.5 and pressure 70 kPa, as shown in Figure 4.61. Estimate the pressure at point A.

[Answer: 96.33 kPa, 597.1 kPa]

- 4.48** Calculate the lift and drag coefficient experienced by a flat plate kept at an angle of attack of 5° to an air stream at Mach 2.3 and pressure 101 kPa, using (a) shock–expansion theory and (b) Ackeret's theory.

[Answer: (a) 0.1735, 0.0152, (b) 0.1685, 0.0147]

- 4.49** Calculate the  $C_L$  and  $C_D$  for a half-wedge of wedge angle 5° kept in an air stream at Mach 2 and 101 kPa at (a) 0° angle of attack and (b) at 3° angle of attack.

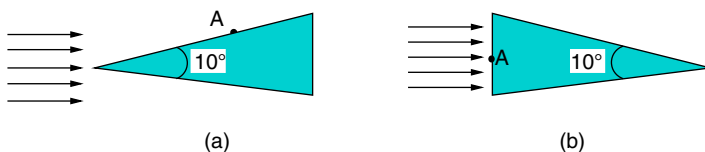
[Answer: (a)  $C_L = -0.054$ ,  $C_D = 0.00497$ , (b)  $C_L = 0.1778$ ,  $C_D = 0.01554$ ]

- 4.50** Mach 3 air at 101 kPa and  $-30^\circ\text{C}$  flows over a symmetrical wedge of semi-vertex angle 5°, leading to the generation of oblique shocks. The right-running shock impinges on a wall which “turns away from the flow” by 5° exactly at the point where the oblique shock wave impinges on it, i.e. the wall has a 5° sharp convex corner at the point where the incident shock impinges on it. Sketch the flow pattern. If the leading edge of the wedge is 1 m above the wall, how far behind this leading edge would the change in wall angle have to occur?

[Answer: 2.34 m]

- 4.51** An oblique shock in air causes an entropy increase of  $11.5 \text{ J}/(\text{kg K})^{-1}$ . If the shock angle is 25°, determine the Mach number ahead of the shock and the flow deflection angle.

[Answer: 3.29, 9°]



**Figure 4.61** A symmetrical wedge, with (a) vertex and (b) base, facing flow.

## 5

## Compressible Flow Equations

### 5.1 Introduction

The one-dimensional analysis given in the earlier chapters is valid only for flow through infinitesimal streamtubes. In many real flow situations, the assumption of one-dimensionality for the entire flow is at best an approximation. In problems such as flow in ducts, the one-dimensional treatment is adequate. However, in many other practical cases, the one-dimensional methods are neither adequate nor do they provide information about the important aspects of the flow. For example, in the case of flow past the wings of an aircraft, flow through the blade passages of turbines and compressors, and flow through ducts of rapidly varying cross-sectional area, the flow field must be thought of as two-dimensional or three-dimensional in order to obtain results of practical interest.

Because of the mathematical complexities associated with the treatment of the most general case of three-dimensional motion – including shocks, friction, and heat transfer – it becomes necessary to conceive simple models of flow, which lend themselves to analytical treatment but at the same time furnish valuable information concerning the real and difficult flow patterns. We know that by using Prandtl's boundary layer concept, it is possible to neglect friction and heat transfer for the region of potential flow outside the boundary layer (see Section 1.11).

In this chapter, we discuss the differential equations of motion for irrotational, inviscid, adiabatic, and shock-free motion of a perfect gas.

### 5.2 Crocco's Theorem

Consider two-dimensional, steady, inviscid flow in natural coordinates  $(l, n)$  such that  $l$  is along the streamline direction and  $n$  is perpendicular to the direction of the streamline. The advantage of using the natural coordinate system is that the flow velocity is always along the streamline direction and the velocity normal to the streamline is zero.

Though this is a two-dimensional flow, we can apply one-dimensional analysis, by considering the portion between the two streamlines 1 and 2 (as shown in Figure 5.1) as a streamtube and taking the third dimension to be  $\infty$ .

Let us consider unit width in the third direction for the present study. For this flow, the equation of continuity is

$$\rho V \Delta n = \text{constant} \quad (5.1)$$



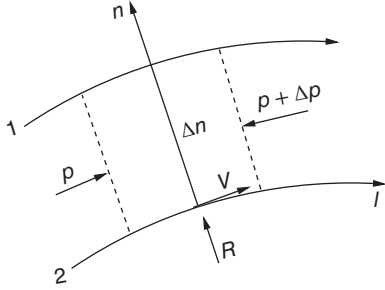


Figure 5.1 Flow between two streamlines.

The  $l$ -momentum equation is<sup>1</sup>

$$\rho V \Delta n dV = -dp \Delta n$$

The  $l$ -momentum equation can also be expressed as

$$\rho V \frac{\partial V}{\partial l} = -\frac{\partial p}{\partial l} \quad (5.2)$$

The  $n$ -momentum equation is

$$dV = 0$$

But there will be centrifugal force acting in the  $n$ -direction. Therefore,

$$\frac{\rho V^2}{R} = -\frac{\partial p}{\partial n} \quad (5.3)$$

The energy equation is

$$h + \frac{V^2}{2} = h_0 \quad (5.4)$$

Also, by Eq. (1.55),

$$T ds = dh - \frac{dp}{\rho}$$

Differentiation of Eq. (5.4) gives  $dh + VdV = dh_0$ . Therefore, the entropy equation becomes

$$T ds = -\left(V dV + \frac{dp}{\rho}\right) + dh_0$$

This equation can be split as follows.

(i)

$$T \frac{\partial s}{\partial l} = -\left(V \frac{\partial V}{\partial l} + \frac{1}{\rho} \frac{\partial p}{\partial l}\right)$$

because  $\frac{dh_0}{dl} = 0$  along the streamlines.

<sup>1</sup> Momentum equation. For incompressible flow,

$$\sum F_i = \rho \int V_x dQ$$

where  $Q$  is the volume flow rate. For compressible flow,

$$\begin{aligned} \sum F_i &= \int \rho V_x dQ \\ \sum dF_i &= \rho V_x dQ = \dot{m} V_x \end{aligned}$$

(ii)

$$T \frac{\partial s}{\partial n} = - \left( V \frac{\partial V}{\partial n} + \frac{1}{\rho} \frac{\partial p}{\partial n} \right) + \frac{dh_0}{dn}$$

Introducing  $\partial p / \partial l$  from Eq. (5.2) and  $\partial p / \partial n$  from Eq. (5.3) into the above two equations, we get

$$T \frac{\partial s}{\partial l} = 0 \quad (5.5a)$$

$$T \frac{\partial s}{\partial n} = -V \left( \frac{\partial V}{\partial n} - \frac{V}{R} \right) + \frac{dh_0}{dn} \quad (5.5b)$$

But  $\left( \frac{V}{R} - \frac{\partial V}{\partial n} \right) = \zeta$  is the vorticity of the flow. Therefore,

$$\boxed{T \frac{\partial s}{\partial n} = \frac{dh_0}{dn} + V\zeta} \quad (5.6)$$

This is known as *Crocco's theorem for two-dimensional flows*. From this it can be seen that the rotation depends on the rate of change of entropy and stagnation enthalpy normal to the streamlines.

Crocco's theorem essentially relates entropy gradients to vorticity, in steady, frictionless, non-conducting, adiabatic flows. In this form Crocco's equation shows that if the entropy ( $s$ ) is a constant, the vorticity ( $\zeta$ ) must be zero. Likewise, if vorticity  $\zeta$  is zero, the entropy gradient in the direction normal to the streamline ( $ds/dn$ ) must be zero, implying that the entropy  $s$  is a constant. That is, isentropic flows are irrotational, and irrotational flows are isentropic. This result is true, in general, only for steady flows of inviscid fluids in which there are no body forces acting and the stagnation enthalpy is a constant.

From Eq. (5.5a) it can be seen that the entropy does not change along a streamline. Also, Eq. (5.5b) shows how entropy varies normal to the streamlines.

The circulation is

$$\Gamma = \oint_c V \, dl = \iint_s \text{curl } V \, ds = \iint_s \zeta \, ds \quad (5.7)$$

By Stokes's theorem, the vorticity  $\zeta$  is given by

$$\boxed{\zeta = \text{curl } V}$$

$$\begin{aligned} \zeta_x &= \left( \frac{\partial V_z}{\partial y} - \frac{\partial V_y}{\partial z} \right) \\ \zeta_y &= \left( \frac{\partial V_x}{\partial z} - \frac{\partial V_z}{\partial x} \right) \\ \zeta_z &= \left( \frac{\partial V_y}{\partial x} - \frac{\partial V_x}{\partial y} \right) \end{aligned} \quad (5.8)$$

where  $\zeta_x, \zeta_y, \zeta_z$  are the vorticity components. The two conditions that are necessary for a frictionless flow to be isentropic throughout are

- $h_0 = \text{constant}$ , throughout the flow.
- $\zeta = 0$ , throughout the flow.

From Eq. (5.8),  $\zeta = 0$  for irrotational flow. That is, if a frictionless flow is to be isentropic, the total enthalpy should be constant throughout and the flow should be irrotational.

**When  $\zeta \neq 0$** 

Since  $h_0 = \text{constant}$ ,  $T_0 = \text{constant}$  (perfect gas). For this type of flow we can show that,

$$\zeta = \frac{T}{V} \frac{ds}{dn} = -\frac{R T_0}{V p_0} \frac{dp_0}{dn} \quad (5.9)$$

From Eq. (5.9), it can be seen that in an irrotational flow (that is with  $\zeta = 0$ ) stagnation pressure does not change normal to the streamlines. Even when there is a shock in the flow field,  $p_0$  changes along the streamlines at the shock but does not change normal to the streamlines.

Let  $h_0 = \text{constant}$  (isoenergetic flow). Then Eq. (5.6) can be written in vector form as

$$T \text{ grad } s + V \times \text{curl } V = \text{grad } h_0 \quad (5.10a)$$

where  $\text{grad } s$  stands for increase of entropy  $s$  in the  $n$ -direction. For a steady, inviscid, and isoenergetic flow,

$$\begin{aligned} T \text{ grad } s + V \times \text{curl } V &= 0 \\ V \times \text{curl } V &= -T \text{ grad } s \end{aligned} \quad (5.10b)$$

If  $s = \text{constant}$ ,  $V \times \text{curl } V = 0$ . This implies that (a) the flow is irrotational, that is  $\text{curl } V = 0$ , or (b)  $V$  is parallel to  $\text{curl } V$ .

**Irrotational flow**

For irrotational flows ( $\text{curl } V = 0$ ), a potential function  $\phi$  exists such that,

$$\boxed{V = \text{grad } \phi} \quad (5.11)$$

Therefore, the velocity components are given by

$$V_x = \frac{\partial \phi}{\partial x}, \quad V_y = \frac{\partial \phi}{\partial y}, \quad V_z = \frac{\partial \phi}{\partial z},$$

The advantage of introducing  $\phi$  is that the three unknowns  $V_x$ ,  $V_y$ , and  $V_z$  in a general three-dimensional flow are reduced to a single unknown  $\phi$ . With  $\phi$ , the irrotationality conditions defined by Eq. (5.8) may be expressed as follows.

$$\zeta_x = \frac{\partial V_z}{\partial y} - \frac{\partial V_y}{\partial z} = 0 = \frac{\partial}{\partial y} \left( \frac{\partial \phi}{\partial z} \right) - \frac{\partial}{\partial z} \left( \frac{\partial \phi}{\partial y} \right) = 0$$

Also, the incompressible continuity equation  $\nabla \cdot V = 0$  becomes

$$\boxed{\frac{\partial^2 \phi}{\partial x^2} + \frac{\partial^2 \phi}{\partial y^2} + \frac{\partial^2 \phi}{\partial z^2} = 0}$$

This is Laplace's equation. With the introduction of  $\phi$ , the three equations of motion can be replaced, at least for incompressible flow, by one Laplace equation, which is a linear equation.

**5.2.1 Basic Solutions of Laplace's Equation**

We know from our basic studies on fluid flows (reference [9]) that,

- For uniform flow (toward positive  $x$ -direction), the potential function is

$$\phi = V_\infty x$$

- For a source of strength  $Q$ , the potential function is

$$\phi = \frac{Q}{2\pi} \ln r$$

- For a doublet of strength  $\mu$  (issuing in the negative  $x$ -direction), the potential function is

$$\phi = \frac{\mu \cos \theta}{r}$$

- For a potential (free) vortex (counterclockwise) with circulation  $\Gamma$ , the potential function is

$$\phi = \frac{\Gamma}{2\pi} \theta$$

### 5.3 General Potential Equation for Three-Dimensional Flow

For a steady, inviscid, three-dimensional flow, by continuity equation,

$$\nabla \cdot (\rho \mathbf{V}) = 0$$

that is

$$\frac{\partial(\rho V_x)}{\partial x} + \frac{\partial(\rho V_y)}{\partial y} + \frac{\partial(\rho V_z)}{\partial z} = 0 \quad (5.12)$$

Euler's equations of motion (neglecting body forces) are:

$$\rho \left( V_x \frac{\partial V_x}{\partial x} + V_y \frac{\partial V_x}{\partial y} + V_z \frac{\partial V_x}{\partial z} \right) = -\frac{\partial p}{\partial x} \quad (5.13a)$$

$$\rho \left( V_x \frac{\partial V_y}{\partial x} + V_y \frac{\partial V_y}{\partial y} + V_z \frac{\partial V_y}{\partial z} \right) = -\frac{\partial p}{\partial y} \quad (5.13b)$$

$$\rho \left( V_x \frac{\partial V_z}{\partial x} + V_y \frac{\partial V_z}{\partial y} + V_z \frac{\partial V_z}{\partial z} \right) = -\frac{\partial p}{\partial z} \quad (5.13c)$$

For incompressible flows, the density  $\rho$  is a constant. Therefore, the above four equations are sufficient for solving the four unknowns  $V_x$ ,  $V_y$ ,  $V_z$ , and  $p$ . But for compressible flows,  $\rho$  is also an unknown. Therefore, the unknowns are  $\rho$ ,  $V_x$ ,  $V_y$ ,  $V_z$ , and  $p$ . Hence, the additional equation, namely the isentropic process equation, is used. That is,  $p/\rho^\gamma = \text{constant}$  is the additional equation used along with continuity and momentum equations.

Introducing the potential function  $\phi$ , we have the velocity components as

$$V_x = \frac{\partial \phi}{\partial x} = \phi_x, \quad V_y = \frac{\partial \phi}{\partial y} = \phi_y, \quad V_z = \frac{\partial \phi}{\partial z} = \phi_z \quad (5.14)$$

Equation (5.12) may also be written as

$$\rho \left( \frac{\partial V_x}{\partial x} + \frac{\partial V_y}{\partial y} + \frac{\partial V_z}{\partial z} \right) + V_x \frac{\partial \rho}{\partial x} + V_y \frac{\partial \rho}{\partial y} + V_z \frac{\partial \rho}{\partial z} = 0 \quad (5.12a)$$

From isentropic process relation,  $\rho = \rho(p)$ . Hence,

$$\frac{\partial \rho}{\partial x} = \frac{d\rho}{dp} \frac{\partial p}{\partial x} = -\frac{1}{a^2} \rho \left( V_x \frac{\partial V_x}{\partial x} + V_y \frac{\partial V_x}{\partial y} + V_z \frac{\partial V_x}{\partial z} \right)$$

because from Eq. (5.13a),

$$\frac{\partial p}{\partial x} = -\rho \left( V_x \frac{\partial V_x}{\partial x} + V_y \frac{\partial V_x}{\partial y} + V_z \frac{\partial V_x}{\partial z} \right), \quad \frac{dp}{d\rho} = a^2$$

Similarly,

$$\begin{aligned}\frac{\partial \rho}{\partial y} &= -\frac{1}{a^2} \rho \left( V_x \frac{\partial V_y}{\partial x} + V_y \frac{\partial V_y}{\partial y} + V_z \frac{\partial V_y}{\partial z} \right) \\ \frac{\partial \rho}{\partial z} &= -\frac{1}{a^2} \rho \left( V_x \frac{\partial V_z}{\partial x} + V_y \frac{\partial V_z}{\partial y} + V_z \frac{\partial V_z}{\partial z} \right)\end{aligned}$$

With the above relations for  $\frac{\partial \rho}{\partial x}$ ,  $\frac{\partial \rho}{\partial y}$ , and  $\frac{\partial \rho}{\partial z}$ , Eq. (5.12a) can be expressed as

$$\begin{aligned}\frac{\partial V_x}{\partial x} \left( 1 - \frac{V_x^2}{a^2} \right) + \frac{\partial V_y}{\partial y} \left( 1 - \frac{V_y^2}{a^2} \right) + \frac{\partial V_z}{\partial z} \left( 1 - \frac{V_z^2}{a^2} \right) - \frac{V_x V_y}{a^2} \left( \frac{\partial V_x}{\partial y} + \frac{\partial V_y}{\partial x} \right) \\ - \frac{V_y V_z}{a^2} \left( \frac{\partial V_y}{\partial z} + \frac{\partial V_z}{\partial y} \right) - \frac{V_z V_x}{a^2} \left( \frac{\partial V_z}{\partial x} + \frac{\partial V_x}{\partial z} \right) = 0\end{aligned}$$

But the velocity components and their derivatives in terms of potential function are the following.

$$\begin{aligned}V_x &= \frac{\partial \phi}{\partial x} = \phi_x, \quad V_y = \frac{\partial \phi}{\partial y} = \phi_y, \quad V_z = \frac{\partial \phi}{\partial z} = \phi_z \\ \frac{\partial V_x}{\partial x} &= \phi_{xx}, \quad \frac{\partial V_y}{\partial y} = \phi_{yy}, \quad \frac{\partial V_z}{\partial z} = \phi_{zz} \\ \frac{\partial V_x}{\partial y} &= \phi_{xy}, \quad \frac{\partial V_y}{\partial z} = \phi_{yz}, \quad \frac{\partial V_z}{\partial x} = \phi_{zx}\end{aligned}$$

Therefore, in terms of potential function  $\phi$ , the above equation can be expressed as

$$\begin{aligned}\left( 1 - \frac{\phi_x^2}{a^2} \right) \phi_{xx} + \left( 1 - \frac{\phi_y^2}{a^2} \right) \phi_{yy} + \left( 1 - \frac{\phi_z^2}{a^2} \right) \phi_{zz} \\ - 2 \left( \frac{\phi_x \phi_y}{a^2} \phi_{xy} + \frac{\phi_y \phi_z}{a^2} \phi_{yz} + \frac{\phi_z \phi_x}{a^2} \phi_{zx} \right) = 0\end{aligned}\tag{5.15}$$

This is the *basic potential equation* for compressible flow, and it is nonlinear.

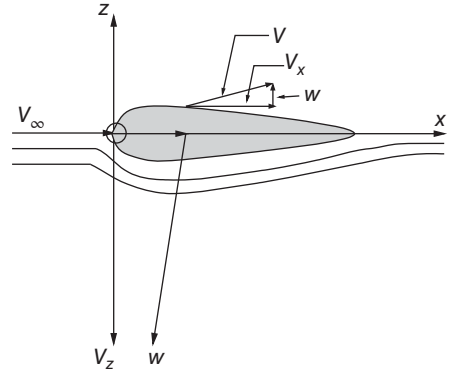
The difficulties associated with compressible flow stem from the fact that the basic equation is nonlinear. Hence the superposition of solutions is not valid. Further, in Equation (5.15), the local speed of sound,  $a$ , is also a variable. By Eq. (2.9e), we have

$$\left( \frac{a}{a_\infty} \right)^2 = 1 - \frac{\gamma - 1}{2} M_\infty^2 \left( \frac{V_x^2 + V_y^2 + V_z^2}{V_\infty^2} - 1 \right)\tag{5.16}$$

To solve a compressible flow problem, we have to solve Eq. (5.15) using Eq. (5.16), but this is not possible analytically. However, numerical solution is possible for given boundary conditions (BCs).

## 5.4 Linearization of the Potential Equation

The general equation for compressible flows, Eq. (5.15), can be simplified for flow past slender or planar bodies. Airfoils, slender bodies of revolution, and so on are typical examples of *slender bodies*. Bodies like wings, where one dimension is smaller than others, are called *planar bodies*. These bodies introduce small disturbances. The airfoil contour becomes the stagnation streamline.

**Figure 5.2** Airfoil in a uniform flow.

For the airfoil shown in Figure 5.2, with the exception of nose region, the perturbation velocity  $w$  is small everywhere.

### 5.4.1 Small Perturbation Theory

Assume that the velocity at any point in the flow field is given by the vector sum of the freestream velocity  $V_\infty$  along the  $x$ -axis and the perturbation velocity components  $u$ ,  $v$ , and  $w$  along the  $x$ -,  $y$ -, and  $z$ -directions, respectively. Consider the flow around an airfoil shown in Figure 5.2. The velocity components around the airfoil are

$$V_x = V_\infty + u, \quad V_y = v, \quad V_z = w \quad (5.17)$$

where  $V_x$ ,  $V_y$ , and  $V_z$  are the main flow velocity components and  $u$ ,  $v$ , and  $w$  are the perturbation (disturbance) velocity components along the  $x$ -,  $y$ -, and  $z$ -directions, respectively.

The small perturbation theory postulates that the perturbation velocities are small compared to the main velocity components, that is

$$u \ll V_\infty, \quad v \ll V_\infty, \quad w \ll V_\infty \quad (5.18a)$$

Therefore,

$$V_x \approx V_\infty, \quad V_y \ll V_\infty, \quad V_z \ll V_\infty \quad (5.18b)$$

Now, consider a flow at a small angle of attack or yaw as shown in Figure 5.3. Here,

$$V_x = V_\infty \cos \alpha + u, \quad V_y = V_\infty \sin \alpha + v$$

Since the angle of attack  $\alpha$  is small, the above equations reduce to

$$V_x = V_\infty + u, \quad V_y = v$$

Thus, Eq. (5.17) can be used for this case also.

With Eq. (5.17), linearization of Eq. (5.15) gives

$$(1 - M^2)\phi_{xx} + \phi_{yy} + \phi_{zz} = 0 \quad (5.19)$$

neglecting all higher-order terms, where  $M$  is the local Mach number. Therefore, Eq. (5.16) should be used in solving Eq. (5.19).

The perturbation velocities may also be written in potential form, as follows.

Let  $\phi = \phi_\infty + \phi$ , where

$$\phi_\infty = V_\infty x : \phi_{xx} = \phi_{\infty xx}^{(0)} + \phi_{xx} \dots$$

Therefore,  $\phi$  may be called the disturbance (perturbation) potential and hence the perturbation velocity components are given by

$$u = \frac{\partial \phi}{\partial x}, v = \frac{\partial \phi}{\partial y}, w = \frac{\partial \phi}{\partial z} \quad (5.20)$$

With the assumptions of this small perturbation theory, Eq. (5.16) can be expressed as

$$\begin{aligned} \left(\frac{a}{a_\infty}\right)^2 &= 1 - (\gamma - 1)M_\infty^2 \frac{u}{V_\infty} \\ \left(\frac{a_\infty}{a}\right)^2 &= \left(1 - (\gamma - 1)M_\infty^2 \frac{u}{V_\infty}\right)^{-1} \end{aligned} \quad (5.21)$$

Using binomial theorem,  $(a_\infty/a)^2$  can be expressed as

$$\left(\frac{a_\infty}{a}\right)^2 = 1 + (\gamma - 1)\frac{u}{V_\infty}M_\infty^2 + O\left(M_\infty^4 \frac{u^2}{V_\infty^2}\right) \quad (5.22)$$

Substitute the above expression for  $(a_\infty/a)$  in the equation

$$M = \left(1 + \frac{u}{V_\infty}\right) \left(\frac{a_\infty}{a}\right) M_\infty$$

the relation between the local Mach number  $M$  and freestream Mach number  $M_\infty$  may be expressed (neglecting small terms) as

$$M^2 = \left[1 + 2\frac{u}{V_\infty} \left(1 + \frac{\gamma - 1}{2}M_\infty^2\right)\right] M_\infty^2 \quad (5.23)$$

The combination of Eqs. (5.23) and (5.19) gives

$$(1 - M_\infty^2)\phi_{xx} + \phi_{yy} + \phi_{zz} = \frac{2}{V_\infty} M_\infty^2 \phi_x \phi_{xx} \left(1 + \frac{\gamma - 1}{2}M_\infty^2\right) \quad (5.24)$$

Equation (5.24) is a nonlinear equation and is valid for subsonic, transonic, and supersonic flow under the framework of small perturbations with  $u \ll V_\infty$ ,  $v \ll V_\infty$ , and  $w \ll V_\infty$ . It is, however, not valid for hypersonic flow even for slender bodies (since  $u \approx V_\infty$  in the hypersonic flow regime). The equation is called the *linearized potential flow equation*, though it is not linear.

Equation (5.24) may also be written as

$$(1 - M_\infty^2)\phi_{xx} + \phi_{yy} + \phi_{zz} = 2\frac{M_\infty^2}{1 - M_\infty^2} \frac{u}{V_\infty} \left(1 + \frac{\gamma - 1}{2}M_\infty^2\right) (1 - M_\infty^2)\phi_{xx} \quad (5.25)$$

Further linearization is possible if

$$\frac{M_\infty^2}{1 - M_\infty^2} \frac{u}{V_\infty} \ll 1 \quad (5.26)$$

With this condition, Eq. (5.25) results in

$$(1 - M_\infty^2)\phi_{xx} + \phi_{yy} + \phi_{zz} = 0 \quad (5.27)$$

This is the fundamental equation governing most of the compressible flow regime. Equation (5.27) is valid only when Eq. (5.26) is valid, and Eq. (5.26) is valid only when the freestream

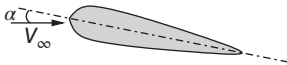


Figure 5.3 Airfoil at an angle of attack in a uniform flow.

Mach number  $M_\infty$  is sufficiently different from 1. Hence, Eq. (5.26) is valid for subsonic and supersonic flows only. For transonic flows, Eq. (5.24) can be used. For  $M_\infty \approx 1$ , Eq. (5.24) reduces to

$$\boxed{-\frac{\gamma+1}{V_\infty} \phi_x \phi_{xx} + \phi_{yy} + \phi_{zz} = 0} \quad (5.28)$$

The nonlinearity of Eq. (5.28) makes transonic flow problems much more difficult than subsonic or supersonic flow problems.

Equation (5.27) is elliptic (that is all terms are positive) for  $M_\infty < 1$  and hyperbolic (that is not all terms are positive) for  $M_\infty > 1$ . But in both the cases, the governing differential equation is linear. This is the advantage of Eq. (5.27).

## 5.5 Potential Equation for Bodies of Revolution

Airplanes fuselages, rocket shells, missile bodies, and circular ducts are the few bodies of revolutions that are commonly used in practice. The general three-dimensional Cartesian equations can be used for these problems. But it is much simpler to use cylindrical polar coordinates than Cartesian coordinates. Cartesian coordinates are  $x$ ,  $y$ , and  $z$ , and the corresponding velocity components are  $V_x$ ,  $V_y$ , and  $V_z$ . Cylindrical polar coordinates are  $x$ ,  $r$ , and  $\theta$  and the corresponding velocity components are  $V_x$ ,  $V_r$ , and  $V_\theta$ . For axisymmetric flows with cylindrical coordinates, the equations will be independent of  $\theta$ . Thus, mathematically, cylindrical coordinates reduce the problem to become two-dimensional. However, for flows that are not axially symmetric (e.g. a missile at an angle of attack),  $\theta$  will be involved. The continuity equation in cylindrical coordinates is

$$\frac{\partial(\rho V_x)}{\partial x} + \frac{1}{r} \frac{\partial(\rho r V_r)}{\partial r} + \frac{1}{r} \frac{\partial(\rho V_\theta)}{\partial \theta} = 0 \quad (5.29)$$

Expressing the velocity components in terms of the potential function  $\phi$  as

$$V_x = \frac{\partial \phi}{\partial x}, \quad V_r = \frac{\partial \phi}{\partial r}, \quad V_\theta = \frac{1}{r} \frac{\partial \phi}{\partial \theta} \quad (5.30)$$

The potential Eq. (5.25) can be written, in cylindrical polar coordinates, as

$$\begin{aligned} & \left(1 - \frac{\phi_x^2}{a^2}\right) \phi_{xx} + \left(1 - \frac{\phi_r^2}{a^2}\right) \phi_{rr} + \left(1 - \frac{1}{r^2} \frac{\phi_\theta^2}{a^2}\right) \frac{1}{r^2} \phi_{\theta\theta} \\ & - 2 \left( \frac{\phi_x \phi_r}{a^2} \phi_{xr} + \frac{\phi_x \phi_\theta}{a^2} \frac{1}{r^2} \phi_{x\theta} + \frac{\phi_r \phi_\theta}{a^2} \frac{1}{r^2} \phi_{r\theta} \right) + \left(1 + \frac{1}{r^2} \frac{\phi_\theta^2}{a^2}\right) \frac{1}{r} \phi_r = 0 \end{aligned} \quad (5.31)$$

Also,

$$\left(\frac{a}{a_\infty}\right)^2 = 1 - \frac{\gamma-1}{2} M_\infty^2 \left( \frac{V_x^2 + V_r^2 + V_\theta^2}{V_\infty^2} - 1 \right) \quad (5.32)$$

The small perturbation assumptions are

$$\begin{aligned} V_x &= V_\infty + u, \quad V_r = v_r, \quad V_\theta = v_\theta \\ u &\ll V_\infty, \quad v_r \ll V_\infty, \quad v_\theta \ll V_\infty \end{aligned}$$



where  $V_x$ ,  $V_r$ , and  $V_\theta$  are the mean velocity components and  $u$ ,  $v_r$ , and  $v_\theta$  are the perturbation velocity components along the  $x$ -,  $r$ -, and  $\theta$ -direction, respectively. Introduction of these relations in Eq. (5.31) results in

$$(1 - M^2)\phi_{xx} + \phi_{rr} + \frac{1}{r}\phi_r + \frac{1}{r^2}\phi_{\theta\theta} = 0 \quad (5.33)$$

where  $M$  is the local Mach number after Eq. (5.23). The relations for  $u$ ,  $v_r$ , and  $v_\theta$  in polar coordinates, under small perturbation assumption, are

$$u = \frac{\partial\phi}{\partial x} = \phi_x, v_r = \frac{\partial\phi}{\partial r} = \phi_r, v_\theta = \frac{1}{r} \frac{\partial\phi}{\partial\theta} = \frac{1}{r}\phi_\theta$$

With these expressions for  $u$ ,  $v_r$ , and  $v_\theta$ , Eq. (5.24) can be written as

$$(1 - M_\infty^2)\phi_{xx} + \phi_{rr} + \frac{1}{r}\phi_r + \frac{1}{r^2}\phi_{\theta\theta} = \frac{2}{V_\infty} M_\infty^2 \phi_x \phi_{xx} \left(1 + \frac{\gamma - 1}{2} M_\infty^2\right) \quad (5.34)$$

This equation corresponds to Eq. (5.24) with the same term on the right-hand side. Therefore, with

$$\frac{M_\infty^2}{1 - M_\infty^2} \frac{u}{V_\infty} \ll 1$$

Equation (5.34) simplifies to

$$(1 - M_\infty^2)\phi_{xx} + \phi_{rr} + \frac{1}{r}\phi_r + \frac{1}{r^2}\phi_{\theta\theta} = 0 \quad (5.35)$$

This is the governing equation for subsonic and supersonic flows in cylindrical coordinates. For transonic flow, Eq. (5.34) becomes

$$-\frac{\gamma + 1}{V_\infty} \phi_x \phi_{xx} + \phi_{rr} + \frac{1}{r}\phi_r + \frac{1}{r^2}\phi_{\theta\theta} = 0 \quad (5.36)$$

For axially symmetric subsonic and supersonic flows,  $\phi_{\theta\theta} = 0$ . Therefore, Eq. (5.35) reduces to

$$(1 - M_\infty^2)\phi_{xx} + \phi_{rr} + \frac{1}{r}\phi_r = 0 \quad (5.37)$$

Similarly, Eq. (5.36) reduces to

$$-\frac{\gamma + 1}{V_\infty} \phi_x \phi_{xx} + \phi_{rr} + \frac{1}{r}\phi_r = 0 \quad (5.38)$$

Equation (5.38) is the equation for axially symmetric transonic flows. All these equations are valid only for small perturbations, that is for small values of angle of attack and angle of yaw ( $< 15^\circ$ ).

### 5.5.1 Conclusions

From the above discussions on potential flow theory for compressible flows, we can draw the following conclusions.

- The small perturbation equations for subsonic and supersonic flows are linear, but for transonic flows the equation is nonlinear.
- Subsonic and supersonic flow equations do not contain the specific heats ratio  $\gamma$ , but transonic flow equation contains  $\gamma$ . This shows that the results obtained for subsonic and supersonic flows, with small perturbation equations, can be applied to any gas, but this cannot be done for transonic flows.

- All these equations are valid for slender bodies. This is true of rockets, missiles, and so on.
- These equations can also be applied to airfoils, but not to bluff shapes such as the circular cylinder.
- For nonslender bodies, the flow can be calculated by using the original nonlinear equation.

### 5.5.2 Solution of Nonlinear Potential Equation

#### (i) Numerical methods

The nonlinearity of Eq. (5.24) makes it tedious to solve the equation analytically. However, solutions for the equation can be obtained by numerical methods. But a numerical solution is not a general solution, and is valid only for a specific configuration of flow field with a fixed Mach number and specified geometry.

#### (ii) Transformation (hodograph) methods

When one velocity component is plotted against another velocity component, the resulting curve may be linear, whereas in the physical plane, the relation may be nonlinear. This method is used for solving certain transonic flow problems.

#### (iii) Similarity methods

In these methods, the boundary conditions need to be specified for solving the equation. Detailed discussion of this method can be found in Chapter 6 on similarity methods.

## 5.6 Boundary Conditions

Examine the streamlines around an airfoil kept in a flow field as shown in Figure 5.4. In inviscid flow the streamline near the boundary is similar to the body contour. The flow must satisfy the following boundary conditions (BCs).

#### Boundary condition 1 – Kinematic flow condition

The flow velocity at all surface points is tangential to the body contour. The component of velocity normal to the body contour is zero.

#### Boundary condition 2

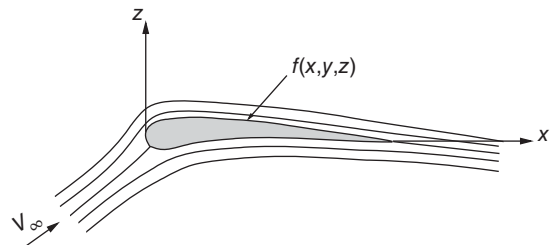
At  $z \rightarrow \pm\infty$ , perturbation velocities are zero or finite. The kinematic flow condition for the airfoil shown in Figure 5.4, with small perturbation assumptions, may be written as follows.

Body contour:  $f = f(x, y, z)$

The velocity vector  $V$  at any point on the body is tangential to the surface. Therefore, on the surface of the airfoil ( $V \cdot \text{grad } f$ ) = 0, that is

$$(V_\infty + u) \frac{\partial f}{\partial x} + v \frac{\partial f}{\partial y} + w \frac{\partial f}{\partial z} = 0 \quad (5.39)$$

**Figure 5.4** Cambered airfoil at an angle of attack.



But  $u/V_\infty \ll 1$ ; therefore, Eq. (5.39) simplifies to

$$V_\infty \frac{\partial f}{\partial x} + v \frac{\partial f}{\partial y} + w \frac{\partial f}{\partial z} = 0 \quad (5.40)$$

For two-dimensional flows,  $v = 0$ ;  $\partial f / \partial y = 0$ . Therefore, Eq. (5.39) reduces to

$$\frac{w}{V_\infty + u} = - \frac{\partial f / \partial x}{\partial f / \partial z} = \left( \frac{\partial z}{\partial x} \right)_c \quad (5.41)$$

where the subscript  $c$  refers to the body contour,  $(\partial z / \partial x)$  is the slope of the body, and  $u$  and  $w$  are the tangential and normal components of velocity, respectively. Expressing  $u$  and  $w$  as power series of  $z$ , we get

$$\begin{aligned} u(x, z) &= u(x, 0) + a_1 z + a_2 z^2 + \dots \\ w(x, z) &= w(x, 0) + b_1 z + b_2 z^2 + \dots \end{aligned}$$

The coefficients  $a$ 's and  $b$ 's in these series are functions of  $x$ . If the body is sufficiently slender,

$$\frac{w(x, 0)}{V_\infty + u(x, 0)} = \left( \frac{dz}{dx} \right)_c$$

that is for sufficiently slender bodies it is not necessary to fulfill the BC on the contour of the airfoil. It is sufficient if the BC on the  $x$ -axis of the body is satisfied, that is on the axis of a body of revolution or the chord of an airfoil. With  $u/V_\infty \ll 1$ , the above condition becomes

$$\frac{w(x, 0)}{V_\infty} = \left( \frac{dz}{dx} \right)_c \quad (5.42)$$

For *planar bodies*,  $\partial f / \partial y = 0$  and therefore,

$$\frac{w(x, y, 0)}{V_\infty} = \left( \frac{dz}{dx} \right)_c \quad (5.43)$$

that is, the condition is satisfied in the plane of the body. In Eqs. (5.42) and (5.43), the elevation of the body above the  $x$ -axis is neglected.

### 5.6.1 Bodies of Revolution

For bodies of revolution, the term  $\frac{1}{r} \frac{\partial}{\partial r}(rv_r)$  present in the continuity Eq. (5.29) becomes finite. Because of this term the perturbations near the body become significant. Therefore, a power series for velocity components is not possible. However, we can apply the following approximation to express the perturbation velocity as a power series. For axisymmetric bodies,

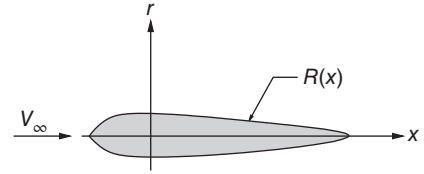
$$\frac{1}{r} \frac{\partial}{\partial r}(rv_r) \sim \frac{\partial u}{\partial x}, \quad \frac{\partial}{\partial r}(rv_r) \sim r \frac{\partial u}{\partial x}$$

when  $r \rightarrow 0$ ;  $\frac{\partial}{\partial r}(rv_r) \approx 0$  or  $rv_r = a_0(x)$ . Thus, even though the radial component of velocity  $v_r$  on the axis of a body of revolution is of the order of  $1/r$ , it can be estimated near the axis similar to a potential vortex. For a potential vortex, the radial velocity is

$$v_r \propto \frac{1}{r}$$

Now,  $v_r$  can be expressed in terms of a power series as

$$rv_r = a_0 + a_1 r + a_2 r^2 + \dots$$

**Figure 5.5** An axisymmetric body in a flow.

For the axisymmetric body with its surface profile contour given by the function  $R(x)$ , we have

$$\frac{v_r}{V_\infty + u} = \left( \frac{dR(x)}{dx} \right)_c$$

The simplified kinematic flow condition for the body in Figure 5.5 is

$$\frac{(rv_r)_0}{V_\infty} = R(x) \frac{dR(x)}{dx} \quad (5.44)$$

where subscript 0 refers to the axis of the body.

Equation (5.44) is called the *simplified kinematic flow condition* in the sense that the kinematic flow condition is fulfilled on the axis, rather than on the surface of the body contour.

On the axis of the body, Eq. (5.44) gives

$$\lim_{r \rightarrow 0} (rv_r) = V_\infty R(x) \frac{dR(x)}{dx} \quad (5.45)$$

From the above discussions, it may be summarized that the BCs for this kind of problem are the following.

For two-dimensional (planar) bodies,

$$\left( \frac{w}{V_\infty + u} \right)_c \approx \frac{(w)_0}{V_\infty} = \left( \frac{\partial z}{\partial x} \right)_c \quad (5.46)$$

For bodies of revolution (elongated bodies),

$$R(x) \left( \frac{v_r}{V_\infty + u} \right)_c \approx \frac{(rv_r)_0}{V_\infty} = R(x) \frac{dR(x)}{dx} \quad (5.47)$$

## 5.7 Pressure Coefficient

Pressure coefficient is the nondimensional difference between a local pressure and the freestream pressure. The idea of finding the velocity distribution is to find the pressure distribution and then integrate it to get lift, moment, and pressure drag. For three-dimensional flows, the pressure coefficient  $C_p$ , as given by (Eq. 2.54), is

$$C_p = \frac{2}{\gamma M_\infty^2} \left\{ \left[ \frac{\gamma - 1}{2} M_\infty^2 \left( 1 - \frac{(V_\infty + u)^2 + v^2 + w^2}{V_\infty^2} \right) + 1 \right]^{\gamma/(\gamma-1)} - 1 \right\}$$

or

$$C_p = \frac{2}{\gamma M_\infty^2} \left\{ \left[ 1 - \frac{\gamma - 1}{2} M_\infty^2 \left( \frac{2u}{V_\infty} + \frac{u^2 + v^2 + w^2}{V_\infty^2} \right) \right]^{\gamma/(\gamma-1)} - 1 \right\}$$

where  $M_\infty$  and  $V_\infty$  are the freestream Mach number and velocity, respectively;  $u$ ,  $v$ , and  $w$  are the  $x$ -,  $y$ -, and  $z$ -components of perturbation velocity; and  $\gamma$  is the ratio of specific heats. Expanding

the right-hand side of this equation binomially and neglecting the third and higher-order terms of the perturbation velocity components, we get

$$C_p = - \left( 2 \frac{u}{V_\infty} + (1 - M_\infty^2) \frac{u^2}{V_\infty^2} + \frac{v^2 + w^2}{V_\infty^2} \right) \quad (5.48a)$$

For two-dimensional or planar bodies, the  $C_p$  simplifies further, resulting in

$$\boxed{C_p = -2 \frac{u}{V_\infty}} \quad (5.48b)$$

This is a fundamental equation applicable to three-dimensional compressible (subsonic and supersonic) flows, as well as for low-speed two-dimensional flows.

### 5.7.1 Bodies of Revolution

For bodies of revolution, by small perturbation assumption, we have  $u \ll V_\infty$ , but  $v$  and  $w$  are not negligible. Therefore, Eq. (5.48a) simplifies to

$$C_p = -2 \frac{u}{V_\infty} - \frac{v^2 + w^2}{V_\infty^2} \quad (5.49)$$

The above equation, which is in Cartesian coordinates, may also be expressed as

$$C_p = -2 \frac{u}{V_\infty} - \left( \frac{v_r}{V_\infty} \right)^2 \quad (5.50)$$

Combining Eqs. (5.47) and (5.50), we get

$$C_p = - \left[ 2 \frac{u}{V_\infty} + \left( \frac{dR(x)}{dx} \right)^2 \right] \quad (5.51)$$

where  $R(x)$  is the expression for the body contour.

## 5.8 Summary

In this chapter we have presented some of the aspects of linearized compressible flow. It is important to recognize the fundamental nature of the approximations introduced to linearize the basic potential equation for compressible flow. Although modern numerical techniques are capable of yielding accurate solutions for flows with complex geometries, linearized solutions still play a vital role in the field of compressible flows.

By Crocco's theorem, we have, for two-dimensional flows,

$$T \frac{\partial s}{\partial n} = \frac{dh_0}{dn} + V\zeta$$

where  $s$  is entropy,  $h_0$  is stagnation enthalpy, and  $\zeta$  is vorticity. This equation relates the velocity of a flow field to the entropy of the fluid. Also, it stipulates the conditions under which a frictionless flow will have the same entropy on different streamlines, that is it will be isentropic. The conditions are

$$h_0 = \text{constant, throughout the flow}$$

$$\zeta = 0, \text{ throughout the flow}$$

That is, isentropic flows are irrotational and irrotational flows are isentropic. This result is true, in general, only for steady flows of inviscid fluids in which there are no body forces and in which the stagnation enthalpy is constant. For irrotational flows, by Laplace's equation, we have

$$\frac{\partial^2 \phi}{\partial x^2} + \frac{\partial^2 \phi}{\partial y^2} + \frac{\partial^2 \phi}{\partial z^2} = 0$$

The basic solutions for this equations are the following.

- For uniform flow (toward positive  $x$ -direction), the potential function is

$$\phi = V_{\infty} x$$

- For a source of strength  $Q$ , the potential function is

$$\phi = \frac{Q}{2\pi} \ln r$$

- For a doublet of strength  $\mu$  (issuing in negative  $x$ -direction), the potential function is

$$\phi = \frac{\mu \cos \theta}{r}$$

- For a potential (free) vortex (counterclockwise) with circulation  $\Gamma$ , the potential function is

$$\phi = \frac{\Gamma}{2\pi} \theta$$

The governing equations for three-dimensional potential flow in Cartesian coordinates are the following.

The continuity equation

$$\frac{\partial(\rho V_x)}{\partial x} + \frac{\partial(\rho V_y)}{\partial y} + \frac{\partial(\rho V_z)}{\partial z} = 0$$

The Euler's equation of motion (neglecting body forces) or the momentum equations are

$$\rho \left( V_x \frac{\partial V_x}{\partial x} + V_y \frac{\partial V_x}{\partial y} + V_z \frac{\partial V_x}{\partial z} \right) = -\frac{\partial p}{\partial x}$$

$$\rho \left( V_x \frac{\partial V_y}{\partial x} + V_y \frac{\partial V_y}{\partial y} + V_z \frac{\partial V_y}{\partial z} \right) = -\frac{\partial p}{\partial y}$$

$$\rho \left( V_x \frac{\partial V_z}{\partial x} + V_y \frac{\partial V_z}{\partial y} + V_z \frac{\partial V_z}{\partial z} \right) = -\frac{\partial p}{\partial z}$$

and the isentropic process relation is

$$\frac{p}{p_0} = \left( \frac{\rho}{\rho_0} \right)^\gamma$$

Instead of the energy equation, we have the isentropic relation. The isentropic relation given above is for a perfect gas. The more general form of the isentropic relation is, simply,  $s = \text{constant}$ .

In terms of the velocity potential, the momentum equation becomes

$$\begin{aligned} & \left( 1 - \frac{\phi_x^2}{a^2} \right) \phi_{xx} + \left( 1 - \frac{\phi_y^2}{a^2} \right) \phi_{yy} + \left( 1 - \frac{\phi_z^2}{a^2} \right) \phi_{zz} \\ & - 2 \left( \frac{\phi_x \phi_y}{a^2} \phi_{xy} + \frac{\phi_y \phi_z}{a^2} \phi_{yz} + \frac{\phi_z \phi_x}{a^2} \phi_{zx} \right) = 0 \end{aligned}$$

This is the *basic potential equation* for compressible flow and it is nonlinear. Because of the nonlinearity of this equation, the superposition of solutions is not valid. Furthermore, the local speed of sound in this equation is also a variable.

With small perturbation theory, Eq. (5.15) reduces to

$$(1 - M_\infty^2)\phi_{xx} + \phi_{yy} + \phi_{zz} = 0$$

This is an approximate equation; it no longer represents the exact physics of the flow. However, the original nonlinear equation – Eq. (5.15) – has been reduced to a linear equation – Eq. (5.19). It is also called the *linearized perturbation velocity potential equation*. It is important to note that Eq. (5.19) is valid for subsonic and supersonic flows only. It is not valid for transonic flows.

The linearized potential flow equation valid for subsonic, supersonic, and transonic flows is

$$(1 - M_\infty^2)\phi_{xx} + \phi_{yy} + \phi_{zz} = \frac{2}{V_\infty} M_\infty^2 \phi_x \phi_{xx} \left( 1 + \frac{\gamma - 1}{2} M_\infty^2 \right)$$

Equation (5.24) is nonlinear, unlike Eq. (5.19), which is linear.

From the above governing equations it is evident that subsonic and supersonic flows lend themselves to approximate, linearized theory for the case of irrotational, isentropic flow with small perturbations. But transonic and hypersonic flows cannot be linearized, even with small perturbations.

The potential equations for bodies of revolution in cylindrical polar coordinates are the following.

The continuity equation:

$$\frac{\partial(\rho V_x)}{\partial x} + \frac{1}{r} \frac{\partial(\rho r V_r)}{\partial r} + \frac{1}{r} \frac{\partial(\rho V_\theta)}{\partial \theta} = 0$$

The momentum equation:

$$\begin{aligned} & \left( 1 - \frac{\phi_x^2}{a^2} \right) \phi_{xx} + \left( 1 - \frac{\phi_r^2}{a^2} \right) \phi_{rr} + \left( 1 - \frac{1}{r^2} \frac{\phi_\theta^2}{a^2} \right) \frac{1}{r^2} \phi_{\theta\theta} \\ & - 2 \left( \frac{\phi_x \phi_r}{a^2} \phi_{xr} + \frac{\phi_x \phi_\theta}{a^2} \frac{1}{r^2} \phi_{x\theta} + \frac{\phi_r \phi_\theta}{a^2} \frac{1}{r^2} \phi_{r\theta} \right) + \left( 1 + \frac{1}{r^2} \frac{\phi_\theta^2}{a^2} \right) \frac{1}{r} \phi_r = 0 \end{aligned}$$

With the small perturbation assumption, this equation reduces to

$$(1 - M_\infty^2)\phi_{xx} + \phi_{rr} + \frac{1}{r}\phi_r + \frac{1}{r^2}\phi_{\theta\theta} = 0$$

This equation is valid for subsonic and supersonic flows in cylindrical coordinates. For transonic flows the governing equation is

$$-\frac{\gamma + 1}{V_\infty} \phi_x \phi_{xx} + \phi_{rr} + \frac{1}{r}\phi_r + \frac{1}{r^2}\phi_{\theta\theta} = 0$$

For axially symmetric flows,  $\phi_{\theta\theta} = 0$ ; therefore, Eqs. (5.35) and (5.36) reduce to

$$\begin{aligned} (1 - M_\infty^2)\phi_{xx} + \phi_{rr} + \frac{1}{r}\phi_r &= 0 \\ -\frac{\gamma + 1}{V_\infty} \phi_x \phi_{xx} + \phi_{rr} + \frac{1}{r}\phi_r &= 0 \end{aligned}$$

All these equations are valid only for small perturbations, that is for small values of angle of attack and yaw ( $<15^\circ$ ). The pressure coefficient  $C_p$  given by small perturbation theory is

$$C_p = - \left( 2 \frac{u}{V_\infty} + (1 - M_\infty^2) \frac{u^2}{V_\infty^2} + \frac{v^2 + w^2}{V_\infty^2} \right)$$

For bodies of revolution, the  $C_p$  becomes

$$C_p = - \left[ 2 \frac{u}{V_\infty} + \left( \frac{dR(x)}{dx} \right)^2 \right]$$

where  $R(x)$  is the expression for body contour.

In the light of the discussion of this chapter it may be summarized that

- The small perturbation equations for subsonic and supersonic flows are linear, but for transonic flows the equation is nonlinear.
- Subsonic and supersonic equations do not contain the specific heats ratio  $\gamma$ , but the transonic flow equation contains  $\gamma$ . This implies that the results obtained for subsonic and supersonic flows with small perturbation equations can be applied to any gas, but this cannot be done for transonic flows.

## Exercise Problems

- 5.1 Show that, for compressible flow of a perfect gas, the variation of total pressure across a streamline is given by

$$-\frac{1}{\rho_0} \frac{dp_0}{dn} = \left( 1 + \frac{\gamma-1}{2} M^2 \right) u \zeta + \frac{\gamma-1}{2} c_p M^2 \frac{dT_0}{dn}$$

where  $n$  is the direction normal to the streamline.

- 5.2 The nose of a cylindrical body has the profile  $R = \varepsilon x^{3/2}$ ,  $0 \leq x \leq 1$ . Show that the pressure distribution on the body is given by

$$\frac{C_p}{\varepsilon^2} = 6x \ln \frac{2}{\varepsilon \sqrt{M^2 - 1}} - 3x \ln(x) - \frac{33}{4}x$$

Estimate the drag coefficient for  $M = \sqrt{2}$  and  $\varepsilon = 0.1$ .

(Hint: For obtaining  $C_D$ , use  $C_D S(L) = \int_0^L C_p(x) S'(x) dx$ , where  $S(x)$  is the cross-sectional area of the body at  $x$  and  $L$  is the length of the body.)

[Answer:  $C_D = 0.0786$ ]

- 5.3 For a perfect gas, express the ratio of local and freestream speed of sound in terms of the local velocity components, freestream velocity and freestream Mach number.

$$\left[ \text{Answer : } \left( \frac{a}{a_\infty} \right)^2 = 1 - \frac{\gamma-1}{2} M_\infty^2 \left( \frac{V_x^2 + V_y^2 + V_z^2}{V_\infty^2} - 1 \right) \right]$$

- 5.4 For an isentropic flow of a perfect gas, show that the vorticity  $\zeta$  in terms of flow velocity and stagnation pressure and temperature can be expressed as

$$\zeta = \frac{R}{V} \frac{T_0}{p_0} \frac{dp_0}{dn}$$

where  $n$  is the coordinate normal to streamline.



## 6

## Similarity Rule

### 6.1 Introduction

In Section 5.4, we saw that the governing equation for compressible flow is elliptic for subsonic flows and becomes hyperbolic for supersonic flows. This change in the nature of the partial differential equation, upon going from subsonic to supersonic flow, indicates the possibility of deriving similarity relationships between subsonic compressible flow and the corresponding incompressible flow, and the importance of the Mach wave in a supersonic solution. In this chapter we will derive an expression that relates the subsonic compressible flow past a certain profile to the incompressible flow past a second profile derived from first principles through an *affine transformation*. Such an expression is called a *similarity rule*.

If the governing equations of motion could be solved easily, the solution itself would indicate quite clearly the nature of any similarities that might exist among members of a family of flow patterns. Then there would be no need for a separate derivation of similarity rules.

But in the majority of situations, we are unable to solve the equations of motion. However, even though solutions are lacking, we may use our knowledge of the forms of the differential equations and the related boundary conditions to derive the similarity rules.

### 6.2 Two-Dimensional Flow: The Prandtl–Glauert Rule for Subsonic Flow

#### 6.2.1 Prandtl–Glauert Transformations

Prandtl and Glauert have shown that it is possible to relate the solution of compressible flow around a body to the incompressible flow solution.

The transformation from one to the other is achieved in the following manner. The Laplace equations for two-dimensional compressible and incompressible flows, respectively, are

$$(1 - M_\infty^2)\phi_{xx} + \phi_{zz} = 0 \quad (6.1)$$

$$(\phi_{xx})_{\text{inc}} + (\phi_{zz})_{\text{inc}} = 0 \quad (6.2)$$

where the  $x$ -coordinate is along the flow direction, the  $z$ -coordinate is normal to the flow,  $M_\infty$  is the freestream Mach number, and  $\phi$  is the velocity potential function. These equations, however, are not the complete description of the problem, since it is also necessary to specify the boundary conditions.

Equations (6.1) and (6.2) can be transformed into one another by the following transformation.

$$x_{\text{inc}} = x, \quad z_{\text{inc}} = K_1 z \quad (6.3a)$$

$$\phi(x, z) = K_2 \phi_{\text{inc}}(x_{\text{inc}}, z_{\text{inc}}) \quad (6.3b)$$

In Eq. (6.3), the variables with the subscript “inc” are for incompressible flow and the variables without the subscript are for compressible flow. Combining Eqs. (6.1) and (6.3), we get

$$(1 - M_\infty^2) K_2 \frac{\partial^2 \phi_{\text{inc}}}{\partial x_{\text{inc}}^2} + K_1^2 K_2 \frac{\partial^2 \phi_{\text{inc}}}{\partial z_{\text{inc}}^2} = 0$$

that is

$$K_2 \left( (1 - M_\infty^2) \frac{\partial^2 \phi_{\text{inc}}}{\partial x_{\text{inc}}^2} + K_1^2 \frac{\partial^2 \phi_{\text{inc}}}{\partial z_{\text{inc}}^2} \right) = 0$$

This is identical to the incompressible potential Eq. (6.2) if

$$K_1 = \sqrt{1 - M_\infty^2} \quad (6.4)$$

Now,  $K_2$  is to be determined from the boundary conditions. For slender bodies, by small perturbation theory (see Section 5.6), we have

$$\frac{w}{V_\infty + u} \approx \frac{w}{V_\infty} = \frac{dz}{dx} \quad (6.5)$$

since  $u/V_\infty \ll 1$ . Equation (6.5) can be expressed in terms of the potential function as

$$w = \left( \frac{\partial \phi}{\partial z} \right)_{z=0} = V_\infty \frac{dz}{dx} \quad (6.6a)$$

$$w_{\text{inc}} = \left( \frac{\partial \phi_{\text{inc}}}{\partial z_{\text{inc}}} \right)_{z_{\text{inc}}=0} = V_\infty \frac{dz_{\text{inc}}}{dx_{\text{inc}}} \quad (6.6b)$$

Also, by Eq. (6.3),

$$\left( \frac{\partial \phi}{\partial z} \right)_{z=0} = K_1 K_2 \left( \frac{\partial \phi_{\text{inc}}}{\partial z_{\text{inc}}} \right)_{z_{\text{inc}}=0}$$

With this relation, and Eqs. (6.6), we get

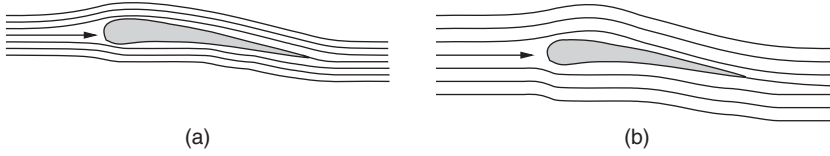
$$\frac{dz}{dx} = K_1 K_2 \left( \frac{dz_{\text{inc}}}{dx_{\text{inc}}} \right) \quad (6.7a)$$

$$\frac{dz}{dx} = K_2 \sqrt{1 - M_\infty^2} \left( \frac{dz_{\text{inc}}}{dx_{\text{inc}}} \right) \quad (6.7b)$$

From Eq. (6.7b), it can be seen that  $K_2$  can be determined from the boundary conditions.

Equation (6.7b) simply means that the slope of the profile in the compressible flow pattern is  $(K_2 \sqrt{1 - M_\infty^2})$  times the slope of the corresponding profile in the related incompressible flow pattern.

For further treatment of similarity rules, let us consider the three specific versions of the problems, namely the direct problem (version I), in which the body profile is treated as invariant; the indirect problem (version II), which is the case of equal potentials (the pressure distribution around the body in incompressible flow and compressible flow are taken as the same); and the streamline analogy (version III), which is also called *Gothert's rule*.



**Figure 6.1** Flow over an airfoil in (a) incompressible flow and (b) compressible flow.

### 6.2.2 The Direct Problem (Version I)

Consider an invariant profile. In this case, there is no transformation of geometry at all. For the profile to be invariant, from Eq. (6.7b), we have the condition

$$K_2 = \frac{1}{\sqrt{1 - M_\infty^2}} \quad (6.8)$$

Therefore, Eq. (6.7b) reduces to

$$\frac{dz}{dx} = \frac{dz_{\text{inc}}}{dx_{\text{inc}}} \quad (6.9)$$

Equation (6.9) contradicts the original transformation Eq. (6.3). However, the error involved in this contradiction is not large, since the Prandtl–Glauert (P–G) transformation is valid only for small perturbations.

By Eq. (6.3), we have

$$Z = \frac{Z_{\text{inc}}}{\sqrt{1 - M_\infty^2}} \quad (6.10)$$

Equation (6.3) is valid only for streamlines away from the body. Since the P–G transformation is based on small perturbation theory, the error increases with increasing thickness of the body. In addition to this, some error is introduced by the above contradiction – see Eq. (6.9).

Equation (6.10) shows that the streamlines around a body in a compressible flow are more separated than those around a body in incompressible flow by an amount given by  $1/\sqrt{1 - M_\infty^2}$ . In other words, by the existence of a body in the flow field, the streamlines are more displaced in a compressible flow than in an incompressible flow, as shown in Figure 6.1, that is the disturbances introduced by an object are larger in compressible flow than in incompressible flow and they increase with the rise in Mach number. This is so because in compressible flow there is a density decrease as the flow passes over the body, owing to acceleration, whereas in incompressible flow there is no change in density at all. That is to say, across the body there is a drop in density, and hence by streamtube area–velocity relation (Section 2.4), the streamtube area increases as the density decreases. At  $M_\infty = 1$ , this disturbance becomes infinitely large and this treatment is no longer valid.

The potential function for compressible flow given by Eq. (6.3) is

$$\phi = \frac{\phi_{\text{inc}}}{\sqrt{1 - M_\infty^2}} \quad (6.11a)$$

By Eqs. (5.20) and (5.48b), we have the velocity  $u$  and the pressure coefficient  $C_p$  as

$$u = \frac{\partial \phi}{\partial x}, \quad C_p = -2 \frac{u}{V_\infty}$$

Using Eq. (6.11a), the perturbation velocity and the pressure coefficient may be expressed as follows.

$$\frac{\partial \phi}{\partial x} = \frac{1}{\sqrt{1 - M_\infty^2}} \frac{\partial \phi_{\text{inc}}}{\partial x_{\text{inc}}}$$

Therefore,

$$\begin{aligned} u &= \frac{u_{\text{inc}}}{\sqrt{1 - M_\infty^2}} \\ C_p &= \frac{C_{p_{\text{inc}}}}{\sqrt{1 - M_\infty^2}} \end{aligned} \quad (6.11b)$$

Since the lift coefficient  $C_L$  and pitching moment coefficient  $C_M$  are integrals of  $C_p$ , they can be expressed following Eq. (6.11b) as

$$C_L = \frac{C_{L_{\text{inc}}}}{\sqrt{1 - M_\infty^2}} \quad (6.11c)$$

$$\frac{dC_L}{d\alpha} = \frac{(dC_L/d\alpha)_{\text{inc}}}{\sqrt{1 - M_\infty^2}} \quad (6.11d)$$

For a flat plate in compressible flow,

$$\frac{dC_L}{d\alpha} = \frac{2\pi}{\sqrt{1 - M_\infty^2}} \quad (6.11e)$$

$$C_M = \frac{C_{M_{\text{inc}}}}{\sqrt{1 - M_\infty^2}} \quad (6.11f)$$

Similarly, we can express the circulation in compressible flow in terms of circulation in incompressible flow as

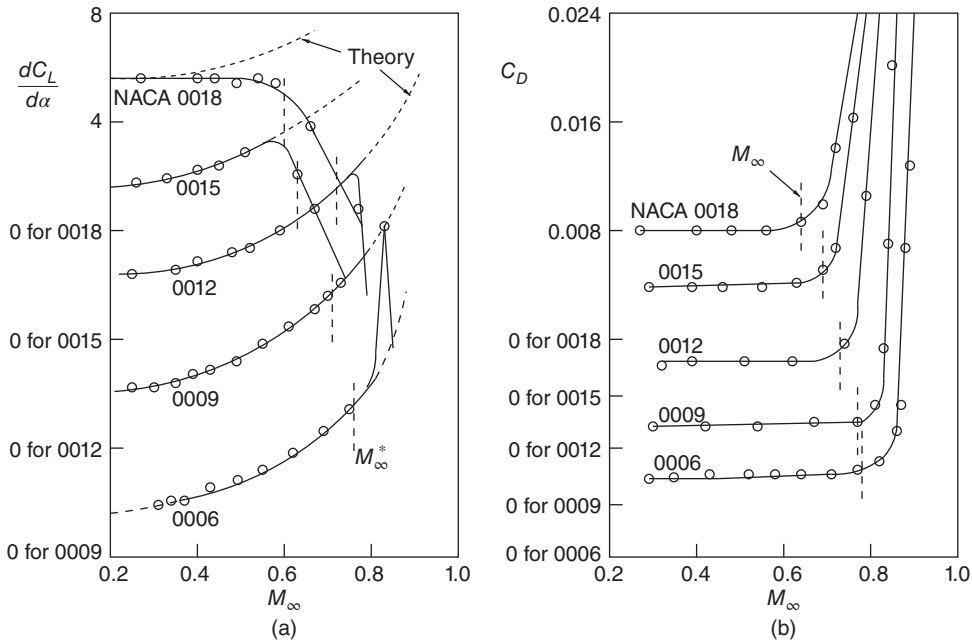
$$\Gamma = \frac{\Gamma_{\text{inc}}}{\sqrt{1 - M_\infty^2}} \quad (6.11g)$$

From the discussion on version I of the P–G transformation, the following two statements can be made.

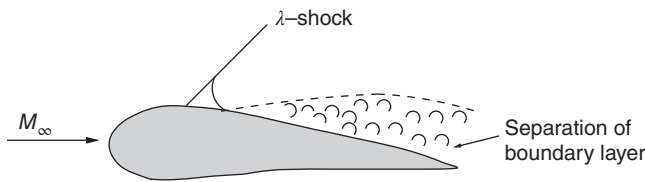
- Streamlines for compressible flow are farther apart from each other by  $1/\sqrt{1 - M_\infty^2}$  than in incompressible flow.
- The ratio between aerodynamic coefficients in compressible and incompressible flows is also  $1/\sqrt{1 - M_\infty^2}$ .

From Eqs. (6.11c) and (6.11f), we infer that the locations of the aerodynamic center and the center of pressure do not change with the freestream Mach number  $M_\infty$ , as they are ratios between  $C_M$  and  $C_L$ .

The theoretical lift-curve slope and drag coefficient from the P–G rule and the measured  $C_L$  and  $C_D$  versus Mach number for symmetrical NACA profiles of different thickness are shown in Figure 6.2. From this figure it can be seen that the thinner the airfoil the better is the accuracy of the P–G rule. For 6% airfoil there is good agreement up to  $M_\infty = 0.8$ ; for 12% airfoil, the agreement is also good up to  $M_\infty = 0.8$ ; thus 12% may be taken as the limit of applicability of the P–G rule. For 15% airfoil, there is good agreement up to  $M_\infty = 0.6$ . But above Mach 0.6, there is no more agreement. However, for supersonic aircraft the profiles used are very thin; so, from



**Figure 6.2** Variation of (a) lift-curve slope and (b) drag coefficient with Mach number ( $\circ$  measured).



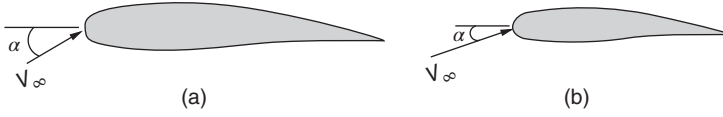
**Figure 6.3** Flow separation caused by  $\lambda$ -shock.

a practical point of view, the P–G rule is very good even with the contradicting assumptions involved.

Beyond a certain Mach number, there is decrease in lift. This can be explained by Figure 6.2b. There is a sudden increase in drag when the local speed increases beyond sonic speed. This is because, at the sonic point on the profile, there is a  $\lambda$ -shock which gives rise to a separation of the boundary layer, as shown in Figure 6.3. The freestream Mach number which gives sonic velocity somewhere on the boundary is called the *critical Mach number*  $M_\infty^*$ . The critical Mach number decreases with increasing thickness ratio of profile. The P–G rule is valid only up to about  $M_\infty^*$ .

### 6.2.3 The Indirect Problem (Case of Equal Potentials): P–G Transformation (Version II)

In the indirect problem, the requirement is to find a transformation, for the profile, by which we can obtain a body in incompressible flow with exactly the same pressure distribution as in the compressible flow.



**Figure 6.4** Airfoils in (a) incompressible and (b) compressible flow.

For two-dimensional or planar bodies, the pressure coefficient  $C_p$  is given by Eq. (5.48b) as

$$C_p = -2 \frac{u}{V_\infty}$$

and the perturbation velocity component,  $u$ , is

$$u = \frac{\partial \phi}{\partial x}$$

But in this case,  $C_p = C_{p_{inc}}$ ; therefore, from the above expressions for  $C_p$  and  $u$ , we have

$$C_p = C_{p_{inc}}, \quad u = u_{inc}, \quad \phi = \phi_{inc}$$

For this situation, the transformation Eq. (6.3) gives

$$K_2 = 1 \quad (6.12)$$

From Eq. (6.7b) with  $K_2 = 1$ , we get

$$\frac{dz}{dx} = \sqrt{1 - M_\infty^2} \frac{dz_{inc}}{dx_{inc}} \quad (6.13)$$

Equation (6.13) is the relation between the geometries of the actual profile in compressible flow and the transformed profile in the incompressible flow, resulting in the same pressure distribution around them.

From Eq. (6.13), we see that, in a compressible flow, the body must be thinner by the factor  $\sqrt{1 - M_\infty^2}$  than the body in incompressible flow, as shown in Figure 6.4. Also, the angle of attack in compressible flow must be smaller by the same factor than in incompressible flow.

From the above relation for  $C_p$ , we have

$$\frac{C_p}{C_{p_{inc}}} = \frac{C_L}{C_{L_{inc}}} = \frac{C_M}{C_{M_{inc}}} = 1 \quad (6.14)$$

That is, the lift coefficient and pitching moment coefficient are also the same in both the incompressible and compressible flows. But, because of decreased  $\alpha$  in compressible flow,

$$\frac{dC_L}{d\alpha} = \frac{1}{\sqrt{1 - M_\infty^2}} \left( \frac{dC_L}{d\alpha} \right)_{inc}$$

This is because the disturbances introduced in a compressible flow are larger than those in an incompressible flow and, therefore, we must reduce  $\alpha$  and the geometry by that amount (the difference in the magnitude of disturbance in a compressible and an incompressible flow). In other words, because of Eq. (6.3) ( $z = K_1 z_{inc}$ ), every dimension in the  $z$ -direction must be reduced and so the angle of attack  $\alpha$  should also be transformed.

## 6.2.4 Streamline Analogy (Version III): Gothert's Rule

Gothert's rule states that the slope of a profile in a compressible flow pattern is larger by the factor  $1/\sqrt{1 - M_\infty^2}$  than the slope of the corresponding profile in the related incompressible

flow pattern [7]. But if the slope of the profile at each point is greater by the factor  $1/\sqrt{1-M_\infty^2}$ , it is also true that the camber ( $f$ ) ratio, angle of attack ( $\alpha$ ) ratio, and the thickness ( $t$ ) ratio must all be greater for the compressible airfoil by the factor  $1/\sqrt{1-M_\infty^2}$ .

Thus, by Gothert's rule we have

$$\frac{\alpha_{\text{inc}}}{\alpha} = \frac{f_{\text{inc}}}{f} = \frac{t_{\text{inc}}}{t} = \sqrt{1-M_\infty^2}$$

Compute the aerodynamic coefficients for this transformed body for incompressible flow. The aerodynamic coefficients of the given body at the given compressible flow Mach number are given by

$$\frac{C_p}{C_{p_{\text{inc}}}} = \frac{C_L}{C_{L_{\text{inc}}}} = \frac{C_M}{C_{M_{\text{inc}}}} = \frac{1}{1-M_\infty^2} \quad (6.15)$$

The application of Gothert's rule is much more complicated than the application of version I of the P-G rule. This is because, for finding the behavior of a body with respect to  $M_\infty$ , we have to calculate for each  $M_\infty$  at a time, whereas by the P-G rule (version I) the complete variation is obtained in one go. However, only Gothert's rule is exact with the framework of linearized theory and the P-G rule is only approximate because of the contradicting assumptions involved.

Now, we can see some aspects of the practical significance of these results. A fairly good amount of theoretical and experimental information on the properties of classes of affinely related profiles in incompressible flow – with variations in camber, thickness ratio, and angle of attack – is available. If it is necessary to find the  $C_L$  of one of these profiles at a finite Mach number  $M_\infty$ , either theoretically or experimentally, we first find the lift coefficient in incompressible flow of an affinely related profile. The camber, thickness, and angle of attack are smaller than the corresponding values for the original profile by the factor  $\sqrt{1-M_\infty^2}$ . Then, by multiplying this  $C_L$  for incompressible flow profile by  $1/(1-M_\infty^2)$ , we find the desired lift coefficient for the compressible flow.

This method of collecting data for incompressible flow is cumbersome, since data for a large number of thickness ratios are required. It would be more convenient in many respects to know how the Mach number affects the performance of the profile of a fixed shape. The direct problem, discussed in Section 6.2.2, yields information of this type.

### 6.3 Prandtl–Glauert Rule for Supersonic Flow: Versions I and II

In Section 6.2, we have seen the similarity rules for subsonic flows. Now let us examine the similarity rules for supersonic flows. We can visualize from our previous discussions on similarity rules for subsonic compressible flows that the factor  $K_1$  in the transformation Eq. (6.3) should have the following relations depending on the flow regime.

$$K_1 = \sqrt{1-M_\infty^2} \quad \text{for subsonic flow}$$

$$K_1 = \sqrt{M_\infty^2 - 1} \quad \text{for supersonic flow}$$

Therefore, in general, we can write

$$K_1 = \sqrt{|1-M_\infty^2|} \quad (6.16)$$

However, there is one important difference between the treatment of supersonic flow and subsonic flow: we cannot find any incompressible flow in the supersonic flow regime.

### 6.3.1 Subsonic Flow

We know that for subsonic flow the transformation relations are given by Eq. (6.3) as

$$x_{\text{inc}} = x, \quad z_{\text{inc}} = K_1 z, \quad \phi = K_2 \phi_{\text{inc}}$$

The transformed equation is

$$K_2[(1 - M_\infty^2)(\phi_{xx})_{\text{inc}} + K_1^2(\phi_{zz})_{\text{inc}}] = 0$$

and the condition to be satisfied by this equation in order to be identical to Eq. (6.2) is

$$K_1 = \sqrt{1 - M_\infty^2}$$

For this case the above transformed equation becomes the Laplace equation.

### 6.3.2 Supersonic Flow

The transformation relations for supersonic flow are

$$x' = x, \quad z' = K_1 z, \quad \phi = K_2 \phi'$$

where the variables with a prime are the transformed variables. The aim in writing these transformations is to make the Mach number  $M_\infty$  in the governing Eq. (6.1) vanish.

With the above transformation relations, the governing equation becomes

$$K_2[(1 - M_\infty^2)\phi'_{xx} + K_1^2\phi'_{zz}] = 0$$

For supersonic flow,  $M_\infty > 1$ , therefore the above equation becomes

$$K_2[(M_\infty^2 - 1)\phi'_{xx} - K_1^2\phi'_{zz}] = 0$$

By inspection of this equation, we can see that the Mach number  $M_\infty$  can be eliminated from the above equation with

$$K_1 = \sqrt{M_\infty^2 - 1}$$

The equation becomes

$$\phi'_{xx} - \phi'_{zz} = 0 \tag{6.17a}$$

Now we must find out to which supersonic Mach number this flow belongs.

The original form of the governing differential equation for this kind of flow, given by Eq. (6.1), is

$$(M_\infty^2 - 1)\phi_{xx} - \phi_{zz} = 0 \tag{6.17b}$$

For Eqs. (6.17a) and (6.17b) to be identical, it is necessary that

$$M_\infty = \sqrt{2}$$

By following the arguments of the P–G rule for subsonic compressible flow, we can show the following results for versions I and II of the Prandtl–Glauert rule for supersonic flow.

#### 6.3.2.1 Analogy Version I

For this case of invariant profile in supersonic flow,

$$K_2 = \frac{1}{\sqrt{M_\infty^2 - 1}}$$



Compute the flow around the given body at  $M_\infty = \sqrt{2}$ . For any other supersonic Mach number, the aerodynamics coefficients are given by

$$\frac{C_p}{C'_p} = \frac{C_L}{C'_L} = \frac{C_M}{C'_M} = \frac{1}{\sqrt{M_\infty^2 - 1}} \quad (6.18a)$$

where  $C_p$ ,  $C_L$ , and  $C_M$  are at  $M_\infty = \sqrt{2}$  and  $C'_p$ ,  $C'_L$ , and  $C'_M$  are at any other supersonic Mach number.

### 6.3.2.2 Analogy Version II

Here the requirement is to find a transformation for the profile, by which we can obtain a body, for which the governing equation is Eq. (6.17a) with exactly the same pressure distribution as the actual body for which the governing equation is Eq. (6.17b). For this

$$K_2 = 1$$

The derivation of the above two results is left to the reader as an exercise. From the above results, we see that in supersonic flow  $M_\infty = \sqrt{2}$  plays the same role as  $M_\infty = 0$  in subsonic flow.

For version II, we can write

$$\frac{C_p}{C'_p} = \frac{C_L}{C'_L} = \frac{C_M}{C'_M} = 1 \quad (6.18b)$$

### 6.3.2.3 Analogy Version III: Gothert's Rule

For any given body, at given Mach number  $M_\infty$ , find the transformed shape by using the rule

$$\frac{\alpha'}{\alpha} = \frac{f'}{f} = \frac{t'}{t} = \sqrt{M_\infty^2 - 1} \quad (6.19)$$

where  $\alpha$  is the angle of attack, and  $f$  and  $t$  are the camber and thickness of the given body, respectively. The primed quantities are for the transformed body and the unprimed ones are for the actual body.

Compute the aerodynamic coefficients of the transformed body for  $M_\infty = \sqrt{2}$ . The aerodynamic coefficients of the given body at the given Mach number  $M_\infty$  follow from

$$\frac{C_p}{C'_p} = \frac{C_L}{C'_L} = \frac{C_M}{C'_M} = \frac{1}{M_\infty^2 - 1} \quad (6.20)$$

We can state the Gothert rule for subsonic and supersonic flows by using a modulus:  $|1 - M_\infty^2|$ .

From the discussion on similarity rules for compressible subsonic and supersonic flows it is clear that, in subsonic flow, there is a ready-made linearized solution for  $M_\infty = 0$ . Hence, for such cases we can use the P-G rule. But for supersonic flow the linear theory equations are very simple and, therefore, we can conveniently use the Gothert rule.

### Example 6.1

A given profile has, at  $M_\infty = 0.29$ , the following lift coefficients:

$$C_L = 0.2 \text{ at } \alpha = 3^\circ$$

$$C_L = -0.1 \text{ at } \alpha = -2^\circ$$

where  $\alpha$  is the angle of attack. Plot the relation showing  $dC_L/d\alpha$  vs  $M_\infty$  for the profile for values of  $M_\infty$  up to 1.0.

**Solution:**

At  $M_\infty = 0.29$ ,

$$\begin{aligned}\frac{dC_L}{d\alpha} &= \frac{0.2 + 0.1}{3 + 2} = 0.06/\text{degree} \\ &= 3.438/\text{radian} \\ &= 1.094\pi/\text{radian}\end{aligned}$$

By the P–G rule,

$$\left(\frac{dC_L}{d\alpha}\right)_{M=M_\infty} = \frac{\left(\frac{dC_L}{d\alpha}\right)_{\text{inc}}}{\sqrt{1 - M_\infty^2}}$$

Therefore,

$$\left(\frac{dC_L}{d\alpha}\right)_{\text{inc}} = 1.047\pi/\text{radian}$$

For any other subsonic Mach number, by the P–G rule,

$$\frac{dC_L}{d\alpha} = \frac{\left(\frac{dC_L}{d\alpha}\right)_{\text{inc}}}{\sqrt{1 - M_\infty^2}} = \frac{1.047\pi}{\sqrt{1 - M_\infty^2}}$$

Therefore, we have the following variation:

$M$	0.1	0.2	0.3	0.4	0.5	0.6	0.7	0.8	0.9	1.0
$\frac{dC_L}{d\alpha}$	$1.05\pi$	$1.07\pi$	$1.10\pi$	$1.14\pi$	$1.21\pi$	$1.31\pi$	$1.46\pi$	$1.74\pi$	$2.40\pi$	$\infty$

## 6.4 The von Karman Rule for Transonic Flow

The potential Eq. (5.24), for the present case of two-dimensional transonic flow, reduces to

$$(1 - M_\infty^2)\phi_{xx} + \phi_{zz} = \frac{2}{V_\infty} \left(1 + \frac{\gamma - 1}{2} M_\infty^2\right) M_\infty^2 \phi_x \phi_{xx} \quad (6.21a)$$

Equation (6.21a) results in a form due to Spreiter (see also [10]) for  $M_\infty \approx 1$ , as

$$C_p = \frac{\left(\frac{t}{c}\right)^{2/3}}{[(\gamma + 1)M_\infty^2]^{1/3}} \tilde{C}_p(\chi) \quad (6.21b)$$

where

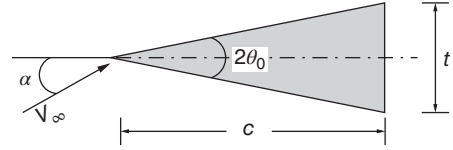
$$\chi = \frac{1 - M_\infty^2}{\left[\left(\frac{t}{c}\right)(\gamma + 1)M_\infty^2\right]^{2/3}} \quad (6.21c)$$

and  $\tilde{C}_p$  is the similarity pressure coefficient. It follows from Eq. (6.21b) that the lift and drag coefficients are given by

$$C_L = \frac{\left(\frac{t}{c}\right)^{2/3}}{[(\gamma + 1)M_\infty^2]^{1/3}} \tilde{C}_L(\chi) \quad (6.21d)$$

$$C_D = \frac{\left(\frac{t}{c}\right)^{5/3}}{[(\gamma + 1)M_\infty^2]^{1/3}} \tilde{C}_D(\chi) \quad (6.21e)$$

**Figure 6.5** Wedge at an angle of attack.



Equations (6.21b), (6.21d), and (6.21e) are valid for local as well as for total values. Sometimes, instead of thickness ratio  $t/c$ , fineness ratio, defined in Figure 6.5, is used.

For the wedge shown in Figure 6.5,

$$\frac{1}{2} \frac{t}{c} = \tan \theta_0, \quad \frac{t}{c} = 2 \tan \theta_0$$

The ratio  $t/c$  is called the *fineness ratio* (at angle of attack = 0).

$$\tan(\theta_0 \pm \alpha) = \tan \left( \frac{1}{2} \frac{t}{c} \left( 1 \pm \frac{2\alpha}{t/c} \right) \right) \quad (6.22)$$

where the plus sign is for the upper surface and the minus sign is for the lower surface. For finding the local values of  $C_p$ ,  $C_L$ , and  $C_D$ , we must use the fineness ratio defined by these equations.

#### 6.4.1 Use of the von Karman Rule

If we know the solution for one profile, we can find solutions for other affinely related profiles. For example, the NACA profiles designated by 8405, 8410, and 8415 all have the same distribution, same nose radius, and so on; only the absolute magnitude of  $t/c$  is different. This rule can be extended to transonic flow range also. From Figure 6.6, it can be seen that in the transonic range the aerodynamic coefficients change very quickly with Mach number, so that the proper values to be considered are not  $M_\infty$ ,  $C_L$ ,  $C_D$ , and  $C_p$ ; instead they are  $\chi$ ,  $\tilde{C}_L$ ,  $\tilde{C}_D$ , and  $\tilde{C}_p$ .

From the discussion so far, we can make the following remarks.

- For subsonic and supersonic flows, the governing equation  $(1 - M_\infty^2) \phi_{xx} + \phi_{zz} = 0$  is independent of  $\gamma$ , so that the results from similarity rules can be applied to any gas; but for transonic flow, the potential equations are not independent of  $\gamma$ . Therefore, the results have to be properly applied to different gases, with suitable correction for  $\gamma$ , for example a probe used for air in transonic range can be calibrated for steam.
- For transonic flow,

$$C_p \sim C_L \sim \left( \frac{t}{c} \right)^{2/3}$$

- For subsonic flow,

$$C_p \sim C_L \sim \left( \frac{t}{c} \right)$$

- For supersonic flow,

$$C_p \sim C_L \sim \left( \frac{t}{c} \right)$$

Transonic flow is characterized by the occurrence of shock and boundary layer separation. This explains the steep increase in  $C_D$  at transonic range. We should also recall that the shock should be sufficiently weak for small perturbation. This theory cannot be applied, say, to the circular cylinder because the perturbations are not small.

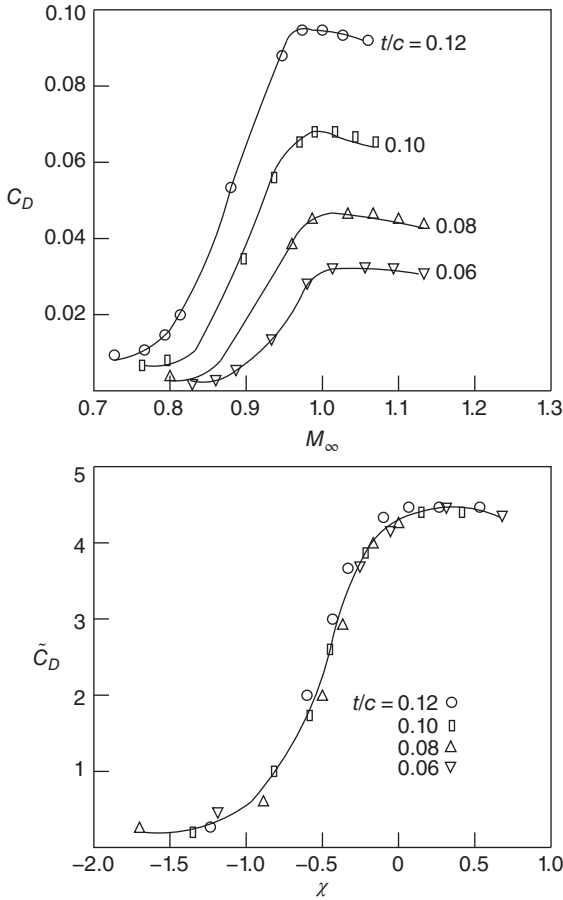


Figure 6.6 The transonic similarity rule.

## 6.5 Hypersonic Similarity

The linear theory is not valid at high supersonic Mach numbers, since

$$\frac{u}{V_\infty} \ll 1 \text{ is true only for supersonic flow, and}$$

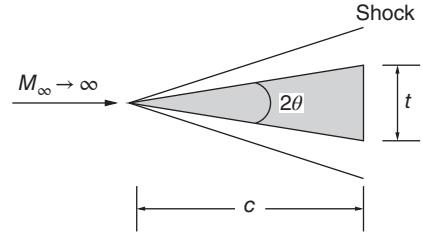
$$\frac{u}{V_\infty} \approx 1 \text{ for hypersonic flow.}$$

Even slender bodies produce large disturbances in hypersonic flow. The original nonlinear equations have to be used for such flows. So, mathematically, hypersonic flow is similar to transonic flow. In supersonic flow, slender bodies produce weak shocks and so these can be considered as Mach lines. But in hypersonic flow even slender bodies produce strong shocks and, therefore, in hypersonic flow we can no longer deal with Mach lines and must deal with the actual shock waves. At high Mach numbers the Mach angle  $\mu$  may be of the same order or less than the maximum deflection angle  $\theta$  of the body.

From these considerations, the similarity rule can be obtained for hypersonic flow. The Mach angle  $\mu$  is given by the relation

$$\sin \mu = \frac{1}{M_\infty}$$

**Figure 6.7** Slender body in hypersonic flow.



For the present case of flow shown in Figure 6.7,

$$\sin \mu \approx \mu = \frac{1}{M_\infty} \leq \theta$$

where  $\theta$  is the half angle of the wedge in the figure, that is for hypersonic flow,

$$M_\infty \theta \geq 1 \quad (6.23)$$

But in hypersonic flows, even for small disturbances, there are shock lines, and the angle of shock is always less than the angle of the Mach line. Therefore, in reality, the inequality in Eq. (6.23), obtained with the approximation that Mach angle  $\mu$  is of the same order or less than the flow turning angle  $\theta$ , has to be modified since the shock angle is always less than  $\mu$ . In other words, it can be stated that  $M_\infty \theta$  is greater than some quantity  $K$ , whose numerical value can be less than unity also.

It is a common practice to express

$$K = M_\infty \theta \geq 0.5 \quad (6.24)$$

$$\boxed{K = M\theta} \quad (6.25)$$

where  $K$  is called the *hypersonic similarity parameter*.

### Example 6.2

For  $\theta = 10^\circ$  ( $\approx 0.174$  radian),  $M_\infty = 4$ , the hypersonic similarity parameter  $K = M_\infty \theta = 0.7$ . For  $\theta = 20^\circ$  and  $M_\infty = 2$ ,

$$K = M_\infty \theta \approx 0.7$$

That is, for a wedge with half-angle  $20^\circ$ ,  $M_\infty = 2$  should be considered as hypersonic. This implies that  $M \geq 5$  for hypersonic flow is only a crude limit. For  $\theta = 5^\circ$  and  $M_\infty = 8$ ,

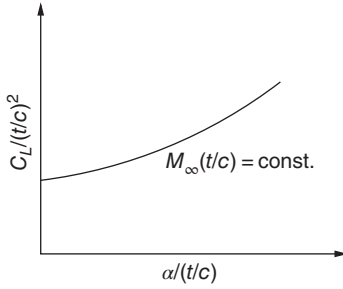
$$K = M_\infty \theta \approx 0.7$$

Thus, a wedge with half-angle  $5^\circ$  in a flow with  $M_\infty = 8$  produces shocks as strong as a wedge with half-angle  $20^\circ$  in a flow with  $M_\infty = 2$ .

Also, by Eq. (6.22),

$$\theta = \theta_0 \pm \alpha = \frac{1}{2} \frac{t}{c} \left( 1 \pm \frac{2\alpha}{t/c} \right) \quad (6.26)$$

Whenever  $M_\infty \theta$  is the same for a number of bodies, the flow about them will be dynamically similar, that is to investigate the hypersonic flow about a wedge with half-angle  $5^\circ$  and  $M_\infty = 8$ , we can use a supersonic tunnel with  $M_\infty = 2$  and  $\theta = 20^\circ$ . This is of paramount importance in testing; of course, the two bodies should be affinely related (geometrically similar). Consider

Figure 6.8 Variation of  $C_L/(t/c)^2$  with  $\alpha/(t/c)$ .

two models, 1 and 2:

$$\frac{K_1}{K_2} = \frac{M_{\infty 1} \left( \frac{t}{c} \right)_1 \left( 1 \pm 2 \frac{\alpha}{(t/c)_1} \right)}{M_{\infty 2} \left( \frac{t}{c} \right)_2 \left( 1 \pm 2 \frac{\alpha}{(t/c)_2} \right)}$$

$$\frac{K_1}{K_2} = 1 \text{ for dynamic similarity}$$

This condition for dynamic similarity will be satisfied only when

$$M_{\infty 1} \left( \frac{t}{c} \right)_1 = M_{\infty 2} \left( \frac{t}{c} \right)_2$$

$$\left( \frac{\alpha}{(t/c)_1} \right) = \left( \frac{\alpha}{(t/c)_2} \right)$$

That is, these two conditions should be satisfied for dynamic similarity, when there is geometric similarity

$$C_p \approx C_L = \left( \frac{t}{c} \right)^2 F_1 \left( \frac{x}{c}, M_{\infty} \left( \frac{t}{c} \right), \frac{\alpha}{t/c} \right) \quad (6.27)$$

The total lift and drag coefficients are given by

$$C_L = \left( \frac{t}{c} \right)^2 F_2 \left( M_{\infty} \left( \frac{t}{c} \right), \frac{\alpha}{t/c} \right) \quad (6.28)$$

$$C_D = \left( \frac{t}{c} \right)^3 F_3 \left( M_{\infty} \left( \frac{t}{c} \right), \frac{\alpha}{t/c} \right) \quad (6.29)$$

Equations (6.27)–(6.29) give the functional dependence of various aerodynamic coefficients for hypersonic flow.

A plot like the one shown in Figure 6.8 gives the correct representation of the different parameters. This similarity rule is valid for axially symmetric bodies like rockets and missiles also.

The transonic and hypersonic similarity rules discussed here are just a few glimpses, highlighting some of the vital features associated with them. Those who are looking for a deeper understanding of these problems should consult standard books on these topics.

## 6.6 Three-Dimensional Flow: Gothert's Rule

### 6.6.1 General Similarity Rule

The P–G rule is approximate because it satisfies the boundary conditions only on the axis and not on the contour. But the Gothert rule is exact and valid for both two-dimensional and

three-dimensional bodies. The potential equation is (for  $M_\infty < \text{or} > 1$ )

$$(1 - M_\infty^2)\phi_{xx} + \phi_{yy} + \phi_{zz} = 0 \quad (6.30)$$

For  $M_\infty < 1$ , the equation is elliptic in nature, and for  $M_\infty > 1$ , it is hyperbolic. Here also we make a transformation by which the transformed equation does not contain  $M_\infty$  explicitly any more. Let

$$x' = x, \quad y' = K_1 y, \quad z' = K_1 z, \quad \phi' = K_2 \phi$$

With the above new variables, Eq. (6.30) transforms into

$$(1 - M_\infty^2)\phi'_{x'x'} + K_1^2(\phi'_{y'y'} + \phi'_{z'z'}) = 0$$

$M_\infty$  vanishes from the above equation for

$$K_1 = \sqrt{|1 - M_\infty^2|} \quad (6.31)$$

With Eq. (6.31), the resulting potential flow equation for subsonic flow is

$$\phi'_{x'x'} + \phi'_{y'y'} + \phi'_{z'z'} = 0$$

and for supersonic flow,

$$\phi'_{x'x'} - \phi'_{y'y'} - \phi'_{z'z'} = 0$$

Again, for subsonic flow, the equation is exactly the same as the Laplace equation. For supersonic flow, the equation is identical with the compressible flow equation (Eq. (6.30)) with  $M_\infty = \sqrt{2}$ .

Now,

$$u' = \frac{\partial \phi'}{\partial x} = K_2 \frac{\partial \phi}{\partial x} = K_2 u \quad (6.32a)$$

$$v' = \frac{\partial \phi'}{\partial y} = \frac{K_2}{K_1} \frac{\partial \phi}{\partial y} = \frac{K_2}{K_1} v \quad (6.32b)$$

$$w' = \frac{\partial \phi'}{\partial z'} = \frac{K_2}{K_1} \frac{\partial \phi}{\partial z} = \frac{K_2}{K_1} w \quad (6.32c)$$

$$C_p = \frac{p - p_\infty}{\frac{1}{2} \rho V_\infty^2} = -2 \frac{u}{V_\infty} = -\frac{2}{V_\infty} \frac{\partial \phi}{\partial x} \quad (6.33)$$

and

$$C'_p = -2 \frac{u'}{V_\infty} \quad (6.34)$$

with the assumption that  $V_\infty = V'_\infty$ . This assumption really does not impose any restriction on the rule, because in supersonic flow the velocity itself is not important (that is  $V/a$  is more relevant than  $V$ ). The introduction of Eq. (6.32a) into Eq. (6.34) results in

$$C'_p = -2K_2 \frac{u}{V_\infty}$$

that is

$$C'_p = K_2 C_p \quad (6.35)$$

The kinematic flow condition, Eq. (6.6), states that

$$\frac{w}{V_\infty} = \frac{\partial z}{\partial x}$$

$$w = V_{\infty} \frac{\partial z}{\partial x} \quad (6.36a)$$

$$w' = V_{\infty} \frac{\partial z'}{\partial x'} \quad (6.36b)$$

Combining Eqs. (6.36a) and (6.36b), we get

$$w' = \frac{\partial x}{\partial z} \frac{\partial z'}{\partial x'} w = K_1 w$$

since  $x' = x$  and  $z'/z = K_1$ . But  $w' = (K_2/K_1)w$  by Eq. (6.32c); therefore,

$$K_1 = \frac{K_2}{K_1}$$

that is

$$K_2 = K_1^2$$

$$K_2 = |1 - M_{\infty}^2| \quad (6.37)$$

Therefore,

$$C_p = \frac{C'_p}{|1 - M_{\infty}^2|} \quad (6.38)$$

Equation (6.38) is valid (exactly) at any point on the boundary of the body, as well as in the flow field. Therefore,

$$\boxed{\frac{C_p}{C'_p} = \frac{C_L}{C'_L} = \frac{C_M}{C'_M} = \frac{1}{|1 - M_{\infty}^2|}} \quad (6.39)$$

Equation (6.39) is an important equation, relating the aerodynamic coefficients for the actual and transformed bodies.

### 6.6.2 Gothert's Rule

The aerodynamic coefficients of a body in three-dimensional compressible flow are obtained as follows.

The geometry of the given body is transformed in such a way that its lateral and normal dimensions (both in  $y$ - and  $z$ -directions) are multiplied by  $\sqrt{|1 - M_{\infty}^2|}$ . If the flow is subsonic, compute the compressible flow about the transformed body; if the flow is supersonic, compute the field with  $M_{\infty} = \sqrt{2}$  about the transformed body. The aerodynamic coefficients of the given body in a given flow follow from transformed flow with Eq. (6.39).

The Gothert rule can be applied to two-dimensional flows also (stated as version III of the P–G rule).

It is exact in the framework of linear theory, whereas the P–G rule is only approximate. For thicker bodies, when there is doubt about the accuracy with P–G rule, Gothert's rule should be used even though it is tedious.

The coefficient of pressure is

$$C_p = -2 \frac{u}{V_{\infty}}$$



The error involved in the pressure coefficients ratio is

$$\frac{C_p}{C'_p} = O\left(\left(\frac{u}{V_\infty}\right)^2\right)$$

That is why the P–G rule, though approximate, can be used quite satisfactorily up to  $t/c = 15\%$  (because the error is less). The Gothert rule is still superior and is applicable not only to flow past bodies but also to flow through ducts where the diameter is small.

### 6.6.3 Application to Wings of Finite Span

Consider a wing planform transformation described as follows.

#### 6.6.3.1 Planform

Taper ratio:  $\lambda' = \lambda$

$$\text{Aspect ratio: } A' = A\sqrt{|1 - M_\infty^2|} \quad (6.40)$$

$$\text{Sweep angle: } \cot \phi' = \cot \phi \sqrt{|1 - M_\infty^2|}$$

$$A' \tan \phi' = A \tan \phi \quad (6.41)$$

For subsonic flow, the transformation decreases  $A$ , and for supersonic flow, the transformation increases  $A$ . Note that  $\phi$  is the sweep angle here.

#### 6.6.3.2 Profile

The profile is given by the relations

$$\frac{\alpha'}{\alpha} = \frac{f'}{f} = \frac{t'}{t} = \sqrt{|1 - M_\infty^2|} \quad (6.42)$$

Thus, for wings (three-dimensional bodies), the Gothert rule is even more complicated: we have to transform not only the profile but also the planform for each  $M_\infty$ . But this is the only reasonable method for wing analysis. In subsonic flow, these similarity rules are of great importance, but in supersonic flow they are not so important because even in two-dimensional subsonic flow the elliptical equation is very difficult to solve, but in supersonic flow the hyperbolic equation can be easily solved.

After making the transformations with Eqs. (6.40) and (6.42), find  $C_L$ ,  $C_M$ , and so on, for the incompressible case, and then the corresponding coefficients for the compressible case will be determined by the relations

$$\frac{C_p}{C'_p} = \frac{C_L}{C'_L} = \frac{C_M}{C'_M} = \frac{1}{|1 - M_\infty^2|}$$

But it is tedious to find the variation of  $C_p$ ,  $C_L$ , and  $C_M$  with  $M_\infty$  because for every  $M_\infty$  we have to make the above transformations.

### 6.6.4 Application to Bodies of Revolution and Fuselages

The general, three-dimensional equations can be applied to these shapes. But it is more convenient to use polar coordinates for bodies of revolution and fuselages.

The potential equation in cylindrical polar coordinates, for incompressible flow, is

$$\frac{\partial^2 \phi}{\partial x^2} + \frac{\partial^2 \phi}{\partial r^2} + \frac{1}{r} \frac{\partial \phi}{\partial r} + \frac{1}{r^2} \frac{\partial^2 \phi}{\partial \theta^2} = 0 \quad (6.43)$$

where  $x$ ,  $r$ , and  $\theta$  are the axial, radial, and angular (circumferential) coordinates, respectively. For compressible flow, the equation is

$$(1 - M_\infty^2) \frac{\partial^2 \phi}{\partial x^2} + \frac{\partial^2 \phi}{\partial r^2} + \frac{1}{r} \frac{\partial \phi}{\partial r} + \frac{1}{r^2} \frac{\partial^2 \phi}{\partial \theta^2} = 0 \quad (6.44)$$

The transformation is

$$x' = x, \quad r' = K_1 r, \quad \theta' = \theta, \quad \phi = K_2 \phi' \quad (6.45)$$

where the primed parameters are the transformed ones. Equation (6.44) is independent of  $M_\infty$  for

$$K_1 = \sqrt{|1 - M_\infty^2|}$$

From the streamline analogy,

$$K_2 = \frac{1}{|1 - M_\infty^2|}$$

Here again, as in Cartesian coordinates, *transform the geometry* and then calculate the aerodynamic coefficients for the incompressible case and then the values for the compressible case are given by Eq. (6.39). If  $f = 0$ , the only transformation required will be  $t'/t = \sqrt{|1 - M_\infty^2|}$ . The variations of  $\frac{u_{\max}}{V_\infty}$ ,  $\left(\frac{dC_L}{d\alpha}\right)_{C_L=0}$  and  $\frac{u_{\max}}{V_\infty} / \left(\frac{u_{\max}}{V_\infty}\right)_{\text{inc}}$  with  $M_\infty$  are shown in Figure 6.9a–c, respectively.

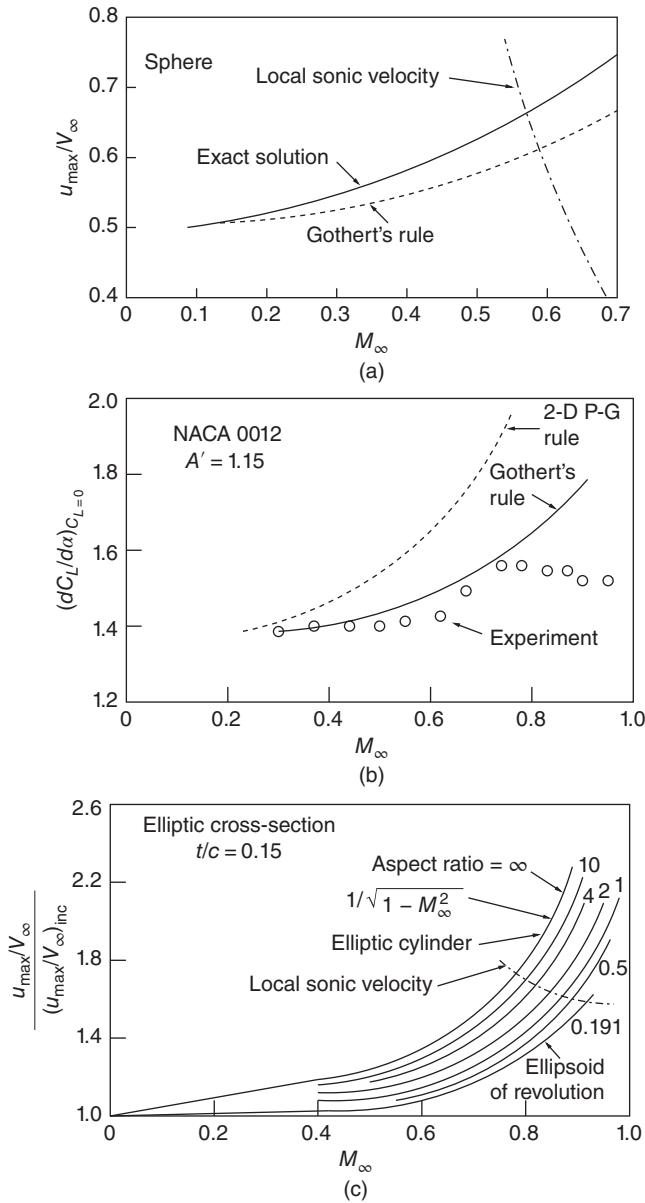
In Figure 6.9a, it can be seen that beyond the chain line the results cannot be applied because, once the speed of sound is reached locally, there will be a shock somewhere and this is certainly a nonlinear effect. Though the plot is for a sphere, which is not a slender body, the results of the Gothert rule are quite good (at  $M_\infty = 0.5$ , the error is only ~5%). For slender bodies, Gothert's rule applies very well.

In Figure 6.9b, the results for the NACA 0012 profile with aspect ratio ( $A'$ )1.15 are shown. For those Mach numbers for which locally the speed of sound is not reached anywhere on the profile, Gothert's rule checks very well with experimental values. The P–G rule for  $A' = \infty$  shows that for large  $A'$  the  $dC_L/d\alpha$  obtained is much higher.

The three-dimensional relief effect is shown in Figure 6.9c. For an infinitely long circular cylinder in a stream of velocity  $V_\infty$ ,  $u_{\max} = V_\infty$ , but for a sphere  $u_{\max} = 0.5V_\infty$ . From the plot, the three-dimensional relief effect increases with an increase in  $M_\infty$ . A slender body (small  $A'$ ) introduces smaller perturbations, that is the disturbances produced by wings are much more as compared to a fuselage. This difference in disturbances of wings and fuselage is greater at larger  $M_\infty$ . So, locally, the speed of sound is reached first on the wings and not on the fuselage. That is, we should find out the critical Mach number for the wings and not for the fuselage since only the former is significant. The critical Mach number  $M_{cr}$  for the fuselage will be much higher than the  $M_{cr}$  for the wing.

#### 6.6.4.1 Comparison of Two-Dimensional Symmetric Body and Axially Symmetric Body

For an axisymmetric body, in any cross-section the flow will be same. But this will not be so for a two-dimensional body. Also, at any cross-section, the disturbances produced by an axisymmetric body will be much smaller, that is the acceleration of flow will be much less and



**Figure 6.9** Results of Gothert's rule for a three-dimensional subsonic flow.

hence the drop in the pressure coefficient  $C_p$  is much smaller compared to a two-dimensional body.

### 6.6.5 The Prandtl–Glauert Rule

This is only an approximation and a greater simplification compared to Gothert's rule. Here we need not effect any transformation in the  $z$ -direction at all. That means Eq. (6.42) is no longer necessary. Only Eq. (6.40), which gives transformation to the planform alone, is necessary.

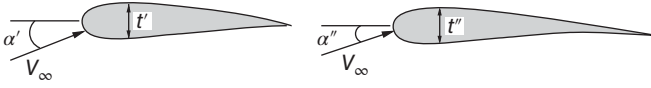


Figure 6.10 Affinely related airfoils.

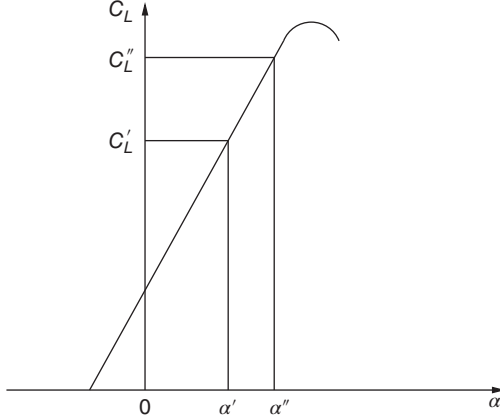


Figure 6.11 Lift coefficient variation with angle of attack.

#### 6.6.5.1 General Considerations

The P–G rule introduces the concept of affinely related profiles in incompressible flow. Affinely related profiles are those for which, for example, the  $t/c$  ratio alone is different and  $\alpha$  and  $f$  are the same, that is all the ordinates of the two profiles are related simply by a constant.

Similarly, we can obtain affinely related profiles by changing  $\alpha$  alone or  $f$  alone. In general, affinely related profiles, as shown in Figure 6.10, can be obtained by using

$$\frac{t'}{t''} = \frac{f'}{f''} = \frac{\alpha'}{\alpha''} = K_1 \quad (6.46)$$

We should effect only one of these parameters in Eq. (6.46) in order to get affinely related profiles. For such profiles, it follows from theory and experiment that

$$\frac{C'_p}{C''_p} = \frac{C'_L}{C''_L} = \frac{C'_M}{C''_M} = K_1 \quad (6.47)$$

This can be thought as: if  $\alpha$  for one wing is  $K$  times  $\alpha$  for the second wing then the  $C_L$ ,  $C_p$ , and  $C_M$  for the first wing should be correspondingly  $K$  times larger than those for the second wing. This is so because of the linearity of lift curve, as shown in Figure 6.11.

These relationships hold only for the linear portion, because of the linearity involved in the theory.

#### 6.6.5.2 P–G Rule for Two-Dimensional Flow, Using Eqs. (6.46) and (6.47)

We have to use Eq. (6.46) with (6.42), and (6.47) with (6.39), and set  $K_1 = \sqrt{|1 - M_\infty^2|}$  in Eqs. (6.46) and (6.47). What we have to prescribe now is our postulation for P–G rule versions I and II:

**Version I**  $M_\infty = 0$  for subsonic flow and, therefore,

$$\frac{t}{t'} = \frac{f}{f'} = \frac{\alpha}{\alpha'} = 1 \quad (6.48)$$

where the prime refers to the incompressible case.

**Version II**  $M_\infty = \sqrt{2}$  for supersonic flow and

$$\frac{t}{t''} = \frac{t}{t'} \frac{t'}{t''} = K_1 = \sqrt{|1 - M_\infty^2|}$$

Therefore,

$$\frac{C_p}{C_p''} = \frac{C_p}{C_p'} \frac{C_p'}{C_p''} = \frac{1}{K_1} = \frac{1}{\sqrt{|1 - M_\infty^2|}} \quad (6.49)$$

where the double prime refers to a transformed profile.

### 6.6.5.3 Application to Wings

The general relation between the pressure coefficients of closely related wing profiles (Eq. (6.39)) is

$$\frac{(C_p)_{A,\alpha,t/c,f/c,x/c,y/s,z/t}}{(C_p')_{k_1 A, k_1 \alpha, k_1(t/c), k_1(f/c), x/c, y/s, z/t}} = \frac{1}{|1 - M_\infty^2|}$$

where  $s$  is the semi-span of the wing. This transformed pressure coefficient ratio corresponds to  $M_\infty = 0$  (version I of the P-G rule), for subsonic flow.

For  $M_\infty = \sqrt{2}$  (supersonic flow), by Eq. (6.49) of version II, we get

$$\frac{(C_p)_{A,\alpha,t/c,f/c,x/c,y/s,z/t}}{(C_p')_{k_1 A, k_1 \alpha, k_1(t/c), k_1(f/c), x/c, y/s, z/t}} = \frac{1}{\sqrt{|1 - M_\infty^2|}} \quad (6.50)$$

$$\frac{(C_L)_{A,t/c,\alpha}}{(C_L')_{k_1 A, t/c,\alpha}} = \frac{(C_M)_{A,t/c,\alpha}}{(C_M')_{k_1 A, t/c,\alpha}} = \frac{1}{\sqrt{|1 - M_\infty^2|}} \quad (6.51)$$

By Gothert's rule, we have

$$\frac{C_p}{C_p'} = \frac{C_L}{C_L'} = \frac{C_M}{C_M'} = \frac{1}{|1 - M_\infty^2|} \quad (6.39)$$

$$\frac{\alpha'}{\alpha} = \frac{f'}{f} = \frac{t'}{t} = \sqrt{|1 - M_\infty^2|} \quad (6.42)$$

By the similarity rule for affinely related profiles in incompressible flow, if

$$\frac{t'}{t''} = \frac{f'}{f''} = \frac{\alpha'}{\alpha''} = K_1 \quad (6.46)$$

then

$$\frac{C_p'}{C_p''} = \frac{C_L'}{C_L''} = \frac{C_M'}{C_M''} = K_1 \quad (6.47)$$

This is an empirical rule. For low-speed flows, this can be explained with respect to  $\alpha$ . But these equations are only approximate. Actually, for supersonic flow,  $C_L$  does not depend on  $t$  at all. It depends only on  $f$  and  $\alpha$ . We relate the given profile in compressible flow (unprimed) to the transformed profile (double primed) by

$$\frac{t}{t''} = \frac{f}{f''} = \frac{\alpha}{\alpha''} = 1 \quad (6.48a)$$

With Eqs. (6.48a) and (6.42), we find that

$$\frac{t'}{t''} = \frac{t'}{t} \frac{t}{t''} = 1 \sqrt{|1 - M_\infty^2|} \quad \text{or} \quad K_1 = \sqrt{|1 - M_\infty^2|}$$

Then the aerodynamic coefficients of the given profile in compressible flow are related to those of the transformed profile (which has the same geometry) in incompressible flow or at  $M_\infty = \sqrt{2}$  by

$$\frac{C_p}{C_p''} = \frac{C_L}{C_L''} = \frac{C_M}{C_M''} = \frac{1}{\sqrt{|1 - M_\infty^2|}} \quad (6.49a)$$

because

$$\frac{C_p}{C_p''} = \frac{C_p}{C_p'} \frac{C_p'}{C_p''} = \frac{1}{|1 - M_\infty^2|} \sqrt{|1 - M_\infty^2|} \text{ by Eqs. (6.39) and (6.47).}$$

#### 6.6.5.4 Application to Wings of Finite Span

Gothert's rule – Eq. (6.39) – states that

$$\frac{(C_p)_{A,\alpha,t/c,f/c,x/c,y/s,z/t}}{(C_p')_{k_1 A, k_1 \alpha, k_1(t/c), k_1(f/c), x/c, y/s, z/t}} = \frac{1}{|1 - M_\infty^2|}$$

and by P–G rule, we have

$$\frac{(C_p)_{A,\alpha,t/c,f/c,x/c,y/s,z/t}}{(C_p'')_{k_1 A, \alpha, t/c, f/c, x/c, y/s, z/t}} = \frac{1}{\sqrt{|1 - M_\infty^2|}} \quad (6.50a)$$

Equation (6.50a) is only an approximate relation. Further,

$$\frac{(C_L)_{A,\alpha,t/c,f/c}}{(C_L'')_{k_1 A, \alpha, t/c, f/c}} = \frac{(C_M)_{A,\alpha,t/c,f/c}}{(C_M'')_{k_1 A, \alpha, t/c, f/c}} = \frac{1}{\sqrt{|1 - M_\infty^2|}} \quad (6.51a)$$

The P–G rule is only approximate, but Gothert's rule, though exact, is very tedious, especially in three dimensions, because here we have to transform the profile also. For the P–G rule, only the planform has to be transformed.

From the P–G rule, for three-dimensional wings we obtain a similarity rule in the following way. If the relation

$$C_p' = \theta' F_1 \left( \lambda', A', \cot \phi', \frac{x'}{c}, \frac{y'}{s} \right) \quad (6.52)$$

for a wing is known at  $M_\infty = 0$  and  $M_\infty = \sqrt{2}$ , then it follows for an arbitrary Mach number from Eqs. (6.40), (6.41), and (6.50), that

$$C_p = \frac{\theta}{\sqrt{|1 - M_\infty^2|}} F_2 \left( \lambda, A \tan \phi, A \sqrt{|1 - M_\infty^2|}, \frac{x}{c}, \frac{y}{s} \right) \quad (6.53a)$$

$$C_L = \frac{\theta}{\sqrt{|1 - M_\infty^2|}} F_3 \left( \lambda, A \tan \phi, A \sqrt{|1 - M_\infty^2|} \right) \quad (6.53b)$$

$$C_{D_0} = \frac{\theta}{\sqrt{|1 - M_\infty^2|}} F_4 \left( \lambda, A \tan \phi, A \sqrt{|1 - M_\infty^2|} \right) \quad (6.53c)$$

where  $\lambda$  is the taper ratio.

In Eq. (6.53a):  $\theta$  means  $\alpha$  or  $f/c$  or  $t/c$ .

In Eq. (6.53b):  $\theta$  means  $\alpha$  or  $f/c$  or  $t/c$ , but  $t/c$  only in subsonic flow.

In Eq. (6.53c):  $\theta$  means either  $t/c$  or  $f/c$ .

In Eqs. (6.52) and (6.53),  $\phi$  is the angle of sweep for the wing.

### 6.6.5.5 Application to Bodies of Revolution

Application of the P–G rule to bodies of revolution is similar to that for airfoils (two-dimensional), that is no transformation of the body is necessary. The aerodynamic coefficients in compressible flow are the same as in incompressible flow or at  $M_\infty = \sqrt{2}$ . Hence, there is no Mach number effect at all and the results are the same as those for slender body theory.

This contradicts the more exact Gothert rule. A closer examination shows that the P–G rule for bodies of revolution is valid only for very slender and extremely pointed (sharp-nosed) bodies. This theory is applied to rockets, very small aspect ratio wings, and so on. Of course, wave drag is influenced by  $M$  even for slender bodies. We can use the results of incompressible flow when calculating pressure distribution, and so on.

From Figure 6.9c, it can be seen that, for very small aspect ratios, the effect of the Mach number is very small and at  $A = 0$  the Mach number effect vanishes.

## 6.6.6 The von Karman Rule for Transonic Flow

### 6.6.6.1 Application to Wings

For  $M_\infty = 1$ ,

$$C_p = \theta^{2/3} F_5(\lambda, A \tan \phi, A\theta^{1/3}, x/c, y/s) \quad (6.54a)$$

$$C_L = \theta^{2/3} F_6(\lambda, A \tan \phi, A\theta^{1/3}) \quad (6.54b)$$

$$C_D = \theta^{5/3} F_7(\lambda, A \tan \phi, A\theta^{1/3}) \quad (6.54c)$$

Mathematically, these can be derived from the nonlinear differential Eq. (5.24). These laws are also approximately valid in the vicinity of  $M_\infty = 1$ . The main advantage of these similarity rules is that we have to investigate the influence of  $\lambda$ ,  $A \tan \phi$ , and  $A\theta^{1/3}$  only and not the influence of  $\lambda$ ,  $A$ ,  $\phi$ , and  $\theta$  separately, which is very tedious. Thus, the rules are very important for experimental investigations.

### 6.6.6.2 Application to Bodies of Revolution

The pressure distribution of a body (unprimed) is related to the pressure distribution of an affinely related body (primed) at  $M_\infty = 1$ , by the relation

$$C_p = C'_p \left( \frac{\theta_f}{\theta'_f} \right)^2 \quad (6.55)$$

where the subscript  $f$  stands for fuselage. This rule was derived by von Karman, but later on it was shown that a correction factor should be applied.

## 6.7 Critical Mach Number

In Section 6.2, we saw that the freestream subsonic Mach number which gives a sonic Mach number somewhere on the boundary of the body is called the *critical Mach number*  $M_\infty^*$ , and this decreases with the increasing thickness to chord ratio of the profile, without going into the details about the calculation of this important parameter. Calculating  $M_\infty^*$  for a given wing is extremely important because a local transonic flow zone over the profile will influence the aerodynamic efficiency of the wing considerably. Let us have a closer look at this vital parameter, influencing the performance of flying objects.

We are familiar with the definition of the critical Reynolds number. The critical Reynolds number is the Reynolds number at which the nature of the flow field begins to change from laminar to turbulent. Also, we know that any transition is gradual, and hence the transition would take place over a range of Reynolds number, and both laminar and turbulent pockets will prevail in the flow field over this range of Reynolds number. This leads to the definition of lower and upper critical Reynolds numbers. The lower critical Reynolds number is that Reynolds number below which the entire flow field is laminar, and the upper critical Reynolds number is that Reynolds number above which the entire field is turbulent. The laminar and turbulent flows dictated by the lower and upper critical Reynolds numbers can be precisely encountered in practice. In an analogous manner, one may say that the critical Mach number is that at which both subsonic and supersonic zones exist in the flow field. The lower critical Mach number is that below which the entire flow field is subsonic, and the upper critical Mach number is that above which the entire flow field is supersonic. But these definitions of lower and upper critical Mach numbers are only of mathematical interest, because the upper critical Mach number cannot be encountered in any physical flow process. This is essentially due to the waves present in the supersonic field. Therefore, it will be of great value, from a design point of view, to have a thorough understanding of the critical Mach number.

The Mach number ( $M$ ) refers to the method of measuring airspeed that was developed by the Austrian physicist Ernst Mach. It is used to indicate flight velocities in high-speed flight and is related to the speed of sound. The actual speed of sound varies depending on the altitude above sea level, because sound travels at slightly different speeds at different temperatures, and the temperature varies according to altitude. At sea level, the speed of sound is about  $1225 \text{ km h}^{-1}$  ( $a = \sqrt{\gamma RT} = \sqrt{1.4 \times 287 \times 288.15} = 340.26 \text{ m s}^{-1}$  or  $340.26 \times 3.6 \approx 1225 \text{ km h}^{-1}$ ). At 20 000 ft (6096 m), the speed of sound is  $1062 \text{ km h}^{-1}$ .

If an aircraft is traveling at one half of the speed of sound, it is said to be traveling at Mach 0.5. A speed of Mach 2 is twice the speed of sound. Because the speed of sound varies, a particular speed at sea level expressed as a Mach number would be faster than the same speed at 30 000 ft (9144 m), which would be faster than the same speed at 40 000 ft (12 192 m). In other words, the velocity of Mach 2 stream at sea level is greater (in magnitude) than Mach 2 stream at 30 000 ft. That is, the flow velocity for a given Mach number at a specified altitude will be smaller than that at a lower altitude. When an aircraft reaches Mach 1, it is said to *break the sound barrier*.

The following breakdowns have been generally accepted to classify speeds:  $M$  less than 0.8 is subsonic,  $M = 0.8$  to 1.2 is transonic,  $M$  from 1.2 to 5.0 is supersonic, and  $M$  greater than 5.0 is hypersonic.

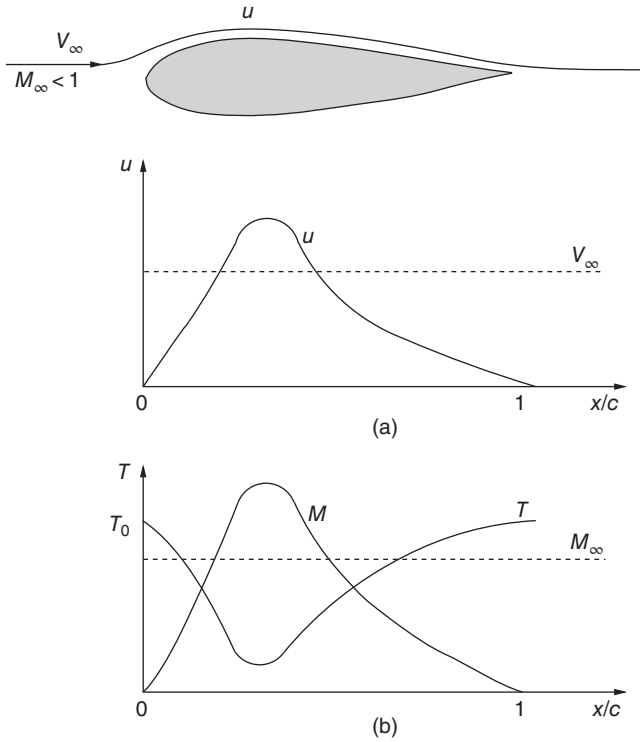
A critical Mach number is the speed of an aircraft (below Mach 1) when the air flowing over some area of the airfoil has reached the speed of sound. For instance, if the air flowing over a wing reaches Mach 1 when the wing is only moving at Mach 0.8 then the wing's critical Mach number is 0.8.

Examine the subsonic flow past an airfoil, illustrated in Figure 6.12. The flow accelerates from the leading edge to a maximum value at the maximum thickness location and then decelerates toward the trailing edge, as shown in Figure 6.12a. The corresponding variations of temperature and Mach number, from the leading edge to the trailing edge of the airfoil, are shown in Figure 6.12b.

This flow process can be treated as adiabatic, with the stagnation temperature  $T_0 = \text{constant}$ . Therefore, by energy equation, we have

$$h + \frac{u^2}{2} = h_0$$





**Figure 6.12** (a) Variation of flow velocity and (b) variation of Mach number and temperature.

where  $h$  and  $h_0$  are the static and total enthalpies, respectively, and  $u$  is the local velocity. Assuming air to be a perfect gas, we can express,  $h = c_p T$  and  $h_0 = c_p T_0$ . Thus,

$$\begin{aligned}
 h &= h_0 - \frac{u^2}{2} \\
 c_p T &= c_p T_0 - \frac{u^2}{2} \\
 T &= T_0 - \frac{u^2}{2c_p} \\
 &= T_0 - \frac{u^2}{2 \frac{\gamma}{\gamma-1} R} \\
 &= T_0 - \frac{(\gamma-1)}{2} \frac{u^2}{\gamma R} \\
 &= T_0 - \frac{(\gamma-1)}{2} \frac{u^2 T}{\gamma R T} \\
 &= T_0 - \frac{(\gamma-1)}{2} M^2 T
 \end{aligned}$$

since  $c_p = \gamma/(\gamma-1) R$ ,  $a = \sqrt{\gamma R T}$ .

This shows that the temperature is maximum at the leading edge, which is a stagnation point, assumes a minimum at the maximum thickness location and then increases toward the trailing edge, as shown in Figure 6.12b. The Mach number of the flow increases from zero at the leading edge to the maximum level at the maximum thickness location and then decreases toward the

trailing edge. The Mach number variation over the profile depends on the airfoil shape and the angle of attack. Thus, it is evident that as the freestream Mach number  $M_\infty$  is increased the highest local  $M$  on the surface may exceed 1 long before  $M_\infty$  reaches 1. The value of the freestream Mach number  $M_\infty$  at which the highest  $M$  on the airfoil first reaches 1 is called the *critical Mach number* and is represented as  $M_\infty^*$ . Note that  $M_\infty^*$  is a value of the freestream Mach number.  $M_\infty^*$  is less than 1 for any object with finite thickness.

### 6.7.1 Calculation of $M_\infty^*$

If the pressure coefficient  $C_p$  is known at a lower freestream Mach number  $M_\infty$ , the critical Mach number can be calculated as follows.

We know that the isentropic pressure–Mach number relation is,

$$\frac{p_0}{p} = \left(1 + \frac{\gamma - 1}{2} M^2\right)^{\gamma/(\gamma-1)}$$

where  $p$  and  $p_0$  are the local static and stagnation pressures, respectively. If  $p_\infty$  and  $M_\infty$  are the freestream static pressure and Mach number, respectively, then we can express the local pressure as

$$\frac{p}{p_\infty} = \left(\frac{1 + \frac{\gamma - 1}{2} M_\infty^2}{1 + \frac{\gamma - 1}{2} M^2}\right)^{\gamma/(\gamma-1)}$$

since  $p_0 = p_{0\infty}$ , for isentropic flows. The pressure coefficient is defined as

$$C_p = \frac{p - p_\infty}{\frac{1}{2} \rho_\infty V_\infty^2}$$

where  $\rho_\infty$  and  $V_\infty$  are the freestream density and velocity, respectively. The  $C_p$  can be expressed in terms of  $M_\infty$ , as

$$\begin{aligned} C_p &= \frac{2}{\rho_\infty V_\infty^2} p_\infty \left(\frac{p}{p_\infty} - 1\right) \\ &= \frac{2}{\rho_\infty V_\infty^2} \rho_\infty R T_\infty \left(\frac{p}{p_\infty} - 1\right) \\ &= \frac{2}{\gamma V_\infty^2} \gamma R T_\infty \left(\frac{p}{p_\infty} - 1\right) \\ &= \frac{2}{\gamma M_\infty^2} \left(\frac{p}{p_\infty} - 1\right) \end{aligned}$$

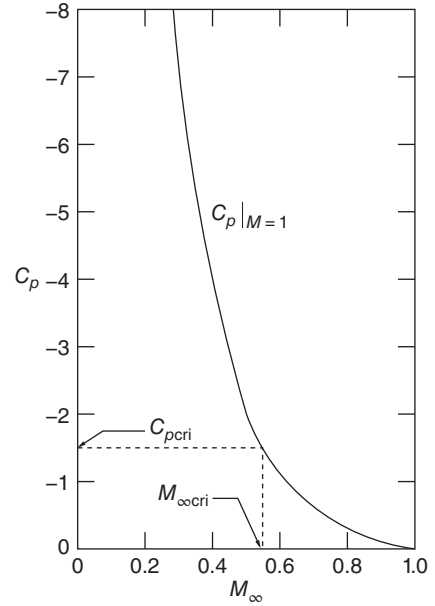
Substituting for  $p/p_\infty$ , we get the pressure coefficient as

$$C_p = \frac{2}{\gamma M_\infty^2} \left( \left( \frac{2 + (\gamma - 1) M_\infty^2}{2 + (\gamma - 1) M^2} \right)^{\gamma/(\gamma-1)} - 1 \right) \quad (6.56)$$

At the point where the local Mach number  $M = 1$ , the local pressure coefficient becomes

$$C_p|_{M=1} = \frac{2}{\gamma M_\infty^2} \left( \left( \frac{2 + (\gamma - 1) M_\infty^2}{\gamma + 1} \right)^{\gamma/(\gamma-1)} - 1 \right) \quad (6.57)$$

**Figure 6.13** Pressure coefficient variation with freestream Mach number.



This equation can be used to find the critical Mach number, once  $C_p$  at the minimum pressure point is known.

At  $M_\infty = M_\infty^*$ , the local Mach number  $M$  reaches 1 somewhere over the airfoil. The value of  $C_p$  at this point can be found by setting  $M = 1$ .

For any given airfoil, the value of  $M_\infty^*$  can be found from the value of the minimum  $C_p$  on the airfoil.

If the incompressible pressure distribution is known, the  $C_{pinc}$  data on the airfoil can be used to get the  $C_p$  values at the desired higher freestream Mach number using the Prandtl–Glauert relation, Eq. (6.11b),

$$C_p = \frac{C_{pinc}}{\sqrt{1 - M_\infty^2}}$$

A plot of a  $C_p$  variation with freestream Mach number is shown in Figure 6.13.

### Example 6.3

If the value of the pressure coefficient at the maximum velocity location on a profile is  $-2.3$ , determine the critical Mach number.

#### Solution:

Given,  $C_{pmin} = -2.13$ . If this is taken as the pressure coefficient corresponding to  $M = 1$  then the freestream Mach number becomes the critical Mach number. Therefore, from Eq. (6.57), we have

$$C_p|_{M=1} = \frac{2}{\gamma M_\infty^2} \left( \left( \frac{2 + (\gamma - 1)M_\infty^2}{\gamma + 1} \right)^{\gamma/(\gamma-1)} - 1 \right)$$

$$-2.13 = \frac{2}{1.4 M_\infty^2} \left( \left( \frac{2 + 0.4 M_\infty^2}{2.4} \right)^{3.5} - 1 \right)$$

$$\begin{aligned}
 -M_\infty^2 &= \frac{2}{1.4 \times 2.13} \left( \left( \frac{2 + 0.4M_\infty^2}{2.4} \right)^{3.5} - 1 \right) \\
 &= 0.67 \left( \left( \frac{2 + 0.4M_\infty^2}{2.4} \right)^{3.5} - 1 \right)
 \end{aligned}$$

Solving, we get the critical Mach number as

$$M_\infty^* = \boxed{0.5}$$

## 6.8 Summary

In this chapter, the basic facts about the similarity rule for *affinely transformed shapes* is outlined. In a geometrical transformation, if all coordinates in a given direction are changed by a uniform ratio then the transformation involved is termed *affine*. We have demonstrated in this chapter that it is possible to derive an expression that relates the subsonic compressible flow past a certain profile to the incompressible flow past a second profile derived from the first through an affine transformation. Such an expression is called a *similarity rule*.

In many practical applications, the similarity rules may be useful. For instance, Gothert's rule for subsonic flow allows us to predict the details of the compressible subsonic flow past a body at subsonic speeds if we know the details of an incompressible flow past an affinely related body. In the same manner, the supersonic similarity rule shows how experimental data for a certain body at a certain  $M_\infty$  can be made applicable to a related body at a different  $M_\infty$ .

The derivation of similarity rules is a form of dimensional analysis involving *distorted models* rather than geometrically similar models. However, there are a number of differences between these two methods. Dimensional analysis simply lists the dimensionless parameters that are involved, whereas similarity analysis goes much further, showing how to group these dimensionless quantities in such a way as to reduce the number of independent variables. For dimensional analysis we need to know or guess the variables involved in a problem. But for similarity analysis, we need to know more, for instance the different equations and the boundary conditions. Sometimes similarity rules come from a set of experiments.

The Laplace equations for two-dimensional compressible and incompressible flows, respectively, are

$$(1 - M_\infty^2)\phi_{xx} + \phi_{zz} = 0$$

$$(\phi_{xx})_{\text{inc}} + (\phi_{zz})_{\text{inc}} = 0$$

The generalized transformation which transforms Eqs. (6.1) and (6.2) into one another is

$$X_{\text{inc}} = x$$

$$Z_{\text{inc}} = K_1 z$$

$$\phi(x, z) = K_2 \phi_{\text{inc}}(x_{\text{inc}}, z_{\text{inc}})$$

where  $K_1 = \sqrt{1 - M_\infty^2}$  and  $K_2$  have to be determined from the boundary conditions.

The relation between the geometries of the corresponding profile is

$$\frac{dz}{dx} = K_2 \sqrt{1 - M_\infty^2} \left( \frac{dz_{\text{inc}}}{dx_{\text{inc}}} \right)$$

which means that the shape of the profile in the compressible flow pattern is  $(K_2 \sqrt{1 - M_\infty^2})$  times the slope of the corresponding profile in the related incompressible flow pattern.

In similarity analysis, three types of problems are considered:

- the direct problem (version I of the P–G rule), in which the body profile is treated as invariant
- the indirect problem (version II of the P–G rule), which is the case of equal potential (the pressure distribution around the body in incompressible flow and compressible flow are taken to be the same)
- the streamline analogy (version III), which is also called *Gothert's rule*.

In the direct problem, there is no transformation of geometry at all. Therefore,

$$\frac{dz}{dx} = \frac{dz_{\text{inc}}}{dx_{\text{inc}}}$$

In other words, the ratios of the angle of attack  $\alpha$ , the thickness  $t$ , and the camber  $f$  are

$$\frac{\alpha}{\alpha_{\text{inc}}} = \frac{t}{t_{\text{inc}}} = \frac{f}{f_{\text{inc}}} = 1$$

Then the forces acting in the two flows are related through

$$\frac{C_p}{C_{p_{\text{inc}}}} = \frac{C_L}{C_{L_{\text{inc}}}} = \frac{C_M}{C_{M_{\text{inc}}}} = \frac{1}{\sqrt{1 - M_\infty^2}}$$

These equations mean that, for the same profile at the same angle of attack, the pressure coefficient, lift coefficient, and moment coefficient are all affected by the Mach number in proportion to the factor  $1/\sqrt{1 - M^2}$ .

The P–G rule also implies that the streamlines around a given profile in compressible flow are farther apart from each other by  $1/\sqrt{1 - M_\infty^2}$  than in incompressible flow. The freestream Mach number which gives sonic velocity somewhere on the boundary of an object placed in the fluid stream is called the critical Mach number  $M_\infty^*$ , and this decreases with increasing thickness of the body. The freestream Mach number for which the entire flow around the body is subsonic is called the *lower critical Mach number*. The freestream Mach number for which the entire flow around the body is supersonic called the *upper critical Mach number*.

In the *indirect problem*, the requirement is to find a transformation, for the profile, by which we can obtain a body in incompressible flow with exactly the same pressure distribution as in the compressible flow. The compressible profile is affinely related to the incompressible profile in such a way that

$$\frac{dz}{dx} = \sqrt{1 - M_\infty^2} \frac{dz_{\text{inc}}}{dx_{\text{inc}}}$$

$$\frac{\alpha}{\alpha_{\text{inc}}} = \frac{t}{t_{\text{inc}}} = \frac{f}{f_{\text{inc}}} = \sqrt{1 - M_\infty^2}$$

Then

$$\frac{C_p}{C_{p_{\text{inc}}}} = \frac{C_L}{C_{L_{\text{inc}}}} = \frac{C_M}{C_{M_{\text{inc}}}} = 1$$

These equations mean that the dimensionless pressure distribution, lift coefficient, and moment coefficient will be the same for compressible and incompressible flow if the profiles are affinely related in such a way that the compressible profile is smaller in camber ratio, thickness ratio, and angle of attack by the factor  $\sqrt{1 - M_\infty^2}$ .

By Gothert's rule, we have

$$\frac{\alpha}{\alpha_{\text{inc}}} = \frac{t}{t_{\text{inc}}} = \frac{f}{f_{\text{inc}}} = \frac{1}{\sqrt{1 - M_{\infty}^2}}$$

The aerodynamic coefficients of the given body at the given Mach number  $M_{\infty}$  are given by

$$\frac{C_p}{C_{p_{\text{inc}}}} = \frac{C_L}{C_{L_{\text{inc}}}} = \frac{C_M}{C_{M_{\text{inc}}}} = \frac{1}{1 - M_{\infty}^2}$$

This means that if the two profiles are related affinely the pressure, lift, and moment coefficient for the compressible flow pattern will be greater than those for the related incompressible flow pattern by the factor  $1/(1 - M_{\infty}^2)$ . In this method, if the lift coefficient of one of these profiles at a finite Mach number  $M_{\infty}$  is required, we have to find, either theoretically or experimentally, the lift coefficient in incompressible flow of an affinely related profile whose camber, thickness ratio, and angle of attack are all smaller than the corresponding values for the original profile by the ratio  $\sqrt{1 - M_{\infty}^2}$ . Then by multiplying this lift coefficient by  $1/(1 - M_{\infty}^2)$ , we find the desired lift coefficient for the compressible flow.

This method of projecting experimental data for incompressible flow is sometimes tedious, since it requires incompressible data for a large range of the thickness ratio. It would be more convenient in many cases to know how the Mach number affects the performance of a profile of fixed slope. The P-G rule version I yields information of this type.

The similarity rules for supersonic flow are the following.

For version I:

$$\frac{C_p}{C'_p} = \frac{C_L}{C'_L} = \frac{C_M}{C'_M} = \frac{1}{\sqrt{M_{\infty}^2 - 1}}$$

For version II:

$$\frac{C_p}{C'_p} = \frac{C_L}{C'_L} = \frac{C_M}{C'_M} = 1$$

For version III:

$$\frac{C_p}{C'_p} = \frac{C_L}{C'_L} = \frac{C_M}{C'_M} = \frac{1}{M_{\infty}^2 - 1}$$

In the above relations, the primed quantities are for the transformed body and the unprimed ones are for the actual body. Compute the flow about the given body at  $M_{\infty} = \sqrt{2}$ . For any other supersonic Mach number, the aerodynamic coefficient are given by Eq. (6.18). In supersonic flow  $M_{\infty} = \sqrt{2}$  plays the same role as  $M_{\infty} = 0$  does in subsonic flow. In version II, the ratios of the aerodynamic coefficients are equal to unity. In version III, compute the aerodynamic coefficients of the transformed body for  $M_{\infty} = \sqrt{2}$ . The aerodynamic coefficients of the given body at the given Mach number  $M_{\infty}$  follow from Eq. (6.20).

For transonic flows, by the von Karman rule, we have

$$C_p = \frac{\left(\frac{t}{c}\right)^{2/3}}{[(\gamma + 1)M_{\infty}^2]^{1/3}} \tilde{C}_p(\chi)$$

$$C_L = \frac{\left(\frac{t}{c}\right)^{2/3}}{[(\gamma + 1)M_{\infty}^2]^{1/3}} \tilde{C}_L(\chi)$$

$$C_D = \frac{\left(\frac{t}{c}\right)^{5/3}}{[(\gamma + 1)M_\infty^2]^{1/3}} \tilde{C}_D(\chi)$$

where

$$\chi = \frac{1 - M_\infty^2}{\left[\left(\frac{t}{c}\right)(\gamma + 1)M_\infty^2\right]^{2/3}}$$

By hypersonic similarity, we have

$$K = M\theta$$

where  $K$  is the *hypersonic similarity parameter*.

It is evident from the discussions of this chapter that, if the equations of motion could be solved, the solutions themselves would indicate quite clearly the nature of any similarities that might exist among members of a family of flow patterns. A separate derivation of similarity rules would, therefore, be superfluous. But, in many flow situations of practical interest, we are unable to solve the equations of motion. However, even though solutions are lacking, we may use our knowledge of the forms of the differential equations, along with the associated boundary conditions, and thus derive the similarity rules.

## Exercise Problems

**6.1** An airfoil has the following lift-curve slopes at the Mach numbers given (measurements):

M	0.2	0.3	0.4	0.5	0.6	0.7	0.75
$\frac{dC_L}{d\alpha} / \text{deg}$	0.108	0.113	0.115	0.124	0.130	0.127	0.100

Plot  $\frac{dC_L}{d\alpha}$  vs  $M$ -curve.

**6.2** A slender model with semi-vertex angle  $\theta = 3^\circ$  has to operate at  $M_\infty = 10$  with an angle of attack of  $\alpha = 3^\circ$ . What are the respective angles of attack required to simulate the conditions if a wind tunnel test has to be carried out at (a)  $M_\infty = 3.0$ ,  $\theta = 12^\circ$  and (b)  $M_\infty = 3.0$ ,  $\theta = 3^\circ$ ?

[Answer: (a)  $7.3^\circ$ , (b)  $16.3^\circ$ ]

**6.3** A missile has a conical nose with a semi-vertex angle of  $4^\circ$  and is subjected to a Mach number of 12 under actual conditions. A model of the missile has to be tested in a supersonic wind tunnel at a test section Mach number of 2.5. Calculate the semi-vertex angle of the conical nose of the model.

[Answer:  $19.2^\circ$ ]

**6.4** Show that the results of the linearized supersonic theory for flow past a wedge of semi-wedge angle  $\theta$  may be put into the following similarity form

$$C_p \frac{((\gamma + 1)M_\infty^2)^{1/3}}{\theta^{2/3}} = \frac{2}{\chi^{1/2}}$$

where

$$\chi = \frac{M_\infty^2 - 1}{(\theta(\gamma + 1)M_\infty^2)^{2/3}}$$

- 6.5** Determine the minimum  $C_p$  for a wing, if the critical Mach number is (a) 0.3 and (b) 0.4.  
[Answer: (a)  $-6.95$ , (b)  $-3.66$ ]
- 6.6** If the distance between the streamlines around an airfoil are displaced 30% more than the streamlines for the incompressible flow around the airfoil, determine the compressible flow Mach number.  
[Answer: 0.64]
- 6.7** If the lift-curve slope of an airfoil in a subsonic compressible flow is 8, determine the freestream Mach number.  
[Answer: 0.619]
- 6.8** Determine the decrease in thickness-to-chord ratio required for an airfoil in a Mach 0.6 freestream to experience drag equal to that experienced by it if the freestream is incompressible.  
[Answer: 20%]
- 6.9** If the lift coefficient of an airfoil in a Mach 0.29 flow is 0.2, determine the angle attack of the transformed airfoil in a compressible flow that would experience the same lift coefficient.  
[Answer:  $1.822^\circ$ ]
- 6.10** If the drag coefficient of an airfoil in a Mach  $\sqrt{2}$  stream is 0.09, determine the drag the airfoil would experience when placed in a Mach 2.2 stream.  
[Answer: 0.176]
- 6.11** If the lift coefficient of an affinely transformed airfoil is Mach  $\sqrt{2}$  air stream is 0.9, determine the lift coefficient that the original airfoil in a Mach 1.9 stream would experience.  
[Answer: 0.345]



## 7

## Two-Dimensional Compressible Flows

### 7.1 Introduction

The equations of motion in terms of velocity potential for steady, irrotational isentropic motion, as derived in Chapter 5, turn out to be nonlinear partial differential equations. Although the equations were derived quite easily, exact solutions of these equations for particular flow problems often involve tedious mathematical procedures; in many cases, solutions are not possible. To solve this problem, the following two courses of action seem to be open:

- Find exact solutions for a simplified problem with the hope of obtaining a qualitative understanding of the nature of other flow patterns for which solutions are not available.
- Find simple, though approximate, solutions suitable for practical applications. Both methods of approach yield useful information and in a sense complement each other, as the few exact solutions serve as a check on the validity and reliability of the approximate methods. In this chapter we will see how the second method may be applied to some important problems of two-dimensional flow.

The assumption of two-dimensionality itself serves as a first approximation to the flow past the wings of an airplane, the flow through the blade system of propellers and of axial-flow in compressors and turbines. In many such applications the velocity of perturbations produced by the body immersed in the flow are small, because the bodies are very thin. In this fact lies the essence of the linearized method – that the flow pattern may be thought of as the combination of a uniform, parallel velocity on which small perturbation velocities are superposed.

The advantage of making such an assumption, as seen in Chapter 5, lies in the fact that the governing equation of motion is greatly simplified and also becomes linear. Further, it was shown in Chapter 5 that from this linearized theory or small perturbation theory, we can draw useful approximate information as to the effect of Mach number for subsonic flow. The linearized theory also makes evident an approximate similarity law for different flow fields.

### 7.2 General Linear Solution for Supersonic Flow

The fundamental equation governing most of the compressible flow regime, within the frame of small perturbations, is, from Eq. (5.27),

$$(1 - M_\infty^2)\phi_{xx} + \phi_{zz} = 0 \quad (7.1)$$

Equation (7.1) is elliptic for  $M_\infty < 1$  and hyperbolic for  $M_\infty > 1$ . There is hardly any method available for obtaining the analytical solution of this equation for  $M_\infty < 1$ . But for  $M_\infty > 1$ , analytical solutions are available for Eq. (7.1).

**Solutions of Eq. (7.1) for  $M_\infty > 1$** 

For  $M_\infty > 1$ , Eq. (7.1) is of the hyperbolic type, with the form being similar to that of the wave equation. The general solution to this equation can be written as the sum of two arbitrary functions,  $f$  and  $g$ , such that

$$\phi(x, z) = f(z - x \tan \mu) + g(z + x \tan \mu) \quad (7.2)$$

where  $\mu$  is the Mach angle and

$$\tan \mu = \frac{1}{\sqrt{M_\infty^2 - 1}} \quad (7.3)$$

The arbitrary functions  $f$  and  $g$  are to be determined from the boundary conditions for the specific problems.

**Proof**

To show that Eq. (7.2) is the solution to Eq. (7.1) when  $M_\infty > 1$ , rewrite Eq. (7.2) as

$$\phi = f(\xi) + g(\eta)$$

where  $\xi$  and  $\eta$  are the new variables, defined as

$$\xi = z - x \tan \mu, \quad \eta = z + x \tan \mu$$

Therefore,

$$\begin{aligned} \phi_x &= \frac{\partial f}{\partial \xi} \frac{\partial \xi}{\partial x} + \frac{\partial g}{\partial \eta} \frac{\partial \eta}{\partial x} \\ &= -f' \tan \mu + g' \tan \mu \\ &= \tan \mu (g' - f') \\ \phi_{xx} &= \frac{\partial \phi_x}{\partial x} = \tan \mu \left( \frac{\partial g'}{\partial \eta} \frac{\partial \eta}{\partial x} - \frac{\partial f'}{\partial \xi} \frac{\partial \xi}{\partial x} \right) \end{aligned}$$

On simplification this yields

$$\begin{aligned} \phi_{xx} &= \tan^2 \mu (f'' + g'') \\ \phi_z &= \frac{\partial f}{\partial \xi} \frac{\partial \xi}{\partial z} + \frac{\partial g}{\partial \eta} \frac{\partial \eta}{\partial z} \\ \phi_z &= f' + g' \end{aligned} \quad (7.4a)$$

Differentiation of the above expression for  $\phi_z$  with respect to  $z$  gives

$$\phi_{zz} = f'' + g'' \quad (7.4b)$$

Substituting Eqs. (7.4a) and (7.4b) into (7.1), we get

$$(1 - M_\infty^2) \tan^2 \mu (f'' + g'') + (f'' + g'') = 0$$

This equation is satisfied for  $\tan \mu$  from Eq. (7.3). That is, Eq. (7.2) is the general solution of Eq. (7.1). However, the functions  $f$  and  $g$  differ from problem to problem. As well as Eq. (7.2), the solution to Eq. (7.1) can also be written as

$$\phi(x, z) = f(x - \beta z) + g(x + \beta z) \quad (7.5)$$

where

$$\beta = \cot \mu = \sqrt{M_\infty^2 - 1} \quad (7.6)$$

On inspection of the solution Eqs. (7.2) and (7.5), it can be seen that  $\phi$  is constant, and hence all the flow properties are constant, along the straight lines given by the equation

$$z = \pm x \tan \mu + \text{constant}$$

This equation gives two families of straight lines, as shown in Figure 7.1, one family running to the left of the object and the other family running to the right, when viewed in the flow direction.

These are called *Mach lines* or *characteristics*. The lines of constant  $f$  that make a positive angle with the flow direction and run to the left of the disturbance (object) are called *left-running characteristics* and *lines of constant g*, making a negative angle with the flow direction and running to the right of object are called *right-running characteristics*. Depending on the geometry of the object, there will only be left-running or right-running. or both, characteristics present in the field, as shown in Figure 7.2.

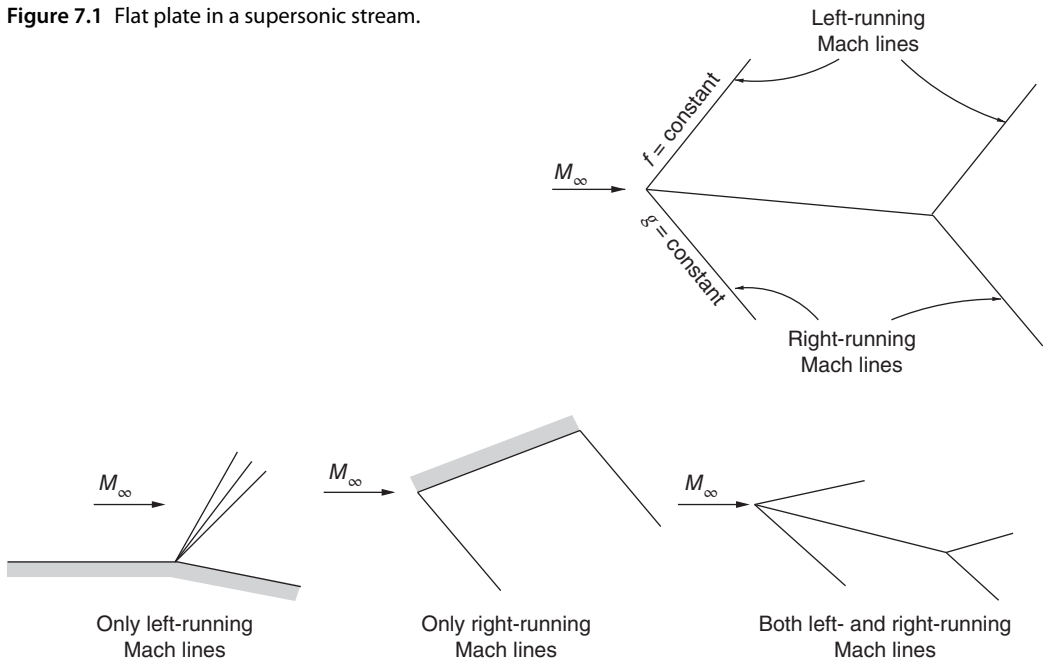
### 7.2.1 Existence of Characteristics in a Physical Problem

From the above discussions it is observed that

- disturbances and Mach lines can be produced only by boundaries
- disturbances can travel only in the downstream direction.

In Figure 7.2, we have shown that the characteristics of two families are independent of each other. This is because the geometries chosen are such that on one side of the boundary there is

**Figure 7.1** Flat plate in a supersonic stream.



**Figure 7.2** Characteristics on different objects in a supersonic flow.



**Figure 7.3** Coexistence of left-running ( $l-r$ ) and right-running ( $r-r$ ) characteristics.

only one family of Mach lines. This is not always the case. In fact, in many situations of practical importance, the opposite characteristics will intersect each other, as shown in Figure 7.3.

By knowing the type of Mach lines present in the problems, the equations can be suitably taken.

From Eq. (7.5), we have the potential function as

$$\phi(x, z) = f(x - \beta z) + g(x + \beta z)$$

where  $f$  represents the left-running Mach lines, on which  $g = 0$ , and  $g$  represents the right running Mach lines, on which  $f = 0$ . The perturbation velocities are

$$u = \frac{\partial \phi}{\partial x} = \phi_x = f' + g' \quad (7.7a)$$

$$w = \frac{\partial \phi}{\partial z} = \phi_z = \beta(g' - f') \quad (7.7b)$$

Then the pressure coefficient is given by Eq. (5.48) as

$$C_p = -2 \frac{u}{V_\infty} = -\frac{2}{V_\infty} (f' + g') \quad (7.8)$$

That is, to compute the pressure distribution, we need to know only the derivatives of  $f$  and  $g$ . There is no need to know the functions  $f$  and  $g$  themselves.

### 7.2.2 Equation for the Streamlines from Kinematic Flow Condition

From Section 5.6, by kinematic flow condition we know that

$$\frac{dz}{dx} = \frac{w}{V_\infty + u} = \frac{w/V_\infty}{1 + u/V_\infty}$$

To make the integration of this equation easier, we write the equation as follows.

$$\frac{dz}{dx} = \frac{w/V_\infty}{1 + \frac{u}{V_\infty} - M_\infty^2 \frac{u}{V_\infty}} = \frac{w/V_\infty}{1 - \beta^2 \frac{u}{V_\infty}}$$

where  $\beta = \sqrt{M_\infty^2 - 1}$ , and the denominator  $\left(1 + \frac{u}{V_\infty}\right)$  has been written as  $\left(1 + \frac{u}{V_\infty} - M_\infty^2 \frac{u}{V_\infty}\right)$ . This is possible because  $\frac{u}{V_\infty} \ll 1$  and so  $\left(M_\infty^2 \frac{u}{V_\infty}\right) < 1$ . Hence, the error introduced by this change is not significant. Rearranging the above equation, we get

$$V_\infty dz \left(1 - \beta^2 \frac{u}{V_\infty}\right) = w dx$$

Substituting for  $u$  and  $w$  from Eqs. (7.7a) and (7.7b), we obtain

$$\begin{aligned} V_\infty dz \left( 1 - \frac{\beta^2}{V_\infty} (f' + g') \right) &= \beta(g' - f') dx \\ V_\infty dz &= \beta(g' dx - f' dx) + \beta^2(f' dz + g' dz) \\ &= \beta((g' dx + \beta g' dz) - (f' dx - \beta f' dz)) \\ &= \beta(dg - df) \end{aligned}$$

since

$$\begin{aligned} df &= \frac{\partial f}{\partial x} dx + \frac{\partial f}{\partial z} dz = f' dx - \beta f' dz \\ dg &= \frac{\partial g}{\partial x} dx + \frac{\partial g}{\partial z} dz = g' dx + \beta g' dz \end{aligned}$$

Hence,

$$dz = \frac{\beta}{V_\infty} (dg - df)$$

Integrating, we get the result

$$\boxed{z = \frac{\beta}{V_\infty} (g - f) + \text{constant}} \quad (7.9)$$

This is the general solution of supersonic flow. Once the geometry is known, Eq. (7.9) gives  $g$  and  $f$  and then from Eq. (7.8)  $C_p$  and hence the lift and drag can be calculated. Therefore, in any problem if we are not interested in the geometry of the body present, then it is not necessary to find  $f$  and  $g$ . It is sufficient if  $f'$  and  $g'$  are found, to get the  $C_p$ , which is very much simpler.

### Example 7.1

The upper and lower surfaces of a symmetrical two-dimensional airfoil are given by  $z = \pm \epsilon x(1 - x/c)^2$ , where  $c$  is the chord and  $\epsilon \ll 1$ . The airfoil is at zero incidence in a steady supersonic stream of Mach number  $M_\infty$  in positive  $x$ -direction. (a) Find the velocity components according to the linear theory in the upper region of disturbance. (b) Show that the drag coefficient of the airfoil is given by

$$C_D = \frac{8}{15} \frac{\epsilon^2}{\sqrt{M_\infty^2 - 1}}$$

**Solution:**

(a)

$$z = \pm \epsilon x(1 - x/c)^2 \quad (i)$$

The governing equation is

$$\begin{aligned} \beta^2 \frac{\partial^2 \phi}{\partial x^2} - \frac{\partial^2 \phi}{\partial z^2} &= 0 \\ \phi(x, z) &= f(x - \beta z) \quad \text{for } z > 0 \quad (\text{that is above the airfoil}) \end{aligned}$$

where  $\beta = \sqrt{M_\infty^2 - 1}$ . On the upper surface, the boundary condition is

$$\left( \frac{\partial \phi}{\partial z} \right)_{z=0} = -\beta f'(x) \equiv U \left( \frac{dz}{dx} \right)_{z=0}$$

With Eq. (i) the boundary condition becomes

$$\left(\frac{\partial \phi}{\partial z}\right)_{z=0} \equiv U\epsilon \left(1 - 4\frac{x}{c} + 3\left(\frac{x}{c}\right)^2\right)$$

Therefore,

$$\begin{aligned} f'(x) &= -\frac{U}{\beta}\epsilon \left(1 - 4\frac{x}{c} + 3\left(\frac{x}{c}\right)^2\right) \\ \phi_x &= f'(x - \beta z) = -\frac{U}{\beta}\epsilon \left(1 - \frac{4}{c}(x - \beta z) + \frac{3}{c^2}(x - \beta z)^2\right) \\ \phi_z &= -\beta f'(x - \beta z) = U\epsilon \left(1 - \frac{4}{c}(x - \beta z) + \frac{3}{c^2}(x - \beta z)^2\right) \end{aligned}$$

(b)

$$\begin{aligned} C_D &= \frac{2}{\beta c} \int_0^c (\lambda_u^2 + \lambda_l^2) dx = \frac{4}{\beta c} \int_0^c \lambda_t^2 dx \\ \lambda_t &= \frac{dz}{dx} = \epsilon \left(1 - 4\frac{x}{c} + 3\left(\frac{x}{c}\right)^2\right) \end{aligned}$$

Substituting  $\lambda_t^2$  in the equation for  $C_D$  and simplifying, we get

$$C_D = \frac{8}{15} \frac{\epsilon^2}{(\sqrt{M_\infty^2 - 1})}$$

## 7.3 Flow over a Wave-Shaped Wall

Consider a uniform flow of velocity  $V_\infty$  over a two-dimensional wave-shaped wall, as shown in Figure 7.4, with wavelength  $L$  and amplitude  $h$ .

Let the wall shape be defined by the equation

$$z_w = h \sin(\lambda x) \quad (7.10)$$

In Eq. (7.10), subscript  $w$  stands for wall and  $\lambda = 2\pi/L$ . Let us assume  $h \ll L$ , so that linear theory can be applied. By kinematic flow condition, Eq (5.43), for  $z \rightarrow 0$ , we have

$$\frac{w}{V_\infty} = \frac{dz_w}{dx} = h\lambda \cos(\lambda x) \quad (7.11)$$

Now, with this background, let us try to solve the governing equation for incompressible flow, compressible subsonic flow and supersonic flow.

### 7.3.1 Incompressible Flow

The governing equation for incompressible flow is the Laplace equation

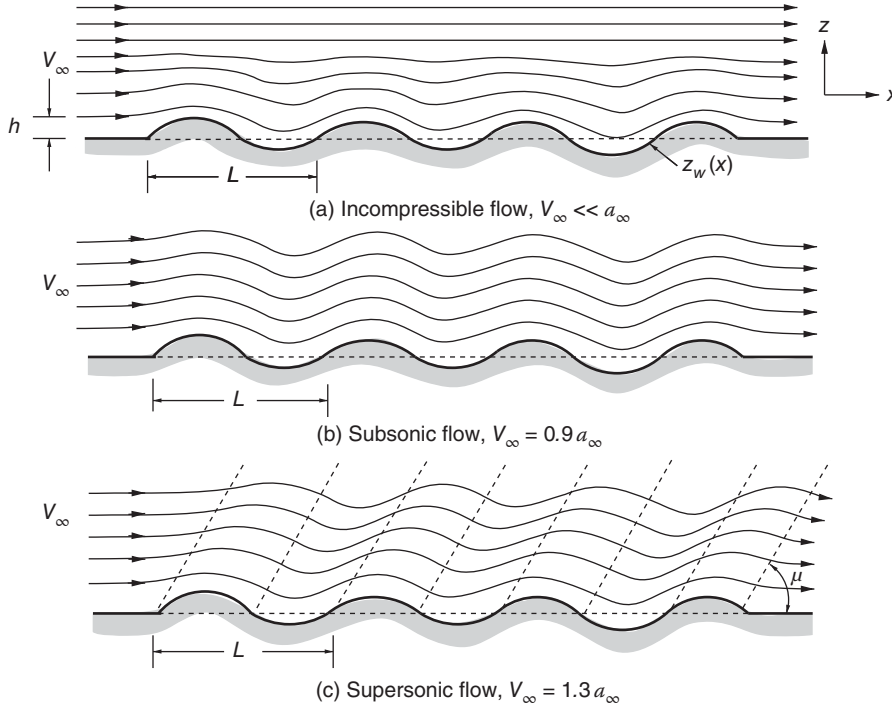
$$\phi_{xx} + \phi_{zz} = 0$$

This can be solved by expressing the potential function as

$$\phi(x, z) = F(x)G(z)$$

Solving by separation of variables, we get

$$\phi(x, z) = -V_\infty h e^{-\lambda z} \cos(\lambda x) \quad (7.12)$$



**Figure 7.4** Flow past a wave-shaped wall.

where this is only the perturbation potential. Obtaining the expression for  $\phi$ , given by Eq. (7.12), is left as an exercise for the reader.

Using Eq. (7.12), we can easily get the resultant velocity  $U$  and perturbation velocity  $w$  as

$$U = V_\infty + u = V_\infty (1 + h\lambda e^{-\lambda z} \sin(\lambda x)) \quad (7.13a)$$

$$w = V_\infty h\lambda e^{-\lambda z} \cos(\lambda x) \quad (7.13b)$$

### 7.3.2 Compressible Subsonic Flow

The governing equation for this flow is

$$(1 - M_\infty^2)\phi_{xx} + \phi_{zz} = 0$$

Solving as before, we get the result

$$\phi(x, z) = -\frac{V_\infty h}{\sqrt{1 - M_\infty^2}} \exp\left(-\lambda z \sqrt{1 - M_\infty^2}\right) \cos(\lambda x) \quad (7.14)$$

Hence, we have

$$U = V_\infty + u = V_\infty \left(1 + \frac{h\lambda}{\sqrt{1 - M_\infty^2}} \exp\left(-\lambda z \sqrt{1 - M_\infty^2}\right) \sin(\lambda x)\right) \quad (7.15a)$$

$$w = V_\infty h\lambda \exp\left(-\lambda z \sqrt{1 - M_\infty^2}\right) \cos(\lambda x) \quad (7.15b)$$

### 7.3.3 Supersonic Flow

For supersonic flow the governing potential equation is

$$(M_\infty^2 - 1)\phi_{xx} - \phi_{zz} = 0 \quad (7.16)$$

For this equation, by Eq. (7.5), we have the solution as

$$\phi(x, z) = f(x - \beta z) + g(x + \beta z)$$

where  $\beta = \cot \mu = \sqrt{1 - M_\infty^2}$ .

From the geometry of the problem under consideration, since the disturbances can move only in the direction of flow, there can only be left-running Mach lines, as shown in Figure 7.4c. Therefore,

$$\phi(x, z) = f(x - \beta z), g = 0$$

Hence, the perturbation velocity  $w$  on the wall is

$$w_w = \left( \frac{\partial \phi}{\partial z} \right)_{z=0} = -\beta(f'(x - \beta z))_{z=0} = -\beta f'(x)$$

Equating this to  $w$  given by Eq. (7.11), we get

$$\begin{aligned} f'(x) &= -\frac{V_\infty}{\beta} \lambda h \cos(\lambda x) \\ f(x) &= -\frac{V_\infty h \sin(\lambda x)}{\beta} \end{aligned}$$

This is only on the wall. In general,

$$\begin{aligned} \phi(x, z) &= f(x - \beta z) \\ \phi(x, z) &= -\frac{V_\infty}{\beta} h \sin(\lambda(x - \beta z)) \end{aligned} \quad (7.17)$$

that is

$$\phi(x, z) = -\frac{V_\infty h}{\sqrt{M_\infty^2 - 1}} \sin \left( \lambda \left( x - \sqrt{M_\infty^2 - 1} z \right) \right) \quad (7.18)$$

Therefore,

$$U = V_\infty + u = V_\infty \left( 1 - \frac{h\lambda}{\sqrt{M_\infty^2 - 1}} \right) \cos \left( \lambda \left( x - \sqrt{M_\infty^2 - 1} z \right) \right) \quad (7.19a)$$

$$w = V_\infty h \lambda \cos \left( \lambda \left( x - \sqrt{M_\infty^2 - 1} z \right) \right) \quad (7.19b)$$

The  $\phi$  here is only the disturbance potential, and if the total potential is required, add  $(V_\infty x)$  to  $\phi$ .

### 7.3.4 Pressure Coefficient

The fundamental form of expression for the coefficient of pressure applicable to two-dimensional compressible flow, with the frame of small perturbations, given by Eq. (5.48b), is

$$C_p = -2 \frac{u}{V_\infty}$$

Therefore, in the present problem:



1.  $C_p = -2h\lambda e^{-\lambda z} \sin(\lambda x)$  for incompressible flow
2.  $C_p = -\frac{2h\lambda}{\sqrt{1-M_\infty^2}} \exp\left(-\lambda z \sqrt{1-M_\infty^2}\right) \sin(\lambda x)$  for subsonic compressible flow
3.  $C_p = \frac{2h\lambda}{\sqrt{M_\infty^2-1}} \cos\left(\lambda\left(x - \sqrt{M_\infty^2-1} z\right)\right)$  for supersonic flow

On the surface of the wall ( $z=0$ ) and the above results reduce to

$$C_p = -2h\lambda \sin(\lambda x) \quad \text{for incompressible flow} \quad (7.20)$$

$$C_p = -\frac{2h\lambda}{\sqrt{1-M_\infty^2}} \sin(\lambda x) \quad \text{for subsonic flow} \quad (7.21)$$

$$C_p = \frac{2h\lambda}{\sqrt{M_\infty^2-1}} \cos(\lambda x) \quad \text{for supersonic flow} \quad (7.22)$$

In the above solution we did not get  $f$  directly. The results are obtained from  $f'$ . If only  $C_p$  on the wall is needed, it is not necessary to find  $f$ , since the  $C_p$  on the wall is given by Eq. (7.8).

$$C_p = -\frac{2}{V_\infty}(f' + g')$$

Usually, for aerodynamic applications, only  $C_p$  on the wall is necessary.

From the plots of incompressible, compressible subsonic, and supersonic flow over a wave-shaped wall, shown in Figure 7.4, the following observations can be made.

- For  $M_\infty = 0$ , the disturbances die down rapidly because of the  $e^{-\lambda z}$  term in the  $C_p$  expression.
- For  $M_\infty < 1$ , the larger the  $M_\infty$ , the slower is the dying down of disturbances in the direction perpendicular to the wall.
- For  $M_\infty = 1$ , the disturbances do not die down at all (of course the equations derived in this chapter cannot be used for transonic flows).
- For  $M_\infty > 1$ , the disturbances do not die down at all. The disturbance can be felt even at  $\infty$  (far away from the wall) if the flow is inviscid.

Further, for equal perturbations, we have

$$x - z\sqrt{M_\infty^2 - 1} = \text{constant}$$

As  $z \rightarrow \infty$ ,

- for  $M_\infty < 1$ , the disturbances vanish
- for  $M_\infty > 1$ , the disturbances are finite and they do not die down at all.

Equation (7.21) is symmetric with respect to wall geometry and Eq. (7.22) is asymmetric with respect to wall geometry. Therefore, when  $C_p$  is integrated along  $x$ , for  $M_\infty < 1$ , the integral goes to zero and for  $M_\infty > 1$ , the integral  $> 0$ . In other words, in subsonic flow, the pressure coefficient is in phase with the wall shape so that there is no drag force on the wall, but in supersonic flow, the pressure coefficient is out of phase with the wall shape and hence there is drag force acting on the wall.

## 7.4 Summary

In this chapter, the governing equation for compressible flow, derived with small perturbation assumption, has been solved for the specific flow situation of flow past a wave-shaped wall, highlighting the importance of Mach number in compressible flow analysis.

The governing equation for compressible flow, within the frame of small perturbation, is

$$(1 - M_\infty^2)\phi_{xx} + \phi_{zz} = 0$$

This equation is elliptic for  $M_\infty < 1$  and hyperbolic for  $M_\infty > 1$ .

For  $M_\infty > 1$ , Eq. (7.1) is similar to the wave equation. The general solution can be written as

$$\phi(x, z) = f(z - x \tan \mu) + g(z + x \tan \mu)$$

where  $f$  and  $g$  are arbitrary functions and  $\mu$  is the Mach angle.

It can be inferred from Eq. (7.2) that the velocity potential  $\phi$ , and hence all the flow properties, is constant along the straight lines given by the equation

$$z = \pm x \tan \mu + \text{constant}$$

This equation gives the left-running and right-running characteristics.

The general solution for supersonic flow is given by

$$z = \frac{\beta}{V_\infty}(g - f) + \text{constant}$$

Once the geometry is known, Eq. (7.9) gives  $f$  and  $g$ , and then from Eq. (7.8),  $C_p$  and hence the lift and drag can be calculated.

For flow along a wave-shaped wall, the solutions are the following.

- For incompressible flow the perturbation potential is

$$\phi(x, z) = -V_\infty h e^{-\lambda z} \cos(\lambda x)$$

- For compressible subsonic flow,

$$\phi(x, z) = -\frac{V_\infty h}{\sqrt{1 - M_\infty^2}} \exp\left(-\lambda z \sqrt{1 - M_\infty^2}\right) \cos(\lambda x)$$

- For supersonic flow,

$$\phi(x, z) = -\frac{V_\infty h}{\sqrt{M_\infty^2 - 1}} \sin\left(\lambda \left(x - \sqrt{M_\infty^2 - 1} z\right)\right)$$

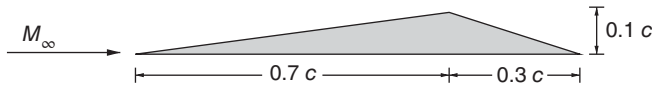
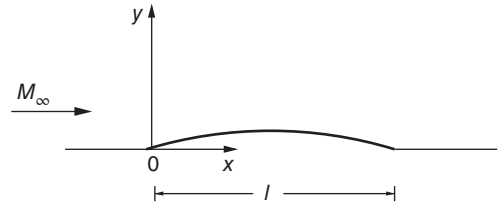
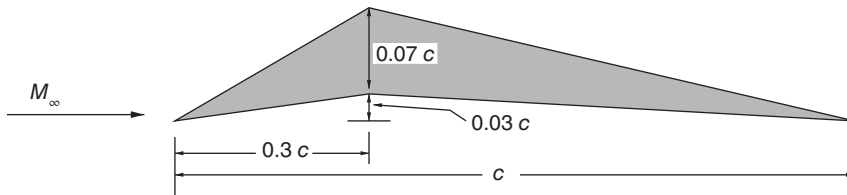
In subsonic flow, the pressure coefficient is in phase with the wall shape, and so there is no drag force on the wall. But in supersonic flow, the pressure coefficient is out of phase with the wall and therefore there is drag force acting on the wall.

## Exercise Problems

- 7.1** A shallow irregularity of length  $l$ , in a plane wall, shown in Figure 7.5, is given by the expression  $y = kx(1 - x/l)$ , where  $0 < x < l$  and  $k \ll 1$ . A uniform supersonic stream with freestream Mach number  $M_\infty$  is flowing over it. Using linearized theory, show that the velocity potential due to disturbance in the flow is

$$\phi(x, y) = -\frac{U_\infty}{\beta} k(x - \beta y) \left(1 - \frac{x - \beta y}{l}\right)$$

where  $\beta = \sqrt{M_\infty^2 - 1}$ .

**Figure 7.5** A shallow irregularity in a plane wall.**Figure 7.6** A two-dimensional wing profile.**Figure 7.7** A two-dimensional thin airfoil.

- 7.2** A two-dimensional wing profile, shown in Figure 7.6, is placed in a Mach 2.5 air stream at an incidence of  $2^\circ$ . Using linearized theory, calculate the lift coefficient  $C_L$  and the drag coefficient  $C_D$ .  
[Answer: 0.06096 and 0.04372]
- 7.3** A two-dimensional thin airfoil, shown in Figure 7.7, is placed in a Mach 3.0 air stream at an angle of attack of  $2^\circ$ . Using linearized theory, estimate  $C_{pu}$  and  $C_{pl}$ .  
[Answer:  $C_{pu} = 0.211$ ,  $C_{pl} = 0.046$  ( $0 \leq x \leq 0.3c$ );  $C_{pu} = -0.1258$ ,  $C_{pl} = -0.0551$  ( $0.3c \leq x \leq c$ )]

## 8

## Flow with Friction and Heat Transfer

### 8.1 Introduction

So far, we have discussed the compressible flow of gases in ducts, where changes in flow properties were brought about solely by area change, that is where effects of viscosity are neglected. But, in a real flow situation, like stationary power plants, aircraft propulsion engines, high vacuum technology, transport of natural gas in long pipelines, transport of fluids in chemical process plants, and various types of flow systems, the high-speed flow travels through passages of sufficient length that the effects of viscosity (friction) cannot be neglected. In many practical flow situations, friction may even have a decisive effect on the resultant flow characteristics. The inclusion of friction terms in the equations of motion makes the analysis of the problem far more complex.

Like area-change and friction, energy effects such as external heat exchange, combustion, or moisture condensation can also produce continuous changes in the state of a flowing stream. Here in our discussion of the energy effect, we will consider processes involving change in the stagnation temperature or the stagnation enthalpy of a gas stream that flows at constant area and without frictional effects. Though a process involving simple  $T_0$  change is difficult to achieve in practice, many useful conclusions of practical significance may be drawn by analyzing the process of simple  $T_0$  change. Flow where the energy effect is the sole cause of a change of state is termed *Rayleigh flow*.

In this chapter, we intend to discuss flows with friction alone and simple  $T_0$  change alone as the primary factors causing change of states from a simple one-dimensional point of view.

### 8.2 Flow in Constant Area Duct with Friction

Consider the one-dimensional steady flow of a perfect gas, with constant specific heats, through a constant-area duct. Also, let there be neither external heat exchange nor external shaft work and assume that differences in elevation produce negligible changes as compared with frictional effects. The flow with the above-mentioned conditions, namely *adiabatic flow with no external work*, is called *Fanno line flow*.

Let the wall friction (due to viscosity) be the chief factor bringing about changes in fluid properties, for the adiabatic compressible flow through ducts of constant area under consideration.

The energy equation of steady flow under the above assumptions may be written, from Eq. (1.39), as

$$h + \frac{V^2}{2} = h_0 \quad (8.1)$$

where  $h$  and  $V$  are respectively the corresponding values of the enthalpy and velocity at an arbitrary section of the duct and  $h_0$  (the stagnation enthalpy) has a constant value for all sections of the duct.

By equation of continuity,

$$\frac{\dot{m}}{A} = \rho V = G \quad (8.2)$$

where  $\rho$  is the density at the section where  $V$  and  $h$  are measured and  $G$  is called the *mass velocity*, which has a constant value for all sections of the duct.

Combining Eqs. (7.1) and (7.2), we get the equation of the Fanno line in terms of the enthalpy and density as

$$h = h_0 - \frac{G^2}{2\rho^2} \quad (8.3)$$

Because  $h_0$  and  $G$  are constants for a given flow, Eq. (8.3) defines a relation between the local density and the local enthalpy. This relation defines families of curves (the particular curve depending on the choice of the parameters  $G$  and  $h_0$ ) in the plane of any two thermodynamic variables. In Figure 8.1, this relation is shown graphically in the  $h$ - $v$  plane, for a single value of  $h_0$  and for several values of  $G$ . Such curves are, in general, called *Fanno lines*.

### 8.2.1 The Fanno Line

For a pure substance,

$$s = s(h, \rho)$$

That is, the entropy is determined by the enthalpy and the density. The curves of Figure 8.1 may thus be transferred to the enthalpy–entropy diagram, giving the familiar *Fanno curves* of Figure 8.2. For all substances so far investigated, the Fanno curves have the same general shape. The three curves shown in Figure 8.2 have the same stagnation enthalpy but different mass flow rates per unit area.

We know by the second law of thermodynamics that for an adiabatic flow the entropy may increase but cannot decrease. Thus, in Figure 8.2, the path of states along any one of the Fanno curves must be toward the right. Therefore, if the flow at some point in the duct is subsonic (point  $a$  of Figure 8.2), the effect of friction will be to increase the velocity and Mach number and to decrease the enthalpy and pressure of the stream. On the other hand, if the flow is initially supersonic (point  $b$ ), the effect of friction will be to decrease the velocity and Mach number and to increase the enthalpy and pressure of the stream. A subsonic flow may therefore never

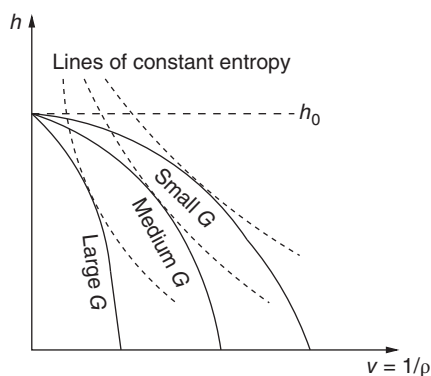
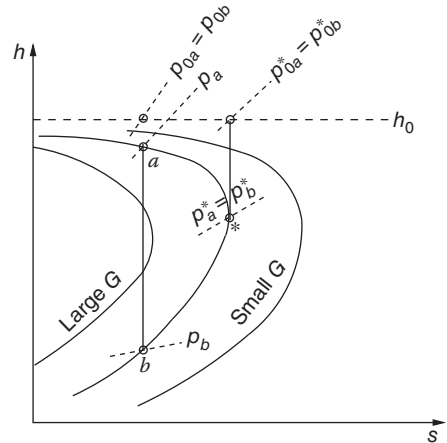


Figure 8.1 Fanno lines on an  $h$ - $v$  plane.

**Figure 8.2** Fanno lines on an  $h$ - $s$  diagram.

become supersonic and a supersonic flow may never become subsonic, unless a discontinuity is present. Thus, we observe that, as in the case of isentropic flow, the qualitative character of the flow is markedly influenced by the flow speed, that is whether it is subsonic or supersonic.

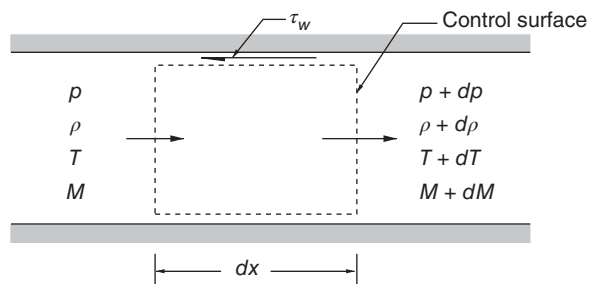
The limiting pressure, beyond which the entropy would decrease, occurs at Mach number unity and is denoted by  $p^*$ . The asterisk here denotes the state where  $M = 1$ , for the particular case of adiabatic flow through ducts of constant area.

From Figure 8.2 it can be seen that the isentropic stagnation pressure is reduced as a result of friction, irrespective of whether the flow is subsonic or supersonic.

### 8.3 Adiabatic, Constant-Area Flow of a Perfect Gas

In this section, the fluid is assumed to be perfect so as to make the analytical treatment of the problem simpler. Further, with this assumption, it becomes possible to draw broad conclusions which would not be otherwise apparent. The aim here is to express the variations in flow characteristics along the length of a duct of constant area in analytical form. This requires the introduction of the momentum equation, with a term accounting for the frictional forces acting on the control volume, since the rate of change of flow properties depends on the amount of friction. In Chapter 1, the isentropic relations were derived by writing the various physical relations for two sections a finite distance apart. To demonstrate another method of approach, let us carry out the present analysis in differential form.

Select an infinitesimal control volume, as shown in Figure 8.3. In the figure,  $\tau_w$  is the shear stress due to friction acting on the wall of the duct.

**Figure 8.3** Control surface for analysis of adiabatic, constant-area flow.

For a perfect gas,

$$p = \rho RT$$

This may also be expressed as

$$\frac{dp}{p} = \frac{d\rho}{\rho} + \frac{dT}{T} \quad (8.4)$$

By definition of the Mach number,

$$M^2 = \frac{V^2}{\gamma RT}$$

This gives

$$\frac{dM^2}{M^2} = \frac{dV^2}{V^2} - \frac{dT}{T} \quad (8.5)$$

The energy equation for a perfect gas gives

$$c_p dT + d\left(\frac{V^2}{2}\right) = 0$$

Dividing throughout by  $c_p T$  and using the definition of Mach number, we get

$$\frac{dT}{T} + \frac{\gamma - 1}{2} M^2 \frac{dV^2}{V^2} = 0 \quad (8.6)$$

The continuity equation, Eq. (8.2), is

$$G = \frac{\dot{m}}{A} = \rho V$$

Noting that  $G$  is a constant, this equation can be expressed as

$$\frac{d\rho}{\rho} + \frac{1}{2} \frac{dV^2}{V^2} = 0 \quad (8.7)$$

Referring to Figure 8.3, the momentum balance gives

$$-A dp - \tau_w dA_w = \dot{m} dV$$

where  $A$  is the cross-sectional area of duct and  $dA_w$  is the wetted wall surface area of the duct over which the shear stress  $\tau_w$  acts.

### 8.3.1 Definition of Friction Coefficient

The *coefficient of drag*, or the *coefficient of friction*, as it is generally referred to for flow in ducts, is defined as

$$f \equiv \frac{\text{Wall shear stress}}{\text{Dynamic pressure head of the stream}}$$

$$f \equiv \frac{\tau_w}{\frac{1}{2} \rho V^2}$$

It is common practice in such analysis to use a parameter called *hydraulic diameter*  $D$ , defined as

$$D \equiv \frac{4(\text{cross-sectional area})}{\text{wetted perimeter}}$$

$$D \equiv \frac{4A}{\left(\frac{dA_w}{dx}\right)} = 4 \frac{A}{dA_w} dx$$

The advantage of using hydraulic diameter is that the equations in terms of hydraulic diameter are valid even for ducts with noncircular cross-section.

Introducing the above  $f$  and  $D$  along with the continuity equation into the momentum equation, we get

$$-dp - 4f \frac{\rho V^2}{2} \frac{dx}{D} = \frac{\dot{m}}{A} dV = \rho V^2 \frac{dV}{V}$$

Dividing throughout by  $p$  and expressing  $\rho V^2$  as  $\gamma p M^2$ , we obtain

$$\frac{dp}{p} + \frac{\gamma M^2}{2} 4f \frac{dx}{D} + \frac{\gamma M^2}{2} \frac{dV^2}{V^2} = 0 \quad (8.8)$$

The isentropic stagnation pressure  $p_0$  is given by Eq. (1.73) as

$$p_0 = p \left( 1 + \frac{\gamma - 1}{2} M^2 \right)^{\gamma/(\gamma-1)}$$

that is

$$\frac{dp_0}{p_0} = \frac{dp}{p} + \frac{\gamma M^2/2}{1 + \frac{\gamma-1}{2} M^2} \frac{dM^2}{M^2} \quad (8.9)$$

Now, we may define a new parameter called *impulse function*  $F$  as

$$F \equiv pA + \rho AV^2 = pA(1 + \gamma M^2)$$

After noting that  $A$  is a constant, this may be expressed in differential form in terms of  $p$  and  $M$ , as

$$\frac{dF}{F} = \frac{dp}{p} + \frac{\gamma M^2}{1 + \gamma M^2} \frac{dM^2}{M^2} \quad (8.10)$$

### 8.3.2 Effects of Wall Friction on Fluid Properties

Now we see that the simultaneous algebraic Eqs. (8.4)–(8.10) relate eight differential variables:

$$\frac{dp}{p}, \quad \frac{d\rho}{\rho}, \quad \frac{dT}{T}, \quad \frac{dM^2}{M^2}, \quad \frac{dV^2}{V^2}, \quad \frac{dp_0}{p_0}, \quad \frac{dF}{F}, \quad \frac{4f dx}{D}$$

The physical phenomenon causing changes in flow properties is the *viscous friction*. Hence, we choose the variable  $4f dx/D$  as independent. Now, solving the seven equations as simultaneous equations for the remaining seven variables, we can obtain

$$\frac{dM^2}{M^2} = \frac{\gamma M^2 \left( 1 + \frac{\gamma - 1}{2} M^2 \right)}{1 - M^2} 4f \frac{dx}{D} \quad (8.11)$$

$$\frac{dp}{p} = -\frac{\gamma M^2 (1 + (\gamma - 1) M^2)}{2(1 - M^2)} 4f \frac{dx}{D} \quad (8.12)$$

$$\frac{dV}{V} = \frac{\gamma M^2}{2(1 - M^2)} 4f \frac{dx}{D} \quad (8.13)$$

$$\frac{dT}{T} = \frac{1}{2} \frac{da}{a} = -\frac{\gamma(\gamma - 1) M^4}{2(1 - M^2)} 4f \frac{dx}{D} \quad (8.14)$$



$$\frac{d\rho}{\rho} = -\frac{\gamma M^2}{2(1-M^2)} 4f \frac{dx}{D} \quad (8.15)$$

$$\frac{dp_0}{p_0} = -\frac{\gamma M^2}{2} 4f \frac{dx}{D} \quad (8.16)$$

$$\frac{dF}{F} = -\frac{\gamma M^2}{2(1-\gamma M^2)} 4f \frac{dx}{D} \quad (8.17)$$

### 8.3.3 Second Law of Thermodynamics

For an adiabatic flow, the stagnation temperature is invariant. Therefore, from Eq. (1.57), the entropy change can be expressed as

$$\frac{ds}{c_p} = -\frac{\gamma-1}{\gamma} \frac{dp_0}{p_0} \quad (8.18)$$

Substituting for  $dp_0/p_0$ , from Eq. (8.16), we have

$$\frac{ds}{c_p} = \frac{(\gamma-1)M^2}{2} 4f \frac{dx}{D} \quad (8.19)$$

The second law of thermodynamics states that the entropy should not decrease in an adiabatic flow process. Therefore, from Eq. (8.19), it follows that the friction coefficient  $f$  must always be a positive quantity, since by convention  $dx$  in Eq. (8.19) is positive in the direction of flow.

In Figure 8.3 we have marked the shear stress in a direction opposite to that of the flow. Since  $f$  must always be positive, we conclude that the shear stress must always act in a direction opposite to the flow, as marked in the figure.

From Eqs. (8.11)–(8.17), for flow parameters in terms of friction coefficient  $f$ , it may be summarized as follows.

For *subsonic inlet flow*, the effect of friction on the downstream flow is such that:

- Pressure  $p$  decreases
- Mach number  $M$  increases
- Velocity  $V$  increases
- Temperature  $T$  decreases
- Density  $\rho$  decreases
- Stagnation pressure  $p_0$  decreases
- Impulse function  $F$  decreases.

For *supersonic inlet flow*, the effect of friction on the downstream flow is such that:

- Pressure  $p$  increases
- Mach number  $M$  decreases
- Velocity  $V$  decreases
- Temperature  $T$  increases
- Density  $\rho$  increases
- Stagnation pressure  $p_0$  decreases
- Impulse function  $F$  decreases.

From the above summary we may observe that the friction has the net effect of accelerating a subsonic stream and causes a rise in static pressure at supersonic speeds.

### 8.3.4 Working Relations

Equations (8.11)–(8.19) can be integrated to result in formulae suitable for practical calculations. Let the Mach number be the independent variable for this purpose. Then Eq. (8.11) may be rearranged to give

$$\int_0^{L_{\max}} 4f \frac{dx}{D} = \int_{M^2}^1 \frac{1 - M^2}{\gamma M^4 \left(1 + \frac{\gamma - 1}{2} M^2\right)} dM^2$$

where the integration limits are taken as the section where the Mach number is  $M$  and where  $x$  is arbitrarily set equal to zero, and as the section where Mach number is unity and  $x$  is the maximum possible length of duct,  $L_{\max}$ .

On integration, the above equation yields

$$4\bar{f} \frac{L_{\max}}{D} = \frac{1 - M^2}{\gamma M^2} + \frac{\gamma + 1}{2\gamma} \ln \left[ \frac{(\gamma + 1)M^2}{2 \left(1 + \frac{\gamma - 1}{2} M^2\right)} \right] \quad (8.20)$$

where  $\bar{f}$  is the mean friction coefficient with respect to duct length defined by

$$\bar{f} = \frac{1}{L_{\max}} \int_0^{L_{\max}} f dx$$

Equation (8.20) gives the maximum value of  $4\bar{f}(L/D)$  corresponding to any initial Mach number  $M$ .

Because  $4\bar{f}(L_{\max}/D)$  is a function only of  $M$ , the duct length required for the flow to pass from a given initial Mach number  $M_1$  to a given final Mach number  $M_2$  is obtained from the expression

$$4\bar{f} \frac{L}{D} = \left(4\bar{f} \frac{L_{\max}}{D}\right)_{M_1} - \left(4\bar{f} \frac{L_{\max}}{D}\right)_{M_2} \quad (8.21)$$

Similarly, the local flow properties can be found in terms of local Mach number. Indicating the properties at  $M = 1$  as superscripted with asterisk and integrating between the duct sections with Mach number  $M$  and 1, we obtain, from Eqs. (8.12)–(8.17) and (8.19):

$$\frac{p}{p^*} = \frac{1}{M} \left[ \frac{\gamma + 1}{2 \left(1 + \frac{\gamma - 1}{2} M^2\right)} \right]^{1/2} \quad (8.22)$$

$$\frac{V}{V^*} = M \left[ \frac{\gamma + 1}{2 \left(1 + \frac{\gamma - 1}{2} M^2\right)} \right]^{1/2} \quad (8.23)$$

$$\frac{T}{T^*} = \frac{a^2}{a^{*2}} = \frac{\gamma + 1}{2 \left(1 + \frac{\gamma - 1}{2} M^2\right)} \quad (8.24)$$

$$\frac{\rho}{\rho^*} = \frac{V^*}{V} = \frac{1}{M} \left[ \frac{2 \left( 1 + \frac{\gamma-1}{2} M^2 \right)}{\gamma+1} \right]^{1/2} \quad (8.25)$$

$$\frac{p_0}{p_0^*} = \frac{1}{M} \left[ \frac{2 \left( 1 + \frac{\gamma-1}{2} M^2 \right)}{\gamma+1} \right]^{(\gamma+1)/2(\gamma-1)} \quad (8.26)$$

$$\frac{F}{F^*} = \frac{1 + \gamma M^2}{M \left[ 2(\gamma+1) \left( 1 + \frac{\gamma-1}{2} M^2 \right) \right]^{1/2}} \quad (8.27)$$

$$\frac{s-s^*}{c_p} = \ln M^2 \left[ \frac{(\gamma+1)}{2M^2 \left( 1 + \frac{\gamma-1}{2} M^2 \right)} \right]^{(\gamma+1)/(2\gamma)} \quad (8.28)$$

We know that the quantities marked with an asterisk in these equations are constants for a given adiabatic constant-area flow. Therefore, they may be regarded as convenient reference values for normalizing the equations. To find the change in a flow property, say the density, between sections of the duct where the Mach numbers are  $M_1$  and  $M_2$ , we set

$$\frac{\rho_2}{\rho_1} = \frac{\left( \frac{\rho}{\rho^*} \right)_{M_2}}{\left( \frac{\rho}{\rho^*} \right)_{M_1}}$$

where  $\left( \frac{\rho}{\rho^*} \right)_{M_1}$  is the value on the right-hand side of Eq. (8.25) corresponding to  $M_1$  and so on.

The variation of dimensionless ratios given by Eqs. (8.20) and (8.22)–(8.27) with Mach number is tabulated in Table A.4 in the Appendix.

### Example 8.1

Atmospheric air at 101.35 kPa and 300 K is drawn through a frictionless bell-mouth entrance into a 3 m long tube having a 0.05 m diameter. The average friction coefficient  $\bar{f} = 0.005$  for the tube. The system is perfectly insulated. (a) Find the maximum mass flow rate and the range of backpressure that will produce this flow. (b) What is the exit pressure required to produce 90% of the maximum mass flow rate and what will be the stagnation pressure and the velocity at the exit for that mass flow rate?

### Solution:

(a) The mass flow rate will be maximum for choked flow conditions.

For choked flow,

$$4\bar{f} \frac{L_{\max}}{D} = \frac{4 \times 0.005 \times 3}{0.05} = 1.2$$

For  $4\bar{f}\frac{L_{\max}}{D} = 1.2$ , from the Fanno flow table (Table A.4),

$$M_1 = 0.485, \quad \frac{p_1}{p^*} = 2.2076, \quad \frac{T_1}{T^*} = 1.146$$

From the isentropic table (Table A.1) for  $M_1 = 0.485$ ,

$$\frac{p_1}{p_0} = 0.851, \quad \frac{T_1}{T_0} = 0.955$$

Therefore,

$$p_1 = (0.851)(101.35) = 86.25 \text{ kPa}$$

$$T_1 = (0.955)(300) = 286.5 \text{ K}$$

$$p^* = \frac{p_1}{2.2076} = 39.07 \text{ kPa}$$

$$T^* = \frac{T_1}{1.146} = 250 \text{ K}$$

$$\rho^* = \frac{p^*}{RT^*} = 0.544 \text{ kg m}^{-3}$$

$$a^* = \sqrt{\gamma RT^*} = \sqrt{1.4 \times 287 \times 250} \\ = 316.94 \text{ m s}^{-1}$$

The maximum flow rate is

$$\dot{m}^* = \rho^* a^* A = 0.544 \times 316.96 \times \frac{\pi}{4} (0.05)^2$$

$$\dot{m}^* = \boxed{0.3385 \text{ kg s}^{-1}}$$

The range of backpressure ( $p_b$ ) that would produce this flow is

$$\boxed{p_b \leq p^* (39.07 \text{ kPa})}$$

(b) 90% of  $\dot{m}^*$  is

$$\dot{m} = 0.9 \times 0.3385 = 0.3047 \text{ kg s}^{-1}$$

$$G = \frac{\dot{m}}{A} = 155.18 \text{ kg (s m}^2)^{-1}$$

$$\rho_1 V_1 = G = \frac{\dot{m}}{A}, \quad p_1 M_1 \sqrt{\frac{\gamma}{RT_1}} = G$$

$$\frac{p_1}{p_0} \sqrt{\frac{T_0}{T_1}} M_1 = \sqrt{\frac{R}{\gamma}} \frac{\sqrt{T_0}}{p_0} G = \frac{\sqrt{\gamma RT_0}}{\gamma} \frac{G}{p_0} \\ = \frac{\sqrt{1.4 \times 287 \times 300}}{1.4} \frac{155.16}{1.0135 \times 10^5} \\ = 0.3797$$

Solving this for  $M_1$ , by a trial and error method, we get

$$M_1 = 0.42$$

From the isentropic table, for  $M_1 = 0.42$ ,

$$\frac{p_1}{p_0} = 0.886, \quad p_1 = 89.8 \text{ kPa}$$

$$\frac{T_1}{T_0} = 0.966, \quad T_1 = 289.8 \text{ K}$$

By Eq. (8.21),

$$4\bar{f}\frac{L}{D} = 1.2 = \left(4\bar{f}\frac{L_{\max}}{D}\right)_{M_1} - \left(4\bar{f}\frac{L_{\max}}{D}\right)_{M_2}$$

Using Eq. (8.20) or the Fanno flow table, we get for  $M_1 = 0.42$ ,

$$\left(4\bar{f}\frac{L_{\max}}{D}\right)_{M_1} = 1.9744$$

Hence,

$$1.2 = 1.9744 - \left(4\bar{f}\frac{L_{\max}}{D}\right)_{M_2}$$

that is

$$\left(4\bar{f}\frac{L_{\max}}{D}\right)_{M_2} = 0.7744$$

For this value of  $4\bar{f}(L_{\max}/D)$ , from the Fanno flow table,

$$M_2 = 0.541$$

Now, using the Fanno table (Table A.4), for  $M_1 = 0.42$ ,

$$\frac{p_1}{p^*} = 2.563, \quad \frac{T_1}{T^*} = 1.159, \quad \frac{p_{01}}{p_0^*} = 1.529$$

For  $M_2 = 0.541$ ,

$$\frac{p_2}{p^*} = 1.96, \quad \frac{T_2}{T^*} = 1.134, \quad \frac{p_{02}}{p_0^*} = 1.264$$

Therefore,

$$p_2 = \frac{p_2}{p^*} \frac{p^*}{p_1} p_1$$

$$= \boxed{68.67 \text{ kPa}}$$

$$T_2 = \frac{T_2}{T^*} \frac{T^*}{T_1} T_1 = 283.5 \text{ K}$$

$$p_{02} = \frac{p_{02}}{p_0^*} \frac{p_0^*}{p_{01}} p_{01}$$

$$= \boxed{83.78 \text{ kPa}}$$

$$a_2 = \sqrt{\gamma R T_2} = 337.5 \text{ m s}^{-1}$$

The exit velocity

$$V_2 = M_2 a_2 = 0.541 \times 337.5$$

$$= \boxed{182.59 \text{ m s}^{-1}}$$

**Example 8.2**

A straight pipe of 0.05 m diameter is attached to a large air reservoir at 1.38 MPa and 310 K. The exit of the pipe is open to atmosphere. Assuming an adiabatic flow with an average friction coefficient of 0.005, calculate the pipe length necessary to obtain a mass flow rate of  $2.25 \text{ kg s}^{-1}$ .

**Solution:**

Let the subscripts 1 and 2 refer to conditions at entry and exit of the pipe, respectively. Given:

$$\dot{m} = 2.25 \text{ kg s}^{-1}$$

By Eq. (8.2), the mass velocity is

$$\begin{aligned} G &= \frac{\dot{m}}{A} = \frac{2.25}{(\pi/4)(0.05)^2} \\ &= 0.1146 \times 10^4 \text{ kg(m}^2\text{s)}^{-1} \end{aligned}$$

Also,

$$G = p_1 M_1 \left( \frac{\gamma}{RT_1} \right)^{1/2} = p_2 M_2 \left( \frac{\gamma}{RT_2} \right)^{1/2} = \text{constant}$$

Now the relation

$$p_1 M_1 \left( \frac{\gamma}{RT_1} \right)^{1/2} = G$$

can be rewritten as

$$\begin{aligned} \frac{p_1}{p_0} \left( \frac{T_0}{T_1} \right)^{1/2} M_1 &= \left( \frac{R}{\gamma} \right)^{1/2} G \frac{T_0^{1/2}}{p_0} = \frac{\sqrt{\gamma RT_0}}{\gamma} \frac{G}{p_0} \\ &= \frac{352.9}{1.4} \times \frac{0.1146 \times 10^4}{13.8 \times 10^5} \\ &= 0.209 \end{aligned} \quad (i)$$

The left-hand side of Eq. (i) has three parameters and out of them the pressure ratio and temperature ratio are uniquely related to Mach number. By trial and error, we can solve this equation as follows:

Let  $M_1 = 0.21$ . Then

$$\text{LHS} = \frac{0.21 \times 0.9697}{\sqrt{0.9913}} = 0.2045$$

$$\text{LHS} < \text{RHS}$$

Let  $M_1 = 0.22$ . Then

$$\text{LHS} = \frac{0.22 \times 0.9668}{\sqrt{0.9904}} = 0.2136$$

$$\text{LHS} > \text{RHS}$$

Hence,  $M_1$  lies between 0.21 and 0.22. For  $M_1 = 0.213$ , LHS is nearly equal to RHS. Therefore,  $M_1 = 0.213$  can be taken as the correct solution. For this value of  $M_1$ ,

$$\frac{p_1}{p_0} = 0.969, \quad \frac{p_1}{p^*} = 5.12$$

Thus,

$$p_1 = 1.337 \text{ MPa}$$

$$p^* = 261.1 \text{ kPa}$$

For  $M_1 = 0.213$ , from Eq. (8.20),

$$4f \frac{L_{\max}}{D} = 12.11$$

Therefore,

$$\begin{aligned} L_{\max} &= \frac{12.11 \times 0.05}{4 \times 0.005} \\ &= \boxed{30.275 \text{ m}} \end{aligned}$$

## 8.4 Flow with Heating or Cooling in Ducts

So far, we have considered only the effect of area change and friction on the gas flow process. From a one-dimensional aspect, there is yet another effect producing continuous changes in the state of flowing stream, and this third factor is called the *energy effect*. External heat exchange, combustion, or moisture condensation are examples of energy effects. In the discussion on the effects of area change on flow state, we considered the process to be isentropic with frictional and energy effects absent. In Section 8.2 we dealt with the effects of wall friction in the absence of area change and energy effects; the corresponding process is described by the Fanno curve and may aptly be termed *simple friction*.

In this section, we discuss processes involving change in the stagnation temperature or the stagnation enthalpy of a gas stream that flows at constant area and without frictional effects. Though a process involving simple  $T_0$  change is difficult to achieve in practice, many useful conclusions of practical significance may be drawn by analyzing the process of simple  $T_0$  change. These conclusions can be expected to have a higher degree of validity when the departures from the assumptions of the model are small.

### 8.4.1 Governing Equations

For the flow of gas through a constant-area duct without friction, the momentum equation may be written as

$$p + \rho V^2 = \frac{F}{A} = \text{constant} \quad (8.29)$$

By continuity,

$$\rho V = \frac{\dot{m}}{A} = G = \text{constant} \quad (8.30)$$

Combining Eqs. (8.29) and (8.30), we get

$$p + \frac{G^2}{\rho} = \frac{F}{A} \quad (8.31)$$

For constant values of  $G$  and  $F/A$ , Eq. (8.31) defines a unique relation between pressure and density, called the *Rayleigh line*. Since both the enthalpy  $h$  and entropy  $s$  are functions of  $p$  and  $\rho$ , Eq. (8.31) may be used for representing a Rayleigh line on the  $h-s$  diagram, as illustrated in

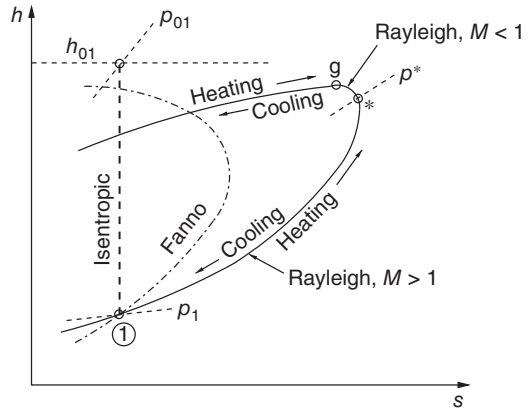
**Figure 8.4** Rayleigh curve for simple  $T_0$  change.

Figure 8.4. In general, most of the fluids in practical use have Rayleigh curves of the general form shown in Figure 8.4.

The portion of the Rayleigh curve above the point of maximum entropy usually corresponds to subsonic flow and the portion below to supersonic flow. The process of simple heating is thermodynamically reversible; therefore, heat addition should correspond to an entropy increase, and heat rejection must correspond to an entropy decrease. Therefore, the Mach number is increased by heating and decreased by cooling, at subsonic speeds. On the other hand, the Mach number is decreased by heating and increased by cooling, at supersonic speeds. Thus, like friction, heat addition also always tends to make the Mach number in the duct approach unity. Cooling always causes the Mach number to change in the direction away from unity.

For heat addition at either subsonic or supersonic speeds, the amount of heat input cannot be greater than that for which the leaving Mach number is unity. If the heat addition is too large, the flow will be *choked*, that is the initial Mach number will be reduced to a magnitude that is consistent with the specified amount of heat input.

#### 8.4.2 Simple-Heating Relations for a Perfect Gas

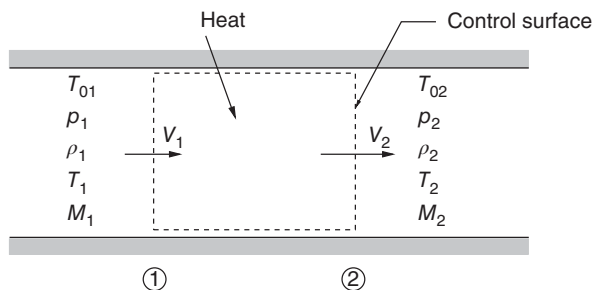
As in Section 8.3, we shall describe the flow of a perfect gas through a constant-area duct. Let there be no friction. Consider the control volume shown in Figure 8.5.

For the flow through a constant-area duct, by continuity,

$$\frac{\rho_2}{\rho_1} = \frac{V_1}{V_2} \quad (8.32)$$

The momentum balance in the absence of friction gives

$$p_1 - p_2 = \frac{\dot{m}}{A}(V_2 - V_1)$$

**Figure 8.5** Control volume for Rayleigh flow.



But  $\dot{m}/A = \rho V$  and  $\rho V^2 = \gamma p M^2$  (for perfect gas). Using these relations, the above momentum equation may be rewritten as

$$\frac{p_2}{p_1} = \frac{1 + \gamma M_1^2}{1 + \gamma M_2^2} \quad (8.33)$$

By the state equation,

$$\frac{p_2}{p_1} = \frac{\rho_2 T_2}{\rho_1 T_1} \quad (8.34)$$

The Mach number ratio between states 1 and 2 can be expressed as

$$\frac{M_2}{M_1} = \frac{V_2 a_1}{V_1 a_2} = \frac{V_2}{V_1} \sqrt{\frac{T_1}{T_2}} \quad (8.35)$$

Similarly, for impulse function,

$$\frac{F_2}{F_1} = \frac{p_2(1 + \gamma M_2^2)}{p_1(1 + \gamma M_1^2)}$$

Using, Eq. (8.33), we get

$$\frac{F_2}{F_1} = 1 \quad (8.36)$$

The isentropic stagnation pressure ratio is given by Eq. (1.73) as

$$\frac{p_{02}}{p_{01}} = \frac{p_2 \left(1 + \frac{\gamma-1}{2} M_2^2\right)^{\gamma/(\gamma-1)}}{p_1 \left(1 + \frac{\gamma-1}{2} M_1^2\right)^{\gamma/(\gamma-1)}} \quad (8.37)$$

The entropy change may be found from Eq. (1.59) as

$$\frac{s_2 - s_1}{c_p} = \ln \frac{T_2/T_1}{(p_2/p_1)^{(\gamma-1)/\gamma}} \quad (8.38)$$

So far, we have seen the relation between the parameters at two different states of the process. All these changes are brought about by changes in stagnation temperature. That is, the rate of change of stream properties along Rayleigh lines is a function of the rate of change of the stagnation temperature. From the energy relation, the stagnation temperature  $T_0$  is

$$\begin{aligned} T_0 &= T + \frac{V^2}{2c_p} = T \left(1 + \frac{V^2}{2c_p T}\right) \\ &= T \left(1 + \frac{\gamma-1}{2} M^2\right) \end{aligned}$$

Therefore,

$$\frac{T_{02}}{T_{01}} = \frac{T_2}{T_1} \frac{1 + \frac{\gamma-1}{2} M_2^2}{1 + \frac{\gamma-1}{2} M_1^2} \quad (8.39)$$

For the process involving only heat exchange, the change in stagnation temperature is a direct measure of the amount of heat transfer. If  $Q$  is the heat added to the control volume, then by the energy equation,

$$Q = c_p(T_2 - T_1) + \frac{V_2^2 - V_1^2}{2} = c_p(T_{02} - T_{01}) \quad (8.40)$$

Equations (8.32)–(8.34) may be combined to result in

$$\frac{T_2}{T_1} = \frac{M_2^2 (1 + \gamma M_1^2)^2}{M_1^2 (1 + \gamma M_2^2)^2} \quad (8.41)$$

Using Eq. (8.41) in Eq. (8.39), we get

$$\frac{T_{02}}{T_{01}} = \frac{M_2^2 (1 + \gamma M_1^2)^2 \left(1 + \frac{\gamma - 1}{2} M_2^2\right)}{M_1^2 (1 + \gamma M_2^2)^2 \left(1 + \frac{\gamma - 1}{2} M_1^2\right)} \quad (8.42)$$

Equations (8.41) and (8.42) express the static and stagnation temperature ratios between states 1 and 2 in terms of Mach numbers at these states.

Following the same procedure as that in Section 8.3, we can get the following *normalized* expressions (working formulae) for the present flow process involving only heat transfer:

$$\frac{T}{T^*} = \frac{(\gamma + 1)^2 M^2}{(1 + \gamma M^2)^2} \quad (8.43)$$

$$\frac{T_0}{T_0^*} = \frac{2(\gamma + 1)M^2 \left(1 + \frac{\gamma - 1}{2} M^2\right)}{(1 + \gamma M^2)} \quad (8.44)$$

$$\frac{V}{V^*} = \frac{\rho^*}{\rho} = \frac{(\gamma + 1)M^2}{1 + \gamma M^2} \quad (8.45)$$

$$\frac{p}{p^*} = \frac{\gamma + 1}{1 + \gamma M^2} \quad (8.46)$$

$$\frac{p_0}{p_0^*} = \frac{\gamma + 1}{1 + \gamma M^2} \left[ \frac{2 \left(1 + \frac{\gamma - 1}{2} M^2\right)}{1 + \gamma} \right]^{\gamma/(\gamma - 1)} \quad (8.47)$$

$$\frac{s - s^*}{c_p} = \ln M^2 \left( \frac{\gamma + 1}{1 + \gamma M^2} \right)^{(\gamma + 1)/\gamma} \quad (8.48)$$

Also,

$$\frac{T_{02}}{T_{01}} = \frac{(T_0/T_0^*)_{M_2}}{(T_0/T_0^*)_{M_1}} \quad (8.49)$$

where  $(T_0/T_0^*)_{M_2}$  is given by Eq. (8.44) and so on. The variation of the dimensionless ratios given by Eqs. (8.43)–(8.47) with Mach number is given in Table A.5 in the Appendix.

From our discussions on Rayleigh flow and property relations, the physical trends associated with flow with simple  $T_0$  change may be summarized as follows.

For *subsonic flow* ( $M_1 < 1$ ), when heat is added:

- Pressure decreases,  $p_2 < p_1$
- Mach number increases,  $M_2 > M_1$
- Velocity increases,  $V_2 > V_1$
- Temperature increases for  $M_1 < \gamma^{-1/2}$  and temperature decreases for  $M_1 > \gamma^{-1/2}$
- Total temperature increases,  $T_{02} > T_{01}$
- Total pressure decreases,  $p_{02} < p_{01}$ .

For *supersonic flow* ( $M_1 > 1$ ), when heat is added:

- Pressure increases,  $p_2 > p_1$
- Mach number decreases,  $M_2 < M_1$
- Velocity decreases,  $V_2 < V_1$
- Temperature increases,  $T_2 > T_1$
- Total temperature increases,  $T_{02} > T_{01}$
- Total pressure decreases,  $p_{02} < p_{01}$ .

Note that for subsonic flow when heat is added, the temperature increases for  $M_1 < \gamma^{-1/2}$  and decreases for  $M_1 > \gamma^{-1/2}$ . This is due to the fact that the value of  $T/T^*$  goes through a maximum at  $M = 1/\sqrt{\gamma}$ , corresponding to point g on Figure 8.4. In the case of air, therefore, for the values of  $M$  between 0.85 and 1, heat addition results in a decrease of stream temperature and heat rejection results in an increase of stream temperature.

### Example 8.3

Air at standard sea level conditions enters the tube shown in Figure 8.6, at Mach 0.68 and reaches a value of Mach 0.25 at the exit of the diffuser (station B). The entrance area is  $1 \text{ m}^2$ .

(a) Assuming no dissipative losses in the diffuser, show that the area at station B is  $2.16 \text{ m}^2$ . Will the area be larger or smaller if losses are present? (b) Show that, assuming no losses, the static pressure at B is  $132.2 \text{ kPa}$  and the density is  $1.48 \text{ kg m}^{-3}$ . If losses are present, will the stagnation pressure rise or fall from station A to station B? Will the stagnation density rise or fall? Give reason for your answer. (c) Heat is added at Mach 0.25 between stations B and C until thermal choking occurs. Show that the heat added is  $9.15 \times 10^5 \text{ J kg}^{-1}$  and the stagnation temperature at station C is  $1225 \text{ K}$ .

### Solution:

Given,

$$p_A = 101.33 \text{ kPa}, \quad M_A = 0.68$$

$$T_A = 288 \text{ K}, \quad M_B = 0.25$$

$$\rho_A = 1.225 \text{ kg m}^{-3}, \quad A_A = 1 \text{ m}^2$$

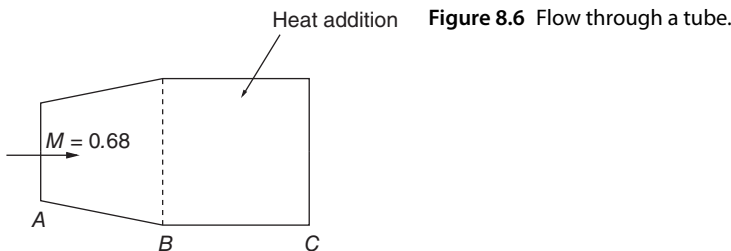


Figure 8.6 Flow through a tube.

(a) From the isentropic flow table,

$$\frac{A_A}{A^*} = 1.110 \quad \text{for } M_A = 0.68$$

$$\frac{A_B}{A^*} = 2.403 \quad \text{for } M_B = 0.25$$

Therefore,

$$\begin{aligned} A_B &= \frac{A_B}{A^*} \frac{A^*}{A_A} A_A = \frac{2.403}{1.11} \times 1 \\ &= \boxed{2.165 \text{ m}^2} \end{aligned}$$

If losses were present, the area would have been larger, since

$$\dot{m} = \frac{\Gamma}{\sqrt{\gamma R T_0}} p_0 f(M) A$$

where

$$\Gamma = \gamma \left( \frac{2}{\gamma + 1} \right)^{(\gamma+1)/2(\gamma-1)}$$

$\dot{m}$ ,  $T_0$ , and  $M$  being constants,  $p_0$  decreases with losses; hence  $A_B$  has to increase.

(b) From the isentropic table,

$$\frac{p_A}{p_0} = 0.7338, \quad \frac{\rho_A}{\rho_0} = 0.8016 \quad \text{for } M_A = 0.68$$

$$\frac{p_B}{p_0} = 0.9575, \quad \frac{\rho_B}{\rho_0} = 0.9694 \quad \text{for } M_B = 0.25$$

Therefore,

$$p_B = \frac{p_B}{p_0} \frac{p_0}{p_A} p_A = \boxed{132.2 \text{ kPa}}$$

$$\rho_B = \frac{\rho_B}{\rho_0} \frac{\rho_0}{\rho_A} \rho_A = \boxed{1.48 \text{ kg m}^{-3}}$$

$$\Delta s = R \ln \frac{p_{0A}}{p_{0B}} \quad \text{for } \Delta s > 0, \quad p_{0A} > p_{0B}$$

Hence, if losses were present, the stagnation pressure would have decreased from  $A$  to  $B$ :

$$\begin{aligned} \frac{p_{0A}}{\rho_{0A}} &= R T_{0A}, \quad \frac{p_{0B}}{\rho_{0B}} = R T_{0B} \\ \frac{\rho_{0B}}{\rho_{0A}} \frac{p_{0A}}{p_{0B}} &= 1 \quad \text{since } T_{0A} = T_{0B} \\ \frac{\rho_{0B}}{\rho_{0A}} &= \frac{p_{0B}}{p_{0A}} < 1 \end{aligned}$$

Therefore, the stagnation density falls from  $A$  to  $B$ .

(c) For  $M_A = 0.68$ , from the isentropic table, we have

$$\frac{T_A}{T_{0A}} = 0.9153$$

Hence,

$$T_{0A} = 314.7 \text{ K} = T_{0B}$$

For thermal choking, from Table A.5,

$$\frac{T_{0B}}{T_0^*} = 0.25684 \quad \text{at } M_B = 0.25$$

Therefore,

$$T_0^* = \boxed{1225.3 \text{ K}} = T_{0C}$$

Heat added is given by Eq. (8.40) as

$$Q = c_p(T_{0C} - T_{0B})$$

Also,

$$c_p = \frac{\gamma}{\gamma - 1} R = 1004.5 \text{ m}^2 (\text{s}^2 \text{ K})^{-1}$$

Thus,

$$\begin{aligned} Q &= 1004.5(1225.3 - 314.7) \\ &= \boxed{9.147 \times 10^5 \text{ J kg}^{-1}} \end{aligned}$$

## 8.5 Summary

From our discussions in Chapters 1–8, it is clear that the change of state in flow properties is achieved by three means: (i) with area change, treating the fluid to be inviscid and passage to be frictionless; (ii) with friction, considering the heat transfer between the surrounding and system to be negligible; and (iii) with heat transfer, assuming the fluid to be inviscid and passage to be frictionless. These three types of flows are called *isentropic flow*, *frictional* or *Fanno type flow*, and *Rayleigh type flow*, respectively.

All gas dynamic problems encountered in practice can be classified under these three flow processes, of course with the assumptions mentioned. Although it is impossible to have a flow process that is purely isentropic or Fanno type or Rayleigh type, in practice it is justified in assuming so, since the results obtained from these processes prove to be accurate enough for most of the practical situations in gas dynamics.

Flows in which wall friction is the chief factor bringing about changes in flow properties, assuming that no heat is transferred to or from the fluid stream, are termed *Fanno-type flows*. When the ducts are short, the flow is approximately adiabatic. However, when the ducts are extremely long, as in the case of natural-gas pipelines, there is sufficient area for heat transfer to make the flow nonadiabatic and approximately isothermal.

Considering one-dimensional steady flow of a perfect gas through a constant area duct, with the assumption that there is no external heat exchange or external shaft work and that differences in elevation produce negligible changes as compared to frictional effects, we can write

$$h = h_0 - \frac{G^2}{2\rho^2}$$

where  $h$  and  $h_0$  are the static and stagnation enthalpy,  $\rho$  is density, and  $G$  is mass velocity. This equation shows that, for a given initial condition, the relation between the local density  $\rho$  and local enthalpy  $h$  is fixed. This implies that the relation between any two properties of the flowing gas is also fixed. Thus, all the states that satisfy Eq. (8.3) can be plotted on an  $h$ – $s$  diagram. The

locus of these states on such a diagram is called the *Fanno line*. Figure 8.2 shows such lines for a certain value of  $h_0$ .

The friction coefficient  $f$  is defined as

$$f = \frac{\text{Wall shear stress}}{\text{Dynamic pressure head of the stream}}$$

The hydraulic diameter  $D$  is defined as

$$D = \frac{4 (\text{cross-sectional area})}{\text{wetted perimeter}}$$

The advantage of using hydraulic diameter is that the equations, in terms of hydraulic diameter, are valid even for ducts with noncircular cross-section.

The maximum length of the duct required for the flow to choke for a given initial Mach number is given by

$$4\bar{f}\frac{L_{\max}}{D} = \frac{1-M^2}{\gamma M^2} + \frac{\gamma+1}{2\gamma} \ln \left[ \frac{(\gamma+1)M^2}{2 \left(1 + \frac{\gamma-1}{2}M^2\right)} \right]$$

where  $\bar{f}$  is the mean friction coefficient with respect to duct length, defined by

$$\bar{f} = \frac{1}{L_{\max}} \int_0^{L_{\max}} f dx$$

The duct length required for the flow to pass from a given initial Mach number  $M_1$  to a given final Mach number  $M_2$  can be obtained from the expression

$$4\bar{f}\frac{L}{D} = \left(4\bar{f}\frac{L_{\max}}{D}\right)_{M_1} - \left(4\bar{f}\frac{L_{\max}}{D}\right)_{M_2}$$

At the maximum entropy point of the Fanno curve, the velocity is sonic velocity. For subsonic flow, the enthalpy decreases as the velocity increases in the direction of the flow. For supersonic flow, the enthalpy increases as the velocity decreases in the direction of the flow. Thus, the upper part of the Fanno line represents the state of subsonic flow, while the lower part of the line represents the states of supersonic flow.

The physical significance of the point of maximum entropy may be illustrated by considering the flow in a pipe with friction. If in such a case both the initial pressure and the discharge pressure are maintained constant, there is a maximum pipe length that we can use for a given mass flow rate. However, the variation of pressure, velocity, entropy, and so on, of the fluid as a function of pipe length can be predicted if the friction coefficient for the pipe is known.

From the discussion on Fanno flow it is clear that friction always drives the Mach number toward unity, decelerating a supersonic flow and accelerating a subsonic flow. In Figure 8.2, the  $h-s$  diagram of one-dimensional flow with friction, the above-mentioned effect of friction on Mach number is emphasized. For any given initial Mach number, for a certain value of  $L$  the flow becomes sonic. For this condition the flow is said to be *choked*, since any further increase in  $L$  is not possible without causing a drastic change of the inlet conditions. For instance, if the inlet conditions were achieved by expansion through a supersonic nozzle, and if  $L$  were larger than that allowed for attaining Mach 1 at the exit, then a normal shock would form inside the supersonic nozzle and the duct inlet conditions would suddenly become subsonic.

It is important to note that friction always causes the total pressure to decrease whether the inlet flow is subsonic or supersonic. Further, unlike the Rayleigh curve for flow with heating

or cooling, the upper and lower portions of the Fanno curve cannot be traversed by the same one-dimensional flow. In other words, it is not possible to first decelerate a supersonic flow to sonic condition by friction, and then further retard it to subsonic speeds also by friction, since such a subsonic deceleration violates the second law of thermodynamics.

A process involving changes in the stagnation enthalpy or stagnation temperature of a gas stream that flows at constant area and without frictional effects is called a process with *simple*  $T_0$  *change*. In this process, energy effects such as external heat exchange, combustion, or moisture condensation are the prime parameters causing changes in the state of a flowing gas.

For fixed values of the flow per unit area and the impulse function per unit area, a unique relation between the pressure and the density is defined as

$$p + \frac{G^2}{\rho} = \frac{F}{A}$$

This equation is called the *Rayleigh line relation*. Since both the enthalpy and entropy are functions of pressure and density, it follows that Eq. (8.31) may be used for representing the Rayleigh line on the enthalpy–entropy diagram, as shown in Figure 8.4.

From a physical point of view, the changes in stream properties are due primarily to changes in stagnation temperature. That is, the rate of change of stream properties along a Rayleigh line is a function of the rate of change of stagnation temperature.

The stagnation temperature corresponding to a given state is that temperature that the stream would assume if it were adiabatically decelerated to zero velocity. The ratio of stagnation temperatures at sections 1 and 2 in terms of Mach numbers at these sections, for a Rayleigh flow, can be expressed as

$$\frac{T_{02}}{T_{01}} = \frac{M_2^2 (1 + \gamma M_1^2)^2}{M_1^2 (1 + \gamma M_2^2)^2} \frac{\left(1 + \frac{\gamma - 1}{2} M_2^2\right)}{\left(1 + \frac{\gamma - 1}{2} M_1^2\right)}$$

It is important to note that heat addition always drives the Mach numbers toward 1, accelerating a subsonic flow and decelerating a supersonic flow. This is emphasized on the Rayleigh curve in Figure 8.4. Heating always acts to reduce the stagnation pressure, irrespective of whether the speed is subsonic or supersonic. An increase in stagnation pressure, on the other hand, may be obtained at either subsonic or supersonic speeds by a cooling process which reduces to stagnation temperature; in practice, this is difficult because other effects are always present which tend to reduce the stagnation pressure.

Finally, it is extremely important to realize that we have considered only simple types of flow to study the flow processes in which only a simple independent parameter was allowed to change, for example isentropic flow in Chapter 2, where effects of area change alone were considered, and Fanno and Rayleigh flows in this chapter, where the effects of friction alone and the effects of changes in stagnation temperature alone, respectively, have been considered. But in many practical problems of interest, these effects occur simultaneously and there may also be such other phenomena as chemical reaction, change of phase, injection or withdrawal of gases, and changes in molecular weight and specific heats. Rocket nozzles, ramjets, combustion chambers of gas turbine engines, moving flame fronts, moisture condensation shocks, injectors and ejectors, detonation waves, and heat exchangers are typical examples of flow passages in which simultaneous effects are present. For solving such flows all the effects associated with such processes must be taken into account simultaneously. For solving such flows, readers are encouraged to consult books specializing on such topics, see, for instance, [7].

## Exercise Problems

- 8.1** The stagnation chamber of a wind tunnel is connected to a high-pressure air reservoir by a long pipe of 100 mm diameter, with a friction coefficient of 0.005. If the static pressure ratio between the reservoir and the stagnation chamber is 10 and the reservoir static pressure is 101.35 MPa, how long can the pipe be without choking? Assume the flow to be adiabatic, subsonic, and one-dimensional.

[Answer:  $L_{\max} = 1034.4 \text{ m}$ ]

- 8.2** Air at a pressure of 350 kPa and 300 K is to be transported at the rate of  $0.090 \text{ kg s}^{-1}$  over a distance of 600 m through a pipe. The final pressure has to be at least 140 kPa. Assuming isothermal flow and the average friction coefficient of the pipe  $\bar{f} = 0.004$ , determine the minimum pipe diameter.

[Answer: 0.0402 m]

- 8.3** With an experimental rig comprising a convergent–divergent nozzle attached to a smooth round tube, the following data were measured with the aim of measuring the friction coefficient for the supersonic flow of air: stagnation pressure and temperature upstream of the nozzle are  $p_0 = 6.73 \text{ MPa}$  and  $T_0 = 312 \text{ K}$ ; throat diameter = 0.0061 m; diameter of nozzle exit and tube  $D = 0.0127 \text{ m}$ ; pressure of streams at stations  $x_1/D = 1.75$  and  $x_2/D = 29.60$  from the tube inlet:  $p_1 = 238 \text{ kPa}$  and  $p_2 = 485 \text{ kPa}$ . Calculate the average friction coefficient between stations  $x_1$  and  $x_2$ . Assume that the flow to the throat of the nozzle is isentropic and that the flow in the entire system is adiabatic.

[Answer: 0.002577]

- 8.4** An isentropic nozzle having an area ratio of 2 discharges air into an insulated pipe of length  $L$  and diameter  $D$ . The nozzle is supplied at 700 kPa and 300 K and the duct discharges into a space where the pressure is 280 kPa. Calculate the  $4\bar{f}L/D$  of the pipe and the mass flow rate per unit area in the pipe for the cases where a normal shock stands: (a) at the nozzle throat, (b) at the nozzle exit plane, and (c) at the duct exit plane.

[Answer: (a)  $4.8576$ ,  $816.5 \text{ kg (m}^2 \text{ s)}^{-1}$ , (b)  $0.5251$ ,  $815.9 \text{ kg (m}^2 \text{ s)}^{-1}$ , (c)  $0.21312$ ,  $815.6 \text{ kg (m}^2 \text{ s)}^{-1}$ ]

- 8.5** A gaseous mixture of air and fuel enters a ramjet combustion chamber with a velocity of  $73.15 \text{ m s}^{-1}$ , at a static temperature and pressure of 333.3 K and 55.16 kPa. The heat of reaction  $\Delta H$  of the fuel–air mixture is  $1395.5 \text{ kJ kg}^{-1}$ . Assuming that the working fluid has the same thermodynamic properties as air before and after combustion, the friction is negligible and the cross-sectional area of the combustion chamber is constant, calculate: (a) the stagnation temperature after combustion, (b) the Mach number after combustion, (c) the final static temperature, (d) the loss in stagnation pressure due to heat addition, (e) the entropy change, (f) the final velocity of the combustion mixture, and (g) the maximum heat of reaction for which flow with the specified initial conditions can be maintained.

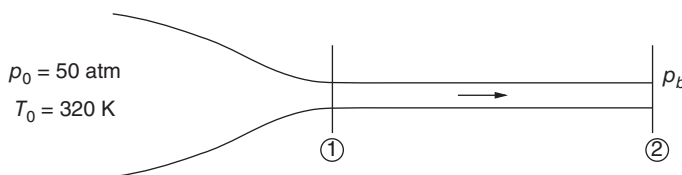
[Hint:  $\Delta H = c_p(T_{02} - T_{01})$ ]

[Answer: (a) 1725.2 K, (b) 0.68, (c) 1583.2 K, (d) 8.53 kPa, (e)  $1690.1 \text{ J (kg K)}^{-1}$ , (f)  $542.1 \text{ m s}^{-1}$ , (g)  $1607.2 \text{ kJ kg}^{-1}$ ]



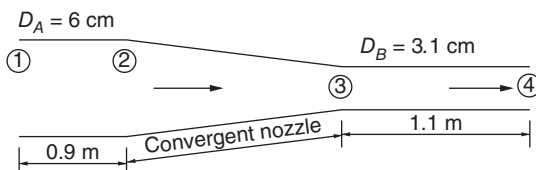
- 8.6** Air flows adiabatically through a duct of diameter 20 mm. At station 1 in the duct,  $M_1 = 0.2$ ,  $p_1 = 5$  atm, and  $T_1 = 300$  K. Compute  $p_2$ ,  $T_2$ ,  $V_2$ , and  $p_{02}$  at station 2, where  $M_2 = 0.5$ .  
[Answer: 198.558 kPa, 288 K, 170.09 m s<sup>-1</sup>, 235.52 kPa]
- 8.7** Air flows through a perfectly insulated square tube of cross-section 0.1 m by 0.1 m. At section 1 inside the tube,  $M_1 = 0.2$ ,  $T_1 = 72^\circ\text{C}$ , and  $p_1 = 2$  atm. At downstream section 2,  $M_2 = 0.76$ . Determine the mass flow rate through the tube and the drag force acting on the duct between sections 1 and 2.  
[Answer: 1.524 kg s<sup>-1</sup>, 1223.43 N]
- 8.8** Carbon dioxide gas enters an insulated circular tube of length-to-diameter ratio 50. At the entrance, the flow velocity is 195 m s<sup>-1</sup> and temperature is 310 K. If the flow at the tube exit is choked, determine the average friction factor of the tube.  
[Answer: 0.00105]
- 8.9** Air flows through a pipe of 25 mm diameter and 51 m length. The conditions at the exit of the pipe are  $M_2 = 0.8$ ,  $p_2 = 1$  atm, and  $T_2 = 270$  K. Assuming adiabatic one-dimensional flow, calculate  $M_1$ ,  $p_1$ , and  $T_1$  at the pipe entrance. Take the local friction coefficient to be 0.005.  
[Answer: 0.13, 6.56 atm, 303.52 K]
- 8.10** Air enters a perfectly insulated tube of 5 cm diameter with a stagnation state at  $p_0 = 135$  kPa and  $T_0 = 359$  K. The velocity at the entrance is  $V_1 = 135$  m s<sup>-1</sup>. If the average friction factor is 0.02, determine (a) the minimum length of the duct required for the flow to choke and (b) the mass flow rate and the stagnation pressure at the exit if the tube length is 0.6 m.  
[Answer: (a) 1.99 m, (b) 0.326 kg s<sup>-1</sup>, 121.23 kPa]
- 8.11** Hydrogen enters an insulated tube of 25 mm diameter with  $V_1 = 200$  m s<sup>-1</sup>,  $p_1 = 250$  kPa, and  $T_1 = 303$  K. What is the length of the tube required for this flow to choke? Determine the exit pressure. The friction factor of the tube  $\bar{f} = 0.03$ .  
[Answer: 5.82 m, 34.31 kPa]
- 8.12** An air stream flowing out of a convergent nozzle at 200 m s<sup>-1</sup> and 30 °C is made to enter an insulated pipe of diameter 20 mm. Determine the length of the pipe at which the flow will become sonic if the average friction factor is 0.02.  
[Answer: 15.6 cm]
- 8.13** Methane gas flows in a commercial steel pipe of 25 mm diameter. At the inlet  $p_1 = 1.0$  MPa,  $T_1 = 320$  K, and  $V_1 = 25$  m s<sup>-1</sup>. Determine the velocity and pressure at the pipe length at which the flow just chokes. Treat the flow as being adiabatic. For methane  $R = 518.4$  J (kg K)<sup>-1</sup> and the viscosity coefficient  $\mu = 0.011 \times 10^{-3}$  kg (m s)<sup>-1</sup> at the given inlet condition. Take the average friction coefficient to be  $\bar{f} = 0.004$ .  
[Answer: 432.87 m s<sup>-1</sup>, 50.18 kPa]
- 8.14** Argon gas enters an insulated, constant area duct with a Mach number of 0.6, static pressure 90 kPa, and static temperature 300 K. The duct diameter is 30 cm and the length is 1.9 m. If the average friction factor for the duct is 0.02, determine the Mach number, pressure, and temperature at the duct exit.  
[Answer: 0.73, 72.78 kPa, 290.51 K]

- 8.15** Air flows through a pipe of 50 mm diameter with a friction factor of 0.006. At a certain point along the pipe length the Mach number is 0.2. Find the maximum permissible distance from the point to the exit of the pipe if choking is to be avoided.  
[Answer: 30.277 m]
- 8.16** Air flows adiabatically at the rate of  $2.7 \text{ kg s}^{-1}$  through a 100 mm diameter pipe with a mean friction coefficient of 0.006. If the initial pressure and temperature are 1.8 bar and  $50^\circ\text{C}$ , (a) what is the limiting maximum length of the pipe up to which choking will not occur? What are the  $p$  and  $T$  at the (b) exit end and (c) half way along the pipe?  
[Answer: (a) 4.8 m, (b) 82.4 kPa,  $9.08^\circ\text{C}$ , (c) 150.6 kPa,  $44.19^\circ\text{C}$ ]
- 8.17** Air flows adiabatically through a long pipe of 50 mm diameter. If the entrance Mach number is 0.2, calculate the distance from the entrance at which the Mach number will be (a) 1.0 and (b) 0.6. Assume the friction coefficient to be 0.00375.  
[Answer: (a) 48.44 m, (b) 46.8 m]
- 8.18** Air at a stagnation temperature of 380 K is to be transported through a duct of 55 m length. What is the minimum diameter of the duct for the flow to remain unchoked for velocity at the duct entrance of (a)  $30 \text{ m s}^{-1}$ , (b)  $90 \text{ m s}^{-1}$ , and (c)  $425 \text{ m s}^{-1}$ . The average friction factor for the duct is 0.02. Assume the flow to be adiabatic.  
[Answer: (a) 4.12 cm, (b) 42.2 cm, (c) 96.77 m]
- 8.19** Air enters a square duct of side 3 cm with velocity  $1000 \text{ m s}^{-1}$  and temperature 350 K. The friction factor for the duct is 0.0025. Determine the duct length required for the flow to decelerate to Mach 1.0.  
[Answer: 1.40 m]
- 8.20** A constant area duct of 25 mm diameter and 250 mm length is connected to a reservoir at 50 atm and 320 K, through a convergent nozzle, as shown in Figure 8.7. Determine the maximum air flow rate through the system. Also, determine the range of backpressure over which the mass flow rate will remain maximum. Assume the average friction factor for the duct to be 0.023.  
[Answer:  $4.3 \text{ kg s}^{-1}$ ,  $0 < p_b < 2.05 \text{ MPa}$ ]
- 8.21** Air flows through an insulated duct of diameter 30 mm. Determine the duct length required to accelerate the flow from (a) Mach 0.2 to Mach 0.5 and (b) Mach 0.2 to Mach 1.0. The average friction factor for the duct is 0.025.  
[Answer: (a) 16.157 m, (b) 17.44 m]
- 8.22** A compressor delivers air into a pipe of 5 cm diameter and 18 m length. The average friction factor for the pipe is 0.02. If the air leaves the pipe with  $p_e = 1 \text{ atm}$  and  $T_e = 195^\circ\text{C}$ , compute the mass flow rate through the pipe.  
[Answer:  $0.096 \text{ kg s}^{-1}$ ]



**Figure 8.7** Flow from a reservoir passing through a constant area duct.

- 8.23** Argon gas from a large tank at 5 atm (gauge) and 300 K is discharging through an insulated tube of 30 cm diameter into an ambient atmosphere at nearly zero pressure. What will be the mass flow rate through the tube if its length is (a) 0 m and (b) 2.22 m? Assume the average friction factor for the tube to be 0.005.  
[Answer: (a)  $125 \text{ kg s}^{-1}$ , (b)  $115.68 \text{ kg s}^{-1}$ ]
- 8.24** The settling chamber of a wind tunnel and a high-pressure air storage tank are connected by a long pipe of 100 mm diameter. If the static pressure ratio between the storage tank and the settling chamber is 15 and the settling chamber static pressure is 150 atm, how long can the pipe be without choking? Assume one-dimensional flow in the pipe and a friction coefficient of 0.005.  
[Answer: 703.3 m]
- 8.25** Air at a stagnation state of 600 kPa and 390 K is expanded through a piping system, shown in Figure 8.8, to a pressure of 45 kPa. Estimate the mass flow rate through the system if the average friction factor for pipe A is 0.015 and that for pipe B is 0.013.  
[Answer:  $0.596 \text{ kg s}^{-1}$ ]
- 8.26** Natural gas with specific heats ratio 1.3 flows through a pipeline of diameter 0.05 m, isothermally at 300 K. At the inlet the Mach number and pressure are 0.1 and 1.2 MPa, respectively. The pressure at the exit is 300 kPa and the average friction factor for the pipe is 0.002. Calculate (a) the length of the pipeline, (b) the exit Mach number, and (c) the maximum length of the pipeline for which isothermal flow is possible and the corresponding total pressure at the end of this isothermal length.  
[Answer: (a) 435.5 m, (b) 0.4, (c) 447.38 m, 136.82 kPa]
- 8.27** Air flows adiabatically through a 0.3 m diameter and 5 m long constant-area duct. The Mach number at the duct entrance is 2.4 and the pressure is 100 kPa. Determine (a) the Mach number and pressure at the duct exit when the entire flow is shock-free and (b) the backpressure required to keep a normal shock at the duct exit. Take the average friction factor for the duct to be 0.003.  
[Answer: (a) 1.71, 163.6 kPa, (b) 530.85 kPa]
- 8.28** Air enters an insulated tube of 25 mm diameter and length 30 m at  $V_1 = 15 \text{ m s}^{-1}$ ,  $p_1 = 400 \text{ kPa}$ , and  $T_1 = 350 \text{ K}$ . Determine  $p_2$ ,  $T_2$ ,  $p_{02}$ , and  $V_2$  at the tube exit. Is the flow at the tube exit choked? If not, how much additional length of the tube is required for the flow to choke? Take the average friction coefficient to be 0.005.  
[Answer: 99.76 kPa, 348.34 K, 101.56 kPa,  $59.86 \text{ m s}^{-1}$ , 520.44 m]
- 8.29** Air from a tank is discharged into another tank through a perfectly insulated tube of diameter 10 mm and length 3 m. At the tube entrance the flow is subsonic with  $p_1 = 4 \text{ atm}$



**Figure 8.8** Flow through a piping system.

and  $T_1 = 400$  K. When the pressure in the second tank is 1.5 atm, what will be the mass flow rate through the tube. The average friction factor for the tube is  $\bar{f} = 0.022$ .  
[Answer:  $0.0155 \text{ kg s}^{-1}$ ]

- 8.30** Air enters a combustion chamber at  $80 \text{ m s}^{-1}$ , 300 K, and 76 kPa. Combustion adds  $610 \text{ kJ kg}^{-1}$  of heat to the air. Calculate the velocity, Mach number, and stagnation pressure loss at the exit of the combustion chamber. Also, determine the amount of heat addition required for the flow to choke.  
[Answer:  $283.94 \text{ m s}^{-1}$ , 0.48, 6.59 kPa,  $1064.5 \text{ kJ kg}^{-1}$ ]

- 8.31** Air at  $p_1 = 1$  atm and  $T_1 = 288$  K enters a heated duct. Neglecting friction, calculate the amount of heat per unit mass necessary to choke the flow at the duct exit. Also, determine the pressure and temperature at the duct exit, for inlet Mach number of (a)  $M_1 = 2.5$  and (b)  $M_1 = 0.5$ .  
[Answer: (a)  $265.788 \text{ kJ kg}^{-1}$ , 4.0625 atm, 760.5 K, (b)  $135.607 \text{ kJ kg}^{-1}$ , 0.849 atm, 364.5 K]

- 8.32** The flow of air at  $20^\circ\text{C}$  and Mach 1.5 in a constant-area duct is decelerated to Mach 1.0 by heating. Determine the change in temperature and the quantity of heat added.  
[Answer: 96.42 K,  $42.60 \text{ kJ kg}^{-1}$ ]

- 8.33** Air at 101 kPa and  $30^\circ\text{C}$  enters a rectangular frictionless tube of cross-section 10 cm by 15 cm at  $90 \text{ m s}^{-1}$ . After heat addition, it leaves the duct at  $220 \text{ m s}^{-1}$ . Calculate the pressure and temperature at the duct exit and the amount of heat added per second. How much heat addition per second would cause the flow to choke at the duct exit?  
[Answer: 86.98 kPa, 643.9 K, 569.2 kW, 1278.5 kW]

- 8.34** Air enters a 100 mm diameter frictionless duct. At the inlet,  $p_1 = 110$  kPa,  $T_1 = 20^\circ\text{C}$ , and  $V_1 = 75 \text{ m s}^{-1}$ . What quantity of heat must be added per second in order to have the exit temperature  $T_2 = 217^\circ\text{C}$ ? What will be the pressure, velocity, and Mach number at the duct exit for this heat addition?  
[Answer:  $157 \text{ kJ s}^{-1}$ , 104.30 kPa,  $132.35 \text{ m s}^{-1}$ , 0.3]

- 8.35** A fuel–air mixture enters a combustion chamber, in the form of a duct, at  $80 \text{ m s}^{-1}$  and 325 K. Estimate the amount of heat addition at the combustion chamber required for this flow to exit as a choked flow. Assume the fuel–air mixture to be equivalent to air.  
[Answer:  $1272.7 \text{ kJ kg}^{-1}$ ]

- 8.36** Determine the heat transfer required to decelerate an air stream at Mach 3, which corresponds to a speed of  $800 \text{ m s}^{-1}$  to a velocity of  $700 \text{ m s}^{-1}$ , resulting in Mach 1.5.  
[Answer:  $291.65 \text{ kJ kg}^{-1}$ ]

- 8.37** A Rayleigh flow of air is taking place through a rectangular tube of cross-section 0.5 m by 0.2 m. At section 1 in the tube,  $p_1 = 9.36$  kPa (gauge) and  $T_1 = 300^\circ\text{C}$ . At the tube exit, the speed is subsonic with  $p_e = 1$  atm. If the mass flow rate is  $10 \text{ kg s}^{-1}$ , determine the heat transferred per kg of air,  $q$ , between section 1 and the tube exit. Assume  $\gamma = 1.4$  and  $c_p = 1004.5 \text{ J (kg K)}^{-1}$ .  
[Answer:  $291.2 \text{ kJ kg}^{-1}$ ]

- 8.38** Air at a stagnation state of 300 kPa and 350 K flows through a convergent nozzle of exit diameter 15 mm, into a constant-area frictionless duct of the same diameter as that of the nozzle exit. Heat is transferred to the duct at a rate of  $175 \text{ kJ kg}^{-1}$  of air. Determine (a) the maximum mass flow rate through the duct and (b) the range of backpressure for the mass flow rate maximum. Assume air to be a perfect gas.  
[Answer: (a)  $0.08299 \text{ kg s}^{-1}$ , (b)  $0 < p_b < 141.2 \text{ kPa}$ ]
- 8.39** Air enters a constant-area duct at Mach 3 and a stagnation state of 1.3 MPa and 750 K. Assume that the flow through the duct undergoes a frictionless energy transfer process such that the exit Mach number is unity. Determine the total temperature and pressure at the exit if (a) a normal shock is positioned at the duct inlet and (b) the flow process is shock-free supersonic heating. Will there be any difference in the exit total temperature and pressure between the two cases?  
[Answer: (a) 1154 K, 0.38 MPa, (b) 1154 K, 1.157 MPa]
- 8.40** Air flows through a 20 mm diameter pipe of length 2 m. The Mach number at the pipe exit is 0.8. If the mean friction factor for the pipe is 0.0025, determine the Mach number at the pipe inlet.  
[Answer: 0.519]
- 8.41** Air at a total pressure and temperature of 8 atm and 450 K enters a frictionless constant cross-section duct. If a heat addition of  $850 \text{ kJ kg}^{-1}$  makes the flow to choke at the duct exit, determine the inlet Mach number and total pressure and total temperature at the exit.  
[Answer: 0.3, 6.678 atm, 1296.6 K]
- 8.42** A ramjet engine flies at Mach 4 in an atmosphere at 222 K. At the entrance to the burner, the Mach number of the flow is 0.3. Combustion in the burner may be represented approximately as heating of a perfect gas with constant specific heats ratio of  $\gamma = 1.4$ . At the exit of the burner the stagnation temperature of the gas is 2462 K. Assuming the burner to be a constant area duct and neglecting the frictional effects, determine the Mach number of the gas leaving the burner. Also, find the stagnation pressure loss due to heating.  
[Answer: 0.71, 12.9%]
- 8.43** Air is flowing through a tube of diameter 12 mm. At station 1 the static and stagnation pressures are measured as 2.38 and 3.4 atm, respectively, and at station 2, which is 300 mm downstream of station 1, the static pressure is 1.76 atm. If the flow at the tube exit is choked, determine the friction factor of the pipe segment from station 1 to station 2.  
[Answer: 0.001534]

## 9

## Method of Characteristics

### 9.1 Introduction

*Method of characteristics* is a numerical method for solving the full nonlinear equations of motion for inviscid, irrotational flow. As we have already discussed, except the Prandtl–Meyer expansion, all other problems have been solved by linear theory. If we are looking for better accuracy of results than that obtained by using the approximate linearized equations, it is necessary to work out improved solutions by including higher-order terms in the approximate equations or by considering the exact equations. However, in the latter case, it is rarely possible to get solutions in analytical form because of the nonlinear nature of the equations. We must then resort to numerical techniques, the method of characteristics being one such technique.

### 9.2 The Concepts of Characteristics

In the previous chapters, Mach lines were identified as characteristic lines, and they have been labeled as *left-running* and *right-running*, according to whether they run to the left or right with respect to an observer looking in the flow direction. Now, let us see some of the important features of the characteristics. From the earlier discussions on the properties of Mach lines and expansion flows, we may infer the following *general features of characteristics*.

- They exist only in a supersonic flow field.
- Characteristics are coincident with Mach lines. (Mach lines are lines along which very weak disturbances propagate, and across a Mach line the flow property changes are small but finite.)
- While the derivatives of the flow properties are discontinuous, the flow properties themselves are continuous on the characteristics.
- Given the characteristics or Mach lines, the dependent variables satisfy a relation known as the *compatibility relation*. This provides the key to the method of computation.
- Because the characteristics are lines across which there is a jump (even if small) in flow properties, the downstream flow does not affect the upstream flow. Therefore, it is sufficient to calculate the flow for different regions of the flow field and then they can be patched up.

But in a subsonic flow, any downstream flow affects the upstream flow. So the entire flow has to be solved simultaneously.

### 9.3 The Compatibility Relation

Consider a steady, adiabatic, two-dimensional, irrotational supersonic flow. The governing equations for this flow are

$$(V_x^2 - a^2) \frac{\partial V_x}{\partial x} + V_x V_z \left( \frac{\partial V_x}{\partial z} + \frac{\partial V_z}{\partial x} \right) + (V_z^2 - a^2) \frac{\partial V_z}{\partial z} = 0 \quad (9.1)$$

$$\frac{\partial V_z}{\partial x} - \frac{\partial V_x}{\partial z} = 0 \quad (9.2)$$

If  $(V_x^2 + V_z^2)/a^2 < 1$ , the equations are of an *elliptic type*, and the *relaxation method* of solution is appropriate. If  $(V_x^2 + V_z^2)/a^2 > 1$ , the equations are of a *hyperbolic type*. The numerical solution may be obtained by the method of characteristics.

Using the natural coordinate system, in which the velocity is expressed in terms of its magnitude and direction  $(V, \theta)$ , and the independent variables are the streamline coordinates  $(l, n)$ , with  $l$  varying along the streamline and  $n$  varying normal to streamline, Eqs. (9.1) and (9.2) can be written as

$$\left( \frac{V^2}{a^2} - 1 \right) \frac{1}{V} \frac{\partial V}{\partial l} - \frac{\partial \theta}{\partial n} = 0 \quad (9.3)$$

$$\frac{\partial V}{\partial n} - V \frac{\partial \theta}{\partial l} = 0 \quad (9.4)$$

which are, respectively, the momentum and irrotationality equations.

With the introduction of Mach angle  $\mu$ , we can write Eqs. (9.3) and (9.4) as

$$\frac{\cot^2 \mu}{V} \frac{\partial V}{\partial l} - \frac{\partial \theta}{\partial n} = 0 \quad (9.5)$$

$$\frac{1}{V} \frac{\partial V}{\partial n} - \frac{\partial \theta}{\partial l} = 0 \quad (9.6)$$

where

$$\cot^2 \mu = M^2 - 1 \quad (9.7)$$

In Section 4.6, it was shown that for a finite deflection angle  $\theta$  the direction of a weak oblique shock wave differs from the Mach wave direction  $\mu$  by an amount  $\varepsilon$ , which is of the same order as  $\theta$ . The change of flow speed across such a wave may be found as follows. From Figure 4.2, we have

$$\frac{V_2}{V_1} = \frac{V_{x2}^2 + V_y^2}{V_{x1}^2 + V_y^2} = \frac{(V_{x2}/V_y)^2 + 1}{(V_{x1}/V_y)^2 + 1} = \frac{\tan^2(\beta - \theta) + 1}{\tan^2 \beta + 1} = \frac{\cos^2 \beta}{\cos^2(\beta - \theta)}$$

From Eq. (4.27) we have

$$\cos^2 \beta = 1 - \sin^2 \beta = \frac{M_1^2 - 1}{M_1^2} \left[ 1 - \frac{2\varepsilon}{\sqrt{M_1^2 - 1}} \right]$$

A similar expression for  $\cos^2(\beta - \theta)$  can be obtained by replacing  $\varepsilon$  by  $(\varepsilon - \theta)$  in the above expression. Substituting the expressions for  $\cos^2 \beta$  and  $\cos^2(\beta - \theta)$  in terms of  $\varepsilon$  and  $\theta$  in the above expression for velocity ratio, and dropping all terms of order  $\theta^2$  and higher, we obtain

$$\begin{aligned} \frac{V_2}{V_1} &\approx 1 - \frac{\theta}{\sqrt{M_1^2 - 1}} \\ \frac{\Delta V}{V_1} &\approx -\frac{\theta}{\sqrt{M_1^2 - 1}} \end{aligned} \quad (9.8)$$

In Section 4.9, it was defined that the Prandtl–Meyer function  $\nu = \pm\theta$ , where the plus sign holds for a right-running characteristic and the minus sign holds for a left-running characteristic.

Now, the Prandtl–Meyer function  $\nu$ , which is a dimensionless measure of the speed, may be defined, using Eq. (9.8), as

$$\nu = \int \frac{\cot \mu}{V} dV \quad (9.9)$$

where  $\cot \mu = \sqrt{M^2 - 1}$ . In differential form, Eq. (9.9) becomes

$$d\nu = \cot \mu \frac{dV}{V} \quad (9.10)$$

Now it will be seen that, for the method of characteristics, the Prandtl–Meyer function  $\nu$  is the most appropriate of the many functions that are related to the velocity  $V$  (or the Mach number  $M$ ).

Substitution of Eq. (9.10) into Eqs. (9.5) and (9.6) results in

$$\frac{\partial \nu}{\partial l} - \tan \mu \frac{\partial \theta}{\partial n} = 0 \quad (9.11)$$

$$\tan \mu \frac{\partial \nu}{\partial n} - \frac{\partial \theta}{\partial l} = 0 \quad (9.12)$$

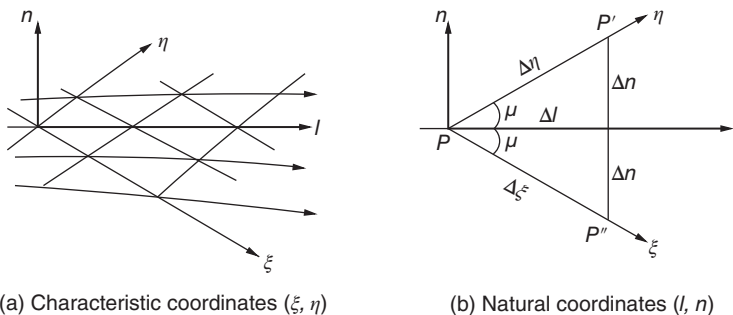
The objective here is to find the *compatibility relation* between the Prandtl–Meyer function  $\nu$  and the flow turning angle  $\theta$ , which, according to the theory of hyperbolic equations, must exist on the characteristics, or Mach lines. Though the theory gives rules for finding the compatibility condition, here we shall obtain it by *inspection*, since our interest is only from the application point of view.

We are familiar with the fact that the Mach lines are inclined to the streamlines at an angle  $\pm \mu$ . Therefore, we may expect to get the compatibility relations by rewriting Eqs. (9.11) and (9.12) in a coordinate system  $(\xi, \eta)$  consisting of the network of Mach lines, as shown in Figure 9.1. The change in any function,  $f$ , in going from point  $P$  to point  $P'$  along an  $\eta$  coordinate may be written as

$$\Delta f = \frac{\partial f}{\partial n} \Delta \eta$$

$\Delta f$  may also be calculated by going along the streamline coordinate system as

$$\Delta f = \frac{\partial f}{\partial l} \Delta l + \frac{\partial f}{\partial n} \Delta n = \left( \frac{\partial f}{\partial l} + \frac{\partial f}{\partial n} \frac{\Delta n}{\Delta l} \right) \Delta l$$



**Figure 9.1** Characteristic and natural coordinate systems.



From the above two equations,

$$\frac{\partial f}{\partial \eta} \frac{\Delta \eta}{\Delta l} = \frac{\partial f}{\partial l} + \frac{\partial f}{\partial n} \frac{\Delta n}{\Delta l}$$

From the geometry of Figure 9.1b, this may be expressed as

$$\sec \mu \frac{\partial f}{\partial \eta} = \frac{\partial f}{\partial l} + \tan \mu \frac{\partial f}{\partial n} \quad (9.13)$$

Similarly, we can write

$$\sec \mu \frac{\partial f}{\partial \xi} = \frac{\partial f}{\partial l} - \tan \mu \frac{\partial f}{\partial n} \quad (9.14)$$

which give the rules that relate the derivatives of any function,  $f$ , in the two coordinate systems. Adding and subtracting Eqs. (9.11) and (9.12), we get

$$\frac{\partial}{\partial l}(\nu - \theta) + \tan \mu \frac{\partial}{\partial n}(\nu - \theta) = 0$$

$$\frac{\partial}{\partial l}(\nu + \theta) - \tan \mu \frac{\partial}{\partial n}(\nu + \theta) = 0$$

Comparing the above equations with Eqs. (9.13) and (9.14), respectively, we obtain

$$\frac{\partial}{\partial \eta}(\nu - \theta) = 0, \quad \frac{\partial}{\partial \xi}(\nu + \theta) = 0$$

That is,

$$\nu - \theta = R \text{ (constant) along } \eta\text{-characteristic}$$

$$\nu + \theta = Q \text{ (constant) along } \xi\text{-characteristic}$$

(9.15)

These are the compatibility relations between  $\nu$  and  $\theta$ . They simply mean that the functions  $Q = \nu + \theta$  and  $R = \nu - \theta$  are invariants on the  $\xi$ - and  $\eta$ -characteristics, respectively.

*Note:* at this juncture we should note that the compatibility relations are not always obtained in such convenient form as Eq. (9.15). Generally, they are obtained in differential form and cannot always be integrated in this way, independently of the specific flow field to be solved.

## 9.4 The Numerical Computational Method

Consider the element from a characteristic network, illustrated in Figure 9.2. Flow properties along  $AB$  are given. To find the flow properties at point  $P$ , consider the right-running characteristic  $AP$ , with  $Q = \text{constant}$ , and left-running characteristic  $BP$ , with  $R = \text{constant}$ .

For the above element we can write

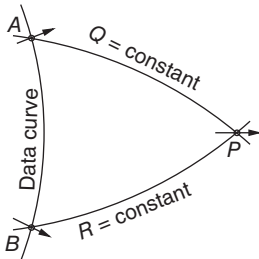
$$Q_P = Q_A, \quad R_P = R_B$$

But by Eq. (9.15),

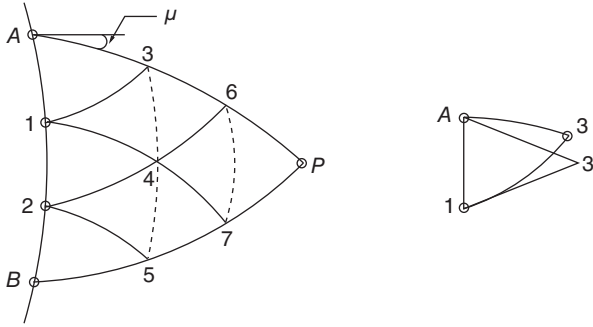
$$Q = \nu + \theta, \quad R = \nu - \theta$$

Hence,

$$\nu = \frac{1}{2}(Q + R), \quad \theta = \frac{1}{2}(Q - R)$$



**Figure 9.2** Characteristic network element.



**Figure 9.3** Characteristic network.

Therefore,

$$v_P = \frac{1}{2}(Q_P + R_P), \quad \theta_P = \frac{1}{2}(Q_P - R_P)$$

Now, the problem is solved since, once  $v$  is known,  $M$ ,  $\mu$ ,  $p/p_0$  are all known from the isentropic relations (or table). Also, once  $\theta$  is known, the flow inclination with respect to the data line is known. The location of point  $P$ , which is an unknown, is found by a numerical technique. In this technique, the space is divided into parts to result in a characteristic network, as illustrated in Figure 9.3. As a first approximation, the characteristics are replaced by straight line segments. Because of this linear approximation, we arrive at point  $3'$  instead of 3, as shown in Figure 9.3. The error adds up and finally we get a point  $P'$  instead of  $P$ . To minimize the error, the dimensions of the meshes should be of a smaller size. Applying a step-by-step procedure, starting from the data curve, giving the data or boundary conditions we can identify the flow field at point  $P$ . For instance, point 3 is located by using the known Mach angles and flow directions at points 1 and  $A$  to draw the characteristic segments. Flow conditions at point 3 are determined from the data at points  $A$  and 1. Similarly, point 4 is found, and then point 6 is found from points 3 and 4. Thus, starting from the data curve the computation proceeds outwards.

The “working outward” computation from the data curve indicates that the nature of the boundary condition is such that it influences the flow only in the downstream direction. This is in contrast to the Laplacian or elliptic type of field, in which the region of computation must be completely bounded, and in which each point is influenced by all other points in the region.

### 9.4.1 Solid and Free Boundary Points

From the characteristic network shown in Figure 9.3, it can be seen that for computing  $v$  and  $\theta$  at point 3, the invariants  $Q$  and  $R$  at points  $A$  and 1 must be known. These points  $A$  and 1 may lie on a solid wall or a free boundary, such as the edge of a jet, that is the boundary conditions fit into the computation quite readily. Consider the characteristic network element shown in Figure 9.4.

In Figure 9.4, the properties on the data curve arc 1–2 is known, that is  $v_1$ ,  $\theta_1$ ,  $v_2$ , and  $\theta_2$  are known. In other words, the invariants  $Q$  on the arc 1–3 and  $R$  on the arc 2–3 are known. Therefore, the flow properties ( $v_3$ ,  $\theta_3$ ) at point 3 can easily be obtained from the relations of Eq. (9.15) as follows.

$$Q_1 = v_1 + \theta_1, \quad R_2 = v_2 - \theta_2 \quad (9.16a)$$

Hence,

$$v_3 = \frac{1}{2}(Q_1 + R_2), \quad \theta_3 = \frac{1}{2}(Q_1 - R_2) \quad (9.16b)$$

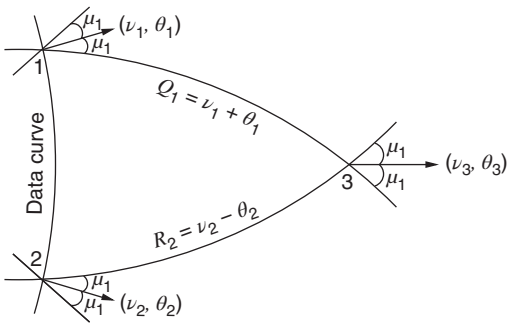


Figure 9.4 Characteristic network element.

With Eqs. (9.16a)–(9.16b), we can form the data given in Figure 9.5, which should be known for computing data for point 3, depending on whether 3 is an interior point or a point on a solid wall, or a point on a free boundary.

From Figure 9.5, it can be seen that, if any two of the quantities in the table are known, the other two may be calculated with the relations in Eqs. (9.16a)–(9.16b).

Sometimes it may be necessary to compute flows in which shocks appear. On such occasions, the method illustrated in Figure 9.6 may be employed. As seen from the figure, point 3 is just behind the shock. One invariant  $R$  is obtained from point 1, since arc 1–3 is a left-running characteristic. The other is determined by the shock equations (see Section 4.3); it is not given explicitly, but as a relation between  $\nu_3$  and  $\theta_3$ . Thus, the flow at point 3 may be solved. These then determine the shock angle  $\beta$ , which is used to draw the next shock segment.

If the shock is strongly curved, the flow downstream of it will have vorticity and the isentropic equations are not valid in this region, and they must be replaced by appropriate equations accounting for vorticity effects.

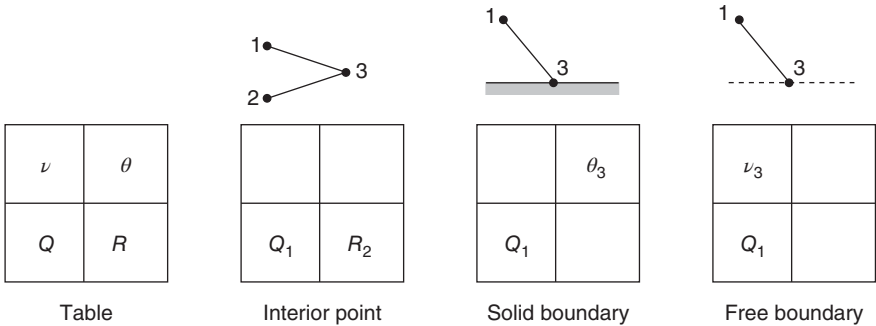


Figure 9.5 Known data for computing flow at point 3.

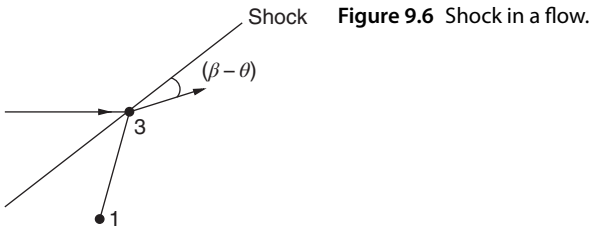


Figure 9.6 Shock in a flow.

**Example 9.1**

Compute the flow in a diverging channel, shown in Figure 9.7, with walls diverging by  $15^\circ$  and  $M_{\text{data}} = 1.348$ . Divide the data curve into three equal segments, that is  $\Delta\theta = 5^\circ$ .

**Solution:**

The values of  $\nu$  and  $\theta$  are known at points 1 to 4 (data curve). Therefore, the invariants  $Q$  and  $R$  on all left- and right-running characteristics originating from the above points may be calculated with the relations

$$Q = \nu + \theta, \quad R = \nu - \theta$$

Hence, the Prandtl–Meyer function  $\nu$  and turning angle  $\theta$  at points 5–14 may be obtained from the corresponding values of  $Q$  and  $R$  for each point using the relations

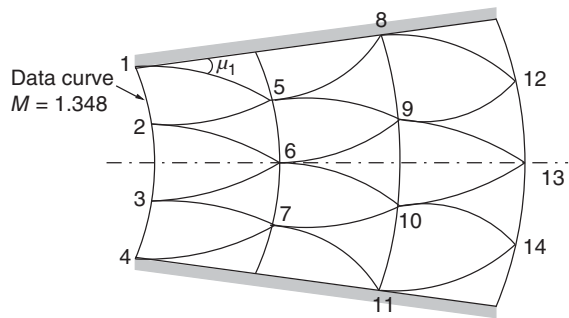
$$\nu = \frac{1}{2}(Q + R), \quad \theta = \frac{1}{2}(Q - R)$$

Table 9.1 gives the computed values of  $\nu$ ,  $\theta$ ,  $\mu$ , and  $M$  at points 5–14 following the above procedure.

**Remarks**

- The compatibility conditions  $Q = \nu + \theta$  and  $R = \nu - \theta$  make the whole procedure simple. These conditions are simple only for two-dimensional irrotational flows.
- A drawing should always be made along with the computation, to locate the points.

**Figure 9.7** A divergent channel.



**Table 9.1** Computed values of  $\nu$ ,  $\theta$ ,  $\mu$ , and  $M$  at points 5 to 14.

Boundary conditions						Point	$Q$	$R$	$\nu^\circ$	$\theta^\circ$	$\mu^\circ$	$M$
Given			Derived			5	15	5	10	5	44.2	1.434
Point	$\mu^\circ$	$\nu^\circ$	$\theta^\circ$	$Q$	$R$	6	10	10	10	0	44.2	1.434
						7	5	15	10	-5	44.2	1.434
1	47.9	7.5	7.5	15	0	8	20	5	12.5	7.5	41.1	1.520
2	47.9	7.5	2.5	10	5	9	15	10	12.5	2.5	41.1	1.520
3	47.9	7.5	-2.5	5	10	10	10	15	12.5	-2.5	41.1	1.520
4	47.9	7.5	-7.5	0	15	11	5	20	12.5	-7.5	41.1	1.520
						12	20	10	15	5	38.5	1.606
						13	15	15	15	0	38.5	1.606
						14	10	20	15	-5	38.5	1.606

### 9.4.2 Sources of Error

- In an actual flow, there will be a boundary layer. This introduces error to the results obtained, since it is not correct to assume the characteristics to be straight near the wall. The error may be corrected by calculating the displacement thickness at different stations and adding it to the contour already calculated.
- Values obtained with  $\Delta\theta = 1^\circ$  and  $\Delta\theta = 0.5^\circ$  are almost the same. Therefore, there is no necessity to take  $\Delta\theta$  less than  $1^\circ$ .

### 9.4.3 Axisymmetric Flow

The important features of the method of characteristics have already been described in our discussion on plane flow. The computations for two-dimensional flow were seen to be very easy because of the simple nature of the compatibility relations – Eq. (9.15). But the theory of characteristics for general three-dimensional flow is quite involved, and the computations are cumbersome. However, for axisymmetric flow, the method is easily extended from two-dimensional flow case.

Consider the fluid element shown in Figure 9.8. The governing equation for this motion may be shown to be

$$\frac{\cot^2 \mu}{V} \frac{\partial V}{\partial l} - \frac{\partial \theta}{\partial n} = \frac{\sin \theta}{r} \quad (9.17)$$

$$\frac{1}{V} \frac{\partial V}{\partial n} - \frac{\partial \theta}{\partial l} = 0 \quad (9.18)$$

where  $(V, \theta)$  define the velocity in the natural coordinates plane. Equation (9.17) differs from Eq. (9.5) only in the final term. The irrotationality equation, (Eq. 9.18), is the same as Eq. (9.6). Multiplication of Eq. (9.17) by  $\tan \mu$  and Eq. (9.18) by  $\tan \mu \cot \mu$  yields

$$\frac{\cot \mu}{V} \frac{\partial V}{\partial l} - \tan \mu \frac{\partial \theta}{\partial n} = \tan \mu \frac{\sin \theta}{r} \quad (9.17a)$$

$$\tan \mu \frac{\cot \mu}{V} \frac{\partial V}{\partial n} - \frac{\partial \theta}{\partial l} = 0 \quad (9.18a)$$

With the help of relations (9.9) and (9.10), Eqs. (9.17a) and (9.18a) become

$$\frac{\partial v}{\partial l} - \tan \mu \frac{\partial \theta}{\partial n} = \tan \mu \frac{\sin \theta}{r}$$

$$\tan \mu \frac{\partial v}{\partial n} - \frac{\partial \theta}{\partial l} = 0$$

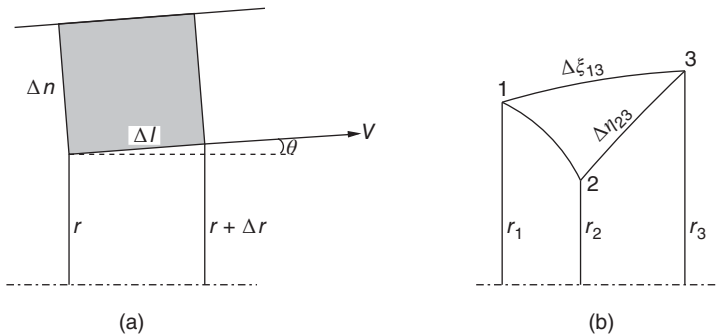


Figure 9.8 Axisymmetric flow coordinates: (a) natural coordinates and (b) characteristic network.

The above two relations correspond to Eqs. (9.11) and (9.12) for the two-dimensional case. Following the same procedure as that adopted for two-dimensional flow, we can obtain the following equations.

$$\frac{\partial}{\partial \eta}(\nu - \theta) = \sin \mu \frac{\sin \theta}{r} \quad (9.19)$$

$$\frac{\partial}{\partial \xi}(\nu + \theta) = \sin \mu \frac{\sin \theta}{r} \quad (9.20)$$

Now the integration has to be done numerically, step by step, simultaneously with the construction of the characteristic network.

Consider the characteristic mesh element shown in Figure 9.8b. Point 3 is to be solved from the known data at 2 and 1. From Eqs. (9.19) and (9.20) we may write

$$\begin{aligned} \int_2^3 d(\nu - \theta) &= \int_2^3 \left( \sin \mu \frac{\sin \theta}{r} \right) d\eta \\ \int_1^3 d(\nu + \theta) &= \int_1^3 \left( \sin \mu \frac{\sin \theta}{r} \right) d\xi \end{aligned}$$

Now assume that, for small-size mesh, the quantities in parentheses on the RHS are approximately constant, over the interval of integration, and have the known values at 1 and 2, respectively. The integrations yield

$$\begin{aligned} (\nu_3 - \theta_3) - (\nu_2 - \theta_2) &= \sin \mu_2 \frac{\sin \theta_2}{r_2} \Delta \eta_{23} \\ (\nu_3 + \theta_3) - (\nu_1 + \theta_1) &= \sin \mu_1 \frac{\sin \theta_1}{r_1} \Delta \xi_{13} \end{aligned}$$

From the above two equations, we get

$$\nu_3 = \frac{1}{2}(\nu_1 + \nu_2) + \frac{1}{2}(\theta_1 - \theta_2) + \frac{1}{2} \left( \sin \mu_1 \frac{\sin \theta_1}{r_1} \Delta \xi_{13} + \sin \mu_2 \frac{\sin \theta_2}{r_2} \Delta \eta_{23} \right) \quad (9.21)$$

$$\theta_3 = \frac{1}{2}(\nu_1 - \nu_2) + \frac{1}{2}(\theta_1 + \theta_2) + \frac{1}{2} \left( \sin \mu_1 \frac{\sin \theta_1}{r_1} \Delta \xi_{13} - \sin \mu_2 \frac{\sin \theta_2}{r_2} \Delta \eta_{23} \right) \quad (9.22)$$

Equations (9.21) and (9.22) differ from the two-dimensional Eq. (9.15) only in the additional terms that depend on the geometry of the particular problem. In these terms, the radial distances  $r_1$  and  $r_2$  of the points under consideration, and the length of the mesh sides,  $\Delta \eta_{23}$  and  $\Delta \xi_{13}$ , must be obtained from the flow field by measurement on a drawing or by computation.

#### 9.4.4 Nonisentropic Flow

For a nonisentropic flow, the governing equation of motion becomes

$$\frac{\cot^2 \mu}{V} \frac{\partial V}{\partial l} - \frac{\partial \theta}{\partial n} = \frac{\sin \theta}{r} \quad (9.23)$$

and the vorticity equation follows from relation (5.6) as

$$\frac{1}{V} \frac{\partial V}{\partial n} - \frac{\partial \theta}{\partial l} = -\frac{T}{V^2} \frac{ds}{dn} + \frac{1}{V^2} \frac{dh_0}{dn} \quad (9.24)$$

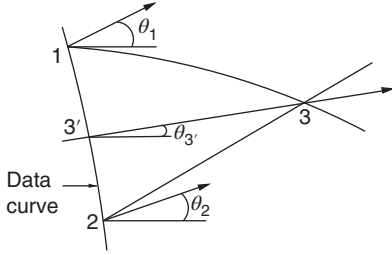


Figure 9.9 Characteristic mesh and a streamline.

Transforming Eqs. (9.23) and (9.24) into characteristic coordinates, we get

$$\begin{aligned}\frac{\partial}{\partial \eta}(\nu - \theta) &= \sin \mu \frac{\sin \theta}{r} - \frac{\cos \mu}{V^2} \left( T \frac{ds}{dn} - \frac{dh_0}{dn} \right) \\ \frac{\partial}{\partial \xi}(\nu + \theta) &= \sin \mu \frac{\sin \theta}{r} + \frac{\cos \mu}{V^2} \left( T \frac{ds}{dn} - \frac{dh_0}{dn} \right)\end{aligned}$$

The final terms in each equation may be written as derivatives along the characteristics with geometry shown in Figure 9.1b;

$$\frac{\partial \eta}{\partial n} = \operatorname{cosec} \mu, \quad \frac{\partial \xi}{\partial n} = -\operatorname{cosec} \mu$$

Integration of the above governing equations over a small-mesh element yields

$$\nu_3 - \theta_3 = \nu_2 - \theta_2 + \sin \mu_2 \frac{\sin \theta_2}{r_2} \Delta \eta_{23} - \frac{\cot \mu_2}{V_2^2} [T_2(s_3 - s_2) - (h_{03} - h_{02})] \quad (9.25)$$

$$\nu_3 + \theta_3 = \nu_1 + \theta_1 + \sin \mu_1 \frac{\sin \theta_1}{r_1} \Delta \xi_{13} - \frac{\cot \mu_1}{V_1^2} [T_1(s_3 - s_1) - (h_{03} - h_{01})] \quad (9.26)$$

$\nu_3$  and  $\theta_3$  may be obtained from Eqs. (9.25) and (9.26). From the above relations, it can be seen that values of  $s_3$  and  $h_{03}$  at point 3 are needed for computation. These may be determined as follows. In Figure 9.9, once point 3 is located, the streamline through it may be approximately located by drawing a line with slope  $\theta_{3'} = (\theta_1 + \theta_2)/2$ , intersecting the data curve at 3'. Since  $s$  and  $h_0$  are invariant along streamlines, their values at 3 are the same as at 3' on the data curve, where they are known.

## 9.5 Theorems for Two-Dimensional Flow

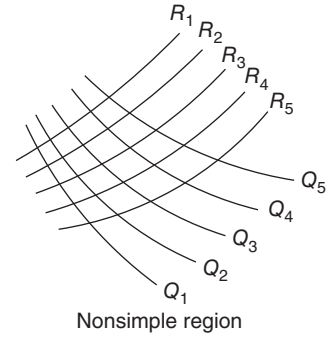
For two-dimensional (plane) supersonic flow, from the compatibility relations (9.15), we have

$$\nu - \theta = R \quad (\text{along } \eta\text{-characteristics})$$

$$\nu + \theta = Q \quad (\text{along } \xi\text{-characteristics})$$

These two relations, which are *independent of the specific flow geometry*, lead to three useful theorems which we now give under three types of flow.

- *General or nonsimple region.* Characteristics of both the families are curved and are physically significant.
- *Simple region (simple wave).* One family of characteristics is straight. The other family (curved) is physically insignificant and not shown (by convention).
- *Uniform flow.* Both families are straight and physically insignificant and not shown (by convention).

**Figure 9.10** Characteristics of a general region.

Consider the *general region* shown in Figure 9.10. The values of  $\nu$  and  $\theta$  at the intersection of any two characteristics are found from the solution of the above equations, as

$$\nu = \frac{1}{2}(Q + R), \quad \theta = \frac{1}{2}(Q - R)$$

Along any  $\eta$ -characteristic,  $R$  is constant and so the changes in  $\nu$  and  $\theta$  depend only on the changes in  $Q$ . Thus,

$$\Delta\nu = \frac{1}{2}\Delta Q = \Delta\theta \quad (9.27a)$$

Similarly, along  $\xi$ -characteristics,

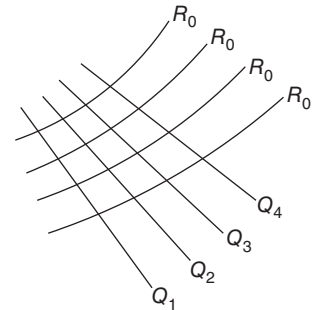
$$\Delta\nu = \frac{1}{2}\Delta R = -\Delta\theta \quad (9.27b)$$

Thus, the entire flow field is known if the values of  $R$  and  $Q$  on the characteristics are known.

Consider next the *simple region* shown in Figure 9.11. In a simple region, by definition, either  $Q$  or  $R$  is constant throughout the region. In the figure, all the  $\eta$ -characteristics have the same value of  $R (= R_0)$ . Then, by Eq. (9.27b),  $\nu$  and  $\theta$  are individually constant along a  $\xi$ -characteristic, which must be straight. Thus, in a simple region, one set of characteristics are straight lines, with uniform conditions on each one. The flow changes encountered in crossing the straight characteristics are given by

$$\Delta\nu = \pm\Delta\theta \quad (9.28)$$

In Eq. (9.28), the plus sign is for  $\xi$ -characteristics and the minus sign for  $\eta$ -characteristics. The relation given by Eq. (9.28) is different from that given by Eq. (9.27) in the sense that Eq. (9.28) is valid on any line that crosses the straight characteristics, and in particular on a streamline.

**Figure 9.11** Characteristics of a simple region.



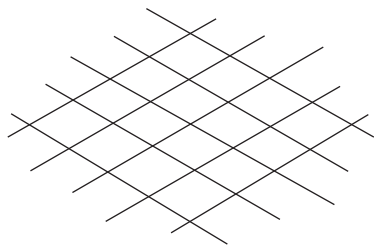


Figure 9.12 Characteristics in a uniform flow region.

Consider now the *uniform flow* shown in Figure 9.12. By definition, uniform flow is that for which  $R = R_0$  and  $Q = Q_0$  throughout. That is,  $v$  and  $\theta$  are uniform, and both  $\xi$ -type and  $\eta$ -type characteristics are straight lines constituting a parallel network, as illustrated in Figure 9.12.

A flow field in which all three regions coexist is given in Figure 4.20. As shown in the figure, the usual convention is to omit the Mach lines in the uniform region, to show only the straight lines in a simple region, and both sets in the nonsimple region.

It can be seen that *the uniform region does not adjoin the nonsimple region* (except at one point). This is a general theorem, which may be easily proved by trying to construct contrary case, if we remember the definitions given above.

## 9.6 Numerical Computation with Weak Finite Waves

The method of constructing two-dimensional, supersonic flows by using waves was outlined in Chapter 4. If the waves are weak, we can set up a computing procedure which is equivalent to the characteristic method (see Section 4.6). In computation with weak waves, the entire gradual change in the flow is assumed to occur discontinuously along a single line given by Mach angle  $\bar{\mu}$ , as shown in Figure 9.13.

It is further assumed that the strength of weak finite waves ( $\Delta\theta$ ) does not change at intersections. This assumption is valid only for two-dimensional flow.

### 9.6.1 Reflection of Waves

- On rigid walls a wave is reflected as a wave of the same sense (of opposite family), as illustrated in Figure 9.14 (see also Section 4.11).
- On an open or free boundary (say the boundary of a free jet), a wave is reflected as a wave of opposite sense, as illustrated in Figure 9.15.

It can be seen from Figure 9.15 that the free boundary itself is deflected at the wave incident point. *The deflection of the free boundary is downwards if an expansion wave hits it and the deflection is upwards when a compression wave hits it.* It is important to note that in Figure 9.15 an expansion ray is shown to reflect as a compression wave from the free boundary and a

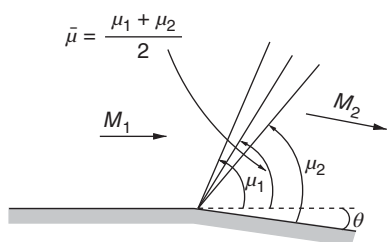
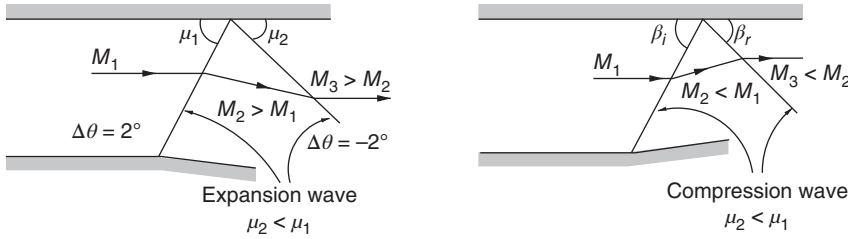
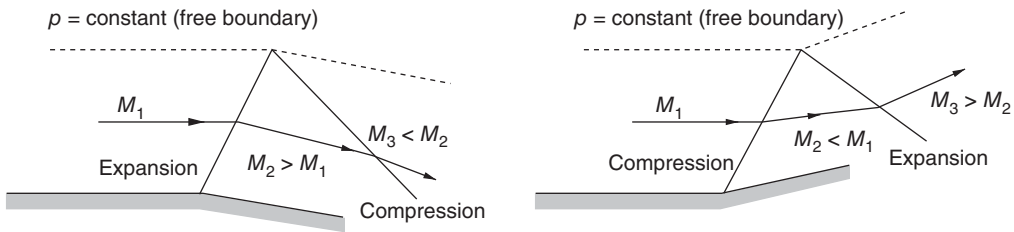


Figure 9.13 Centered expansion.



**Figure 9.14** Reflections of waves from a solid wall.



**Figure 9.15** Reflection of waves from free boundary.

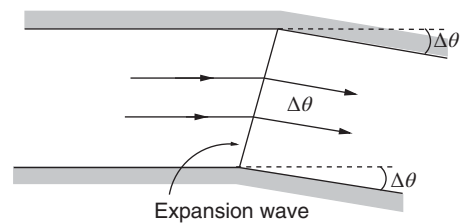
compression wave is shown to reflect as a single expansion wave. This should be taken as a representative expansion wave. In reality, the compression wave will reflect as an expansion fan from a free boundary and not as a single expansion ray.

From the above reflection, it can be seen that, on reflection from a wall, a wave of  $\xi$ -type is changed to a wave of  $\eta$ -type. The turning strength of the reflected wave is the same as that of the incident wave, since the flow must return to the original direction, parallel to the wall. From this process we can visualize that the wave reflection may be “canceled” by suitable accommodation of the portion of the wall after the incident wave, that is there will not be a reflection of the wave, as shown in Figure 9.16. The wall deflection is equal to the strength of the wave.

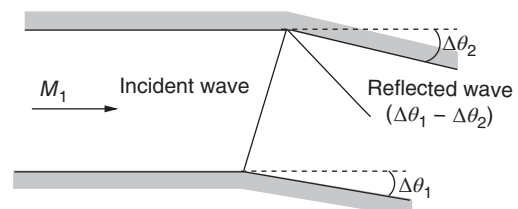
We can summarize the above reflection patterns as follows (Figure 9.17).

If  $\Delta\theta_2 = \Delta\theta_1$ , then there will not be any reflection. If  $\Delta\theta_2 < \Delta\theta_1$ , then the reflected wave will be an expansion wave, and when  $\Delta\theta_2 > \Delta\theta_1$ , the reflected wave will be a compression wave.

**Figure 9.16** Cancellation of wave reflection.



**Figure 9.17** Wave reflection.



In a process involving a large number of reflections of expansion waves, the flow condition at any point in the flow field is given by

$$\theta - \theta_1 = m - n, \quad v - v_1 = m + n \quad (9.29)$$

where  $m$  is the number of expansion waves of equal strength, say  $1^\circ$ , that is one family ( $\xi$ -type) crossed by the flow, and  $n$  is the number of expansion waves of equal strength, say  $1^\circ$ , the other family ( $\eta$ -type) crossed by the flow. The initial flow field is given by  $(v_1, \theta_1)$ .

More generally, the flow field condition  $(M, p, \rho, T)$  at any point in a flow involving multiple reflections of expansion and compression waves of both  $\xi$ -type and  $\eta$ -type is given by

$$\begin{aligned} \theta - \theta_1 &= m - n - k + l \\ v - v_1 &= m + n - k - l \end{aligned}$$

where  $k$  is the number of compression waves on one family ( $\xi$ -type) crossed by the flow, and  $l$  is the number of compression waves of other family ( $\eta$ -type) crossed by the flow.

### Example 9.2

Solve the flow field at the exit of an underexpanded two-dimensional nozzle with air flow, shown in Figure 9.18. At the nozzle exit,  $M_A = 1.435$  and  $\theta_A = 0^\circ$ .

#### Solution:

Because of symmetry, the streamline along the axis of the nozzle must be straight, and may be replaced by a solid wall, as shown in the figure. Given  $M_A = 1.435$  and  $\theta_A = 0$ . For  $M_A = 1.435$ , from the isentropic table, we get  $v_A = 10^\circ$  and  $p_A/p_0 = 0.299$ . In this example, it is assumed that the entire expansion is taking place through a single expansion wave.

From our discussion on the Prandtl–Meyer function (Section 4.9), we know that  $v$  and  $\theta$  are connected by the relation  $v = \pm\theta$ , where the plus sign holds for a right-running characteristic and the minus sign holds for a left-running characteristic.

Now, the entire expansion from region A to region B is taking place across a left-running characteristic and, therefore,  $\theta_B = -v_A = -10^\circ$ .

Also, by Eq. (4.49a), for the expansion

$$v_B = v_A + |\theta_B - \theta_A| = 10 + 10 = 20^\circ$$

With the value of the Prandtl–Meyer function, we can get the flow properties. For  $v_B = 20^\circ$ , from the isentropic table,

$$M_B = 1.775, \quad p_B/p_0 = 0.181$$

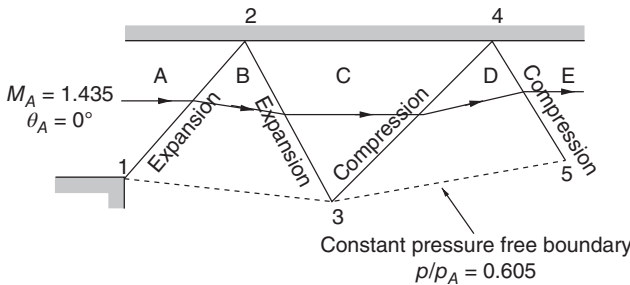


Figure 9.18 Flow from a nozzle hitting a wall.

**Table 9.2** Flow properties at different points.

Field	$\nu$	$M$	$\mu$	$p/p_0$	$\theta$
A	10°	1.435	44.2°	0.299	0°
B	20°	1.775	34.3°	0.181	−10°
C	30°	2.134	27.9°	0.104	0°
D	20°	1.775	34.3°	0.181	10°
E	10°	1.435	44.2°	0.299	0°

After the expansion, the pressure ratio in region  $B$  is 0.181. At the free boundary, the pressure outside the boundary must be equal to  $p_B$ . Therefore, the pressure ratio at the free boundary for the given exit pressure  $p_A$  is

$$\frac{p}{p_A} = \frac{p_B/p_0}{p_A/p_0} = \frac{0.181}{0.299} = 0.605$$

Following the above procedure, we can get the flow field as given in Table 9.2.

The above solution can yield the wave and deflection angles also. The mean Mach angle  $\bar{\mu}$  for an expansion fan with  $\mu_1$  and  $\mu_2$  as the Mach angles at the beginning and end of the fan is given by

$$\bar{\mu} = \frac{\mu_1 + \mu_2}{2}$$

Similarly, the mean deflection angle  $\bar{\theta}$  is given by

$$\bar{\theta} = \frac{\theta_1 + \theta_2}{2}$$

With the above relations, for the present flow field, we have

Wave	$\bar{\mu}$	$\bar{\theta}$
1–2	39.25°	−5°
2–3	31.1°	5°
3–4	31.1°	5°
4–5	39.25°	−5°

*Note:* in the above problem, all the regions are assumed to be simple regions. There is a 10° deflection of the jet boundary as it leaves the nozzle.

## 9.7 Design of Supersonic Nozzle

In the design of a de Laval nozzle, we are looking for a proper geometry of the nozzle to accelerate the flow to result in uniform, parallel, and wave-free supersonic flow. In Section 2.6, it was highlighted that only a shape like the one shown in Figure 9.19 can produce such a uniform and unidirectional flow.

In order to accelerate a flow from subsonic to supersonic speed, the duct has to be convergent–divergent in shape, as shown in Figure 9.19. Further, for a supersonic convergent–divergent nozzle, it is essential to have wave-free and parallel flow in the test-section (at the nozzle exit) at the desired Mach number. An improper contour will result in the

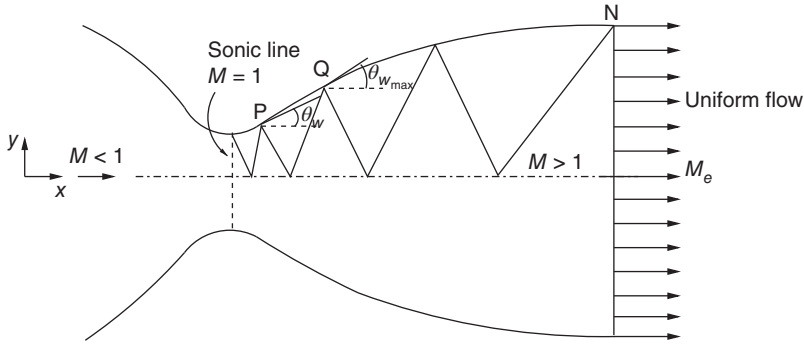


Figure 9.19 Supersonic (de Laval) nozzle.

presence of weak waves, which may coalesce to form a finite shock and prevent a uniform flow in the test-section. Therefore, it is imperative to have a proper design of nozzle contours for the generation of uniform supersonic flows.

The method of characteristics provides a technique for properly designing the contour of a supersonic nozzle for shock-free, isentropic flow, taking into account the multidimensional flow inside the duct. The purpose here is to illustrate the design of a supersonic nozzle by the method of computation with weak waves (characteristics).

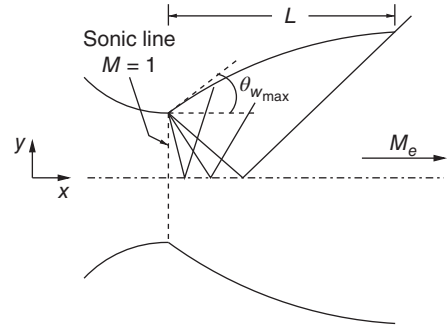
Consider the supersonic nozzle shown in Figure 9.19. The subsonic flow in the convergent portion of the nozzle is accelerated to sonic speed at the throat. Generally, because of the multidimensionality of the converging subsonic flow, the sonic line is gently curved. However, in most applications, we assume the sonic line to be straight, as shown in Figure 9.19. In the divergent portion downstream of the throat, let  $\theta_w$  be the angle at any point P on the duct wall. The portion of the nozzle with increasing  $\theta_w$  is called the *expansion* section, where expansion waves are generated and propagate in the downstream direction, reflecting from the opposite wall. In Figure 9.19, because of symmetry, waves above the center line only are shown. At point Q, there is an inflection of the duct wall contour and  $\theta_w$  is maximum. Downstream of Q,  $\theta_w$  decreases until the wall becomes parallel to the  $x$ -direction at point N.

Supersonic nozzles with gradual expansions as illustrated in Figure 9.19 are characteristics of wind tunnel nozzles where high-quality, uniform, and unidirectional flow is required in the test-section. Hence, wind tunnel nozzles are long, with very smooth gradual expansion. But in applications such as rocket motors, nozzles are comparatively short in order to minimize weight. Also, in applications where rapid expansions are the requirement, such as the nonequilibrium flow in gas dynamic lasers, the nozzle length should be as short as possible. In such cases, the expansion portion of the nozzle is shrunk to a point and the expansion takes place through a centered Prandtl–Meyer wave emanating from a sharp-corner throat with an angle  $\theta_{w_{\max}}$ , as shown in Figure 9.20. The length  $L$  shown in Figure 9.20 is the minimum length possible for shock-free, isentropic flow. If the contour is made within a length shorter than  $L$ , shocks will develop inside the nozzle.

### 9.7.1 Contour Design Details

To illustrate the application of the method of characteristics for supersonic nozzle design, let us consider the specific problem of designing a minimum length nozzle to expand the flow from  $M = 1$  at the throat to  $M = 2.0$  in the test-section (nozzle exit) where the flow is to be uniform and parallel to the flow direction at the throat.

Figure 9.20 Minimum-length nozzle.



Let us employ the region-to-region method of characteristics for designing the contour. Since a minimum length nozzle is to be designed, a sharp-cornered nozzle assumption will be made. For characteristics it can be proved that,

- along left-running characteristic or across right-running characteristic,  $\nu - \theta = \text{constant}$ ;
  - along right-running characteristic or across left-running characteristic,  $\nu + \theta = \text{constant}$ ;
- where  $\nu$  is the Prandtl–Meyer function and  $\theta$  is the flow turning angle.

In the region-to-region method, flow is divided into various regions by the incident and reflected characteristics (from the centerline). Now, with the help of  $\nu$  and  $\theta$ , Mach numbers in the regions can be calculated using the above-mentioned relations between  $\nu$  and  $\theta$ .

The sonic line at the throat is assumed to be straight, and the design is done for one-half of the nozzle, as the other half is only a mirror image of the first, because of symmetry.

The characteristic lines and contour points for the proposed nozzle are shown in Figure 9.21. For a sharp-cornered nozzle,

$$\theta_{\text{fan}} = \frac{\nu_{TS}}{2}$$

where the subscript  $TS$  refers to the test-section.

From Table A.1 in the Appendix, for  $M_{TS} = 2.0$ ,  $\nu_{TS} = 26.38^\circ$ . Hence,

$$\theta_{\text{fan}} = 13.19^\circ$$

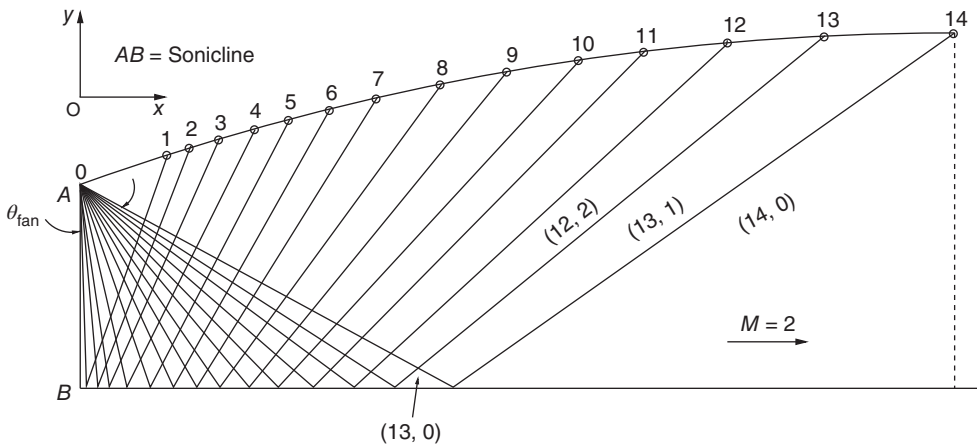


Figure 9.21 Characteristic lines and contour points.

A total of 14 characteristics are considered in the fan, with the first being at an angle of  $0.19^\circ$  with the sonic line and the rest being at a difference of  $1^\circ$  to each other, as illustrated in Figure 9.21, that is all the waves (except the first) are of strength  $1^\circ$ . The reflections from the centerline form the regions. For example, characteristic 1 gives rise to 15 regions, from (0, 0) to (0, 14), as shown in the figure.

The values of  $\nu$  and  $\theta$  at every region can be calculated as follows. For the regions formed by the first wave, we have

$$\begin{aligned}\theta &= 0^\circ, & \nu &= 0 & [\text{region}(0, 0)] \\ \theta &= 0.19^\circ, & \nu &= 0.19^\circ & [\text{region}(0, 1)] \\ \theta &= 1.19^\circ, & \nu &= 1.19^\circ & [\text{region}(0, 2)]\end{aligned}$$

For the regions formed by the second wave,

$$\begin{aligned}\theta &= 0^\circ, & \nu &= 0.38^\circ & [\text{region}(1, 0)] \\ \theta &= 1^\circ, & \nu &= 1.38^\circ & [\text{region}(1, 1)]\end{aligned}$$

and so on.

Similarly, we can go up to region (14, 0).

A computer program can be written for the calculation of  $\theta$  and  $\nu$  in every region. The program can take the input of a number  $n$  and divide the  $\theta_{\text{fan}}$  into  $(13/n + 1)$  characteristics. In the present calculation  $n$  is taken as unity. (The program listing for calculating the values of  $\nu$  and  $\theta$  in the regions considered is given in the Appendix of [6].) Once  $\nu$  is known, the Mach number can be obtained from Table A.1.

The values of  $\nu$  and  $\theta$  at different regions shown in Figure 9.21 and the corresponding Mach numbers can be obtained in this way.

Note that, in the present nozzle design for Mach 2, the computed area ratio (considering the width in the  $z$ -direction as unity) is

$$\begin{aligned}\frac{A_e}{A^*} &= \frac{y_e \times 1}{y^* \times 1} = \frac{14.41}{8.8} \\ &= 1.6375\end{aligned}$$

The corresponding area ratio (for Mach 2 nozzle) from the isentropic area–Mach number relation is  $A_e/A^* = 1.688$ . Thus, the error in the result of  $A_e/A^*$  computed by the method of characteristics is

$$\begin{aligned}\text{error} &= \frac{(A_e/A^*)_{\text{isen}} - (A_e/A^*)_{\text{moc}}}{(A_e/A^*)_{\text{isen}}} \times 100 \\ &= \frac{1.688 - 1.6375}{1.688} \times 100 \\ &= 2.99\%\end{aligned}$$

For calculating the  $x$ -location of a contour point  $i$ , the following formula may be used:

$$\begin{aligned}x_i &= \frac{(A/A^*)_i - (A/A^*)_{i-1}}{2 \tan(\theta_{i-1})} y^* + x_{i-1} \\ y_i &= (A/A^*)_i y^*\end{aligned}$$

where  $i = 1, 2, \dots, 14$ . In these equations,

$\theta_{i-1}$  = turning angle in region  $i - 1$

$(A/A^*)_i$  = area ratio at point  $i$

$(A/A^*)_{i-1}$  = area ratio at point  $i - 1$

$A^*$  = area at the throat

$y^*$  =  $y$ -coordinate at the throat

Also,

$(A/A^*)_0$  = area ratio at the throat = 1

$\theta_0 = 13.19^\circ$  (in the present case)

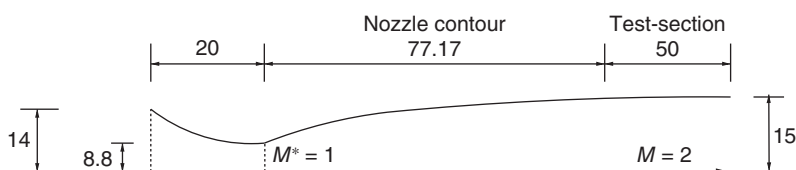
The area ratio at a particular point may be calculated from Eq. (2.32) or Table A.1 in the Appendix as the Mach number at that point is known. The area ratio also gives the  $y$ -location of the point. Table 9.3 shows the  $x$  and  $y$  coordinates of contour points. These contour points along with characteristics are shown in Figure 9.21.

The resulting nozzle contour given by the calculated points is shown in Figure 9.22. A nozzle fabricated as per the contour in this figure generated a uniform parallel supersonic stream with Mach number 1.97 at the gas dynamics laboratory at the Indian Institute of Technology Kanpur.

In the above calculations, viscosity has been neglected. But in actual flow, the boundary layer on the nozzle and side walls will have a displacing effect which will reduce the effective height and width of the nozzle. Allowance for this should be made by adding a correction for boundary layer growth to the designed contour. Finally, we should note that, in the present example, the calculation procedure has been very much simplified by assuming the flow in the nozzle to be two-dimensional. For axisymmetric and three-dimensional flow, the strength of a wave, generally, varies continuously in space, and therefore the simple relations between  $\nu$  and  $\theta$  used in the present case are no longer valid.

**Table 9.3** Coordinates of contour points.

Contour points	Throat	1	2	3	4	5	6	7
$x$ mm	0.0	7.76	7.95	9.01	10.25	11.69	13.38	15.40
$y$ mm	8.8	10.62	10.66	10.89	11.13	11.38	11.65	11.93
		8	9	10	11	12	13	14
		17.84	20.85	24.66	29.69	36.78	48.00	71.70
		12.23	12.55	12.88	13.24	13.61	14.00	14.41



**Figure 9.22** De Laval nozzle contour generated by method of characteristics.



## 9.8 Summary

Method of characteristics is basically a numerical technique. Characteristics are weak waves across which there is a jump in the gradients of flow properties.

The general features of the characteristics are the following.

- They exist only in supersonic flows.
- They are coincident with Mach lines.
- On the characteristics, the derivatives of flow properties are discontinuous, while the flow properties themselves are continuous.
- On the characteristics, the dependent variables satisfy a particular relation known as the compatibility relation.

The compatibility relations are

$$v - \theta = R \text{ (constant) along } \eta\text{-characteristics}$$

$$v + \theta = Q \text{ (constant) along } \xi\text{-characteristics}$$

These relations provide the key to the method of computation. The compatibility relations, which are independent of the specific flow geometry, lead to the result that the flow changes encountered in crossing characteristics that are straight are given by

$$\Delta v = \pm \Delta \theta$$

where the plus sign is for  $\xi$ -characteristics and the minus sign is for  $\eta$ -characteristics.

On a rigid boundary, a wave is reflected as a wave of the same sense (of opposite family), and on an open or free boundary a wave is reflected as a wave of opposite sense.

The deflection of a free boundary is downward if an expansion wave hits it and the deflection is upward when a compression wave hits it.

The wave reflection may be *canceled* by suitable accommodation of the portion of the wall after the incident wave.

The method of characteristics provides a technique for the proper design of supersonic nozzles for shock-free, isentropic flow. Centered expansion of the flow at the throat results in a short-length nozzle and continuous expansion at the throat results in a long nozzle.

For calculating the  $x$ - and  $y$ -coordinates of a contour point  $i$ , the following formulae may be used.

$$x_i = \frac{(A/A^*)_i - (A/A^*)_{i-1}}{2 \tan(\theta_{i-1})} y^* + x_{i-1}$$

$$y_i = (A/A^*)_i y^*$$

where

$$\theta_{i-1} = \text{flow turning angle in region } i - 1$$

$$(A/A^*)_i = \text{area ratio at point } i$$

$$(A/A^*)_{i-1} = \text{area ratio at point } i - 1$$

$$A^* = \text{area at the throat}$$

$$y^* = y\text{-coordinate at the throat}$$

The close agreement between the design and measured Mach numbers experienced by experimental researchers highlights the validity of this method for the design of supersonic nozzles for practical applications such as supersonic wind tunnels.

## 10

## Measurements in Compressible Flow

### 10.1 Introduction

For calibration and use of flow devices such as wind tunnels, we have to do many measurements to define the properties of the flow in the device. Once the calibration of the device is complete, to compute the forces and their distribution on the models that are to be tested by placing them in the known flow field generated by wind tunnel, we again require instruments and techniques for making these measurements. In this chapter we shall study some of the popular techniques and devices used for measuring the properties of a compressible flow. From our basic studies on fluid flows, we know that the important variables that need measurement are pressure, temperature, density, and flow velocity including its direction. We shall discuss the methods available for the measurement of these properties for compressible flows.

### 10.2 Pressure Measurements

The pressure measuring devices used for fluid flow pressure measurements can generally be grouped as manometers and pressure transducers. Various types of liquid manometers are employed, depending on the range of pressures to be measured and the degree of precision required. “U”-type manometers, multitube manometers, micromanometers, and Betz type manometers are some of the popular liquid manometers. The pressure transducers used may be classified as electrical type transducers, mechanical type transducers, and optical type transducers.

#### 10.2.1 Liquid Manometers

In a liquid manometer the pressure is balanced by the weight of the liquid column. The sensitivity of the instrument depends on the density of the fluid used. Water, alcohol, and mercury are the commonly used fluids. For compressible flows with high subsonic and supersonic Mach numbers, mercury is suitable since fluids like water and alcohol will give unmanageable variations in manometer columns for the pressures associated with such speeds.

In addition to these manometers, an accurate *barometer* is essential for pressure measurements, since pressures are invariably measured in terms of a difference in pressure from some known reference. The most common reference is the local atmospheric pressure. For pressures measured with reference to atmospheric pressure, conversions to absolute pressure requires that atmospheric pressure be known. The common mercury barometer, shown in Figure 10.1, is quite satisfactory for this purpose. When equipped with a suitable device for viewing the meniscus of the mercury column and reading the mercury column height scale,

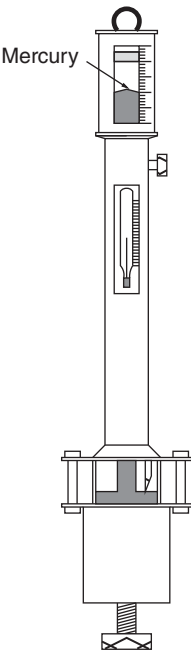


Figure 10.1 A mercury barometer.

a good barometer will allow the measurement of atmospheric pressure with an accuracy of a small fraction of a millimeter of mercury. This is usually quite adequate for the purposes of compressible flow measurements.

10.2.2 Measuring Principle of Manometers

Manometers measure the difference between a known and an unknown pressure by observing the difference in heights of two fluid columns. Two common types of manometers are illustrated in Figure 10.2.

Figure 10.2a consists of two vertical glass tubes joined together with a U-type connection at the bottom. Each tube has a linear scale attached to it, which is usually marked off in

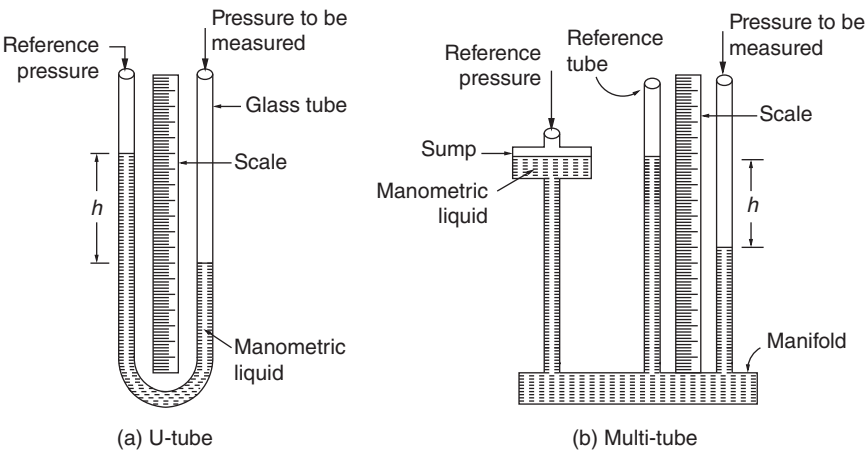


Figure 10.2 Manometers.

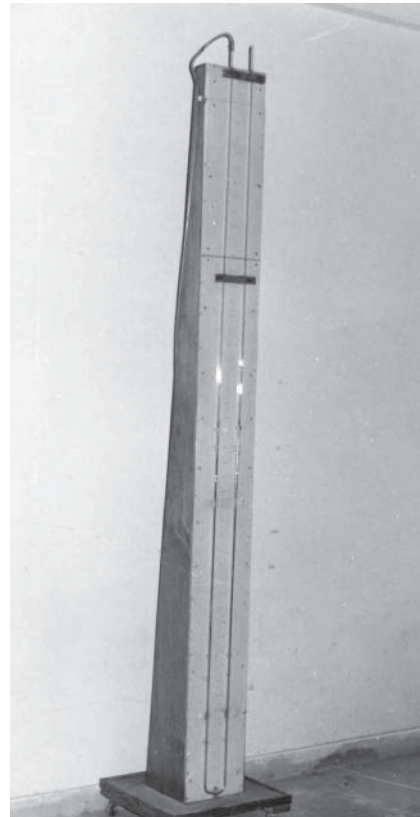
millimeters. The tubes are filled with a fluid until the fluid level in the tube is at the center of the adjacent scales. A reference pressure is applied to the top of one of the tubes and the pressure to be measured is applied to the top of the second tube. The heights of the two columns of fluid will change until the difference between the two heights,  $h$ , is equal to the pressure to be measured in terms of fluid column height. The commonly employed reference pressure for this type of manometer is atmospheric pressure. However, in many cases the difference between atmospheric and measured pressure will represent a much longer column of the manometer fluid than that can be accommodated by the tubes. In such cases, the only way to use the manometer (other than changing the fluid) is to adjust the reference so that a smaller fluid height will be reached. This had the disadvantage of adding an intermediate pressure to be measured.

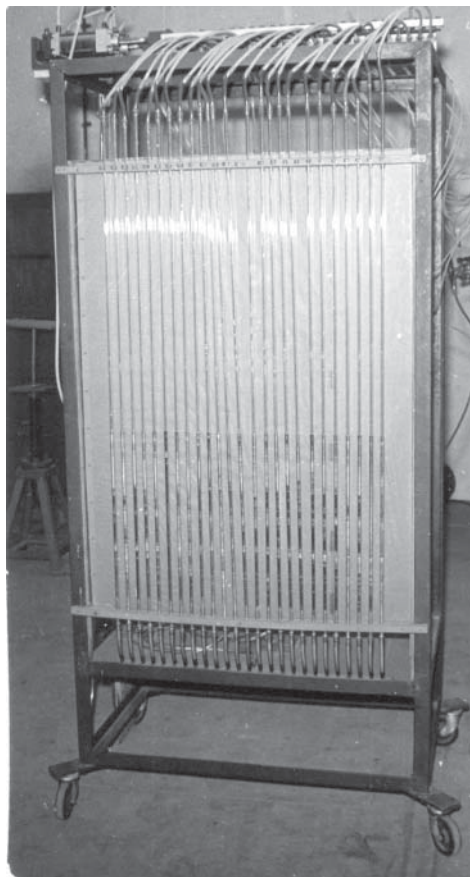
The sump and tube manometer, illustrated in Figure 10.2b, operates on the same principle as the U-tube manometer. However, in this manometer a large cross-sectional area sump takes the place of the tube to which the reference pressure is applied. The sump level is used as a reference, and, frequently, a number of tubes are employed to form a multitube manometer. The sump and tube manometer has the following advantages over the U-tube manometer.

- It can be used for the measurement of more than one differential pressure at a time.
- The reference level can be adjusted so that only one scale has to be read instead of two, to determine fluid column height. Photographs of a U-type and sump and multitube manometers are shown in Figures 10.3 and 10.4, respectively.

Either of the two types of manometer may be constructed with tubes and scales that can be tilted. In this way, an improvement in reading accuracy is obtained, since a given distance

**Figure 10.3** U-tube manometer.





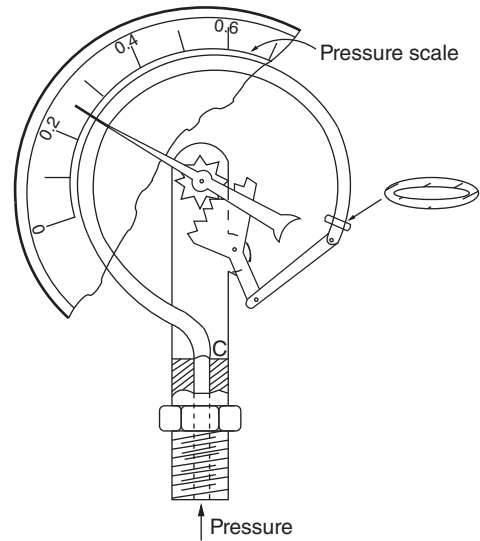
**Figure 10.4** Sump and multitube manometer.

along the scale will represent a smaller vertical height and consequently a smaller pressure difference.

The ordinary liquid manometers are not suitable for very high- or very low-pressure measurements. In addition, they have very poor frequency response. Further, a little dirt in a tube, a bubble in a line, or condensate changing the fluids' specific gravities can all produce anomalous readings. If the user takes care of the above-mentioned problems, the liquid manometers can prove to be an excellent device for pressure measurement in most practical situations barring a few flow situations, such as flow in intermittent tunnels where the accurate measurement of pressure with liquid manometers is very difficult because of the short durations available for measurements. However, these problems can be sorted out if one could arrange to connect an effective pinching mechanism, which could close all the columns of the manometer at an appropriate time, thereby making the liquids in different tubes stay wherever they are. After noting down the readings, the tubes can be opened again ready for the next measurement.

### **10.2.3 Dial-Type Pressure Gauges**

The dial-type pressure gauge, shown in Figure 10.5, usually operates on the principle of a bellows or a Bourdon tube deflecting as a result of a pressure change and driving the needle on a dial through a mechanical linkage. Although gauges of this type may be obtained with accuracies suitable for quantitative pressure measurements, they are not extensively used for this purpose. They are primarily used for the visual monitoring of pressure in plumbing circuits.

**Figure 10.5** Dial-type pressure gauge.

As compared to manometers, dial-type gauges have the advantage of being easier to read. Also, they can be obtained for pressure ranges well beyond those of the manometers. However, they do have the following disadvantages.

- They must be calibrated periodically to ensure that they continue to read correctly.
- The manometers are less expensive when there are a large number of pressures to be read, whereas the dial-type gages are expensive for such measurements.
- Like manometers, they cannot be easily read electronically.

#### 10.2.4 Pressure Transducers

Pressure transducers can be designed and built for almost any pressure generally encountered in fluid flow measurement. These can also be used for remote indication. Pressure transducers are electromechanical devices that convert pressure to electrical signals, which can be recorded with a data system such as that used for recording strain gauge signals. These transducers are generally classified as mechanical, electrical, or optical type.

The commonly used transducers employ an elastic diaphragm (various shapes) which is subjected to a displacement whenever pressure is applied. This movement is generally small and kept within linear range, and is amplified using mechanical, electrical, electronic, or optical systems. A typical diaphragm pressure capsule is illustrated in Figure 10.6.

The local strain produced on the diaphragm is proportional to the pressure applied. For a circular diaphragm, the deflection  $\delta$  at the center is given by

$$\delta = \frac{3p}{16Et^2}a^4(1 - \mu_r^2)$$

where  $a$  is the diaphragm radius,  $t$  is the diaphragm thickness,  $\mu_r$  is Poisson's ratio,  $E$  is Young's modulus, and  $p$  is pressure. This holds good for small deflections only.

For large deflections, corrugated diaphragms have to be used. Usually, the diaphragms are made using beryllium copper or phosphor-bronze sheets. Heat-treated stainless steel diaphragms are also often employed. Photographs of some transducers are shown in Figure 10.7.

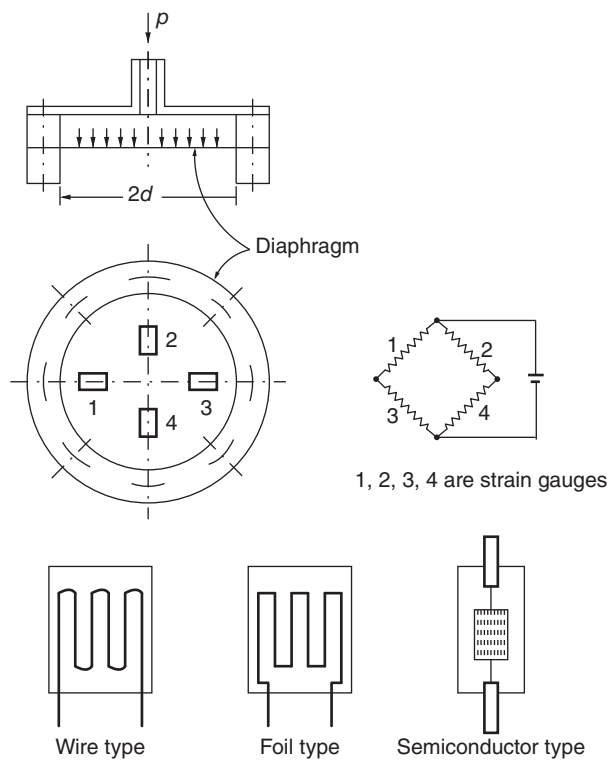


Figure 10.6 Pressure transducer (strain gauge type).

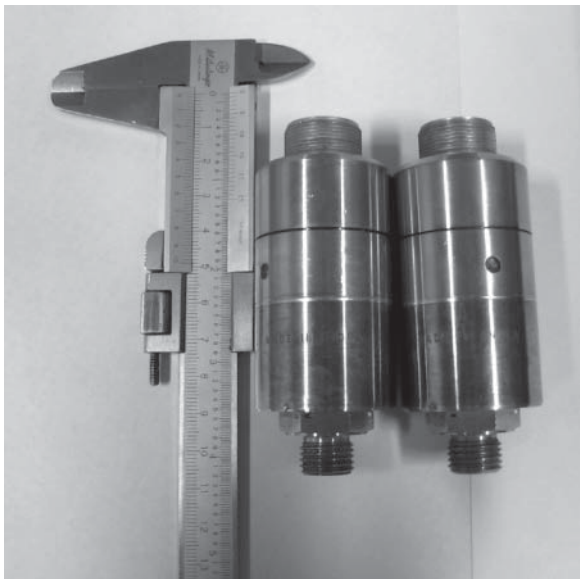


Figure 10.7 Pressure transducers (vernier caliper used to show scale).

The following are the advantages of pressure transducers over manometers and other pressure gauges.

- They provide a signal proportional to pressure which can be automatically recorded by any data system.
- They are relatively low-volume devices and consequently respond more rapidly to pressure changes.
- They are small enough to be mounted inside wind tunnel models.

Their major disadvantage relative to a good manometer is that they must be calibrated, whereas the manometer with a known fluid can be considered as the pressure standard.

Because of the relatively high cost of pressure transducers, a scheme has been devised for using one transducer to measure a number of pressures – up to 48 or more. This scheme is the commutation of pressures using a device known as a *pressure scanner valve*.

In using the scanner valve models, pressures are allowed to stabilize in the lines leading from the model through the stator of the scanner valve. The rotor is then turned through one revolution, connecting each model pressure in turn to the pressure transducer through a slot.

### Example 10.1

The U-type manometer measures total and static pressures of a high-speed flow as 535 mm of mercury (suction) and 610 mm of mercury (suction), respectively. Determine the flow Mach number.

#### Solution:

Assuming the atmospheric pressure to be 760 mm Hg (standard sea level pressure), the total and static pressures of the stream in absolute scale are

$$\begin{aligned} p_{t_{\text{abs}}} &= p_{t_{\text{meas}}} + p_{\text{atm}} \\ &= -535 + 760 = 225 \text{ mm Hg} \end{aligned}$$

$$\begin{aligned} p_{\text{abs}} &= p_{\text{meas}} + p_{\text{atm}} \\ &= -610 + 760 = 150 \text{ mm Hg} \end{aligned}$$

$$\frac{p}{p_t} = \frac{150}{225} = 0.667$$

For this pressure ratio, from Table A.1 in the Appendix,

$$M = \boxed{0.783}$$

## 10.3 Temperature Measurements

For direct measurement of the static temperature, the device that measures the temperature should travel at the velocity of the flow without disturbing the flow. But this is impractical. Therefore, alternatively, the measurement of temperature of high-speed streams is almost invariably made using thermocouples. Thermocouple is a device which operates on the *Seebeck effect*, which states that *a flow of heat in a metal is always accompanied by a flow of electromotive force (emf)*. In other words, the Seebeck principle states that, “heat flow in a metal is always accompanied by an emf.” This is also referred to as the *Seebeck effect*. This forms the basis for the working of the *thermocouple*. In a vast number of metals like copper, platinum, chromel, and iron, both heat and emf flow in the same direction. But in another group of metals, like constantan, alumel, and rhodium, the direction of heat flow is opposite to that of the emf. These two groups are commonly known as *dissimilar metals*. The



thermocouple consists of two dissimilar metals joined together at two points, one point being the place where the temperature is to be measured and the other point being a place where the temperature is known (called the *reference junction*).

First, let us consider the measurement of temperature by locating a thermocouple or other thermometric device at the wall surface, as shown in Figure 10.8.

The thermocouple at the wall surface lies inside the viscous boundary layer, at a fixed wall, where the flow velocity is zero, and we should expect the measured wall temperature to be closer to the freestream total temperature  $T_{t\infty}$ , than the free stream static temperature  $T_\infty$ . A temperature distribution in a compressible-flow boundary layer is as shown in Figure 10.8. Let us assume that the wall is insulated. Therefore,

$$\frac{\partial T}{\partial y} = 0 \quad \text{at } y = 0$$

and the temperature is called the *adiabatic wall temperature*  $T_{aw}$ . There is heat flow in the  $y$ -direction due to conduction. Because of the flow of a high-velocity gas stream near a surface, there can be appreciable frictional heating of the fluid. In other words, the fast-moving layers in the boundary do work on the slowly moving layers. If the heat loss due to conduction and energy gain from viscous heating cancel each other then the flow can be considered brought to rest adiabatically in the boundary layer, and  $T_{aw} = T_{t\infty}$ . A measure of the relative importance of heating is given by the *Prandtl number*, defined as

$$\text{Pr} = \frac{\mu c_p}{K}$$

For a fluid with  $\text{Pr} = 1$ , the adiabatic wall temperature is equal to the freestream stagnation temperature. If  $\text{Pr} < 1$ , then  $T_{aw} < T_{t\infty}$ . This can be summarized by defining a *recovery factor*  $R$ , where

$$R = \frac{T_{aw} - T_\infty}{T_{t\infty} - T_\infty}$$

Since  $T_{t\infty} = T_\infty \left( 1 + \frac{\gamma-1}{2} M_\infty^2 \right)$ , from Eq. (1.72), it follows that

$$T_{aw} = T_\infty \left( 1 + R \frac{\gamma-1}{2} M_\infty^2 \right)$$

It can be shown that for a laminar compressible boundary layer,

$$R = \text{Pr}^{1/2}$$

whereas for a turbulent boundary layer,

$$R \approx \text{Pr}^{1/3}$$

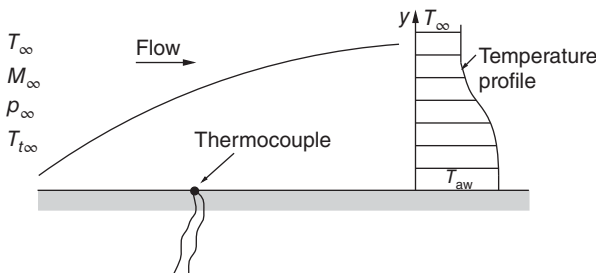
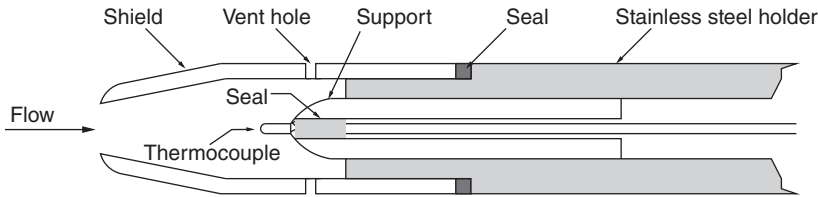


Figure 10.8 Thermocouple at wall.



**Figure 10.9** Stagnation temperature probe.

For air, up to moderately high temperatures,  $Pr = 0.72$ , so that  $R \approx 1$ , for a turbulent boundary layer.

From the foregoing discussion, it is clear that a direct measurement of freestream static temperature is not possible; a measurement of the adiabatic wall temperature can be used to determine  $T_{t\infty}$ ; then by measuring  $p_{t\infty}$  and  $p_{\infty}$ ,  $M_{\infty}$  and  $T_{\infty}$  can be calculated.

For measurement of temperature in the absence of a wall, a stagnation temperature probe, as illustrated in Figure 10.9, can be used to determine  $T_{t\infty}$ . The flow is brought to rest inside the tube. Vent holes are provided in the sides of the probe to allow for the proper ventilation of the space inside the probe. If the air is allowed to be stagnant inside, it may get cooled and yield a false reading. It is necessary that the flow be slowed down to zero velocity at the thermocouple with no gain or loss of heat.

Shields have been provided to prevent radiation heat loss from the thermocouple. The thermocouple lead wires must be made as thin as possible so as to minimize heat flow by conduction back along the wires.

When the flow is supersonic, there will be a detached shock standing in front of the probe. However, the measurement of  $T_{t\infty}$  is unaffected by the presence of the shock, since the flow process across the shock is adiabatic. In such streams, the probes usually measure temperatures from slightly below to considerably below the true stagnation temperatures. The performance of such a probe is usually defined by a *recovery factor*  $k$  as follows.

$$k = \frac{T_{ti} - T_{\infty}}{T_t - T_{\infty}}$$

where  $T_{ti}$  is the indicated or measured total temperature in kelvin,  $T_t$  is the actual total temperature in kelvin, and  $T_{\infty}$  is the static temperature in kelvin. By suitable design,  $k$  can be made very close to unity for air. In any case, such a probe must be calibrated to define  $k$  as a function of  $Re$ ,  $Pr$ , and  $M$ .

The above-mentioned techniques for measuring temperature of a compressible flow stream are only selective representations of the various techniques available for such measurements. For a deeper understanding of these measurement procedures; the reader should refer to books on experimental techniques, such as *Instrumentation, Measurements, and Experiments in Fluids* by Rathakrishnan [5].

### Example 10.2

A total temperature probe measures the temperature of a Mach 1.5 air flow as 520 K. If the probe has a recovery factor of 0.97, determine the stream static temperature.

#### Solution:

From the isentropic table (Table A.1), for  $M_{\infty} = 1.5$ ,  $T_{\infty}/T_{t\infty} = 0.6897$ . Given: the recovery factor is 0.97. Therefore,

$$0.97 = \frac{T_{ti} - T_{\infty}}{T_{t\infty} - T_{\infty}}$$

that is

$$\frac{520 - T_{\infty}}{\left(\frac{1}{0.6897} - 1\right) T_{\infty}} = 0.97$$

This gives the stream static temperature  $T_{\infty}$  as

$$T_{\infty} = \boxed{362 \text{ K}}$$

## 10.4 Velocity and Direction

The velocity or Mach number and flow angularity are essential for calibrating flow devices, such as wind tunnels. With the measured pressure and temperature, the magnitude of the velocity can be calculated with the relation

$$V = M\sqrt{\gamma RT}$$

In order to decide on the quality of the flow device, it is also necessary to know the direction of the velocity vector or the flow angularity. At supersonic speeds, this can be found with a symmetric wedge or cone, as shown in Figure 10.10.

For a uniform flow passing over a symmetrical wedge, the angle of attack of the wedge can be determined from a measurement of the pressure difference ( $p_u - p_l$ ). For a flow without angularity, a symmetrical wedge with its centerline aligned with the flow must read the pressure difference ( $p_u - p_l$ ) as zero.

Instead of obtaining the velocity from the pressure and temperature measurements, we can measure it directly by using a hot-wire probe. The probe consists of a short length of a thin wire kept in the flow stream, with the wire heated by passing electric current through it. An equilibrium of the convective cooling of the wire with electrical energy input is maintained. Therefore,

$$I^2 R_w = hA(T_w - T_{\infty})$$

where  $I$  is the electric current,  $R_w$  is the electrical resistance of the wire,  $A$  is the surface area of the wire exposed to the flow,  $h$  is the convective heat transfer coefficient,  $T_w$  is the wire surface temperature, and  $T_{\infty}$  is the freestream temperature.

Measuring  $R_w$ ,  $I$ , and  $T_{\infty}$ , and knowing the wire temperature as a function of resistance,  $h$  can be calculated from the above relation.

The flow velocity and the convective heat transfer are related in a unique fashion; this is generally known as *King's law*.

$$\text{Nu} = A_1 \text{Pr} + B_1 \text{Pr}(\text{Re})^{1/2}$$

where the Nusselt number  $\text{Nu}$  gives the heat transfer rate and the Prandtl number  $\text{Pr}$  is constant for air at room temperature. Therefore,

$$\text{heat transfer rate} = A_2 + B_2(\text{Re})^{1/2}$$

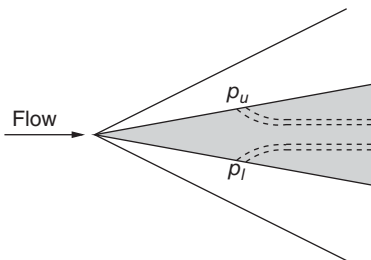


Figure 10.10 Symmetrical wedge.

Using electrical units, we obtain, for a given wire in air flow, the equation

$$\frac{I^2 R_w}{R_w - R_g} = A + B(V)^{1/2}$$

where  $R_g$  is cold resistance of unheated wire at air temperature,  $R_w$  is the wire resistance when exposed to the flow,  $V$  is flow velocity, and  $A$  and  $B$  are constants to be obtained from calibration experiments.

By measuring the quantities on the left-hand side of King's law, the flow velocity can be determined.

The above heat transfer–velocity relation is valid in the Reynolds number range

$$0.1 < \text{Re} < 10^5$$

where  $\text{Re} = Vd/\nu$ , with  $d$  as the diameter of the wire and  $\nu$  the kinematic viscosity of the fluid.

In reality it is difficult to measure  $I$  and  $R_w$  simultaneously, especially at high velocities. Hence, one of the quantities is kept constant and the other allowed to vary. A system where  $I$  is kept constant is called a *constant current hot wire anemometer*; with  $R_w$  constant, it is called a *constant resistance system*. Since the resistance and temperature are uniquely related for a given wire material, the latter is also known as a *constant temperature hot wire anemometer*. For more details about hot-wire anemometry, the reader may refer to [5].

## 10.5 Density Problems

The density of the flow can be calculated by measuring or determining the pressure and temperature. However, apart from the above-discussed methods of experimentally investigating flow patterns by means of pressure and velocity surveys, compressible flows lend themselves particularly well to optical methods of investigation. These optical methods (considered here) depend on the variation of density or its derivatives in the flow field.

The commonly used optical methods for compressible flow analysis – the interferometer, the Schlieren, and the shadowgraph – depend on either of two physical phenomena.

- The speed of light depends on the index of refraction of a gas and this in turn depends on its density.
- Light passing through a density gradient in a gas is deflected in the same manner as though it were passing through a prism. (This is a consequence of the first phenomenon.)

In a high-speed flow, the density changes are sufficient to make these phenomena adequate for optical observation. The interferometer measures directly the changes in density, and is primarily suited for quantitative determination of the density field.

The Schlieren method measures density gradients. Although it is theoretically possible to adapt it for quantitative use, it is inferior to the interferometer in this respect.

The shadowgraph method measures the second derivative of the density. Therefore, it makes visible only those parts of the flow field where the density gradients change very rapidly and is therefore suitable for the study of shock waves.

## 10.6 Compressible Flow Visualization

In supersonic flows, the air density changes are sufficiently large to allow the air to be photographed directly, using optical systems that are sensitive to density changes. In this chapter,

we will study some of the techniques that are often employed for fluid flow analysis. The general principle for flow visualization is to render the “fluid elements” visible by either (i) observing the motion of suitable selected foreign materials added to the flowing fluid or (ii) using an optical pattern resulting from the variation of the optical properties of the fluid, such as refractive index, owing to the variation of the properties of the flowing fluid itself. The first group of techniques is generally used for incompressible flows and the second group for compressible flows.

Some of the popularly used visualization techniques for studying transonic and supersonic flow problems of practical interest are as follows.

- *Interferometry* is an optical technique that gives a qualitative estimate of flow *density* in the field.
- The *Schlieren* technique gives a qualitative estimate of the *density gradient* of the field. This is used to visualize faint shock waves, expansion waves, and so on.
- The *Shadowgraph* method is employed for fields with strong shock waves.

### 10.6.1 Supersonic Flows

For visualizing compressible flows, optical flow visualization techniques are commonly used. Interferometer, Schlieren, and shadowgraph are the three popularly employed optical visualization techniques for visualizing shock and expansion waves in supersonic flows. They are based on the variation of the refractive index, which is related to the fluid density by the Gladstone–Dale relation and consequently to the pressure and velocity of the flow. For making these variations visible, the three different classes of methods mentioned above are generally used. With respect to a reference ray, that is a ray that has passed through a homogeneous field with refractive index  $n$ , the methods do the following.

- The *interferometer* makes visible the *optical phase changes* resulting from the relative retardation of the disturbed rays.
- The *Schlieren* system gives the deflection angles of the incident rays.
- The *shadowgraph* visualizes the *displacement experienced by an incident ray* that has crossed the high-speed flowing gas.

These optical visualization techniques have the advantage of being nonintrusive and thereby in the supersonic regime of flow, avoiding the formation of unwanted shock or expansion waves. They also avoid problems associated with the introduction of foreign particles, which may not accurately follow the fluid motion at high speeds because of inertia effects. However, none of these techniques gives information directly on the velocity field. The optical patterns given by the interferometer, Schlieren, and shadowgraph, respectively, are sensitive to the *flow density*, *its first derivative*, and *its second derivative*. For quantitative evaluation, the interferometry is generally chosen because this evaluation is based upon the precise measurement of fringe pattern distortion instead of the not so precise measurement of change in photographic contrast, as in the Schlieren and shadowgraph. However, Schlieren and shadowgraph visualizations being useful and less expensive are often used to visualize flow patterns, especially at supercritical Reynolds numbers. In particular, they clearly show shock waves and, when associated with ultrashort duration recordings, they also show the flow structure. Although these optical techniques are simple in principle, they are rather difficult to implement. High precision and high optical quality of the setup components, including the wind tunnel test-section windows, are required for proper visualization with these techniques.

## 10.7 Interferometer

The interferometer is an optical method best suited to qualitative determination of the density field of high-speed flows. Several types of interferometer are used for the measurement of the refractive index, but the instrument most widely used for density measurements in gas streams (wind tunnels) is that attributed to Mach and Zehnder.

The fundamental principle of the interferometer is the following. From the wave theory of light we have

$$c = f\lambda \quad (10.1)$$

where  $c$  is the velocity of propagation of light,  $f$  is its frequency, and  $\lambda$  is its wavelength.

From corpuscular properties of light, we know that when light travels through a gas the velocity of propagation is affected by the physical properties of the gas. The velocity of light in a given medium is related to the velocity of light in a vacuum through the index of refraction  $n$ , defined as

$$\frac{c_{\text{vac}}}{c_{\text{gas}}} = n \quad (10.2)$$

The value of refractive index  $n$  is 1.0003 for air and 1.5 for glass.

The Gladstone–Dale empirical equation relates the refractive index  $n$  to the density of the medium as

$$\frac{n - 1}{\rho} = K \quad (10.3)$$

where  $K$  is the Gladstone–Dale constant for the given gas and  $\rho$  is the gas density.

### 10.7.1 Formation of Interference Patterns

Figure 10.11 shows the essential features of the *Mach–Zehnder interferometer*, schematically.

Light from the source is made to pass through lens  $L_1$ , which renders the light parallel. The parallel beam of light leaving the lens passes through a monochromatic filter. The light wave passes through two paths (1–2–4 and 1–3–4) before falling on the screen, as shown in the figure. The light rays from the source are divided into two beams by the half-silvered mirror  $M_1$ . The two beams, after passing through two different paths (the lengths of paths being the same), recombine at lens  $L_2$  and are projected onto the screen. The difference between the two

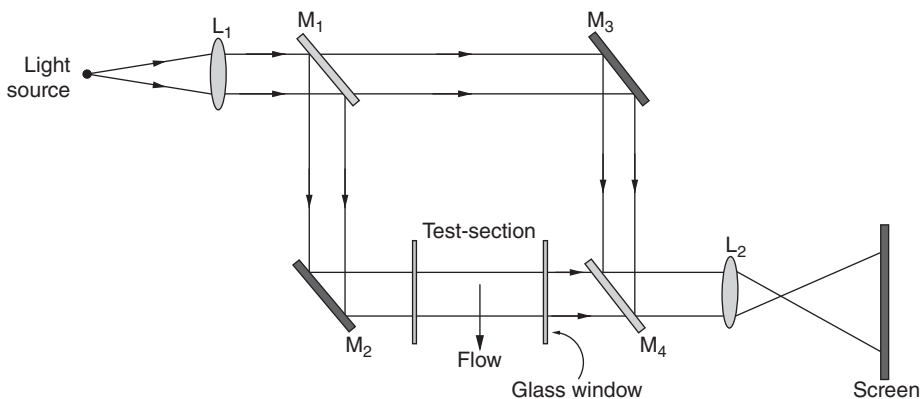


Figure 10.11 Mach-Zehnder interferometer.

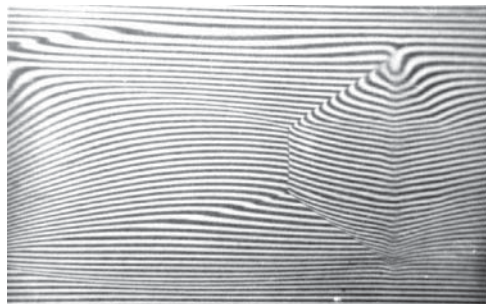
rays is that one (1–3–4) has traveled through room air while the other (1–2–4) has traveled through the test-section. When there is no flow through the test-section, the two rays having passed through identical paths are in phase with each other and recombine constructively. Thus, a uniform patch of light will be seen on the screen. Now, *if the density of the medium of one of the paths is changed (say increased) then the light beam passing through will be retarded and there will be a phase difference between the two beams.* When the magnitude of the phase difference is equal to  $\lambda/2$ , the two rays interfere with each other giving rise to a dark spot on the screen. Hence, if there is appreciable difference in the density, the picture on the screen will consist of dark and white bands, the phase difference between the consecutive dark bands being equal to unity. An interferogram of a two-dimensional supersonic jet is shown in Figure 10.12.

It can be seen that, far away from the jet axis, the fringes (dark and white bands) are parallel, indicating that the flow field has uniform density (in this case, the zone is without flow). The mild kinks in the fringes are the location of the density change. Those who are familiar with a free jet structure will easily be able to observe the barrel shock, the Mach disc, and the reflection of the barrel shock from the Mach disc.

### 10.7.2 Quantitative Evaluation

Before attempting any quantitative evaluation of an interferogram, it is imperative to understand the “bands” on the picture. If the optical path of each ray in one leg of the interferometer is equal to the optical path of the corresponding ray in the other leg, the split beams coming together at  $M_4$  in Figure 10.11 will reinforce each other so as to render the screen uniformly bright. This will also occur if the optical path lengths are different by an integer number of wavelength. Let us assume that this is the condition of the interferometer when there is no flow in the test-section. When there is flow in the test-section, the optical path lengths of each ray through the test-section may change depending on the density change encountered by the ray traversing the flow. If a ray going through the test-section has an optical path length that is an integer plus one-half of a wavelength difference from the corresponding ray through the other leg of the interferometer, there will be complete destructive interference of the two rays as they emerge from the mirror  $M_4$ . This will give rise to a black band on the screen. Similarly, a complete constructive interference will result in a white band on the screen. Therefore, there is a possibility of a range of partially constructive and partially destructive interference, giving rise to a gray zone on the screen. The picture then will be a series of black and white fringes with a variation of hue between the fringes.

At this stage, we must note that a slight rotation of the mirrors  $M_1$  and  $M_4$  about their vertical axes will result in a series of equally spaced vertical fringes. In practice, this is the initial setting usually taken, since the use of such an initial setting makes it easier to ascertain the amount of



**Figure 10.12** Interferogram of a two-dimensional supersonic jet at  $M = 1.62$ .

retardation associated with each fringe when there is a flow present, which makes it easier to determine the density field of the flow.

With this background we can now attempt to evaluate the interferogram quantitatively. We know that, on the dark bands of Figure 10.12, the light waves passing through the test-section are out of phase with those that pass through the room air in the compensating chamber by  $1/2, 3/2, 5/2, \dots$  of the wavelength  $\lambda_{\text{room}}$  of light in the room atmosphere. Therefore, the light beams passing through the adjacent dark bands of the test-section are out of phase by one wavelength ( $1 \times \lambda_{\text{room}}$ ). Hence, if  $a$  represents the fluid lying in one dark band and  $b$  the fluid in an adjacent dark band, the difference in time for a light beam to pass through  $a$  as compared to that passing through  $b$  is given by

$$t_b - t_a = \frac{\lambda_{\text{room}}}{c_{\text{room}}} \quad (10.4)$$

where  $t_a$  is the time for the light to pass through a region of density  $a$ , and  $t_b$  is the time required for the light to pass through a region of density  $b$ . Let  $c_a$  and  $c_b$  be the velocities of propagation of light through regions  $a$  and  $b$ , and  $L$  be the length of the test-section along the light direction.

We know that the frequency  $f$  of a given monochromatic light is constant. Therefore,

$$f = \frac{V}{\lambda} = \frac{c_{\text{room}}}{\lambda_{\text{room}}} = \frac{c_a}{\lambda_a} = \frac{c_b}{\lambda_b} = \frac{c_{\text{vac}}}{\lambda_{\text{vac}}} \quad (10.5)$$

The difference in travel time given by Eq. (10.4) may also be expressed in terms of the difference in speed of light in the test-section, using Eq. (10.5), as

$$t_b - t_a = \frac{1}{f} = \frac{\lambda_{\text{vac}}}{c_{\text{vac}}} \quad (10.6)$$

Also,

$$t_b - t_a = \frac{L}{c_b} - \frac{L}{c_a} = \frac{\lambda_{\text{vac}}}{c_{\text{vac}}}$$

where  $L$  is the test-section width.

The velocity of light in a given medium is related to the velocity of light in a vacuum through the index of refraction  $n$  defined as

$$n \equiv \frac{c_{\text{vac}}}{c}, n_a \equiv \frac{c_{\text{vac}}}{c_a}, n_b \equiv \frac{c_{\text{vac}}}{c_b} \quad (10.7)$$

that is

$$n_b - n_a = c_{\text{vac}} \left( \frac{1}{c_b} - \frac{1}{c_a} \right) = \frac{c_{\text{vac}}}{L} \frac{\lambda_{\text{vac}}}{c_{\text{vac}}}$$

That is,

$$n_b - n_a = \frac{\lambda_{\text{vac}}}{L} \quad (10.8)$$

Now, the index of refraction may be connected to the gas density through the empirical Gladstone–Dale equation, Eq. (10.3), to result in

$$\boxed{\rho_b - \rho_a = \frac{\lambda_{\text{vac}}}{LK}} \quad (10.9)$$

The right-hand side of this equation can easily be computed from the dimension of the test-section, the color of the monochromatic light used, and the value of  $K$  for air. The density in the low-speed flow upstream of the nozzle throat may be found by measuring



the temperature and pressure in that region. With that region as a reference, the density on each dark band in the nozzle may be computed from Eq. (10.9). This kind of interferogram is also termed *infinite-fringe*, which signifies that the light field is uniform in the absence of flow through the test-section. Although, in principle, it is possible to compute the density field quantitatively, as discussed above, using interferograms, the accuracy of this procedure using the infinite-fringe interferogram will not be high unless the optical components are extraordinarily accurate. In fact, this is one of the major hurdles in the use of this technique for the quantitative evaluation of compressible flow fields.

### 10.7.3 Fringe-Displacement Method

This method is used when a more accurate quantitative estimate is required. This is just a modified version of the infinite-fringe technique described above. Let us consider the interferometer arrangement shown in Figure 10.11. Let the mirror  $M_3$  be rotated through a small angle with respect to mirror  $M_1$ . The two rays of light which were in phase at  $M_1$  will now be out of phase at the screen. Thus, the image on the screen (with no flow in the test-section) will consist of alternate white and dark bands, uniformly spaced, with each fringe lying parallel to the axis of rotation. The spacing of successive dark fringes may be shown to be equal to  $\lambda/2\delta$ , where  $\delta$  is the difference in the angles of rotation between the two splitters (that is mirrors  $M_1$  and  $M_3$ ).

Now, assume that the air density in the test-section is increased uniformly. This will result in a uniform displacement of all the wavefronts passing through the test-section. This displacement in turn will cause the interference bands on the screen to shift in a direction normal to the bands, even though the bands will remain parallel and uniformly spaced. The fringe shift is a measure of density change in the test-section. It can be shown that

$$\rho_2 - \rho_1 = \frac{\lambda_{\text{vac}}}{LK} \frac{l}{d} \quad (10.10)$$

where  $\rho_1$  and  $\rho_2$  are the density at the initial reference condition and the density in the test-section, respectively,  $d$  is the distance between the dark fringes in the reference condition, and  $l$  is the distance shifted by a dark fringe in passing from condition 1 to condition 2.

When there is flow in the test-section, nonuniform fringe shift will occur corresponding to the density field, and the resultant fringes will be curved. Eq. (10.10) may then be applied at each point in the flow. If both flow and no-flow photographs are taken, Eq. (10.10) may be used to determine the density change at each point, with respect to the no-flow density.

## 10.8 Schlieren System

The Schlieren method is a technique for visualizing the density gradients in a transparent medium. Figure 10.13 shows a typical Schlieren arrangement, usually employed for supersonic flow visualization.

Light from a source is collimated by the first lens and then passed through the test-section. It is then brought to a focus by the second lens and projected on the screen. At the focal point of the second lens, where the image of the source is formed, a knife-edge (which is an opaque object) is introduced to cut off part of the light. The screen is made to be uniformly illuminated by the portion of the light escaping the knife-edge, by suitably adjusting it to intercept about half the light, when there is no flow in the test-section. For the sake of simplicity, for instance, let us assume the test-section to be two-dimensional, with each light ray passing through a path

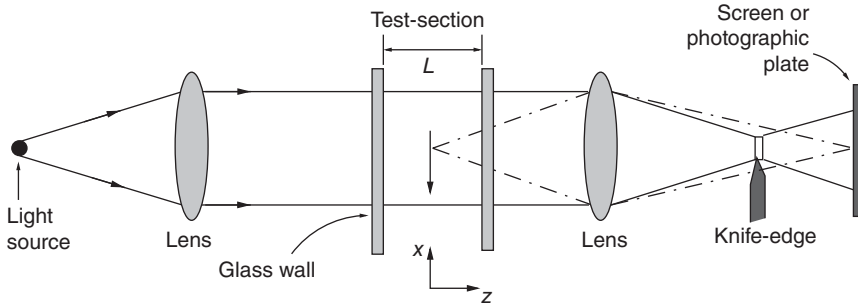


Figure 10.13 Schlieren system.

of constant air density. When flow is taking place through the test-section, the light rays will get deflected, since any light ray passing through a region in which there is a density gradient normal to the light direction will be deflected as though it had passed through a prism. In other words, if the medium in the test-section is homogeneous (constant density) the rays from the source will continue in their straight line path. If there is density gradient in the medium, the rays will follow a curved path, *bending toward the region of higher density and away from the region of lower density*. Therefore, depending on the orientation of the knife-edge with respect to the density gradient, and on the sign of the density gradient, more or less of the light passing through each part of the test-section will escape the knife-edge and illuminate the screen. Thus, *the Schlieren system makes density gradients visible in terms of variations of intensity of illumination*. A photographic plate at the viewing screen records density gradients in the test-section as different shades of gray.

Let us assume that the flow through the test-section is parallel and in the  $xy$ -plane. Assume the light to be passing through the test-section in the  $z$ -direction. From the theory of light, it is known that *the speed of a wavefront of light varies inversely with the index of refraction of the medium through which the light travels*. Therefore, a given wavefront will rotate as it passes through a gradient in the refractive index  $n$ . Hence, the normal to the wavefront will follow a curved path. This effect is stated earlier in other words as “the ray will follow a curved path bending toward the region of higher density and away from the region of lower density.” In such a case, the radius of curvature  $R$  of the light ray is proportional to  $1/n$ . It can be shown that

$$\frac{1}{R} = \text{gradient } n$$

The total angular deflection  $\epsilon$  of the ray in passing through the test-section of width  $L$  is therefore given by

$$\epsilon = \frac{L}{R} = L \text{ grad } n$$

Resolving this into Cartesian components, we have

$$\epsilon_x = L \frac{\partial n}{\partial x} \quad \epsilon_y = L \frac{\partial n}{\partial y}$$

Using Eq. (10.3), these equations can be expressed as

$$\epsilon_x = LK \frac{\partial \rho}{\partial x} \quad (10.11a)$$

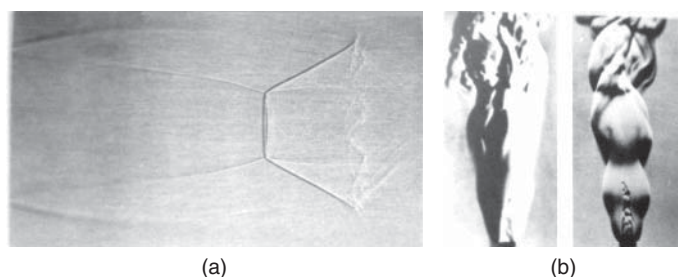
$$\epsilon_y = LK \frac{\partial \rho}{\partial y} \quad (10.11b)$$

From Eqs. (10.11a) and (10.11b) it can be seen that the Schlieren is sensitive to the first derivative of the density.

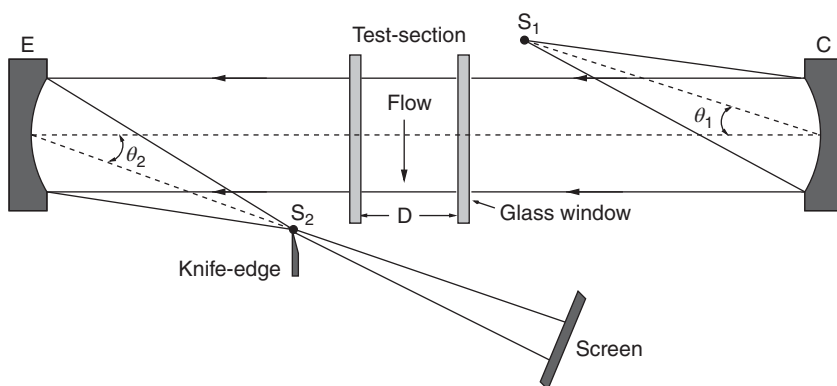
Referring to Figure 10.13 it can be visualized that, if the knife-edge is aligned normal to the flow, that is in the  $y$ -direction, only deflection  $\epsilon_x$  will influence the light passing the knife-edge. Therefore, only density gradients in the  $x$ -direction will be made visible, and the gradients in the  $y$ -direction will not be visible. Similarly, if the knife-edge is aligned parallel to the  $x$ -direction, only the gradients in the  $y$ -direction will be visible. A typical Schlieren picture of a free jet is shown in Figure 10.14a.

At this stage, we should note that the Schlieren lenses must not only be of high optical quality but also have large diameters and long focal lengths. The large diameter is necessary to cover the required portion of the flow field, which is often large (say 200 mm in diameter). The long focal length is necessary in order to get the required precision and image size. Further, the Schlieren lens should be free of chromatic and spherical aberrations. Also, the astigmatism must be as small as possible.

In experiments where the region under study has a large cross-section, as in the case of many modern wind tunnels, it is difficult to obtain lenses of sufficient diameter and focal lengths, and at the same time with the required optical properties, and if such lenses are made specially for such use they will prove to be extremely expensive. As a result, concave mirrors have been widely used instead. They are comparatively free from chromatic aberration and mirrors of large diameters and long focal lengths are much easier to grind and correct than lenses. A twin-mirror Schlieren system that gives good resolving power is shown in Figure 10.15. The mirrors C and E are a carefully matched pair. Usually they are made of glass, and their front



**Figure 10.14** Schlieren picture: (a) a supersonic free jet, (b) a Bunsen flame with knife-edge vertical (left) and horizontal (right).



**Figure 10.15** Twin-mirror Schlieren system.

surfaces are parabolized to better than one-tenth of a wavelength of light. The excellence of their optical quality bears a direct relation to the image quality produced. Also, owing to their size (often more than 300 mm in diameter) and weight, they must be carefully mounted to avoid distortions.

In the Schlieren setup arrangement, it is essential that the angle  $\theta_1$  must be approximately equal to angle  $\theta_2$  and that their value should be as small as possible, although angles up to about  $7^\circ$  are used successfully to obtain flow visualization of acceptable quality. The distance between the mirrors is not critical but it is good practice to make it greater than twice the focal length of the mirrors. Also, the optical system beyond  $S_2$  is simplified if the distance from the disturbance to be observed at test-section D to the mirror E is greater than the focal length of E. The parallel rays entering the region D are bent by the refractive index gradient and are no longer parallel to the beam from mirror C and hence, cannot be focused by the second mirror unless the distance from D to the second mirror E is greater than the focal length of E.

The image of the test-section flow field (containing the model) focused at the focal point at  $S_2$  will diverge and proceed further. This image can be made to fall on a flat screen. The clarity of the image can be modified by adjusting the knife-edge. Proper adjustment of the knife-edge can result in sharp images of the shock (or compression) and expansion waves prevailing in the flow falling on the screen. A still or video camera can record the image on the screen. When a video camera is used, the image can be made to fall on the camera lens. This will avoid the parallax error associated with capturing the image from the screen with a still camera kept at an angle to the screen, without cutting the light rays from  $S_2$ .

### 10.8.1 Range and Sensitivity of the Schlieren System

Let us assume that the contrast on the screen is increased by reducing the size of the image. That is, the knife-edge is made to cut off most of the light, any ray deflecting beyond a certain limit will be completely cut off by the knife-edge and further deflection will have no effect on the contrast. This means that the range gets limited. Increase in sensitivity affects the range of the density gradient for which the system could be used. The contrast or sensitivity requirement depends on the problem to be studied. Hence, to adjust the contrast the knife-edge is generally mounted with a vertical movement so that its position could be altered with respect to the image.

### 10.8.2 Optical Components Quality Requirements

The quality of the optical equipment to be used in the Schlieren setup depends on the type of the investigation carried out. The cost increases rapidly with the quality of the optical components. The vital components are the mirrors and the light source. Now, optical quality mirrors are easily available. The following specifications are sufficient to meet the visualization requirements of a 200 mm diameter flow field.

#### 10.8.2.1 Schlieren Mirrors

- Two parabolic mirrors of 200 mm diameter.
- Focal length of the mirrors about 1.75 m.
- Thickness of the mirror glass about 25 mm.

The reflecting surface of the mirrors should be ground to an accuracy of one-quarter wavelength of sodium light and aluminized. Parabolic mirrors are the most suitable, even though they are more expensive than spherical mirrors, which also will serve the purpose. It is important to note here that, although optical finish of  $\lambda/4$  is good enough for visualization of shock

waves, if it is the aim to study the structure of the flow field (e.g. shear layers in a free jet, and so on) with ultra-short Schlieren photography, a mirror surface finish of the order of  $\lambda/20$  is essential.

#### 10.8.2.2 Light Source

- Small intense halogen lamp of 30 W is commonly used.
- Mercury vapor lamp of suitable intensity (say 200 W) may also be employed.
- Provision to vary the intensity of light will prove useful.

#### 10.8.2.3 Condenser Lens

Any condenser lens pair generally used for projection systems will be sufficient. This need not be of very high quality.

#### 10.8.2.4 Focusing Lens

This lens is positioned in the Schlieren system in such a way that a flow field is focused on the screen. An ordinary double convex lens can be used.

#### 10.8.2.5 Knife-Edge

Any straight sharp-edged opaque object mounted on an adjustable stand will be sufficient to serve as a knife-edge. The Schlieren technique is generally used only for qualitative work, even though in principle it can be used for quantitative work. If quantitative measurements are to be done, the density of the image has to be measured and this can be done with a photodensitometer. This instrument contains a photo cell and it is scanned over the photographic film of the Schlieren image. By properly adjusting the exposure time, the brightness of the pattern on the photographic print can be made proportional to the brightness of the Schlieren system. The effect of the knife-edge on the image obtained with Schlieren is evident from Figure 10.14b.

#### 10.8.2.6 Color Schlieren

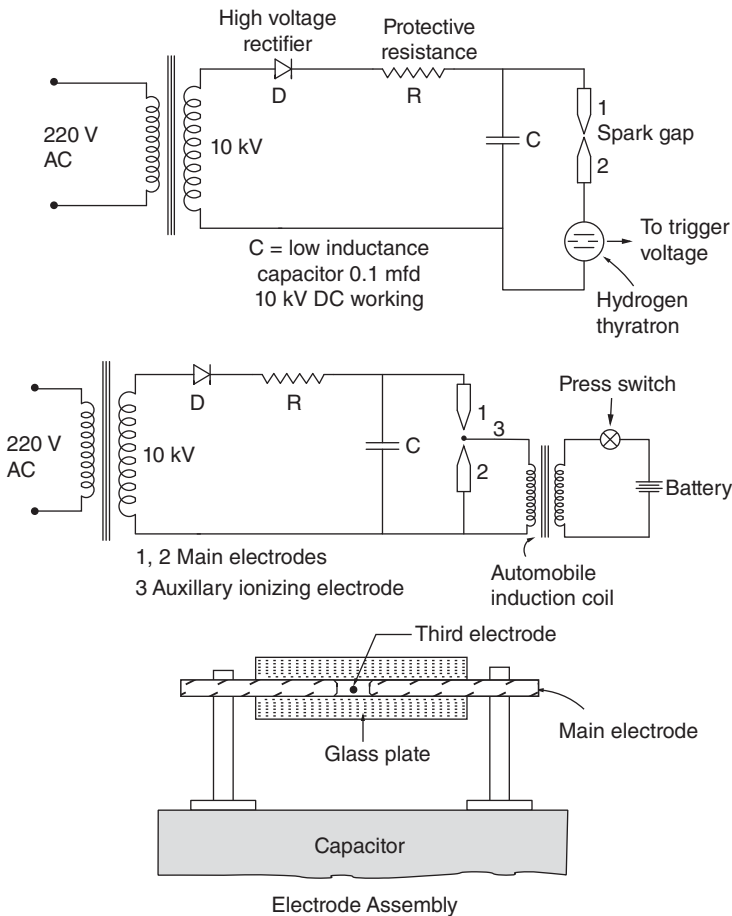
If the knife-edge which is kept at the focal point of the second mirror is replaced by a colored filter containing different colors, and a white-light source is used, the image formed on the screen will have different colors depending on which way the beam bends. The contrast in the ordinary black and white Schlieren will now be represented by colors. Usually the colors red, yellow, and green are used. These filters are 1 or 2 mm wide and placed side by side. When there is no flow, the image of the source is allowed to fall on the yellow portion of the filter. Now the image on the viewing screen will be completely yellow. When the density gradient is introduced the image gets displaced and falls partly on the neighboring filter thus altering the color on the screen. In the three-filter color Schlieren screen, the color indicates the size of the density gradient also. The color effect described can also be achieved with a dispersion prism placed at the knife-edge location.

#### 10.8.2.7 Short-Duration Light Source

To study unsteady phenomena such as flow over a moving object, turbulent fluctuations in the wake of a body, or the mixing shear layer in a jet flow field, it is often necessary to take short-duration exposures of the Schlieren image to arrest (record) the unsteadiness in the image. For this the duration of exposure required is of the order of 1 or 2  $\mu$ s or even less. An ordinary shutter in conjunction with a continuous light source is limited to an exposure time of not more than 1/1000 second. Therefore, to obtain shorter exposures the light sources capable of emitting light of very short duration should be employed. A capacitor discharge type electric spark unit is commonly used for this purpose. Sparks of durations of the order of microseconds could be obtained by capacitor discharge.

A spark light source of short duration can be made in the laboratory. A low-inductance conductor and a high-voltage DC source are the vital components of this unit. The simplest form of spark unit consists of two electrodes separated by an air gap and the electrodes are connected to the terminals of the capacitor. The discharge time depends on the value of the time constant of the system, that is on the  $CR$  value, where  $C$  is the capacitance and  $R$  is the resistance, which includes the effect of the inductance of the circuit. The total energy of the discharge is  $\frac{1}{2}CV^2$ , where  $V$  is the voltage. The energy discharge during the sparking gets partly dissipated into heat and the rest goes into electromagnetic radiation, including the visible range. To obtain a discharge of very short duration it is necessary to use high voltage with a small capacitor having negligible inductance. In addition, the resistance of the overall circuit should be kept to a minimum by mounting the spark gap assembly directly on the capacitor electrodes. A DC voltage of 10 kV and a capacitor of  $0.1 \mu\text{F}$  is sufficient to make a good spark source. If carefully designed, a discharge time of  $1 \mu\text{s}$  could easily be achieved.

A spark source should be capable of being triggered whenever needed. This is generally done by using a hydrogen thyatron capable of conducting high current as well as high voltage. Sometimes a simple third ionizing electrode is employed since hydrogen thyratrons are expensive and have a short life. The electric circuit for the above system is shown in Figure 10.16.



**Figure 10.16** Schlieren spark source circuit.

The electrode is used to reduce the resistance in the path between the two main electrodes by ionization. For the Schlieren system a line source is needed and this could be achieved by placing two electrodes between two glass plates, as shown in Figure 10.16. The glass plates confine the spark instead of allowing it to wander around. The material of the electrodes can be steel, nickel, aluminum, or even tungsten. Aluminum electrodes produce high-intensity light and increase the duration, owing to afterglow. The afterglow is in the low frequency of the visible spectrum and can be filtered out to some extent by using special optical filters.

In general, the Schlieren method is used either for the detection of small refractive index gradients or for the quantitative measurement of these gradients. For the detection of small gradients the apparatus described in Figure 10.15, in which the deviation of the light ray  $\epsilon$  gives rise to the relative light intensity change  $\Delta I/I$  on the photographic plate, is almost universally used for studying phenomena in gas dynamics. The method may also be made quantitative, but careful attention must be paid to the several variables in the experimental arrangement. If the disturbance is to be photographed, the arrangement must give a maximum contrast between the images of the undisturbed and disturbed regions, and at the same time the photograph must be dense enough to be measurable by photometric means. In most cases high contrast photographic plates are preferable even though they are somewhat slower. In order to calibrate the system, a known refractive index gradient, such as a small glass prism, may be inserted in some corner of the median plane of the test-field zone, which allows a check on the formulae used for the optical system. The sensitivity, that is  $\Delta I/I$ , depends directly upon the brightness of the image of  $S_1$  and  $S_2$ , and upon its uniformity of illumination. This, of course, requires as bright and uniform a source as possible to start with and an optical system that sacrifices no more light than necessary. Rectangular sources are usually superior. For proper adjustment, the knife-edges or slits should be of high quality and should be mounted in such a manner that they can be raised and lowered, rotated, or moved forward or backward by micrometer adjustments. Also, the mirrors should be accurately adjustable. The mounting of all components should be rigid. The sensitivity also increases directly with the focal length of the Schlieren mirror or lens.

When the Schlieren method is applied to the study of disturbances such as density gradients in a supersonic wind tunnel in which the flow is two-dimensional, with the flow in the  $x$ -direction and the light beam in the  $z$ -direction, the component of the gradient of the refractive index in the  $z$ -direction vanishes. The index of refraction in air for sodium light can be expressed in terms of density, by the relation

$$n = 1 + 0.000293 \frac{\rho}{\rho_{\text{NTP}}}$$

where  $\rho_{\text{NTP}}$  is the density at 1 atm and  $0^\circ\text{C}$ . The components of the angular deflection  $\epsilon_x$  and  $\epsilon_y$  in the  $x$ - and  $y$ -directions, respectively, are given by

$$\epsilon_x = \int c \frac{\partial \rho}{\partial x} dz, \quad \epsilon_y = \int c \frac{\partial \rho}{\partial y} dz \quad (10.12)$$

where  $c$  is a constant.

When the component of the density gradient in the direction of the light beam does not vanish (as in the case of a three-dimensional flow field), the interpretation of the pictures becomes more complicated.

### 10.8.3 Sensitivity of the Schlieren Method for Shock and Expansion Studies

So far, we have discussed the various aspects of the technical and application details of the Schlieren method. The emphasis has been laid mainly on the qualitative aspects of the flows

with density gradients, such as the supersonic flow over an object. Now we can ask a question. Is the Schlieren method capable of detecting every density gradient irrespective of the intensity of the gradient or is there any threshold below which it is not possible to detect the disturbance with the Schlieren method? To get an answer, let us assume that our interest now is to know: *under what condition will an oblique shock become visible?* Assume the knife-edge to be parallel to the front of the oblique shock and, as a typical value, the angle between the shock and the optic axis  $\theta = 1^\circ = 0.0175$  rad. For the present arrangement, it can be shown that all the light incident upon the shock is refracted and the amount of light reflected is negligible. Let subscripts 0, 1, and 2 refer to the stagnation state at  $20^\circ\text{C}$ , and states upstream and downstream of the shock, respectively. For this flow field, Snell's law of refraction leads to the relation [11]

$$1 + 0.000293 \left( \frac{273}{293} \right) p_0 \left( \frac{\rho_1}{\rho_0} - \frac{\rho_2}{\rho_0} \right) = 1 - \epsilon \tan \theta \quad (10.13)$$

where  $\epsilon$  is the angular deflection of the light ray, owing to the presence of the shock. Let  $\epsilon = 10^{-5}$  rad (which is a typical value). Equation (10.13) becomes

$$\rho_2 - \rho_1 = \rho_0 \frac{\tan \theta}{27.3 p_0} \quad (10.14)$$

The relation between the shock angle  $\beta$  and the Mach angle  $\mu$  can be written as

$$\sin \beta = \frac{M_n}{M_1} = M_n \sin \mu \quad (10.15)$$

where  $M_n$  is the component of upstream Mach number  $M_1$ , normal to the oblique shock. The ratio of the static to stagnation densities upstream of the shock is

$$\frac{\rho_1}{\rho_0} = \left( 1 + \frac{\gamma - 1}{2} M_1^2 \right)^{-1/(\gamma-1)}$$

With  $\gamma = 1.4$ , the density ratio becomes

$$\frac{\rho_1}{\rho_0} = \left( 1 + \frac{M_1^2}{5} \right)^{-5/2}$$

The ratio of downstream to upstream densities of the shock wave is

$$\begin{aligned} \frac{\rho_2}{\rho_1} &= \frac{6M_n^2}{M_n^2 + 5} \\ \frac{\rho_2 - \rho_1}{\rho_0} &= \frac{\rho_2 - \rho_1}{\rho_1} \frac{\rho_1}{\rho_0} = \frac{5(M_n^2 - 1)}{M_n^2 + 5} \frac{\rho_1}{\rho_0} = \frac{\tan \theta}{27.3 p_0} \end{aligned} \quad (10.16)$$

provided the knife-edge is parallel to the shock front. Therefore, for the given values of  $\theta$ ,  $p_0$ , and  $M_1$ , the minimum difference ( $\beta - \theta$ ), which will give a visible Schlieren effect, can be determined.

If the density change across the oblique shock is small, then  $\beta - \theta$  becomes small. Further,  $M_n^2 = 1 + \delta$ , with  $\delta \ll 1$ . For this case, we can show that

$$\beta - \mu = \frac{3}{5} \frac{\rho_0}{\rho_1} \frac{\tan \theta}{27.3 p_0 \sqrt{M_1^2 - 1}} \quad (10.17)$$

If  $\epsilon = 10^{-5}$ , the knife-edge is parallel to the front of the shock wave, and  $\theta = \beta - \mu = 1^\circ$ , the minimum stagnation pressure (for some given Mach numbers) at which shock can be visualized with Schlieren (at the above assumed rather favorable condition) is given in Table 10.1.



**Table 10.1** Limiting stagnation pressure above which waves can be visualized by Schlieren.

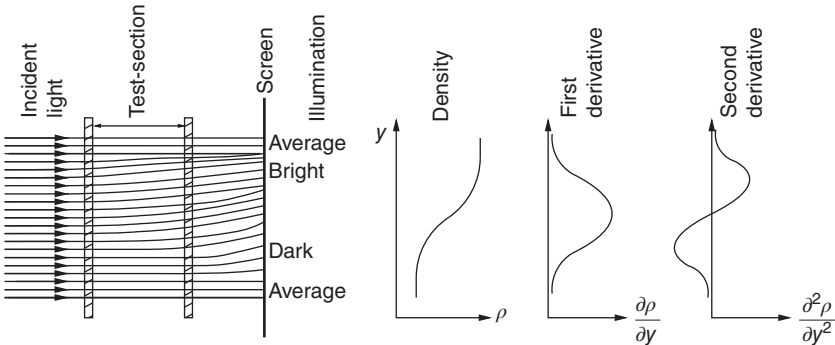
$M$	1.5	2.0	2.5	3.0	3.5	4.0	4.5	5.0	6.0
$p_{0min}, \text{ atm}$	0.050	0.055	0.073	0.102	0.145	0.205	0.287	0.396	0.715
			7.0	8.0	9.0	10.0			
			1.216	1.959	3.015	4.465			

10.9 Shadowgraph

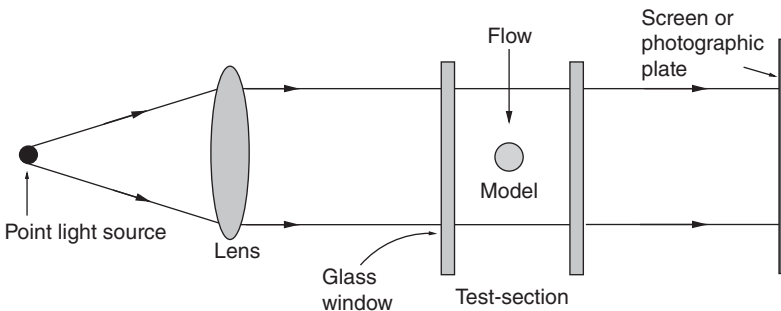
In our discussions on the Schlieren system we have seen that the positions of the image points on the viewing screen are not affected by deflections of light rays in the test-section. This is because the deflected rays are also brought to focus in the focal plane, and that the screen is uniformly illuminated when the knife-edge is not inserted into the light beam. On the other hand, if the screen is placed at a position close to the test-section, the effect of ray deflection will be visible. This effect, termed the *shadow effect*, is illustrated in Figure 10.17.

On the screen there are bright zones, where the rays crowd closer, and dark zones, where the rays diverge. At places where the spacing between the rays is unchanged, the illumination is normal even though there has been refraction. Thus, the shadow effect depends not on the absolute deflection but on the relative deflection of the light rays, that is on the rate at which they converge or diverge on coming out of the test-section.

A shadowgraph consists of a light source, a collimating lens, and a viewing screen, as shown in Figure 10.18.



**Figure 10.17** The shadow effect.



**Figure 10.18** Shadowgraph system.

Let us assume that the test-section has stagnant air in it and that the illumination on the screen is of uniform intensity. When flow takes place through the test-section, the light beam will be refracted wherever there is a density gradient. However, if the density gradient everywhere in the test-section is constant, all light rays would deflect by the same amount, and there would be no change in the illumination of the picture on the screen. Only when there is a gradient in density gradient will there be a tendency for light rays to converge or diverge. In other words, the variations in illumination of the picture on the screen are proportional to the second derivative of the density. For a two-dimensional flow, the increase of light intensity can be expressed as

$$\Delta I = k \left( \frac{\partial^2 \rho}{\partial x^2} + \frac{\partial^2 \rho}{\partial y^2} \right) \quad (10.18)$$

where  $k$  is a constant and  $x$  and  $y$  are the coordinates in a plane normal to the light path.

Therefore, the shadowgraph is only really suited for flow fields with rapidly varying density gradients. A typical shadowgraph of a highly underexpanded circular sonic jet is shown in Figure 10.19. Since the jet is underexpanded, the waves present in the field would be strong enough to result in a large density gradient across them. One such wave, termed a *Mach disc* (a compression front normal to the jet axis), is seen in the field. The Mach disc is essentially a normal shock and hence the shock has positive and negative rates of change of density gradient across it. Therefore, the shock is made up of a dark line followed by a bright line in the shadow picture, in accordance with the *shadow effect*.

### 10.9.1 Comparison of the Schlieren and Shadowgraph Methods

As we saw in the previous sections, the theory shows that the Schlieren technique depends upon the first derivative of the refractive index (flow density), while the shadowgraph method depends upon its second derivative. Consequently, in phenomena where the refractive index varies relatively slowly, the Schlieren method is to be preferred to the shadowgraph method, other things being equal. On the other hand, the shadow method beautifully brings out the rapid changes in the index of refraction. The shadow method also has the advantage of greater simplicity and somewhat wider possible application. The two methods therefore complement each other, and both should be used wherever possible. Fortunately, in many cases the same apparatus or optical parts can be used for both the methods by simple rearrangement and without too much effort on the part of the experimenter. In addition to the first and second derivatives, the refractive index can also be obtained by integration. However, whenever possible, it is preferable to measure the density directly rather than

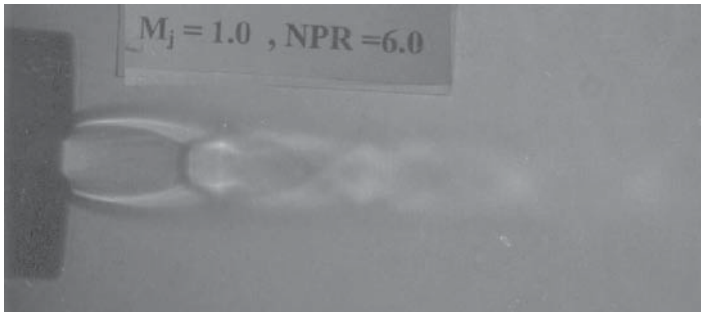


Figure 10.19 Shadowgraph of an underexpanded sonic jet operating at a nozzle pressure ratio 6.

obtaining it from its derivative. For this reason it is clear that the Schlieren and shadow methods should be supplemented by the interference method, which gives the refractive index directly.

## 10.10 Wind Tunnels

Wind tunnels are devices that provide air streams flowing under controlled conditions so that models of interest can be tested using them. From an operational point of view, wind tunnels are generally classified as *low-speed*, *high-speed*, and *special purpose tunnels*. Low-speed tunnels are those with a test-section speed of less than 650 kmph. Depending upon the test-section size, they are referred to as *small-size* or *full-scale tunnels*. They are further classified into the following categories: *open-circuit tunnels*, having no guided return of air, and *closed-circuit* or *return-flow tunnels*, having a continuous path for the air. In low-speed tunnels, the predominant factors influencing the tunnel performance are inertia and viscosity. The effect of compressibility is negligible for these tunnels. Thus, if the Reynolds number of the experimental model and full-scale prototype are equal, any difference in viscosity becomes unimportant.

### 10.10.1 High-Speed Wind Tunnels

Tunnels with a test-section speed of more than 650 kmph are called *high-speed tunnels*. The predominant aspect in a high-speed tunnel operation is that the influence of compressibility is significant. This means that in high-speed flows it is essential to consider the *Mach number* as a more appropriate parameter than velocity. A lower limit of *high-speed* might be considered the flow with a Mach number of approximately 0.5 (about 650 kmph) at standard sea level conditions.

Based on the test-section Mach number  $M$  range, the high-speed tunnels are classified as follows.

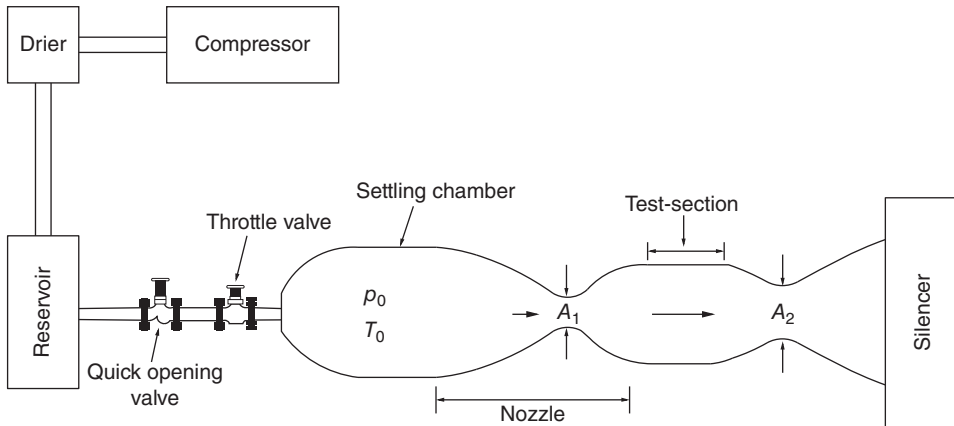
- $0.8 < M < 1.2$             Transonic tunnel
- $1.2 < M < 5$              Supersonic tunnel
- $M > 5$                     Hypersonic tunnel

Like low-speed tunnels, high-speed tunnels are also classified as *intermittent* or *open-circuit tunnels* and *continuous-return-circuit tunnels*, based on the type of operation. The power to drive a low-speed wind tunnel varies as the cube of the test-section velocity. Although this rule does not hold in the high-speed regime, the implication of rapidly increasing power requirements with increasing test-section speed holds for high-speed tunnels also. Because of the power requirements, high-speed wind tunnels are often of the *intermittent type*, in which energy is stored in the form of pressure or vacuum, or both, and is allowed to drive the tunnel only a few seconds out of each pumping hour.

The intermittent blowdown and induction tunnels are normally used for Mach numbers from 0.5 to about 5.0, and the intermittent pressure–vacuum tunnels are normally used for higher Mach numbers. The continuous tunnel is used throughout the speed range. Both intermittent and continuous tunnels have their own advantages and disadvantages.

### 10.10.2 Blowdown Type Wind Tunnels

Essential features of the intermittent blowdown wind tunnel are schematically shown in Figure 10.20.



**Figure 10.20** Schematic layout of intermittent blowdown tunnel.

#### 10.10.2.1 Advantages

The main advantages of blowdown type wind tunnels are the following.

- They are the simplest among the high-speed tunnel types and most economical to build.
- Large-size test-sections and high Mach numbers (up to  $M = 4$ ) can be obtained.
- Constant blowing pressure can be maintained and a running time of considerable duration can be achieved.

These are the primary advantages of intermittent blowdown tunnels. In addition to these, there are many additional advantages for this type of tunnel. For example, a single drive may easily run several tunnels of different capabilities, failure of a model usually will not result in tunnel damage, extra power is available to start the tunnel, and so on.

#### 10.10.2.2 Disadvantages

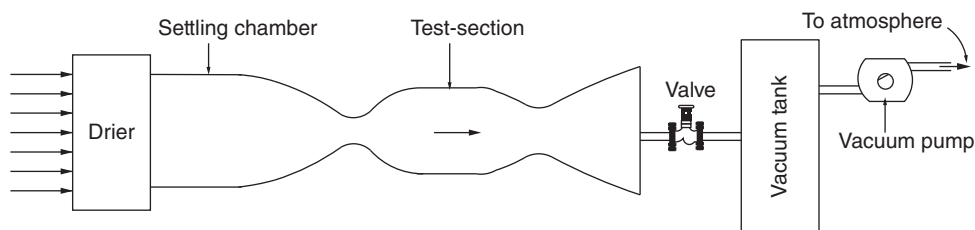
The major disadvantages of blowdown tunnels are the following.

- The ratio of charging time to running time will be very high for large tunnels.
- Stagnation temperature in the reservoir drops during tunnel run, thus changing the Reynolds number of the flow in the test-section.
- An adjustable (automatic) throttling valve between the reservoir and settling chamber is necessary for constant stagnation pressure (temperature varying) operation.
- Starting load is high (no control possible).
- Reynolds number of flow is low, owing to low static pressure in the test-section.

The commonly employed reservoir pressure range is from 600 kPa to 2 MPa for blowdown tunnel operations. As large as 15 MPa is also used where space limitations require it.

### 10.10.3 Induction Type Tunnels

In this type of tunnel, a vacuum created at the downstream end of the tunnel is used to establish the flow in the test-section. A typical induction tunnel circuit is shown schematically in Figure 10.21.



**Figure 10.21** Schematic diagram of induction tunnel.

#### 10.10.3.1 Advantages

The advantages of induction tunnels are the following.

- Stagnation pressure and stagnation temperature are constant.
- No oil contamination in air, since the pump is at the downstream end.
- Starting and shutdown operations are simple.

#### 10.10.3.2 Disadvantages

The disadvantages of induction type supersonic tunnels are the following.

- Size of the air drier required is very large, since it has to handle a large mass flow in a short duration.
- Vacuum tank size required is also very large.
- High Mach numbers ( $M > 2$ ) are not possible because of large suction requirements for such Mach numbers.
- The Reynolds number is very low, since the stagnation pressure is atmospheric.

The blowdown and induction principles can also be employed together for supersonic tunnel operation to derive the benefits of both types.

### 10.10.4 Continuous Supersonic Wind Tunnels

The essential features of a continuous-flow supersonic wind tunnel are shown in Figure 10.22.

Like intermittent tunnels, the continuous tunnels also have some advantages and disadvantages.

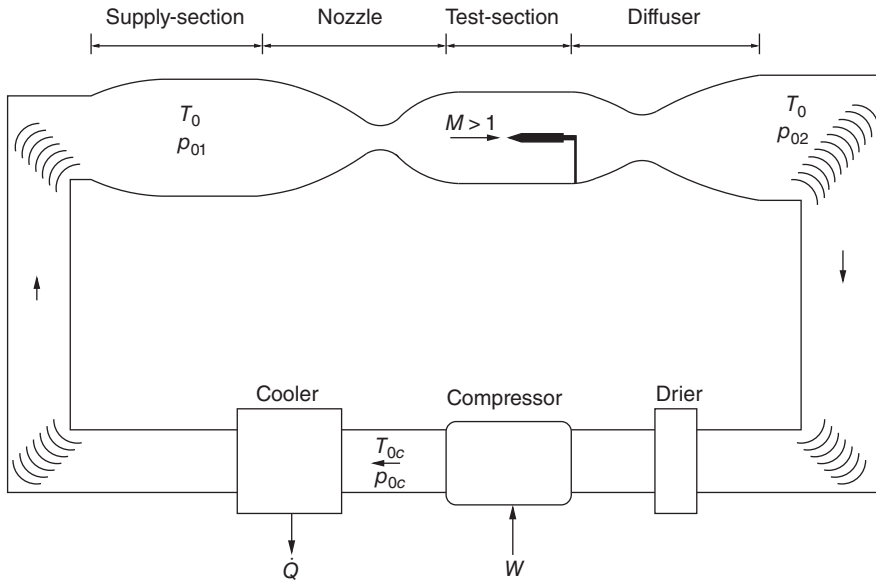
The main *advantages* of continuous supersonic wind tunnels are the following.

- Better control over the Reynolds number is possible, since the shell is pressurized.
- Only a small capacity drier is required.
- Testing conditions can be held the same over a long period of time.
- The test-section can be designed for high Mach numbers ( $M > 4$ ) and large models.
- Starting load can be reduced by starting at low pressure in the tunnel shell.

The major *disadvantages* of continuous supersonic tunnels are the following.

- Power required is very high.
- Temperature stabilization requires a large cooler.
- A compressor drive has to be designed to match the tunnel's characteristics.
- Tunnel design and operation are more complicated.

It can be seen from the foregoing discussions that both intermittent and continuous tunnels have certain specific advantages and disadvantages. Before going into the specific details about supersonic tunnel operation, it will be useful to note the following details about supersonic tunnels.



**Figure 10.22** Schematic diagram of a closed-circuit supersonic wind tunnel.

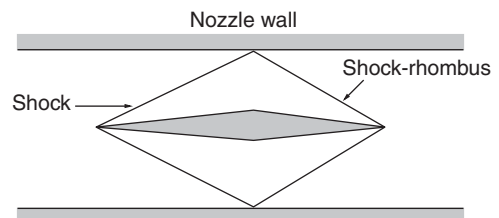
- Axial flow compressor is better suited for large pressure ratio and mass flow.
- Diffuser design is critical since increasing diffuser efficiency will lower the power requirement considerably. The supersonic diffuser portion (geometry) must be carefully designed to decrease the Mach number of the flow as much as possible, before shock formation. The subsonic portion of the diffuser must have an optimum angle, to minimize the frictional and separation losses.
- Proper nozzle geometry is very important to obtain a good distribution of Mach number and freedom from flow angularity in the test-section. Theoretical calculation of a high accuracy and boundary layer compensation, and so on, have to be carefully worked out for large test-sections. Using fixed nozzle blocks for different Mach numbers is simple but very expensive and it is quite laborious for changeover in the case of large test-sections. A flexible wall-type nozzle is complicated and expensive from a design point of view and the Mach number range is limited (usually  $1.5 < M < 3.0$ ).
- Model size is determined from the shock-rhombus, shown in Figure 10.23.

The model must be accommodated inside the rhombus formed by the incident and reflected shocks, for proper measurements.

### 10.10.5 Losses in Supersonic Tunnels

The total power loss in a continuous supersonic wind tunnel may be split into the following components.

**Figure 10.23** Shock-rhombus.



- 1) Frictional losses (in the return circuit)
- 2) Expansion losses (in diffuser)
- 3) Losses in contraction cone and test-section
- 4) Losses in guide vanes
- 5) Losses in cooling system
- 6) Losses due to shock wave (in diffuser supersonic part)
- 7) Losses due to model and support system drag

The first five components of losses represent the usual low-speed tunnel losses. All the five components together constitute only about 10% of the total loss. Components 6 and 7 are additional losses in a supersonic wind tunnel and usually amount to approximately 90% of the total loss, with shock wave losses alone accounting for nearly 80% and model and support system drag constituting nearly 10% of the total loss. Therefore, it is customary, in estimating the power requirements, for determining the pressure ratio required for supersonic tunnel operation that the pressure ratio across the diffuser alone is considered and a correction factor is applied to take care of the rest of the losses.

The pressure ratio across the diffuser multiplied by the correction factor must therefore be equal to the pressure ratio required across the compressor to run the tunnel continuously. The relationship between these two vital pressure ratios, namely the diffuser pressure ratio,  $p_{01}/p_{02}$ , and compressor pressure ratio,  $p_{0c}/p_{03}$ , may be related as follows.

$$\text{Compressor pressure ratio } \frac{p_{0c}}{p_{03}} = \frac{p_{01}}{p_{02}} \frac{1}{\eta} \quad (10.19)$$

where  $p_{0c}$  is the stagnation pressure at compressor exit,  $p_{03}$  is the stagnation pressure at compressor inlet,  $p_{01}$  is the stagnation pressure at diffuser inlet,  $p_{02}$  is the stagnation pressure at diffuser exit, and

$$\eta = \frac{\text{Diffuser losses}}{\text{Total loss}}$$

is the correction factor.

The value of  $\eta$  varies from 0.6 to 0.85, depending on the kind of shock pattern through which the pressure recovery is achieved in the diffuser. The variation of the compressor pressure ratio,  $p_{0c}/p_{03}$ , with the test-section Mach number,  $M$ , is shown in Figure 10.24.

### 10.10.6 Supersonic Wind Tunnel Diffusers

Basically, the diffuser is a device to convert the kinetic energy of a flow to pressure energy. The diffuser efficiency may be defined, in two ways, as

- polytropic efficiency  $\eta_d$
- isentropic efficiency  $\eta_\sigma$ .

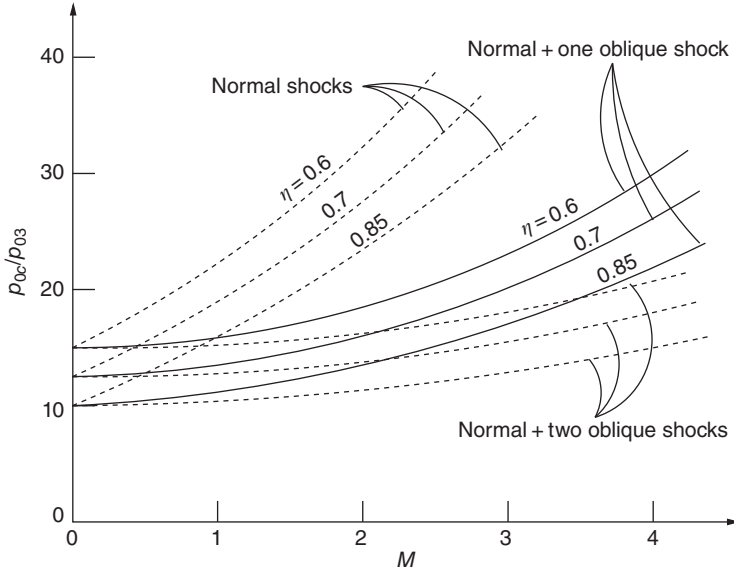
#### 10.10.6.1 Polytropic Efficiency

It is known that, at any point in a diffuser, a small change of kinetic energy of unit mass of fluid results in an increase of pressure energy as per the equation

$$\Delta p = \eta_d d \left( \frac{V^2}{2} \right) \quad (10.20)$$

and the pressure ratio is given by

$$\frac{p_{02}}{p_1} = \left( \frac{T_{02}}{T_1} \right)^{\frac{\gamma}{\gamma-1} \eta_d} = \left( 1 + \frac{\gamma-1}{2} M_1^2 \right)^{\frac{\gamma}{\gamma-1} \eta_d} \quad (10.21)$$



**Figure 10.24** Compressor-pressure ratio variation with test-section Mach number.

where  $p_1$  and  $p_{02}$  are the static and stagnation pressures upstream and downstream of the point under consideration, respectively, and  $\eta_d$  is the polytropic efficiency.  $M_1$ ,  $T_1$ , and  $T_{02}$  are the Mach number and static and stagnation temperatures at the appropriate locations.

#### 10.10.6.2 Isentropic Efficiency

The isentropic efficiency of a diffuser may be defined as

$$\eta_\sigma = \frac{\text{Ideal KE required for observed power}}{\text{Actual KE transferred}}$$

and

$$\text{Ideal KE from } p_1 \text{ to } p_{02} (\text{without loss}) = \int_{p_1}^{p_{02}} \frac{dp}{\rho} = \frac{\gamma}{\gamma - 1} \frac{p_1}{\rho_1} \left( \left( \frac{p_{02}}{p_1} \right)^{\frac{\gamma-1}{\gamma}} - 1 \right) \quad (10.22)$$

Note that, in Eqs. (10.21) and (10.22), the velocity at the diffuser outlet is assumed to be negligible, which is why the pressure at location 2 is taken as  $p_{02}$ , the stagnation pressure. With Eq. (10.22) the isentropic efficiency,  $\eta_\sigma$ , becomes

$$\eta_\sigma = \frac{\frac{\gamma}{\gamma-1} \frac{p_1}{\rho_1} \left( \left( \frac{p_{02}}{p_1} \right)^{\frac{\gamma-1}{\gamma}} - 1 \right)}{\frac{1}{2} V_1^2} = \frac{2}{\gamma - 1} \frac{1}{M_1^2} \left( \left( \frac{p_{02}}{p_1} \right)^{\frac{\gamma-1}{\gamma}} - 1 \right)$$

From the above equation, the pressure ratio  $p_{02}/p_1$  becomes

$$\frac{p_{02}}{p_1} = \left( 1 + \frac{\gamma - 1}{2} M_1^2 \eta_\sigma \right)^{\frac{\gamma}{\gamma-1}} \quad (10.23)$$

From Eqs. (10.21) and (10.23), we get

$$\left( 1 + \frac{\gamma - 1}{2} M_1^2 \right)^{\eta_d} = \left( 1 + \frac{\gamma - 1}{2} M_1^2 \eta_\sigma \right) \quad (10.24)$$



If  $H$  is the total pressure (total head) upstream of the test-section, and  $p_1$  is the static pressure there, then we have by isentropic relation,

$$\frac{H}{p_1} = \left(1 + \frac{\gamma - 1}{2} M^2\right)^{\frac{\gamma}{\gamma - 1}} \quad (10.25)$$

Therefore, the overall pressure ratio,  $H/p_{02}$ , for the tunnel becomes

$$\frac{H}{p_{02}} = \frac{H}{p_1} \frac{p_1}{p_{02}}$$

But this is also *the compressor pressure ratio* required to run the tunnel. Hence, using Eqs. (10.23) and (10.25), the compressor pressure ratio,  $p_\sigma$ , can be expressed as

$$p_\sigma = \frac{H}{p_{02}} = \left( \frac{1 + \frac{\gamma - 1}{2} M_1^2}{1 + \frac{\gamma - 1}{2} M_1^2 \eta_\sigma} \right)^{\frac{\gamma}{\gamma - 1}} \quad (10.26)$$

For continuous and intermittent supersonic wind tunnels, the energy ratio,  $ER$ , may be defined as follows.

1) For continuous tunnel

$$ER = \frac{\text{KE at the test-section}}{\text{Work done in isentropic compression per unit time}}$$

Using Eq. (10.26), this may be expressed as

$$ER = \frac{1}{\left(p_\sigma^{\frac{\gamma}{\gamma - 1}} - 1\right) \left(\frac{2}{(\gamma - 1)M_1^2} + 1\right)} \quad (10.27)$$

2) For intermittent tunnel

$$ER = \frac{(\text{KE in test-section})(\text{Time of tunnel run})}{\text{Energy required for charging the reservoir}} \quad (10.28)$$

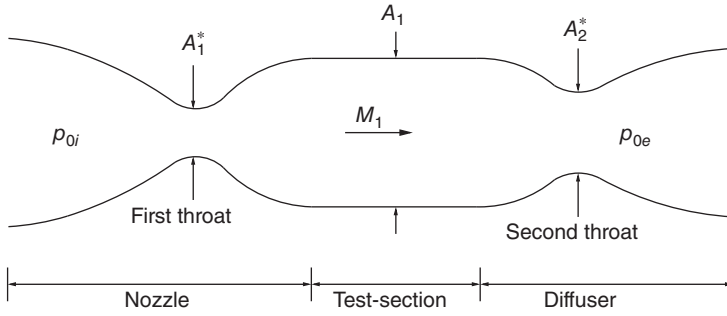
From the above discussions we can infer that, for  $M < 1.7$ , induced flow tunnels are more efficient than blowdown tunnels. In spite of this advantage, most of the supersonic tunnels even over this Mach number range are operated as blowdown tunnels and not as induced flow tunnels. This is because vacuum tanks are more expensive than compressed air storage tanks.

### 10.10.7 Effects of Second Throat

A typical supersonic tunnel with second throat is shown schematically in Figure 10.25.

The second throat is used to provide isentropic deceleration and highly efficient pressure recovery after the test-section. Neglecting frictional and boundary layer effects, a wind tunnel can theoretically be run at design conditions indefinitely, with no pressure difference requirement to maintain the flow, once started. But this is an ideal situation which cannot be achieved in practice. Even under the assumptions of this ideal situation, during start-up a pressure difference must be maintained across the entire system to establish the flow. For the supersonic tunnel sketched in Figure 10.25, the following observation may be made.

- As the pressure ratio  $p_{0e}/p_{0i}$  is decreased below 1.0, the flow situation is the same as that in a convergent–divergent nozzle, where  $p_{0i}$  and  $p_{0e}$  are the stagnation pressures at the nozzle inlet and the diffuser exit, respectively.



**Figure 10.25** Schematic of supersonic wind tunnel with second throat.

- Now any further decrease in  $p_{0e}/p_{0i}$  would cause a shock to appear downstream of the nozzle throat.
- Further decrease in  $p_{0e}/p_{0i}$  moves the shock downstream, toward the nozzle exit.
- With a shock in the diverging portion of the nozzle, there is a severe stagnation pressure loss in the system.
- To pass the flow after the shock, the second throat must be at least of an area  $A_2^*$ .
- The worst case causing maximum loss of stagnation pressure is when there is a normal shock in the test-section. For this case, the second throat area must be at least  $A_2^*$ .
- If the second throat area is less than this, it cannot pass the required flow, and the shock can never reach the test-section, and will remain in the divergent part of the nozzle.
- Under these conditions, supersonic flow can never be established in the test-section.
- As  $p_{0e}/p_{0i}$  is further lowered, the shock jumps to an area in the divergent portion of the diffuser which is greater than the test-section area, that is the shock is swallowed by the diffuser.
- To maximize the pressure recovery in the diffuser,  $p_{0e}/p_{0i}$  can now be increased, which makes the shock to move upstream to the diffuser throat, and the shock can be positioned at the location where the shock strength is the minimum.

From the above observations, it is evident that the second throat area must be large enough to accommodate the mass flow when a normal shock is present in the test-section. Assuming the flow to be one-dimensional in the tunnel sketched in Figure 10.25, it can be shown from continuity equation that

$$\rho_1^* a_1^* A_1^* = \rho_2^* a_2^* A_2^*$$

The flow process across a normal shock is adiabatic, and therefore

$$T_1^* = T_2^*$$

and

$$\rho_1^*/\rho_2^* = p_1^*/p_2^* = p_{01}/p_{02}$$

Also,

$$a_2^* = a_1^*$$

since  $T_1^* = T_2^*$ . Therefore, the minimum area of the second throat required for starting the tunnel becomes

$$\boxed{\frac{A_2^*}{A_1^*} = \frac{p_{01}}{p_{02}}} \quad (10.29)$$

where  $p_{01}$  and  $p_{02}$  are the stagnation pressures upstream and downstream, respectively, of the normal shock just ahead of the second throat. The pressures  $p_{01}$  and  $p_{02}$  are identically equal to  $p_{0i}$  and  $p_{0e}$ , respectively. Instead of the ratio of the throats area, it is convenient to deal with the ratio of the test-section area  $A_1$  to the diffuser throat area  $A_2^*$ . This is called the *diffuser contraction ratio*,  $\psi$ . Thus, the maximum permissible contraction ratio for starting the tunnel is given by

$$\psi_{\max} = \frac{A_1}{A_2^*} = \frac{A_1}{A_1^*} \times \frac{A_1^*}{A_2^*} = \frac{A_1}{A_1^*} \times \frac{p_{02}}{p_{01}} = f(M_1) \quad (10.30)$$

When the second throat area is larger than the minimum required for any given condition, the shock wave is able to jump from the test-section to the downstream side of the diffuser throat. This is termed *shock swallowing*. The complete test-section has supersonic flow, which is the required state for a supersonic wind tunnel test-section. However, the second throat and part of the diffuser also have supersonic flow. Apparently, we have only shifted the shock from the test-section to the diffuser. This again will result in considerable loss. In principle, it is possible to bring down the loss to a very low level by reducing the area of the second throat after starting the tunnel. As  $A_2^*$  is reduced, the shock becomes weaker – as seen from Eq. (10.29) – and moves upstream toward the second throat. When  $A_2^* = A_1^*$ , the shock just reaches the second throat, and its strength becomes vanishingly small. This is the ideal situation, resulting in supersonic flow in the test-section and isentropic flow in the diffuser.

At this stage, we should realize that the above model is based on the assumption that the flow is one-dimensional and inviscid, with a normal shock in the test-section. A more realistic model might have to take into account the nonstationary effects of the shock, the possibility of oblique shocks, and the role of boundary layer development. Further, reduction of  $A_2^*$  to  $A_1^*$ , which is the ideal value, is not possible in practice. However, some contraction after starting is possible, up to a limiting value at which the boundary layer effects prevent the maintenance of sufficient mass flow for maintaining a supersonic test-section, and beyond that the flow *breaks down*.

Experimental studies confirm, in a general way, the theoretical considerations outlined above, although there are modifications, owing to viscous effects.

The skin friction at the wall, of course, causes some additional loss of stagnation pressure. Some of the diffuser problems outlined here may be avoided to a large extent by

- using a variable-geometry diffuser
- using a variable-geometry diffuser in conjunction with a variable-geometry nozzle
- driving the shock through the diffuser throat by means of a large-amplitude pressure pulse
- taking advantage of effects that are not one-dimensional.

### 10.10.8 Compressor Tunnel Matching

Usually, the design of a continuous supersonic wind tunnel has either of the following two objectives.

- Choose a compressor for specified test-section size, Mach number, and pressure level.
- Determine the best utilization of an already available compressor.

In the first case, wind tunnel characteristics govern the selection of the compressor and in the second case it is the other way about. In either case the characteristics to be matched are the *overall pressure ratio* and *mass flow*.

The compressor characteristics are usually given in terms of the volumetric flow  $V$  rather than the mass flow  $m$ . Therefore, it is convenient to give the wind tunnel characteristics also in

terms of  $V$ . We know that the volume can be expressed as

$$V = \frac{m}{\rho}$$

since the density  $\rho$  varies in the tunnel circuit, the volumetric flow also varies for a given constant mass flow  $m$ . For the compressor, we specify the intake flow as

$$V_i = \frac{m}{\rho_i} \quad (10.31)$$

which is essentially the same as the volume flow at the diffuser exit.

On the other hand, the volume flow at the supply section (wind tunnel settling chamber) is

$$V_0 = \frac{m}{\rho_0} \quad (10.32)$$

Using the throat as the reference section, the mass flow can be expressed as

$$m = \rho^* a^* A^* = \left( \frac{2}{\gamma + 1} \right)^{\frac{\gamma+1}{2(\gamma-1)}} \rho_0 a_0 A^* \quad (10.33)$$

where  $a^*$  and  $a_0$  are the sonic speeds at the throat and stagnation state, respectively.

With Eq. (10.33), Eq. (10.32) can be rewritten as

$$\begin{aligned} V_0 &= \left( \frac{2}{\gamma + 1} \right)^{\frac{\gamma+1}{2(\gamma-1)}} a_0 A^* \\ &= \left( \frac{2}{\gamma + 1} \right)^{\frac{\gamma+1}{2(\gamma-1)}} \sqrt{\gamma R T_0} \frac{A^*}{A} A \\ &= \text{constant} \sqrt{T_0} A \left( \frac{A^*}{A} \right) \end{aligned}$$

From this equation it can be seen that the volume flow rate  $V_0$  depends on the stagnation temperature, test-section area, and test-section Mach number (since  $A/A^*$  is a function of  $M$ ).

The compressor intake flow and the supply section (settling chamber) flow may easily be related, using Eqs. (10.31) and (10.32), to result in

$$\frac{V_i}{V_0} = \frac{\rho_0}{\rho_i} = \frac{p_0}{p_i} \times \frac{T_i}{T_0} = \Lambda \quad (10.34)$$

Since  $T_i = T_0$ ,  $\Lambda$  is simply the pressure ratio at which the tunnel is actually operating. This pressure ratio  $\Lambda$  must always be more than the minimum pressure ratio  $\lambda$  required for supersonic operation at any desired Mach number.

Equation (10.34) gives the relation between the operating pressure ratio,  $\Lambda$ , and the compressor intake volume,  $V_0$ , as

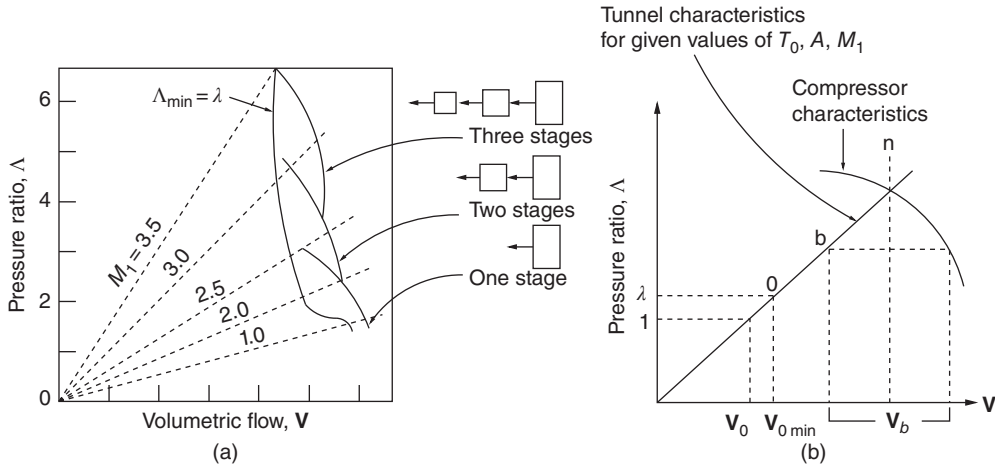
$$\Lambda = \left( \frac{1}{V_0} \right) V_i$$

The plot of  $\Lambda$  versus  $V_i$  is a straight line, through the origin, with slope  $1/V_0$ , as shown in Figure 10.26 [10].

The power requirement for a multistage compressor is given by

$$\left( \frac{1}{746} \right) \left( \frac{N\gamma}{\gamma - 1} \right) \dot{m} R T_s \left[ \left( \frac{p_{0c}}{p_{03}} \right)^{\frac{\gamma-1}{\gamma N}} - 1 \right] \quad (10.35)$$

where  $\dot{m}$  is the mass flow rate of air in  $\text{kg s}^{-1}$ ,  $p_{03}$  and  $p_{0c}$  are the total pressures at the inlet and outlet of the compressor, respectively,  $N$  is the number of stages, and  $T_s$  is the stagnation temperature.



**Figure 10.26** Wind tunnel and compressor characteristics: (a) operation over a range of  $M_1$  using multistage compressor and (b) matching of wind tunnel compressor characteristics (one test-section condition):  $n$ , matching point;  $b$ , matching point with by-pass; and  $0$ , matching point at minimum operating pressure ratio. Source: Reprinted from [10] (Figure 5.11), © 1957, with the permission of John Wiley & Sons, Inc.

### Example 10.3

Determine the minimum possible diffuser contraction ratio and the power required for a two-stage compressor to run a closed-circuit supersonic tunnel at  $M = 2.2$ . The efficiency of the compressor is 85%,  $p_{01} = 4$  atm,  $T_0 = 330$  K, and  $A_{TS} = 0.04$  m<sup>2</sup>.

#### Solution:

The compressor pressure ratio is

$$\frac{p_{0c}}{p_{03}} = \frac{p_{01}}{p_{02}} \frac{1}{\eta}$$

Given:  $M = 2.2$ ,  $\eta = 0.85$ ,  $N = 2$ ,  $T_0 = 330$  K,  $p_{01} = 4$  atm,  $A_{TS} = 0.04$  m<sup>2</sup>.

For  $M_1 = 2.2$ ,  $\frac{p_{02}}{p_{01}} = 0.6281$ , from the normal shock table, and  $\frac{A_1}{A_1^*} = 2.005$ , from the isentropic table.

Therefore, the maximum possible contraction ratio becomes

$$\begin{aligned} \psi_{\max} &= \frac{A_1}{A_1^*} \times \frac{p_{02}}{p_{01}} \\ &= 2.005 \times 0.6281 \\ &= \boxed{1.26} \end{aligned}$$

The mass flow rate is given by

$$\begin{aligned} \dot{m} &= \frac{0.6847}{\sqrt{RT_0}} p_0 A^* \\ &= \frac{0.6847 \times 4 \times 101325}{\sqrt{287 \times 330}} \times \frac{0.04}{2.005} \\ &= 17.99 \text{ kg s}^{-1} \end{aligned}$$

The power required to run the tunnel is

$$\begin{aligned} \text{Power} &= \frac{1}{746} \times \frac{2 \times 1.4}{0.4} \times 17.99 \times 287 \times 330 \left[ \left( \frac{\left( \frac{1}{0.6281} \right)^{\frac{0.2857}{2}}}{0.85} \right) - 1 \right] \\ &= \boxed{1499.50 \text{ hp}} \end{aligned}$$

### Basic Formulae for Supersonic Wind Tunnel Calculations

From our discussions so far, it is easy to identify that the following are the important relations required for supersonic tunnel calculations.

$$\begin{aligned} \frac{p_1}{p_2} &= \left( \frac{\rho_1}{\rho_2} \right)^\gamma = \left( \frac{T_1}{T_2} \right)^{\frac{\gamma}{\gamma-1}} \\ a &= \sqrt{\gamma RT} = 20.04 \sqrt{T} \text{ m s}^{-1} \\ \frac{\gamma}{\gamma-1} \frac{p}{\rho} + \frac{V^2}{2} &= \text{constant} = \frac{\gamma}{\gamma-1} \frac{p_t}{\rho_t} \end{aligned}$$

where  $p_t$  and  $\rho_t$  are the stagnation pressure and density, respectively.

$$\begin{aligned} \frac{p_2}{p_1} &= \left( \frac{1 + \frac{\gamma-1}{2} M_1^2}{1 + \frac{\gamma-1}{2} M_2^2} \right)^{\frac{\gamma}{\gamma-1}} \\ \frac{p_t}{p} &= \left( 1 + \frac{\gamma-1}{2} M^2 \right)^{\frac{\gamma}{\gamma-1}} \\ \frac{\rho_t}{\rho} &= \left( 1 + \frac{\gamma-1}{2} M^2 \right)^{\frac{1}{\gamma-1}} \\ \frac{T_t}{T} &= \left( 1 + \frac{\gamma-1}{2} M^2 \right) \end{aligned}$$

where  $p$ ,  $\rho$ , and  $T$  are the local pressure, density, and temperature, respectively, and  $p_1$  and  $p_2$  are the pressures upstream and downstream of a normal shock.

#### 10.10.9 The Mass Flow Rate

The mass flow rate is one of the primary considerations in sizing a wind tunnel test-section and the associated equipment, such as compressor and diffuser. The mass flow rate is given by

$$\dot{m} = \rho AV$$

From isentropic relations, for air with  $\gamma = 1.4$ , we have

$$\rho = \rho_t (1 + 0.2M^2)^{-\frac{5}{2}}$$

where  $\rho_t$  is the total or stagnation density. By the perfect gas state equation, we have

$$\rho_t = \frac{p_t}{RT_t}$$

Therefore,

$$\rho = \left( \frac{p_t}{R T_t} \right) (1 + 0.2M^2)^{-\frac{5}{2}}$$

where  $R = 287 \text{ m}^2(\text{s}^2 \text{ K})^{-1}$  is the gas constant for air,  $p_t$  is the total pressure in pascals, and  $T_t$  is the total temperature in degrees kelvin.

Also, the local temperature and velocity are given by

$$T = T_t(1 + 0.2M^2)^{-1}$$

$$V = M(1.4 R T)^{\frac{1}{2}}$$

Substituting the above expression for a  $T$  into a  $V$  expression, we get

$$V = M \left[ \frac{1.4 R T_t}{(1 + 0.2M^2)} \right]^{\frac{1}{2}}$$

Using the above expressions for  $V$  and  $\rho$  in the  $\dot{m}$  equation, we get the mass flow rate as

$$\dot{m} = \left( \frac{1.4}{R T_t} \right)^{\frac{1}{2}} \frac{M p_t A}{(1 + 0.2M^2)^3} \quad (10.36)$$

This equation is valid for both subsonic and supersonic flows. When the mass flow rate being calculated is for subsonic Mach number, Eq. (10.36) is evaluated using the test-section Mach number in conjunction with the total temperature and pressure. For supersonic flows, it is usually convenient to make the calculations at the nozzle throat, where the Mach number is 1.0. Further, it should be noted that blowdown tunnels are usually operated at a constant pressure during the run. The main objective of a constant pressure run is to obtain a steady flow while data is being recorded. Thus, the total pressures to be used in the evaluation of Eq. (10.36) are the minimum allowable (or required) operating pressures.

#### Example 10.4

A continuous wind tunnel operates at Mach 2.5 at test-section, with static conditions corresponding to 10 000 m altitude. The test-section is 150 mm × 150 mm in cross-section, with a supersonic diffuser downstream of the test-section. Determine the power requirements of the compressor during start-up and during steady-state operation. Assume the compressor inlet temperature to be the same as the test-section stagnation temperature.

#### Solution:

At the test-section,  $M = 2.5$ . At 10 000 m altitude, from the atmospheric table in [3], we have

$$p = 26.452 \text{ kPa}, \quad T = 223.15 \text{ K}$$

These are the pressure and temperature at the test-section.

From the isentropic table (Table A.1), for  $M = 2.5$ , we have

$$\frac{p}{p_0} = 0.058528, \quad \frac{T}{T_0} = 0.4444$$

Therefore, the stagnation pressure and temperature at the test-section are

$$p_0 = \frac{26.452}{0.058528} = 451.95 \text{ kPa}$$

$$T_0 = \frac{223.15}{0.44444} = 502.1 \text{ K}$$

During steady-state operation, the mass flow rate through the test-section is

$$\begin{aligned}
 \dot{m} &= \rho A V \\
 &= \frac{p}{RT} A M \sqrt{\gamma R T} \\
 &= \frac{26452}{287 \times 223.15} (0.15 \times 0.15) (2.5) \sqrt{1.4 \times 287 \times 223.15} \\
 &= 6.96 \text{ kg s}^{-1}
 \end{aligned}$$

From the isentropic table, for  $M = 2.5$ , we have

$$\frac{A}{A^*} = 2.63671$$

Therefore,

$$\begin{aligned}
 A^* &= \frac{0.15 \times 0.15}{2.63671} \\
 &= 0.00853 \text{ m}^2
 \end{aligned}$$

This is the area of the first throat.

During start-up, a shock wave is formed when the flow becomes supersonic. The pressure loss due to this shock is maximum when it is at the test-section.

For  $M = 2.5$ , from the normal shock table (Table A.2), we have

$$\frac{p_{02}}{p_{01}} = 0.499$$

Also, we know that

$$\frac{p_{02}}{p_{01}} = \frac{A_1^*}{A_2^*}$$

Therefore,

$$\begin{aligned}
 \frac{A_1^*}{A_2^*} &= 0.499 \\
 A_2^* &= \frac{A_1^*}{0.499} = \frac{0.00853}{0.499}
 \end{aligned}$$

Thus,

$$\begin{aligned}
 \frac{A}{A_2^*} &= \frac{0.15 \times 0.15}{0.00853} \times 0.499 \\
 &= 1.316
 \end{aligned}$$

For this area ratio, from the isentropic table, we get  $M = 1.68$ . This is the Mach number ahead of the shock when the shock is at the second throat.

For  $M = 1.68$ , from the normal shock table, we have

$$\frac{p_{02}}{p_{01}} = 0.86394$$

This pressure loss must be compensated by the compressor. The power input required for the compressor to compensate for this loss is

$$\text{Power} = h_0 - h_i = c_p (T_0 - T_i)$$



where the subscripts 0 and  $i$  refer to compressor outlet and inlet conditions, respectively. For an isentropic compressor,

$$\begin{aligned}\frac{T_0}{T_i} &= \left(\frac{p_0}{p_i}\right)^{\frac{(\gamma-1)}{\gamma}} \\ T_0 - T_i &= T_i \left[ \left(\frac{p_0}{p_i}\right)^{\frac{(\gamma-1)}{\gamma}} - 1 \right] \\ &= 502.1 \left[ \left(\frac{1}{0.86394}\right)^{0.286} - 1 \right] \\ &= 21.45 \text{ K}\end{aligned}$$

Thus, the power input required becomes

$$\text{Power} = 1004.5(21.45) = 21546.52 \text{ J kg}^{-1}$$

The horse power required for the compressor is

$$\begin{aligned}\text{Power} &= \frac{\dot{m} W}{746} \\ &= \frac{6.96 \times 21546.52}{746} \\ &= \boxed{201 \text{ hp}}\end{aligned}$$

This is the running horse power required for the compressor.

During start-up,  $M_1 = 2.5$ , the corresponding  $p_{02}/p_{01} = 0.499$ , from the normal shock table. The isentropic work required for the compressor during start-up is

$$\begin{aligned}W &= \left[ \left(\frac{1}{0.499}\right)^{0.286} - 1 \right] 502.1 c_p \\ &= 110.4 c_p \\ &= 1004.5 \times 110.4 \\ &= 110896.8 \text{ J kg}^{-1}\end{aligned}$$

Thus, the power required is

$$\begin{aligned}\text{Power} &= \frac{6.96 \times 110896.8}{746} \\ &= \boxed{1034.6 \text{ hp}}\end{aligned}$$

### Example 10.5

Estimate the settling chamber pressure and temperature and the area ratio required to operate a Mach 2 tunnel under standard sea-level conditions. Assume the flow to be one-dimensional and the tunnel to be operating with correct expansion.

#### Solution:

The tunnel is operating with correct expansion. Therefore, the sea-level pressure and temperature become the pressure and temperature in the test-section (that is at the nozzle exit). Thus,  $p_e = 101.325 \text{ kPa}$  and  $T_e = 15^\circ\text{C}$ .

Let subscripts  $e$  and 0 refer to nozzle exit and stagnation states, respectively.

From the isentropic relations, we have the temperature and pressure ratio as

$$\begin{aligned}
 \frac{T_0}{T_e} &= 1 + \frac{\gamma - 1}{2} M_e^2 \\
 &= 1 + \frac{1.4 - 1}{2} \times 2^2 = 1.8 \\
 T_0 &= 1.8 T_e = 1.8 \times 288.15 \\
 &= \boxed{518.67 \text{ K}} \\
 \frac{p_0}{p_e} &= \left( 1 + \frac{\gamma - 1}{2} M_e^2 \right)^{\gamma/\gamma-1} \\
 &= 1.8^{3.5} = 7.824 \\
 p_0 &= 7.824 p_e \\
 &= \boxed{792.77 \text{ Pa}}
 \end{aligned}$$

From the isentropic relations we have the area ratio as

$$\begin{aligned}
 \left( \frac{A_e}{A_{th}} \right)^2 &= \frac{1}{M_e^2} \left[ \frac{2}{\gamma + 1} \left( 1 + \frac{\gamma - 1}{2} M_e^2 \right) \right]^{\frac{\gamma+1}{\gamma-1}} \\
 &= \frac{1}{2^2} \left[ \frac{2}{2.4} \times 1.8 \right]^6 = 2.8476 \\
 \frac{A_e}{A_{th}} &= \boxed{1.687}
 \end{aligned}$$

### 10.10.10 Blowdown Tunnel Operation

In a blowdown tunnel circuit, the pressure and temperature of air in the compressed air reservoir (also called a *storage tank*) change during operation. This change of reservoir pressure causes the following effects.

- The tunnel stagnation and settling chamber pressures fall correspondingly.
- The tunnel is subjected to dynamic conditions.
- Dynamic pressure in the test-section falls and hence the forces acting on the model change during test.
- The Reynolds number of the flow changes during the tunnel run.

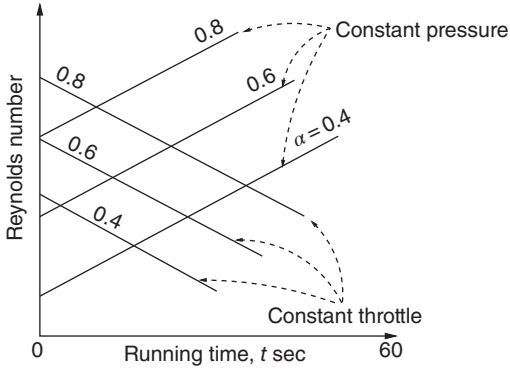
Usually, the following three methods of operation are adopted for blowdown tunnel operation:

- constant Reynolds number operation
- constant pressure operation
- constant throttle operation.

The ratio between the settling chamber initial pressure  $p_{bi}$  and reservoir initial pressure  $p_{0i}$  is an important parameter influencing the test-section Reynolds number. Let

$$\frac{p_{bi}}{p_{0i}} = \frac{\text{Settling chamber initial pressure}}{\text{Reservoir initial pressure}} = \alpha$$

The variation of Reynolds number with tunnel running time  $t$ , as a function of  $\alpha$ , is as shown in Figure 10.27.



**Figure 10.27** Reynolds number variation with tunnel running time.

As seen from Figure 10.27, the Reynolds number increases with the running time for constant pressure operation and decreases with the running time for constant throttle operation. The change in Reynolds number results in the change of boundary layer thickness, which in turn causes area and Mach number change in the test-section. Usually, the Mach number variation due to the above causes is small.

#### 10.10.10.1 Reynolds Number Control

By definition, Reynolds number is the ratio between the inertia and viscous forces.

$$\text{Re} = \frac{\text{Inertia force}}{\text{Viscous force}}$$

It can be shown that

$$\text{Re} = \frac{\rho V L}{\mu}$$

where  $\rho$ ,  $V$ , and  $\mu$  are the density, velocity, and viscosity, respectively, and  $L$  is a characteristic dimension of the model being tested. The above equation may be expressed as

$$\frac{\text{Re}}{L} = \frac{\rho V}{\mu} \quad (10.37)$$

Also, the viscosity coefficient may be expressed as

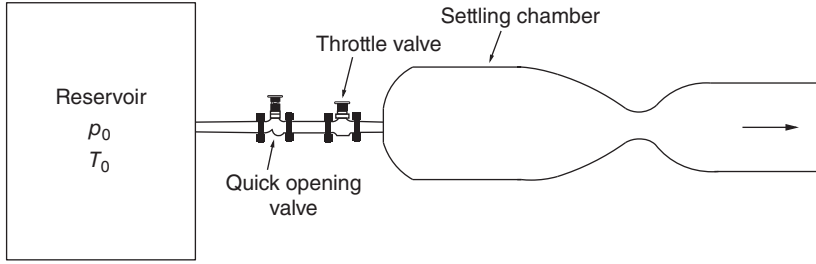
$$\mu = C T^m V = C T^m M \sqrt{\gamma R T} = c_1 f(M) \sqrt{T}$$

In the above expression,  $c_1$  and  $C$  are constants,  $m$  is the viscosity index,  $\gamma$  is the isentropic index, and  $R$  is the gas constant.

Let  $p_b$  and  $p_{bi}$  be the instantaneous and initial pressures in the settling chamber, respectively, and  $T_b$  and  $T_{bi}$  be the corresponding temperatures. With the above relations for  $\mu$ , Eq. (10.37) can be expressed as

$$\frac{\text{Re}}{L} = g_1 f(M, m) \left[ \frac{p_b/p_{bi}}{(T_b/T_{bi})^{(m+\frac{1}{2})}} \right] \quad (10.38)$$

where  $g_1$  is a function of initial (starting) conditions ( $p_{bi}$ ,  $p_{oi}$ ). From Eq. (10.38) it can be seen that the Reynolds number during tunnel run is influenced only by the quantities within the square brackets. These quantities can easily be held constant by suitable manipulation of a throttling valve located between the reservoir and the settling chamber, as shown in Figure 10.28.



**Figure 10.28** Blowdown tunnel layout.

The throttling process may be expressed by the following equation.

$$p_{bi} = \alpha p_0^\beta \quad (10.39)$$

where  $p_{bi}$  and  $p_0$  are the total pressures after (stagnation pressure in the settling chamber) and before (stagnation pressure in the reservoir) throttling, respectively, and  $\alpha$  and  $\beta$  are constants.

The function  $g$  in Eq. (10.38), at settling chamber conditions, is

$$g_i = \left( \frac{\gamma p_{bi}}{a_{bo} \mu_{bo}} \right)$$

where  $a_{bo}$  is the proportionality constant and  $\mu_{bo}$  is the viscosity coefficient of air in the settling chamber.

The function  $f(M, m)$ , from isentropic relations, is

$$f(M, m) = \frac{M}{\left[ 1 + \frac{\gamma-1}{2} M^2 \right]^{\left( \frac{\gamma+1}{2(\gamma-1)} - m \right)}}$$

Now, applying the polytropic law for the expansion of gas in the storage tank, we can write

$$\frac{p_0}{p_{0i}} = \left( \frac{T_0}{T_{0i}} \right)^{\frac{n}{n-1}}$$

where subscripts 0 and 0i refer for instantaneous and initial conditions in the reservoir and  $n$  is the polytropic index.

Also, from Eq. (10.39), we have

$$\frac{p_b}{p_{bi}} = \left( \frac{p_0}{p_{0i}} \right)^\beta$$

Therefore, with the above relations, Eq. (10.38) can be expressed as,

$$\boxed{\frac{\text{Re}}{L} = g_1 f(M, m) \left[ \left( \frac{p_0}{p_{0i}} \right)^{\left( \beta - \frac{(2m+1)(n-1)}{2n} \right)} \right]} \quad (10.40)$$

This is the general relation between test-section Reynolds number and reservoir pressure. From this equation, the following observations can be made.

- For  $\text{Re} = \text{constant}$ ,  $\beta = \frac{(2m+1)(n-1)}{2n}$
- For “constant  $p_b$ ” operation,  $p_b = \alpha p_0^\beta = \text{constant}$  and  $\beta = 0$ . Thus, Eq. (10.40) simplifies to

$$\frac{\text{Re}}{L} = K_3 \left( \frac{p_{0i}}{p_0} \right)^{\frac{(2m+1)(n-1)}{2n}}$$

where  $K_3$  is a constant. This implies that  $Re$  increases with time  $t$ , since  $p_0$  decreases with  $t$ .

- For constant throttle operation,  $\beta = 1$  and

$$p_b = \alpha p_0^\beta = \alpha p_0$$

Therefore,

$$\frac{Re}{L} = K_3 \left( \frac{p_0}{p_{0i}} \right)^{\left[ 1 - \frac{(2m+1)(n-1)}{2n} \right]} \quad 0 < \frac{(2m+1)(n-1)}{2n} < 1$$

This implies that  $Re$  decreases with  $t$  for constant throttle operation.

From the above observations it can be inferred that, for a given settling chamber pressure and temperature, the running time is

- shortest for constant throttle operation
- longest for constant Reynolds number operation
- in between the above two for constant pressure operation.

### 10.10.11 Optimum Conditions

For optimum performance of a tunnel in terms of running time  $t$ , the drop in reservoir pressure should be as slow as possible. To achieve this slow rate of fall in reservoir pressure, the pressure regulating valve (PRV) should be adjusted after the tunnel has been started, in such a manner that the pressure in the settling chamber is the minimum pressure  $p_{bmin}$  required for the run.

The performance of the tunnel, that is the test-section Mach number  $M$  versus the tunnel run time  $t$ , for different methods of control mentioned above should be evaluated for the entire range of operation. This performance can be recorded in the form of graphs for convenient reference. From such graphs, the best-suited method of operation for any particular test and the required settings of the throttle valve ( $\alpha$ ,  $\beta$ , and so on) can be chosen. A typical performance chart will look like the one shown in Figure 10.29.

For a given test-section Mach number  $M$  there is a  $p_b$  minimum in the settling chamber, given by the pressure ratio relation. The Reynolds number in the test-section depends on this  $p_b$  value and constant Reynolds number operation is possible only if

- the  $p_{bi}$  value is so chosen that as  $t$  proceeds (increases) both  $p_0$  and  $p_b$  reach  $p_{bmin}$  value simultaneously (to result in an optimum constant Reynolds number)

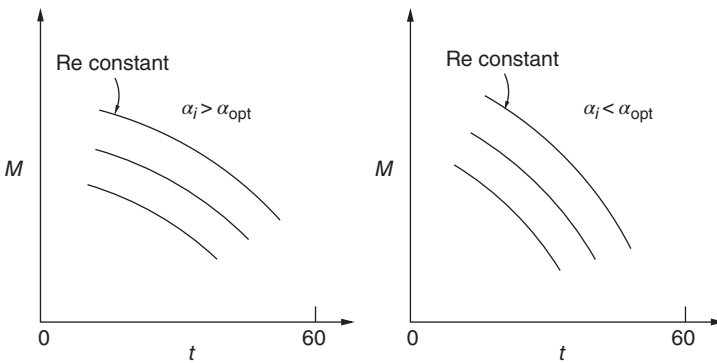


Figure 10.29 Wind tunnel performance chart.

- $p_{bi} > p_{b\text{opt}}$ , the reservoir pressure will become equal to  $p_b$  at some instant, and from then onwards constant Reynolds number operation is not possible.
- $p_{bi} < p_{b\text{opt}}$ , the  $p_b = p_{b\text{min}}$  state will be reached at time  $t$  when  $p_0 > p_b$  and supersonic operation will no longer be possible.

### 10.10.12 Running Time of Blowdown Wind Tunnels

Blowdown supersonic wind tunnels are usually operated with either constant dynamic pressure ( $q$ ) or constant mass flow rate ( $\dot{m}$ ).

For constant  $q$  operation, the only control necessary is a PRV that holds the stagnation pressure in the settling chamber at a constant value. The stagnation pressure in the storage tank falls according to the polytropic process  $pV^n = \text{constant}$ . For short-duration runs with high mass flow rates, the polytropic index is 1.4. For long-duration runs with thermal mass<sup>1</sup> in the tank, the polytropic index  $n$  approaches 1.

For a constant mass flow run, the stagnation temperature and pressure in the settling chamber must be held constant. For this, either a heater or a thermal mass external to the storage tank is essential. The addition of heat energy to the pressure energy in the storage tank results in a longer running time of the tunnel. Another important consequence of this heat addition is that the constant settling chamber temperature of the constant mass run keeps the test-section Reynolds number at a constant value.

For calculating the running time of a tunnel, let us make the following assumptions.

- Expansion of the gas in the storage tank is polytropic.
- Gas temperature in the storage tank is held constant with a heater.
- Gas pressure in the settling chamber is kept constant with a PRV.
- No heat is lost in the pipelines from the storage tank to the test-section.
- Expansion of the gas from the settling chamber to the test-section is isentropic.
- Test-section speed is supersonic.

The mass flow rate  $\dot{m}$  through the tunnel, as given by Eq. (10.36), is

$$\dot{m} = \left( \frac{1.4}{R T_t} \right)^{1/2} \frac{M p_t A}{(1 + 0.2M^2)^3}$$

where  $M$  is the test-section Mach number,  $p_t$  and  $T_t$  are the pressure and temperature in the settling chamber.

We know that for supersonic flows it is convenient to calculate the mass flow rate with nozzle throat conditions. At the throat,  $M = 1.0$ , and Eq. (10.36) becomes

$$\dot{m} = 0.0404 \frac{p_t A^*}{\sqrt{T_t}} \quad (10.41)$$

The value of gas constant used in the above equation is  $R = 287 \text{ m}^2 (\text{s}^2 \text{ K})^{-1}$ , which is the gas constant for air.

The product of mass flow rate and run time gives the change of mass in the storage tank. Therefore,

$$\dot{m}t = (\rho_i - \rho_f)V_t \quad (10.42)$$

where  $V_t$  is the tank volume and  $\rho_i$  and  $\rho_f$  are the initial and final densities in the tank, respectively.

<sup>1</sup> Thermal mass is a material that has a high value of thermal capacity.

From Eq. (10.42), the running time  $t$  is obtained as

$$t = \frac{(\rho_i - \rho_f)}{\dot{m}} V_t$$

Substituting for  $\dot{m}$  from Eq. (10.41) and arranging the above equation, we get

$$t = 24.728 \frac{\sqrt{T_t} V_t}{p_t A^*} \rho_i \left( 1 - \frac{\rho_f}{\rho_i} \right) \quad (10.43)$$

For polytropic expansion of air in the storage tank, we can write

$$\frac{\rho_f}{\rho_i} = \left( \frac{p_f}{p_i} \right)^{\frac{1}{n}}; \quad \rho_i = \frac{p_i}{RT_i}$$

where subscripts  $i$  and  $f$  denote the initial and final conditions in the tank, respectively. Substitution of the above relations into Eq. (10.43) results in

$$t = 0.086 \frac{V_t}{A^*} \frac{\sqrt{T_t} p_i}{T_i p_t} \left( 1 - \left( \frac{p_f}{p_i} \right)^{\frac{1}{n}} \right) \quad (10.44)$$

with  $V_t$  in  $\text{m}^3$ ; this gives the run time in seconds for the general case of blowdown tunnel operation with the constant mass flow rate condition.

From Eq. (10.44) it is obvious that, for  $t_{\max}$ , the condition required is  $p_t$  minimum. At this stage, we should realize that the above equation for running time has to be approached from a practical point of view and not from a purely mathematical point of view. Realizing this, it can be seen that the tunnel run does not continue until the tank pressure drops to the settling chamber stagnation pressure  $p_t$ , but stops when the storage pressure reaches a value that is appreciably higher than  $p_t$ , that is when  $p_f = p_t + \Delta p$ . This  $\Delta p$  is required to overcome the frictional and other losses in the piping system between the storage tank and the settling chamber. The value of  $\Delta p$  varies from about  $0.1p_t$  for very-small-mass-flow runs to somewhere around  $1.0p_t$  for high-mass-flow runs.

The proper value of the polytropic index  $n$  in Eq. (10.44) depends on the rate at which the stored high-pressure air is used, the total amount of air used and the shape of the storage tank. The value of  $n$  tends toward 1.4 as the storage tank shape approaches spherical shape. With heat storage material in the tank (that is for isothermal condition), the index  $n$  approaches unity. Equation (10.44) may also be used with reasonable accuracy for constant-pressure runs in which the change in total temperature is small, since these runs approach the constant-mass flow rate situation.

### Example 10.6

Determine the running time for a Mach 2 blowdown wind tunnel with test-section cross-section of  $300 \text{ mm} \times 300 \text{ mm}$ . The storage tank volume is  $20 \text{ m}^3$  and the pressure and temperature of air in the tank are 20 atm and  $25^\circ\text{C}$ , respectively. The tank is provided with a heat sink material inside. Take the starting pressure ratio required for Mach 2.0 to be 3.0, the loss in PRV to be 50% and the polytropic index  $n = 1.0$ .

### Solution:

Given: the settling chamber pressure required to start the tunnel is  $p_t = 3.0 \times 101.3 \text{ kPa}$ . The pressure loss in the PRV is 50%; therefore,

$$p_f = 1.5 \times 303.9 = 455.85 \text{ kPa}$$

From the isentropic table, for  $M = 2.0$ , we have  $A^*/A = 0.593$ . Therefore,

$$A^* = 0.593 \times 0.09 = 0.0534 \text{ m}^2$$

By Eq. (10.44), the running time,  $t$ , is given by

$$\begin{aligned} t &= 0.086 \left( \frac{20}{0.0534} \right) \left( \frac{\sqrt{298}}{298} \right) \left( \frac{2026}{303.9} \right) \left[ 1 - \left( \frac{455.85}{2026} \right) \right] \\ &= \boxed{9.64 \text{ s}} \end{aligned}$$

## 10.11 Hypersonic Tunnels

Hypersonic tunnels are those that operate with test-section Mach numbers above 5. Generally, they operate with stagnation pressures in the range of 10 to 100 atm and stagnation temperatures in the range of  $-50$  to  $2000^\circ\text{C}$ . Contoured nozzles that are more often axially symmetric are used in hypersonic tunnels.

Models that can be tested in hypersonic tunnels are usually larger than those meant for testing in supersonic tunnels. The model frontal area can go up to 10% of the test-section cross-sectional area. The model size will probably be restricted by the wake behind it, which takes too much flow area in the diffuser and blocks it during tunnel starting.

Use of dry and heated air is necessary for hypersonic operation to avoid condensation effects and liquefaction during expansion to the high Mach number and corresponding low temperatures. The requirement of heated air is the major factor making hypersonic tunnel operation more complicated than supersonic tunnel operation. To get a feel for the drastic changes in the flow properties at hypersonic speeds, let us examine the parameters listed in Table 10.2, for isentropic index  $\gamma = 1.4$ .

Now, we should note this table is based on isentropic relations. As we know, in the isentropic relations the index  $\gamma$  is treated as a constant. However, we are familiar with the fact that  $\gamma$  is constant only for gases that are thermally as well as calorically perfect, simply termed perfect gases [6]. Therefore, in hypersonic flows if the test-section flow temperatures are to be at room temperature, the storage temperature has to be increased to very high values, which will pose metallurgical problems. Because of these considerations, the temperatures in the test-section of hypersonic tunnels are usually quite low, in spite of the fact that the storage temperature is kept appreciably above the ambient temperature.

**Table 10.2** Area ratio, pressure ratio, and temperature ratio at certain hypersonic Mach numbers.

$M$	$A/A^*$	$p_0/p$	$T_0/T$
5	25.00 E 00	529.10 E 00	6.000
10	53.59 E 01	424.39 E 03	21.000
15	37.55 E 02	660.15 E 03	46.000
20	15.38 E 03	478.29 E 04	80.998
25	46.31 E 03	224.54 E 05	126.000



**Example 10.7**

Find the test-section temperature for a hypersonic stream of air at Mach 7 with a stagnation temperature of 700 K.

**Solution:**

From the isentropic table ( $\gamma = 1.4$ ), for  $M = 7.0$ , we have

$$\frac{T}{T_0} = 0.09592$$

Therefore, the temperature of air in the test-section is

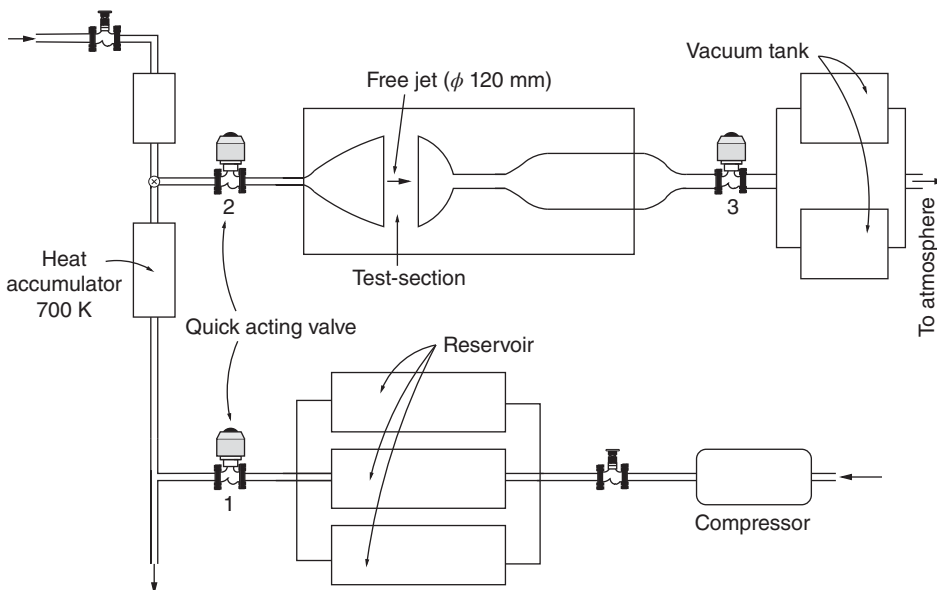
$$T = (0.09592)(700) = 67.144 \text{ K}$$

$$= \boxed{-206^\circ \text{C}}$$

It can be seen from Table 10.2 that the pressure ratios involved in the hypersonic tunnel flow process are very high. In order to achieve these pressure ratios, it is customary to employ a combination of high pressure and vacuum together in hypersonic tunnel operations. A typical hypersonic tunnel circuit is schematically shown in Figure 10.30.

From the above discussions on hypersonic tunnel operation, the following observations can be made.

- The pressure ratio, area ratio, and temperature ratio for  $M > 5$  increase very steeply with increases of  $M$ . Usually, both a high-pressure tank at the nozzle inlet and a vacuum tank at the diffuser end are necessary for hypersonic operations.
- The very low temperatures encountered in the test-section result in liquefaction of air and hence preheating of air to 700–1000 K is common in hypersonic tunnel operation. For air, up to Mach 8 preheating to about 1300 K is satisfactory. For  $M > 10$ , a gas such as helium is better suited.
- Because of the very low density in the test-section, optical flow visualization of viscous shock waves, and so on, becomes more difficult.
- Shock wave angle (e.g. on wedge, cone, and so on) changes appreciably with moisture content of air and hence measurements have to be done with extra care.



**Figure 10.30** Hypersonic tunnel circuit.

- The heating of air introduces additional problems, such as material requirement for settling chamber, nozzle, test-section glass window, and other parts (the tunnel structure, test-section walls, and so on) to withstand high temperatures.
- Because of low pressure and temperature, the flow at the test-section has a low Reynolds number and hence the boundary layer thickness increases to a large extent.
- Determining the exact value of Mach numbers at high Mach number is quite difficult, since heating expands tunnel walls and, therefore, the area ratio is changed. In addition, the boundary layer (which is quite thick) makes it more difficult to calculate  $M$ . Also, the specific heats ratio  $\gamma$  is changing, owing to the drastic changes of temperature encountered in the tunnel, and hence accurate computation of the total pressure  $p_0$  and static pressure  $p$  is difficult.

### 10.11.1 Hypersonic Nozzle

For hypersonic operations, axisymmetric nozzles are better suited than two-dimensional nozzles. For high Mach numbers of the order 10 the throat size becomes extremely narrow and forming the shape itself becomes very difficult. Because of the high temperatures, the material to be used also poses a problem. Material liners scale and pit easily at these high speeds. Though porcelain-coated nozzles are good for these high temperatures and speeds, they do not provide the smoothness that is required for hypersonic speeds. A minimum diameter of around 12 mm for the nozzle throat is arrived at from practical considerations. A typical shape for hypersonic nozzles is shown schematically in Figure 10.31.

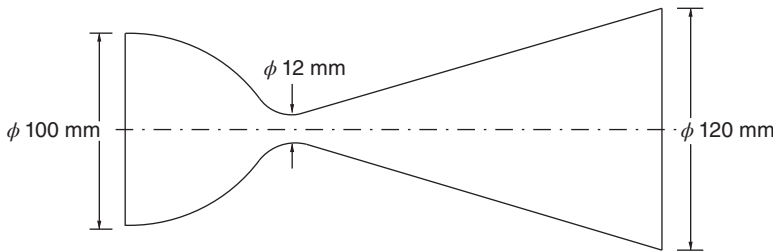


Figure 10.31 Hypersonic nozzle.

### Example 10.8

(a) Design a nozzle to deliver Mach 1.6 air flow with inlet diameter 40 mm, semi-convergence angle  $30^\circ$ , and semi-divergence angle  $7^\circ$ , to be run by a reservoir at 6 atm and  $35^\circ\text{C}$  with a mass flow rate of  $0.11\text{ kg s}^{-1}$ , discharging to atmospheric pressure. (b) Calculate the Reynolds number at the exit, based on the exit diameter? (c) What will be the type of expansion at the nozzle exit? Sketch the waves at the exit, and (d) Determine the maximum theoretical Mach number possible for the flow after exiting the nozzle.

#### Solution:

(a) Given,  $M_e = 1.6$ ,  $\dot{m} = 0.11\text{ kg s}^{-1}$ ,  $p_0 = 6\text{ atm}$ ,  $T = 35 + 273 = 308\text{ K}$ ,  $\theta_c = 30^\circ$ ,  $\theta_d = 7^\circ$  and  $p_b = 1\text{ atm}$ .

The mass flow rate is given by

$$\dot{m} = \frac{0.6847 p_0 A_{\text{th}}}{\sqrt{RT_0}}$$

Therefore,

$$\begin{aligned}
 A_{th} &= \frac{\dot{m} \sqrt{RT_0}}{0.6847 p_0} \\
 &= \frac{0.11 \times \sqrt{287 \times 308}}{0.6847 \times (6 \times 101325)} \\
 &= 7.857 \times 10^{-5} \text{ m}^2 \\
 d_{th} &= \sqrt{\frac{(7.857 \times 10^{-5}) \times 4}{\pi}} \\
 &= 0.01 \text{ m} \\
 &= 10 \text{ mm}
 \end{aligned}$$

The convergent portion of the nozzle is as shown in Figure 10.32. The length of the convergent portion is

$$\begin{aligned}
 x_c &= \frac{15}{\tan \theta_c} = \frac{15}{\tan 30} \\
 &= 26 \text{ mm}
 \end{aligned}$$

For  $M_e = 1.6$ , from the isentropic table, we have  $\frac{A_e}{A_{th}} = 1.25$ . Thus,

$$\begin{aligned}
 A_e &= 1.25 A_{th} \\
 d_e &= \sqrt{1.25} d_{th} \\
 &= \sqrt{1.25} \times 10 \\
 &= 11.18 \text{ mm}
 \end{aligned}$$

The divergent portion of the nozzle is as shown in Figure 10.33. The length of the divergent portion is

$$\begin{aligned}
 x_d &= \frac{1.18/2}{\tan \theta_d} = \frac{0.59}{\tan 7^\circ} \\
 &= 4.805 \text{ mm}
 \end{aligned}$$

The dimensions of the desired nozzle are shown Figure 10.34.

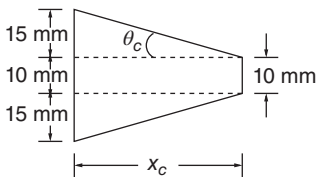


Figure 10.32 Convergent part of the C-D nozzle.

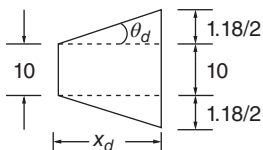
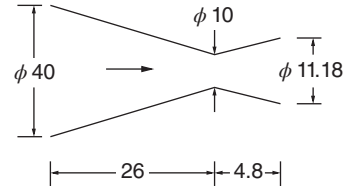


Figure 10.33 Divergent portion of the C-D nozzle.

**Figure 10.34** Convergent–divergent nozzle (all dimensions are in mm).

(b) For  $M_e = 1.6$ , from the isentropic table,

$$\frac{T_e}{T_0} = 0.6614, \quad \frac{\rho_e}{\rho_0} = 0.3557, \quad \frac{p_e}{p_0} = 0.2353$$

Therefore, the exit temperature is

$$\begin{aligned} T_e &= 0.6614 T_0 = 0.6614 \times 308 \\ &= 203.7 \text{ K} \end{aligned}$$

The viscosity of the flow at the nozzle exit, by the Sutherland relation, is

$$\begin{aligned} \mu &= 1.46 \times 10^{-6} \frac{T_e^{3/2}}{T_e + 111} \\ &= (1.46 \times 10^{-6}) \times \frac{203.7^{3/2}}{203.7 + 111} \\ &= 1.35 \times 10^{-5} \text{ kg (m s)}^{-1} \end{aligned}$$

The speed of sound at the nozzle exit is

$$\begin{aligned} a_e &= \sqrt{\gamma R T_e} \\ &= \sqrt{1.4 \times 287 \times 203.7} \\ &= 286.1 \text{ m s}^{-1} \end{aligned}$$

The flow speed at the nozzle exit is

$$\begin{aligned} V_e &= M_e a_e = 1.6 \times 286.1 \\ &= 457.76 \text{ m s}^{-1} \end{aligned}$$

The flow density at the nozzle exit is

$$\begin{aligned} \rho_e &= 0.3557 \rho_0 = 0.3557 \frac{p_0}{R T_0} \\ &= 0.3557 \times \frac{6 \times 101325}{287 \times 308} \\ &= 2.446 \text{ kg m}^{-3} \end{aligned}$$

Thus, the Reynolds number of the flow delivered by the nozzle, based on  $d_e$ , is

$$\begin{aligned} \text{Re}_{d_e} &= \frac{\rho_e V_e d_e}{\mu_e} \\ &= \frac{2.446 \times 457.76 \times (11.18 \times 10^{-3})}{1.35 \times 10^{-5}} \\ &= 927262 \\ &= \boxed{9.27 \times 10^5} \end{aligned}$$

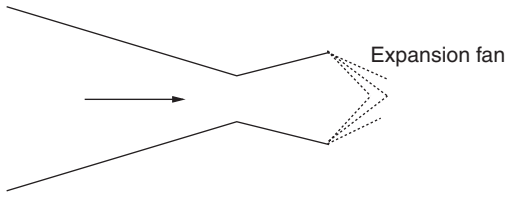


Figure 10.35 Expansion at the nozzle exit.

- (c) The flow pressure at the nozzle exit is

$$\begin{aligned} p_e &= 0.2353 p_0 = 0.2353 \times (6 \times 101325) \\ &= 143050.6 \text{ Pa} \end{aligned}$$

The backpressure  $p_b = 101325 \text{ Pa}$ , thus,  $p_e > p_b$  and the nozzle is underexpanded. Therefore, there will be an expansion fan at the nozzle exit, as shown in Figure 10.35.

- (d) The theoretical Mach number  $M_{\max}$  possible for the flow leaving the nozzle is the Mach number that can be achieved by expanding the stagnation air at 6 atm to 1 atm. Thus,  $\frac{p_0}{p} = 6$ . By isentropic relation, we have

$$\frac{p_0}{p} = \left( 1 + \frac{\gamma - 1}{2} M^2 \right)^{\gamma/(\gamma-1)}$$

That is,

$$\begin{aligned} 6 &= (1 + 0.2 M_{\max}^2)^{3.5} \\ 1 + 0.2 M_{\max}^2 &= 6^{1/3.5} = 1.668 \\ M_{\max} &= \sqrt{\frac{1.668 - 1}{0.2}} \\ &= \boxed{1.83} \end{aligned}$$

## 10.12 Instrumentation and Calibration of Wind Tunnels

Calibration of a wind tunnel test-section to ensure uniform flow characteristics throughout the test-section is an essential requirement in wind tunnel operation.

### 10.12.1 Calibration of Supersonic Wind Tunnels

Supersonic tunnels operate in the Mach number range of about 1.4–5.0. They usually have operating total pressures from about atmospheric to 2 MPa ( $\approx 300 \text{ psi}$ ) and operating total temperatures of about ambient to  $100^\circ\text{C}$ . A maximum model cross-section area (projected area of the model, normal to the test-section axis) of the order of 4% of the test-section area is quite common for supersonic tunnels. *Model size is limited by tunnel choking and wave reflection considerations.* When proper consideration is given to choking and wave reflection while deciding on the size of a model, there will be no effects of the wall on the flow over the models (unlike low-speed tunnels), since the reflected disturbances will propagate only downstream of the model. However, there will be a buoyancy effect if there is a pressure gradient in the tunnel. Luckily, typical pressure gradients associated with properly designed tunnels are small, and the buoyancy effects in such tunnels are usually negligible. The Mach number in a supersonic tunnel with solid walls cannot be adjusted, because it is set by the geometry of the nozzle. Small

increases in Mach number usually accompany large increases in operating pressure (the stagnation pressure in the settling chamber in the case of constant back pressure or the nozzle pressure ratio in the case of blowdown indraft combination), in that the boundary layer thickness is reduced and consequently the effective area ratio is increased.

During calibration as well as testing, the condensation of moisture in the test gas must be avoided. To ensure that condensation will not be present in significant amounts, the air dew point in the tunnel should be continuously monitored during tunnel operation. The amount of moisture that can be held by a cubic meter of air increases with increasing temperature, but is independent of the pressure. The moist atmospheric air cools as it expands isentropically through a wind tunnel. The air may become supercooled (cooled to a temperature below the dew-point temperature) and the moisture will then condense out. If the moisture content is sufficiently high, it will appear as a dense fog in the tunnel. Detailed information about the effect of condensation on the flow quality in the test-section of a tunnel can be found in [5].

### 10.12.2 Calibration

The calibration of a supersonic wind tunnel includes determining the test-section flow Mach number throughout the range of operating pressure of each nozzle, determining flow angularity and determining an indication of turbulence level effects.

### 10.12.3 Mach Number Determination

The following methods may be employed for determining the test-section Mach number of supersonic wind tunnels.

- Mach numbers from close to the speed of sound to 1.6 are usually obtained by measuring the static pressure  $p$  in the test-section and the total pressure  $p_{01}$  in the settling chamber and using the isentropic relation

$$\frac{p_{01}}{p} = \left( 1 + \frac{\gamma - 1}{2} M^2 \right)^{\frac{\gamma}{\gamma - 1}}$$

- For Mach numbers above 1.6, it is more accurate to use the pitot pressure in the test-section  $p_{02}$  with the total head in the settling chamber  $p_{01}$  and the normal shock relation.

$$\frac{p_{02}}{p_{01}} = \left[ 1 + \frac{2\gamma}{\gamma + 1} (M_1^2 - 1) \right]^{-\frac{1}{\gamma - 1}} \left[ \frac{(\gamma + 1)M_1^2}{(\gamma - 1)M_1^2 + 2} \right]^{\frac{\gamma}{\gamma - 1}}$$

- Measurement of static pressure  $p_1$  using a wall pressure tap in the test-section and measurement of pitot pressure  $p_{02}$  at the test-section axis, above the static tap can be used through the Rayleigh pitot formula,

$$\frac{p_1}{p_{02}} = \frac{\left( \frac{2\gamma}{\gamma + 1} M_1^2 - \frac{\gamma - 1}{\gamma + 1} \right)^{\frac{1}{\gamma - 1}}}{\left( \frac{\gamma + 1}{2} M_1^2 \right)^{\frac{\gamma}{\gamma - 1}}}$$

for an accurate determination of the Mach number.

- Measurement of shock wave angle  $\beta$  from a Schlieren and shadowgraph photograph of flow past a wedge or cone of angle  $\theta$  can be used to obtain the Mach number through  $\theta - \beta - M$  relation:

$$\tan \theta = 2 \cot \beta \left( \frac{M_1^2 \sin^2 \beta - 1}{M_1^2 (\gamma + \cos 2\beta) + 2} \right)$$

- The Mach angle  $\mu$  measured from a Schlieren photograph of a clean test-section can also be used for determining the Mach number with the relation

$$\sin \mu = \frac{1}{M_1}$$

For this, the Schlieren system used must be powerful enough to capture the Mach waves in the test-section.

- The Mach number can also be obtained by measuring pressures on the surface of cones or two-dimensional wedges, although this is rarely done in calibration.

#### 10.12.4 Pitot Pressure Measurement

Pitot pressures are measured by using a *pitot probe*. The pitot probe is simply a tube with a blunt end facing into the air stream. The tube will normally have an inside to outside diameter ratio of 0.5–0.75, and a length aligned with the air stream of 15–20 times the tube diameter. The inside diameter of the tube forms the pressure orifice. For test-section calibration, a rake consisting of a number of pitot probes is usually employed. The pitot tube is simple to construct and accurate to use. It should always have a squared-off entry and the largest practical ratio of hole (inside) diameter to outside diameter.

At this stage, it is important to note that an open-ended tube facing into the air stream always measures the stagnation pressure (a term identical in meaning to the *total head*) it sees. For flows with Mach number greater than 1, a bow shock wave will be formed ahead of the pitot tube nose. Therefore, the flow reaching the probe nose is not the actual freestream flow but the flow traversed by the bow shock at the nose. Thus, what the pitot probe measures is not the actual static pressure but the total pressure behind a normal shock (the portion of the bow shock at the nose hole can be approximated to a normal shock). This new value is called the *pitot pressure* and in modern terminology refers to pressure measured by a pitot probe in a supersonic stream. The pressure measured by a pitot probe is significantly influenced by very low Reynolds numbers based on probe diameter. However, this effect is seldom a problem in supersonic tunnels, since a reasonable-size probe will usually have a Reynolds number well above 500; Reynolds numbers below 500 are troublesome for pitot pressure measurements.

#### 10.12.5 Static Pressure Measurement

Supersonic flow static pressure measurements are much more difficult than the measurement of pitot and static pressures in a subsonic flow. The primary problem in the use of static pressure probes at supersonic speeds is that the probe will have a shock wave (either attached or detached shock) at its nose, causing a rise in static pressure. The flow passing through the oblique shock at the nose will be decelerated. However, the flow will continue to be supersonic because all naturally occurring oblique shocks are weak shocks with supersonic flow on either side of them. The supersonic flow of reduced Mach number will get decelerated further

while passing over the nose-cone of the probe because a decrease of streamtube area would decelerate a supersonic stream. This progressively decelerating flow over the nose-cone would be expanded by the expansion fan at the nose-cone shoulder junction of the probe. Therefore, the distance over the shoulder should be sufficient for the flow to get accelerated to the level of the undisturbed freestream static pressure, in order to measure the correct static pressure of the flow. The static pressure hole should be located at the point where the flow comes to the level of a freestream Mach number. Here, it is essential to note that the flow deceleration process through the oblique shock at the probe nose and over the nose-cone portion can be made to be approximately isentropic if the flow turning angles through these compression waves are kept at less than  $5^\circ$ .

Static pressures on the walls of supersonic tunnels are often used for a rough estimation of test-section Mach numbers. However, it should be noted that the wall pressures will not correspond to the pressures on the tunnel center line if compression or expansion waves are present between the wall and the center line. When a Mach number is to be determined from static pressure measurements, the total pressure of the stream is measured in the settling chamber simultaneously with the test-section static pressure. The Mach number is then calculated using the isentropic relation.

### 10.12.6 Determination of Flow Angularity

The flow angularity in a supersonic tunnel is usually determined by using either cone or wedge yaw meters. Sensitivities of these yaw meters are maximum when the wedge or cone angles are maximum. They work below Mach numbers for which wave detachment occurs, and are so used. The cone yaw meter is more extensively used than the wedge yaw meter, since it is easier to fabricate.

### 10.12.7 Determination of Turbulence Level

Measurements with a hot-wire anemometer demonstrate that there are high-frequency fluctuations in the air stream of supersonic tunnels that do not occur in free air. These fluctuations, broadly grouped under the heading of *turbulence*, consist of small oscillations in velocity, stream temperature (entropy), and static pressure (sound). Some typical values of these fluctuations are given in Table 10.3.

The PRV, drive system, after cooler, and test-section boundary layer are the major causes for the fluctuations. Velocity fluctuations due to upstream causes may be reduced at low and moderate Mach numbers by the addition of screens in the settling chambers. At high Mach numbers, upstream pressure and velocity effects are usually less, since the large nozzle contraction ratios damp them out. Temperature fluctuations are unaffected by contraction ratio.

**Table 10.3** Turbulence level in the settling chamber and test-section of a supersonic tunnel.

Parameter	Settling chamber	Test-section
M	all	2.2–4.5
Sound, $\frac{\Delta p}{p}$	<0.1%	0.2–1%
Entropy, $\frac{\Delta T}{T}$	<0.1%	<0.1–<1%
Velocity, $\frac{\Delta V}{V}$	0.5–1%	<0.1–<1%



### 10.12.8 Determination of Test-Section Noise

Test-section noise is defined as the fluctuations of pressure. Noise may result from unsteady settling chamber pressure fluctuations due to upstream flow conditions. It may also be due to weak unsteady shocks originating in a turbulent boundary layer on the tunnel wall. Noise in the test-section is very likely to influence the point of boundary layer transition on a model. Also, it is probable that the noise will influence the other test results as well.

Test-section noise can be detected by either hot-wire anemometry measurements or by high-response pitot pressure measurements. It is a usual practice to make measurements in both the test-section and the settling chamber of the tunnel to determine whether the noise is coming from the test-section boundary layer. It is then possible to determine whether fluctuations in the two places are related. The test-section noise usually increases with increasing tunnel operating pressure, and test-section noise originating in the settling chamber usually decreases as tunnel Mach number increases.

### 10.12.9 Use of Calibration Results

The Mach number in the vicinity of a model during a test is assumed to be equal to an average of those obtained in the same portion of the test-section during calibrations. With this Mach number and the total pressure ( $p_{01}$ ) measured in the settling chamber, it is possible to define the dynamic pressure  $q$  as

$$\frac{q}{p_{01}} = \frac{\gamma}{2} M^2 \left( 1 + \frac{\gamma - 1}{2} M^2 \right)^{-\frac{\gamma}{\gamma - 1}}$$

for use in data reduction. If the total temperature is also measured in the settling chamber, all properties of the flow in the test-section can be obtained using isentropic relations. The flow angularities measured during calibration are used to adjust model angles set with respect to the tunnel axis to a mean flow direction reference. The transition point and noise measurements made during the calibration may be used to decrease the tunnel turbulence and noise level.

### 10.12.10 Starting of Supersonic Tunnels

Supersonic tunnels are usually started by operating a quick-operating valve, which causes air to flow through the tunnel. In continuous operation tunnels, the compressors are normally brought up to the desired operating speed with air passing through a bypass line. When operating speed is reached, a valve in the by-pass line is closed, which forces the air through the tunnel. In blowdown tunnels a valve between the pressure storage tanks and the tunnel is opened.

Quick starting is desirable for supersonic tunnels, since the model is subjected to high loads during the starting process. Also, a quick start of blowdown tunnel conserves air. To determine when the tunnel is started, the pressure at an orifice in the test-section wall near the model nose is usually observed. When this pressure suddenly drops to a value close to the static pressure for the design Mach number, the tunnel is started. If the model is blocking the tunnel, the pressure will not drop. We can easily identify the starting of the tunnel from the sound it makes.

Some tunnels are provided with variable second-throat diffusers, designed to decrease the pressure ratio required for tunnel operation. These diffusers are designed to allow the setting of a cross-sectional area large enough for starting the tunnel and to allow the setting of a smaller

cross-sectional area for more efficient tunnel operation. When used as designed, the variable diffuser throat area is reduced to a predetermined area as soon as the tunnel has started.

### 10.12.11 Starting Loads

Whenever a supersonic tunnel is being started or stopped, a normal shock passes through the test-section, and large forces are imposed on the model. The model oscillates violently at the natural frequency of the model support system and normal force loads of about five times those which the model would experience during steady flow in the same tunnel at an angle of attack of  $10^\circ$  are not uncommon. The magnitudes of starting loads on a given model in a given tunnel are quite random, and exactly what causes the large loads is not yet understood.

Starting loads pose a serious problem in the design of balances for wind tunnel models. If the balances are designed to be strong enough to withstand these severe starting loads, it is difficult to obtain sensitivities adequate for resolving the much smaller aerodynamic loads during tests. A number of methods have been used for alleviating this problem. Among them the more commonly used methods are

- starting at a reduced total pressure in continuous tunnels
- shielding the model with retractable protective shoes, during start-up
- injecting the model into the air stream after the tunnel has started.

### 10.12.12 Reynolds Number Effects

The primary effects of Reynolds number in supersonic wind tunnel testing are on drag measurements. The aerodynamic drag of a model is usually made up of the following four parts.

- Skin friction drag, which is equal to the momentum loss of air in the boundary layer.
- Pressure drag, which is equal to the integration of pressure loads in the axial direction, over all surfaces of the model ahead of the base.
- Base drag, which is equal to the product of base pressure differential and base area.
- Drag due to lift, which is equal to the component of normal force in the flight direction.

The pressure drag and drag due to lift are essentially independent of model scale or Reynolds number and can be evaluated from wind tunnel tests of small models. But the skin friction and base drags are influenced by Reynolds number. In the supersonic regime, the skin friction is only a small proportion of the total drag due to the increased pressure drag over the fore-body of the model. However, it is still quite significant and needs to be accounted for. Although the probability of downstream disturbances affecting the base pressure and hence the base drag is reduced because of the inability of downstream disturbances to move upstream in supersonic flow, enough changes make their way through the subsonic wake to cause significant base interference effects.

### 10.12.13 Model Mounting-Sting Effects

Any sting extending downstream from the base of a model will have an effect on the flow and therefore is likely to affect model base pressure. For actual tests, the sting must be considerably larger than that to withstand the tunnel starting loads and to allow testing to the maximum steady load condition, with a reasonable model deflection. Sting diameters of  $1/4$  to  $3/4$  model base diameters are typical in wind tunnel tests. The effects on the base pressure of typical sting diameters are significant but represent less than 1% of the dynamic pressure and therefore a small amount of the total drag of most of the models.

## 10.13 Calibration and Use of Hypersonic Tunnels

Hypersonic tunnels operate in the Mach number range of 5–10 or more. The stagnation pressure varies from 1 to 10 MPa, and the stagnation temperature varies from 60 to 2000 °C. They mostly have solid-walled test-sections and require contoured nozzles, which are most frequently axially symmetric instead of two-dimensional. Models that are larger than those that can be tested in supersonic tunnels can be tested in hypersonic tunnels. Hypersonic tunnel models sometimes have a frontal area as high as 10% of the test-section area. Model size will probably be limited by the large model wake, which takes up too much flow area in the diffuser and blocks it during tunnel starting. The tunnel wall effect is unlikely to affect the flow over the model.

The air used in a hypersonic tunnel is heated to avoid liquefaction during expansion to the high Mach number and the corresponding low-temperatures, and to facilitate heat transfer studies. In fact, the use of heated air is the major factor that makes the hypersonic tunnel operation more complicated than supersonic tunnel operation. The air in hypersonic tunnels must also be dry to avoid condensation effects due to the expansion of the air to high Mach numbers and the associated low temperatures. However, this problem is less serious here than in supersonic tunnels, because in the process of compressing the air to the necessary high pressures for hypersonic flow most of the natural water will be simply squeezed out.

### 10.13.1 Calibration of Hypersonic Tunnels

The calibration procedure for hypersonic tunnel test-sections is generally the same as that of a supersonic tunnel. However, in hypersonic tunnels it is much more important to calibrate over the complete range of conditions through which the tunnel will operate. The boundary layers at the nozzle wall are much thicker and subject to larger changes in thickness than in supersonic tunnels, owing to operating pressure and temperature. Also, the real gas effects make the test-section Mach number very sensitive to total temperature. Further, a significant axial temperature gradient may exist in the settling chamber, with the temperature decaying as the nozzle throat is approached. In addition to axial gradients, serious lateral temperature gradient is also present in the settling chamber. These must be eliminated before uniform flow can be achieved in the test-section.

### 10.13.2 Mach Number Determination

As in the supersonic tunnels, Mach numbers in hypersonic tunnels are usually obtained by using pitot pressure measurements, which differ from those in supersonic tunnels in pressure and Reynolds number ranges. Pitot pressure in hypersonic tunnels will usually be lower. It should be ensured that the Reynolds number based on probe diameter is above 500 (or preferably 1000), since inaccurate measurements are likely if it is lower.

The determination of Mach number from the measured pitot and total pressures becomes highly complicated if the air temperature is 500 °C or above, because of the real gas effects. The procedure for determining the Mach number from the measured pitot and total pressures and a measured total temperature is as follows.

- 1) From the measured  $p_{02}/p_{01}$ , determine the corresponding Mach number from the normal shock table for perfect gas.
- 2) From the chart of  $(p_{02}/p_{01})_{\text{thermpert}}/(p_{02}/p_{01})_{\text{perf}}$  versus  $M$ , determine this ratio of pressure ratios at the above  $M$  and measured  $T_0$ .

- 3) Divide the experimental pressure ratio by the ratio determined above to obtain the corresponding value of  $(p_{02}/p_{01})_{\text{perf}}$ .
- 4) For the new  $(p_{02}/p_{01})_{\text{perf}}$ , determine the corresponding  $M$  from the perfect gas normal shock table.
- 5) If the Mach number obtained above is not equal to that used in step 2, enter step 2 with the Mach number from step 4 and repeat. When the two Mach numbers agree closely, the interpolation is complete.

Note that, for an accurate determination of  $M$ , we need pressure–Mach number charts for the high temperature ( $>500^\circ\text{C}$ ) regime. For this we should refer to books specializing in high-temperature gases. This method of determining the Mach number from a measured pressure ratio is cumbersome and inaccurate. A high-speed computer may be used for this purpose.

The following facts about hypersonic tunnel operation will be of value for experimentation with hypersonic tunnels. If the air in the settling chamber is at room temperature, we can achieve a test-section Mach number of 5 without liquefaction of air. But to avoid liquefaction of air as it expands to the test-section conditions where the Mach number is 10, the stagnation temperature (that is the temperature in the settling chamber) should be approximately 1060 K. Because of the limitation of heater capacity, the maximum Mach number for a continuous-flow wind tunnel using air as the test gas is approximately 10. However, using better insulation and heater build-up methods, there are tunnels operating at Mach numbers of 12 and even 14 with air as the test gas.

One of the major concerns in hypersonic tunnel operations is the combination of maximum Mach number and minimum stagnation temperature for which condensation-free flow can be generated. Experimental studies show that, in a rapidly expanding nozzle (air) flow at low stream pressures (less than about 0.05 mm Hg), significant supercooling of the air would be encountered, since the onset of condensation was due to the spontaneous condensation of nitrogen. At these low pressures, an approximately constant experimental supercooling value of about 22 K was obtained.

To achieve higher Mach number flows, the stagnation temperature must be in excess of 1060 K. The high-pressure/high-temperature condition required for hypersonic tunnels can be generated in many ways, for example by the use of flow conditions downstream of the reflected shock wave in a shock tube as the reservoir conditions for a shock tunnel. But the tunnel run time for such facilities is very short. The short run time reduces the energy requirements and alleviates tunnel and model thermal–structural interactions.

Based on run time, hypersonic wind tunnels are classified into the following three categories.

- Impulse facilities, which have runtime of about one second or less.
- Intermittent tunnels (blowdown or indraft), which have run times of a few seconds to several minutes.
- Continuous tunnels, which can operate for hours (only of theoretical interest, since continuous hypersonic tunnels are extremely expensive to build and operate).

The facilities with the shortest run times have the higher stagnation temperatures. Arc discharge or reflected shock waves in a shock tube are used to generate the short-duration, high-temperature stagnation conditions.

The flow quality (including uniformity, noise, cleanliness, and steadiness) in the test-section can affect the results obtained in a ground-test program. Disturbance modes in hypersonic tunnels include vorticity (turbulence fluctuations), entropy fluctuations (temperature spottiness) which are traceable to the settling chamber, and pressure fluctuations (radiated aerodynamic

**Table 10.4** Stagnation temperature ( $T_{01}$ ) variation with  $M_1$  for  $T_1 = 50$  K, based on perfect gas assumption.

$M_1$	5	6	7	8	9	10	11	12	13	14	15
$T_{01}$ (K)	300	410	540	690	860	1050	1260	1490	1740	2010	2300

noise). These disturbances can affect the results of boundary layer transition studies conducted in hypersonic wind tunnels.

It is known that even the high-enthalpy, short-duration facilities operate on the borderline between perfect gas and real gas flow. Let us look at the reservoir temperature required to maintain perfect air at a test-section temperature of 50 K and Mach number  $M_1$ . Table 10.4 gives these values for different values of  $M_1$ .

When the test-section Mach number is 8.5, the stagnation temperature for a perfect air must be 772 K. However, it is well established that the vibrational state is exited beginning approximately at 770 K. Thus, for the high Mach number facilities, vibrational excitation occurs in the settling chamber, followed by vibrational freezing downstream of the throat, and subsequent rapid relaxation in the downstream section of the nozzle. This kind of improper characteristic of hypersonic flow field manifests itself as an error in the Mach number. Hypersonic tunnels heated by conventional clean air heaters have exhibited a Mach number error of as much as 1.5% compared to that predicted by isentropic flow using the ratio of freestream pitot pressure to reservoir pressure. Even these relatively small errors in Mach number can result in significant errors in the nondimensionalized data, if they are ignored.

It is important to note that hypersonic wind tunnels usually operate such that the static temperature in the test-section approaches the liquefaction limit. Thus, hypersonic Mach numbers are achieved with relatively low freestream velocities (which is related to the kinetic energy), because the speed of sound (which is related to the static temperature) is relatively low.

### 10.13.3 Determination of Flow Angularity

Flow angularity in hypersonic tunnels is usually determined by cones with included angle in the range of  $20^\circ - 90^\circ$ . The shock waves on cones with higher angles are detached throughout the hypersonic Mach number range, and the surface pressure variation with angle of attack cannot be easily calculated.

### 10.13.4 Determination of Turbulence Level

The large contraction ratios of hypersonic tunnels have a tendency to reduce the turbulence percentage level in the test-section to insignificant values. Therefore, there is no need to determine the turbulence level of hypersonic tunnels.

#### 10.13.4.1 Blockage Tests

Blockage tests are made during the calibration phase to determine the size of the models that may be tested in the tunnel and to find the effect of model size on the starting and operating pressure ratios of the tunnel.

#### 10.13.4.2 Starting Loads

There is no published data available on starting loads in hypersonic tunnels. But from experience it is found that at Mach 7 the starting loads are not so severe as indicated for supersonic tunnels.

### 10.13.5 Reynolds Number Effects

At hypersonic speeds the boundary layers are relatively thicker and more prone to separate in the presence of unfavorable (adverse) pressure gradients than they are at supersonic speeds. Also, there is likely to be an intense interaction between the shock waves and boundary layers. For example, on a wedge or cone leading edge, the shock at hypersonic speeds will be very close to the surface. The boundary layer on the wedge or cone will be an important part of the distance between the surface and the shock. Under these conditions, loads on the model can no longer be considered simply as those due to an inviscid flow field that exerts pressure through the boundary layer and onto the model surface. Since the boundary layer primarily depends on the Reynolds number, we can say that the complete flow field around a vehicle at hypersonic speeds is dependent to a significant extent on the Reynolds number. Thus, force and moment coefficients in addition to drag are likely to be influenced significantly by the Reynolds number.

The boundary layers on models in hypersonic tunnels are mostly, if not entirely, laminar. However, it is not clear that tripping the boundary layer is the answer to the problem of obtaining comparable flow fields over the model in the tunnel and the full-scale vehicle in flight. In flight, at hypersonic speeds, the full-scale vehicle is likely to have long runs of laminar flow if it has reasonably smooth surfaces. Reynolds numbers as high as  $7 \times 10^7$  without transition have been reported on rockets. This highlights the difficulty of predicting the location where the transition will occur on the model in flight and consequently where or if a boundary layer trip should be used. The usual practice at present is to test models without transition strips in hypersonic tunnels. If it is found that the smooth model has extensive boundary layer separation at some point at which it is not expected on the vehicle in flight, then a transition strip may be tried as a means of eliminating separation.

### 10.13.6 Force Measurements

Force measurements in hypersonic tunnels are similar to those of subsonic and supersonic tunnels. However, there are a few problems in hypersonic tunnel force measurements which do not exist in the lower-speed tunnels. They are the following.

- Models will get heated up during the tests, because hypersonic tunnels use heated air.
- It is essential to ensure that the model heating and the heated air do not affect the electrical signals from the strain gauge balance.
- There are possibilities of significant temperature effects on balance readout at temperatures well below those for which the cement holding the gauges to the flexures fails.
- With the model at an angle of attack, surface heating rates on the model will be higher on the windward side than on the leeward side. Air circulating from the model base through the balance cavity will also heat the gauges on one side of the balance more than the gauges on the other side.

These cases of uneven heating of the balance are not taken care of by temperature compensation of the bridges of the balance. Keeping the balance temperature essentially constant at a near-ambient value during the test is the remedy for the variable balance temperature problem.

In addition to effects on balance readings, uneven heating on the windward and leeward model surfaces may cause model distortion of significant magnitude, especially when the length-to-diameter ratio of the model is large. This effect is usually avoided by cooling the model. In intermittent operating tunnels it may be eliminated by increasing model wall thickness or by using a material such as Invar, which has a low coefficient of thermal expansion.

Low model loads at high Mach numbers is another problem in hypersonic force tests. Aerodynamic loads in some cases may be considerably less than the model weight. This poses

a problem in balance design. The balance must be strong enough to hold the model but it must also be weak enough to be sensitive to loads smaller than the model weight. Under these conditions, there is likelihood of continuous low-frequency oscillations of the model during a test. These oscillations may cause inertia loads to become a significant portion of the aerodynamic loads to be measured, and satisfactory data cannot be obtained unless the data acquisition system is equipped with suitable electronic filtering.

## 10.14 Flow Visualization

Schlieren systems for high-speed tunnels are often designed for passing the light through the test-section twice using a *double-pass system*. This is accomplished by using a circular arc mirror adjacent to one wall of the test-section and a light source and mirror focal point as close together as possible on the opposite side of the test-section, in order to increase the system's sensitivity. However, it is found that obtaining good Schlieren pictures of the flow around a model when the test-section pressures are less than about 1 mm Hg (absolute) is difficult, even with a double-pass system. Pressures below 1 mm Hg are common in wind tunnels operating at Mach 8 and above.

To obtain better flow visualization at low test-section pressures, the air in the flow field of the model may be ionized using an electric current (used by the Jet Propulsion Laboratory, USA). An electrode is placed a few centimeters upstream and a few centimeters above the model in the test-section. A potential of 5000 V DC is established between the electrode and the model with a current flow of 0.4 amp. The flow of current ionizes the flow field, with the result that shock waves are clearly shown in regular photographs, and are much more clearly visible in these Schlieren photographs than in Schlieren photographs taken without ionization. Care must be taken to interlock (possibly with a low-pressure switch) the power system to prevent injury to personnel.

## 10.15 Summary

In this chapter we have outlined some of the major measurement techniques that are commonly employed for compressible flow analysis. In any flow field the prime quantities of interest are the pressure, temperature, density, velocity, and its direction.

The devices used for pressure measurements in fluid flows may broadly be grouped as manometers and pressure transducers. Some of the popular manometers are the "U" type manometers, multitube manometer, micro manometers, and Betz manometer. The pressure transducers used are of electrical type, mechanical type, and optical type.

The thermocouple is the most commonly used device for temperature measurements in fluid flow. It operates on the principle that a flow of current in a metal accompanies a flow of heat. In some metals, heat and current flow in the same direction. In some other metals, heat flow and current flow are in opposite directions. These are called *dissimilar metals*. Thermocouples are made with dissimilar metals like copper–constantan, iron–constantan, and so on.

The flow velocity may be calculated from the measured pressure and temperature through the relation

$$V = M\sqrt{\gamma RT}$$

The flow direction may be obtained using a symmetric wedge or cone with pressure taps at directly opposite locations, as shown in Figure 10.10.

The velocity may also be measured using a hot wire anemometer. By King's law,

$$\frac{I^2 R_w}{R_w - R_g} = A + B(V)^{1/2}$$

By measuring the resistance  $R_w$  and  $R_g$ , keeping the current constant or measuring  $I$ , and by keeping the resistances constant, the flow velocity can be determined. The hot-wire system with  $I$  constant is called the *constant-current hot-wire anemometer*, and the system with  $R_w$  constant is called the *constant-temperature hot-wire anemometer*.

The density of a flow can be calculated by measuring the pressure and temperature. Supersonic flows with significant density changes can be visualized with optical systems such as interferometer, Schlieren, and shadowgraph. These techniques may be used to get a considerable insight into the qualitative aspects of the flow field. Even though these optical techniques have been thought of as qualitative visualization methods for supersonic flows in classical literature, today they are being used for quantitative analysis also, with suitable transformation and image-processing techniques. The present understanding is that, out of these, interferometer is very much more amenable to quantitative studies. When proper methods are developed for quantitative studies of the field with these kinds of optical techniques – which are nonintrusive and do not require any seeding like laser Doppler anemometers – they will stay as the most reliable high-tech experimental methods for supersonic flow studies.

For visualizing compressible flows, *interferometer*, *Schlieren*, and *shadowgraph* are the three popularly employed techniques. The interferometer makes visible the optical phase changes resulting from the relative retardation of the disturbed rays. The Schlieren system gives the deflection angles of the incident rays. The shadowgraph visualizes the displacement experienced by an incident ray which has crossed the high-speed gas flow.

The quality of the optical equipment needed in the Schlieren set-up depends on the type of investigation to be carried out. The cost increases rapidly with the quality of the optical components. The vital components are the mirrors and the light source.

The interferometer is an optical method best suited to qualitative determination of the density field of high-speed flows.

In general, the Schlieren method is used either for the detection of small refractive index gradients or for the quantitative measurement of these gradients.

The shadowgraph is best suited only for flow fields with rapidly varying density gradients.

The theory shows that the Schlieren technique depends upon the first derivative of the refractive index (flow density), while the shadowgraph method depends upon its second derivative. Consequently, in phenomena where the refractive index varies relatively slowly, the Schlieren method is to be preferred to the shadowgraph method, other things being equal. On the other hand, the shadow method beautifully brings out the rapid changes in the index of refraction. The shadow method also has the advantage of greater simplicity and somewhat wider possible application. The two methods therefore complement each other and both should be used wherever possible.

Wind tunnels are devices that provide air streams flowing under controlled conditions so that models of interest can be tested using them.

*Low-speed tunnels* are those with test-section speed less than 650 kmph. The effect of compressibility is negligible for these tunnels. Thus, if the Reynolds number of the experimental model and full-scale prototype are equal, any difference in viscosity becomes unimportant.

Tunnels with test-section speed more than 650 kmph are called *high-speed tunnels*. The predominant aspect in high-speed tunnel operation is that the influence of compressibility is significant. This means that in high-speed flows it is essential to consider the *Mach number* as a more appropriate parameter than velocity.



All modern wind tunnels have four important components: the *contraction cone*, the *working or test-section*, the *diffuser*, and the *driving unit*.

High-speed tunnels are generally grouped into intermittent and continuous operation tunnels, based on the type of operation.

Blowdown tunnels are the simplest among the high-speed tunnel types and most economical to build. But the charging-time-to-running-time ratio will be very high for large tunnels, and the stagnation temperature in the reservoir drops during tunnel run, thus changing the Reynolds number of the flow. Reservoir pressure range is from 100 to 300 psi for blowdown tunnel operations.

In the induction tunnels the stagnation pressure and stagnation temperature are constants, there is no oil contamination in the air, owing to the pump being at the downstream end, and starting and shutdown operations are simple. But the size of the air drier required is very large because it has to handle a large mass flow in a short duration, and the vacuum tank size required is also very large.

In continuous supersonic wind tunnels better control over the Reynolds number is possible. Test conditions can be held the same over a long period of time. But the power required is very high, temperature stabilization requires a large-size cooler, the compressor drive has to be designed to match the tunnel characteristics and design, and operation is more complicated.

The model size for a supersonic tunnel is dictated by the test-rhombus formed by the incident and reflected shocks.

The power loss in a continuous supersonic wind tunnel is due to friction, expansion, shock wave, model, and support system drag.

The second throat in a supersonic tunnel is to provide isentropic deceleration and highly efficient pressure recovery after the test-section.

Usually, blowdown tunnels are operated at constant Reynolds number, constant pressure, or constant throttle. For a given settling chamber pressure and temperature, the running time is the shortest for constant-throttle operation, the longest for constant-Reynolds-number operation, and in between for constant-pressure operation.

Hypersonic tunnels generally operate with stagnation pressures from 10 to 100 atm and stagnation temperatures from 50 to 2000 °C. The model frontal area can go up to 10% of the test-section cross-sectional area.

Supersonic tunnels operate in the Mach number range of about 1.4–5.0. Maximum model cross-section areas up to 4% of the test-section area are quite common for supersonic tunnels.

At subsonic speeds, the Mach number decreases and the pressure increases with condensation, whereas at supersonic speeds the reverse is true.

Calibration of a supersonic wind tunnel includes determining the flow Mach number throughout the range of operating pressures of each nozzle, determining flow angularity and determining an indication of turbulence level effects.

Pitot pressures are measured by using a pitot tube. A pitot tube will normally have an inside-to-outside-diameter ratio of 0.5–0.75, and a length aligned with the air stream of 15–20 tube diameters.

Supersonic flow static pressure measurements become difficult because of the shock wave (either attached or detached shock) at its nose, which causes a rise in static pressure.

The flow angularity in a supersonic tunnel is usually determined by using either cone or wedge yaw meters.

There are high-frequency fluctuations in the air stream of supersonic tunnels that do not occur in free air. These fluctuations, broadly grouped under the heading *turbulence*, consist of small oscillations in velocity, stream temperature (entropy), and static pressure (sound).

The test-section noise may result from unsteady settling chamber pressures and weak unsteady shocks originating in a turbulent boundary layer on the tunnel wall.

The primary effects of Reynolds number in supersonic wind tunnel testing are on drag measurements. The pressure drag and drag due to lift are essentially independent of model scale or Reynolds number and can be evaluated from wind tunnel tests of small models. But the skin friction and base drag are influenced by Reynolds number.

Hypersonic tunnel models sometimes have frontal areas as high as 10% of the test-section area. The air used in a hypersonic tunnel is heated to avoid liquefaction during expansion to the high Mach number and corresponding low temperatures, and to facilitate heat transfer studies. The calibration procedure for a hypersonic tunnel test-section is generally the same as that of a supersonic tunnel.

Flow angularity in a hypersonic tunnel is usually determined by cones with included angles in the range  $20^\circ - 90^\circ$ . The large contraction ratios of hypersonic tunnels have a tendency to reduce the turbulence percentage level in the test-section to insignificant values.

At hypersonic speeds the boundary layers are relatively thicker and are more prone to separate in the presence of adverse pressure gradients than at supersonic speeds. Also, there is likely to be intense interaction between shock waves and boundary layers. Under these conditions, loads on the model can no longer be considered simply as those due to an inviscid flow field which exerts pressure through the boundary layer and onto the model surface. Therefore, force and moment coefficients in addition to drag are likely to be influenced significantly by the Reynolds number.

Force measurements in hypersonic tunnels are similar to those of subsonic and supersonic tunnels. But having low model loads at high Mach numbers is a problem in hypersonic force tests. Aerodynamic loads in some cases may be considerably less than the model weight. This poses a problem in balance design. The balance must be strong enough to hold the model, but it must also be weak enough to be sensitive to loads smaller than the model weight. Under these conditions, there is a likelihood of continuous low-frequency oscillations of the model during a test.

## Exercise Problems

- 10.1** The Mach number of a compressible air flow is to be determined from static probe and pitot probe measurements. If the static and pitot probes indicate 500 mm Hg suction and 350 mm Hg suction, respectively, (a) determine the flow Mach number and (b) repeat the calculation for a pitot probe that indicates of 275 mm Hg compression.  
[Answer: (a) 0.835, (b) 1.56]
- 10.2** A pitot-static tube in an air stream records a dynamic pressure of 50 cm of mercury. The static pressure and stagnation temperature of the air stream are  $3.6 \times 10^4 \text{ N m}^{-2}$  (gauge) and  $27^\circ\text{C}$ , respectively. If the barometer reads 75.6 cm of mercury, compute the air velocity, assuming the air to be (a) compressible and (b) incompressible.  
[Answer: (a)  $256.06 \text{ m s}^{-1}$ , (b)  $237.55 \text{ m s}^{-1}$ ]
- 10.3** Air flows through an adiabatic frictionless passage. At station 1 the Mach number is 0.9 and the static pressure is  $4.15 \times 10^5 \text{ N m}^{-2}$ . At station 2 the Mach number is 0.2. Calculate the change in static pressure between stations 1 and 2.  
[Answer:  $2.676 \times 10^5 \text{ Pa}$ ]

- 10.4** Air flows at a speed of  $400 \text{ m s}^{-1}$  and a static pressure of 1 atm. The air is isentropically brought to rest in a steady flow process. Find the Mach number and stagnation pressure if the static temperature is (a)  $500^\circ\text{C}$ , (b)  $-50^\circ\text{C}$ .  
[Answer: (a) 0.718,  $1.428 \times 10^5 \text{ Pa}$ , (b) 1.336,  $2.949 \times 10^5 \text{ Pa}$ ]
- 10.5** An airplane flies at a constant speed of 900 kmph at 10 000 m altitude. A pressure traverse shows that the air is brought to rest at a particular location on the fuselage. Calculate (a) the temperature of air in the stagnation region and (b) the temperature rise caused by the impact. Assume air to be a perfect gas and  $\gamma = 1.4$ .  
[Answer: (a) 254.17 K, (b) 31.02 K]
- 10.6** An intermittent wind tunnel is designed for a Mach number of 4 at the test-section. The tunnel operates by sucking air from the atmosphere through a duct into a vacuum tank. The tunnel is located at an altitude of 1650 m, where  $\rho = 1.044 \text{ kg m}^{-3}$ . If the flow is isentropic, show that the density at the test section is  $0.029 \text{ kg m}^{-3}$ .
- 10.7** A stationary temperature probe inserted into a duct where air is flowing at  $250 \text{ m s}^{-1}$  reads  $100^\circ\text{C}$ . What is the actual temperature of the air?  
[Answer:  $68.89^\circ\text{C}$ ]
- 10.8** If the specific power required to run a closed circuit supersonic tunnel maintaining the test-section total temperature at 430 K is  $149.2 \text{ kJ kg}^{-1}$  (a) determine the test-section Mach number. (b) If the mass flow rate through the test-section of area  $0.002 \text{ m}^2$  has to be  $0.8 \text{ kg s}^{-1}$ , what should be the total pressure in the settling chamber? also, determine the running power required. Assume the compression in the compressor is isentropic.  
[Answer: (a) 2.82, (b) 7.2 atm, 160 hp]

## 11

## Ramjet

## 11.1 Introduction

Ramjet is a simple air-breathing engine. It consists of a diffuser, a combustion chamber, and an exhaust nozzle, as shown in Figure 11.1. Air entering the diffuser is compressed to attain the low-speed level required for combustion. Fuel is mixed with air in the combustion chamber and burned. The hot gas mixture after the combustion is expanded through the nozzle which converts the high-pressure energy of the combustion gases to kinetic energy, resulting in the generation of thrust. It is important to note that in the diffuser the incoming air is decelerated from the high flight speed  $M_\infty$ , which is usually supersonic, to a relatively low velocity through the compression caused by the shock system at the intake and the ramming action inside the duct from just downstream of the inlet to the combustion chamber entrance. Therefore, although ramjets can operate at subsonic flight speeds, the increasing pressure rise accompanying higher flight speeds renders ramjets more suitable for supersonic flights.

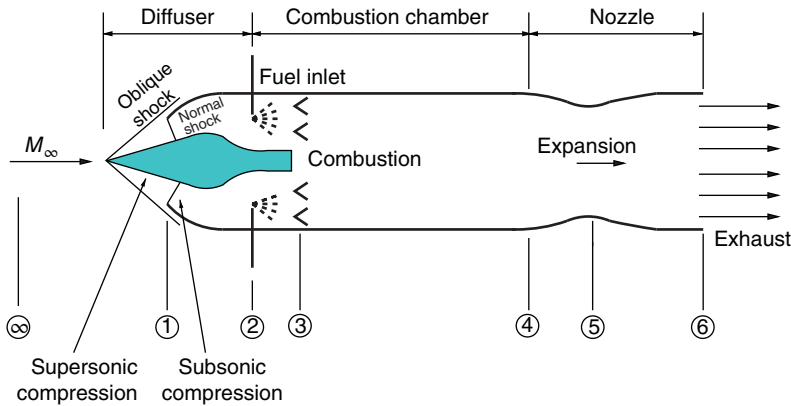
The ramjet engine shown in Figure 11.1 is typical of supersonic ramjets that employ supersonic diffusion through a system of shocks. Since the supersonic flow stream entering the intake has to be decelerated to about Mach 0.2–0.3 before entry to the combustion chamber, the pressure rise can be substantial. For example, for isentropic deceleration from Mach 4 to Mach 0.3, the static pressure ratio between the ambient and the combustion chamber should be around 145. But, in reality, only a fraction of the isentropic pressure ratio is actually achieved. This is because at high Mach numbers the total pressure losses associated with shocks are substantial.

The air after compression passes over the fuel injectors which spray fuel in the form of fine droplets. The fuel and air mix rapidly and the mixture is then burned in the combustion chamber. A flameholder is placed in the combustion chamber to stabilize the flame. The combustion raises the temperature of the fuel-air mixture to about 3000 K before the combustion products expand to a high velocity in the nozzle. The reaction caused by the momentum of the combustion products leaving the nozzle is the thrust generated by the engine. The thrust generated can be expressed as

$$Th = \dot{m}u_e + (p_e - p_\infty)A_e$$

where  $\dot{m}$  is the mass flow rate through the nozzle,  $u_e$  is the flow velocity at the nozzle exit,  $p_e$  is the pressure at the nozzle exit,  $p_\infty$  is the ambient pressure to which the nozzle discharges, and  $A_e$  is the nozzle exit area. A part of this thrust is used to overcome the shear force acting over the internal surface of the engine.

As we know, the gas turbine engines cannot be operated at high temperatures of the order of 3000 K. This is because the turbine blades are subjected to high centrifugal stresses and cannot be cooled easily. Whereas, the walls of the combustion chamber and the nozzle of a ramjet engine can be cooled by a fuel-injection pattern that leaves a shielding layer of relatively cool



**Figure 11.1** Schematic of a ramjet engine.

air next to the wall surface to maintain the wall temperature around 1000 K, which can be tolerated by the material used at present. This relatively higher-operating temperature of the ramjet allows operation at high flight Mach numbers. However, the combustion chamber inlet temperature also increases with the flight Mach number. This sets a limiting Mach number for ramjet operation, since beyond the limiting Mach number the temperature will approach the limit set by the wall material and cooling methods. For example, at a flight Mach number of 8 in an atmosphere at 225 K, the stagnation temperature is about 2500 K.

At temperatures greater than 2500 K, dissociation of combustion products becomes significant. At such temperatures the further addition of fuel will result in dissociation enhancement rather than temperature rise.

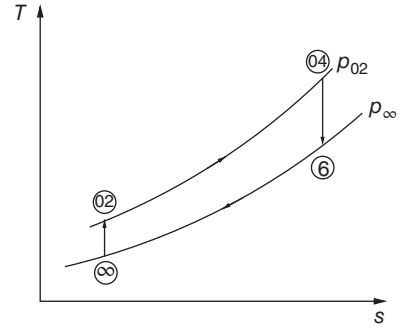
A major disadvantage of the ramjet is the pressure rise in the engine and is solely governed by the flight speed and diffuser performance. Owing to this, the ramjet cannot develop static thrust and hence cannot accelerate a vehicle from zero velocity (standing start). Also, designing a diffuser of high efficiency is difficult, owing to detrimental boundary layer behavior in rising pressure gradients especially in the presence of shocks, which cannot be avoided during supersonic operation, since a supersonic flow is essentially wave dominated. However, the complicated thermodynamic process associated with the ramjet can be greatly simplified if some simplifying assumptions are made. A ramjet designed with such simplified thermodynamic analysis is termed an *ideal ramjet*.

## 11.2 The Ideal Ramjet

It is essentially a hypothetical engine with simplified process cycles involving isentropic process. The complicated thermodynamic processes involved in the ramjet flow and combustion can be greatly simplified by making the following assumptions.

- The compression and expansion processes in the engine are reversible and adiabatic.
- The combustion process takes place at constant pressure.

Even though these assumptions are not realistic, they simplify the analysis of the processes in the ideal ramjet engine. Furthermore, the ideal ramjet is a useful concept and serves as a standard for comparing the performance of actual ramjet engines, i.e. the ideal ramjet can be regarded as identical to the Carnot engine model used in thermodynamics. In the diffusers of

**Figure 11.2**  $T$ - $s$  diagram of an ideal ramjet process.


the actual engines there are irreversibilities due to the shock waves, fuel air mixing, and wall friction. Also, unless the combustion takes place at very low velocities, both static and total pressures will drop, owing to friction and heat transfer.

In the ramjet engine shown in Figure 11.1 the air is isentropically compressed from the freestream state  $\infty$  to stagnation state 02 at station 2, as shown on the  $T$ - $s$  diagram in Figure 11.2. It is essential to realize that in the ideal process assumed the compression through the oblique shock and normal shock from stations 1 to 2 is regarded as isentropic. This is reasonable only when the oblique shock at the nose of the intake spike is very weak, causing flow turning of less than  $5^\circ$ , and the Mach number upstream of the normal shock is just about unity. Even after meeting these stringent requirements, the compression process is only approximately close to isentropic. In spite of these assumptions, of weak oblique and normal shocks, the actual process is nonisentropic. But the entropy increase associated with the compression process would be small enough to approximate it as isentropic. The combustion process is represented by a constant-pressure heat and mass addition process from state 02 to state 04, where the temperature is a maximum at  $T_{04}$ . The combustion products expand isentropically through the nozzle to the ambient pressure  $p_\infty$  to which the flow is discharged. That is, in the ideal process the nozzle is assumed to be correctly expanded with the exit pressure  $p_e$  equal to the backpressure  $p_\infty$ .

The general thrust equation is

$$\text{Th} = \dot{m}_\infty [(1+f)u_e - u] + (p_e - p_\infty)A_e \quad (11.1)$$

For an ideal ramjet engine with  $p_e = p_\infty$ , this simplifies to

$$\text{Th} = \dot{m}_\infty [(1+f)u_e - u] \quad (11.2)$$

where  $\dot{m}_\infty$  is the mass flow rate of air entering the engine,  $f$  is the fuel-air ratio,  $u_e$  is the velocity at the nozzle exit, and  $u$  is the flow velocity at the nozzle inlet (flight velocity, here  $u$ , is written without subscript  $\infty$  for convenience).

For the case of isentropic compression and expansion processes, and low-speed constant-pressure heat and mass addition, the stagnation pressure must be constant throughout the engine. Therefore,  $p_{0\infty} = p_{06}$ .

Treating the gas constant  $R$  and the specific heats ratio  $\gamma$  for the flow throughout the engine as invariants, we can express the pressure ratios  $p_{06}/p_\infty$  and  $p_{06}/p_e$ , using isentropic relations, as

$$\frac{p_{06}}{p_\infty} = \left( 1 + \frac{\gamma-1}{2} M_\infty^2 \right)^{\frac{\gamma}{\gamma-1}}$$

$$\frac{p_{06}}{p_e} = \left( 1 + \frac{\gamma-1}{2} M_e^2 \right)^{\frac{\gamma}{\gamma-1}}$$

where  $M_\infty$  is the flight Mach number and  $M_e$  is the nozzle exit Mach number. Note that air enters the engine at the inlet, fuel is added at station 2, the fuel-air mixture is burned from 3 to 4, and the combustion products are expanded in the nozzle. The temperature associated with the combustion is quite large to treat the specific heats ratio  $\gamma$  to be a constant. Also, the gas constant  $R$  for the air, for the fuel-air mixture and the combustion products are different. Therefore, assuming  $R$  for the entire flow as invariant and  $\gamma$  at all temperatures associated with the flow through the entire engine as invariant at best could be a crude approximation to simplify the analysis.

When the flow at the nozzle exit is correctly expanded, i.e. when  $p_e = p_\infty$ , from the above pressure ratio equations we get

$$\frac{p_{06}}{p_\infty} = \frac{p_{06}}{p_e}$$

and

$$M_e = M_\infty$$

Thus, the nozzle exit velocity becomes

$$u_e = \frac{a_e}{a_\infty} u_\infty$$

where  $a_\infty$  is the freestream speed of sound and  $a_e$  is the speed of sound at the nozzle exit. Also, treating the flow to be an isentropic flow of a perfect gas, we have the speed of sound at the inlet and exit as  $a_\infty = \sqrt{\gamma R T_\infty}$  and  $a_e = \sqrt{\gamma R T_e}$ . Therefore,

$$\frac{a_\infty}{a_e} = \sqrt{\frac{T_\infty}{T_e}}$$

Also, for the case of  $M_e = M_\infty$ ,

$$\frac{T_{0\infty}}{T_\infty} = 1 + \frac{\gamma - 1}{2} M_\infty^2$$

where  $T_{0\infty}$  and  $T_\infty$ , respectively, are the stagnation and static temperatures of the freestream air.

$$\frac{T_{06}}{T_e} = 1 + \frac{\gamma - 1}{2} M_e^2$$

But  $T_{06} = T_{04}$ ; therefore,

$$\frac{T_{04}}{T_{0\infty}} = \frac{T_e}{T_\infty}$$

Thus,

$$\frac{a_\infty}{a_e} = \sqrt{\frac{T_{0\infty}}{T_{04}}}$$

Hence the nozzle exit velocity can be written as

$$u_e = \sqrt{\frac{T_{04}}{T_{0\infty}}} u \quad (11.3)$$

For the idealized combustion process, neglecting the enthalpy of the incoming fuel, the energy equation can be written as

$$(1 + f)h_{04} = h_{02} + f Q_R \quad (11.4)$$

where  $f$  is the fuel-air ratio, defined as the ratio of mass flow rate of fuel  $\dot{m}_f$  to the mass flow rate of air  $\dot{m}_a$  (i.e.  $f = \dot{m}_f / \dot{m}_a$ ) and  $Q_R$  is the heating value (HV) of the fuel. The HV, defined as “the amount of energy released when a fuel is burnt completely in a steady-flow process and the products are returned to the state of the reactants,” is another commonly used term in combustion study of fuels. The HV of a fuel is equal to the absolute value of the enthalpy of combustion of the fuel, that is

$$\text{HV} = |h_c| \text{ (kJ kg}^{-1} \text{ fuel)}$$

The HV depends on the phase of the  $\text{H}_2\text{O}$  in the products. The HV is called the *higher heating value* HHV when the  $\text{H}_2\text{O}$  in the products is in liquid form, and it is called the *lower heating value* LHV when the  $\text{H}_2\text{O}$  in the products is in vapor form. They are related by

$$\text{HHV} = \text{LHV} + (N\bar{h}_{fg})_{\text{H}_2\text{O}} \text{ (kJ kg}^{-1} \text{ fuel)}$$

where  $N$  is the number of moles of  $\text{H}_2\text{O}$  in the products and  $\bar{h}_{fg}$  is the enthalpy of vaporization of water at the specified temperature.

Assuming the specific heat  $c_p$  to be a constant and the fuel-air mixture before combustion and the combustion products to be perfect gases ( $h = c_p T$ ), Eq. (11.4) may be solved for  $f$  as follows.

$$\begin{aligned} (1+f)c_p T_{04} &= c_p T_{02} + f Q_R \\ c_p (T_{04} - T_{02}) &= f(Q_R - c_p T_{04}) \\ f &= \frac{c_p (T_{04} - T_{02})}{Q_R - c_p T_{04}} \\ &= \frac{c_p T_{02} (T_{04}/T_{02} - 1)}{Q_R - c_p T_{04}} \end{aligned}$$

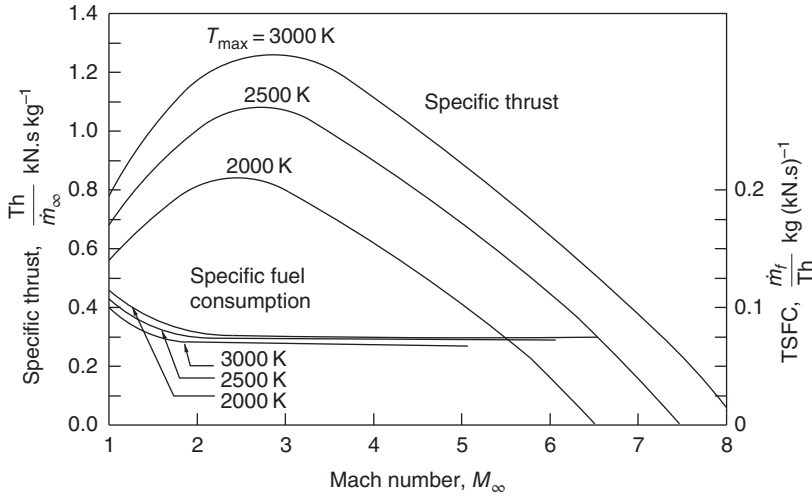
But  $T_{02} = T_{0\infty}$ ; therefore,

$$f = \frac{(T_{04}/T_{0\infty}) - 1}{[Q_R/(c_p T_{0\infty})] - T_{04}/T_{0\infty}} \quad (11.5)$$

Equations (11.2) and (11.3) can be combined to express the thrust per unit mass of air as

$$\begin{aligned} \frac{\text{Th}}{\dot{m}_\infty} &= [(1+f)u_e - u] \\ &= (1+f)\sqrt{\frac{T_{04}}{T_{0\infty}}}u - u \\ &= u \left( (1+f)\sqrt{\frac{T_{04}}{T_{0\infty}}} - 1 \right) \\ &= M_\infty a \left( (1+f)\sqrt{\frac{T_{04}}{T_\infty}}\sqrt{\frac{T_\infty}{T_{0\infty}}} - 1 \right) \\ &= M_\infty a \left( (1+f)\sqrt{\frac{T_{04}}{T_\infty}} \left( 1 + \frac{\gamma-1}{2} M_\infty^2 \right)^{-\frac{1}{2}} - 1 \right) \\ \frac{\text{Th}}{\dot{m}_\infty} &= M_\infty \sqrt{\gamma R T_\infty} \left( (1+f)\sqrt{T_{04}/T_\infty} \left( 1 + \frac{\gamma-1}{2} M_\infty^2 \right)^{-\frac{1}{2}} - 1 \right) \end{aligned} \quad (11.6)$$





**Figure 11.3** Variation of thrust and fuel consumption with flight Mach number for ideal ramjet engine, for  $Q_R = 45\,000 \text{ kJ kg}^{-1}$ ,  $\gamma = 1.4$ , and  $T_\infty = 220 \text{ K}$ . Source: Hill, P.G. and Peterson, C.R., *Mechanics and Thermodynamics of Propulsion*, 2/E, ©1992, pp. 160, 161. Reprinted by permission of Pearson Education, Inc., Upper Saddle River, New Jersey.

The thrust specific fuel consumption (TSFC) is defined as

$$\text{TSFC} = \frac{\dot{m}_f}{Th} = \frac{f}{Th/\dot{m}_\infty} \quad (11.7)$$

where  $Th/\dot{m}_\infty$  is called *specific thrust* and  $\dot{m}_\infty$  is the freestream air mass flow rate entering the engine. The effect of flight Mach number  $M_\infty$  and maximum temperature on the specific thrust and fuel-air ratio of ideal ramjets is shown in Figure 11.3.

It is essential to note that the calculations used for plotting Figure 11.3 are quite approximate, owing to the following assumptions.

- The dissociation of the combustion products is neglected.
- Frictional and shock losses are ignored.
- Variation of specific heat with temperature change is assumed to be zero.

In spite of these assumptions, Figure 11.3 shows qualitatively the same behavior as that of actual ramjets, which require supersonic flight speed for achieving reasonably significant thrust and reasonably low specific fuel consumption.

Some other performance parameters of a propulsive device are the propulsive efficiency  $\eta_p$ , the thermal efficiency  $\eta_{th}$ , and the overall efficiency  $\eta_o$ . They are defined as follows.

For a single propellant system the propulsive efficiency [12] is

$$\eta_p = \frac{Th \times u}{\dot{m}_\infty [(1+f)(u_e^2/2) - u^2/2]}$$

where  $u$  is the flow velocity at the engine inlet and  $u_e$  is the velocity at the nozzle exit. The propulsive efficiency, defined as the ratio of the thrust power ( $Th \times u$ ) to the rate of generation of propellant kinetic energy, is a measure of the performance of a propulsion system.

The product of thrust and flight speed is termed *thrust power*. In general for air-breathing engines,  $f \ll 1$  and therefore may be ignored in the above expression for  $\eta_p$  and in Eq. (11.1) without leading to significant error. Also, the pressure term in Eq. (11.1) is usually much smaller

than the other two terms. Therefore, the thrust becomes

$$\text{Th} \approx \dot{m}_\infty(u_e - u)$$

Thus, the propulsive efficiency simplifies to

$$\begin{aligned}\eta_p &= \frac{(u_e - u)u}{u_e^2/2 - u^2/2} \\ &= \frac{2u/u_e}{1 + u/u_e}\end{aligned}$$

For a single propellant system the thermal efficiency is

$$\begin{aligned}\eta_{th} &= \frac{\text{Rate of addition of kinetic energy to the propellant}}{\text{Total energy consumption rate}} \\ &= \frac{\dot{m}_\infty((1+f)(u_e^2/2) - u^2/2)}{\dot{m}_f Q_R}\end{aligned}$$

where  $\dot{m}_f$  is the mass flow rate of fuel,  $\dot{m}_\infty$  is the mass flow rate of air, and  $Q_R$  is the heat of reaction of the fuel, defined as the difference between the enthalpy of the products and the enthalpy of the reactants.

The overall efficiency is the product of  $\eta_p \eta_{th}$ , i.e.

$$\eta_o = \eta_p \eta_{th} = \frac{\text{Th} \times u}{\dot{m}_f Q_R}$$

For air-breathing engines such as ramjet,  $f \ll 1$ . Therefore, replacing the propulsive efficiency in the above expression in terms of  $u$  and  $u_e$ , we get

$$\eta_o = 2\eta_{th} \left( \frac{u/u_e}{1 + u/u_e} \right)$$

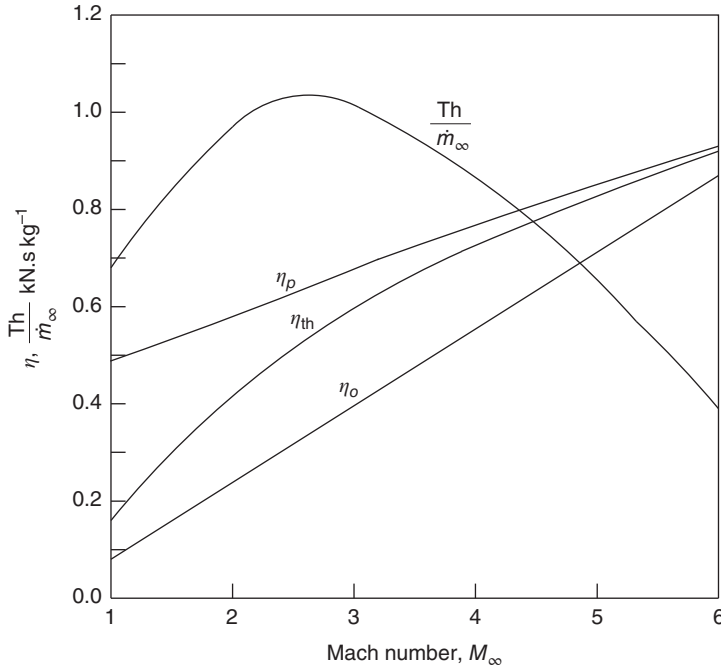
The specific thrust and overall efficiency of an ideal ramjet as a function of a flight Mach number is shown in Figure 11.4. It can be seen that the highest specific thrust occurs at a flight Mach number of about 2.6. But even though the specific thrust falls for higher Mach numbers, a much better range could be obtained for Mach numbers well above 3. Furthermore, it can be seen that the overall efficiency increases sharply, with an increasing Mach number. This is a typical example for the case that the conditions for maximum fuel consumption (i.e. maximum range) are quite different from those for which engine size per unit thrust is minimum. Also, from Figure 11.3 it can be seen that the TSFC remains finite as the specific thrust approaches zero.

### 11.3 Aerodynamic Losses

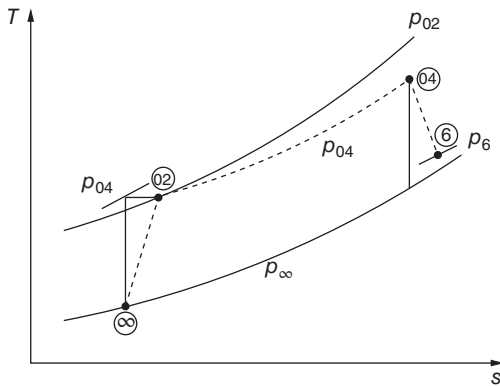
Unlike the ideal ramjet engine, the air, the fuel-air mixture, and the combustion products in an actual ramjet engine suffer stagnation pressure loss, owing to shock waves and wall friction, as they pass through the engine. The effect of these irreversibilities on the process of compression, combustion, and expansion is shown on the  $T-s$  diagram in Figure 11.5.

The actual compression process from state  $\infty$  to state 2 is nonisentropic and the stagnation pressure at the end of the process is lower than that for an isentropic process. The diffuser performance may be characterized by a stagnation pressure ratio  $r_d$ , defined as

$$r_d = \frac{p_{02}}{p_{0\infty}} \quad (11.8)$$



**Figure 11.4** Variation of efficiency and specific thrust with flight Mach number for ideal ramjet, for  $Q_R = 45\,000 \text{ kJ kg}^{-1}$ ,  $T_{\max} = 2500 \text{ K}$ , and  $T_{\infty} = 220 \text{ K}$ . Source: Hill, P.G. and Peterson, C.R., *Mechanics and Thermodynamics of Propulsion*, 2/E, ©1992, pp. 160, 161. Reprinted by permission of Pearson Education, Inc., Upper Saddle River, New Jersey.



**Figure 11.5**  $T$ - $s$  diagram illustrating aerodynamic losses during ramjet processes.

The stagnation pressure ratio  $r_c$  for the combustor is

$$r_c = \frac{p_{04}}{p_{02}} \quad (11.9)$$

The stagnation pressure ratio  $r_n$  for the nozzle is

$$r_n = \frac{p_{06}}{p_{04}} \quad (11.10)$$

Therefore, the overall stagnation pressure ratio can be expressed as

$$\frac{p_{06}}{p_{0\infty}} = \frac{p_{06}}{p_{04}} \frac{p_{04}}{p_{02}} \frac{p_{02}}{p_{0\infty}}$$

that is

$$\frac{p_{06}}{p_{0\infty}} = r_d r_c r_n \quad (11.11)$$

where  $r_d = p_{02}/p_{0\infty}$  is the stagnation pressure ratio caused by the diffusion process from the intake to the combustion chamber entrance.

By isentropic relation, we have

$$\begin{aligned} \frac{p_{06}}{p_e} &= \left(1 + \frac{\gamma-1}{2} M_e^2\right)^{\gamma/(\gamma-1)} \\ 1 + \frac{\gamma-1}{2} M_e^2 &= \left(\frac{p_{06}}{p_e}\right)^{(\gamma-1)/\gamma} \\ M_e^2 &= \frac{2}{\gamma-1} \left( \left(\frac{p_{06}}{p_{0\infty}} \frac{p_{\infty}}{p_e}\right)^{(\gamma-1)/\gamma} \left(\frac{p_{0\infty}}{p_{\infty}}\right)^{(\gamma-1)/\gamma} - 1 \right) \end{aligned}$$

But

$$\left(\frac{p_{0\infty}}{p_{\infty}}\right)^{(\gamma-1)/\gamma} = \left(1 + \frac{\gamma-1}{2} M_{\infty}^2\right)$$

The nozzle exhaust Mach number  $M_e$  becomes

$$M_e^2 = \frac{2}{\gamma-1} \left[ \left(1 + \frac{\gamma-1}{2} M_{\infty}^2\right) \left(\frac{p_{06}}{p_{0\infty}} \frac{p_{\infty}}{p_e}\right)^{\frac{\gamma-1}{\gamma}} - 1 \right]$$

Using Eq. (11.11), the above equation can be rewritten as

$$M_e^2 = \frac{2}{\gamma-1} \left[ \left(1 + \frac{\gamma-1}{2} M_{\infty}^2\right) \left(r_d r_c r_n \frac{p_{\infty}}{p_e}\right)^{\frac{\gamma-1}{\gamma}} - 1 \right] \quad (11.12)$$

If the heat transfer from the engine is assumed to be negligible, the nozzle exhaust velocity  $u_e$  can be expressed as

$$\begin{aligned} u_e &= M_e a_e \\ &= M_e \sqrt{\gamma R T_e} \end{aligned}$$

In terms of exhaust stagnation temperature  $T_{04}$ , the nozzle exhaust velocity becomes

$$u_e = M_e \sqrt{\frac{\gamma R T_{04}}{\left(1 + \frac{\gamma-1}{2} M_e^2\right)}} \quad (11.13)$$

The irreversibilities have no effect on the stagnation temperatures throughout the engine. Therefore, the fuel-air ratio necessary to produce the desired value of  $T_{04}$  is given by the modified form of Eq. (11.5) and becomes

$$f = \frac{(T_{04}/T_{0\infty}) - 1}{(\eta_b Q_R / c_p T_{0\infty}) - (T_{04}/T_{0\infty})}$$

where  $\eta_b$  is the combustion efficiency and  $\eta_b Q_R$  is the actual heat release per unit mass of fuel. The engine thrust per unit air flow becomes

$$\frac{\text{Th}}{\dot{m}_{\infty}} = [(1+f)u_e - u] + \frac{1}{\dot{m}_{\infty}}(p_e - p_{\infty})A_e$$

Using Eqs. (11.12) and (11.13), the above equation can be expressed as

$$\frac{Th}{\dot{m}_\infty} = (1+f) \sqrt{\frac{2\gamma RT_{04}(\lambda-1)}{(\gamma-1)\lambda}} - M_\infty \sqrt{\gamma RT_\infty} + \frac{p_e A_e}{\dot{m}_\infty} \left(1 - \frac{p_\infty}{p_e}\right) \quad (11.14)$$

where

$$\lambda = \left(1 + \frac{\gamma-1}{2} M_\infty^2\right) \left(r_d r_c r_n \frac{p_\infty}{p_e}\right)^{\frac{\gamma-1}{\gamma}}$$

Also, the TSFC becomes

$$TSFC = \frac{f}{Th/\dot{m}_\infty} \equiv \frac{\text{Fuel-air ratio}}{\text{Specific thrust}}$$

So far in our discussions on the ideal ramjet, all the sources of irreversibilities were assumed to not cause stagnation pressure loss. But for calculating the performance of actual engines, the irreversibilities and the associated losses at different components of the engine must be taken into account.

## 11.4 Aerothermodynamics of Engine Components

The inlet, combustor, and nozzle are the three major components of gas turbine and ramjet engines. For a ramjet, Eq. (11.14) indicates that a given percentage loss in stagnation pressure has the same effect on engine performance. Therefore, the efficient performance of the engine components is of prime importance for the good performance of the engine. But designing the components to perform with high efficiency is more difficult in the regions requiring an increase of static pressure (adverse pressure gradient) compared to regions which require a decrease of static pressure (favorable pressure gradient). This is because of the boundary layer behavior and the tendency for separation in the presence of adverse pressure gradients. Thus, inlets where the pressure usually rises may be more difficult to design for efficient operation than passages experiencing favorable gradients, such as nozzles.

### 11.4.1 Engine Inlets

Depending on the flight Mach number of the vehicle, the engine inlets are called *subsonic* or *supersonic inlets*. Though we are concerned with ramjets, it will be beneficial to know the performance of inlets meant for both gas turbine and ramjet engines. In the discussions to follow we will study the details of the process associated with both subsonic and supersonic inlets.

#### 11.4.1.1 Subsonic Inlets

An air-breathing engine installed in an aircraft or a missile must be provided with an air intake and a ducting system. We know that for turbojet engines the air flow entering the compressor or fan must have a Mach number in the range of 0.4–0.7. Usually the upper part of this range is suitable only for transonic compressors. For engines designed for subsonic cruise, say Mach 0.8, the inlet must act as a diffuser with a gradual diffusion from Mach 0.8 to 0.6. Usually part of this deceleration occurs upstream of the inlet entrance.

Some of the primary considerations in the inlet design are the following.

- The inlet must be designed to operate without boundary layer separation, even when the air of the intake is not in the direction of the flow far upstream of the inlet. In other words,

the inlet performance must not be adversely influenced by the pitch and yaw motions of the aircraft.

- The stagnation pressure loss in the inlet must be small.
- The velocity and direction of the flow leaving the inlet must be uniform, i.e. the flow at the exit of the inlet should be uniform and unidirectional. This is an essential requirement, because distortions in the velocity profile at the compressor inlet can cause severe adverse effects to the aerodynamic performance of the compressor and may even lead to failure of the blades due to vibration.

These requirements for the inlet pose challenging problems in the design of both subsonic and supersonic inlets. To get a clear idea of the flow process through inlets let us look into them in detail in the following section.

## 11.5 Flow Through Inlets

The inlet may have to operate over a wide range of freestream conditions, depending on the flight speed and mass flow requirements of the engine. To gain an insight about the inlet performance, let us examine the streamline patterns and the corresponding thermodynamic path of an “average” fluid element for two typical subsonic conditions shown in Figure 11.6.

In this figure station  $\infty$  refers to the freestream or undisturbed flow ahead of the inlet duct and  $A_\infty$  is the cross-sectional area of the *capture streamtube*. To see the nature of this problem in aerodynamic terms, the concept of capture streamtube – also called an *aerodynamic duct* – is introduced. The air mass flowing through the capture streamtube gets accelerated or decelerated before entering the intake. For example, during level cruise flight, the flow in the streamtube may experience some deceleration external to the engine intake. Thus, as shown in Figure 11.6a, the cross-sectional area of the streamtube increases from freestream to intake entry. In another flight mode, like take-off and climb, which is a low-speed high-thrust operation, the engine will require more mass flow of air. For this case the streamtube will resemble a converging duct, as shown in Figure 11.6b, resulting in acceleration of the air stream upstream

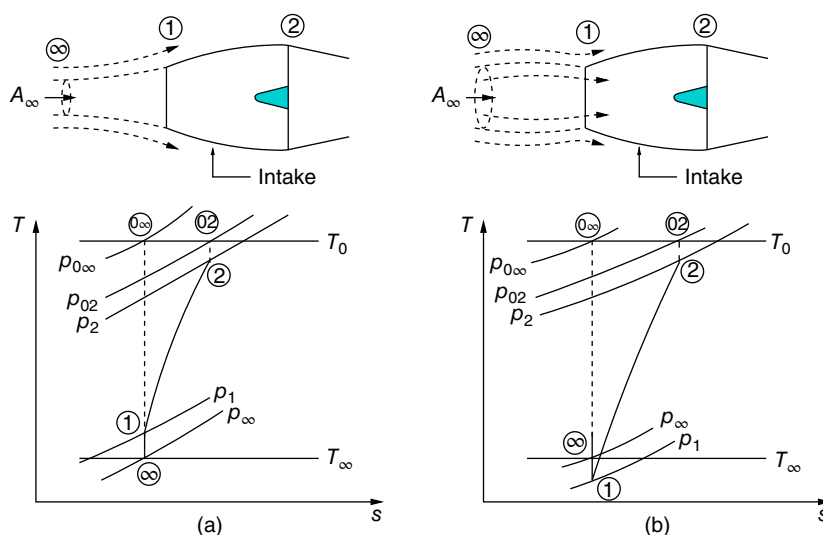


Figure 11.6 Streamline patterns and the corresponding  $T-s$  diagrams for subsonic inlets.

of the inlet. In both cases there is an external change of state (outside of the intake duct). Further, this change is isentropic, since there is no solid wall to introduce friction.

In Figure 11.6a, the streamtube ahead of the intake will decelerate the flow from location  $\infty$  to 1 and in Figure 11.6b the flow will accelerate in the portion ahead of the inlet entrance. The external acceleration lowers the pressure at the entry to the inlet. Therefore, for given velocities at stations  $\infty$  and 2, external acceleration increases the internal pressure rise across the diffuser. If this pressure rise is too large, the diffuser may stall, owing to boundary layer separation. Usually stall causes a loss of stagnation pressure of the stream. The external deceleration (Figure 11.6a) requires less internal pressure rise and thus results in lesser loading on the boundary layer in the diffuser. Therefore, the inlet area has to be so chosen to minimize the external acceleration during take-off, with the result that external deceleration occurs during cruise level flight. Under these conditions the upstream capture area  $A_\infty$  is less than the inlet area  $A_1$ , and some flow is “spilled over” the inlet, accelerating as it passes over the outer surface.

### 11.5.1 Inlet Flow Process

The flow in the inlet essentially decelerates. In other words, the inlet duct acts as a “diffuser.” The fluid momentum decreases and pressure increases, with no work being done, as it passes through the inlet. At this stage, it is important to note that even though a substantial amount of experimental and analytical work has been done on axisymmetric diffusers, they are not directly applicable to aircraft inlets. This is because most work on diffusers focuses on maximum pressure recovery, which is usually associated with a highly nonuniform exit velocity profile and even with some flow unsteadiness. But in subsonic inlets meant for aircraft engines the flow velocity entering the compressor should be strictly steady and uniform.

### 11.5.2 Boundary Layer Separation

Consider the inlet shown in Figure 11.7. In actual inlets flow separation can take place in any of the three zones shown as 1, 2, and 3. Separation of the external flow at zone 1 will cause high nacelle drag. Inside the duct the separation may take place in zone 2 or 3 depending on the duct geometry and operating conditions.

Separation at zone 3 is more probable, owing to large adverse pressure gradients, due to flow acceleration around the nose of the center body and deceleration at the rear of the body as the curvature decreases.

### 11.5.3 Flow Over the Inlet

The streamline pattern of subsonic flow over a typical inlet is shown in Figure 11.8. The dotted line shown in Figure 11.8 is an imaginary control volume around the inlet duct. At the inlet lip the external flow gets accelerated to high velocity, and accompanying low pressure can adversely affect the boundary layer in the following ways.

- When the entire flow is subsonic, if the low pressure region is followed by a region of rising pressure then the boundary layer may separate. Thus, the maximum velocity due to flow

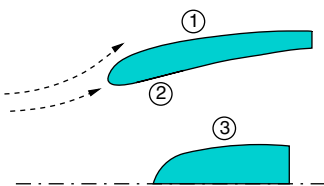
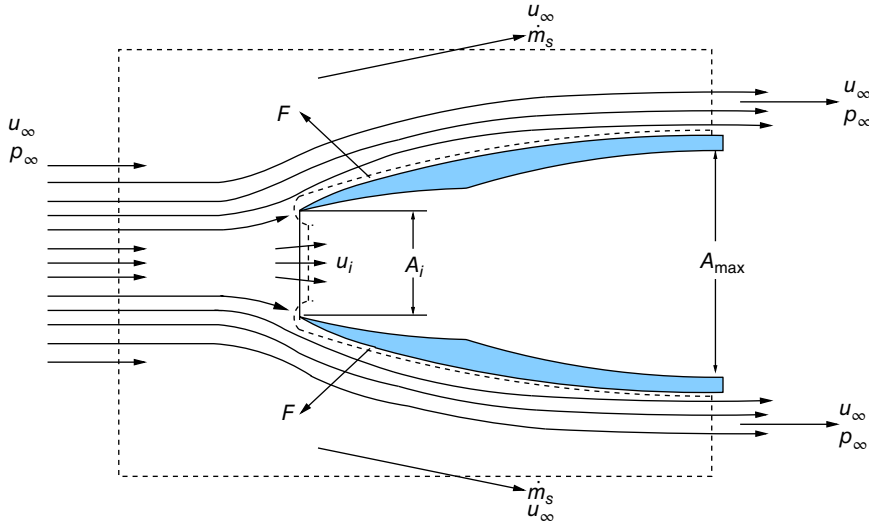


Figure 11.7 Boundary layer separation location.



**Figure 11.8** Flow past an inlet.

acceleration at the lip must be below a certain limiting value beyond which boundary layer separation can be expected downstream of the lip.

- When the flow around the inlet is partly supersonic, the local supersonic region will usually end abruptly in a shock, and the shock–wall interaction may cause boundary layer separation. Thus, for this case also the local Mach number must be below a certain limiting value. Otherwise, the boundary layer will separate.

The boundary layer separation is undesirable and should be avoided, since it results in poor pressure recovery in the flow over the after portions of the aircraft or engine housing. This process results in a net rearward force, termed as *drag on the body*.

In Figure 11.8  $u$  and  $p$ , respectively, are the velocity and pressure of the flow,  $F$  is the force acting on the inlet, and  $A$  is cross-sectional area. Subscripts  $\infty$  and  $i$  refer to the freestream and entrance of the inlet. As shown in the figure, all external flow enters and leaves the control volume with an axial velocity of  $u_\infty$ . Neglecting the changes in air density, the net momentum flux out of the control volume can be expressed as

$$\dot{m}_\infty u_\infty + \rho u_i^2 A_i - \rho u_\infty^2 A_{\max}$$

where  $A_{\max}$  is the area of the inlet duct at its exit.

The mass flow escaping the control volume through its side is

$$\dot{m}_s = \rho u_\infty A_{\max} - \rho u_i A_i$$

The momentum flux associated with this mass is

$$\rho A_i (u_i^2 - u_i u_\infty)$$

The net force in the axial direction, acting on the control volume is

$$p_\infty A_{\max} - p_i A_i - F_x$$

where  $F_x$  is the axial component of the force acting on the control volume. Neglecting friction, the net force acting on the control volume in the axial direction can be expressed as

$$F_x = - \int_{\text{inlet}} p(x.n) dA = \int_{A_i}^{A_{\max}} p dA_x$$



where  $p$  is the pressure,  $x$  is the unit vector in the flow direction,  $n$  is the outward normal pointing unit vector to the inlet area,  $dA$  is the elemental area external to the surface, and  $dA_x$  is the projection of  $dA$  in the axial direction.

With the above equations, the momentum equation can be rewritten as

$$p_\infty A_{\max} - p_i A_i - \int_{A_i}^{A_{\max}} p dA_x = \rho A_i (u_i^2 - u_i u_\infty)$$

or

$$\int_{A_i}^{A_{\max}} (p_\infty - p) dA_x = \rho A_i (u_i^2 - u_i u_\infty) + (p_i - p_\infty) A_i \quad (11.15)$$

By the incompressible Bernoulli's equation, we have

$$p_i - p_\infty = \rho \left( \frac{u_\infty^2 - u_i^2}{2} \right)$$

Thus,

$$\begin{aligned} \int_{A_i}^{A_{\max}} (p_\infty - p) dA_x &= \rho A_i (u_i^2 - u_i u_\infty) + \rho A_i \left( \frac{u_\infty^2}{2} - \frac{u_i^2}{2} \right) \\ &= \frac{1}{2} \rho u_\infty^2 A_i \left( 2 \frac{u_i^2}{u_\infty^2} - 2 \frac{u_i}{u_\infty} + 1 - \frac{u_i^2}{u_\infty^2} \right) \\ &= \frac{1}{2} \rho u_\infty^2 A_i \left( 1 - 2 \frac{u_i}{u_\infty} + \frac{u_i^2}{u_\infty^2} \right) \\ &= \frac{1}{2} \rho u_\infty^2 A_i \left( 1 - \frac{u_i}{u_\infty} \right)^2 \end{aligned}$$

The incremental thrust due to flow is

$$\Delta \text{Th} = \int_{A_i}^{A_{\max}} (p_\infty - p) dA_x$$

From the above two equations, we get

$$\frac{\Delta \text{Th}}{\frac{1}{2} \rho u_\infty^2 A_i} = \left( 1 - \frac{u_i}{u_\infty} \right)^2 \quad (11.16)$$

Equation (11.16) shows that the thrust generated by the engine can be increased by lowering the flow speed at the intake entry.

At the outer surface of the nozzle, the pressure must rise from the  $p_{\min}$  value at the inlet lip to the ambient value  $p_\infty$  at some downstream location. Now define an average pressure difference for the outer surface of the nacelle, as

$$\begin{aligned} \overline{p_\infty - p} &= \frac{\int_{A_i}^{A_{\max}} (p_\infty - p) dA_x}{A_{\max} - A_i} \\ &= s(p_\infty - p_{\min}) \end{aligned}$$

where  $s$  is a constant with a magnitude of between 0 and 1. We can express the incremental thrust as

$$\Delta Th = s(p_\infty - p_{\min})(A_{\max} - A_i)$$

Thus, Eq. (11.16) becomes

$$\frac{s(p_\infty - p_{\min})(A_{\max} - A_i)}{\frac{1}{2}\rho u_\infty^2 A_i} = \left(1 - \frac{u_i}{u_\infty}\right)^2$$

This equation can be rewritten as

$$\frac{A_{\max}}{A_i} = 1 + \frac{\left(1 - \frac{u_i}{u_\infty}\right)^2}{sC_{p_{\max}}\left(\frac{u_{\max}}{u_\infty}\right)^2}$$

where

$$C_{p_{\max}} = \frac{p_\infty - p_{\min}}{\frac{1}{2}\rho u_{\max}^2}$$

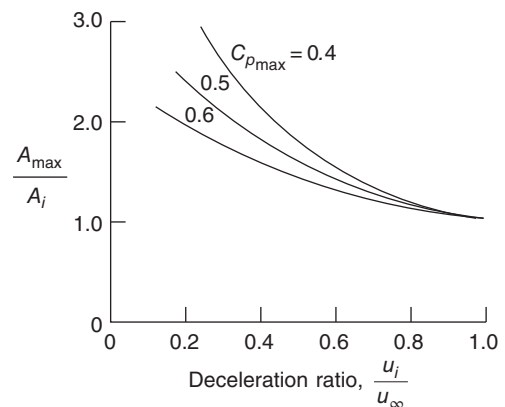
or

$$\frac{A_{\max}}{A_i} = 1 + \frac{\left(1 - \frac{u_i}{u_\infty}\right)^2 (1 - C_{p_{\max}})}{sC_{p_{\max}}} \quad (11.17)$$

The value of  $s$  in Eq. (11.17) depends on the nacelle shape. For example, taking  $s = 0.5$ , we can show the dependence of the size of the external surface necessary to prevent external boundary layer separation, for any given value of  $u_i/u_\infty$ , as shown in Figure 11.9.

From Figure 11.9, it can be seen that, to prevent excessive drag, the size of the nacelle should increase with an increase of external deceleration (i.e. with decrease of  $u_i/u_\infty$ ). Even without separation, larger nacelle will experience high aerodynamic drag. But if the external deceleration is modest (for example  $u_i/u_\infty > 0.8$ ), its effect on minimum nacelle size is quite small. The use of partial internal deceleration is very effective in reducing the maximum diameter, because it permits reduction in both  $A_i$  and  $A_{\max}/A_i$ .

**Figure 11.9** Variation of  $A_{\max}/A_i$  with velocity ratio  $u_i/u_\infty$  for  $s = 0.5$ .



Even though the above analysis of intake (nacelle) flow is based on many simplifications, it shows that the performance of an intake depends on the pressure gradient on both internal and external compression and  $A_{\max}/A_i$  ratio. The internal pressure rise depends on the flow deceleration between entry to the inlet diffuser and entry to the compressor (or burner, for a ramjet). Nacelle size required for low drag strongly depends on the degree of external deceleration.

## 11.6 Performance of Actual Intakes

The differences between the ideal and actual performance of aircraft engine intakes may be characterized by using *diffuser efficiency* or by using stagnation pressure ratio.

### 11.6.1 Isentropic Efficiency

Consider the intake and the corresponding  $T$ - $s$  diagram shown in Figure 11.10.

For the intake shown in Figure 11.10, the isentropic efficiency can be defined as

$$\eta_d = \frac{h_{02s} - h_\infty}{h_{0\infty} - h_\infty} \approx \frac{T_{02s} - T_\infty}{T_{0\infty} - T_\infty}$$

where  $h_{0\infty}$  and  $h_\infty$  are the stagnation and static enthalpy of the freestream air,  $h_{02s}$  is the stagnation enthalpy after isentropically decelerating the flow from station 1 to station 2 of the intake, and  $T_{02s}$  is the temperature attained by isentropic deceleration of the outlet flow to stagnation state. Therefore, by isentropic relations, we have

$$\frac{T_{02s}}{T_\infty} = \left( \frac{p_{02}}{p_\infty} \right)^{\frac{\gamma-1}{\gamma}}$$

and

$$\frac{T_{02}}{T_\infty} = 1 + \frac{\gamma-1}{2} M_\infty^2$$

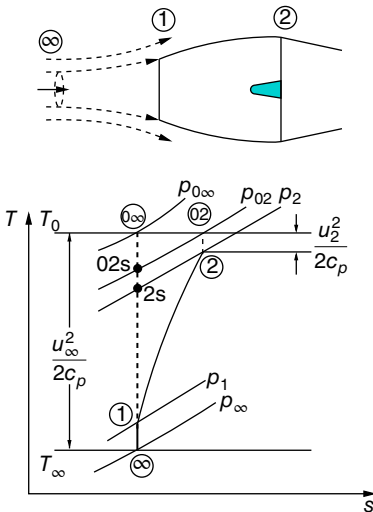


Figure 11.10 An intake and  $T$ - $s$  diagram for the flow through it.

Thus, the diffuser efficiency becomes

$$\eta_d = \frac{\left(\frac{p_{02}}{p_\infty}\right)^{\frac{\gamma-1}{\gamma}} - 1}{\frac{\gamma-1}{2}M_\infty^2} \quad (11.18)$$

### 11.6.2 Stagnation Pressure Ratio

The stagnation pressure ratio  $r_d$ , defined as the ratio of the stagnation pressure at the intake exit to the freestream stagnation pressure, is used as a measure of diffuser performance.

$$r_d = \frac{p_{02}}{p_{0\infty}} \quad (11.19)$$

This ratio can be expressed as

$$\frac{p_{02}}{p_{0\infty}} = \frac{p_{02}}{p_\infty} \frac{p_\infty}{p_{0\infty}}$$

or

$$\begin{aligned} \frac{p_{02}}{p_\infty} &= \frac{p_{02}}{p_{0\infty}} \frac{p_{0\infty}}{p_\infty} \\ &= \frac{p_{02}}{p_{0\infty}} \left(1 + \frac{\gamma-1}{2}M_\infty^2\right)^{\frac{\gamma}{\gamma-1}} \end{aligned}$$

Using this and Eq. (11.18), we get

$$\eta_d = \frac{\left(1 + \frac{\gamma-1}{2}M_\infty^2\right) (r_d)^{\frac{\gamma}{\gamma-1}} - 1}{\frac{\gamma-1}{2}M_\infty^2} \quad (11.20)$$

It can be seen from this relation that the diffuser efficiency is governed by the stagnation pressure ratio  $r_d$  and the freestream Mach number  $M_\infty$ . Variation of  $r_d$  and  $\eta_d$  with  $M_\infty$  is shown in Figure 11.11.

### 11.6.3 Supersonic Inlets

For gas turbine engines the flow leaving the engine inlet system should be subsonic, even when they fly at supersonic speeds. This is because it is difficult to pass a fully supersonic stream through the compressor without excessive shock losses. Furthermore, the development of a fully supersonic compressor is still only in the research stage. Designing such a compressor will be of great advantage, because it could provide very high mass flow per unit area and a very high pressure ratio per stage. Currently, the Mach number of the axial flow approaching a subsonic compressor should be around 0.4 and for the transonic stage it can be about 0.6. Here the term *transonic* refers to the flow velocity relative to the blade tip and not to the entrance velocity.

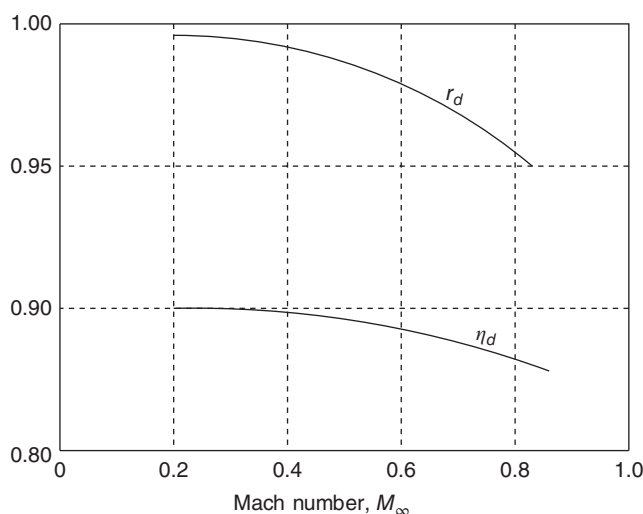
The ramjet engine is free from the above-mentioned restriction, since it does not use a compressor. Also, in ramjets it is possible to have combustion in a supersonic stream without severe aerodynamic losses. The name SCRAMJET denotes the supersonic combustion ramjet, a concept that is being investigated for high flight Mach numbers. However, this concept is yet to become practical, and to date ramjet combustion requires a subsonic airstream to provide stable combustion without excessive aerodynamic losses.

In our discussions in this chapter, we will be studying the means of decelerating supersonic flow to subsonic speed suitable for the existing gas turbine compressors and ramjet combustors.

### 11.6.4 Supersonic Diffusers

We know that in the supersonic flow regime decrease in the area of a duct will result in deceleration of flow. This phenomenon is exploited in the form of a second throat in supersonic wind tunnels, that is attaching a convergent–divergent duct at the end of the wind tunnel test-section will decelerate the supersonic flow by forming a normal shock in the duct. To minimize the pressure loss it is usual to position the shock just downstream of the second throat where the Mach number is slightly greater than 1. The concept of using a convergent–divergent duct, which is usually referred to as a *nozzle* in supersonic flow studies, for decelerating supersonic flow to subsonic speed is termed a *reverse nozzle diffuser* in inlet studies. The main difference between the second throat and the reverse nozzle diffuser is that in the case of supersonic wind tunnel application there is no *aerodynamic duct* effect ahead of the diffusers, but in supersonic inlets there is an aerodynamic duct effect upstream of the diffuser. Even though the use of a convergent–divergent duct appears simple and impressive, in principle, from a theoretical point of view, there are formidable challenges from a practical point of view. The main cause for these difficulties is the need for the successful operation of the reversed nozzle inlet over a range of flight Mach numbers and the problem which stems from shock–boundary layer interactions. Furthermore, under certain conditions, flow can become highly oscillatory.

In wind tunnel applications, we can see that the shock which is initially formed at the entry to the reversed-nozzle diffuser need be pushed to the second throat in order to minimize the pressure loss caused by the shock. It is achieved either by increasing the operating stagnation pressure or by temporarily increasing the second throat area. In the case of inlet diffusers the positioning of the shock at the throat can be achieved by momentarily over-speeding the inlet air or by varying the diffuser geometry. The process of positioning the shock can be viewed as a problem independent of the boundary layer effect. Therefore, for the present let us ignore the boundary layer effects and examine the starting problem of a convergent–divergent diffuser from a one-dimensional point of view, treating the flow to be isentropic.



**Figure 11.11** Variation of diffuser efficiency and stagnation pressure ratio with freestream Mach number.

### 11.6.5 Starting Problem

Consider a supersonic flow entering a convergent–divergent diffuser. Let us assume the flow to be one-dimensional and isentropic. Therefore, we need to consider only the loss due to the normal shock present in the passage. Even though this is a simplified analysis, the results can be applied to actual flow through diffusers where the wall boundary layer is carefully removed by suction through porous walls. Examine the flow through a fixed geometry convergent–divergent inlet, which is accelerated from subsonic to supersonic speeds in steps, shown schematically in Figure 11.12.

In Figure 11.12a, low subsonic flow passes through the inlet. The upstream capture area  $A_\infty$  is dictated by conditions downstream of the inlet. As the flow accelerates, the streamtube upstream of the intake gets adjusted, as shown in Figure 11.12b. Owing to this variation of streamtube area, the flow gets accelerated to sonic velocity at the minimum area,  $A_{th}$ , of the inlet. The mass flow rate through the intake is limited by the choking at  $A_{th}$ . When the flow is choked, we have  $A_{th} = A^*$  and the upstream capture area  $A_\infty$  can be expressed, using the isentropic area–Mach number relation as

$$\frac{A_\infty}{A^*} = \frac{A_\infty}{A_{th}} = \frac{1}{M_\infty} \left[ \frac{2}{\gamma + 1} \left( 1 + \frac{\gamma - 1}{2} M_\infty^2 \right) \right]^{\frac{\gamma + 1}{2(\gamma - 1)}} \quad (11.21)$$

where  $M_\infty$  is the freestream Mach number.

For high subsonic values of  $M_\infty$ , we have

$$\frac{A_\infty}{A^*} = \frac{A_\infty}{A_{th}} < \frac{A_i}{A_{th}}$$

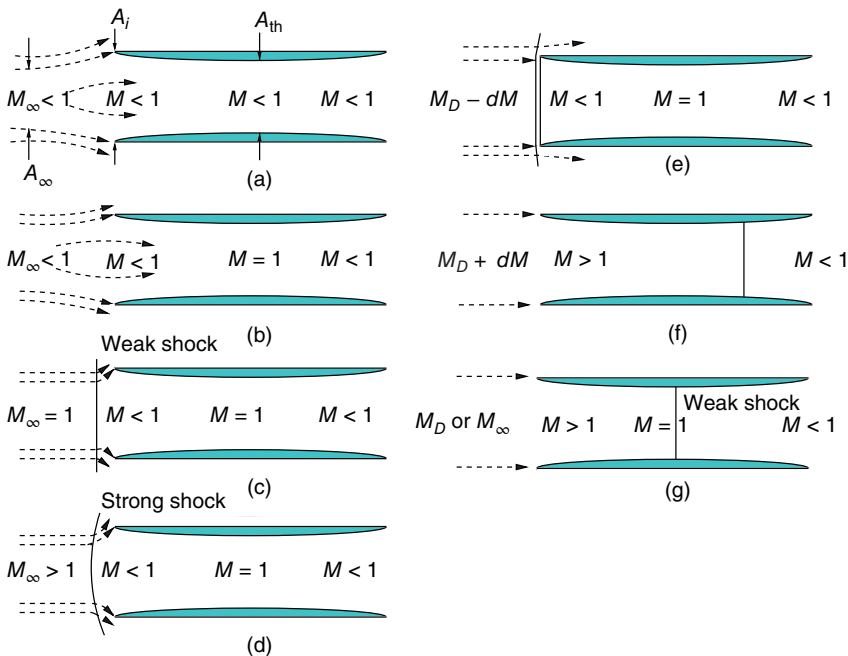


Figure 11.12 Flow through a convergent–divergent inlet.

Thus, the capture area  $A_\infty$  should be less than the inlet area  $A_i$ , for high subsonic freestream Mach numbers.

As the freestream flow accelerates further and  $M_\infty = 1$ , a weak shock forms and stands upstream of the inlet (Figure 11.12c). For further acceleration leading to  $M_\infty > 1$ , the shock is moved toward the inlet and also becomes bow-shaped, as shown in Figure 11.12d. There is a specific value  $M_D$  for the freestream Mach number at which the shock is positioned exactly at the inlet throat as shown in Figure 11.12g, and the corresponding  $M_\infty$  is termed the design Mach number  $M_D$ . For  $M_\infty$  slightly less than  $M_D$ , that is for  $M_D - dM$ , the shock is slightly ahead of the inlet entrance, as shown in Figure 11.12e. For  $M_\infty$  slightly greater than  $M_D$ , that is for  $M_D + dM$ , the shock is pushed downstream of the intake throat and positioned at a location downstream of the throat, as shown in Figure 11.12f.

From Figure 11.12 it can be seen that for both subsonic and supersonic Mach numbers the same mass of air “spills” over the intake. Also, this spillage process is nonisentropic. To have a better picture of the flow process illustrated in Figure 11.12, let us consider the supersonic flow through an aerodynamic duct, as shown in Figure 11.13.

- When the exit of the duct is closed with a plug, as shown in Figure 11.13a, the duct will act like a blunt body with a bow-shock ahead of it. The flow behind the detached shock will have a subsonic region up to the duct entrance. The flow will accelerate to attain sonic speed and finally will become supersonic, as illustrated in Figure 11.13a.
- When the entrance is partially opened by retracting the plug (allowing a small opening  $A_e$  at the exit), some quantity of air will flow through the duct, forming a narrow streamtube, effectively thinning the body and thereby allowing the shock to stand closer to the duct mouth, as shown in Figure 11.13b. The total pressure  $p_{02}$  behind the shock will be given by the normal shock relation

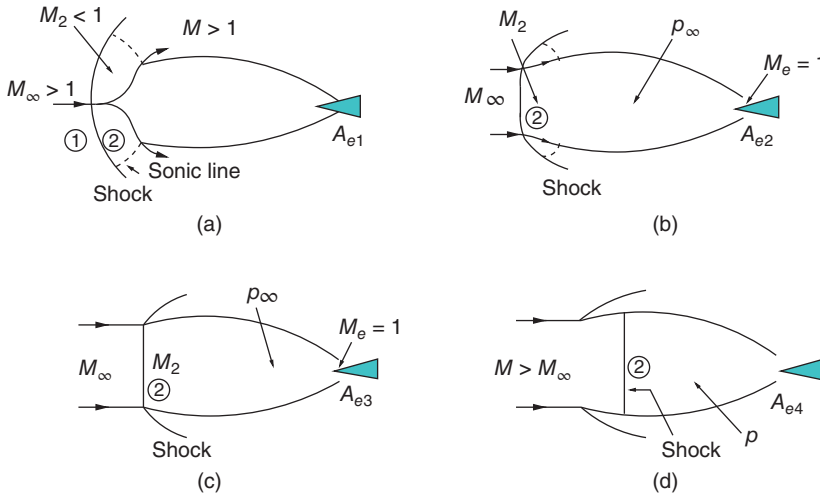
$$\frac{p_{02}}{p_{01}} = \left[ 1 + \frac{2\gamma}{\gamma + 1}(M_1^2 - 1) \right]^{-1/(\gamma-1)} \left[ \frac{(\gamma + 1)M_1^2}{(\gamma - 1)M_1^2 + 2} \right]^{\gamma/(\gamma-1)}$$

Flow in the streamtube becomes subsonic with Mach number  $M_2$  just behind the shock and decelerates further in the intake portion of the duct. After crossing the maximum cross-section of the duct, the flow accelerates up to the duct exit. If  $p_{02}/p_e$  is more than 1.89 (assuming no friction), the Mach number will reach 1.0 at the exit. In other words, the flow at the duct exit is choked.

- As the exit area  $A_e$  is further increased by withdrawing the plug more, the shock moves upstream, approaching the duct entry. At some value of  $A_e$  (which is less than the duct entry cross-section area  $A_c$ ), the shock lies across the entry plane, as shown in Figure 11.13c. This happens when the ratio of the duct inlet area  $A_c$  to the exit area  $A_e$  has the value of the area ratio  $A/A^*$  required for the flow to choke for Mach number  $M_2$ , the subsonic Mach number behind the normal shock. At this stage, the flow condition inside the duct is subsonic throughout but choked at the exit. The area ratio  $A_\infty/A_c$  is 1.0 and the duct is said to be *running full*.
- For further increase of  $A_e$ , more flow tries to leave the duct, creating a depression which sucks the shock inside the duct. The shock would be positioned inside the duct at a station where the total pressure downstream of the shock had decreased sufficiently to compensate for the increase in area and would leave the mass flow unchanged, as shown in Figure 11.13d. That is, when

$$p \times A_{e4} = p_\infty \times A_{e3}$$

At this stage, it is important to note that no solution exists for a flow ratio  $(A_c/A_e)$  greater than 1.0. This is because, since the duct design aims at experiencing subsonic



**Figure 11.13** Flow through an aerodynamic duct in a supersonic stream.

flow, the supersonic flow must pass through a shock. If the shock is outside the duct, a station upstream of the duct, with  $A_\infty$  greater than  $A_c$ , the pressure in the subsonic stream behind the shock will decrease toward entry because of flow acceleration in the contracting streamtube. Such a shock position will not be stable, any small disturbance will drive it toward the entry. If the shock is inside the duct, any increase of suction downstream cannot be transmitted forward through the shock. An increase of pressure upstream can increase pressure throughout the system, causing an increase of mass flow, without affecting the flow-area ratio.

The flow and pressure recovery in the aerodynamic duct, owing to the process described above, are as shown in Figure 11.14. Neglecting fictional effects, these are the characteristics of a *pitot intake* (intakes resembling open-ended tubes such as the one shown in Figure 11.13 are referred to as *pitot intakes*) at supersonic speeds.

- The operating condition (state 3 in Figure 11.14) which corresponds to maximum pressure recovery and maximum flow rate is termed the *critical point* or *critical operation*.
- Operation for which the mass flow rate through the inlet is less than the critical operation mass flow rate (state 2 in Figure 11.14) is called *subcritical operation*.
- Operation (state 4 in Figure 11.14) for which the mass flow rate is maximum but the pressure recovery is lower than the critical operation is termed *supercritical operation*.

The pitot intakes have the specific advantages of *low drag* and *a stable flow characteristics with good flow distribution*. But the level of pressure recovery achieved is limited by the total pressure ratio  $\frac{p_{02}}{p_{01}}$  across a normal shock, as shown in Figure 11.14b. This is a serious disadvantage, since the pressure loss across a normal shock increases steeply with an increase of flow Mach number. The pressure loss across a normal shock at different Mach numbers given in Table 11.1 illustrates this aspect.

We know that a 1% loss of intake total pressure results in between a 1 and 1.5% loss of engine gross thrust [13]. Therefore, from Table 11.1 it is evident that a pitot intake is probably not acceptable, even at Mach 1.5. Indeed this requirement dictates most supersonic theory and practice.

From the above discussion, it is evident that, at the design Mach number, the throat will have Mach 1, and isentropic deceleration from supersonic level to subsonic level will prevail.



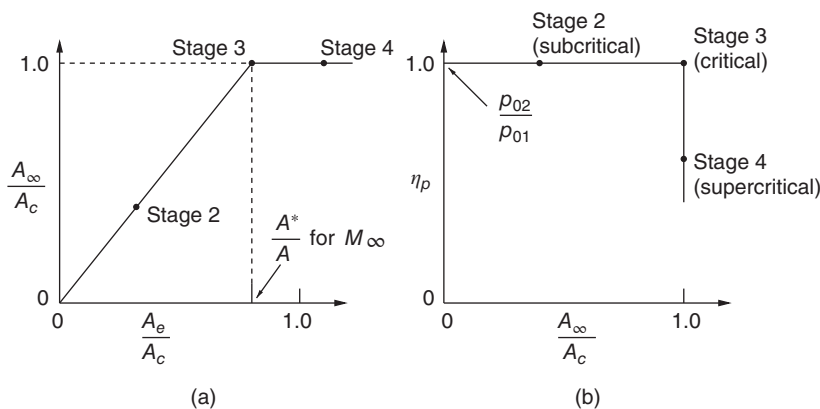


Figure 11.14 Flow and shock pressure recovery of a pitot intake.

Table 11.1 Total pressure ratio across normal shock.

$M_\infty$	1	1.5	2.0	2.5	3.0	3.5	4.0
$\frac{p_{02}}{p_{01}}$	1.0	0.9298	0.7209	0.4990	0.3283	0.2129	0.1388

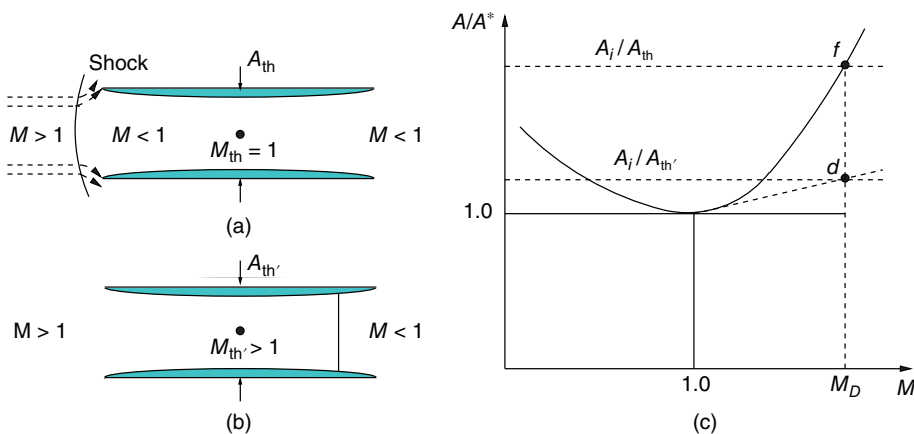


Figure 11.15 Shock swallowing.

However, this condition would be unstable even for this simplified model. A slight decrease of flight speed or even a marginal increase of backpressure would result in spillage and the shock would move rapidly out through the inlet to reestablish a shock in front of the intake, as shown in Figure 11.15.

Therefore, it would be preferable to maintain the throat Mach number slightly greater than unity while reaching subsonic velocities through a weak shock just downstream of the throat. An inlet having  $\frac{A_i}{A_{th}}$  greater than one (that is a convergent duct) will always require spillage upon reaching supersonic flight speed since  $\frac{A_\infty}{A_{th}}$  will always pass through a minimum of 1 just as sonic flight velocity is attained. Under such situation, *shock swallowing* is a means

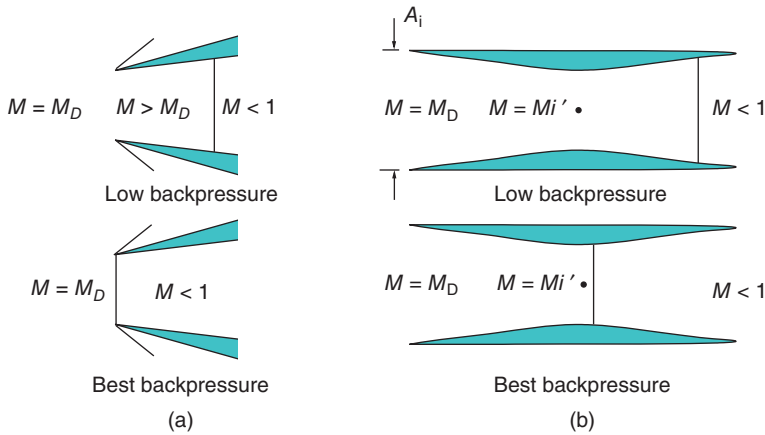
to establish isentropic flow (of course, excluding the shock zone). Shock swallowing is the process in which the normal shock formed at the divergent portion of the duct is made to move out of the duct. This can be achieved by the following two means.

- By over-speeding the flight to a higher Mach number than the design value.
- By varying the duct geometry at constant flight speed.

The process of shock swallowing can easily be decided in terms of one-dimensional analysis. Let us assume that the inlet is accelerated to the design Mach number  $M_D$  with a starting shock present as a bow shock standing ahead of the inlet entry (Figure 11.15a). Now, if the area ratio  $\frac{A_i}{A_{th}}$  is decreased – by increasing the throat area  $A_{th}$  and keeping the inlet area unaltered – to the value that can ingest the entire inlet flow behind the shock, the shock will be swallowed by inlet and the shock will be positioned downstream of the throat. This process of momentary increase of throat area from  $A_{th}$  to the new value  $A_{th'}$  establishes isentropic flow within the convergent portion of the inlet. Also, the throat Mach number  $M_{th'}$  is greater than 1, and a relatively strong shock occurs downstream of the throat, as shown in Figure 11.15b. Completely isentropic flow can be established by reducing the throat area to its original value. The operating condition moves from  $d$  to  $f$ , as shown in Figure 11.15c which shows the variation of  $A/A^*$  with Mach number.

The increase and decrease of throat geometry to swallow the shock and establish isentropic flow throughout the inlet passage, even though impressive, is difficult to achieve mechanically for axisymmetric flows. But an effect similar to a variable throat area can be achieved by moving a central plug between nonparallel walls of a passage. Use of porous convergent walls can also result in a somewhat similar effect to that of a variable throat area. When the shock is ahead of the passage, the high static pressure within the convergence causes considerable “leakage” through the walls, thus effectively increasing the throat area to permit shock swallowing. Once this occurs, the lower static pressure within the convergence somewhat decreases the flow loss. But since the porosity area required is more than that of the throat [14], this results in high mass flow loss under operating conditions. But this has the advantage of removing the boundary layer fluid; however, the loss associated with porosity is more than that associated with the boundary layer removal. Also, flow that is decelerated but not used internally contributes substantially to the drag of the propulsion device. From the above discussion it is clear that the starting problem can be avoided by using a divergent inlet with  $\frac{A_i}{A_{th}} = 1$ , as shown in Figure 11.16.

For supersonic flight speeds and low backpressure, the internal flow within the divergent portion can be accelerated before decelerating it through a shock. In such a process, the Mach number ahead of the shock has to be as low as possible for low stagnation pressure loss. In other words, the shock has to be positioned just downstream of the throat for minimizing the total pressure loss. This is because when the shock is just upstream of the throat the flow would experience acceleration up to the throat and then would decelerate in the divergent portion of the diffuser. This kind of acceleration followed by deceleration can be avoided if the shock is positioned just downstream of the throat, leading to monotonic deceleration behind the shock. This can be achieved by adjusting the backpressure. For engines operating in a free field where adjustment of backpressure cannot be made by varying the ambient pressure, unlike wind tunnels in the laboratory where the pressure of the storage chamber from which the tunnel flow is discharged can be controlled. In the case of engines the required backpressure can be achieved by varying the engine exhaust area. One of the popular techniques employed for this is positioning a taper plug at the nozzle exit. By adjusting the backpressure the shock can be positioned just on the inlet tip for simple diverging inlets and just downstream of the throat for the convergent–divergent outlet, as shown in Figure 11.16b.



**Figure 11.16** Fixed-geometry diffuser with normal shock inside (a) simple diverging duct and (b) Kantrowitz–Donaldson inlet.

The operating condition in which a detached shock is positioned ahead of the inlet and there is flow spillage is called *subcritical operation*. Operation where the shock is just at the inlet tip is called *critical operation*, and the operation where the shock is swallowed is termed *supercritical operation*. At this stage, we should note that a detached shock will be formed ahead of the inlet (if the operation of the above inlet is considered) as a result of choking in the inlet. For a complete engine, formation of detached shock can take place as a result of any downstream flow restriction that cannot accept the entire mass flow  $\rho_\infty U_\infty A_i$ .

## 11.7 Shock–Boundary Layer Interaction

In the discussion so far, we have assumed that there is no boundary layer in the passage. But in reality there will be a boundary layer present, and the shocks in the duct will have to interact with that. We know from our basic studies on gas dynamics that, across a shock wave of appreciable strength, the boundary layer will separate, and the separation may have a strong effect on the structure of the shock. For example, a turbulent boundary layer will separate when the shock-induced velocity reduction is between 20 and 30% ( $0.36 < C_p < 0.51$ ) [13]. Using the normal shock relations (see [6]), it can be seen that this would correspond to an upstream Mach number of 1.15 (20% reduction in velocity) and 1.25 (30% reduction in velocity).

Now let us have a closer look at one of the most important and least-understood practical problems, namely the shock–boundary layer interaction. We know that, when the pressures at the inlet and exit of a duct in which a gas flows supersonically are adjusted, it is possible to establish a shock in the duct. This shock will be radically different from a plane compression front. This is because of an interaction between the shock wave and the boundary layer on the duct walls.

Even though the phenomenon of shock–boundary layer interaction is most complicated, the outstanding physical features can be readily explained. In our discussion so far we have ignored the effects of viscosity on the nature of flow pattern. But in an actual flow process the viscous effects play a dominant role. It is important to keep track of viscous effects, especially when shocks are present. Prandtl's concept of the boundary layer is one of the great inventions in modern fluid mechanics. The essence of the boundary layer is that viscous stresses in a fluid

of low viscosity (e.g. air) are small everywhere compared with other terms in the momentum equation, except in comparatively thin layers near solid boundaries where large velocity gradients, and hence appreciable viscous stresses, must necessarily exist. Therefore, viscous effects are assumed to be important only in boundary layers adjacent to solid surfaces, and the flow outside the boundary layer is assumed to be frictionless.

This assumption offers a great simplification when the boundary layer flow does not affect the external flow significantly. For this case, the two regions of flow, the external flow and boundary layer flow, may be calculated separately, assuming that the boundary of the frictionless flow coincides with the solid boundary. Such is often the case for problems of subsonic flow, especially when the boundary is very thin compared with other significant length dimensions, like the thickness of an airfoil or the diameter of a duct. The presence of the boundary layer then has only a second-order effect on the exterior flow. But when separation of the boundary layer occurs owing to adverse pressure gradients, as in the stalling of a wing profile, the boundary layer thickens to such an extent that it materially affects the exterior flow, and it is no longer possible to assume that the boundary layer coincides with the solid boundary. In such cases, the simplicity of the boundary layer concept breaks down, and the boundary layer effect on exterior flow becomes very significant and cannot be ignored.

## 11.8 Oblique Shock Wave Incident on Flat Plate

When a shock wave impinges on a boundary layer near solid bodies, the interaction between the shock wave and the boundary layer is usually strong and produces first-order effects on both the boundary layer and the exterior flow. The large pressure gradients in the neighborhood of the shock wave violently distort the boundary layer flow. These distortions, which are propagated both upstream and downstream in the subsonic part of the boundary layer, in turn influence the conditions outside the boundary layer by means of expansion and compression waves generated by the disturbed boundary layer. Thus there is a mutual interaction between a shock wave and a boundary layer, an interaction which may lead to a flow pattern radically different from what might be anticipated if no boundary layer were present.

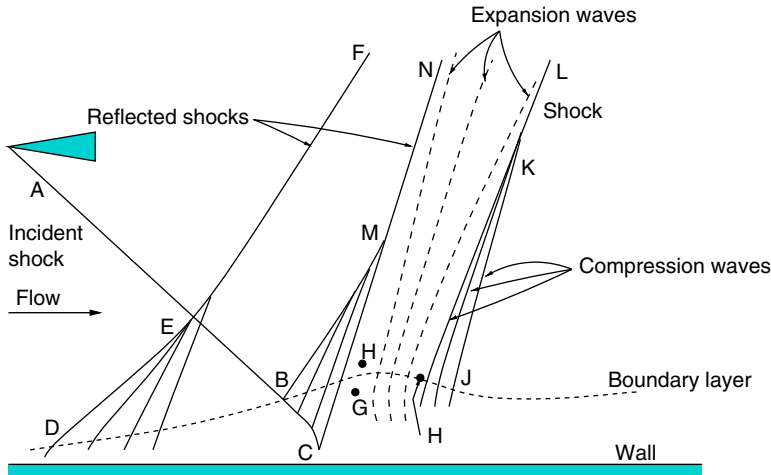
Examine the flow field with a shock–boundary layer interaction, as shown in Figure 11.17.

The oblique shock AB impinges on a flat plate on which there is a boundary layer. If the boundary layer were not present, the incident shock would be reflected as an oblique shock and the reflection would be specular (when the wall is assumed to be smooth). When a boundary layer is present, this simple type of reflection cannot occur, because of the following reasons.

- The shock bends as it enters the region of changing velocity in the boundary layer, and must terminate at the sonic line in the boundary layer.
- The effect of the shock can be propagated upstream through the subsonic zone within the boundary layer.

Because of the second effect, the pressure in the boundary layer begins to rise before the point of incidence of shock AB. The pressure rise is accompanied by a velocity decrease and hence a thickening of the boundary layer along DB. Oblique compression wavelets are generated along DB, owing to the turning of the streamlines. The wavelets coalesce to form the shock EF.

As the shock AB enters the boundary layer, it is refracted along BC because it is in a region of changing Mach number. Owing to this refraction, wavelets are generated along BC. Some of these are rarefaction wavelets, but often they are compression wavelets which coalesce into the shock MN.



**Figure 11.17** Schematic representation of reflection of oblique shock from boundary layer on a flat plate. Source: Reprinted from A.H. Shapiro, *The Dynamics and Thermodynamics of Compressible Fluid Flow*, vol. 1, p. 582 (Figure 16.49a), © 1953, with the permission of John Wiley & Sons, Inc.

The pressure at F is usually larger than that at G because the stream at F has passed through a shock of comparatively higher strength. Such a pressure gradient, if present, causes the streamlines to turn back toward the wall. This streamline curvature in turn produces expansion waves in the supersonic flow.

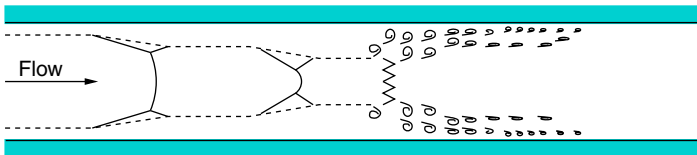
When the pressure difference between F and G is quite large the flow may be turned toward the wall. Because of this turning, compression wavelets are generated along the concave part of the boundary layer HJ. These compression waves coalesce into the shock KL.

The above discussion is qualitatively realized with experimental observations. The nature of the interaction depends upon Mach number, shock strength, velocity profile in the boundary layer, and specially on whether the boundary layer is laminar or turbulent.

## 11.9 Normal Shocks in Ducts

While dealing with one-dimensional supersonic flows in ducts, we often speak of a normal shock standing in a duct when the backpressure is high. In practice it is observed that the pressure rise through the shock occurs over an axial distance of several duct diameters.

The normal shock could not possibly extend to the wall when a boundary layer is present, because a rapid thickening of the boundary layer upstream of the shock gives rise to an oblique shock. The reflected shock at the juncture of the normal and oblique shocks, as shown in Figure 11.18, are necessary as a result of continuity requirements. Thus, a series of forked normal shocks appeared, and the length of the normal shock becomes progressively smaller as the



**Figure 11.18** Normal shock in a duct.

boundary layer thickens. Finally, the sonic velocity is reached and the stream then decelerates subsonically as it refills the passage. Therefore, the stream decelerates through a combination of normal and oblique shocks to Mach number unity and then decelerates further to subsonic speeds.

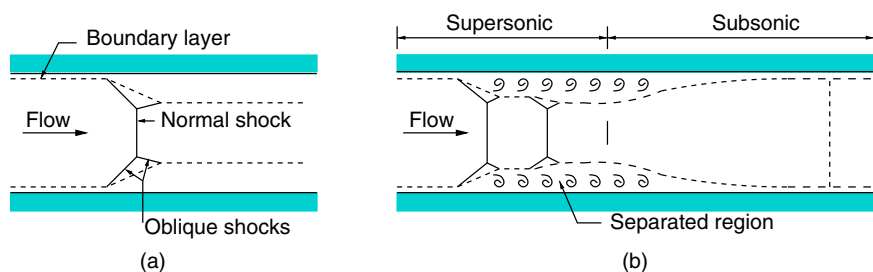
When the inlet and exit pressures of a duct, in which a gas flows at supersonic speed, are adjusted so that a compression shock appears in the duct, the latter is found to be radically different from a plane shock. This difference is due to an interaction between the shock wave and the boundary layer on the wall of the duct. The details of the phenomenon are very complicated, but the overall physical features can be readily explained. The normal shock in the core of the stream imposes a severe adverse pressure gradient on the stream as a whole. As the boundary layer flow has been retarded by wall friction, it does not have sufficient momentum to negotiate this adverse pressure gradient. Consequently, apart from the thickening of the boundary layer produced by the adverse pressure gradient, there is often a back flow in the boundary layer near the shock. This back flow results in a separation of the stream from the walls. The boundary layer effects lead to the formation of oblique waves and consequently the flow is far from one-dimensional.

Flow pattern due to shock–boundary layer interaction in a duct will typically resemble that shown in Figure 11.19.

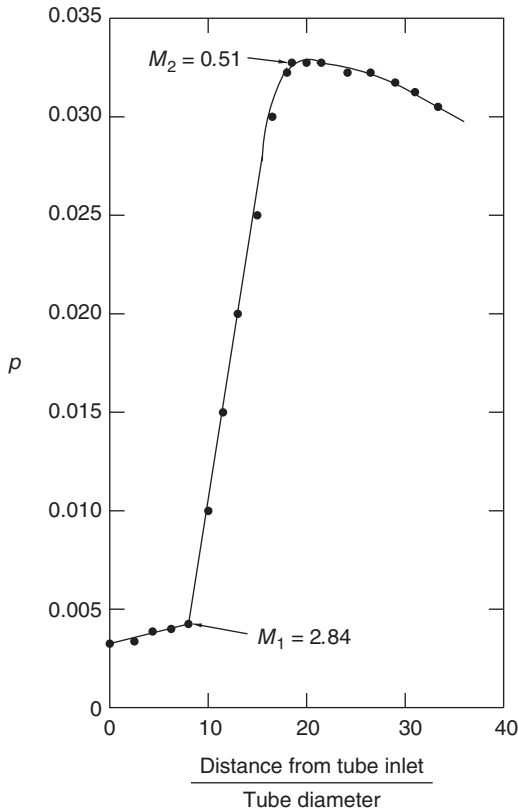
When a weak shock interacts with a thin boundary layer, the normal shock extends over most of the stream and a thickening of the boundary layer occurs, as shown in Figure 11.19a. This kind of interaction can be encountered slightly downstream of the throats of supersonic nozzles. When the shock is strong and the boundary layer is thick, the shock–boundary layer interaction will cause back flow and flow separation, as illustrated in Figure 11.19b. This type of interaction can be realized in long ducts fed by supersonic nozzles. The main flow stream separates from the walls, alternately passes through a series of acceleration zones and shocks, and, finally, after reaching subsonic speeds, diverges and fills the duct again.

A typical static pressure distribution measured at the wall of a duct containing a shock is shown in Figure 11.20. The pressure distribution shown is with Mach 2.84 at the beginning of the shock. About 10 diameters of duct length was required for attaining the pressure rise.

Measurements of the maximum pressure rise for the steeply ascending part of the pressure–distance curve indicate that the measured  $p_2/p_1$  is about 6% less than the value corresponding to the normal shock equation. This agreement is fairly good, considering the fact that at neither Section 1 nor Section 2 is the flow strictly one-dimensional. The good agreement between the measured and calculated pressure rise implies that the wall shearing forces in the region of separation in Figure 11.19b are very small, and hence the normal shock relations are reasonably applicable between Sections 1 and 2.



**Figure 11.19** Typical shock–boundary layer interactions in a duct. (a) Thin boundary layer and weak shock. (b) Thick boundary layer and strong shock.



**Figure 11.20** Measured static pressure distribution at the wall of a duct with compression waves as in Figure 11.19b. Source: Reprinted from A.H. Shapiro, *The Dynamics and Thermodynamics of Compressible Fluid Flow*, vol. 1, p. 136 (Figure 5.18), ©1953, with permission of John Wiley & Sons, Inc.

From the above discussions on shock–boundary layer interaction, we see that strong shocks can have significant effects on duct flow. Also, if a shock wave has been placed in a supersonic stream of a given Mach number,

- It is preferable to have an oblique shock than a normal shock because the pressure rise across an oblique shock is much less than that across a normal shock.
- The shock should interact with the wall at the point where the boundary layer thickness is smallest, that is the backpressure should be kept at a level so that the shock is made to interact with the boundary layer where the boundary layer is thin.

## 11.10 External Supersonic Compression

Even though there is no starting problem for the normal shock inlet, there is a severe pressure loss associated with normal shocks. The loss becomes large for high Mach numbers. For example, for gases with  $\gamma = 1.4$ , the pressure loss associated with normal shock is 28% at Mach 2 ( $p_{02}/p_{01} = 0.7209$ ). Therefore, it is preferable and beneficial if the Mach number before the normal shock is reduced to a low supersonic value. In other words, some external deceleration should be established and the Mach number ahead of the normal shock should be reduced to a low value to obtain a reasonable performance while maintaining the starting characteristics of a simple divergent inlet. That is, compressing the flow ahead of the intake in stages will prove to be beneficial from the pressure loss point of view. The simplest and most practical external deceleration mechanism is an oblique shock or, in some case, a series of oblique shocks.

Even though oblique shocks are not isentropic, the pressure loss in reaching subsonic velocity through a series of oblique shocks followed by a normal shock is less than that associated with a simple normal shock at a given flight Mach number. The losses decrease with an increase of the number of oblique shocks, especially at high flight Mach numbers.

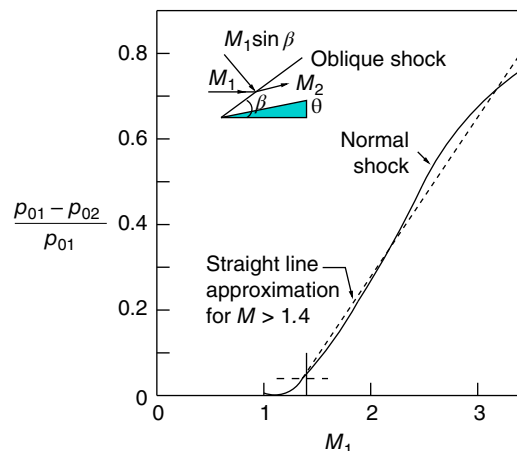
## 11.11 Two-Shock Intakes

Let us take a closer look at normal-shock pressure recovery to have an insight into the principle of staging a supersonic compression to achieve a reduction of total pressure loss. Total pressure loss through a normal shock at upstream Mach number  $M_1$  is shown in Figure 11.21.

It can be seen that, up to Mach 1.4, the loss is less than 4%. Above Mach 1.4 the curve is reasonably well approximated by a straight line giving a loss rate of 4% per 0.1 Mach number. Now, for a two-dimensional oblique shock with wave angle  $\beta$ , the loss is that corresponding to the component Mach number normal to the shock,  $M_1 \sin \beta$ . For turning angle  $\theta$  up to  $10^\circ$  (say), the shock angle  $\beta$  (oblique shock table and chart; Table A.3) lies in a band between  $25^\circ$  and  $50^\circ$ . It follows that the product  $M_1 \sin \beta$  varies only slightly with  $M_1$ , and up to Mach 3 does not in fact exceed the value 1.4, so that the oblique shock loss is not greater than 4%. The reduction in Mach number value from  $M_1$  to  $M_2$  is, however, very significant. For example, a  $10^\circ$  turning lowers the Mach number by about 0.6, which is sufficient to reduce normal shock loss by about 24%. This kind of benefits makes it attractive to devise systems of supersonic compression in stages, yielding high pressure recovery overall. The number and types of such stages used depend upon the freestream Mach number and other factors. Compression may be internal or external to the duct. In our discussions here we are concerned with only external compression systems. Two-shock intake is the simplest form of staged compression. In this intake, a single-angled wedge or cone projects forward of the duct. This generates an oblique shock to reduce the flow Mach number from the freestream value to a lower supersonic value. This flow passes through a normal shock at or near the entry and becomes subsonic. Examine the flow fields over a wedge and a cone, as illustrated in Figure 11.22.

It can be seen that the flow behind the oblique shock is different in the two cases. Over the wedge the flow is at a constant Mach number and parallel to the wedge surface. Over the cone, the flow behind the conical shock is itself conical. For the same apex angle the conical shock is weaker than the wedge shock. As seen in Figure 11.22c, for the wedge the pressure jumps across

**Figure 11.21** Character of normal shock loss.





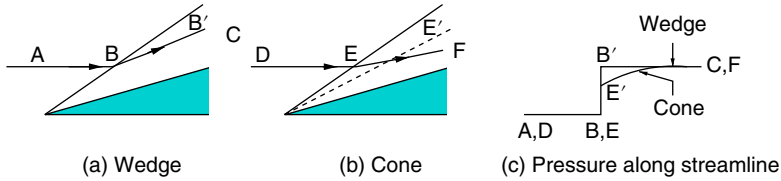


Figure 11.22 Flow past a wedge and a cone.

the shock and remains constant, but for the cone the pressure jump across the shock is followed by isentropic compression in the conical flow. Thus, the conical system is more efficient of the two. However, in practice, the choice is governed more by factors of engineering convenience.

It is obvious that the gas dynamic process of flow past the wedge and cone illustrated in Figure 11.22 are the same. The wedge or cone sits centrally with respect to the duct entry, which accounts for the term *center-body intake* being sometimes used. It is also referred to as *forebody intake* as it is synonymous with *external compression intake* of wedge or cone form.

The entry area  $A_c$  (streamtube “capture” area at entry) is defined as the area enclosed by the leading edge of the intake cowl, including the cross-sectional area of the forebody in the plane. As with a pitot intake, the maximum mass flow ratio achievable at supersonic speed occurs if and when the *boundary of the free streamtube  $A_\infty$  arrives undisturbed at the lip*, that is when

$$\frac{A_\infty}{A_c} = 1.0 \quad (11.22)$$

This condition is referred to as *full flow*. Maximum mass flow occurs when the flow remains supersonic up to the intake entry. This implies that the normal shock is at the intake lip or inside. The magnitude of mass flow depends on the Mach number, forebody apex angle, and the position of the lip. Basically, there are two possible combinations of shock angle  $\beta$  and the angle  $\theta$  subtended by the lip at the apex of the forebody. They are  $\beta \leq \theta$  and  $\beta > \theta$ . The flow fields corresponding to these conditions are illustrated in Figure 11.23.

For  $\beta \leq \theta$ , the capture streamtube can be increased until the flow arrives at the lip with the freestream Mach number. This condition is analogous to that for a pitot intake and we have

$$\left( \frac{A_\infty}{A_c} \right)_{\max} = 1.0 = \left( \frac{A_\infty}{A_c} \right)_{\text{full}} \quad (11.23)$$

For  $\beta > \theta$ , the maximum mass flow achievable is restricted by the necessary deflection of the bounding streamline in passing through the oblique shock. Hence

$$\left( \frac{A_\infty}{A_c} \right)_{\max} < 1.0 \quad (11.24)$$

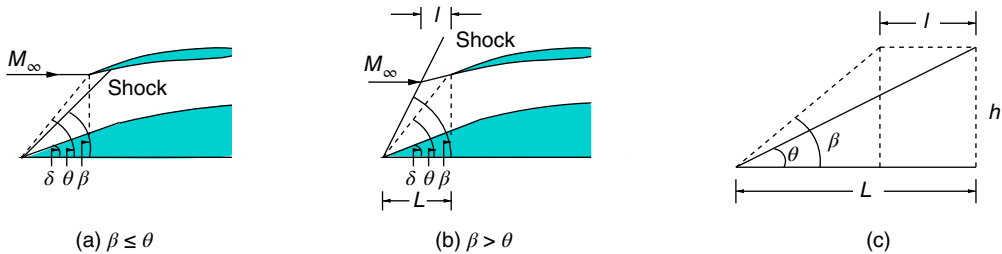


Figure 11.23 Maximum flow conditions for a single-wedge intake.

That is, the maximum mass flow achievable is less than full mass flow. The maximum mass flow is a function of Mach number; therefore, at some Mach numbers higher than that marked in Figure 11.23b, the oblique shock would fall on the lip and allow full flow through the intake. For a wedge forebody, it is easy to calculate the maximum flow when  $\beta > \theta$ . Let the distance from the forebody nose tip to the intake entry plane be  $L$  and that from the intersection point of the bounding streamline and oblique shock to the entry plane be  $l$ , as shown in Figure 11.23. From Figure 11.23, we have,

$$h = L \tan \theta$$

Also,

$$h = (L - l) \tan \beta$$

The area  $A_\infty$  and  $A_c$  become

$$A_c = L \tan \theta$$

$$A_\infty = (L - l) \tan \beta$$

Therefore,

$$\frac{A_\infty}{A_c} = \frac{(L - l) \tan \beta}{L \tan \theta} \quad (11.25)$$

Also, the flow behind the shock is parallel to the wedge surface, thus we have

$$1 - \frac{A_\infty}{A_c} = \frac{l \tan \delta}{L \tan \theta} \quad (11.26)$$

From Eqs. (11.25) and (11.26), eliminating  $L$  and  $l$ , we can obtain the flow ratio,  $A_\infty/A_c$ , as

$$\left( \frac{A_\infty}{A_c} \right)_{\max} = \frac{\cot \delta - \cot \theta}{\cot \delta - \cot \beta} \quad (11.27)$$

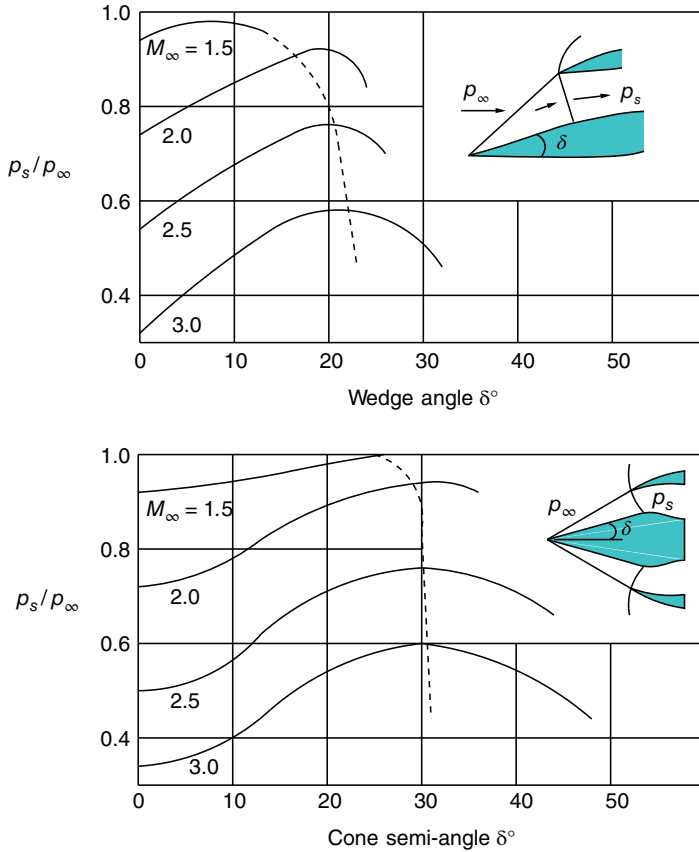
For a cone intake, an analytical solution can be obtained by assuming that the stream lines behind the conical shocks are portions of hyperbola. The formula arrived at by a process analogous to that for the wedge intake is [13]

$$\left( \frac{A_\infty}{A_c} \right)_{\max} = \frac{\cot^2 \delta - \cot^2 \theta}{\cot^2 \delta - \cot^2 \beta} \quad (11.28)$$

The pressure recovery of the shock system at the critical point (maximum pressure recovery at maximum flow) is the product of the separate total pressure ratios across oblique and normal shocks. The pressure recovery for a wedge forebody can be defined explicitly. For a cone the normal shock Mach number varies to a small extent from cone surface to cowl lip but a mean of the end value is normally adequate for the calculation of pressure recovery. Pressure recovery as a function of apex angle for wedge and cone forebodies with two-shocks is shown in Figure 11.24, for freestream Mach numbers up to 3.0.

From these plots we can see the following.

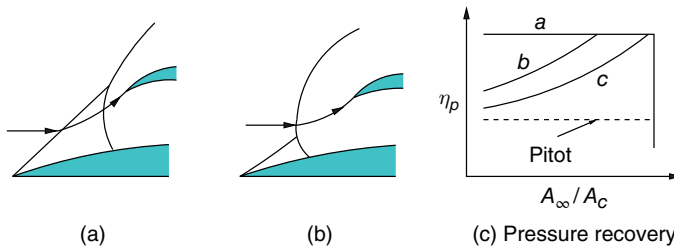
- At optimum angles, the conical intake is about 1.5% more efficient than the wedge type intake.
- For a given Mach number, large improvement can be achieved with forebodies compared to pitot intake ( $\delta = 0$ ). For instance, at Mach 2.0 the pressure recovery increases from 72 to 90% with forebody.
- It should be realized that boundary layer losses have not been taken into account. A two-shock intake is only moderately good at Mach 2.0. But it is unlikely to be efficient at higher Mach numbers – though the performance very much depends, of course, on the type of aircraft mission to be performed.



**Figure 11.24** Shock pressure recovery for wedge and cone forebodies.

The nature of pressure recovery at subcritical operation can be examined as follows. As the flow ratio proceeds from a critical point, the normal shock moves forward from the intake entry, allowing subsonic flow spillage behind it. There are three possible cases for this situation, as shown schematically in Figure 11.25.

- When  $\beta \gg \theta$ , at all reduced flows the capture streamline passes wholly through the two-shock system, as illustrated in Figure 11.25a. Shock pressure recovery remains constant, as in curve *a* in Figure 11.25c; therefore, similar to the variation of a pitot intake (Figure 11.14) but at the higher value corresponding to two-shock compression.
- When  $\beta$  is slightly larger than  $\theta$ , as the flow is reduced from the critical value, the flow pattern, as shown in Figure 11.25a, prevails for a time. After a certain time interval, the shock intersection point moves inside the capture streamtube, as shown in Figure 11.25b. Now, part of the intake flow passes through a single strong outer shock and encounters lower pressure recovery. Thus, the flow characteristic (curve *b* in Figure 11.25c) follows that of case Figure 11.25a, near critical flow, but at lower flows falls away, approaching that of the pitot intake value.
- When  $\beta \leq \theta$ , the shock intersection point lies inside the capture streamtube at all subcritical flows, the flow ratio is reduced, and the pressure recovery falls steadily from the critical value toward the pitot intake level.



**Figure 11.25** Pressure recovery at subcritical operation.

To calculate the shock pressure recovery in cases *b* and *c* in Figure 11.25c, details about the normal shock position as a function of flow ratio is essential. When the shock position is known, the properties of flow passing through the single outer shock and two inner shocks can be calculated, for both cone- and wedge-type intakes. Hence, suitably weighted mean pressure recovery can be derived.

## 11.12 Multi-Shock Intakes

In principle, an external shock system can be broken into any desired number of stages. In this section, let us examine a three-shock intake with two oblique shocks and one normal shock. For this shock system the center body should be a double-wedge or double-cone. The theoretical shock pressure recoveries of these two types constitute useful standards. The advantage of these systems is that a double-cone intake can be designed to yield a pressure recovery of as high as 96% at Mach 2.0 and about 88% at Mach 2.5.

The shock configurations for a double-wedge intake is shown in Figure 11.26. Determination of the shock configuration for this case is not simple. Because of this, any calculation of the maximum flow ratio for a three-shock intake with the position of the junction between first and second compression surfaces is generally complex. However, if we assume that there exists a Mach number  $M_D$ , at which the two-wedge shocks fall simultaneously on the cowl lip, as shown in Figure 11.26b, the expression for maximum flow ratio at any Mach number below  $M_D$  can be written as [13]

$$\left( \frac{A_\infty}{A_c} \right)_{\max} = \frac{\cot \delta_1 - \cot \beta_{1D}}{\cot \delta_1 - \cot \beta_1} \frac{\cot \delta_2 - \cot \beta_{2D}}{\cot \delta_2 - \cot \beta_2} \quad (11.29)$$

where the first and second wedge angles  $\delta_1$  and  $\delta_2$ , respectively, determine the angle  $\beta_{1D}$  and  $\beta_{2D}$  and the geometry is such that

$$\frac{L_w}{L} = \frac{L_w}{h_c} \tan \beta_{1D} = \frac{\tan(\beta_{2D} + \delta_1) - \tan \beta_{1D}}{\tan(\beta_{2D} + \delta_1) - \tan \delta_1} \quad (11.30)$$

In Eq. (11.29) the value of the maximum flow ratio assumes the flow to be two-dimensional. Close to the design Mach number, this assumption is valid if the oblique shocks are enclosed by end walls, swept from the tip of the compression surface to the cowl lip. For Mach numbers well below the design Mach number, or if the end walls are cut away, supersonic spillage occurs across the end walls, reducing the maximum flow attainable. McGregor [15] proposed a correlation parameter  $G$  for the amount of this sideways spillage as

$$G = \frac{A_1}{A_c} \left( \frac{p_1}{p_\infty} - 1 \right) + \frac{A_2}{A_c} \left( \frac{p_2}{p_\infty} - 1 \right) \quad (11.31)$$

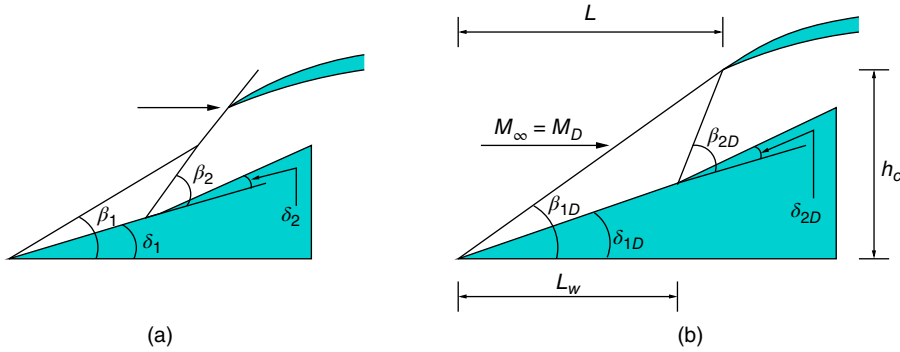


Figure 11.26 Shock configuration in a double-wedge intake.

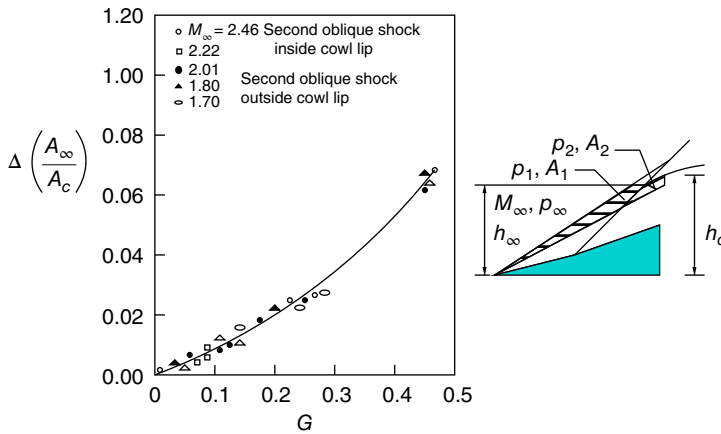


Figure 11.27 Maximum mass flow deficiency variation with  $G$ .

where  $A_1$  and  $A_2$  are the spillage area behind the first and second oblique shocks, respectively, and  $p_1$  and  $p_2$  are the pressures in those areas corresponding to two-dimensional flow. Measured deficiencies in maximum flow  $\Delta \left( \frac{A_\infty}{A_c} \right)$  as a function of  $G$  and the deficiencies calculated with Eq. (11.31) are compared in Figure 11.27, for a set of freestream Mach numbers.

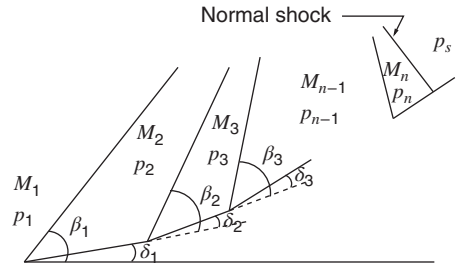
In principle, the external shock system can be broken down and three or more oblique shocks can be used ahead of the normal shock. For a shock system with  $(n - 1)$  oblique shocks, as shown in Figure 11.28, the shock pressure recovery is given by the product of the individual total-pressure ratios, that is

$$\frac{p_{\theta s}}{p_{\theta \infty}} = \frac{p_{0s}}{p_{01}} = \frac{p_{02}}{p_{01}} \frac{p_{03}}{p_{02}} \dots \dots \frac{p_{0n}}{p_{0(n-1)}} \frac{p_{0s}}{p_{0n}}$$

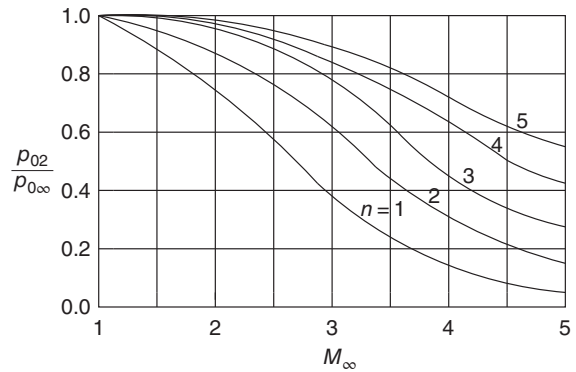
Oswatitsch [16] showed that, for such a system in two-dimensions, maximum shock pressure recovery is obtained when the oblique shocks are of equal strength. This means that Mach numbers perpendicular to the shocks are equal, that is

$$M_1 \sin \beta_1 = M_2 \sin \beta_2 = \dots = M_{n-1} \sin \beta_{n-1}$$

**Figure 11.28** Schematic of  $(n - 1)$  oblique shocks for Oswatitsch optimization.



**Figure 11.29** Shock pressure recovery for optimum arrangement of two-dimensional shocks.



This method of optimization is complex. But Hermann [17] has simplified the procedure. He pointed out that the Mach number ahead of the normal shock,  $M_{1n}$  cannot be included in the equality of Eq. (11.30). Numerical evaluation provides the approximate result that

$$M_{1n} \approx 0.94 M_1 \sin \beta_1$$

in a range of  $M_1$  from 1.5 to 5.0 for  $n = 2, 3$ , or 4. The method for evaluating an optimum arrangement is indirect. That is, a value for  $M_{1n}$  has to be assumed, from which a value of  $M_\infty$  can be determined using the functional relationship for pressure recovery. A value of  $\beta_1$  follows, hence the first wedge angle  $\delta_1$ , and then the rest of the geometry, Mach numbers, and pressure ratios. For this procedure, iteration is necessary to arrive at the required value of the freestream Mach number  $M_\infty$ .

Optimum shock pressure recovery as a function of freestream Mach number for two-dimensional systems with up to five shocks is given in Figure 11.29. In general, up to about Mach 2, equal deflections give the best results. For higher Mach numbers, the first deflection has to be the smallest and the last the largest for best results.

For axisymmetric intakes, optimum shock systems may be determined by graphical methods. Details of design criteria for axisymmetric intake can be found in [18].

### 11.13 Isentropic Compression

Isentropic compression is the limiting case of a multi-shock compression scheme. In isentropic compression the pressure recovery is achieved through a large number of weak shocks, also

termed *isentropic compression waves*. For isentropic compression the forebody should have a smooth contour to generate an infinitely large number of weak oblique shocks of infinitesimal strength throughout its length, as shown in Figure 11.30. These waves compress the supersonic stream isentropically, that is without any loss of total pressure. In a two-dimensional flow, for a continuous system of zero-strength shocks, or characteristic lines, the process is the reverse of a Prandtl–Meyer expansion flow around a sharp corner and the profile required for this process can be calculated by assuming the profile as a streamline of the Prandtl–Meyer flow. In  $(r, \phi)$  coordinates, the profile is obtained from the relations [13]

$$\frac{x}{r_0} = \frac{r}{r_0} \cos(\mu - \nu)$$

and

$$\frac{y}{r_0} = \frac{r}{r_0} \sin(\mu - \nu)$$

where  $x$  and  $y$  are the axial and transverse coordinates in Cartesian coordinates,  $\mu$  is the Mach angle,  $\nu$  is the Prandtl–Meyer function.

Also, we have

$$\nu = \phi + \mu - \frac{\pi}{2}$$

and

$$\phi = \frac{1}{k} \tan^{-1}(k\sqrt{M^2 - 1})$$

where

$$k = \sqrt{\frac{\gamma - 1}{\gamma + 1}}$$

Profiles calculated on this basis have been tabulated by Connors and Meyer for Mach numbers up to 4.0 [18]. In practice, the leading edge of a forebody inevitably has a finite (non-zero) thickness or angle, thus a shock of finite strength is generated there, Connors and Meyer's calculations assume 1% loss of total pressure for this initial shock.

Axisymmetric center body calculations are more involved, as the characteristic lines are not straight and the flow conditions are not constant. Connors and Meyer's method suggests that an initial characteristic line is determined from the known flow field generated by a conical nose considering 1% pressure loss, as in the case of a two-dimensional wedge flow, and at the focal

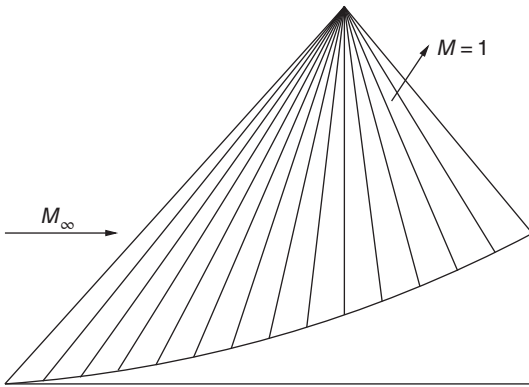
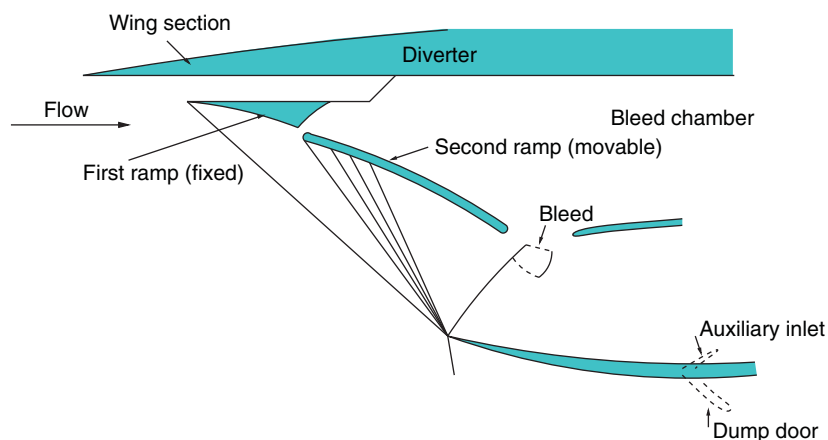


Figure 11.30 Isentropic compression.



**Figure 11.31** Aerodynamic features of Concorde intake.

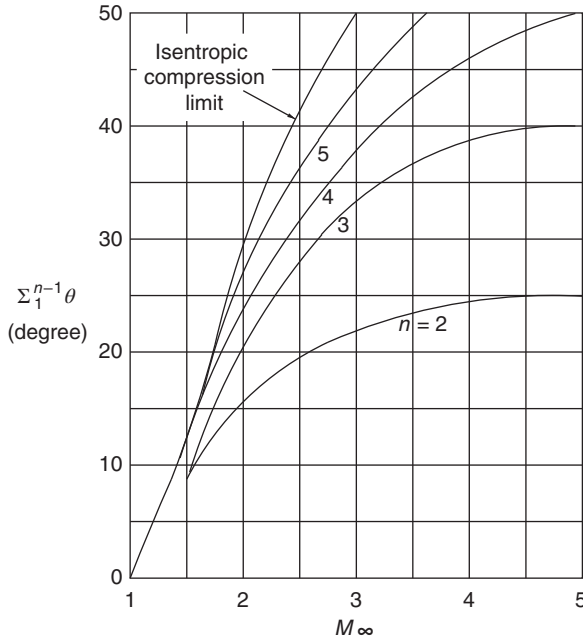
point of the characteristic two-dimensional reverse Prandtl–Meyer relations are assumed. With these two conditions the isentropic flow field is calculated using the method of characteristics for potential flow with axial symmetry. Streamlines of the flow are traced by applying continuity considerations, and hence the surface contour is determined.

Theoretically, it is possible to decelerate the flow all the way down to sonic speed, using isentropic compression. But, in practice, such fully isentropic compression is not possible, owing to compatibility conditions imposed by other parts of the flow. In practice, the supersonic compression is always terminated with a strong shock at low supersonic Mach numbers. This implies that the use of isentropic compression is restricted to intermediate stages, as in the second wedge of a multi-shock system. In such a context, isentropic compression can be both practical and useful and it has been adopted in practice for a number of aircraft requiring high intake performance. The Concorde aircraft intake shown in Figure 11.31 is an example of intake with isentropic compression. As can be seen in the figure, at the design operation, the oblique shock from the nose of the first ramp and the compression waves from the second ramp will meet at the lip of the bottom wall. But at off-design conditions it is possible to adjust second ramp orientation and control the oblique shock from the first ramp and the compression waves from the second ramp to meet at the lip of the bottom wall, as in the case of design operation. However, it is essential to note that, even though in principle it is possible to achieve this kind of wave manipulation to resemble the design operation, in actual situations making the compression waves from the first and second ramps to meet at the lip of the bottom wall is practically impossible. Therefore, the variable second ramp can at best be taken as a mechanism to reduce the pressure loss by generating continuous compression.

## 11.14 Limits of External Compression

We know that, in passing through the compression system generated by the forebody (whether isentropic or in discrete shocks), the flow is turned away from the intake axis. Therefore, at the intake entry the flow is not parallel to the intake axis but at an inclination corresponding to the total turning angle. Now, the flow has to be turned back to the axial direction within the





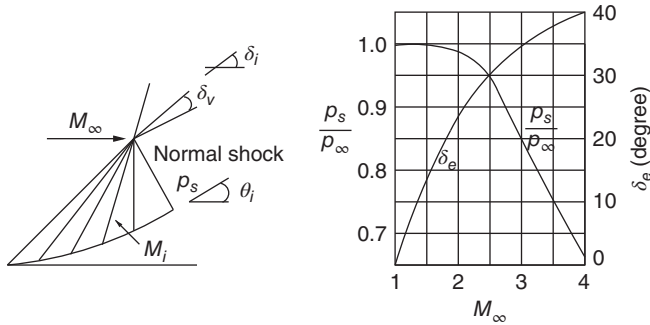
**Figure 11.32** Flow turning angle for optimum two-dimensional shock.

subsonic diffuser. For an efficient compression system the turning angles can be quite large. For optimum multi-shock systems causing complete isentropic compression, the total turning angle as a function of freestream Mach number is shown in Figure 11.32. As can be seen in Figure 11.32, the number of compression waves  $n$  required for a desired turning angle  $\theta$  increases steeply with flight Mach number  $M_\infty$ . This is because, as we saw in Chapter 4, a compression wave can be regarded as isentropic when the flow turning angle  $\Delta\theta$  caused by the wave is small, since the entropy increase due to the wave is proportional to  $\Delta\theta^3$ . Therefore,  $\Delta\theta$  should be kept as low as possible to achieve compressions which can be regarded as isentropic, resulting in very low pressure loss. For this the  $n$ , which represents the number of compression waves (that is the number of turnings on the ramp), has to be large. At this stage it is essential to realize that in devices such as supersonic intakes we need to consider the losses due to skin friction along with the pressure loss. Thus, even though  $n \rightarrow \infty$  would result in completely isentropic compression, leading to insignificant pressure loss, this would require a ramp of very large length, causing severe skin friction drag. Therefore, in the design it is necessary to strike a balance between  $\Delta\theta$  and the ramp length, which will result in significant minimization of pressure loss, without causing severe skin friction drag.

For isentropic compression, the full angle of turn is given explicitly by the Prandtl–Meyer function  $\nu$ , as

$$\nu = \sqrt{\frac{\gamma+1}{\gamma-1}} \arctan \sqrt{\frac{\gamma+1}{\gamma-1}(M^2-1)} - \arctan(M^2-1)$$

Unlike the multi-shock systems, there is no terminal strong shock in the isentropic compression. Therefore, the flow turning angle corresponds to a sector of the Prandtl–Meyer curve lying between the initial and final Mach number of the isentropic compression system. Realization of an efficient compression through a large turning angle depends on factors involving either the *external stream* around the cowl or conditions of the *internal flow* immediately within the duct entry.



**Figure 11.33** Cowl external angle limit for shock attachment and corresponding maximum pressure recovery with isentropic compression.

## 11.15 External Shock Attachment

An efficient external compression can be achieved when the shock formed by coalescing the isentropic compression waves generated at the surface of the center-body attaches with the inlet lip. If the duct inner surface (continuation of the forebody) is aligned so as to maintain a constant cross-sectional area (that is the surface of the wedge center-body and the inner surface of the cowl are parallel), a normal shock will sit across the entry and flow in the duct will become wholly subsonic. To achieve this the shock wave generated by the cowl in the external flow (that is outside the capture streamtube) must be attached to the lip. If the shock is detached, it will modify the nature of the compression system and increase the cowl external drag. The external angle of the cowl, therefore, should not exceed the minimum required for shock attachment at a given freestream Mach number. The shock attachment criterion can in all cases be taken to be that for a two-dimensional flow, since the flow locally at the cowl lip is effectively two-dimensional even for three-dimensional geometries of the inlet. The limit angle (external flow) is given in Figure 11.33.

The shock attachment criterion is relevant to all forms of forebody compression. For isentropic compression, the limiting pressure recovery can be calculated easily. The flow turning angle  $\theta_i$  is given by

$$\theta_i = \nu_\infty - \nu_i$$

where  $\nu_\infty$  is the Prandtl–Meyer function of the freestream flow at  $M_\infty$  and  $\nu_i$  is the Prandtl–Meyer function for the entry Mach number  $M_i$ . It is evident from this relation that the maximum pressure recovery is for minimum  $\nu_i$  ( $\approx 0$ ) with the inlet Mach number just above unity ( $M_i \approx 1$ ). The plot of  $p_s/p_\infty$ , with  $p_s/p_\infty$  calculated for two-dimensional isentropic compression with normal shock at the inlet and cowl vertex angle ( $\delta_v$ )  $3^\circ$ , variation with Mach number illustrates that the pressure recovery is maximum at  $M_\infty = 1$ .

## 11.16 Internal Shock Attachment

If the initial part of the duct is designed without internal contraction, as shown in Figure 11.34a, an attached normal shock will be generated at the critical operation. For supercritical and highly supercritical operation, the waves will be as shown in Figure 11.34b and c (in these sketches the expansion fan from the forebody is not considered). Designing the duct this way, the turning

angle of the forebody has to be increased to a value at which the internal oblique shock at the cowl lip is on the point of detachment.

In principle the cowl angle can be set to any value below the maximum angle required for external shock attachment. But in practice, a forebody angle larger than a cowl angle results in complications. The normal-shock pressure recovery would fall rapidly with a decrease of cowl internal angle, but a lower cowl angle implies a lower cowl drag. Therefore, the design has to optimize between pressure recovery and cowl drag.

## 11.17 Pressure Loss

In our discussions on Fanno and Rayleigh flows in Chapter 8, we saw that both friction and stagnation temperature change would cause significant total pressure loss to flow in a constant area duct. The ramjet combustion chamber is a typical device involving both Fanno and Rayleigh processes. In addition to these causes, the flameholder, which is essential for stable combustion, also causes some pressure loss due to the drag it offers. Therefore, the pressure loss caused by the flame-holder also has to be accounted for. These contributions to the pressure loss can be related to the upstream flow Mach number  $M_2$  and the total temperature rise, by considering the flow in the ramjet burner zone as one-dimensional, as illustrated in Figure 11.35.

As shown in Figure 11.35, the flow at the inlet and exit of the combustion chamber is assumed to be at uniform velocity and temperature. That is, any flow through the porous side walls of the combustion chamber is not accounted for in the analysis.

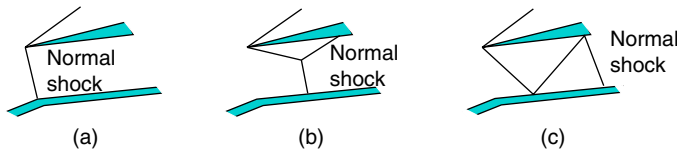
The drag  $D$  due to the flameholders will be proportional to the inlet dynamic pressure  $\frac{1}{2}\rho_2 u_2^2$ . Therefore, the momentum equation for the burner can be expressed as

$$(p_2 - p_4)A - D = \dot{m}_4 u_4^2 - \dot{m}_2 u_2^2$$

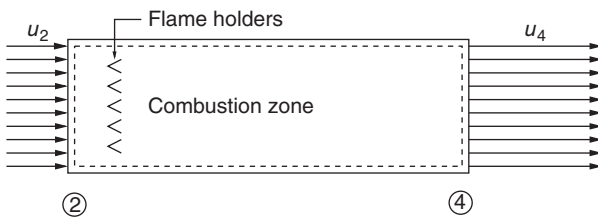
where  $A$  is the cross-sectional area of the burner.

Also, the drag can be expressed as

$$D = c \frac{1}{2} \rho_2 u_2^2$$



**Figure 11.34** Waves at the entry of a duct without internal contraction: (a) critical operation, (b) supercritical operation, and (c) highly supercritical operation.



**Figure 11.35** Simplified one-dimensional model of a ramjet burner.

where  $c$  is the proportionality constant, which can be taken as the ratio of the pressure drop due to friction to the upstream dynamic pressure. Now, substituting for drag in the momentum equation, we get

$$(p_2 - p_4)A - c \frac{1}{2} \rho_2 u_2^2 = \rho_4 A u_4^2 - \rho_2 A u_2^2$$

$$p_2 - p_4 = \rho_4 u_4^2 - \rho_2 u_2^2 + \frac{c}{A} \frac{1}{2} \rho_2 u_2^2$$

We can express  $\rho_4 u_4^2$  as

$$\rho_4 u_4^2 = \frac{p_4}{RT_4} u_4^2 = \frac{\gamma_4 p_4}{\gamma_4 RT_4} u_4^2$$

$$= \gamma_4 p_4 \frac{u_4^2}{a_4^2} = \gamma_4 p_4 M_4^2$$

Similarly,

$$\rho_2 u_2^2 = \gamma_2 p_2 M_2^2$$

Now, assuming  $\gamma_4 = \gamma_2 = \gamma$ , the momentum equation can be expressed as

$$p_2 - p_4 = \gamma p_4 M_4^2 - \gamma p_2 M_2^2 + k \gamma p_2 M_2^2$$

where  $k = \frac{c}{A}$ . This equation can be arranged as

$$\frac{p_2}{p_4} = 1 + \gamma M_4^2 - \gamma M_2^2 \frac{p_2}{p_4} + k \frac{\gamma M_2^2}{2} \frac{p_2}{p_4}$$

$$= 1 + \gamma M_4^2 + \frac{p_2}{p_4} \gamma M_2^2 \left( \frac{k}{2} - 1 \right)$$

$$\frac{p_2}{p_4} \left( 1 + \gamma M_2^2 \left( 1 - \frac{k}{2} \right) \right) = 1 + \gamma M_4^2$$

or

$$\frac{p_2}{p_4} = \frac{1 + \gamma M_4^2}{1 + \gamma M_2^2 \left( 1 - \frac{k}{2} \right)} \quad (11.32)$$

By Eq. (8.37), we have

$$\frac{p_{04}}{p_{02}} = \frac{p_4}{p_2} \frac{\left( 1 + \frac{\gamma-1}{2} M_4^2 \right)^{\gamma/(\gamma-1)}}{\left( 1 + \frac{\gamma-1}{2} M_2^2 \right)^{\gamma/(\gamma-1)}}$$

Substituting for  $p_4/p_2$  from Eq. (11.32), we get

$$\frac{p_{04}}{p_{02}} = \frac{1 + \gamma M_2^2 \left( 1 - \frac{k}{2} \right) \left( 1 + \frac{\gamma-1}{2} M_4^2 \right)^{\gamma/(\gamma-1)}}{1 + \gamma M_4^2 \left( 1 + \frac{\gamma-1}{2} M_2^2 \right)^{\gamma/(\gamma-1)}} \quad (11.33)$$

The fuel flow rate  $\dot{m}_f$  to the burner is much smaller than the air mass flow rate  $\dot{m}_2$  ( $\dot{m}_f \ll \dot{m}_2$ ). Therefore, we can take  $\dot{m}_4$  to be approximately equal to  $\dot{m}_2$  ( $\dot{m}_4 \approx \dot{m}_2$ ), and

$$\rho_4 u_4 = \rho_2 u_2 \quad (11.34)$$

By the thermal state equation we have  $p = \rho RT$ . Therefore, Eq. (11.34) becomes

$$\frac{p_2}{p_4} = \frac{u_4}{u_2} \frac{T_2}{T_4} = \frac{M_4}{M_2} \sqrt{\frac{T_2}{T_4}} \quad (11.35)$$

By isentropic relation, we have the temperature ratio  $T_2/T_4$  as

$$\frac{T_2}{T_4} = \frac{T_{02}}{T_{04}} \frac{\left(1 + \frac{\gamma-1}{2} M_4^2\right)}{\left(1 + \frac{\gamma-1}{2} M_2^2\right)}$$

Substituting this into Eq. (11.35), we get

$$\frac{p_2}{p_4} = \frac{M_4}{M_2} \sqrt{\frac{T_{02}}{T_{04}} \frac{\left(1 + \frac{\gamma-1}{2} M_4^2\right)}{\left(1 + \frac{\gamma-1}{2} M_2^2\right)}} \quad (11.36)$$

Now, equating the right-hand sides of Eqs. (11.32) and (11.36), we get

$$\frac{T_{02}}{T_{04}} = \frac{M_4^2 \left(1 + \frac{\gamma-1}{2} M_4^2\right)}{M_2^2 \left(1 + \frac{\gamma-1}{2} M_2^2\right)} \frac{\left(1 + \gamma M_2^2 \left(1 - \frac{k}{2}\right)\right)^2}{(1 + \gamma M_4^2)^2} \quad (11.37)$$

In Chapter 8, we saw that both friction and  $T_0$  change would accelerate a subsonic flow to the limiting maximum of  $M_4 = 1$ . Therefore, for a given burner with a known value of  $k$ , it is possible to identify the value of  $M_2$  to result in the desired value of  $T_{04}/T_{02}$ , by substituting  $M_4 = 1$  in Eq. (11.37).

It is important to realize that the above analysis is with the simple burner model of constant cross-sectional area. If the cross-sectional area of the burner were to increase in the flow direction, the inlet Mach number  $M_2$  will change and thus would result in the increase of the overall cross-sectional area of the engine.

### Example 11.1

A two-dimensional diffuser is to be designed for a ramjet to fly at Mach 2.2. At the design Mach number an oblique shock has to be attached to the vertex of the wedge, and a normal shock at the inlet lip of the diffuser. Determine (a) the wedge angle for obtaining the maximum possible pressure recovery and (b) the maximum total pressure ratio across the oblique shock attached to the wedge.

#### Solution:

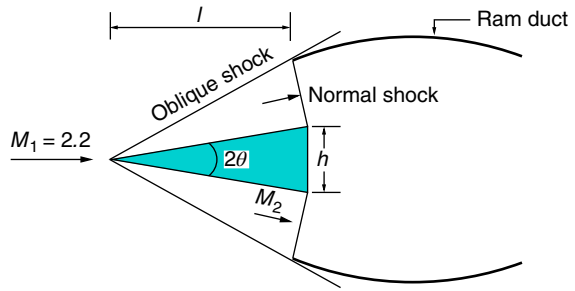
(a) The flow field with oblique shocks attached to the vertex of the wedge and normal shocks at the lip of the ramjet duct are shown in Figure 11.36.

For  $M_1 = 2.2$ , from Table A.1, the isentropic table,

$$\frac{A_1}{A_1^*} = 2.005$$

The pressure loss across the normal shock at the ramjet lip will be minimal if  $M_2 \approx 1$ .

**Figure 11.36** Flow past a ramjet wedge.



For  $M_2 = 1$ , from the isentropic table,

$$\frac{A_2}{A_2^*} = 1.00$$

Therefore,

$$\frac{A_1}{A_1^*} - \frac{A_2}{A_2^*} = h$$

$$2.005 - 1 = h$$

$$h = 1.005$$

Assuming  $l$  to be equal to unity, we have

$$\tan 2\theta = 1.005$$

This gives

$$2\theta = \tan^{-1}(1.005)$$

$$= 45.14^\circ$$

- (b) For  $M_1 = 2.2$  and  $\theta = 22.57^\circ$ , from the oblique shock chart 1 (Figure A.1 in the Appendix), we have the shock angle as  $\beta = 52^\circ$ .

Therefore, the Mach number normal to oblique shock is

$$\begin{aligned} M_{1n} &= M_1 \sin \beta \\ &= 2.2 \times \sin 52^\circ \\ &= 1.73 \end{aligned}$$

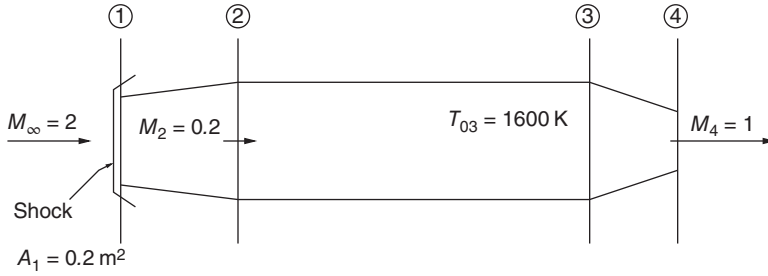
For  $M_{1n} = 1.73$ , from the normal shock table (Table A.2),

$$\frac{p_{02}}{p_{01}} = 0.843$$

That is, the pressure recovery is 84.3%.

### Example 11.2

The ramjet, shown in Figure 11.37, is designed to operate at Mach 2 at 6000 m altitude. At the design point, the Mach number of air entering the combustion chamber is 0.2 and the total temperature of the combustion gas entering the exhaust nozzle is 1600 K. The calorific value of the fuel is  $20\,000 \text{ kJ kg}^{-1}$  and the combustion efficiency is 1.0. At the design operation the exhaust nozzle is choked. Neglecting the weight of the fuel, assuming the flow inside the ramjet to be frictionless and the specific heats ratio for both the air and the combustion gas to be 1.4,



**Figure 11.37** A ramjet engine.

determine (a) the cross-sectional area of the combustion chamber  $A_2$ , (b) the area ratio of the exhaust nozzle  $A_3/A_4$ , (c) the mass flow rate of air, (d) the ratio of total pressure at the nozzle entry to freestream static pressure ( $p_{03}/p_\infty$ ), (e) the jet velocity  $u_e$ , (f) the fuel flow rate and the specific thrust, (g) the overall efficiency, (h) the TSFC, and (i) the propulsive and thermal efficiencies.

**Solution:**

(a) At 6000 m altitude, from the gas tables in [3],

$$p_\infty = 47.2 \text{ kPa}, \quad T_\infty = 249.15 \text{ K}, \quad \rho = 0.660 \text{ kg m}^{-3}$$

For  $M_\infty = 2$ , from the isentropic table (Table A.1),

$$\frac{p_\infty}{p_{0\infty}} = 0.1278, \quad \frac{T_\infty}{T_{0\infty}} = 0.5556, \quad \frac{A_\infty}{A^*} = 1.688$$

For  $M_\infty = 2$ , from the normal shock table (Table A.2),

$$M_1 = 0.58, \quad \frac{p_1}{p_\infty} = 4.5.$$

For  $M_1 = 0.58$ , from the isentropic table,

$$\frac{A_1}{A^*} = 1.213, \quad \frac{p_1}{p_{01}} = 0.7962$$

For  $M_2 = 0.2$ , from the isentropic table,

$$\frac{A_2}{A^*} = 2.964, \quad \frac{T_2}{T_{02}} = 0.9921$$

Therefore,

$$\begin{aligned} \frac{A_2}{A_1} &= \frac{A_2/A^*}{A_1/A^*} \\ &= \frac{2.964}{1.213} \\ &= 2.444 \end{aligned}$$

$$\begin{aligned} A_2 &= 2.444 \times A_1 \\ &= 2.444 \times 0.2 \\ &= \boxed{0.489 \text{ m}^2} \end{aligned}$$

(b) Flow through the ram duct is friction free; therefore,

$$\begin{aligned} T_{02} &= T_{0\infty} = \frac{T_{\infty}}{0.5556} \\ &= \frac{249.15}{0.5556} \\ &= 448.43 \text{ K} \end{aligned}$$

The flow from 2 to 3 is a Rayleigh flow. Therefore,

$$\frac{T_{03}}{T_0^*} = \frac{T_{03}}{T_{02}} \times \frac{T_{02}}{T_0^*}$$

From the Rayleigh flow table (Table A.5), for  $M_2 = 0.2$ ,  $\frac{T_{02}}{T_0^*} = 0.1735$ .

$$\begin{aligned} \frac{T_{03}}{T_0^*} &= \frac{1600}{448.43} \times 0.1735 \\ &= 0.619 \end{aligned}$$

For  $\frac{T_{03}}{T_0^*} = 0.619$ , from the Rayleigh flow table,  $M_3 \approx 0.45$ .

From the isentropic table, for  $M_3 = 0.45$ ,  $\frac{A_3}{A^*} = 1.45$ , and for  $M_4 = 1$ ,  $\frac{A_4}{A^*} = 1$ . Hence,

$$\begin{aligned} \frac{A_3}{A_4} &= \frac{A_3}{A^*} \times \frac{A^*}{A_4} \\ &= 1.45 \times 1 \\ &= \boxed{1.45} \end{aligned}$$

(c) The mass flow rate is

$$\dot{m} = \rho_{\infty} A_{\infty} V_{\infty}$$

The velocity  $V_{\infty}$  is

$$\begin{aligned} V_{\infty} &= M_{\infty} a_{\infty} \\ &= M_{\infty} \times \sqrt{\gamma R T_{\infty}} \\ &= 2 \times \sqrt{1.4 \times 287 \times 249.15} \\ &= 632.8 \text{ m s}^{-1} \end{aligned}$$

Therefore,

$$\begin{aligned} \dot{m} &= 0.660 \times 0.2 \times 632.8 \\ &= \boxed{83.53 \text{ kg s}^{-1}} \end{aligned}$$

(d) The pressure ratio  $\frac{p_{03}}{p_{\infty}}$  can be expressed as

$$\frac{p_{03}}{p_{\infty}} = \frac{p_{03}}{p_{02}} \times \frac{p_{02}}{p_{0\infty}} \times \frac{p_{0\infty}}{p_{\infty}}$$

For  $M_{\infty} = 2$ , from the isentropic table,  $\frac{p_{0\infty}}{p_{\infty}} = \frac{1}{0.1278}$ , and from the normal shock table,  $\frac{p_{01}}{p_{0\infty}} = 0.7209$ .



There is no pressure loss from 1 to 2; therefore,

$$\frac{p_{02}}{p_{0\infty}} = \frac{p_{01}}{p_{0\infty}}$$

For the Rayleigh flow table, for  $M_3 = 0.45$ ,  $\frac{p_{03}}{p_0^*} = 1.135$ , and for  $M_3 = 0.2$ ,  $\frac{p_{02}}{p_0^*} = 1.235$ . Thus,

$$\begin{aligned} \frac{p_{03}}{p_{02}} &= \frac{p_{03}/p_0^*}{p_{02}/p_0^*} \\ &= \frac{1.135}{1.235} \\ &= 0.919 \end{aligned}$$

Hence,

$$\begin{aligned} \frac{p_{03}}{p_{\infty}} &= 0.919 \times 0.7209 \times \frac{1}{0.1278} \\ &= \boxed{5.18} \end{aligned}$$

(e) By Eq. (11.3), the exit velocity is

$$u_e = \sqrt{\frac{T_{04}}{T_{0\infty}}} \times u$$

where  $u$  is the freestream velocity,

$$\begin{aligned} u &= M_{\infty} a_{\infty} \\ &= 2 \times \sqrt{1.4 \times 287 \times 249.15} \\ &= 632.8 \text{ m s}^{-1} \end{aligned}$$

Therefore,

$$\begin{aligned} u_e &= \sqrt{\frac{1600}{448.43}} \times 632.8 \\ &= \boxed{1195.30 \text{ m s}^{-1}} \end{aligned}$$

(f) By Eq. (11.5)

$$\begin{aligned} f &= \frac{(T_{03}/T_{0\infty}) - 1}{Q_R/(c_p T_{0\infty}) - T_{03}/T_{0\infty}} \\ &= \frac{(1600/448.43) - 1}{20000/(1.0045 \times 448.43) - 1600/448.43} \\ &= \frac{2.568}{44.4 - 3.568} \\ &= 0.063 \end{aligned}$$

Therefore, the fuel flow rate is

$$\begin{aligned} \dot{m}_f &= f \times \dot{m} \\ &= 0.063 \times 83.53 \\ &= \boxed{5.26 \text{ kg s}^{-1}} \end{aligned}$$

The specific thrust is

$$\begin{aligned}
 \frac{\text{Th}}{\dot{m}} &= (1 + f)u_e - u \\
 &= (1 + 0.063) \times 1195.30 - 632.8 \\
 &= 1.063 \times 1195.30 - 632.8 \\
 &= 637.8 \text{ N s kg}^{-1} \\
 &= \boxed{0.6378 \text{ kN s kg}^{-1}}
 \end{aligned}$$

(g) The overall efficiency is

$$\begin{aligned}
 \eta_o &= \frac{\text{Th} \times u}{\dot{m}_f \times Q_R} \\
 &= \frac{(\text{Th}/\dot{m}) \times u}{(\dot{m}_f/\dot{m}) \times Q_R} \\
 &= \frac{637.8 \times 632.8}{0.063 \times (20000 \times 10^3)} \\
 &= \boxed{0.32}
 \end{aligned}$$

(h) The TSFC is

$$\begin{aligned}
 \text{TFSC} &= \frac{f}{\text{Th}/\dot{m}} \\
 &= \frac{0.063}{0.6378} \\
 &= \boxed{0.0988 \text{ kg (s kN)}^{-1}} \\
 &= 3.6 \times 0.0988 \\
 &= \boxed{0.3557 \text{ kg (hr N)}^{-1}}
 \end{aligned}$$

(i) The propulsive efficiency is

$$\begin{aligned}
 \eta_p &= \frac{\text{Th} \times u}{\dot{m}[(1 + f)(u_e^2/2) - u^2/2]} \\
 &= \frac{(\text{Th}/\dot{m}) \times u}{[(1 + f)(u_e^2/2) - u^2/2]} \\
 &= \frac{637.8 \times 632.8}{[(1 + 0.063) \times (1195.3^2/2) - 632.8^2/2]} \\
 &= \frac{403599.84}{559158.50} \\
 &= \boxed{0.72}
 \end{aligned}$$

The thermal efficiency is

$$\begin{aligned}
 \eta_{th} &= \frac{\dot{m}[(1+f)(u_e^2/2) - u^2/2]}{\dot{m}_f Q_R} \\
 &= \frac{[(1+f)(u_e^2/2) - u^2/2]}{(\dot{m}_f/\dot{m})Q_R} \\
 &= \frac{(1+0.063) \times (1195.3^2/2) - 632.8^2/2}{0.063 \times (20000 \times 10^3)} \\
 &= \boxed{0.444}
 \end{aligned}$$

## 11.18 Supersonic Combustion

We saw in Chapter 4 that the pressure loss associated with the deceleration of a supersonic or hypersonic stream through shocks can be severe. Because of this, the losses involved in subsonic ramjet combustor can be substantial. Furthermore, if the ramjet has to be used for hypersonic flight, in addition to the losses caused by the shocks in decelerating the flow, the temperature at the combustor entrance will become extremely high. This resultant high temperature, caused by the deceleration, in addition to making vehicle cooling difficult, leads to the dissociation of oxygen and nitrogen in the air stream, which will result in severe combustion loss. For hypersonic flights with a Mach number greater than 8, the temperature of air entering the combustion chamber becomes quite large and a strong function of pressure. This high pressure proves to be an advantage because the dissociation of the mixture in the combustion chamber at high temperatures is retarded by the high pressure. Furthermore, the temperature of the combustion product also becomes pressure dependent. It has been found that, for Mach 10 flight and a combustion pressure of 10 atm, there is no temperature rise due to combustion because at this condition all the combustion energy is absorbed by dissociation [12]. Indeed, at a sufficiently high Mach number, the temperature of the combustion products can be lower than that of the incoming air. The low speed at which the fuel and air can be converted into dissociation products may show that there is sufficient residence time in the combustion chamber to approach equilibrium composition. But once the combustion products enter the nozzle, because of the fast expansion encountered in the nozzle, there is no possibility of the mixture's approaching equilibrium composition at any location in the nozzle. Indeed, in practical situations the expansion in the nozzle is quite rapid for the composition of the combustion products to readjust, after each step of the temperature and pressure reduction, to a new equilibrium composition. When the expansion in the nozzle is extremely rapid, the mixture may be effectively *frozen* with the initial high-temperature composition. This clearly reveals that, at flight Mach numbers of order 10, only an insignificant amount of combustion energy of the fuel would be available for the acceleration of the combustion products to generate thrust. It is important to note that because of the rapid acceleration encountered, the combustion products at high temperature will experience a significant decrease of temperature. This rapid decrease of temperature will result in the recombination of the dissociated products. The chemical kinetics of the recombination process in the nozzle, in general, will have a strong influence on the thrust and propulsive efficiency of the ramjet engine.

The concept of SCRAMJET is considered a means to avoid or minimize this dissociation loss and the pressure loss associated with the deceleration of supersonic or hypersonic incoming

stream to subsonic level, through compression waves, before entering the combustion chamber. With supersonic combustion, the product temperatures are relatively low and, because of this, dissociation loss decreases since the dissociation depends on the static temperature rather than the stagnation temperature. However, the wall heat transfer depends mainly on the stagnation temperature, and thus the wall-cooling problem is not eased by employing supersonic combustion. The cooling caused by liquid hydrogen on its path from the fuel tank to the engine has been envisaged as a means to keep the engine and vehicle cool enough to survive the period of hypersonic flight.

Supersonic combustion demands that the fuel be injected and mixed with the oxidizer (usually air) flowing at a supersonic speed. The air stream enters the combustor at supersonic speed. Hydrogen fuel in a gaseous state is injected at an angle to the airflow direction. The combined perturbation of fuel injection, fuel air mixing, and combustion results in a complex shock pattern. In hypersonic missile programs the aim is to establish supersonic combustion with kerosene as the fuel. In this conceptual engine the hypersonic air stream decelerated in the intake enters the combustor at a supersonic Mach number of about 2. The kerosene is injected into this supersonic stream as tiny droplets. These droplets will position a bow shock ahead of them. Also, these droplets would vaporize rapidly. Therefore, the detached shock ahead of a droplet will undergo a rapid change in its shape and strength. There are a large number of droplets in the combustor. We know that a shock causes a significant increase of entropy and thus the shocks in the combustor cause a large increase of entropy of the fuel-air mixture. This increase of entropy will induce a thorough mixing of the fuel and air, leading to high combustion efficiency. However, the unsteadiness caused by the tremendous increase of entropy and the associated perturbation will be transmitted in the upstream direction. At this stage, we may wonder how perturbation can travel upstream in a supersonic stream. The answer to this is the following.

Even though the flow speed of the air-fuel mixture is supersonic in the combustor, at the wall of the chamber there is a boundary layer caused by the viscous effect. As we know, the boundary layer is that thin layer adjacent to a solid surface in which the flow velocity increases from zero to freestream level. Thus, there is a subsonic layer within the boundary layer. Through this subsonic layer, the perturbation due to entropy increase caused by the fuel-air mixing and the shocks at the fuel droplets can easily travel upstream and even reach the intake entrance. If the disturbances are severe, on reaching the intake entrance they can disturb the flow to such an extent that they cause breakdown of the flow through the intake. When this happens, the combustion in the combustor will stop and the consequence will be disastrous. Therefore, it is essential to prevent the upstream propagation of the perturbation in the combustor in the upstream direction. To ensure this, it is usual practice to position a constant area duct between the intake exit and the combustor inlet, in which a series of oblique shocks will be positioned. These oblique shocks are usually weak shocks so that they will not cause any significant pressure loss. But these shocks will cause a considerable increase of static pressure of the air stream entering the combustor, which is an advantage for the combustor performance. Essentially, the interaction of these shocks with the boundary layer at the wall of the parallel duct and the complex wave pattern established due to this shock-boundary layer interaction prevents the upstream propagation of the perturbation from the combustor. Thus, the constant area duct essentially isolates the intake from getting disturbed by the instabilities from the combustor and hence is called an *isolator*. The oblique shock system in the isolator is referred to as an *oblique shock-train* or simply as a *shock-train*.

The isolator has to be carefully designed to accommodate a shock-train which will prevent combustion-induced perturbations from seriously distorting the flow in the inlet without causing any other adverse effect. Especially, the pressure rise caused by the shock-train has to be kept within the limit so that it will not cause separation of the incoming boundary layer. Because of the advantages envisaged, active research is being carried out in many countries to establish supersonic combustion. Once developed, this supersonic combustion technology will prove to be a boon to propulsive efficiency of engines meant for supersonic and hypersonic flights.

## 11.19 Summary

Ramjet is a simple air-breathing engine. It consists of a diffuser, a combustion chamber, and an exhaust nozzle. The incoming air at high flight speed is decelerated to a low velocity by the shock system at the intake and the ramming action inside the duct from just downstream of the inlet to the combustion chamber entrance. Since the supersonic flow stream entering the intake has to be decelerated to about Mach 0.2–0.3 before entry to the combustion chamber, the pressure rise can be substantial.

The thrust generated can be expressed as

$$Th = \dot{m}u_e + (p_e - p_\infty)A_e$$

A part of this thrust is applied to overcome the shear force acting over the internal surface of the engine.

A ramjet designed with simplified thermodynamic analysis is termed an *ideal ramjet*. It is essentially a hypothetical engine with a simplified process cycles involving an isentropic process.

- The compression and expansion processes in the engine are reversible and adiabatic.
- The combustion process takes place at constant pressure.

Even though these assumptions are not realistic, they simplify the analysis of the processes in the ideal ramjet engine.

The TSFC is defined as

$$TSFC = \frac{\dot{m}_f}{Th} = \frac{f}{Th/\dot{m}_\infty}$$

where  $Th/\dot{m}_\infty$  is called *specific thrust* and  $f$  is the *fuel-air ratio*.

For a single propellant system the propulsive efficiency is

$$\eta_p = \frac{Th \times u}{\dot{m}_\infty[(1+f)(u_e^2/2) - u^2/2]}$$

The propulsive efficiency, defined as the ratio of the thrust power ( $Th \times u$ ) to the rate generation by the propellant kinetic energy, is a measure of the performance of a propulsion system.

The product of thrust and flight speed is termed *thrust power*. In general for air-breathing engines,  $f \ll 1$  and therefore may be ignored in the expression for  $\eta_p$  and in Eq. (11.1) without leading to significant error. Also, the pressure term in Eq. (11.1) is usually much smaller than the other two terms. Therefore, the thrust becomes

$$Th \approx \dot{m}_\infty(u_e - u)$$

Thus, the propulsive efficiency simplifies to

$$\begin{aligned}\eta_p &= \frac{(u_e - u)u}{u_e^2/2 - u^2/2} \\ &= \frac{2u/u_e}{1 + u/u_e}\end{aligned}$$

For a single propellant system the thermal efficiency is

$$\begin{aligned}\eta_{th} &= \frac{\text{Rate of addition of kinetic energy to the propellant}}{\text{Total energy consumption rate}} \\ &= \frac{\dot{m}_\infty((1+f)(u^2/2) - u^2/2)}{\dot{m}_f Q_R}\end{aligned}$$

where  $Q_R$  is the heat of reaction of the fuel.

The overall efficiency is the product of  $\eta_p \eta_{th}$ , i.e.

$$\eta_o = \eta_p \eta_{th} = \frac{Th \times u}{\dot{m}_f Q_R}$$

For air-breathing engines such as ramjet,  $f \ll 1$ . Therefore, replacing the propulsion efficiency by this expression in terms of  $u$  and  $u_e$ , we get

$$\eta_o = 2\eta_{th} \left( \frac{u/u_e}{1 + u/u_e} \right)$$

Unlike the ideal ramjet engine, the propellant in a real engine suffers stagnation pressure losses, owing to shock waves and wall friction, as it passes through the engine.

An air-breathing engine installed in an aircraft or a missile must be provided with an air intake and a ducting system. We know that for turbojet engines the air flow entering the compressor or fan must have a Mach number in the range of 0.4–0.7. Usually, the upper part of this range is suitable only for transonic compressors. For engines designed for subsonic cruise, say Mach 0.8, the inlet must act as a diffuser with a gradual diffusion from Mach 0.8 to 0.6. Usually, part of this deceleration occurs upstream of the inlet entrance.

- The inlet must be designed to operate without boundary layer separation, even when the air of the intake is not in the direction of the flow far upstream of the inlet.
- The stagnation pressure loss in the inlet must be small.
- The flow at the exit of the inlet should be uniform and unidirectional.

The inlet may have to operate over a wide range of freestream conditions, depending on the flight speed and mass flow requirements of the engine. The flow in the inlet essentially decelerates. In other words, the inlet duct acts as a diffuser.

In actual inlets flow separation can take place. Separation of the external flow will cause high nacelle drag. Inside the duct, separation may take place, depending on the duct geometry and operating conditions.

At the inlet lip the external flow gets accelerated to a high velocity, and accompanying low pressure can adversely affect the boundary layer in the following ways.

- When the entire flow is subsonic, if the low pressure region is followed by a region of rising pressure then the boundary layer may separate.
- When the flow around the inlet is partly supersonic, the local supersonic region will usually end abruptly in a shock, and the shock–wall interaction may cause boundary layer separation.

Boundary layer separation is undesirable and should be avoided, since it results in poor pressure recovery in the flow over the after portions of the aircraft or engine housing. This process results in a net rearward force, termed *drag on the body*.

For gas turbine engines the flow leaving the engine inlet system should be subsonic, even when they fly at supersonic speeds. This is because it is difficult to pass a fully supersonic stream through the compressor without excessive shock losses. Furthermore, the development of a fully supersonic compressor is still only at the research stage. Such a compressor would be of great benefit, because it could provide very high mass flow per unit area and very high pressure ratio per stage. At time of writing (2018), the Mach number of the axial flow approaching a subsonic compressor should be around 0.4 and for the transonic stage it should be about 0.6. Here the term *transonic* refers to the flow velocity relative to the blade tip and not to the entrance velocity.

The ramjet engine is free from the above-mentioned restriction, since it does not use a compressor. Also, in ramjets it is possible to have combustion in a supersonic stream without severe aerodynamic losses. The name SCRAMJET denotes the supersonic combustion ramjet, a concept that is under investigation for high flight Mach numbers.

We know that in the supersonic flow regime a decrease in the area of a duct will result in a deceleration of flow. This phenomenon is exploited in the form of the second throat in supersonic wind tunnels. To minimize the pressure loss it is usual practice to position the shock just downstream of the second throat where the Mach number is slightly greater than 1. The concept of using a convergent–divergent duct, which is usually referred to as a *nozzle* in supersonic flow studies, for decelerating supersonic flow to subsonic speeds is termed a *reverse nozzle diffuser* in inlet studies. The main difference between the second throat and reverse nozzle diffuser is that in the case of supersonic wind tunnel application there is no *aerodynamic duct* effect ahead of the diffusers, but in supersonic inlets there is an aerodynamic duct effect upstream of the diffuser.

In wind tunnel applications, we can see that the shock which is initially formed at the entry to the reversed-nozzle diffuser needs to be pushed to the second throat in order to minimize the pressure loss it causes. Shock movement is achieved either by increasing the operating stagnation pressure or by temporarily increasing the second throat area. In the case of inlet diffusers the positioning of the shock at the throat can be achieved by momentarily over-speeding the inlet air or by varying the diffuser geometry. The process of positioning the shock can be viewed as a problem independent of the boundary layer effect.

- The condition of maximum pressure recovery at maximum mass flow rate is termed the *critical point* or *critical operation*.
- Operation at a lower flow rate is called *subcritical operation*.
- Operation at the maximum flow rate but with a lower pressure recovery is termed *supercritical operation*.

The pitot intakes have the specific advantages of low drag and stable flow characteristics with good flow distribution.

The operating condition in which a detached shock is positioned ahead of the inlet and there is flow spillage is called *subcritical operation*. The operation where the shock is just at the inlet tip is called *critical operation* and the operation where the shock is swallowed is termed *supercritical operation*.

The concept of SCRAMJET is considered a means of avoiding or minimizing the dissociation loss and the pressure loss associated with the deceleration of supersonic or hypersonic incoming stream to a subsonic level, through compression waves, before entering the combustion chamber.

Supersonic combustion demands that the fuel is injected and mixed with the oxidizer (usually air) at a supersonic stream. The air stream enters the combustor at a supersonic speed. Hydrogen fuel in a gaseous state is injected at an angle to the airflow direction. The combined perturbation of fuel injection, fuel-air mixing, and combustion results in a complex shock pattern. In hypersonic missile programs the aim is to establish supersonic combustion with kerosene as the fuel. In this conceptual engine the hypersonic air stream decelerated in the intake enters the combustor at a supersonic Mach number of about 2. The kerosene is injected into this supersonic stream as tiny droplets. These droplets would position a bow shock ahead of them. Also, these droplets would vaporize rapidly. Therefore, the detached shock ahead of a droplet would undergo a rapid change in its shape and strength. There are a large number of droplets in the combustor. We know that a shock causes a significant increase of entropy and thus the shocks in the combustor cause a large increase of entropy in the fuel-air mixture. This increase of entropy would induce a thorough mixing of the fuel and air, leading to high combustion efficiency.

It is essential to prevent the upstream propagation of the perturbation in the combustor in the upstream direction. To ensure this, it is usual practice to position a constant area duct between the intake exit and the combustor inlet, in which a series of oblique shocks will be positioned. These oblique shocks usually are weak shocks so that they will not cause any significant pressure loss. But these shocks will cause a considerable increase of static pressure of the air stream entering the combustor, which is an advantage for the combustor performance. Essentially, the interaction of these shocks with the boundary layer at the wall of the parallel duct and the complex wave pattern established due to this shock–boundary layer interaction prevents the upstream propagation of the perturbation from the combustor. Thus, the constant area duct essentially isolates the intake from getting disturbed by the instabilities from the combustor and hence is called an *isolator*. The oblique shock system in the isolator is referred to as an *oblique shock-train* or simply as a *shock-train*.

## Exercise Problems

- 11.1 Calculate the minimum value of the ratio of the inlet height to the throat height of a two-dimensional convergent–divergent diffuser designed to start a Mach 2 supersonic air stream.  
[Answer: 1.217]
- 11.2 A ramjet flies at an altitude of 6900 m with a freestream Mach number of 2.2. If the propulsive efficiency is 0.6, find the nozzle exit velocity.  
[Answer:  $1604.98 \text{ ms}^{-1}$ ]
- 11.3 A ramjet flies at an altitude where the temperature is 200 K with a Mach number of 3.0. If the fuel-air ratio is 0.05 and the thermal efficiency is 0.5, find the heat addition due to combustion when the exit velocity is  $1400 \text{ ms}^{-1}$ . Also, find the overall efficiency  
[Answer: 26695.04 kJ, 38%]
- 11.4 A ramjet cruises at 6000 m at Mach 2.5. The fuel-air ratio to the combustion chamber is 0.055. If the total temperature difference between the entry and exit of the combustion chamber is 1250 K, (a) determine the HV of the fuel assuming the flow through the engine as adiabatic and the gas constant of the combustion product as the same as that



- of air and  $c_p = 1.005 \text{ kJ (kg K)}^{-1}$  for both air and combustion product. (b) If the flow through the nozzle is isentropic and correctly expanded, determine the exit velocity.  
[Answer: 24 660.6 kJ, 1421.51  $\text{ms}^{-1}$ ]
- 11.5** A ramjet of entrance diameter 0.2 m flies at 20 km altitude at a speed of 430  $\text{ms}^{-1}$ . The temperature at the nozzle entry is 1900 K. If the nozzle is correctly expanded, what would be (a) the thrust per unit mass of air and (b) the propulsive efficiency of the engine. Assume that the fuel-air ratio is very small compared to unity.  
[Answer: (a) 0.6375 kN s  $\text{kg}^{-1}$ , (b) 57.4%]
- 11.6** If the isentropic efficiency of a subsonic intake is 0.95, determine the pressure loss in the intake when the freestream flow of Mach number 0.9 and pressure 1 atm enters it.  
[Answer: 2.4%]
- 11.7** If the stagnation pressure ratio across a subsonic intake in a Mach 0.82 air stream is 0.9, determine the diffuser efficiency.  
[Answer: 74.4%]
- 11.8** An intake of an engine has inlet and maximum diameters of 0.2 m and 0.5 m, respectively. (a) If the freestream flow is at 230  $\text{ms}^{-1}$  280 K and 90 kPa what should be the required decrease in the flow speed at the intake entry to increase the thrust by 10%? (b) Find the velocity at the exit of the intake if the density there is 20% higher than the density at the entry. Assume the density at the inlet is the same as the freestream density.  
[Answer: (a) 1.19%, (b) 26.38  $\text{ms}^{-1}$ ]
- 11.9** A convergent–divergent supersonic intake of entrance diameter 0.25 m is designed to position a weak shock at the throat. (a) If the design value of a freestream Mach number is 2.2, determine the throat diameter. (b) If the exit diameter is 0.4 m, what will be the exit Mach number?  
[Answer: (a) 0.177 m, (b) 0.115]
- 11.10** A Mach 2.5 air stream at 5 kPa and 200 K is made to enter an intake. If the isentropic efficiency of the diffuser is 0.95, determine the heat loss from the intake for a unit mass of air.  
[Ans: 12.56 kJ  $\text{kg}^{-1}$ ]
- 11.11** If the entropy increase due to the diffusion process in an intake is 5%, can the total pressure at the intake exit be taken as the total pressure at the inlet?  
[Answer: Yes]
- 11.12** Air stream at 200  $\text{ms}^{-1}$ , 100 kPa and 300 K through the capture area of an intake is accelerated to 230  $\text{ms}^{-1}$  before entering the intake. The flow from the entry to the exit of the intake is decelerated to 20  $\text{ms}^{-1}$ . Assuming the flow to be isentropic, determine the additional pressure rise caused by the acceleration in the capture streamtube.  
[Answer: 27.85%]
- 11.13** Determine the specific fuel consumption of the ramjet flying at Mach 1.5 in an altitude where the pressure and temperature are 11.6 kPa and 205 K, respectively, if the

maximum temperature in the combustion chamber is 2500 K and the HV of the fuel is 45 000 kJ kg<sup>-1</sup>. Assume  $\gamma = 1.4$  and  $c_p = 1$  kJ kg<sup>-1</sup> and neglect all losses.  
 [Answer: 0.058 972 kg (kN s)<sup>-1</sup>]

- 11.14** A reverse nozzle diffuser or convergent-divergent duct to decelerate a Mach 1.8 supersonic air stream to subsonic speed is to be designed to deliver a Mach 0.2 stream. If the inlet area is 0.2 m<sup>2</sup>, determine the throat and exit area of the diffuser.  
 [Answer: 0.172 m<sup>2</sup>, 0.5096 m<sup>2</sup>]
- 11.15** A nacelle with  $s = 0.5$  has its maximum area as twice its inlet area. If the velocity at the nacelle inlet is half of the freestream value, determine the maximum pressure coefficient.  
 [Answer: 0.33]
- 11.16** A supersonic intake operates with a shock across the entry plane. The flow inside the duct is subsonic throughout but choked at the exit. The freestream Mach number is 2 with pressure 40 kPa. If the exit area is 0.003 and the exit mass flow rate is 1.4 kg s<sup>-1</sup>, determine the inlet area.  
 [Answer: 0.003 66 m<sup>2</sup>]
- 11.17** If the efficiency of a subsonic diffuser at a freestream Mach number of 0.8 is 0.88 determine the stagnation pressure ratio across the diffuser.  
 [Answer: 0.953]
- 11.18** The incremental thrust associated with the lowering of flow speed at the intake entry is 50 kPa for an intake with an inlet area of 0.2 m<sup>2</sup> and a maximum area of 0.4 m<sup>2</sup> while flying at Mach 2.0 at 10 km altitude. Assuming the constant  $s = 0.62$ , determine the  $C_{p_{\max}}$ .  
 [Answer: 0.845]

## 12

## Jets

## 12.1 Introduction

A jet may be defined as a *pressure-driven shear flow that exhibits a characteristic that the width-to-axial distance is a constant*. This constant assumes a value of 8 for jet Mach numbers  $< 0.2$  and the constant decreases with an increase of Mach number.

When a jet is issuing into a still environment it is termed a *free jet* or *submerged jet*. If it is issuing into a flow, constituting a field that has the jet surrounded by a flow field of different velocity, it is referred to as a *co-flowing jet*. When the jet is issuing normal to a boundary (either a solid or a fluid boundary), it is referred to as an *impinging jet*. If the jet axis is at an oblique angle to the boundary, and the boundary is a wall, it is called a *wall jet*. If a jet is opposed by another jet, the combination is termed *opposing jets*.

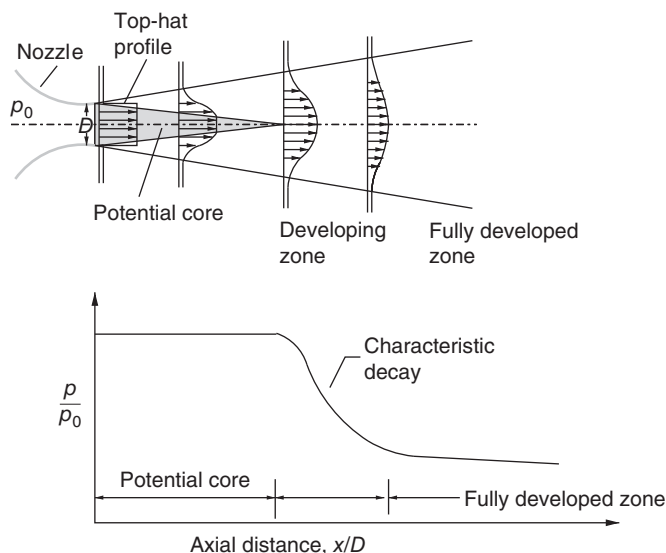
The jet may also be defined as a *continuous fluid flow issuing from an orifice into a medium of lower speed fluid*. As the jet fluid travels further away from its origin, it slows down, owing to mixing with the stagnant ambient fluid entrained and inducted into the jet field. This is due to the boundary layer at the nozzle exit which develops roll-up structures, or ring vortices, that grow in size when they move downstream, owing to the entrainment of ambient fluid into the jet stream. Thus, mass flow at any cross-section of the jet progressively increases along the downstream direction. Hence, to conserve momentum, the centerline velocity decreases with downstream distance. The resulting centerline velocity decay is proportional to the gradient across the shear layer and is a strong function of the distance downstream of the jet exit. The vast quantity of knowledge presently available and the continuous research currently being carried out stand as testimony to the importance of jet flows. This is due to the extensive nature of their applicability, from household appliances to hi-tech rockets. In terms of academic interest, studies of jets have provided insight into the understanding of the dynamics of free shear layers and vortical structures.

The differential shear at the jet boundary forms vortices, and they bring fluid mass from the surrounding environment into the jet field. This transport of mass from the surroundings into the jet is called *entrainment*. There are vortices all over the jet boundary and thus a large number of eddies induct mass into the jet. This entrainment process clearly reveals that the law of conservation of mass is not valid for jet flow. The entrained mass is at a lower momentum compared to the momentum of the fluid elements in the jet issuing from the nozzle or orifice. Therefore, the fluid masses of higher and lower momentum will try to come to an equilibrium, leading to a decrease in the momentum of the jet mass issuing from the nozzle. Thus, the mass and momentum transports become active soon after the jet comes out of the nozzle. This process will try to carry the entrained mass toward the jet axis. This action causes large-size mass-entraining vortices formed at the jet boundary to be fragmented into small-size eddies that move toward the jet axis. Smaller vortices being efficient mixing promoters assist the low momentum mass

entrained at the jet boundary to gain momentum from the jet mass at higher momentum and travel toward the jet axis. Thus, the viscous activity progressively spreads toward the axis of the jet. The viscous action ultimately reaches the jet axis at an axial distance downstream of the nozzle exit. Up to this location the jet velocity (the velocity at the nozzle exit) remains unaffected along the jet axis. The jet flow that has uniform velocity all over the exit plane of the nozzle or orifice is said to *exhibit a top-hat* (that is resembling its shape) at the nozzle exit and thus can be assumed to be inviscid. But soon after exiting the nozzle the flow experiences vortex formation at the boundaries, because of the differential shear. The relatively large vortices formed at the jet boundary entrain the surrounding mass into the jet and get fragmented to mixing-promoting small vortices. Thus, the top-hat velocity profile at the nozzle exit shrinks in size as the jet propagates downstream from the nozzle exit. In other words, the mixing initiated at the jet periphery spreads toward the jet axis, as the jet propagates downstream.

For subsonic jets, the axial distance up to which the jet velocity along the axis is unaffected is called the *jet core*. In other words, the axial distance from the nozzle exit at which the jet velocity (that is the nozzle exit velocity) begins to decrease is termed the *jet core*. For subsonic jets, after the core the axial velocity decreases continuously, owing to the mixing process. This decay is rapid and is inversely proportional to the axial distance when the jet Mach number is subsonic. This is popularly called *characteristic decay*. The jet core is essentially a potential region where the jet retains its axial velocity at all axial points in the region. After the core, the entire jet field is dominated by viscous action. The core for a subsonic free jet usually extends up to about six times the nozzle exit diameter ( $D$ ). After that, the characteristic decay begins and that dominates from about  $6D$  to about  $12D$ . After that, the jet decays very slowly, and gradually approaches zero velocity at a far downstream location. Theoretically, this extends up to infinity. But in reality, the velocity becomes insignificant after about  $30D$ . The region from the end of characteristic decay to infinity is also referred to as the *self-similar region* or *fully developed region*.

The features of the jet flow field – the jet core, characteristic decay, and fully developed zones – are shown schematically in Figure 12.1.



**Figure 12.1** Different zones of a subsonic jet and the corresponding pitot pressure variation along the centerline.

It is seen that the jet develops with an included angle of about  $10^\circ$ . This is a typical value for subsonic jets. At the boundary, vortices are formed because of differential shear. These vortices are the mass carriers that carry the fluid mass from the surroundings into the jet.

From vortex dynamics, we know that large-scale vortices (this implies that the size of the vortex is large) are efficient suction creators and thus efficient in engulfing the fluid from the surroundings into the jet. This process of bringing mass from the surroundings into the jet is termed *mass entrainment* or simply *entrainment*. The fluid mass with zero momentum from the surrounding zone entrained by the large vortex structures will interact with the jet fluid at a finite momentum. In the process, the jet fluid will exchange momentum with the entrained mass. Thus, the momentum of the jet fluid will decrease and that of the entrained fluid will increase, but the total momentum of the jet is conserved. During the process, the large vortices get fragmented into small eddies. That is, even though the large-size vortices are efficient entrainers, the life of the large-size structure is very short. On the other hand, small-scale eddies have a longer life and also serve as good transporters of mass and momentum. Therefore, in a jet flow, large- and small-scale structures must be present in suitable proportions to result in an efficient mixing of the jet flow with the surrounding fluid. In other words, the mass-entraining large-scale structures and mass transporting small-scale structures should be present in proper proportions in the jet field in order to achieve the best mixing. At this stage, it is important to realize that identifying this proportion in a turbulent field like a jet is an impossible task. Hence, it is a usual practice to ensure the existence of these structures in appropriate proportion by indirect means. One of the popular means for this is the measurement of jet centerline decay. Jet centerline decay is a direct measure of the mixing taking place in the jet field. A fast decay implies rapid mixing, and vice versa. Thus, for efficient mixing of the jet with the surrounding fluid, there should be a proper combination of large- and small-scale vortices. In other words, a proper combination of the mass entrainers and mass distributors should be present inside the jet.

At this stage, it is important to realize that generation and manipulation of this kind of combination of small and large eddies is not a practically possible one. But we can try to generate proper proportions of mixed-size vortices to enhance the jet mixing to a large extent. It is usual practice in jet research to observe the decay of jet centerline velocity or pressure to quantify the decay of jet. A jet with a faster decay of its centerline pressure implies that it contains a mixture of the proper combination of large and small vortices compared to an identical jet with a slower decay of centerline pressure. Enhancement of jet decay can be achieved with controls that are passive or active in nature.

Basically, jets can be classified into incompressible jets and compressible jets, as shown in Figure 12.2. The jets with a Mach number of less than 0.3, up to which the compressibility effects are negligible, are called *incompressible jets*. Jets with a Mach number of more than 0.3 are termed *compressible jets*. Compressible jets can be further subdivided into subsonic, sonic, and supersonic jets. Jets with a Mach number of less than 1.0 are called *subsonic jets* and jets with a Mach number of 1.0 are called *sonic jets*, which can either be correctly expanded or under-expanded. Jets with a Mach number of more than 1.0 are called *supersonic jets*. These can be further classified into overexpanded, correctly expanded, and underexpanded jets. The classifications described above are listed in Figure 12.2.

### 12.1.1 Subsonic Jets

Subsonic jets are those with Mach numbers of between 0.3 and 1.0, and are always correctly expanded, and develop with an included angle of about  $10^\circ$ . A schematic diagram of a typical subsonic jet and the different flow zones in the jet are shown in Figure 12.1.

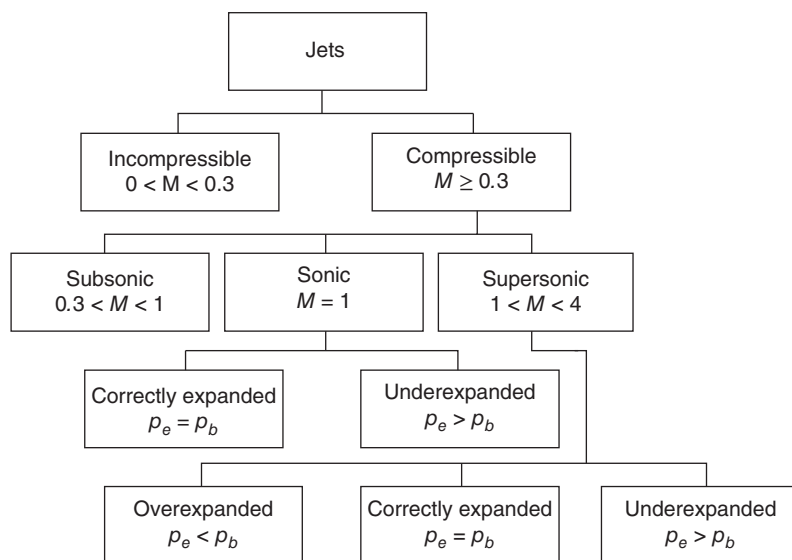


Figure 12.2 Classification of jets.

The flow regimes in a subsonic jet are classified as follows.

- *Potential core region.* This region consists of a core zone of constant axial velocity equal to the jet (nozzle) exit velocity, surrounded by a rapidly growing and predominantly shear dominated annulus of mixing layer or shear layer with intense turbulence. The potential core of a subsonic jet typically extends to about six times the nozzle exit diameter ( $D_e$ ) downstream from the nozzle exit. This is because the mixing initiated at the jet boundary (periphery) has not yet permeated into the entire flow field, thus leaving a region that is characterized by a constant axial velocity.
- *Transition region.* This is the region where the centerline velocity begins to decay. This characteristic decay zone extends from about  $5D_e$  to  $10D_e$  downstream over which the turbulence changes from its annular to a somewhat pseudo-cylindrical distribution. As a result, the velocity difference between the ambient fluid and the high-speed core region of the jet decreases and attenuates the shear that supports the vortical rings in the jet, and thus the velocity profiles become smoother with jet propagation.

The transition region is characterized by a growth of three-dimensional flow due to wave instability of the cores of the vortex rings. The merging of these distorted vortices produces large eddies which can remain coherent around the potential core region of the jet.

- *Fully developed region.* Beyond the transition region the jet becomes similar in appearance to a flow of fluid from a source of infinitely small thickness (in an axially symmetric case the source is a point, and in a plane parallel case it is a straight line perpendicular to the plane of flow of the jet). In reality, the jet velocity becomes insignificant after about  $30D_e$ .

## 12.2 Mathematical Treatment of Jet Profiles

We saw that a jet propagating through a medium at rest is called a *submerged jet*. The velocity at the center of the section of an axially symmetric submerged jet is inversely proportional to

the distance from the pole [19].

$$u_m = \frac{\text{constant}}{x} \quad (12.1)$$

The velocity variation along the axis of a plane-parallel jet is inversely proportional to the square root of the distance from the pole.

$$u_m = \frac{\text{constant}}{\sqrt{x}} \quad (12.2)$$

The distribution of temperature along the axis of the main region of a jet can be established in the same way as for velocities, except that instead of the constant value of the momentum the constant heat content of the jet must be used. Indeed, in the determination of the heat content of the jet from the temperature difference, the fluid sucked by the jet from the surrounding space does not contribute to the heat transfer, since the temperature difference is equal to zero ( $\Delta T_u = 0$ ). In other words, the surplus heat content of the entire mass of fluid passing through a jet section chosen at random is equal to the surplus heat content of the initial mass emerging over the same interval of time from the nozzle.

For a circular jet, the temperature drop along the jet axis is given by

$$\Delta T_m = \frac{\text{constant}}{x} \quad (12.3)$$

For a plane-parallel jet, the temperature drop along the jet axis is given by

$$\Delta T_m = \frac{\text{constant}}{\sqrt{x}} \quad (12.4)$$

From the above expressions for the temperature and velocity decay, it can be seen that the drop in the mean temperature along the axis of a free jet conforms to the same law as the drop in mean velocity. It is important to note that the above equation describing the relationship between the mean values still holds, despite the fact that the temperature and velocity profiles in the submerged jet are dissimilar.

## 12.3 Theory of Turbulent Jets

Some of the well-known theories around jets or so-called free turbulence are

- Prandtl's old theory
- Taylor's theory
- Prandtl's new theory
- Richard's theory
- Mattioli's theory.

Prandtl's "old" theory of free turbulence was published in 1925, and Tollmien applied it in 1926 to solve the following three problems concerning the propagation of free mixed jets of an incompressible fluid.

- Boundary layer of an infinite plane-parallel jet.
- Parallel jet issuing from a very narrow orifice.
- Axially symmetric jet issuing from a very small orifice.

The investigation of free turbulent flow is of great interest because it is the simplest case of turbulence and the least dependent on the effect of viscosity. The study of free turbulence may be regarded as the preliminary stage in the study of turbulent flow.

The successful development of the mechanics of turbulent jets stimulated applications of the theory jets to the solutions of heat problems, such as the problem of temperature distribution along the axis of the jet and in its lateral cross-sections, the problem of heat diffusion from the jet into the adjoining space, and so on.

In addition, a direct conclusion of Prandtl's theory for the cases of the free jet, and of the wake behind a body, is the complete similarity between velocity and temperature fields. Experimental studies of the distributions of the velocity of flow and temperature of a gas in the wake behind long circular and lens-shaped cylinders proved that the theoretical Prandtl–Schlichting velocity fields are well verified by the experimental data, whereas no similarity between the velocity and temperature fields occur, and the heat transfer from the wake of the streamlined body is twice as great as predicted by Prandtl's theory.

Taylor, after noticing a contradiction in Prandtl's theory of free turbulence, assumed that the turbulent shearing stress in a stream must be determined by the lateral transfer of vorticity and not, as Prandtl assumed, by momentum transfer. Thus, Taylor removed an inconsistency of Prandtl's theory, namely its neglect of local instantaneous pressure gradient that substantially influences momentum exchange but does not affect vorticity transfer.

In 1942, Prandtl published a new theory of free turbulence, in which Newton's law of viscous friction was used, as Boussinesq had suggested in the nineteenth century, to determine the turbulent shearing stress in a jet. He assumed the coefficient of *turbulence viscosity* to be proportional to the product of density, velocity difference, and jet thickness. Using Prandtl's new theory, Görtler solved two new problems of the theory of the submerged turbulent jet:

- the problem of a plan jet with an infinite parallel stream
- the problem of a plan jet with an infinitely narrow initial cross-section.

If Prandtl's old theory of free turbulence led Tollmien to an understanding of a jet of finite thickness, then, by applying Prandtl's new theory, Görtler obtained asymptotic velocity profiles (Gaussian) at the lateral cross-section of the jet, characteristics of an infinitely thick jet.

The main advantage of the new Prandtl–Görtler theory of the flow of a jet compared with the old Prandtl–Tollmien theory is that in the former velocity profiles are described by relatively simple analytical formulae while in the old theory they were determined numerically.

In 1939, Abramovich published his work on the theory of the turbulent two-dimensional jet of a compressible gas. Following him, Van Driest developed a method of analyzing the turbulent boundary layer in a compressible gas. Van Driest's innovation consists of the hypothesis that, in addition to fluctuations of velocity, density, pressure, and temperature, there are fluctuations of mass flow ( $\rho u$ ), ( $\rho v$ ) regarded as single properties; thus the continuity equation for the average values of mass flow has the same form as in the case of the steady flow of an ideal gas.

What we have discussed so far is just a glimpse of the vast array of material available on incompressible jets. For a detailed compilation of the characteristics of incompressible jets, we can refer to books such as [19–21].

### 12.3.1 Mean Velocity and Mean Temperature

Generally speaking, mean velocity can be calculated in different ways; here, the results obtained are not the same but depend on the physical meaning attributed to the word *mean*.



Often, the mean velocity is taken to be the mean arithmetic velocity  $u_{cA}$ , which is represented by the ratio of fluid mass flow rate to the cross-sectional area

$$u_{cA} = \frac{m}{\rho_c A} = \frac{\int_0^A \rho u dA}{\rho_c A} \quad (12.5)$$

The mean arithmetic velocity is obtained by averaging with respect to area. The mean velocity  $u_{cm}$  can also be obtained as a ratio of the momentum per second to the mass flow per second.

$$u_{cm} = \frac{\int_0^m u dm}{\int_0^A \rho u dA} = \frac{\int_0^A \rho u^2 dA}{\int_0^A \rho u dA} \quad (12.6)$$

The value found from this equation is termed the *mean-square velocity*. It is found by averaging with respect to the fluid mass flow rate. Naturally, the values  $u_{cA}$  and  $u_{cm}$  need not be the same, and the difference between them increases as the nonuniformity of the velocity field increases. In the case of a submerged jet, the mean arithmetic and mean-square velocities differ considerably.

In practical calculations the average temperature according to mass flow of the fluid is almost always applied; hence, the mean temperature is taken as the ratio of the heat content of the mass flow rate to the mass flow rate.

$$\Delta T_{cm} = \frac{\int_0^m \Delta T dm}{m} = \frac{\int_0^A \Delta T \rho u dA}{\int_0^A \rho u dA} \quad (12.7)$$

Returning to Eq. (12.5), we should note that the equality of the dimensionless mean temperature difference and the mean velocity is valid only for the mean-square velocity, that is for cases in which the latter is derived by averaging with respect to the mass flow rate.

### 12.3.2 Turbulence Characteristics of Free Jets

It is interesting to note that all free jets are turbulent even at Reynolds numbers close to zero. This is because of the differential shear experienced by the jet at its periphery. In fact, the generation of a laminar jet requires a lot of arrangement and skill. So far laminar jets have been demonstrated with special equipment up to Reynolds numbers of about 60. In general, free jets – even at Reynolds numbers as low as 2 – prove to be turbulent. Therefore, the laws governing the distribution of different pulsation characteristics of the stream and their interrelationships are very important in the theory of a turbulent jet in particular, and in the theory of turbulence in general. The perturbations of the velocity vector (or one of its components), averaged with respect to time, are equal to zero; hence, it is usual to determine the turbulence of the flow from the non-disappearing mean-square pulsation in velocity, temperature, and other parameters  $\sqrt{\overline{u'^2}}$ ,  $\sqrt{\overline{v'^2}}$ ,  $\sqrt{\overline{w'^2}}$ , and so on.

The interrelationship between the turbulent characteristics is determined by the mean values of their products (correlation)  $\overline{u'v'}$ ,  $\overline{v'w'}$ ,  $\overline{w'u'}$ ,  $\overline{u'T'}$ ,  $\overline{v'T'}$ , and so on. The averaged mixing length, which is described below and can be determined in the following way, serves as a measure of the scale of turbulence.

$$l_u = \frac{\sqrt{\overline{u'^2}}}{\frac{\partial \overline{u}}{\partial y}}, l_v = \frac{\sqrt{\overline{v'^2}}}{\frac{\partial \overline{v}}{\partial y}}, l_T = \frac{\sqrt{\overline{T'^2}}}{\frac{\partial \overline{T}}{\partial y}}$$

### 12.3.3 Mixing Length

In a turbulent jet the components of velocity at any point can be decomposed into a time-averaged value plus a randomly varying perturbation:

$$u = \bar{u} + u', \quad v = \bar{v} + v'$$

When averaged over some finite time interval, the fluctuation or pulsation components are equal to zero:

$$\overline{u'} = \overline{v'} = 0$$

If the mean free path of a fluid particle (mixing length) in a turbulent stream is equal to  $l$ , when moved in the transverse direction, the particle reaches a layer in which the mean velocity differs from what it was in the layer from which it separated by the following value:

$$\Delta \bar{u} = l \frac{\partial \bar{u}}{\partial y}$$

The loss of individuality of the fluid particle (its merging with the mass of the new layer) should be accompanied by a discontinuous variation (perturbation) in velocity of

$$u' = \Delta \bar{u}$$

In other words, the perturbation of a stream-wise velocity component is of the order

$$u' \sim l \frac{\partial \bar{u}}{\partial y}$$

It is usually assumed that the transverse perturbation in velocity  $v'$  is proportional to the stream-wise perturbations  $u'$  but having the opposite sign

$$-v' \sim u', \quad \text{that is } -v' \sim l \frac{\partial \bar{u}}{\partial y}$$

The absence of solid boundaries in the free stream that might damp the oscillations of the particles led Prandtl to assume that, in this case, the mixing length at any cross-section of the stream was constant [22]:

$$l(y) = \text{constant}$$

The variation in the mixing length along the  $x$ -axis  $l = l(x)$  may be established by means of available experimental data. The sufficient basis for Prandtl's assumption is provided by the similarity of boundary layers in different cross-sections of a free stream. This similarity was established by a large number of experiments in which the velocity profiles proved universal when plotted in dimensionless coordinates

$$\frac{u}{u_m} = f\left(\frac{y}{b}\right) \quad (12.8)$$

That is, they coincide for different sections of the jet. The similarity of boundary layers in the section of the given free stream implies, among other things, the similarity of geometric dimensions. In other words, equality may be expected between the dimensionless mixing lengths for different sections of the stream.

$$\frac{l_1}{b_1} = \frac{l_2}{b_2} = \dots = \text{constant} \quad (12.9)$$

Thus, it is sufficient to establish a law for the growth of the jet as a function of distance along the  $x$ -axis in order to define the way in which the mixing length increases. Prandtl assumed that

the growth of the jet (that is the rate at which the thickness of the jet boundary layer increases) is controlled by the transverse perturbation velocity [23]

$$\frac{db}{dt} \sim v' \sim -l \frac{\partial \bar{u}}{\partial y} \quad (12.10)$$

Because of the similarity of velocity profiles in different cross-sections of the jet, it is possible to write

$$\frac{\partial \bar{u}}{\partial y} \sim \frac{u_m}{b} \quad (12.11)$$

and, hence, according to Eqs. (12.10) and (12.11),

$$\frac{db}{dt} \sim \frac{l}{b} u_m \sim u_m \quad (12.12)$$

On the other hand, the rate of growth of the jet

$$\frac{db}{dt} = \frac{db}{dx} \frac{dx}{dt} \sim \frac{db}{dx} u_m \quad (12.13)$$

A comparison of Eqs. (12.12) and (12.13) provides a solution of the problem of establishing the law governing the increase in thickness of the submerged jet and the mixing length in the direction of flow

$$\boxed{\frac{db}{dx} = \text{constant}, \quad b = x \times \text{constant}, \quad l = c x} \quad (12.14)$$

This linear law for the increase in the jet thickness and mixing length along the stream holds jets of different shapes: the boundary layer of an infinite plane stream, the plane parallel, and the axially symmetric jet. In all three cases, the law applies only when the velocity profiles in the submerged jets are universal.

Experimental results of mean velocities and temperature differences at various cross-sections of the jets in the Reynolds number range from  $30 \times 10^3$  to  $59 \times 10^3$  at the conditions listed in Table 12.1 are shown in Figure 12.3a–c. Here the local velocities and temperature differences are referred to the velocity and the temperature difference on the axis of each section.

$$\frac{u}{u_m} = f\left(\frac{y}{b}\right)$$

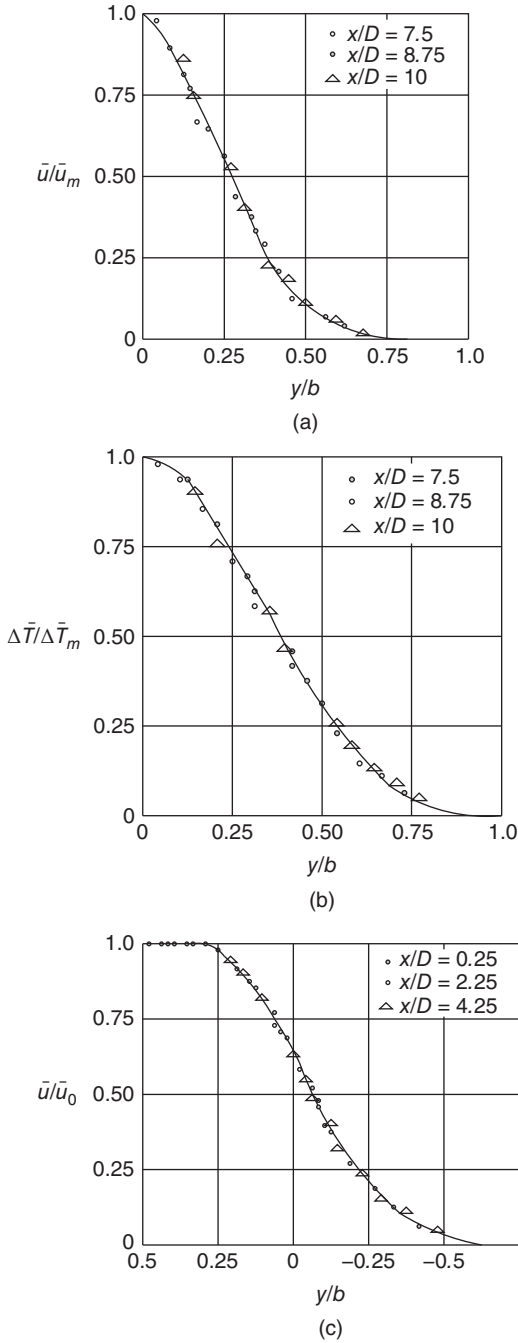
$$\frac{\Delta T}{\Delta T_m} = f\left(\frac{y}{b}\right)$$

where  $y$  is the distance between the jet axis and the point investigated, and  $b$  is the half-thickness (radius) of the jet at the given cross-section of the main region (that is downstream of the core).

Since the range over which the  $Re_d$  were varied is fairly narrow, no conclusions with regard to the similarity of the mean-square pulsation of the longitudinal component of the velocity vector can be drawn on the basis of these experiments.

**Table 12.1** Test conditions and the corresponding regions.

Condition	$u_0$ (m s <sup>-1</sup> )	$T$ °C	$Re$ ( $u_0 D$ )/ $\nu$	Main region ( $x/D$ )	Initial region ( $x/D$ )
1	35	225	$39.3 \times 10^3$	7.50	0.25
2	35	100	$59.0 \times 10^3$	8.75	2.25
3	30	125	$30.5 \times 10^3$	10.0	4.25



**Figure 12.3** (a) Mean velocity in the transition zone; (b) mean temperature in the transition zone; and (c) mean velocity in the initial region. (Source: Reprinted with permission from [19] [Figure 1.35]. The MIT Press, Massachusetts. © 1963.)

If it is assumed that the following equality holds

$$\sqrt{\overline{u'^2}} = l_u \frac{\partial \bar{u}}{\partial y} \quad (12.15)$$

then we can find the value of  $l_u$ , known as the *mixing length*.

The dimensionless quantity  $l_u/b$ , found from the given experiments and from Eq. (12.15), remains roughly constant for most of the cross-sections and is 0.12–0.13 [19].

In the initial region of the jet, the distribution of the pulsation of the longitudinal component of the velocity vector, shown in dimensionless coordinates

$$\frac{\sqrt{u'^2}}{u_0} = f\left(\frac{y}{b}\right)$$

can also be described with reasonable accuracy by a simple curve. The assumption of the validity of Eq. (12.15) in the boundary layer of the initial region made it possible to determine  $l_u/b_1$ , which proved to be approximately 0.1 [19] for most of the cross-section of the boundary layer.

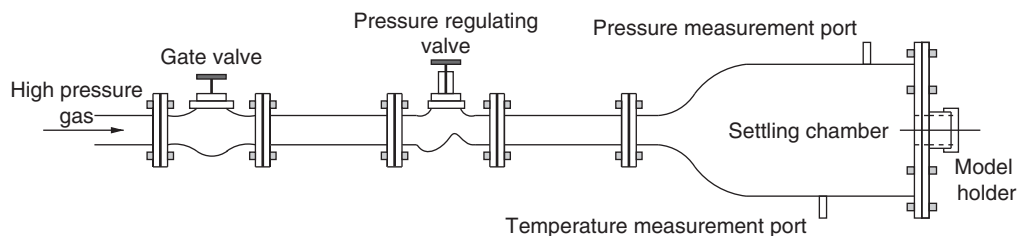
Similarly, assuming the validity of the relation

$$\sqrt{v'^2} = l_v \frac{\partial \bar{u}}{\partial y}$$

we can also find the mixing length  $l_v$ . The ratio of  $l_v/b$  is more or less constant for most of the section, and is equal to 0.1. The mixing length of the transverse velocity vector component in the boundary layer of the initial region is approximately equal to  $0.08b$ . Experimental results suggested that there is no universal curve for the temperature pulsation profile in different cross-sections of the jet. What is given in this section is just a glimpse of the vast amount of information on turbulent jets compiled by Abramovich. Detailed information on low-speed jets is given in [19].

## 12.4 Experimental Methods for Studying Jets and the Techniques Used for Analysis

We have seen that a jet is a turbulent flow. Because of the complexity of the flow, jets are mostly studied experimentally. The major parameters considered for analyzing a jet are the centerline pressure or velocity decay and pressure or velocity profiles. These are done using the pitot pressure measured along the jet axis and across the jet in the direction normal to the jet axis. For subsonic jets the measured pitot pressure can be converted to velocity using the pressure of the atmosphere to which the jet is discharging as the static pressure. This is possible because the subsonic jets are correctly expanded. The isentropic pressure–Mach number relation can be used to convert the measure pitot pressure to Mach number, and the Mach number can be converted to velocity. But in supersonic jets the pitot probe will measure the total pressure behind the bow shock positioned at the nose. Also, because of the complex pattern of the waves prevailing in the jet field, the static pressure varies from point to point. Also, it is not possible to measure the static pressure in a supersonic jet field. Therefore, it is usual practice to use the measured pitot pressure data as it is to study the decay and spread characteristics of supersonic jets. In addition to pitot pressure measurement, the waves present in the flow field can be visualized using optical visualization techniques such as Schlieren or shadowgraph. The measured pitot pressure distribution is usually plotted in the form of centerline pressure decay or (Mach number decay for subsonic jets) and isobar or iso-Mach contours. From these plots, the vital characteristics of the jet – namely the core length, characteristic decay, spread of the jet, length of the shock cells, number of shock cells present in the core, and the strength of the waves present in the core – can be discerned. The optical visualization pictures can authenticate the presence of shock cells, and the wave strengths can be estimated from the pressure plot.



**Figure 12.4** Schematic diagram of a free jet test facility.

The jet noise is another important parameter to be considered in the study of high-speed jets. For subsonic jets the turbulent mixing noise is the major component of the noise. But for supersonic jets, in addition to the mixing noise the shock-associated noise can contribute significantly to the overall jet noise. The shock-associated noise can contain broadband shock noise and screech noise. The jet noise can be studied by measuring the noise with a sound level meter.

A typical experimental facility for studying free jets is shown in Figure 12.4.

The experimental set-up consists of an air supply system (which consists of compressor and storage tanks) and an open jet test facility. Compressed dry air stored in tanks is usually used for jet studies. The tunnel control section generally includes a gate valve followed by a pressure-regulating valve. The pressure-regulating valve is connected to a mixing tube, which delivers the air to the settling chamber. The settling chamber is connected to the mixing tube by a wide-angle diffuser followed by a few screens or closely meshed grids set a few centimeters apart for minimizing the turbulence at the nozzle inlet. These screens are inserted in the settling chamber to make the air come to a settled equilibrium in the chamber. The settling chamber is usually provided with ports (tapings) for measuring the stagnation pressure and temperature of the air in the settling chamber. Test models can be fixed at the end of the settling chamber by a slot holder arrangement, which is a short pipe-like protrusion with an embedded O-ring to prevent leakage. The model to be studied can be placed over the O-ring, over which an annular retaining sleeve with internal threads can be screwed tightly. The settling chamber total pressure ( $p_0$ ), which is the controlling parameter in an investigation, has to be maintained constant during a run by controlling the pressure regulating valve. The stagnation pressure ( $p_0$ ) level in the settling chamber gives the different nozzle pressure ratios (NPR), defined as the ratio of stagnation pressure to the backpressure ( $p_b$ ), required for any study.

### 12.4.1 Pressure Measurement

A pitot probe is used for pressure measurement in jets. We know that the pitot probe is a most useful and widely used instrument in experimental fluid mechanics. The accuracy of a pitot probe depends on its shape, the Reynolds number, the magnitude of transverse shear, turbulence intensity and length scale, and the orientation with respect to the mean flow direction and the Mach number. A typical pitot probe used in the author's lab has an outer diameter of 0.6 mm and an inner diameter of 0.4 mm. It is important to make sure that the ratio of the jet cross-sectional area to the projected area of the pitot probe is more than 64 to treat the probe blockage effect as being negligible. For example, if the exit diameter of the nozzle used to deliver a supersonic jet is 10 mm, the probe blockage ratio for this case is  $(10/0.6)^2 = 278$ , which is well above the blockage limit of 64 for regarding the probe blockage as negligible. Another point to be noted in pitot pressure measurements is that in the supersonic regime what the probe measures is the total pressure behind the bow shock that stands ahead of the probe. Thus, what the pitot probe measures is not the actual total pressure. If the actual total pressure is required,

we have to correct for the pressure loss across the shock. Since a supersonic jet core is wave dominated, the Mach number in the core varies from point to point and also the waves in a different shock well are of varying strength. Therefore, usually no attempt would be made to correct the measured total pressure for shock loss. Also, it has to be emphasized that in supersonic regions there would be some measurement error due to probe interference with the shock structure and so the measured pressure data in supersonic regions should be considered only qualitative and good enough for comparative study. In all pressure measurements the sensing probe has to be oriented parallel to the transverse axis ( $y$ -axis) with the sensing probe facing the jet axis ( $x$ -axis). If the pitot probe is mounted on a rugged traverse which has six degrees of freedom (three translational and three rotational), the pressure at any point in a jet field can be measured comfortably.

#### 12.4.1.1 Precautions Observed

It is essential to observe the following precautions during the experiments.

- The horizontal alignment of the settling chamber has to be ensured.
- The pitot probe has to be carefully aligned with the flow direction to the  $x$ -axis of the nozzle geometry, facing the nozzle exit.
- Care has to be exercised in the alignment of the models, to ensure proper positioning of the measurement planes.
- The nearest wall has to be 150 nozzle exit diameters away, to avoid wall effects.
- The pressure pipelines and the settling chamber ports have to be leak free.
- During the experiment, the settling chamber stagnation pressure reading has to be constantly monitored.
- The stagnation pressure and the air flow rate in the settling chamber have to be kept constant during the experiments by adjusting the pressure regulating valve.
- The experiments have to be conducted in a large room with constant ambient temperature.

In jet noise experiments, free-field conditions become essential, for scaling laws to be derived, which would enable a comparison of results obtained at different power settings (e.g. model and full-scale jets). The anechoic chambers used for jet acoustic experiments are different from those used for purely acoustic or electronics experiments such as the calibration of a microphone. Jet experiments involve mass flow through the chamber, and since jets entrain ambient fluid, it is necessary to provide ventilation for mass entrainment. Similarly, ventilation should be provided for the passage of jet mass flow outside the enclosure.

Jet noise can be measured using a precision integrating sound level meter with a tiny (say 6 mm) condenser microphone. It is preferable to use sound level meter having an amplitude range of  $-10$  to  $140$  dB (currently this range is available) with some user-selectable ranges and three standard weighting networks: A, C, and linear weightings. Most of the researchers use C weighting. The instrument gives output signals in both AC and DC form. The AC output follows all signal-conditioning circuits, including the bandpass filters. The AC output can be used to drive the inputs of external signal analyzers, such as fast Fourier transforms (FFTs). Usually jet sound pressures are measured in fast mode and sound pressure levels are referred to  $20$  Pa.

The acoustic measurements are usually made at two locations: in the nozzle exit plane and far-field. In the nozzle exit plane, the microphone should be positioned at  $30D$  (where  $D$  is the nozzle exit diameter) radial distance. For the far-field case acoustic data should be acquired at a radial distance of  $100D$  in the azimuthal plane, with the microphone tip positioned at  $30^\circ$  orientation to the jet axis. For both cases, acoustic data should be acquired in two planes, namely along the control (say the tabs) and normal to the control, for the jets with controls such as tabs located at the nozzle exit.

## 12.5 Expansion Levels of Jets

The NPR, which is the ratio of the stagnation pressure in the settling chamber, which runs the jet-delivering nozzle to the pressure of the environment to which the jet is discharged, dictates the level of expansion at the nozzle exit. If the static pressure at the nozzle exit is lower than the pressure of the environment, the jet is termed *overexpanded*; if the exit pressure is equal to the environmental pressure the jet is called *correctly expanded*, and if the exit pressure is greater than the environmental pressure the jet is termed *underexpanded*.

### 12.5.1 Overexpanded Jets

A jet is said to be overexpanded when the nozzle exit pressure  $p_e$  is lower than the ambient pressure  $p_a$  to which it is discharging. To increase  $p_e$  to the level of  $p_a$ , oblique shock waves are formed at the edge of the nozzle exit. These shocks of opposite family cross each other at the jet axis and travel to the jet boundary and are reflected as expansion waves. The oblique shocks at the nozzle exit compress the jet flow at a pressure  $p_e$ , which is less than the ambient pressure  $p_a$ , in order to make the exit pressure  $p_e$  come to equilibrium with the ambient pressure  $p_a$ . Figure 12.5 schematically shows the shock and expansion waves prevailing in an overexpanded jet. Owing to these waves, a periodic shock-cell structure is generated in the jet flow field and the cell length of these periodic structures is found to increase with an increase of jet Mach number. It is essential to note that overexpansion is possible only for supersonic jets; subsonic jets are always correctly expanded and a sonic jet can be either correctly expanded or underexpanded but can never be overexpanded.

It can be seen that there is an oblique shock at the nozzle exit in a bid to increase the exit pressure  $p_e$  to the level of the backpressure by compressing the jet flow leaving the nozzle. But the flow also encounters an expansion fan due to the relaxation offered by the large space of the environment to which the jet propagates. Therefore, at the nozzle exit the flow passes through the oblique shock which compresses the flow and turns the flow toward the jet centerline and soon after passes through the expansion fan, owing to the relaxation effect, experiencing an acceleration and the associated pressure decrease. Further, the flow slightly away from the nozzle exit edge encounters the oblique shock from the opposite edge of the nozzle exit. This shock is of the opposite family and is influenced by the shock from the opposite end. Thus, the flow around the jet axis is compressed twice by the two families of oblique shocks. But the flow at the zone near the nozzle azimuth encounters an oblique shock and an expansion fan soon after exiting. The flow turned away from the nozzle axis (by the expansion fan) has to be turned back toward the nozzle axis in order to flow parallel to the nozzle axis in the far field, satisfying basic flow physics. To enable this, a compression wave is generated at the nozzle exit. But this compression wave has to regulate the flow, which is suddenly turned away by the vertex of the expansion fan as well the flow in the zones away from the expansion fan vertex, which are gently turned.

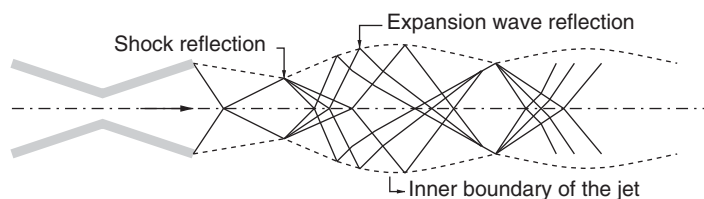


Figure 12.5 Schematic of the waves prevailing in an overexpanded jet.

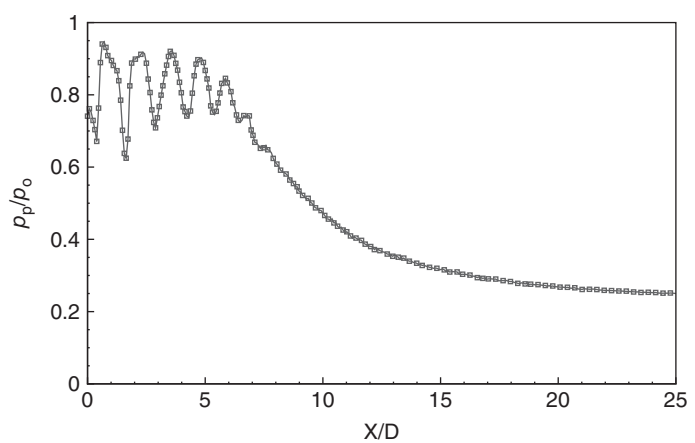


Therefore, the compression wave assumes a curved shape. The curved compression waves from opposite edges resembling a barrel, this is popularly known as *barrel shock*. At high levels of overexpansion, two such barrels can be seen in the near field. The inner one is the edge of the flow traversed by the oblique shocks of the opposite family, and the outer one is the edge of the flow traversed by an oblique shock and the expansion fan. Both oblique shock and expansion rays cross each other along the jet centerline and hit the inner barrel shock. Part of the incident wave experiences unlike reflection and part of it gets transmitted through the barrel wave. The transmitted portion of the wave passing through the barrel wave experiences a compression and a deflection toward the barrel wave (that is toward the jet axis) and travels to the outer barrel. On incidence upon the outer barrel the wave gets reflected again. These reflections from the inner and outer barrel waves are unlike. Thus, an incident shock (compression wave) reflects as an expansion fan and an expansion ray reflects as a compression wave. There is a “kink” at the point where a shock gets reflected and a “bulge” where the expansion rays get reflected, owing to their number.

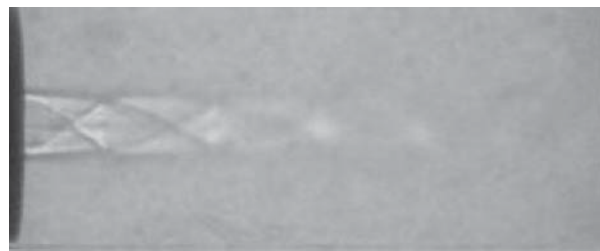
The quantitative and qualitative natures of a Mach 1.88 axisymmetric free jet of air are given as the centerline pitot pressure decay and shadowgraph pictures in Figure 12.6.

From the centerline pitot pressure decay and the shadowgraph pictures of the overexpanded supersonic jet shown in Figure 12.6, it can be seen that the waves in the jet core become stronger with the increase of NPR. Also, the shock cell length and number of shock cells both increase with NPR.

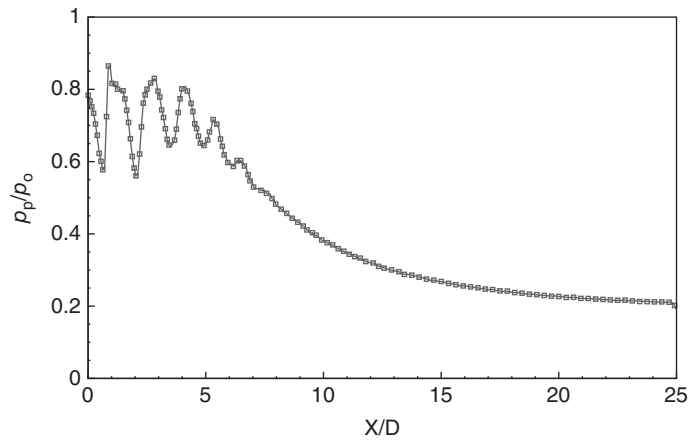
It is interesting to see that the experimental results of centerline pitot pressure distribution shown in Figure 12.6a and c show an oscillatory nature. In these plots,  $p_p$  is the measured pitot pressure distribution along the jet axis and  $p_0$  is the stagnation pressure in the settling chamber which runs the jet,  $X$  is the axial distance from the nozzle exit, and  $D$  is the nozzle exit diameter. The pressure variation is oscillatory because, on exiting the nozzle, the jet finds large space to relax. But the flow at the nozzle exit is overexpanded with the exit pressure less than the pressure of the environment to which the jet is discharging. Thus, the flow encounters a relaxation, owing to the larger space and a compression to increase the lower pressure associated with its overexpanded state to come to an equilibrium with the environmental pressure (backpressure). It is seen that the pitot pressure decreases to some distance from the nozzle exit (that is from  $X/D = 0$ ). This implies that the supersonic flow accelerates. Because the pitot pressure measures essentially the total pressure behind the detached shock at the nose of the pitot probe, it is bound to decrease with the increase of supersonic Mach number. After accelerating monotonically up to some axial distance, the pressure ratio assumes the first minimum. This is the point of a local maximum for the Mach number. This can be taken as the location just upstream of the point where the oblique shocks from the opposite ends meet on the jet axis. Just downstream of this shock intersection point, the flow along the jet axis is traversed by two oblique shocks. Even though the individual oblique shocks are weak in nature, their combined strength proves to be strong, causing the flow to become subsonic behind the intersection point. The subsonic flow downstream of the shock crossover point receives momentum from the higher momentum flow zones around it. Because of this momentum exchange, the subsonic flow accelerates. The region of increasing pitot pressure from the first pressure minimum point is the zone of subsonic acceleration, because in a subsonic flow the increase of pitot pressure is an indication of flow acceleration. The subsonic flow accelerates and attains a sonic state at the point of first peak in the pressure plot. The sonic flow continues to accelerate to supersonic levels, as indicated by the progressive decrease of pitot pressure from the first peak point. The supersonic flow attains the second local maximum at the second minimum point on the pressure plot, which is just ahead of the second crossover point of the compression waves from opposite ends. Behind this point, the flow becomes subsonic and begins to accelerate to sonic



(a) NPR 4.5 (overexpanded)



(b) NPR 4.5 (overexpanded)



(c) NPR 5.5 (overexpanded)



(d) NPR 5.5 (overexpanded)

**Figure 12.6** Centerline pitot pressure decay and shadowgraph pictures of a Mach 1.88 circular free jet at two levels of overexpansion.

level and further accelerates to supersonic levels. This kind of flow acceleration cycle continues up to the point where the flow begins to show a monotonic decrease of pitot pressure.

For a supersonic jet, there is nothing like a constant velocity zone or potential core as there is in the case of a subsonic jet. Therefore, the core for a supersonic jet is usually taken as the axial extent up to which supersonic flow prevails [24]. In other words, the supersonic core may be defined as the axial distance from the nozzle exit at which the characteristic decay begins. From the beginning of the characteristic decay onwards, the supersonic jet characteristics are identical to those of a subsonic jet. This is natural, since the flow has become subsonic. The supersonic core contains a complex wave pattern. This complicates the analysis of a supersonic jet core. Even though the pitot pressure distribution in any plane normal to the jet axis can be measured accurately, it is not possible to determine the local Mach numbers at the corresponding points, because the corresponding static pressures cannot be measured by any technique, because of the wave domination. Also, the stagnation pressure in the settling chamber cannot be taken as the total pressure upstream of the points where the pitot pressures were measured. This is because the compression waves present in the field cause pressure loss when the flow passes through them. Therefore, neither the isentropic relation

$$\frac{p_0}{p} = \left(1 + \frac{\gamma - 1}{2} M^2\right)^{\gamma/(\gamma-1)}$$

nor the normal shock relation

$$\frac{p_{02}}{p_{01}} = \left(1 + \frac{2\gamma}{\gamma + 1} (M_1^2 - 1)\right)^{-1/(\gamma-1)} \left(\frac{(\gamma + 1)M_1^2}{(\gamma - 1)M_1^2 + 2}\right)^{\gamma/(\gamma-1)}$$

which relate the local Mach number to the local static and stagnation pressures and local stagnation pressure and local pitot pressure, respectively, can be used to determine the Mach number. Therefore, it is usual practice to analyze the jet with the measured pitot pressure ( $p_p$ ) nondimensionalized with the stagnation pressure ( $p_0$ ) in the settling chamber as a function of nondimensional axial distance, as in Figure 12.6a. The distance between adjacent pressure peaks (maximum or minimum) is referred to as a *shock cell*. The quantitative details about the overexpanded supersonic jet discussed above can be discerned from the shadowgraph picture of the jet shown in Figure 12.6b and d.

### 12.5.2 Correctly Expanded Jets

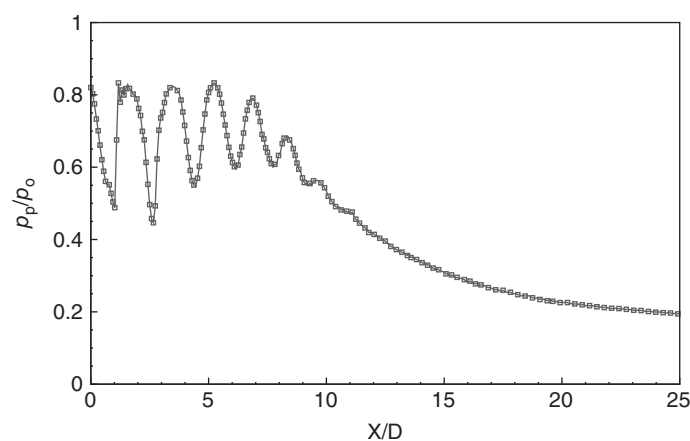
A jet is said to be correctly expanded when the nozzle exit pressure is equal to the ambient pressure. This jet is also wave dominated, as is an imperfectly expanded jet, even though we might think that there would not be any waves. The reason for this is that, as the jet is issuing from the confined area to an infinite area, it tries to expand through expansion waves and after that gets compressed through compression waves (the reflected waves from the jet boundary), which results in a periodic wave structure, as discussed in Chapter 2.

In Chapter 2 we saw that, for a correctly expanded condition, the nozzle exit pressure  $p_e$  is equal to the backpressure ( $p_e = p_b$ ). Therefore, there is no need for the flow to be compressed or expanded after exiting the nozzle, as in the case of overexpanded or underexpanded states, respectively, to come to a pressure equilibrium with the backpressure. This gives an impression that, when the flow is correctly expanded, there are no compression or expansion waves generated at the nozzle exit. Indeed, we tend to think that the correctly expanded sonic and supersonic flow exiting a nozzle is wave-free. But in the actual flow process it is not true. This is because, even though the flow is correctly expanded, soon after exiting the nozzle the flow encounters a large space to relax. Therefore, the flow turns away from the nozzle axis in a bid

to occupy the space available downstream of the nozzle exit. We know that supersonic flow is essentially wave dominated and any change in the state (change of  $p$ ,  $T$ ,  $\rho$ ) or mode (direction) of the flow will take place only through these waves. In the case of correctly expanded flow exiting a nozzle, the flow has to turn away from the nozzle axis to occupy the free space available. This leads to the formation of expansion waves at the nozzle exit. It is important to note that the expansion strength in the case of correctly expanded flow is much less than that for an underexpanded flow. Thus, both correctly expanded and underexpanded flows encounter expansion at the nozzle exit. However, the expansion for a correctly expanded flow is to turn the flow away from the nozzle axis, but for an underexpanded flow the expansion has to reduce the static pressure and turn the flow away from the nozzle axis. The expansion rays formed at the nozzle exit will travel some distance and be reflected from the jet boundary as compression waves, as illustrated in Figure 2.12a and b. To quantify the effect of the expansion of correctly expanded sonic and supersonic flows some representative experimental results of centerline pitot pressure distribution are shown in Figure 2.13a and b.

The centerline pitot pressure decay and shadowgraph picture of correctly expanded Mach 1.88 jet are shown in Figure 12.7.

The pressure distribution and the waves prevailing in the jet field clearly demonstrate that correctly expanded supersonic jet is also wave dominated.



(a) NPR 6.5 (correctly expanded)



(b) NPR 6.5 (correctly expanded)

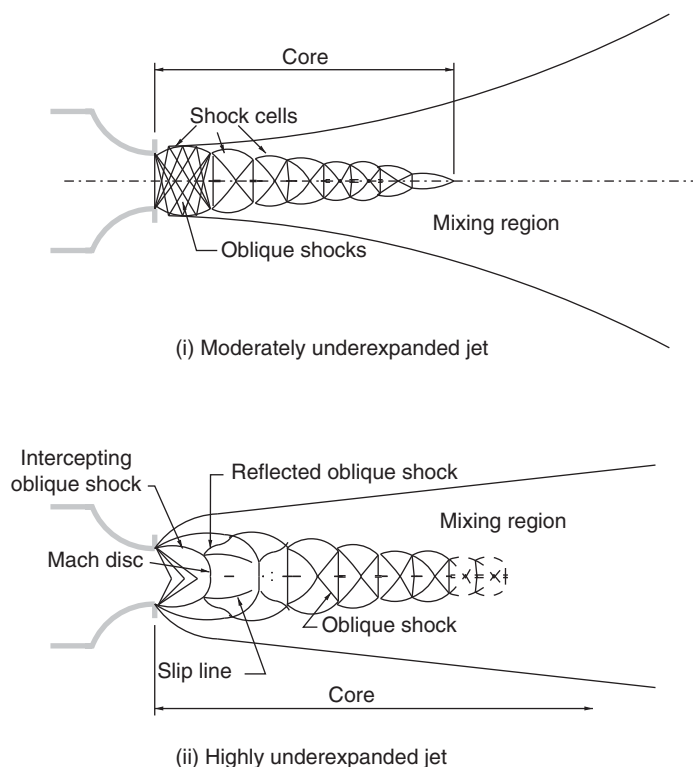
**Figure 12.7** Centerline pitot pressure decay and shadowgraph picture of a correctly expanded Mach 1.88 circular free jet.

### 12.5.3 Underexpanded Jets

A jet is said to be underexpanded, when the nozzle exit pressure ( $p_e$ ) is higher than the backpressure ( $p_b$ ). Since the nozzle exit pressure is higher than the backpressure, wedge-shaped expansion waves occur at the edge of the nozzle. These waves cross one another and are reflected from the boundaries of the jet flow field as compression waves. The compression waves again cross one another and are reflected on the boundaries of the jet as expansion waves. Figure 12.8 shows a sketch of an underexpanded jet. For an underexpanded jet, in addition to the expansion fan caused by the level of underexpansion, there will be another expansion effect due to the relaxation experienced by the jet on exiting the nozzle into a large space. Thus, the combined effect of these two causes establishes a stronger expansion fan than what the underexpansion level alone can establish. The essential difference between the moderately underexpanded and highly underexpanded jet is that at the end of the first shock cell there is no Mach disc in the former but there is a Mach disc in the latter.

Let us examine the shadowgraph pictures of the circular sonic jet at NPRs of 2–8, shown in Figure 12.9.

For a sonic jet, the isentropic limiting NPR for correct expansion is 1.89. Therefore, sonic jets in the NPR range of 2–8 are underexpanded. With the increase of NPR, the underexpansion level increases progressively. Therefore, the expansion fan strength increases with the increase of NPR. At NPR 2, the expansion is only mild and thus the waves prevailing in the jet flow are weak. At NPR 3 the waves become stronger. The expansion rays in the fans from the opposite edges of the nozzle exit are clearly seen in Figure 12.9a. These rays get reflected from the



**Figure 12.8** Schematic of the waves prevailing in an underexpanded jet.



(a) NPR 2



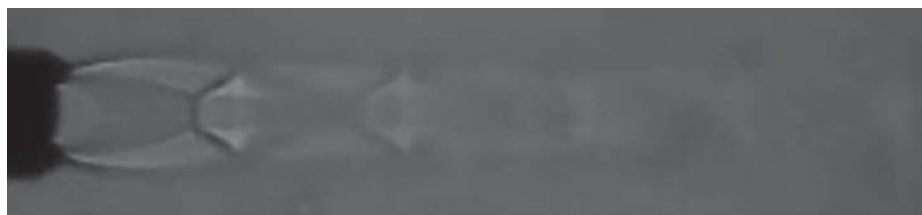
(b) NPR 3



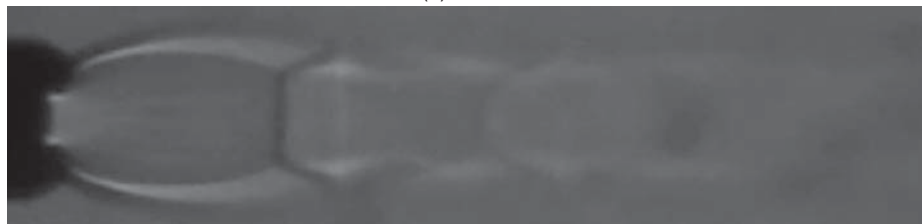
(c) NPR 4



(d) NPR 4.25



(e) NPR 5



(f) NPR 8

**Figure 12.9** Shadowgraph pictures of an underexpanded sonic jet at different NPRs.

barrel waves as compression waves. The angles of these reflected compression waves decrease progressively because of the angle of the incident expansion rays and the shape of the barrel wave from which they get reflected. Because of this continuous change in the angle, the reflected rays coalesce, forming an oblique shock. The oblique shocks thus formed from the opposite sides intersect at the jet axis and pass through. While passing through, the shocks influence each other and experience a change in their direction of propagation, as seen in Figure 12.9b. Even though the oblique shocks formed by the reflected waves are weak shocks at the point of intersection, the flow encounters the combined effect of all the intersecting shocks. Thus, the intersecting point decelerates the flow severely and depending upon the NPR the deceleration can be to subsonic level.

At NPR 4, as seen in Figure 12.9c, the expansion fan at the nozzle exit has become stronger than at NPR 3. Also, the shock crossover point has become larger because, with increasing NPR, the expansion rays get reflected as compression waves and coalesce, forming oblique shocks of increased strength. Therefore, the flow velocity behind the intersecting shocks decreases progressively with the increase of NPR. This calls for a larger shock intersecting zone for momentum exchange, causing the intersecting point to become larger, as seen in this figure.

Beyond some limiting NPR, the shock intersecting point becomes an intersecting zone, which resembles a disc, as seen in Figure 12.9d for NPR 4.25. This disc is termed a *Mach disc*. The Mach disc is essentially a compression wave identical to a normal shock across which the flow decelerates to subsonic level. A sonic or supersonic jet with a Mach disc in the core is termed a *highly underexpanded jet*. An underexpansion level of about 2 ( $p_e/p_b \approx 2$ ) can be taken as the lower limit of an underexpansion level for the formation of a Mach disc. It is important to note that this limiting level of underexpansion is strongly influenced by the nozzle geometry and the settling chamber (stagnation chamber) condition.

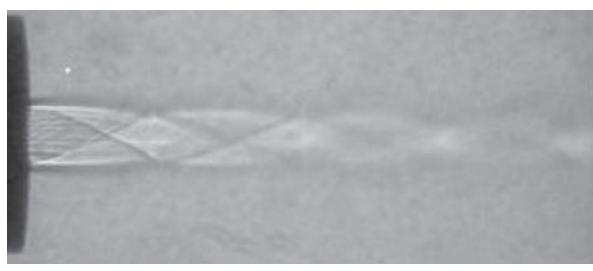
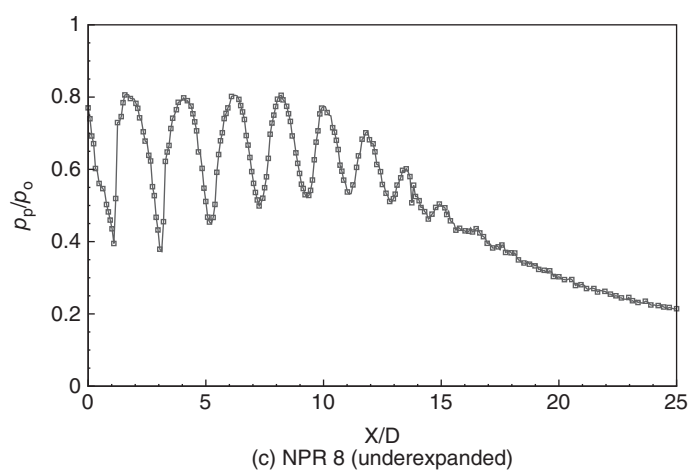
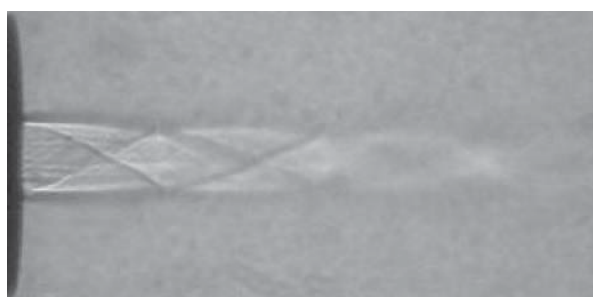
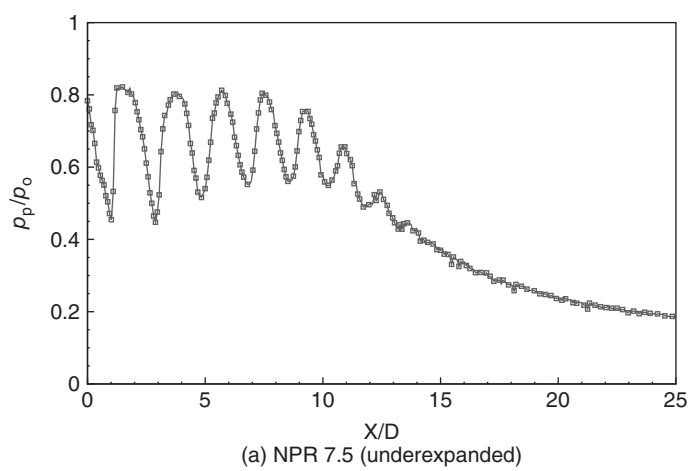
At NPRs 5 and 8, as seen in Figure 12.9e and f, the Mach disc becomes progressively larger with an increase of NPR beyond the limiting value. The flow behind the Mach disc is subsonic. This subsonic zone of low momentum receives momentum from the higher momentum flow around it and gradually gets accelerated to supersonic level slightly downstream of the disc. Because of this process, the pitot pressure behind the Mach disc remains constant up to some downstream distance. This distance increases with an increase in the underexpansion level.

The distance from the nozzle exit to the first shock crossover (or Mach disc) is called the *first shock cell length*. The distance from one shock crossing point to the next is called the *shock cell length*. As can easily be seen, the expansion and compression waves in the first shock cell are stronger than those in the subsequent cells.

The centerline pitot pressure decay and a shadowgraph picture of a Mach 1.88 jet at two levels of underexpansion levels corresponding to NPRs 7.5 and 8 are shown in Figure 12.10.

## 12.6 Control of Jets

There are numerous systems, where the ability to enhance the mixing of a jet will greatly improve their performance. For example, by increasing the rate of mixing between air and fuel, the efficiency of a combustion cycle can be improved. In SCRAMJET the entire mixing process has to be completed within a short distance to minimize the size of the combustor and for enhancing the performance of the entire vehicle system. In combustion systems, both large- and small-scale mixing enhancement is sought since large-scale mixing determines the rapidity of the mixing process and small-scale or microscale level mixing ensures effective molecular level mixing for efficient combustion. By increasing the rate of mixing with the ambient fluid, the infrared radiance of the plume can be reduced. Other examples of technological



**Figure 12.10** Centerline pitot pressure decay and shadowgraph pictures of an underexpanded Mach 1.88 circular free jet.



applications requiring control of mixing in compressible flows include thrust augmenting ejectors, thrust vector control, metal deposition, and gas dynamic lasers. The diverse nature of applicability of jets demands that they be made suitable for a specific application by controlling them. Here, *control* may be defined as the ability to modify the jet flow mixing characteristics to achieve engineering efficiency, technological ease, economy, adherence to standards, and so on.

## 12.6.1 Classification of Control Methods

All types of jet controls can be broadly classified into either active or passive controls. In active control, an auxiliary power source (like microjets) is used to control the jet's characteristics. In passive control the controlling energy is drawn directly from the flow to be controlled. Both active and passive controls mainly aim at modifying flow and noise characteristics.

### 12.6.1.1 Active Control

Many active jet control methods use energized actuators to dynamically manipulate flow phenomena by employing open- or closed-loop algorithms. Pulsed jets, piezoelectric actuators, microjets, and oscillating jets are among the most effective controls for active mixing enhancement. The design of an active flow control system requires knowledge of flow phenomenon and the selection of appropriate actuators, sensors, and a control algorithm.

The role of an actuator is to inject perturbations at a prescribed frequency into the flow at locations where the flow is most receptive to these inputs. The actuator leverages or disrupts the flow to bring about a desired effect. For example, the conventional excitation methods rely on exciting instability modes with their most amplified frequency band to bring about jet mixing enhancement. For jet excitation, the conventional philosophy has been to energize the large-scale coherent structures (large suction creators) or bring about vortex interactions that result in the engulfment of surrounding fluid (entrainment), resulting in mixing enhancement.

Active control methods are selected to achieve maximum receptivity for the specific medium considered. The flow can be excited by mechanical means, such as fluctuating flaps, vibrating ribbons, piezoelectric surfaces, acoustical perturbation; hydrodynamic methods, such as periodic suction and blowing; thermal techniques, such as heating strips or electrical discharge; or by modulation of the free stream. To maximize the effect, the external perturbations should match the flow instability band to take advantage of the natural amplification of the flow. Crow and Champagne demonstrated active control of a turbulent jet [25]. They used acoustical excitation at the preferred mode of the jet to enhance the jet's growth rate and produce highly coherent structures. By choosing the proper frequency, the growth rate and entrainment characteristics of the shear layer can be controlled to either enhance or suppress them.

### 12.6.1.2 Passive Control

Among the two main types of jet control, passive controls are mostly desired not only because no external power source is required but also because in some cases the engineer is left with no other option. Passive control usually uses geometrical modifications of the element from which flow separation occurs to change the shear layer stability characteristics. Some examples of these modifications are: trip wires in plane shear layers; convoluted splitter plates; and non-circular jets such as square jets and elliptic jets. Some of the commonly used passive control methods are shown in Figure 12.11.

Passive control techniques range from alterations in the exit shape of the nozzle to the implementation of tooth-like tabs and vortex generators in the jet. Many studies have focused on the placement of small tabs and vortex generators at the exit of axisymmetric and rectangular nozzles. These methods primarily aim at disturbing the boundary layer at the nozzle exit to

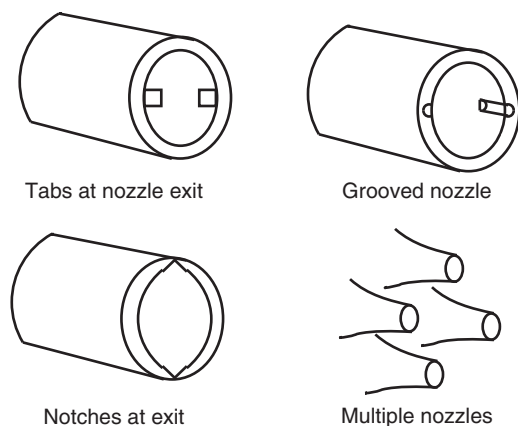


Figure 12.11 Schematic of a few passive controls.

achieve the desired flow behavior. Particularly, the grooves or tabs at the exit trip the boundary layer developing inside the nozzle. This drastically influences the shear layer growth and flow behavior, thus providing a lot of scope for mixing enhancement.

Mixing enhancement has many technological benefits and is, therefore, an area of continuing research. Various control schemes have been examined in an effort to increase mixing in different flows. A common strategy in these schemes has been to manipulate the large-scale vortical motions indigenous to the shear region. Primarily, these are the spanwise vortical structures that characterize all two-dimensional shear layers. Another form of the large-scale structures, receiving attention lately, are the steady streamwise vortices, e.g. those produced by vortex generators. The large structures, in any form, play a crucial role in the dynamics of the shear layer. They are responsible for the bulk of the entrainment and transfer of mass and momentum across the shear region.

### 12.6.2 Role of Shear Layer in Flow Control

When a jet issuing from a nozzle propagates into the stagnant air, at the jet boundary, vortices are generated because of the shear between the fluid elements of the jet which are in motion and the stationary fluid elements of the atmosphere. These vortices entrain the stagnant air mass into the jet. Thus, an active shear zone is established at the jet boundary in the proximity of the nozzle exit. The shear action propagates toward the jet axis and reaches the axis at some downstream distance. From this location onward, the viscous action dominates the entire jet field. A thorough understanding of the shear action is essential to control the mixing and acoustic characteristics of the jets.

#### 12.6.2.1 Large-Scale Structure in Subsonic Shear Layers

The original work of Brown and Roshko on the structure of planar mixing layers triggered extensive research during the past three decades that substantiated the idea that large-scale coherent structures control the dynamics of all free shear flows including plane mixing layers, jets of different geometries (axisymmetric, plane, elliptic, rectangular, and so on), and wakes [26]. These two-dimensional structures were found to play an important role in entrainment and mixing processes in incompressible shear layers.

The formation of coherent structures in a shear layer is initiated by Kelvin–Helmholtz instability, governed by Rayleigh's equation for inviscid flows. The exponential growth of the velocity and vorticity perturbations leads to a nonlinear process that eventually causes the roll-up of the shear layer vortices. The initial vortex shedding frequency  $f_i$ , which is also called the *most*

*amplified frequency*, is determined by various characteristics of the exit velocity profile, such as shape, turbulence structure, initial shear layer momentum thickness ( $\theta_o$ ), and the jet exit velocity ( $U_o$ ).

The initial vortices grow in the shear layer and coalesce as they are convected downstream in a “pairing” process [27]. Owing to merging and entrainment, the shear layer spreads and the frequency associated with the large vortices decreases. The irrotational entrainment by the large-scale structures leaves the entrained fluids essentially unmixed during the lifetime of the vortices [28]. Nonetheless, intense mixing occurs during pairing or other amalgamation processes. Some distance downstream of the splitter plate trailing edge, a secondary, spanwise instability appears, leading to the development of streamwise vortices [29]. The appearance of these vortices enhances the mixing process, which is referred to as the *mixing transition*. The streamwise vorticity, which is organized in *ribs*, interacts with the spanwise structures. With increasing downstream distance, the interaction increases the three-dimensional structure in the shear layer, leading to high-order instabilities and transition to a small-scale dominated flow.

In the shear layer of the jet, the physical dimensions of the nozzle introduce new length scales, which are not present in a plane shear layer. The number of vortex interactions is limited by the distance between the nozzle and the location where the shear layer surrounding the potential core merges (the typical length of the potential core of an initially laminar jet is about five diameters, or slot-widths). The jet flow characteristics at the end of the potential core are determined by jet-column instability [25].

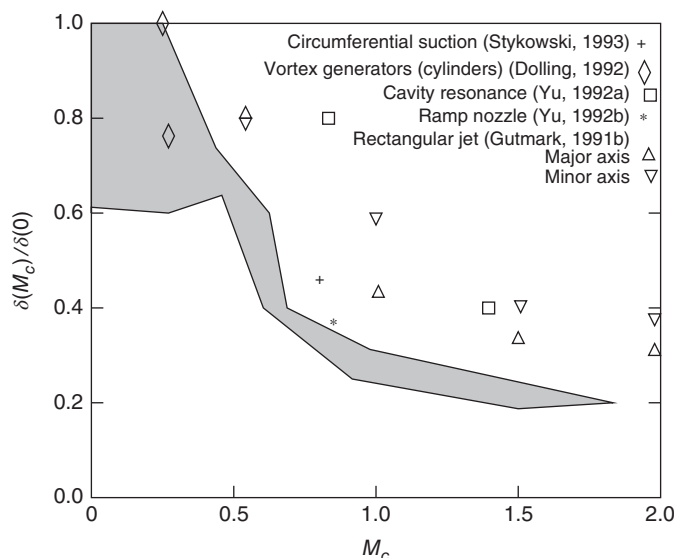
### 12.6.2.2 Role of Large-Scale Structures in Subsonic Mixing Enhancement

Existence of large-scale structures in the shear layer and their relation to the flow stability make it possible to control the development of the shear layer and, thus, affect its mixing characteristics. In general, large-scale structures are beneficial for the enhancement of bulk mixing, but they hinder fine-scale or molecular mixing, which is necessary, for example, in reacting flow applications. Enhancement of both large- and small-scale mixing can be achieved by exciting a combination of unstable modes.

### 12.6.3 Supersonic Shear Layers

Mixing in supersonic shear layers is critically dependent upon the compressibility effects in addition to the velocity and density ratios across the shear layer. The compressibility level is best described by a parameter called the *convective Mach number* ( $M_c$ ) [30, 31]. This parameter is defined as the relative convection speed of the large-scale structures in shear layer to one of the freestreams, normalized by the speed of sound of that stream. The two convective Mach numbers of the streams (designated as 1 and 2) are:  $M_{c1} = (U_1 - U_c)/a_1$  and  $M_{c2} = (U_2 - U_c)/a_2$ , where  $U_c$  is the convective velocity of the structures,  $U$  is the mean velocity of the freestream, and  $a$  is the speed of sound. These convective Mach numbers are equal to each other in shear layers with equal static pressures and specific heats ratio in the two streams,  $M_{c1} = M_{c2} = M_c = (U_1 - U_2)/(a_1 + a_2)$ .

The ratio of compressible to incompressible spreading rates of the shear layer has been described as a function of the convective Mach number, as illustrated in Figure 12.12. This figure shows that compressibility effects cause the spreading rate to drop significantly, reaching an asymptotic value close to 20% of the spreading rate observed in incompressible shear layers for  $M_c > 0.8$ . One potential mechanism for the stabilization of the compressible shear layer relative to incompressible flow is the suppression of upstream and cross-flow communication paths within the shear layer due to the high Mach number [31]. Acoustic interaction between



**Figure 12.12** Summary of some mixing-enhancement techniques in supersonic shear flows. The enhanced normalized shear-layer spreading rates compared with baseline data (shaded area) is combined from several references showing the normalized spreading rate of the unforced compressible shear layer as a function of the convective Mach number.

different regions of the shear layer, which is possible in an elliptic subsonic flow, are inhibited, thus stabilizing the compressible flow.

Compressible shear layers are subjected to density gradients. However, Brown and Roshko showed that the growth rate of an incompressible shear layer with a density ratio alone cannot explain the much larger decrease in the growth rate of compressible shear layers [26]. The density gradients in compressible shear layers, coupled with large pressure gradients across shocks, produce vorticity, owing to the baroclinic torque  $-1/\rho^2(\nabla\rho \times \nabla p)$ , which is uncommon in incompressible flows.

Mixing enhancement has many technological benefits and is, therefore, an area of continuing research. The mixing process in jet shear layers involves bulk mixing driven by large-scale coherent structures and small-scale mixing dominated by turbulent velocity fluctuations. Large-scale structures, characterized by organized vorticity distributions, are intrinsic features of the high Reynolds number mixing layer [26]. Control of jet development for practical applications is largely dependent on understanding the dynamics and topology of coherent structures, in particular how jet properties can be affected by control of the formation, interaction, merging, and breakdown of coherent structures.

Formation of circular, azimuthally coherent vortex rings and their sequential merging dominate the shear-layer growth and the entrainment in axisymmetric jet configurations at moderately high Reynolds number [25]. At a short distance downstream of the jet exit, three-dimensionality becomes the crucial feature of the jet structure, and the streamwise vorticity has the dominant role in entraining fluid from the surroundings [32]. Self-induction, vortex stretching, and reconnection become the dominant fluid dynamical processes involved [33]. Azimuthal nonuniformities at the jet exit add complexity to the evolution of the jet shear layer; the three-dimensional development of the jet is particularly sensitive to initial conditions, for example the nozzle geometry or upstream disturbances. In noncircular jets, deformation dynamics of asymmetric vortices play an important role in the jet evolution. Asymmetric jets

are naturally more unstable than their axisymmetric counterparts. Amplification of high-order instability modes, rather than the axisymmetric mode that dominates the near-field region of a circular jet, brings about complex vortex topologies.

Substantial efforts have been devoted to investigating the properties of jets emerging from noncircular nozzles. Verma and Rathakrishnan studied elliptic nozzles with corners, e.g. rectangular and triangular, and observed that as the jet spreads its cross-section can regularly evolve through shapes similar to those of the jet nozzle, but with axes successively rotated at angles characteristic of the jet geometry, referred to as the *axis-switching phenomenon* [34]. This main underlying mechanism for the enhanced entrainment properties of noncircular jets, relative to comparable circular jets, results from self-induced Biot–Savart deformation of vortex rings with nonuniform azimuthal curvature and interaction between azimuthal and streamwise vortices. Owing to Biot–Savart self-induction, portions of the vortex with small radius of curvature, such as the major axis section of elliptic rings or the vortices in square or triangular rings, will move downstream faster than the rest, leading to their deformation. As the vortex convects downstream, the deformations yield a complex topology, which results in redistribution of energy between azimuthal and streamwise vortices whose subsequent interaction increases the small-scale vorticity content of the jet.

In supersonic planar, axisymmetric, and noncircular shear layers, the effect of compressibility on mixing becomes important and adds to the effects of velocity and density gradients and azimuthal distribution. The convective Mach number ( $M_c$ ) [30, 35] quantifies the compressibility effect. The spreading rate of a plane shear layer drops sharply to about 20% of the incompressible spreading rate as  $M_c > 0.6$ . Supersonic shear layers exhibit augmented three-dimensional vortical structures, owing to preferential amplification of high modes of instability. Therefore, noncircular jets that are inherently dominated by high azimuthally unstable modes are particularly suitable for enhancing mixing in supersonic flows.

Shear-flow control methods seek to enhance the three-dimensionality of the flow, and thus entrainment and mixing, by manipulating the natural development of large-scale coherent structures and their breakdown into turbulence. Passive mixing-control strategies are based on geometrical modifications of the jet nozzle, which alter the flow development downstream of the nozzle relative to a conventional circular nozzle. Interest in noncircular jets was driven primarily by the potential to obtain enhanced mixing between the jet flow and the surroundings. Elliptic and rectangular jets were shown to have entrainment rates significantly larger than those of circular or two-dimensional jets, owing to vortex self-induction effects [36]. Enhanced mixing was observed in both subsonic and supersonic jets. Large-scale coherent structures in natural planar shear layers [29] and axisymmetric jets [32] were altered and deformed by interaction with secondary streamwise vortices, with streamwise-vortex generation locations dependent on upstream disturbances. The interaction between azimuthal and streamwise vortices constitutes an important process, which can be used as an independent method of mixing enhancement in circular, plane jets, or in conjunction with noncircular jet geometries to achieve additional enhanced mixing. Controlled streamwise vortex generation can be achieved using different azimuthal perturbation methods, including corrugated, lobed, or indented nozzle edges, vortex generators, or other nozzle shaping concepts.

#### 12.6.4 Use of Tabs for Jet Control

Bradbury and Khadem were among the first to document the effect of tabs in a low-speed jet [37]. With square tabs placed normal to the flow at the nozzle exit, they observed a significant increase in the centerline velocity decay caused by the tabs. With the use of two tabs, the apparent potential core length was reduced to about two diameters followed by a rapid decay

of the centerline mean velocity. They considered the stirring action of trailing vortex motions shed from the tabs as a possible mechanism for the observed effect. However, they could not detect such vortex motion using wool tufts, which led to the inference that the effect was likely to be due to the circumferential variations in flow angle produced by the tabs. It would be fair to say that the flow mechanism responsible for the effect of the tab was far from clear when the investigation was started.

Ahuja and Brown reported that, for a round jet flow of Mach number 1.12 and total temperature 664 K, the potential core length of the jet flow could be reduced from six diameters to under two diameters by using two diametrically opposed mechanical tabs [38]. They found that the mixing enhancement produced by the two mechanical tabs can reduce the temperature along the jet centerline from 655 to about 472 K at a distance of five jet diameters downstream, and the mechanical tabs can reduce low-frequency noise by up to 5 or 6 dB. However, most of these investigations were focused on the overall mixing enhancement performance of mechanical tabs and the application of mechanical tabs to jet noise reduction. Not until 1993, based on the flow visualization laser sheet and cigar smoke illumination and pressure measurement of a jet flow, did Zaman propose that the distortion introduced by a mechanical tab is due to a pair of streamwise vortices and which must be responsible for the phenomenal entrainment [39]. They found that the tabs can distort the jet cross-section and increase the jet spread significantly. They conjectured that a tab with a height as small as 2% of the jet diameter, but larger than the efflux boundary layer thickness, produces a significant effect. They further explained that tabs are ineffective in the overexpanded flow, as in that case an adverse pressure gradient exists near the nozzle exit which reduces the pressure differential produced by tabs. From their centerline pitot pressure measurements, the drastic reduction of the jet potential core length and alteration of the shock-expansion train with reduced shock-cell spacing can be clearly seen under the action of the tabs. They identified that variation of tab length for a given width did not seem to make much difference as long as the length was larger than the boundary layer thickness.

Subsequent researchers have clearly determined that the tab produces a pair of counter-rotating streamwise vortices [40–42]. The sense of rotation of the vortex pair is such that, fluid from the center of the tab base flows toward its tip. The relative magnitude of the peak streamwise vorticity was found to be about 20% of that of the peak azimuthal vorticity for a tabbed circular jet at a Mach number of 0.3 [39].

Zaman, Reeder, and Samimy surmised two possible sources of streamwise vorticity for the flow over a tab [40, 41]. The dominant source comes from the *pressure hill* formed upstream of the tab. The flow deceleration by the tab creates a pressure hill, which together with the presence of the wall produces the pair of counter rotating streamwise vortices. This mechanism is described mathematically by the Navier–Stokes equation at the wall,

$$\left. \frac{1}{\rho} \frac{\partial p}{\partial z} \right|_{y=0} = \nu \left. \frac{\partial}{\partial y} (\omega) \right|_{y=0}$$

where  $y$  and  $z$  are the lateral (normal to the wall) and spanwise coordinates, respectively, and the substitution,  $\omega_x|_{y=0} = \frac{\partial w}{\partial y}$ , has been made. The secondary source, again owing to the pressure gradients on the tab's surface, is the vorticity shed from the sides of the tab. Initially, vorticity is shed parallel to the edge; as it convects downstream, it becomes reoriented by the velocity gradients in the shear layer. Thus, if the tab is tilted downstream, vorticity from primary and secondary sources adds together, improving the tab's effectiveness [40]. In addition to the pressure gradients which induce streamwise vorticity into the flow, the well-known *necklace* or *horseshoe* vortices due to boundary layer reorientation can also be important in the flow over a tab. Several researchers have detected the cores of necklace vortices [41, 43]. It should be noted

that the sense of rotation of the vortex pair from the pressure hill is always opposite to that of the necklace vortex pair.

Several studies have reported results with variations in flow field conditions, as well as tab shape, size, number, and angle. The following is a summary of published results [37, 38, 40]:

- Appreciably faster decay of the centerline velocity for one-, two-, four-, and six-tab cases, relative to the reference case.
- Mixing enhancement greater for supersonic cases than subsonic cases.
- Heating the jet provides no significant change in the effectiveness of the tabs.
- Smaller tabs have less effect in distorting the jet. tab width is more critical than tab height. Tab height greater than the boundary layer thickness is required, to be effective.
- Tab is effective in the presence of a favorable pressure gradient at the nozzle exit.
- Tab shape (rectangular vs triangular) has little effect on tab performance.
- Orientation or angle of the tab is more critical than shape; triangular tab leaning  $45^\circ$  down-stream, referred to as a *delta tab*, has the greatest effect.

Several other observations regarding optimal tab placement and shape have been made. Reeder and Samimy found that the tab is best placed at the trailing edge [43]. Upstream or detached settings interfere with the pressure hill source of vorticity. Also, the tab height must exceed the boundary layer thickness to generate streamwise vorticity effectively. However, tabs with a much smaller height can produce noticeable effects. After brief parametric studies, Zaman et al. found the optimal tab shape to be triangular [40]. In the usage of the base of the tab was attached to the exit edge of a nozzle, and the apex tilted downstream  $45^\circ$ . This configuration not only worked as effectively as a square tab placed normal to the flow but also incurred less thrust penalty [44].

Kumar Singh and Rathakrishnan [45] investigated the finding of Zaman [39] that, for the same projected area, the width of the tab is more effective in enhancing the mixing than its length. They found that, for the same projected area, the length of the tab is more effective in enhancing the mixing than its width. In addition to the influence of tab geometry on mixing, they had postulated that, when the streamwise vortices are introduced right up to the jet centerline, it may prove to be an advantage in enhancing the mixing as high as 80%. Further work was done by Lovaraju, Paparao, and Rathakrishnan based on the above postulation [46]. Instead of tabs, a wire running across a diameter (cross-wire) was used as the passive control to enhance the jet mixing. The streamwise vortices introduced by the cross-wire led to a more rapid decay of the centerline pitot pressure. Also, the cross-wire was found to weaken the shocks in the jet core significantly. This passive control was found to be effective at all levels of expansion. An as high as 50% reduction in core length was achieved for Mach 1.79 at NPR 5.66. The authors had authentically proved that the limit for tab length is the nozzle exit radius and not the boundary layer thickness. This limit of tab length is termed the *Rathakrishnan limit*. However, it must be noted that the wire causes momentum thrust loss, owing to area blockage caused by the wire. Also, the drag caused by the wire in a supersonic stream must be accounted for. Hence, the thinnest effective tab has to be identified and used to minimize both the thrust loss and drag caused by the wire.

Most of the studies cited in the foregoing were conducted in free jets discharging into quiescent surroundings. Ahuja [47] and Carletti, Rogers, and Parekh [23] investigated the effect of tabs for a circular jet with a cylindrical ejector surrounding the jet. Both found an increased mixing within the ejector under the influence of the tabs. While most of the investigations on the effect of tabs have been conducted experimentally, there have also been a few numerical studies. Steffen, Reddy, and Zaman compared numerical results with corresponding experimental results and noted good agreement in terms of the vorticity field as well as overall jet

entrainment [48]. These results lent further credence to the postulations made on the basic flow dynamics as discussed above.

Design of large and jet-propelled aircraft and large booster rocket engines has focused on noise problems. Difficulties in devising satisfactory solutions stem from the inherent complexities of the phenomena of jet noise generation. Consequently, over the past two decades extensive theoretical and experimental studies have been attempted to understand the basic mechanism of jet noise generation and its abatement. Supersonic jets normally possess complex shock patterns. Therefore, the role of shock waves in noise generation becomes significant. The main sources of high-speed jet noise are: the turbulent nature of the flow, shock–turbulence interaction, flow-induced oscillations of shocks, and resonance effects. Noise from such jets is complex and may even be nonlinearly interdependent. Noise prediction for such flows for a wide range of operating conditions is not possible as yet. An intense discrete acoustic emission termed *screech* or *whistle* as a consequence of oscillating shock waves within a supersonic jet usually dominates the noise emitted by a cold model converging jet operated slightly above the choked flow condition. From the literature, it is evident that supersonic noise reduction can be achieved by enhancing mixing and eliminating or weakening and/or reducing the effective axial extent of the shock structure. To enhance jet mixing and reduce jet noise, many studies have focused on the placement of small tabs and vortex generators at the exit of axisymmetric and rectangular nozzles. These introduce streamwise vortices to transport the low-speed fluid entrained at the jet periphery toward the centerline while forcing out higher-speed core fluid. The main difference between the two methods is the type of vortex generated. Tabs (which are placed normal to the flow) generate a pair of counter-rotating vortices, but a half delta-wing vortex generator produces only a simple vortex. A tab is a small protrusion into the flow which produces a counter-rotating streamwise vortex pair that can affect the jet flow development significantly. The streamwise vortices usually have a long life and, once introduced into the flow, tend to persist over tens of jet diameters downstream. This is in contrast to azimuthal vortical structures that are more energetic but have a shorter lifespan. The generation mechanism of the streamwise vortex pairs by the tabs, and their effect on the entrainment and spreading of free jets, have been discussed in the literature [38, 41, 43, 49, 50]. In the studies carried out so far, various factors have been found to influence the jet decay. Also, the nozzle boundary layer thickness, turbulence level, and convergence were found to have insignificant influence on the jet development. In contrast, the insertion of small rectangular tabs at the exit was found to have a profound effect on jet development.

In a continuing effort to increase the mixing in free shear flows, vortex generators in the form of tabs have been investigated by several researchers [38, 41, 43, 49–52]. In the study of the effect of tabs on turbulent boundary layer, Greta and Smith also found that a tab generates a pair of counter rotating streamwise vortices that stimulate a strong ejection of boundary layer flow into the high speed flow, resulting in a rapid cross-stream mixing and a significantly thickened turbulent boundary layer [53]. In particular, it was found that just two tabs produced gross distortions in the jet development, compared to four, six, or eight tabs [37]. Also, another study, conducted by Krothapalli and Wishart discovered that placing two tabs in symmetry along the exit diameter leads to a more rapid jet development compared to asymmetrical placement [54]. Further, for overexpanded flow through a nozzle, tabs have little or no influence at low Mach numbers, whereas, at higher Mach numbers, significant flow discretions were observed. From the above discussions, it is evident that tabs are identified as a passive control with the potential to enhance mixing and attenuate jet noise. As the jet fluid travels further away from its origin, it slows down, owing to its mixing with the ambient fluid. The interaction between the jet and the ambient fluid forms the mixing layer or the shear layer. As the primary structures or ring vortices roll up and move downstream, they grow in size, owing to the entrainment of ambient



fluid. The resulting jet decay is proportional to the velocity gradient across the shear layer and is a strong function of the distance downstream of the jet exit. Liepmann and Gharib showed that streamwise vorticity drastically alters the mass entrainment of a jet, and the efficiency of this vorticity in entraining fluid increases relative to that of azimuthal vorticity as the jet evolves downstream [32]. From a jet noise point of view, alteration of the coherent structures of the jet can produce a significant reduction in far-field noise or can change the directivity or spectral characteristics of the noise field [55]. Further, for an underexpanded flow, the width of the tab was found to have a more profound effect on jet decay for the same blockage area ratios. Also, the end shape of the tab has only an insignificant effect on the distortion produced, as long as the blockage area to the flow was kept constant.

### 12.6.5 Evaluation of the Effectiveness of Some Specific Passive Controls

From the above discussions on tabs and the survey of some major findings of the effectiveness of tabs on the mixing and acoustic characteristics, it is evident that the generation of mixing-promoting vortices with the right geometry of the tabs plays a vital role in the control of the mixing and noise characteristics of jets. Also, if the size of the vortices shed can be manipulated that would prove to be an important advantage from a jet mixing point of view. These two aspects – introducing the mixing-promoting vortices up to the nozzle centerline, right from the nozzle exit, and shedding mixing-promoting vortices of varying size – were studied as two specific investigations with limiting tab, running across the diameter of convergent–divergent nozzles of three supersonic Mach numbers, and with corrugated tabs capable of shedding vortices of mixed sizes located at the exit of a convergent–divergent nozzle. The findings of these experimental studies are discussed below.

#### 12.6.5.1 Jet Control with the Limiting Tab

To gain an insight into the physics of the vortices shed by the control in the form of a cross-wire, popularly known as the *Rathakrishnan limit*, a detailed experimental investigation was carried out by Rathakrishnan [24]. The effect of the vortex shed by the cross-wire on the mixing and acoustic aspects was clearly brought out in this investigation. A pitot probe was used to measure the pressure along the jet centerline at various operating conditions. In the supersonic flow region, the measured pitot pressure  $p$  corresponds to the stagnation pressure behind the bow shock in front of the pitot probe. It is important to note that, in a supersonic jet core, what the probe measures is the total pressure behind the bow shock that stands ahead of the probe. Thus, it is not the actual total pressure. If the actual total pressure is required, one has to correct the measured pressure for the pressure loss across the shock. But the jet core is wave dominated and the Mach number in the core varies from point to point; also, the shocks in different shock cells are of different strength. Therefore, it is difficult to correct the measured total pressure for shock loss. Furthermore, in supersonic regions there is some measurement error due to probe interference with shock-structure. Hence, the results in supersonic regions should be considered only as qualitative and are good enough for comparative purposes [56]. Nevertheless, the data are accurate enough to capture the overall features, such as the number of shock-cells and the spacing between them, and so on. In a steady supersonic flow with a single normal shock ahead of the pitot tube, a sharp drop in total pressure followed by a rise signifies the presence of a strong shock wave. The measured data consist of the settling chamber pressure, the pitot pressure along the jet centerline, and the stagnation temperature.

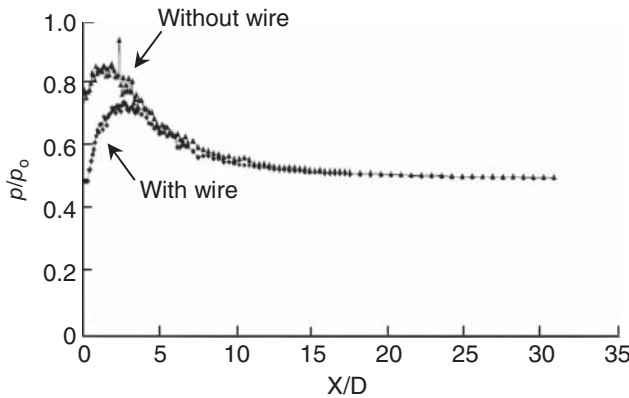
The effectiveness of the limiting tab on the mixing and acoustic characteristics of three supersonic jets is discussed here. The Mach numbers 1.6, 1.79, and 2 were specifically chosen to study the cross-wire effect jets which are screech prone (Mach 1.6 and 1.79 jets) and jets without

screech. A Mach 2 jet is also studied, since, even though a Mach 2 jet without control is free from screech, when the wire is introduced the Mach number downstream of the wire may be such as to fall into the range of 1.6–2.0 to become screech prone. Another aspect of interest in jet control is the control effectiveness in the presence of an adverse pressure gradient. To achieve this goal the NPRs considered were such that the jets generated were underexpanded, correctly expanded, and overexpanded, exhibiting a favorable pressure gradient and adverse pressure gradient with underexpanded and overexpanded conditions, respectively. Mach 1.6 and 1.79 jets were tested at NPRs 2, 4, 6, and 8. In addition to these NPRs, they were also tested at correct expansion. The tested NPRs for Mach 2 were 4, 7.82, and 9.

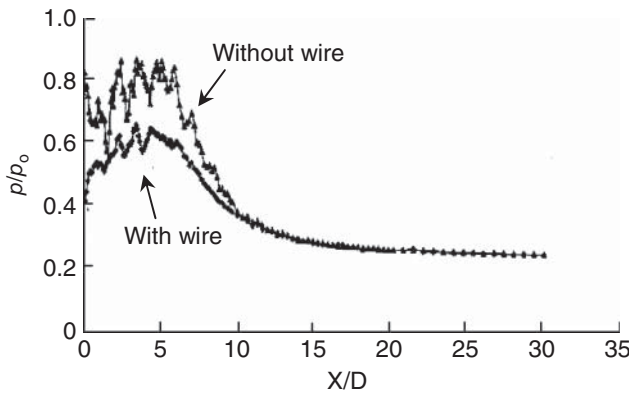
### 12.6.5.2 Centerline Decay

The jet centerline pitot pressure decay is a measure of jet mixing. Therefore, to investigate the effect of the cross-wire on jet mixing the measured pitot pressure ( $p$ ) along the jet axis ( $X$ -direction) is nondimensionalized with the settling chamber pressure ( $p_0$ ) and plotted as a function of nondimensionalized axial distance,  $X/D$  (where  $D$  is the nozzle exit diameter) in Figures 12.13–12.17. Centerline pressure decay for a Mach 1.6 jet operated NPR 2, with and without cross-wire is compared in Figure 12.13.

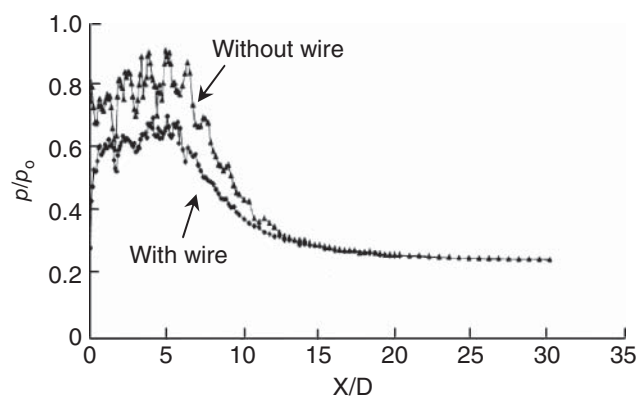
For the uncontrolled jet, the core is the axial extent up to which supersonic flow prevails. But when the cross-wire is introduced, the core can be taken as the axial extent from the nozzle



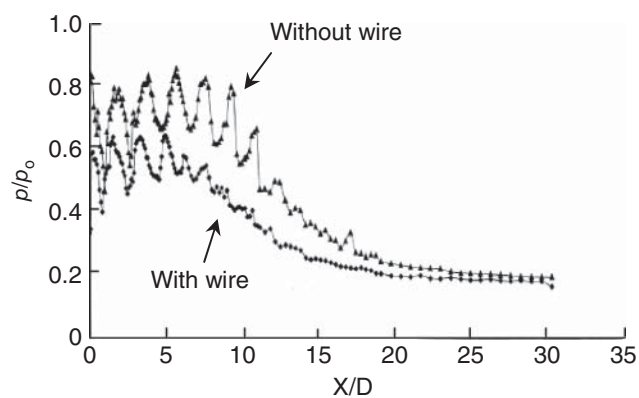
**Figure 12.13** Centerline decay for a Mach 1.6 jet at NPR 2 (overexpanded).



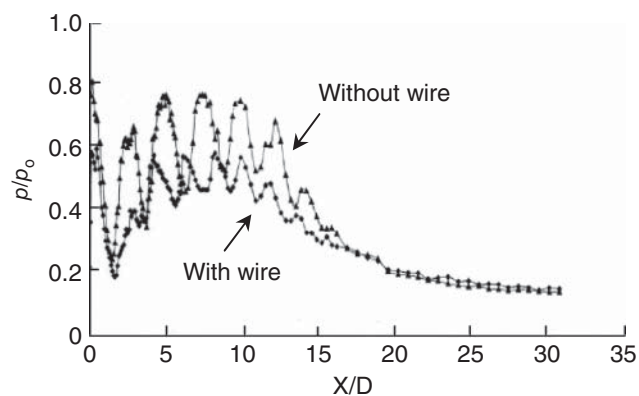
**Figure 12.14** Centerline decay for a Mach 1.6 jet at NPR 4 (overexpanded).



**Figure 12.15** Centerline decay for a Mach 1.6 jet at NPR 4.24 (correctly expanded).



**Figure 12.16** Centerline decay for a Mach 1.6 jet at NPR 6 (underexpanded).



**Figure 12.17** Centerline decay for a Mach 1.6 jet at NPR 8 (underexpanded).

exit at which the characteristic decay begins. The cross-wire essentially divides the jet into two smaller jets. Because of this bifurcation and the associated initiation of enhanced transverse momentum exchange, the flow along the centerline behind the wire gains momentum rapidly, attains a peak followed by characteristic decay, typical of a free jet. Therefore, the axial extent at which characteristic decay begins can be justifiably taken as the core length for the jet from a nozzle with a cross-wire [56]. It can be seen that the uncontrolled jet core has only mild oscillations in the centerline pitot pressure. This implies that the shocks prevailing in the jet core are very weak. But the jet from the nozzle with the wire does not exhibit any pitot pressure oscillation. This reveals that there are no waves of significant strength along the jet centerline downstream of the wire. After the core, the jet without wire experiences a faster decay than the jet with wire. It should be noted that all the above-mentioned differences in the jet behavior are taking place within  $10D$  axial distance. Beyond  $10D$ , jets from nozzles with wire and without wire behave very similarly. It is well established that weakening the shocks in the jet core will result in a reduction of shock-associated noise, and hence a reduction in the overall noise [56]. Therefore, weakening the mild shocks in the core by the presence of wire can be expected to result in jet noise reduction. The faster decay of the jet from the plain nozzle (without wire) is because the jet passes through a number of mild shocks before the core ends, thereby resulting in a lower subsonic Mach number compared to the wired for which the core does not possess any shock of significant strength. The jet with wire has a marginally shorter core than the plain nozzle jet. It is essential to be cautious here about the arguments given for the larger pressure loss at the nozzle exit when the wire is introduced. Because of the wire there is a detached shock generated. This shock is positioned upstream of the wire. Therefore, the pitot pressure just behind the wire is the pressure in the subsonic wake of the wire. Hence, what is measured is essentially the pressure in the wake of the wire. Thus, the magnitude assumes significantly lower values than the plain nozzle jet.

The centerline decay for NPR 4 is given in Figure 12.14. This is again an overexpanded state for a Mach 1.6 jet. It can be seen that the shocks in the jet core become significantly weaker when the wire is introduced. Also, the core length is reduced considerably with the introduction of the wire. It should be noted that, even though both NPR 2 and NPR 4 generate overexpanded jets, the level of overexpansion comes down with an increase of NPR, that is with NPR increase the adverse pressure gradient comes down and the cross-wire becomes more effective in reducing the core length and weakening the shocks.

These results agree well with the observation made by Samimy and Reeder that passive control will be effective in the presence of a favorable pressure gradient [57]. Even though the above NPR increase from 2 to 4 does not establish a favorable pressure gradient, the adverse pressure gradient level decreases when the NPR is increased from 2 to 4 and hence the passive control becomes more effective. For NPR 4, the core has decreased from  $7.2D$  (plain nozzle) to  $4.6D$  (nozzle with wire), that is the presence of the wire causes a reduction of about 36% in core length.

The centerline decay for NPR 4.24 (correctly expanded) is shown in Figure 12.15.

For the plain nozzle, the core exhibits shocks of significant strength, even though at the nozzle exit there is no shock present for the correct expansion. This is because, even though the nozzle is correctly expanded, the flow exiting the nozzle finds a larger area to relax. This would cause the flow to encounter an associated expansion fan. Because of this expansion fan at the nozzle exit, the flow accelerates to a higher Mach number downstream of the nozzle exit and the expansion waves getting reflected as compression waves from the jet boundary coalesce to form a shock at the jet axis and the shock gets reflected as an expansion fan, and the cycle repeats. As a result, in the uncontrolled jet, the initial shocks are weaker compared to some of the downstream shocks. But when the wire is introduced, the shock envelope in front of

the wire results in significant reduction in total pressure and hence a much lower pressure at  $x/D = 0$ , compared to the plain nozzle jet. The shocks were found to be very weak for the wired case and the core decreases from  $9.2D$  to  $6.3D$ . Here again the wire does not influence the jet propagation beyond  $13D$ .

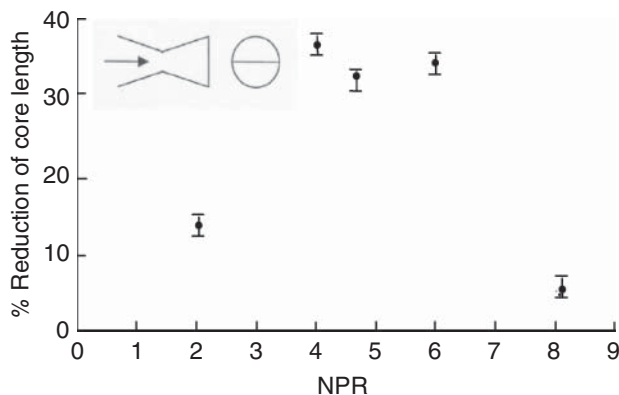
The centerline decay for an underexpanded jet with and without wire, at NPR 6, is compared in Figure 12.16.

This is the case with a favorable pressure gradient, since the jet is underexpanded. As reported by Zaman et al. [39, 40, 44], Samimy and Reeder [57], and Kumar Singh and Rathakrishnan [45], the passive control causes significant core reduction. For the plain nozzle large numbers of strong shocks are present in the core and the core extends up to about  $17D$ . Whereas, when the wire is introduced, the core length comes down to around  $12D$ . Further, the numbers of shock-cells are reduced and shocks become significantly weaker. Also, the effect of wire results in different decay than the plain nozzle even beyond  $13D$ .

When the underexpansion level increases, the favorable pressure gradient also increases and the shocks in the core for the plain nozzle become stronger, as seen in Figure 12.17, for NPR 8.

At this level of underexpansion also, the cross-wire causes the shocks to become considerably weaker. But the core length reduction achieved is only marginal for this case. For both with wire and without wire, the jet decay retains its identity as far as  $30D$ .

From the above discussions on centerline pressure decay, it can be inferred that the wire is effective in promoting jet mixing at all levels of expansion. However, the expansion level significantly influences the degree of wire effectiveness in promoting mixing. The physical reason for the wire performance may be summarized as follows. The azimuthal radius of curvature of a plain nozzle exit is uniform. Therefore, azimuthal vortices of uniform size are shed at the nozzle exit. Owing to this, the vortices would be able to promote the mixing only from a downstream station where they interact with the mass-entraining vortices at the jet periphery. But the cross-wire, as reported by Lovaraju et al. [56], to begin with introduces four sharp corners with the nozzle exit, at their root ends, thus spoiling the uniformity of the azimuthal radius of curvature of the nozzle exit. These four corners would shed vortices of a smaller size than the azimuthal vortices. Thus, vortices of varying size are generated right at the nozzle exit. It is well known that large vortices are efficient entrainers but are highly unstable, and then they easily get fragmented into small vortices. In other words, large structures have a comparatively short lifespan and cannot travel long distances [56]. In contrast, small vortices are efficient mixing promoters and are capable of traveling longer distances before losing their identity, even though they are poor entrainers. Therefore, the mass-entraining large structures and mass-transporting small structures should exist in proper proportion for the efficient mixing of the jet mass with the ambient fluid. But identifying an optimum combination of large and small vortices is very difficult because the vortices are extremely sensitive to both flow and geometrical parameters, and in a jet the flow parameters vary at a rapid rate, which cannot be predicted explicitly. Owing to the complex nature of the vortex dynamics, it is usual practice to quantify the mixing by measuring flow parameters such as pitot pressure, which is amenable for physical measurements. In addition to introducing the sharp corners, the wire in a supersonic stream positions a detached shock all along its length. The flow over the wire assumes a reduced velocity after passing through the shock envelop. Owing to this flow, the wire sheds a row of spanwise vortices (rotational axis along the wire length) on either side. Even though these vortices are spanwise while shedding, they become streamwise soon after shedding, owing to the inertia of the jet flow. These spanwise vortices, being small and shed right up to the jet centerline, are able to promote significant mixing. Another aspect of the control with cross-wire is that the geometry of the nozzle is essentially rendered asymmetrical, as reported by Lovaraju and Rathakrishnan [58]. Because of this, even though the flow encounters greatly reduced velocity



**Figure 12.18** Percentage reduction of the core length with NPR for a Mach 1.6 jet.

due to the shock envelop at the wire and due to the wire wake, on either side of the wire the flow has high inertia. The low momentum fluid behind the wire receives momentum from the neighboring high momentum streams on either side of the wire through the active momentum exchange process associated with the turbulent jet flow. All these favorable mixing promotion aspects make the controlled jet decay faster than its uncontrolled counterpart. To quantify the above results on core length reduction, the parameter, and percentage reduction of core length, defined as

$$\text{Percentage reduction} = \frac{(\text{Core length without wire} - \text{Core length with wire})}{(\text{Core length without wire})} \times 100$$

has been used. The variation of percentage reduction in core length as a function of NPR for a Mach 1.6 jet is shown in Figure 12.18.

It can be seen that the cross-wire is highly effective in reducing the core length in the range of NPR from about 4–6. It is interesting to note that this range of NPR covers overexpanded, correctly expanded, and underexpanded conditions for the jet. Hence, the literature stating that passive control will not be efficient under adverse pressure gradient and will be very efficient under a favorable pressure gradient should be looked into again. From the above results, it can be seen that the passive control in the form of cross-wire extending up to the nozzle centerline can reduce the core length and weaken the shocks in the core very efficiently for some combinations of Mach number and level of expansion. A closer look into the physical phenomenon taking place in the jet when the wire is present may explain the reason for this control achieved with a cross-wire. Basically, when a cylinder is placed in a subsonic stream it will shed vortices alternately. These vortices are streamwise in nature and can travel a long distance compared to spanwise or azimuthal vortices. Therefore, the streamwise vortices can efficiently serve as a mixing enhancement mechanism for jets [56]. This aspect is exploited for faster decay with passive control in subsonic jets. But in supersonic jets the core consists of a mixture of subsonic and supersonic Mach number zones. Further, when a passive control in the form of a cylindrical cross-wire is introduced at the nozzle exit, a detached shock is positioned ahead of the wire. This makes the flow behind the shock subsonic, thereby enabling the wire to shed streamwise vortices, as in the case of subsonic flow. However, these streamwise vortices shed by the cross-wire have to pass through different Mach number zones in the jet flow field before losing their identity. This process results in mixing enhancement. The mixing level would vary from place to place in the supersonic jet because of the presence of mixed subsonic and supersonic zones. Nevertheless, the mixing initiated by these streamwise vortices will result in significantly

enhanced mixing of the supersonic jet, especially in the core region. This is the main cause for the shocks in the core becoming weaker compared to the plain nozzle jet. The effectiveness of the cross-wire is strongly influenced by the level of expansion since the Mach number zones in the jet core strongly depend on the expansion level, that is the level of NPR.

### 12.6.5.3 Flow Development

To understand the physics of the generation of streamwise vortices and their effect on jet mixing, the pitot pressures measured at different planes normal to the jet axis were studied by constructing isobars using the measured pressures. The isobaric contours for a Mach 1.6 jet, with and without wire,  $X/D = 0$  and 1 for NPR 4, 4.24, and 6 are shown in Figure 12.19a–c. The outermost isobaric contour in these figures is with  $p/p_0 = 0.2$ , with intermediate contours uniformly stepped up by a value of  $p/p_0 = 0.1$ .

The isobars for NPR 2 at different axial distances from  $X/D = 0$  to 6 exhibited that, at  $X/D = 0$ , the introduction of the wire introduces a relatively low-speed zone across the jet. As the jet moves downstream the low-speed zone introduced gets bifurcated and forms two counter-rotating zones toward the jet periphery. Because of this, the jet with cross-wire behaves like a noncircular jet, showing a tendency of axis switching, which is a well-known phenomenon in jet mixing. An earlier axis switching implies a faster mixing. For NPR 2, the axis switching with wire was at about  $6D$ , whereas for the plain nozzle case there was no tendency of axis switching. This validates the discussion (Figure 12.13) indicating almost no shocks in the core.

The isobars for NPR 4 (Figure 12.19a) show axis switching at  $X/D$  of less than 1. This implies a greater enhancement in mixing compared to NPR 2. This is reflected as a drastically reduced core length and significantly weakened shocks in the core, as seen in Figure 12.14. The slower jet decay compared to the plain nozzle case was also evident from the larger jet width of the plain nozzle compared to the wired nozzle at  $X/D = 5$  and 6. The bifurcation of the jet by the cross-wire is evident from these isobars. A similar effect of cross-wire bifurcating the jet with high Mach number cores on either side of the wire was reported by Lovaraju and Rathakrishnan [58]. For the correctly expanded case at NPR 4.24 (Figure 12.19b), the axis switching is taking place at  $X/D$  of less than 1. The observation of considerable reduction in core length and decrease of shock strength due to wire control are supported by these isobars. The faster decay of the jet after the core for the plain nozzle compared to the controlled nozzle was evident from the isobars.

The isobars at an underexpanded condition with NPR 6 (Figure 12.19c) show that the jet core for the plain nozzle contains no low-speed zones, but low-speed zones are introduced at the centerline when the wire is introduced. However, because of the favorable pressure gradient the jet travels faster and the axis switching takes place at about  $3D$  compared to less than  $1D$  for the lower NPR cases. The streamwise vortices could not weaken the shock to the extent that they could for the lower NPR cases. However, the effect of the vortices introduced by the wire on core length reduction and shock weakening became better after the fourth cell, that is beyond  $5D$ . For NPR 8, the axis switching is taking place at  $3D$ . The streamwise vortices introduced by the wire could only have a marginal control over the shock strength and jet mixing in the near field.

From these isobaric contours it can be seen that the circular geometry of the nozzle is made noncircular by the wire. As discussed earlier, the wire introduces four sharp corners to the nozzle exit. This makes the uniform azimuthal radius of curvature at the nozzle exit asymmetric. This leads to the formation of vortices of mixed sizes. This mixed size of vortices initiates mixing right at the nozzle exit. In addition to this, unlike tabs, the wire sheds streamwise vortices all along the diameter of the nozzle exit. Also, the vortices shed by the wire encounter a low-momentum zone in the wake of the wire, thus finding more residential time for their

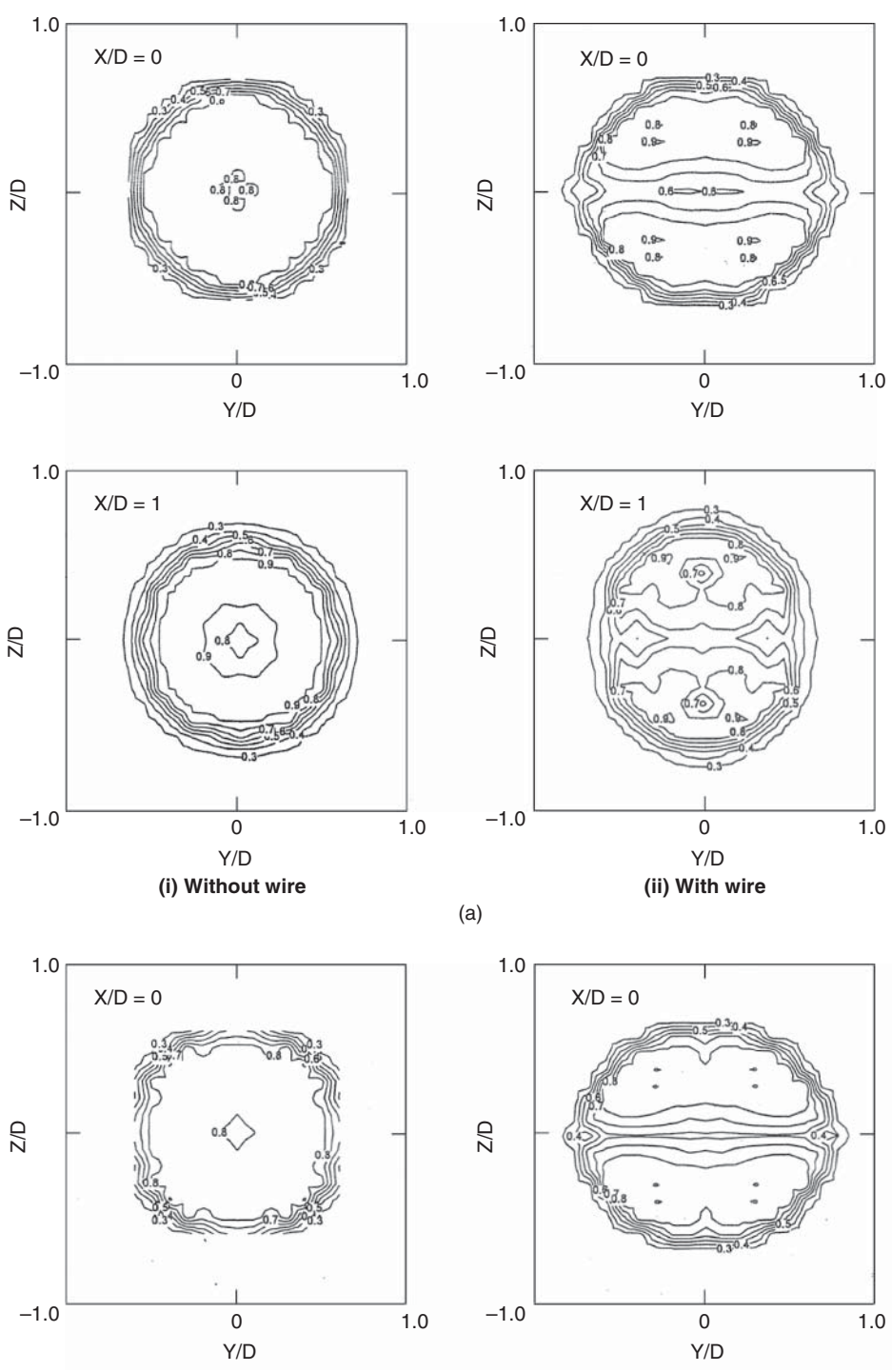


Figure 12.19 Isopitot pressure contours for (a)  $M = 1.6$  at NPR 4; (b)  $M = 1.6$  at NPR 4.24; and (c)  $M = 1.6$  at NPR 6.



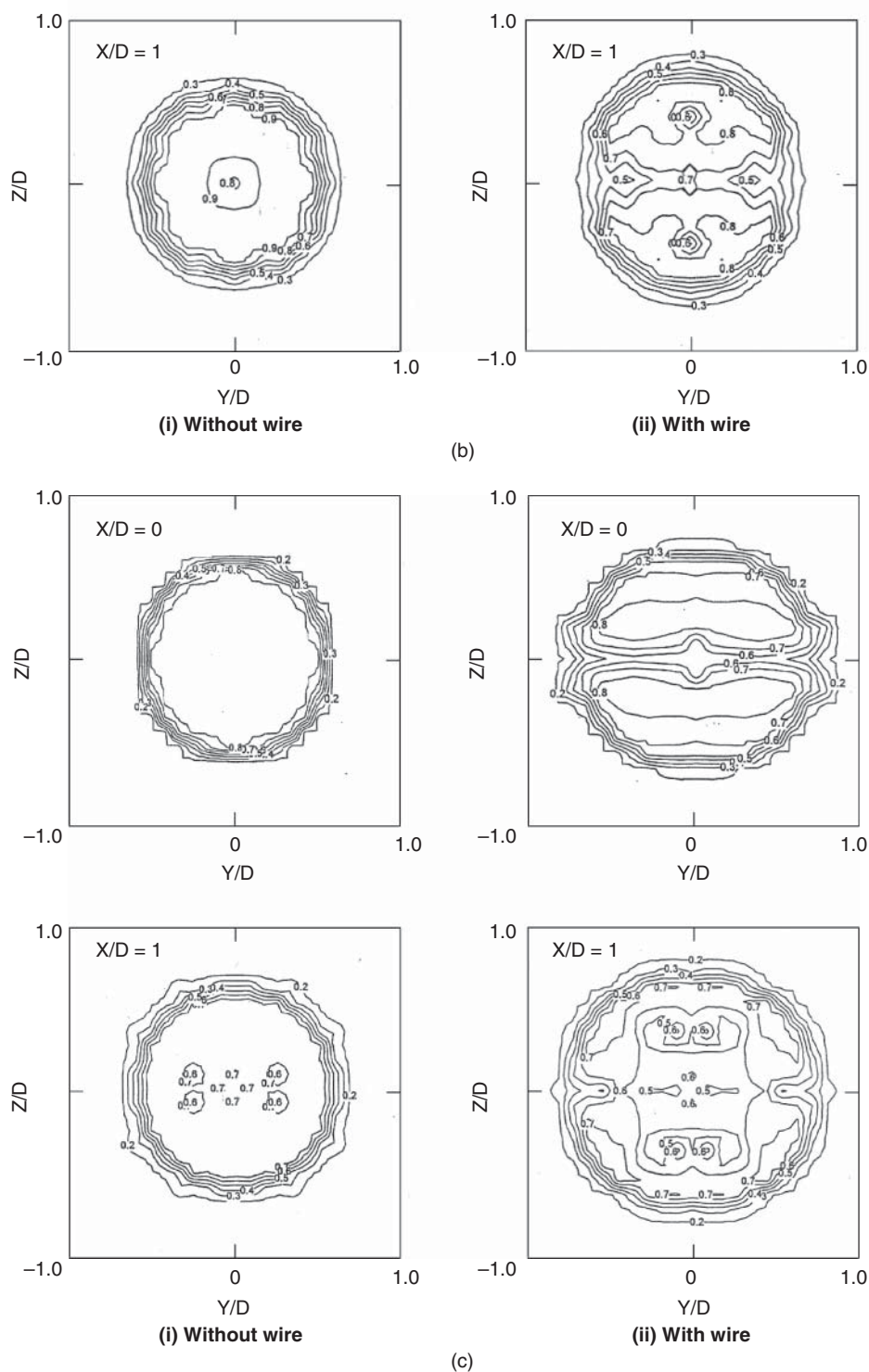
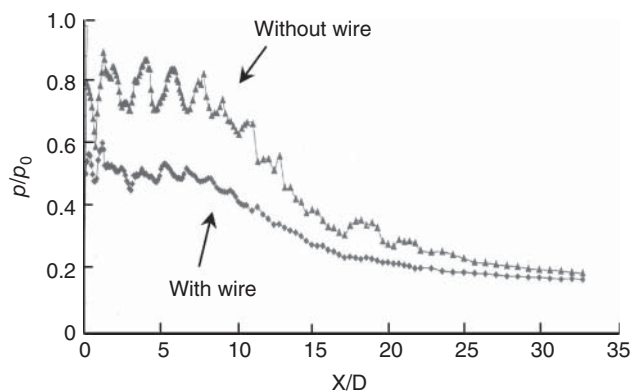


Figure 12.19 (Continued)



**Figure 12.20** Centerline decay for a Mach 1.79 jet at NPR 5.66 (correctly expanded).

interaction to promote mixing. The combined influence of the noncircular effect introduced, the introduction of vortices right up to the nozzle centerline, and providing the vortices with more time for interaction leads to enhanced mixing. The effect of mixing enhancement is clearly seen from the isobaric contours as axis switching.

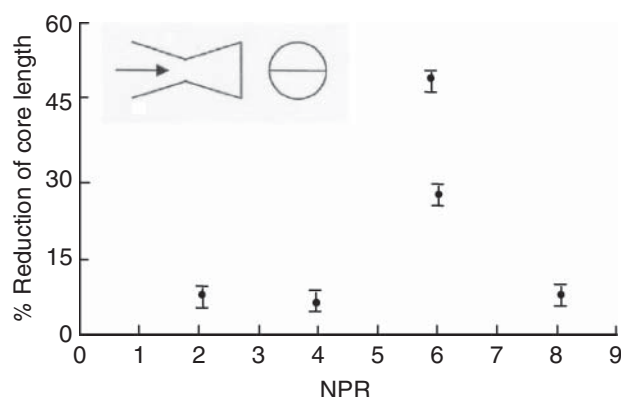
The centerline decay of a Mach number 1.79 jet at different levels of expansion (the plots are not shown here) shows that at NPR 2 there is no significant reduction in the core length except that the pressure level with wire is always lower than without wire. This is because the presence of the wire generates a detached shock and the flow experiences considerable pressure loss, owing to the detached shock. At NPR 4 the shocks in the jet core have been made very weak by the wire. This reduction of shock strength can result in significant reduction of jet noise, since the shock-associated noise forms a significant portion of the jet noise for supersonic jets. The core length reduction achieved is not significant in this case, even though the shocks get weakened. The results for NPR 5.66, that is the correctly expanded case, reveal that the wire is effective in weakening the shocks in the core. Also, the core length comes down from  $20D$  to  $10D$ , as seen in Figure 12.20.

Supersonic flow prevails up to about  $20D$  for the plain nozzle as it has been brought down to just about  $10D$  when wire is introduced. This may be considered as a very good aerodynamic advantage in terms of mixing. For NPR 6, which is an underexpanded case, the strong shocks in the plain nozzle core have been made significantly weaker with the introduction of the wire. The core comes down from  $13.2D$  to  $9.8D$ . For NPR 8, which is again an underexpanded condition, the results show that the strong shocks in the jet core have been significantly diffused by the wire and the core length has come down from nearly  $11.2D$  to  $10.2D$ .

The percentage reduction of core length with NPR is shown in Figure 12.21. It is interesting to note that, for the overexpanded case, the core length reduction is only marginally influenced by NPR. The maximum core length reduction is at correct expansion. For underexpanded condition the core length reduction comes down with an increase of NPR.

#### 12.6.5.4 Acoustic Characteristics of a Mach 1.6 Jet

As summarized in [46], except for jets operating at a correctly expanded condition, the noise of a supersonic jet comprises three basic components: the turbulent mixing noise, the broadband shock-associated noise, and the screech tones. The appearance of a screech tone is usually accompanied by its harmonics. Sometimes, even the fourth or fifth harmonics can be detected. The relative magnitude of this noise intensity is a strong function of the direction of observation. In the downstream direction of the jet, turbulent mixing noise is the most dominant noise



**Figure 12.21** Percentage reduction in core length with NPR for a Mach 1.79 jet.

component. In the upstream direction, the broadband shock-associated noise is more intense. For circular jets, the screech tones radiate primarily in the upstream direction.

As mentioned in the literature review, screech tones from supersonic jets were first observed by Powel [59, 60]. Since then, the phenomenon has been studied experimentally by a large number of investigators. It has been found that the fundamental screech tones radiate primarily in the upstream direction, whereas the principal direction of radiation of the first harmonic is at  $90^\circ$  to the jet flow [61].

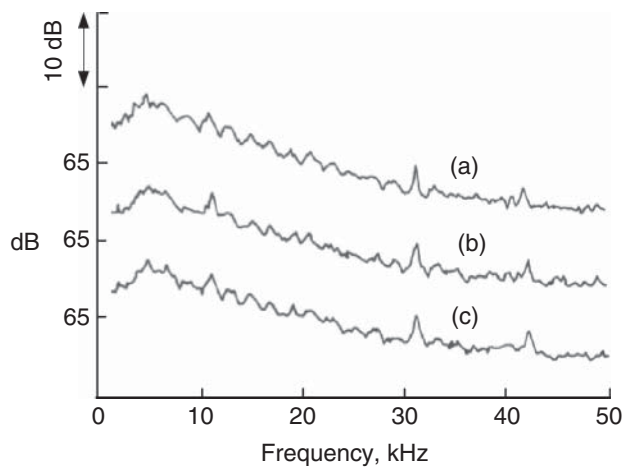
The turbulent mixing noise is from both large-scale turbulence structures and fine-scale turbulence of the jet flow. The large-scale turbulence structures generate the dominant part of the turbulent mixing noise. The fine-scale turbulence is responsible for the background noise.

Broadband shock-associated noise and screech tones are generated only when a quasi-periodic shock cell structure is present in the jet core. The quasi-periodicity of the shock-cells plays a crucial role in defining the characteristics of both the broadband and discrete frequency shock noises. The shock cell structure in an imperfectly expanded supersonic jet is formed by oblique/normal shock and expansion fans. These shocks or expansion fans are generated at the nozzle lip because of the mismatch of the static pressures inside and outside of the nozzle exit. For an underexpanded jet an expansion fan is positioned at the nozzle lip. The expansion fan or shock, once formed, propagates across the jet flow until it impinges on the mixing layer on the other side. Since the flow outside the jet is stationary, either a shock or an expansion fan is not allowed in that zone. The impinging shock or expansion fan is therefore reflected back into the jet field. The reflection process gets repeated many times downstream until the shock/expansion fan is dissipated by turbulence. These repeated reflections of the shock/expansion fans by the mixing layer of the jet give rise to quasi-periodic shock cells. From this point of view, the disturbances get trapped inside the jet by the mixing layer surrounding the jet core zone. In other words, one may consider the jet flow as behaving like a waveguide for the disturbances that form the shock cell.

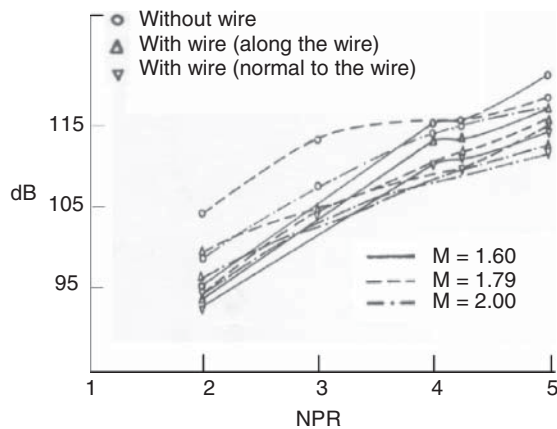
The frequency spectra for a Mach number 1.6 jet at NPR 2 and  $X/D=0$  are presented in Figure 12.22, for the cases of without wire, along the wire, and normal to the wire.

It can be seen that the introduction of the wire results in a reduction of shock-associated noise, as seen at frequency 5 kHz for these cases. Also, the fact that the jet noise is sensitive to the direction of measurement is evident from Figure 12.22b and c.

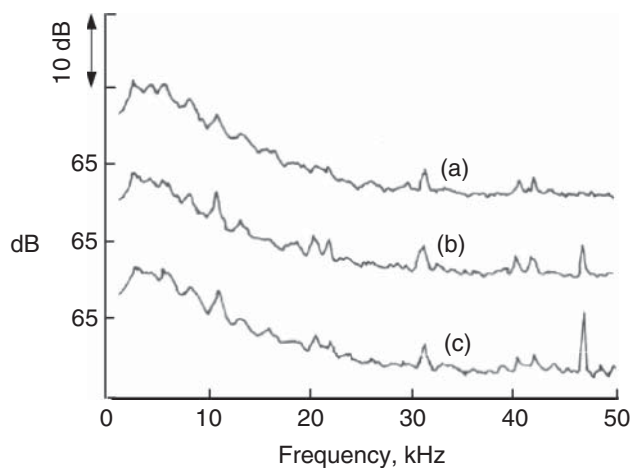
The jet noise (also called the *overall sound pressure level*, OASPL) measured at  $R/D=100$  is presented in Figure 12.23, for Mach 1.6, 1.79, and 2.0 jets as function NPR. The frequency spectra at  $R/D=100$  and NPR 2 are shown in Figure 12.24.



**Figure 12.22** Frequency spectrum for  $M = 1.6$ ,  $NPR = 2$ ,  $X/D = 0$ ,  $R/D = 30$ : (a) without wire; (b) along the wire; and (c) normal to the wire.



**Figure 12.23** Overall sound pressure level variation with NPR.



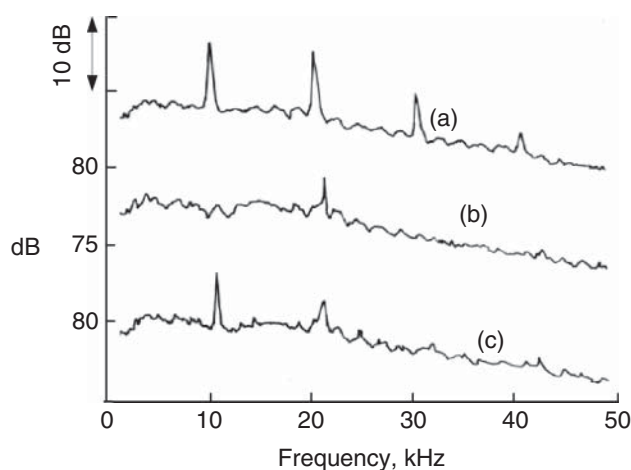
**Figure 12.24** Frequency spectrum for  $M = 1.6$ ,  $NPR = 2$ ,  $R/D = 100$ ,  $\theta = 30$  degrees: (a) without wire; (b) along the wire; and (c) normal to the wire.

From these results it can be seen that the jet noise comes down by nearly 2 dB when wire is introduced. This is mainly due to the reduction of shock-associated noise owing to a weakening of the shocks by the cross-wire as seen from the centerline pitot pressure distribution shown in Figure 12.13.

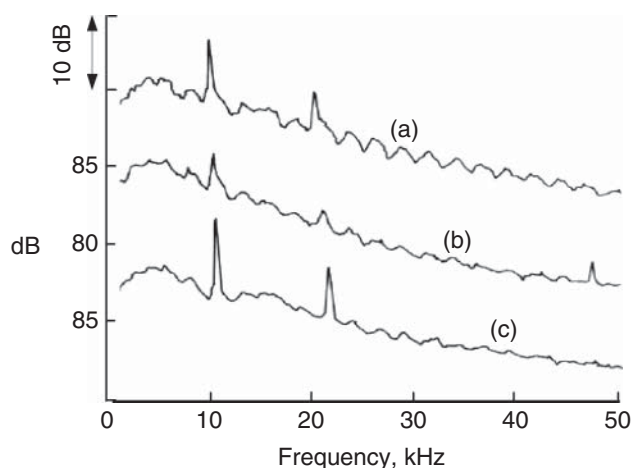
The frequency spectra at  $X/D = 0$  for NPR 4 are shown in Figure 12.25.

For the plain nozzle, screech tones with four harmonics are seen in the spectrum. When the cross-wire is introduced in the direction along the wire the screech is suppressed to a large extent, and at low frequencies it is totally eliminated. In the direction normal to the wire the screech is reduced to a single peak screech, and its amplitude has come down by 8 dB (from 98 dB to about 90 dB). This is mainly due to the weakening of the shocks by the cross-wire as seen from Figure 12.13.

The far field ( $R/D = 100$ ) spectra for NPR 4 are shown in Figure 12.26.



**Figure 12.25** Frequency spectrum for  $M = 1.6$ , NPR 4,  $X/D = 0$ ,  $R/D = 30$ : (a) without wire; (b) along the wire; and (c) normal to the wire.



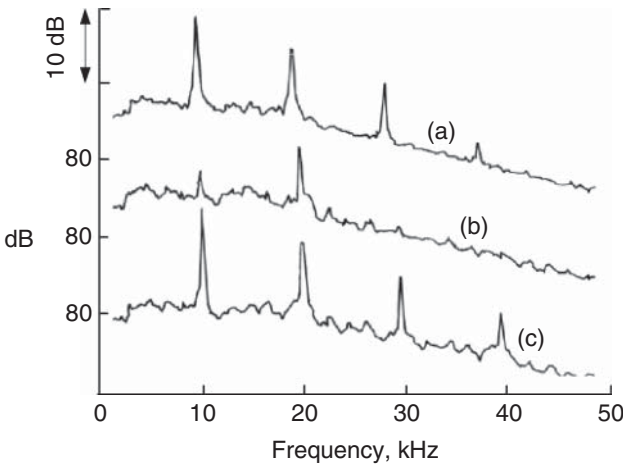
**Figure 12.26** Frequency spectrum for  $M = 1.6$ , NPR 4,  $R/D = 100$ ,  $\theta = 30$  degrees: (a) without wire; (b) along the wire; and (c) normal to the wire.

In this case the OASPL comes down by 5 dB along the wire and 2.1 dB normal to the wire. For the plain nozzle, screech tones with two frequencies are present. It reduces to screech with single frequency in the wire plane, resulting in a nearly 5 dB reduction in jet noise. However, in the direction normal to the wire, there is no screech suppression; both harmonics are prevailing with a slight reduction in their amplitudes.

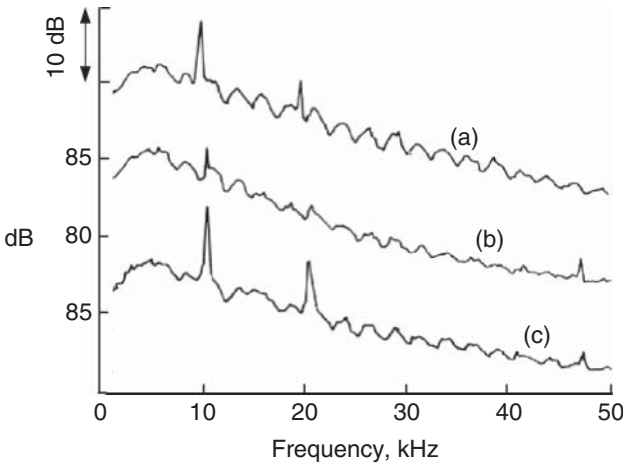
For the correctly expanded (NPR 4.24,  $X/D=0$ ), as seen from Figure 12.27, the spectra for plain nozzle as well as wired nozzle exhibit screech tones.

For the plain nozzle four screech harmonics are seen. But along the wire the harmonics are reduced to two, and the amplitude of the screech tones come down significantly. However, normal to the wire even though the screech amplitudes have come down, the four harmonics present in the plain nozzle case are seen for this case also.

The far field ( $R/D=100$ ) spectra for correct expansion (NPR 4.24) are given in Figure 12.28.



**Figure 12.27** Frequency spectrum for  $M = 1.6$ , NPR 4.24,  $X/D = 0$ ,  $R/D = 30$ : (a) without wire; (b) along the wire; and (c) normal to the wire.

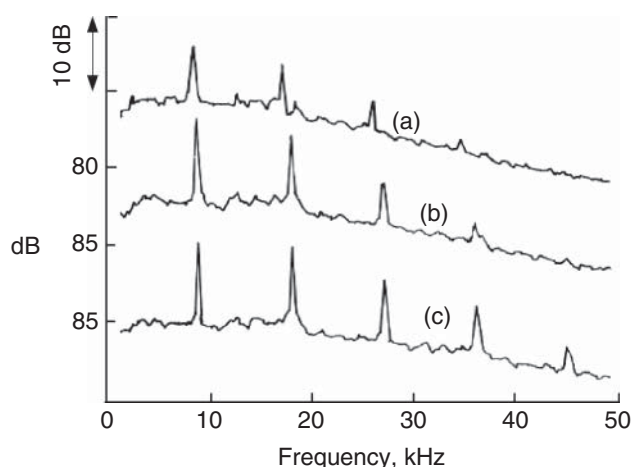


**Figure 12.28** Frequency spectrum for  $M = 1.6$ , NPR 4.24,  $R/D = 100$ ,  $\theta = 30$  degrees: (a) without wire; (b) along the wire; and (c) normal to the wire.

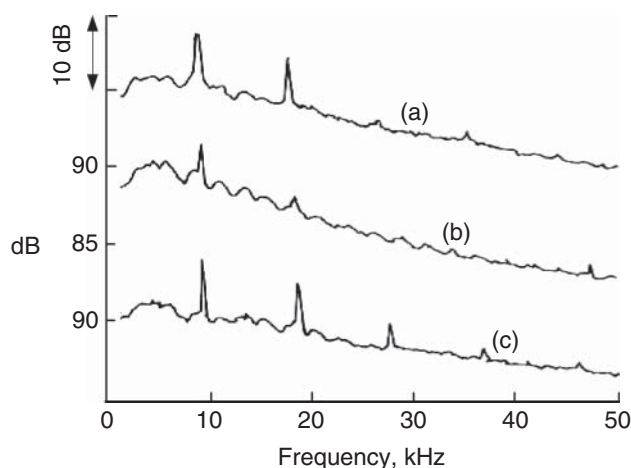
For the plain nozzle two screech tones are present. The screech is suppressed to a large extent along the wire, but normal to the wire, though the shock-associated noise is reduced marginally, the screech amplitude remains unaffected. For this case an OASPL reductions of 4.5 dB along the wire and 2.1 dB normal to the wire are achieved, as seen from Figure 12.23. The frequency spectra for NPR 5 that correspond to an underexpanded condition are shown for  $X/D = 0$  in Figure 12.29.

The behavior for this NPR is slightly different from the correctly expanded and overexpanded cases. For the plain nozzle, three prominent screech frequencies are seen, but when the wire is introduced the screech amplitude increases along the wire as well as normal to the wire, as seen from Figure 12.29. However, at low frequencies, the noise (dB) content comes down. Further, at high frequencies the noise level shows some increase when the wire is introduced.

The far field ( $R/D = 100$ ) spectra for NPR 5 are shown in Figure 12.30.



**Figure 12.29** Frequency spectrum for  $M = 1.6$ , NPR 5,  $X/D = 0$ ,  $R/D = 30$ : (a) without wire; (b) along the wire; and (c) normal to the wire.



**Figure 12.30** Frequency spectrum for  $M = 1.6$ , NPR 5,  $R/D = 100$ ,  $\theta = 30$  degrees: (a) without wire; (b) along the wire; and (c) normal to the wire.

For the plain nozzle, two screech tones are present, also the shock-associated noise content is significant. The introduction of wire brings down the screech amplitude from 109 to 98 dB along the wire. Also, the shock-associated noise and mixing noise are reduced significantly when the wire is introduced. This results in an OASPL reduction of 6.9 dB along the wire. Normal to the wire the screech frequencies are unaffected for the first two harmonics and also a third harmonic is seen. But the shock-associated noise and mixing noise get reduced in this plane also. This results in an OASPL reduction of about 4 dB.

#### 12.6.5.5 Acoustic Characteristics of a Mach 1.79 Jet

The frequency spectra for a plain nozzle and along the wire and normal to the wire at  $X/D = 0$  and NPR 2 reveal that introduction of the wire results in an increase of the amplitude of shock-associated noise both along and normal to the wire compared to the plain nozzle. A probable reason for this is that the detached shock generated by the wire also contributes to the shock-associated noise. However, from the spectral content it can be seen that introduction of wire results in reduction of OASPL.

The frequency spectra for NPR 2 at  $R/D = 100$  show that for the plain nozzle there is a screech at sounds of 6 kHz. introduction of wire reduces the screech amplitude from 90 dB to about 82 dB, along the wire. The spectrum normal to the wire shows that the screech is completely suppressed in this direction, but the shock-associated noise takes a wider band of frequencies. From these spectra, it is evident that the introduction of wire results in an OASPL reduction of 4.8 dB along the wire and 8.9 dB normal to the wire, which is a substantial reduction.

Similar results for NPR 3 at  $X/D = 0$  show that the screech present for the plain nozzle is completely suppressed by the wire introduction. Also, there is a significant reduction in the amplitude at all frequencies. At  $R/D = 100$ , for the plain nozzle there are two screech harmonics and significant broadband shock noise. The introduction of wire completely eliminates the screech and even the shock-associated noise amplitude comes down significantly. Because of these effects OASPL reductions of 8.9 dB along the wire and 9 dB normal to the wire are achieved.

The frequency spectra for  $X/D = 0$  and NPR 4 exhibit screech tones with four harmonics for the plain nozzle. When the wire is introduced the screech tone amplitude is reduced significantly along the wire and to some extent normal to the wire. This reduction in screech tone amplitude is reflected as a reduction in OASPL in the far field. The spectra of far-field noise at  $R/D = 100$  and NPR 4 show that, in the far field also, introduction of wire suppresses the screech amplitude along the wire but normal to the wire the screech tones are not affected by the wire. However, introduction of the wire results in an OASPL reduction of 5.2 dB along the wire and 3.5 dB normal to the wire, as seen in Figure 12.23.

At NPR 5, introduction of the wire increases the screech amplitude. However, the frequency band of shock-associated noise becomes narrower with the introduction of the wire. This results in an OASPL reduction of 4.2 dB along the wire and 3.2 dB normal to the wire.

#### 12.6.5.6 Acoustic Characteristics of a Mach 2 Jet

To investigate the effect of streamwise vortices introduced by the cross-wire on the acoustic characteristics of a jet, which is considered the limiting end of the screech-prone Mach number, noise measurements were made for a Mach number 2 jet from a nozzle with and without wire. Here again, as in the case of Mach numbers 1.6 and 1.79 jets, the measurements were made for NPRs 2–5 only.

The frequency spectra at  $X/D = 0$  show no screech tone, even for the plain nozzle. The introduction of wire brings down the mixing noise amplitude at lower frequencies, along the wire. However, the amplitude of the mixing noise has been increased at all frequency levels normal



to the wire. This may be due to the direct effect of the convection of the streamwise vortices away from the wire in the direction normal to it.

The frequency spectra for  $R/D = 100$  and NPR 2 show that the shock-associated noise amplitude comes down significantly along the wire and marginally normal to the wire. An OASPL reduction of 3.2 dB along the wire and 2.1 dB normal to the wire are experienced in this case.

The frequency spectra at  $X/D = 0$  and NPR 3 exhibit screech with three harmonics, with the second harmonic having the highest amplitude. The introduction of the wire suppresses the screech completely and the amplitudes at all frequency levels come down along the wire; however, normal to the wire, the amplitudes go up. It is important to note that screech at Mach 2 is unusual and, as per the literature, is not probable. Hence, this aspect of screech appearance at Mach 2 calls for a deeper investigation.

The far-field ( $R/D = 100$ ) spectra at NPR 3 show that the amplitudes of both shock-associated and mixing noises come down when the wire is introduced. This results in an OASPL reduction of 4 dB along the wire and 4.5 dB normal to the wire.

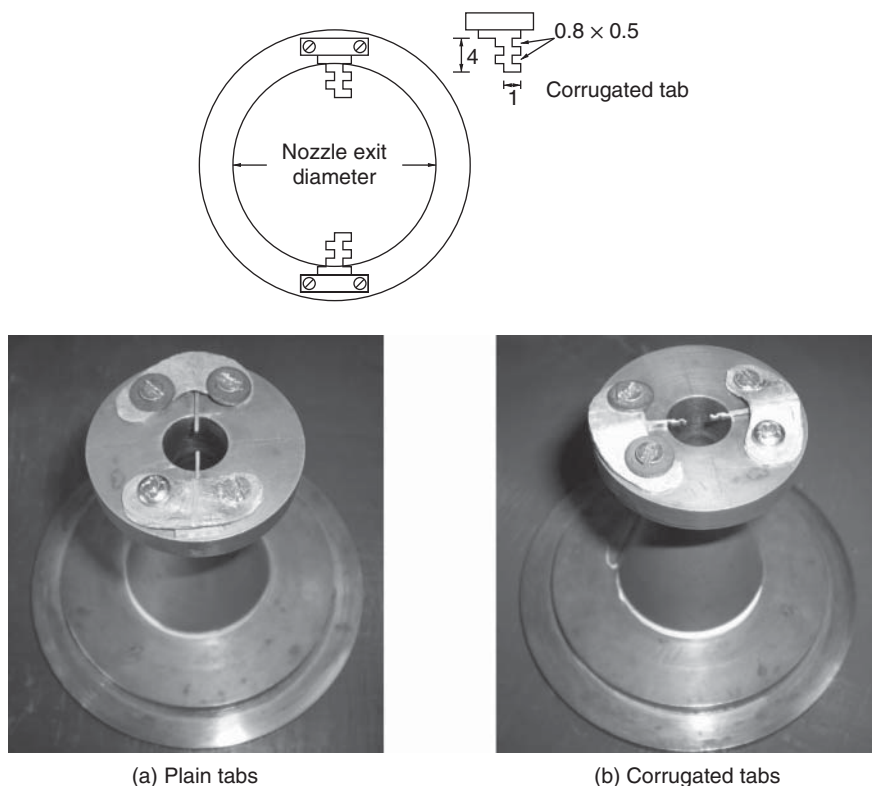
The frequency spectra at  $X/D = 0$  for NPR 4 show four harmonics for the screech for the plain nozzle, but the screech is completely suppressed when the wire is introduced. The corresponding frequency spectra for  $R/D = 100$  show a screech tone for the plain nozzle, whereas the screech is completely eliminated along the wire and screech amplitude is reduced from 102 to 88 dB normal to the wire. The amplitude of the shock-associated noise has also been reduced significantly both along the wire and normal to the wire. This is because the shocks have been made significantly weaker by the wire, as seen in Figure 12.23. An OASPL reduction of 6.1 dB along the wire and 5.9 dB normal to the wire are achieved for this case. The frequency spectra for NPR 4 at  $X/D = 0$  show that for the plain nozzle there are three harmonics for the screech. The screech is suppressed by the wire and the amplitudes come down at all frequency levels along the wire but they go up significantly at all frequencies in the direction normal to the wire.

Frequency spectra for  $R/D = 100$  and NPR 5 reveal that the introduction of wire brings down the amplitude of both shock-associated and mixing noises at all frequencies in the directions along and normal to the wire. For this case an OASPL reduction of 6 dB along the wire and 5 dB normal to the wire are achieved.

### 12.6.5.7 Use of Corrugated Tabs

It is well known that the manipulation of the size of the vortices shed by the tabs play a dominant role in promoting the mixing of free jets. The smaller the vortex size, the better its mixing efficiency. To investigate the effect of introducing mixing-promoting vortices of varying size at the nozzle exit, Chiranjeevi Panindra and Rathakrishnan studied a Mach 1.8 jet from a convergent-divergent nozzle with two corrugated tabs fixed at the nozzle exit [62]. Corrugations were provided at the edges of rectangular tabs with the intention of making the tabs shed smaller vortices compared to identical tabs without corrugation and demonstrated the effect of these vortices of reduced size on the mixing enhancement of a Mach 1.8 free jet.

The experimental model used in this investigation was a Mach 1.8 axisymmetric convergent-divergent nozzle of semi-divergence angle  $7^\circ$ , made of brass. The exit diameter of the nozzle was 13 mm. The Reynolds numbers of the Mach 1.8 jet coming out of the nozzle, based on nozzle exit diameter, were 6.6 and 1.34 million, respectively, for the minimum and maximum NPRs of 4 and 8 of this investigation. The tabs were made of 1 mm thick aluminum sheet. Two plain rectangular tabs of length 4 mm and width 0.7 mm offering a blockage of 4% (defined as the ratio of the projected area of the two tabs at the nozzle exit to the nozzle exit area) and two rectangular tabs of identical blockage with corrugation were used in the present investigation.



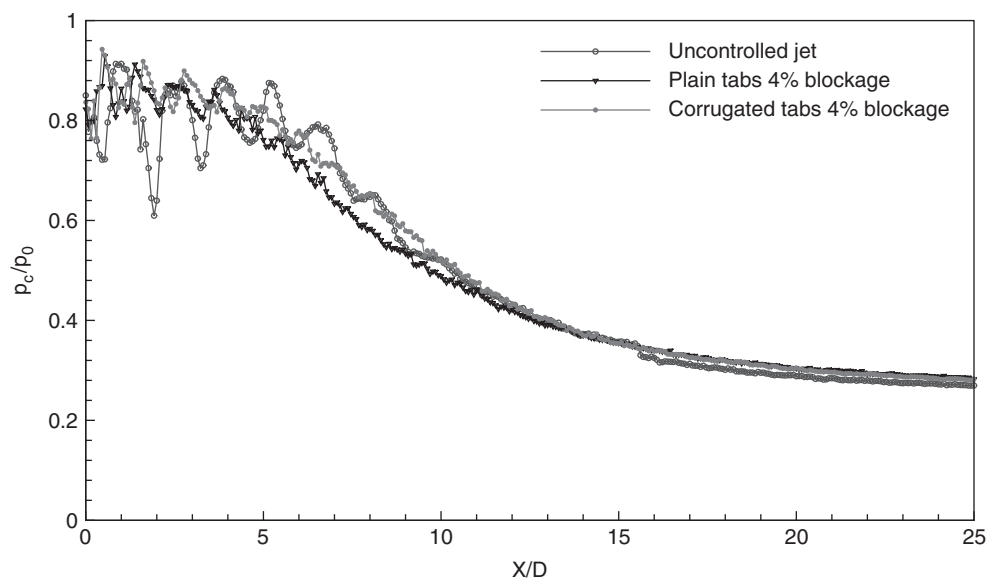
**Figure 12.31** Schematic of corrugated tab and photographic views of the nozzle with (a) uncorrugated tabs and (b) corrugated tabs.

The details of the corrugation and photographic views of the nozzle with uncorrugated and corrugated tabs at its exit are shown in Figure 12.31a and b, respectively.

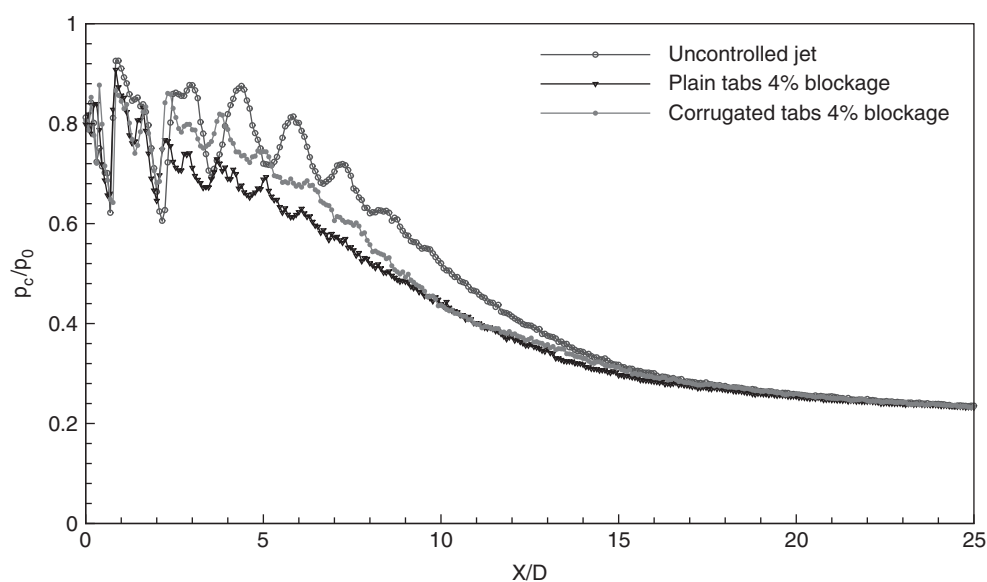
These tabs were located diametrically opposite to the nozzle exit, as shown in Figure 12.31. Lovaraju et al. showed that the momentum thrust loss suffered, owing to a cross-wire, is approximately equal to the projected area of the wire [46]. Also, it is essential to realize that, in addition to momentum thrust loss, there is a penalty in the form of increased base drag. Thus, the corrugated tabs offering a blockage of 4% will cause a momentum loss of around 4%.

The centerline pitot pressure ( $p_c/p_0$ ) decay for the uncontrolled jet, controlled jet with plain tabs, and controlled jet with corrugated tabs are given in Figure 12.32–12.37.

At NPR 4, the Mach 1.8 jet is overexpanded with overexpansion ratio  $p_c/p_b = 0.696$ . For this level of expansion, there will be an oblique shock at the nozzle exit to increase the pressure to come to equilibrium with the backpressure, which is the pressure of the atmosphere to which the jet is discharged. The oblique shock from the opposite edges of the nozzle exit would cross each other at a distance downstream of nozzle exit. For the present case of axisymmetric nozzle, this shock crossover point would be at the jet axis, which is also the nozzle axis. After crossing over, the oblique shock would be reflected from the barrel shock as expansion waves, since reflection from a free boundary is unlike (opposite in nature). These expansion waves would travel up to the opposite boundary of the jet and be reflected as compression waves, and these waves travel from one boundary to another boundary and reflect as expansion waves. Thus, there are a large number of compression and expansion waves prevailing in the near field of the jet, where the flow Mach number is supersonic. It is essential to realize that the flow Mach

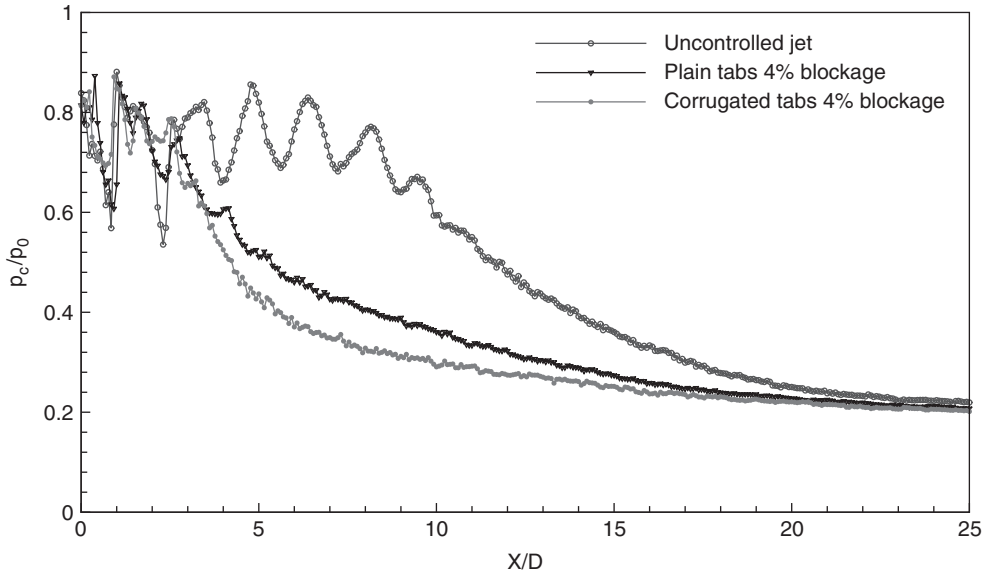


**Figure 12.32** Centerline decay for a Mach 1.8 jet at NPR 4 (overexpanded).

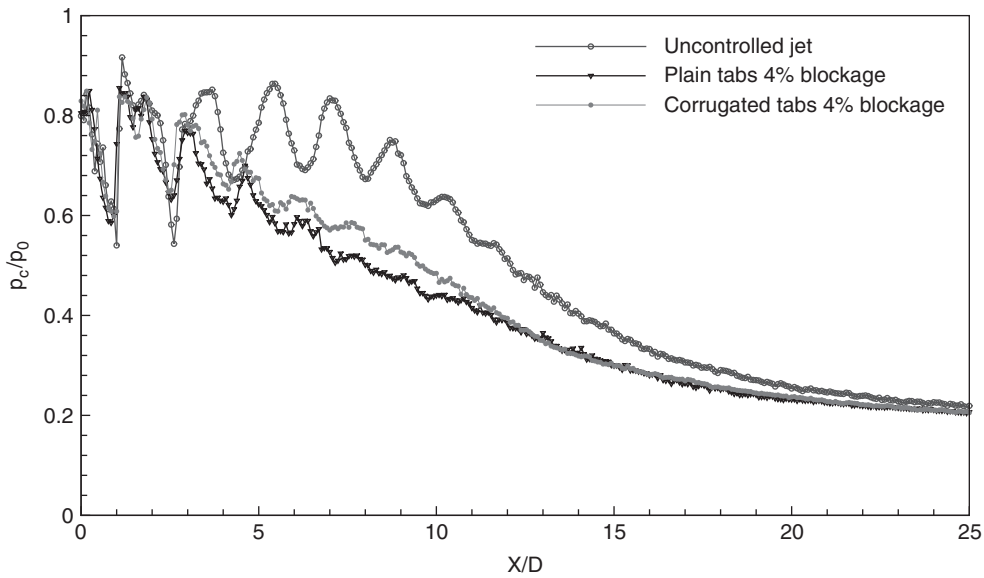


**Figure 12.33** Centerline decay for a Mach 1.8 jet at NPR 5 (overexpanded).

number downstream of the oblique shocks at the nozzle exit would be supersonic but with a magnitude of less than the Mach number upstream of the shock. This is because all the naturally occurring oblique shocks are weak shocks [6]. Thus, along the jet axis, the flow passes through a number of compression wave crossover points and expansion wave crossover points. It is well known that the pressure measured by a pitot probe will decrease with increase in Mach number. As seen in Figure 12.32, for the uncontrolled jet, the pitot pressure decreases over a very narrow range of  $X/D$  from 0 to about 0.5. This is because, at the exit of the nozzle, there is an oblique

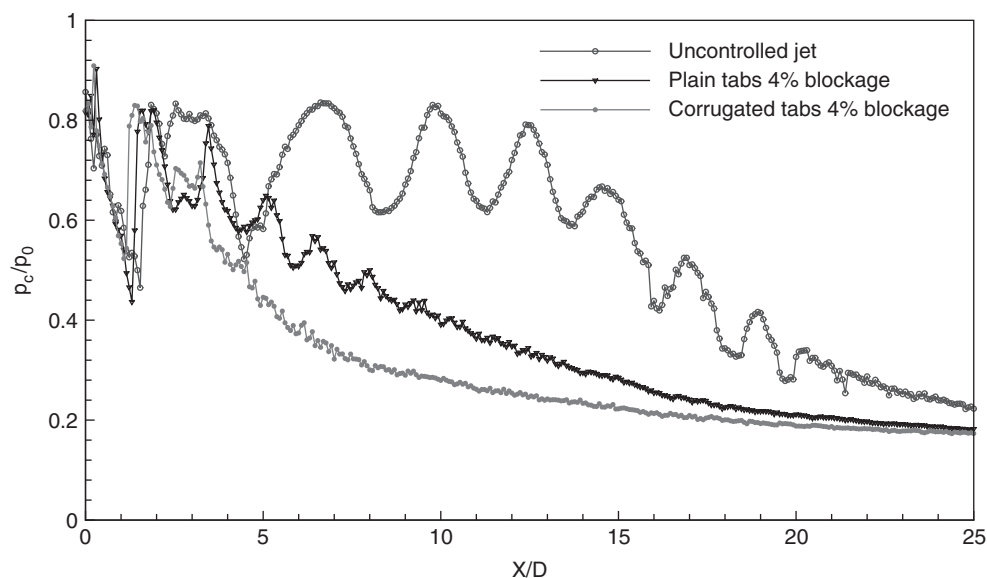


**Figure 12.34** Centerline decay for a Mach 1.8 jet at NPR 5.74 (correctly expanded).

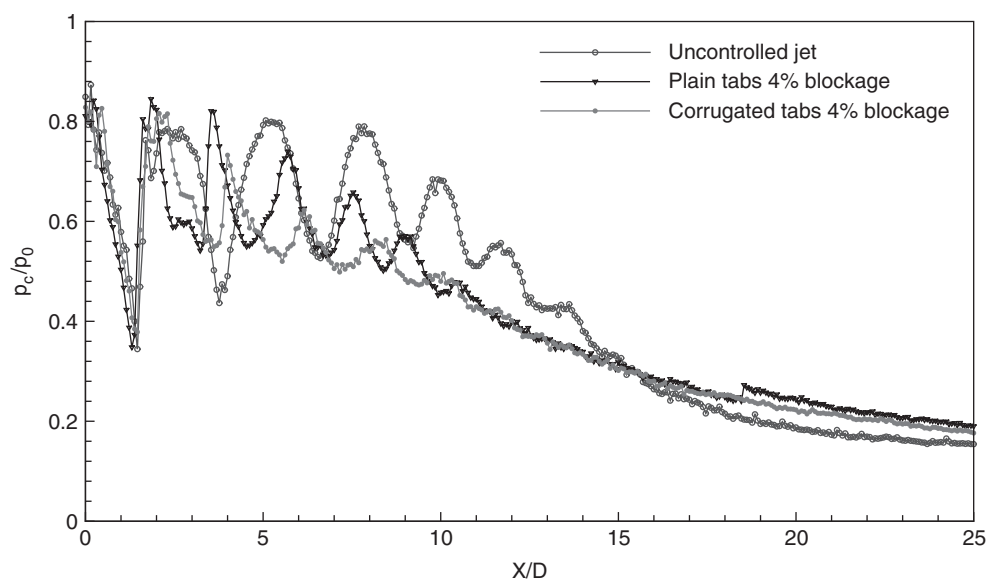


**Figure 12.35** Centerline decay for a Mach 1.8 jet at NPR 6 (underexpanded).

shock caused by overexpansion and an expansion fan caused by the relaxation effect due to the larger space available for the flow to expand soon after exiting the nozzle [63]. Therefore, the combined effect of the compression caused by the oblique shock and the expansion caused by relaxation dictates the flow Mach number. From  $X/D=0$  to about  $0.5$ , the pitot pressure decrease indicates acceleration of the flow. The pitot pressure attains a minimum at  $X/D=0.5$ . This should be the location just downstream of the shock crossover point, where the flow experiences deceleration, owing to the combined effect of two waves crossing. The flow behind the



**Figure 12.36** Centerline decay for a Mach 1.8 jet at NPR 7 (underexpanded).



**Figure 12.37** Centerline decay for a Mach 1.8 jet at NPR 8 (underexpanded).

crossover point essentially becomes subsonic as it moves downstream. The subsonic flow acceleration is indicated by an increase of pitot pressure from  $X/D = 0.5$  onwards. At about  $X/D = 1$ , the flow attains transonic level, followed by acceleration to supersonic Mach numbers. The first pressure maximum peak is a location of transonic Mach number. It is important to note that the subsonic flow downstream of a shock crossover point accelerates to higher Mach numbers by gaining momentum from the higher momentum fluid mass around the jet axis, where the flow was traversed by only one compression wave. After attaining the transonic Mach number,

the flow encounters acceleration due to momentum gain as well as through being traversed by expansion waves, which are the reflections of compression waves from the jet boundary. The accelerating flow attains a maximum Mach number at the location where the pitot pressure shows minimum peak at  $X/D$  slightly less than 2. Downstream of this minimum pressure point, flow accelerates again, attains transonic Mach number, and continues to accelerate to attain a third supersonic Mach number, which is at about  $X/D = 3.2$ . This cycle of acceleration continues exhibiting a wavy nature of pitot pressure up to about  $X/D = 8.4$ . Beyond that, there is a continuous decrease of pitot pressure, indicating the jet undergoing characteristic decay. Beyond  $X/D$  of about 14, the pitot pressure asymptotically approaches the fully developed region. Thus, for the uncontrolled jet, the supersonic core (axial extent up to which the wavy nature of the supersonic flow prevails) extends to about  $X/D = 8.4$ . From  $X/D = 8.4$  to 14, the flow exhibits characteristic decay and  $X/D$  beyond 14 could be taken as the fully developed zone. The distance from one minimum peak to another minimum peak can be taken as the shock cell length [58]. Thus there are about six shock cells for the uncontrolled jet at NPR 4, and the shocks in the jet core are of considerable strength. When, the plain tab is placed at the nozzle exit, as expected, the waves in the jet core become weaker, and the core length comes down from  $X/D = 8.4$  for the plain to about  $X/D = 6.4$ , for the jet with plain tabs, and to about  $X/D = 6$  for corrugated tabs of the same blockage as the plain tab of 4%. At NPR 4, both plain and corrugated tabs influence the jet mixing significantly, making the waves in the jet core weaker compared to the uncontrolled jet.

Centerline pitot pressure decays of the uncontrolled and controlled jets, at NPR 5, are compared in Figure 12.33. This NPR is also the case of overexpanded condition. But the overexpansion level comes down from  $p_e/p_b = 0.696$  for NPR 4 to  $p_e/p_b = 0.87$  for NPR 5. In other words, the adverse pressure gradient for NPR 5 is lower than that for NPR 4.

For the plain jet, the core extends up to about  $X/D = 8.5$ , and the waves present in the core are of considerable strength. For the plain tabs, the core length is about  $6D$ , whereas for the corrugated tabs, the core length is about  $5.2D$ . For both the tabs, the waves in the jet core are weaker than the uncontrolled jet. Furthermore, the characteristic decays for the uncontrolled and controlled jets with plain and corrugated tabs are distinctly different.

For the correctly expanded jet at NPR 5.74, as seen in Figure 12.34, the tabs can bring down the core length from about  $10D$  to  $4D$  for the plain tabs and  $3D$  for the corrugated tabs. Even in the presence of zero pressure gradient at the nozzle exit, the corrugated tabs can promote mixing to a greater extent than the plain tabs. Also the mixing efficiency of the corrugated tabs is much better than the plain tabs which cause a core length reduction of only about 60%. The characteristic decay for the corrugated tabs is found to be faster than the plain tabs, but in the flow field beyond  $X/D = 14$  both the tabs influence the field almost identically.

As seen from Figure 12.35, at NPR 6, which is with marginal favorable pressure gradient at the nozzle exit, the core length for an uncontrolled jet extends up to about  $11.4D$ , whereas for the jet from a nozzle with plain tabs the core length comes down to about  $9.2D$  and with corrugated tabs to  $8.4D$ . That is, the plain tabs reduce the core length to about 19% and the corrugated tabs reduce the core length to about 26%. Also, the waves in the first three shock cells are weaker for the corrugated tabs than the plain tabs.

At NPR 7, as seen from Figure 12.36, the waves in the core of the uncontrolled become very strong and the core extends as far as about  $20D$ . For the plain tabs, the core comes down to about  $9.2D$ . Also, the waves in the core beyond the first shock cell are made significantly weaker. The corrugated tabs result in a drastic reduction of jet core to about  $4D$ . This is about a 78% decrease in the core length. Another interesting fact is that the shocks in the core, including the first cell, are made considerably weaker by the corrugated tabs. The difference in the area enclosed by the pitot pressure curve is larger for the corrugated tabs, indicating that the mixing provided by the corrugated tabs is much larger than the plain tabs. For this case, the jets with tabs show their individual identity up to about  $18D$ .

At the largest tested NPR of 8, the favorable pressure gradient is  $p_e/p_b = 1.392$ . The results shown in Figure 12.37, show that the core length for the uncontrolled jet extends to about  $13.6D$ , whereas for the jet from the nozzle with plain tabs, the core length comes down to about  $12.8D$  and with corrugated tabs to about  $11.2D$ . Even though the core length achieved with corrugated tabs is not drastic, the corrugated tabs cause the waves in the jet core to become weaker compared to the plain jet. Though acoustic measurements are not made in the present investigation, weakening the waves in the jet core can be taken as an advantage from a noise reduction point of view [64].

From the above discussions of centerline pressure decay of uncontrolled and controlled jets, it is evident that the effectiveness of tabs is greatly dictated by the level of expansion at the nozzle exit. One interesting feature is that, while the literature suggests that the control effectiveness increases with an increase of favorable pressure gradient, the tabs here are found to be most efficient at and around correctly expanded condition. This kind of observation was also reported by Kumar Singh and Rathakrishnan for the limiting case of the tab length, namely a tab running across the diameter of the nozzle exit – a cross-wire [45]. Therefore, it is essential to look again into the statement that the control effectiveness increases with an increase of a favorable pressure gradient, as reported in the literature. The core length reductions achieved with the plain tabs and corrugated tabs are calculated for all the NPRs.

For the uncontrolled jet, the core length increases with NPR up to 7 and then comes down drastically at NPR 8. For the plain tabs, the core length shows an oscillatory nature, as seen from Figure 12.38.

For the corrugated tabs also, the variation is oscillatory, but at all levels of expansion (that is at all NPRs), the core length of the jet from nozzle with corrugated tabs is less than that with the plain tabs. This clearly reveals that the mixing efficiency of corrugated tabs is higher than that of plain tabs at all three levels of expansion: overexpanded, correctly expanded, and underexpanded. In other words, in the presence of adverse pressure gradient, zero pressure gradient (no pressure gradient) as well as favorable pressure gradient, the corrugated tabs are more efficient in mixing promotion than the plain tabs. However, the effectiveness of corrugated tabs is strongly influenced by the level of expansion.

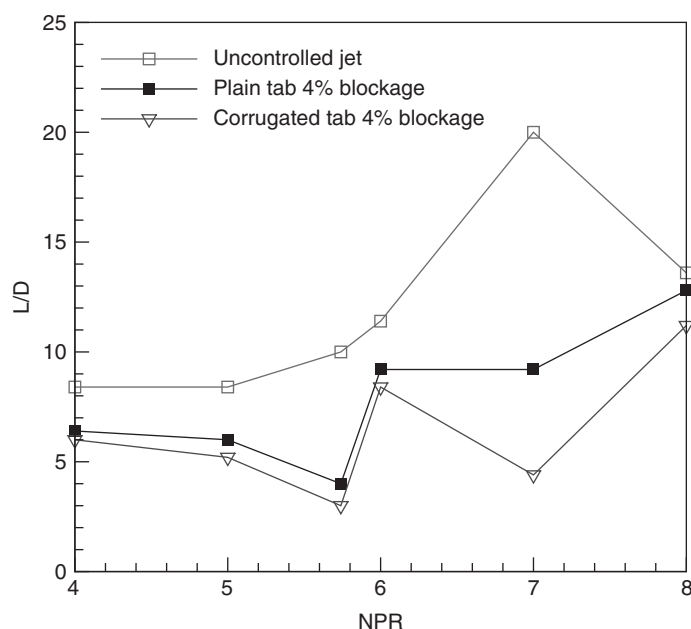


Figure 12.38 Variation of core length with NPR.

Thus, it can be summarized that a generation of smaller vortices by the corrugated tabs, compared to uniform size vortices shed by the plain tabs, is more efficient in promoting mixing, in accordance with the vortex dynamics, that is the smaller the vortex size, the better the mixing efficiency.

### 12.6.5.8 Pressure Profiles

The pitot pressure ( $p_c$ ) distribution, measured along the tabs and normal to the tab directions for the controlled jets and along the radial direction for uncontrolled jets, are made nondimensional by dividing by the settling chamber pressure ( $p_0$ ). The radial distance ( $R$ ), transverse distance ( $y$ ), that is, along the tab, and normal ( $z$ ), that is, normal to the tab, are made nondimensional by dividing them with a nozzle exit diameter ( $D$ ).

The pitot pressure profiles for the uncontrolled jet at NPR 4, at axial distances of  $X/D = 0.5, 1, 2, 4, 6$ , and  $10$  are presented in Figure 12.39.

At  $X/D = 0.5$ , at the jet axis, the pitot pressure is the minimum; this implies that the jet velocity is maximum at that point. Away from the jet axis, the pitot pressure shows an almost constant level up to about  $R/D = 0.5$ , followed by a steep decrease from  $0.5$  to  $0.6$ . Beyond  $R/D = 0.6$ , the pitot pressure remains almost a constant with a magnitude of  $p_c/p_0 = 0.25$ . At  $X/D = 1$ , around the axis, the pitot pressure exhibits almost a constant pressure zone. This implies that there is a uniform Mach number zone around the jet axis. This prevails from  $R/D = 0$  to about  $0.3$ . For  $R/D$  greater than  $0.3$ , the pitot pressure decreases sharply up to about  $R/D = 0.6$ . Beyond that, the pressure remains almost the same. At  $X/D = 2$ , the constant pitot pressure magnitude around the jet axis is higher than  $X/D = 1$ . But the radial extent of this peak pressure is only from  $R/D = 0$  to about  $0.25$ . At  $X/D = 4$ , the pitot pressure peak value comes down to  $0.8$ , and also the decrease of pressure shows a relatively gradual variation than the near field profiles upstream of this location. At  $X/D = 6$ , there is no constant pressure zone around the axis, as exhibited by the single peak pitot pressure profile. Also, in the radial direction pressure decreases gradually, attaining a minimum pressure level of  $p_c/p_0 = 0.22$  at  $R/D = 1$  around  $1$ . At  $X/D = 10$ , the jet has encountered the characteristic decay, and the pitot pressure decay shows an almost fully

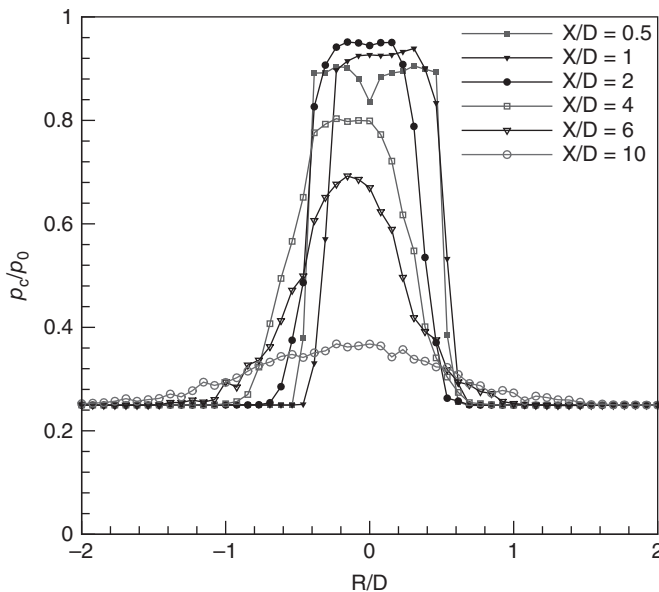
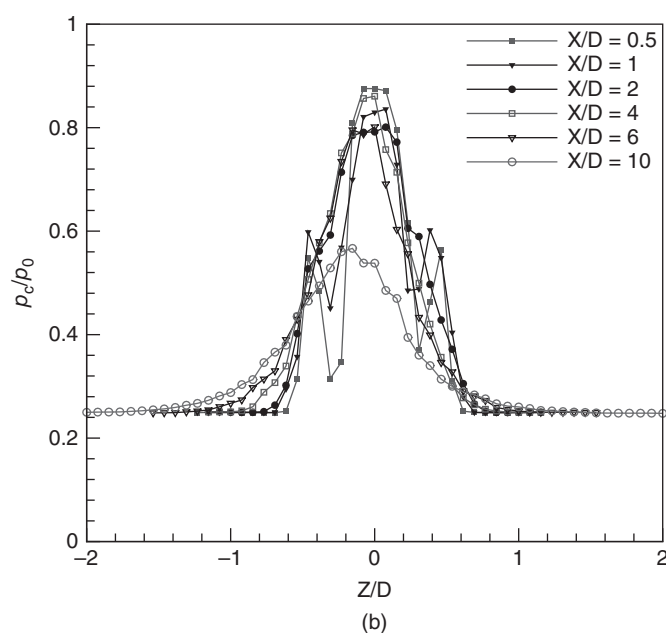
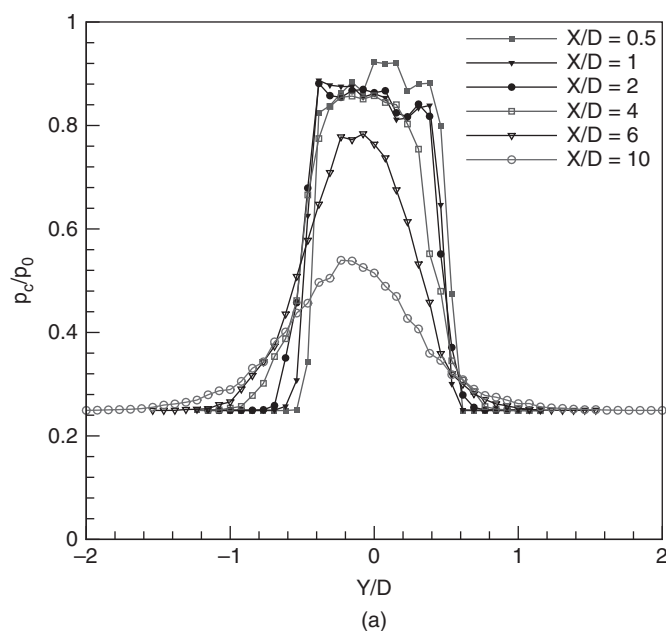


Figure 12.39 Pressure profiles for an uncontrolled jet at NPR 4.



developed nature. In all these profiles, it is interesting to note that the pressure profiles are not symmetric about the jet axis. This is because the jet field is essentially vortex dominated and hence, owing to the vortex action, the field is rendered asymmetric. Even so, the jet at  $X/D = 0$  is essentially axisymmetric.

For the controlled jet with plain tabs, the pitot pressures along the tab direction ( $z$ -profiles), normal to the tabs ( $y$ -profiles), for NPR 4, at  $X/D = 0.5, 1, 2, 4, 6$ , and  $10$  are shown in Figure 12.40a and b.



**Figure 12.40** Pressure profiles for a jet with plain tabs at NPR 4: (a)  $y$ -profiles and (b)  $z$ -profiles.

The  $y$ -profile at  $X/D = 0.5$  does not exhibit any dip as in the case of the uncontrolled jet. Further, there is a constant pressure zone around the jet axis. This is a clear indication of the mixing caused by the vortices shed from the tabs right at the nozzle exit. Further, the fall after the peak pressure is also slightly reduced compared to the uncontrolled jet. The jet is rendered more asymmetrical compared to the uncontrolled jet. Another interesting feature is that the pressure profiles at  $X/D = 1, 2$ , and  $4$  are with marginal variation in the peak pressure around the jet axis. This is a clear indication of momentum transport caused by the control tabs. For  $X/D = 6$ , the peak pressure is much higher than the uncontrolled jet. This is because the shock cells are made weaker by the tabs, as seen in the centerline pressure decay plots. Owing to these weakened waves, the flow retains its pressure level to a greater distance compared to the uncontrolled jet. For a similar reason, at  $X/D = 10$  also, the peak pressure is much larger than the uncontrolled jet. However, in the far field, the pressure levels are almost comparable to the uncontrolled jet. This feature was observed as an almost similar asymptotic decay of controlled and uncontrolled jets in the far field from the centerline pitot pressure decay results. The  $z$ -profiles (Figure 12.40b) are distinctly different from the  $y$ -profiles. This is a clear indication of the asymmetry to the jet propagation introduced by the tabs. In the  $z$ -profiles, the peak profile zone is narrower at all axial distances compared to the  $y$ -profiles. This is because, in the direction normal to the tabs, the flow can spread greatly without the influence of the vortices shed by the tabs. In other words, as in the case of the direction along the tab, normal to the tab, the flow can relax because of the absence of any solid body. In the  $z$ -profiles, at about  $X/D = 2, 4$ , and  $6$ , the profiles exhibit off-center peaks. This shows that, slightly downstream of the tabs, the jet is essentially bifurcated with high-velocity zones on either side of the jet axis. But at  $X/D = 10$ , the  $z$  pressure profile is almost identical to that of the  $y$ -profile. In the far field,  $z$ -profiles are identical to the radial profiles for uncontrolled jets as well as  $y$ -profiles.

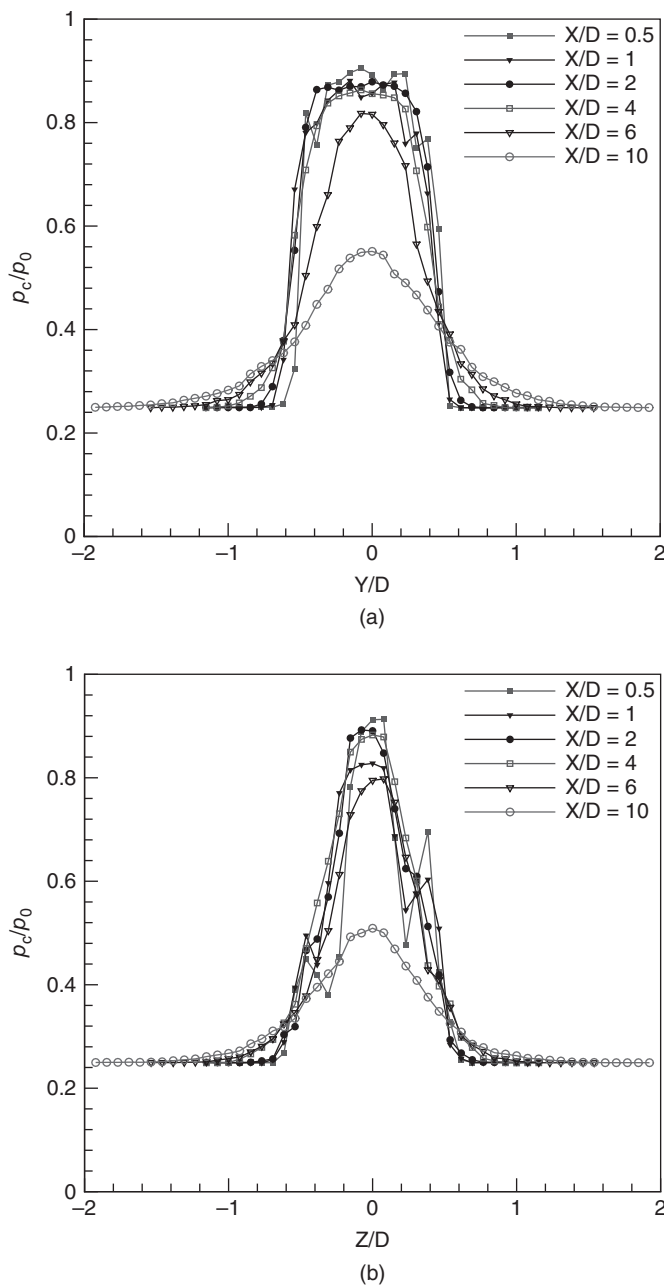
The pressure profiles along the  $y$ - and  $z$ -directions for the jet with corrugated tabs are shown in Figure 12.41a and b.

These show that, in the  $y$ -direction, the space between the tabs experiences more uniform flow than the plain tabs. Also, at  $X/D = 1$  and  $2$ , the pressure profiles show a wider uniform pressure zone compared to the plain tabs. The pressure profile peak at  $X/D = 6$  is higher than that of the plain tabs. These features clearly demonstrate that the mixing caused by the corrugated tabs is much better than the plain tabs. For corrugated tabs, the pressure profiles retain their signature even beyond  $Y/D = 1$ . The  $z$ -profiles, shown in Figure 12.41b, exhibit similar features to the plain tabs in the near field. But the off-center peaks show drastically different magnitudes on either side of the jet axis. Because of this, the mixing beyond the off-center peak locations is bound to become greater than a field with almost identical off-center peaks. Thus, the differential off-center peaks can be regarded as the direct indication of the better mixing caused by the corrugated tabs. The far field behavior of  $z$ -profile is almost identical to the plain tabs.

The pressure profiles for the correctly expanded jets from a nozzle without and with tabs are presented in Figures 12.42–12.44.

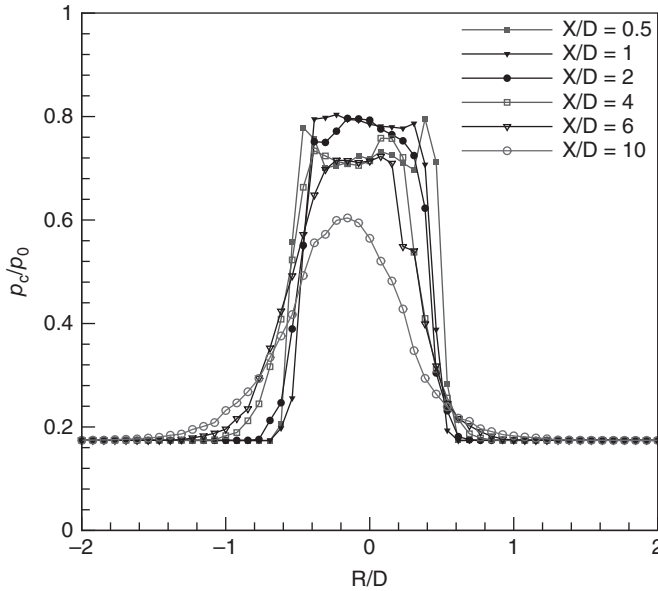
At NPR 5.74, the jet is correctly expanded with zero pressure gradient at the nozzle exit. Therefore, it might be expected that the pitot pressure profile at  $X/D = 0.5$  is of uniform magnitude over a radial distance from the jet axis.

For correctly expanded Mach 1.8 supersonic flow, the pitot pressure is supposed to read  $p_c/p_0 = 0.8127$ , as per the isentropic theory. However, in the results shown in Figure 12.42 at  $X/D = 0.5$ , the  $p_c/p_0$  is around 0.72 over a radial distance around the jet axis followed by a gradual increase reaching about 0.8. This clearly implies that, around the jet axis, the Mach number



**Figure 12.41** Pressure profiles for a jet with corrugated tabs at NPR 4: (a) y-profiles and (b) z-profiles.

is higher than 1.8. This is in accordance with the results of Rathakrishnan [63], which state that a flow, even at correctly expanded condition, encounters an expansion fan at the nozzle exit, owing to the relaxation experienced by the flow, because of the availability of larger space. Therefore, the flow accelerates to begin with and then encounters the reflected compression

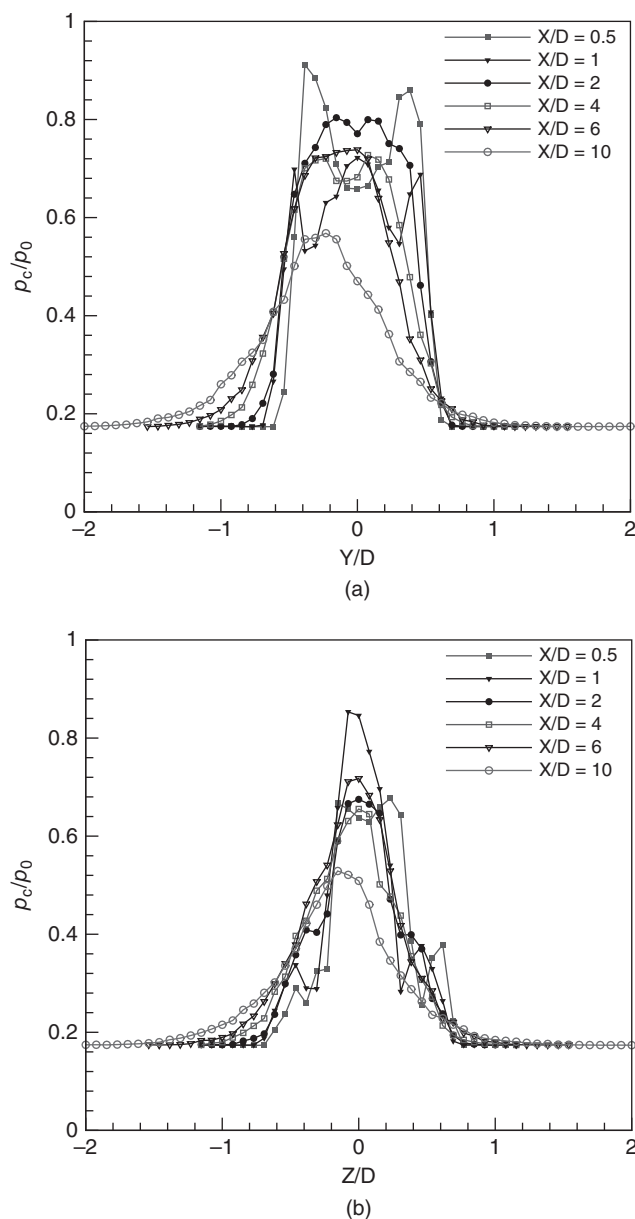


**Figure 12.42** Pressure profiles for an uncontrolled jet at NPR 5.74.

waves from the jet boundary. These features are reflected as  $p_c/p_0$  corresponding to Mach number 1.8 around the jet axis, followed by the increase of  $p_c/p_0$  (decrease of Mach number). The flow process at  $X/D = 1$  is similar to  $X/D = 0.5$ . At  $X/D = 2$ , the pressure peak is around the axis, followed by a gradual decrease and a subsequent steep fall. The waves prevailing in the near field, for this case, are of marginal strength. At  $X/D = 10$ , the pressure profiles show a single peak followed by a gradual but considerable decay up to  $R/D = 0.5$ . Beyond  $R/D = 0.5$ , the decay is asymptotic. For this case also, the pressure profiles for an uncontrolled jet exhibits asymmetry as in the case of overexpanded jets.

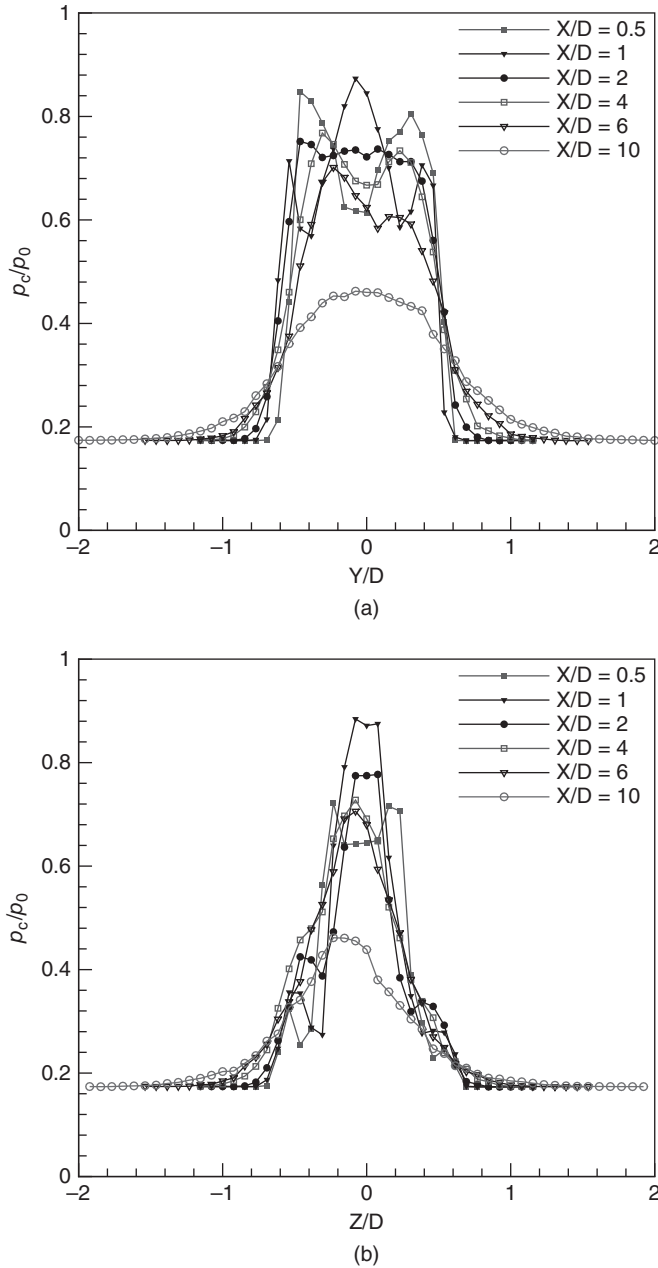
When the plain tabs are placed at the nozzle exit, the jet experiences mixing right from the nozzle exit. However, the mixing initiation by the tabs is just in the proximity of the tabs. Because of this, in the near field, waves continue to prevail. However, the strength of the waves is greatly reduced by the mixing process initiated by the tabs. At  $X/D = 5$ , the minimum pressure dip is lower than the uncontrolled jet. But this cannot be taken as an indication of larger Mach number than the uncontrolled since the flow encounters severe loss, owing to the additional shocks caused by the presence of the tabs. The waves at  $X/D = 2$  are found to be much weaker than the uncontrolled jet. This is due to the mixing augmentation caused by the tabs. The asymmetry of the pressure profiles in the  $y$ -direction is considerable. The  $z$ -profiles shown in Figure 12.43b show that the spread in the direction normal to the tabs is less than that in the direction along the tabs. Also, normal to the tabs the jet continues to exhibit asymmetry.

The pressure profiles for corrugated tabs are shown in Figure 12.44. In the near field, the waves are seen, but as early as  $X/D = 2$  the jet spread is more extensive than with the plain tabs. Also, at  $X/D = 10$  the jet momentum is greatly reduced by the efficient mixing caused by the corrugated tabs, compared to the plain tabs. Furthermore, because of efficient mixing the jet



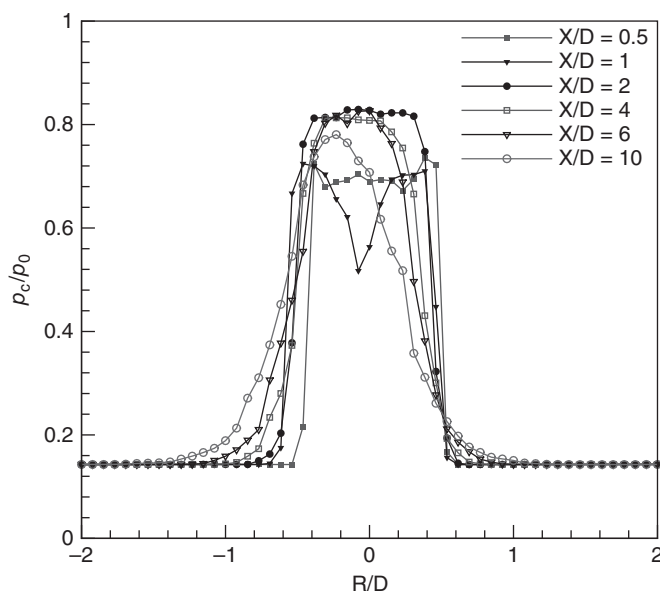
**Figure 12.43** Pressure profiles for a jet with plain tabs at NPR 5.74: (a) y-profiles and (b) z-profiles.

asymmetry is greatly reduced, as seen in Figure 12.44a. In the direction normal to the tabs, as seen from z-profiles in Figure 12.44b, the jet spread is considerably larger at  $X/D = 0.5$  and 1, compared to the plain tabs. In this direction also, the jet diffuses faster than the plain tabs, as shown by the peak pressure value of about 0.46 at  $X/D = 10$ , against 0.58 at the same axial distance for the plain tabs. Thus, even in the presence of no pressure gradient, the corrugated tabs perform better than the plain tabs.



**Figure 12.44** Pressure profiles for a jet with corrugated tabs at NPR 5.74: (a) y-profiles and (b) z-profiles.

At NPR 7, the Mach 1.8 jet is considerably underexpanded with a favorable pressure gradient of  $p_e/p_b = 1.218$ . Therefore, the expansion fan at the nozzle exit has to be powerful. Because of this, the Mach number at the nozzle axis in the near field would be much higher than the jet at Mach number 1.8.



**Figure 12.45** Pressure profiles for an uncontrolled jet at NPR 7.

As seen in Figure 12.45, the  $p_c/p_0$  along the axis at  $X/D = 0.5$  is about 0.52, which is very much lower than for NPR 6. At  $X/D = 1$ , the pressure level is almost identical to NPR 6 around the jet axis, and the same is true for  $X/D = 2, 4, 6$ , and 10. But the almost uniform Mach number zone at  $X/D = 1$  and 2 for NPR 7 is much wider than for NPR 6. Asymmetry is well pronounced for this underexpanded state also.

The pressure profiles for the plain tabs shown in Figure 12.46 reveal that the jet spread at NPR 7 is slightly higher than at NPR 6, both along and normal to the tabs. Also, the waves prevail as far as  $X/D = 6$ , and the asymmetry is also larger than NPR 6.

For the corrugated tabs, as seen in the pressure profiles shown in Figure 12.47, the jet spread is larger than that of the plain tabs at corresponding NPR.

Also, mild waves are observed even at  $X/D = 10$ ; this may be because the initial waves are made weaker by the corrugated tabs. Therefore, flow traversed by the weaker waves can possess considerable momentum over a longer distance than the field traversed by the initially stronger waves as with plain tabs. As in the case of lower NPRs, the jet asymmetry is greatly reduced by the corrugated tabs. This once again emphasizes that the mixing caused by the corrugated tabs is superior to that with plain tabs.

#### 12.6.5.9 Optical Flow Visualization

The shadowgraph technique was employed to visualize the waves prevailing in the jet with and without control at different NPRs. For the controlled jets, visualization was carried out viewing along the tabs and normal to the tabs.

At NPR 4, which is an overexpanded state for a Mach 1.8 jet, the oblique shocks at the nozzle exit can be clearly seen (Figure 12.48).

These oblique shocks cross each other at the jet axis and reach the barrel shock. On reaching the barrel shock, the oblique shock reflects as an expansion fan, since reflection from fluid

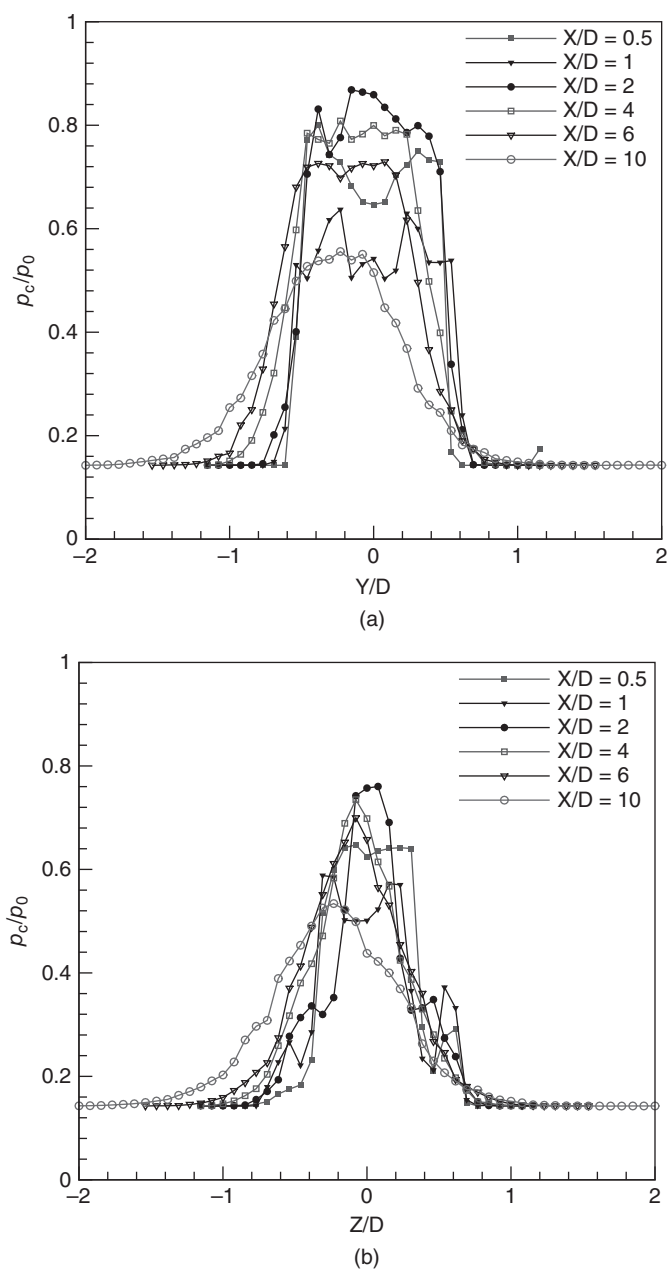
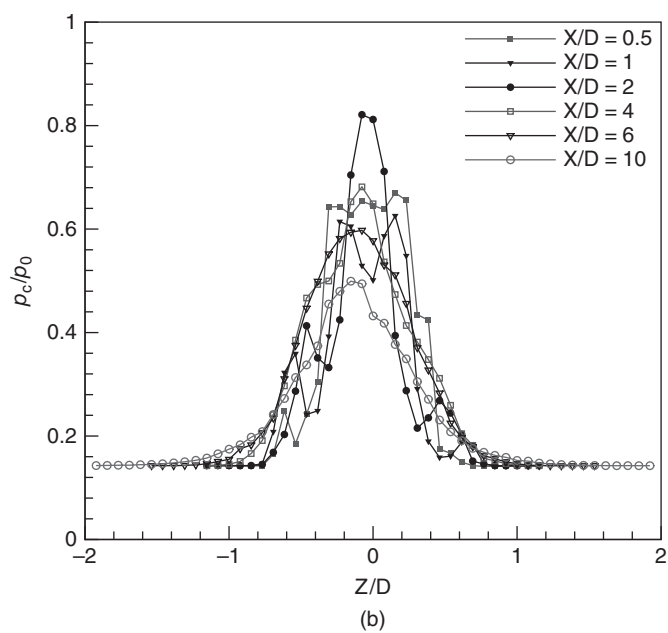
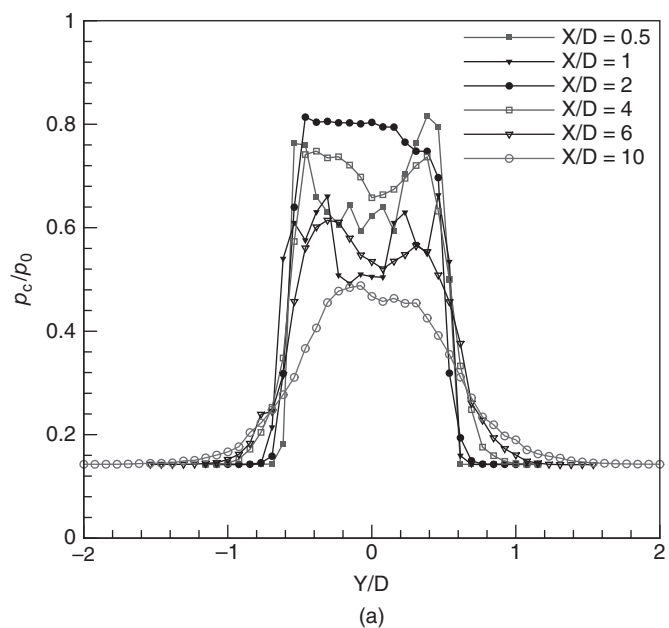


Figure 12.46 Pressure profiles for a jet with plain tabs at NPR 7: (a) y-profiles and (b) z-profiles.





**Figure 12.47** Pressure profiles for a jet with corrugated tabs at NPR 7: (a) y-profiles and (b) z-profiles.



**Figure 12.48** Shadowgraph picture for an uncontrolled jet at NPR 4.

boundary is unlike [24]. The kink formed at the shock reflection points is clearly seen in the picture. The expansion waves cross each other and reach the boundary and reflect back as compression waves. The reflected compression waves once again cross each other at the jet axis and reflect back as an expansion fan from the barrel shock boundary. This kind of wave reflection continues for some distance downstream. The distance between successive shock reflection points (kinks) is taken as a shock cell. At NPR 4, four cells are visible. The first two cells are prominent and the third and fourth are weak cells.

For the controlled jets with plain tabs and corrugated tabs, the visualization pictures in the direction normal to the tabs are shown in Figure 12.49a, for NPR 4.

It is interesting to note that the shock cells prevailing in the uncontrolled jet are greatly disturbed, resulting in a number of smaller diamond-shaped structures for both plain and



With plain tabs



With corrugated tabs

(a)

**Figure 12.49** Shadowgraph pictures for a controlled jet at NPR 4: (a) viewed normal to the tabs,  $xz$ -plane and (b) viewed along the tabs,  $xy$ -plane.



With plain tabs



With corrugated tabs

(b)

**Figure 12.49** (Continued)

corrugated tabs. However, as can be seen in Figure 12.49a, the first diamond for the plain tabs is longer, but the second diamond for the corrugated tabs is larger than that of the plain tabs, and it alternates. This kind of number of wave crossings is seen up to some downstream distance for both the tabs. There are four prominent diamonds along the centerline for the plain tabs, but for the corrugated tabs only three such diamonds are prominent.

The visualization pictures in the direction along the tabs are shown in Figure 12.49b, and the wave pattern is completely different from normal to the tabs. Furthermore, the waves in the plain tab case are relatively stronger than for the corrugated tabs.

At NPR 5.74, which is the correctly expanded condition for a Mach 1.8 jet, the waves prevailing in an uncontrolled field are shown in Figure 12.50.

It is interesting to note that, even at the correctly expanded condition, the jet field is wave dominated. This is because, as explained by Rathakrishnan [63], the jet encounters an expansion


**Figure 12.50** Shadowgraph picture for uncontrolled at NPR 5.74.

fan due to the relaxation effect. These expansion waves get reflected as compression waves and the process continues. For this case also, two prominent shock cells are visible.

The waves prevailing in the correctly expanded controlled jet operated at NPR 5.74 are shown in Figure 12.51.



With plain tabs



With corrugated tabs

(a)



With plain tabs



With corrugated tabs

(b)

**Figure 12.51** Shadowgraph pictures for controlled jet at NPR 5.74: (a) viewed normal to the tabs,  $xz$ -plane and (b) viewed along the tabs,  $xy$ -plane.



**Figure 12.52** Shadowgraph picture for a controlled jet at NPR 7.

As discussed in the pressure profiles, there are waves in the jet core due to the relaxation effect. For the plain tabs, in the direction normal to the tabs, the waves are seen up to a considerable distance downstream of the nozzle exit. This may be because of the expansion at the exit not being strong, as it is only caused by the relaxation effect. As a result, the flow Mach number changes caused by the waves are not too pronounced. The supersonic nature of a jet can therefore continue over a longer distance compared to NPR 4, which is an over-expanded condition. Along the tabs also, the shock cells continue over a longer distance than at NPR 4.

At NPR 7 (an underexpanded state for a jet) the expansion fan at the nozzle exit is stronger. Because of the stronger expansion, the centerline Mach number reaches a much higher value, resulting in longer shock cells. For this case, even the third cell is considerably longer and stronger, as seen in Figure 12.52.

At NPR 7, which is a highly underexpanded operation, strong waves are visible in the first few cells for the plain tabs in the direction normal to the tabs (Figure 12.53a).

For the corrugated tabs, however, the waves are considerably weaker, owing to the enhanced mixing efficiency of these tabs. In the direction along the tabs, for the plain tabs, even the third cell shows a shock crossover point, but for the corrugated tabs, the third cell has only very weak waves. For both plain tabs and corrugated tabs, the jet spread is more in the direction normal to the tabs ( $xy$ -plane) compared to the direction along the tabs ( $xz$ -plane).

The shadowgraph pictures clearly demonstrate the difference in the wave domination in the supersonic core and the effect of additional or augmented mixing of the corrugated tabs compared to the plain tabs. It is well known that shock cell length reduction and weakening of waves in the jet core can be taken as an indication of reduced shock-associated noise. Therefore, it can be justifiably stated that, even though jet noise has not been measured, the control with corrugated tabs is advantageous for jet noise reduction also.

#### 12.6.5.10 Water Flow Visualization

It was found that the corrugated tab causes better mixing than the plain tab. The physical reason for this was speculated to be that the vortices shed from the corrugated tab were relatively smaller than those shed by the plain tab. To evaluate this speculation, a modest experimental visualization with water stream as the flow medium was conducted. Flow past identical rectangular tabs, one with corrugation and one without corrugation, were visualized. The plain and corrugated tabs were placed in the test-section with a water stream speed of  $20 \text{ cm s}^{-1}$ . By injecting water color dye, the flow fields behind the plain and corrugated tabs were visualized. The two pictures of flow field around the plain and corrugated tabs are given in Figure 12.54.



With plain tabs



With corrugated tabs

(a)



With plain tabs

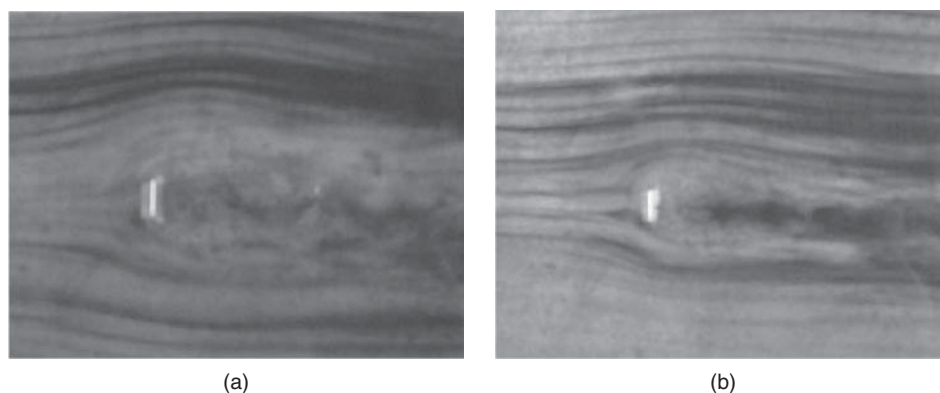


With corrugated tabs

(b)

**Figure 12.53** Shadowgraph pictures for a controlled jet at NPR 7: (a) viewed normal to the tabs,  $xz$ -plane and (b) viewed along the tabs,  $xy$ -plane.

It can be seen that, in the wake of the corrugated tab, the vortices are smaller, thus causing a better mixing compared to the plain tab. Furthermore, the flow deviation caused by the plain tab is found to be much larger than for the corrugated tab. It is important to note that these results are only qualitative in nature. Also, the Reynolds number of the water stream, based on the width of the tab, is just 2238. However, the corrugated tab shedding smaller vortices can



**Figure 12.54** Water flow visualization pictures: (a) plain tab and (b) corrugated tab.

be taken as supportive evidence for the speculation in the discussion of results of centerline pitot pressure decay and pitot pressure profiles of jets controlled with a plain rectangular or a corrugated rectangular tab.

### 12.6.6 Grooves and Cutouts

The tabs and cross-wires discussed in the previous sections are passive controls that shed mixing-promoting vortices to enhance the mixing. But there is thrust loss due to the blockage to exit area caused by the tabs or the wire. Also, the drag of the tab or wire causes an additional penalty. In an attempt to overcome these shortcomings of the tab and cross-wire, controls in the form of grooves provided by removing material from the exit plane to some upstream distance at the nozzle wall, as shown in Figure 12.11, and cut out at the nozzle wall at the exit plane have been investigated [34]. The grooves generate mixing-promoting vortices right from the beginning of its geometry. These vortices are found to enhance the mixing significantly. But entropy generation associated with the perturbation caused by the mixing promotion spoils the uniformity of the flow at the nozzle exit and leads to thrust loss. Thus, even for grooves, there is a thrust penalty.

## 12.7 Noncircular Jets and Shifted Tabs

Noncircular jets, such as elliptic jets, owing to the continuous variation in the azimuthal radius of curvature, form flow structures of different sizes at the jet boundary and the jet spreads differently along different planes [65, 66]. Studies of noncircular jets show that the jet experiences fine-scale mixing at the corners and at high curvature regions and large suction at the low curvature/flat side regions, owing to the formation of large-scale vortices, resulting in large entrainment [67, 68]. Extensive research has been done on square and rectangular jets in the past several decades. Rectangular slot jets, of a Mach number in the range 1.4–1.8 ( $M_j = 1.4$  to 1.8), exhibit large spreading rates when operating at moderately underexpanded conditions [69, 70]. At this state, the jet generates intense discrete tones called *screech*. The interaction of these tones with the jet's shear layer results in the formation of large-scale vortices which develop alternatively on the two sides of the jet along its wide side. The resulting flapping motion yields a high spreading rate and accelerates the mixing process.

Rectangular supersonic jets with various designs of the divergent section of the nozzle were tested over a wide range of convective Mach numbers ( $0.5 < M_c < 2.20$ ) by Gutmark et al. [66]. The nozzle design with internal divergence along the wide side of the nozzle increased the spreading rate by a factor of 2 throughout the entire range of  $M_c < 1.8$ . Srinivasan and Rathakrishnan [71] carried out experimental studies on rectangular slot jets of aspect ratio (AR) 1, 2, 4, and 6, at correctly expanded and underexpanded sonic conditions, with an aim of understanding the core region of the jet, particularly the pitot pressure oscillations in the core. The results show that the AR of the orifice is a crucial parameter for rectangular jets. The amplitudes of pressure oscillation showed a monotonic variation for AR 1:1 and 2:1 rectangular jets, and an oscillatory variation for AR 4:1 and 6:1 jets, indicating the possibility of entirely different mechanisms in the core of the jet issuing from lower AR and higher AR rectangular orifices. However, elliptic jets have not received as much attention as square and rectangular jets have. The limited number of studies reported on elliptic jet clearly demonstrate their superior mixing capabilities compared to circular jets. The enhanced mixing capability of elliptic jets compared to their circular counterpart is due to the generation of azimuthal vortices of continuously varying size generated at the nozzle exit [72]. These mixed size vortices promote both large- and small-scale mixing, whereas in circular jets the curvature is the same across the jet boundary; therefore, the mixing is not as rapid as in elliptic jets. Earlier studies on elliptic jets support this fact. Schadow and co-workers studied an elliptic jet of AR 3:1 and found enhanced mixing characteristics of the elliptic jet compared to a circular jet at subsonic, sonic, and supersonic underexpanded conditions [73]. Quinn showed that the mixing in an elliptic jet issuing from a sharp-edged orifice plate is higher than elliptic jets issuing from contoured elliptic nozzles and round jets [74]. Mitchell et al., using planar particle image velocimetry, studied a low AR underexpanded elliptical jet and reported a vortex bifurcation process at the highest pressure ratio of NPR = 4.2, which was previously observed only for jets with higher AR [75]. Yoon and Lee investigated the near field structure of an elliptic jet using stereoscopic particle image velocimetry and reported that the total entrainment rate of the elliptic jet was about 1.5% larger than that of the round jet [76]. The enhanced mixing of elliptic jets is reflected in the form of axis-switching. In axis-switching, the major and minor axes of jets switch after a certain distance downstream of the nozzle exit. Many researchers have observed axis-switching. Hussain and Husain observed that the locations and number of axis-switching were strongly dependent on the initial conditions of the jet [77]. Ho and Gutmark reported three axis-switching for 2:1 AR elliptic jet and found that the mass entrainment of the elliptic jet was several times higher than that of circular jet [36]. Quinn observed two axis-switching and found that the jet attains an axisymmetric shape at about 30 equivalent slot diameters downstream of the exit plane [78]. Menon and Skews found that the phenomenon of axis-switching in elliptical nozzles was exacerbated on increasing the pressure ratio [79].

Passive controls – such as nozzle exit geometry modification and vortex generators in the form of tabs, notches, and grooves – are popular because of their efficient mixing-promoting capability. Among the various passive control techniques, the use of noncircular geometries has gained importance, owing to their capability to generate mixing-promoting vortices right from the nozzle exit. It is well known that, for mixing enhancement, the jet should have the mass entraining large-scale vortices and mass-transporting small-scale vortices in proper proportions. Also, mass transporting or mixing-promoting small-scale vortices of mixed size will result in an immense mixing enhancement. The noncircular nozzle exit geometries, such as rectangular and square shapes, were found to shed both small- and large-scale vortices, owing to the presence of sharp corners. To exploit this inbuilt advantage, many researchers have carried out extensive studies on the use of rectangular geometry for effective jet control. But, even



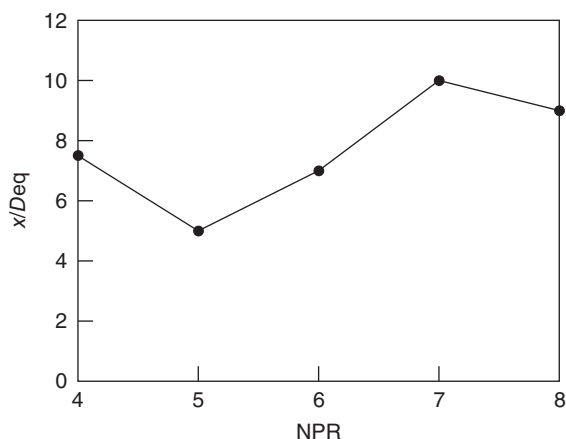
though the rectangular and square exits shed vortices of mixed size at the sharp corners, the vortices shed from the straight edges would be of uniform size and hence might not be efficient in promoting mixing right from the nozzle exit. Use of elliptic geometry as a passive jet control technique has also attracted many researchers because of its increased entrainment and enhanced mixing capabilities [36, 73, 77, 78, 80, 81]. The studies on supersonic elliptic jets proved that the mixing characteristics of supersonic elliptic jets were similar to that of subsonic jets.

The increased entrainment and enhanced mixing capabilities of the elliptic jet (noncircular jets) relative to the equivalent circular jet are due to the phenomenon known as *axis-switching*, which was unanimously supported by the literature. Axis-switching is a phenomenon in which the cross-section of an asymmetric jet evolves in such a manner that, after a certain distance from the nozzle exit, the major and the minor axes are interchanged [82]. The curvature-dependent self-advection of the vortical structures in an elliptic jet produces three-dimensional deformation leading to the switching of axes and enhanced large-scale mixing. Since the self-induced motion depends on the local curvature and on the core radius, the effect of initial boundary layer characteristics (which controls the core radius of rolled-up vortices) is more pronounced in elliptic jets than in circular jets [77].

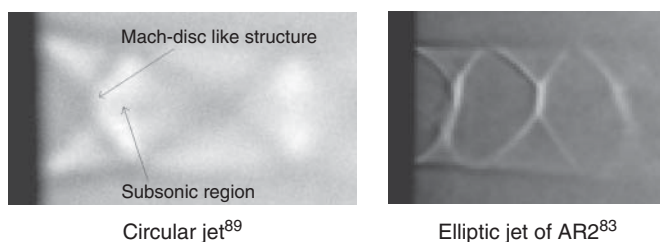
From the literature, it is explicit that most of the studies on elliptic jets are for subsonic incompressible elliptic jets from elliptic slots and nozzles. Also, the investigations reported on sonic and supersonic elliptic jets correspond to jets issuing from elliptic slots and convergent nozzles with a smooth transition from circular inlet to elliptic exit. The supersonic Mach numbers reported in these studies are equivalent jet Mach numbers ( $M_j$ ) corresponding to correctly expanded flow. Thus, it can be stated that characterizing supersonic elliptic jets from a convergent–divergent nozzle of elliptic cross-section from its entry to exit, at different levels of expansion of supersonic jets, would be of great value to high-speed jet literature. With this aim, Aravindh Kumar and Rathakrishnan studied a Mach 2 jet issuing from a straight convergent–divergent elliptic nozzle of AR 2, with elliptic cross-section right from the inlet to the exit [83]. The results of this study show that the continuously varying size of the mixing-promoting vortices shed by the elliptic nozzle exit is an advantage from a mixing enhancement point of view, compared to an equivalent circular nozzle. Except at NPRs 4 and 5, the centerline pressure decay of the elliptic jet at all the NPRs is faster than the equivalent circular jet, in all the three zones of the jet field, namely the core, characteristic decay, and fully developed regions. However, the elliptic jet continues to enjoy better near-field mixing at NPRs 4 and 5 also. The elliptic jet spreads faster along the minor axis plane than the major axis plane and exhibits axis-switching at all levels of expansion, indicating faster near-field mixing. Indeed, the axis-switching phenomenon is strongly influenced by the expansion level at the nozzle exit. The axis-switching location, which initially shifts upstream with an increase in NPR from 4 to 5, moves downstream from NPRs 5 to 7, at a faster rate. When the NPR is increased from 7 to 8, the level of expansion changes from an overexpanded state to a marginally underexpanded state, followed by a slight upstream movement of the axis-switching location, as seen in Figure 12.55, which shows the variation of axis-switching locations with the NPR.

A shadowgraph image of the waves present in the Mach 2 elliptic jet of AR 2 at NPR 4 is compared with the waves present in the core of a Mach 2 circular jet of the same mass flow rate and expansion level in Figure 12.56. It can be seen that the waves (expansion/compression) present in the elliptic jet core are unsymmetrical and the waves in the circular jet core are symmetrical about the jet axis. This asymmetrical nature of the waves in the elliptic jet is due to the azimuthal asymmetry of the elliptic nozzle.

Also, the shock cells in the core of the elliptic jet are shorter than the circular jet. Shorter shock cell presence can be taken as an advantage from an aero-acoustic point of view, since,



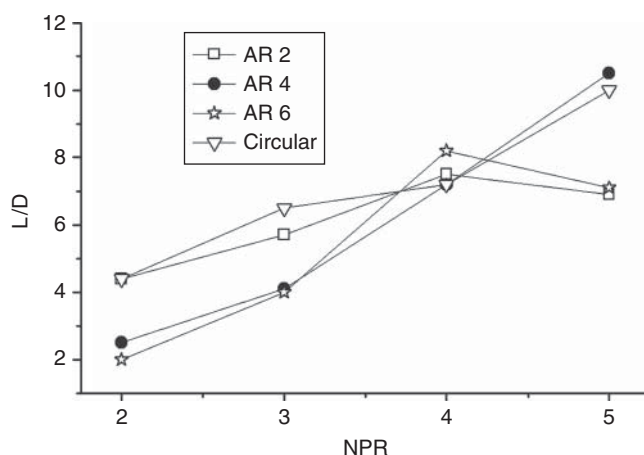
**Figure 12.55** Variation of axis-switching location with NPR of a supersonic jet elliptic jet of AR 2 [83].



**Figure 12.56** Shadowgraph image of a Mach 2 circular and elliptic jets at NPR 4 (overexpanded).

in accordance with Tam's theory [84], shorter shock cells would result in less shock-associated noise than longer shock cells.

To get an insight into the characteristics of elliptic jets in the presence of different levels of favorable pressure gradients and in the presence and absence of a boundary layer, Chauhan et al. studied the mixing characteristics of underexpanded elliptic sonic jets issuing from the orifice and nozzle [85]. Mixing of the jet issuing from the nozzle is found to be higher than the jet from the orifice. The jet from the nozzle showed a higher spread rate along the minor axis plane than the major axis plane. As a result of this differential spread, the jet switches axes at a certain distance downstream of the nozzle exit. For NPR above 2, the jet issuing from the nozzle shows two axis-switching, whereas the orifice jet shows only one axis-switching. Also, axis-switching location shifts upstream with an increase of favorable pressure gradient, indicating that the mixing becomes faster with an increase of NPR. The difference in the propagation of the jets from the nozzle and orifice of identical geometry, at a given pressure ratio, demonstrates that the boundary layer in the passage has a strong influence on jet mixing. Further work on the AR effect on elliptical sonic jet mixing has focused on the influence of AR on the sonic jet decay, at different levels of underexpansion [86]. This study is on elliptical sonic jets issuing from orifices of the same exit area, with exit ARs, ratios of major axis to minor axis, of 2, 4, and 6, at NPRs 2–5, in steps of 1. The results of elliptical jets were compared with identical jets from a circular orifice. Elliptic geometry was found to be effective in enhancing the mixing compared to circular geometry. This mixing superiority of elliptic jet over the circular jet was found to be independent of the levels of underexpansion. Also, the elliptical jets from orifices of ARs 4 and 6 experienced significantly higher mixing than the jet from AR 2 orifice, up to the level of the underexpansion level corresponding to Mach disc formation. For higher underexpansion levels, the mixing of AR 4 and AR 6 jets becomes inferior to that of the AR 2 jet.



**Figure 12.57** Variation of core length with NPR of a sonic jet elliptic jet of AR 2, 4, 6, and a sonic circular jet [86].

Jet core length variation with NPR, for the sonic jets, studied by Chauhan et al. [86], are shown in Figure 12.57. The core length ( $L$ ) is nondimensionalized with the equivalent diameter ( $D$ ). It can be seen that, for all the elliptical jets and the circular jet, the core length increases with NPR from the almost correctly expanded state (NPR 2) to the NPR at which the Mach disc forms (NPR 4).

For NPR beyond 4, for the AR 4 elliptical jet and circular jet, the core length continues to increase with NPR, whereas for elliptic jets of AR 2 and 6, the core length decreases with an increase in NPR. At NPR 2 and 3, the core length of an AR 4 and AR 6 jet is much shorter than that of AR 2 and the circular jet. Beyond NPR 4, the core length of AR 4 becomes significantly larger than AR 2 and AR 6 jets, and nearly equal to circular jet core. The core length of an AR 6 and AR 2 jet is almost the same at NPR 5. Also, the core length of an AR 4 and AR 6 jet are the same at NPR 3. At NPR 4, the core length of AR 2, AR 4, and the circular jet are almost the same. At NPR 2 the core length of AR 2 jet coincides with the core length of the circular jet.

Further, the unsymmetrical spread of elliptic jets results in axis-switching, and the distance from the orifice exit where axis-switching takes place depends on the orifice AR and expansion level of the orifice. An increase of a favorable pressure gradient at the orifice exit results in the upward shifting of the axis-switching location, indicating an increase in near-field mixing. The lesser amplitudes of pitot pressure oscillation in an elliptic jet core indicate that the shock cell structure of an elliptic jet is weaker than that of a circular jet.

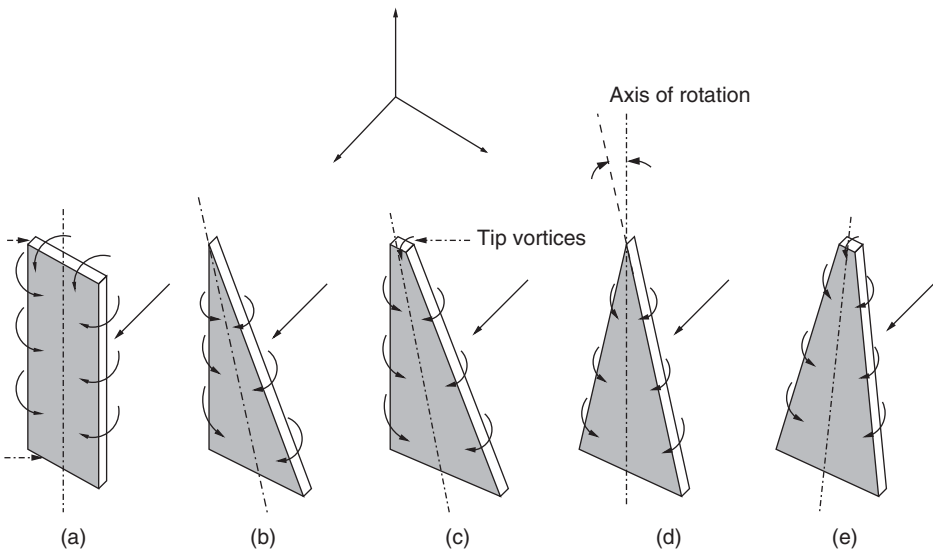
### 12.7.1 Jet Control with Tabs

From the jet literature it is known that tabs are effective in mixing the jet fluid with the mass entrained from the surrounding, owing to the differential shear at the jet boundary. The mechanism of mixing enhancement is identified as the mixing-promoting small-scale vortices shed from the edges of the tab. Further, it has been envisaged that, if the mixing-promoting vortices shed are of mixed-size, it would result in better mixing than an environment containing mass transporting small-scale vortices of uniform size. To study this aspect, the rectangular tabs, usually employed for mixing promotion, were provided with corrugation [62] and it was found that the corrugated tabs caused better mixing than the uncorrugated tabs of identical blockage. This triggered the research on corrugated tabs. Arun Kumar and Rathakrishnan studied the mixing-promoting capability of right-angled triangular tabs with a sharp and truncated vertex

by placing two identical tabs at the exit of a Mach 2 axisymmetric nozzle and found that, at all levels of expansion, the core length reduction caused by both the tabs was appreciable, but the mixing caused by the truncated tab was superior [87]. The mixing-promoting efficiency of the truncated tab was found to increase with an increase of NPR (that is a decrease of an adverse pressure gradient). This study showed that the mixing-promoting capability of the triangular tab is better than that of a rectangular tab of identical blockage area, at any specified flow condition.

A closer look into the flow physics of the momentum transfer process associated with the small-scale vortices shed from the tab would explain the reason for its mixing-promoting superiority. It is well known that the size of vortices shed from an object is proportional to the half-width of the object normal to the stream direction [88]. For a rectangular tab the half-width is uniform all along the tab length from the root end to the tip end. Therefore, the tab would shed mixing-promoting vortices of only uniform size all along its edges, except the tip, where there are two sharp corners and the vortices shed from the flat tip end and side wall are of different sizes and would interact intensely (Figure 12.58). Also, the vortices shed from the tip would be of a transverse type ( $y$ -direction), whereas those shed from the edges would be of a normal type ( $z$ -direction). Therefore, the uniform vortices shed by the rectangular tab would travel some distance downstream before becoming active in promoting mixing. Conversely, the triangular tab, owing to its geometry, would shed vortices of continuously varying size all along its edges, with the largest at the root end and continuously decreasing in size toward the tip end. The isosceles triangular tab, capable of shedding vortices of continuously varying size along its edges, at every height from the base would be of an identical size, though of the opposite family. But, the mixing-promoting vortices shed from the right-angled triangular tab would be of different size at all heights, in addition to being of the opposite family (Figure 12.58).

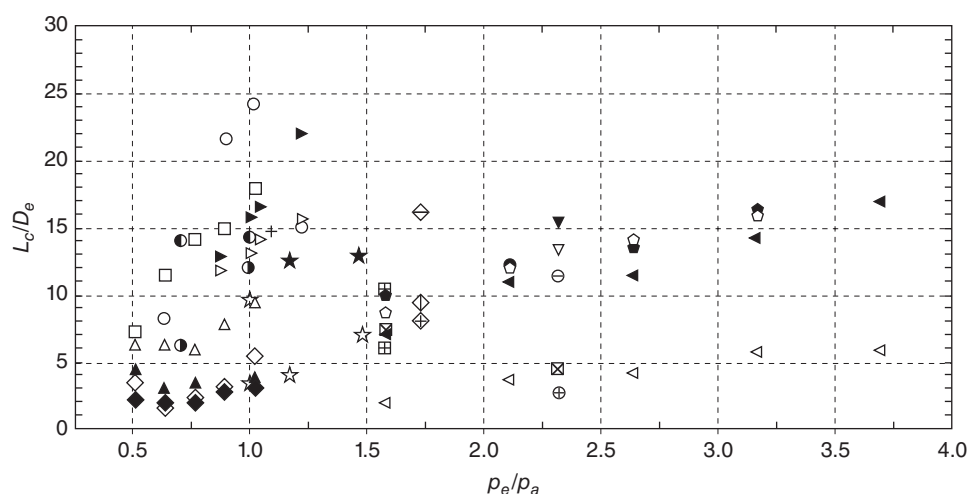
Moreover, the vortices of continuously varying size shed from the opposite sides of an isosceles triangular tab are inclined at an equal angle ( $\phi$ ) with respect to the axis of the tab. But the vortices from the opposite edges of the right-angled triangular tab are inclined with respect to



**Figure 12.58** Schematic representation of vortex formation from (a) rectangular tab; (b) right-angled triangular tab with sharp vertex; (c) right-angled triangular tab with truncated vertex; (d) isosceles triangular tab with sharp vertex; and (e) isosceles triangular tab with truncated vertex.

the tab axis at different angles ( $\phi$ ). These combinations – continuously varying size of vortices of opposite family, with their axes at unequal inclination to the tab axis – might be the reason for the reduced mixing-promoting efficiency of a right-angled triangular tab compared to an isosceles triangular tab. Another important feature to be noted is that near the sharp vertex tip, though the vortices are of a different size and from an opposite family, their closer proximity would make them interact intensely, which would lead to the loss of vorticity content. This might be the reason of reduced mixing-promoting efficiency of the sharp vertex triangular tab compared to the truncated vertex triangular tab. When the vertex is truncated, even at the tip, vortices of an opposite family would not interact among themselves. This might be an advantage because almost the entire vorticity content available with the mixing-promoting vortices would be used for mixing promotion [89, 90]. This can be regarded as the primary reason for the better efficiency of the triangular tab with a truncated vertex rather than a sharp vertex. However, the mixing-promoting efficiency of a sharp triangular tab is higher than the rectangular tab, owing to the mixed size of vortices shed from the triangular tab.

The variation of nondimensionalized core length ( $L_c/D_e$ ;  $L_c$  is the core length and  $D_e$  is the equivalent diameter of the nozzle/orifice exit) with the expansion ratio and the ratio of the pressure  $p_e$  at the nozzle exit to the backpressure  $p_a$ , to which the jet issuing from the nozzle is discharged,  $p_e/p_a$ , for the uncontrolled and controlled jets are shown in Figure 12.59 [90].



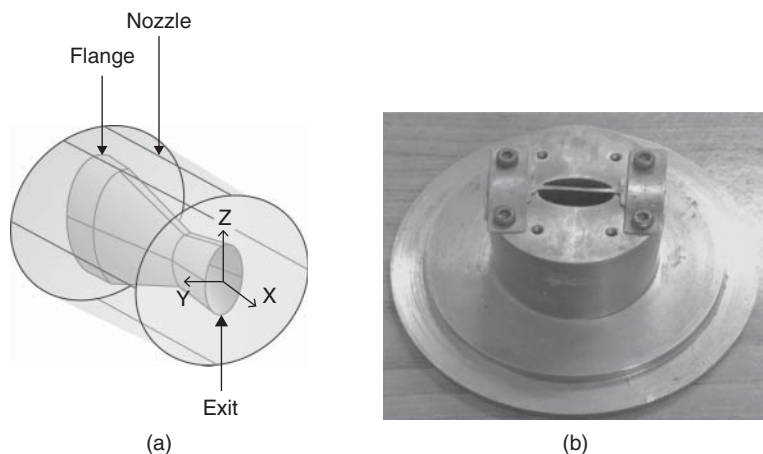
Variation of supersonic core length with expansion ratios ( $p_e/p_a$ ); ○ - Uncontrolled jet, □ - Jet controlled with rectangular tabs, △ - Jet controlled with sharp vertex right-angled triangular tabs, ◇ - Jet controlled with truncated vertex right-angled triangular tabs; ⊖ - no control, ⊗ - rectangular tabs and ⊕ - delta tabs (Zaman *et al.*<sup>(61)</sup>,  $M_d = 1.0$ ); ▼ - no control, and ▽ - grooves (Krothapalli *et al.*<sup>(28)</sup>,  $M_d = 1.0$ ); ▢ - no control, ⊠ - microjets with  $\phi_i = 0.02$  and ⊞ - microjets with  $\phi_i = 0.04$  (Mohammed K Ibrahim *et al.*<sup>(5)</sup>,  $M_d = 1.0$ ); ◀ - no control, and ▶ - rectangular tabs (Shibu Clement and Rathakrishnan<sup>(105)</sup>,  $M_d = 1.0$ ); ● - no control, and ○ - square grooves (Mrinal *et al.*<sup>(37)</sup>,  $M_d = 1.0$ ); ◆ - no control, ◇ - rectangular tabs, and ⬠ - rotating rectangular tabs (Mohammed K Ibrahim, and Yoshiaki Nakamura<sup>(106)</sup>,  $M_d = 1.35$ ); ★ - no control, and ☆ - rectangular tabs (Samimy *et al.*<sup>(58)</sup>,  $M_d = 1.35$ ); + - no control (Munday *et al.*<sup>(99)</sup>,  $M_d = 1.5$ ); ► - no control, and ◄ - rectangular tabs (Chiranjeevi and Rathakrishnan<sup>(102)</sup>,  $M_d = 1.8$ ); ● - no control, and ⊙ - square grooves (Vishnu and Rathakrishnan<sup>(36)</sup>,  $M_d = 1.8$ ); ▲ - delta tabs with sharp vertex, and ◆ - delta tabs with truncated vertex (Arun Kumar and Rathakrishnan<sup>(71)</sup>,  $M_d = 2.0$ ).

Figure 12.59 Variation of supersonic core length with expansion ratio [90].

For the uncontrolled jet and the rectangular tabs, the core length shows a monotonic increase with an increase in the expansion ratio, but for the triangular tabs with sharp and truncated vertex, there is no such variation in core length with the expansion ratio. The core length for the rectangular tab is the highest among the tabs studied, implying the least mixing-promoting efficiency, at all the expansion ratios of the present investigation. That is, the performance of triangular tabs is superior to that of rectangular tabs, at all levels of expansion. Zaman et al. also observed that triangular tabs perform better than rectangular tabs [49]. The core length variation of an isosceles triangular tab with a sharp or truncated vertex, studied by Arun Kumar and Rathakrishnan [90], is also shown in Figure 12.59. Among the triangular tabs studied, the core length for the truncated isosceles triangular tabs is the lowest, implying maximum mixing-promoting efficiency. Moreover, the performance of isosceles triangular tabs is better than the performance of right-angled triangular tabs, for both the sharp and the truncated vertex, at all levels of expansion. A point to be noted is that the core length of isosceles triangular tabs with sharp and truncated vertex is less than  $5D_e$ , at all levels of expansion of the present study.

The efficiency of tabs of two geometries in promoting the mixing of a Mach 2 elliptic jet has been studied by Bajpai and Rathakrishnan [91]. The experimental model used is a Mach 2.0 convergent–divergent elliptic nozzle of AR 2 : 1. The equivalent throat and exit diameters of the nozzle are 10 and 13 mm, respectively. An isometric view of the nozzle and a photographic view of the nozzle with a tab placed along the major axis are shown in Figure 12.60.

Limiting tabs of triangular and circular (crosswire) cross-sectional geometry of a projected area of 5% of the nozzle exit area (that is a tab of 5% geometrical blockage), placed along the major and minor axes at the nozzle exit, were tested for NPR (the ratio of the pressure in the settling chamber to which the jet nozzle is attached to the pressure of the environment to which the jet issuing from the nozzle is discharged) from 4 to 8, in steps of one. Both tabs are efficient mixing promoters, at all the tested NPRs, when placed along the minor axis. But for orientation along the major axis, the crosswire retards the mixing, at all the NPRs. The triangular tab along the major axis is also found to retard the mixing at NPRs 4 and 5, but for NPRs above 5 it causes mixing enhancement even when placed along the major axis. The crosswire is found to be a better mixing promoter than the triangular tab. A maximum core length reduction of 88% is caused by the triangular tab along the minor axis, at NPR 4. The corresponding core length reduction for the crosswire is only 72%. Shadowgraph images of controlled jets show



**Figure 12.60** (a) An isometric view of the exit of AR 2 : 1 convergent–divergent elliptical nozzle; (b) a photographic view of nozzle with limiting tab, of triangular cross-section, along the major axis.

that both tabs weaken the waves in the jet core. The geometry and orientation of the tab and the expansion level influence the mixing caused by the tab.

The better mixing-promoting capability of the triangular tab compared to the crosswire may be because of the vertex of the triangle facing the flow, which might result in a reduced extent of pressure hill at the face. The smaller pressure hill might have enabled the streamlines to comfortably negotiate the tab and reach the tab base, forming smaller vortices than the crosswire, for which the pressure hill at the leading edge is bound to be larger.

Further, even for a given tab geometry, the tab width can play a dominant role in modifying the mixing. This aspect was addressed by using triangular tabs of different width, having identical geometrical blockage, by placing them along the minor and major axis of an elliptic nozzle exit plane [91]. Shadowgraph images of a Mach 2.0 elliptic jet controlled with a limiting triangular tab, placed along the minor and major axes, at NPR 8, are shown in Figures 12.61 and 12.62, respectively. From these images, the strong influence of the vortex size difference, caused by the pressure hill shape at the face of the tab (resulting in a completely different wave pattern in the core of the jet controlled by the narrower triangular tab along the major axis and wider triangular tab along the minor axis) can be clearly seen.

### 12.7.2 Shifted Tabs

One of the serious shortcomings associated with the control of a jet with tabs is the momentum thrust loss caused by the blockage of the nozzle exit area by the tabs. It is important to note that, though placing triangular tabs at the nozzle exit was found to enhance the mixing of both circular and elliptic supersonic jets, in the presence of different levels of the present gradient at the nozzle exit, the tabs at the nozzle exit blocks a portion of the nozzle exit area. Also, there is a detached shock at the face of each tab. The reduced area at the nozzle exit will result in a decrease of a Mach number that the nozzle would deliver if there were no tab and the exit was clean, in accordance with isentropic flow theory. Furthermore, the detached shock envelope formed ahead of the tab will make the flow deviate away from the nozzle centerline. Both of these effects – the reduction of the nozzle exit area and the divergence of the jet – will lead to loss of momentum thrust that the nozzle is capable of generating if the tabs are not at the nozzle exit, since the thrust generated by the nozzle is

$$\text{Thrust} = \dot{m} \times V_j + A_e(p_e - p_a)$$

where  $\dot{m}$  is the mass flow rate through the nozzle, and is given by

$$\begin{aligned} \dot{m} &= (\text{density} \times \text{area} \times \text{velocity})_{\text{throat}} \\ &= \rho^* A^* V^* \end{aligned}$$

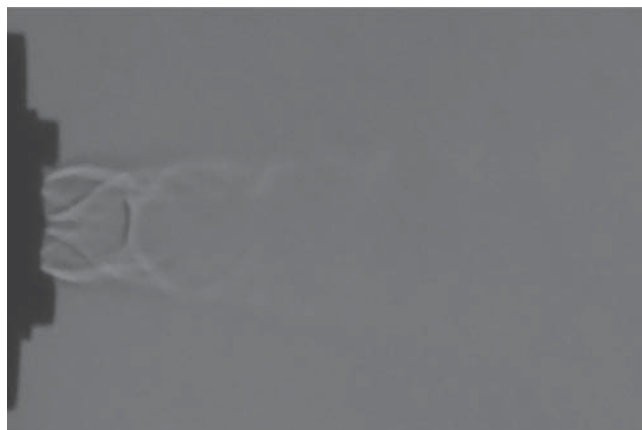
$A_e$  is the nozzle exit area,  $p_e$  is the static pressure at nozzle exit, and  $p_a$  is the backpressure to which the jet is discharged. For a correctly expanded state,  $p_e = p_a$ , for an overexpanded state,  $p_e < p_a$ , and for an underexpanded state,  $p_e > p_a$ . Thus, when the jet is operating at off design conditions, the term  $A_e(p_e - p_a)$  will contribute to the thrust generation positively when the jet is underexpanded and negatively when the jet is overexpanded. But the magnitude of this contribution is negligibly small compared to the first term  $\dot{m} \times V_j$  in the above thrust equation, and hence usually ignored at all levels of expansion. For the choked throat, such as the present one,  $\rho^*$ ,  $A^*$ , and  $V^*$  are constant, for a given settling chamber pressure  $p_0$ , hence the thrust generated by the nozzle is almost solely dictated by the jet velocity  $V_j$ . Therefore, even a marginal decrease of jet velocity is undesirable from a propulsion point of view. But enhancing jet mixing is preferable from the point of view of applications, such as stealth capability, reduction of base-heating, and so on. Therefore, it will be of great value, from both a propulsion and an application point

of view, if the aerodynamic mixing of the jet with the surrounding environment to which it is discharged is enhanced using a control, which will augment the jet mixing without any adverse effect, such as a decrease of jet velocity.

It will be of great value if the desired mixing enhancement of the jet is achieved by placing the mixing-promoting tabs downstream of the nozzle exit, establishing a situation which leaves the nozzle exit clean, without disturbing the velocity of the jet issuing out, and at the same time the small-scale vortices necessary for enhancing the mixing of the jet flow mass with the mass entrained by it through the mass entraining large-scale vortices formed at the boundary, due to the differential shear caused by the jet mass moving with finite momentum and the surrounding fluid mass at zero momentum. With the aim of mixing augmentation without thrust loss, the effect of a cross-wire placed downstream of a sonic nozzle exit was studied. The shifted cross-wire was found to influence the near-field mixing significantly, resulting in an appreciable reduction of jet core length. The shifted cross-wire was found to cause mixing enhancement even in the far field. Also, the shocks in the jet core were weakened by the wire. But these studies were limited to subsonic and sonic jets only.



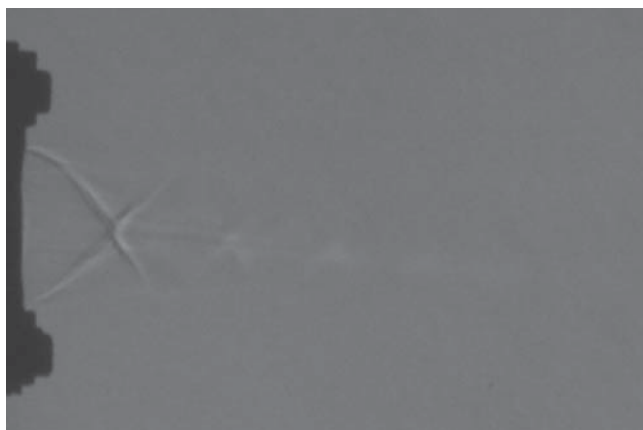
(a) view direction normal to major axis



(b) view direction normal to minor axis

**Figure 12.61** Shadowgraph images of a Mach 2.0 elliptic jet, at NPR 8, with a limiting triangular tab along the minor axis [91].





(a) view direction normal to major axis

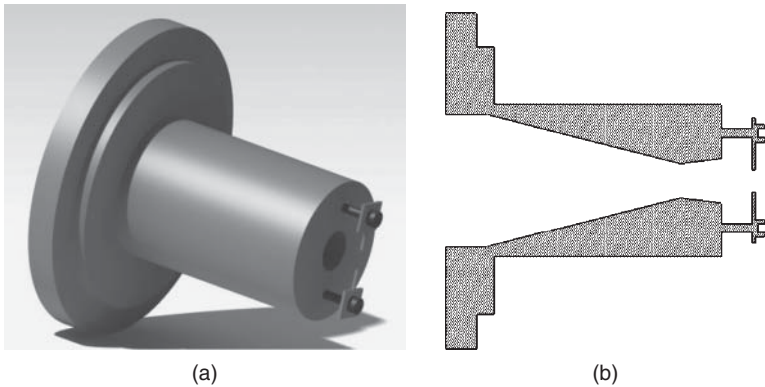


(b) view direction normal to minor axis

**Figure 12.62** Shadowgraph images for a Mach 2.0 elliptic jet, at NPR 8, with a triangular limiting tab along a major axis [91].

It is important to note that, in addition to thrust loss due to the presence of tab at nozzle exit, there is another penalty due to the drag of the tab. Thus, a portion of the momentum thrust generated by the jet would be spent to overcome this drag component, when the tab is used for jet control. In the shifted tab concept, the disadvantage of momentum loss can be avoided by shifting the tab from the nozzle exit, but the penalty due to the drag experienced by the tab is intact for both the tab at the nozzle exit and at a location downstream of the nozzle exit.

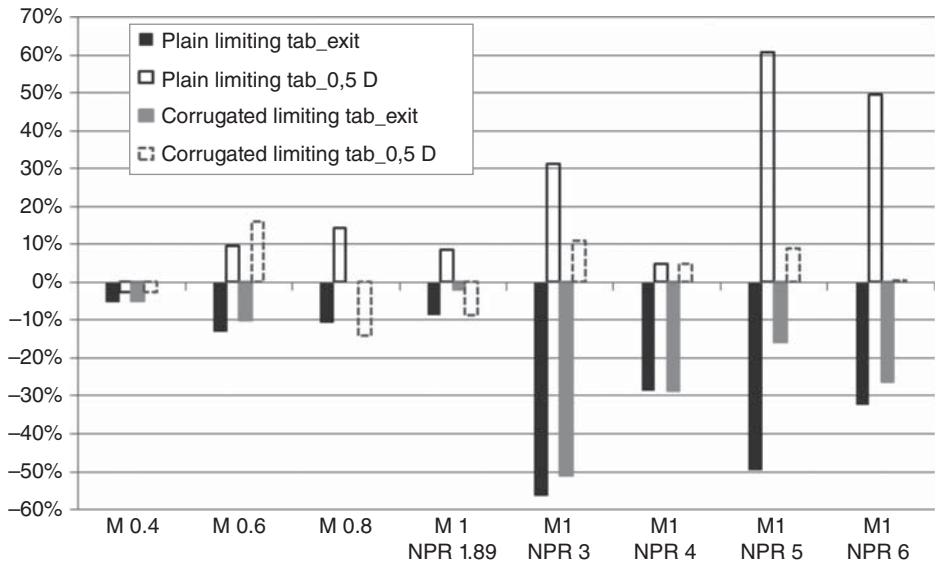
This concept of jet control with the tab positioned slightly downstream of the nozzle exit, as illustrated in Figure 12.63, was used by Parveen Kumar for a supersonic jet control [92]. Two rectangular tabs of a projected area of 2% each of the nozzle exit area were used to control the mixing of a Mach 1.9 circular jet, by placing the tabs at  $0.5D$  downstream of the nozzle exit plane. It was found that the mixing-promoting effectiveness of parallel shifted tabs is inferior to both an uncontrolled jet and one controlled with tabs at the nozzle exit. A jet controlled with tabs at  $0.5D$ , at overexpanded states, is found to retard the mixing, but as the jet approaches underexpansion state, the mixing-promoting efficiency of parallel-shifted tabs is found to be superior than the tabs at the nozzle exit. The shadowgraph pictures for the uncontrolled and



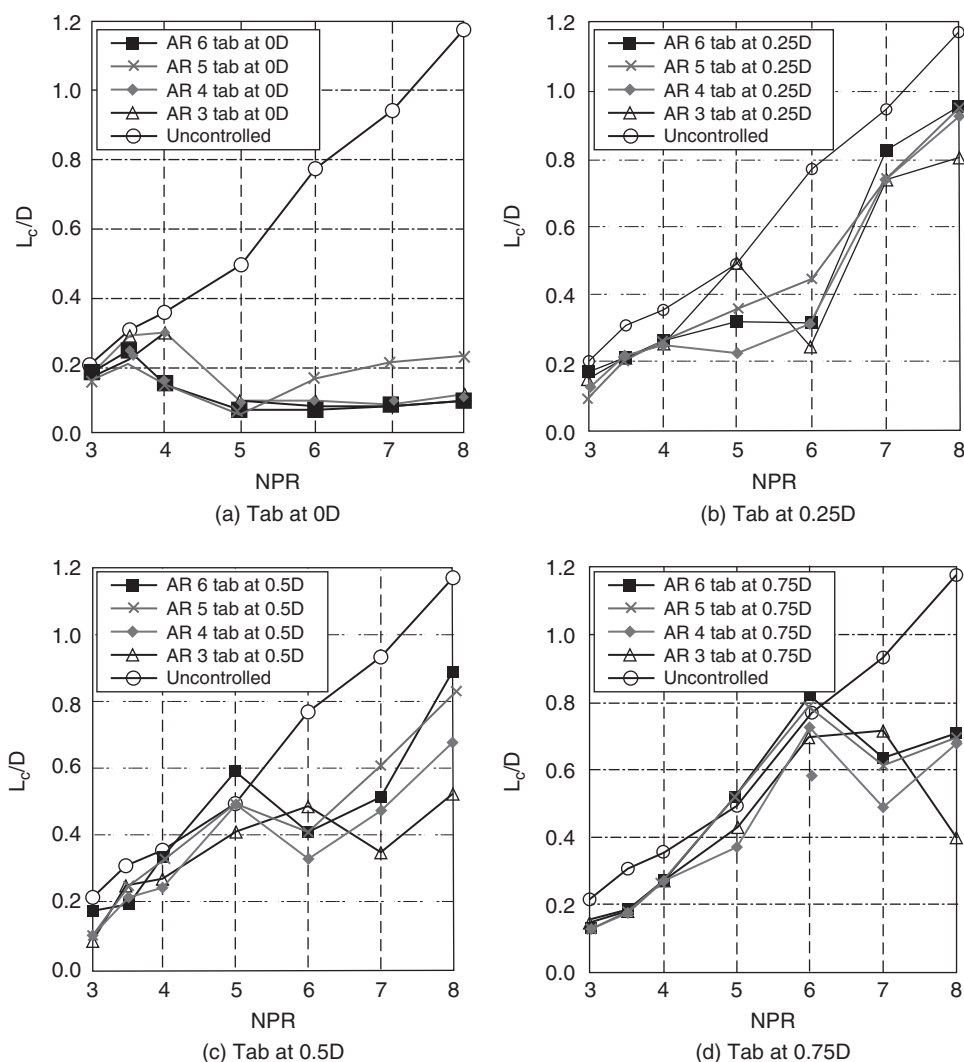
**Figure 12.63** Nozzle with shifted tabs (a) an artistic view and (b) a schematic diagram of a section view [93].

controlled jet clearly demonstrate the effectiveness of shifted tabs in weakening the waves in the jet core.

Mixing modification caused by a limiting rectangular tab with and without corrugations located at the nozzle exit and at 0.5D, downstream of the nozzle exit, for subsonic and sonic jet was studied by Berrueta and Rathakrishnan [93]. It was found that the mixing caused by the tab at the nozzle exit was better than the tab at 0.5D, for both plain and corrugated geometries. Also, both tabs caused better mixing for underexpanded sonic jets than the correctly expanded sonic jet and subsonic jets. At NPR 3 the plain tab at the nozzle exit reduced the core length by about 56% and the corrugated tab reduced the core by about 51%. But when the plain tab is placed at 0.5D the jet mixing is retarded. However, the corrugated tab at 0.5D enhances the mixing, though not up to the level of the same tab at 0D, at all Mach numbers except 0.6. The maximum reduction of core caused by a shifted corrugated tab is 14% for a Mach 0.8 jet. The results showing the mixing performance of the tabs at nozzle exit and 0.5D are summarized in Figure 12.64.



**Figure 12.64** Increasing/decreasing of the core length with the introduction of the tab [93].



**Figure 12.65** Variation of core length of a Mach 2 jet without control and with a rectangular tab of different AR, placed at a different axial location from the nozzle exit for different NPR [94].

Mixing characteristics of a Mach 2 jet controlled by shifted tabs has been studied at different levels of expansion at the nozzle exit by Maruthupandiyar and Rathakrishnan [94]. Two identical rectangular flat tabs of AR (length/width) 3–6, offering 2.5% blockage each, located diametrically opposite, at axial locations 0.25D, 0.5D, and 0.75D downstream of the nozzle exit have been studied. Core length variation of the uncontrolled and controlled jets as a function of NPR is shown in Figure 12.65. The core length ( $L_c$ ) is nondimensionalized with the nozzle exit diameter  $D$ . For the uncontrolled jet the core length increases monotonically with an increase of NPR.

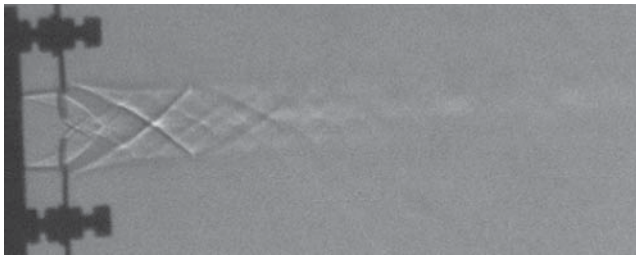
It can be seen that the mixing promotion caused by the shifted tab increases with an increase of adverse pressure gradient (that is below NPR 5). On the contrary, the mixing enhancement caused by the tab placed at the nozzle exit decreases with the increase of an adverse pressure gradient. At higher NPRs from 5 to 8 for a shifted tab configuration, the magnitude of oscillation



(a)



(b)



(c)

**Figure 12.66** Waves in (a) uncontrolled jet, (b) for tab at 0D, (c) for tab at 0.5D, at NPR 8 [94].

in the centerline pitot pressure is reduced considerably compared to the uncontrolled jet. At lower NPRs, that is in the presence of a high level of adverse pressure gradient, corresponding to expansion level,  $p_e/p_a$ , from 0.383 to 0.511, a shifted tab is found to be a better mixing promoter than the tab at the nozzle exit. But for an expansion level from 0.511 to 1.022, the tab at the nozzle exit proves to be a better mixing promoter. Also, among the shifted tab locations, 0.5D is found to be the best mixing promoter, resulting in a 55.56% reduction of core length at NPR 3, and the corresponding core length reduction for tabs at 0.25D, 0.75D, and 0D are only 25.93, 22.2, and 14.81%, respectively.

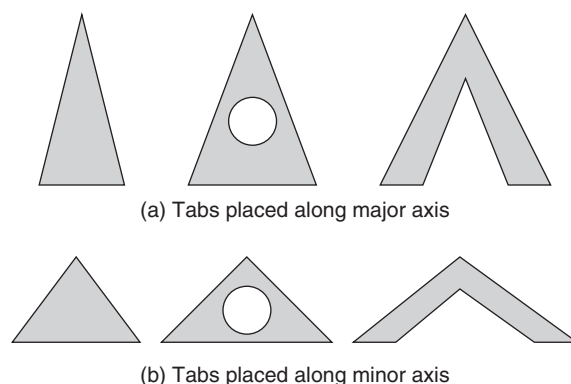
The waves in the core of the jet are strongly influenced by the tab position. Waves in the core of the uncontrolled jet and the controlled jet with tabs at 0D and 0.5D, at NPR 8, are shown in Figure 12.66.

### 12.7.3 Ventilated Triangular Tabs

The efficacy of passive control in the form of a ventilated triangular tab on mixing characteristics of supersonic jets to apprehend the governing flow physics and to capture the flow structure, in the presence of different levels of expansion at the exit of a Mach 1.5 elliptic nozzle of AR 3,

**Table 12.2** Core length/equivalent diameter of the nozzle exit.

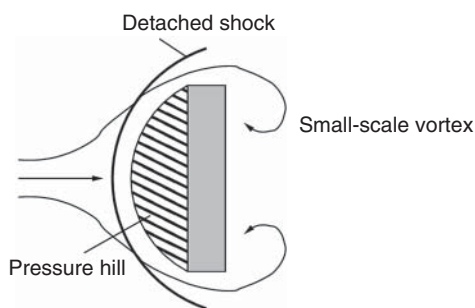
NPR	No control	No vent		Circular hole		Triangular hole	
		Major	Minor	Major	Minor	Major	Minor
3	3.01	2.48	0.52	3.08	0.60	2.63	1.13
4	4.32	2.23	1.13	4.70	1.13	5.60	1.50
5	4.37	3.84	1.50	4.00	1.80	5.42	1.73
6	4.97	4.60	2.26	4.30	2.33	5.65	1.88

**Figure 12.67** Triangular tabs without ventilation and with circular and triangular ventilation placed along the major and minor axes [95].


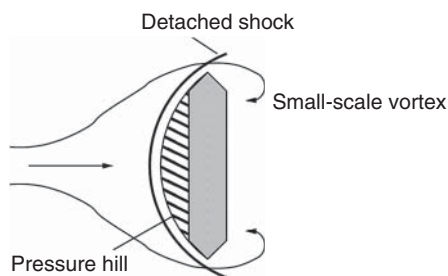
was investigated by Dadhich [95]. The effects of the tab configurations – triangular tabs placed along the major axis, triangular tabs placed along the minor axis, triangular tabs with a circular hole placed along the major axis, triangular tabs with a circular hole placed along the minor axis, triangular tabs with a triangular hole placed along the major axis, and triangular tabs with a triangular hole placed along the minor axis – were studied, in the range of NPR from 3 to 6. The core lengths for the different tab configurations studied, at different NPRs, are listed in Table 12.2. In this study an important geometrical feature, which influenced the mixing modification caused by both ventilated and unventilated triangular tabs, is its vertex angle. To keep the geometrical blockage due to the tab as 5% for all the configurations, the vertex angle for the tabs along the major axis is kept smaller than the tabs along the minor axis. Schematic sketches of the tabs used in this study are shown in Figure 12.67.

The effect of modifying the shape of tab edges on the aerodynamic mixing characteristics of a circular Mach 2.0 jet controlled with a rectangular tab has been studied recently [96]. The tabs used in this investigation are rectangular strips of AR 2 : 1 (AR 2), with square and sharp edges (Figure 12.68).

To overcome the disadvantage of momentum thrust loss due to blockage of the nozzle exit area, the concept of positioning the tabs slightly downstream of the nozzle exit has also been investigated. Jet mixing with tabs placed at shifted locations of 0.25D, 0.5D, and 0.75D from the nozzle exit plane was investigated for both square- and sharp-edged tabs. It was found that, when placed at the same location from the nozzle exit, a sharp-edged tab is a better mixing promoter than a square-edged tab, for a highly overexpanded jet (NPR 3). Profile plots of a controlled jet at higher NPRs reveal that, when positioned at nozzle exit (0D), square-edged tabs



(a) Square-edged tab



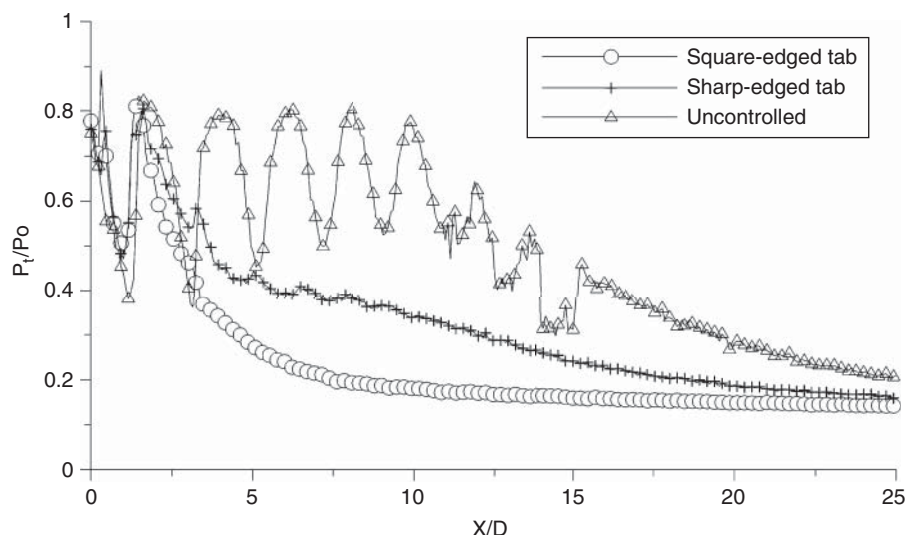
(b) Sharp-edged tab

**Figure 12.68** A cartoon illustrating the detached shock envelope over the tab, pressure hill at the tab face and the vortices leaving the tab edges [96].

split the jet into two high-speed regions, thereby causing significantly enhanced mixing, leading to a shorter core length, compared to sharp-edged tabs at  $0D$ . Such bifurcation is observed neither with sharp-edged tabs positioned at exit nor with square-/sharp-edged tabs positioned at shifted locations. For NPRs 3 and 4, at shifted locations, the vortices shed from the sharp-edged tab result in a marginally lower centerline pressure ratio than that shed from a square-edged tab, and it is the other way around for NPRs 5–8.

Variation of the pitot pressure ( $P_t/P_0$ ;  $P_t$  is the pitot pressure along the jet axis and  $P_0$  is the stagnation chamber pressure) along the axis of an uncontrolled jet and a jet controlled with 2 sharp-edged and square-edged identical rectangular tabs (length 2.56 mm, width 1.28 mm, and thickness 0.5 mm), of a projected area of 2.5% of the nozzle exit area, and located at diametrically opposite locations at the nozzle exit with an axial distance  $X/D$  ( $X$  is the distance from the nozzle exit and  $D$  is nozzle exit diameter), at NPR 8, is shown in Figure 12.69.

NPR 8 for a Mach 2 jet is a case of about 2% favorable pressure gradient at the nozzle exit. At this marginal level of the positive pressure gradient, the square-edged tab is found to be a far superior mixing promoter than the sharp-edged tab, in all the three zones of the jet. The core length of the uncontrolled jet at NPR 8 is about  $15D$ , whereas the core lengths for the jets controlled with square- and sharp-edged tabs are only about  $1.5D$  and  $8D$ , respectively. Thus, the core length reductions associated with the square- and sharp-edged tabs are 90 and 47%, respectively. Decay results at different levels of the pressure gradient of this study show that, in the presence of both adverse and favorable pressure gradients, the square-edged tab is a better mixing promoter than the sharp-edged tab in all the three zones of the jet. Also, this mixing-promoting superiority of the square-edged tab increases with a decrease of an adverse pressure gradient and an increase of a favorable pressure gradient.



**Figure 12.69** Centerline pressure plot of jet at NPR 8; tabs at exit [96].

### 12.7.4 Tab Edge Effect

The vortices shed by the tab would be strongly influenced by the geometry of the edge. Both the types of tabs used in the present study were made of 0.5 mm thick brass sheets; one with a square-edge and the other with a sharp-edge, as shown in Figure 12.68. The figure also shows that there would be a detached shock ahead of the tab. But the shock shape would be different for each tab, with the wave closer to the edge for the tab with the sharp-edge compared to that of the square-edged tab, as illustrated in Figure 12.68. Any difference in the shock shape will result in the formation of pressure hills of different types, as shown in the figure. Owing to the shape of the hill, for the detached shock with its edges closer to the tab, the streamlines negotiating the pressure hill would shed a smaller vortex from the edge of the sharp-edged tab than the square-edged tab. From vortex theory, it is known that the smaller the size of the mass transporting small-scale vortices, the better the mixing promoted by them. Thus, the vortices shed along the edges of the sharp-edged tab may be expected to cause better mixing promotion than the relatively larger small-scale vortices shed from the edges of the square-edged tab. As seen from the results in Figure 12.69, the decay results of centerline pitot pressure can quantify the mixing-promoting capability of the vortices shed from the edges of these tabs with square- and sharp-edges. From the results shown in Figure 12.69, it is seen that, for tabs at the nozzle exit (0D), at NPR 8, the core length reduction amounts to as high as 90%, for the square-edged tabs and only to about 47% for the sharp-edged tabs. These results demonstrate that it is not just the size of the small-scale vortices shed from the tab but also the combined effect of the environment established by the proportion of the mass entraining large-scale vortices formed at the edge of the jet boundary, owing to the differential shear between the jet and the surrounding to which the jet is discharged and the mass transporting small-scale vortices shed from the edges of the tab and the level of the pressure gradient present at the nozzle exit is the dictating factor for the aerodynamic mixing of the mass entrained at the jet boundary with jet fluid mass. In the presence of a 2% favorable pressure gradient, the size of small-scale vortices shed by the square-edged tab at 0D seems to establish the environment which is better than that established by the relatively smaller vortices shed by the sharp-edged tab, for mixing promotion.



(a)



(b)

**Figure 12.70** Shadowgraph images of a Mach 2 circular jet at NPR 4, with square-edged tabs at nozzle exit (0D): (a) viewed normal to the tab; (b) viewed along the tab [96].

At all NPRs, when the square-/sharp-edged tabs are shifted from the exit to  $0.25D$ , there is an increase in the core length of the controlled jet. At some NPRs, jets controlled with sharp-edged tabs at  $0.5D$  or  $0.75D$  showed a smaller core length compared to the jet controlled with sharp-edged tabs at  $0.25D$ . But this is accompanied by a presence of strong shocks in the core of the jet.

Shadowgraph images of the waves present in the controlled jet core, at NPR 4 and 5, for the case of square-edged tab at  $0D$  and  $0.5D$  are shown in Figures 12.70 and 12.71, respectively.

For the jet running at NPR 4, controlled with tabs at nozzle exit ( $0D$ ), the additional waves formed due to the presence of the tabs can be seen in Figure 12.70. The larger spread in the direction normal to the tab is clearly seen in this figure. Shadowgraph images of the jet at the same level of overexpansion (corresponding to NPR 4), controlled with a tab at a shifted location of  $0.5D$  downstream of the nozzle exit, are shown in Figure 12.71. It can be seen that there is a detached shock at the tab face and, after negotiating the tabs, the shocks from opposite ends cross each other at the jet axis, at a station downstream of the tabs. These shock crossover points become a Mach disc in the direction normal to the tabs, as can be seen in Figure 12.71.

Shadowgraph images of the jet controlled with sharp-edged tabs at  $0D$  and  $0.5D$ , at NPR 4 and 5, are shown in Figures 12.72 and 12.73, respectively.

It is interesting to note that the waves present in the core of the jet with sharp-edged tabs are different from those with square-edged tabs. At NPR 4, and tab location  $0D$ , as seen in Figures 12.70–12.73, the spread of the jet with sharp-edged tabs is less than the spread of the jet with square-edged tabs. This demonstrates that it is not just the level of pressure gradient





(a)



(b)

**Figure 12.71** Shadowgraph images of a Mach 2 circular jet at NPR 5, with square-edged tabs at 0.5D: (a) viewed normal to the tab; (b) viewed along the tab [96].



(a)



(b)

**Figure 12.72** Shadowgraph images of a Mach 2 circular jet at NPR 4, with sharp-edged tabs at nozzle exit (0D): (a) viewed normal to the tab; (b) viewed along the tab [96].



(a)



(b)

**Figure 12.73** Shadowgraph images of a Mach 2 circular jet at NPR 5, with sharp-edged tabs at  $0.5D$ : (a) viewed normal to the tab; (b) viewed along the tab [96].

at the nozzle exit but also the combined effect of the pressure hill at the tab face and the level of expansion at the nozzle exit which dictates the size of the mixing-promoting small-scale vortices shed by the tab.

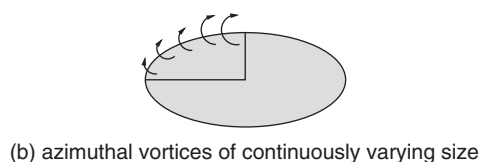
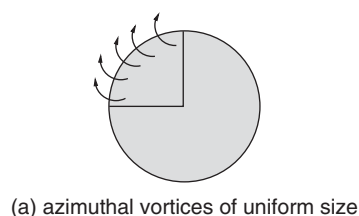
In the case of the uncontrolled elliptic nozzle, the size of the vortices shed at the nozzle exit would vary continuously from one end of the major axis to the adjacent end of the minor axis, in accordance with vortex theory, which states that the size of the vortex shed from an edge is proportional to the radius of curvature of the edge [97].

Thus, the azimuthal vortices shed around the ends of the major axis would be smaller than those shed around the ends of the minor axis. Schematic diagrams illustrating the azimuthal vortices shed from the exit of a circular and elliptic nozzle are shown in Figure 12.74.

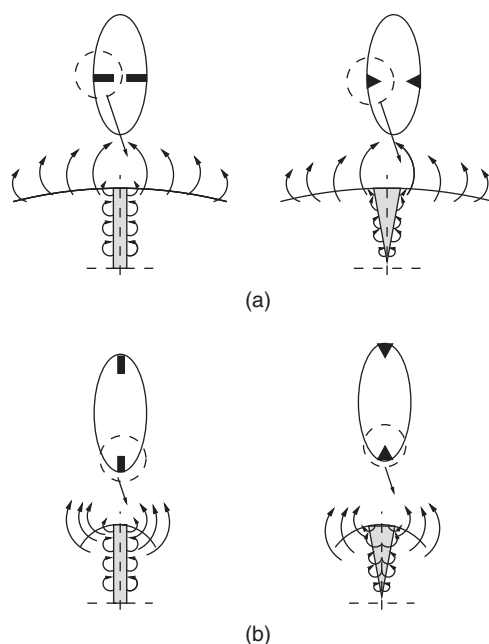
It can be seen that the circular nozzle sheds only vortices of uniform size compared with the elliptic nozzle, which sheds vortices of a continuously varying size from one end of the major axis to the adjacent end of the minor axis. Because of this, the jet issuing from an elliptic nozzle will have a better mixing environment than a circular nozzle of identical area and inlet condition. This will enable the jet issuing from an elliptic nozzle to enjoy better aerodynamic mixing than an identical jet issuing from a circular nozzle.

When a tab is placed normal to a flow, it will shed vortices from its edges. These small-scale transverse vortices leaving the tab will become streamwise soon after shedding, owing to the inertia of the jet. The size of the vortex shed from a tab is proportional to its local half-width. The results of centerline pressure decay of the elliptic jet controlled with two identical rectangular and triangular tabs placed diametrically opposite, along the major and minor axes at the exit of nozzle, show that the tabs (rectangular and triangular) along the minor axis are more efficient

**Figure 12.74** Schematic of vortices shed from (a) a circular nozzle exit and (b) an elliptic nozzle exit.



**Figure 12.75** Schematic diagram of vortices shed from an elliptic nozzle exit and tabs: (a) rectangular and triangular tabs along the minor axis; (b) rectangular and triangular tabs along the major axis.



in enhancing the mixing of the jet with the ambient fluid than the tabs along the major axis [97]. This is because the azimuthal vortices shed at the minor axis side of the nozzle exit are relatively larger compared with the azimuthal vortices shed at the major axis side, owing to the curvature effect of the elliptic geometry. The relatively larger size of the azimuthal vortices shed around the minor axis, along with the relatively smaller small-scale vortices shed from the tabs placed along the minor axis (Figure 12.75a), seem to create a better mixing-promoting environment compared with those associated with the tabs along the major axis (Figure 12.75b). This might be the reason for the better mixing caused by the tabs along the minor axis. As can be seen in Figure 12.75, the width of the tab remains the same from base to tip for the rectangular tab compared with the triangular tab with varying width from base to vertex. Therefore, a triangular tab sheds vortices of continuously varying size from base to vertex, whereas a rectangular tab can shed only vortices of uniform size along its length [97].

Another important feature that dictates the size of the vortex shed from an object is the pressure hill at the front face [88]. For the triangular tab, the pressure hill at its face varies in size from

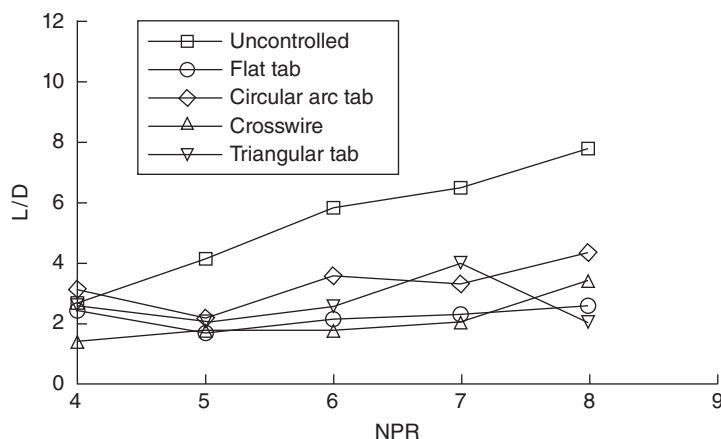
its base to tip. Therefore, the environment required for mixing-promoting vortices of mixed size is built in for the triangular shape. The mixing promotion caused by triangular tabs along the minor axis would be better than that of rectangular tabs along the same orientation because of the mixed size of the mixing-promoting small-scale vortices shed by the triangular tab compared with the rectangular tab, which would shed small-scale vortices of uniform size only (Figure 12.75a). The small-scale vortices of continuously varying size from base to vertex, introduced by the triangular tabs, along with the small-scale azimuthal vortices of relatively larger size shed from the nozzle exit, would provide an environment of mixed-size vortices favorable for promoting mixing of the mass entrained by the large-scale vortices at the jet boundary with the jet mass.

The tabs in limit length are found to be effective in promoting the mixing. However, the studies on the mixing efficiency of limiting tabs are only few, especially on the use of limiting tabs for promoting the mixing of noncircular jets. The control effectiveness of a limiting tab on a supersonic elliptic jet issuing from an elliptic nozzle of AR 4 was studied by Rathakrishnan [98]. The dominant source for the generation of the mixing-promoting streamwise vortices shed by the tab is the pressure hill formed at the tab face of the tab. The size of the pressure hill is governed not only by the projected area of the tab normal to the flow but also by the shape of the tab. The pressure hills formed at the face of the flat, triangular, circular arc, and circular (crosswire) geometry of the same projected area will be different. The effect of this difference in the shape of the pressure hill is to make the tabs shed streamwise vortices of different sizes. The influence of this change in the size of mixing-promoting vortices shed by tabs on jet mixing was studied in the presence of various levels of pressure gradient, without going into the details of the actual size of the pressure hill.

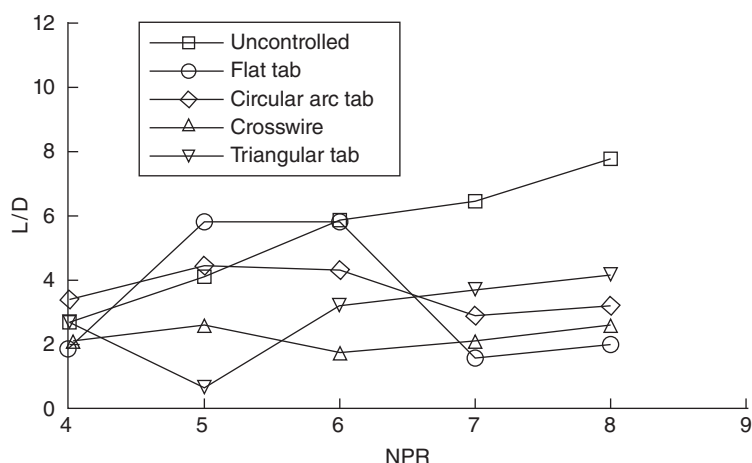
Among the tabs studied, the triangular tab was found to be the most efficient mixing promoter for this Mach 2 elliptical jet. The triangular tab promotes mixing to the largest extent when placed along the minor axis, leading to a core length reduction of about 82%, in the presence of an adverse pressure gradient of about 36%, at the nozzle exit, that is at NPR 5. At this NPR, circular arc and flat tabs protect the core, that is these tabs retard the jet mixing, leading to an elongation of the core by 8.7 and 42.4% respectively, whereas the core reduction caused by crosswire is only 36.8% at this NPR. The triangular tab is also found to be the most efficient mixing promoter for tab orientation along the major axis, but for this orientation the best core length reduction caused is only 73.4%, at NPR 8. The efficient mixing promotion caused by the triangular tab does not introduce any abnormal level of asymmetry to jet propagation.

Core length variations caused by the limiting tabs of different geometries, placed along the major and minor axes of the AR 4 elliptic Mach 2 jet, at different levels of expansion, are quantified in Figures 12.76 and 12.77, respectively. The plots in Figure 12.76 show the variation of non-dimensional core length  $L/D$  with NPR, for tabs along the major axis. It can be seen that for an uncontrolled jet the core length increases monotonically with NPR, which is typical for a free jet. For controlled jets, the effect of NPR on the core length is less pronounced than for an uncontrolled jet. However, at the overexpanded state corresponding to NPR 4, establishing a high level of adverse pressure gradient at the nozzle exit, the circular arc tab is found to retard the mixing, but this retardation is only at NPR 4. For NPRs above 4, all the tabs enhance the mixing considerably, as can be seen from Figure 12.76.

Variation of the non-dimensional core length of the controlled and uncontrolled jets with NPR, for tab orientation along the minor axis, is shown in Figure 12.77. For this orientation of the tab also, at NPR 4, the circular arc tab is found to retard the mixing. Furthermore, the mixing caused by the flat tab is found to be insignificant at NPR 6, but the same flat tab is found to enhance the mixing to the highest level compared to other tabs for NPRs 7 and 8. Other tabs



**Figure 12.76** Jet core length variation with NPR, for tabs along the major axis [98].



**Figure 12.77** Core length variation with NPR for tabs along the minor axis [98].

also enhance the mixing considerably, but the mixing enhancement caused by the triangular tab at NPR 5 is the highest over the range of NPR, as well as across the tab geometries.

From these results it is evident that the mixing-promoting environment, established by the momentum-transporting small-scale vortices shed from the edges of the tabs and mass entraining large-scale vortices formed at the jet boundary, is strongly influenced by the combined effect of the pressure hill at the tab face, which is governed by the geometry of the tab, and the pressure gradient present at the nozzle exit, which governs the convection of mixing-promoting small-scale vortices shed by the tabs.

## 12.8 Summary

A jet may be defined as a *pressure-driven shear flow with the characteristic that the width-to-axial distance is a constant*. This constant assumes a value of 8 for jet Mach numbers  $< 0.2$  and the constant decreases with an increase of Mach number.

When a jet is issuing into a still environment it is termed a *free jet* or a *submerged jet*. If it is issuing into a flow, constituting a field that has the jet surrounded by a flow field of different velocity, it is referred to as a *co-flowing jet*. When the jet is issuing normal to a boundary (either a solid or a fluid boundary), it is referred to as an *impinging jet*. If the jet axis is at an oblique angle to the boundary and the boundary is a wall, it is called a *wall jet*. If a jet is opposed by another jet, the combination is termed *opposing jets*.

For subsonic jets, the axial distance up to which the jet velocity along the axis is unaffected is called the *jet core*. The jet core is essentially a potential region where the jet retains its axial velocity at all axial points in the region. After the core the entire jet field is dominated by viscous action. The core for a subsonic free jet usually extends up to about six times the nozzle exit diameter ( $D$ ). After that, the characteristic decay begins and that dominates from about  $6D$  to about  $12D$ . The region from the end of characteristic decay to infinity is also referred to as a *self-similar region* or a *fully developed region*.

Large-scale vortices are efficient suction creators and thus efficient in engulfing the fluid from the surroundings into the jet. This process of bringing mass from the surroundings into the jet is termed *mass entrainment* or simply *entrainment*. The fluid mass with zero momentum from the surrounding zone, entrained by the large vortex structures, will interact with the jet fluid at a finite momentum. In the process the jet fluid will exchange momentum with the entrained mass. Thus, the momentum of the jet fluid will decrease and that of the entrained fluid will increase, but the total momentum of the jet is conserved. During the process, the large vortices get fragmented into small eddies. Small-scale eddies have a longer life and they also serve as good transporters of mass and momentum. Therefore, in a jet flow large- and small-scale structures must be present in suitable proportion to result in an efficient mixing of the jet flow with the surrounding fluid. However, identifying this proportion in a turbulent field such as a jet is an impossible task. Hence, it is usual practice to ensure the existence of these structures in appropriate proportion by indirect means. One of the popular means for this is the measurement of jet centerline decay, which is a direct measure of the mixing taking place in the jet field. A fast decay implies rapid mixing, and vice versa.

A jet with faster decay of its centerline pressure implies that it contains a proper combination of large and small vortices compared to an identical jet with a slower decay of centerline pressure. Enhancement of jet decay can be achieved with controls which are passive or active in nature. An *active control* is one which requires an additional source of energy for its action and a *passive control* is one that does not require any external energy for its action. Most of the passive control techniques make use of geometrical modification of the nozzle exit.

The velocity at the center of the section of an axially symmetric submerged jet is inversely proportional to the distance from the pole.

$$u_m = \frac{\text{constant}}{x}$$

The velocity decay along the axis of a plane-parallel jet is inversely proportional to the square root of the distance from the pole.

$$u_m = \frac{\text{constant}}{\sqrt{x}}$$

All free jets are turbulent, even at Reynolds numbers close to zero. This is because of the differential shear experienced by the jet at its periphery. Therefore, the laws governing the distribution of different pulsation characteristics of the stream and their interrelationships are very important in the theory of the turbulent jet in particular, and in the theory of turbulence in general.

Some of the well-known theories of the jet or the so-called free turbulence are

- Prandtl's old theory
- Taylor's theory
- Prandtl's new theory
- Richard's theory
- Mattioli's theory.

Basically, jets can be classified into incompressible jets and compressible jets. The jets with a Mach number of less than 0.3, up to which the compressibility effects are negligible, are called *incompressible jets*. Jets with a Mach number of more than 0.3 are termed *compressible jets*. Compressible jets can further be subdivided into subsonic, sonic, and supersonic jets. Jets with a Mach number of less than 1.0 are called *subsonic jets*, and jets with a Mach number of 1.0 are called *sonic jets*, which can be correctly expanded or underexpanded. Jets with a Mach number of more than 1.0 are called *supersonic jets*, and these can be further classified into *overexpanded*, *correctly expanded*, and *underexpanded jets*.

Subsonic jets are those with Mach numbers of between 0.3 and 1.0, and are always correctly expanded, and develop with an included angle of about  $10^\circ$ . The flow regimes in a subsonic jet are classified as follows.

- *Potential core region.* This region consists of a core zone of constant axial velocity equal to the jet (nozzle) exit velocity, surrounded by a rapidly growing and predominantly shear dominated annulus of mixing layer or shear layer with intense turbulence. The potential core of a subsonic jet typically extends to about five times the nozzle exit diameter ( $D_e$ ) downstream of the nozzle exit. This is because the mixing initiated at the jet boundary (periphery) has not yet permeated into the entire flow field, thus leaving a region that is characterized by a constant axial velocity.
- *Transition region.* This is the region where the centerline velocity begins to decay. This characteristic decay zone extends from about  $5D_e$  to  $10D_e$  downstream, over which the turbulence changes from its annular to a somewhat pseudo-cylindrical distribution. As a result, the velocity difference between the ambient fluid and the high-speed core region of the jet decreases and attenuates the shear that supports the vortical rings in the jet, and thus the velocity profiles become smoother with jet propagation.  
The transition region is characterized by a growth of three-dimensional flow due to wave instability of the cores of the vortex rings. The merging of these distorted vortices produces large eddies which can remain coherent around the potential core region of the jet.
- *Fully developed region.* Beyond the transition region the jet becomes similar in appearance to a flow of fluid from a source of infinitely small thickness (in an axially symmetric case the source is a point, and in a plane parallel case it is a straight line perpendicular to the plane of flow of jet). In practice, the jet velocity becomes insignificant after about  $30D_e$ .

A jet is said to be overexpanded when the nozzle exit pressure  $p_e$  is lower than the ambient pressure  $p_a$  to which it is discharging.

A jet is said to be correctly expanded when the nozzle exit pressure is equal to the ambient pressure. This jet is also wave dominated, as is an imperfectly expanded jet, even though we think that there would not be any waves. The reason for this is that, as the jet is issuing from a confined area to an infinite area, it tries to expand through expansion waves and after that gets compressed through compression waves (the reflected waves from the jet boundary), and this results in a periodic wave structure.

A jet is said to be underexpanded when the nozzle exit pressure ( $p_e$ ) is higher than the backpressure ( $p_b$ ). Since the nozzle exit pressure is higher than the backpressure, wedge-shaped

expansion waves occur at the edge of the nozzle. These waves cross one another and are reflected from the boundaries of the jet flow field as compression waves. The compression waves again cross one another and are reflected on the boundaries of the jet as expansion waves. For an underexpanded jet also, in addition to the expansion fan caused by the level of underexpansion, there will be another expansion effect, owing to the relaxation experienced by the jet on exiting from the nozzle into a large space. Thus, the combined effect of these two causes establishes a stronger expansion fan than the underexpansion level alone can establish. Beyond some limiting NPR, the shock intersecting point becomes an intersecting zone, which resembles a disc, as seen in Figure 12.9d for NPR 4.25. This disc is termed a *Mach disc*. The Mach disc is essentially a compression wave identical to a normal shock, across which the flow decelerates to a subsonic level. A sonic or supersonic jet with a Mach disc in the core is termed *highly underexpanded*.

The diverse nature of applicability jets demands that they be made suitable for a specific application, by controlling them. Here, control may be defined as the ability to modify the jet flow mixing characteristics to achieve engineering efficiency, technological ease, economy, adherence to standards, and so on.

Jet controls can be broadly classified into active and passive controls, but passive controls are the more desirable, partly because they require no external power source.

Large-scale coherent structures control the dynamics of all free shear flows, including plane mixing layers, jets of different geometries (axisymmetric, plane, elliptic, rectangular, and so on), and wakes. These two-dimensional structures were found to play an important role in entrainment and mixing processes in incompressible shear layers.

Mixing in supersonic shear layers is critically dependent upon the compressibility effects in addition to the velocity and density ratios across the shear layer. The compressibility level is best described by a parameter called the *convective Mach number*.

Supersonic jets normally possess complex shock patterns. Therefore, the role of shock waves in noise generation becomes significant. The main sources of high-speed noise are the turbulent nature of the flow, shock-turbulence interaction, flow-induced oscillations of shocks, and resonance effects. An intense, discrete acoustic emission termed *screech* or *whistle*, as a consequence of oscillating shock waves within a supersonic jet, usually dominates the noise emitted by a cold model converging jet operated at slightly above a choked flow condition.

The turbulent mixing noise is from both large-scale turbulence structures and fine-scale turbulence of the jet flow. The large-scale turbulence structures generate the dominant part of the turbulent mixing noise. The fine-scale turbulence is responsible for the background noise.

Broadband shock-associated noise and screech tones are generated only when a quasi-periodic shock cell structure is present in the jet core. The quasi-periodicity of the shock cells plays a crucial role in defining the characteristics of both the broadband and discrete frequency shock noises.

Noncircular jets, such as elliptic jets, owing to the continuous variation in the azimuthal radius of curvature, form flow structures of different size at the jet boundary and the jet spreads differently along different planes. Studies on noncircular jets show that the jet experiences fine-scale mixing at the corners and at high curvature regions and large suction at the low curvature/flat side regions, owing to the formation of large-scale vortices, resulting in large entrainment.

The increased entrainment and enhanced mixing capabilities of the elliptic jet (noncircular jets) relative to the equivalent circular jet are due to the phenomenon known as *axis-switching*, which is unanimously supported by the literature. Axis-switching is a phenomenon in which the cross-section of an asymmetric jet evolves in such a manner that, after a certain distance from the nozzle exit, the major and the minor axes are interchanged.



Waves (expansion/compression) present in the elliptic jet core are unsymmetrical and the waves in the circular jet core are symmetrical about the jet axis. This asymmetrical nature of the waves in the elliptic jet is due to the azimuthal asymmetry of the elliptic nozzle. Also, the shock cells in the core of the elliptic jet are shorter than the circular jet.

The distance from the orifice exit where axis-switching takes place depends on the orifice AR and the expansion level of the orifice. The increase of a favorable pressure gradient at the orifice exit results in the upward shifting of the axis-switching location, indicating an increase in near-field mixing.

The size of vortices shed from an object is proportional to the half-width of the object normal to the stream direction. For rectangular tab the half-width is uniform all along the tab length from the root end to the tip end, whereas the triangular tab, owing to its geometry, would shed vortices of continuously varying size all along its edges, with the largest at the root end and continuously decreasing in size toward the tip end. The isosceles triangular tab, capable of shedding vortices of continuously varying size along its edges, at every height from the base, would be of identical size, though of an opposite family. But, the mixing-promoting vortices shed from the right-angled triangular tab would be of a different size at all heights, in addition to being of an opposite family. Moreover, the vortices of continuously varying size shed from the opposite sides of the isosceles triangular tab would be inclined at an equal angle with respect to the axis of the tab. But the vortices from the opposite edges of the right-angled triangular tab are inclined with respect to the tab axis at different angles. Another important feature to be noted is that, near the sharp vertex tip, though the vortices shed would be of different size and opposite family, their closer proximity would make them interact intensely, leading to a loss of vorticity content. When the vertex is truncated, even at the tip, vortices of an opposite family would not interact among themselves. This might be an advantage because almost the entire vorticity content available with the mixing-promoting vortices would be used for mixing promotion.

Limiting tabs of triangular and circular (crosswire) cross-sectional geometry of a projected area of 5% of the nozzle exit area (that is a tab of 5% geometrical blockage), placed along the minor axis at the nozzle exit, were found to be efficient mixing promoters. The better mixing-promoting capability of the triangular tab compared to the crosswire may be because of the vertex of the triangle facing the flow, which might result in a reduced extent of pressure hill at the face. For a given tab geometry, the tab width can play a dominant role in modifying the mixing.

One of the serious shortcomings associated with the control of a jet with tabs is the momentum thrust loss caused by the blockage of the nozzle exit area by the tabs. Also, the detached shock envelope formed ahead of the tab will make the flow to deviate away from the nozzle centerline. Both the effects – the reduction of the nozzle exit area and the divergence of the jet – will lead to a loss of momentum thrust that the nozzle is capable of generating if the tabs are not at the nozzle exit. Therefore, it will be of great value, from both the propulsion and application points of view, if the aerodynamic mixing of the jet with the surrounding environment to which it is discharged is enhanced using a control, which will augment the jet mixing without any adverse effect (such as a decrease of jet velocity). This concept of jet control with the tab positioned slightly downstream of the nozzle exit is termed *shifted tabs*.

Mixing modification caused by limiting rectangular tab with and without corrugations located at the nozzle exit and at 0.5D, downstream of the nozzle exit, for subsonic and sonic jet was found to be inferior to a tab at the nozzle exit.

For the case of a Mach 2 jet, mixing promotion caused by a shifted tab was found to increase with an increase of adverse pressure gradient. In fact, the mixing enhancement caused by a tab placed at the nozzle exit decreases with an increase of the adverse pressure gradient.

The efficacy of passive control in the form of a ventilated triangular tab on the mixing characteristics of supersonic jets to apprehend the governing flow physics and to capture the flow structure, in the presence of different levels of expansion at the exit of a Mach 1.5 elliptic nozzle of AR 3, revealed that an important geometrical feature, which influenced the mixing modification caused by both ventilated and unventilated triangular tab, is its vertex angle.

Study of the effect of modifying the shape of tab edges, on the aerodynamic mixing characteristics of a circular Mach 2.0 jet, controlled with a rectangular tab, revealed that when placed at the same location from the nozzle exit a sharp-edged tab is a better mixing promoter than a square-edged tab, for a highly overexpanded jet. At a marginal level of a positive pressure gradient, the square-edged tab is found to be a far superior mixing promoter than the sharp-edged tab, in all the three zones of the jet. This mixing-promoting superiority of the square-edged tab increases with a decrease of the adverse pressure gradient and an increase of a favorable pressure gradient.

An important feature that dictates the size of the vortex shed from an object is the pressure hill at the front face. For the triangular tab, the pressure hill at its face varies in size from its base to its tip. Therefore, the environment required for mixing-promoting vortices of mixed size is built in for the triangular shape. The mixing promotion caused by triangular tabs along the minor axis would be better than that of rectangular tabs along the same orientation because of the mixed size of the mixing-promoting small-scale vortices shed by the triangular tab compared with the rectangular tab, which would shed small-scale vortices of uniform size only. The small-scale vortices of continuously varying size from base to vertex, introduced by the triangular tabs, along with the small-scale azimuthal vortices of a relatively larger size shed from the nozzle exit, would provide an environment of mixed-size vortices, which is favorable for promoting mixing of the mass entrained by the large-scale vortices at the jet boundary with the jet mass.

## Appendix A

**Table A.1** Isentropic flow of perfect gas ( $\gamma = 1.4$ ).

$M$	$p/p_0$	$T/T_0$	$\rho/\rho_0$	$A/A^*$	$a/a_0$	$M^*$	$\mu$	$\nu$
0.00	1.0000	1.0000	1.0000	$\infty$	1.0000	0.0000		
0.01	0.9999	1.0000	1.0000	57.874	1.0000	0.0110		
0.02	0.9997	0.9999	0.9998	28.942	1.0000	0.0219		
0.03	0.9994	0.9998	0.9996	19.301	0.9999	0.0329		
0.04	0.9989	0.9997	0.9992	14.481	0.9998	0.0438		
0.05	0.9983	0.9995	0.9988	11.591	0.9998	0.0548		
0.06	0.9975	0.9993	0.9982	9.666	0.9996	0.0657		
0.07	0.9966	0.9990	0.9976	8.292	0.9995	0.0766		
0.08	0.9955	0.9987	0.9968	7.262	0.9994	0.0876		
0.09	0.9944	0.9984	0.9960	6.461	0.9992	0.0985		
0.10	0.9930	0.9980	0.9950	5.822	0.9990	0.1094		
0.11	0.9916	0.9976	0.9940	5.299	0.9988	0.1204		
0.12	0.9900	0.9971	0.9928	4.864	0.9986	0.1313		
0.13	0.9883	0.9966	0.9916	4.497	0.9983	0.1422		
0.14	0.9864	0.9961	0.9903	4.182	0.9980	0.1531		
0.15	0.9844	0.9955	0.9888	3.910	0.9978	0.1639		
0.16	0.9823	0.9949	0.9873	3.673	0.9974	0.1748		
0.17	0.9800	0.9943	0.9857	3.464	0.9971	0.1857		
0.18	0.9776	0.9936	0.9840	3.278	0.9968	0.1965		
0.19	0.9751	0.9928	0.9822	3.112	0.9964	0.2074		
0.20	0.9725	0.9921	0.9803	2.964	0.9960	0.2182		
0.21	0.9697	0.9913	0.9783	2.829	0.9956	0.2290		
0.22	0.9668	0.9904	0.9762	2.708	0.9952	0.2398		
0.23	0.9638	0.9895	0.9740	2.597	0.9948	0.2506		
0.24	0.9607	0.9886	0.9718	2.496	0.9943	0.2614		
0.25	0.9575	0.9877	0.9694	2.403	0.9938	0.2722		
0.26	0.9541	0.9867	0.9670	2.317	0.9933	0.2829		
0.27	0.9506	0.9856	0.9645	2.238	0.9928	0.2936		
0.28	0.9470	0.9846	0.9619	2.166	0.9923	0.3043		

(continued)

Table A.1 (Continued)

$M$	$p/p_0$	$T/T_0$	$\rho/\rho_0$	$A/A^*$	$a/a_0$	$M^*$	$\mu$	$\nu$
0.29	0.9433	0.9835	0.9592	2.098	0.9917	0.3150		
0.30	0.9395	0.9823	0.9564	2.035	0.9911	0.3257		
0.31	0.9355	0.9811	0.9535	1.977	0.9905	0.3364		
0.32	0.9315	0.9799	0.9506	1.922	0.9899	0.3470		
0.33	0.9274	0.9787	0.9476	1.871	0.9893	0.3576		
0.34	0.9231	0.9774	0.9445	1.823	0.9886	0.3682		
0.35	0.9188	0.9761	0.9413	1.778	0.9880	0.3788		
0.36	0.9143	0.9747	0.9380	1.736	0.9873	0.3893		
0.37	0.9098	0.9733	0.9347	1.696	0.9866	0.3999		
0.38	0.9052	0.9719	0.9313	1.659	0.9859	0.4104		
0.39	0.9004	0.9705	0.9278	1.623	0.9851	0.4209		
0.40	0.8956	0.9690	0.9243	1.590	0.9844	0.4313		
0.41	0.8907	0.9675	0.9207	1.559	0.9836	0.4418		
0.42	0.8857	0.9659	0.9170	1.529	0.9828	0.4522		
0.43	0.8807	0.9643	0.9132	1.501	0.9820	0.4626		
0.44	0.8755	0.9627	0.9094	1.474	0.9812	0.4729		
0.45	0.8703	0.9611	0.9055	1.449	0.9803	0.4833		
0.46	0.8650	0.9594	0.9016	1.425	0.9795	0.4936		
0.47	0.8596	0.9577	0.8976	1.402	0.9786	0.5038		
0.48	0.8541	0.9559	0.8935	1.380	0.9777	0.5141		
0.49	0.8486	0.9542	0.8894	1.359	0.9768	0.5243		
0.50	0.8430	0.9524	0.8852	1.340	0.9759	0.5345		
0.51	0.8374	0.9506	0.8809	1.321	0.9750	0.5447		
0.52	0.8317	0.9487	0.8766	1.303	0.9740	0.5548		
0.53	0.8259	0.9468	0.8723	1.286	0.9730	0.5649		
0.54	0.8201	0.9449	0.8679	1.270	0.9721	0.5750		
0.55	0.8142	0.9430	0.8634	1.255	0.9711	0.5851		
0.56	0.8082	0.9410	0.8589	1.240	0.9700	0.5951		
0.57	0.8022	0.9390	0.8544	1.226	0.9690	0.6051		
0.58	0.7962	0.9370	0.8498	1.213	0.9680	0.6150		
0.59	0.7901	0.9349	0.8451	1.200	0.9669	0.6249		
0.60	0.7840	0.9328	0.8405	1.188	0.9658	0.6348		
0.61	0.7778	0.9307	0.8357	1.177	0.9647	0.6447		
0.62	0.7716	0.9286	0.8310	1.166	0.9636	0.6545		
0.63	0.7654	0.9265	0.8262	1.155	0.9625	0.6643		
0.64	0.7591	0.9243	0.8213	1.145	0.9614	0.6740		
0.65	0.7528	0.9221	0.8164	1.136	0.9603	0.6837		
0.66	0.7465	0.9199	0.8115	1.127	0.9591	0.6934		
0.67	0.7401	0.9176	0.8066	1.118	0.9579	0.7031		
0.68	0.7338	0.9153	0.8016	1.110	0.9567	0.7127		

(continued)

Table A.1 (Continued)

$M$	$p/p_0$	$T/T_0$	$\rho/\rho_0$	$A/A^*$	$a/a_0$	$M^*$	$\mu$	$\nu$
0.69	0.7274	0.9131	0.7966	1.102	0.9555	0.7223		
0.70	0.7209	0.9107	0.7916	1.094	0.9543	0.7318		
0.71	0.7145	0.9084	0.7865	1.087	0.9531	0.7413		
0.72	0.7080	0.9061	0.7814	1.081	0.9519	0.7508		
0.73	0.7016	0.9037	0.7763	1.074	0.9506	0.7602		
0.74	0.6951	0.9013	0.7712	1.068	0.9494	0.7696		
0.75	0.6886	0.8989	0.7660	1.062	0.9481	0.7789		
0.76	0.6821	0.8964	0.7609	1.057	0.9468	0.7883		
0.77	0.6756	0.8940	0.7557	1.052	0.9455	0.7975		
0.78	0.6691	0.8915	0.7505	1.047	0.9442	0.8068		
0.79	0.6625	0.8890	0.7452	1.043	0.9429	0.8160		
0.80	0.6560	0.8865	0.7400	1.038	0.9416	0.8251		
0.81	0.6495	0.8840	0.7347	1.034	0.9402	0.8343		
0.82	0.6430	0.8815	0.7295	1.030	0.9389	0.8433		
0.83	0.6365	0.8789	0.7242	1.027	0.9375	0.8524		
0.84	0.6300	0.8763	0.7189	1.024	0.9361	0.8614		
0.85	0.6235	0.8737	0.7136	1.021	0.9347	0.8704		
0.86	0.6170	0.8711	0.7083	1.018	0.9333	0.8793		
0.87	0.6106	0.8685	0.7030	1.015	0.9319	0.8882		
0.88	0.6041	0.8659	0.6977	1.013	0.9305	0.8970		
0.89	0.5977	0.8632	0.6924	1.011	0.9291	0.9058		
0.90	0.5913	0.8606	0.6870	1.009	0.9277	0.9146		
0.91	0.5849	0.8579	0.6817	1.007	0.9262	0.9233		
0.92	0.5785	0.8552	0.6764	1.006	0.9248	0.9320		
0.93	0.5721	0.8525	0.6711	1.004	0.9233	0.9407		
0.94	0.5658	0.8498	0.6658	1.003	0.9219	0.9493		
0.95	0.5595	0.8471	0.6604	1.002	0.9204	0.9578		
0.96	0.5532	0.8444	0.6551	1.001	0.9189	0.9663		
0.97	0.5469	0.8416	0.6498	1.001	0.9174	0.9748		
0.98	0.5407	0.8389	0.6445	1.000	0.9159	0.9833		
0.99	0.5345	0.8361	0.6392	1.000	0.9144	0.9916		
1.00	0.5283	0.8333	0.6339	1.000	0.9129	1.0000	90.000	0.000
1.01	0.5221	0.8306	0.6287	1.000	0.9113	1.0083	81.931	0.045
1.02	0.5160	0.8278	0.6234	1.000	0.9098	1.0166	78.635	0.126
1.03	0.5099	0.8250	0.6181	1.001	0.9083	1.0248	76.138	0.229
1.04	0.5039	0.8222	0.6129	1.001	0.9067	1.0330	74.058	0.351
1.05	0.4979	0.8193	0.6077	1.002	0.9052	1.0411	72.247	0.487
1.06	0.4919	0.8165	0.6024	1.003	0.9036	1.0492	70.630	0.637
1.07	0.4860	0.8137	0.5972	1.004	0.9020	1.0573	69.160	0.797
1.08	0.4800	0.8108	0.5920	1.005	0.9005	1.0653	67.808	0.968

(continued)

**Table A.1** (Continued)

$M$	$p/p_0$	$T/T_0$	$\rho/\rho_0$	$A/A^*$	$a/a_0$	$M^*$	$\mu$	$\nu$
1.09	0.4742	0.8080	0.5869	1.006	0.8989	1.0733	66.553	1.148
1.10	0.4684	0.8052	0.5817	1.008	0.8973	1.0812	65.380	1.336
1.11	0.4626	0.8023	0.5766	1.010	0.8957	1.0891	64.277	1.532
1.12	0.4568	0.7994	0.5714	1.011	0.8941	1.0970	63.234	1.735
1.13	0.4511	0.7966	0.5663	1.013	0.8925	1.1048	62.246	1.944
1.14	0.4455	0.7937	0.5612	1.015	0.8909	1.1126	61.306	2.160
1.15	0.4398	0.7908	0.5562	1.017	0.8893	1.1203	60.408	2.381
1.16	0.4343	0.7879	0.5511	1.020	0.8877	1.1280	59.550	2.607
1.17	0.4287	0.7851	0.5461	1.022	0.8860	1.1356	58.727	2.839
1.18	0.4232	0.7822	0.5411	1.025	0.8844	1.1432	57.936	3.074
1.19	0.4178	0.7793	0.5361	1.028	0.8828	1.1508	57.176	3.314
1.20	0.4124	0.7764	0.5311	1.030	0.8811	1.1583	56.443	3.558
1.21	0.4070	0.7735	0.5262	1.033	0.8795	1.1658	55.735	3.806
1.22	0.4017	0.7706	0.5213	1.037	0.8778	1.1732	55.052	4.057
1.23	0.3964	0.7677	0.5164	1.040	0.8762	1.1806	54.391	4.312
1.24	0.3912	0.7648	0.5115	1.043	0.8745	1.1879	53.751	4.569
1.25	0.3861	0.7619	0.5067	1.047	0.8729	1.1952	53.130	4.830
1.26	0.3809	0.7590	0.5019	1.050	0.8712	1.2025	52.528	5.093
1.27	0.3759	0.7561	0.4971	1.054	0.8695	1.2097	51.943	5.359
1.28	0.3708	0.7532	0.4923	1.058	0.8679	1.2169	51.375	5.627
1.29	0.3658	0.7503	0.4876	1.062	0.8662	1.2240	50.823	5.898
1.30	0.3609	0.7474	0.4829	1.066	0.8645	1.2311	50.285	6.170
1.31	0.3560	0.7445	0.4782	1.071	0.8628	1.2382	49.761	6.445
1.32	0.3512	0.7416	0.4736	1.075	0.8611	1.2452	49.251	6.721
1.33	0.3464	0.7387	0.4690	1.080	0.8595	1.2522	48.753	7.000
1.34	0.3417	0.7358	0.4644	1.084	0.8578	1.2591	48.268	7.279
1.35	0.3370	0.7329	0.4598	1.089	0.8561	1.2660	47.795	7.561
1.36	0.3323	0.7300	0.4553	1.094	0.8544	1.2729	47.332	7.844
1.37	0.3277	0.7271	0.4508	1.099	0.8527	1.2797	46.880	8.128
1.38	0.3232	0.7242	0.4463	1.104	0.8510	1.2864	46.439	8.413
1.39	0.3187	0.7213	0.4418	1.109	0.8493	1.2932	46.007	8.699
1.40	0.3142	0.7184	0.4374	1.115	0.8476	1.2999	45.585	8.987
1.41	0.3098	0.7155	0.4330	1.120	0.8459	1.3065	45.171	9.276
1.42	0.3055	0.7126	0.4287	1.126	0.8442	1.3131	44.767	9.565
1.43	0.3012	0.7097	0.4244	1.132	0.8425	1.3197	44.371	9.855
1.44	0.2969	0.7069	0.4201	1.138	0.8407	1.3262	43.983	10.146
1.45	0.2927	0.7040	0.4158	1.144	0.8390	1.3327	43.603	10.438
1.46	0.2886	0.7011	0.4116	1.150	0.8373	1.3392	43.230	10.731
1.47	0.2845	0.6982	0.4074	1.156	0.8356	1.3456	42.865	11.023
1.48	0.2804	0.6954	0.4032	1.163	0.8339	1.3520	42.507	11.317
1.49	0.2764	0.6925	0.3991	1.169	0.8322	1.3583	42.155	11.611

(continued)

Table A.1 (Continued)

$M$	$p/p_0$	$T/T_0$	$\rho/\rho_0$	$A/A^*$	$a/a_0$	$M^*$	$\mu$	$\nu$
1.50	0.2724	0.6897	0.3950	1.176	0.8305	1.3646	41.810	11.905
1.51	0.2685	0.6868	0.3909	1.183	0.8287	1.3708	41.472	12.200
1.52	0.2646	0.6840	0.3869	1.190	0.8270	1.3770	41.140	12.495
1.53	0.2608	0.6811	0.3829	1.197	0.8253	1.3832	40.813	12.790
1.54	0.2570	0.6783	0.3789	1.204	0.8236	1.3894	40.493	13.086
1.55	0.2533	0.6754	0.3750	1.212	0.8219	1.3955	40.178	13.381
1.56	0.2496	0.6726	0.3710	1.219	0.8201	1.4015	39.868	13.677
1.57	0.2459	0.6698	0.3672	1.227	0.8184	1.4075	39.564	13.973
1.58	0.2423	0.6670	0.3633	1.234	0.8167	1.4135	39.265	14.269
1.59	0.2388	0.6642	0.3595	1.242	0.8150	1.4195	38.971	14.565
1.60	0.2353	0.6614	0.3557	1.250	0.8133	1.4254	38.682	14.860
1.61	0.2318	0.6586	0.3520	1.258	0.8115	1.4313	38.398	15.156
1.62	0.2284	0.6558	0.3483	1.267	0.8098	1.4371	38.118	15.452
1.63	0.2250	0.6530	0.3446	1.275	0.8081	1.4429	37.843	15.747
1.64	0.2217	0.6502	0.3409	1.284	0.8064	1.4487	37.572	16.043
1.65	0.2184	0.6475	0.3373	1.292	0.8046	1.4544	37.305	16.338
1.66	0.2151	0.6447	0.3337	1.301	0.8029	1.4601	37.043	16.633
1.67	0.2119	0.6419	0.3302	1.310	0.8012	1.4657	36.784	16.928
1.68	0.2088	0.6392	0.3266	1.319	0.7995	1.4713	36.530	17.222
1.69	0.2057	0.6364	0.3232	1.328	0.7978	1.4769	36.279	17.516
1.70	0.2026	0.6337	0.3197	1.338	0.7961	1.4825	36.032	17.810
1.71	0.1996	0.6310	0.3163	1.347	0.7943	1.4880	35.789	18.103
1.72	0.1966	0.6283	0.3129	1.357	0.7926	1.4935	35.549	18.396
1.73	0.1936	0.6256	0.3095	1.367	0.7909	1.4989	35.312	18.689
1.74	0.1907	0.6229	0.3062	1.376	0.7892	1.5043	35.080	18.981
1.75	0.1878	0.6202	0.3029	1.386	0.7875	1.5097	34.850	19.273
1.76	0.1850	0.6175	0.2996	1.397	0.7858	1.5150	34.624	19.565
1.77	0.1822	0.6148	0.2964	1.407	0.7841	1.5203	34.400	19.855
1.78	0.1794	0.6121	0.2931	1.418	0.7824	1.5256	34.180	20.146
1.79	0.1767	0.6095	0.2900	1.428	0.7807	1.5308	33.963	20.436
1.80	0.1740	0.6068	0.2868	1.439	0.7790	1.5360	33.749	20.725
1.81	0.1714	0.6041	0.2837	1.450	0.7773	1.5411	33.538	21.014
1.82	0.1688	0.6015	0.2806	1.461	0.7756	1.5463	33.329	21.302
1.83	0.1662	0.5989	0.2776	1.472	0.7739	1.5514	33.124	21.590
1.84	0.1637	0.5963	0.2745	1.484	0.7722	1.5564	32.921	21.877
1.85	0.1612	0.5936	0.2715	1.495	0.7705	1.5614	32.720	22.163
1.86	0.1587	0.5910	0.2686	1.507	0.7688	1.5664	32.523	22.449
1.87	0.1563	0.5884	0.2656	1.519	0.7671	1.5714	32.328	22.734
1.88	0.1539	0.5859	0.2627	1.531	0.7654	1.5763	32.135	23.019
1.89	0.1516	0.5833	0.2598	1.543	0.7637	1.5812	31.945	23.303
1.90	0.1492	0.5807	0.2570	1.555	0.7620	1.5861	31.757	23.586

(continued)

**Table A.1** (Continued)

$M$	$p/p_0$	$T/T_0$	$\rho/\rho_0$	$A/A^*$	$a/a_0$	$M^*$	$\mu$	$\nu$
1.91	0.1470	0.5782	0.2542	1.568	0.7604	1.5909	31.571	23.869
1.92	0.1447	0.5756	0.2514	1.580	0.7587	1.5957	31.388	24.151
1.93	0.1425	0.5731	0.2486	1.593	0.7570	1.6005	31.207	24.432
1.94	0.1403	0.5705	0.2459	1.606	0.7553	1.6052	31.028	24.712
1.95	0.1381	0.5680	0.2432	1.619	0.7537	1.6099	30.852	24.992
1.96	0.1360	0.5655	0.2405	1.633	0.7520	1.6146	30.677	25.271
1.97	0.1339	0.5630	0.2378	1.646	0.7503	1.6192	30.505	25.549
1.98	0.1318	0.5605	0.2352	1.660	0.7487	1.6239	30.335	25.827
1.99	0.1298	0.5580	0.2326	1.674	0.7470	1.6284	30.166	26.104
2.00	0.1278	0.5556	0.2300	1.688	0.7454	1.6330	30.000	26.380
2.01	0.1258	0.5531	0.2275	1.702	0.7437	1.6375	29.836	26.655
2.02	0.1239	0.5506	0.2250	1.716	0.7420	1.6420	29.673	26.930
2.03	0.1220	0.5482	0.2225	1.730	0.7404	1.6465	29.512	27.203
2.04	0.1201	0.5458	0.2200	1.745	0.7388	1.6509	29.353	27.476
2.05	0.1182	0.5433	0.2176	1.760	0.7371	1.6553	29.196	27.748
2.06	0.1164	0.5409	0.2152	1.775	0.7355	1.6597	29.041	28.020
2.07	0.1146	0.5385	0.2128	1.790	0.7338	1.6640	28.888	28.290
2.08	0.1128	0.5361	0.2104	1.806	0.7322	1.6683	28.736	28.560
2.09	0.1111	0.5337	0.2081	1.821	0.7306	1.6726	28.585	28.829
2.10	0.1094	0.5313	0.2058	1.837	0.7289	1.6769	28.437	29.097
2.11	0.1077	0.5290	0.2035	1.853	0.7273	1.6811	28.290	29.364
2.12	0.1060	0.5266	0.2013	1.869	0.7257	1.6853	28.145	29.630
2.13	0.1043	0.5243	0.1990	1.885	0.7241	1.6895	28.001	29.896
2.14	0.1027	0.5219	0.1968	1.902	0.7225	1.6936	27.859	30.161
2.15	0.1011	0.5196	0.1946	1.919	0.7208	1.6977	27.718	30.425
2.16	0.0996	0.5173	0.1925	1.935	0.7192	1.7018	27.578	30.688
2.17	0.0980	0.5150	0.1903	1.953	0.7176	1.7059	27.441	30.951
2.18	0.0965	0.5127	0.1882	1.970	0.7160	1.7099	27.304	31.212
2.19	0.0950	0.5104	0.1861	1.987	0.7144	1.7139	27.169	31.473
2.20	0.0935	0.5081	0.1841	2.005	0.7128	1.7179	27.036	31.732
2.21	0.0921	0.5059	0.1820	2.023	0.7112	1.7219	26.903	31.991
2.22	0.0906	0.5036	0.1800	2.041	0.7097	1.7258	26.773	32.249
2.23	0.0892	0.5014	0.1780	2.059	0.7081	1.7297	26.643	32.507
2.24	0.0878	0.4991	0.1760	2.078	0.7065	1.7336	26.515	32.763
2.25	0.0865	0.4969	0.1740	2.096	0.7049	1.7374	26.388	33.018
2.26	0.0851	0.4947	0.1721	2.115	0.7033	1.7412	26.262	33.273
2.27	0.0838	0.4925	0.1702	2.134	0.7018	1.7450	26.138	33.527
2.28	0.0825	0.4903	0.1683	2.154	0.7002	1.7488	26.014	33.780
2.29	0.0812	0.4881	0.1664	2.173	0.6986	1.7526	25.892	34.032
2.30	0.0800	0.4859	0.1646	2.193	0.6971	1.7563	25.771	34.283
2.31	0.0787	0.4837	0.1628	2.213	0.6955	1.7600	25.652	34.533

(continued)



Table A.1 (Continued)

$M$	$p/p_0$	$T/T_0$	$\rho/\rho_0$	$A/A^*$	$a/a_0$	$M^*$	$\mu$	$\nu$
2.32	0.0775	0.4816	0.1609	2.233	0.6940	1.7637	25.533	34.782
2.33	0.0763	0.4794	0.1592	2.254	0.6924	1.7673	25.416	35.031
2.34	0.0751	0.4773	0.1574	2.274	0.6909	1.7709	25.300	35.279
2.35	0.0740	0.4752	0.1556	2.295	0.6893	1.7745	25.184	35.526
2.36	0.0728	0.4731	0.1539	2.316	0.6878	1.7781	25.070	35.771
2.37	0.0717	0.4709	0.1522	2.338	0.6863	1.7817	24.957	36.017
2.38	0.0706	0.4688	0.1505	2.359	0.6847	1.7852	24.845	36.261
2.39	0.0695	0.4668	0.1488	2.381	0.6832	1.7887	24.734	36.504
2.40	0.0684	0.4647	0.1472	2.403	0.6817	1.7922	24.624	36.747
2.41	0.0673	0.4626	0.1456	2.425	0.6802	1.7956	24.515	36.988
2.42	0.0663	0.4606	0.1439	2.448	0.6786	1.7991	24.407	37.229
2.43	0.0653	0.4585	0.1424	2.471	0.6771	1.8025	24.300	37.469
2.44	0.0643	0.4565	0.1408	2.494	0.6756	1.8059	24.195	37.708
2.45	0.0633	0.4544	0.1392	2.517	0.6741	1.8092	24.090	37.946
2.46	0.0623	0.4524	0.1377	2.540	0.6726	1.8126	23.985	38.183
2.47	0.0613	0.4504	0.1362	2.564	0.6711	1.8159	23.882	38.420
2.48	0.0604	0.4484	0.1346	2.588	0.6696	1.8192	23.780	38.655
2.49	0.0594	0.4464	0.1332	2.612	0.6682	1.8225	23.679	38.890
2.50	0.0585	0.4444	0.1317	2.637	0.6667	1.8257	23.578	39.124
2.51	0.0576	0.4425	0.1302	2.661	0.6652	1.8290	23.479	39.357
2.52	0.0567	0.4405	0.1288	2.686	0.6637	1.8322	23.380	39.589
2.53	0.0559	0.4386	0.1274	2.712	0.6622	1.8354	23.282	39.820
2.54	0.0550	0.4366	0.1260	2.737	0.6608	1.8386	23.185	40.050
2.55	0.0542	0.4347	0.1246	2.763	0.6593	1.8417	23.089	40.280
2.56	0.0533	0.4328	0.1232	2.789	0.6578	1.8448	22.993	40.508
2.57	0.0525	0.4309	0.1218	2.815	0.6564	1.8479	22.899	40.736
2.58	0.0517	0.4289	0.1205	2.842	0.6549	1.8510	22.805	40.963
2.59	0.0509	0.4271	0.1192	2.869	0.6535	1.8541	22.712	41.189
2.60	0.0501	0.4252	0.1179	2.896	0.6521	1.8571	22.620	41.415
2.61	0.0493	0.4233	0.1166	2.923	0.6506	1.8602	22.528	41.639
2.62	0.0486	0.4214	0.1153	2.951	0.6492	1.8632	22.438	41.863
2.63	0.0478	0.4196	0.1140	2.979	0.6477	1.8662	22.348	42.086
2.64	0.0471	0.4177	0.1128	3.007	0.6463	1.8691	22.259	42.307
2.65	0.0464	0.4159	0.1115	3.036	0.6449	1.8721	22.170	42.529
2.66	0.0457	0.4141	0.1103	3.065	0.6435	1.8750	22.082	42.749
2.67	0.0450	0.4122	0.1091	3.094	0.6421	1.8779	21.995	42.968
2.68	0.0443	0.4104	0.1079	3.123	0.6406	1.8808	21.909	43.187
2.69	0.0436	0.4086	0.1067	3.153	0.6392	1.8837	21.823	43.405
2.70	0.0430	0.4068	0.1056	3.183	0.6378	1.8865	21.738	43.621
2.71	0.0423	0.4051	0.1044	3.213	0.6364	1.8894	21.654	43.838
2.72	0.0417	0.4033	0.1033	3.244	0.6350	1.8922	21.571	44.053

(continued)

**Table A.1** (Continued)

$M$	$p/p_0$	$T/T_0$	$\rho/\rho_0$	$A/A^*$	$a/a_0$	$M^*$	$\mu$	$\nu$
2.73	0.0410	0.4015	0.1022	3.275	0.6337	1.8950	21.488	44.267
2.74	0.0404	0.3998	0.1010	3.306	0.6323	1.8978	21.405	44.481
2.75	0.0398	0.3980	0.0999	3.338	0.6309	1.9005	21.324	44.694
2.76	0.0392	0.3963	0.0989	3.370	0.6295	1.9033	21.243	44.906
2.77	0.0386	0.3945	0.0978	3.402	0.6281	1.9060	21.162	45.117
2.78	0.0380	0.3928	0.0967	3.434	0.6268	1.9087	21.083	45.327
2.79	0.0374	0.3911	0.0957	3.467	0.6254	1.9114	21.003	45.537
2.80	0.0368	0.3894	0.0946	3.500	0.6240	1.9140	20.925	45.746
2.81	0.0363	0.3877	0.0936	3.534	0.6227	1.9167	20.847	45.954
2.82	0.0357	0.3860	0.0926	3.567	0.6213	1.9193	20.770	46.161
2.83	0.0352	0.3844	0.0916	3.601	0.6200	1.9219	20.693	46.368
2.84	0.0347	0.3827	0.0906	3.636	0.6186	1.9246	20.617	46.573
2.85	0.0341	0.3810	0.0896	3.671	0.6173	1.9271	20.541	46.778
2.86	0.0336	0.3794	0.0886	3.706	0.6159	1.9297	20.466	46.982
2.87	0.0331	0.3777	0.0877	3.741	0.6146	1.9323	20.391	47.185
2.88	0.0326	0.3761	0.0867	3.777	0.6133	1.9348	20.318	47.388
2.89	0.0321	0.3745	0.0858	3.813	0.6119	1.9373	20.244	47.589
2.90	0.0317	0.3729	0.0849	3.850	0.6106	1.9398	20.171	47.790
2.91	0.0312	0.3712	0.0840	3.887	0.6093	1.9423	20.099	47.990
2.92	0.0307	0.3696	0.0831	3.924	0.6080	1.9448	20.027	48.190
2.93	0.0302	0.3681	0.0822	3.961	0.6067	1.9472	19.956	48.388
2.94	0.0298	0.3665	0.0813	3.999	0.6054	1.9497	19.885	48.586
2.95	0.0293	0.3649	0.0804	4.038	0.6041	1.9521	19.815	48.783
2.96	0.0289	0.3633	0.0796	4.076	0.6028	1.9545	19.745	48.980
2.97	0.0285	0.3618	0.0787	4.115	0.6015	1.9569	19.676	49.175
2.98	0.0281	0.3602	0.0779	4.155	0.6002	1.9593	19.607	49.370
2.99	0.0276	0.3587	0.0770	4.194	0.5989	1.9616	19.539	49.564
3.00	0.0272	0.3571	0.0762	4.235	0.5976	1.9640	19.471	49.757
3.01	0.0268	0.3556	0.0754	4.275	0.5963	1.9663	19.404	49.950
3.02	0.0264	0.3541	0.0746	4.316	0.5951	1.9686	19.337	50.142
3.03	0.0260	0.3526	0.0738	4.357	0.5938	1.9709	19.271	50.333
3.04	0.0256	0.3511	0.0730	4.399	0.5925	1.9732	19.205	50.523
3.05	0.0253	0.3496	0.0723	4.441	0.5913	1.9755	19.139	50.713
3.06	0.0249	0.3481	0.0715	4.483	0.5900	1.9777	19.074	50.902
3.07	0.0245	0.3466	0.0707	4.526	0.5887	1.9800	19.010	51.090
3.08	0.0242	0.3452	0.0700	4.570	0.5875	1.9822	18.946	51.277
3.09	0.0238	0.3437	0.0692	4.613	0.5862	1.9844	18.882	51.464
3.10	0.0234	0.3422	0.0685	4.657	0.5850	1.9866	18.819	51.650
3.11	0.0231	0.3408	0.0678	4.702	0.5838	1.9888	18.756	51.835
3.12	0.0228	0.3393	0.0671	4.747	0.5825	1.9910	18.694	52.020
3.13	0.0224	0.3379	0.0664	4.792	0.5813	1.9931	18.632	52.203

(continued)

Table A.1 (Continued)

$M$	$p/p_0$	$T/T_0$	$\rho/\rho_0$	$A/A^*$	$a/a_0$	$M^*$	$\mu$	$\nu$
3.14	0.0221	0.3365	0.0657	4.838	0.5801	1.9953	18.571	52.386
3.15	0.0218	0.3351	0.0650	4.884	0.5788	1.9974	18.509	52.569
3.16	0.0215	0.3337	0.0643	4.930	0.5776	1.9995	18.449	52.751
3.17	0.0211	0.3323	0.0636	4.977	0.5764	2.0016	18.388	52.932
3.18	0.0208	0.3309	0.0630	5.025	0.5752	2.0037	18.329	53.112
3.19	0.0205	0.3295	0.0623	5.073	0.5740	2.0058	18.269	53.291
3.20	0.0202	0.3281	0.0617	5.121	0.5728	2.0079	18.210	53.470
3.21	0.0199	0.3267	0.0610	5.170	0.5716	2.0099	18.151	53.649
3.22	0.0196	0.3253	0.0604	5.219	0.5704	2.0119	18.093	53.826
3.23	0.0194	0.3240	0.0597	5.268	0.5692	2.0140	18.035	54.003
3.24	0.0191	0.3226	0.0591	5.319	0.5680	2.0160	17.977	54.179
3.25	0.0188	0.3213	0.0585	5.369	0.5668	2.0180	17.920	54.355
3.26	0.0185	0.3199	0.0579	5.420	0.5656	2.0200	17.863	54.529
3.27	0.0183	0.3186	0.0573	5.472	0.5645	2.0220	17.807	54.704
3.28	0.0180	0.3173	0.0567	5.523	0.5633	2.0239	17.751	54.877
3.29	0.0177	0.3160	0.0561	5.576	0.5621	2.0259	17.695	55.050
3.30	0.0175	0.3147	0.0555	5.629	0.5609	2.0278	17.640	55.222
3.31	0.0172	0.3134	0.0550	5.682	0.5598	2.0297	17.585	55.393
3.32	0.0170	0.3121	0.0544	5.736	0.5586	2.0317	17.530	55.564
3.33	0.0167	0.3108	0.0538	5.790	0.5575	2.0336	17.476	55.734
3.34	0.0165	0.3095	0.0533	5.845	0.5563	2.0355	17.422	55.904
3.35	0.0163	0.3082	0.0527	5.900	0.5552	2.0373	17.368	56.073
3.36	0.0160	0.3069	0.0522	5.956	0.5540	2.0392	17.315	56.241
3.37	0.0158	0.3057	0.0517	6.012	0.5529	2.0411	17.262	56.409
3.38	0.0156	0.3044	0.0511	6.069	0.5517	2.0429	17.209	56.576
3.39	0.0153	0.3032	0.0506	6.126	0.5506	2.0447	17.157	56.742
3.40	0.0151	0.3019	0.0501	6.184	0.5495	2.0466	17.105	56.908
3.41	0.0149	0.3007	0.0496	6.242	0.5484	2.0484	17.053	57.073
3.42	0.0147	0.2995	0.0491	6.301	0.5472	2.0502	17.002	57.237
3.43	0.0145	0.2982	0.0486	6.360	0.5461	2.0520	16.950	57.401
3.44	0.0143	0.2970	0.0481	6.420	0.5450	2.0537	16.900	57.564
3.45	0.0141	0.2958	0.0476	6.480	0.5439	2.0555	16.849	57.726
3.46	0.0139	0.2946	0.0471	6.541	0.5428	2.0573	16.799	57.888
3.47	0.0137	0.2934	0.0466	6.602	0.5417	2.0590	16.749	58.050
3.48	0.0135	0.2922	0.0462	6.664	0.5406	2.0607	16.700	58.210
3.49	0.0133	0.2910	0.0457	6.727	0.5395	2.0625	16.651	58.370
3.50	0.0131	0.2899	0.0452	6.790	0.5384	2.0642	16.602	58.530
3.51	0.0129	0.2887	0.0448	6.853	0.5373	2.0659	16.553	58.689
3.52	0.0127	0.2875	0.0443	6.917	0.5362	2.0676	16.505	58.847
3.53	0.0126	0.2864	0.0439	6.982	0.5351	2.0693	16.456	59.005
3.54	0.0124	0.2852	0.0434	7.047	0.5340	2.0709	16.409	59.162

(continued)

**Table A.1** (Continued)

$M$	$p/p_0$	$T/T_0$	$\rho/\rho_0$	$A/A^*$	$a/a_0$	$M^*$	$\mu$	$\nu$
3.55	0.0122	0.2841	0.0430	7.113	0.5330	2.0726	16.361	59.318
3.56	0.0120	0.2829	0.0426	7.179	0.5319	2.0743	16.314	59.474
3.57	0.0119	0.2818	0.0421	7.246	0.5308	2.0759	16.267	59.629
3.58	0.0117	0.2806	0.0417	7.313	0.5298	2.0775	16.220	59.784
3.59	0.0115	0.2795	0.0413	7.381	0.5287	2.0792	16.174	59.938
3.60	0.0114	0.2784	0.0409	7.450	0.5276	2.0808	16.128	60.091
3.61	0.0112	0.2773	0.0405	7.519	0.5266	2.0824	16.082	60.244
3.62	0.0111	0.2762	0.0401	7.589	0.5255	2.0840	16.036	60.397
3.63	0.0109	0.2751	0.0397	7.659	0.5245	2.0856	15.991	60.549
3.64	0.0108	0.2740	0.0393	7.730	0.5234	2.0871	15.946	60.700
3.65	0.0106	0.2729	0.0389	7.802	0.5224	2.0887	15.901	60.850
3.66	0.0105	0.2718	0.0385	7.874	0.5213	2.0903	15.856	61.001
3.67	0.0103	0.2707	0.0381	7.947	0.5203	2.0918	15.812	61.150
3.68	0.0102	0.2697	0.0378	8.020	0.5193	2.0933	15.768	61.299
3.69	0.0100	0.2686	0.0374	8.094	0.5183	2.0949	15.724	61.447
3.70	0.0099	0.2675	0.0370	8.169	0.5172	2.0964	15.680	61.595
3.71	0.0098	0.2665	0.0367	8.244	0.5162	2.0979	15.637	61.743
3.72	0.0096	0.2654	0.0363	8.320	0.5152	2.0994	15.594	61.889
3.73	0.0095	0.2644	0.0359	8.397	0.5142	2.1009	15.551	62.036
3.74	0.0094	0.2633	0.0356	8.474	0.5132	2.1024	15.508	62.181
3.75	0.0092	0.2623	0.0352	8.552	0.5121	2.1039	15.466	62.326
3.76	0.0091	0.2613	0.0349	8.630	0.5111	2.1053	15.424	62.471
3.77	0.0090	0.2602	0.0345	8.709	0.5101	2.1068	15.382	62.615
3.78	0.0089	0.2592	0.0342	8.789	0.5091	2.1082	15.340	62.758
3.79	0.0087	0.2582	0.0339	8.869	0.5081	2.1097	15.299	62.901
3.80	0.0086	0.2572	0.0335	8.951	0.5072	2.1111	15.258	63.044
3.81	0.0085	0.2562	0.0332	9.032	0.5062	2.1125	15.217	63.186
3.82	0.0084	0.2552	0.0329	9.115	0.5052	2.1140	15.176	63.327
3.83	0.0083	0.2542	0.0326	9.198	0.5042	2.1154	15.135	63.468
3.84	0.0082	0.2532	0.0323	9.282	0.5032	2.1168	15.095	63.608
3.85	0.0081	0.2522	0.0320	9.366	0.5022	2.1182	15.055	63.748
3.86	0.0080	0.2513	0.0316	9.451	0.5013	2.1195	15.015	63.887
3.87	0.0078	0.2503	0.0313	9.537	0.5003	2.1209	14.975	64.026
3.88	0.0077	0.2493	0.0310	9.624	0.4993	2.1223	14.936	64.164
3.89	0.0076	0.2484	0.0307	9.711	0.4984	2.1236	14.896	64.302
3.90	0.0075	0.2474	0.0304	9.799	0.4974	2.1250	14.857	64.440
3.91	0.0074	0.2464	0.0302	9.888	0.4964	2.1263	14.818	64.576
3.92	0.0073	0.2455	0.0299	9.977	0.4955	2.1277	14.780	64.713
3.93	0.0072	0.2446	0.0296	10.067	0.4945	2.1290	14.741	64.848
3.94	0.0071	0.2436	0.0293	10.158	0.4936	2.1303	14.703	64.984
3.95	0.0070	0.2427	0.0290	10.250	0.4926	2.1316	14.665	65.118

(continued)

Table A.1 (Continued)

$M$	$p/p_0$	$T/T_0$	$\rho/\rho_0$	$A/A^*$	$a/a_0$	$M^*$	$\mu$	$\nu$
3.96	0.0069	0.2418	0.0287	10.342	0.4917	2.1329	14.627	65.253
3.97	0.0069	0.2408	0.0285	10.435	0.4908	2.1342	14.589	65.386
3.98	0.0068	0.2399	0.0282	10.529	0.4898	2.1355	14.552	65.520
3.99	0.0067	0.2390	0.0279	10.623	0.4889	2.1368	14.515	65.652
4.00	0.0066	0.2381	0.0277	10.719	0.4880	2.1381	14.478	65.785
4.01	0.0065	0.2372	0.0274	10.815	0.4870	2.1394	14.441	65.917
4.02	0.0064	0.2363	0.0271	10.912	0.4861	2.1406	14.404	66.048
4.03	0.0063	0.2354	0.0269	11.009	0.4852	2.1419	14.367	66.179
4.04	0.0062	0.2345	0.0266	11.108	0.4843	2.1431	14.331	66.309
4.05	0.0062	0.2336	0.0264	11.207	0.4833	2.1444	14.295	66.439
4.06	0.0061	0.2327	0.0261	11.307	0.4824	2.1456	14.259	66.569
4.07	0.0060	0.2319	0.0259	11.408	0.4815	2.1468	14.223	66.698
4.08	0.0059	0.2310	0.0256	11.509	0.4806	2.1480	14.188	66.826
4.09	0.0058	0.2301	0.0254	11.611	0.4797	2.1493	14.152	66.954
4.10	0.0058	0.2293	0.0252	11.715	0.4788	2.1505	14.117	67.082
4.11	0.0057	0.2284	0.0249	11.819	0.4779	2.1517	14.082	67.209
4.12	0.0056	0.2275	0.0247	11.923	0.4770	2.1529	14.047	67.336
4.13	0.0055	0.2267	0.0245	12.029	0.4761	2.1540	14.012	67.462
4.14	0.0055	0.2258	0.0242	12.135	0.4752	2.1552	13.978	67.588
4.15	0.0054	0.2250	0.0240	12.243	0.4743	2.1564	13.943	67.713
4.16	0.0053	0.2242	0.0238	12.351	0.4735	2.1576	13.909	67.838
4.17	0.0053	0.2233	0.0236	12.460	0.4726	2.1587	13.875	67.963
4.18	0.0052	0.2225	0.0234	12.570	0.4717	2.1599	13.841	68.087
4.19	0.0051	0.2217	0.0231	12.680	0.4708	2.1610	13.808	68.210
4.20	0.0051	0.2208	0.0229	12.792	0.4699	2.1622	13.774	68.333
4.21	0.0050	0.2200	0.0227	12.904	0.4691	2.1633	13.741	68.456
4.22	0.0049	0.2192	0.0225	13.017	0.4682	2.1644	13.708	68.578
4.23	0.0049	0.2184	0.0223	13.131	0.4673	2.1655	13.675	68.700
4.24	0.0048	0.2176	0.0221	13.246	0.4665	2.1667	13.642	68.821
4.25	0.0047	0.2168	0.0219	13.362	0.4656	2.1678	13.609	68.942
4.26	0.0047	0.2160	0.0217	13.479	0.4648	2.1689	13.576	69.063
4.27	0.0046	0.2152	0.0215	13.597	0.4639	2.1700	13.544	69.183
4.28	0.0046	0.2144	0.0213	13.715	0.4631	2.1711	13.512	69.303
4.29	0.0045	0.2136	0.0211	13.835	0.4622	2.1721	13.480	69.422
4.30	0.0044	0.2129	0.0209	13.955	0.4614	2.1732	13.448	69.541
4.31	0.0044	0.2121	0.0207	14.076	0.4605	2.1743	13.416	69.659
4.32	0.0043	0.2113	0.0205	14.198	0.4597	2.1754	13.384	69.777
4.33	0.0043	0.2105	0.0203	14.322	0.4588	2.1764	13.353	69.895
4.34	0.0042	0.2098	0.0202	14.446	0.4580	2.1775	13.321	70.012
4.35	0.0042	0.2090	0.0200	14.571	0.4572	2.1785	13.290	70.129
4.36	0.0041	0.2083	0.0198	14.697	0.4563	2.1796	13.259	70.245

(continued)

**Table A.1** (Continued)

$M$	$p/p_0$	$T/T_0$	$\rho/\rho_0$	$A/A^*$	$a/a_0$	$M^*$	$\mu$	$\nu$
4.37	0.0041	0.2075	0.0196	14.823	0.4555	2.1806	13.228	70.361
4.38	0.0040	0.2067	0.0194	14.951	0.4547	2.1816	13.198	70.476
4.39	0.0040	0.2060	0.0193	15.080	0.4539	2.1827	13.167	70.591
4.40	0.0039	0.2053	0.0191	15.210	0.4531	2.1837	13.137	70.706
4.41	0.0039	0.2045	0.0189	15.341	0.4522	2.1847	13.106	70.820
4.42	0.0038	0.2038	0.0187	15.472	0.4514	2.1857	13.076	70.934
4.43	0.0038	0.2030	0.0186	15.605	0.4506	2.1867	13.046	71.048
4.44	0.0037	0.2023	0.0184	15.739	0.4498	2.1877	13.016	71.161
4.45	0.0037	0.2016	0.0182	15.873	0.4490	2.1887	12.986	71.274
4.46	0.0036	0.2009	0.0181	16.009	0.4482	2.1897	12.957	71.386
4.47	0.0036	0.2002	0.0179	16.146	0.4474	2.1907	12.927	71.498
4.48	0.0035	0.1994	0.0178	16.284	0.4466	2.1917	12.898	71.610
4.49	0.0035	0.1987	0.0176	16.422	0.4458	2.1926	12.869	71.721
4.50	0.0035	0.1980	0.0174	16.562	0.4450	2.1936	12.840	71.832
4.51	0.0034	0.1973	0.0173	16.703	0.4442	2.1946	12.811	71.942
4.52	0.0034	0.1966	0.0171	16.845	0.4434	2.1955	12.782	72.052
4.53	0.0033	0.1959	0.0170	16.988	0.4426	2.1965	12.753	72.162
4.54	0.0033	0.1952	0.0168	17.132	0.4418	2.1974	12.725	72.271
4.55	0.0032	0.1945	0.0167	17.277	0.4411	2.1984	12.696	72.380
4.56	0.0032	0.1938	0.0165	17.423	0.4403	2.1993	12.668	72.489
4.57	0.0032	0.1932	0.0164	17.570	0.4395	2.2002	12.640	72.597
4.58	0.0031	0.1925	0.0163	17.718	0.4387	2.2012	12.612	72.705
4.59	0.0031	0.1918	0.0161	17.867	0.4380	2.2021	12.584	72.812
4.60	0.0031	0.1911	0.0160	18.018	0.4372	2.2030	12.556	72.919
4.61	0.0030	0.1905	0.0158	18.169	0.4364	2.2039	12.528	73.026
4.62	0.0030	0.1898	0.0157	18.322	0.4357	2.2048	12.501	73.132
4.63	0.0029	0.1891	0.0156	18.476	0.4349	2.2057	12.473	73.238
4.64	0.0029	0.1885	0.0154	18.630	0.4341	2.2066	12.446	73.344
4.65	0.0029	0.1878	0.0153	18.786	0.4334	2.2075	12.419	73.449
4.66	0.0028	0.1872	0.0152	18.943	0.4326	2.2084	12.392	73.554
4.67	0.0028	0.1865	0.0150	19.101	0.4319	2.2093	12.365	73.659
4.68	0.0028	0.1859	0.0149	19.261	0.4311	2.2102	12.338	73.763
4.69	0.0027	0.1852	0.0148	19.421	0.4304	2.2110	12.311	73.867
4.70	0.0027	0.1846	0.0146	19.583	0.4296	2.2119	12.284	73.970
4.71	0.0027	0.1839	0.0145	19.746	0.4289	2.2128	12.258	74.073
4.72	0.0026	0.1833	0.0144	19.910	0.4281	2.2136	12.232	74.176
4.73	0.0026	0.1827	0.0143	20.075	0.4274	2.2145	12.205	74.279
4.74	0.0026	0.1820	0.0141	20.241	0.4267	2.2154	12.179	74.381
4.75	0.0025	0.1814	0.0140	20.408	0.4259	2.2162	12.153	74.482
4.76	0.0025	0.1808	0.0139	20.577	0.4252	2.2170	12.127	74.584
4.77	0.0025	0.1802	0.0138	20.747	0.4245	2.2179	12.101	74.685

(continued)

**Table A.1** (Continued)

$M$	$p/p_0$	$T/T_0$	$\rho/\rho_0$	$A/A^*$	$a/a_0$	$M^*$	$\mu$	$\nu$
4.78	0.0025	0.1795	0.0137	20.918	0.4237	2.2187	12.076	74.786
4.79	0.0024	0.1789	0.0135	21.090	0.4230	2.2196	12.050	74.886
4.80	0.0024	0.1783	0.0134	21.264	0.4223	2.2204	12.025	74.986
4.81	0.0024	0.1777	0.0133	21.438	0.4216	2.2212	11.999	75.086
4.82	0.0023	0.1771	0.0132	21.614	0.4208	2.2220	11.974	75.185
4.83	0.0023	0.1765	0.0131	21.792	0.4201	2.2228	11.949	75.285
4.84	0.0023	0.1759	0.0130	21.970	0.4194	2.2236	11.924	75.383
4.85	0.0023	0.1753	0.0129	22.150	0.4187	2.2245	11.899	75.482
4.86	0.0022	0.1747	0.0128	22.331	0.4180	2.2253	11.874	75.580
4.87	0.0022	0.1741	0.0126	22.513	0.4173	2.2261	11.849	75.678
4.88	0.0022	0.1735	0.0125	22.696	0.4166	2.2268	11.825	75.775
4.89	0.0022	0.1729	0.0124	22.881	0.4159	2.2276	11.800	75.872
4.90	0.0021	0.1724	0.0123	23.067	0.4152	2.2284	11.776	75.969
4.91	0.0021	0.1718	0.0122	23.254	0.4145	2.2292	11.751	76.066
4.92	0.0021	0.1712	0.0121	23.443	0.4138	2.2300	11.727	76.162
4.93	0.0021	0.1706	0.0120	23.633	0.4131	2.2308	11.703	76.258
4.94	0.0020	0.1700	0.0119	23.824	0.4124	2.2315	11.679	76.353
4.95	0.0020	0.1695	0.0118	24.017	0.4117	2.2323	11.655	76.449
4.96	0.0020	0.1689	0.0117	24.211	0.4110	2.2331	11.631	76.544
4.97	0.0020	0.1683	0.0116	24.406	0.4103	2.2338	11.608	76.638
4.98	0.0019	0.1678	0.0115	24.603	0.4096	2.2346	11.584	76.732
4.99	0.0019	0.1672	0.0114	24.801	0.4089	2.2353	11.560	76.826
5.00	0.0019	0.1667	0.0113	25.000	0.4082	2.2361	11.537	76.920

Note: In Table A.1  $\mu$  and  $\nu$  values are in degrees.

**Table A.2** Normal shock in perfect gas ( $\gamma = 1.4$ ).

$M_1$	$M_2$	$P_2/P_1$	$\rho_2/\rho_1$	$T_2/T_1$	$a_2/a_1$	$P_{02}/P_{01}$
1.01	0.9901	1.0234	1.0167	1.0066	1.0033	1.0000
1.02	0.9805	1.0471	1.0334	1.0132	1.0066	1.0000
1.03	0.9712	1.0710	1.0502	1.0198	1.0099	1.0000
1.04	0.9620	1.0952	1.0671	1.0263	1.0131	0.9999
1.05	0.9531	1.1196	1.0840	1.0328	1.0163	0.9999
1.06	0.9444	1.1442	1.1009	1.0393	1.0195	0.9998
1.07	0.9360	1.1690	1.1179	1.0458	1.0226	0.9996
1.08	0.9277	1.1941	1.1349	1.0522	1.0258	0.9994
1.09	0.9196	1.2194	1.1520	1.0586	1.0289	0.9992
1.10	0.9118	1.2450	1.1691	1.0649	1.0320	0.9989
1.11	0.9041	1.2708	1.1862	1.0713	1.0350	0.9986

(continued)

**Table A.2** (Continued)

$M_1$	$M_2$	$P_2/P_1$	$\rho_2/\rho_1$	$T_2/T_1$	$a_2/a_1$	$P_{02}/P_{01}$
1.12	0.8966	1.2968	1.2034	1.0776	1.0381	0.9982
1.13	0.8892	1.3230	1.2206	1.0840	1.0411	0.9978
1.14	0.8820	1.3495	1.2378	1.0903	1.0442	0.9973
1.15	0.8750	1.3762	1.2550	1.0966	1.0472	0.9967
1.16	0.8682	1.4032	1.2723	1.1029	1.0502	0.9961
1.17	0.8615	1.4304	1.2896	1.1092	1.0532	0.9953
1.18	0.8549	1.4578	1.3069	1.1154	1.0561	0.9946
1.19	0.8485	1.4854	1.3243	1.1217	1.0591	0.9937
1.20	0.8422	1.5133	1.3416	1.1280	1.0621	0.9928
1.21	0.8360	1.5414	1.3590	1.1343	1.0650	0.9918
1.22	0.8300	1.5698	1.3764	1.1405	1.0680	0.9907
1.23	0.8241	1.5984	1.3938	1.1468	1.0709	0.9896
1.24	0.8183	1.6272	1.4112	1.1531	1.0738	0.9884
1.25	0.8126	1.6562	1.4286	1.1594	1.0767	0.9871
1.26	0.8071	1.6855	1.4460	1.1657	1.0797	0.9857
1.27	0.8016	1.7150	1.4634	1.1720	1.0826	0.9842
1.28	0.7963	1.7448	1.4808	1.1783	1.0855	0.9827
1.29	0.7911	1.7748	1.4983	1.1846	1.0884	0.9811
1.30	0.7860	1.8050	1.5157	1.1909	1.0913	0.9794
1.31	0.7809	1.8354	1.5331	1.1972	1.0942	0.9776
1.32	0.7760	1.8661	1.5505	1.2035	1.0971	0.9758
1.33	0.7712	1.8970	1.5680	1.2099	1.0999	0.9738
1.34	0.7664	1.9282	1.5854	1.2162	1.1028	0.9718
1.35	0.7618	1.9596	1.6028	1.2226	1.1057	0.9697
1.36	0.7572	1.9912	1.6202	1.2290	1.1086	0.9676
1.37	0.7527	2.0230	1.6376	1.2354	1.1115	0.9653
1.38	0.7483	2.0551	1.6549	1.2418	1.1144	0.9630
1.39	0.7440	2.0874	1.6723	1.2482	1.1172	0.9607
1.40	0.7397	2.1200	1.6897	1.2547	1.1201	0.9582
1.41	0.7355	2.1528	1.7070	1.2612	1.1230	0.9557
1.42	0.7314	2.1858	1.7243	1.2676	1.1259	0.9531
1.43	0.7274	2.2190	1.7416	1.2741	1.1288	0.9504
1.44	0.7235	2.2525	1.7589	1.2807	1.1317	0.9476
1.45	0.7196	2.2862	1.7761	1.2872	1.1346	0.9448
1.46	0.7157	2.3202	1.7934	1.2938	1.1374	0.9420
1.47	0.7120	2.3544	1.8106	1.3003	1.1403	0.9390
1.48	0.7083	2.3888	1.8278	1.3069	1.1432	0.9360
1.49	0.7047	2.4234	1.8449	1.3136	1.1461	0.9329
1.50	0.7011	2.4583	1.8621	1.3202	1.1490	0.9298
1.51	0.6976	2.4934	1.8792	1.3269	1.1519	0.9266
1.52	0.6941	2.5288	1.8963	1.3336	1.1548	0.9233

(continued)



Table A.2 (Continued)

$M_1$	$M_2$	$P_2/P_1$	$\rho_2/\rho_1$	$T_2/T_1$	$a_2/a_1$	$p_{02}/p_{01}$
1.53	0.6907	2.5644	1.9133	1.3403	1.1577	0.9200
1.54	0.6874	2.6002	1.9303	1.3470	1.1606	0.9166
1.55	0.6841	2.6362	1.9473	1.3538	1.1635	0.9132
1.56	0.6809	2.6725	1.9643	1.3606	1.1664	0.9097
1.57	0.6777	2.7090	1.9812	1.3674	1.1694	0.9062
1.58	0.6746	2.7458	1.9981	1.3742	1.1723	0.9026
1.59	0.6715	2.7828	2.0149	1.3811	1.1752	0.8989
1.60	0.6684	2.8200	2.0317	1.3880	1.1781	0.8952
1.61	0.6655	2.8574	2.0485	1.3949	1.1811	0.8915
1.62	0.6625	2.8951	2.0653	1.4018	1.1840	0.8877
1.63	0.6596	2.9330	2.0820	1.4088	1.1869	0.8838
1.64	0.6568	2.9712	2.0986	1.4158	1.1899	0.8799
1.65	0.6540	3.0096	2.1152	1.4228	1.1928	0.8760
1.66	0.6512	3.0482	2.1318	1.4299	1.1958	0.8720
1.67	0.6485	3.0870	2.1484	1.4369	1.1987	0.8680
1.68	0.6458	3.1261	2.1649	1.4440	1.2017	0.8639
1.69	0.6431	3.1654	2.1813	1.4512	1.2046	0.8599
1.70	0.6405	3.2050	2.1977	1.4583	1.2076	0.8557
1.71	0.6380	3.2448	2.2141	1.4655	1.2106	0.8516
1.72	0.6355	3.2848	2.2304	1.4727	1.2136	0.8474
1.73	0.6330	3.3250	2.2467	1.4800	1.2165	0.8431
1.74	0.6305	3.3655	2.2629	1.4873	1.2195	0.8389
1.75	0.6281	3.4062	2.2791	1.4946	1.2225	0.8346
1.76	0.6257	3.4472	2.2952	1.5019	1.2255	0.8302
1.77	0.6234	3.4884	2.3113	1.5093	1.2285	0.8259
1.78	0.6210	3.5298	2.3273	1.5167	1.2315	0.8215
1.79	0.6188	3.5714	2.3433	1.5241	1.2346	0.8171
1.80	0.6165	3.6133	2.3592	1.5316	1.2376	0.8127
1.81	0.6143	3.6554	2.3751	1.5391	1.2406	0.8082
1.82	0.6121	3.6978	2.3909	1.5466	1.2436	0.8038
1.83	0.6099	3.7404	2.4067	1.5541	1.2467	0.7993
1.84	0.6078	3.7832	2.4224	1.5617	1.2497	0.7948
1.85	0.6057	3.8262	2.4381	1.5693	1.2527	0.7902
1.86	0.6036	3.8695	2.4537	1.5770	1.2558	0.7857
1.87	0.6016	3.9130	2.4693	1.5847	1.2588	0.7811
1.88	0.5996	3.9568	2.4848	1.5924	1.2619	0.7765
1.89	0.5976	4.0008	2.5003	1.6001	1.2650	0.7720
1.90	0.5956	4.0450	2.5157	1.6079	1.2680	0.7674
1.91	0.5937	4.0894	2.5310	1.6157	1.2711	0.7627
1.92	0.5918	4.1341	2.5463	1.6236	1.2742	0.7581
1.93	0.5899	4.1791	2.5616	1.6314	1.2773	0.7535

(continued)

**Table A.2** (Continued)

$M_1$	$M_2$	$P_2/P_1$	$\rho_2/\rho_1$	$T_2/T_1$	$a_2/a_1$	$P_{02}/P_{01}$
1.94	0.5880	4.2242	2.5767	1.6394	1.2804	0.7488
1.95	0.5862	4.2696	2.5919	1.6473	1.2835	0.7442
1.96	0.5844	4.3152	2.6069	1.6553	1.2866	0.7395
1.97	0.5826	4.3610	2.6220	1.6633	1.2897	0.7349
1.98	0.5808	4.4071	2.6369	1.6713	1.2928	0.7302
1.99	0.5791	4.4534	2.6518	1.6794	1.2959	0.7255
2.00	0.5774	4.5000	2.6667	1.6875	1.2990	0.7209
2.01	0.5757	4.5468	2.6815	1.6956	1.3022	0.7162
2.02	0.5740	4.5938	2.6962	1.7038	1.3053	0.7115
2.03	0.5723	4.6410	2.7109	1.7120	1.3084	0.7069
2.04	0.5707	4.6885	2.7255	1.7203	1.3116	0.7022
2.05	0.5691	4.7362	2.7400	1.7285	1.3147	0.6975
2.06	0.5675	4.7842	2.7545	1.7369	1.3179	0.6928
2.07	0.5659	4.8324	2.7689	1.7452	1.3211	0.6882
2.08	0.5643	4.8808	2.7833	1.7536	1.3242	0.6835
2.09	0.5628	4.9294	2.7976	1.7620	1.3274	0.6789
2.10	0.5613	4.9783	2.8119	1.7704	1.3306	0.6742
2.11	0.5598	5.0274	2.8261	1.7789	1.3338	0.6696
2.12	0.5583	5.0768	2.8402	1.7875	1.3370	0.6649
2.13	0.5568	5.1264	2.8543	1.7960	1.3402	0.6603
2.14	0.5554	5.1762	2.8683	1.8046	1.3434	0.6557
2.15	0.5540	5.2262	2.8823	1.8132	1.3466	0.6511
2.16	0.5525	5.2765	2.8962	1.8219	1.3498	0.6464
2.17	0.5511	5.3270	2.9101	1.8306	1.3530	0.6419
2.18	0.5498	5.3778	2.9238	1.8393	1.3562	0.6373
2.19	0.5484	5.4288	2.9376	1.8481	1.3594	0.6327
2.20	0.5471	5.4800	2.9512	1.8569	1.3627	0.6281
2.21	0.5457	5.5314	2.9648	1.8657	1.3659	0.6236
2.22	0.5444	5.5831	2.9784	1.8746	1.3691	0.6191
2.23	0.5431	5.6350	2.9918	1.8835	1.3724	0.6145
2.24	0.5418	5.6872	3.0053	1.8924	1.3756	0.6100
2.25	0.5406	5.7396	3.0186	1.9014	1.3789	0.6055
2.26	0.5393	5.7922	3.0319	1.9104	1.3822	0.6011
2.27	0.5381	5.8450	3.0452	1.9194	1.3854	0.5966
2.28	0.5368	5.8981	3.0584	1.9285	1.3887	0.5921
2.29	0.5356	5.9514	3.0715	1.9376	1.3920	0.5877
2.30	0.5344	6.0050	3.0845	1.9468	1.3953	0.5833
2.31	0.5332	6.0588	3.0976	1.9560	1.3986	0.5789
2.32	0.5321	6.1128	3.1105	1.9652	1.4019	0.5745
2.33	0.5309	6.1670	3.1234	1.9745	1.4052	0.5702
2.34	0.5297	6.2215	3.1362	1.9838	1.4085	0.5658

(continued)

Table A.2 (Continued)

$M_1$	$M_2$	$P_2/P_1$	$\rho_2/\rho_1$	$T_2/T_1$	$a_2/a_1$	$p_{02}/p_{01}$
2.35	0.5286	6.2762	3.1490	1.9931	1.4118	0.5615
2.36	0.5275	6.3312	3.1617	2.0025	1.4151	0.5572
2.37	0.5264	6.3864	3.1743	2.0119	1.4184	0.5529
2.38	0.5253	6.4418	3.1869	2.0213	1.4217	0.5486
2.39	0.5242	6.4974	3.1994	2.0308	1.4251	0.5444
2.40	0.5231	6.5533	3.2119	2.0403	1.4284	0.5401
2.41	0.5221	6.6094	3.2243	2.0499	1.4317	0.5359
2.42	0.5210	6.6658	3.2367	2.0595	1.4351	0.5317
2.43	0.5200	6.7224	3.2489	2.0691	1.4384	0.5276
2.44	0.5189	6.7792	3.2612	2.0788	1.4418	0.5234
2.45	0.5179	6.8362	3.2733	2.0885	1.4452	0.5193
2.46	0.5169	6.8935	3.2855	2.0982	1.4485	0.5152
2.47	0.5159	6.9510	3.2975	2.1080	1.4519	0.5111
2.48	0.5149	7.0088	3.3095	2.1178	1.4553	0.5071
2.49	0.5140	7.0668	3.3215	2.1276	1.4586	0.5030
2.50	0.5130	7.1250	3.3333	2.1375	1.4620	0.4990
2.51	0.5120	7.1834	3.3452	2.1474	1.4654	0.4950
2.52	0.5111	7.2421	3.3569	2.1574	1.4688	0.4911
2.53	0.5102	7.3010	3.3686	2.1674	1.4722	0.4871
2.54	0.5092	7.3602	3.3803	2.1774	1.4756	0.4832
2.55	0.5083	7.4196	3.3919	2.1875	1.4790	0.4793
2.56	0.5074	7.4792	3.4034	2.1976	1.4824	0.4754
2.57	0.5065	7.5390	3.4149	2.2077	1.4858	0.4715
2.58	0.5056	7.5991	3.4263	2.2179	1.4893	0.4677
2.59	0.5047	7.6594	3.4377	2.2281	1.4927	0.4639
2.60	0.5039	7.7200	3.4490	2.2383	1.4961	0.4601
2.61	0.5030	7.7808	3.4602	2.2486	1.4995	0.4564
2.62	0.5022	7.8418	3.4714	2.2590	1.5030	0.4526
2.63	0.5013	7.9030	3.4826	2.2693	1.5064	0.4489
2.64	0.5005	7.9645	3.4937	2.2797	1.5099	0.4452
2.65	0.4996	8.0262	3.5047	2.2902	1.5133	0.4416
2.66	0.4988	8.0882	3.5157	2.3006	1.5168	0.4379
2.67	0.4980	8.1504	3.5266	2.3111	1.5202	0.4343
2.68	0.4972	8.2128	3.5374	2.3217	1.5237	0.4307
2.69	0.4964	8.2754	3.5482	2.3323	1.5272	0.4271
2.70	0.4956	8.3383	3.5590	2.3429	1.5307	0.4236
2.71	0.4949	8.4014	3.5697	2.3536	1.5341	0.4201
2.72	0.4941	8.4648	3.5803	2.3642	1.5376	0.4166
2.73	0.4933	8.5284	3.5909	2.3750	1.5411	0.4131
2.74	0.4926	8.5922	3.6015	2.3858	1.5446	0.4097
2.75	0.4918	8.6562	3.6119	2.3966	1.5481	0.4062

(continued)

**Table A.2** (Continued)

$M_1$	$M_2$	$P_2/P_1$	$\rho_2/\rho_1$	$T_2/T_1$	$a_2/a_1$	$P_{02}/P_{01}$
2.76	0.4911	8.7205	3.6224	2.4074	1.5516	0.4028
2.77	0.4903	8.7850	3.6327	2.4183	1.5551	0.3994
2.78	0.4896	8.8498	3.6431	2.4292	1.5586	0.3961
2.79	0.4889	8.9148	3.6533	2.4402	1.5621	0.3928
2.80	0.4882	8.9800	3.6636	2.4512	1.5656	0.3895
2.81	0.4875	9.0454	3.6737	2.4622	1.5691	0.3862
2.82	0.4868	9.1111	3.6838	2.4733	1.5727	0.3829
2.83	0.4861	9.1770	3.6939	2.4844	1.5762	0.3797
2.84	0.4854	9.2432	3.7039	2.4955	1.5797	0.3765
2.85	0.4847	9.3096	3.7139	2.5067	1.5833	0.3733
2.86	0.4840	9.3762	3.7238	2.5179	1.5868	0.3701
2.87	0.4833	9.4430	3.7336	2.5292	1.5903	0.3670
2.88	0.4827	9.5101	3.7434	2.5405	1.5939	0.3639
2.89	0.4820	9.5774	3.7532	2.5518	1.5974	0.3608
2.90	0.4814	9.6450	3.7629	2.5632	1.6010	0.3577
2.91	0.4807	9.7128	3.7725	2.5746	1.6046	0.3547
2.92	0.4801	9.7808	3.7821	2.5861	1.6081	0.3517
2.93	0.4795	9.8490	3.7917	2.5976	1.6117	0.3487
2.94	0.4788	9.9175	3.8012	2.6091	1.6153	0.3457
2.95	0.4782	9.9862	3.8106	2.6206	1.6188	0.3428
2.96	0.4776	10.0552	3.8200	2.6322	1.6224	0.3398
2.97	0.4770	10.1244	3.8294	2.6439	1.6260	0.3369
2.98	0.4764	10.1938	3.8387	2.6555	1.6296	0.3340
2.99	0.4758	10.2634	3.8479	2.6673	1.6332	0.3312
3.00	0.4752	10.3333	3.8571	2.6790	1.6368	0.3283
3.01	0.4746	10.4034	3.8663	2.6908	1.6404	0.3255
3.02	0.4740	10.4738	3.8754	2.7026	1.6440	0.3227
3.03	0.4734	10.5444	3.8845	2.7145	1.6476	0.3200
3.04	0.4729	10.6152	3.8935	2.7264	1.6512	0.3172
3.05	0.4723	10.6862	3.9025	2.7383	1.6548	0.3145
3.06	0.4717	10.7575	3.9114	2.7503	1.6584	0.3118
3.07	0.4712	10.8290	3.9203	2.7623	1.6620	0.3091
3.08	0.4706	10.9008	3.9291	2.7744	1.6656	0.3065
3.09	0.4701	10.9728	3.9379	2.7865	1.6693	0.3038
3.10	0.4695	11.0450	3.9466	2.7986	1.6729	0.3012
3.11	0.4690	11.1174	3.9553	2.8108	1.6765	0.2986
3.12	0.4685	11.1901	3.9639	2.8230	1.6802	0.2960
3.13	0.4679	11.2630	3.9725	2.8352	1.6838	0.2935
3.14	0.4674	11.3362	3.9811	2.8475	1.6875	0.2910
3.15	0.4669	11.4096	3.9896	2.8598	1.6911	0.2885
3.16	0.4664	11.4832	3.9981	2.8722	1.6948	0.2860

(continued)

Table A.2 (Continued)

$M_1$	$M_2$	$P_2/P_1$	$\rho_2/\rho_1$	$T_2/T_1$	$a_2/a_1$	$p_{02}/p_{01}$
3.17	0.4659	11.5570	4.0065	2.8846	1.6984	0.2835
3.18	0.4654	11.6311	4.0149	2.8970	1.7021	0.2811
3.19	0.4648	11.7054	4.0232	2.9095	1.7057	0.2786
3.20	0.4643	11.7800	4.0315	2.9220	1.7094	0.2762
3.21	0.4639	11.8548	4.0397	2.9345	1.7131	0.2738
3.22	0.4634	11.9298	4.0479	2.9471	1.7167	0.2715
3.23	0.4629	12.0050	4.0561	2.9598	1.7204	0.2691
3.24	0.4624	12.0805	4.0642	2.9724	1.7241	0.2668
3.25	0.4619	12.1562	4.0723	2.9851	1.7277	0.2645
3.26	0.4614	12.2322	4.0803	2.9979	1.7314	0.2622
3.27	0.4610	12.3084	4.0883	3.0106	1.7351	0.2600
3.28	0.4605	12.3848	4.0963	3.0234	1.7388	0.2577
3.29	0.4600	12.4614	4.1042	3.0363	1.7425	0.2555
3.30	0.4596	12.5383	4.1120	3.0492	1.7462	0.2533
3.31	0.4591	12.6154	4.1198	3.0621	1.7499	0.2511
3.32	0.4587	12.6928	4.1276	3.0751	1.7536	0.2489
3.33	0.4582	12.7704	4.1354	3.0881	1.7573	0.2468
3.34	0.4578	12.8482	4.1431	3.1011	1.7610	0.2446
3.35	0.4573	12.9262	4.1507	3.1142	1.7647	0.2425
3.36	0.4569	13.0045	4.1583	3.1273	1.7684	0.2404
3.37	0.4565	13.0830	4.1659	3.1405	1.7721	0.2383
3.38	0.4560	13.1618	4.1734	3.1537	1.7759	0.2363
3.39	0.4556	13.2408	4.1809	3.1669	1.7796	0.2342
3.40	0.4552	13.3200	4.1884	3.1802	1.7833	0.2322
3.41	0.4548	13.3994	4.1958	3.1935	1.7870	0.2302
3.42	0.4544	13.4791	4.2032	3.2069	1.7908	0.2282
3.43	0.4540	13.5590	4.2105	3.2203	1.7945	0.2263
3.44	0.4535	13.6392	4.2179	3.2337	1.7982	0.2243
3.45	0.4531	13.7196	4.2251	3.2472	1.8020	0.2224
3.46	0.4527	13.8002	4.2323	3.2607	1.8057	0.2205
3.47	0.4523	13.8810	4.2395	3.2742	1.8095	0.2186
3.48	0.4519	13.9621	4.2467	3.2878	1.8132	0.2167
3.49	0.4515	14.0434	4.2538	3.3014	1.8170	0.2148
3.50	0.4512	14.1250	4.2609	3.3150	1.8207	0.2129
3.51	0.4508	14.2068	4.2679	3.3287	1.8245	0.2111
3.52	0.4504	14.2888	4.2749	3.3425	1.8282	0.2093
3.53	0.4500	14.3710	4.2819	3.3562	1.8320	0.2075
3.54	0.4496	14.4535	4.2888	3.3701	1.8358	0.2057
3.55	0.4492	14.5362	4.2957	3.3839	1.8395	0.2039
3.56	0.4489	14.6192	4.3026	3.3978	1.8433	0.2022
3.57	0.4485	14.7024	4.3094	3.4117	1.8471	0.2004

(continued)

**Table A.2** (Continued)

$M_1$	$M_2$	$P_2/P_1$	$\rho_2/\rho_1$	$T_2/T_1$	$a_2/a_1$	$p_{02}/p_{01}$
3.58	0.4481	14.7858	4.3162	3.4257	1.8509	0.1987
3.59	0.4478	14.8694	4.3229	3.4397	1.8546	0.1970
3.60	0.4474	14.9533	4.3296	3.4537	1.8584	0.1953
3.61	0.4471	15.0374	4.3363	3.4678	1.8622	0.1936
3.62	0.4467	15.1218	4.3429	3.4819	1.8660	0.1920
3.63	0.4463	15.2064	4.3496	3.4961	1.8698	0.1903
3.64	0.4460	15.2912	4.3561	3.5103	1.8736	0.1887
3.65	0.4456	15.3762	4.3627	3.5245	1.8774	0.1871
3.66	0.4453	15.4615	4.3692	3.5388	1.8812	0.1855
3.67	0.4450	15.5470	4.3756	3.5531	1.8850	0.1839
3.68	0.4446	15.6328	4.3821	3.5674	1.8888	0.1823
3.69	0.4443	15.7188	4.3885	3.5818	1.8926	0.1807
3.70	0.4439	15.8050	4.3949	3.5962	1.8964	0.1792
3.71	0.4436	15.8914	4.4012	3.6107	1.9002	0.1777
3.72	0.4433	15.9781	4.4075	3.6252	1.9040	0.1761
3.73	0.4430	16.0650	4.4138	3.6397	1.9078	0.1746
3.74	0.4426	16.1522	4.4200	3.6543	1.9116	0.1731
3.75	0.4423	16.2396	4.4262	3.6689	1.9154	0.1717
3.76	0.4420	16.3272	4.4324	3.6836	1.9193	0.1702
3.77	0.4417	16.4150	4.4385	3.6983	1.9231	0.1687
3.78	0.4414	16.5031	4.4447	3.7130	1.9269	0.1673
3.79	0.4410	16.5914	4.4507	3.7278	1.9307	0.1659
3.80	0.4407	16.6800	4.4568	3.7426	1.9346	0.1645
3.81	0.4404	16.7688	4.4628	3.7575	1.9384	0.1631
3.82	0.4401	16.8578	4.4688	3.7723	1.9423	0.1617
3.83	0.4398	16.9470	4.4747	3.7873	1.9461	0.1603
3.84	0.4395	17.0365	4.4807	3.8022	1.9499	0.1589
3.85	0.4392	17.1262	4.4866	3.8172	1.9538	0.1576
3.86	0.4389	17.2162	4.4924	3.8323	1.9576	0.1563
3.87	0.4386	17.3064	4.4983	3.8473	1.9615	0.1549
3.88	0.4383	17.3968	4.5041	3.8625	1.9653	0.1536
3.89	0.4380	17.4874	4.5098	3.8776	1.9692	0.1523
3.90	0.4377	17.5783	4.5156	3.8928	1.9730	0.1510
3.91	0.4375	17.6694	4.5213	3.9080	1.9769	0.1497
3.92	0.4372	17.7608	4.5270	3.9233	1.9807	0.1485
3.93	0.4369	17.8524	4.5326	3.9386	1.9846	0.1472
3.94	0.4366	17.9442	4.5383	3.9540	1.9885	0.1460
3.95	0.4363	18.0362	4.5439	3.9694	1.9923	0.1448
3.96	0.4360	18.1285	4.5494	3.9848	1.9962	0.1435
3.97	0.4358	18.2210	4.5550	4.0003	2.0001	0.1423

(continued)

Table A.2 (Continued)

$M_1$	$M_2$	$P_2/P_1$	$\rho_2/\rho_1$	$T_2/T_1$	$a_2/a_1$	$p_{02}/p_{01}$
3.98	0.4355	18.3138	4.5605	4.0157	2.0039	0.1411
3.99	0.4352	18.4068	4.5660	4.0313	2.0078	0.1399
4.00	0.4350	18.5000	4.5714	4.0469	2.0117	0.1388
4.01	0.4347	18.5934	4.5769	4.0625	2.0156	0.1376
4.02	0.4344	18.6871	4.5823	4.0781	2.0194	0.1364
4.03	0.4342	18.7810	4.5876	4.0938	2.0233	0.1353
4.04	0.4339	18.8752	4.5930	4.1096	2.0272	0.1342
4.05	0.4336	18.9696	4.5983	4.1253	2.0311	0.1330
4.06	0.4334	19.0642	4.6036	4.1412	2.0350	0.1319
4.07	0.4331	19.1590	4.6089	4.1570	2.0389	0.1308
4.08	0.4329	19.2541	4.6141	4.1729	2.0428	0.1297
4.09	0.4326	19.3494	4.6193	4.1888	2.0467	0.1286
4.10	0.4324	19.4450	4.6245	4.2048	2.0506	0.1276
4.11	0.4321	19.5408	4.6296	4.2208	2.0545	0.1265
4.12	0.4319	19.6368	4.6348	4.2368	2.0584	0.1254
4.13	0.4316	19.7330	4.6399	4.2529	2.0623	0.1244
4.14	0.4314	19.8295	4.6450	4.2690	2.0662	0.1234
4.15	0.4311	19.9262	4.6500	4.2852	2.0701	0.1223
4.16	0.4309	20.0232	4.6550	4.3014	2.0740	0.1213
4.17	0.4306	20.1204	4.6601	4.3176	2.0779	0.1203
4.18	0.4304	20.2178	4.6650	4.3339	2.0818	0.1193
4.19	0.4302	20.3155	4.6700	4.3502	2.0857	0.1183
4.20	0.4299	20.4133	4.6749	4.3666	2.0896	0.1173
4.21	0.4297	20.5115	4.6798	4.3830	2.0936	0.1164
4.22	0.4295	20.6098	4.6847	4.3994	2.0975	0.1154
4.23	0.4292	20.7084	4.6896	4.4159	2.1014	0.1144
4.24	0.4290	20.8072	4.6944	4.4324	2.1053	0.1135
4.25	0.4288	20.9063	4.6992	4.4489	2.1092	0.1126
4.26	0.4286	21.0056	4.7040	4.4655	2.1132	0.1116
4.27	0.4283	21.1051	4.7087	4.4821	2.1171	0.1107
4.28	0.4281	21.2048	4.7135	4.4988	2.1210	0.1098
4.29	0.4279	21.3048	4.7182	4.5155	2.1250	0.1089
4.30	0.4277	21.4050	4.7229	4.5322	2.1289	0.1080
4.31	0.4275	21.5055	4.7275	4.5490	2.1328	0.1071
4.32	0.4272	21.6062	4.7322	4.5658	2.1368	0.1062
4.33	0.4270	21.7071	4.7368	4.5827	2.1407	0.1054
4.34	0.4268	21.8083	4.7414	4.5995	2.1447	0.1045
4.35	0.4266	21.9096	4.7460	4.6165	2.1486	0.1036
4.36	0.4264	22.0113	4.7505	4.6335	2.1525	0.1028
4.37	0.4262	22.1131	4.7550	4.6505	2.1565	0.1020
4.38	0.4260	22.2152	4.7595	4.6675	2.1604	0.1011

(continued)

**Table A.2** (Continued)

$M_1$	$M_2$	$P_2/P_1$	$\rho_2/\rho_1$	$T_2/T_1$	$a_2/a_1$	$P_{02}/P_{01}$
4.39	0.4258	22.3175	4.7640	4.6846	2.1644	0.1003
4.40	0.4255	22.4201	4.7685	4.7017	2.1683	0.0995
4.41	0.4253	22.5229	4.7729	4.7189	2.1723	0.0987
4.42	0.4251	22.6259	4.7773	4.7361	2.1763	0.0979
4.43	0.4249	22.7291	4.7817	4.7533	2.1802	0.0971
4.44	0.4247	22.8326	4.7861	4.7706	2.1842	0.0963
4.45	0.4245	22.9363	4.7904	4.7879	2.1881	0.0955
4.46	0.4243	23.0403	4.7948	4.8053	2.1921	0.0947
4.47	0.4241	23.1445	4.7991	4.8227	2.1961	0.0940
4.48	0.4239	23.2489	4.8034	4.8401	2.2000	0.0932
4.49	0.4237	23.3535	4.8076	4.8576	2.2040	0.0924
4.50	0.4236	23.4584	4.8119	4.8751	2.2080	0.0917
4.51	0.4234	23.5635	4.8161	4.8926	2.2119	0.0910
4.52	0.4232	23.6689	4.8203	4.9102	2.2159	0.0902
4.53	0.4230	23.7745	4.8245	4.9279	2.2199	0.0895
4.54	0.4228	23.8803	4.8287	4.9455	2.2239	0.0888
4.55	0.4226	23.9864	4.8328	4.9632	2.2278	0.0881
4.56	0.4224	24.0926	4.8369	4.9810	2.2318	0.0874
4.57	0.4222	24.1992	4.8410	4.9988	2.2358	0.0867
4.58	0.4220	24.3059	4.8451	5.0166	2.2398	0.0860
4.59	0.4219	24.4129	4.8492	5.0344	2.2438	0.0853
4.60	0.4217	24.5201	4.8532	5.0523	2.2477	0.0846
4.61	0.4215	24.6276	4.8572	5.0703	2.2517	0.0839
4.62	0.4213	24.7353	4.8612	5.0883	2.2557	0.0832
4.63	0.4211	24.8432	4.8652	5.1063	2.2597	0.0826
4.64	0.4210	24.9513	4.8692	5.1243	2.2637	0.0819
4.65	0.4208	25.0597	4.8731	5.1424	2.2677	0.0813
4.66	0.4206	25.1683	4.8771	5.1605	2.2717	0.0806
4.67	0.4204	25.2772	4.8810	5.1787	2.2757	0.0800
4.68	0.4203	25.3863	4.8849	5.1969	2.2797	0.0793
4.69	0.4201	25.4956	4.8887	5.2152	2.2837	0.0787
4.70	0.4199	25.6051	4.8926	5.2335	2.2877	0.0781
4.71	0.4197	25.7149	4.8964	5.2518	2.2917	0.0775
4.72	0.4196	25.8249	4.9002	5.2701	2.2957	0.0769
4.73	0.4194	25.9352	4.9040	5.2885	2.2997	0.0762
4.74	0.4192	26.0457	4.9078	5.3070	2.3037	0.0756
4.75	0.4191	26.1564	4.9116	5.3255	2.3077	0.0750
4.76	0.4189	26.2673	4.9153	5.3440	2.3117	0.0745
4.77	0.4187	26.3785	4.9190	5.3625	2.3157	0.0739
4.78	0.4186	26.4900	4.9227	5.3811	2.3197	0.0733
4.79	0.4184	26.6016	4.9264	5.3998	2.3237	0.0727

(continued)



**Table A.2** (Continued)

$M_1$	$M_2$	$P_2/P_1$	$\rho_2/\rho_1$	$T_2/T_1$	$a_2/a_1$	$P_{02}/P_{01}$
4.80	0.4183	26.7135	4.9301	5.4184	2.3277	0.0721
4.81	0.4181	26.8256	4.9338	5.4372	2.3318	0.0716
4.82	0.4179	26.9380	4.9374	5.4559	2.3358	0.0710
4.83	0.4178	27.0505	4.9410	5.4747	2.3398	0.0705
4.84	0.4176	27.1634	4.9446	5.4935	2.3438	0.0699
4.85	0.4175	27.2764	4.9482	5.5124	2.3478	0.0694
4.86	0.4173	27.3897	4.9518	5.5313	2.3519	0.0688
4.87	0.4172	27.5032	4.9553	5.5502	2.3559	0.0683
4.88	0.4170	27.6170	4.9589	5.5692	2.3599	0.0677
4.89	0.4169	27.7310	4.9624	5.5882	2.3639	0.0672
4.90	0.4167	27.8452	4.9659	5.6073	2.3680	0.0667
4.91	0.4165	27.9596	4.9694	5.6264	2.3720	0.0662
4.92	0.4164	28.0743	4.9728	5.6455	2.3760	0.0657
4.93	0.4162	28.1893	4.9763	5.6647	2.3801	0.0652
4.94	0.4161	28.3044	4.9797	5.6839	2.3841	0.0647
4.95	0.4160	28.4198	4.9831	5.7032	2.3881	0.0642
4.96	0.4158	28.5354	4.9865	5.7225	2.3922	0.0637
4.97	0.4157	28.6513	4.9899	5.7418	2.3962	0.0632
4.98	0.4155	28.7673	4.9933	5.7612	2.4002	0.0627
4.99	0.4154	28.8837	4.9967	5.7806	2.4043	0.0622
5.00	0.4152	29.0002	5.0000	5.8000	2.4083	0.0617

**Table A.3** Oblique shock in perfect gas ( $\gamma = 1.4$ ).

Weak solution				Strong solution			
$M_1$	$\theta$	$\beta$	$p_2/p_1$	$M_2$	$\beta$	$p_2/p_1$	$M_2$
1.05	0	72.07	0.998	1.052	89.66	1.120	0.953
1.10	0	65.28	0.998	1.101	89.83	1.245	0.912
1.10	1	69.80	1.077	1.039	83.57	1.227	0.925
1.15	0	60.34	0.998	1.151	89.89	1.376	0.875
1.15	1	63.16	1.062	1.102	85.98	1.369	0.880
1.15	2	67.00	1.141	1.043	81.17	1.340	0.901
1.20	0	56.39	0.998	1.201	89.92	1.513	0.842
1.20	1	58.55	1.056	1.158	87.04	1.509	0.845
1.20	2	61.05	1.120	1.111	83.86	1.494	0.855
1.20	3	64.34	1.198	1.056	80.03	1.463	0.876
1.25	0	53.08	0.999	1.251	89.94	1.656	0.813
1.25	1	54.88	1.053	1.211	87.65	1.653	0.815
1.25	2	56.85	1.111	1.170	85.21	1.644	0.821

(continued)

Table A.3 (Continued)

Weak solution				Strong solution			
$M_1$	$\theta$	$\beta$	$p_2/p_1$	$M_2$	$\beta$	$p_2/p_1$	$M_2$
1.25	3	59.13	1.176	1.124	82.55	1.626	0.832
1.25	4	61.99	1.254	1.072	79.39	1.594	0.852
1.25	5	66.50	1.366	0.999	74.64	1.528	0.895
1.30	0	50.24	0.999	1.301	89.95	1.805	0.786
1.30	1	51.81	1.051	1.263	88.05	1.803	0.787
1.30	2	53.47	1.106	1.224	86.06	1.796	0.792
1.30	3	55.32	1.167	1.184	83.95	1.783	0.800
1.30	4	57.42	1.233	1.140	81.65	1.763	0.812
1.30	5	59.96	1.311	1.090	78.97	1.733	0.831
1.30	6	63.46	1.411	1.027	75.37	1.679	0.864
1.35	0	47.76	0.999	1.351	89.96	1.960	0.762
1.35	1	49.17	1.050	1.314	88.34	1.958	0.763
1.35	2	50.63	1.104	1.277	86.65	1.952	0.766
1.35	3	52.22	1.162	1.239	84.89	1.943	0.772
1.35	4	53.97	1.224	1.199	83.03	1.928	0.781
1.35	5	55.93	1.292	1.157	80.99	1.907	0.793
1.35	6	58.23	1.370	1.109	78.66	1.877	0.811
1.35	7	61.18	1.465	1.052	75.72	1.830	0.839
1.35	8	66.91	1.632	0.954	70.02	1.711	0.909
1.40	0	45.55	0.999	1.401	89.96	2.120	0.740
1.40	1	46.84	1.050	1.365	88.55	2.119	0.741
1.40	2	48.17	1.103	1.329	87.08	2.114	0.743
1.40	3	49.59	1.159	1.293	85.57	2.106	0.748
1.40	4	51.12	1.219	1.255	83.99	2.095	0.754
1.40	5	52.78	1.283	1.216	82.31	2.079	0.764
1.40	6	54.63	1.354	1.174	80.49	2.057	0.776
1.40	7	56.76	1.433	1.128	78.41	2.028	0.793
1.40	8	59.37	1.526	1.074	75.89	1.984	0.818
1.40	9	63.18	1.655	1.003	72.19	1.906	0.863
1.45	0	43.57	0.999	1.451	89.97	2.286	0.720
1.45	1	44.77	1.050	1.416	88.71	2.285	0.720
1.45	2	46.00	1.103	1.381	87.41	2.281	0.722
1.45	3	47.30	1.158	1.345	86.08	2.275	0.726
1.45	4	48.68	1.217	1.309	84.70	2.265	0.732
1.45	5	50.16	1.279	1.272	83.27	2.252	0.739
1.45	6	51.76	1.346	1.232	81.73	2.236	0.749
1.45	7	53.52	1.419	1.191	80.07	2.213	0.761
1.45	8	55.52	1.500	1.146	78.20	2.184	0.778
1.45	9	57.89	1.593	1.095	75.98	2.142	0.801

(continued)

Table A.3 (Continued)

Weak solution				Strong solution			
$M_1$	$\theta$	$\beta$	$p_2/p_1$	$M_2$	$\beta$	$p_2/p_1$	$M_2$
1.45	10	61.05	1.711	1.032	72.99	2.076	0.837
1.50	0	41.78	0.999	1.501	89.97	2.458	0.701
1.50	1	42.91	1.050	1.466	88.84	2.457	0.702
1.50	2	44.07	1.103	1.432	87.67	2.454	0.704
1.50	3	45.27	1.158	1.397	86.48	2.448	0.707
1.50	4	46.54	1.216	1.362	85.26	2.440	0.711
1.50	5	47.89	1.278	1.325	83.99	2.430	0.717
1.50	6	49.33	1.343	1.288	82.66	2.415	0.725
1.50	7	50.88	1.413	1.249	81.25	2.398	0.735
1.50	8	52.57	1.489	1.208	79.71	2.375	0.748
1.50	9	54.47	1.572	1.164	78.00	2.345	0.764
1.50	10	56.68	1.666	1.114	76.00	2.305	0.785
1.50	11	59.46	1.781	1.055	73.44	2.245	0.817
1.50	12	64.35	1.967	0.961	68.79	2.115	0.885
1.55	0	40.15	0.999	1.551	89.97	2.636	0.684
1.55	1	41.23	1.051	1.516	88.95	2.635	0.685
1.55	2	42.32	1.104	1.482	87.88	2.632	0.686
1.55	3	43.45	1.159	1.448	86.80	2.628	0.689
1.55	4	44.64	1.217	1.413	85.70	2.620	0.693
1.55	5	45.89	1.278	1.378	84.57	2.611	0.698
1.55	6	47.21	1.343	1.341	83.39	2.599	0.705
1.55	7	48.62	1.411	1.304	82.15	2.584	0.713
1.55	8	50.13	1.484	1.265	80.83	2.565	0.723
1.55	9	51.77	1.563	1.224	79.40	2.541	0.736
1.55	10	53.60	1.649	1.180	77.81	2.511	0.752
1.55	11	55.69	1.746	1.132	75.97	2.471	0.772
1.55	12	58.24	1.860	1.076	73.69	2.415	0.801
1.55	13	61.98	2.018	0.999	70.24	2.316	0.852
1.60	0	38.66	0.999	1.601	89.97	2.820	0.668
1.60	1	39.69	1.051	1.566	89.03	2.819	0.669
1.60	2	40.72	1.105	1.532	88.06	2.817	0.670
1.60	3	41.81	1.160	1.498	87.07	2.812	0.673
1.60	4	42.93	1.219	1.464	86.06	2.806	0.676
1.60	5	44.11	1.280	1.429	85.03	2.798	0.681
1.60	6	45.34	1.345	1.393	83.97	2.787	0.686
1.60	7	46.65	1.412	1.357	82.86	2.774	0.693
1.60	8	48.03	1.484	1.320	81.69	2.758	0.702
1.60	9	49.51	1.561	1.281	80.45	2.738	0.712
1.60	10	51.12	1.643	1.240	79.10	2.713	0.725

(continued)

Table A.3 (Continued)

Weak solution				Strong solution			
$M_1$	$\theta$	$\beta$	$p_2/p_1$	$M_2$	$\beta$	$p_2/p_1$	$M_2$
1.60	11	52.88	1.732	1.196	77.61	2.682	0.741
1.60	12	54.89	1.832	1.148	75.90	2.643	0.761
1.60	13	57.28	1.947	1.094	73.82	2.588	0.789
1.60	14	60.54	2.097	1.023	70.90	2.500	0.832
1.65	0	37.28	0.999	1.651	89.98	3.010	0.654
1.65	1	38.27	1.052	1.616	89.10	3.009	0.654
1.65	2	39.27	1.106	1.582	88.20	3.006	0.656
1.65	3	40.30	1.162	1.548	87.29	3.002	0.658
1.65	4	41.38	1.221	1.514	86.37	2.997	0.661
1.65	5	42.50	1.283	1.479	85.42	2.989	0.665
1.65	6	43.67	1.347	1.444	84.45	2.980	0.670
1.65	7	44.89	1.415	1.409	83.44	2.968	0.676
1.65	8	46.18	1.487	1.372	82.39	2.954	0.683
1.65	9	47.55	1.562	1.334	81.28	2.937	0.692
1.65	10	49.01	1.643	1.295	80.10	2.916	0.703
1.65	11	50.58	1.729	1.254	78.83	2.890	0.716
1.65	12	52.31	1.822	1.210	77.41	2.859	0.732
1.65	13	54.26	1.926	1.163	75.80	2.818	0.752
1.65	14	56.54	2.044	1.109	73.86	2.764	0.778
1.65	15	59.52	2.192	1.042	71.25	2.681	0.818
1.70	0	36.01	0.999	1.701	89.98	3.205	0.641
1.70	1	36.96	1.052	1.666	89.17	3.204	0.641
1.70	2	37.93	1.107	1.632	88.33	3.202	0.642
1.70	3	38.92	1.164	1.598	87.48	3.198	0.644
1.70	4	39.96	1.224	1.564	86.62	3.193	0.647
1.70	5	41.03	1.286	1.529	85.75	3.186	0.650
1.70	6	42.15	1.351	1.495	84.85	3.178	0.655
1.70	7	43.31	1.420	1.459	83.93	3.167	0.660
1.70	8	44.53	1.491	1.423	82.97	3.154	0.667
1.70	9	45.81	1.567	1.386	81.97	3.139	0.675
1.70	10	47.17	1.647	1.348	80.91	3.121	0.684
1.70	11	48.61	1.731	1.309	79.78	3.099	0.695
1.70	12	50.17	1.822	1.267	78.56	3.072	0.708
1.70	13	51.87	1.919	1.233	77.21	3.040	0.724
1.70	14	53.77	2.027	1.176	75.67	2.998	0.744
1.70	15	55.98	2.150	1.122	73.84	2.944	0.770
1.70	16	58.79	2.300	1.057	71.43	2.863	0.808
1.70	17	64.61	2.585	0.933	65.99	2.647	0.905
1.75	0	34.83	0.999	1.751	89.98	3.406	0.628

(continued)

Table A.3 (Continued)

Weak solution				Strong solution			
$M_1$	$\theta$	$\beta$	$p_2/p_1$	$M_2$	$\beta$	$p_2/p_1$	$M_2$
1.75	1	35.76	1.053	1.716	89.22	3.406	0.628
1.75	2	36.69	1.109	1.682	88.43	3.404	0.629
1.75	3	37.65	1.167	1.648	87.64	3.400	0.631
1.75	4	38.65	1.227	1.613	86.84	3.395	0.634
1.75	5	39.68	1.290	1.579	86.03	3.389	0.637
1.75	6	40.76	1.356	1.544	85.19	3.381	0.641
1.75	7	41.87	1.425	1.509	84.34	3.361	0.646
1.75	8	43.04	1.497	1.473	83.45	3.360	0.652
1.75	9	44.25	1.573	1.437	82.53	3.349	0.659
1.75	10	45.53	1.653	1.400	81.57	3.329	0.667
1.75	11	46.88	1.737	1.361	80.55	3.310	0.677
1.75	12	48.32	1.826	1.321	79.47	3.287	0.688
1.75	13	49.86	1.922	1.279	78.29	3.259	0.701
1.75	14	51.55	2.024	1.235	76.99	3.225	0.718
1.75	15	53.42	2.137	1.187	75.51	3.183	0.738
1.75	16	55.59	2.265	1.133	73.76	3.127	0.763
1.75	17	58.30	2.419	1.068	71.48	3.046	0.800
1.75	18	62.94	2.667	0.965	67.27	2.873	0.877
1.80	0	33.73	0.998	1.801	89.98	3.613	0.617
1.80	1	34.63	1.054	1.766	89.27	3.613	0.617
1.80	2	35.54	1.110	1.731	88.53	3.611	0.618
1.80	3	36.48	1.169	1.697	87.78	3.608	0.619
1.80	4	37.44	1.231	1.662	87.03	3.603	0.622
1.80	5	38.44	1.295	1.628	86.27	3.597	0.625
1.80	6	39.48	1.361	1.593	85.49	3.590	0.628
1.80	7	40.56	1.431	1.558	84.69	3.581	0.633
1.80	8	41.67	1.504	1.523	83.87	3.570	0.638
1.80	9	42.84	1.581	1.486	83.02	3.557	0.644
1.80	10	44.06	1.661	1.449	82.13	3.542	0.652
1.80	11	45.34	1.745	1.412	81.20	3.525	0.660
1.80	12	46.69	1.834	1.373	80.22	3.504	0.670
1.80	13	48.12	1.929	1.332	79.16	3.480	0.682
1.80	14	49.66	2.029	1.290	78.02	3.450	0.696
1.80	15	51.34	2.138	1.245	76.76	3.415	0.712
1.80	16	53.20	2.257	1.196	75.33	3.371	0.733
1.80	17	55.34	2.391	1.142	73.62	3.313	0.759
1.80	18	57.99	2.551	1.077	71.42	3.230	0.796
1.80	19	62.30	2.797	0.977	67.58	3.063	0.867
1.85	0	32.70	0.998	1.851	89.98	3.826	0.606

(continued)

Table A.3 (Continued)

Weak solution				Strong solution			
$M_1$	$\theta$	$\beta$	$p_2/p_1$	$M_2$	$\beta$	$p_2/p_1$	$M_2$
1.85	1	33.58	1.055	1.815	89.31	3.826	0.606
1.85	2	34.47	1.112	1.781	88.61	3.824	0.607
1.85	3	35.38	1.172	1.746	87.91	3.821	0.608
1.85	4	36.32	1.234	1.711	87.20	3.817	0.610
1.85	5	37.30	1.299	1.677	86.48	3.811	0.613
1.85	6	38.30	1.367	1.642	85.74	3.704	0.617
1.85	7	39.34	1.438	1.607	84.99	3.796	0.621
1.85	8	40.42	1.512	1.571	84.22	3.786	0.626
1.85	9	41.55	1.590	1.535	83.43	3.774	0.631
1.85	10	42.72	1.671	1.498	82.61	3.760	0.638
1.85	11	43.94	1.756	1.461	81.75	3.744	0.646
1.85	12	45.22	1.845	1.422	80.85	3.725	0.655
1.85	13	46.58	1.940	1.383	79.89	3.703	0.665
1.85	14	48.00	2.039	1.341	78.86	3.677	0.677
1.85	15	49.56	2.146	1.298	77.75	3.646	0.692
1.85	16	51.23	2.261	1.252	76.51	3.609	0.709
1.85	17	53.09	2.386	1.203	75.11	3.562	0.729
1.85	18	55.23	2.527	1.148	73.44	3.502	0.756
1.85	19	67.87	2.696	1.082	71.28	3.415	0.793
1.85	20	62.10	2.952	0.982	67.54	3.244	0.865
1.90	0	31.73	0.998	1.901	89.98	4.045	0.596
1.90	1	32.60	1.056	1.865	89.34	4.044	0.596
1.90	2	33.47	1.114	1.830	88.68	4.043	0.597
1.90	3	34.36	1.175	1.995	88.01	4.040	0.598
1.90	4	35.28	1.238	1.760	87.34	4.036	0.600
1.90	5	36.23	1.304	1.725	86.66	4.031	0.603
1.90	6	37.21	1.373	1.690	85.97	4.024	0.606
1.90	7	38.22	1.446	1.655	85.26	4.016	0.610
1.90	8	39.27	1.521	1.619	84.54	4.007	0.614
1.90	9	30.39	1.600	1.583	83.79	3.996	0.620
1.90	10	41.49	1.682	1.546	83.02	3.983	0.626
1.90	11	42.67	1.768	1.509	82.22	3.968	0.633
1.90	12	43.90	1.858	1.471	81.38	3.950	0.641
1.90	13	45.19	1.953	1.432	80.50	3.930	0.650
1.90	14	46.55	2.053	1.391	79.57	3.907	0.661
1.90	15	48.00	2.159	1.349	78.56	3.879	0.674
1.90	16	49.54	2.272	1.305	77.47	3.847	0.688
1.90	17	51.23	2.393	1.258	76.25	3.807	0.706
1.90	18	53.10	2.526	1.208	74.86	3.758	0.727

(continued)

Table A.3 (Continued)

Weak solution				Strong solution			
$M_1$	$\theta$	$\beta$	$p_2/p_1$	$M_2$	$\beta$	$p_2/p_1$	$M_2$
1.90	19	55.24	2.676	1.151	73.21	3.693	0.755
1.90	20	57.90	2.856	1.084	71.06	3.601	0.794
1.90	21	62.25	3.132	0.979	67.22	3.414	0.869
1.95	0	30.83	0.998	1.951	89.98	4.270	0.586
1.95	1	31.68	1.057	1.914	89.37	4.269	0.586
1.95	2	32.53	1.116	1.879	88.74	4.267	0.587
1.95	3	33.40	1.178	1.844	88.11	4.265	0.589
1.95	4	34.30	1.242	1.809	87.47	4.261	0.590
1.95	5	35.23	1.310	1.773	86.82	4.256	0.593
1.95	6	36.19	1.380	1.738	86.17	4.250	0.596
1.95	7	37.18	1.454	1.702	85.50	4.242	0.599
1.95	8	38.20	1.530	1.667	84.81	4.233	0.604
1.95	9	39.26	1.610	1.630	84.11	4.223	0.609
1.95	10	40.36	1.694	1.594	83.38	4.211	0.614
1.95	11	41.50	1.781	1.557	82.63	4.197	0.621
1.95	12	42.69	1.873	1.519	81.85	4.180	0.628
1.95	13	43.93	1.968	1.480	81.03	4.162	0.637
1.95	14	45.23	2.069	1.440	80.17	4.140	0.647
1.95	15	46.60	2.175	1.398	79.25	4.115	0.658
1.95	16	48.06	2.288	1.355	78.25	4.086	0.671
1.95	17	49.62	2.408	1.310	77.17	4.051	0.686
1.95	18	51.32	2.537	1.262	75.97	4.009	0.705
1.95	19	53.21	2.678	1.210	74.58	3.956	0.727
1.95	20	55.38	2.838	1.152	72.93	3.887	0.756
1.95	21	58.10	3.030	1.082	70.74	3.787	0.796
1.95	22	62.85	3.346	0.966	66.52	3.565	0.883
2.00	0	29.98	0.998	2.001	89.99	4.500	0.577
2.00	1	30.81	1.058	1.964	89.40	4.499	0.578
2.00	2	31.65	1.118	1.928	88.80	4.498	0.578
2.00	3	32.51	1.181	1.892	88.19	4.495	0.580
2.00	4	33.39	1.247	1.857	87.58	4.492	0.581
2.00	5	34.30	1.315	1.821	86.97	4.487	0.584
2.00	6	35.24	1.387	1.786	86.34	4.481	0.586
2.00	7	36.21	1.462	1.750	85.70	4.474	0.590
2.00	8	37.21	1.540	1.714	85.05	4.465	0.594
2.00	9	38.24	1.621	1.677	84.39	4.455	0.598
2.00	10	39.31	1.707	1.641	83.70	4.444	0.604
2.00	11	40.42	1.795	1.603	82.99	4.431	0.610
2.00	12	41.58	1.888	1.565	82.26	4.415	0.617

(continued)

Table A.3 (Continued)

Weak solution				Strong solution			
$M_1$	$\theta$	$\beta$	$p_2/p_1$	$M_2$	$\beta$	$p_2/p_1$	$M_2$
2.00	13	42.78	1.986	1.526	81.49	4.398	0.625
2.00	14	44.03	2.087	1.487	80.69	4.378	0.634
2.00	15	45.34	2.195	1.446	79.83	4.355	0.644
2.00	16	46.73	2.307	1.403	78.92	4.328	0.656
2.00	17	48.20	2.427	1.359	77.94	4.296	0.669
2.00	18	49.79	2.554	1.313	76.86	4.259	0.685
2.00	19	51.51	2.692	1.264	75.66	4.214	0.704
2.00	20	53.42	2.843	1.210	74.27	4.157	0.728
2.00	21	55.64	3.014	1.150	72.59	4.082	0.758
2.00	22	58.46	3.223	1.076	70.33	3.971	0.802
2.10	0	28.42	0.998	2.101	89.99	4.978	0.561
2.10	1	29.22	1.060	2.063	89.45	4.978	0.561
2.10	2	30.03	1.122	2.026	88.90	4.976	0.562
2.10	3	30.87	1.187	1.989	88.34	4.974	0.563
2.10	4	31.72	1.256	1.953	87.78	4.971	0.565
2.10	5	32.61	1.327	1.917	87.21	4.966	0.567
2.10	6	33.51	1.402	1.880	86.64	4.961	0.569
2.10	7	34.45	1.480	1.844	86.06	4.954	0.572
2.10	8	35.41	1.561	1.807	85.47	4.946	0.576
2.10	9	36.41	1.646	1.770	84.86	4.937	0.580
2.10	10	37.43	1.734	1.733	84.24	4.926	0.585
2.10	11	38.49	1.827	1.695	83.60	4.914	0.590
2.10	12	39.59	1.923	1.656	82.94	4.901	0.596
2.10	13	40.73	2.024	1.617	82.26	4.885	0.603
2.10	14	41.91	2.129	1.578	81.54	4.867	0.611
2.10	15	43.14	2.239	1.537	80.79	4.847	0.620
2.10	16	44.43	2.355	1.495	80.00	4.823	0.630
2.10	17	45.78	2.476	1.452	79.16	4.796	0.641
2.10	18	47.21	2.604	1.408	78.26	4.765	0.654
2.10	19	48.73	2.740	1.361	77.28	4.729	0.669
2.10	20	50.36	2.885	1.312	76.19	4.685	0.687
2.10	21	52.16	3.042	1.260	74.96	4.632	0.708
2.10	22	54.17	3.215	1.202	73.52	4.564	0.735
2.10	23	56.55	3.415	1.136	71.72	4.472	0.770
2.10	24	59.77	3.674	1.049	69.10	4.324	0.824
2.20	0	27.01	0.998	2.201	89.99	5.480	0.547
2.20	1	27.80	1.062	2.162	89.49	5.480	0.547
2.20	2	28.59	1.127	2.124	88.98	5.478	0.548
2.20	3	29.40	1.194	2.086	88.46	5.476	0.549

(continued)



Table A.3 (Continued)

Weak solution				Strong solution			
$M_1$	$\theta$	$\beta$	$p_2/p_1$	$M_2$	$\beta$	$p_2/p_1$	$M_2$
2.20	4	30.24	1.265	2.049	87.94	5.473	0.550
2.20	5	31.10	1.340	2.011	87.42	5.468	0.552
2.20	6	31.98	1.417	1.974	86.89	5.463	0.554
2.20	7	32.89	1.498	1.936	86.35	5.457	0.557
2.20	8	33.83	1.583	1.899	85.80	5.450	0.561
2.20	9	34.79	1.672	1.861	85.24	5.441	0.564
2.20	10	35.79	1.764	1.823	84.67	5.431	0.569
2.20	11	36.81	1.860	1.784	84.09	5.420	0.573
2.20	12	37.87	1.961	1.745	83.48	5.407	0.579
2.20	13	38.96	2.066	1.706	82.86	5.393	0.585
2.20	14	40.10	2.176	1.666	82.22	5.376	0.592
2.20	15	41.27	2.290	1.625	81.55	5.358	0.600
2.20	16	42.29	2.409	1.583	80.84	5.337	0.609
2.20	17	43.76	2.535	1.540	80.10	5.313	0.618
2.20	18	45.09	2.666	1.496	79.31	5.286	0.630
2.20	19	46.49	2.804	1.451	78.47	5.254	0.642
2.20	20	47.98	2.949	1.404	77.55	5.217	0.657
2.20	21	49.56	3.104	1.354	76.55	5.174	0.674
2.20	22	51.28	3.270	1.301	75.42	5.122	0.694
2.20	23	53.18	3.451	1.244	74.13	5.057	0.718
2.20	24	55.36	3.655	1.181	72.56	4.973	0.749
2.20	25	58.05	3.899	1.104	70.49	4.850	0.793
2.20	26	62.69	4.291	0.980	66.48	4.581	0.885
2.30	0	25.75	0.998	2.301	89.99	6.005	0.534
2.30	1	26.52	1.064	2.260	89.52	6.005	0.535
2.30	2	27.29	1.131	2.221	89.04	6.003	0.535
2.30	3	28.09	1.201	2.182	88.56	6.001	0.536
2.30	4	28.91	1.275	2.144	88.07	5.998	0.537
2.30	5	29.75	1.353	2.105	87.58	5.994	0.599
2.30	6	30.61	1.434	2.067	87.09	5.989	0.541
2.30	7	31.50	1.518	2.028	86.59	5.983	0.544
2.30	8	32.42	1.607	1.990	86.08	5.976	0.547
2.30	9	33.36	1.699	1.951	85.56	5.968	0.550
2.30	10	34.33	1.796	1.912	85.03	5.959	0.554
2.30	11	35.33	1.897	1.872	84.49	5.948	0.559
2.30	12	36.35	2.002	1.833	83.93	5.936	0.564
2.30	13	37.42	2.112	1.792	83.36	5.922	0.569
2.30	14	38.51	2.226	1.751	82.77	5.907	0.576
2.30	15	39.64	2.345	1.710	82.15	5.890	0.583

(continued)

Table A.3 (Continued)

Weak solution				Strong solution			
$M_1$	$\theta$	$\beta$	$p_2/p_1$	$M_2$	$\beta$	$p_2/p_1$	$M_2$
2.30	16	40.82	2.470	1.668	81.51	5.870	0.591
2.30	17	42.03	2.600	1.625	80.84	5.849	0.599
2.30	18	43.30	2.736	1.580	80.14	5.824	0.609
2.30	19	44.62	2.878	1.535	79.39	5.796	0.620
2.30	20	46.01	3.028	1.488	78.58	5.763	0.633
2.30	21	47.47	3.185	1.440	77.72	5.726	0.647
2.30	22	49.03	3.351	1.389	76.77	5.682	0.663
2.30	23	50.70	3.529	1.336	75.72	5.629	0.683
2.30	24	52.54	3.721	1.279	74.51	5.565	0.706
2.30	25	54.61	3.934	1.216	73.09	5.482	0.735
2.30	26	57.08	4.182	1.143	71.27	5.368	0.774
2.30	27	60.55	4.513	1.044	68.46	5.173	0.839
2.40	0	24.60	0.998	2.401	89.99	6.553	0.523
2.40	1	25.36	1.066	2.359	89.55	6.553	0.523
2.40	2	26.12	1.136	2.318	89.10	6.552	0.524
2.40	3	26.90	1.209	2.278	88.64	6.550	0.525
2.40	4	27.70	1.286	2.238	88.18	6.547	0.526
2.40	5	28.53	1.366	2.199	87.72	6.543	0.528
2.40	6	29.38	1.450	2.159	87.26	6.538	0.530
2.40	7	30.25	1.539	2.119	86.79	6.532	0.532
2.40	8	31.15	1.631	2.079	86.31	6.525	0.535
2.40	9	32.07	1.728	2.040	85.82	6.518	0.538
2.40	10	33.02	1.829	1.999	85.33	6.509	0.542
2.40	11	34.00	1.935	1.959	84.82	6.499	0.546
2.40	12	35.01	2.045	1.918	84.30	6.487	0.550
2.40	13	36.04	2.160	1.877	83.77	6.474	0.556
2.40	14	37.11	2.280	1.835	83.22	6.460	0.561
2.40	15	38.21	2.405	1.793	82.65	6.443	0.568
2.40	16	39.35	2.535	1.750	82.06	6.425	0.575
2.40	17	40.53	2.671	1.706	81.45	6.405	0.583
2.40	18	41.75	2.813	1.661	80.80	6.382	0.592
2.40	19	43.02	2.961	1.616	80.12	6.356	0.602
2.40	20	44.34	3.115	1.569	79.40	6.326	0.613
2.40	21	45.72	3.277	1.521	78.63	6.292	0.625
2.40	22	47.17	3.448	1.471	77.80	6.253	0.640
2.40	23	48.72	3.628	1.419	76.90	6.208	0.656
2.40	24	50.37	3.819	1.364	75.89	6.154	0.675
2.40	25	52.17	4.026	1.306	74.75	6.088	0.698
2.40	26	54.18	4.252	1.243	73.40	6.005	0.726

(continued)

Table A.3 (Continued)

Weak solution				Strong solution			
$M_1$	$\theta$	$\beta$	$p_2/p_1$	$M_2$	$\beta$	$p_2/p_1$	$M_2$
2.40	27	56.54	4.511	1.170	71.72	5.892	0.763
2.40	28	59.65	4.838	1.078	69.29	5.713	0.820
2.50	0	23.56	0.998	2.501	89.99	7.125	0.513
2.50	1	24.30	1.068	2.457	89.57	7.125	0.513
2.50	2	25.05	1.140	2.415	89.14	7.123	0.514
2.50	3	25.82	1.216	2.374	88.71	7.121	0.514
2.50	4	26.61	1.296	2.333	88.28	7.118	0.516
2.50	5	27.42	1.380	2.292	87.84	7.115	0.517
2.50	6	28.26	1.468	2.251	87.40	7.110	0.519
2.50	7	29.12	1.560	2.210	86.96	7.104	0.521
2.50	8	30.01	1.657	2.169	86.50	7.098	0.524
2.50	9	30.92	1.758	2.127	86.05	7.090	0.527
2.50	10	31.85	1.864	2.086	85.58	7.082	0.530
2.50	11	32.81	1.974	2.044	85.10	7.072	0.534
2.50	12	33.80	2.090	2.002	84.61	7.061	0.539
2.50	13	34.82	2.211	1.960	84.11	7.048	0.544
2.50	14	35.87	2.336	1.917	83.60	7.034	0.549
2.50	15	36.95	2.467	1.874	83.07	7.019	0.555
2.50	16	38.06	2.604	1.830	82.52	7.001	0.562
2.50	17	39.20	2.746	1.785	81.95	6.982	0.569
2.50	18	40.39	2.895	1.739	81.35	6.960	0.577
2.50	19	41.62	3.049	1.693	80.73	6.936	0.586
2.50	20	42.89	3.211	1.646	80.07	6.908	0.596
2.50	21	44.22	3.379	1.597	79.37	6.877	0.607
2.50	22	45.60	3.556	1.548	78.63	6.841	0.620
2.50	23	47.06	3.741	1.496	77.82	6.800	0.634
2.50	24	48.60	3.936	1.443	76.94	6.753	0.651
2.50	25	50.25	4.143	1.387	75.96	6.696	0.670
2.50	26	52.04	4.365	1.327	74.86	6.627	0.693
2.50	27	54.02	4.609	1.262	73.56	6.541	0.721
2.50	28	56.33	4.884	1.189	71.95	6.425	0.757
2.50	29	59.31	5.225	1.098	69.68	6.246	0.812
2.60	0	22.60	0.998	2.601	89.99	7.720	0.504
2.60	1	23.34	1.071	2.556	89.59	7.720	0.504
2.60	2	24.07	1.145	2.512	89.18	7.718	0.505
2.60	3	24.83	1.224	2.469	88.77	7.716	0.505
2.60	4	25.61	1.307	2.427	88.36	7.714	0.506
2.60	5	26.42	1.394	2.384	87.95	7.710	0.508
2.60	6	27.24	1.486	2.342	87.53	7.705	0.510

(continued)

Table A.3 (Continued)

Weak solution				Strong solution			
$M_1$	$\theta$	$\beta$	$p_2/p_1$	$M_2$	$\beta$	$p_2/p_1$	$M_2$
2.60	7	28.09	1.582	2.299	87.10	7.700	0.512
2.60	8	28.97	1.683	2.257	86.67	7.693	0.514
2.60	9	29.87	1.789	2.214	86.24	7.686	0.517
2.60	10	30.79	1.900	2.172	85.79	7.678	0.520
2.60	11	31.74	2.016	2.129	85.34	7.668	0.524
2.60	12	32.71	2.137	2.085	84.88	7.657	0.528
2.60	13	33.72	2.263	2.041	84.41	7.645	0.533
2.60	14	34.75	2.395	1.997	83.92	7.632	0.538
2.60	15	35.81	2.533	1.953	83.42	7.616	0.543
2.60	16	36.90	2.677	1.908	82.91	7.600	0.550
2.60	17	38.03	2.826	1.862	82.37	7.581	0.557
2.60	18	39.19	2.982	1.815	81.82	7.560	0.564
2.60	19	40.38	3.144	1.768	81.24	7.537	0.572
2.60	20	41.62	3.313	1.720	80.63	7.511	0.582
2.60	21	42.91	3.489	1.671	79.98	7.481	0.592
2.60	22	44.24	3.672	1.621	79.30	7.448	0.604
2.60	23	45.64	3.864	1.569	78.57	7.410	0.616
2.60	24	47.10	4.066	1.516	77.78	7.367	0.631
2.60	25	48.65	4.278	1.460	76.92	7.316	0.648
2.60	26	50.31	4.503	1.403	75.96	7.255	0.667
2.60	27	52.10	4.744	1.341	74.87	7.182	0.690
2.60	28	54.09	5.007	1.274	73.59	7.091	0.719
2.60	29	56.39	5.304	1.199	72.01	6.967	0.756
2.60	30	59.35	5.670	1.106	69.78	6.778	0.811
2.70	0	21.72	0.998	2.701	89.99	8.338	0.496
2.70	1	22.44	1.073	2.654	89.61	8.338	0.496
2.70	2	23.17	1.150	2.609	89.22	8.337	0.496
2.70	3	23.92	1.232	2.564	88.83	8.335	0.497
2.70	4	24.70	1.318	2.520	88.43	8.332	0.498
2.70	5	25.49	1.409	2.476	88.03	8.328	0.499
2.70	6	26.31	1.504	2.432	87.63	8.324	0.501
2.70	7	27.15	1.605	2.388	87.23	8.318	0.503
2.70	8	28.02	1.710	2.344	86.82	8.312	0.506
2.70	9	28.91	1.821	2.300	86.40	8.305	0.508
2.70	10	29.82	1.937	2.256	85.98	8.296	0.511
2.70	11	30.76	2.058	2.212	85.55	8.287	0.515
2.70	12	31.73	2.185	2.167	85.11	8.276	0.519
2.70	13	32.72	2.318	2.122	84.66	8.265	0.523
2.70	14	33.74	2.457	2.076	84.20	8.251	0.528

(continued)

Table A.3 (Continued)

Weak solution				Strong solution			
$M_1$	$\theta$	$\beta$	$p_2/p_1$	$M_2$	$\beta$	$p_2/p_1$	$M_2$
2.70	15	34.79	2.601	2.030	83.73	8.237	0.533
2.70	16	35.86	2.752	1.984	83.24	8.220	0.539
2.70	17	36.97	2.909	1.937	82.74	8.202	0.546
2.70	18	38.11	3.073	1.889	82.21	8.182	0.553
2.70	19	39.28	3.243	1.841	81.67	8.160	0.560
2.70	20	40.50	3.420	1.792	81.10	8.135	0.569
2.70	21	41.75	3.604	1.742	80.50	8.106	0.579
2.70	22	43.05	3.796	1.691	79.86	8.075	0.589
2.70	23	44.40	3.997	1.638	79.19	8.039	0.601
2.70	24	45.81	4.206	1.585	78.47	7.998	0.614
2.70	25	47.29	4.425	1.530	77.69	7.951	0.630
2.70	26	48.85	4.656	1.472	76.83	7.897	0.647
2.70	27	50.52	4.900	1.412	75.88	7.832	0.667
2.70	28	52.33	5.162	1.349	74.79	7.753	0.691
2.70	29	54.35	5.449	1.280	73.51	7.653	0.720
2.70	30	56.69	5.773	1.202	71.92	7.519	0.759
2.70	31	59.72	6.176	1.104	69.63	7.307	0.817
2.80	0	20.91	0.999	2.801	89.99	8.980	0.488
2.80	1	21.62	1.075	2.752	89.63	8.980	0.488
2.80	2	22.34	1.155	2.706	89.25	8.978	0.489
2.80	3	23.09	1.240	2.659	88.87	8.976	0.489
2.80	4	23.85	1.329	2.613	88.49	8.974	0.491
2.80	5	24.64	1.423	2.568	88.11	8.970	0.492
2.80	6	25.46	1.523	2.522	87.73	8.966	0.493
2.80	7	26.29	1.628	2.477	87.34	8.960	0.495
2.80	8	27.15	1.738	2.431	86.95	8.954	0.498
2.80	9	28.03	1.854	2.386	86.55	8.947	0.500
2.80	10	28.94	1.975	2.340	86.14	8.939	0.503
2.80	11	29.87	2.102	2.294	85.73	8.929	0.507
2.80	12	30.83	2.236	2.248	85.31	8.919	0.510
2.80	13	31.81	2.375	2.201	84.88	8.907	0.514
2.80	14	32.82	2.520	2.154	84.44	8.894	0.519
2.80	15	33.86	2.672	2.107	83.99	8.880	0.524
2.80	16	34.92	2.831	2.059	83.53	8.864	0.530
2.80	17	36.02	2.996	2.010	83.05	8.846	0.536
2.80	18	37.14	3.168	1.961	82.55	8.826	0.543
2.80	19	38.30	3.346	1.911	82.04	8.804	0.550
2.80	20	39.49	3.532	1.861	81.50	8.780	0.558
2.80	21	40.72	3.726	1.810	80.93	8.753	0.567

(continued)

Table A.3 (Continued)

Weak solution				Strong solution			
$M_1$	$\theta$	$\beta$	$p_2/p_1$	$M_2$	$\beta$	$p_2/p_1$	$M_2$
2.80	22	41.99	3.927	1.758	80.34	8.722	0.577
2.80	23	43.31	4.136	1.705	79.71	8.688	0.588
2.80	24	44.68	4.355	1.651	79.04	8.649	0.600
2.80	25	46.10	4.583	1.595	78.33	8.605	0.614
2.80	26	47.60	4.822	1.538	77.55	8.554	0.630
2.80	27	49.19	5.073	1.479	76.69	8.495	0.648
2.80	28	50.89	5.340	1.416	75.73	8.424	0.668
2.80	29	52.73	5.625	1.350	74.63	8.337	0.693
2.80	30	54.79	5.938	1.278	73.33	8.227	0.724
2.80	31	57.20	6.295	1.197	71.68	8.076	0.766
2.80	32	60.43	6.752	1.091	69.21	7.828	0.831
2.90	0	20.15	0.998	2.901	89.99	9.645	0.481
2.90	1	20.86	1.078	2.851	89.64	9.645	0.482
2.90	2	21.58	1.160	2.802	89.28	9.643	0.482
2.90	3	22.32	1.248	2.754	88.91	9.641	0.483
2.90	4	23.08	1.341	2.706	88.55	9.639	0.484
2.90	5	23.86	1.439	2.659	88.18	9.635	0.485
2.90	6	24.67	1.542	2.612	87.81	9.631	0.486
2.90	7	25.50	1.651	2.565	87.44	9.625	0.488
2.90	8	26.35	1.766	2.518	87.06	9.619	0.491
2.90	9	27.23	1.887	2.470	86.67	9.612	0.493
2.90	10	28.13	2.014	2.423	86.28	9.604	0.496
2.90	11	29.06	2.148	2.375	85.89	9.595	0.499
2.90	12	30.01	2.287	2.327	85.49	9.584	0.503
2.90	13	30.98	2.433	2.279	85.07	9.573	0.507
2.90	14	31.99	2.586	2.230	84.65	9.560	0.511
2.90	15	33.01	2.746	2.181	84.22	9.545	0.516
2.90	16	34.07	2.912	2.132	83.78	9.530	0.521
2.90	17	35.15	3.086	2.082	83.32	9.512	0.527
2.90	18	36.26	3.266	2.031	82.85	9.493	0.533
2.90	19	37.41	3.454	1.980	82.36	9.471	0.540
2.90	20	38.58	3.649	1.928	81.85	9.447	0.548
2.90	21	39.80	3.853	1.876	81.31	9.421	0.557
2.90	22	41.04	4.064	1.823	80.70	9.391	0.566
2.90	23	42.34	4.283	1.769	80.16	9.358	0.576
2.90	24	43.67	4.512	1.714	79.54	9.321	0.588
2.90	25	45.06	4.750	1.658	78.87	9.279	0.601
2.90	26	46.51	4.998	1.600	78.14	9.231	0.615
2.90	27	48.04	5.258	1.540	77.36	9.175	0.631

(continued)

Table A.3 (Continued)

Weak solution				Strong solution			
$M_1$	$\theta$	$\beta$	$p_2/p_1$	$M_2$	$\beta$	$p_2/p_1$	$M_2$
2.90	28	49.65	5.533	1.479	76.49	9.109	0.650
2.90	29	51.39	5.823	1.414	75.52	9.031	0.672
2.90	30	53.27	6.136	1.345	74.39	8.935	0.699
2.90	31	55.40	6.480	1.270	73.04	8.810	0.732
2.90	32	57.93	6.879	1.183	71.29	8.635	0.777
2.90	33	61.57	7.420	1.063	68.44	8.319	0.855
3.00	0	19.45	0.998	3.001	89.99	10.333	0.475
3.00	1	20.16	1.080	2.949	89.65	10.333	0.475
3.00	2	20.87	1.165	2.898	89.30	10.332	0.476
3.00	3	21.60	1.256	2.848	88.95	10.330	0.476
3.00	4	22.35	1.352	2.799	88.60	10.327	0.477
3.00	5	23.13	1.454	2.750	88.24	10.323	0.479
3.00	6	23.94	1.562	2.701	87.88	10.319	0.480
3.00	7	24.76	1.675	2.652	87.52	10.314	0.482
3.00	8	25.61	1.795	2.603	87.16	10.307	0.484
3.00	9	26.49	1.922	2.554	86.79	10.300	0.486
3.00	10	27.38	2.054	2.505	86.41	10.292	0.489
3.00	11	28.30	2.194	2.456	86.03	10.283	0.492
3.00	12	29.25	2.340	2.406	85.64	10.273	0.496
3.00	13	30.22	2.494	2.356	85.24	10.261	0.500
3.00	14	31.22	2.654	2.306	84.84	10.248	0.504
3.00	15	32.24	2.821	2.255	84.42	10.234	0.508
3.00	16	33.29	2.996	2.204	84.00	10.218	0.514
3.00	17	34.36	3.179	2.152	83.56	10.201	0.519
3.00	18	35.47	3.368	2.100	83.11	10.182	0.525
3.00	19	36.60	3.566	2.047	82.64	10.161	0.532
3.00	20	37.76	3.771	1.994	82.15	10.137	0.539
3.00	21	38.96	3.984	1.940	81.64	10.111	0.547
3.00	22	40.19	4.206	1.886	81.11	10.082	0.556
3.00	23	41.46	4.436	1.831	80.55	10.050	0.566
3.00	24	42.78	4.676	1.774	79.96	10.014	0.577
3.00	25	44.14	4.925	1.717	79.33	9.973	0.589
3.00	26	45.55	5.184	1.659	78.65	9.927	0.602
3.00	27	47.03	5.455	1.599	77.92	9.874	0.617
3.00	28	48.59	5.739	1.537	77.13	9.812	0.635
3.00	29	50.24	6.038	1.473	76.24	9.739	0.654
3.00	30	52.01	6.356	1.406	75.24	9.652	0.678
3.00	31	53.96	6.699	1.334	74.07	9.542	0.706
3.00	32	56.18	7.081	1.254	72.64	9.399	0.743

(continued)

Table A.3 (Continued)

Weak solution				Strong solution			
$M_1$	$\theta$	$\beta$	$p_2/p_1$	$M_2$	$\beta$	$p_2/p_1$	$M_2$
3.00	33	58.91	7.533	1.160	70.71	9.188	0.794
3.00	34	63.67	8.267	1.003	66.75	8.697	0.908
3.10	0	18.80	0.998	3.102	89.99	11.045	0.470
3.10	1	19.50	1.083	3.047	89.66	11.045	0.470
3.10	2	20.20	1.171	2.994	89.32	11.043	0.470
3.10	3	20.93	1.264	2.942	88.98	11.041	0.471
3.10	4	21.68	1.364	2.891	88.64	11.039	0.472
3.10	5	22.46	1.470	2.840	88.30	11.035	0.473
3.10	6	23.26	1.581	2.789	87.95	11.031	0.474
3.10	7	24.08	1.700	2.739	87.60	11.025	0.476
3.10	8	24.93	1.825	2.688	87.24	11.019	0.478
3.10	9	25.80	1.957	2.637	86.89	11.012	0.480
3.10	10	26.69	2.096	2.586	86.52	11.004	0.483
3.10	11	27.61	2.241	2.535	86.15	10.994	0.486
3.10	12	28.55	2.395	2.484	85.78	10.984	0.489
3.10	13	29.52	2.555	2.432	85.39	10.973	0.493
3.10	14	30.51	2.724	2.380	85.00	10.960	0.497
3.10	15	31.53	2.899	2.327	84.60	10.946	0.502
3.10	16	32.57	3.083	2.274	84.19	10.930	0.507
3.10	17	33.64	3.274	2.221	83.77	10.913	0.512
3.10	18	34.74	3.474	2.167	83.33	10.894	0.518
3.10	19	35.86	3.681	2.113	82.88	10.873	0.524
3.10	20	37.02	3.897	2.058	82.42	10.850	0.531
3.10	21	38.20	4.121	2.003	81.93	10.824	0.539
3.10	22	39.42	4.354	1.947	81.42	10.795	0.548
3.10	23	40.67	4.596	1.890	80.89	10.764	0.557
3.10	24	41.97	4.847	1.833	80.33	10.728	0.567
3.10	25	43.31	5.108	1.775	79.73	10.688	0.578
3.10	26	44.69	5.379	1.715	79.09	10.643	0.591
3.10	27	46.14	5.661	1.655	78.41	10.592	0.605
3.10	28	47.65	5.956	1.593	77.67	10.533	0.621
3.10	29	49.24	6.265	1.529	76.85	10.465	0.639
3.10	30	50.93	6.592	1.462	75.94	10.383	0.661
3.10	31	52.77	6.940	1.392	74.90	10.284	0.686
3.10	32	54.80	7.319	1.316	73.66	10.158	0.717
3.10	33	57.15	7.747	1.230	72.11	9.987	0.758
3.10	34	60.20	8.276	1.124	69.87	9.717	0.820
3.20	0	18.19	0.998	3.202	89.99	11.780	0.464
3.20	1	18.89	1.085	3.145	89.67	11.780	0.464

(continued)



Table A.3 (Continued)

Weak solution				Strong solution			
$M_1$	$\theta$	$\beta$	$p_2/p_1$	$M_2$	$\beta$	$p_2/p_1$	$M_2$
3.20	2	19.59	1.176	3.090	89.34	11.778	0.465
3.20	3	20.31	1.273	3.036	89.01	11.776	0.466
3.20	4	21.06	1.376	2.983	88.68	11.774	0.466
3.20	5	21.83	1.485	2.930	88.34	11.770	0.468
3.20	6	22.63	1.602	2.878	88.01	11.765	0.469
3.20	7	23.45	1.725	2.825	87.67	11.760	0.471
3.20	8	24.29	1.855	2.773	87.32	11.754	0.473
3.20	9	25.16	1.993	2.720	86.97	11.747	0.475
3.20	10	26.05	2.138	2.667	86.62	11.738	0.478
3.20	11	26.97	2.290	2.614	86.26	11.729	0.480
3.20	12	27.91	2.451	2.561	85.90	11.719	0.484
3.20	13	28.87	2.619	2.507	85.53	11.707	0.487
3.20	14	29.86	2.795	2.453	85.15	11.694	0.491
3.20	15	30.88	2.980	2.398	84.76	11.680	0.496
3.20	16	31.92	3.172	2.344	84.36	11.665	0.500
3.20	17	32.98	3.373	2.289	83.96	11.647	0.506
3.20	18	34.07	3.583	2.233	83.54	11.628	0.511
3.20	19	35.19	3.801	2.177	83.10	11.608	0.517
3.20	20	36.34	4.027	2.121	82.65	11.584	0.524
3.20	21	37.51	4.263	2.064	82.18	11.559	0.532
3.20	22	38.72	4.507	2.006	81.70	11.531	0.540
3.20	23	39.96	4.761	1.948	81.19	11.499	0.549
3.20	24	41.24	5.024	1.889	80.65	11.464	0.558
3.20	25	42.56	5.297	1.830	80.08	11.425	0.569
3.20	26	43.92	5.581	1.770	79.48	11.381	0.581
3.20	27	45.34	5.876	1.708	78.83	11.332	0.595
3.20	28	46.81	6.184	1.645	78.13	11.275	0.610
3.20	29	48.36	6.505	1.581	77.37	11.209	0.627
3.20	30	49.99	6.842	1.514	76.53	11.131	0.646
3.20	31	51.74	7.200	1.445	75.58	11.039	0.669
3.20	32	53.65	7.583	1.371	74.48	10.924	0.697
3.20	33	55.79	8.004	1.291	73.15	10.776	0.731
3.20	34	58.35	8.490	1.198	71.41	10.566	0.779
3.20	35	62.06	9.157	1.069	68.52	10.178	0.863
3.30	0	17.62	0.998	3.302	89.99	12.538	0.460
3.30	1	18.31	1.088	3.242	89.68	12.538	0.460
3.30	2	19.01	1.181	3.186	89.36	12.537	0.460
3.30	3	19.73	1.281	3.130	89.04	12.535	0.461
3.30	4	20.48	1.388	3.075	88.71	12.532	0.462

(continued)

Table A.3 (Continued)

Weak solution				Strong solution			
$M_1$	$\theta$	$\beta$	$p_2/p_1$	$M_2$	$\beta$	$p_2/p_1$	$M_2$
3.30	5	21.25	1.501	3.020	88.39	12.528	0.463
3.30	6	22.04	1.622	2.965	88.06	12.524	0.464
3.30	7	22.86	1.750	2.911	87.73	12.518	0.466
3.30	8	23.70	1.886	2.856	87.39	12.512	0.468
3.30	9	24.57	2.029	2.802	87.05	12.505	0.470
3.30	10	25.46	2.181	2.747	86.71	12.496	0.472
3.30	11	26.37	2.340	2.692	86.36	12.487	0.475
3.30	12	27.31	2.508	2.636	86.01	12.477	0.478
3.30	13	28.27	2.684	2.581	85.65	12.465	0.482
3.30	14	29.26	2.869	2.525	85.28	12.452	0.486
3.30	15	30.27	3.062	2.469	84.90	12.438	0.490
3.30	16	31.31	3.264	2.412	84.52	12.422	0.495
3.30	17	32.37	3.475	2.355	84.12	12.405	0.500
3.30	18	33.46	3.695	2.297	83.72	12.386	0.505
3.30	19	34.57	3.923	2.240	83.30	12.365	0.511
3.30	20	35.71	4.161	2.181	82.86	12.342	0.518
3.30	21	36.88	4.409	2.123	82.41	12.317	0.525
3.30	22	38.08	4.665	2.064	81.94	12.288	0.533
3.30	23	39.31	4.932	2.004	81.45	12.257	0.541
3.30	24	40.57	5.208	1.944	80.93	12.223	0.551
3.30	25	41.88	5.494	1.883	80.39	12.184	0.561
3.30	26	43.22	5.792	1.822	79.81	12.141	0.572
3.30	27	44.61	6.100	1.759	79.20	12.092	0.585
3.30	28	46.06	6.421	1.696	78.54	12.036	0.599
3.30	29	47.57	6.755	1.631	77.82	11.973	0.615
3.30	30	49.16	7.105	1.564	77.03	11.898	0.634
3.30	31	50.85	7.474	1.495	76.15	11.810	0.655
3.30	32	52.67	7.865	1.422	75.15	11.704	0.680
3.30	33	54.67	8.289	1.344	73.97	11.569	0.710
3.30	34	56.96	8.762	1.258	72.50	11.390	0.750
3.30	35	59.85	9.333	1.153	70.45	11.115	0.809
3.40	0	17.09	0.998	3.402	89.99	13.320	0.455
3.40	1	17.77	1.090	3.340	89.69	13.320	0.455
3.40	2	18.47	1.187	3.281	89.37	13.318	0.456
3.40	3	19.19	1.290	3.224	89.06	13.316	0.456
3.40	4	19.93	1.400	3.166	88.74	13.313	0.457
3.40	5	20.70	1.518	3.109	88.43	13.310	0.458
3.40	6	21.49	1.643	3.053	88.10	13.305	0.460
3.40	7	22.31	1.776	2.996	87.78	13.300	0.461

(continued)

Table A.3 (Continued)

Weak solution				Strong solution			
$M_1$	$\theta$	$\beta$	$p_2/p_1$	$M_2$	$\beta$	$p_2/p_1$	$M_2$
3.40	8	23.15	1.917	2.940	87.46	13.293	0.463
3.40	9	24.01	2.067	2.883	87.13	13.286	0.465
3.40	10	24.90	2.224	2.826	86.79	13.278	0.468
3.40	11	25.82	2.391	2.769	86.45	13.268	0.471
3.40	12	26.75	2.566	2.712	86.11	13.258	0.474
3.40	13	27.72	2.751	2.654	85.76	13.246	0.477
3.40	14	28.70	2.944	2.596	85.40	13.233	0.481
3.40	15	29.71	3.146	2.537	85.03	13.219	0.485
3.40	16	30.75	3.358	2.479	84.66	13.203	0.489
3.40	17	31.81	3.571	2.420	84.27	13.186	0.494
3.40	18	32.89	3.810	2.360	83.88	13.166	0.500
3.40	19	34.00	4.050	2.301	83.47	13.145	0.506
3.40	20	35.13	4.300	2.241	83.05	13.122	0.512
3.40	21	36.30	4.559	2.180	82.61	13.097	0.519
3.40	22	37.49	4.829	2.120	82.16	13.069	0.526
3.40	23	38.71	5.108	2.058	81.68	13.038	0.535
3.40	24	39.97	5.398	1.997	81.19	13.003	0.544
3.40	25	41.26	5.698	1.934	80.66	12.965	0.554
3.40	26	42.59	6.009	1.872	80.11	12.922	0.565
3.40	27	43.96	6.332	1.808	79.52	12.874	0.577
3.40	28	45.39	6.667	1.744	78.89	12.819	0.590
3.40	29	46.87	7.016	1.678	78.21	12.757	0.605
3.40	30	48.42	7.380	1.611	77.47	12.685	0.623
3.40	31	50.06	7.761	1.541	76.65	12.600	0.642
3.40	32	51.81	8.164	1.469	75.72	12.499	0.665
3.40	33	53.71	8.595	1.393	74.65	12.374	0.693
3.40	34	55.84	9.067	1.310	73.35	12.213	0.728
3.40	35	58.36	9.608	1.215	71.67	11.986	0.775
3.40	36	61.91	10.330	1.088	68.96	11.582	0.856
3.50	0	16.58	0.997	3.502	89.99	14.125	0.451
3.50	1	17.27	1.092	3.438	89.70	14.125	0.451
3.50	2	17.96	1.192	3.377	89.39	14.123	0.452
3.50	3	18.67	1.298	3.317	89.08	14.121	0.452
3.50	4	19.42	1.412	3.257	88.77	14.118	0.453
3.50	5	20.18	1.534	3.198	88.46	14.115	0.454
3.50	6	20.97	1.664	3.140	88.15	14.110	0.456
3.50	7	21.79	1.802	3.081	87.83	14.104	0.457
3.50	8	22.63	1.949	3.022	87.51	14.098	0.459
3.50	9	23.49	2.105	2.963	87.19	14.091	0.461

(continued)

Table A.3 (Continued)

Weak solution				Strong solution			
$M_1$	$\theta$	$\beta$	$p_2/p_1$	$M_2$	$\beta$	$p_2/p_1$	$M_2$
3.50	10	24.38	2.269	2.904	86.86	14.082	0.463
3.50	11	25.30	2.443	2.845	86.53	14.073	0.466
3.50	12	26.24	2.626	2.786	86.20	14.062	0.469
3.50	13	27.20	2.819	2.726	85.85	14.050	0.473
3.50	14	28.18	3.021	2.666	85.50	14.037	0.476
3.50	15	29.19	3.233	2.605	85.15	14.023	0.480
3.50	16	30.22	3.455	2.545	84.78	14.007	0.485
3.50	17	31.28	3.686	2.484	84.41	13.989	0.489
3.50	18	32.36	3.928	2.422	84.02	13.970	0.495
3.50	19	33.47	4.180	2.361	83.63	13.949	0.500
3.50	20	34.60	4.442	2.299	83.22	13.926	0.506
3.50	21	35.76	4.714	2.236	82.79	13.900	0.513
3.50	22	36.95	4.997	2.174	82.35	13.872	0.521
3.50	23	38.16	5.290	2.111	81.90	13.841	0.529
3.50	24	39.41	5.593	2.048	81.41	13.806	0.537
3.50	25	40.69	5.908	1.984	80.91	13.768	0.547
3.50	26	42.01	6.234	1.920	80.38	13.725	0.557
3.50	27	43.37	6.572	1.855	79.81	13.678	0.569
3.50	28	44.77	6.922	1.789	79.21	13.624	0.582
3.50	29	46.23	7.286	1.723	78.56	13.562	0.596
3.50	30	47.76	7.665	1.655	77.85	13.492	0.613
3.50	31	49.36	8.061	1.585	77.08	13.410	0.631
3.50	32	51.05	8.477	1.513	76.21	13.313	0.653
3.50	33	52.88	8.919	1.438	75.22	13.194	0.678
3.50	34	54.89	9.396	1.357	74.05	13.046	0.710
3.50	35	57.19	9.928	1.268	72.59	12.846	0.750
3.50	36	60.09	10.571	1.159	70.55	12.539	0.810
3.60	0	16.11	0.997	3.602	89.99	14.953	0.447
3.60	1	16.79	1.095	3.536	89.70	14.953	0.448
3.60	2	17.48	1.197	3.472	89.40	14.952	0.448
3.60	3	18.19	1.307	3.410	89.10	14.950	0.448
3.60	4	18.93	1.425	3.348	88.80	14.947	0.449
3.60	5	19.70	1.551	3.287	88.49	14.943	0.450
3.60	6	20.49	1.686	3.226	88.19	14.938	0.452
3.60	7	21.30	1.829	3.165	87.88	14.933	0.453
3.60	8	22.14	1.981	3.104	87.56	14.926	0.455
3.60	9	23.01	2.143	3.043	87.25	14.918	0.457
3.60	10	23.90	2.315	2.982	86.93	14.910	0.460
3.60	11	24.81	2.496	2.921	86.61	14.900	0.462

(continued)

Table A.3 (Continued)

Weak solution				Strong solution			
$M_1$	$\theta$	$\beta$	$p_2/p_1$	$M_2$	$\beta$	$p_2/p_1$	$M_2$
3.60	12	25.75	2.687	2.859	86.28	14.889	0.465
3.60	13	26.71	2.888	2.797	85.94	14.878	0.468
3.60	14	27.70	3.100	2.735	85.60	14.864	0.472
3.60	15	28.71	3.322	2.672	85.25	14.850	0.476
3.60	16	29.74	3.554	2.609	84.90	14.834	0.480
3.60	17	30.80	3.796	2.546	84.53	14.816	0.485
3.60	18	31.88	4.050	2.483	84.16	14.796	0.490
3.60	19	32.98	4.314	2.419	83.77	14.775	0.495
3.60	20	34.11	4.588	2.355	83.37	14.752	0.501
3.60	21	35.27	4.873	2.291	82.96	14.726	0.508
3.60	22	36.45	5.170	2.227	82.53	14.698	0.515
3.60	23	37.66	5.477	2.162	82.08	14.666	0.523
3.60	24	38.90	5.795	2.097	81.62	14.632	0.531
3.60	25	40.17	6.125	2.032	81.13	14.594	0.541
3.60	26	41.48	6.466	1.966	80.62	14.551	0.551
3.60	27	42.83	6.820	1.900	80.07	14.504	0.562
3.60	28	44.22	7.186	1.834	79.49	14.450	0.575
3.60	29	45.65	7.566	1.766	78.87	14.389	0.588
3.60	30	47.15	7.961	1.697	78.19	14.320	0.604
3.60	31	48.72	8.372	1.627	77.45	14.240	0.622
3.60	32	50.38	8.803	1.555	76.64	14.145	0.642
3.60	33	52.14	9.259	1.480	75.71	14.032	0.666
3.60	34	54.07	9.746	1.400	74.64	13.892	0.695
3.60	35	56.22	10.279	1.314	73.33	13.709	0.731
3.60	36	58.79	10.894	1.215	71.62	13.450	0.780
3.60	37	62.54	11.738	1.078	68.73	12.963	0.869
3.70	0	15.66	0.997	3.702	89.99	15.805	0.444
3.70	1	16.34	1.098	3.633	89.71	15.805	0.444
3.70	2	17.03	1.203	3.567	89.41	15.803	0.444
3.70	3	17.74	1.316	3.503	89.12	15.801	0.445
3.70	4	18.48	1.438	3.439	88.82	15.798	0.446
3.70	5	19.24	1.568	3.375	88.52	15.794	0.447
3.70	6	20.03	1.707	3.312	88.22	15.790	0.448
3.70	7	20.85	1.856	3.249	87.92	15.784	0.450
3.70	8	21.69	2.014	3.186	87.61	15.777	0.451
3.70	9	22.55	2.183	3.123	87.30	15.770	0.454
3.70	10	23.44	2.361	3.059	86.99	15.761	0.456
3.70	11	24.36	2.550	2.995	86.67	15.751	0.458
3.70	12	25.30	2.750	2.931	86.35	15.740	0.461

(continued)

Table A.3 (Continued)

Weak solution				Strong solution			
$M_1$	$\theta$	$\beta$	$p_2/p_1$	$M_2$	$\beta$	$p_2/p_1$	$M_2$
3.70	13	26.26	2.960	2.867	86.02	15.728	0.464
3.70	14	27.25	3.181	2.803	85.69	15.715	0.468
3.70	15	28.25	3.412	2.738	85.35	15.700	0.472
3.70	16	29.29	3.655	2.673	85.00	15.684	0.476
3.70	17	30.34	3.909	2.608	84.64	15.666	0.481
3.70	18	31.42	4.174	2.542	84.28	15.646	0.486
3.70	19	32.53	4.451	2.476	83.90	15.624	0.491
3.70	20	33.65	4.738	2.411	83.51	15.601	0.497
3.70	21	34.81	5.037	2.344	83.11	15.575	0.503
3.70	22	35.99	5.347	2.278	82.69	15.546	0.510
3.70	23	37.19	5.669	2.212	82.26	15.515	0.518
3.70	24	38.43	6.002	2.145	81.80	15.480	0.526
3.70	25	39.69	6.348	2.079	81.33	15.442	0.535
3.70	26	40.99	6.705	2.011	80.83	15.399	0.545
3.70	27	42.33	7.075	1.944	80.30	15.352	0.556
3.70	28	43.70	7.458	1.876	79.74	15.298	0.568
3.70	29	45.13	7.854	1.807	79.14	15.238	0.581
3.70	30	46.61	8.266	1.738	78.49	15.169	0.596
3.70	31	48.15	8.694	1.667	77.79	15.090	0.613
3.70	32	49.77	9.142	1.594	77.01	14.998	0.632
3.70	33	51.49	9.612	1.519	76.14	14.888	0.655
3.70	34	53.34	10.112	1.440	75.14	14.754	0.681
3.70	35	55.39	10.653	1.356	73.95	14.584	0.714
3.70	36	57.76	11.259	1.262	72.44	14.352	0.758
3.70	37	60.82	12.007	1.146	70.25	13.982	0.824
3.80	0	15.24	0.997	3.802	89.99	16.680	0.441
3.80	1	15.92	1.100	3.731	89.71	16.680	0.441
3.80	2	16.60	1.208	3.662	89.42	16.678	0.441
3.80	3	17.31	1.325	3.595	89.13	16.676	0.442
3.80	4	18.05	1.450	3.529	88.84	16.673	0.443
3.80	5	18.81	1.585	3.463	88.55	16.669	0.444
3.80	6	19.60	1.729	3.398	88.25	16.664	0.445
3.80	7	20.42	1.883	3.332	87.96	16.658	0.446
3.80	8	21.26	2.048	3.267	87.66	16.652	0.448
3.80	9	22.13	2.223	3.201	87.35	16.644	0.450
3.80	10	23.02	2.409	3.135	87.05	16.635	0.452
3.80	11	23.93	2.605	3.069	86.73	16.625	0.455
3.80	12	24.87	2.813	3.003	86.42	16.614	0.458
3.80	13	25.83	3.032	2.937	86.10	16.602	0.461

(continued)

Table A.3 (Continued)

Weak solution				Strong solution			
$M_1$	$\theta$	$\beta$	$p_2/p_1$	$M_2$	$\beta$	$p_2/p_1$	$M_2$
3.80	14	26.82	3.263	2.870	85.77	16.588	0.464
3.80	15	27.83	3.505	2.803	85.44	16.573	0.468
3.80	16	28.86	3.759	2.735	85.09	16.557	0.472
3.80	17	29.92	4.025	2.668	84.74	16.538	0.477
3.80	18	31.00	4.302	2.600	84.39	16.519	0.482
3.80	19	32.10	4.591	2.532	84.02	16.497	0.487
3.80	20	33.23	4.892	2.464	83.64	16.473	0.493
3.80	21	34.38	5.205	2.396	83.24	16.447	0.499
3.80	22	35.56	5.530	2.328	82.84	16.418	0.506
3.80	23	36.76	5.867	2.260	82.41	16.386	0.513
3.80	24	37.99	6.216	2.192	81.97	16.351	0.521
3.80	25	39.25	6.577	2.123	81.51	16.313	0.530
3.80	26	40.54	6.951	2.055	81.02	16.270	0.540
3.80	27	41.87	7.337	1.986	80.51	16.222	0.550
3.80	28	43.23	7.737	1.917	79.97	16.169	0.562
3.80	29	44.64	8.152	1.847	79.39	16.108	0.575
3.80	30	46.10	8.581	1.776	78.76	16.040	0.589
3.80	31	47.63	9.027	1.704	78.09	15.962	0.605
3.80	32	49.22	9.492	1.631	77.34	15.871	0.624
3.80	33	50.90	9.979	1.556	76.52	15.764	0.645
3.80	34	52.70	10.494	1.478	75.57	15.634	0.670
3.80	35	54.67	11.045	1.395	74.47	15.472	0.700
3.80	36	56.89	11.654	1.304	73.12	15.259	0.739
3.80	37	59.60	12.367	1.198	71.28	14.944	0.795
3.80	38	64.18	13.485	1.030	67.57	14.227	0.913
3.90	0	14.84	0.997	3.902	89.99	17.578	0.438
3.90	1	15.51	1.103	3.828	89.72	17.578	0.438
3.90	2	16.20	1.214	3.757	89.43	17.577	0.438
3.90	3	16.91	1.334	3.688	89.15	17.574	0.439
3.90	4	17.64	1.463	3.619	88.86	17.571	0.440
3.90	5	18.41	1.602	3.551	88.57	17.567	0.441
3.90	6	19.20	1.752	3.483	88.28	17.562	0.442
3.90	7	20.01	1.911	3.415	87.99	17.556	0.443
3.90	8	20.85	2.082	3.347	87.70	17.550	0.445
3.90	9	21.72	2.264	3.279	87.40	17.542	0.447
3.90	10	22.61	2.457	3.211	87.10	17.533	0.449
3.90	11	23.53	2.662	3.143	86.79	17.523	0.452
3.90	12	24.47	2.878	3.074	86.48	17.511	0.455
3.90	13	25.44	3.107	3.005	86.16	17.499	0.458

(continued)

Table A.3 (Continued)

Weak solution				Strong solution			
$M_1$	$\theta$	$\beta$	$p_2/p_1$	$M_2$	$\beta$	$p_2/p_1$	$M_2$
3.90	14	26.42	3.347	2.936	85.84	17.485	0.461
3.90	15	27.43	3.600	2.866	85.51	17.470	0.465
3.90	16	28.47	3.865	2.797	85.18	17.453	0.469
3.90	17	29.53	4.143	2.727	84.84	17.434	0.473
3.90	18	30.61	4.433	2.657	84.49	17.414	0.478
3.90	19	31.71	4.735	2.587	84.12	17.392	0.483
3.90	20	32.83	5.050	2.517	83.75	17.368	0.489
3.90	21	33.98	5.377	2.447	83.37	17.341	0.495
3.90	22	35.16	5.717	2.377	82.97	17.312	0.502
3.90	23	36.36	6.069	2.307	82.55	17.280	0.509
3.90	24	37.58	6.434	2.237	82.12	17.245	0.517
3.90	25	38.84	6.812	2.167	81.67	17.206	0.525
3.90	26	40.13	7.203	2.097	81.20	17.163	0.535
3.90	27	41.45	7.607	2.026	80.70	17.115	0.545
3.90	28	42.80	8.025	1.956	80.17	17.061	0.556
3.90	29	44.20	8.458	1.885	79.61	17.001	0.569
3.90	30	45.65	8.906	1.813	79.01	16.933	0.583
3.90	31	47.15	9.370	1.741	78.36	16.855	0.598
3.90	32	48.72	9.853	1.667	77.64	16.765	0.616
3.90	33	50.37	10.358	1.591	76.85	16.660	0.636
3.90	34	52.13	10.890	1.513	75.96	16.533	0.660
3.90	35	54.03	11.456	1.431	74.92	16.378	0.688
3.90	36	56.15	12.072	1.343	73.68	16.177	0.724
3.90	37	58.64	12.773	1.242	72.06	15.895	0.772
3.90	38	62.08	13.689	1.111	69.50	15.402	0.853
4.00	0	14.46	0.997	4.002	89.99	18.500	0.435
4.00	1	15.13	1.105	3.925	89.72	18.500	0.435
4.00	2	15.81	1.219	3.852	89.44	18.498	0.435
4.00	3	16.52	1.343	3.780	89.16	18.496	0.436
4.00	4	17.26	1.476	3.709	88.88	18.493	0.437
4.00	5	18.02	1.620	3.638	88.60	18.489	0.438
4.00	6	18.81	1.774	3.568	88.31	18.484	0.439
4.00	7	19.63	1.940	3.498	88.02	18.478	0.440
4.00	8	20.47	2.117	3.427	87.73	18.471	0.442
4.00	9	21.34	2.305	3.357	87.44	18.463	0.444
4.00	10	22.23	2.506	3.286	87.14	18.453	0.446
4.00	11	23.15	2.719	3.215	86.84	18.443	0.449
4.00	12	24.10	2.944	3.144	86.54	18.432	0.452
4.00	13	25.06	3.182	3.073	86.23	18.419	0.455

(continued)



Table A.3 (Continued)

Weak solution				Strong solution			
$M_1$	$\theta$	$\beta$	$p_2/p_1$	$M_2$	$\beta$	$p_2/p_1$	$M_2$
4.00	14	26.05	3.433	3.001	85.91	18.405	0.458
4.00	15	27.06	3.697	2.929	85.59	18.389	0.462
4.00	16	28.10	3.974	2.857	85.26	18.372	0.466
4.00	17	29.16	4.264	2.785	84.92	18.354	0.470
4.00	18	30.24	4.566	2.713	84.58	18.333	0.475
4.00	19	31.34	4.882	2.641	84.22	18.311	0.480
4.00	20	32.46	5.211	2.569	83.86	18.286	0.485
4.00	21	33.61	5.553	2.497	83.48	18.259	0.491
4.00	22	34.79	5.909	2.425	83.09	18.230	0.498
4.00	23	35.98	6.277	2.353	82.68	18.197	0.505
4.00	24	37.21	6.659	2.281	82.26	18.161	0.513
4.00	25	38.46	7.054	2.209	81.82	18.122	0.521
4.00	26	39.74	7.462	2.137	81.36	18.079	0.530
4.00	27	41.05	7.885	2.066	80.88	18.030	0.540
4.00	28	42.40	8.321	1.994	80.36	17.976	0.551
4.00	29	43.79	8.772	1.921	79.81	17.916	0.563
4.00	30	45.22	9.239	1.849	79.23	17.848	0.577
4.00	31	46.71	9.723	1.775	78.60	17.770	0.592
4.00	32	48.26	10.226	1.701	77.91	17.681	0.609
4.00	33	49.88	10.749	1.625	77.15	17.576	0.628
4.00	34	51.61	11.299	1.546	76.30	17.452	0.651
4.00	35	53.46	11.881	1.465	75.32	17.301	0.678
4.00	36	55.50	12.509	1.378	74.16	17.109	0.711
4.00	37	57.84	13.210	1.281	72.70	16.849	0.754
4.00	38	60.83	14.064	1.164	70.60	16.441	0.820
4.10	0	14.10	0.997	4.102	89.99	19.445	0.432
4.10	1	14.77	1.108	4.023	89.73	19.445	0.432
4.10	2	15.45	1.225	3.947	89.45	19.443	0.433
4.10	3	16.16	1.352	3.872	89.17	19.441	0.433
4.10	4	16.89	1.489	3.798	88.90	19.438	0.434
4.10	5	17.66	1.638	3.725	88.62	19.433	0.435
4.10	6	18.45	1.797	3.652	88.33	19.428	0.436
4.10	7	19.27	1.968	3.580	88.05	19.422	0.438
4.10	8	20.11	2.152	3.507	87.77	19.415	0.439
4.10	9	20.98	2.347	3.434	87.48	19.407	0.441
4.10	10	21.88	2.556	3.360	87.18	19.398	0.444
4.10	11	22.80	2.777	3.287	86.89	19.387	0.446
4.10	12	23.74	3.012	3.213	86.59	19.375	0.449
4.10	13	24.71	3.260	3.139	86.28	19.362	0.452

(continued)

Table A.3 (Continued)

Weak solution				Strong solution			
$M_1$	$\theta$	$\beta$	$p_2/p_1$	$M_2$	$\beta$	$p_2/p_1$	$M_2$
4.10	14	25.70	3.521	3.065	85.97	19.348	0.455
4.10	15	26.71	3.796	2.991	85.65	19.332	0.459
4.10	16	27.75	4.085	2.916	85.33	19.315	0.462
4.10	17	28.81	4.387	2.842	85.00	19.296	0.467
4.10	18	29.89	4.703	2.768	84.66	19.275	0.471
4.10	19	30.99	5.033	2.693	84.31	19.252	0.476
4.10	20	32.12	5.377	2.619	83.95	19.227	0.482
4.10	21	33.27	5.734	2.545	83.58	19.200	0.488
4.10	22	34.44	6.105	2.471	83.20	19.170	0.494
4.10	23	35.64	6.490	2.397	82.80	19.137	0.501
4.10	24	36.86	6.889	2.323	82.39	19.101	0.509
4.10	25	38.10	7.301	2.250	81.96	19.061	0.517
4.10	26	39.38	7.728	2.177	81.51	19.017	0.526
4.10	27	40.69	8.169	2.103	81.03	18.968	0.536
4.10	28	42.03	8.625	2.030	80.53	18.914	0.547
4.10	29	43.41	9.095	1.956	80.00	18.853	0.558
4.10	30	44.83	9.582	1.883	79.43	18.785	0.572
4.10	31	46.31	10.086	1.808	78.82	18.707	0.586
4.10	32	47.84	10.609	1.733	78.15	18.618	0.603
4.10	33	49.44	11.152	1.656	77.42	18.514	0.621
4.10	34	51.13	11.722	1.578	76.60	18.392	0.643
4.10	35	52.94	12.322	1.496	75.67	18.244	0.669
4.10	36	54.91	12.965	1.410	74.58	18.059	0.700
4.10	37	57.15	13.672	1.316	73.24	17.814	0.739
4.10	38	59.86	14.501	1.207	71.42	17.452	0.796
4.10	39	64.50	15.811	1.031	67.66	16.611	0.919
4.20	0	13.76	0.997	4.202	89.99	20.413	0.430
4.20	1	14.42	1.110	4.120	89.73	20.413	0.430
4.20	2	15.10	1.231	4.041	89.46	20.411	0.430
4.20	3	15.81	1.361	3.964	89.18	20.409	0.431
4.20	4	16.55	1.503	3.888	88.91	20.406	0.432
4.20	5	17.31	1.655	3.812	88.63	20.402	0.433
4.20	6	18.10	1.820	3.736	88.36	20.396	0.434
4.20	7	18.92	1.997	3.661	88.08	20.390	0.435
4.20	8	19.77	2.187	3.586	87.80	20.383	0.437
4.20	9	20.64	2.390	3.510	87.51	20.374	0.439
4.20	10	21.54	2.607	3.434	87.22	20.365	0.441
4.20	11	22.46	2.837	3.358	86.93	20.354	0.443
4.20	12	23.41	3.081	3.282	86.64	20.342	0.446

(continued)

Table A.3 (Continued)

Weak solution				Strong solution			
$M_1$	$\theta$	$\beta$	$p_2/p_1$	$M_2$	$\beta$	$p_2/p_1$	$M_2$
4.20	13	24.38	3.339	3.205	86.33	20.329	0.449
4.20	14	25.37	3.611	3.128	86.03	20.314	0.452
4.20	15	26.38	3.897	3.052	85.72	20.298	0.456
4.20	16	27.42	4.198	2.975	85.40	20.281	0.460
4.20	17	28.48	4.513	2.898	85.07	20.261	0.464
4.20	18	29.56	4.843	2.821	84.74	20.240	0.468
4.20	19	30.67	5.187	2.745	84.40	20.217	0.473
4.20	20	31.79	5.546	2.668	84.04	20.191	0.479
4.20	21	32.94	5.919	2.592	83.68	20.164	0.485
4.20	22	34.11	6.306	2.516	83.30	20.133	0.491
4.20	23	35.31	6.708	2.440	82.91	20.100	0.498
4.20	24	36.53	7.124	2.365	82.51	20.063	0.505
4.20	25	37.77	7.555	2.290	82.09	20.023	0.513
4.20	26	39.05	8.000	2.215	81.64	19.978	0.522
4.20	27	40.35	8.461	2.140	81.18	19.929	0.532
4.20	28	41.69	8.936	2.065	80.69	19.874	0.542
4.20	29	43.06	9.427	1.990	80.17	19.813	0.554
4.20	30	44.47	9.934	1.915	79.61	19.744	0.567
4.20	31	45.93	10.459	1.840	79.02	19.666	0.581
4.20	32	47.45	11.002	1.764	78.37	19.577	0.597
4.20	33	49.03	11.567	1.686	77.66	19.474	0.615
4.20	34	50.70	12.157	1.608	76.88	19.352	0.636
4.20	35	52.47	12.777	1.526	75.99	19.207	0.660
4.20	36	54.39	13.437	1.441	74.96	19.026	0.690
4.20	37	56.54	14.156	1.349	73.70	18.793	0.726
4.20	38	59.07	14.977	1.244	72.07	18.461	0.777
4.20	39	62.66	16.072	1.104	69.37	17.859	0.864
4.30	0	13.43	0.997	4.302	89.99	21.405	0.428
4.30	1	14.10	1.113	4.217	89.73	21.405	0.428
4.30	2	14.77	1.236	4.136	89.46	21.403	0.428
4.30	3	15.48	1.370	4.056	89.20	21.401	0.429
4.30	4	16.22	1.516	3.977	88.92	21.397	0.429
4.30	5	16.98	1.674	3.898	88.65	21.393	0.430
4.30	6	17.78	1.844	3.820	88.38	21.388	0.432
4.30	7	18.60	2.027	3.742	88.10	21.381	0.433
4.30	8	19.44	2.223	3.664	87.82	21.374	0.435
4.30	9	20.32	2.434	3.586	87.54	21.365	0.436
4.30	10	21.22	2.658	3.507	87.26	21.356	0.439
4.30	11	22.14	2.897	3.428	86.97	21.345	0.441

(continued)

Table A.3 (Continued)

Weak solution				Strong solution			
$M_1$	$\theta$	$\beta$	$p_2/p_1$	$M_2$	$\beta$	$p_2/p_1$	$M_2$
4.30	12	23.09	3.151	3.349	86.68	21.333	0.444
4.30	13	24.06	3.419	3.270	86.38	21.319	0.447
4.30	14	25.06	3.702	3.191	86.08	21.304	0.450
4.30	15	26.07	4.000	3.111	85.77	21.288	0.453
4.30	16	27.11	4.314	3.032	85.46	21.270	0.457
4.30	17	28.18	4.642	2.953	85.14	21.250	0.461
4.30	18	29.26	4.986	2.874	84.81	21.228	0.466
4.30	19	30.36	5.345	2.795	84.47	21.205	0.471
4.30	20	31.49	5.719	2.716	84.12	21.179	0.476
4.30	21	32.64	6.108	2.638	83.77	21.150	0.482
4.30	22	33.81	6.512	2.560	83.40	21.120	0.488
4.30	23	35.00	6.931	2.482	83.01	21.086	0.495
4.30	24	36.22	7.366	2.405	82.62	21.048	0.502
4.30	25	37.47	7.815	2.328	82.20	21.007	0.510
4.30	26	38.74	8.280	2.251	81.77	20.962	0.518
4.30	27	40.04	8.759	2.175	81.31	20.912	0.528
4.30	28	41.37	9.255	2.099	80.83	20.857	0.538
4.30	29	42.73	9.766	2.023	80.32	20.795	0.550
4.30	30	44.14	10.295	1.947	79.78	20.726	0.562
4.30	31	45.59	10.841	1.870	79.20	20.647	0.576
4.30	32	47.09	11.406	1.793	78.57	20.558	0.592
4.30	33	48.66	11.993	1.715	77.89	20.455	0.609
4.30	34	50.30	12.604	1.636	77.13	20.334	0.629
4.30	35	52.05	13.245	1.554	76.27	20.190	0.653
4.30	36	53.92	13.924	1.469	75.29	20.013	0.681
4.30	37	56.00	14.658	1.378	74.11	19.787	0.715
4.30	38	58.40	15.481	1.277	72.61	19.477	0.761
4.30	39	61.54	16.506	1.151	70.37	18.969	0.833
4.40	0	13.12	0.997	4.402	90.00	22.420	0.426
4.40	1	13.78	1.116	4.314	89.74	22.419	0.426
4.40	2	14.46	1.242	4.230	89.47	22.418	0.426
4.40	3	15.17	1.380	4.147	89.20	22.416	0.426
4.40	4	15.90	1.529	4.065	88.94	22.412	0.427
4.40	5	16.67	1.692	3.984	88.67	22.408	0.428
4.40	6	17.46	1.867	3.903	88.40	22.402	0.429
4.40	7	18.29	2.057	3.823	88.13	22.396	0.431
4.40	8	19.13	2.260	3.742	87.85	22.388	0.432
4.40	9	20.01	2.478	3.661	87.57	22.379	0.434
4.40	10	20.91	2.711	3.579	87.29	22.370	0.436

(continued)

Table A.3 (Continued)

Weak solution				Strong solution			
$M_1$	$\theta$	$\beta$	$p_2/p_1$	$M_2$	$\beta$	$p_2/p_1$	$M_2$
4.40	11	21.84	2.959	3.498	87.01	22.358	0.439
4.40	12	22.79	3.222	3.416	86.72	22.346	0.441
4.40	13	23.76	3.501	3.334	86.43	22.332	0.444
4.40	14	24.76	3.795	3.252	86.13	22.317	0.447
4.40	15	25.78	4.106	3.170	85.83	22.300	0.451
4.40	16	26.82	4.432	3.088	85.52	22.282	0.455
4.40	17	27.89	4.774	3.007	85.20	22.262	0.459
4.40	18	28.97	5.132	2.925	84.88	22.240	0.463
4.40	19	30.08	5.506	2.844	84.54	22.216	0.468
4.40	20	31.20	5.896	2.763	84.20	22.189	0.473
4.40	21	32.35	6.301	2.683	83.85	22.160	0.479
4.40	22	33.53	6.723	2.602	83.48	22.129	0.485
4.40	23	34.72	7.160	2.523	83.11	22.094	0.492
4.40	24	35.94	7.612	2.444	82.72	22.057	0.499
4.40	25	37.18	8.081	2.365	82.31	22.015	0.507
4.40	26	38.45	8.565	2.287	81.88	21.969	0.515
4.40	27	39.74	9.065	2.209	81.43	21.919	0.524
4.40	28	41.07	9.581	2.132	80.96	21.863	0.535
4.40	29	42.43	10.114	2.054	80.47	21.800	0.546
4.40	30	43.83	10.664	1.977	79.94	21.730	0.558
4.40	31	45.27	11.233	1.899	79.37	21.651	0.572
4.40	32	46.76	11.820	1.821	78.76	21.561	0.587
4.40	33	48.31	12.429	1.743	78.09	21.457	0.604
4.40	34	49.94	13.063	1.663	77.35	21.337	0.623
4.40	35	51.66	13.726	1.581	76.53	21.194	0.646
4.40	36	53.50	14.426	1.496	75.58	21.019	0.673
4.40	37	55.51	15.178	1.406	74.47	20.800	0.705
4.40	38	57.81	16.010	1.308	73.07	20.504	0.748
4.40	39	60.68	17.004	1.190	71.11	20.051	0.811
4.50	0	12.82	0.997	4.503	90.00	23.458	0.424
4.50	1	13.49	1.118	4.411	89.74	23.458	0.424
4.50	2	14.16	1.248	4.324	89.48	23.456	0.424
4.50	3	14.87	1.389	4.238	89.21	23.454	0.424
4.50	4	15.61	1.543	4.154	88.95	23.450	0.425
4.50	5	16.37	1.710	4.070	88.68	23.446	0.426
4.50	6	17.17	1.891	3.986	88.42	23.440	0.427
4.50	7	17.99	2.087	3.903	88.15	23.434	0.429
4.50	8	18.84	2.297	3.819	87.88	23.426	0.430
4.50	9	19.72	2.523	3.735	87.60	23.417	0.432

(continued)

Table A.3 (Continued)

Weak solution				Strong solution			
$M_1$	$\theta$	$\beta$	$p_2/p_1$	$M_2$	$\beta$	$p_2/p_1$	$M_2$
4.50	10	20.62	2.764	3.651	87.32	23.407	0.434
4.50	11	21.55	3.021	3.567	87.04	23.395	0.437
4.50	12	22.50	3.294	3.482	86.76	23.383	0.439
4.50	13	23.48	3.584	3.397	86.47	23.369	0.442
4.50	14	24.48	3.890	3.313	86.18	23.353	0.445
4.50	15	25.50	4.213	3.228	85.88	23.336	0.449
4.50	16	26.55	4.552	3.144	85.57	23.317	0.452
4.50	17	27.61	4.908	3.059	85.26	23.297	0.456
4.50	18	28.70	5.281	2.975	84.94	23.274	0.461
4.50	19	29.81	5.671	2.892	84.61	23.250	0.465
4.50	20	30.94	6.076	2.809	84.27	23.223	0.471
4.50	21	32.09	6.499	2.726	83.92	23.193	0.476
4.50	22	33.26	6.938	2.644	83.57	23.161	0.482
4.50	23	34.45	7.393	2.563	83.19	23.126	0.489
4.50	24	35.67	7.865	2.482	82.81	23.088	0.496
4.50	25	36.91	8.353	2.401	82.41	23.046	0.504
4.50	26	38.17	8.857	2.321	81.99	22.999	0.512
4.50	27	39.47	9.378	2.242	81.55	22.948	0.521
4.50	28	40.79	9.916	2.163	81.09	22.891	0.531
4.50	29	42.15	10.470	2.084	80.60	22.827	0.542
4.50	30	43.54	11.043	2.006	80.08	22.757	0.554
4.50	31	44.97	11.634	1.927	79.52	22.677	0.567
4.50	32	46.45	12.244	1.848	78.92	22.586	0.582
4.50	33	47.99	12.877	1.769	78.27	22.482	0.599
4.50	34	49.60	13.534	1.689	77.56	22.361	0.618
4.50	35	51.30	14.220	1.606	76.76	22.219	0.640
4.50	36	53.10	14.943	1.521	75.85	22.046	0.665
4.50	37	55.07	15.714	1.432	74.79	21.831	0.697
4.50	38	57.29	16.559	1.335	73.47	21.546	0.736
4.50	39	59.98	17.543	1.223	71.70	21.129	0.793
4.50	40	64.33	19.026	1.052	68.25	20.214	0.909
4.60	0	12.54	0.997	4.603	90.00	24.520	0.422
4.60	1	13.20	1.121	4.508	89.74	24.519	0.422
4.60	2	13.88	1.253	4.418	89.48	24.518	0.422
4.60	3	14.58	1.398	4.329	89.22	24.515	0.423
4.60	4	15.32	1.557	4.242	88.96	24.512	0.423
4.60	5	16.09	1.729	4.155	88.70	24.507	0.424
4.60	6	16.88	1.916	4.069	88.43	24.501	0.425
4.60	7	17.71	2.118	3.982	88.17	24.495	0.427

(continued)

Table A.3 (Continued)

Weak solution				Strong solution			
$M_1$	$\theta$	$\beta$	$p_2/p_1$	$M_2$	$\beta$	$p_2/p_1$	$M_2$
4.60	8	18.56	2.335	3.896	87.90	24.487	0.428
4.60	9	19.44	2.568	3.809	87.63	24.478	0.430
4.60	10	20.35	2.818	3.722	87.35	24.467	0.432
4.60	11	21.28	3.085	3.635	87.08	24.456	0.435
4.60	12	22.24	3.368	3.547	86.79	24.443	0.437
4.60	13	23.21	3.669	3.460	86.51	24.428	0.440
4.60	14	24.22	3.987	3.372	86.22	24.412	0.443
4.60	15	25.24	4.322	3.285	85.92	24.395	0.446
4.60	16	26.29	4.675	3.198	85.62	24.376	0.450
4.60	17	27.36	5.045	3.111	85.31	24.355	0.454
4.60	18	28.44	5.433	3.025	84.99	24.332	0.458
4.60	19	29.55	5.838	2.939	84.67	24.307	0.463
4.60	20	30.68	6.261	2.853	84.34	24.279	0.468
4.60	21	31.83	6.701	2.769	83.99	24.250	0.474
4.60	22	33.00	7.158	2.685	83.64	24.217	0.480
4.60	23	34.20	7.632	2.601	83.27	24.181	0.486
4.60	24	35.41	8.123	2.518	82.89	24.142	0.493
4.60	25	36.65	8.631	2.436	82.50	24.099	0.501
4.60	26	37.92	9.156	2.355	82.09	24.052	0.509
4.60	27	39.21	9.698	2.274	81.65	23.999	0.518
4.60	28	40.53	10.258	2.193	81.20	23.942	0.528
4.60	29	41.88	10.835	2.114	80.72	23.877	0.539
4.60	30	43.27	11.430	2.034	80.21	23.806	0.550
4.60	31	44.69	12.044	1.954	79.66	23.725	0.563
4.60	32	46.17	12.679	1.874	79.08	23.633	0.578
4.60	33	47.69	13.335	1.794	78.44	23.529	0.594
4.60	34	49.29	14.017	1.713	77.75	23.408	0.613
4.60	35	50.96	14.727	1.630	76.97	23.265	0.634
4.60	36	52.74	15.473	1.545	76.09	23.094	0.659
4.60	37	54.67	16.265	1.457	75.07	22.881	0.689
4.60	38	56.83	17.128	1.361	73.83	22.605	0.726
4.60	39	59.37	18.111	1.253	72.20	22.212	0.778
4.60	40	62.99	19.429	1.107	69.49	21.489	0.868
4.70	0	12.27	0.997	4.703	90.00	25.605	0.420
4.70	1	12.93	1.123	4.605	89.75	25.604	0.420
4.70	2	13.60	1.259	4.512	89.49	25.603	0.420
4.70	3	14.31	1.408	4.420	89.23	25.600	0.421
4.70	4	15.05	1.571	4.330	88.97	25.597	0.422
4.70	5	15.82	1.748	4.240	88.71	25.592	0.422

(continued)

Table A.3 (Continued)

Weak solution				Strong solution			
$M_1$	$\theta$	$\beta$	$p_2/p_1$	$M_2$	$\beta$	$p_2/p_1$	$M_2$
4.70	6	16.61	1.940	4.151	88.45	25.586	0.424
4.70	7	17.44	2.149	4.061	88.19	25.579	0.425
4.70	8	18.30	2.373	3.972	87.92	25.571	0.427
4.70	9	19.18	2.615	3.882	87.65	25.562	0.428
4.70	10	20.09	2.873	3.792	87.38	25.551	0.430
4.70	11	21.02	3.149	3.702	87.11	25.539	0.433
4.70	12	21.98	3.443	3.612	86.83	25.526	0.435
4.70	13	22.96	3.755	3.522	86.54	25.511	0.438
4.70	14	23.97	4.085	3.431	86.26	25.495	0.441
4.70	15	24.99	4.434	3.341	85.96	25.477	0.444
4.70	16	26.04	4.800	3.251	85.67	25.458	0.448
4.70	17	27.11	5.185	3.162	85.36	25.436	0.452
4.70	18	28.20	5.588	3.073	85.05	25.413	0.456
4.70	19	29.31	6.010	2.985	84.73	25.387	0.461
4.70	20	30.44	6.449	2.897	84.40	25.359	0.466
4.70	21	31.59	6.907	2.810	84.06	25.329	0.472
4.70	22	32.77	7.382	2.724	83.71	25.295	0.477
4.70	23	33.96	7.875	2.639	83.35	25.259	0.484
4.70	24	35.18	8.386	2.554	82.97	25.219	0.491
4.70	25	36.42	8.915	2.470	82.58	25.175	0.498
4.70	26	37.68	9.461	2.387	82.18	25.127	0.506
4.70	27	38.97	10.025	2.305	81.75	25.074	0.515
4.70	28	40.28	10.607	2.223	81.30	25.015	0.525
4.70	29	41.63	11.207	2.142	80.83	24.950	0.535
4.70	30	43.01	11.826	2.061	80.33	24.878	0.547
4.70	31	44.43	12.464	1.980	79.80	24.796	0.560
4.70	32	45.90	13.123	1.899	79.22	24.703	0.574
4.70	33	47.42	13.804	1.818	78.60	24.598	0.590
4.70	34	49.00	14.511	1.737	77.92	24.476	0.608
4.70	35	50.66	15.246	1.654	77.17	24.333	0.629
4.70	36	52.41	16.016	1.568	76.31	24.162	0.653
4.70	37	54.31	16.832	1.480	75.33	23.952	0.682
4.70	38	56.40	17.714	1.385	74.15	23.682	0.717
4.70	39	58.84	18.705	1.280	72.63	23.307	0.765
4.70	40	62.09	19.956	1.146	70.30	22.676	0.842
4.80	0	12.01	0.997	4.803	90.00	26.713	0.418
4.80	1	12.67	1.126	4.701	89.75	26.713	0.418
4.80	2	13.34	1.265	4.605	89.49	26.711	0.419
4.80	3	14.05	1.417	4.511	89.24	26.709	0.419

(continued)



Table A.3 (Continued)

Weak solution				Strong solution			
$M_1$	$\theta$	$\beta$	$p_2/p_1$	$M_2$	$\beta$	$p_2/p_1$	$M_2$
4.80	4	14.79	1.585	4.418	88.98	26.705	0.420
4.80	5	15.56	1.767	4.325	88.72	26.700	0.421
4.80	6	16.36	1.965	4.232	88.46	26.694	0.422
4.80	7	17.19	2.180	4.140	88.20	26.687	0.423
4.80	8	18.04	2.412	4.047	87.94	26.679	0.425
4.80	9	18.93	2.662	3.955	87.68	26.669	0.427
4.80	10	19.84	2.929	3.862	87.41	26.658	0.429
4.80	11	20.78	3.215	3.769	87.13	26.646	0.431
4.80	12	21.74	3.520	3.676	86.86	26.632	0.433
4.80	13	22.72	3.843	3.582	86.58	26.617	0.436
4.80	14	23.73	4.186	3.489	86.29	26.601	0.439
4.80	15	24.76	4.547	3.396	86.00	26.583	0.443
4.80	16	25.81	4.928	3.304	85.71	26.563	0.446
4.80	17	26.88	5.328	3.212	85.41	26.541	0.450
4.80	18	27.97	5.747	3.121	85.10	26.517	0.454
4.80	19	29.08	6.185	3.030	84.78	26.491	0.459
4.80	20	30.22	6.641	2.940	84.46	26.462	0.464
4.80	21	31.37	7.117	2.851	84.12	26.431	0.469
4.80	22	32.54	7.611	2.762	83.78	26.397	0.475
4.80	23	33.74	8.124	2.675	83.42	26.360	0.482
4.80	24	34.95	8.655	2.589	83.05	26.319	0.488
4.80	25	36.19	9.205	2.503	82.66	26.275	0.496
4.80	26	37.45	9.773	2.418	82.26	26.226	0.504
4.80	27	38.74	10.359	2.334	81.84	26.172	0.513
4.80	28	40.05	10.964	2.251	81.40	26.112	0.522
4.80	29	41.40	11.588	2.169	80.94	26.046	0.533
4.80	30	42.78	12.231	2.087	80.44	25.972	0.544
4.80	31	44.19	12.894	2.005	79.92	25.889	0.557
4.80	32	45.65	13.578	1.923	79.35	25.796	0.571
4.80	33	47.16	14.284	1.841	78.75	25.689	0.586
4.80	34	48.73	15.016	1.759	78.08	25.566	0.604
4.80	35	50.37	15.777	1.675	77.34	25.422	0.624
4.80	36	52.11	16.573	1.590	76.52	25.252	0.647
4.80	37	53.97	17.413	1.501	75.57	25.043	0.675
4.80	38	56.02	18.317	1.408	74.43	24.777	0.709
4.80	39	58.37	19.321	1.304	73.00	24.416	0.754
4.80	40	61.37	20.542	1.179	70.93	23.842	0.823
4.90	0	11.76	0.997	4.903	90.00	27.845	0.417
4.90	1	12.42	1.129	4.798	89.75	27.844	0.417

(continued)

Table A.3 (Continued)

Weak solution				Strong solution			
$M_1$	$\theta$	$\beta$	$p_2/p_1$	$M_2$	$\beta$	$p_2/p_1$	$M_2$
4.90	2	13.09	1.271	4.699	89.50	27.843	0.417
4.90	3	13.80	1.427	4.601	89.24	27.840	0.418
4.90	4	14.54	1.599	4.505	88.99	27.836	0.418
4.90	5	15.31	1.786	4.409	88.74	27.831	0.419
4.90	6	16.11	1.990	4.314	88.48	27.825	0.420
4.90	7	16.94	2.212	4.218	88.22	27.818	0.422
4.90	8	17.80	2.451	4.123	87.96	27.809	0.423
4.90	9	18.69	2.709	4.027	87.70	27.800	0.425
4.90	10	19.60	2.986	3.931	87.43	27.789	0.427
4.90	11	20.54	3.282	3.835	87.16	27.776	0.429
4.90	12	21.50	3.597	3.739	86.89	27.762	0.432
4.90	13	22.49	3.933	3.642	86.61	27.747	0.434
4.90	14	23.50	4.288	3.546	86.33	27.730	0.438
4.90	15	24.53	4.663	3.451	86.04	27.711	0.441
4.90	16	25.59	5.058	3.356	85.75	27.691	0.444
4.90	17	26.66	5.473	3.261	85.45	27.668	0.448
4.90	18	27.76	5.908	3.167	85.14	27.644	0.453
4.90	19	28.87	6.363	3.074	84.83	27.617	0.457
4.90	20	30.00	6.837	2.982	84.51	27.588	0.462
4.90	21	31.16	7.331	2.890	84.18	27.556	0.467
4.90	22	32.33	7.845	2.800	83.84	27.522	0.473
4.90	23	33.53	8.378	2.711	83.48	27.484	0.479
4.90	24	34.74	8.930	2.622	83.12	27.442	0.486
4.90	25	35.98	9.501	2.535	82.74	27.397	0.494
4.90	26	37.24	10.091	2.449	82.34	27.347	0.501
4.90	27	38.53	10.700	2.363	81.93	27.292	0.510
4.90	28	39.84	11.329	2.279	81.49	27.231	0.519
4.90	29	41.18	11.976	2.195	81.03	27.164	0.530
4.90	30	42.55	12.644	2.112	80.55	27.089	0.541
4.90	31	43.96	13.332	2.029	80.03	27.005	0.553
4.90	32	45.42	14.042	1.946	79.48	26.910	0.567
4.90	33	46.92	14.775	1.864	78.88	26.803	0.582
4.90	34	48.47	15.533	1.780	78.23	26.679	0.600
4.90	35	50.10	16.320	1.696	77.51	26.534	0.619
4.90	36	51.82	17.143	1.611	76.70	26.363	0.642
4.90	37	53.66	18.009	1.522	75.78	26.155	0.669
4.90	38	55.67	18.936	1.429	74.69	25.892	0.702
4.90	39	57.95	19.957	1.327	73.33	25.540	0.745
4.90	40	60.77	21.166	1.207	71.44	25.005	0.807
5.00	0	11.52	0.996	5.003	90.00	29.000	0.415
5.00	1	12.18	1.131	4.895	89.75	28.999	0.415

(continued)

Table A.3 (Continued)

Weak solution				Strong solution			
$M_1$	$\theta$	$\beta$	$p_2/p_1$	$M_2$	$\beta$	$p_2/p_1$	$M_2$
5.00	2	12.85	1.277	4.792	89.50	28.998	0.416
5.00	3	13.56	1.437	4.692	89.25	28.995	0.416
5.00	4	14.30	1.613	4.592	89.00	28.991	0.417
5.00	5	15.07	1.806	4.493	88.75	28.986	0.418
5.00	6	15.88	2.016	4.395	88.49	28.980	0.419
5.00	7	16.71	2.244	4.296	88.24	28.972	0.420
5.00	8	17.57	2.491	4.197	87.98	28.964	0.422
5.00	9	18.46	2.757	4.098	87.72	28.954	0.423
5.00	10	19.38	3.043	3.999	87.45	28.942	0.425
5.00	11	20.32	3.350	3.900	87.19	28.930	0.428
5.00	12	21.28	3.676	3.801	86.91	28.915	0.430
5.00	13	22.27	4.024	3.702	86.64	28.900	0.433
5.00	14	23.29	4.392	3.603	86.36	28.882	0.436
5.00	15	24.32	4.781	3.504	86.08	28.863	0.439
5.00	16	25.38	5.190	3.406	85.79	28.842	0.443
5.00	17	26.45	5.621	3.309	85.49	28.819	0.447
5.00	18	27.55	6.072	3.212	85.19	28.794	0.451
5.00	19	28.67	6.544	3.117	84.88	28.767	0.455
5.00	20	29.80	7.037	3.022	84.56	28.737	0.460
5.00	21	30.96	7.550	2.929	84.23	28.705	0.465
5.00	22	32.13	8.083	2.836	83.89	28.670	0.471
5.00	23	33.33	8.637	2.745	83.54	28.631	0.477
5.00	24	34.54	9.210	2.655	83.18	28.589	0.484
5.00	25	35.78	9.803	2.566	82.81	28.542	0.491
5.00	26	37.04	10.416	2.478	82.41	28.591	0.499
5.00	27	38.32	11.048	2.391	82.01	28.435	0.508
5.00	28	39.63	11.701	2.305	81.58	28.374	0.517
5.00	29	40.97	12.373	2.220	81.12	28.305	0.527
5.00	30	42.34	13.066	2.136	80.65	28.229	0.538
5.00	31	43.75	13.780	2.052	80.14	28.144	0.550
5.00	32	45.20	14.516	1.968	79.59	28.048	0.564
5.00	33	46.69	15.276	1.885	79.00	27.938	0.579
5.00	34	48.24	16.061	1.801	78.37	27.813	0.596
5.00	35	49.86	16.876	1.716	77.66	27.668	0.615
5.00	36	51.56	17.725	1.630	76.88	27.496	0.638
5.00	37	53.37	18.618	1.542	75.98	27.287	0.664
5.00	38	55.35	19.570	1.449	74.93	27.027	0.695
5.00	39	57.57	20.612	1.349	73.63	26.683	0.736
5.00	40	60.26	21.821	1.233	71.87	26.175	0.794
5.00	41	64.65	23.652	1.055	68.40	25.048	0.914

Note: In Table A.3  $\theta$  and  $\beta$  values are in degrees.

**Table A.4** One-dimensional flow with friction ( $\gamma = 1.4$ ).

$M$	$T/T^*$	$p/p^*$	$p_0/p_0^*$	$\rho^*/\rho$	$F/F^*$	$4 f l_{\max}/D$
0.02	1.19990	54.77007	28.94214	0.02191	22.83364	1778.4498
0.04	1.19962	27.38175	14.48149	0.04381	11.43462	440.3522
0.06	1.19914	18.25085	9.66591	0.06570	7.64285	193.0311
0.08	1.19847	13.68431	7.26161	0.08758	5.75288	106.7182
0.10	1.19760	10.94351	5.82183	0.10944	4.62363	66.9216
0.12	1.19655	9.11559	4.86432	0.13126	3.87473	45.4080
0.14	1.19531	7.80932	4.18240	0.15306	3.34317	32.5113
0.16	1.19389	6.82907	3.67274	0.17482	2.94743	24.1978
0.18	1.19227	6.06618	3.27793	0.19654	2.64223	18.5427
0.20	1.19048	5.45545	2.96352	0.21822	2.40040	14.5333
0.22	1.18850	4.95537	2.70760	0.23984	2.20464	11.5961
0.24	1.18633	4.53829	2.49556	0.26141	2.04344	9.3865
0.26	1.18399	4.18506	2.31729	0.28291	1.90880	7.6876
0.28	1.18147	3.88199	2.16555	0.30435	1.79503	6.3572
0.30	1.17878	3.61906	2.03506	0.32572	1.69794	5.2993
0.32	1.17592	3.38874	1.92185	0.34701	1.61440	4.4467
0.34	1.17288	3.18529	1.82288	0.36822	1.54200	3.7520
0.36	1.16968	3.00422	1.73578	0.38935	1.47888	3.1801
0.38	1.16632	2.84200	1.65870	0.41039	1.42356	2.7054
0.40	1.16279	2.69582	1.59014	0.43133	1.37487	2.3085
0.42	1.15911	2.56338	1.52890	0.45218	1.33184	1.9744
0.44	1.15527	2.44280	1.47400	0.47293	1.29371	1.6915
0.46	1.15128	2.33256	1.42463	0.49357	1.25981	1.4509
0.48	1.14714	2.23135	1.38010	0.51410	1.22962	1.2453
0.50	1.14286	2.13809	1.33984	0.53452	1.20268	1.0691
0.52	1.13843	2.05187	1.30339	0.55483	1.17860	0.9174
0.54	1.13387	1.97192	1.27032	0.57501	1.15705	0.7866
0.56	1.12918	1.89755	1.24029	0.59507	1.13777	0.6736
0.58	1.12435	1.82820	1.21301	0.61501	1.12050	0.5757
0.60	1.11940	1.76336	1.18820	0.63481	1.10504	0.4908
0.62	1.11433	1.70261	1.16565	0.65448	1.09120	0.4172
0.64	1.10914	1.64556	1.14515	0.67402	1.07883	0.3533
0.66	1.10383	1.59187	1.12653	0.69342	1.06777	0.2979
0.68	1.09842	1.54126	1.10965	0.71268	1.05792	0.2498
0.70	1.09290	1.49345	1.09437	0.73179	1.04915	0.2081
0.72	1.08727	1.44823	1.08057	0.75076	1.04137	0.1721
0.74	1.08155	1.40537	1.06814	0.76958	1.03449	0.1411
0.76	1.07573	1.36470	1.05700	0.78825	1.02844	0.1145
0.78	1.06982	1.32606	1.04705	0.80677	1.02314	0.0917
0.80	1.06383	1.28928	1.03823	0.82514	1.01853	0.0723
0.82	1.05775	1.25423	1.03046	0.84335	1.01455	0.0559
0.84	1.05160	1.22080	1.02370	0.86140	1.01115	0.0423

(continued)

Table A.4 (Continued)

$M$	$T/T^*$	$p/p^*$	$p_0/p_0^*$	$\rho^*/\rho$	$F/F^*$	$4 f l_{\max}/D$
0.86	1.04537	1.18888	1.01787	0.87929	1.00829	0.0310
0.88	1.03907	1.15835	1.01294	0.89703	1.00591	0.0218
0.90	1.03270	1.12913	1.00886	0.91460	1.00399	0.0145
0.92	1.02627	1.10114	1.00560	0.93201	1.00248	0.0089
0.94	1.01978	1.07430	1.00311	0.94925	1.00136	0.0048
0.96	1.01324	1.04854	1.00136	0.96633	1.00059	0.0026
0.98	1.00664	1.02379	1.00034	0.98325	1.00014	0.0005
1.00	1.00000	1.00000	1.00000	1.00000	1.00000	0.0000
1.02	0.99331	0.97711	1.00033	1.01658	1.00014	0.0005
1.04	0.98658	0.95507	1.00130	1.03300	1.00053	0.0018
1.06	0.97982	0.93383	1.00291	1.04925	1.00116	0.0038
1.08	0.97302	0.91335	1.00512	1.06533	1.00200	0.0066
1.10	0.96618	0.89359	1.00792	1.08124	1.00305	0.0099
1.12	0.95932	0.87451	1.01131	1.09698	1.00429	0.0138
1.14	0.95244	0.85608	1.01527	1.11256	1.00569	0.0182
1.16	0.94554	0.83827	1.01978	1.12797	1.00726	0.0230
1.18	0.93861	0.82104	1.02484	1.14321	1.00897	0.0281
1.20	0.93168	0.80436	1.03044	1.15828	1.01081	0.0336
1.22	0.92473	0.78822	1.03657	1.17319	1.01278	0.0394
1.24	0.91777	0.77258	1.04323	1.18792	1.01486	0.0455
1.26	0.91080	0.75743	1.05041	1.20249	1.01705	0.0517
1.28	0.90383	0.74274	1.05810	1.21690	1.01933	0.0582
1.30	0.89686	0.72848	1.06630	1.23114	1.02170	0.0648
1.32	0.88989	0.71465	1.07502	1.24521	1.02414	0.0716
1.34	0.88292	0.70122	1.08424	1.25912	1.02666	0.0785
1.36	0.87596	0.68818	1.09396	1.27286	1.02925	0.0855
1.38	0.86901	0.67551	1.10419	1.28645	1.03189	0.0926
1.40	0.86207	0.66320	1.11493	1.29987	1.03459	0.0997
1.42	0.85514	0.65122	1.12616	1.31313	1.03733	0.1069
1.44	0.84822	0.63958	1.13790	1.32623	1.04012	0.1142
1.46	0.84133	0.62825	1.15015	1.33917	1.04295	0.1215
1.48	0.83445	0.61722	1.16290	1.35195	1.04581	0.1288
1.50	0.82759	0.60648	1.17617	1.36458	1.04870	0.1360
1.52	0.82075	0.59602	1.18994	1.37705	1.05162	0.1433
1.54	0.81393	0.58583	1.20423	1.38936	1.05456	0.1506
1.56	0.80715	0.57591	1.21904	1.40152	1.05752	0.1579
1.58	0.80038	0.56623	1.23438	1.41353	1.06049	0.1651
1.60	0.79365	0.55679	1.25023	1.42539	1.06348	0.1724
1.62	0.78695	0.54759	1.26662	1.43710	1.06647	0.1795
1.64	0.78028	0.53862	1.28355	1.44866	1.06948	0.1867
1.66	0.77363	0.52986	1.30102	1.46008	1.07249	0.1938

(continued)

Table A.4 (Continued)

$M$	$T/T^*$	$p/p^*$	$p_0/p_0^*$	$\rho^*/\rho$	$F/F^*$	$4 fl_{\max}/D$
1.68	0.76703	0.52131	1.31904	1.47135	1.07550	0.2008
1.70	0.76046	0.51297	1.33761	1.48247	1.07851	0.2078
1.72	0.75392	0.50482	1.35673	1.49345	1.08152	0.2147
1.74	0.74742	0.49686	1.37643	1.50429	1.08453	0.2216
1.76	0.74096	0.48909	1.39670	1.51499	1.08753	0.2284
1.78	0.73454	0.48149	1.41754	1.52555	1.09053	0.2352
1.80	0.72816	0.47407	1.43898	1.53598	1.09351	0.2419
1.82	0.72181	0.46681	1.46101	1.54626	1.09649	0.2485
1.84	0.71551	0.45972	1.48365	1.55642	1.09946	0.2551
1.86	0.70925	0.45278	1.50689	1.56644	1.10241	0.2616
1.88	0.70304	0.44600	1.53076	1.57633	1.10536	0.2680
1.90	0.69686	0.43936	1.55525	1.58609	1.10829	0.2743
1.92	0.69074	0.43287	1.58039	1.59572	1.11120	0.2806
1.94	0.68465	0.42651	1.60617	1.60523	1.11410	0.2868
1.96	0.67861	0.42030	1.63261	1.61460	1.11698	0.2929
1.98	0.67262	0.41421	1.65972	1.62386	1.11984	0.2990
2.00	0.66667	0.40825	1.68750	1.63299	1.12268	0.3050
2.02	0.66076	0.40241	1.71597	1.64200	1.12551	0.3109
2.04	0.65491	0.39670	1.74514	1.65090	1.12831	0.3168
2.06	0.64910	0.39110	1.77501	1.65967	1.13110	0.3225
2.08	0.64334	0.38562	1.80561	1.66833	1.13387	0.3282
2.10	0.63762	0.38024	1.83694	1.67687	1.13661	0.3339
2.12	0.63195	0.37498	1.86902	1.68530	1.13933	0.3394
2.14	0.62633	0.36982	1.90184	1.69362	1.14204	0.3449
2.16	0.62076	0.36476	1.93543	1.70182	1.14471	0.3503
2.18	0.61523	0.35980	1.96981	1.70992	1.14737	0.3556
2.20	0.60976	0.35494	2.00497	1.71791	1.15001	0.3609
2.22	0.60433	0.35017	2.04094	1.72579	1.15262	0.3661
2.24	0.59895	0.34550	2.07773	1.73357	1.15521	0.3712
2.26	0.59361	0.34091	2.11535	1.74125	1.15777	0.3763
2.28	0.58833	0.33641	2.15381	1.74882	1.16032	0.3813
2.30	0.58309	0.33200	2.19313	1.75629	1.16284	0.3862
2.32	0.57790	0.32767	2.23332	1.76366	1.16533	0.3911
2.34	0.57276	0.32342	2.27440	1.77093	1.16780	0.3959
2.36	0.56767	0.31925	2.31638	1.77811	1.17025	0.4006
2.38	0.56262	0.31516	2.35927	1.78519	1.17268	0.4053
2.40	0.55762	0.31114	2.40310	1.79218	1.17508	0.4099
2.42	0.55267	0.30720	2.44787	1.79907	1.17746	0.4144
2.44	0.54777	0.30332	2.49360	1.80587	1.17981	0.4189
2.46	0.54291	0.29952	2.54031	1.81258	1.18214	0.4233
2.48	0.53810	0.29579	2.58801	1.81921	1.18445	0.4277

(continued)

Table A.4 (Continued)

$M$	$T/T^*$	$p/p^*$	$p_0/p_0^*$	$\rho^*/\rho$	$F/F^*$	$4 f l_{\max}/D$
2.50	0.53333	0.29212	2.63671	1.82574	1.18673	0.4320
2.52	0.52862	0.28852	2.68645	1.83219	1.18899	0.4362
2.54	0.52394	0.28498	2.73722	1.83855	1.19123	0.4404
2.56	0.51932	0.28150	2.78906	1.84483	1.19344	0.4445
2.58	0.51474	0.27808	2.84197	1.85103	1.19563	0.4486
2.60	0.51020	0.27473	2.89597	1.85714	1.19780	0.4526
2.62	0.50572	0.27143	2.95108	1.86318	1.19995	0.4565
2.64	0.50127	0.26818	3.00733	1.86913	1.20207	0.4604
2.66	0.49687	0.26500	3.06471	1.87501	1.20417	0.4643
2.68	0.49251	0.26186	3.12327	1.88081	1.20625	0.4681
2.70	0.48820	0.25878	3.18300	1.88653	1.20830	0.4718
2.72	0.48393	0.25576	3.24394	1.89218	1.21033	0.4755
2.74	0.47971	0.25278	3.30611	1.89775	1.21235	0.4791
2.76	0.47553	0.24985	3.36951	1.90325	1.21433	0.4827
2.78	0.47139	0.24697	3.43417	1.90868	1.21630	0.4863
2.80	0.46729	0.24414	3.50012	1.91404	1.21825	0.4898
2.82	0.46324	0.24135	3.56736	1.91933	1.22017	0.4932
2.84	0.45922	0.23861	3.63593	1.92455	1.22208	0.4966
2.86	0.45525	0.23592	3.70584	1.92970	1.22396	0.5000
2.88	0.45132	0.23326	3.77711	1.93479	1.22582	0.5033
2.90	0.44743	0.23066	3.84976	1.93981	1.22766	0.5065
2.92	0.44358	0.22809	3.92382	1.94477	1.22948	0.5097
2.94	0.43977	0.22556	3.99931	1.94966	1.23128	0.5129
2.96	0.43600	0.22307	4.07625	1.95449	1.23307	0.5160
2.98	0.43226	0.22063	4.15465	1.95925	1.23483	0.5191
3.00	0.42857	0.21822	4.23456	1.96396	1.23657	0.5222
3.02	0.42492	0.21585	4.31598	1.96861	1.23829	0.5252
3.04	0.42130	0.21351	4.39894	1.97319	1.23999	0.5281
3.06	0.41772	0.21121	4.48347	1.97772	1.24168	0.5310
3.08	0.41418	0.20895	4.56958	1.98219	1.24334	0.5339
3.10	0.41068	0.20672	4.65730	1.98661	1.24499	0.5368
3.12	0.40721	0.20453	4.74666	1.99097	1.24662	0.5396
3.14	0.40378	0.20237	4.83768	1.99527	1.24823	0.5424
3.16	0.40038	0.20024	4.93038	1.99952	1.24982	0.5451
3.18	0.39703	0.19814	5.02480	2.00371	1.25139	0.5478
3.20	0.39370	0.19608	5.12095	2.00786	1.25295	0.5504
3.22	0.39041	0.19405	5.21886	2.01195	1.25449	0.5531
3.24	0.38716	0.19204	5.31855	2.01599	1.25601	0.5557
3.26	0.38394	0.19007	5.42006	2.01998	1.25752	0.5582
3.28	0.38075	0.18812	5.52342	2.02392	1.25901	0.5607
3.30	0.37760	0.18621	5.62863	2.02781	1.26048	0.5632

(continued)

Table A.4 (Continued)

$M$	$T/T^*$	$p/p^*$	$p_0/p_0^*$	$\rho^*/\rho$	$F/F^*$	$4 fl_{\max}/D$
3.32	0.37448	0.18432	5.73574	2.03165	1.26193	0.5657
3.34	0.37139	0.18246	5.84478	2.03545	1.26337	0.5681
3.36	0.36833	0.18063	5.95576	2.03920	1.26479	0.5705
3.38	0.36531	0.17882	6.06872	2.04290	1.26620	0.5729
3.40	0.36232	0.17704	6.18368	2.04656	1.26759	0.5752
3.42	0.35936	0.17528	6.30068	2.05017	1.26897	0.5775
3.44	0.35643	0.17355	6.41974	2.05374	1.27033	0.5798
3.46	0.35353	0.17185	6.54090	2.05727	1.27167	0.5820
3.48	0.35066	0.17016	6.66418	2.06075	1.27300	0.5842
3.50	0.34783	0.16851	6.78961	2.06419	1.27432	0.5864
3.52	0.34502	0.16687	6.91721	2.06759	1.27562	0.5886
3.54	0.34224	0.16526	7.04704	2.07094	1.27691	0.5907
3.56	0.33949	0.16367	7.17911	2.07426	1.27818	0.5928
3.58	0.33677	0.16210	7.31345	2.07754	1.27944	0.5949
3.60	0.33408	0.16055	7.45010	2.08077	1.28068	0.5970
3.62	0.33141	0.15903	7.58908	2.08397	1.28191	0.5990
3.64	0.32877	0.15752	7.73043	2.08713	1.28313	0.6010
3.66	0.32616	0.15604	7.87419	2.09026	1.28433	0.6030
3.68	0.32358	0.15458	8.02038	2.09334	1.28552	0.6049
3.70	0.32103	0.15313	8.16904	2.09639	1.28670	0.6068
3.72	0.31850	0.15171	8.32021	2.09941	1.28787	0.6087
3.74	0.31600	0.15030	8.47391	2.10238	1.28902	0.6106
3.76	0.31352	0.14892	8.63018	2.10533	1.29016	0.6125
3.78	0.31107	0.14755	8.78905	2.10824	1.29128	0.6143
3.80	0.30864	0.14620	8.95057	2.11111	1.29240	0.6161
3.82	0.30624	0.14487	9.11475	2.11395	1.29350	0.6179
3.84	0.30387	0.14355	9.28164	2.11676	1.29459	0.6197
3.86	0.30151	0.14225	9.45128	2.11954	1.29567	0.6214
3.88	0.29919	0.14097	9.62371	2.12228	1.29674	0.6231
3.90	0.29688	0.13971	9.79895	2.12499	1.29779	0.6248
3.92	0.29460	0.13846	9.97704	2.12767	1.29883	0.6265
3.94	0.29235	0.13723	10.15803	2.13032	1.29987	0.6282
3.96	0.29011	0.13602	10.34194	2.13294	1.30089	0.6298
3.98	0.28790	0.13482	10.52883	2.13553	1.30190	0.6315
4.00	0.28571	0.13363	10.71872	2.13809	1.30290	0.6331
4.02	0.28355	0.13246	10.91166	2.14062	1.30389	0.6346
4.04	0.28140	0.13131	11.10768	2.14312	1.30487	0.6362
4.06	0.27928	0.13017	11.30681	2.14560	1.30583	0.6378
4.08	0.27718	0.12904	11.50912	2.14804	1.30679	0.6393
4.10	0.27510	0.12793	11.71463	2.15046	1.30774	0.6408
4.12	0.27304	0.12683	11.92337	2.15285	1.30868	0.6423
4.14	0.27101	0.12574	12.13540	2.15522	1.30960	0.6438

(continued)



Table A.4 (Continued)

$M$	$T/T^*$	$p/p^*$	$p_0/p_0^*$	$\rho^*/\rho$	$F/F^*$	$4\,fl_{\max}/D$
4.16	0.26899	0.12467	12.35076	2.15756	1.31052	0.6452
4.18	0.26699	0.12362	12.56947	2.15987	1.31143	0.6467
4.20	0.26502	0.12257	12.79160	2.16215	1.31233	0.6481
4.22	0.26306	0.12154	13.01719	2.16442	1.31322	0.6495
4.24	0.26112	0.12052	13.24626	2.16665	1.31410	0.6509
4.26	0.25921	0.11951	13.47888	2.16886	1.31497	0.6523
4.28	0.25731	0.11852	13.71505	2.17105	1.31583	0.6536
4.30	0.25543	0.11753	13.95487	2.17321	1.31668	0.6550
4.32	0.25357	0.11656	14.19835	2.17535	1.31752	0.6563
4.34	0.25172	0.11560	14.44554	2.17747	1.31836	0.6576
4.36	0.24990	0.11466	14.69648	2.17956	1.31919	0.6589
4.38	0.24809	0.11372	14.95123	2.18163	1.32000	0.6602
4.40	0.24631	0.11279	15.20983	2.18368	1.32081	0.6615
4.42	0.24453	0.11188	15.47233	2.18571	1.32161	0.6627
4.44	0.24278	0.11097	15.73875	2.18771	1.32241	0.6640
4.46	0.24105	0.11008	16.00916	2.18970	1.32319	0.6652
4.48	0.23933	0.10920	16.28361	2.19166	1.32397	0.6664
4.50	0.23762	0.10833	16.56215	2.19360	1.32474	0.6676
4.52	0.23594	0.10746	16.84483	2.19552	1.32550	0.6688
4.54	0.23427	0.10661	17.13165	2.19742	1.32625	0.6700
4.56	0.23262	0.10577	17.42273	2.19930	1.32700	0.6712
4.58	0.23098	0.10494	17.71807	2.20116	1.32773	0.6723
4.60	0.22936	0.10411	18.01775	2.20300	1.32846	0.6734
4.62	0.22775	0.10330	18.32179	2.20482	1.32919	0.6746
4.64	0.22616	0.10249	18.63027	2.20662	1.32990	0.6757
4.66	0.22459	0.10170	18.94323	2.20841	1.33061	0.6768
4.68	0.22303	0.10091	19.26071	2.21017	1.33131	0.6779
4.70	0.22148	0.10013	19.58277	2.21192	1.33201	0.6790
4.72	0.21995	0.09936	19.90947	2.21365	1.33269	0.6800
4.74	0.21844	0.09860	20.24085	2.21536	1.33338	0.6811
4.76	0.21694	0.09785	20.57698	2.21705	1.33405	0.6821
4.78	0.21545	0.09711	20.91790	2.21872	1.33472	0.6831
4.80	0.21398	0.09637	21.26365	2.22038	1.33538	0.6842
4.82	0.21252	0.09564	21.61431	2.22202	1.33603	0.6852
4.84	0.21108	0.09492	21.96992	2.22365	1.33668	0.6862
4.86	0.20965	0.09421	22.33055	2.22526	1.33732	0.6872
4.88	0.20823	0.09351	22.69624	2.22685	1.33796	0.6881
4.90	0.20683	0.09281	23.06705	2.22842	1.33859	0.6891
4.92	0.20543	0.09212	23.44304	2.22998	1.33921	0.6901
4.94	0.20406	0.09144	23.82427	2.23153	1.33983	0.6910
4.96	0.20269	0.09077	24.21077	2.23306	1.34044	0.6920
4.98	0.20134	0.09010	24.60265	2.23457	1.34104	0.6929
5.00	0.20000	0.08944	24.99994	2.23607	1.34164	0.6938

**Table A.5** One-dimensional frictionless flow with change in stagnation temperature ( $\gamma = 1.4$ ).

$M$	$T_0/T_0^*$	$T/T^*$	$p/p^*$	$p_0/p_0^*$	$\rho^*/\rho$
0.00	0.00000	0.00000	2.40000	1.26788	0.00000
0.02	0.00192	0.00230	2.39866	1.26752	0.00096
0.04	0.00765	0.00917	2.39464	1.26646	0.00383
0.06	0.01712	0.02053	2.38796	1.26470	0.00860
0.08	0.03022	0.03621	2.37869	1.26226	0.01522
0.10	0.04678	0.05602	2.36686	1.25915	0.02367
0.12	0.06661	0.07970	2.35257	1.25539	0.03388
0.14	0.08947	0.10695	2.33590	1.25103	0.04578
0.16	0.11511	0.13743	2.31696	1.24608	0.05931
0.18	0.14324	0.17078	2.29586	1.24059	0.07439
0.20	0.17355	0.20661	2.27273	1.23460	0.09091
0.22	0.20574	0.24452	2.24770	1.22814	0.10879
0.24	0.23948	0.28411	2.22091	1.22126	0.12792
0.26	0.27446	0.32496	2.19250	1.21400	0.14821
0.28	0.31035	0.36667	2.16263	1.20642	0.16955
0.30	0.34686	0.40887	2.13144	1.19855	0.19183
0.32	0.38369	0.45119	2.09908	1.19045	0.21495
0.34	0.42056	0.49327	2.06569	1.18215	0.23879
0.36	0.45723	0.53482	2.03142	1.17371	0.26327
0.38	0.49346	0.57553	1.99641	1.16517	0.28828
0.40	0.52903	0.61515	1.96078	1.15658	0.31373
0.42	0.56376	0.65346	1.92468	1.14796	0.33951
0.44	0.59748	0.69025	1.88822	1.13936	0.36556
0.46	0.63007	0.72538	1.85151	1.13082	0.39178
0.48	0.66139	0.75871	1.81466	1.12238	0.41810
0.50	0.69136	0.79012	1.77778	1.11405	0.44444
0.52	0.71990	0.81955	1.74095	1.10588	0.47075
0.54	0.74695	0.84695	1.70425	1.09789	0.49696
0.56	0.77249	0.87227	1.66778	1.09011	0.52302
0.58	0.79648	0.89552	1.63159	1.08256	0.54887
0.60	0.81892	0.91670	1.59574	1.07525	0.57447
0.62	0.83983	0.93584	1.56031	1.06822	0.59978
0.64	0.85920	0.95298	1.52532	1.06147	0.62477
0.66	0.87708	0.96816	1.49083	1.05503	0.64941
0.68	0.89350	0.98144	1.45688	1.04890	0.67366
0.70	0.90850	0.99290	1.42349	1.04310	0.69751
0.72	0.92212	1.00260	1.39069	1.03764	0.72093
0.74	0.93442	1.01062	1.35851	1.03253	0.74392
0.76	0.94546	1.01706	1.32696	1.02777	0.76645
0.78	0.95528	1.02198	1.29606	1.02337	0.78853
0.80	0.96395	1.02548	1.26582	1.01934	0.81013
0.82	0.97152	1.02763	1.23625	1.01569	0.83125

(continued)

Table A.5 (Continued)

$M$	$T_0/T_0^*$	$T/T^*$	$p/p^*$	$p_0/p_0^*$	$\rho^*/\rho$
0.84	0.97807	1.02853	1.20734	1.01241	0.85190
0.86	0.98363	1.02826	1.17911	1.00951	0.87207
0.88	0.98828	1.02689	1.15154	1.00699	0.89175
0.90	0.99207	1.02452	1.12465	1.00486	0.91097
0.92	0.99506	1.02120	1.09842	1.00311	0.92970
0.94	0.99729	1.01702	1.07285	1.00175	0.94797
0.96	0.99883	1.01205	1.04793	1.00078	0.96577
0.98	0.99971	1.00636	1.02365	1.00019	0.98311
1.00	1.00000	1.00000	1.00000	1.00000	1.00000
1.02	0.99973	0.99304	0.97698	1.00019	1.01645
1.04	0.99895	0.98554	0.95456	1.00078	1.03245
1.06	0.99769	0.97756	0.93275	1.00175	1.04804
1.08	0.99601	0.96913	0.91152	1.00311	1.06320
1.10	0.99392	0.96031	0.89087	1.00486	1.07795
1.12	0.99148	0.95115	0.87078	1.00699	1.09230
1.14	0.98871	0.94169	0.85123	1.00952	1.10626
1.16	0.98564	0.93196	0.83222	1.01243	1.11984
1.18	0.98230	0.92200	0.81374	1.01573	1.13305
1.20	0.97872	0.91185	0.79576	1.01941	1.14589
1.22	0.97492	0.90153	0.77827	1.02349	1.15838
1.24	0.97092	0.89108	0.76127	1.02795	1.17052
1.26	0.96675	0.88052	0.74473	1.03280	1.18233
1.28	0.96243	0.86988	0.72865	1.03803	1.19382
1.30	0.95798	0.85917	0.71301	1.04366	1.20499
1.32	0.95341	0.84843	0.69780	1.04967	1.21585
1.34	0.94873	0.83766	0.68301	1.05608	1.22642
1.36	0.94398	0.82689	0.66863	1.06288	1.23669
1.38	0.93914	0.81613	0.65464	1.07007	1.24669
1.40	0.93425	0.80539	0.64103	1.07765	1.25641
1.42	0.92931	0.79469	0.62779	1.08563	1.26587
1.44	0.92434	0.78405	0.61491	1.09401	1.27507
1.46	0.91933	0.77346	0.60237	1.10278	1.28402
1.48	0.91431	0.76294	0.59018	1.11196	1.29273
1.50	0.90928	0.75250	0.57831	1.12154	1.30120
1.52	0.90424	0.74215	0.56673	1.13153	1.30945
1.54	0.89920	0.73189	0.55553	1.14193	1.31748
1.56	0.89418	0.72174	0.54458	1.15274	1.32530
1.58	0.88917	0.71168	0.53393	1.16397	1.33291
1.60	0.88419	0.70174	0.52356	1.17561	1.34031
1.62	0.87922	0.69190	0.51346	1.18768	1.34753
1.64	0.87429	0.68219	0.50363	1.20017	1.35455
1.66	0.86939	0.67259	0.49405	1.21309	1.36139

(continued)

Table A.5 (Continued)

$M$	$T_0/T_0^*$	$T/T^*$	$p/p^*$	$p_0/p_0^*$	$\rho^*/\rho$
1.68	0.86453	0.66312	0.48472	1.22644	1.36806
1.70	0.85971	0.65377	0.47562	1.24023	1.37455
1.72	0.85493	0.64455	0.46677	1.25447	1.38088
1.74	0.85019	0.63545	0.45813	1.26915	1.38705
1.76	0.84551	0.62649	0.44972	1.28428	1.39306
1.78	0.84087	0.61765	0.44152	1.29987	1.39891
1.80	0.83628	0.60894	0.43353	1.31592	1.40462
1.82	0.83174	0.60036	0.42573	1.33244	1.41019
1.84	0.82726	0.59191	0.41813	1.34943	1.41562
1.86	0.82283	0.58359	0.41072	1.36690	1.42092
1.88	0.81846	0.57540	0.40349	1.38486	1.42608
1.90	0.81414	0.56734	0.39643	1.40330	1.43112
1.92	0.80987	0.55941	0.38955	1.42224	1.43604
1.94	0.80567	0.55160	0.38283	1.44168	1.44083
1.96	0.80152	0.54392	0.37628	1.46164	1.44551
1.98	0.79742	0.53636	0.36988	1.48210	1.45008
2.00	0.79339	0.52893	0.36364	1.50310	1.45455
2.02	0.78941	0.52161	0.35754	1.52462	1.45890
2.04	0.78549	0.51442	0.35158	1.54668	1.46315
2.06	0.78162	0.50735	0.34577	1.56928	1.46731
2.08	0.77782	0.50040	0.34009	1.59244	1.47136
2.10	0.77406	0.49356	0.33454	1.61616	1.47533
2.12	0.77037	0.48684	0.32912	1.64045	1.47920
2.14	0.76673	0.48023	0.32382	1.66531	1.48298
2.16	0.76314	0.47373	0.31865	1.69076	1.48668
2.18	0.75961	0.46734	0.31359	1.71680	1.49029
2.20	0.75613	0.46106	0.30864	1.74345	1.49383
2.22	0.75271	0.45488	0.30381	1.77070	1.49728
2.24	0.74934	0.44882	0.29908	1.79858	1.50066
2.26	0.74602	0.44285	0.29446	1.82708	1.50396
2.28	0.74276	0.43698	0.28993	1.85623	1.50719
2.30	0.73954	0.43122	0.28551	1.88602	1.51035
2.32	0.73638	0.42555	0.28118	1.91647	1.51344
2.34	0.73326	0.41998	0.27695	1.94759	1.51646
2.36	0.73020	0.41451	0.27281	1.97939	1.51942
2.38	0.72718	0.40913	0.26875	2.01187	1.52232
2.40	0.72421	0.40384	0.26478	2.04505	1.52515
2.42	0.72129	0.39864	0.26090	2.07895	1.52793
2.44	0.71842	0.39352	0.25710	2.11356	1.53065
2.46	0.71558	0.38850	0.25337	2.14891	1.53331
2.48	0.71280	0.38356	0.24973	2.18499	1.53591
2.50	0.71006	0.37870	0.24615	2.22183	1.53846

(continued)

Table A.5 (Continued)

$M$	$T_0/T_0^*$	$T/T^*$	$p/p^*$	$p_0/p_0^*$	$\rho^*/\rho$
2.52	0.70736	0.37392	0.24266	2.25943	1.54096
2.54	0.70471	0.36923	0.23923	2.29781	1.54341
2.56	0.70210	0.36461	0.23587	2.33698	1.54581
2.58	0.69953	0.36007	0.23258	2.37696	1.54816
2.60	0.69700	0.35561	0.22936	2.41774	1.55046
2.62	0.69451	0.35122	0.22620	2.45934	1.55272
2.64	0.69206	0.34691	0.22310	2.50179	1.55493
2.66	0.68964	0.34266	0.22007	2.54509	1.55710
2.68	0.68727	0.33849	0.21709	2.58925	1.55922
2.70	0.68494	0.33439	0.21417	2.63428	1.56131
2.72	0.68264	0.33035	0.21131	2.68021	1.56335
2.74	0.68037	0.32638	0.20850	2.72703	1.56536
2.76	0.67815	0.32248	0.20575	2.77478	1.56732
2.78	0.67595	0.31864	0.20305	2.82345	1.56925
2.80	0.67380	0.31486	0.20040	2.87307	1.57114
2.82	0.67167	0.31114	0.19780	2.92365	1.57300
2.84	0.66958	0.30749	0.19525	2.97521	1.57482
2.86	0.66752	0.30389	0.19275	3.02775	1.57661
2.88	0.66550	0.30035	0.19029	3.08129	1.57836
2.90	0.66350	0.29687	0.18788	3.13585	1.58008
2.92	0.66154	0.29344	0.18552	3.19144	1.58178
2.94	0.65960	0.29007	0.18319	3.24808	1.58343
2.96	0.65770	0.28675	0.18091	3.30578	1.58506
2.98	0.65583	0.28349	0.17867	3.36457	1.58666
3.00	0.65398	0.28028	0.17647	3.42445	1.58824
3.02	0.65216	0.27711	0.17431	3.48544	1.58978
3.04	0.65037	0.27400	0.17219	3.54755	1.59129
3.06	0.64861	0.27094	0.17010	3.61081	1.59278
3.08	0.64687	0.26792	0.16806	3.67524	1.59425
3.10	0.64516	0.26495	0.16604	3.74084	1.59568
3.12	0.64348	0.26203	0.16407	3.80763	1.59709
3.14	0.64182	0.25915	0.16212	3.87564	1.59848
3.16	0.64018	0.25632	0.16022	3.94487	1.59985
3.18	0.63858	0.25353	0.15834	4.01536	1.60119
3.20	0.63699	0.25078	0.15649	4.08711	1.60250
3.22	0.63543	0.24808	0.15468	4.16014	1.60380
3.24	0.63389	0.24541	0.15290	4.23448	1.60507
3.26	0.63237	0.24279	0.15115	4.31013	1.60632
3.28	0.63088	0.24021	0.14942	4.38713	1.60755
3.30	0.62941	0.23766	0.14773	4.46548	1.60877
3.32	0.62795	0.23515	0.14606	4.54521	1.60996
3.34	0.62652	0.23268	0.14442	4.62634	1.61113

(continued)

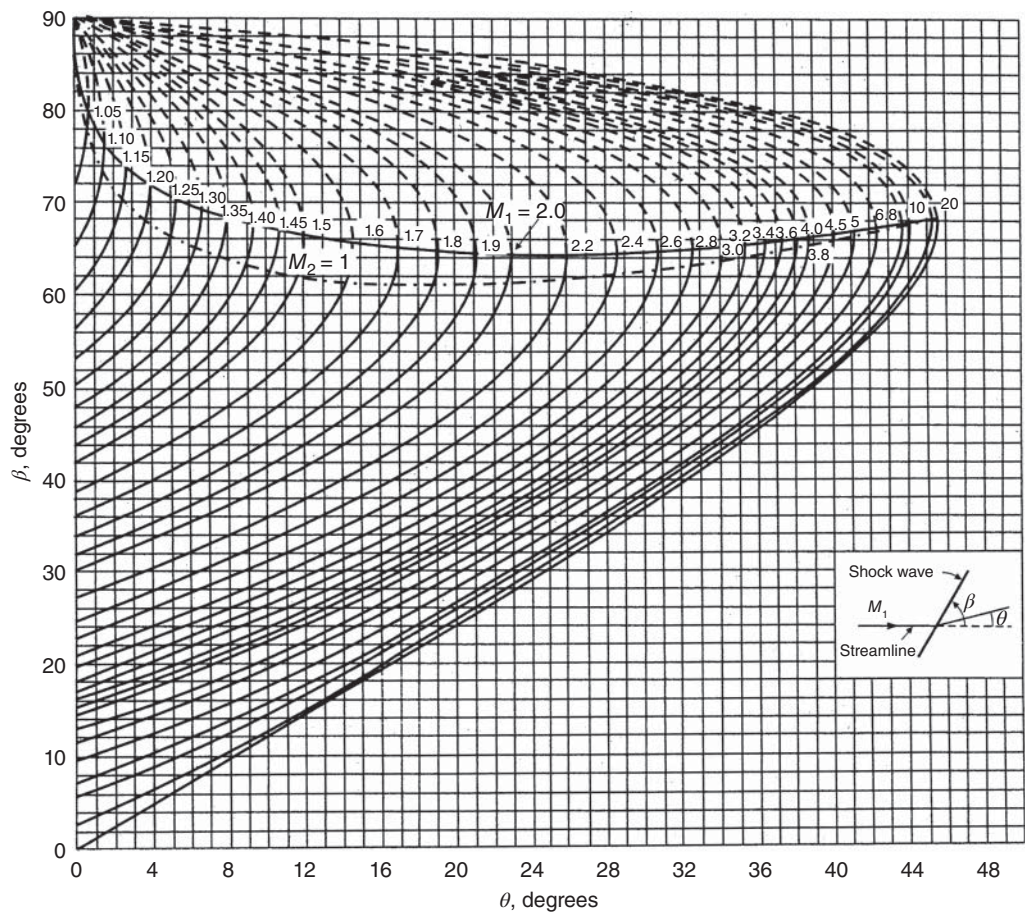
Table A.5 (Continued)

$M$	$T_0/T_0^*$	$T/T^*$	$p/p^*$	$p_0/p_0^*$	$\rho^*/\rho$
3.36	0.62512	0.23025	0.14281	4.70888	1.61228
3.38	0.62373	0.22785	0.14122	4.79286	1.61341
3.40	0.62236	0.22549	0.13966	4.87829	1.61452
3.42	0.62101	0.22317	0.13813	4.96520	1.61562
3.44	0.61968	0.22087	0.13662	5.05361	1.61670
3.46	0.61837	0.21861	0.13513	5.14354	1.61776
3.48	0.61708	0.21639	0.13367	5.23500	1.61881
3.50	0.61581	0.21419	0.13223	5.32802	1.61983
3.52	0.61455	0.21203	0.13081	5.42263	1.62085
3.54	0.61331	0.20990	0.12942	5.51883	1.62184
3.56	0.61209	0.20780	0.12805	5.61666	1.62282
3.58	0.61089	0.20573	0.12670	5.71614	1.62379
3.60	0.60970	0.20369	0.12537	5.81729	1.62474
3.62	0.60853	0.20167	0.12406	5.92012	1.62567
3.64	0.60738	0.19969	0.12277	6.02467	1.62660
3.66	0.60624	0.19773	0.12150	6.13096	1.62750
3.68	0.60512	0.19581	0.12024	6.23900	1.62840
3.70	0.60401	0.19390	0.11901	6.34883	1.62928
3.72	0.60292	0.19203	0.11780	6.46046	1.63014
3.74	0.60184	0.19018	0.11660	6.57393	1.63100
3.76	0.60078	0.18836	0.11543	6.68925	1.63184
3.78	0.59973	0.18656	0.11427	6.80645	1.63267
3.80	0.59870	0.18478	0.11312	6.92555	1.63348
3.82	0.59768	0.18303	0.11200	7.04658	1.63429
3.84	0.59667	0.18131	0.11089	7.16956	1.63508
3.86	0.59568	0.17961	0.10979	7.29452	1.63586
3.88	0.59470	0.17793	0.10871	7.42149	1.63663
3.90	0.59373	0.17627	0.10765	7.55048	1.63739
3.92	0.59278	0.17463	0.10661	7.68154	1.63814
3.94	0.59184	0.17302	0.10557	7.81467	1.63888
3.96	0.59091	0.17143	0.10456	7.94991	1.63960
3.98	0.58999	0.16986	0.10355	8.08729	1.64032
4.00	0.58909	0.16831	0.10256	8.22683	1.64103
4.02	0.58819	0.16678	0.10159	8.36856	1.64172
4.04	0.58731	0.16527	0.10063	8.51250	1.64241
4.06	0.58644	0.16378	0.09968	8.65869	1.64309
4.08	0.58558	0.16231	0.09875	8.80716	1.64375
4.10	0.58473	0.16086	0.09782	8.95792	1.64441
4.12	0.58390	0.15943	0.09691	9.11101	1.64506
4.14	0.58307	0.15802	0.09602	9.26647	1.64570
4.16	0.58225	0.15662	0.09513	9.42431	1.64633
4.18	0.58145	0.15524	0.09426	9.58456	1.64696

(continued)

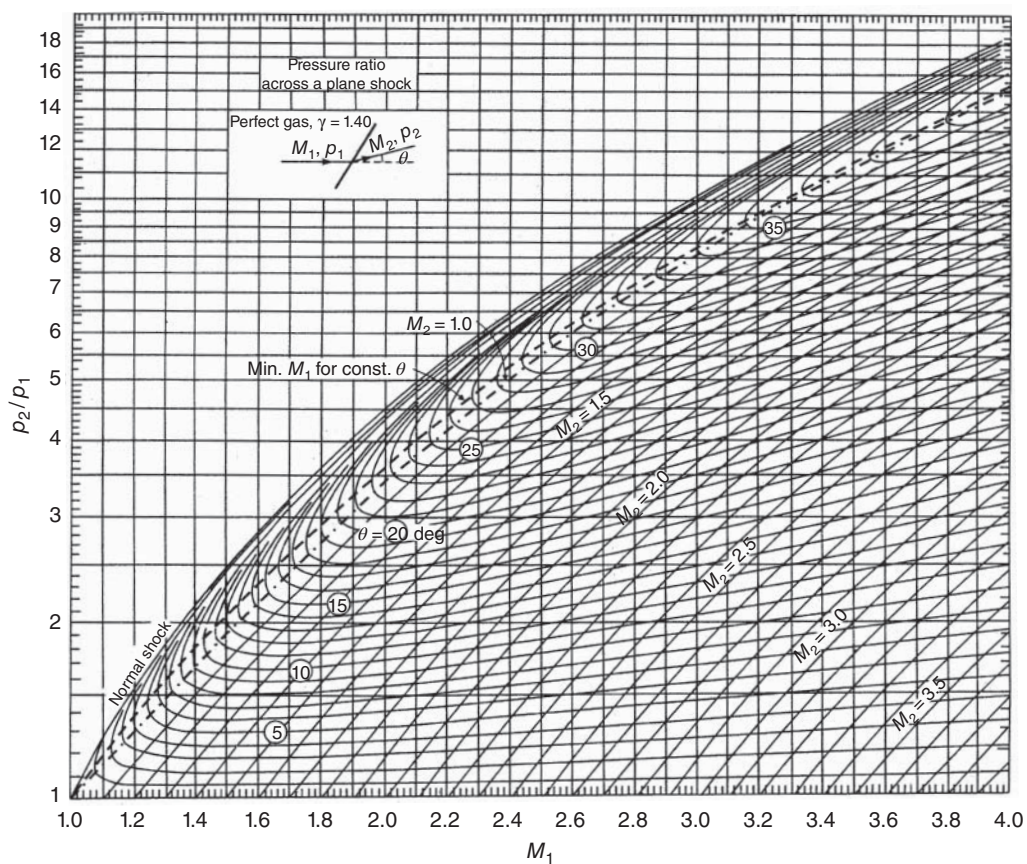
Table A.5 (Continued)

$M$	$T_0/T_0^*$	$T/T^*$	$p/p^*$	$p_0/p_0^*$	$\rho^*/\rho$
4.20	0.58065	0.15388	0.09340	9.74726	1.64757
4.22	0.57987	0.15254	0.09255	9.91244	1.64818
4.24	0.57909	0.15121	0.09171	10.08013	1.64878
4.26	0.57832	0.14990	0.09089	10.25035	1.64937
4.28	0.57757	0.14861	0.09007	10.42314	1.64995
4.30	0.57682	0.14734	0.08927	10.59851	1.65052
4.32	0.57608	0.14607	0.08847	10.77653	1.65109
4.34	0.57535	0.14483	0.08769	10.95721	1.65165
4.36	0.57463	0.14360	0.08691	11.14057	1.65220
4.38	0.57392	0.14239	0.08615	11.32666	1.65275
4.40	0.57322	0.14119	0.08540	11.51551	1.65329
4.42	0.57252	0.14000	0.08465	11.70714	1.65382
4.44	0.57183	0.13883	0.08392	11.90160	1.65434
4.46	0.57116	0.13767	0.08319	12.09891	1.65486
4.48	0.57049	0.13653	0.08248	12.29911	1.65537
4.50	0.56982	0.13540	0.08177	12.50222	1.65588
4.52	0.56917	0.13429	0.08107	12.70830	1.65638
4.54	0.56852	0.13319	0.08039	12.91737	1.65687
4.56	0.56789	0.13210	0.07971	13.12946	1.65735
4.58	0.56726	0.13102	0.07903	13.34460	1.65783
4.60	0.56663	0.12996	0.07837	13.56284	1.65831
4.62	0.56602	0.12891	0.07771	13.78422	1.65878
4.64	0.56541	0.12787	0.07707	14.00875	1.65924
4.66	0.56480	0.12685	0.07643	14.23648	1.65969
4.68	0.56421	0.12583	0.07580	14.46746	1.66014
4.70	0.56362	0.12483	0.07517	14.70170	1.66059
4.72	0.56304	0.12384	0.07456	14.93925	1.66103
4.74	0.56246	0.12286	0.07395	15.18016	1.66146
4.76	0.56190	0.12190	0.07335	15.42444	1.66189
4.78	0.56133	0.12094	0.07275	15.67216	1.66232
4.80	0.56078	0.12000	0.07217	15.92333	1.66274
4.82	0.56023	0.11906	0.07159	16.17798	1.66315
4.84	0.55969	0.11814	0.07101	16.43619	1.66356
4.86	0.55915	0.11722	0.07045	16.69797	1.66397
4.88	0.55862	0.11632	0.06989	16.96336	1.66437
4.90	0.55809	0.11543	0.06934	17.23241	1.66476
4.92	0.55758	0.11455	0.06879	17.50515	1.66515
4.94	0.55706	0.11367	0.06825	17.78162	1.66554
4.96	0.55655	0.11281	0.06772	18.06187	1.66592
4.98	0.55605	0.11196	0.06719	18.34592	1.66629
5.00	0.55556	0.11111	0.06667	18.63384	1.66667



**Figure A.1** Oblique shock chart 1. Variation of shock angle ( $\beta$ ) with flow deflection angle ( $\theta$ ) at various upstream Mach numbers (for perfect gas with  $\gamma = 1.4$ ).





**Figure A.2** Oblique shock chart 2. Variation of pressure ratio and downstream Mach number with flow deflection angle and upstream Mach number.

## References

- 1 Rathakrishnan, E. (2005). *Fundamentals of Engineering Thermodynamics*, 2e. New Delhi: Prentice Hall of India.
- 2 Tsien, H.S. (1946). Superaerodynamics, mechanics of rarefied gases. *Journal of the Aeronautical Sciences* 13 (2): 653.
- 3 Rathakrishnan, E. (2012). *Gas Tables*, 3e. Hyderabad, India: Universities Press.
- 4 Rathakrishnan, E. (2008). Physics of nozzle flow process. *International Review of Aerospace Engineering (IREASE)* 1 (5): 489–491.
- 5 Rathakrishnan, E. (2017). *Instrumentation, Measurements and Experiments in Fluids*, 2e. Boca Raton, FL: CRC Press.
- 6 Rathakrishnan, E. (2017). *Gas Dynamics*, 6e. New Delhi: Prentice Hall of India.
- 7 Shapiro A.H., Dynamics and Thermodynamics of Compressible Fluid Flow: Volumes I & II, Ronald Press, New York, 1953.
- 8 Thompson, P.A. (1972). *Compressible Fluid Dynamics*. New York: McGraw-Hill.
- 9 Rathakrishnan, E. (2012). *Fluid Mechanics: An Introduction*, 3e. New Delhi: Prentice Hall of India.
- 10 Liepmann, H.W. and Roshko, A. (1963). *Elements of Gas Dynamics*. New York: Wiley.
- 11 Ladenburg, R.W. (ed.) (1954). *Physical Measurement in Gas Dynamics and Combustion: Part I*. Princeton: Princeton University Press.
- 12 Hill, P.G. and Peterson, C. (1999). *Mechanics and Thermodynamics of Propulsion*. Addison-Wesley.
- 13 Seddon, J. and Goldsmith, E.L. (1999). *Intake Aerodynamics*. Blackwell Science.
- 14 Wu, J.H.T. (1962). On a two-dimensional perforated intake diffuser. *Aerospace Engineering* 21: 58.
- 15 McGregor I., Some theoretical parameters relevant to the performance of rectangular intakes with double-ramp compression surfaces at supersonic speeds, RAE Technical Report 71237, 1971.
- 16 Oswatitsch K.L., Der Druckruckgewinn bei Geschossen mit Ruckstossantrieb bei hohen Uber-schallgeschwindigkeiten [der Wirkungsgrad von Stossdiffusoren]. Forschungen und Entwicklungen des Heereswaffenamtes, Bericht, Nr. 1005, 1944.
- 17 Hermann, R. (1956). *Supersonic Inlet Diffusers and Introduction to Internal Aerodynamics*. Minneapolis-Honeywell Regulator Company.
- 18 Connors J.F. and Meyer R.C., Design Criteria for Axisymmetric and Two-Dimensional Supersonic Inlets and Exits, NACA TN Note 3589, 1956.
- 19 Abramovich, G.N. (1963). *The Theory of Turbulent Jets*. Boston: The MIT Press.
- 20 Pai, S. (1954). *Fluid Dynamics of Jets*. Toronto: Van Nostrand.
- 21 Rajaratnam, N. (1976). *Turbulent Jets*. Amsterdam: Elsevier Scientific Publishing Co.

- 22 Browand, F.K. and Weidman, P.D. (1976). Large scales in the developing mixing layer. *Journal of Fluid Mechanics* 76: 127–144.
- 23 Carletti, M.J., Rogers, C.B., and Parekh, D.E. (1995). Use of streamwise vorticity to increase mass entrainment in a cylindrical ejector. *AIAA Journal* 33: 1641–1645.
- 24 Rathakrishnan, E. (2009). Experimental studies on the limiting tab. *AIAA Journal* 47 (10): 2475–2485.
- 25 Crow, S.C. and Champagne, F.H. (1971). Orderly structures in jet turbulence. *Journal of Fluid Mechanics* 48 (3): 547–591.
- 26 Brown, G.L. and Roshko, A. (1974). On density effects and large structure in turbulent mixing layers. *Journal of Fluid Mechanics* 64 (4): 775–816.
- 27 Winant, C.D. and Browand, F.K. (1974). Vortex pairing: the mechanism of turbulent mixing layer growth at moderate Reynolds numbers. *Journal of Fluid Mechanics* 63 (2): 237–255.
- 28 Dimotakis, P.E. and Brown, G.J. (1976). The mixing layers at high Reynolds numbers: large structures dynamics and entrainment. *Journal of Fluid Mechanics* 78: 535–560.
- 29 Bernal, L. and Roshko, A. (1986). Streamwise vortex structures in plane mixing layers. *Journal of Fluid Mechanics* 170: 499–525.
- 30 Bogdanoff, D.W. (1983). Compressibility effects in turbulent shear layers. *AIAA Journal* 21: 926–927.
- 31 Papamoschou, D. and Debiasi, M. (1999). Noise measurements in supersonic jets treated with the Mach wave elimination method. *AIAA Journal* 37 (2): 154–160.
- 32 Liepmann, D. and Gharib, M. (1992). The role of streamwise vorticity in the near-field entrainment of round jets. *Journal of Fluid Mechanics* 245: 643–668.
- 33 Hussain, A.K.M.F. (1986). Coherent structures and turbulence. *Journal of Fluid Mechanics* 173: 303–356.
- 34 Verma, S.B. and Rathakrishnan, E. (1998). Mixing enhancement and noise attenuation in notched elliptic-slot jets. *International Journal of Turbo and Jet Engines* 15: 7–25.
- 35 Roshko A. and Papamoschou D., Observation of Supersonic Free Shear Layers, AIAA Paper 86–0162, 1986.
- 36 Ho, C.M. and Gutmark, E.J. (1987). Vortex induction and mass entrainment in a small-aspect ratio elliptic jet. *Journal of Fluid Mechanics* 179: 383–405.
- 37 Bradbury, L.J.S. and Khadem, A.H. (1975). The distortion of a jet by tabs. *Journal of Fluid Mechanics* 70: 801–813.
- 38 Ahuja K.K. and Brown W.H., Shear Flow Control by Mechanical Tabs, AIAA Paper 89–0994, 1989.
- 39 Zaman K.B.M.Q., Streamwise Vorticity Generation and Mixing Enhancement in Free Jets by Delta-Tabs, AIAA Paper 93–3253, 1993.
- 40 Zaman, K.B.M.Q., Reeder, M.F., and Samimy, M. (1994). Control of an axisymmetric jet using vortex generators. *Physics of Fluids* 6: 778–793.
- 41 Bohl D. and Foss J.F., Enhancement of Passive Mixing Tabs by the Addition of Secondary Tabs, AIAA Paper 96–054, 1996.
- 42 Wishart, D.P., Krothapalli, A., and Mungal, M.G. (1993). Supersonic jet control disturbances inside the nozzle. *AIAA Journal* 31 (7): 1340–1341.
- 43 Reeder, M.F. and Samimy, M. (1996). The evolution of a jet with vortex-generating tabs: real-time visualization and quantitative measurements. *Journal of Fluid Mechanics* 311: 73–118.
- 44 Zaman K.B.M.Q., Reeder M.F., and Samimy M., Supersonic Jet Mixing Enhancement by Delta Tabs, AIAA Paper 92–3548, 1992.
- 45 Kumar Singh, N. and Rathakrishnan, E. (2002). Sonic jet control with tabs. *Journal of Turbo and Jet Engines* 19: 107–118.

- 46 Lovaraju P., Paparao K.P.V., and Rathakrishnan E., Shifted Cross-Wire for Supersonic Jet Control, *AIAA Paper 2004-4080*, 2004.
- 47 Ahuja K.K., Mixing Enhancement and Jet Noise Reduction Through Tabs Plus Ejectors, *AIAA Paper 93-4347*, 1993.
- 48 Steffen C.J., Reddy D.R., and Zaman K.B.M.Q., Numerical Modeling of Jet Entrainment for Nozzles Fitted with Delta Tabs, *AIAA Paper 97-0709*, 1997.
- 49 Zaman, K.B.M.Q., Reeder, M.F., and Samimy, M. (1993). Control of an axisymmetric jet using vortex generators. *Physics of Fluids A* 6: 778-793.
- 50 Zaman K.B.M.Q., Spreading Characteristics and Thrust of Jets from Asymmetric Nozzles, *AIAA Paper 96-0200*, 1996.
- 51 Surks, P., Rogers, C.B., and Parekh, D.E. (1994). Entrainment and acoustic variation in a round jet from introduced streamwise vorticity. *AIAA Journal* 32 (10): 2108-2110.
- 52 Jhang S. and Schneider S.P., Molecular-Mixing Measurement and Turbulent-Structure Visualizations in a Round Jet with Tabs, *AIAA Paper 94-3082*, 1994.
- 53 Gretta, W.J. and Smith, C.R. (1993). The flow structure and statistics of a passive mixing tab. *Journal of Fluid Engineering* 115 (2): 255-263.
- 54 Krothapalli, A. and Wishart, D.P. (1993). Supersonic jet control via point disturbances inside the nozzle. *AIAA Journal* 31 (7): 1340-1341.
- 55 Csanady, G.T. (1996). The effect of mean velocity variation on jet noise. *Journal of Fluid Mechanics* 26 (1): 183-197.
- 56 Lovaraju, P., Clement, S., and Rathakrishnan, E. (2007). Effect of cross-wire and tabs on sonic jet structure. *Journal of Shock Waves* 17 (1-2): 71-83.
- 57 Samimy, M. and Reeder, M.F. (1993). Effects of tabs on the flow and noise field of an axisymmetric jet. *AIAA Journal* 31 (5): 609-619.
- 58 Lovaraju, P. and Rathakrishnan, E. (2006). Subsonic and transonic jet control with cross-wire. *AIAA Journal* 44 (11): 2700-2705.
- 59 Mrinal, K., Pankaj, S.T., and Rathakrishnan, E. (2006). Studies on the effect of notches on circular sonic jet mixing. *Journal of Propulsion and Power* 22: 211-214.
- 60 Clement, S. and Rathakrishnan, E. (2006). Characteristics of sonic jets with tabs. *Shock Waves* 15 (3-4): 211-214.
- 61 Srinivasan, K. and Rathakrishnan, E. (2001). A simple mobile anechoic chamber for experiments in jet acoustics. *Journal of Turbo and Jet Engines* 18 (1): 59-64.
- 62 Chiranjeevi Panindra, B. and Rathakrishnan, E. (2010). Corrugated tabs for supersonic jet control. *AIAA Journal* 48 (2): 453-465.
- 63 Rathakrishnan, E. (2008). Waves in correctly expanded supersonic jets. *International Review of Aerospace Engineering (IREASE)* 1 (6): 536-538.
- 64 Verma, S.B. and Rathakrishnan, E. (1999). Experimental study on the noise characteristics of notched circular-slot jets. *Journal of Sound and Vibration* 226 (2): 383-396.
- 65 Grinstein, F.F., Gutmark, E., and Parr, T. (1995). Near field dynamics of subsonic free square jets: a computational and experimental study. *Physics of Fluids* 7 (6): 1483-1497.
- 66 Gutmark, E., Schadow, K.C., and Wilson, K.J. (1991). Subsonic and supersonic combustion using non-semi-circular injectors. *Journal of Propulsion and Power* 7 (2): 240-249.
- 67 Miller, R.S., Madnia, C.K., and Givi, P. (1995). Numerical simulation of non-semi-circular jets. *Computer & Fluids* 24 (1): 1-25.
- 68 Koshigoe, S., Gutmark, E., and Schadow, K.C. (1989). Initial development of non-semi-circular jets leading to axis-switching. *AIAA Journal* 27 (4): 411-419.
- 69 Gutmark, E.J., Schadow, K.C., and Bicker, C.J. (1990). Near acoustic field and shock structure of rectangular supersonic jet. *AIAA Journal* 28 (7): 1163-1170.

- 70 Krothapalli, A., Hsia, Y., Baganoff, D., and Karamcheti, K. (1986). The role of screech tones on mixing of an underexpanded jet. *Journal of Sound Vibration* 106: 119–143.
- 71 Srinivasan, K. and Rathakrishnan, E. (2001). Studies on underexpanded rectangular slot jets. *Journal of the Aeronautical Society of India* 53 (1): 39–43.
- 72 Clement, S., Murugan, K.N., and Rathakrishnan, E. (2005). Superiority of elliptical jets. *Journal of the Institution of Engineers (India): Aerospace Engineering Division* 86: 1–7.
- 73 Schadow, K.C., Gutmark, E., Koshigoe, S., and Wilson, K.J. (1989). Combustion-related shearflow dynamics in elliptic supersonic jets. *AIAA Journal* 27 (10): 1347–1353.
- 74 Quinn, W.R. (2007). Experimental study of the near field and transition region of a free jet issuing from a sharp-edged elliptic orifice plate. *European Journal of Mechanics* 26: 583–614.
- 75 Mitchell, D.M., Honnery, D.R., and Soria, J. (2013). Near-field structure of underexpanded elliptic jets. *Experiments in Fluids* 54 (1578).
- 76 Yoon, J.H. and Lee, S.J. (2003). Investigation of the near-field structure of an elliptic jet using stereoscopic particle image velocimetry. *Measurement Science and Technology* 14: 2034–2046.
- 77 Hussain, A.K.M.F. and Husain, H.S. (1989). Elliptic jets: part 1: characteristics of unexcited and excited jets. *Journal of Fluid Mechanics* 208: 257–320.
- 78 Quinn, W.R. (1989). On mixing in an elliptic turbulent free jet. *Physics of Fluids* 1 (10): 1716–1722.
- 79 Menon, N. and Skews, B.W. (2010). Shock wave configurations and flow structures in non-axisymmetric underexpanded sonic jets. *Shock Waves* 20: 175–190.
- 80 Hussain, A.K.M.F. and Husain, H.S. (1991). Elliptic jets: part 2: dynamics of coherent structures: pairing. *Journal of Fluid Mechanics* 233: 439–482.
- 81 Gutmark, E.J., Schadow, K.C., Parr, T.P. et al. (1989). Non-semi-circular jets in combustion systems. *Experiments in Fluids* 7: 248–258.
- 82 Zaman, K.B.M.Q. (1996). Axis switching and spreading of an asymmetric jet: the role of coherent structure dynamics. *Journal of Fluid Mechanics* 316: 1–27.
- 83 Aravindh Kumar, S.M. and Rathakrishnan, E. (2016). Characteristics of a supersonic elliptic jet. *The Aeronautical Journal* 120 (1225): 495–519. <https://doi.org/10.1017/aer.2016.7>.
- 84 Tam, C.K.W. (1995). Supersonic jet noise. *Annual Review of Fluid Mechanics* 27: 17–43.
- 85 Chauhan, V., Aravindh Kumar, S.M., and Rathakrishnan, E. (2015). Mixing characteristics of underexpanded elliptic sonic jets from orifice and nozzle. *Journal of Propulsion and Power* 31 (2): 496–504.
- 86 Chauhan, V., Aravindh Kumar, S.M., and Rathakrishnan, E. (2016). Aspect ratio effect on elliptical sonic jet mixing. *The Aeronautical Journal* 120 (1230): 1197–1214. <https://doi.org/10.1017/aer.2016.55>.
- 87 Aravindh Kumar, S.M. and Rathakrishnan, E. (2014). Triangular tabs for supersonic jet mixing enhancement. *The Aeronautical Journal* 118 (1209): 1245–1278. <https://doi.org/10.1017/S0001924000009969>.
- 88 Takama, Y., Suzuki, K., and Rathakrishnan, E. (2010). Visualization and size measurement of vortex shed by flat and arc plates in a uniform flow. *International Review of Aerospace Engineering* 1: 55–60.
- 89 Chow, W.L. and Chang, I.S. (1972). Mach reflection from overexpanded nozzle flows. *AIAA Journal* 10 (9): 1261–1263.
- 90 Arun Kumar, P. and Rathakrishnan, E.. Triangular tabs for supersonic jet mixing enhancement, *The Aeronautical Journal* November 2014, Vol. 118, No. 1209, pp. 1245–1278, DOI: 10.1017/S0001924000009969.

- 91 Bajpai, A. and Rathakrishnan, E. (2017). Tab geometry effect on supersonic elliptic jet control. *International Journal of Turbo and Jet Engines* 34 (4): 395–408.
- 92 Kumar P., Shifted tabs for supersonic jet control, Master's thesis, Department of Aerospace Engineering, Indian Institute of Technology Kanpur, India, 2015.
- 93 Berrueta, T. and Rathakrishnan, E. (2017). Control of subsonic and sonic jets with limiting tabs. *International Journal of Turbo and Jet Engines* 34 (1): 103–113.
- 94 Maruthupandiyan, K. and Rathakrishnan, E. (2016). Supersonic jet control with shifted tabs. *Proceedings of the Institution of Mechanical Engineers, Part G: Journal of Aerospace Engineering* 0 (0): 1–15 <https://doi.org/10.1177/0954410016679197>.
- 95 Dadhich U, Jet control with ventilated triangular tabs, Master's thesis, Department of Aerospace Engineering, Indian Institute of Technology Kanpur, India, 2015.
- 96 Manideep A., Shifted sharp-edged rectangular tab for supersonic jet control, Master's thesis, Department of Aerospace Engineering, Indian Institute of Technology Kanpur, India, 2016.
- 97 Aravindh Kumar, S.M. and Rathakrishnan, E. (2017). Control of elliptic supersonic jet of aspect ratio 3. *Journal of Aerospace Engineering* 30 (5): [https://doi.org/10.1061/\(ASCE\)AS.1943-5525.0000762](https://doi.org/10.1061/(ASCE)AS.1943-5525.0000762).
- 98 Rathakrishnan, E. (2018). AR 4 elliptic jet control with limiting tab. *Fluid Dyn. Res.* 50 (2018) 025505 (20pp) <https://doi.org/10.1088/1873-7005/aa9b96>.

## Index

### **a**

absolute units 7, 27  
 acceleration 6, 44  
   convective 44  
   local 44  
   substantial 44  
   zones 421  
 Ackeret's theory 203  
 action, zone of 9, 32  
 active control 473, 542  
 adiabatic ellipse 31  
 adiabatic flow process 14, 16, 288  
 adiabatic wall temperature 336  
 aerodynamic coefficients 242, 252, 268  
 aerodynamic duct 405  
 aerodynamic forces 197  
 aerodynamic losses 401, 411  
 aerothermodynamics of  
   engine components 404  
 aerothermodynamic theory 33  
 affine transformation 239  
 airfoil  
   circular arc 206  
   diamond wedge 197  
 analogy  
   version I 267, 268  
   version II 267, 268  
   version III 267, 268  
 area blockage 479  
 area-Mach number relation 58, 98  
 area-velocity relation 55, 241  
 axis-switching 477, 520  
 axisymmetric flows 229

### **b**

backpressure 48, 59  
 barometer 329

barotropic fluid 45  
 barrel shock 66, 67, 342, 465, 498  
 base drag 385  
 Bernoulli's equation 3, 14, 20, 44  
 blockage effect 462  
 blockage test 388  
 blowdown tunnel 142  
   intermittent 355  
   operation 369  
   running time of 374  
 blunt-faced cylinder 114  
 blunt-nosed body 189, 190  
 bodies of revolution 232, 234, 255, 261  
   potential equation for 229  
 boundary conditions 231  
 boundary layer 22, 28  
 boundary layer separation 243, 249, 389,  
   406  
 bow shock 382, 461

### **c**

calibration 380, 381  
   of hypersonic tunnels 386  
   of supersonic tunnels 380  
 calorically perfect gas 17, 18, 33  
 caloric properties 16  
 camber effect on drag 206  
 cancellation of wave reflection 321  
 capture streamtube 405  
 centered expansion 67, 320  
   process 170  
   wave 138, 147  
    $x$ - $t$  diagram of 138  
 characteristic decay 452  
 characteristic Mach number 53, 116  
   expression for 58

characteristics 138, 164, 273  
     left-running 211  
     right-running 211  
         method of 309  
 chemically reacting gas 118, 122, 147  
 choked flow 60, 94, 480  
 choked state 65  
 circulation 223, 242  
 classification  
     control methods 473  
     of flow regimes 32  
     of jets 454  
 closed system 12, 33  
 coefficient of  
     discharge 71  
     drag 203, 206  
     friction 286  
     heat transfer 338  
     lift 203, 205  
     nozzle discharge 73  
     pressure 95, 233  
     turbulence viscosity 456  
     viscosity 28  
 color Schlieren 348  
 combustion  
     chamber 396  
     efficiency 403  
     supersonic 411, 442  
 compatibility relation 310  
 compressible Bernoulli equation 99  
 compressibility 2, 32  
     correction to dynamic pressure 91  
     limiting conditions 3  
 compressible flow 1, 31  
     basic potential equation 226  
     measurements in 329  
     regimes 30  
     visualization 339  
 compression corner 155, 156, 163  
 compression wave 1, 27, 62  
     isentropic 165  
 compressor pressure ratio 358, 360  
 compressor tunnel matching 362  
 conservation of  
     energy principle 33  
     mass 3, 71  
 contact surface 134, 140, 180 *see also*  
     slipstream  
 continuity equation 54, 57, 171, 224

continuous  
     compression 167, 177  
     expansion 67, 169, 328  
 continuum flow 97, 114  
 continuum hypothesis 28  
 contoured nozzle 57, 64  
 contraction cone 392  
 contraction ratio 79  
     of diffuser 79, 362  
 control mass 33  
 control of jets 471  
     active 473  
     passive 473  
 control volume 33  
 convective Mach number 475, 476  
 convergent–divergent nozzle 56, 57  
     contoured 97  
         design 324  
     elliptic nozzle 477, 520, 526  
     flow in 60  
     mass flow through 65, 66  
     straight 64  
 core of jet 452, 454  
     subsonic jet 452  
     supersonic jet 467, 469  
 correction coefficient 99  
 corrugated tabs 481, 497, 498  
 critical Mach number 243, 261  
 critical operation 415, 418  
     critical pressure ratio 51  
     subcritical operation 415, 418  
     supercritical operation 415, 418  
 critical values 48, 51  
 Crocco's theorem 221, 223  
 crossing of waves 180, 212  
 curved shock 190

## **d**

D'Alembert's paradox 198  
 de Laval nozzle 57, 67, 68, 78, 97  
     design of 323  
 density problems 339  
 design of supersonic nozzle 323  
 detached shock 113, 160, 189–192  
 determination of  
     flow angularity 383, 388  
     Mach number 381, 386  
     test-section noise 384, 388  
     turbulence level 383



dial-type pressure gauge 332  
 diffuser 75  
     contraction ratio 79, 362  
     efficiency 84  
         relation for 85  
     isentropic efficiency of 358, 359  
     normal shock 77, 215  
     oblique shock 77, 215  
     polytropic efficiency of 358  
     supersonic 76, 78, 412  
         special features of 77  
     of supersonic tunnel 78, 358  
 discharge coefficient of nozzle 73  
 discharge from reservoir 45  
 discontinuity surface 180  
 dissimilar metals 335  
 disturbance waves 10, 155  
     propagation of 9, 10  
 double wedge 199, 427  
 drag coefficient 203, 206, 242, 252  
     due to camber 206  
     due to lift 206, 385  
     due to thickness 206  
     intake 415, 432  
     per unit span 198  
     wave drag 198, 211, 261  
 dynamic pressure 4, 88, 203  
     compressibility correction for 91  
     correction coefficient 92

## e

effects of second throat 360  
 efficiency  
     aerodynamic 261  
     of diffuser 84  
         isentropic 358, 410  
         polytropic 358  
     of nozzle 71  
 elliptic equation 229, 239, 253, 271, 310  
 elliptic jet 473, 519, 523  
     shadowgraph image of 522, 529  
 energy equation 1, 7, 11, 19, 115  
     for an adiabatic flow 14  
     for isentropic flow process 45  
     for an open system 12, 33  
 engine inlets 404  
     subsonic inlets 404  
     supersonic inlets 411  
 enthalpy 7, 12, 223

    specific 14  
     stagnation 13  
     static 13  
 entrainment 451, 453  
 entropy 11  
     calculation 18  
     definition of 15  
     discontinuity 180  
     equation 15  
 equation of state  
     calorical 16  
     for perfect or ideal gas 3  
     thermal 16  
 Euler's equation 171, 225, 235  
 expansion  
     centered 67, 138  
     continuous 67  
     corner 156  
     fan 66, 156  
         reflection of 184  
         strength of 139  
     Prandtl-Meyer 170  
     wave 1, 61  
     work 14

## f

Fanno  
     curves 284  
     flow 283  
     line 284  
     table of 604  
 first law of thermodynamics 11  
     for an open system 13  
 fixed-geometry inlets 83  
 flow  
     adiabatic 14  
     deflection angle 155, 165  
     with friction 283  
     with heating or cooling 294  
     inviscid 44  
     isentropic 2  
     mass rate of 2, 44, 47  
     one-dimensional 43  
     potential 228 *see also* potential flow  
     two-dimensional 27, 155, 164, 169  
 flow through inlets 405  
 flow visualization 192, 339, 390  
 force measurement 389  
 free molecular flow 130

friction coefficient  
 definition of 286  
 fringe-displacement method 344

**g**

gas  
 calorically perfect 17  
 calorical properties 16  
 perfect 6, 17  
 thermally perfect 16  
 thermal properties 16  
 gas constant 7, 16  
 universal 49  
 gas dynamics 1  
 definition of 1  
 general region 319  
 Gladstone-Dale constant 341  
 Gladstone-Dale equation 341  
 Gothert's rule 240, 244, 247, 252, 254  
 for finite wings 260  
 for subsonic flow 244  
 for supersonic flow 247  
 three-dimensional flow 252  
 two-dimensional flow 244

**h**

heating value (HV) definition of 399  
 higher heating value (HHV) 399  
 high-speed  
 flow 11, 139, 283, 335  
 tunnels 354  
 hodograph plane 161  
 hot-wire anemometer 383  
 constant current type (CCA) 391  
 constant temperature  
 type (CTA) 391  
 Hugoniot  
 curve 122  
 equation 121, 122, 147  
 hyperbolic equation 255, 311  
 hypersonic 31  
 flow 31, 64, 168, 228, 236, 250  
 nozzle 377  
 similarity 250  
 similarity parameter 251, 269  
 tunnel 354, 375, 376

**i**

ideal gas 3, 26

ideal ramjet 396  
 incompressible  
 Bernoulli's equation 3, 14  
 flow 1, 2, 11, 26  
 intake  
 center body 424  
 Concorde 431  
 double-wedge 428  
 inlet flow process 406  
 multi-shock 427  
 pitot 415  
 single-wedge 424  
 two-shock 423  
 interferometer 340, 341  
 introduction to free jets 451  
 irreversible processes 33  
 irrotational flow 224  
 isenthalpic flow 1  
 isentropic compression 24, 167, 429  
 waves 165, 167  
 isentropic efficiency 358, 359, 410  
 isentropic flow 2  
 table 547  
 isentropic index 6  
 isentropic process 12  
 definition of 15  
 equation for 6  
 isentropic relations 20

**j**

jet 451  
 acoustic characteristics 490, 496  
 centerline decay 451, 453, 461, 468  
 characteristic decay 452  
 classification of 454  
 co-flowing 451  
 compressible 453  
 control of 453  
 active control 473  
 with the limiting tab 481  
 passive control 473  
 control with tabs 471  
 core 452  
 correctly expanded 61, 467  
 centerline decay 63  
 waves in 62  
 definition of 451  
 elliptic 519  
 entrainment 451

- expansion levels of 464
  - flow development 477, 480
  - free 451
    - turbulence characteristics 457
  - fully developed zone 452, 454
  - impinging 451
  - incompressible 453
  - noise 462
    - amplitude 463, 493
    - frequency 491
    - mixing 462
    - screech 462, 480
    - shock associated 462
  - noncircular 519
  - opposing 451
  - overexpanded 453, 454, 464–467
    - centerline decay 466
  - potential core 454
  - pressure profiles 504
  - shadowgraph picture 470
  - sonic 453
  - submerged 451
  - subsonic 453
  - supersonic 453
  - theory of 455, 456
  - transition region 454
  - turbulence characteristics of 457
  - underexpanded 469
    - centerline decay 472
    - shadowgraph picture 470
    - water flow visualization 517
- k**
- King's law 338
  - knife-edge 344, 348
  - Knudsen number 130
- l**
- Laplace's equation 6, 224
    - basic solutions of 224
  - lift 198, 202
    - coefficient of 203, 205
  - light source 341, 348
  - like reflection 183, 185, 192, 211
  - limits of external compression 431
  - linearized potential flow equation 228, 236
  - liquid manometers 329
    - measuring principle 330
  - losses in supersonic tunnels 357
    - expansion loss 358
    - frictional losses 358
    - losses in contraction cone 358
    - losses in cooling system 358
    - losses in guide vanes 358
    - losses in test-section 358
  - losses due to model and support system drag 358
  - losses due to shock wave 358
  - lower heating value (LHV) 399
- m**
- Mach angle 8, 157
    - Mach cone 10, 27
    - Mach number relation 163
  - Mach disc 342, 353, 469, 471, 536
  - Mach line 9, 32, 163, 171
  - Mach number 4, 28
    - characteristic 53
    - critical 243, 256, 261
    - definition of 4, 5
    - determination 381, 388
    - relation to area 58
    - relation to density 22
    - relation to pressure 22
    - relation to temperature 21
    - relation to total pressure 76
    - of shock wave 126
  - Mach reflection 191
  - Mach wave 9, 27, 32, 116, 157, 189
  - manometers 329
    - measuring principle of 330
    - multi-tube 330
    - U-tube 330
  - mass flow rate 2
    - maximum 65
    - per unit area 47
    - relation 65
  - mass-motion velocity 126
  - material boundary 180
  - maximum velocity 46, 53, 406
  - measurements in compressible flow 329
    - density problems 339
    - pressure measurements 329
    - temperature measurements 335
    - velocity and direction 338
  - method of characteristics 309
    - axisymmetric flow 316
    - boundary points 313

method of characteristics (*contd.*)  
 compatibility relations 310  
 computational method 312  
 concepts of characteristics 309  
 design of supersonic nozzle 323  
 nonisentropic flow 317  
 numerical computation 312, 320  
 sources of error 316  
 theorem for 2-D flow 318  
 mixing length 457, 458  
 momentum equations 1, 171, 235  
 momentum thrust 74  
 loss 479, 533  
 relation of 527  
 most amplified frequency 473  
 moving shock 123  
 density ratio across 126  
 governing equations 124  
 Mach number 126  
 temperature ratio across 125  
 velocity 126

## **n**

natural coordinates 221, 311  
 noncircular jets 473, 519, 544  
 nonsimple region 178, 211  
 normal shock 113  
 density ratio across 116  
 diffuser 76  
 in ducts 420  
 entropy change across 119, 146  
 equation for 113  
 flow through 114  
 Hugoniot equation 121  
 Prandtl relation of 116  
 pressure ratio across 117  
 reflected 133  
 Mach number 135  
 relations 115  
 speed of 123, 126  
 stagnation pressure ratio  
 across 76, 119  
 strength of 117  
 strong 130  
 table 559  
 thickness of 113, 148  
 wave 113  
 weak 128  
 nozzle 57

contoured 67  
 flow process 69  
 convergent 65, 68, 70, 97  
 convergent–divergent 60  
 correctly expanded 61  
 de Laval 57  
 design 323  
 discharge coefficient 73  
 efficiency 71  
 flow process 69  
 isentropic expansion 60, 66  
 overexpanded 61, 70, 98  
 pressure ratio (NPR) 69  
 sharp cornered 325  
 straight 68  
 supersonic 164, 323  
 underexpanded 61  
 Nusselt number 338

## **o**

oblique shock 155  
 chart 1 616  
 chart 2 617  
 flow through 156  
 intersection of 178, 180  
 limit as Mach wave 157, 159, 163  
 maximum deflection for 157, 159  
 reflection of 178  
 relations 156  
 solution 159  
 strong 160  
 table 569  
 transformed from normal shock 156  
 wave 155  
 weak 160  
 one-dimensional approximation 43  
 one-dimensional flow 43  
 with area change 54  
 with friction 283  
 with heating 294  
 open system 33  
 energy equation 13  
 optical methods 339  
 overall efficiency 401  
 overall sound pressure  
 level (OASPL) 491

## **p**

passive control 473

- perfect gas 33
    - adiabatic flow 14
    - calorically perfect gas 17, 18
    - definition of 17
    - entropy of 18
    - isentropic flow of 2
    - limitations of 25
    - normal shock in 114
    - specific heats of 6, 7, 18
    - speed of sound in 27
  - performance of actual intakes 410
  - perturbation
    - potential 228, 236, 277, 280
    - velocities 227, 230, 233
  - P–G rule 242, 243, 245–248, 252, 254, 258–261, 267, 268
  - piston problem 123
  - pitot
    - intakes 415
    - pressure 88, 382
      - measurement 382
    - tube 88, 382, 481
  - pitot-static tube 91
  - plane waves 123
  - polytropic efficiency 358
  - potential equation
    - for bodies of revolution 229
    - linearization of 226
    - supersonic flow 278
    - for 3-D flow 225
  - potential flow 28, 221, 228, 230, 235, 236, 253, 431
  - potential function 224
    - for doublet 225
    - for free vortex 225
    - for source 225
    - for uniform flow 224
  - Prandtl–Glauert (P-G) rule
    - for subsonic flow 239
    - for supersonic flow 245
  - Prandtl–Meyer expansion 170
  - Prandtl–Meyer flow 171
  - Prandtl–Meyer function 175
  - Prandtl number 28, 336
  - Prandtl relation 116
  - pressure
    - dynamic 4, 88, 204
    - geometric 88
    - hill 478, 534
    - pitot 88, 381
      - indicated 89
    - static 88
      - measurement of 89, 382
    - total 88
    - transducers 329, 333
  - pressure coefficient 95, 203
    - for incompressible flows 97
  - pressure ratio, critical 52, 98
  - process
    - adiabatic 12
    - constant pressure 33
    - constant volume 33
    - irreversible 12, 15, 33
    - isentropic 12, 15, 20
    - reversible 15, 20, 33
  - propagation of disturbance
    - waves 8, 9, 27
  - propulsive efficiency 400, 401
- q**
- quasi-one-dimensional flow 43, 54
- r**
- ramjet 395
    - engine 396
    - ideal 396
  - Rathakrishnan limit 479
  - Rayleigh flow 283
    - equations 294
  - Rayleigh line 294
    - relation 302
  - Rayleigh supersonic pitot formula 89, 99
  - recovery factor 336, 337
  - reflection
    - of an expansion fan 184
    - from free boundary 185, 321
      - like 185, 192
      - unlike 185, 465
    - Mach 191
    - of oblique shock 184
      - unlike 185, 211, 465
    - of waves 321
  - reservoir
    - discharge from 45
  - reversible process 12
  - revolution
    - body of 229, 232, 234
    - boundary condition 233

revolution (*contd.*)

coefficient of pressure 237

Reynolds number 28

control 370

effects 385

rotation 156, 223

## S

Schlieren method 339, 344, 350

sensitivity of 350

scramjet 411, 442, 446, 471

second throat 76, 361

effects of 360

Seebeck effect 335

principle 335

self-similar

flow 452

motion 211

region 452, 542

shadowgraph 352, 391

shaft work 12, 13

sharp cornered nozzle 325

shear layer 348, 451, 454, 473

role in flow control 474

subsonic 474

supersonic 475

shear stress 29, 285–288

shifted tabs 519, 527, 530–536

shock 9, 27

angle 10

barrel 66

definition of 113

detached 119, 160, 189–190

Mach number 126

moving 123

normal 113

equations of motion 113

oblique 70

reflected 133

speed 128

strength 117

strong 130

velocity 126

weak 128

shock cell 66

shock expansion theory 197

shock polar 160, 211

relation 162

shock-rhombus 357

shock swallowing 362, 416

shock tube 139

applications 142

diaphragm pressure ratio 140

driver section of 147

equation 141, 147

expansion section 147

flow motion in 140

short duration light source 348

silence zone 9

similarity parameters 28

similarity rule 239, 245, 252 *see also* P-G rule;  
Gothert's rule

simple region 178, 211

simple  $T_0$  change 294

relations for a perfect gas 295

simple waves 178, 211

slender bodies 226

slipstream 180, 184, 191

slip surface 180

small perturbation theory 227, 236

sonic velocity 10, 59, 97

specific enthalpy 14

specific heats 7, 18

ratio 6, 19

ratio for thermally perfect gas 18

ratio value range of 19

specific thrust 400

specific volume 14

speed of sound 5

expression 7

stagnation enthalpy 14

stagnation pressure 14 *see also* total pressure

stagnation pressure ratio 411

stagnation temperature 21 *see also* total  
temperature

stagnation temperature probe 337

starting load 355, 356, 385

starting problem 413

state equation

calorical state equation 17

for perfect gas 7

for a thermally perfect gas 16, 17

thermal state equation 17

static pressure definition of 88

measurement 382

probe 90

streamline 43

streamtube 43

- strength of shock 117
- strong shock 130
  - solution 159, 192
- subsonic flow
  - definition of 27
- subcritical operation 84, 415, 418
- submerged jet 451
- subsonic flow 27
- subsonic jet 453
- substantial acceleration 44
- substantial derivative 44
- supercritical operation 84, 415
- supersonic combustion 442
- supersonic diffusers 412
  - starting problem 412–418, 422
- supersonic flow 27
  - in duct with friction 283
  - in duct with simple  $T_0$  change 294
  - general linear solution for 271
  - generation 57, 66
  - linearized theory 32, 236
  - over a wave-shaped wall 277, 279
- supersonic inlets 81, 404, 411
- supersonic jet 453, 467
  - correctly expanded 467
  - overexpanded 464
  - underexpanded 469
- supersonic nozzle 56, 77
  - contoured 67
  - design of 323
  - flow in 60
  - straight C-D 64
- supersonic shear layers 475, 477
- supersonic static tube 90
- supersonic tunnels 68, 89, 354
  - blowdown type 354
  - continuous (closed-circuit) 356
  - induction type 355
  - losses in 357
- supersonic wind tunnel diffusers 78, 358
- surface discontinuity 180 *see also* slipstream
- symmetrical wedge 163, 338
- system
  - closed (or control mass) 11, 14, 33
  - open (or control volume) 12, 13, 33
- t**
- tab 474, 480
  - corrugated 481, 497, 498
- limit 503, 526
- sharp-edged 534
- shifted 545
- square-edged 534
- triangular 526, 527
  - ventilated 532, 533
- table
  - for Fanno flow 604
  - for isentropic flow 547
  - for normal shock 559
  - for oblique shock 569
  - for Rayleigh flow 610
- tangential discontinuity 180
- temperature
  - adiabatic wall 336
  - measurement of 335
  - ratio of total to static 21
  - rise 7, 396, 434
  - stagnation 8, 20, 53
  - total 8, 118, 168
- theory of turbulent jets 455
- thermal efficiency 401, 445
- thermocouple 335, 337, 390
- thermodynamics 11
  - first law of 11, 18
  - second law of 15
- thickness of normal shock 113, 148
- thin airfoil theory 202
  - application of 203
- thrust 168, 395, 527
  - general equation of 397, 400
  - specific 400
  - specific fuel consumption (TSFC) 400
- total pressure 77–79, 88
  - friction effect on 288
  - heat transfer effect on 298
- total temperature 8, 118, 168, 298, 336, 337, 366, 374, 380, 384, 386, 434, 437, 478
- transformation affine 239
- transonic flow 27, 31, 32
- u**
- underexpanded
  - jet 186, 453, 469
  - nozzle 61, 70, 98
- uniform flow 318

unlike reflection 185, 211, 465  
upper critical Mach number 267

## V

variable-geometry inlet 83  
velocity  
    critical 48, 51  
    dimensionless 28  
    maximum 31, 46, 53, 97  
    perturbation 227, 228  
    of shock  $C_s$  123, 126, 128  
    of sound 4, 5, 26  
        expression 7  
velocity plane 161  
velocity potential 225, 239, 280  
    for bodies of revolution 236, 256  
    equation of 236  
    linearized equation 309  
ventilated triangular tabs 532  
visualization  
    of compressible flow 339  
    of incompressible flows 340  
    von Karman rule for transonic flow 248, 261  
vortex dynamics 453  
vortex manipulation 453, 497  
vortices  
    large-scale (mass entraining) 453, 520, 523, 528, 540–542, 544  
    small-scale (mixing promoting) 453, 520, 523, 528, 540–542  
vorticity components 223

## W

wave  
    cancellation of 321  
    centered 67, 138 *see also* centered  
        expansion waves  
    compression 1, 6, 113  
    expansion 138, 155 *see also* expansion,  
        waves  
    intersection of 178, 180, 181  
    left-running 27, 175, 181, 211  
    Mach 1, 9, 10, 27, 32, 116  
    normal shock 113 *see also* normal shock  
    oblique shock 155 *see also* oblique shock  
    propagation 9, 26

    reflection from free boundary 183  
    reflection from rigid wall 179  
    right-running 27, 175, 181, 191  
wave drag 198  
wave equation 272  
wave motion 123  
wave shaped wall 276, 277  
    subsonic flow 277  
    supersonic flow 277  
wave speed 123  
weak shock 128  
    solution 159  
wedge  
    double 198, 199  
    symmetrical 163  
    unsymmetrical 163  
wind tunnels 354  
    blockage test 388  
    blowdown type 354  
    calibration of 380  
        supersonic tunnels 380  
    constant throttle operation 369, 392  
    continuous 356, 387  
        constant pressure operation  
            369, 392  
        constant Reynolds number operation  
            369, 392  
    determination of  
        flow angularity 388  
        test-section noise 384  
        turbulence level 383, 388  
    flow angularity 383, 388  
    flow visualization 390  
    force measurements 389  
    high-speed 354  
    hypersonic 354, 375  
    induction type 355  
    intermittent 354  
    low-speed 354  
Mach number determination 381, 386  
    optimum conditions 372  
    Reynolds number control 370  
    Reynolds number effects 385, 389  
    running time 370, 372, 373  
    special purpose 354  
    starting load 388  
    starting of 384



supersonic 59, 350, 354, 356, 357  
turbulence level 383  
wind tunnel nozzle 73, 324  
    characteristics of 324

**Z**

zone of action 9, 32  
zone of silence 9, 32